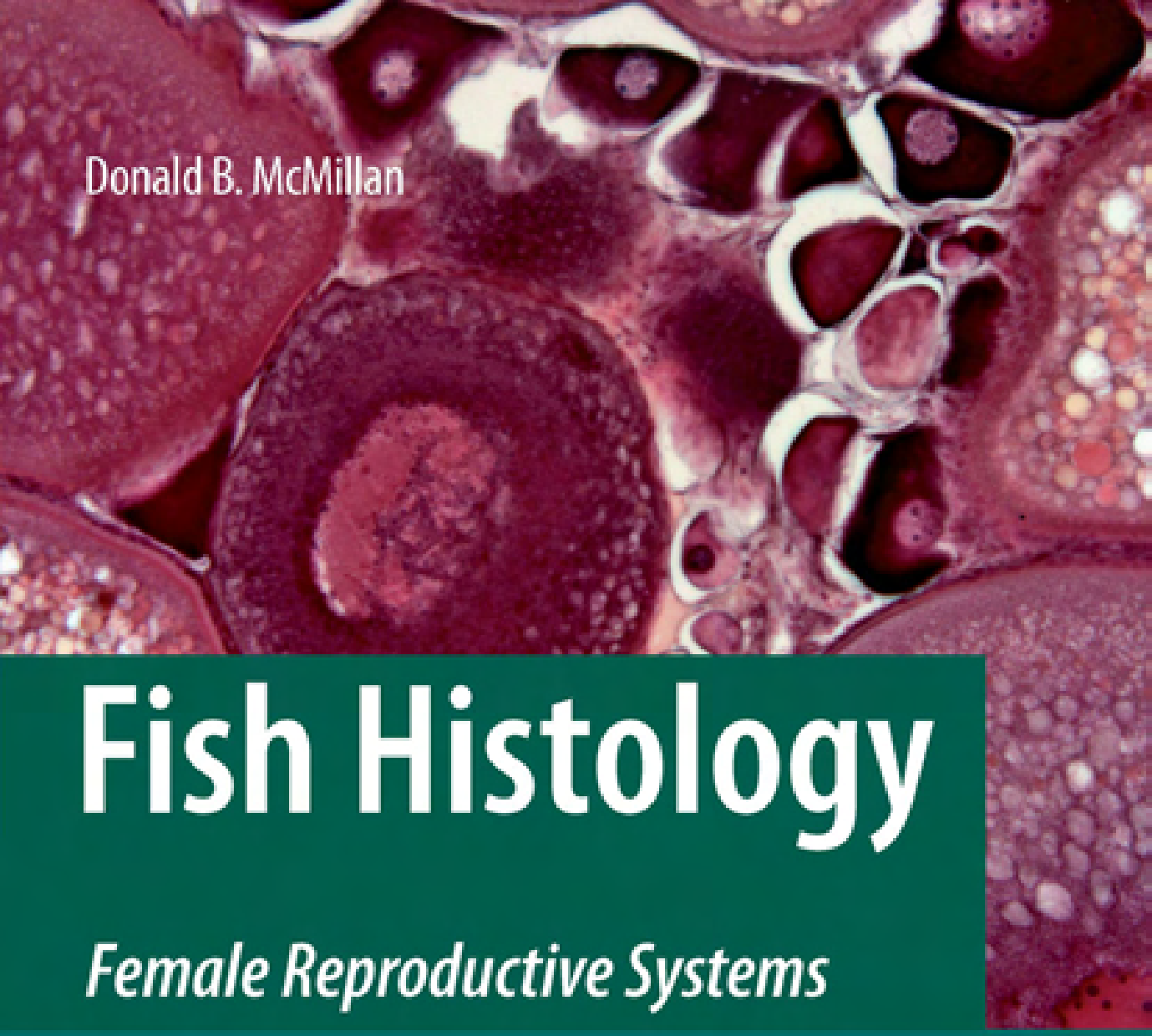

Donald B. McMillan

Fish Histology

Female Reproductive Systems

Springer

Fish Histology

Fish Histology

Female Reproductive Systems

Donald B. McMillan
Department of Biology
The University of Western Ontario
London, Ontario
Canada

Springer

Western
Science

A C.I.P. Catalogue record for this book is available from the Library of Congress.

ISBN 978-1-4020-5415-0 (HB)
ISBN 978-1-4020-5715-1 (e-book)

Published by Springer,
P.O. Box 17, 3300 AA Dordrecht, The Netherlands.

www.springer.com

Printed on acid-free paper

FOR LONE

TABLE OF CONTENTS

PREFACE

Over the past 50 years or so, the techniques of microscopy have attained a high degree of excellence resulting in the accumulation of masses of information on the histology of fishes. This golden age of descriptive morphology, however, is drawing to a close and the time is ripe to draw this material together in a form that can be used by researchers who are studying the diverse aspects of the world's dwindling stocks of fish. For several years, I have been accumulating material on fish histology and, more recently, have been compiling a textbook on the female reproductive systems. My ambition has been to parallel the excellent texts available on mammalian histology and eventually produce similar volumes on other systems. As "fish", I have included Agnatha, Chondrichthyes, and Osteichthyes. Nomenclature used follows that of the authors being cited; in other cases I have used *Fishes of the World*, 2nd ed., by J.S. Nelson, published by John Wiley & Sons.

Although histology deals in visual images, one of the problems that has beset this discipline in the past has been the high cost and difficulty of publishing micrographs. The advent of digital technology and the storage of images on compact discs (CDs), however, has solved this problem and I have rescued many classic and beautiful images from the dust and obscurity of library stacks, making them once again readily available to the present-day scientist. I have embraced this technology with abandon and large numbers of illustrations are included with this work. It should be noted that magnifications given in the legends are taken from the original sources; the actual values will vary depending on the computer being used.

Dr. W.J.R. Lanzing, formerly of the School of Biological Sciences of the University of Sydney, Australia, provided suggestions and encouragement at the outset of the project. I acknowledge, with gratitude, the patient assistance of my colleagues at the University of Western Ontario, especially the Dean of Science, Dr. F.J. Longstaffe, and the Chair of the Department of Biology, Dr. M.B. Fenton, who made excellent facilities available for my research. Messrs. R.J. Harris and I.C. Craig, provided patient and generous technical assistance. I am grateful to the obliging staff of the Taylor Science Library at the University of Western Ontario for their cheerful attention to my needs. Thanks are owed to the many authors and publishers who readily gave permission to copy their material; specific acknowledgements are included with the legends.

CHAPTER 1

FEMALE GENITAL SYSTEMS OF FISH

1.1 Introduction

There is an amazing variation in methods of reproduction in fishes[1]. Some species, at large outlays of energy, release enormous numbers of moderately yolky, mesolecithal eggs that are subjected to subsequent parental neglect. A single ocean sunfish, *Mola mola,* for example, by a prodigious feat of productivity, is said to spawn over 300,000,000 eggs (Nelson, 1984). Other fish may produce relatively small numbers of much yolkier, telolecithal eggs, often improving their chances of survival by providing parental support. Elaborate nest-building activities may precede sexual behaviour and parental care may continue for some time after hatching. The young may be sheltered, for varying periods, within the body of the female and even the male. Some viviparous[2] teleosts produce only one to four well-developed young at a time (Thibault and Schultz, 1978). An amazing array of structural adaptations has evolved for the protection and nourishment of these developing young.

A remarkable reproductive strategy is seen in bitterlings (Cyprinidae, Acheilognathinae) where parents transfer responsibility for the care of their young to a freshwater unionid mussel (Aldridge, 1998). The female bitterling extends her long ovipositor into the mantle cavity of the mussel and deposits her eggs between the gill filaments. The male then ejects his sperm into the mussel's inhalent water current and fertilization takes place within the gills of the host. Early developmental stages are protected from the risk of predation within the body of the mussel; subsequently the larvae swim away from the host to continue life on their own.

Although external fertilization is usual among fishes, copulation may occur in some species. Sometimes this merely ensures that spermatozoa are shed near the eggs but more often it involves insemination of the females. Internal fertilization may be followed immediately by the laying of newly fertilized eggs or some time later by the release of embryos at various stages of development.

Viviparity is highly specialized in some groups of elasmobranchs and teleosts and the developing young may be housed within the ovary or in the genital ducts. Viviparous species of elasmobranchs range from internal incubators that simply retain large, yolked eggs to other species in which the complexity of placentation and egg yolk retention approaches the eutherian condition (Callard et al., 1989). The cartilaginous fishes are of particular interest to reproductive biologists because of their structural and functional similarities in patterns of reproduction and development with those of amniotes (Wourms, 1977). In these highly advanced animals, several processes either made their appearance for the first time among vertebrates or became well established: internal fertilization, viviparity, placental mechanisms for foetal maintenance, patterns of genital tract development and sex differentiation, and the vertebrate type of reproductive endocrinology.

Although most fish are dioecious or gonochoristic, HERMAPHRODITISM does occur where ovarian and testicular tissues appear in the same individual (Atz, 1964; Greenwood, 1975; Chan and Yeung, 1983; Grandi and Colombo, 1997). It is found especially among cyclostomes and teleosts and, in some species, is the normal way of life. Male and female sex cells ripen at the same time in SYNCHRONOUS HERMAPHRODITES. In CONSECUTIVE HERMAPHRODITES, however, there is sex reversal: PROTOGYNOUS HERMAPHRODITES function first as females, then as males while PROTANDROUS HERMAPHRODITES transform from males into females.

Reproduction in most fishes is cyclic, although the length of the cycle is extremely variable (see reviews by Greenwood, 1975; Wourms, 1977; Billard and Breton, 1978; Dodd and Sumpter, 1984; Hamlett and

[1] Detailed in an exhaustive chart, see Breder and Rosen, 1966.

[2] Producing living young instead of eggs.

Koob, 1999). Some, like the lampreys and certain salmonid and eel species, spawn only once and then die; others may breed every two or three years, but most breed once or several times a year. Some hagfishes, some teleosts, and some species of oviparous skates appear to breed throughout the year.

The appearance of the ovary of cyclical breeders varies greatly at different times of the cycle and three ovarian types have been recognized on the basis of the pattern of oocyte development (Wallace and Selman, 1981; Nagahama, 1983). Fish that spawn once and then die, as lampreys, anadromous salmon species, *Oncorhynchus* spp., or catadromous eels, *Anguilla* spp., have SYNCHRONOUS OVARIES in which all oocytes are at the same stage of development. Species that generally spawn once per year during a short breeding season display GROUP-SYNCHRONOUS OVARIES with at least two populations of oocytes at different developmental stages; this is the commonest situation in teleosts. Ovulation of group synchronous ovaries may occur at intervals over the breeding season so that the oocytes are released in "batches". The yellowtail flounder *Pleuronectes ferrugineus* of the continental shelf of the western North Atlantic is such a BATCH SPAWNER (Manning and Crim, 1998). An ASYNCHRONOUS OVARY contains oocytes at all stages of development and occurs in species that spawn many times during a long breeding season: e.g., medaka *Oryzias* spp., killifish, *Fundulus heteroclitus,* and goldfish, *Carassius auratus.*

Many fish, in both temperate and tropical regions, exhibit an annual rhythm of reproduction that is correlated with photoperiod and temperature variations; in the tropics the increased productivity of the rainy season is also an influence (Billard and Breton, 1978). The breeding seasons of marine teleosts of the northern hemisphere are characteristically shorter in northern (3 to 4 months) than in southern forms (5 to 6 months) (Qasim, 1955). Oocytes in the northern species develop synchronously and are probably released in a single spawning; there is a wide range in sizes of maturing oocytes in asynchronous ovaries of southern species indicating that several spawnings occur in a single season. The appearance of continuous breeding, however, may be deceptive in that individuals or populations may exhibit synchronized annual reproductive cycles that are simply out of phase with one another (Scott, 1974).

1.2 Origin of the Genital Systems

Ovaries and testes develop from paired masses of mesodermal tissue on either side of the dorsal mesentery in the dorsolateral lining of the peritoneal cavity (Figure 1.1). These indifferent GENITAL RIDGES bulge into the developing coelom and are later invaded by PRIMORDIAL GERM CELLS that will eventually give rise to oogonia or spermatogonia (Nieuwkoop and Sutasurya, 1979; Nakamura et al., 1998). Covering the surface of the ovary is the so-called GERMINAL EPITHELIUM which is continuous with the peritoneum lining the coelom (Figure 1.2). During embryonic development the germinal epithelium is the proliferative layer that gives rise to much of the somatic tissue of the rudimentary gonad. In the common snook *Centropomus undecimalis,* oogonia are distributed among the stratified squamous cells of this epithelium; they proliferate by mitosis and sink into the stroma of the ovary where further development takes place (Figure 1.3) (Grier, 2000). Presumably the germ cells have invaded the epithelium from an external source. Since it is not known at this time whether this epithelium is the source of germ cells in all fish, some authors consider it misleading to refer to it as a "germinal epithelium", preferring the term "GONADAL EPITHELIUM" for this proliferative layer (Nieuwkoop and Sutasurya, 1979).

In most vertebrates, the somatic tissue of each gonad has a double origin, developing from two distinct but closely associated mesenchymal sources: the CORTEX is derived from proliferation of the coelomic epithelium and is destined to become an ovary; the MEDULLA comes from a more medial cellular proliferation and produces the testis (Wourms, 1977; Wolff, 1991)[3]. Usually one of these portions grows rapidly while the other fails to develop and the sex of the individual is determined early. This pattern of gonadal differentiation from two components is characteristic of elasmobranchs and all tetrapods (Chieffi, 1967). In contrast, both male and female gonads of cyclostomes and teleosts develop directly from coelomic epithelium that corresponds to the cortex of other vertebrates (Wolff, 1991) and there appears to be no contribution from medullary tissue (Dodd and Sumpter, 1984). It has been suggested that these differences may account for the widespread occurrence

[3] The phenomenon of sexual differentiation has been discussed at length by Lepori (1980).

of intersexuality among cyclostomes and teleosts (Hoar, 1969).

Primordial germ cells arise early in development within embryonic endoderm or mesoderm, long before the rudiments of the gonads are formed and at a distance from the site they will eventually occupy (Figure 1.4). Their site of origin is extragonadal and, in some fishes, may be extraembryonic. They migrate into the rudimentary gonad and establish residence in the outer margin of the stroma, just beneath the gonadal epithelium (Figure 1.5) (Wourms, 1977; Nieuwkoop and Sutasurya, 1979; Hamaguchi, 1982; Timmermans and Taverne, 1989; Gevers et al., 1992; van Winkoop et al., 1992; Grandi and Colombo, 1997). Later, they will be ensheathed by cells derived from the gonadal epithelium (Figure 1.6). In contrast to other species, where primordial germ cells migrate to previously formed germinal ridges, the primordial germ cells of the carp *Cyprinus carpio* are present at the site of the gonadal ridges before a gonadal anlage appears (Parmentier and Timmermans, 1985).

Various mechanisms have been proposed to explain the migration of primordial germ cells in fish: amoeboid movements of the germ cells themselves, a passive deliverance produced by morphogenetic movements of the surrounding tissues, and transport in the bloodstream. Migration is said to be powered by amoeboid movement in largemouth black bass *Micropterus salmoides salmoides* (Johnston, 1951), and the carp *Cyprinus carpio* (Nedelea and Steopoe, 1970), while in the medaka *Oryzias latipes* (Hamaguchi, 1982) and barbel *Barbus conchonius* (Timmermans and Taverne, 1989), morphogenetic movements of the surrounding tissues are thought to provide the motive force. Suggestions of a vascular route of migration have received no recent substantiation.

Primordial germ cells are mitotically active as they become segregated from somatic cells but mitosis ceases during the period of migration to the gonadal primordia (Hamaguchi, 1982; Parmentier and Timmermans, 1985; Timmermans and Taverne, 1989; Grandi and Colombo, 1997). In some species a second proliferative phase occurs soon after gonadal colonization but in others there may be a period of weeks or months of intragonadal mitotic rest: intragonadal primordial germ cells of the carp *Cyprinus carpio,* for example, remain "mitotically silent" for an extended period making them especially suitable for studies before the onset of proliferation (van Winkoop, et al., 1992).

Primordial germ cells are larger than surrounding cells, are rounded, oval, or pear-shaped, and show a distinct cell boundary (Figure 1.7) (Nedelea and Steopoe, 1970; Hogan, 1978; Nieuwkoop and Sutasurya, 1979; Hamaguchi, 1982; Parmentier and Timmermans, 1985; Timmermans and Taverne, 1989; van Winkoop et al., 1992; Grandi and Colombo, 1997). The large nucleus has a distinct membrane and is often eccentric; it contains one or two prominent nucleoli. The cytoplasm is often homogeneous but, depending upon the stage of development and the species being studied, it may contain yolk granules, oil droplets, or pigment granules. Granular endoplasmic reticulum and abundant ribosomes have been described in the cytoplasm of some species and an active Golgi complex is found in some cells, often near clumps of mitochondria (Figure 1.8). Coated vesicles, suggestive of metabolic exchanges with the gonadal environment, were described in the cytoplasm of primordial germ cells of the carp *Cyprinus carpio,* often near the surface membrane (Figure 1.9) (van Winkoop et al., 1992).

Two cytoplasmic markers of uncertain significance are said to distinguish primoridal germ cells of *Oryzias latipes* from somatic cells: SHEETS OF AGRANULAR ENDOPLASMIC RETICULUM and electron-dense MITOCHONDRIAL-ASSOCIATED GRANULAR MATERIAL (Figure 1.10) (Hogan, 1978). The fenestrated sheets of agranular endoplasmic reticulum, perhaps produced by blebbing of the nuclear envelope, follow the contours of the nuclei, sometimes almost encircling them. In the germ cells of many species, mitochondrial associated granular material forms one or two compact masses that have been designated variously as BALBIANI BODIES, PERINUCLEAR NUAGES, PERINUCLEAR DENSE BODIES, and GERMINAL DENSE BODIES (Timmermans and Taverne, 1989; van Winkoop et al., 1992; Grandi and Colombo, 1997). They are loosely-woven and strand-like in premigratory germinal cells of *Oryzias latipes*; this appearance gradually changes as the cells begin their migration and, in the gonadal anlagen, these bodies are amorphous, of various sizes and shapes, and composed of electron-dense, fine fibrils (Figure 1.11) (Hamaguchi, 1985). In the carp *Cyprinus carpio* they increase in size with development and part of the material becomes more electron dense; these dark masses adhere to mitochondria and may be centres for mitochondrial multiplication (Figure 1.12) (van Winkoop et al., 1992).

1.3 Anatomy of the Female Genital System

The female genital system consists of the OVARIES that produce EGGS or OVA and, in most species, a duct system communicating with the exterior. In addition to its *cytocrine* function of producing fertilizable gametes, the ovary shares with the testis the complementary *endocrine* function of secreting a variety of steroid hormones that regulate development of the germ cells. Oviducts may be simple passageways for the eggs but often their lining is glandular, and forms protective coverings for the eggs. In some viviparous species, young may develop within the ovary and, in others, within the oviducts.

Gonads of vertebrates always originate from bilateral primordia, but many species possess only one gonad as adults (Franchi, Mandl, and Zuckerman, 1962; Harder, 1975). In hagfish, the left gonad degenerates and only the right develops; in lampreys, the two primordia fuse during development forming a single midline gonad. Ovaries of elasmobranchs develop as paired structures along the dorsal wall of the coelom, on each side of the midline (Wourms, 1977; Dodd, 1983; Dodd and Sumpter, 1984; Callard et al., 1989; Hamlett and Koob, 1999). In several species, either the right or left ovary fails to mature. The functional ovary may be the right (as in several viviparous sharks) or the left (some viviparous rays); in some oviparous skates, however, both ovaries are functional. Atrophy of the oviduct may occur on the same side as the nonfunctional ovary. There is a range in teleost fishes from complete fusion to partial fusion, involving only the posterior part of the gonad or just the gonoducts (Franchi, Mandl, and Zuckerman, 1962; Harder, 1975). Sometimes one of the gonads is rudimentary or merely smaller but still present.

The ovaries are suspended in the posterior body cavity, dorsal to the gut, by MESOVARIA that run their entire length (Figure 1.13) (Harder, 1975). The ovaries may be displaced toward the intestine, coming to lie with the intestine within the mesentery (Figure 1.14). Beneath the VISCERAL PERITONEUM that envelops each ovary is a capsule of connective tissue and smooth muscle, the TUNICA ALBUGINEA. The OVARIAN ARTERY arrives by way of the mesovarium and branches repeatedly into the tunica albuginea.

The ovaries of cyclostomes, most elasmobranchs, and some teleosts are solid and ova are shed directly into the body cavity. No duct system is present in cyclostomes and the eggs are expelled from the body through GENITAL PORES that develop in the body wall shortly before spawning and lead into the urinary sinus or urinary duct and thence to the cloaca or urinogenital papilla. In elasmobranchs, a duct system typical of higher vertebrates develops from the mesonephric or Müllerian ducts, gathering up shed eggs or embryos in a funnel-shaped OSTIUM and passing them through an OVIDUCT to the outside, often adding a shell or providing refuge for developing embryos along the way (Figure 1.15) (Hoar, 1969; Dodd, 1983). Two ovaries and two oviducts are present in the chimaera *Hydrolagus colliei.* In general, the reproductive system of this holocephalan resembles that of elasmobranchs.

Although the ovaries of most elasmobranchs are solid, the visceral peritoneal covering of the ovary of lamnid sharks invaginates to create a hollow organ (Matthews, 1950; Pratt, 1988). The hollow is a direct extension of the peritoneal cavity and forms a branching invagination from a pocket on the right side of the outer surface (Figure 1.16). The channels penetrate all parts of the ovary and provide a means of exit for ripe oocytes (Figure 1.17).

Teleosts display two types of ovaries, gymnovarian and cystovarian (Dodd and Sumpter, 1984; Koya, Takano, and Takahashi, 1995). In the simpler GYMNOVARIAN condition, the ovaries are suspended in the coelom and ovulation occurs directly into the coelomic cavity. In CYSTOVARIAN ovaries, adhesions occur which isolate a part of the coelom, thereby forming a closed sac, the OVARIAN CAVITY or LUMEN, into which ovulation occurs directly (Figure 1.18). This ovarian cavity communicates only with its duct and is lined with mesothelium derived from the coelomic peritoneum. Following ovulation, eggs from both types of ovaries are bathed in a fluid. In gymnovarian ovaries, this fluid is COELOMIC FLUID and is synthesized and secreted by the epithelium of the dorsolateral coelomic wall and mesovarium. In the enclosed cavity of cystovarian ovaries, the fluid is designated as OVARIAN FLUID and originates in part from the epithelial lining. Since teleosts display a wide spectrum of reproductive methods, these fluids have manifold functions.

The cavity of cystovarian ovaries may be formed in two ways. An ENDOVARIAN CAVITY is derived from internalized invaginations of the genital ridges where the ribbonlike ovaries roll up in a lateral and dorsal direction so that the side at which ovulation occurs is turned inward surrounding the cavity (Figure 1.18) (Goodrich, 1930). Alternatively, a PAROVARIAN CAVITY arises from a space enclosed by adhesions between the

gential ridge and the parietal peritoneum. A range is seen from a simple ovary, where ova are shed into the ovarian cavity and soon expelled, to the complex, hollow organ of viviparous teleosts that produces eggs, stores spermatozoa, serves as a site for fertilization, and may provide nourishment for developing young for a prolonged period.

Steroid-producing cells are described in the ovary of tilapia *Sarotherodon niloticus* during ovarian differentiation (Nakamura and Nagahama, 1985). As the ovarian cavity is forming, these cells appear near the blood vessels of the stroma on the side facing the mesentery (Figure 1.19). They are presumed to originate from stomal elements and, as the ovary develops, their numbers increase surrounding the blood vessels. These cells display the tubular mitochondrial cristae and tubular agranular endoplasmic reticulum which are characteristic of steroid production (Figure 1.20). It is suggested that the steroids produced by these cells play a role in the formation of the ovarian lumen (Figure 1.21) and in the differentiation of germ cells.

In many teleosts, the visceral peritoneum covering the ovary and the peritoneum lining its cavity often continue posteriorly, beyond the mass of ovarian tissue, to form the unique OVIDUCT (Hoar, 1969; Harder, 1975) (Figure 1.22). This extension of the ovarian cavity continues posteriorly to connect with the GENITAL PORE leading to the exterior. In some teleosts, including Osteoglossidae, Hiodontidae, Notopteridae, Anguillidae, the loach *Misgurnus* (Cobitididae), Galaxiidae, and Salmonidae, the oviducts degenerate in whole or in part so that the ova pass into the body cavity and make their exit by way of funnels or pores, depending upon the degree of degeneration of the oviducts (Hoar, 1969; van Tienhoven, 1983).

1.4 Ovary

The vertebrate ovary is an aggregation of developing FOLLICLES enmeshed in a vascular STROMA of loose connective tissue and enclosed within an envelope of gonadal epithelium (Figure 1.23). The stroma consists of collagenous, elastic, and reticular fibres and becomes greatly distended as the follicles enlarge. Only in a spent ovary, when the stroma is collapsed, is it easily seen. Beneath the ovarian envelope, a condensation of stromal tissue forms the TUNICA ALBUGINEA, a capsule of connective tissue and, sometimes, smooth muscle (Figure 1.24). Collagenous and elastic fibres are most abundant in the peritoneum, less so in the tunica albuginea, and less again in the stroma itself. Reticular fibres are numerous in both the capsule and the stroma, appearing as fine, anastomosing argyrophilic threads surrounding each egg within a basket of fibres (Figure 1.25).

Early follicles consist of primordial germ cells, newly arrived by migration, enclosed within a cluster of FOLLICULAR CELLS derived from divisions of the gonadal epithelial cells. Primordial germ cells divide by mitosis to produce diploid OOGONIA (Figure 1.26). By mitotic division these oogonia form diploid PRIMARY OOCYTES. Meiotic division of a primary oocyte results in a SECONDARY OOCYTE and first POLAR BODY, both diploid (Figure 1.27) (Grandi and Colombo, 1997). The follicular epithelium eventually completely surrounds the secondary oocyte and the follicle increases greatly in size, first by the elaboration of more cytoplasm and later by the accumulation of yolk during the process of VITELLOGENESIS. Finally the secondary oocyte undergoes MATURATION where a second meiotic division yields an OVUM and another polar body, both haploid. The development and maturation of diploid oogonia to produce haploid ova is OOGENESIS. Polar bodies are small, functionless haploid cells resulting from unequal division during oogenesis. They allow most of the cytoplasm to pass to the ovum while providing for disposal of excess chromatin; polar bodies subsequently degenerate.

A detailed description of folliculogenesis in teleosts has been provided for adult females of the common snook *Centropomus undecimalis* (Grier, 2000). Oogonia, presumably having arisen from some external source, are dispersed among the somatic cells of the gonadal (germinal) epithelium that lines the ovarian lumen (Figure 1.3). The oogonia divide by mitosis, often forming nests of cells. At the outset of folliculogenesis, some oogonia begin to divide by meiosis to produce oocytes. These oocytes descend into the deeper, basal regions of the epithelium. Some epithelial cells, whose processes envelop meiotic oocytes, transform into prefollicular cells which become follicular cells at the completion of folliculogenesis (Figure 1.28). The oocyte, surrounded by its simple layer of prefollicular cells, presses on the basement membrane of the gonadal epithelium, evaginating it and eventually causing the pinching off of a discrete follicle consisting of the oocyte surrounded by its layer of folliclar cells and enclosed in a basement membrane. Cells of the stroma aggregate around the basement membrane of the follicle to form the vas-

cular theca interna and avascular theca externa. Folliculogenesis is considered to be concluded when the basement membrane completely encloses the follicular epithelium; the thecal layers may be fragmentary at this time. Ensconced within the ovarian stroma, the follicle continues its development.

In the past it has been proposed that oogonia and early meiotic stages are not present in the ovaries of adult cartilaginous fishes. It has been shown that oogenesis occurs early in the life of the spotted ray *Torpedo marmorata,* an aplacental, viviparous elasmobranch with a reproductive cycle of three years (Prisco, Ricchiari, and Andreuccetti, 2001). The site of origin and migratory route of the primordial germ cells was not determined. Clusters of oogonia and early meiotic oocytes were observed in the gonadal anlage of embryos; germ cells in the clusters were connected by intercellular bridges bordered by an electron-dense membrane about 30 nm thick (Figure 1.29). In ovaries of subadult and adult females, however, all the germ cells were organized into follicles and no clusters of oogonia or early meiotic cells were found with a single exception. In one adult female, the persistence of germ cells not organized into follicles may support the concept of "reproductive plasticity" and represent the variation that is targeted by natural selection, thereby accounting for the different reproductive strategies adopted by cartilaginous fishes.

In lampreys, primary germ cells divide slowly in the gonadal ridge beneath the peritoneum (Lewis and McMillan, 1965; Hardisty, 1971). This is followed by a period of more rapid division when the germ cells form GERM CELL NESTS or cysts. Meiotic prophase begins in both isolated germ cells and in the cell nests. Cells from the peritoneal epithelium give rise to follicular elements. Germ cells may begin cytoplasmic growth or undergo degeneration (atresia) in early stages of meiotic prophase. Oogenesis occurs to some extent in most or all lamprey gonads. In gonads destined to become ovaries, oogenesis is more synchronous than in testes and, eventually, only oocytes are present. In male lampreys, oocytes that have proceeded to the cytoplasmic growth phase are eliminated by atresia so that the testis becomes smaller during differentiation and contains only small numbers of residual germ cells; at metamorphosis these develop, by mitosis, into nests of primary spermatogonia.

Division of developing germ cells in the ovaries of lampreys causes evaginations of the ovarian wall to expand ventrally, subdividing the ovary into lobes and lobules that contain a stroma of vascular connective tissue (Figures 1.30A to C) (Lewis and McMillan, 1965). These flat, leaf-like extensions of ovarian tissue, usually two follicles in thickness, are the OVIGEROUS FOLDS (Figure 1.30D).

The ovary of the hagfish *Myxine glutinosa* is a dorsal, narrow ribbon suspended in the midline from the mesovarium (Walvig, 1963; Patzner, 1974, 1975). It consists of "series" of follicles that develop from oogonia contained within a band of germinal cells that runs along the free edge of the ovary (Figure 1.31A). When the oocytes enter the vascular connective tissue of the inner part of the ovary, undifferentiated epithelial cells from the mesothelium covering the ovary become attached to them, grow, and stretch to enclose them within a follicular epithelium. "Generations" of oocytes develop from oogonia in the germinal ridge; they grow to a diameter of 1 to 2 mm whereupon they enter a resting period, awaiting ovulation of the previous generation of oocytes (Patzner, 1974). The primary follicle consists of an oocyte surrounded by its follicular epithelium and is contained within a connective tissue sheath, the THECA (Figure 1.31E). Two layers can be discerned in this connective tissue: the theca interna and theca externa. The largest and oldest of the immature eggs are found dangling in individual peritoneal slings, the FOLLICULAR LIGAMENTS, in a single row at the ventral boundary of the ovary (Figure 1.31F). Some of these eggs mature, are ovulated, and a new row of follicles develops to take their places (Figure 1.31G). Empty postovulatory follicles remain for a time, hanging from the free surface of the ovary; later they withdraw into the stroma and undergo regression.

The visceral epithelium lining the hollow, cystovarian ovaries of many teleosts is thrown into a complex series of ovigerous folds (Figure 1.32) (Hoar, 1969). In the stickleback *Eucalia inconstans,* the folds project into the centre of the cavity, usually extending the entire length of the ovary, crowding the cavity into a ventrolateral position where no folds originate (Braekevelt and McMillan, 1967). Early germ cells are first found on the edge of the folds bordering the ovarian cavity. As the follicles mature and increase in size, they are pushed deeper into the stroma. When the follicles are mature, they burst through the visceral peritoneum and are ovulated into the ovarian cavity where they remain until spawning. The cavity, which becomes largely obliterated as the eggs reach maturity, continues posteriorly as the lumen of the oviduct.

The ovary of teleosts is supplied with blood from several arteries that branch off the dorsal aorta, entering the dorsal side of the ovary through the mesovarium. Each follicle in the ovary of *Fundulus* is supplied by a primary arteriole that reaches it through a stalk of stromal elements (Figures 1.33A,B) (Brummett, Dumont, and Larkin, 1982). Branches of the arteriole penetrate deeply into the investing layers of the follicle. The superficially located vessels in the apical or luminal hemisphere of the follicle are more readily apparent and are presumed to be venules that collect blood from the intervening capillary bed and transport it to a vessel that forms a loop on the luminal side of the follicle (Figures 1.33C and A). These vessels terminate in a single collecting vessel that courses toward the outer surface of the ovary, merging with others into two large veins that unite in the dorsal, anterior region of the ovary to form the single ovarian vein. Thick bundles of non-myelinated nerves, presumably autonomic, accompany the ovarian artery and vein in the ovary of tilapia *Oreochromis niloticus* (Figure 1.34) (Nakamura, Specker, and Nagahama, 1996). Groups of a few axons ramify from these nerves to terminate among the cells surrounding the follicles.

In the killifish *Fundulus heteroclitus,* the posterior portion of the ovary is a thin-walled nongerminal OVISAC that is continuous with the short oviduct and apparently serves as a receptacle for ovulated eggs prior to their release to the external environment (Brummett, Dumont, and Larkin, 1982). The luminal epithelium of this thin-walled region displays a localized population of unusual cells with long cytoplasmic extensions bearing short microvilli (Figure 1.35). These cells may continue to line at least part of the oviduct and may function in the transport of ovulated eggs or they may secrete a jelly that forms a surface coat for the extruded eggs.

The microscopic structure of the ovarian luminal wall has been described in a few oviparous teleosts. (The ovarian wall of viviparous teleosts is described in the section on *Viviparity*.) In the medaka *Oryzias latipes,* its epithelium displays cyclic changes corresponding to changes in the ovary (Yamamoto, 1963). As the ova mature, the luminal wall thickens and its simple cuboidal epithelium becomes simple columnar as secretory activity increases (Figure 1.36). The underlying tunica albuginea thickens as vascularization increases and smooth muscle develops. It is presumed that the fluids produced by the epithelial cells facilitate extrusion of the eggs at spawning as well as playing some role during external fertilization. After spawning, the epithelium and tunica albuginea undergo involution.

A simple columnar epithelium of MICROVILLOUS CELLS lines the ovarian cavity of the bleak *Alburnus alburnus* (Lahnsteiner, Weismann, and Patzner, 1997). Around the time of ovulation, these cells bulge apically into the lumen and a few small clusters are also found in the oviduct (Figure 1.37). These cells have diverse functions: they are secretory, maintaining the ionic gradient of the ovarian fluid by the secretion of glucose, proteins, and enzymes (acid phosphatase, protease, and β D-glucuronidase); they synthesize glucuronide steroid (which may act as a pheromone that attracts males and increases the volume of milt); and they are phagocytic. Protein production by microvillous cells is indicated by the prominent nucleolus and abundant tubular granular endoplasmic reticulum that forms concentric layers around the basal nucleus (Figure 1.38). Coated vesicles pinched off from the endoplasmic reticulum are associated with the ubiquitous Golgi complexes; secretory vesicles are released from the Golgi cisterns. The involvement of the microvillous cells in ionic regulation of the ovarian fluid is demonstrated by the presence of apical junctional complexes sealing the epithelium, the abundance of apical mitochondria, and positive tests for apical adenosine triphosphatase activity. Maintenance of the inorganic composition of the ovarian fluid is essential to prevent egg activation: closure of the micropyle, swelling of the eggs due to water uptake, and shell hardening. Table 1.1 records analyses of the composition of the ovarian fluid in the bleak[4]. The microvillous cells of the bleak contain heterophagic vacuoles and lamellar bodies and are active in the phagocytosis of débris from the lumen. Autophagy occurs in regions containing secretory vesicles. The cytoplasm also contains lipid vacuoles and accumulations of free ribosomes. Agranular endoplasmic reticulum is rare.

Ovaries of the syngnathids, the pipefish *Syngnathus scovelli,* and seahorse *Hippocampus erectus,* are unusual in that they lack ovigerous lamellae and present a sequential array of developing follicles arranged within a single sheet in order of their developmental maturity (Begovac and Wallace, 1987, 1988; Sel-

[4] Similar values for four species of salmonids are recorded in an earlier paper by these authors (Lahnsteiner, Weismann, and Patzner, 1995).

man, Wallace, and Player, 1991). This feature is especially useful for studies of follicular development. The ovaries are asynchronous and, because these fish are reproductively active throughout the year, a heterogeneous population of follicles is available in all developmental stages.

The ovaries of both species of syngnathids consist of a sheet of follicles, with their supporting vascular stroma, in the form of a tubular scroll extending lengthwise (Figure 1.39) (Begovac and Wallace, 1987; Selman, Wallace, and Player, 1991). A single GERMINAL RIDGE of the pipefish ovary forms the inner margin of the scroll and, extending from this, is a sequential array of follicles arranged according to their developmental age, sandwiched between the outer ovarian wall and the inner luminal epithelium. Mature oocytes are ovulated from the opposite margin of the scroll, the MATURE EDGE, into the ovarian lumen (Begovac and Wallace, 1987, 1988). In the seahorse, there are two germinal ridges that run the length of the tubular ovary on opposite edges of the ovarian sheet (Selman, Wallace, and Player, 1991). Developing follicles arise from each germinal ridge and grow toward a shared mature region near the middle of the sheet. These sequences may be seen in any cross section of sygnathid ovaries (Figure 1.40). In contrast to the random organization of ovaries of other fish, this temporal and spatial correlation of oocyte development, as seen in these two species, facilitates the study of specific events in follicular development. In addition, the earliest events of oogonial proliferation and early follicle formation, because of their specific location within the ovary, are accessible to experimental manipulation.

These syngnathid ovaries are covered on the outside by visceral mesothelium of squamous to low cuboidal cells that is continuous with the mesovarium; these cells have irregular apical surfaces and numerous pits and vesicles on both their apical and basal surfaces (Figure 1.41A). They contain abundant cytoplasmic filaments and have junctional complexes at their apico-lateral surfaces. This epithelium is subtended by variable amounts of collagenous connective tissue connecting it to several layers of smooth muscle (Figure 1.41B). Blood and lymph vessels are visible in this connective tissue, with the larger vessels apparent at the connection with the mesovarium. Smooth mus-

TABLE 1.1. Composition of the ovarian fluid of the bleak *Alburnus alburnus* (n = 10). (From Lahnsteiner, Weismann, and Patzner, 1997)

Component	Value
pH	8.61 ± 0.10
Osmolality (mosmol kg^{-1})	237.0 ± 27.12
Na^{+} (mmol l^{-1})	171.58 ± 25.83
K^{+} (mmol l^{-1})	2.93 ± 0.57
Ca^{++} (mmol l^{-1})	0.63 ± 0.11
Protein (mg x 100 ml^{-1})	158.48 ± 37.27
Glucose (µmol l^{-1})	2064.76 ± 529.23
Fructose (µmol l^{-1})	0
Galactose (µmol l^{-1})	2.54 ± 3.59
Glycerol (µmol l^{-1})	1.58 ± 0.34
Triglycerides (µmol l^{-1})	0
Cholesterol (µmol l^{-1})	4020 ± 142
Phosphatidylcholine (µmol l^{-1})	47.98 ± 31.92
Choline (µmol l^{-1})	732.43 ± 355.66
Alkaline phosphatase (µmol min^{-1} l^{-1})	32.79 ± 4.11
Acid phosphatase (µmol min^{-1} l^{-1})	3.98 ± 1.34
β-D-glucuronidase (µmol min^{-1} l^{-1})	0.46 ± 0.32
Protease (gelatin substrate) (µmol min^{-1} l^{-1})	34.59 ± 25.72
Protease (casein substrate) (µmol min^{-1} l^{-1})	14.43 ± 11.21

cle comprises most of the thickness of the ovarian wall; the fibres are arranged roughly into two layers: an inner circular and an outer longitudinal (Figure 1.41C). Small blood vessels course between the muscle cells as well as bundles of unmyelinated nerves that tend to run parallel to the long axis of the ovary. Vascular connective tissue of variable thickness occurs between the muscle cells and ovarian follicles. It is suggested that ovulation is accompanied by a wave of contraction of this smooth muscle, coordinated by nervous elements, that squeezes eggs from the lumen, beginning cranially and proceeding caudally.

The GERMINAL RIDGES extend the length of the ovary and contain the proliferative stem cells from which the oocytes are derived and follicles formed (Figure 1.42A). The ridges are covered by the luminal epithelium of squamous to cuboidal cells and contain richly vascular connective tissue surrounding each follicle, especially the largest; extensive lymphatic spaces, lined by attenuated endothelial cells, penetrate this stroma (Figure 1.42B). The developing follicles migrate from the germinal ridges and constitute the FOLLICULAR LAMINA of the ovarian sheet.

As in many bony fishes, the lumen of these cystovarian ovaries is lined by an epithelium that is derived from the coelomic mesothelium and is continuous with the oviduct. The epithelial cells lie on a distinct basal lamina and vary in shape from squamous over the germinal ridge to cuboidal or columnar over more mature follicles (Figure 1.43). The apical surfaces may display microvilli, lateral surfaces are highly interdigitated, and there may be basal infoldings of the plasmalemma. Blebs from the apical surface may protrude into the lumen (Figure 1.44). Within the epithelial cells are abundant cytoplasmic filaments and the cells are attached to one another laterally by desmosomes and apically by tight junctions.

A form of APOCRINE SECRETION has been described in some of the columnar epithelial cells of the ovarian lumen of two other species of teleosts. (During apocrine secretion, part of the cell is lost.) Following ovulation in the medaka *Oryzias latipes,* apical "blebs" break off from the rest of the cell and contribute to the secreted material in the lumen (Takano, 1968). There are no microvilli on these special cells and irregular processes containing vacuoles (presumably derived from the Golgi complex) form on their apical surfaces (Figure 1.45A). The processes break off, thereby forming the apocrine secretion. This activity ceases after ovulation and the cytoplasm of the epithelial cells becomes more electron lucent. As the ovary matures in the goldfish *Carassius auratus,* the dorsal epithelial cells develop cilia and large cytoplasmic blebs break away from the surface at the bases of the cilia (Figure 1.45B) (Takahashi and Takano, 1971). It is suggested that the apocrine secretions contribute to the maintenance of the ovulated eggs within the lumen and that the cilia assist in transporting them to the oviduct.

An unusual adaptation is seen in some species of Scorpaeniformes where the lining of the hollow ovary secretes a bilobed, gelatinous mass that provides protection for the eggs (Fishelson, 1977; Erickson and Pikitch, 1993; Koya, Hamatsu, and Matsubara, 1995; Koya and Matsubara, 1995). The paired cystovarian ovaries are sheathed within a wall of smooth muscle and connective tissue and are enclosed by visceral peritoneum. The ovarian walls converge caudally as an oviduct that terminates between the urinary pore and the anus. Anteriorly the ovaries are rounded and each of them is suspended by a spongy, vessel-rich hilus whose vessels penetrate into the lumen to enter the spongy, vascular, OVIGEROUS STROMA,. Suspended by the hilus at the anterior end of each lobe, the ovigerous stroma floats free within the lumen. The ovigerous tissue is covered by an oocyte-producing epithelium that bristles with vascularized "peduncles" that radiate from the stroma (Figures 1.46A,B). These peduncles are extensions of the stroma and accommodate secondary oocyte development (Figures 1.46C,D). Each oocyte is enclosed by its amorphous zona pellucida, a layer of follicular cells, and a theca (Figure 1.46E).

The luminal wall is lined by a simple columnar epithelium; a more delicate simple columnar epithelium covers the ovigerous tissue. During the spawning season, the epithelial cells of both surfaces secrete the gelatinous mass that fills the lumen. These columnar cells increase in height from vitellogenesis to maturation; they decline after ovulation. The gelatinous mass occurs in two layers: a fibrous OUTER LAYER of polysaccharide and lipid and a homogeneous INNER LAYER of glycolipoprotein or proteoglycan associating lipid. The outer, fibrous layer is secreted by the larger, columnar EPITHELIAL CELLS OF THE OVARIAN WALL. These cells contain abundant agranular endoplasmic reticulum and release apical blebs into the lumen (Figures 1.47A,B). The columnar cells of the OVIGEROUS EPITHELIUM secrete the inner layer and are rich in agranular and granular endoplasmic reticulum and Golgi complexes (Figure 1.47C). They release materials by exocytosis.

Peduncle length increases as vitellogenesis proceeds. Within the base of each peduncle are previtellogenic oocytes; when a mature oocyte is released at ovulation, a previtellogenic oocyte moves up inside the peduncle to take its place and undergo vitellogenesis. At ovulation, the oocytes, embedded in the gelatinous mass, are swept from the lumen (Figure 1.48). The gelatinous mass, secreted by the epithelia of the two lobes, is extruded around the ovigerous tissue of both lobes to form the hollow, bilobed egg mass. Three features of these unusual ovaries facilitate the production, shaping, and expulsion of these egg masses: the ovigerous stroma is encircled by oocytes and connected to the ovarian wall only at the anterior end of each lobe; the inner ovarian wall is lined with secretory cells; and vitellogenic oocytes are borne on peduncles that extend into the lumen, becoming embedded in the gelatinous mass. Similar adaptations for the production of gelatinous egg masses have been described in the masked greenling *Hexagrammos octogrammus* (Scorpaeniformes) (Koya, Munehara, and Takano, 1993) and the angler fish *Lophiomus setigerus* (Lophiiformes) (Yoneda et al., 1998).

Several marine cottid species (Scorpaeniformes) have a unique reproductive mode called "internal gametic association" where spermatozoa are introduced into the ovarian cavity by copulation and float freely in the ovarian fluid although fertilization does not occur until the eggs have been spawned into sea water (Koya, Takano, and Takahashi, 1995; Koya, Munehara, and Takano, 1997). The lumen of the ovarian cavity is lined with a simple microvillous epithelium that secretes the ovarian fluid but does not appear to have a specialized structure for sperm storage (Figures 1.49A,B). During the spawning period, the epithelial cells of both the ovigerous lamellae and the luminal wall manifest the appearance of protein production with abundant basal granular endoplasmic reticulum and active apical Golgi complexes (Figures 1.49C to E). Numerous pinocytotic pits and vesicles are seen in the peripheral cytoplasm of these cells; increasing numbers of pits and vesicles are also present in the endothelial cells of adjacent capillary walls at this time indicating that active transcytosis is taking place (Figure 1.49F). Substances transported from the capillaries appear to be taken into the epithelial cells by endocytosis and synthesized in the granular endoplasmic reticulum into materials that are accumulated in the secretory vesicles by way of the Golgi complexes to be released into the ovarian cavity by exocytosis. These secretions may be augmented by microapocrine secretions wherein blebs are released from projections of the apical surfaces of the epithelial cells (Figures 1.49C,E). This secretory activity shows distinct seasonal changes, being most active during the spawning period, declining during the degeneration period to become quiescent during the recovery period. Adjacent epithelial cells are joined by junctional complexes (Figure 1.49G) and it is suggested that these tight junctions isolate the spermatozoa in the lumen from the maternal immune system. After the spawning period, the junctions break down and residual spermatozoa are eliminated by invading maternal leucocytes: plasma cells, polymorphonuclear leucocytes, and monocytes/macrophages (Figure 1.49H). A summary of the cyclic changes in these epithelial is shown in Figure 1.49I.

The mature ovaries of Chondrichthyes are surrounded by the gonadal epithelium and consist of a connective tissue stroma containing developing follicles, postovulatory follicles (corpora lutea), and degenerating follicles (corpora atretica) (Stanley, 1963; Wourms, 1977; Callard et al., 1989; Hamlett and Koob, 1999). Blood vessels and nerves course through the stroma. The stroma also contains lymph spaces or membranous folds that are filled with developing blood cells (Figure 1.50). Although ovarian morphology is variable in Chondrichthyes, differences are superficial and attributable largely to the numbers and sizes of the yolky eggs present (TeWinkel, 1972; Dodd, 1983; Callard et al., 1989). Variations are related not only to the stage of the reproductive cycle, but also to the mode of reproduction of the species: whether oviparous or viviparous. Vitellogenic oocytes dominate the gross appearance of the ovary of reproductively active females (Callard et al., 1989). After ovulation, the volume of the ovary is greatly reduced and it contains only smaller follicles, corpora lutea, and corpora atretica.

Yellowish, irregular masses of haemopoietic tissue, the EPIGONAL ORGANS, are associated with the gonads of elasmobranchs (Figures 1.16 and 1.17) (Fänge, 1977; Fänge and Mattisson, 1981; Zapata, 1981; Fänge and Pulsford, 1983; Zapata et al., 1996). Although sometimes reduced to the point that they are detectable only by microscopic examination, they have been found in all species examined. They occur in the mesovarium and, in young specimens of *Scyliorhinus canicula,* are said to surround the ovary. Aggregations of haemopoietic tissue in the ovarian stroma of some elas-

mobranchs are probably rudimentary epigonal organs (Figure 1.51) (Fänge, 1977). In the basking shark, *Cetorhinus maximus,* where only the right ovary persists, the epigonal organ lies posterior and slightly dorsal to the ovary, being suspended from the dorsal abdominal wall by a backward extension of the mesovarium (Figure 1.16) (Matthews, 1950). The left epigonal organ is of similar size and shape as the right but no ovary is fused to its anterior end and it is suspended by its own peritoneal fold in the corresponding position on the left side of the body cavity (Figure 1.52). No haemopoietic tissue is associated with the urinogenital system of the holocephalan *Hydrolagus colliei* (Stanley, 1963).

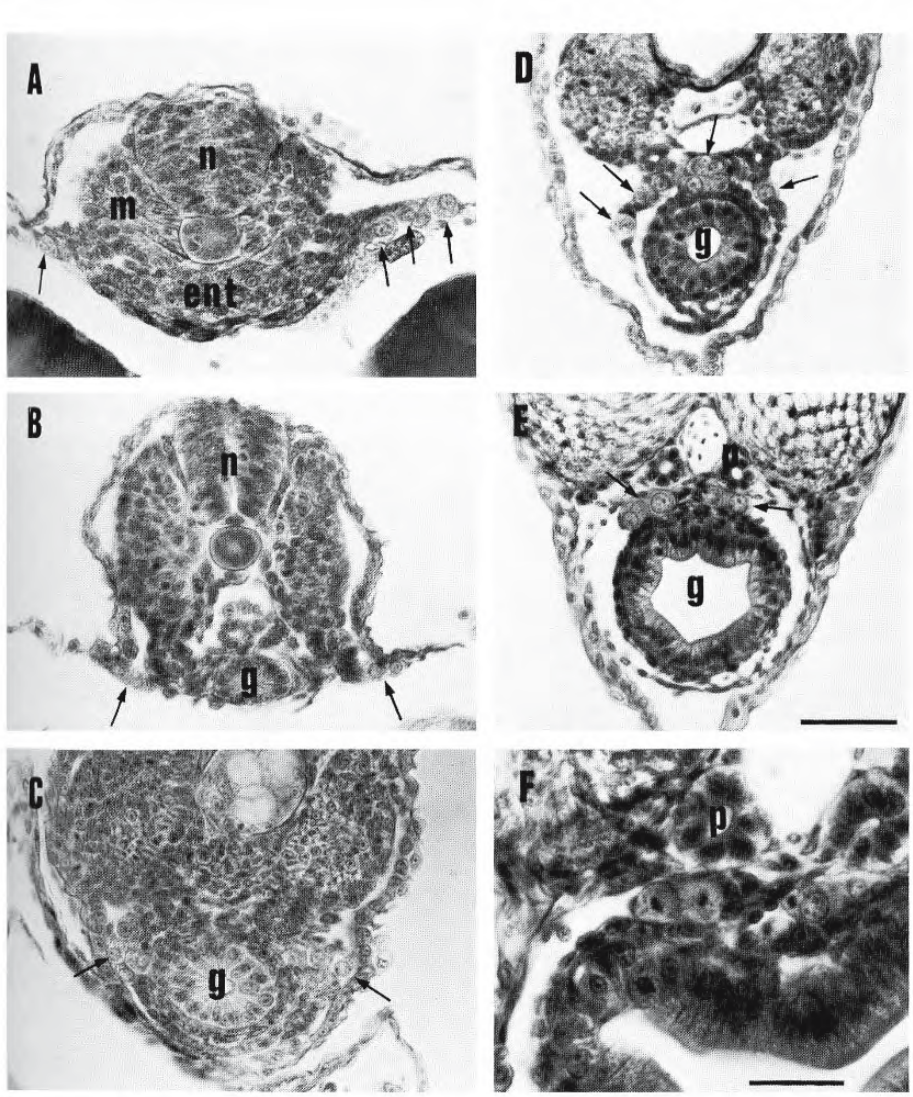

Figure 1.1: Ovaries and testes develop from paired masses of mesodermal tissue on either side of the dorsal mesentery in the dorsolateral lining of the peritoneal cavity. These indifferent genital ridges bulge into the developing coelom and are later invaded by primordial germ cells (arrows) that will eventually give rise to oogonia or spermatogonia. Six stages of this migration are shown in these photomicrographs of cross sections of embryos *Oryzias latipes.* Bar = 40 μm (From Hamaguchi, 1982; reproduced with permission of the author).

A. Primordial germ cells (PGCs) shown in the peripheral endoderm.

B. The PGCs lie alongside the newly-formed gut.

C. The PGCs come together between the lateral plate mesoderm and ectoderm. As the lateral plate mesoderm differentiates into splanchnic and somatic mesoderm, the PGCs migrate through the somatic mesoderm to the dorsal mesentery.

D. Some germ cells have reached the gonadal region, others are in the somatic mesoderm.

E. All germ cells have arrived in the gonadal anlage between the pronephric duct and the gut.

F. One of the germ cells is undergoing mitosis.

Abbreviations: n, neural tube; m, mesoderm; ent, entoderm; g, gut; p, pronephric duct.

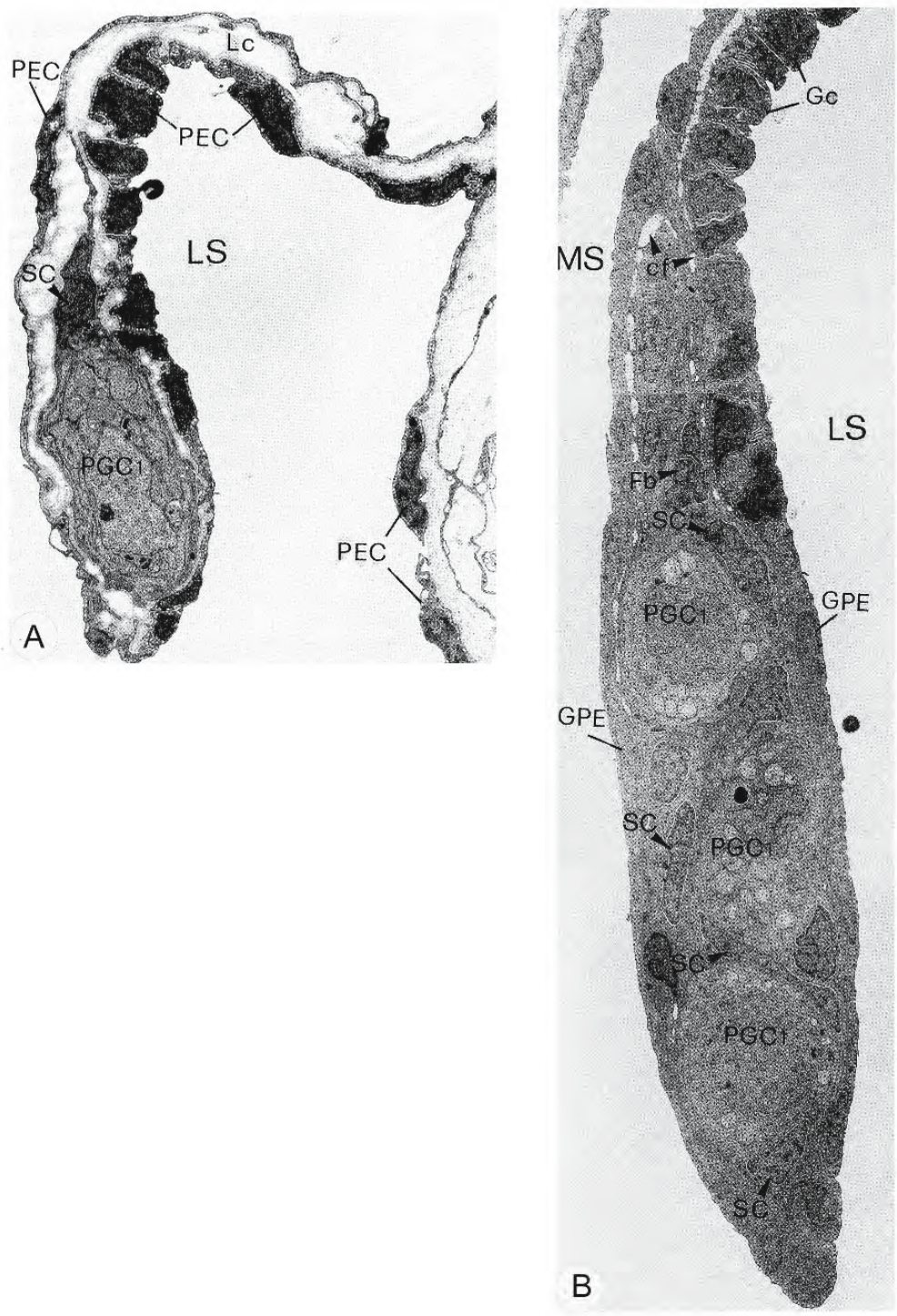

Figure 1.2: Electron micrographs of cross sections through the developing gonad of the eel *Anguilla anguilla* containing primordial germ cells (PGC1) enveloped by somatic cells (SC). The gonad is enclosed by peritoneal epithelium (PEC, GPE) formed of flattened cells on the medial side (MS) and thicker cells on the lateral side (LS). **A**: 6.8 cm elver; X 3,800. **B**: 10.6 cm eel; X 2,800. (From Grandi and Colombo, 1997; © reproduced with permission of John Wiley & Sons, Inc.).

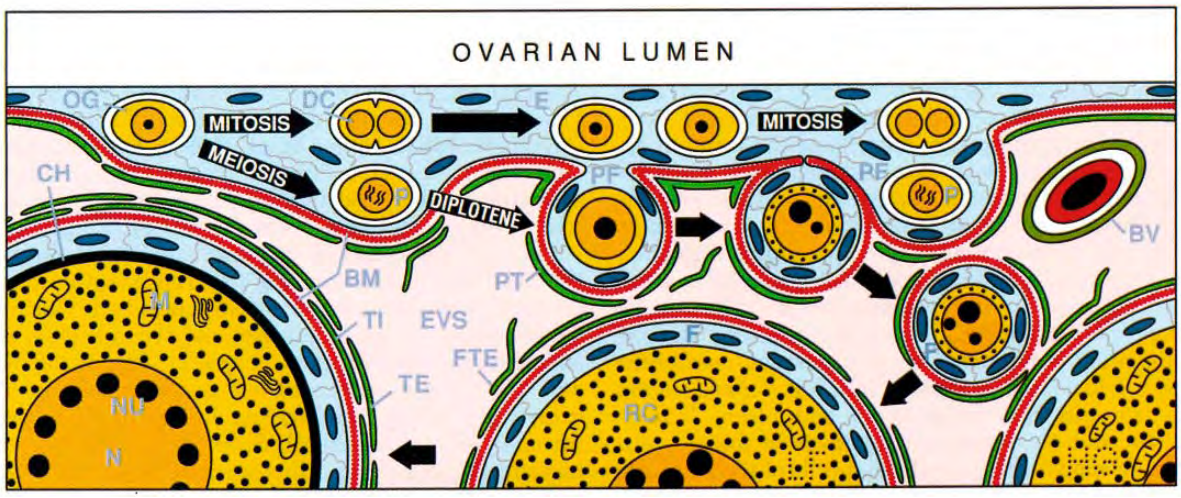

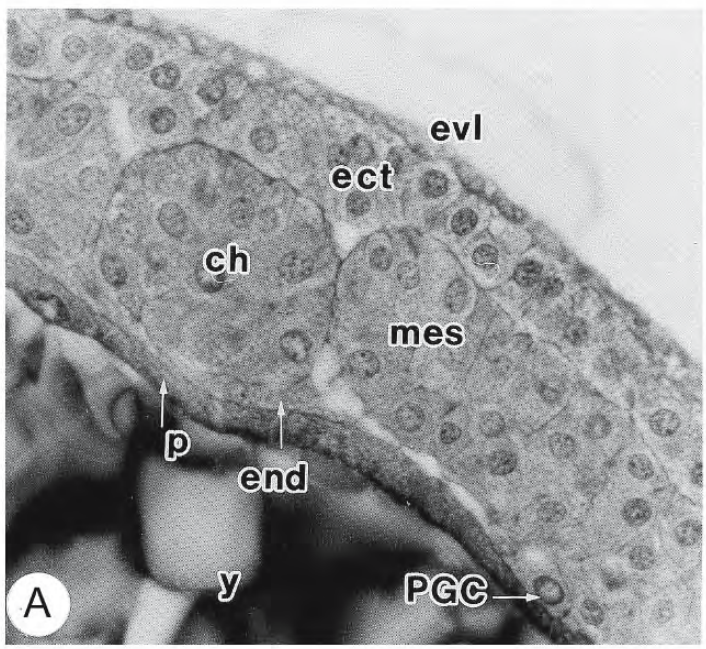

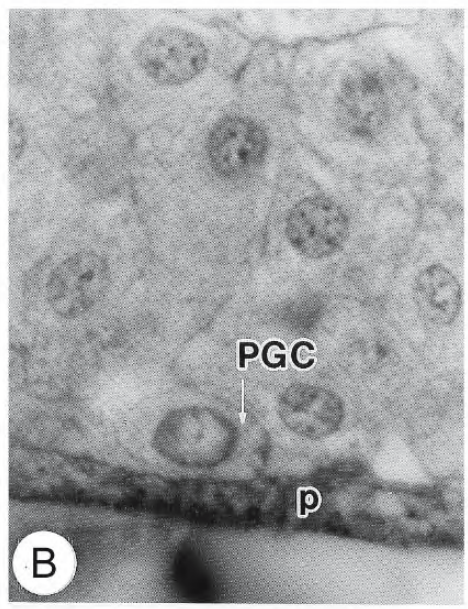

←

Figure 1.3: Diagrammatic representation of the germinal epithelium and the process of oogenesis from a single oogonium in the common snook *Centropomus undecimalis.* Germ cells are yellow and orange; epithelial prefollicle cells and follicle cells are blue; cells within the stroma are green; the basement membrane is red. The germinal epithelium extends between the basement membrane (BM) and the ovarian lumen (OL). It is composed of somatic cells (epithelial cells, E, which become prefollicle cells, PF, during folliculogenesis) and germ cells (oogonia, OG, and pachytene, P, and diplotene oocytes). Oogonia may divide mitotically to maintain their population within the germinal epithelium (mitosis, arrows). They may enter into meiosis, becoming oocytes, and move away from the ovarian lumen. At the initiation of meiosis, the process of folliculogenesis commences (meiosis, arrows). Folliculogenesis is completed when the basement membrane extends up over the forming follicle, its diplotene oocyte, and prefollicle cells, and pinches the follicle off from the germinal epithelium. Prefollicular cells then become follicular cells (F). While within the germinal epithelium, or attached to a cell nest, the oocyte primary growth phase commences when RNA-rich cytoplasm (RC) begins to appear during diplotene. RNA continues to accumulate as both the nuclear and cytoplasmic volumes increase after completion of folliculogenesis coupled with the appearance of multiple nucleoli (NU) and their final orientation around the periphery of the nucleus (N) (perinucleolar stage). Folliculogenesis is complete before this stage of maturation is reached. Beside an RNA-rich cytoplasm, mitochondria (M) and other cellular organelles begin to appear in the oocyte cytoplasm. The follicle is composed of the diplotene oocyte and an encompassing layer of follicular cells. It is separated from the stroma by a basement membrane. In the stroma, prethecal cells (PT) within the extravascular space (EVS) associate with the follicle and form the theca interna. During primary growth, undifferentiated cells within the EVS associate with the surface of the theca. They differentiate into a theca externa (TE). Blood vessels (BV) also reside within the EVS. (From Grier, 2000; © reproduced with permission of John Wiley & Sons, Inc.).

←

Figure 1.4: Primordial germ cells (PGC) arise early in development within embryonic endoderm (end) or mesoderm (mes), long before the rudiments of the gonads are formed and at a distance from the site they will eventually occupy. Photomicrographs of cross sections at the level of the anterior somites through 12-hour embryos of *Barbus conchionus.* (From Timmermans and Taverne, 1989; © reproduced with permission of John Wiley & Sons, Inc.).

A. X 554.

B. X 1,386.

Abbreviations: ch, chorda mesoderm; ect, ectoderm; evl, enveloping layer; p, periblast; y, yolk.

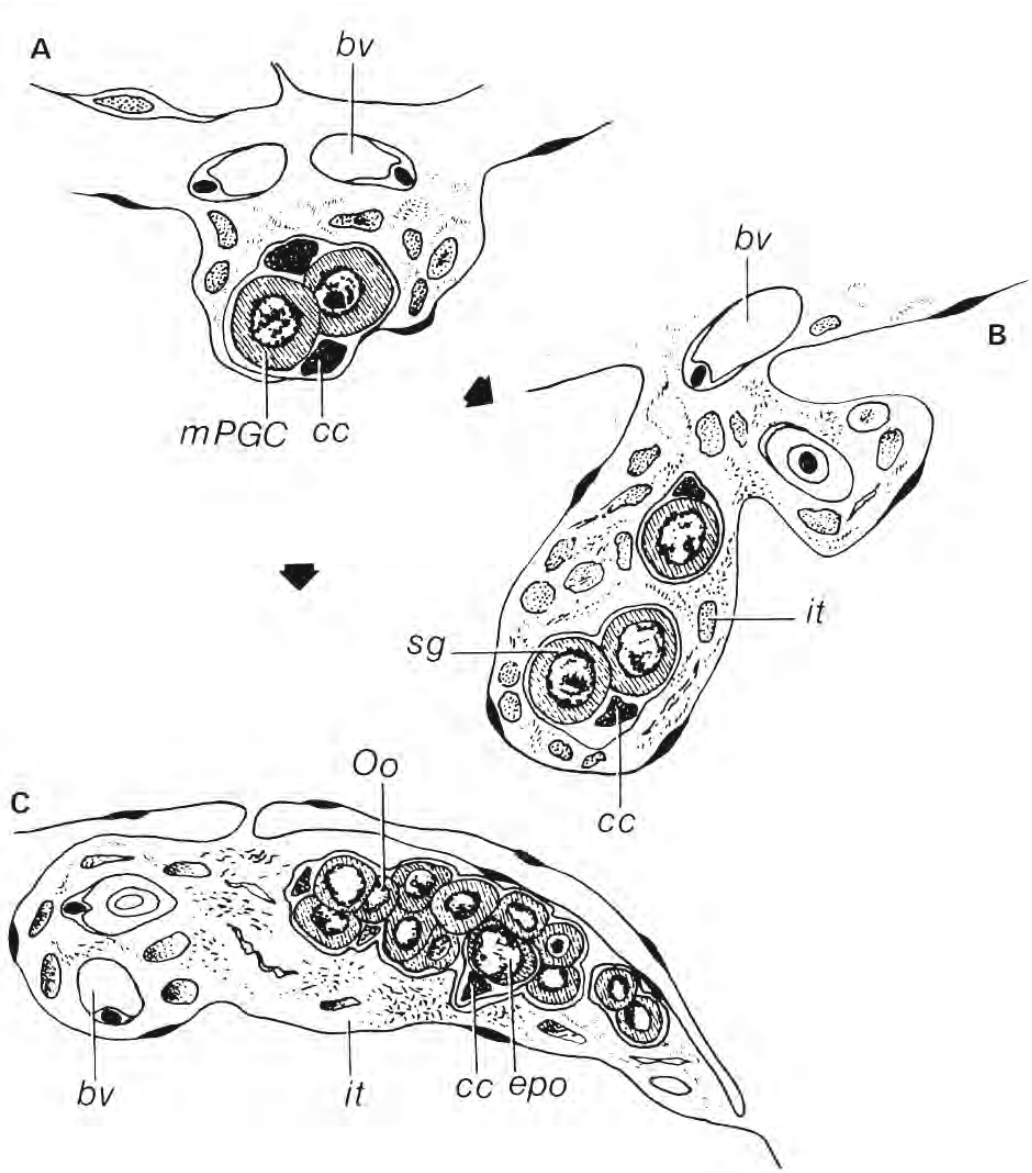

Figure 1.5: The site of origin of primordial germ cells is extragonadal and, in some fishes, may be extraembryonic. These cells migrate into the rudimentary gonad and establish residence in the outer margin of the stroma, just beneath the gonadal epithelium. These are schematic drawings of sections through the carp *Cyprinus carpio* showing male and female gonads during development. (From Parmentier and Timmermans, 1985; reproduced with permission from the Company of Biologists, Ltd.).

A. Indifferent gonad at 8 weeks.

B. Male gonad at 15 weeks.

C. Female gonad at 15 weeks.

Abbreviations: *bv,* blood vessel; *cc,* cyst cell; *epo,* early prophase oocytes; *it,* interstitial tissue; *Oo,* oogonia; *mPGC,* mitotic primordial germ cell; *sg,* spermatogonia.

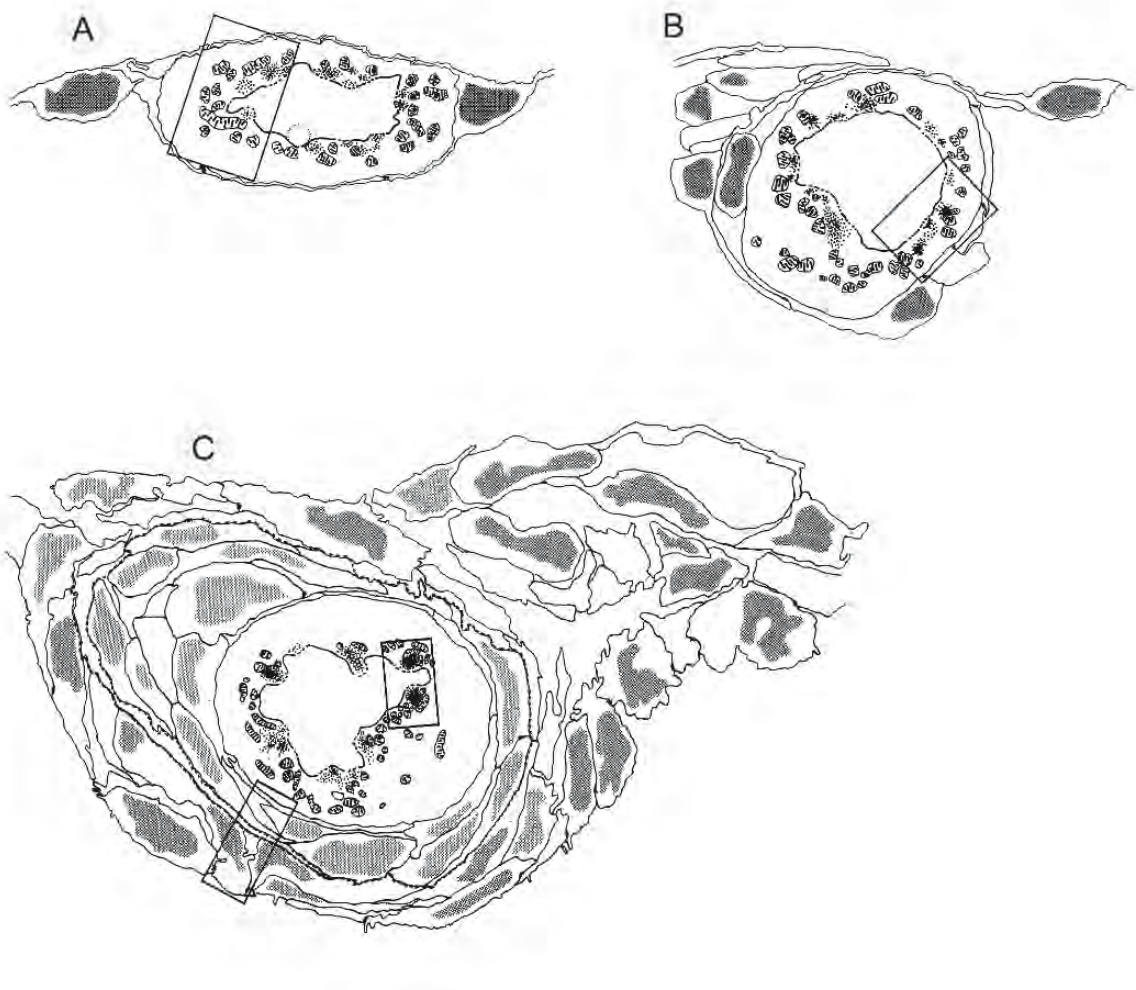

Figure 1.6: Primordial germ cells are ensheathed by cells derived from the gonadal epithelium. Schematic drawings of cross sections through gonadal primordia of the common carp *Cyprinus carpio* at 1, 3, and 5 weeks. (From van Winkoop et al., 1992; reproduced with permission from Springer-Verlag).

A. In the first week the primary germ cell is enclosed by extensions of one or two somatic cells; these form junctional complexes at the side of the coelomic cavity but not at the dorsal side. The outlined area is shown in Figure **D**.

B. By the third week, the number of somatic cells surrounding the primary germ cell has increased. The outlined area is shown in Figure **E**.

C. In the fifth week, a central layer of lighter cells, located close to the primary germ cells, is surrounded by a layer of darker peripheral cells. The upper outlined area is shown in Figure **F** and the lower area is shown in Figure **H**.

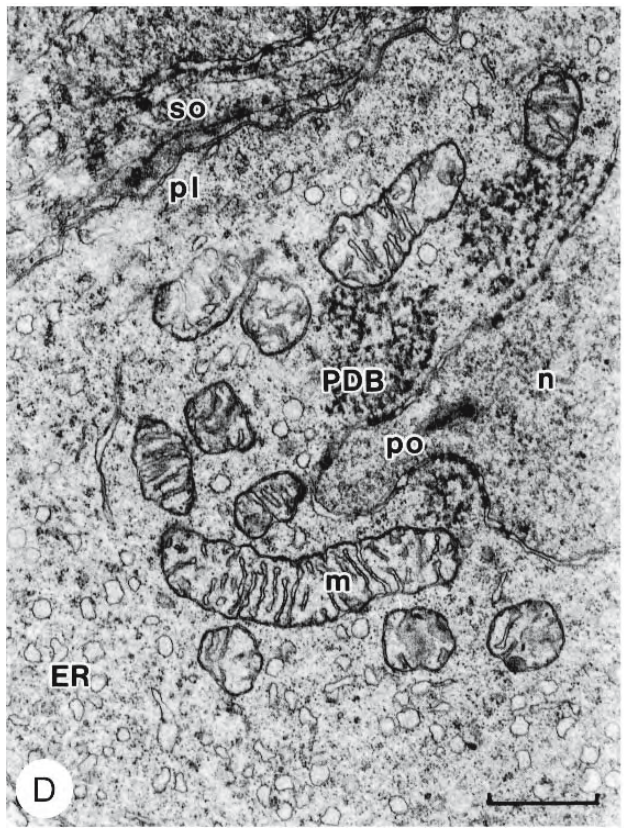

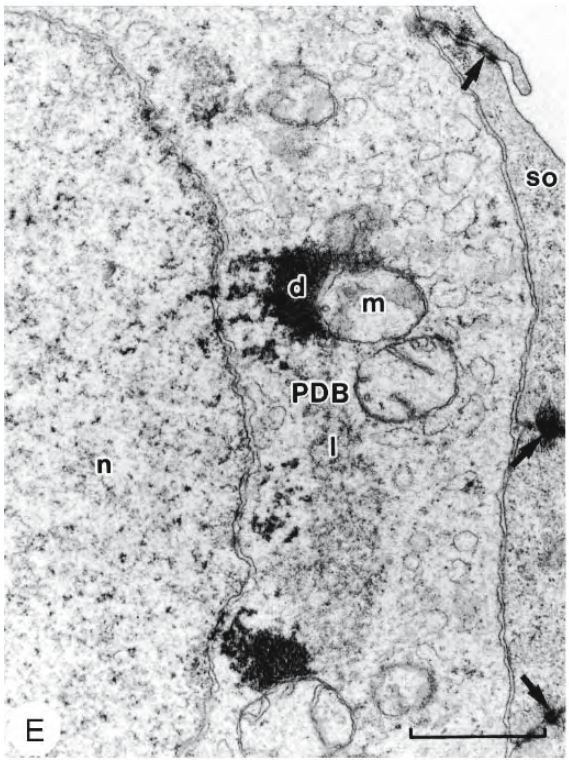

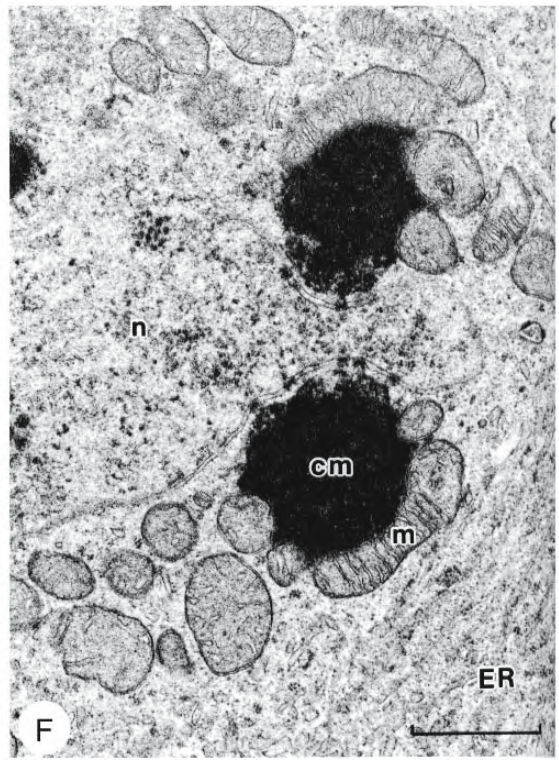

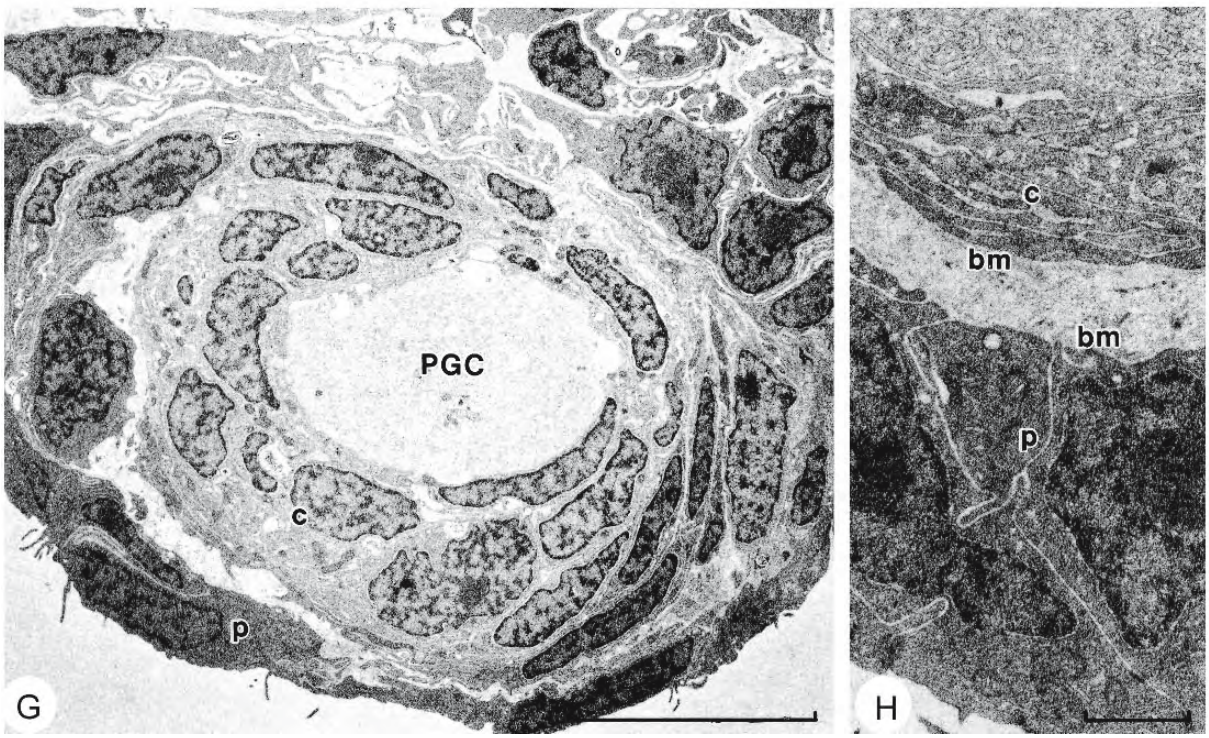

Figure 1.6: Continued.

Figures **D** to **H** are electron micrographs of cross sections through primary germ cells and gonadal primordia.

D. At 3 days a primary germ cell is enveloped by dorsal extensions of a somatic cell (so). Part of the nucleus (n) is shown. Perinuclear dense bodies (PDB), located near nuclear pores (po), are associated with mitochondria (m). The cytoplasm contains agranular endoplasmic reticulum (ER). Bar = 1 μm.

E. A primary germ cell at 3 weeks contains light (l) and dark (d) material; the latter adheres to a mitochondrion (m). Note junctional complexes (arrows) between the extensions of somatic cells (so). The nucleus (n) is at the left. Bar = 1 μm.

F. (upper outline in Figure **C**). Primary germ cell at 4 weeks. Dark cement (cm) is associated with mitochondria (m). Long, agranular cisternae of the endoplasmic reticulum (ER) lie parallel to the cell membrane. The nucleus (n) is at the left. Bar = 1 μm.

G. A primary germ cell (PGC) enveloped by somatic cells at 5 weeks. (The nucleus of the primary germ cell is not visible.) The lighter central somatic cells (c) are surrounded by darker peripheral cells (p). Bar = 10 μm.

H. (lower outline in Figure **C**). Enveloping somatic cells at 5 weeks. Both the lighter central cells (c) and the peripheral cells (p) rest on basement membranes (bm) with connective tissue between. Bar = 1 μm.

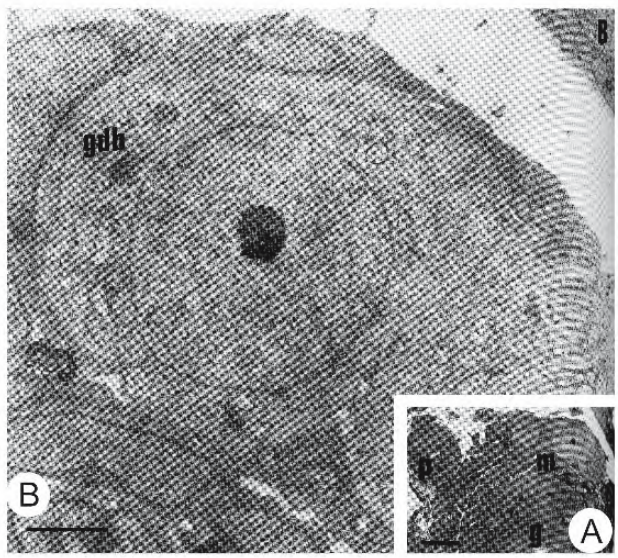

Figure 1.7: Electron micrographs of sections of primordial germ cells of *Oryzias latipes.* (From Hamaguchi, 1982; reproduced with permission of the author).

A. Primary germ cells (g) are larger than surrounding cells, are rounded, oval, or pear-shaped, and show a distinct cell boundary. They are surrounded by somatic cells (m) rich in ribosomes. Pronephric duct, p. Bar = 10 μm.

B. Mesodermal cells surround the primordial germ cell (gdb). The nuclear material is homogeneous. There is a large, round, conspicuous nucleolus. The surrounding somatic cells are richer in ribosomes. Bar = 2 μm.

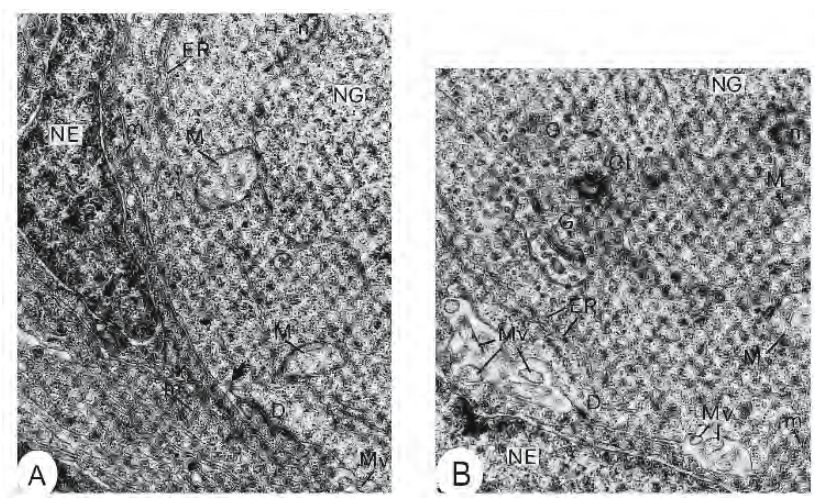

Figure 1.8: Electron micrographs of sections of primordial germ cells of the eel *Anguilla anguilla*. (From Grandi and Colombo, 1997; © reproduced with permission of John Wiley & Sons, Inc.).

A. A primordial germ cell has a nucleus (NG) with irregular outline, a few long cisternae of endoplasmic reticulum (ER), "nuage" (n), a cluster of mitochondria (M) in the cytoplasm, coated pits (arrow), and microvillous extensions (Mv) of the border. An enveloping somatic cell has a flattened nucleus (NE) and many bundles of microfilaments in the cytoplasm. Note the desmosome (D) between the primordial germ cell and the somatic cell. X14,800.

B. Details of a primordial germ cell showing a Golgi complex (G), centriole (Ct), and other organelles. Labelling as in Figure **8A**. X16,400.

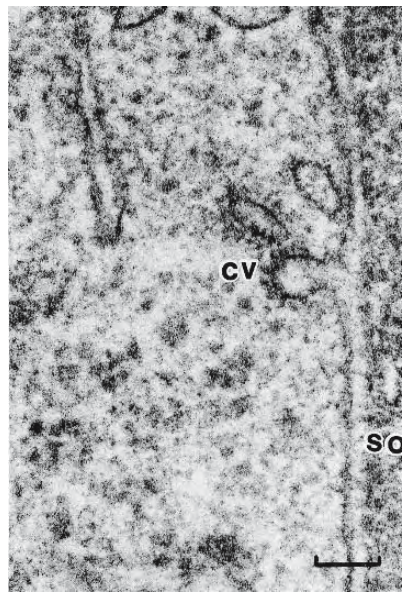

Figure 1.9: Electron micrograph of a section through the cytoplasm of a primordial germ cell of the carp *Cyprinus carpio* of 5 weeks. One coated vesicles (cv) vesicle has fused with the plasma membrane and opens into the narrow intercellular space adjacent to a somatic cell (so). Bar = 0.1 μm. (From van Winkoop et al., 1992; reproduced with permission from Springer-Verlag).

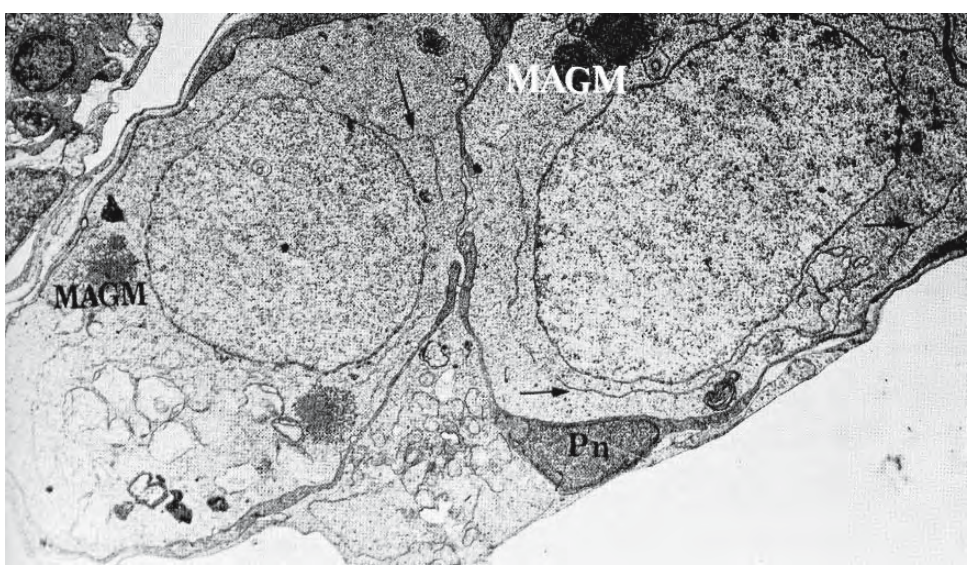

Figure 1.10: Electron micrograph of a section of the indifferent gonad of the genital ridge of *Oryzias latipes.* Two cytoplasmic markers distinguish primordial germ cells from somatic cells (Pn). These are thin sheets of agranular endoplasmic reticulum (arrows) and electron-dense mitochondrial associated granular material (MAGM). X 4,700 (From Hogan, 1978; reproduced with permission from Elsevier Science).

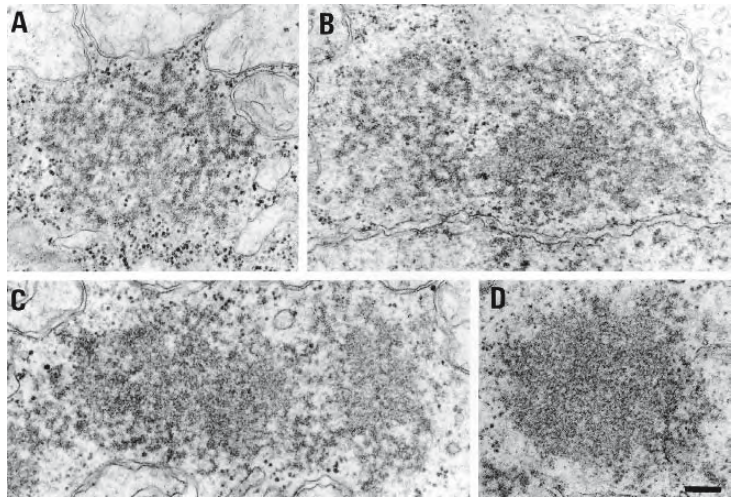

Figure 1.11: These electron micrographs show changes in the appearance of mitochondrial-associated granular material in premigratory germinal cells of *Oryzias latipes* as the cells begin their migration to the gonadal anlagen. X 45,000 (From Hamaguchi, 1985; reproduced with permission of the author).

A. As the cells begin their migration, the material is loosely-woven and strandlike.

B. This appearance gradually changes as a small, amorphous mat of fine, electron-dense fibrils forms.

C. The amorphous mat becomes dominant.

D. The material has become an amorphous body of fine, electron-dense fibrils. In the gonadal anlagen, these bodies are amorphous, of various sizes and shapes. Bar = 0.2 μm.

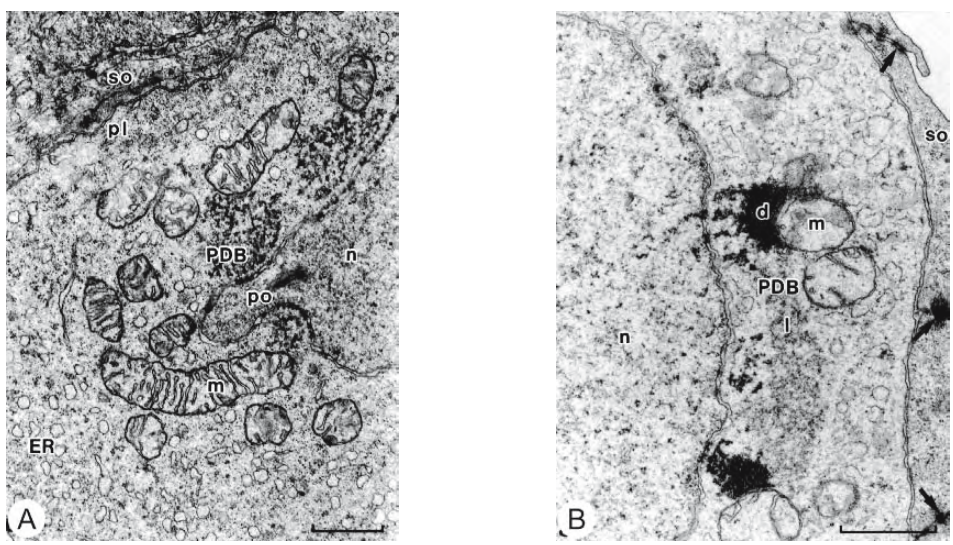

Figure 1.12: In the carp *Cyprinus carpio* the mitochondrial associated granular material increases in size with development and part becomes more electron dense forming dark masses that adhere to mitochondria and may be centres for mitochondrial multiplication. Bar = 1 μm. (From van Winkoop et al., 1992; reproduced with permission from Springer-Verlag).

A. A primordial germ cell at 3 days, showing part of the nucleus (n). The cytoplasm contains agranular endoplasmic reticulum (ER). A dense body (PDB) and associated mitochondrion (m) lies near a nuclear pore (po). Surface membrane of primordial germ cell pl; dorsal extension of enveloping somatic cell, so.

B. Two types of dense material are seen in primordial germ cells at 3 weeks: light (l) and dark (d), the latter adhering to a mitochondrion (m). At the right, junctional complexes (arrows) link extensions of the surrounding somatic cells.

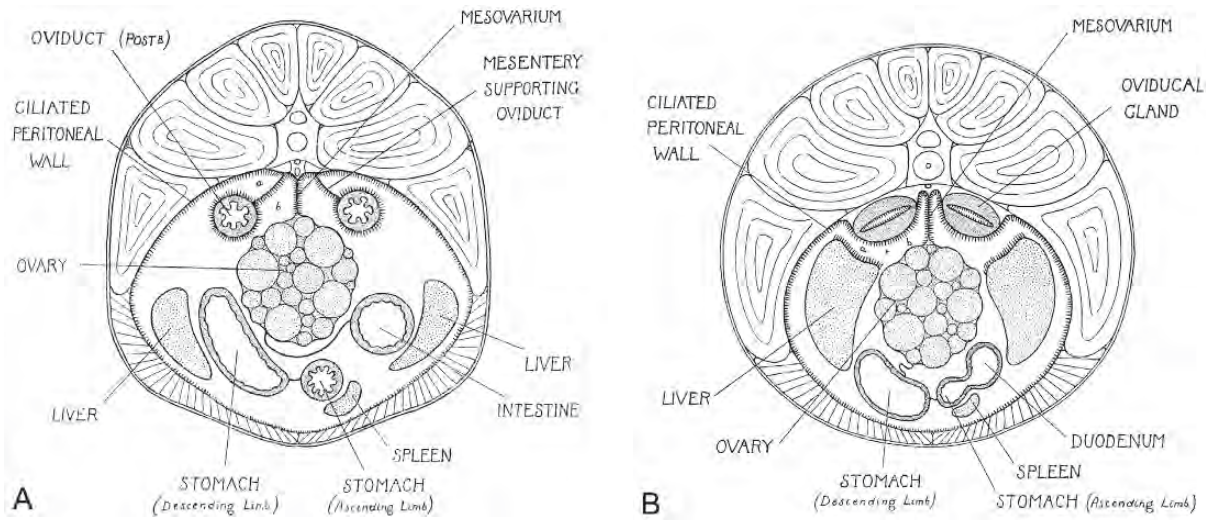

Figure 1.13: The ovaries are suspended in the posterior body cavity, dorsal to the gut, by mesovaria that run their entire length. Diagrammatic cross sections through the body of an adult female shark *Scyliorhinus canicula.* X 1 (From Metten, 1939; reproduced with permission from the Royal Society).

A. Section through the posterior end of the stomach.

B. Section through the duodenum.

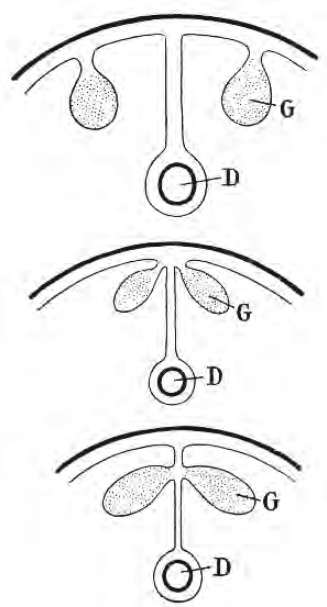

Figure 1.14: The ovaries (G) may be displaced toward the intestine, coming to lie, with the intestine (D), within the mesentery. (From Harder, 1975; reproduced with permission of Schweizerbart'sche Verlagsbuchhandlung, www.schweizerbart.de).

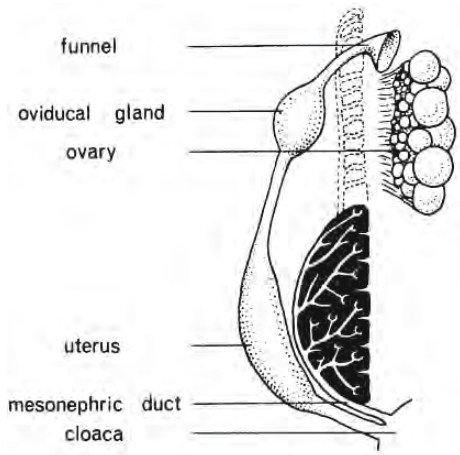

Figure 1.15: In elasmobranchs, a duct system typical of higher vertebrates develops from the mesonephric or Müllerian ducts, gathering up shed eggs or embryos in a funnel-shaped OSTIUM and passing them through an OVIDUCT to the outside, often adding a shell or providing refuge for developing embryos along the way. (From Hoar, 1969; reproduced with permission from Elsevier Science).

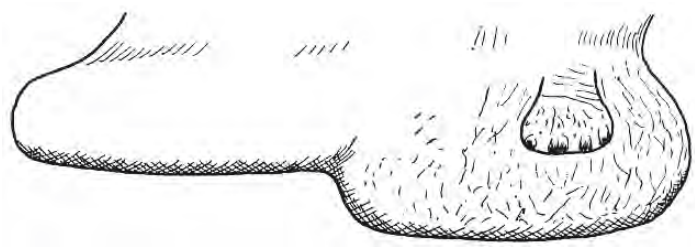

Figure 1.16: Although the ovaries of most elasmobranchs are solid, the visceral peritoneal covering of the ovary of lamnid sharks invaginates to create a hollow organ. The hollow is a direct extension of the peritoneal cavity and forms a branching invagination from a pocket on the right side of the outer surface. Shown is the right ovary and epigonal organ, seen from the right side, of the basking shark *Cetorhinus maximus.* Only the right ovary persists and the epigonal organ lies posterior and slightly dorsal to the ovary, being suspended from the dorsal abdominal wall by a backward extension of the mesovarium. The pocket leading to the interior is visible on the right side. (From Matthews, 1950; reproduced with permission from the Royal Society).

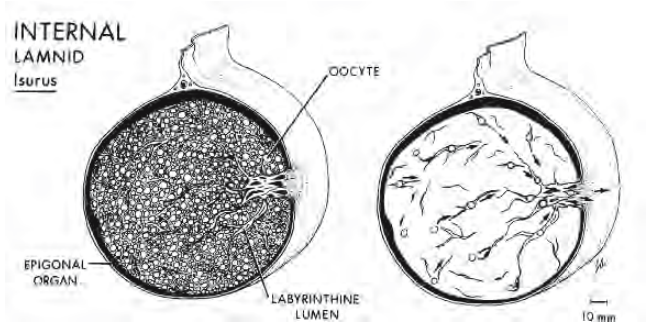

Figure 1.17: Channels penetrate all parts of the ovary and provide a means of exit for ripe oocytes. Posterior view of the ovary of a mature lamnid shark. The left illustration is diagrammatic, the right is schematic. Arrows indicate paths of the oocytes. (From Pratt, 1988; reproduced with permission of the American Society of Ichthyologists and Herpetologists).

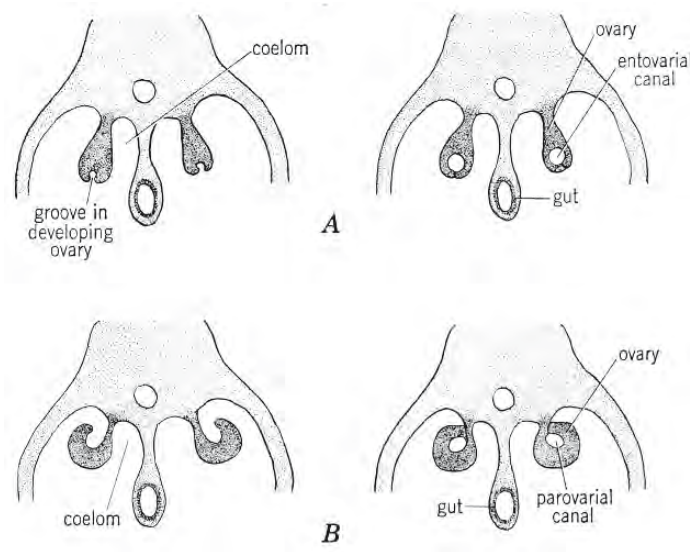

Figure 1.18: The cavity of cystovarian ovaries may be formed in two ways. (From Weichert, 1970; reproduced with permission of the McGraw-Hill Companies).

A. An endovarian cavity is derived from internalized invaginations of the genital ridges where the ribbonlike ovaries roll up in a lateral and dorsal direction so that the side at which ovulation occurs is turned inward surrounding the cavity.

B. Alternatively, a parovarian cavity arises from a space enclosed by adhesions between the genital ridge and the parietal peritoneum.

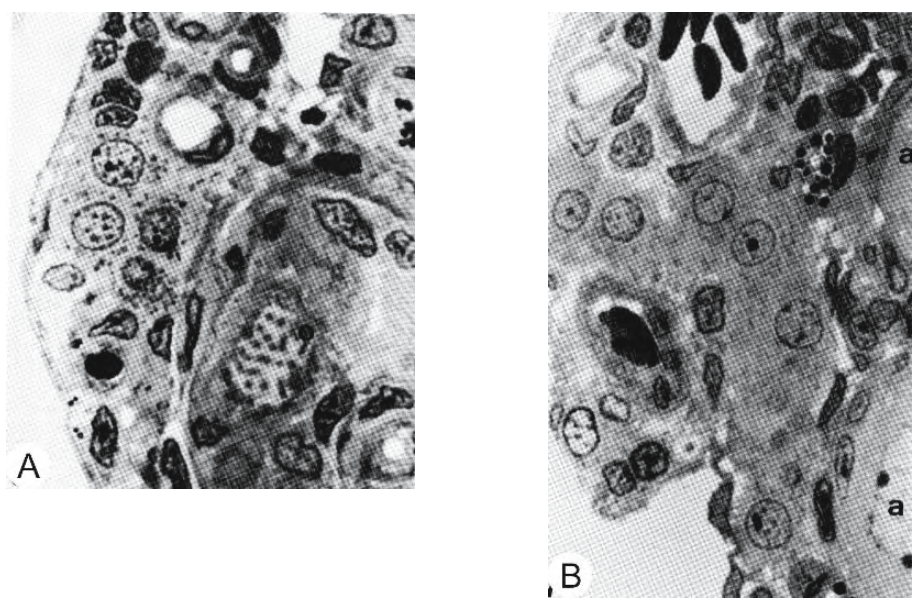

Figure 1.19: Steroid-producing cells are described in the ovary of tilapia *Sarotherodon niloticus* during ovarian differentiation. As the ovarian cavity is forming, these cells appear near the blood vessels of the stroma on the side facing the mesentery. These photomicrographs of cross sections of the ovary show many steroid-producing cells near the blood vessels. (From Nakamura and Nagahama, 1985; reproduced with permission from Blackwell Publishing).

A. 35 days after hatching. Sterioid producing cells at centre left. Premeiotic oocyte, o. X 1,780.

B. 50 days after hatching. Steroid producing cells near centre. Oocyte, a. X 1,700.

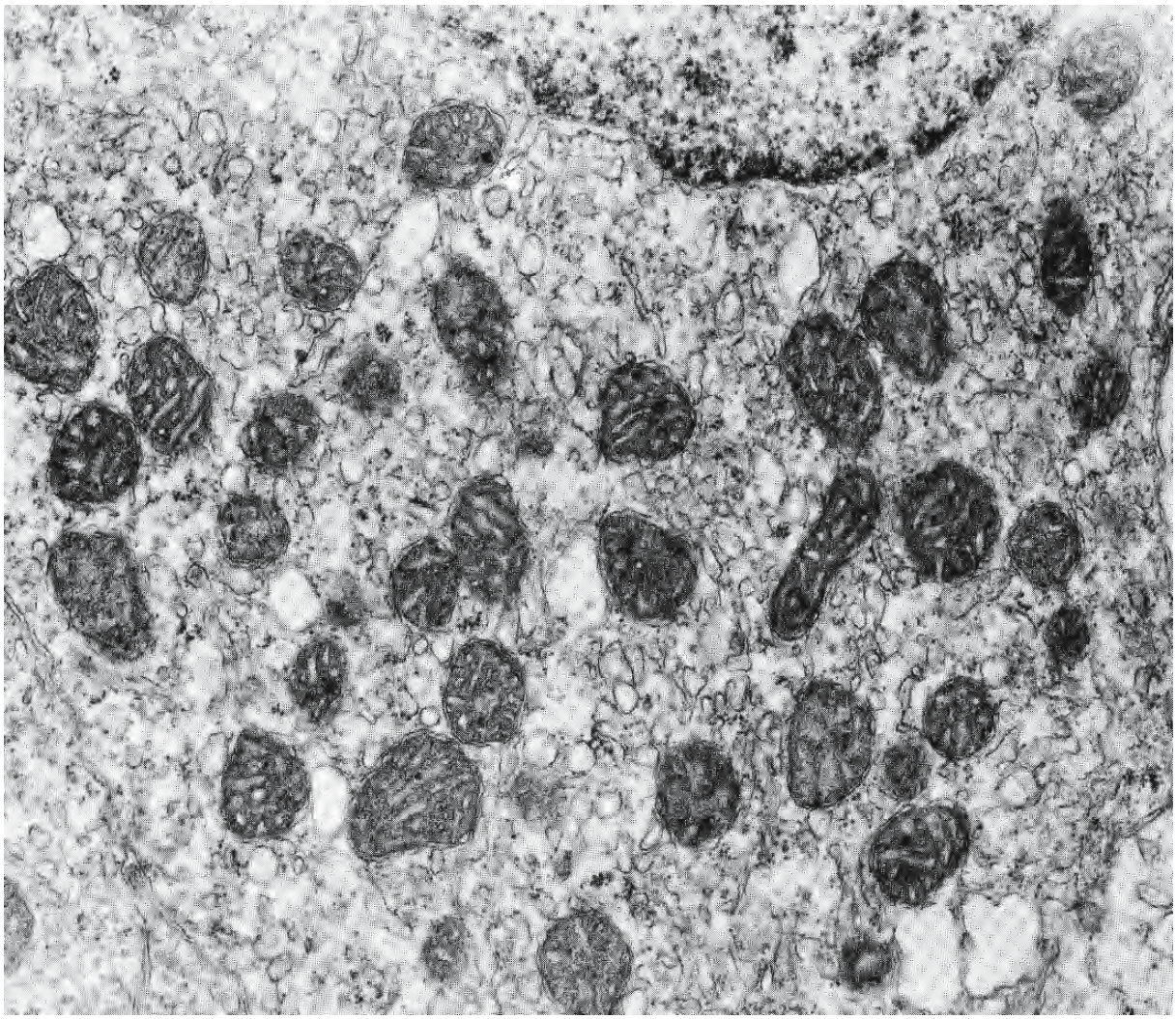

Figure 1.20: Steroid-producing cells are presumed to originate from stromal elements and, as the ovary develops, their numbers increase surrounding the blood vessels. This electron micrograph of a section of a steroid-producing cell from the ovary of tilapia *Sarotherodon niloticus* 50 days after hatching shows the tubular mitochondrial cristae and tubular agranular endoplasmic reticulum which are characteristic of steroid production. X 25,000 (From Nakamura and Nagahama, 1985; reproduced with permission from Blackwell Publishing).

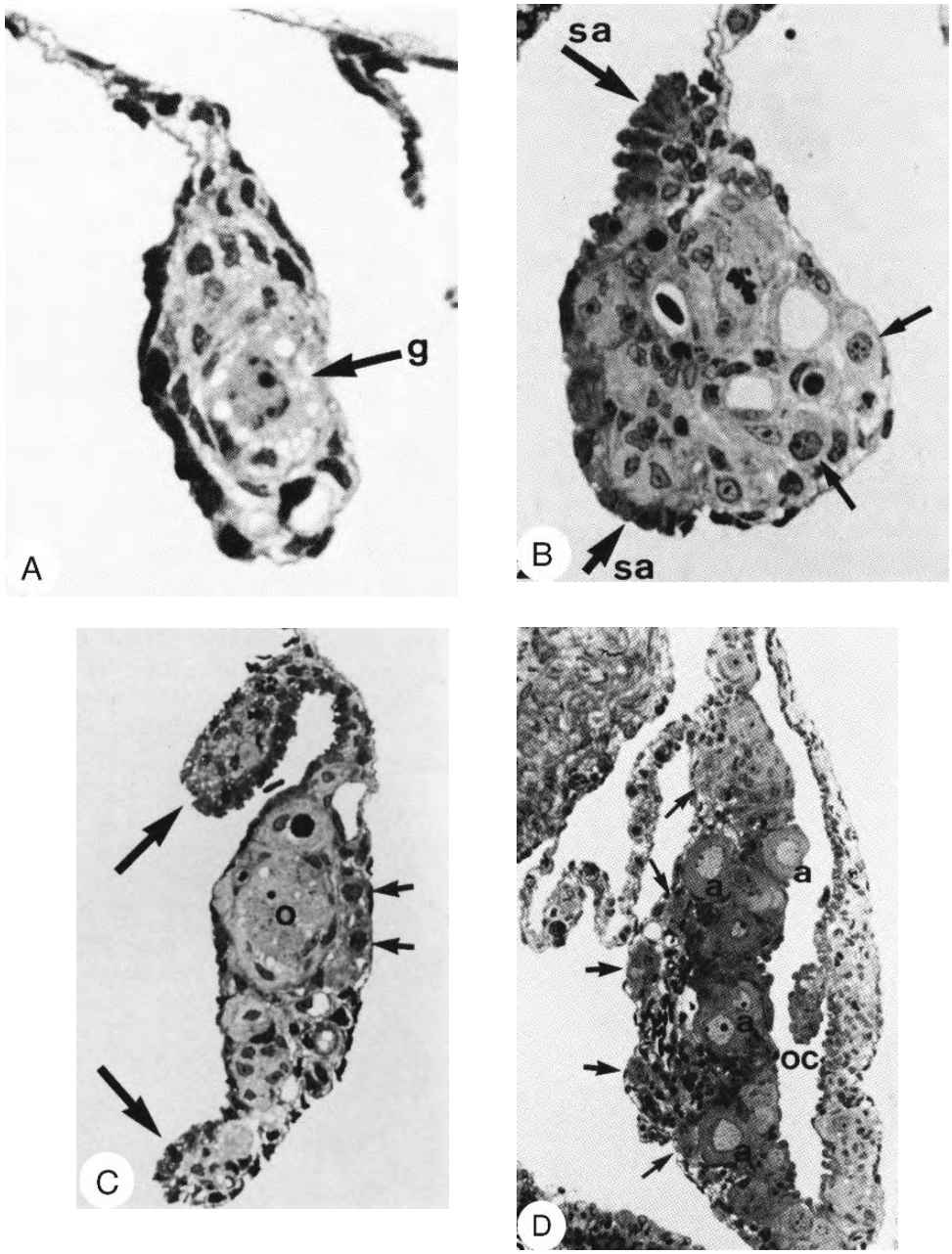

Figure 1.21: Photomicrographs of cross sections of the gonad of developing tilapia *Sarotherodon niloticus.* It is suggested that the steroids produced by steroid-producing cells play a role in the formation of the ovarian lumen and in the differentiation of germ cells. (From Nakamura and Nagahama, 1985; reproduced with permission from Blackwell Publishing).

A. Indifferent gonad 17 days after hatching. A germ cell (g) is surrounded by a few stromal cells. X 1,240.

B. Ovary 26 days after hatching. Steroid-producing cells are seen near the blood vessels. Stromal aggregations (sa large arrow) in the proximal and distal region represent the initial formation of the ovarian cavity. Germ cells are not seen. X 940.

C. Ovary 30 days after hatching showing stromal aggregations (large arrows), cysts containing oogonia and oocytes (o), and steroid-producing cells (small arrows). X 560.

D. Ovary 50 days after hatching showing several oocytes (a) in the perinucleolus stage and numerous steroid-producing cells near blood vessels (arrows). Ovarian cavity, oc. X 340.

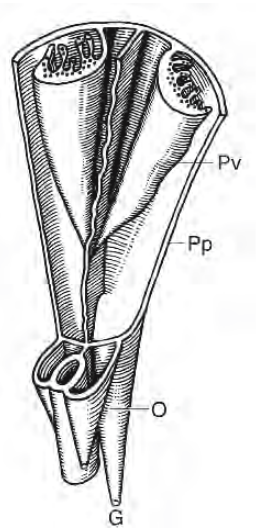

Figure 1.22: In many teleosts, the visceral peritoneum covering the ovary and the peritoneum lining its cavity often continue posteriorly, beyond the mass of ovarian tissue, to form the unique oviduct. This extension of the ovarian cavity continues posteriorly to connect with the genital pore leading to the exterior. (After Giersberg and Rietschel, 1968).
Abbreviations: G, genital pore; O, oviduct; Pp, parietal peritoneum lining ovarian cavity; Pv, visceral peritoneum covering ovary.

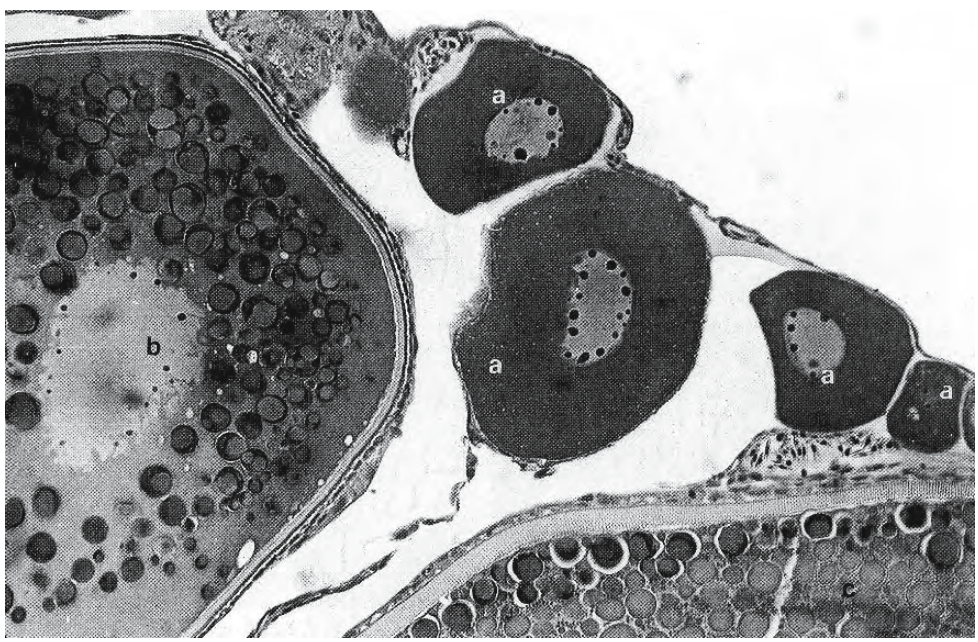

Figure 1.23: Photomicrograph of a section of the ovary of a sexually mature goldfish *Carassius auratus.* The vertebrate ovary is an aggregation of developing follicles enmeshed in a vascular stroma of loose connective tissue and enclosed within an envelope of gonadal epithelium. The stroma consists of collagenous, elastic, and reticular fibres and becomes greatly distended as the follicles enlarge. The clear spaces in the stroma are the result of inevitable shrinkage. X 400 (From Cotelli et al., 1988; reproduced with permission from Elsevier Science).
Abbreviations: a, previtellogenic oocytes; b, vitellogenic oocyte.

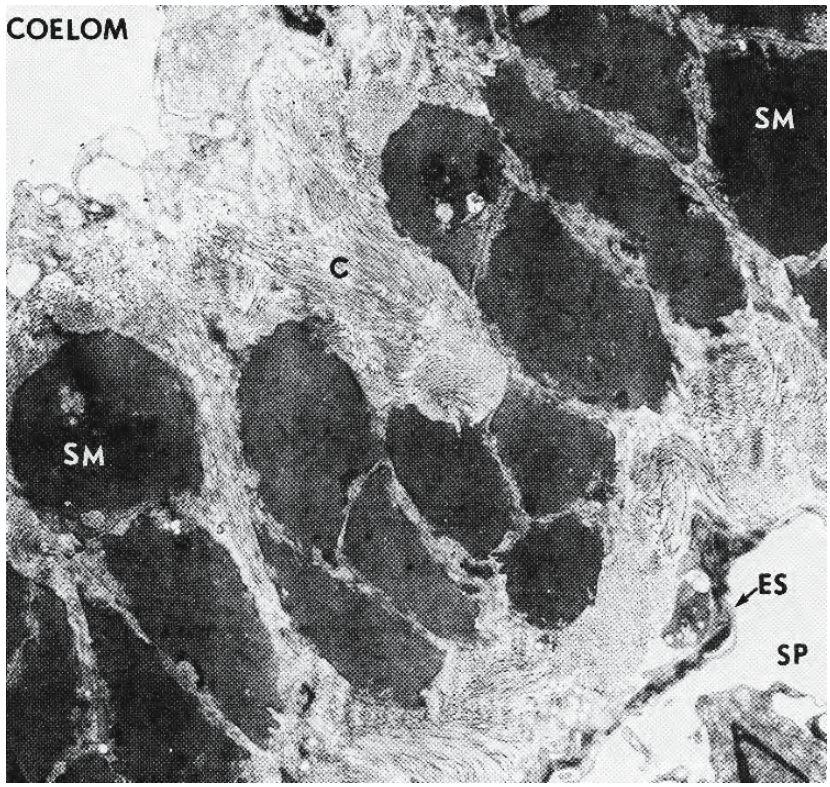

Figure 1.24: Beneath the ovarian envelope, a condensation of stromal tissue forms the capsule or tunica albuginea. This electron micrograph of the well developed capsule of the ovary of *Fundulus heteroclitus* shows abundant collagen (C) and smooth muscle (SM). Inner epithelioid cells (ES) of the stroma line the stromal space (SP). X 7,000 (From Brummett, Dumont, and Larkin, 1982; © reproduced with permission of John Wiley & Sons, Inc.).

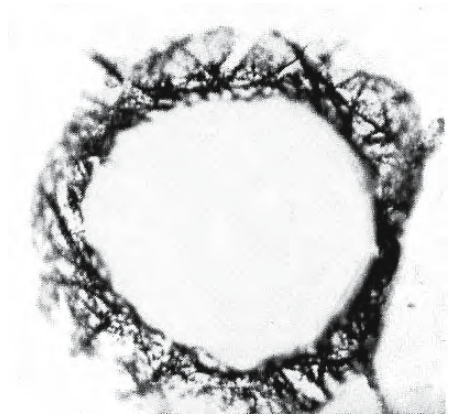

Figure 1.25: Photomicrograph of a section of an ovarian follicle of the brook stickleback *Eucalia inconstans* stained with silver to show the "basket" of reticular fibres surrounding an early oocyte. X 480 (From Braekevelt and McMillan, 1967; © reproduced with permission of John Wiley & Sons, Inc.).

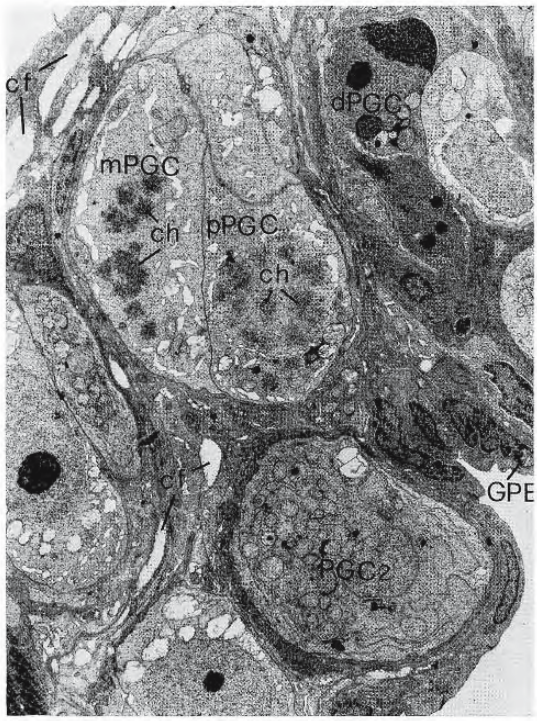

←

Figure 1.26: Early follicles consist of primordial germ cells, newly arrived by migration, enclosed within a cluster of follicular cells derived from divisions of the gonadal epithelial cells. Primordial germ cells in the ovary of the eel *Anguilla anguilla* divide by mitosis to produce diploid oogonia. One germ cell is in metaphase (mPGC), another is in prophase (pPGC). Electron micrograph X 3,000 (From Grandi and Colombo, 1997; © reproduced with permission of John Wiley & Sons, Inc.).
Abbreviations: ch, Chromosomes; cf, bundle of collagen fibrils; dPGC, degenerating germ cell; GPE, gonadal peritoneal epithelium; PGC-2, secondary primordial germ cell.

←

Figure 1.27: Oogonia form diploid primary oocytes by mitotic division. Meiotic division of a primary oocyte in the ovary results in a secondary oocyte and first polar body, both diploid. This section of the ovary of the eel *Anguilla anguilla* shows a cyst of synchronized meiotic oocytes in the zygotene stage, all connected by cytoplasmic bridges (IB). The cyst is enveloped by flattened somatic cells (SC) and is separated by a basal lamina (BL) from the stroma. The oocyte nuclei contain a nucleolus (nu) and synaptonemal complexes (Syc) with chromatin attached to the lateral elements. GPE, gonadic peritoneal epithelium. Electron micrograph X 34,400 (From Grandi and Colombo, 1997; © reproduced with permission of John Wiley & Sons, Inc.).

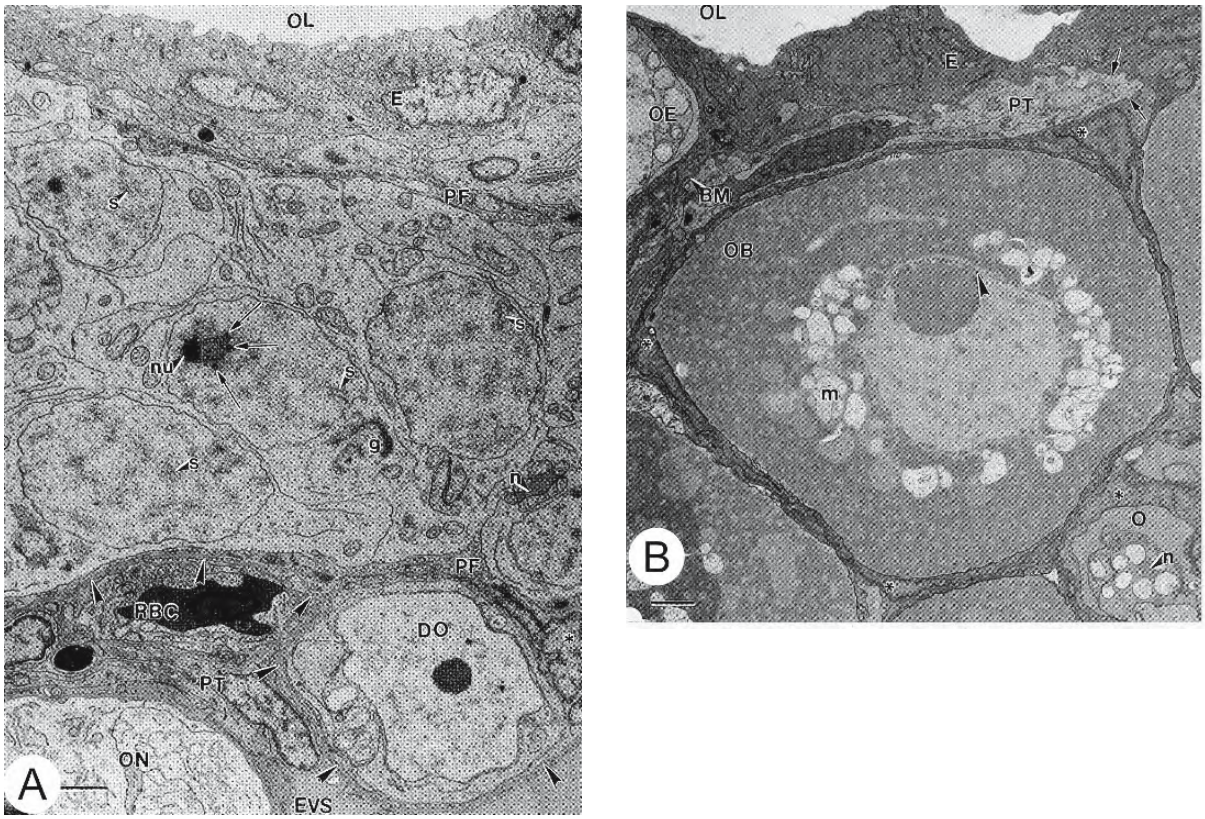

Figure 1.28: Some epithelial cells, whose processes envelop meiotic oocytes, transform into prefollicular cells which become follicular cells at the completion of folliculogenesis. Electron micrographs of the ovary of the common snook *Centropomus unidecimalis.* (From Grier, 2000; © reproduced with permission of John Wiley & Sons, Inc.).

A. The stratified germinal epithelium extends between the ovarian lumen (OL) and the basement membrane (arrowheads) and is composed of epithelial cells (E), a cell nest of meiotic oocytes (in the pachytene stage), and a diplotene oocyte (DO) near the basement membrane. Pachytene oocytes have synaptonemal complexes (s), nucleoli (nu), perhaps multiple nucleoli (arrows), prominent Golgi bodies (g), and nuage (n) surrounded by mitochondria. The single oocyte in diplotene (DO) is being encompassed by prefollicular cells (PF) with pleiomorphic nuclei (*). Newly formed diplotene oocytes have a prominent nucleolus and lack basophilic cytoplasm. The extravascular space (EVS) is nearly occluded by prethecal cells (PT) and a capillary is observed with a single red blood cell (RBC). A nest of oocytes (ON) is seen at the lower left. Bar = 2 μm.

B. Epithelial cells of the germinal epithelium (E) border the ovarian lumen (OL) and encompass an oocyte (OE), isolating it from the lumen. Oocytes with basophilic cytoplasm (OB) and oocytes without (O) are contained within a cell nest still attached to the germinal epithelium. The basement membrane (BM) is continuous over the surface of the nest and also the base of the germinal epithelium (arrows). Prethecal cells (PT) lie within the interstitium. Nuage (n) is present in the smaller oocytes. In the nucleus of a larger oocyte with basophilic cytoplasm, granular material denoting RNA synthesis (arrowhead) is present between the nucleolus and nuclear membrane; the nucleus is ringed by mitochondria (m). These oocytes are not yet enclosed within a follicle although prefollicular cells (*) may completely encompass them. Bar = 1 μm.

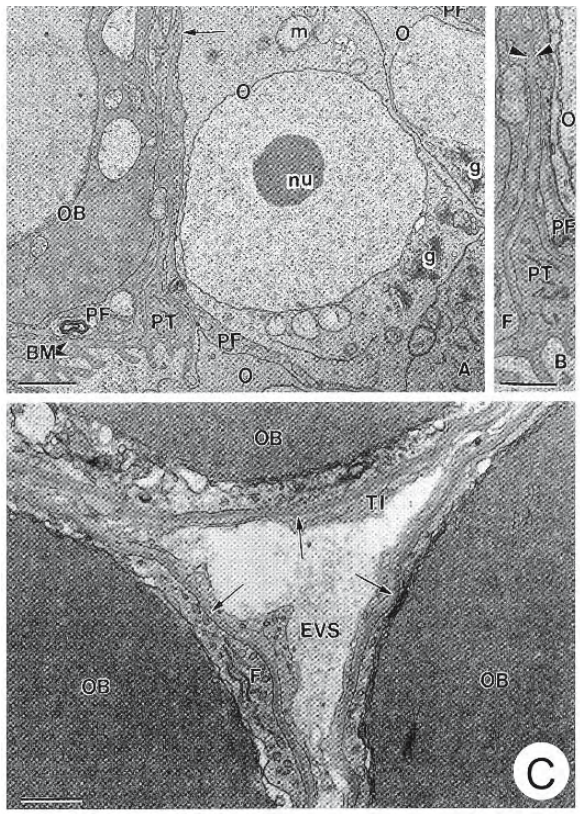

Figure 1.28: Continued.

C. *Upper left*. A portion of an oocyte nest. One diplotene oocyte with basophilic cytoplasm (OB), surrounded by prefollicular cells (PF) is becoming a follicle. Prefollicular cells also surround the nest where oocytes (O) are in contact with each other. These oocytes display prominent nucleoli (nu), vesicular mitochondria (m), and Golgi bodies (g). A prethecal cell (PT) lies between the basement membranes of the forming follicle and cell nest. Bar = 1 μm. *Upper right*. An enlargement of the prethecal cell (PT). The basement membrane extends between the layers of follicular cells (F) that surround the oocyte (O) and the prefollicular cells (PF) around the oocyte nest. Processes from the prethecal cells do not penetrate between these basement membranes (arrowheads). Bar = 1.75 μm. *Lower*. Portions of three follicles, each containing a basophilic oocyte (OB) encompassed by follicular cells (F). Basement membranes (arrows) separate the follicles from the theca interna. EVS, extravascular space. Bar = 1 μm.

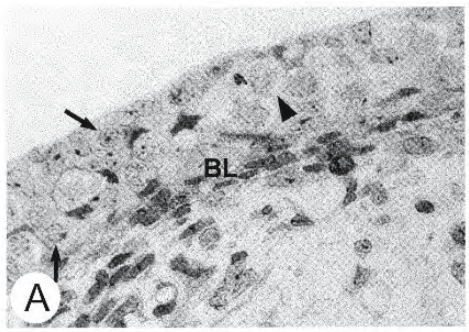

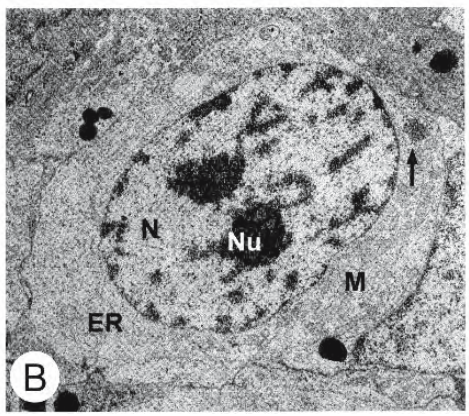

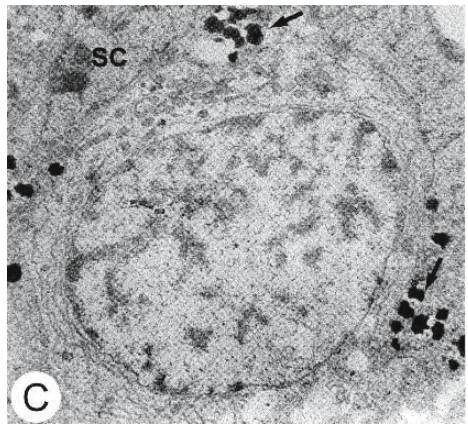

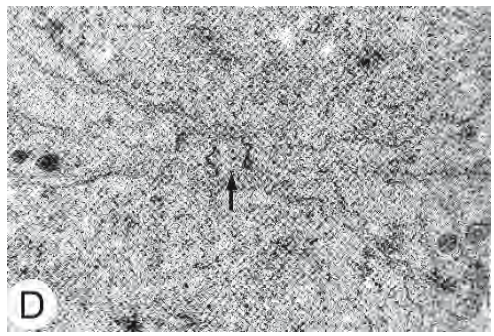

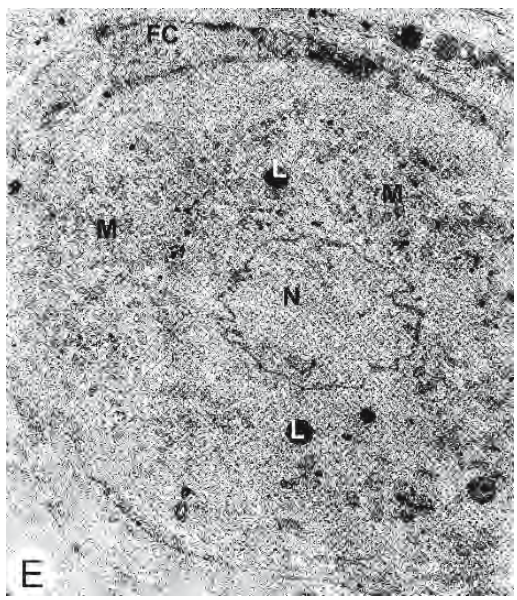

Figure 1.29: Micrographs of sections of the ovarian cortex of 6- to 7-cm embryos of the spotted ray *Torpedo marmorata.* (From Prisco, Ricchiari, and Andreuccetti, 2001; reproduced with permission).

A. Light micrograph of germ cells in the ovarian cortex. Clusters of oogonia (arrows) and meiotic oocytes (arrowhead) are seen. Follicles are absent. X 390.

B. Electron micrograph of an oogonium. The nucleus is round and contains a conspicuous nucleolus and several patches of heterochomatin. Mitochondria, cisternae of granular endoplasmic reticulum, and an aggregate of germ plasm (arrow) are evident in the cytoplasm. X 3,900.

C. Electron micrograph of a leptotene oocyte. Cytoplasmic organelles are initially polarized in a juxtanuclear position. Several osmiophilic vacuoles (arrows) are evident in the surrounding thecal cells. X 4,500.

D. Electron micrograph of an intercellular bridge (arrow) between two oocytes. The membranes bordering the bridge are electron dense and about 30 nm in thickness. X 9,000.

E. Electron micrograph of a primary follicle in the ovary of a neonate. The diplotene oocyte is surrounded by a single layer of squamous follicular cells. X 3,000.

Abbreviations: BL, basal lamina; ER, granular endoplasmic reticulum; FC, follicular cells; L, liposomes; M, mitochondria; N, nucleus; Nu, nucleolus; SC, thecal cells.

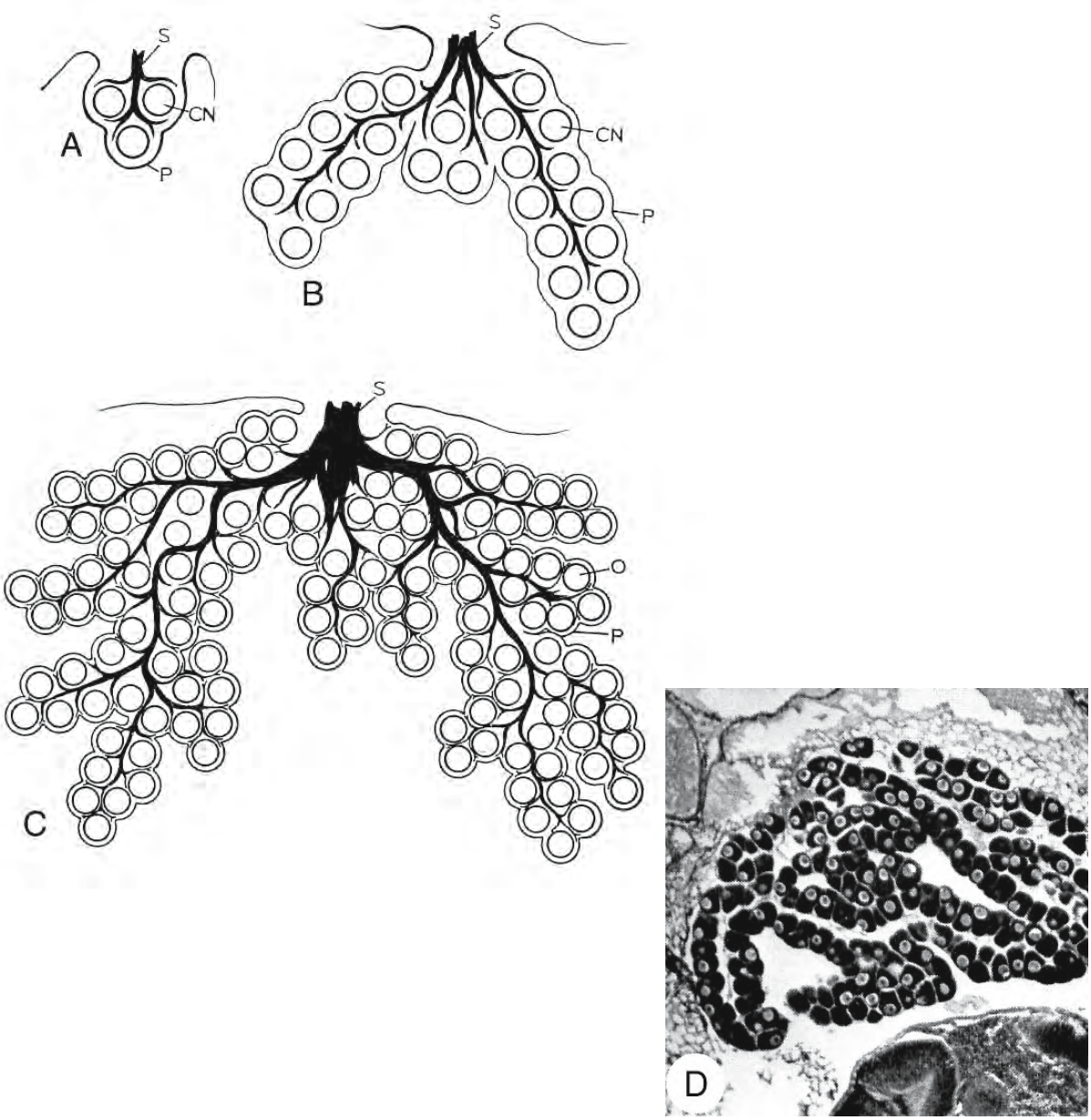

Figure 1.30: Division of developing germ cells in the ovaries of lampreys *Petromyzon marinus* causes evaginations of the ovarian wall to expand ventrally, subdividing the ovary into lobes and lobules that contain a stroma of vascular connective tissue. (From Lewis and McMillan, 1965; © reproduced with permission of John Wiley & Sons, Inc.).

A, B,C. (A) Three cell nests are surrounded by peritoneum and penetrated by a stroma of vascular connective tissue. (B) Each of these cell nests gives rise to a group of cell nests, each of which constitutes a lobe of the ovary; the vascular stroma has penetrated between the cell nests. (C) As division continues, the progeny of each cell nests forms a lobule; the lobule is a discrete group of oocytes (o), roughly two cells in thickness, contained within peritoneum. CN, cell nest; P, peritoneum; S, stroma.

D. Photomicrograph of a section of the ovary of an ammocoete in early metamorphosis showing the ovigerous folds which are flat, leaf-like extensions of ovarian tissue. X 45.

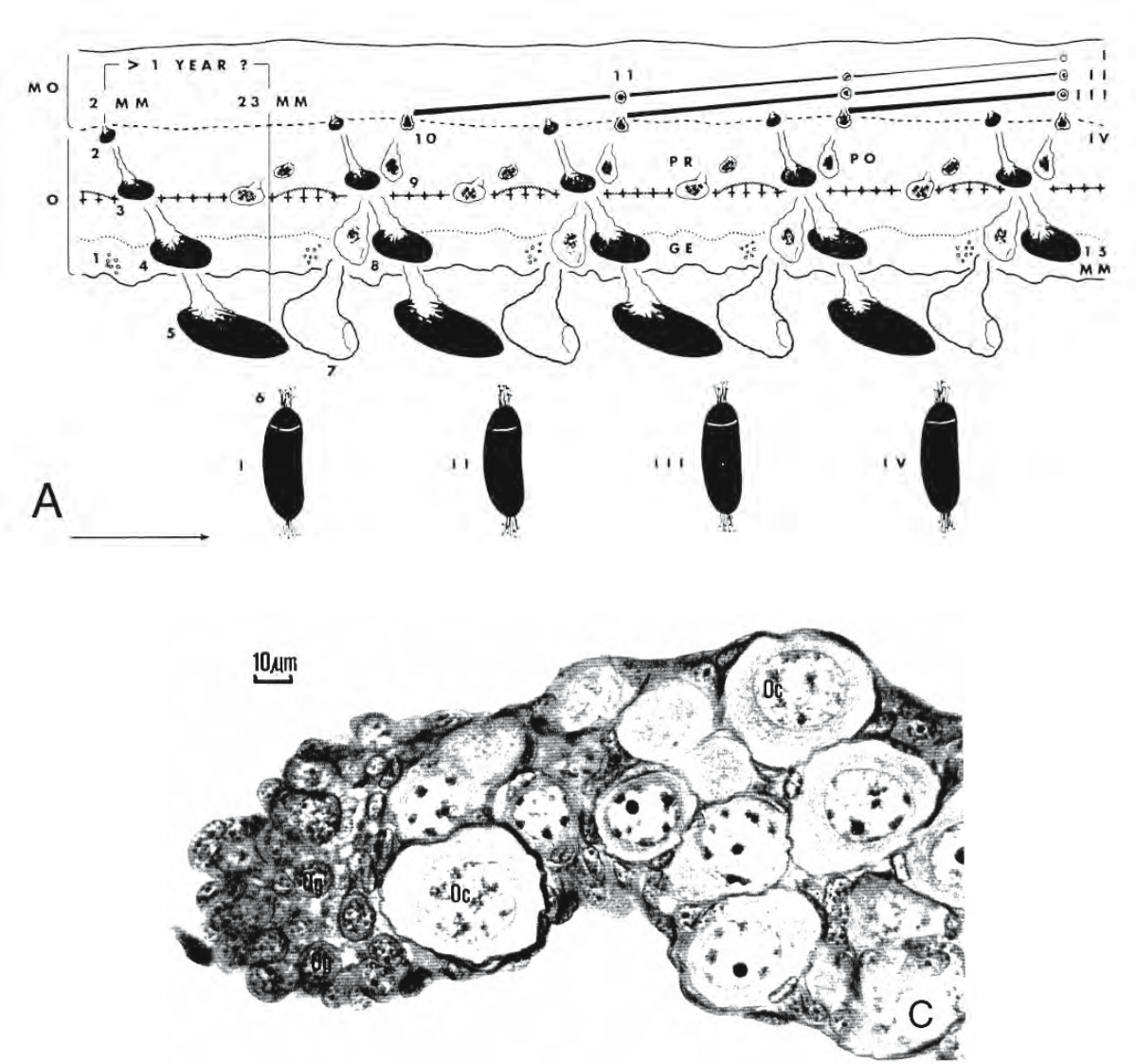

Figure 1.31: The ovary of the hagfish *Myxine glutinosa* forms a dorsal, narrow ribbon suspended from the mesovarium in the midline. (Figures **A** and **G** are from Walvig, 1963; reproduced with permission. **B** to **F** are from Patzner, 1974, and are reproduced, with permission, from the Norwegian Journal of Zoology).

A. The ovary (O) consists of "series" of follicles that develop from oogonia contained within a band of germinal cells that runs along the free edge of the ovary (GE). The movement of oocytes and follicles as well as follicular involution is indicated in this imaginary diagram. Maturing oocytes (1) move from the band of germinal cells into the vascular connective tissue of the inner part of the ovary (2 to 5). Undifferentiated squamous mesothelial cells attach to the oocytes and stretch to enclose them within a follicular epithelium. Four "generations" of oocytes are shown, developing from oogonia in the germinal band (I to IV); they grow to a diameter of 1 to 2 mm whereupon they enter a resting period awaiting ovulation of the previous generation of oocytes. After the mature egg (6) is ovulated, the empty follicle (7) forms a postovulatory corpus luteum (PO) that regresses as it moves toward the mesovarium (MO) (8 to 11). Some follicles undergo atresia at some point in their development (PR).

C. An enlarged portion of **B** showing the oogonia (Og) in the germinal band and oocytes (Oc) within the ovary. X 600.

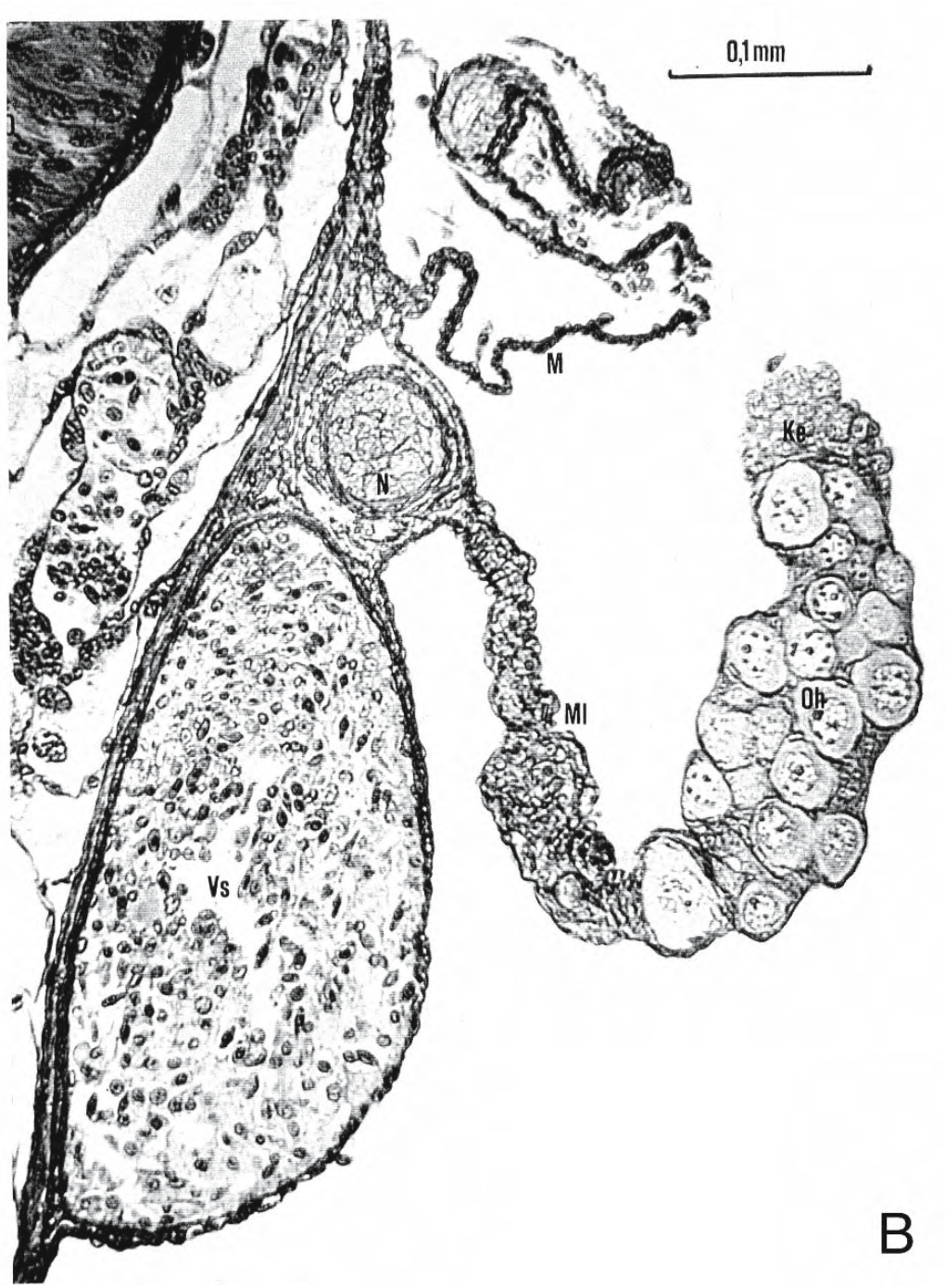

Figure 1.31: Continued.

B. Photomicrograph of a section through the gonad of a 15-cm female. X 290. Oogonia originate in the band of germinal cells (Ke) and migrate to the vascular connective tissue of the inner part of the ovary where they under go meiotic division to become oocytes (Oh).

Abbreviations: D, intestinal epithelium; Ke, germinal cells; M, mesentery; MI, mesovarium; N, nerve; Oh, oocytes; Vs, supra-intestinal vein.

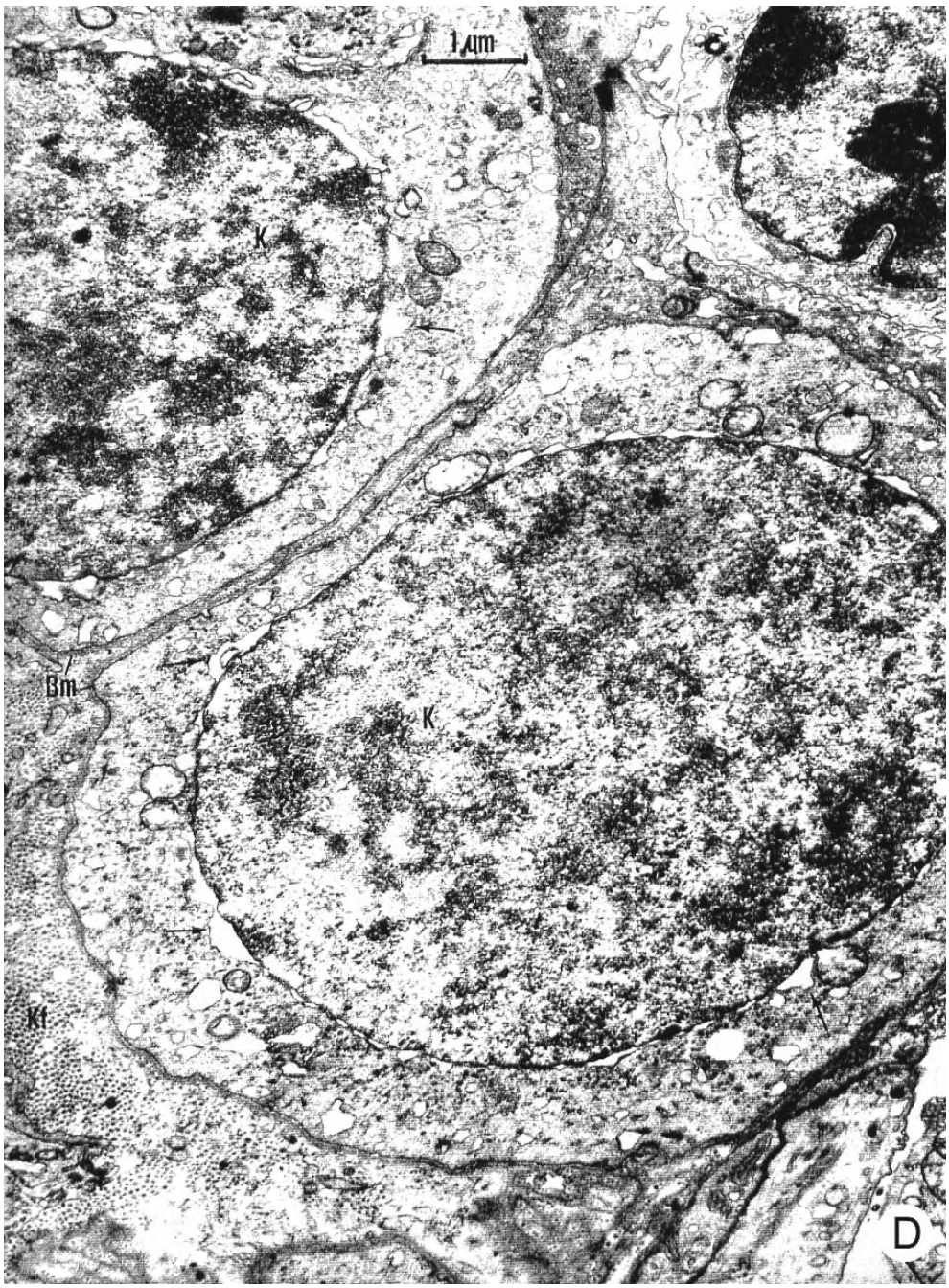

Figure 1.31: Continued.

D. Electron micrograph of a section through the germinal band of a 14-cm female showing two oogonia (K) and one germinal cell. Collagenous fibres (Kf) provide support in the vascular stroma. The basal lamina (Bm) is shown. Arrows indicate undulations of the outer nuclear membrane of an oogonium. X 14,300.

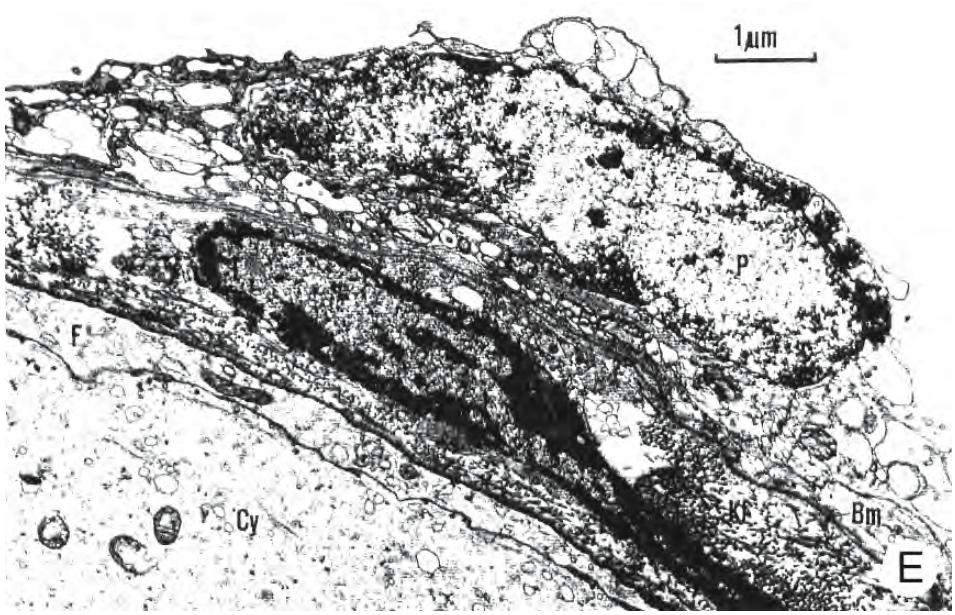

Figure 1.31: Continued.

E. Electron micrograph of a portion of a primary follicle, showing the thin follicular epithelium (F) surrounding an oocyte (Cy). A thecal cell (T) is supported by collagenous fibres (Kf). A peritoneal cell (P) of the mesothelium encloses the ovary. Bm, basement membrane. X 14,200.

Figure 1.31: Continued.

F. Electron micrograph of a portion of a maturing follicle approximately 100 µm in diameter. An oocyte (Cy) is enclosed by a squamous follicular cell (F) resting on its basement membrane. The theca consists of flattened thecal cells (T) and stout collagenous fibres (Kf). A peritoneal cell (P) of the mesothelium rests on its basement membrane (Bm). X 24,000.

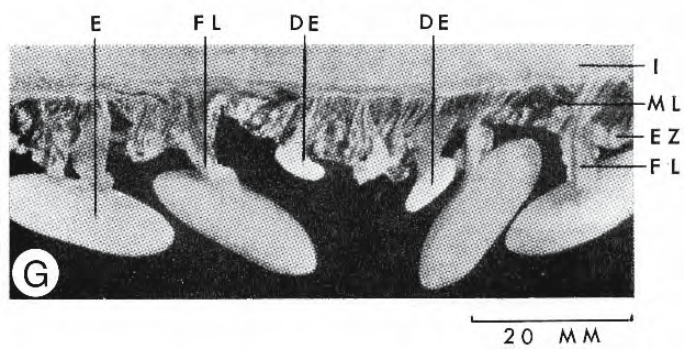

Figure 1.31: Continued.

G. Photograph of the ovary of *Myxine glutinosa.* Nearly mature eggs (E) dangle within individual peritoneal slings (ML) from follicular ligaments (FL) attached to the ovary. Two atretic eggs are shown (DE). The intestine (I) is shown at the top.

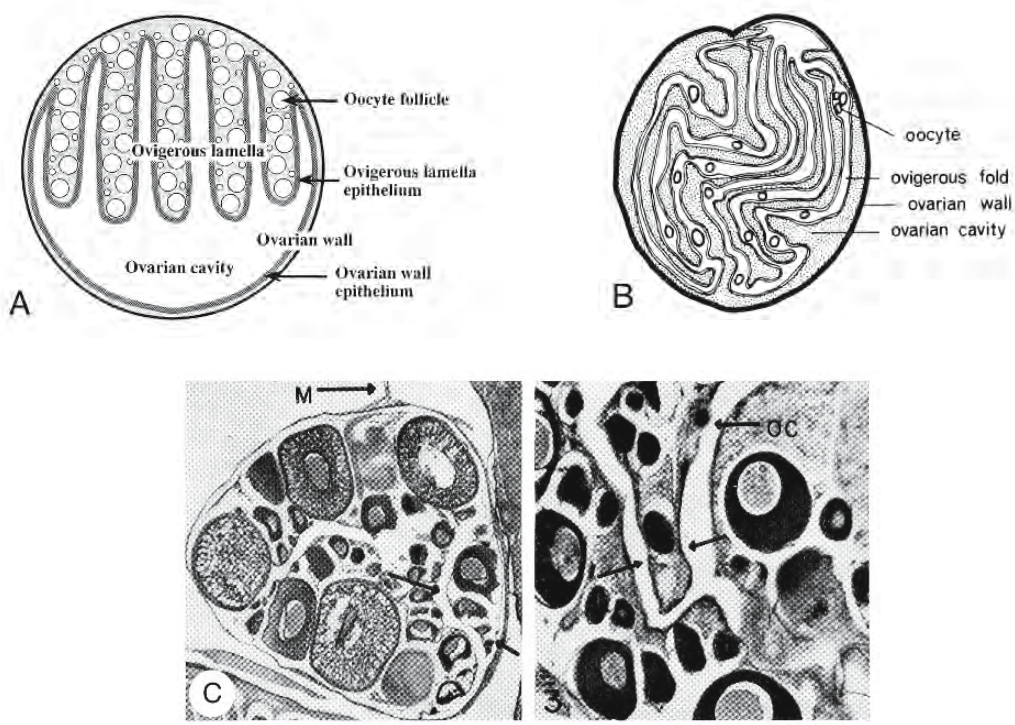

Figure 1.32: The epithelium lining hollow, cystovarian ovaries of many teleosts is thrown into a complex series of ovigerous folds.

A. Schematic diagram of a cross section of one of the paired ovaries of the sculpin, *Alcichthys alcicornis.* (From Koya, Munehara, and Takano, 1997; © reproduced with permission of John Wiley & Sons, Inc.).

B. Complex ovigerous folds in the ovary of the surfperch, *Cymatogaster.* (From Hoar 1969; reproduced with permission from Elsevier Science).

C. Photomicrographs of cross sections of the ovary of the brook stickleback *Eucalia inconstans* showing ovigerous folds (arrows) extending into the ovocoel (OC). Left X 54; right X 155. (From Braekevelt and McMillan, 1967; © reproduced with permission of John Wiley & Sons, Inc.).

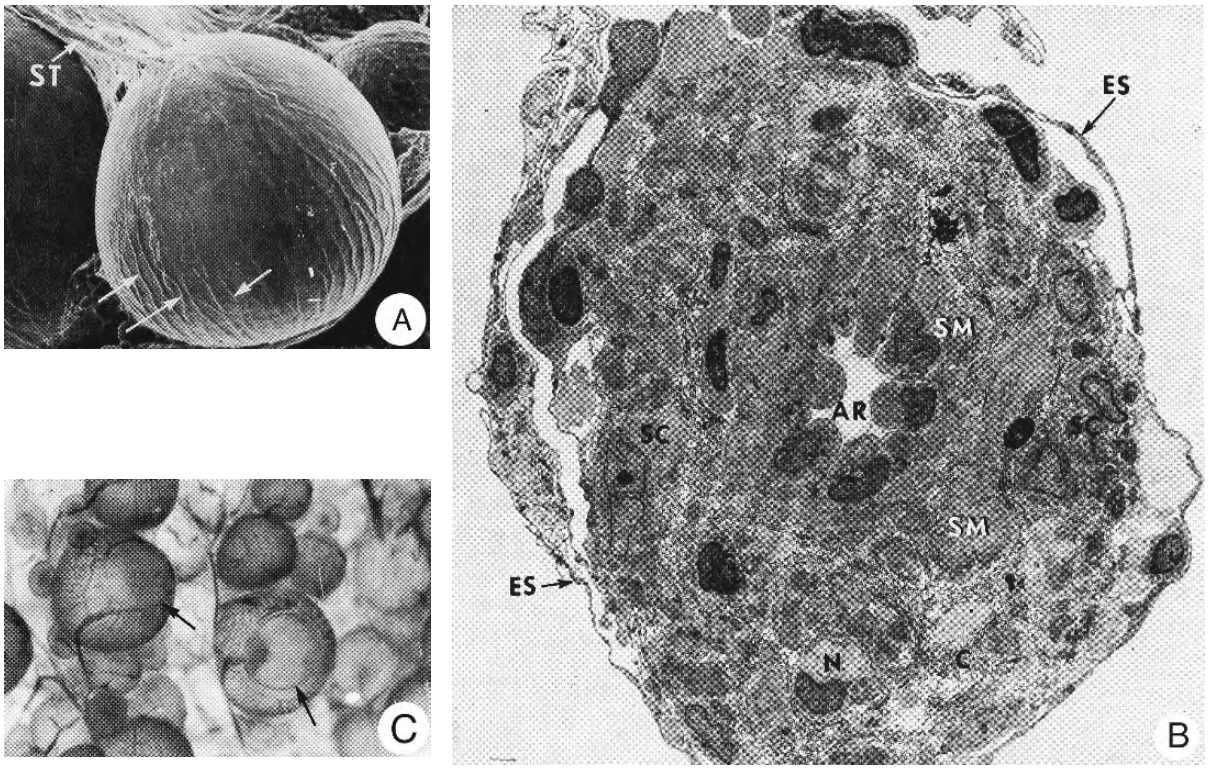

Figure 1.33: The ovary of teleosts is supplied with blood from several arteries that branch off the dorsal aorta, entering the dorsal side of the ovary through the mesovarium. Each follicle in the ovary of the killifish *Fundulus* is supplied by a primary arteriole that reaches it through a stalk of stromal elements. (From Brummett, Dumont, and Larkin, 1982; © reproduced with permission of John Wiley & Sons, Inc.).

A. Scanning electron micrograph of a developing follicle. The follicle is anchored in the stroma by a stalklike structure (ST) surrounded by stromal elements. Blood vessels (arrows) can be seen in the apical hemisphere of the follicle. X 80.

B. Electron micrograph of a cross section the stalklike structure. A central arteriole (AR) is surrounded by smooth muscle (SM), a nerve (N), abundant collagen (C), and stromal cells (SC). An epithelioid layer of stromal cells (ES) encloses the structure. X 4,300.

C. The superficially located vessels in the apical or luminal hemisphere of the follicle are more readily apparent and are presumed to be venules that collect blood from the intervening capillary bed and transport it to a vessel that forms a loop (arrows) surrounding the presumed site of future ovulation on the luminal side of the follicle. These vessels terminate in a single collecting vessel that courses toward the outer surface of the ovary. X 250.

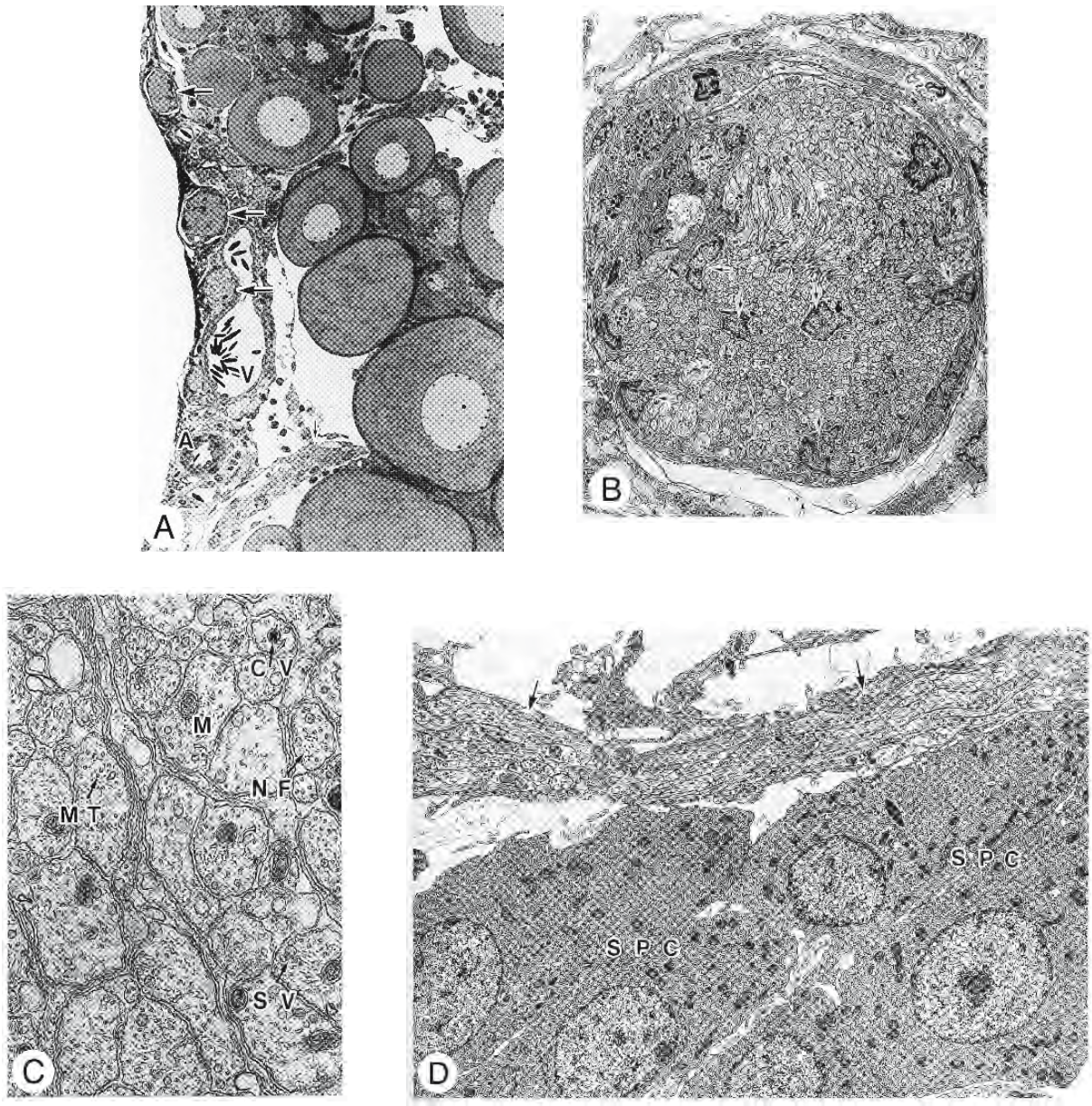

Figure 1.34: Thick bundles of non-myelinated nerves, presumably autonomic, accompany the ovarian artery and vein in the ovary of tilapia *Oreochromis niloticus* (From Nakamura, Specker, and Nagahama, 1996; reproduced with permission from the Zoological Society of Japan).

A. Photomicrograph of a part of the ovary showing thick nerve bundles (large arrows) near the artery (A) and veins (V). Clusters of steroid-producing cells (small arrows) are seen in the interstitial area. X 360.

B. Electron micrograph of a cross section of a thick nerve bundle in the ovary. The bundle consists of more than 1,000 axons and some neurilemma cells (arrows). X 3,800.

C. Cross section of non-myelinated axons in a nerve bundle.
Abbreviations: CV, dense-cored vesicles; M, mitochondria; MT, microtubules; NF, neurofilaments; SV, synaptic vesicles. X 33,200.

D. Nerve bundle (arrows) is distributed near a cluster of steroid-producing cells (SPC) showing well-developed agranular endoplasmic reticulum and mitochondria with tubular cristae. X 41,600.

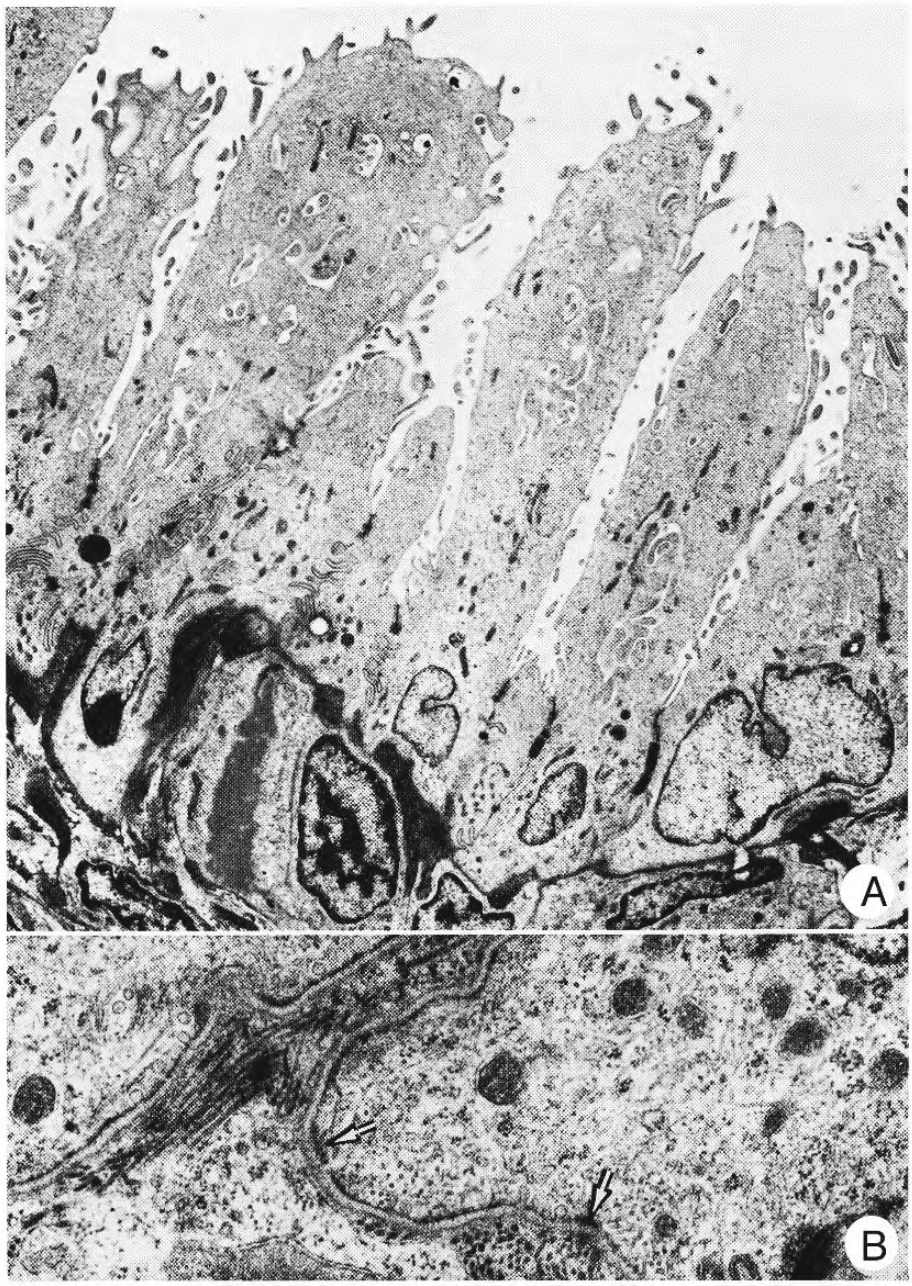

Figure 1.35: In the killifish *Fundulus heteroclitus,* the posterior portion of the ovary is a thin-walled nongerminal ovisac that is continuous with the short oviduct and apparently serves as a receptacle for ovulated eggs prior to their release to the external environment. These cells may function in the transport of ovulated eggs or they may secrete a jelly that forms a surface coat for the extruded eggs. (From Brummett, Dumont, and Larkin, 1982; © reproduced with permission of John Wiley & Sons, Inc.).

A. Electron micrograph of the luminal epithelium of this thin-walled region showing a localized population of unusual cells with long apical cytoplasmic extensions bearing short microvilli and extensive basal interdigitations and desmosomes. Lobate nuclei and numerous mitochondria occupy the basal cytoplasm. X 5,400.

B. Uncoated endocytotic pits and hemidesmosomes (arrows) are seen adjacent to the basal lamina of these cells. There are a few microtubules in the cytoplasm. X 28,300.

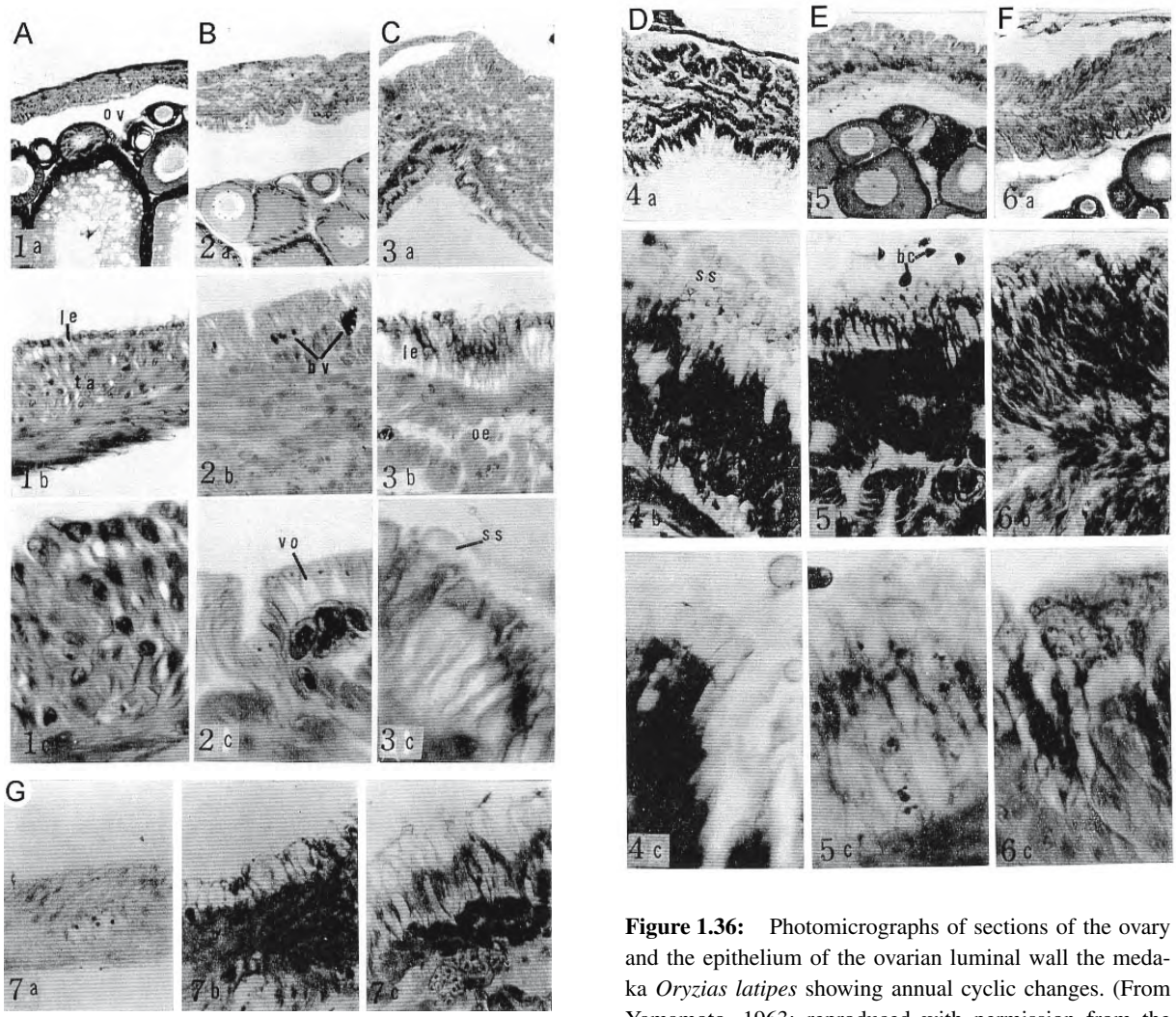

Figure 1.36: Photomicrographs of sections of the ovary and the epithelium of the ovarian luminal wall the medaka *Oryzias latipes* showing annual cyclic changes. (From Yamamoto, 1963; reproduced with permission from the Zoological Society of Japan).

A. Luminal wall during vitellogenesis (January). (1a-c).

B. As the ova mature (February), the luminal wall thickens and its simple cuboidal epithelium becomes simple columnar as secretory activity increases. The underlying tunica albuginea thickens as vascularization increases and smooth muscle develops. (2a-c).

C. The luminal wall continues to thicken (April) and the epithelial cells become taller. (3a-c).

D. Luminal wall in May showing active apocrine secretion. (4a-c).

E. Luminal wall following ovulation (September). (5a-c).

F. After spawning, the epithelium and tunica albuginea undergo involution (November). (6a-c).

G. Rapid changes occur in the luminal wall following spawning. X 440. (7a-c) Immediately after ovulation, the wall becomes thin (left) with a squamous epithelium and reduced tunica submucosa. By the next day, fluid has accumulated in the epithelial cells which once again appear columnar (middle). The vascular subepithelial connective tissue recovers. Two days after spawning (right).

Abbreviations: bc, extravasated blood cells; bv, blood vessel; le, epithelium; oe, oedematous tissue; ov, ovarian lumen; ss, secreted substance; vo, vacuole in columnar epithelium.

Magnification of figures **A** to **F**: top X 110; middle X 440; bottom X 1100.

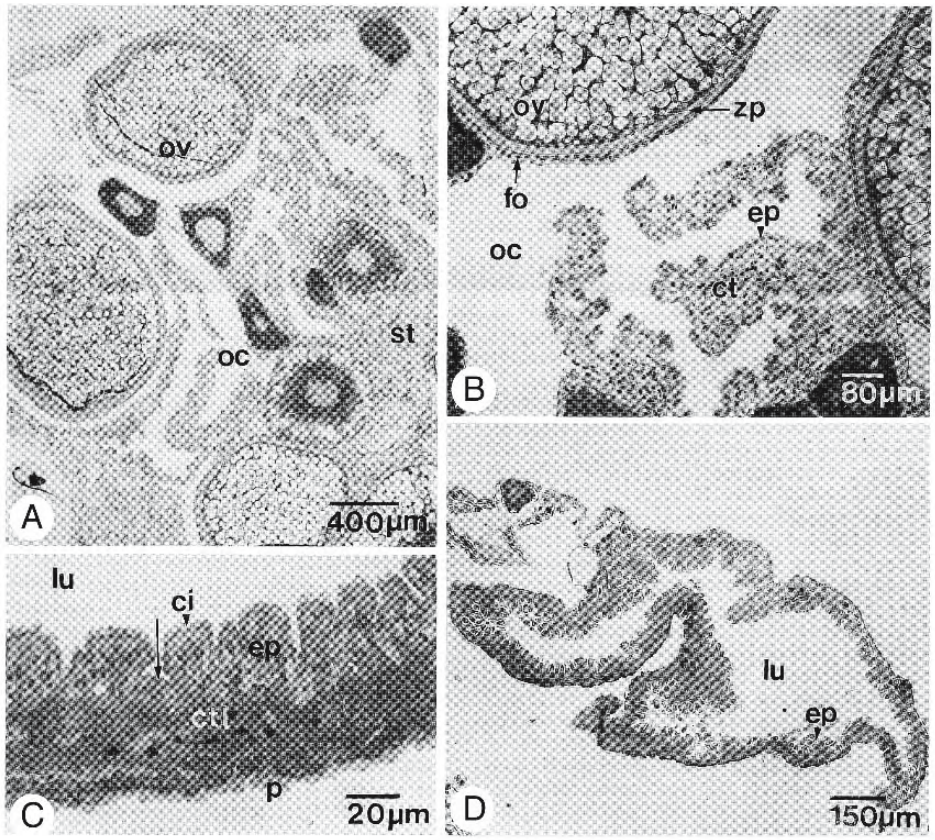

Figure 1.37: Photomicrographs of the simple columnar epithelium of microvillous cells lining the ovarian cavity of the bleak *Alburnus alburnus.* Around the time of ovulation, these cells bulge apically into the lumen and a few small clusters are also found in the oviduct. (From Lahnsteiner, Weismann, and Patzner, 1997; reproduced with permission from Elsevier Science).

A. General view of the ovary showing the labyrinthine ovarian cavity.

B. In some regions, the theca externa of the follicle surrounds the ovarian cavity, not the epithelium of the ovarian cavity.

C. Cross section of the wall of the oviduct. The arrow indicates a cluster of microvillous cells.

D. Wall of the oviduct showing clusters of microvillous cells.

Abbreviations: ci, cilia; ct, connective tissue; ep, epithelium; fo, theca externa of follicle; lu, lumen of oviduct; oc, ovarian cavity; ov, ovum; p, peritoneum; st, stroma; zp, zona pellucida.

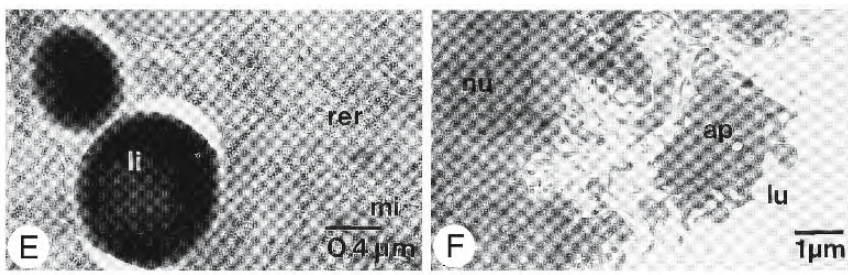

Figure 1.38: Electron micrographs of microvillous cells from the ovarian cavity of *Alburnus alburnus.* (From Lahnsteiner, Weismann, and Patzner, 1997; reproduced with permission from Elsevier Science).

E. Lipid vacuoles in the cytoplasm.

F. A microvillous cell has released a membrane-bound cytoplasmic bleb; this is apocrine secretion.

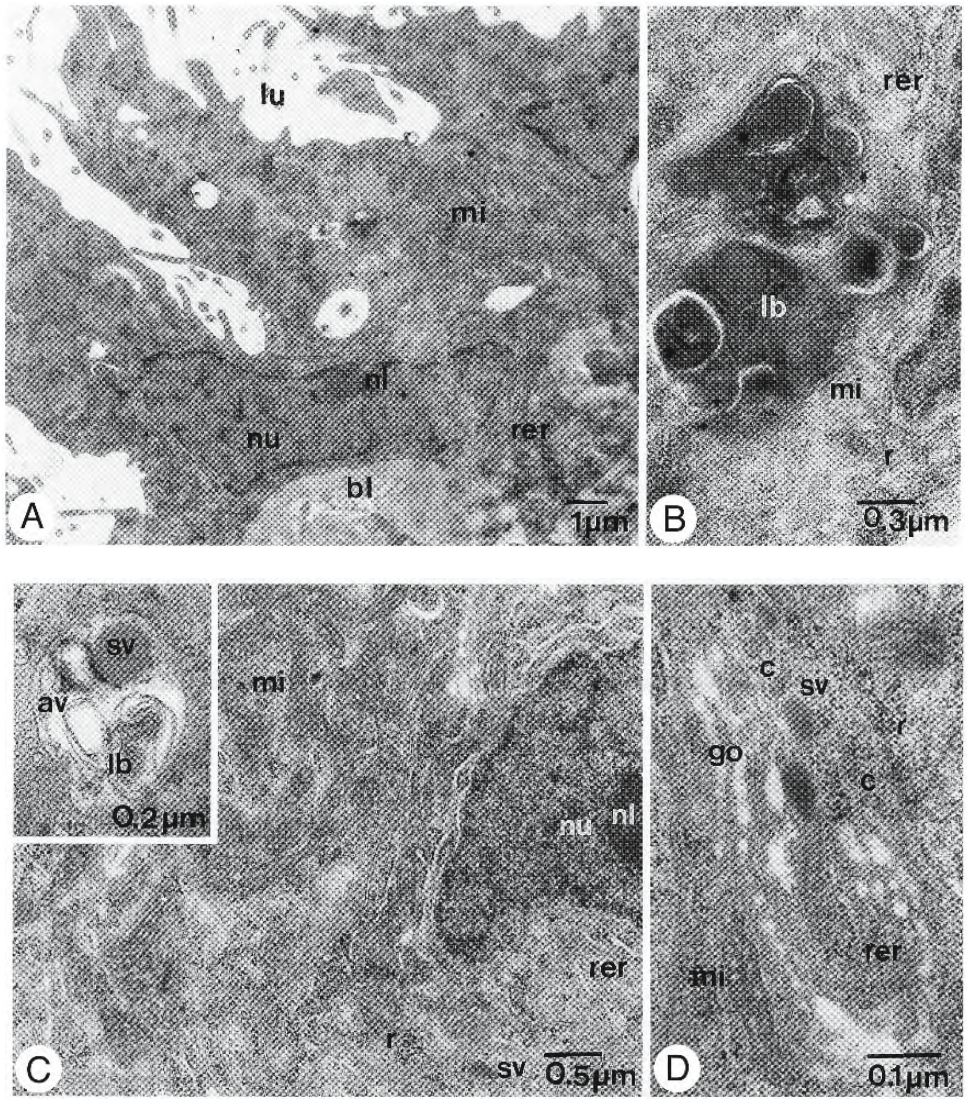

Figure 1.38: Continued.

A. Protein production is indicated by the prominent nucleolus and abundant tubular granular endoplasmic reticulum that forms concentric layers around the basal nucleus.

B. The presence of lamellar bodies in the microvillous cells results from phagocytosis of débris from the lumen.

C. The cytoplasm of a microvillous cell displays the organelles of protein production: nucleolus, agranular endoplasmic reticulum, and free ribosomes. The inset shows an autophagic vesicle in a region containing secretory vesicles.

D. Golgi complex and neighbouring secretory vesicles.**E**. Lipid vacuoles in the cytoplasm.

F. A microvillous cell has released a membrane-bound cytoplasmic bleb; this is apocrine secretion.

Abbreviations: ap, cytoplasmic bleb released by apocrine secretion; av, autophagic vesicle; bl, basal lamina; c, coated vesicles; go, Golgi complex; lb, lamellar bodies; li, lipid vacuoles; lu, lumen; mi, mitochondria; nl, nucleolus; nu, nucleus; r, ribosomes; rer, granular endoplasmic reticulum; sv, secretory vesicle.

Abbreviations: ap, cytoplasmic bleb released by apocrine secretion; av, autophagic vesicle; bl, basal lamina; c, coated vesicles; go, Golgi complex; lb, lamellar bodies; li, lipid vacuoles; lu, lumen; mi, mitochondria; nl, nucleolus; nu, nucleus; r, ribosomes; rer, granular endoplasmic reticulum; sv, secretory vesicle.

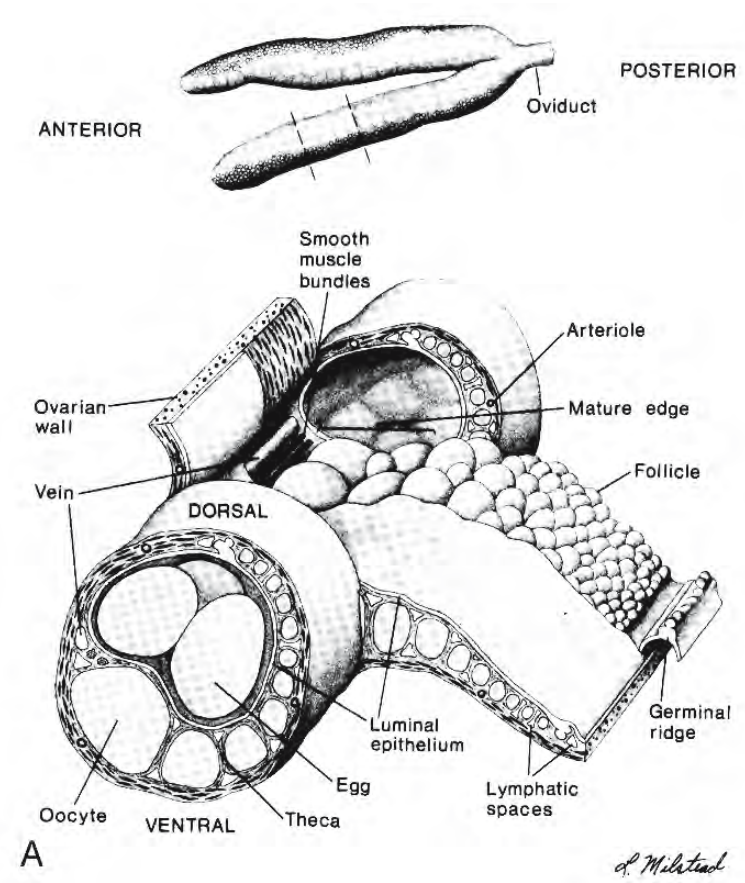

Figure 1.39: The ovaries of syngnathids consist of a sheet of follicles, with their supporting vascular stroma, in the form of a tubular scroll extending lengthwise.

A. The upper drawing shows the paired ovaries of the pipefish *Sygnathus scovelli* which open into the single oviduct. The dashed lines indicate the segment of the ovary that is enlarged below. The middle section has been unfurled to show the follicles and lumen. A single germinal ridge forms the inner margin of the scroll and, extending from this, is a sequential array of follicles arranged according to their developmental age, sandwiched between the outer ovarian wall and the inner luminal epithelium. Mature oocytes are ovulated from the opposite margin of the scroll, the mature edge, into the ovarian lumen. (From Begovac and Wallace, 1987; © reproduced with permission of John Wiley & Sons, Inc.).

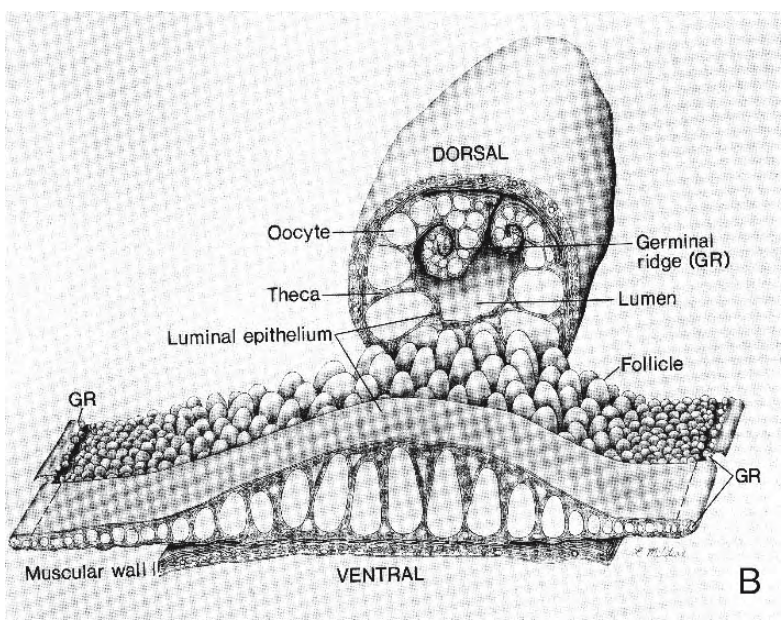

B. In the seahorse *Hippocampus erectus,* there are two germinal ridges that run the length of the tubular ovary on opposite edges of the ovarian sheet. The ovary has been cut along its dorsal midline and both halves have been unrolled. Developing follicles arise from each germinal ridge and grow toward a shared mature region near the middle of the sheet (From Selman, Wallace, and Player, 1991; © reproduced with permission of John Wiley & Sons, Inc.).

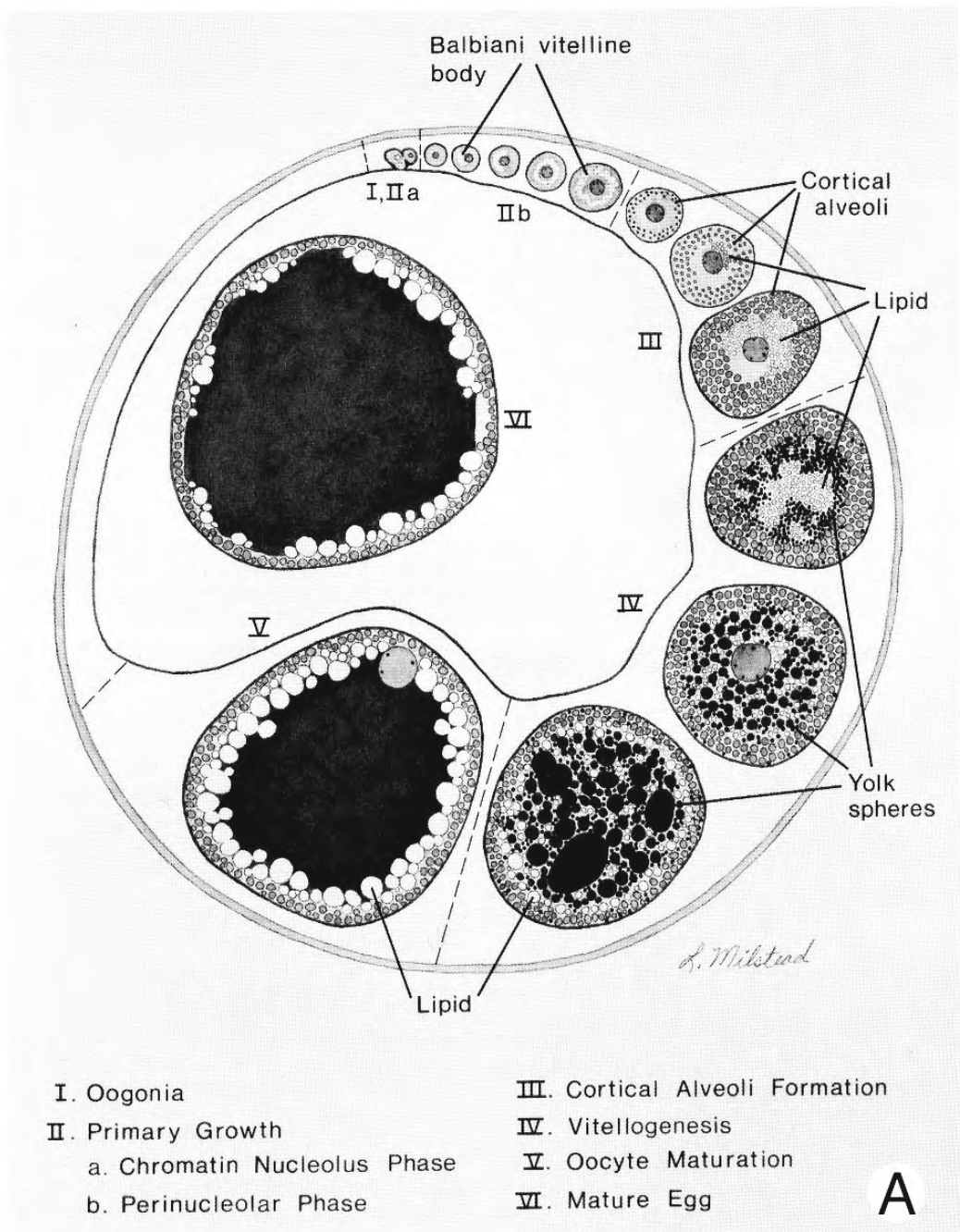

Figure 1.40: In contrast to the random organization of ovaries of other fish, the temporal and spatial correlation of oocyte development, as seen in syngnathids, facilitates the study of specific events in follicular development. These sequences may be seen in any cross section of the ovaries. (Figures **A**, **B**, and **C** © reproduced with permission of John Wiley & Sons, Inc.).

A. Schematic diagram indicating the sequential stages of oocyte development in an optimal section of the ovary of the pipefish *Sygnathus scovelli.* Stage designations are indicated by Roman numerals. (From Begovac and Wallace, 1988).

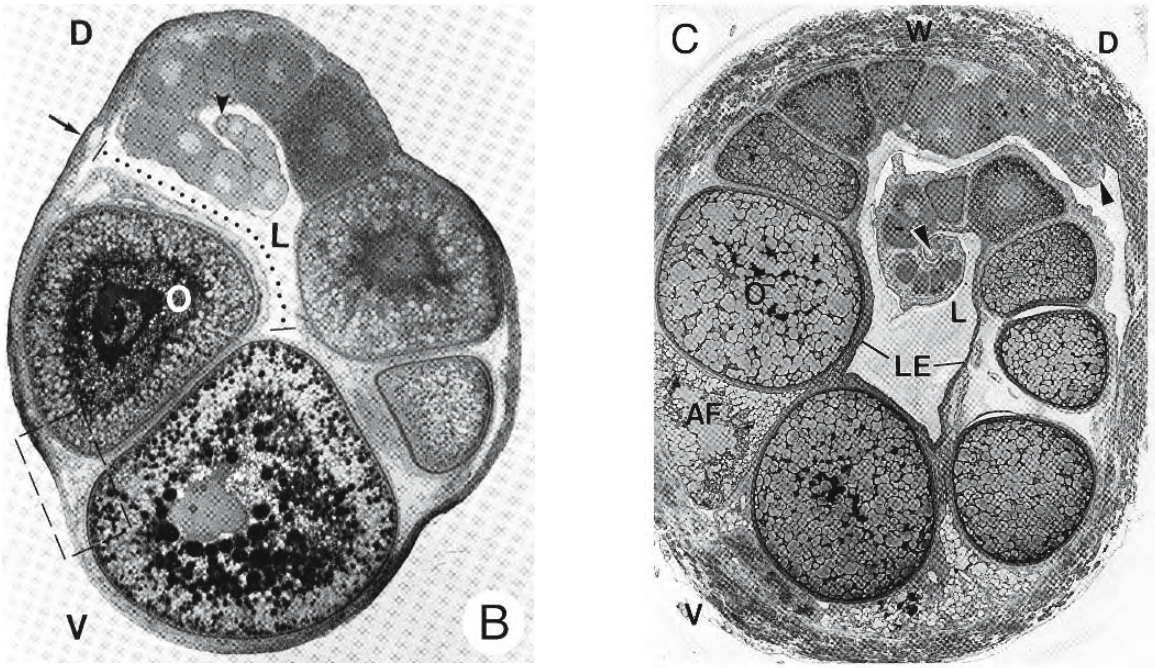

Figure 1.40: Continued.

B. Photomicrograph of a cross section of the ovary of the pipefish. A sequential spiral of developing oocytes is seen, from the earliest stage in the germinal ridge (arrowhead) to the mature edge with the largest oocyte (O) at the dotted line. D, dorsal, L, ovarian lumen; V, ventral. X 100 (From Begovac and Wallace, 1987).

C. Photomicrograph of a cross section through the ovary of the seahorse *Hippocampus erectus.* The follicular lamina has two germinal ridges (arrowheads) from which developing follicles migrate ventrally. D, dorsal; L, lumen; LE, luminal epithelium; O, oocyte in developing follicle; V, ventral; W, muscular wall of the ovary. X 81. (From Selman, Wallace and Player, 1991).

⟶

Figure 1.41: Syngnathid ovaries are covered on the outside by visceral mesothelium of squamous to low cuboidal cells that is continuous with the mesovarium. It is subtended by variable amounts of collagenous connective tissue connecting it to several layers of smooth muscle. (Figures **A**, **B**, and **C** © reproduced with permission of John Wiley & Sons, Inc.).

A. Seahorse, *Hippocampus erectus.* Electron micrograph of a section through a typical mesothelial cell showing its irregular apical surface as well as numerous pits and vesicles (arrowheads) on both their apical and basal surfaces. These cells contain abundant cytoplasmic filaments (arrow). X 20,390 (From Selman, Wallace, and Player, 1991).

B. Seahorse, *Hippocampus erectus.* Photomicrograph of a section through the junction of the mesovarium (M) with the ovarian wall (W). The ovary is covered by visceral peritoneum (arrowheads) which is continuous with the epithelium of

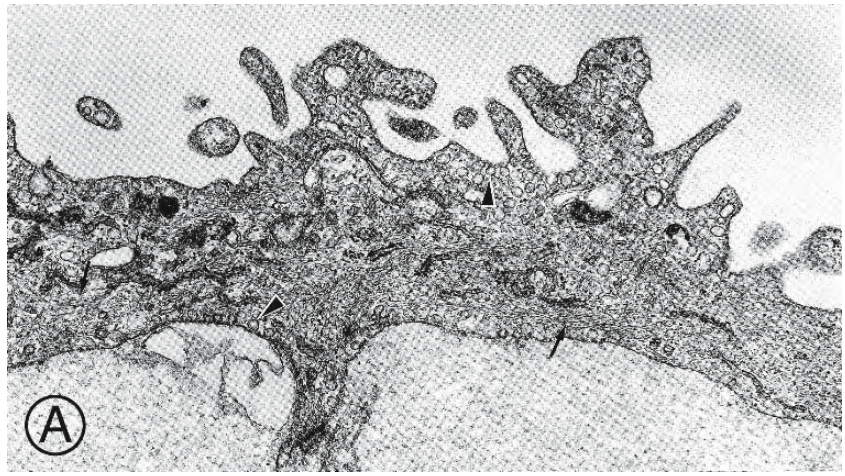

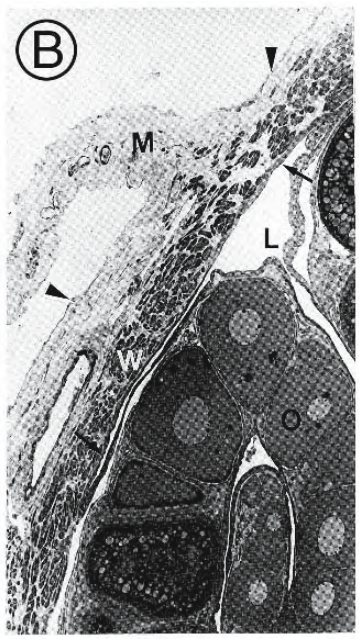

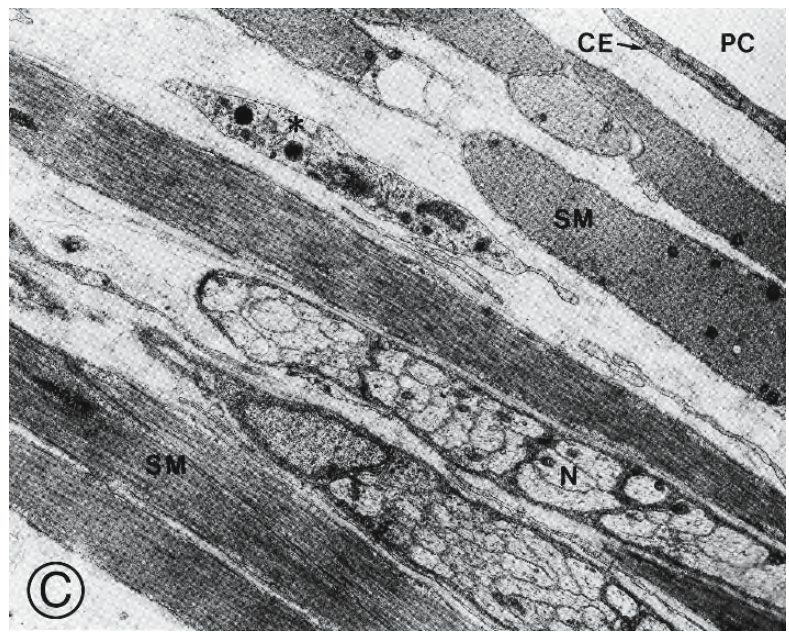

the mesovarium. Blood vessels are abundant within the mesovarium and within the outer layers of the ovarian wall. L, ovarian lumen; O, oocyte. X 140 (From Selman, Wallace, and Player, 1991).

C. Electron micrograph of a section through the ovarian wall of the pipefish, *Syngnathus scovelli.* The simple squamous coelomic epithelium (CE) of the outer ovarian wall faces the peritoneal cavity (PC). It overlies several layers of smooth muscle (SM) which comprise most of the thickness of the ovarian wall; the fibres are arranged roughly into two layers: an inner circular and an outer longitudinal. Small blood vessels course between the muscle cells as well as bundles of unmyelinated nerves (N) that tend to run parallel to the long axis of the ovary. Vascular connective tissue of variable thickness occurs within the wall; a connective tissue cell is shown (*). X 7,980 (From Begovac and Wallace, 1987).

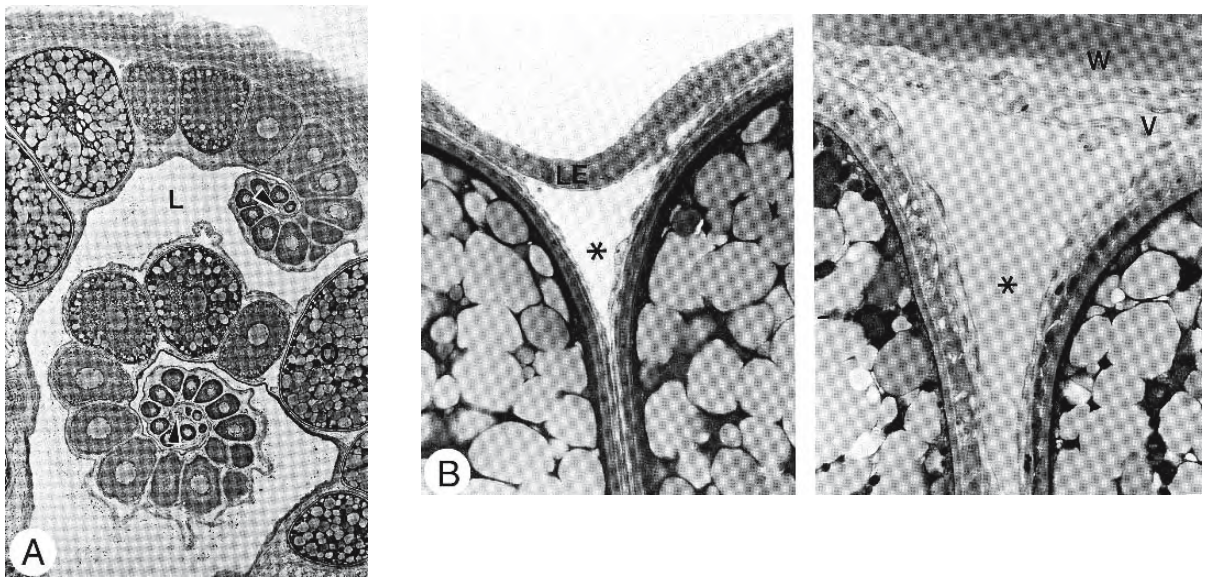

Figure 1.42: The germinal ridges extend the length of the syngnathid ovary and contain the proliferative stem cells from which the oocytes are derived and follicles formed. Photomicrographs of sections through the ovary of the seahorse *Hippocampus erectus.* (From Selman, Wallace, and Player, 1991; © reproduced with permission of John Wiley & Sons, Inc.).

A. Two germinal ridges (arrowheads) project into the ovarian lumen (L). The ridges are covered by the luminal epithelium of squamous to cuboidal cells and contain richly vascular connective tissue surrounding each follicle. The germinal ridges and the follicles arising from each form scrolls that twist in opposite directions. O, oocyte. X 75.

B. Extensive lymphatic spaces (*), lined by attenuated endothelial cells, penetrate the stroma of the ovary. **Left**: a lymphatic vessel lying between adjacent follicles and the overlying luminal epithelium (LE). **Right**: a lymphatic vessel occupies much of the space between adjacent follicles and the ovarian wall (W). V, small vein. X 565.

Figure 1.43: As in many bony fishes, the lumen of the cystovarian ovaries of syngnathids is lined by an epithelium that is derived from the coelomic mesothelium and is continuous with the oviduct. The epithelial cells lie on a distinct basal lamina and vary in shape from squamous over the germinal ridge to cuboidal or columnar over more mature follicles. These electron micrographs show the luminal epithelium from three regions of the ovary of the seahorse *Hippocampus erectus*. Single arrows indicate tight junctions, double arrows, desmosomes. (From Selman, Wallace, and Player, 1991; © reproduced with permission of John Wiley & Sons, Inc.).

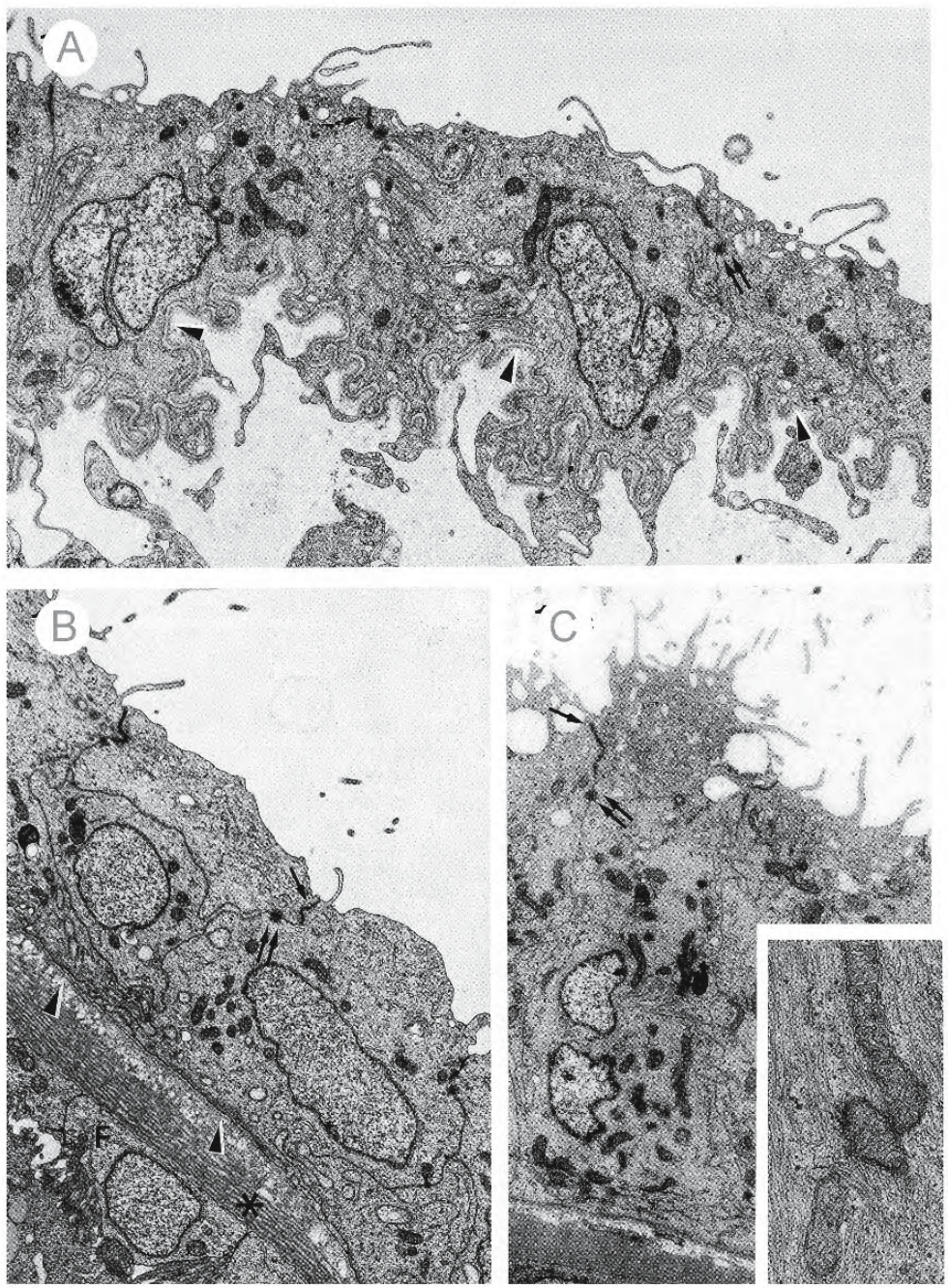

A. Luminal epithelial cells over the germinal ridge are relatively flat and are highly interdigitated on their lateral surfaces. The basal plasmalemma is elaborately infolded. Arrowheads indicate the distinct basal lamina. X 8,170.

B. Cuboidal luminal epithelial cells overlie small follicles. The basal lamina (arrowheads) of the luminal epithelial cells lies next to the thick basal lamina (*) of follicular cells (F) from the underlying follicle. X 7,520.

C. Columnar epithelial cells overlying large follicles display long microvilli, interdigitating lateral membranes, and numerous cytoplasmic filaments. X 6,720. Detail of the cytoplasmic filaments is shown in the inset. X 23,800.

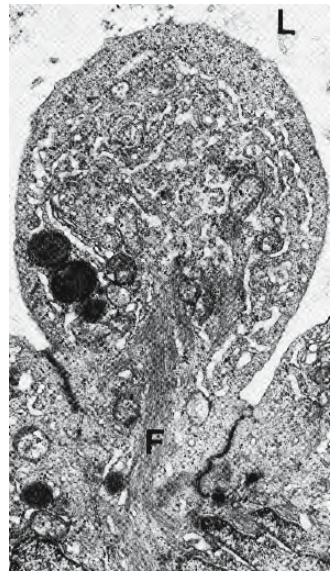

Figure 1.44: Electron micrograph of a luminal epithelial cell from the ovary of the pipefish *Syngnathus scovelli* showing blebbing into the ovarian lumen (L). These cells are highly secretory. Intracellular filaments (F) are abundant. Well developed tight junctions are seen on each side of the bleb. X 9,760 (From Begovac and Wallace, 1987; © reproduced with permission of John Wiley & Sons, Inc.).

——→

Figure 1.45: A form of apocrine secretion has been described in the columnar epithelial cells of the ovarian lumen of teleosts.

A. Electron micrograph of the ovarian wall of the medaka *Oryzias latipes* following ovulation. Apical "blebs" break off from the rest of the cell and contribute to the secreted material in the lumen. X 3,700 (From Takano, 1968; reproduced with permission of the Graduate School of Fisheries Sciences, Hokkaido University).

Abbreviations: L, ovarian lumen; LS, liquid within intercellular spaces; N, nucleus; SM, smooth muscle of subepithelial layer.

B. Electron micrograph of the maturing ovary of the goldfish *Carassius auratus*. The columnar epithelial cells lining the lumen (OL) develop cilia (Ci); large cytoplasmic blebs (Ap) break away from the surface at the bases of the cilia. X 5,700 (From Takahashi and Takano, 1971; reproduced with permission from the Zoological Society of Japan).

Abbreviations: M, mitochondrion; N, nucleus.

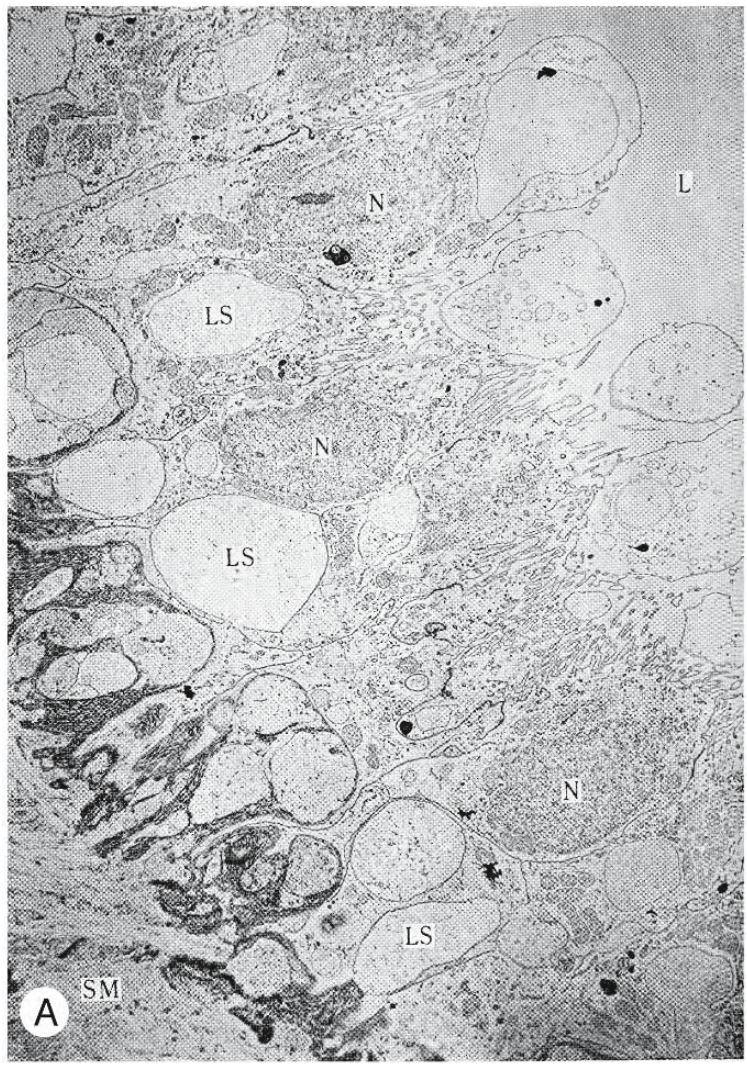

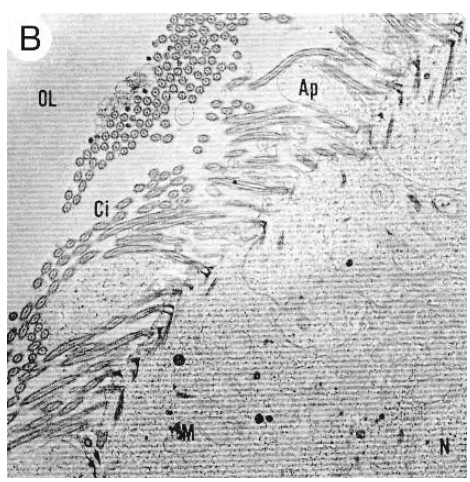

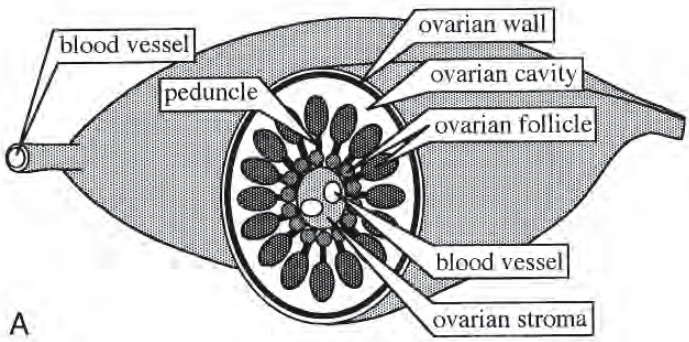

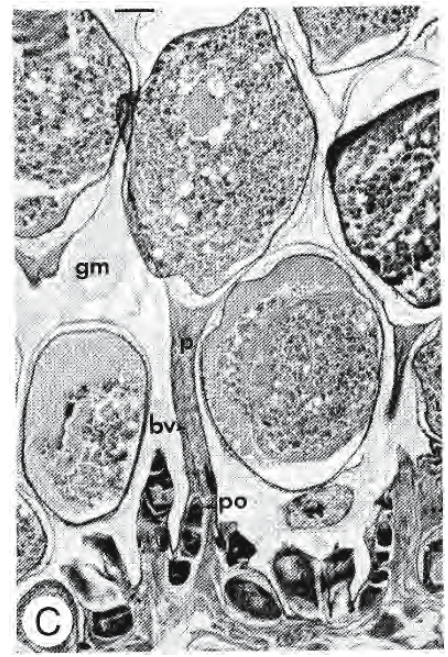

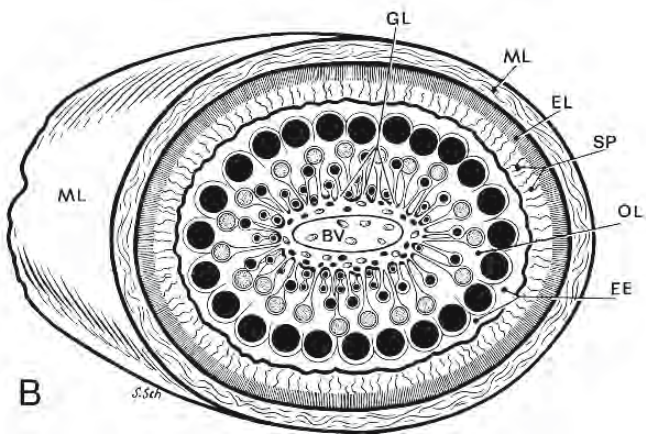

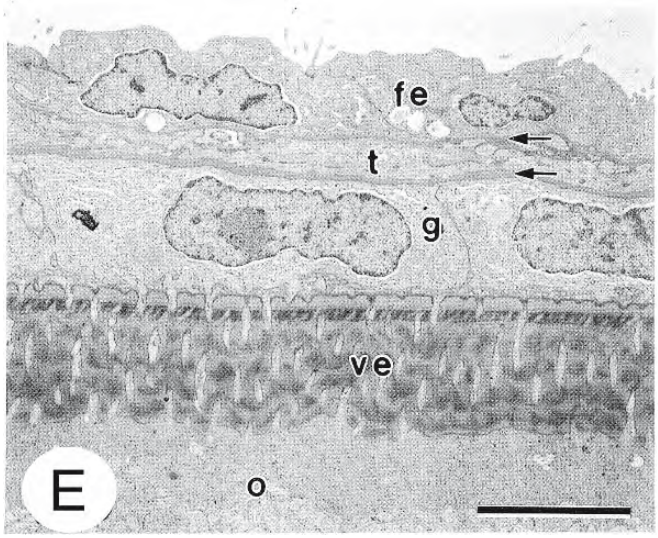

←

Figure 1.46: The lining of the hollow ovary in some species of Scorpaeniformes secretes a bilobed, gelatinous mass that provides protection for the eggs. The paired cystovarian ovaries are sheathed within a wall of smooth muscle and connective tissue and are enclosed by visceral peritoneum. Anteriorly the ovaries are rounded and each of them is suspended by a spongy, vessel-rich hilus whose vessels penetrate into the lumen to enter the spongy, vascular, ovigerous stroma. Suspended by the hilus at the anterior end of each lobe, the ovigerous stroma floats free within the lumen.

A. Schematic diagram of the ovary of the rockfish *Sebastolobus macrochir*. (From Koya and Matsubara, 1995; reproduced with permission of the Graduate School of Fisheries Sciences, Hokkaido University).

B. Diagram of a cross section of the ovary of *Dendrochirus brachypterus* during reproduction. The ovigerous tissue is covered by an oocyte-producing epithelium that bristles with vascularized "peduncles" that radiate from the stroma;. These peduncles are extensions of the stroma and accommodate secondary oocyte development. (From Fishelson, 1977; reproduced with permission of the author).

Abbreviations: BV, blood vessel; EE, egg envelope; EL, epithelial layer; GL, germinative layer; ML, muscle layer; OL, ovarian lumen; SP, secretory processes.

C. Photomicrograph of oocyte and peduncle from the ovary of *Sebastolobus alascanus* collected during an early phase of production of gelatinous material. Scale bar = 104 μm. (From Erickson and Pikitch, 1993; reproduced with kind permission of Kluwer Academic Publishers).

Abbreviations: bv, blood vessel; gm, gelatinous material; po, previtellogenic oocyte.

D. Photomicrograph of an ovarian follicle of S*ebastolobus macrochir* in maturation phase. It projects by a narrow peduncle (p) from the ovarian stroma (s). o, oocyte. Scale bar = 100 μm. (From Koya and Matsubara, 1995; reproduced with permission of the Graduate School of Fisheries Sciences, Hokkaido University).

E. Electron micrograph of a portion of an ovarian follicle of *Sebastolobus macrochir* in maturation phase. The oocyte (o) is enclosed by the amorphous zona pellucida (ve), a layer of follicular cells (g), theca (t), and the simple squamous luminal epithelium (fe). Scale bar = 5 μm. (From Koya and Matsubara, 1995; reproduced with permission of the Graduate School of Fisheries Sciences, Hokkaido University).

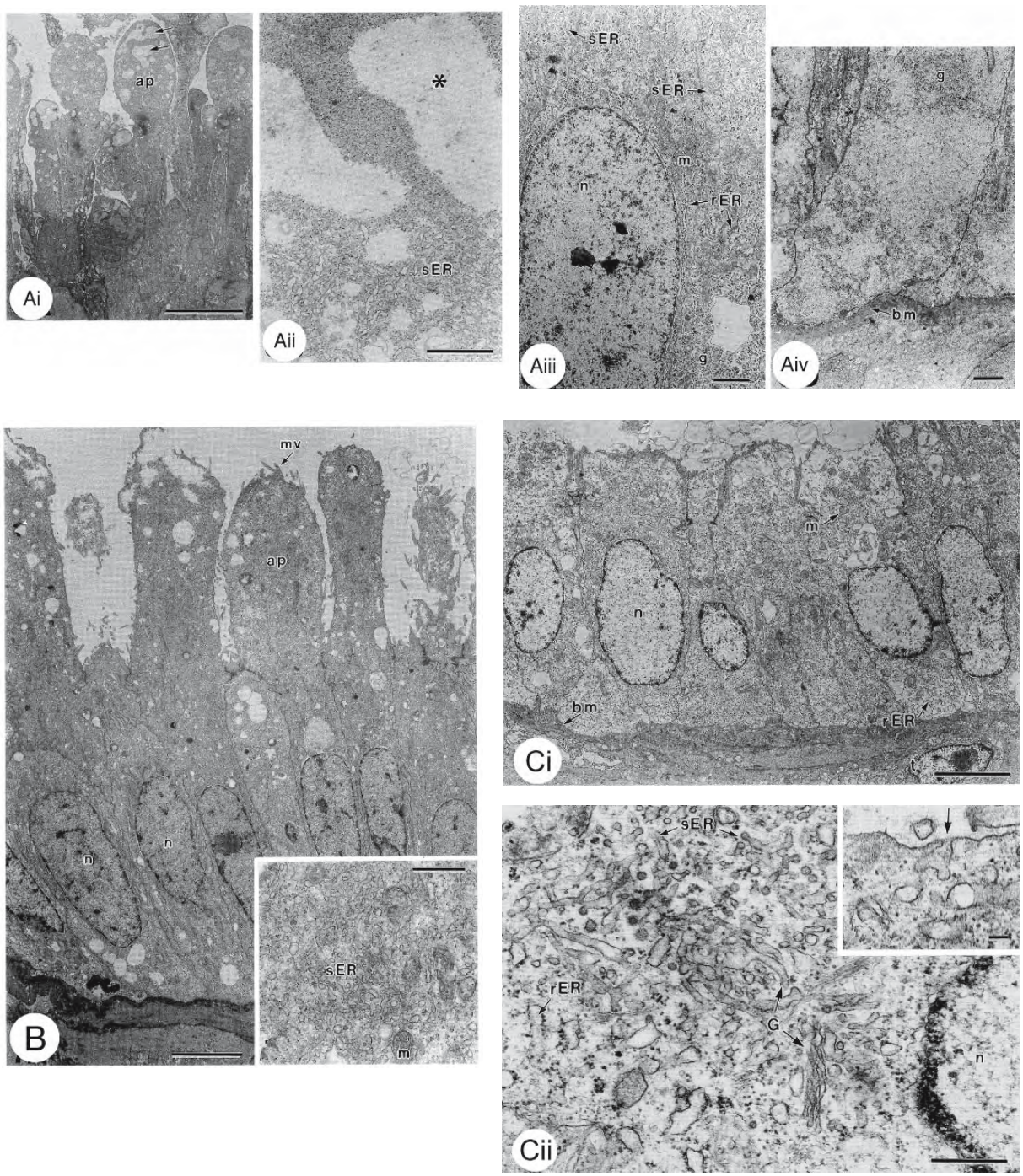

Figure 1.47: Electron micrographs of the epithelia of the ovary of the rockfish *Sebastolobus macrochir*. The luminal wall is lined by a simple columnar epithelium (**A,B**) while a more delicate simple columnar epithelium covers the ovigerous tissue (**C**). (From Koya and Matsubara, 1995; reproduced with permission of the Graduate School of Fisheries Sciences, Hokkaido University).

A. Before ovulation, there is a buildup of the cellular mechanism for protein production in the epithelial cells lining the ovarian wall. These cells produce the outer fibrous layer of the gelatinous mass.

Figure 1.47: Continued.

i: Each epithelial cell bears a large apical projection containing masses of electron-lucent material in the cytoplasm (ap). Bar = 10 μm.

ii: These electron-lucent masses (*) are surrounded by well-developed agranular endoplasmic reticulum (sER). Bar = 1 μm.

iii: The central part of an epithelial cell contains abundant agranular endoplasmic reticulum (sER) and sparse granular endoplasmic reticulum (rER). g, glycogen; m, mitochondria; n, nucleus. Bar = 1 μm.

iv: Numerous glycogen granules (g) are seen in the cytoplasm of the basal part of an epithelial cell. bm, basal lamina. Bar = 1 μm.

B. The apical projections (ap) of the epithelial cells of the luminal wall have decreased in height after the first ovulation. mv, microvilli; n, nucleus. Bar = 5 μm. Inset: the apical cytoplasm contains well-developed agranular endoplasmic reticulum (sER). m, mitochondrion. Bar = 1 μm.

C. The more delicate columnar epithelial cells of the ovigeorous lamella secrete the homogeneous inner layer of the gelatinous mass.

i: These cells lie on a basement lamina (bm) that separates them from the cells of the theca (t). m, mitochondria; n, nucleus; rER, granular endoplasmic reticulum. Bar = 5 μm.

ii: The perinuclear cytoplasm shows well developed agranular endoplasmic reticulum (sER), granular endoplasmic reticulum (rER), and a Golgi complex (G). n, nucleus. Bar = 0.1 μm.

Inset: The apical cytoplasm showing an exocytotic pit (arrow). Bar = 0.1 μm.

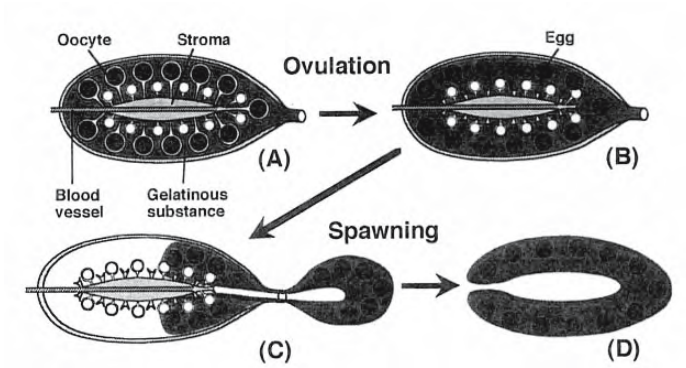

Figure 1.48: Schematic diagram of the formation of gelatinous egg masses in the rockfsh *Sebastolobus macrochir.* (From Koya, Hamatsu, and Matsubara, 1995; reproduced with permission from Blackwell Publishing Asia Pty. Ltd.).

A. Anteriorly the ovaries are rounded and each of them is suspended by a spongy, vessel-rich hilus whose vessels penetrate into the lumen to enter the spongy, vascular, ovigerous stroma which floats free within the lumen. The ovigerous tissue is covered by an oocyte-producing epithelium that bristles with vascularized "peduncles" that radiate from the stroma and bear developing oocytes. During the spawning season, epithelia lining he luminal wall and covering the ovigerous tissue secrete a gelatinous mass that fills the lumen and embeds the oocytes and their stalks. Peduncle length increases as vitellogenesis proceeds.

B. Within the base of each peduncle are previtellogenic oocytes; when a mature oocyte is released at ovulation, a previtellogenic oocyte moves up inside the peduncle to take its place and undergo vitellogenesis.

C. During spawning, the oocytes, embedded in the gelatinous mass, are swept from the lumen. The gelatinous mass, secreted by the epithelia of the two lobes, is extruded around the ovigerous tissue of both lobes.

D. The hollow, bilobed egg mass is extruded.

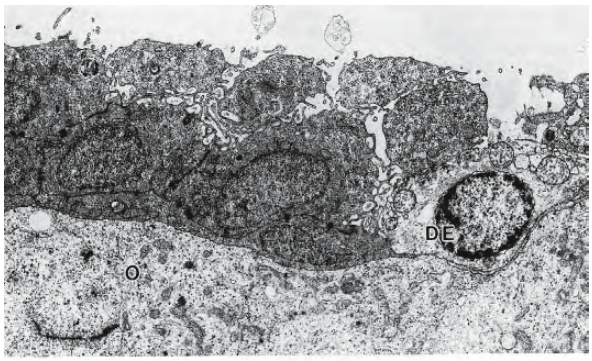

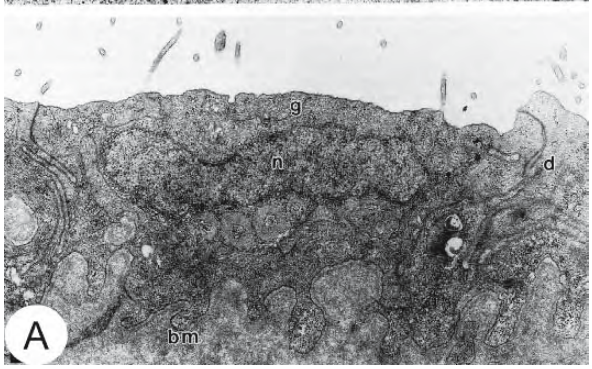

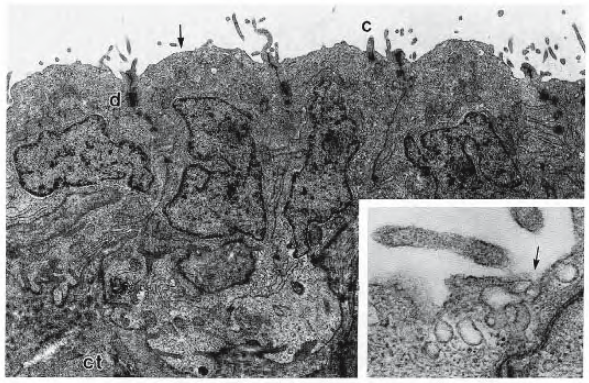

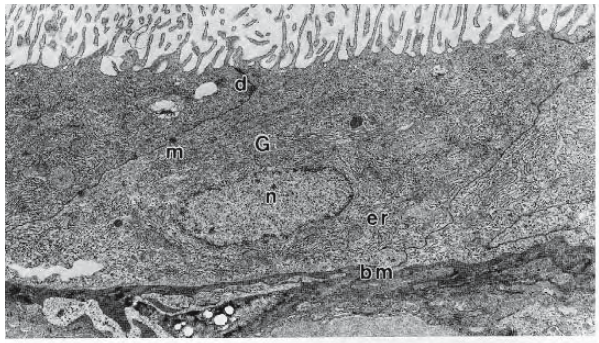

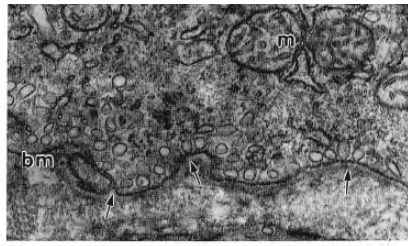

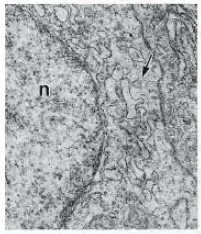

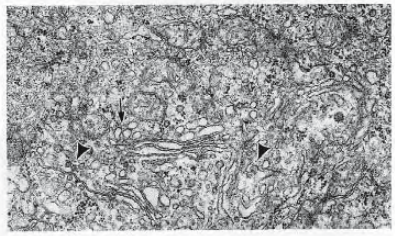

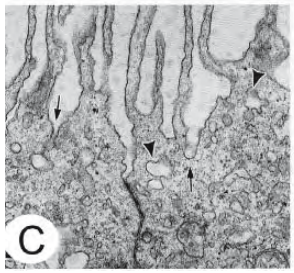

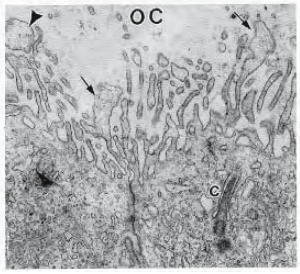

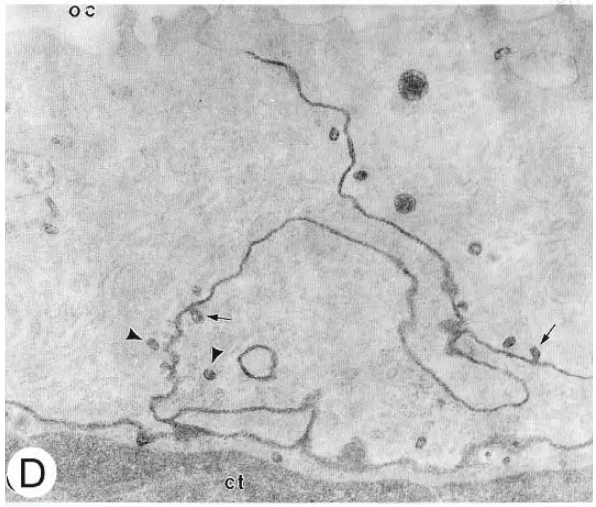

Figure 1.49: Several marine cottid species (Scorpaeniformes) have a unique reproductive mode called "internal gametic association" where spermatozoa are introduced into the ovarian cavity by copulation and float freely in the ovarian fluid although fertilization does not occur until the eggs have been spawned into sea water. These electron micrographs are from the ovary of the marine sculpin *Alcichthys alcicornis.* (From Koya, Takano, and Takahashi, 1995; Koya, Munehara, and Takano, 1997; © reproduced with permission of John Wiley & Sons, Inc.).

A. The epithelium of the ovigerous lamella during the recovery period following spawning.

Upper. The epithelium is stratified during early recovery. X 6,300.

Lower. Later during the recovery period, a simple layer of epithelial cells is arranged on the basal lamina (bm). X 16,000.

B. The epithelium of the ovarian wall early in the recovery period is ciliated (c).

Upper. The epithelium is simple during early recovery. There are few short apical microvilli. The arrow indicates small apical pits on the epithelial cells. X 6,300.

Inset. These pits are shown in greater detail. The vesicles appear to be discharging their contents into the ovarian lumen. X 50,700.

Lower. Microvilli are well developed on the apical surface of the epithelial cells later in the recovery period. The cytoplasm is packed with well-developed granular endoplasmic reticulum (er). X 7,800.

C. Epithelium from the ovigerous lamella during the spawning period. The epithelial cells manifest the appearance of protein production with abundant basal granular endoplasmic reticulum and active apical Golgi complexes. Numerous pinocytotic pits and vesicles are seen in the peripheral cytoplasm of these cells; increasing numbers of pits and vesicles are also present in the endothelial cells of adjacent capillary walls at this time indicating that active transcytosis is taking place.

Upper. Abundant microvilli extend from the apical surface. Granular endoplasmic reticulum (er) and Golgi complexes (G) are well developed. Note the apical desmosomes between adjacent epithelial cells. X 5,800.

Mid left: Granular endoplasmic reticulum near the nucleus (n) appears to be forming a bud-like extension (arrow). X 13,600.

Mid right: Well developed Golgi complex in the apical cytoplasm. Electron-lucent vesicles (arrow) and slightly electron-dense vesicles (arrowheads) lie near the Golgi lamellae. X 22,200.

Lower left: Vesicles in the apical cytoplasm appear to fuse to form secretory vesicles (arrowheads). The contents of these vesicles are released by exocytosis (arrows). X 18,300.

Lower right: Blebbing of the tips of microvilli (arrow). Some vesicular bodies (arrowhead) lie free in the ovarian lumen (OC). X 11,000.

D. Epithelium from the ovigerous lamella during the spawning period.

Upper left: A pinocytotic pit opens into the intercellular space. X 27,300.

Upper right: Numerous pinocytotic pits (arrows) and vesicles are seen in the basal cytoplasm. X 26,000.

Lower: A strong reaction is seen in the connective tissue (ct) and basal intercellular spaces of fish treated with horseradish peroxidase. Reaction products are also observed in the pits (arrows) and vesicles (arrowheads) near the outer surfaces of the cells. X 24,800.

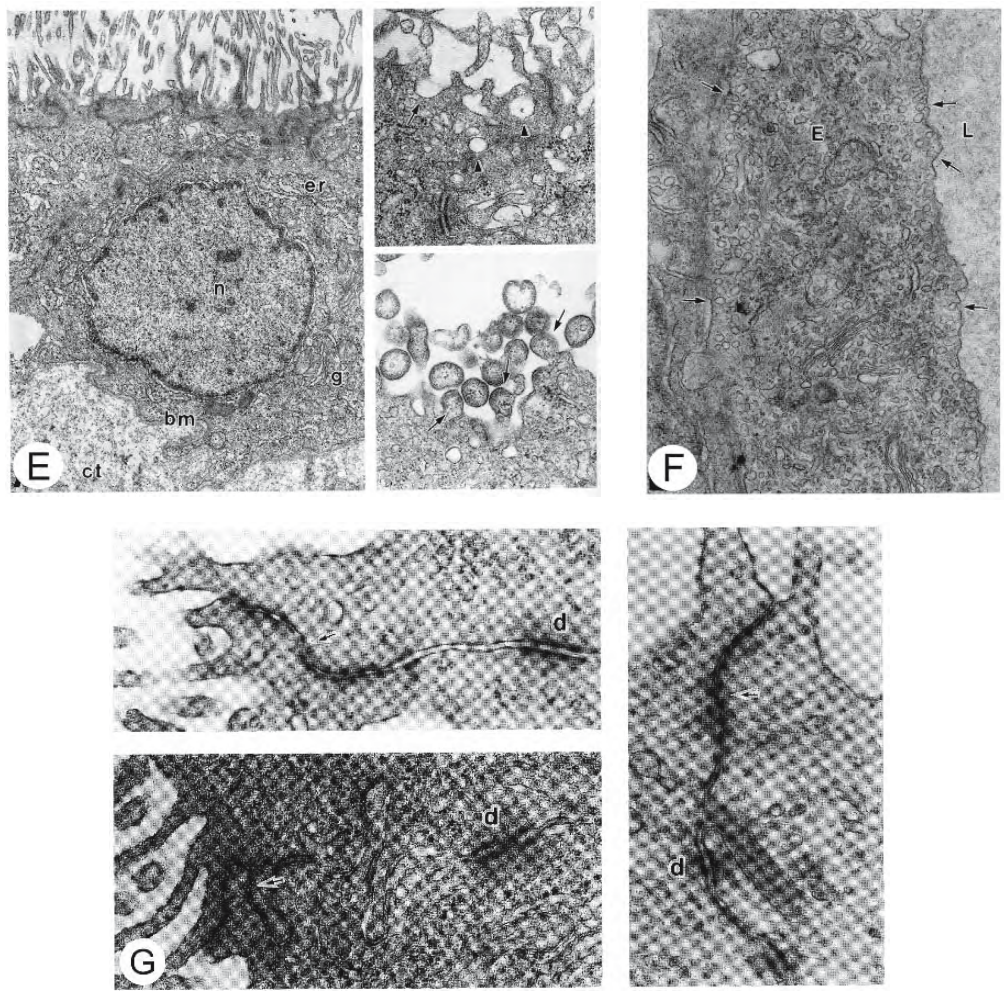

Figure 1.49: Continued.

E. Epithelium from the ovarian wall during spawning.

Left: Numerous microvilli bristle from the apical surface of the epithelial cells; the cytoplasm contains well developed granular endoplasmic reticulum (er) and Golgi complexes (g). X 11,400.

Upper right: The apical surface of the epithelial cells is riddled with exocytotic pits (arrow) and vesicles (arrowheads). X 26,700.

Lower right: Apical blebs (arrows) separate from the surface of the epithelial cells to form a microapocrine secretion. X28,900.

F. During spawning, numerous vesicles pack the cytoplasm of endothelial cells (E) from the capillaries of the ovigerous lamellae. Pits open on both the apical and basal surfaces of the endothelial cells (arrows). The capillary lumen (L) is at the left. X 20,000.

G. Adjacent epithelial cells are joined by junctional complexes and it is suggested that these tight junctions isolate the spermatozoa in the lumen from the maternal immune system.

Upper left; right: The apical borders of epithelial cells of an ovigerous lamella are joined by a junctional complex (arrow) and desmosome (d). X 40,000.

Lower left: Junctional complex (arrow) and desmosome (d) securing the apical borders of epithelial cells from the ovarian wall. X 40,000.

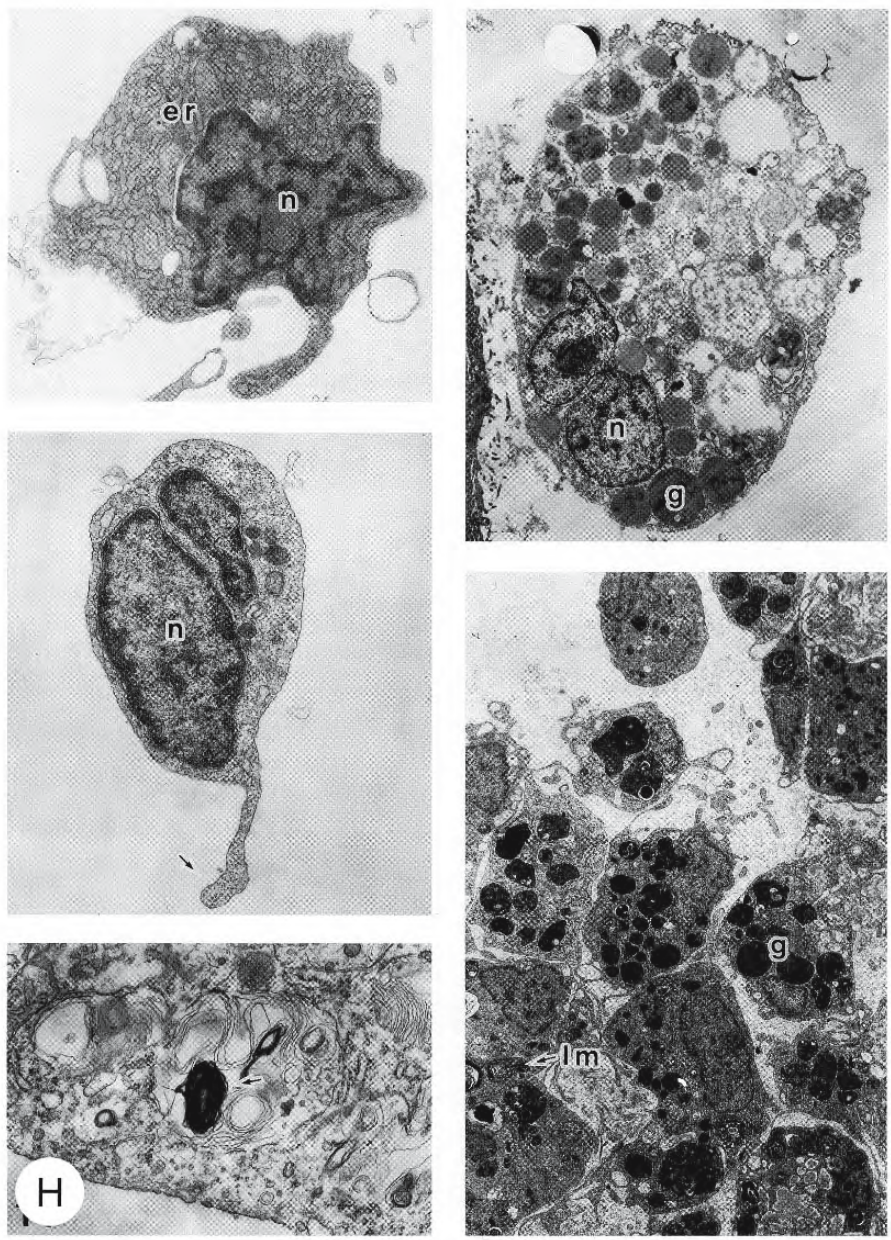

Figure 1.49: Continued.

H. After the spawning period, the junctions break down and residual spermatozoa are eliminated by invading maternal leucocytes.

Upper left: Plasma cell showing characteristic well-developed granular endoplasmic reticulum (er). X 10,000.

Upper right: Polymorphonuclear leucocyte showing lobed nucleus and electron-dense cytoplasmic granules. X 5,000.

Mid left: Monocyte, with few cytoplasmic organelles. The arrow indicates a cytoplasmic extension. X 12,000.

Lower left: The cytoplasm of a macrophage gives evidence of clean-up of cellular breakdown: membranous whorls, multilamellar bodies (arrow), and a heterogeneous collection of vesicles. X 20,000.

Lower right: Masses of macrophages containing lamellar bodies (lm) and electron-dense granules (g) appear during the recovery period. X 3,000.

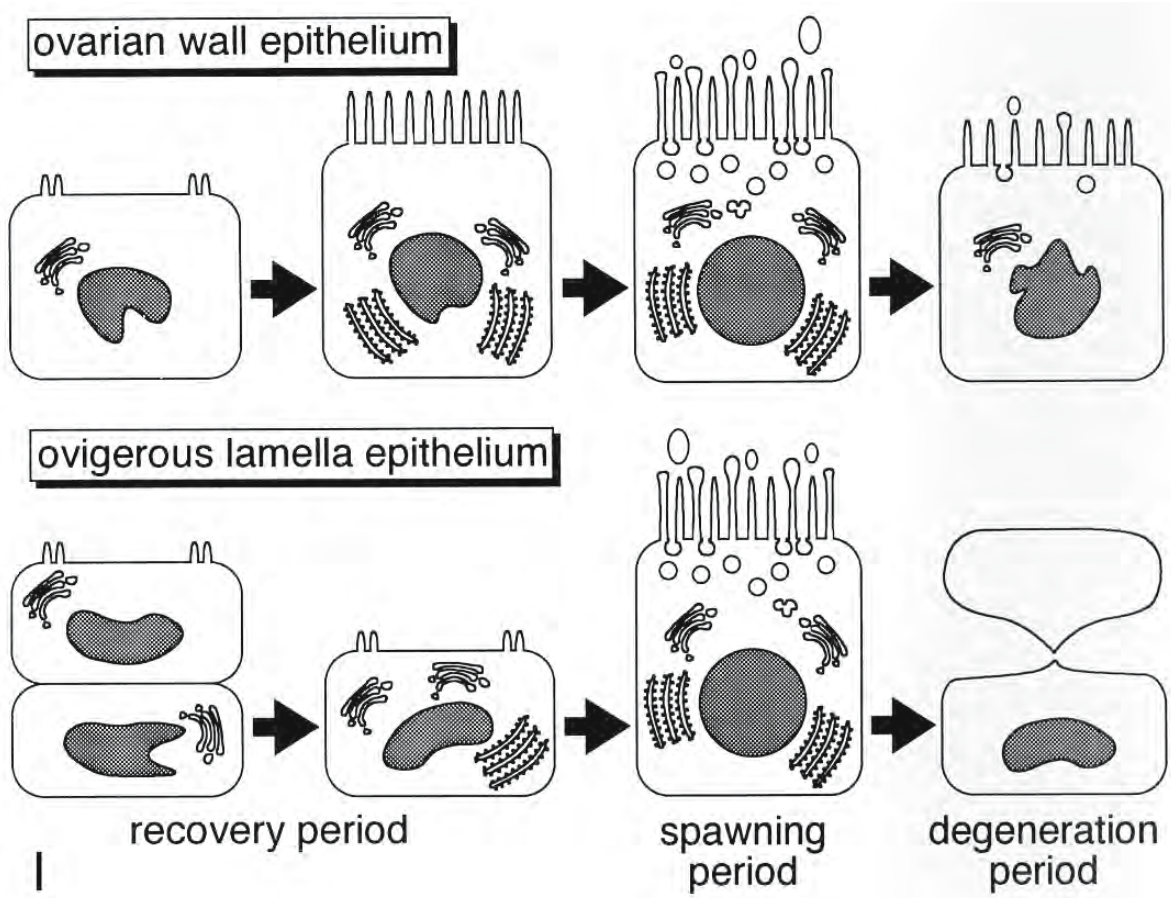

Figure 1.49: Continued.

I. This diagram summarizes the changes that take place during the reproductive cycle of the sculpin *Alcichthys alcicornis*. *Abbreviations*: bm, basal lamina; c, cilium; ct, connective tissue; d, desmosome; DE, degenerating epithelial cell; G,g, Golgi complex; lm, lamellar bodies; n, nucleus; O, oogonium; OC, ovarian cavity.

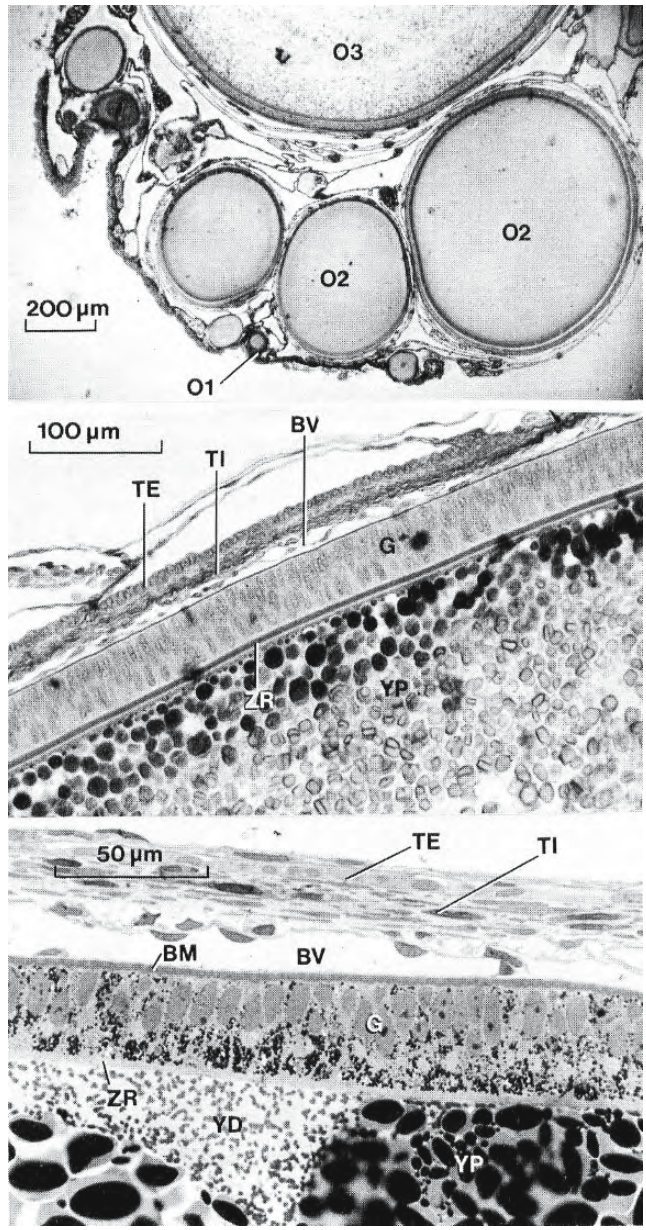

Figure 1.50: Photomicrographs of cross sections of the ovary of *Scyliorhinus canicula.* The ovaries of Chondrichthyes are surrounded by the gonadal epithelium and consist of a connective tissue stroma containing developing follicles, postovulatory follicles (corpora lutea), and degenerating follicles (corpora atretica). Blood vessels and nerves course through the stroma. The stroma also contains lymph spaces or membranous folds that are filled with developing blood cells. (From Dodd and Sumpter, 1984; reproduced with permission of Churchill Livingstone)).

Upper: Oocytes in three stages of development: O1, prior to follicle formation; O2, previtellogenic follicle; and O3, a follicle in early vitellogenesis.

Middle: Cross section of early vitellogenic follicle.

Lower: Cross section of a follicle during early atresia. Dissolution of yolk occurs in patches (YD).

Abbreviations: BM, basement membrane; BV, blood vessel between theca interna and follicular basement membrane; G, follicular epithelium; TE, theca externa; TI, theca interna; YP, yolk platelets; ZR, zona pellucida.

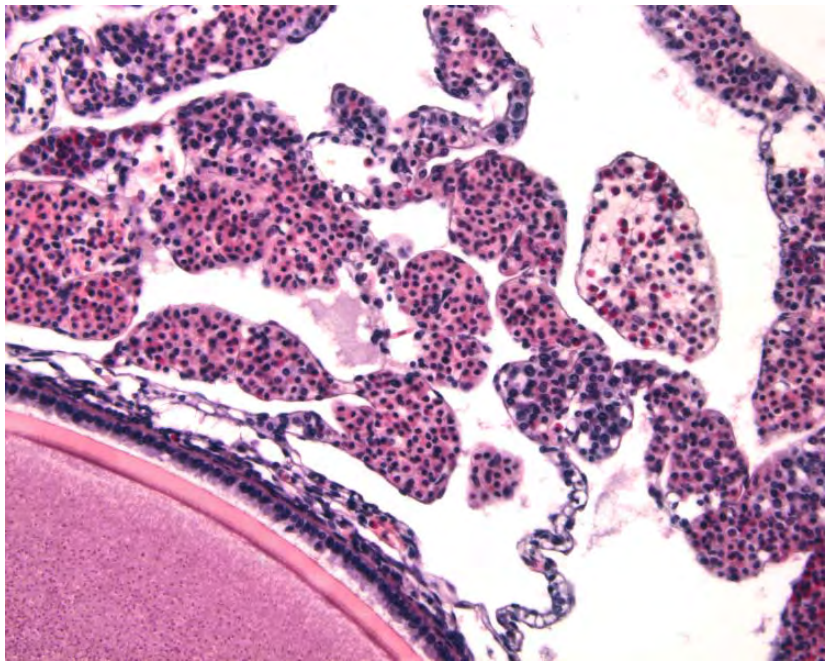

Figure 1.51: Photomicrograph of the spent ovary of the dogfish shark *Squalus acanthias*. An unovulated follicle is seen at the lower left. Abundant haemopoietic activity in seen in the loose connective tissue of the stroma. X 50.

Figure 1.52: General view of the reproductive tract of the basking shark *Cetorhinus maximus*. *Left*: from the ventral surface; the oviduct on the right is opened longitudinally. *Right*: lateral view from the right side. Only the right ovary persists and the epigonal organ lies posterior and slightly dorsal to the ovary, being suspended from the dorsal abdominal wall by a backward extension of the mesovarium. The left epigonal organ is of similar size and shape as the right but no ovary is fused to its anterior end and it is suspended by its own peritoneal fold in the corresponding position on the left side of the body cavity. (From Matthews, 1950; reproduced with permission from the Royal Society).
Abbreviations: AP, abdominal pores; Cl, cloaca; E, epigonal organ; IN, unpaired oviduct; IS, isthmus; K, kidney; MM, mesometrium; O, ovary; OA, ostium; OD, paired oviduct; OE, oesophagus; PO, pocket in right side of ovary; R, rectum; SG, oviductal gland; U, uterus; UP, urinary papilla; UR, uterus lined with folds; UT, uterus lined with trophonemata; VC, common vagina; VP, paired vagina of the left side.

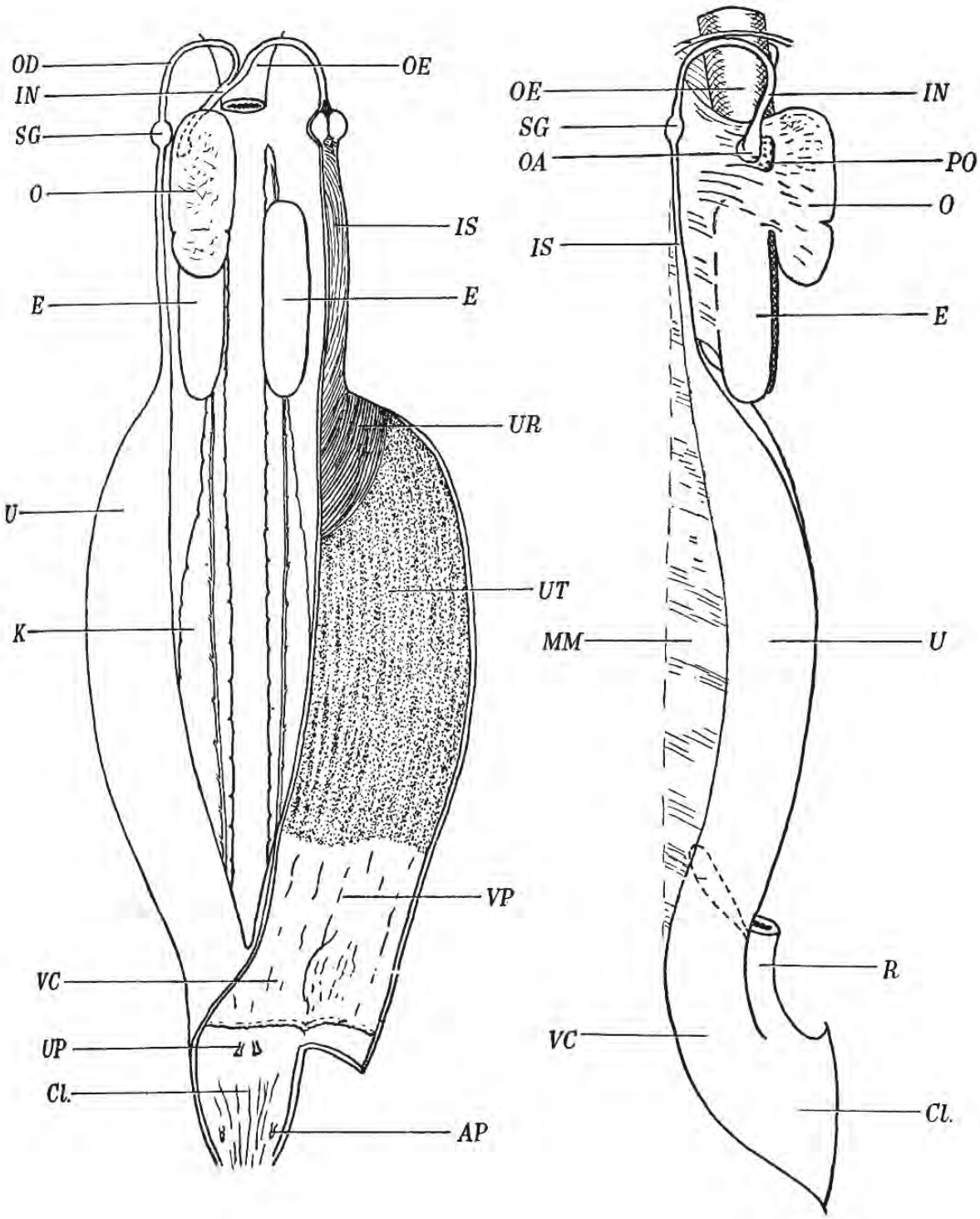

CHAPTER 2

OVARIAN FOLLICLES

2.1 Introduction

Oogonia proliferate by mitosis to become PRIMARY OOCYTES. In these cells the chromosomes are arrested in the diplotene stage of the first meiotic prophase. The oocytes then enter a period of growth that varies from species to species, enlarging chiefly by accumulating yolk. As they grow and mature, various intracellular and extracellular changes occur. Initially the follicular cells form a simple squamous epithelium around each oocyte but, as development proceeds, the cells enlarge and may become cuboidal and even columnar. In cyclostomes and teleosts the FOLLICULAR EPITHELIUM remains single layered but, in Chondrichthyes, it may be composed of several layers (Franchi, 1962). As is typical of many epithelia, desmosomes connect adjacent follicular cells. Follicular cells may also produce ovarian hormones. The follicular epithelium is surrounded by its own basal lamina which separates it from a sheath of condensed vascular connective tissue, the THECA FOLLICULI. As the follicle differentiates, the theca becomes more distinct and may be divided into a THECA INTERNA and THECA EXTERNA. The theca contains fibroblasts, collagenous fibres and capillaries and, in some species, special thecal steroid-producing cells (Figure 2.1).

During development, a thick, translucent, acellular ZONA PELLUCIDA, or VITELLINE ENVELOPE, develops between the oocyte and follicular cells. After hatching, when a simple plasma membrane would be inadequate for such a large cell to withstand the rigours of independent existence, this sheath serves as a tough enclosure for the egg. Even in viviparous forms, where the embryos develop within the body of the female, this envelope is formed during oogenesis (Flegler, 1977). During growth of the oocyte, the zona pellucida becomes perforated by PORE CANALS, enabling an exchange of materials between the oocyte and follicular cells; these channels contain microvilli that extend from the surfaces of both the oocyte and the follicular cells (Figure 2.2).

Polarity is laid down within the oocyte of the medaka *Oryzias latipes* during formation of the zona pellucida, before yolk production begins (Iwamatsu and Nakashima, 1996). This ANIMAL-VEGETAL AXIS consists of an ANIMAL POLE of the most active protoplasm that develops diametrically opposite a VEGETAL POLE of yolky, relatively inert protoplasm. It is suggested that this axis is established during development by reciprocal interactions of the oocyte with the adjacent follicular cells where a group of compactly clustered follicular cells determines the position of the vegetal pole area. A follicular cell at the opposite side of the oocyte differentiates into a MICROPYLAR CELL, thereby determining the position of the MICROPYLE (point of sperm entry) at the animal pole. Indeed, the micropyle is a convenient marker for identifying the animal pole.

In lampreys, possibly all elasmobranchs, and some bony fishes, oogonial proliferation is limited to the larval or embryonic period (Tokarz, 1978). Successive generations of oocytes appear to develop from oogonia in the germinal ridge of adult hagfish *Myxine glutinosa;* these oocytes enter a resting phase while they await ovulation of the previous generation of oocytes (Patzner, 1974). In most bony fishes, oogonial proliferation is found in the adult animal. There is a limited period of peak oogonial division in species with circumscribed annual breeding cycles; in species which do not have restricted breeding cycles, oogonial proliferation occurs either in waves or continuously throughout the year.

At the end of oogonial proliferation, the secondary oogonia become primary oocytes and enter a protracted early prophase. A primary oocyte is surrounded by a single layer of follicular cells to form a PRIMORDIAL FOLLICLE (Tokarz, 1978). This process is similar in all non-mammalian vertebrates and begins at approximately the same stage of meiotic prophase. A scheme of follicular development in the medaka *Oryzias latipes* is shown in Figure 2.3.

Because of the accessiblity of initial stages in the syngnathids — the pipefish and the seahorse — extensive descriptions of folliculogenesis have been carried out on these species, providing much of the information used here (Begovac and Wallace, 1987, 1988; Selman, Wallace, and Player, 1991). Their germinal ridge is well-defined and contains OOGONIA, EARLY PROPHASE I OOCYTES, and SOMATIC PREFOLLICULAR CELLS as well as occasional degenerating cells (Figure 2.4). Oogonia of the germinal ridge divide by mitosis. As the daughter cells move away they are enveloped by FOLLICULAR CELLS which are derived from the proliferation of prefollicular cells that extend processes between contiguous meiotic oocytes. This results in the isolation of the germ cells from other cells, thereby forming a FOLLICLE consisting of an oocyte surrounded by a follicular epithelium enclosed by its own basal lamina (Figure 2.5A). Prefollicular and follicular cells contain cytoplasmic filaments that distinguish them from early meiotic oocytes which contain no filaments. Newly formed follicles are surrounded by a thin THECA of connective tissue elements.

OOGONIA of the pipefish — the stem cells of the germ cell lineage — are oval to spherical cells, about 10 μm in diameter, which occur in the luminal epithelium, near the germinal ridge, and within the germinal ridge itself (Begovac and Wallace, 1988) (Figure 2.6). They are contiguous with other germ cells and somatic cells but are not in contact with the basal lamina of the luminal epithelium. They are the only germ cells within the germinal ridge that incorporate [^{3}H] thymidine, indicating that they are the only germ cells capable of nuclear division; somatic cells, including follicular cells and connective tissue cells incorporate the label as well. Oogonia have the largest nuclear/cytoplasmic ratio of any cells of the germ cell line. The oval nuclei contain one to three nucleoli. Dense-cored granules of unknown composition within the nucleus are specific to nuclei of the germ cell line and are also present in larger oocytes. Oogonial chromatin is more electron-dense than that of meiotic oocytes. Oogonial cytoplasm contains mitochondria, ribosomes, and scant endoplasmic reticulum but appears to lack a Golgi complex. Aggregates of NUAGE material are frequently associated with mitochondria; this is an electron-dense, membraneless organelle consisting of a spongelike aggregation of fine granular material. The function and composition of nuage are uncertain but its presence is a reliable marker of germ cells. Oogonia of the sea lamprey *Petromyzon marinus* appear to be similar to those of teleosts (Okkelberg, 1921; Lewis and McMillan, 1965).

2.2 Stages of Oocyte Development

The process of transformation of oogonia to oocytes is OOGENESIS (Selman and Wallace, 1989). It is generally accepted that the chromosomes become arrested at diplotene of the first meiotic prophase and the initial follicle is established (Wallace and Selman, 1981). It is unclear how oogonial daughter cells are transformed into prophase I meiotic oocytes and whether the oogonial division that produces the oocytes is symmetrical (Begovac and Wallace, 1988). Although it is difficult to distinguish the earliest meiotic oocytes from oogonia, some features are said to characterize newly formed oocytes in the sequentially arranged ovaries of syngnathids: an increase in size along with a decrease in nuclear/cytoplasmic ratio; loss of the perinuclear ring of mitochondria; proliferation of other organelles, especially Golgi complexes; and changes in nuclear morphology, especially condensation of chromatin (Begovac and Wallace, 1988; Selman, Wallace, and Player, 1991) (Figures 2.5B and 2.7A). The most obvious sign of transformation of oogonia to oocytes in the sea lamprey is the increase in the size of the nucleus and the appearance of a prominent nucleolus (Lewis and McMillan, 1965).

Cytoplasmic bridges have been described between oogonia and oocytes of some teleosts (Figure 2.8) (Bruslé and Bruslé, 1978; Grandi and Colombo, 1997); these bridges were no longer observed when follicular cells had enveloped the oocyte (Bruslé, 1980). On the other hand, intercellular bridges were never observed between oogonia or oocytes of the syngnathids (Begovac and Wallace, 1987; Selman, Wallace, and Player, 1991).

An increase in size is the most obvious manifestation of oocyte development (Figure 2.9). The oocyte grows both by an enlargement of the nucleus and the addition of cytoplasm. Later, most growth is due to an increase in the amount of cytoplasm and, in the final stages of maturation, the oocyte has its full complement of yolk and is ready to be ovulated. Four principal stages of oocyte development, as outlined below, have been described in several teleosts (Wallace and Selman, 1981). The major cellular and physiological processes occurring at each stage of the zebrafish *Brachydanio rerio* are outlined by Selman et al. (1993). Average diameters of follicles (oocytes

TABLE 2.1. Average diameters of ovarian follicles in *Fundulus heteroclitus* during the stages of oocyte development (Data from Selman and Wallace, 1986)

1. Primary growth stage	8 — 175 μm
1**A.** Chromatin nucleolus phase	8 — 20 μm
1B. Perinucleolus phase	20 — 175 μm
2. Cortical alveolus stage	175 — 550 μm
3. Vitellogenesis	0.55 — 1.35 mm
4. Oocyte maturation	1.35 — 1.9 mm
4A. Early maturation	1.35 — 1.7 mm
4B. Late maturation	1.7 — 1.9 mm

in early stages), recorded for *Fundulus heteroclitus,* are shown in Table 2.1. Four similar stages have been outlined in the lamprey *Lampetra planeri* (Busson-Mabillot, 1967c). Similar development in the red sea bream *Pagrus major* (Matsuyama, Nagahama, and Matsuura, 1991), the rainbow trout *Salmo gairdneri* (van den Hurk and Peute, 1979), and the summer flounder *Paralichthys dentatus* (Merson et al., 2000) have been assigned to seven stages, nine stages in the medaka *Oryzias latipes* (Figure 2.53) (Iwamatsu et al., 1988) and, in the blenny *Blennius pholis,* eleven (Figure 2.5) (Shackley and King, 1977).

Classification of stages of ovarian maturity by macroscopic observation are useful in fecundity studies (Bagenal and Braum, 1971); these have been adapted, using histological criteria, for the perch *Perca fluviatilis* and pike *Esox lucius* (Figure 2.10) (Treasurer and Holliday, 1981; Treasurer, 1990) and for the bass *Dicentrarchus labrax* (Mayer, Shackley, and Ryland, 1988).

2.2.1 PRIMARY GROWTH

Studies with many teleosts indicate that primary growth is independent of pituitary control (Khoo, 1979). During the primary growth stage, oocytes of most teleosts increase in volume about 1000 fold, growing in diameter from about 10–20 μm at leptotene to 100–200 μm; this is accompanied by a noticeable decrease in nuclear/cytoplasmic ratio (Selman and Wallace, 1989). As the oocyte grows, the definitive follicle forms. Oocytes undergo the early stages of prophase and become arrested in diplotene of the first meiotic division. The primary growth stage may be divided into two phases based on nucleolar morphology: the CHROMATIN-NUCLEOLUS PHASE and the PERINUCLEOLUS PHASE. In the zebrafish *Brachydanio rerio,* the follicular cells do not completely isolate individual oogonia and surround NESTS of early germ cells (Figure 2.11) (Selman et al., 1993). During the primary growth phase, the meiotic oocytes become enclosed by follicular cells thereby forming definitive follicles.

Chromatin-nucleolus stage

Oogonia entering the early stages of meiotic prophase within the germinal ridge of syngnathids transform into oocytes during the chromatin-nucleolus phase (Figure 2.12). DNA replication (pre-leptotene) occurs at this time. Homologous chromosomes pair and begin to condense (leptotene, zygotene); these pairs subsequently shorten and thicken to form synaptonemal complexes (pachytene); finally the chromosomes take on the "lampbrush" configuration (diplotene). The nuclei of pipefish oocytes become more spherical than those of oogonia (Begovac and Wallace, 1988). Nuclei of leptotene oocytes contain dense-cored granules and the chromatin remains electron-dense. Nuclei of oocytes in zygotene and pachytene stages of prophase I are less electron-dense and can be distinguished by the presence of synaptonemal complexes between homologous chromosomes within the nucleus (Figure 2.7B). By the pachytene stage, the synaptonemal complexes are long and the nucleoli have become dispersed and fragmented. Dense-cored granules are still present in the nuclei. Oocytes in zygotene and pachytene grow slightly with an increase in organelles, usually aggregated at one side of the nucleus: mitochondria, Golgi complex, ribosomes, and endoplasmic reticulum. Nuage continues to be present.

Newly formed meiotic oocytes in syngnathids initially are in contact with other oocytes. As the oocytes grow within the germinal ridge, they become separated from adjacent oocytes by processes of PREFOLLICU-

LAR CELLS (Figure 2.4) (Selman, Wallace, and Player, 1991). Soon after the oocytes enter the diplotene, prefollicular cells proliferate, flatten, and eventually form the FOLLICULAR EPITHELIUM that completely envelops the growing oocytes (Bruslé, 1980; Begovac and Wallace, 1988). Each oocyte extends numerous microvilli toward the follicular cells (Figure 2.13E) and later the follicular cells reciprocate by extending microvilli toward the oocyte. The squamous follicular cells have large nuclei with cytoplasm containing mitochondria, granular endoplasmic reticulum, and scant Golgi complexes. The follicular epithelium is enclosed by its basal lamina.

Chromatin-nucleolus oocytes become arrested in late diplotene of meiotic prophase I as the synaptonemal complexes dissociate within the oocyte nucleus (Selman and Wallace, 1989). During this phase, the oocytes begin an extensive period of growth. The ooplasmic matrix increases as well as the organelles which tend to remain juxtanuclear. Nucleoli reappear adjacent to the inner layer of the nuclear envelope. The appearance of multiple nucleoli seems to coincide with the formation of the definitive follicle as it separates from the germinal ridge. Each nucleolus consists of two parts: a cortical region of tightly packed ribosomes, and a central area composed largely of fine filaments and scant amounts of the granular component (Figure 2.14) (Anderson, 1968). The DEFINITIVE FOLLICLE now consists of an oocyte surrounded by a single layer of flattened follicular cells with the entire complex enclosed by a basement lamina. Outside the basal lamina there is a sparse THECAL LAYER of vascular connective tissue and a thin surface epithelium consisting of mesothelial cells. The nucleus of the oocyte is generally spherical with multiple nucleoli in a perinuclear position adjacent to the inner layer of the nuclear envelope (Figure 2.13). Dense-cored granules can still be observed in the nucleus. The nucleus grows and nucleoli increase in number.

Perinucleolus phase

As the oocyte grows, the nucleus enlarges to form the GERMINAL VESICLE[5]; the nuclear membrane becomes undulating and, with further growth of the oocyte, it forms large folds and evaginations and becomes lobed (Guraya, 1986). Soon after the arrest in prophase, ribosomal genes are amplified and several nucleoli appear in the oocytes of most teleosts, generally arranged at the periphery of the germinal vesicle although later they may lie randomly within it (Figure 2.15) (Selman and Wallace, 1989). This is the PERINUCLEOLUS STAGE of primary oocyte growth. These nucleoli are present throughout oocyte growth.

At this stage, the "lampbrush" appearance of the chromosomes becomes more apparent (Figure 2.16). These chromosomes are festooned with loops of DNA that presumably represent unwindings of a single chromosome and are sites of active transcription of heterogeneous RNA in addition to the ribosomal RNA provided by the multiple nucleoli.

Unlike the situation in most teleost oocytes, where large numbers of nucleoli are produced during the chromatin-nucleolus period of primary growth, only one or two nucleoli are present at this time in the viviparous teleost *Xiphophorus helleri* (Azevedo and Coimbra, 1980). These nucleoli display a compact fibrillar core surrounded by a looser, granular periphery (Figure 2.17). Following the diplotene stage, when meiotic activity is suspended and lampbrush chromosomes are present in the nucleus, these nucleoli enlarge from about 6 to 18 μm and become increasingly vacuolated, indicating increased ribosomal production as the cells prepare for vitellogenesis (Figure 2.18). The nucleoli suddenly decrease in size during vitellogenesis; they disappear when the first polar body is emitted and the oocyte II is ready for fertilization.

Oocytes increase in size with the continued elaboration of cytoplasm, mitochondria, Golgi complexes, ribosomes, endoplasmic reticulum, and multivesicular bodies (Begovac and Wallace, 1988). This growth is accommodated by mitotic division of the follicular cells (Figure 2.19). During the primary growth phase most teleost oocytes accumulate extensive aggregations of basophilic and electron-dense material in the perinuclear cytoplasm. This loosely defined structure is the JUXTANUCLEAR COMPLEX OF ORGANELLES (BALBIANI'S VITELLINE BODY)[6] (Figure 2.20) (Clérot, 1976; Bruslé, 1980; Mayer, Shackley, and Ryland, 1988; Selman and Wallace, 1989); there is one report of the juxtanuclear complex in an elasmobranch, the dogfish *Scoliodon sorrakowah* (Guraya, 1979). A conspicuous

[5] The greatly enlarged nucleus of an oocyte during the prophase of the first meiotic division is designated a GERMINAL VESICLE.

[6] The references by Guraya (1979, 1986) discuss Balbiani's vitelline body at length.

"vitelline body" described at the end of the primary growth period in oocytes of the brook lamprey *Entosphenus wilderi* is probably the same structure (Okkelberg, 1921).

The juxtanuclear complex is composed of particles of ribonucleoprotein associated with a heterogeneous population of cytoplasmic organelles: granular endoplasmic reticulum, Golgi elements, mitochondria, lysosomes, multivesicular bodies, and lipid droplets (Figures 2.13C,D). ANNULATE LAMELLAE, of unknown function, have been often described within the juxtanuclear complex (Iwamatsu, 1988). They consist of several parallel smooth cisternae, each containing regularly arranged fenestrations corresponding to the nuclear pores (Figures 2.21 and 2.22). It has been suggested that the cisternae arise from the nuclear envelope and are a special type of endoplasmic reticulum[7].

Depending upon the species of fish, the juxtanuclear complex shows different combinations of various organelles and inclusions. It may be a consequence of this variability that an extensive array of confusing terms has arisen in association with it. These terms include YOLK NUCLEUS, which is sometimes used synonymously with the term juxtanuclear complex; NUAGE or CEMENT, which appears to be a material rich in ribonucleoprotein occupying the ooplasm between the aggregated organelles; and PALLIAL SUBSTANCE, a deeply basophilic cloak enclosing less basophilic material (Beams and Kessel, 1973). The presence of nuage has been used as a criterion for identifying primordial germ cells in the cyprinid *Barbus conchionus* (Gevers et al., 1992) and the centropomid *Centropomus undecimalis* (Grier, 2000).

The substance of the juxtanuclear complex originates as a crescent or cap adjacent to the nuclear membrane and increases in size as the oocyte grows (Figure 2.23) (Guraya, 1963). The complex disappears at the beginning of vitellogenesis. The CIRCUMNUCLEAR RING, seen with the light microscope in oocytes of the cod *Gadus morhua* and the centropomid *Centropomus unidecimalis,* is thought to be homologous to the juxtanuclear complex and is considered to be the first sign that the fish will spawn in the coming season (Figure 2.24) (Kjesbu and Kryvi, 1989; Grier, 2000).

The juxtanuclear complex may assume various shapes in different teleosts. In oocytes of some fish, a single discrete structure develops near the nucleus (e.g., *Channa marulis, Dicentrarchus labrax)* (Guraya, 1963; Mayer, Shackley, and Ryland, 1988); it may expand to form a perinuclear ring (e.g., *Tilapia nilotica, Syngnathus scovelli)* (Begovac and Wallace, 1988); and in some oocytes a single crescent that later becomes ovoid and migrates to the periphery of the oocyte (eight Indian species, but especially *Heteropneustes fossilis)* (Figure 2.25) (Nayyar, 1964). The complex may appear double in oocytes of the Atlantic mackerel *Scomber scombrus* (Coello and Grimm,1990). Nuage of the common snook *Centropomus undecimalis* is a polymorphic organelle associated with mitochondria (Grier, 2000). It occurs as dense cytoplasmic inclusions, generally perinuclear in position (Figure 1.28B).

In the medaka *Oryzias latipes,* the yolk nucleus is an electron-dense, thread-like structure inhabiting the vegetal pole side of the oocyte (Figure 2.26) (Iwamatsu and Nakashima, 1996). It is suggested that the orientation of the vegetal pole may primarily be determined by the random positioning of the yolk nucleus within the oocyte and established by reciprocal interactions between the cytoplasm containing the yolk nucleus and the surrounding follicular cells.

The function of the juxtanuclear complex is enigmatic. It has been suggested that it acts as a centre for metabolic activities related to the formation, multiplication, and accumulation of other organelles and inclusions that are finally distributed in the outer ooplasm before the deposition of yolk, representing a mobilization of the forces needed for laying down yolk (Clérot, 1976; Bruslé, 1980; Selman and Wallace, 1989).

Oocyte volume increases a few hundred fold during primary growth, the nuclear/cytoplasmic ratio decreases, and many membranous organelles are elaborated within the ooplasm (Figures 2.5C,D). At the end of this phase, the oocyte and follicular cells have established an intimate relationship. Patches of translucent material, a precursor of the zona pellucida, accumulate around microvilli that have formed on the surface of the oocyte; follicular cells display fewer microvilli. During oocyte growth, both thecal and follicular cells thicken and multiply.

2.2.2 CORTICAL ALVEOLUS STAGE

The cortical alveolus stage is characterized by the initial appearance of three components: CORTICAL ALVEOLI, the ZONA PELLUCIDA, and LIPID (Figure 2.27A) (Begovac

[7] The topic of annulate lamellae is reviewed extensively by Kessel (1992).

and Wallace, 1988; Selman and Wallace, 1986, 1989; Selman, Wallace, and Player, 1991). Cortical alveoli initially appear circumferentially at various depths in the cytoplasm. They are membrane bound, have a homogeneous appearance, and generally stain for both protein and carbohydrate. Their size and structure are variable; some contain a single large granule within a homogeneous matrix while others contain only the homogeneous matrix (Figures 2.27B and 2.28). They appear to be formed by the granular endoplasmic reticulum and Golgi complex and contain a glycoprotein synthesized within the oocyte (Figures 2.5E,F) (Ulrich, 1969; Tesoriero, 1980; Guraya, 1986; Bruslé, 1985; Selman, Wallace, and Barr, 1986; Selman and Wallace, 1986, 1989). These membrane-bound vesicles are closely associated with the Golgi complex.

As the oocytes grow, the cortical alveoli increase in number and their size becomes more heterogeneous as they fill much of the ooplasm. They enlarge, sometimes to 50+ μm in diameter and, by the end of the cortical alveolus stage, almost fill the cytoplasm of the oocyte. In subsequent stages they continue to form but are displaced to the periphery by yolk protein that accumulates centripetally. The cortical alveoli increase in size and number as they move peripherally in the ooplasm (Figure 2.29) and are found at later stages in variable sizes and numbers beneath the oolemma (see review by Selman and Wallace, 1989). The cortical alveoli will later fuse with the oolemma and, at fertilization, release their glycoprotein into the perivitelline space during the "cortical reaction".

Also in the cortical alveolus stage there is a formation and aggregation of small lipid droplets around the nucleus (Figure 2.27A,D). The lipid mass continues to enlarge in a perinuclear position. Later the lipid droplets increase in size. Lysosome-like bodies of uncertain function are present, often containing electron-dense material. They seem to disappear when yolk begins to accumulate.

The presence of "yolk vesicles" is often described in small oocytes; these appear to be identical in structure and composition with the cortical alveoli that are present in eggs. Since yolk vesicles do not contain yolk as a nutrient source it is suggested that this designation be dropped in favour of "nascent cortical alveoli" or simply "cortical alveoli" (Selman, Wallace, and Barr, 1988).

Pinocytotic vesicles appear during the cortical alveolus stage at the bases of the microvilli (Shackley and King, 1977; Begovac and Wallace, 1988). The zona pellucida is first observed as a thin, PAS-positive band between the oocyte and follicular cells; with the electron microscope it appears as homogeneous material between the microvilli of the oocyte. The microvilli lengthen as the zona pellucida thickens. The follicular cells also form microvilli that interdigitate with the oocyte processes. In some fish the follicular cells remain squamous but in the blenny they become cuboidal to columnar. They contain mitochondria and granular endoplasmic reticulum; Golgi complexes become more abundant. At this stage, one of the follicular cells enlarges and is designated the MICROPYLAR CELL. It later forms the MICROPYLE, a passage for eventual sperm penetration through the zona pellucida.

Cortical alveoli appear to arise in oocytes of the lamprey *Lampetra planeri* just before the beginning of vitellogenesis (Busson-Mabillot, 1967c); they do not form in oocytes of the dogfish *Scoliodon sorrakowah* (Guraya, 1982, 1986).

2.2.3 VITELLOGENESIS

The enlargement of the oocyte that takes place during vitellogenesis is due largely to an accumulation of exogenously derived yolk protein precursors (Begovac and Wallace, 1988). This protein is, in general, called female-specific serum protein (Fujita, Takemura, and Takano, 1998). In teleosts, the relative contribution of protein yolk deposition to oocyte growth is obscured to some extent by the extensive elaboration of cortical alveoli that was initiated prior to vitellogenesis and by the hydration that follows vitellogenesis (Wallace and Selman, 1981). Most proteins appear to be synthesized outside the oocyte (heterosynthetic) although autosynthetic origin of yolk proteins may also occur (Wallace, 1978). The female specific protein, VITELLOGENIN, is a large lipoglycophosphoprotein which is synthesized by the liver, released into the blood, and transported to the ovary. Indeed, the association between liver and ovary is indicated by simultaneous increases in the hepatosomatic and gonadosomatic indexes during vitellogenesis in the catfish *Heteropneustes fossilis* (Srivastava and Saxena, 1996). This phase is dependent on pituitary gonadotropin (Khoo, 1979) which stimulates oestrogen production by the ovary (Wallace, 1985). Oestrogen, especially oestradiol-17β, transported in the blood to the liver, regulates synthesis and secretion of vitellogenin (Nagahama, 1984). Also in response to gonadotropin, vitellogenin is selectively sequestered from the bloodstream by

growing oocytes. Vitellogenin itself is not incorporated into teleost egg yolk but rather is proteolytically cleaved within the oocyte into yolk proteins of which LIPOVITELLIN and PHOSVITIN are the most familiar (Wallace, 1985; Greeley, Calder, and Wallace, 1986). By now, all types of non-mammalian vertebrates, from hagfish (Yu et al., 1981), sharks (Craik, 1978a), and other fish (Wiegand, 1982) to turtles and birds, have been shown to synthesize and secrete vitellogenin as a response to oestrogen.

Macromolecules destined for the production of yolk follow an intercellular route from the maternal circulation to the surface of the oocyte, penetrating between the endothelial cells of the perifollicular capillaries to enter the connective tissue surrounding the follicle (Selman and Wallace, 1982b). On reaching the follicular epithelium they pass between, rather than through, adjacent follicular cells en route to the oocyte. Occasional evidence has been found for the internalization, by micropinocytosis, of electron-dense tracers within the follicular cells but most macromolecules appear to pass through extracellular channels of varying sizes between the follicular cells (Selman and Wallace, 1982a). The molecules then penetrate the patent pore canals of the zona pellucida. Follicular cells do not appear to contribute to yolk formation in teleosts (Selman and Wallace, 1986).

Protein yolk precursors are incorporated into the oocyte by intense micropinocytosis of the oolemma between the bases of the microvilli (Figures 2.30 and 2.31) (Droller and Roth, 1966; Anderson, 1968; Ulrich, 1969; Shackley and King, 1977; Selman and Wallace, 1982a, 1983; Abraham et al., 1984; Bruslé, 1985; Kjesbu, Kryvi, and Norberg, 1996) and translocated to yolk spheres in less than 20 min (Selman and Wallace, 1982b). Coated pits are numerous along the oolemma between the microvilli and micropinocytotic vesicles as well as smooth-surfaced tubules lie together in the cortical ooplasm. Micropinocytosis of external materials by the oocyte is the most characteristic cellular event of vitellogenesis (Selman and Wallace, 1982a).

During vitellogenesis, the zona pellucida thickens and the oocyte continues to form cortical alveoli (Selman and Wallace, 1982a, 1986). The most obvious event marking the initiation of vitellogenesis, however, is the appearance of membrane-bound, fluid-filled yolk spheres lying between the cortical alveoli in the peripheral ooplasm (Figure 2.32).

Two types of yolky inclusions are formed during vitellogenesis: LIPID YOLK DROPLETS and masses of PROTEIN YOLK (Yamamoto, 1964; Shackley and King, 1977, 1979; Wallace and Selman, 1981; Mayer, Shackley, and Ryland, 1988; Selman and Wallace, 1989; Selman et al., 1993). The first type of yolky inclusion to accumulate in most species is lipid yolk in the form of distinct lipid droplets; in the bass these make their appearance in the outer cortex but in most teleosts they first appear in the perinuclear cytoplasm giving rise to suggestions that they are probably formed endogenously (Figure 2.5). Protein yolk accumulation is exogenous in origin and occurs after, and concomitant to, lipid yolk accumulation. In most teleosts, yolk proteins accumulate in fluid-filled yolk spheres that may either maintain their integrity throughout oocyte growth or fuse centripetally, eventually forming a continuous mass of fluid yolk, a process which confers on many teleost eggs their characteristic transparency (Figure 2.33). This coalescence can occur relatively soon after the initial formation of yolk spheres, as in sticklebacks and the pipefish, during the later stages of vitellogenesis, as in the sheepshead minnow, or during maturation, as in those marine teleosts that produce pelagic eggs. Creation of a central mass of fluid yolk displaces the ooplasm, with its cortical alveoli and lipid droplets, to the periphery of the oocyte (Figure 2.5). A few yolk spheres always remain in the peripheral ooplasm, but appear to be reduced in number as the central mass increases (Figure 2.32) (Shackley and King, 1977).

In some species, protein yolk is sequestered in the form of discrete granules that stain intensely for proteins but not for lipids or carbohydrates (Figure 2.34) (Selman and Wallace, 1989; Selman et al., 1993). The surface of the oocyte displays considerable endocytotic activity during this stage and electron-dense material is visible in some endocytotic structures. The yolk platelets of the zebrafish *Brachydanio rerio* are variable in size and some may attain diameters of 40 μm. The contents of most of these yolk bodies are not homogeneous and generally display one to several rectilinear masses embedded in a homogeneous matrix. In appropriately oriented sections, these masses display an orthorhombic crystalline structure with parallel dense bands approximately 10 nm apart (Figure 2.35). This granular yolk becomes the predominant yolk inclusion and densely packs the mid and outer cortex. Unlike the fluid yolk droplets that coalesce as they migrate centripetally, protein yolk granules maintain their structural integrity until maturation, after which they actively coalesce.

YOLK GRANULES are characteristic of freshwater teleosts (Lange et al., 1983) although they have been noted in eggs of the cod *Gadus morhua* (Kjesbu and Kryvi, 1989). As described in a wide range of fishes they consist of one or more crystalline main bodies within an amorphous superficial layer enclosed by a membrane (Figure 2.36) (Yamamoto and Oota, 1967; Wallace, 1978). Elegant crystals have been described within the main body of yolk platelets from a wide variety of fishes (cyclostomes: Karasaki, 1967; Ulrich, 1969; Patzner, 1975; Lange and Richter, 1981; Lange, 1982; teleosts: Lange et al., 1983; and the ancient fishes *Polypterus bichir, Amia calva,* and *Lepisosteus osseus:* Lange, Grodzinski, and Kilarski, 1982). The crystals of cyclostomes appear to be a monoclinic lattice of possibly symmetric lipovitellin-phosvitin dimers whereas those of teleosts and the ancient fishes are an orthorhombic array of lipovitellin-phosvitin complexes consisting of two subunits that are likely not identical. This crystalline structure is rare in marine species, suggesting that the crystals may store essential nutrients, unavailable in fresh water, providing regularly packed microchambers that sequester low molecular weight particles or ions (Lange, Grodzinski, and Kilarski, 1982). X-ray analysis of cryosections indicates the presence of chloride and a variety of cations within the platelets (Lange, 1981, 1982; Lange et al., 1983).

Early vitellogenesis in the pipefish is characterized by the appearance of individual small, membrane-bound yolk spheres in the oocyte periphery and interior (Figures 2.37A to C) (Begovac and Wallace, 1988). As vitellogenesis progresses, the yolk spheres increase in size while the cortical alveoli and lipid are displaced to the peripheral ooplasm. Eventually the yolk spheres coalesce to form a central fluid mass; the cortical alveoli and lipid remain in the peripheral part of the yolk mass. Yolk spheres are moderately electron dense and contain highly electron-dense inclusions that occasionally have a finely granular appearance and provide a specific, reliable marker for following yolk formation (Figures 2.37D,E). There are three types of small yolk spheres: primary, transitional, and mature. PRIMARY YOLK SPHERES appear to contain proteinaceous material interspersed among multivesicular elements. INTERMEDIATE, TRANSIENT YOLK SPHERES contain proteinaceous material, variable vesicular elements, and the yolk-specific, electron-dense inclusion. MATURE YOLK SPHERES contain homogeneous, condensed yolk and a heterogeneous size and distribution of the yolk-specific marker (Figures 2.37D,F). It is suggested that the multivesicular bodies represent a modified lysosomal compartment involved in yolk sphere formation (Begovac and Wallace, 1988). Secondary lysosomes or multivesicular bodies are seen adjacent to cortical alveoli in oocytes of the seahorse and pipefish at about the time of the onset of vitellogenesis (Figure 2.38) and may be required for the proteolytic processing into mature yolk proteins of the vitellogenin taken up by endocytosis (Figure 2.37G) (Selman, Wallace, and Player, 1991). Multivesicular bodies seem to disappear as vitellogenesis progresses.

The involvement of lysosomes or multivesicular bodies in vitellogenesis has been demonstrated in oocytes of the trout *Salmo trutta fario* (Busson-Mabillot, 1984). At an early stage of development, lysosomes arise in the cortical ooplasm and migrate centripetally, almost reaching the nucleus; eventually they constitute the most voluminous compartment of the oocyte (Figure 2.39). They are membrane-bound and contain small vesicles and clumps of finely granular material (Figure 2.40A). Continuities are abundant between the agranular endoplasmic reticulum and the membrane enclosing the lysosomes (Figure 2.40B). At the beginning of vitellogenesis, endocytotic vesicles containing vitellogenin fuse with one another to form larger vesicles and these then fuse with lysosomes to form yolk bodies that may attain diameters up to 10 μm (Figure 2.41). Granular material gradually fills the lysosomes at the onset of vitellogenesis and, over several weeks, this transforms into homogeneous yolk (Figure 2.42).

Other changes are apparent within the follicle during vitellogenesis (Selman and Wallace, 1986; Begovac and Wallace, 1988; Kjesbu, Kryvi, and Norberg, 1996). The germinal vesicle is progressively displaced toward the animal pole as yolk accumulates centripetally within the oocyte. Some small lipid droplets remain associated with the germinal vesicle while others begin to fuse, reaching diameters of 40 to 50 μm, and reside in the peripheral ooplasm. In *Fundulus,* the zona pellucida continues to enlarge, acquiring an elaborate structure whereas, in *Syngnathus,* it undergoes condensation. There is a close structural relationship between bundles of microfilaments and annulate lamellae in vitellogenic oocytes (Kessel, Beams, and Tung, 1984). It is suggested that there is a coparticipation of pores of the annulate lamellae and polyribosomes in the development of microfilament bundles.

Vitellogenesis in the elasmobranch *Scyliorhinus canicula* does not appear to differ fundamentally from

other vertebrates either in the mechanism of vitellogenesis or in its immediate endocrine control (Craik, 1978a,b,c,d,e). Vitellogenin is present in the plasma throughout the year and its uptake by growing ovarian follicles seems to be stimulated by a hormone from the cranial pars distalis of the pituitary.

An unusual form of yolk uptake is described in the lamprey *Petromyzon marinus* where both the oocyte and certain enlarged follicular cells, the "nurse cells", simultaneously form yolk platelets (Lewis and McMillan, 1965). These cells eventually fuse and the yolk-rich cytoplasm from the nurse cells is incorporated into the oocyte. The nucleus of the nurse cell disappears.

2.2.4 MATURATION

Following vitellogenesis, oocytes undergo MATURATION with the resumption of the meiotic or "maturation" division that has been arrested in prophase I since their transformation from oogonia. At this time the follicles appear to attain a critical size, becoming competent to respond to MATURATION-INDUCING HORMONES (MIH) by initiating maturation[8]. Diameters of 0.5 to 0.6 mm have been recorded in seabream *Sparus aurata* (Gothilf et al., 1997), 0.69 to 0.73 mm in zebrafish *Brachydanio rerio* (Selman et al., 1993), 0.8 to 1.2 mm in medaka *Oryzias latipes* (Iwamatsu et al., 1988), 1.5 to 1.9 mm in killifish *Fundulus heteroclitus* (Selman and Wallace, 1986), and 1.1 to 1.3 mm in the pipefish *Syngnathus scovelli* (Begovac and Wallace, 1988). A further increase in size occurs by hydration during maturation in many teleosts, especially marine forms. Maturation division is followed by condensation of the chromosomes and expulsion of the first polar body.

At the beginning of maturation, the oocyte has a large nucleus or GERMINAL VESICLE located centrally or halfway between the centre and periphery (Wallace and Selman, 1978, 1981; Nagahama, 1983; Kjesbu, Kryvi, and Norberg, 1996; Gothilf et al., 1997); it is inconspicuous in whole oocytes of many teleosts (Figure 2.43). The nucleus is in meiotic prophase and contains lampbrush chromosomes. The first visible event associated with final oocyte maturation is the migration of the germinal vesicle to the animal pole at which time it becomes visible under the dissecting microscope. The envelope of the germinal vesicle breaks down (GERMINAL VESICLE BREAKDOWN: GVBD) and the nuclear contents blend with the surrounding cytoplasm. This provides a morphologically identifiable event that may conveniently be used to divide maturation into two physiologically distinct phases: EARLY MATURATION (pre-GVBD) and LATE MATURATION (post-GVBD) (Selman and Wallace, 1986). Germinal vesicle breakdown generally occurs in *Fundulus heteroclitus* when the follicle reaches a diameter of 1.5 to 1.7 mm (Wallace and Selman, 1978).

Early maturation is characterized by a rapid increase in follicular volume, primarily due to hydration but the continued accumulation of heterosynthetic macromolecules by endocytosis accounts for about 16% of this increase (Wallace and Selman, 1985). Protein incorporation appears to stop abruptly at the time of germinal vesicle breakdown. This is consistent with the observation that oocytes in early maturation continue to display endocytotic activity at their surface, whereas those in late maturation do not. During hydration, yolk polypeptides present in early maturational oocytes undergo proteolysis. In late maturation, after germinal vesicle breakdown, the follicle continues to enlarge by hydration. Within the oocyte, lipid droplets continue to coalesce, lose their peripheral attachments, and are able to move freely through the oocyte (Figure 2.44). Immediately prior to ovulation they collect at the upper surface of the oocyte and will float to the opposite pole if the follicle is inverted. During maturation, the yolk bodies of the zebrafish *Brachydanio rerio* lose their crystalline masses and develop a homogeneous interior (Figure 2.45) (Selman et al., 1993).

Follicular maturation is controlled by pituitary gonadotropin which induces a shift in follicular steroidogenesis away from the production of oestradiol-17β, necessary for vitellogenesis and oocyte growth, to the production of the maturation-inducing hormone (MIH) required for the resumption of meiosis (Patiño and Thomas, 1990; Thomas and Patiño, 1991; Nagahama et al., 1994). Oocytes must be primed with gonadotropin before maturation can be induced by MIH. This occurs before coalescence of the lipid droplets and includes synthesis of receptors for the MIH. Considerable evidence has accumulated, especially in Salmoniformes (Jalabert, 1976; Duffey and Goetz, 1980; Nagahama, 1983, 1984; Nagahama and Adachi, 1985; Kanamori, Adachi, and Nagahama, 1988), but in other bony fish as well (Jalabert, 1976; Goetz and Theofan, 1979; Greeley et al., 1986; Levavi-Zermonsky and Yaron, 1986; Asahina, Taguchi, and Hibiya, 1987; Kobayashi et al., 1988; Schoonen et al., 1989; Suzuki, Tan, and Tamaoki, 1989; Haider, 1990; Lessman, 1991; Petrino et al., 1993; Fukada et al., 1994;

[8] The extensive literature on maturation-inducing hormones in teleosts has been reviewed by Goetz (1983), Scott and Canario (1987), Nagahama et al., (1994), and Peter and Yu (1997).

Gothilf et al., 1997), indicating that the major naturally occurring MIH is 17α,20β-dihydroxy-4-pregnen-3-one (17α,20β-DP). This steroid is synthesized collaboratively by both the thecal and follicular layers: gonadotropin stimulates thecal cells to produce 17α-hydroxyprogesterone which is converted within the follicular cells to 17α,20β-dihydroxy-4-pregnene-3-one (Figure 2.46) (Nagahama and Adachi, 1985; Nagahama, 1987; Nagahama et al., 1994). Other C_{21} steroids have been shown to be equally potent in inducing maturation in a number of species, at least *in vitro,* and all have a 17- and 20β-hydroxyl group and are structurally similar to 17α,20β-dihydroxy-4-pregnene-3-one (Scott and Canario, 1987). In two species of sciaenid fish (Perciformes), the predominant steroid produced during final oocyte maturation and the natural MIH is 17α,20β,21-trihydroxy-4-pregnene-3-one (20β-S) (Trant, Thomas, and Shackleton, 1986; Thomas and Trant, 1989; Trant and Thomas, 1989a,b). Both hormones (17α,20β-DP and 20β-S) may play a role in inducing maturation in the striped bass *Morone saxatilis* and white perch *M. americana* (Perciformes) (King et al., 1994; King, Thomas, and Sullivan, 1994; King, Berlinsky, and Sullivan, 1995). Maturation of oocytes of the winter flounder *Pleuronectes americanus* (Pleuronectiformes) appears to be induced by the synergism of several steroids distinct from the progesterones which predominate in other fish (Truscott et al., 1992). It is of interest to note that 17α,20β-dihydroxy-4-pregnene-3-one has been detected in the serum of the sea lamprey *Petromyzon marinus* during the early spawning migration, suggesting a role in maturation and ovulation of this cyclostome (Weisbart et al., 1980).

PROTEASOMES appear to play a role in the maturation of fish oocytes (see review by Tokumoto, 1999). These proteolytic complexes are found in eukaryotic cells and are responsible for the degradation of most cellular proteins, including structural proteins, enzymes, and proteins that regulate cell cycles (Coux, Tanaka, and Goldberg, 1996). Proteasomes help to regulate the amount of a particular protein present in a cell at a given time. There are two types of proteasomes: 20S (700 kDa) and 26S (2000 kDa). The 20S proteasome forms the catalytic core of the 26S which consists of a central cylinder formed from proteases whose active sites are thought to face an inner chamber. Each end of the cylinder is capped by a large protein complex; these complexes are thought to bind proteins destined for digestion and then feed them into the inner chamber. Activity of proteasome 26S increased in oocytes of the goldfish *Carassius auratus* within one hour after exposure to MIH and then declined; it rose again after completion of GVBD (Tokumoto et al., 1997). It was concluded that proteasome 26S is involved in two steps in the meiotic cycle of maturation: the early stage, following stimulation by MIH, before migration of the germinal vesicle, and later at the transition from metaphase I to anaphase I. The nature of the proteins being degraded at these times is still uncertain but proteins critical to the regulation of the cell cycle have been suggested.

The ultrastructure of oocytes approaching the resumption of meiosis has been described *in vitro* and *in vivo* in oocytes of the medaka *Oryzias latipes* (Iwamatsu et al., 1976, 1988). Immediately before germinal vesicle breakdown, tetrad chromosomes may be detected in the central part of the large germinal vesicle. Before maturation begins, there are many mitochondria, annulate lamellae, granular endoplasmic reticulum, and Golgi complexes in the cortical cytoplasm (Figure 2.22). Germinal vesicle breakdown leads to the formation of the spindle of meiosis and, within three hours, meiosis progresses through prometaphase I to metaphase I. Following a short time in anaphase I, the first maturation division is complete by four hours. The oocytes reach metaphase II about five hours after germinal vesicle breakdown and the first polar body is extruded at the animal pole. All cytoplasmic projections of both the oocyte and follicular cells have withdrawn from the zona pellucida by the time of ovulation. Ovulation takes place at the end of this stage. A few Golgi complexes and no annulate lamellae are noted in the ovulated eggs of the medaka (Iwamatsu et al., 1988). (The meiotic process, leading to the expulsion of the second polar body, is resumed at the time of fertilization and sperm penetration.)

Reorganization of the microtubular cytoskeleton during maturation in oocytes of the goldfish *Carassius auratus* has been recorded by confocal immunofluorescence microscopy using an anti-tubulin antibody (Jiang et al., 1996). In fully grown, immature oocytes, the yolk granules appear as dark masses suspended within the glowing meshes of a microtubular network that extends throughout the ooplasm except for the region containing the germinal vesicle. A condensed band of microtubules surrounds the germinal vesicle (Figure 2.47); these microtubules play a role in stabilizing the germinal vesicle at the centre of the oocyte. When the germinal vesicle begins its migration, the

microtubular network disappears, permitting movement toward the animal pole. Cytoplasmic microtubules gradually concentrate in the animal hemisphere. As the germinal vesicle migrates, it trails a glowing "perinuclear tail" of condensed microtubules from its vegetal surface; it appears that the perinuclear tail permits the accumulation of cytoplasmic materials that are necessary for the subsequent maturation (Figure 2.48). It is presumed that cytoplasmic microfilaments contribute the motive power for migration of the germinal vesicle. Coincident with the breakdown of the germinal vesicle (GVBD), numerous microtubules penetrate the germinal vesicle from its vegetal surface and a disc-shaped ring of condensed microtubules is seen at the animal pole region, suggesting a role in spindle formation or the organization of meiotic chromosomes (Figures 2.49 and 2.50).

The marked hydration of oocytes during maturation is especially pronounced in marine teleosts with pelagic or floating eggs, although it occurs to a lesser extent during maturation in many brackish water and marine species with non-floating or demersal eggs (Craik and Harvey, 1984, 1986; Greeley, Calder, and Wallace, 1986; Thorsen and Fyhn, 1996). The floating eggs of many marine teleost species contain about 92% water (Craik and Harvey, 1984, 1986). They owe their buoyancy to this high water content rather than, for example, to low density lipids. Such eggs contain a more dilute aqueous solution than seawater itself and are consequently less dense. In these species, there is a massive and rapid uptake of water during maturation, increasing the volume of the oocyte by a factor of four or five; the resulting mature, buoyant egg is ovulated shortly thereafter. This water uptake is clearly an adaptation leading to wide dispersal of the floating eggs by water currents and is thus related to the high fecundity of these species (Fulton, 1898, cited by Wallace, 1978).

There is evidence of secondary proteolysis of yolk proteins during maturation, being most pronounced in marine species with pelagic eggs where its extent is well correlated with the extent of oocyte hydration (Greeley, Calder, and Wallace, 1986). A large pool of free amino acids that is present in pelagic marine fish eggs originates mainly from the hydrolysis of yolk proteins during final oocyte maturation (Thorsen and Fyhn, 1996). This may assist hydration by increasing osmotic potential within the ooplasm or by supplying energy for hydration to occur, perhaps by breaking high-energy phosphorus bonds.

Three factors have contributed to the enlargement of oocytes: extensive elaboration of cortical alveoli before vitellogenesis, deposition of protein yolk, and hydration following vitellogenesis; the relative contributions of each are difficult to ascertain. Follicular growth in *Fundulus heteroclitus,* from a diameter of 0.55 ± 0.5 up to 1.35 ± 0.5 mm, is due to vitellogenin uptake by the growing oocyte while final enlargement, from 1.35 ± 0.05 up to 1.85 ± 0.05 mm during maturation, is the result of hydration (Wallace and Selman, 1985).

During maturation, the oocyte becomes more translucent as lipid and protein yolk droplets coalesce. Complete fusion of yolk droplets does not occur in all species and it has been noted that the degree of coalescence of the lipid droplets follows a phylogenetic pattern, forming one major droplet in higher teleosts (such as yellow perch *Perca flavescens,* walleye *Stizostedion vitreum,* striped bass *Roccus saxatilis,* and paradisefish *Macropodus opercularis)* but showing less coalescence in lower teleosts (brook trout *Salvelinus fontinalis* and rainbow trout *Salmo gairdneri)* where ovulated oocytes contain a large number of lipid droplets (Goetz, 1983). In some intermediate teleosts (sticklebacks *Gasterosteus aculeatus* and *Apeltes quadracus* and the killifish *Fundulus heteroclitus)* the degree of coalescence is intermediate.

The oocytes soon ovulate into the ovarian lumen and become mature eggs. The vitelline envelope is highly compacted and possesses pore canals prior to maturation (Begovac and Wallace, 1988). At some undefined time during maturation, and before ovulation, the pore canals disappear as the microvilli are retracted or lost from the oocyte and follicular cell. The mature egg is surrounded by the tough CHORION that is derived from remnants of the zona pellucida. The chorion may be decorated with a secondary envelope that appears to have been synthesized by the follicular cells during oocyte growth (Wourms and Sheldon, 1976).

Marine fishes with pelagic eggs differ from other oviparous vertebrates in that a characteristic component of the yolk, protein phosphate, is synthesized and laid down in the ovary in the typical vertebrate manner but does not nourish the young animal (Craik and Harvey, 1984). Instead, it is apparently utilized at a much earlier stage in the life cycle, before the eggs leave the ovary, to provide the energy necessary for the considerable transport of ions by the potassium/sodium pump (K^+ in, Na^+ out). In species such as herring *Clupea harengus,* with demersal eggs, ripening is accompanied by a smaller uptake of water and a signifi-

cant but correspondingly smaller decrease in protein phosphate (Craik and Harvey, 1986).

In captive females of the striped bass *Morone saxatilis,* a certain vulnerability following vitellogenesis presents a problem for the acquaculture industry (Mylonas et al., 1997; Mylonas, Woods, and Zohar, 1997). Final oocyte maturation fails to occur due to an absence of a surge in plasma gonadotropin II so that oocytes become atretic and no ovulation or spawning occurs. Although captive broodstocks would provide more reliable egg production, wild caught females undergoing final oocyte maturation must be used for artificial spawning.

2.3 The Oocyte Envelopes

Development of the follicular envelopes has been described for several species of bony fish, both oviparous and viviparous, and is essentially the same for all (Hurley and Fisher, 1966; Flügel, 1967a,b; Anderson, 1967; Götting, 1967; Ulrich, 1969; Busson-Mabillot, 1973, 1977; Azevedo, 1974; Wourms, 1976; Caporiccio and Connes, 1977; Tesoriero, 1977a; Dumont and Brummett, 1980; Stehr and Hawkes, 1983; Hosokawa, 1983, 1985; Bruslé, 1985; Kessel et al., 1985; Schmehl and Graham, 1987; Iwamatsu et al., 1988; Matsuyama, Nagahama, and Matsuura, 1991; Giulianini and Ferrero, 2000). Oocytes of all species produce a refractile, acellular PRIMARY ENVELOPE around themselves (Wourms, 1976). Several names have been applied to this layer, including "zona pellucida", "zona radiata", "chorion", "vitelline membrane", and "vitelline envelope". The term most commonly used for the homologous structure in mammals is "zona pellucida" and this will be used in this text.[9] Around the zona pellucida, the follicular cells may form a SECONDARY ENVELOPE, often highly ornamented. TERTIARY ENVELOPES, such as jelly coats or leathery egg cases, may be formed by glands in the oviduct, or elsewhere, as the ovum makes its way to the outside world.

2.3.1 PRIMARY ENVELOPE

The zona pellucida of teleosts is secreted by exocytosis around the bases of the microvilli that extend from the surface of the oocyte (Figure 2.51). These microvilli are entrapped in this developing envelope, along with microvilli extending from the follicular cells so that the primary envelope is perforated by PORE CANALS containing microvilli extending perpendicular to its surface (Figure 2.52). These perforations, with their enclosed microvilli, account for the striated pattern of the primary envelope, as seen in sections with the light microscope, giving rise to the term "zona radiata" that is sometimes applied to this layer. The microvilli within the pore canals may be closely apposed (Figures 2.53 and 2.54), even coiling around each other (Kjesbu, Kryvi, and Norberg, 1996). Those from the follicular cells may flatten their tips over the oolemma (Figure 2.55), while the oocyte's microvilli reciprocate by touching the surface of the follicular cells. It is estimated that a single oocyte in the cod *Gadus morhua* bristles with about 1.8 million microvilli, thereby increasing its surface area by a factor of 12.

The zona pellucida transforms during early oocyte development (Figures 2.56 and 2.57) (Götting, 1965; Anderson, 1967; Azevedo, 1974; Hosokawa, 1983; Cotelli et al., 1988; Begovac and Wallace, 1989). During primary growth, prior to its formation, oocytes extend microvilli toward the investing monolayer of follicular cells (Begovac and Wallace, 1988). Initial formation of the zona pellucida occurs at the earliest cortical alveolus stage, with the deposition of a homogeneous electron-lucent layer, designated Z1 by Anderson (1967), between the microvilli (Figure 2.57A). By mid to late cortical alveolus stage, the architecturally complex Z2 and Z3 layers form, giving the zona pellucida a trilaminar appearance (Figure 2.57B). During vitellogenesis, the zona pellucida undergoes compaction, particularly of the Z3 layer (Figure 2.57C) and several layers of alternating electron-dense and electron-lucent lamellae may become apparent. Active exchange of metabolites takes place between the oocyte and perifollicular space by way of the pore canals (Figure 2.58).

When the zona pellucida first appears, the peripheral ooplasm displays enhanced apparatus for protein synthesis and secretion: free ribosomes, granular endoplasmic reticulum, and well developed Golgi complexes (Anderson, 1967; Wourms, 1976). Electron-dense vesicles, apparently formed by the Golgi complex, arise in the peripheral ooplasm prior to deposition of the electron-dense layer of the zona pellucida and are apparent during all subsequent stages of its deposition (Figure 2.59) (Tesoriero, 1977a); this

[9] There may be changes in the egg envelope on contact with the external environment following spawning. The term "chorion" will be reserved, in this text, to designate the structural envelope that encloses the ovulated egg or developing embryo (Hart, Pietri, and Donovan, 1984).

glycoproteinaceous material is presumably deposited by exocytosis and becomes the developing zona pellucida (Figure 2.60) (Tesoriero, 1977b, 1978). No evidence was found in *Cynolebias* spp. that the follicular cells are engaged in the production of extracellular material at this stage (Wourms, 1976).

The innermost, thickest layer of the primary envelope (Z3) in many teleosts develops an elegant, transitory, fibrillar structure, whose appearance in sections suggests "art nouveau arabesques" (Figure 2.61) (Wourms, 1976). The positioning of the pore canals at the centre of the ellipsoid curves of these arches may provide flexibility to withstand expansion of the egg as well as mechanical shocks (Figure 2.62) (Caporiccio and Connes, 1977).

The differences in electron density of the layers of the zona pellucida are likely due to differences in their composition: the outer, more electron-dense layer in *Oryzias latipes* is rich in polysaccharides while the inner layer contains a higher proportion of proteins (Tesoriero, 1977a). In the viviparous teleost *Xiphophorus helleri,* the zona pellucida is homogeneous and shows no layering; it attains a thickness of about 1.0 μm during vitellogenesis, regresses during maturation, and has disappeared before segmentation begins (Azevedo, 1974).

The zona pellucida of the cod is a hydrophobic protein aggregate consisting of three polypeptides, designated, α, β, and γ, with apparent molecular weights of 74, 54, and 47 kDa (Oppen-Berntsen, Helvik, and Walther, 1990). Two to four major proteins with molecular weights ranging from 45 to 130 kDa have been separated from the zona pellucida of other teleosts (Brivio, Bassi, and Cotelli, 1991; Hyllner et al., 1991); minor components with molecular weights ranging from 10 to 100 kDa were also present (Brivio, Bassi, and Cotelli, 1991). The presence of envelope proteins in the plasma of females rises dramatically as sexual maturation proceeds (Oppen-Berntsen et al., 1994) and has been induced in several species of teleosts by oestradiol-17β (Hyllner et al., 1991; Hyllner, Norberg, and Haux, 1994; Larsson, Hyllner, and Haux, 1994; Hyllner, Silversand and Haux, 1994). It has been suggested that these proteins, like vitellogenin, are produced in the liver (Hamazaki, Iuchi, and Tamagami, 1985, 1987; Hamazaki et al., 1989; Oppen-Berntsen, Gram-Jensen, and Walther, 1992). This suggestion is contrary to the conventional understanding of the formation of the teleostean primary envelope: that the constituents of the inner layer are synthesized by the oocyte itself. It is not known whether these proteins are incorporated into the oocyte and then secreted from it to form the inner layer of the zona pellucida, after receiving some molecular modification, or whether they go directly to the site of formation of the egg envelope without passing through the oocyte. Evidence supportive of the conventional view was found in developing oocytes of the pipefish *Syngnathus scovelli* where the proteins of the zona pellucida could not be traced to the liver and it was concluded that they originate within the follicle itself (Figure 2.63) (Begovac and Wallace, 1989).

By the time the oocyte transforms into a mature egg, the microvilli and pore canals are often lost (Figure 2.57D). The Z1 layer is retained throughout oocyte development to maturity, although it becomes much reduced as development progresses. The mature egg envelope (chorion) may retain a lamellar appearance. There is no degeneration of the outermost layer of the zona pellucida of the porgy *Pagras major* prior to maturation, however, nor are the surface pits remaining from the pore canals plugged (Figure 2.64) (Hosokawa, 1983). These pits may also be observed on the surface of the zona pellucida of the flounder and globefish but not on the surface of the medaka, ayu, trout, or salmon.

A simpler, thinner envelope is described in viviparous poeciliids than in oviparous species (Azevedo, 1974), perhaps permitting more intimacy between foetal and maternal circulations. In viviparous *Xiphophorus helleri,* the zona pellucida develops in much the same way as in oviparous forms but forms only a single layer. It reaches its maximum thickness of 1 μm by the end of vitellogenesis, then becomes thinner and almost completely disappears by the end of maturation (Figure 2.56). Microvilli from the oocyte penetrate the pore canals to form a mesh against the follicular cells. The follicular cells of poeciliids may be unique in lacking processes that penetrate the pore canals. The zona pellucida disappears during the first stages of segmentation.

Four distinct layers have been described in the zona pellucida of the white sturgeon *Acipenser transmontanus* where the innermost layer is closely apposed to the oolemma (Cherr and Clark, 1982). The inner two layers are fibrous with filamentous substructures and are similar to layers of the zona pellucida of teleost oocytes. Numerous filamentous, screwlike projections appear to anchor the second layer to the outer layers (Figure 2.65). Electrophoretic separation (SDS-PAGE) shows a range of proteins and glycoproteins in the envelopes (including the jelly coat) of molecular weights

from 21 to ca 300 kDa (Cherr and Clark, 1985). The most prominent band is a 70 kDa protein which resides in the outermost layer of the zona pellucida. After freshwater exposure, this layer contains both the 70 and a 66 kDa glycoprotein, presumably derived by proteolysis of the 70 kDa glycoprotein. This 66 kDa glycoprotein induces a species-specific acrosome reaction in spermatozoa of *A. transmontanus* but not of *A. fulvescens;* no inducer resides in the jelly coat.

A zona pellucida has been described in the developing follicle of a viviparous elasmobranch, the yellow spotted stingray *Urolophus jamaicensis* (Hamlett, Jezior, and Spieler, 1999). It is more delicate than the zona pellucida of teleosts and never becomes as structurally complex or rigid. There is no surface ornamentation and no micropyle. It is most likely a composite layer, being produced cooperatively by both the oocyte and follicular cells. Perforations containing processes from the follicular cells produce the typical striated appearance in sections but, unlike the condition in teleosts, there are no processes extending from the ovum. The processes extending from the follicular cells make contact with the oolemma, indent it, and even penetrate this membrane (Figure 2.66).

The primary envelope of the lamprey follicle is similar to those described for teleosts (Lewis and McMillan, 1965). The oocyte lays down a double, translucent, fibrous zona pellucida whose outer layer is more electron-dense than the inner (Busson-Mabillot, 1967a; Afzelius, Nicander, and Sjödén, 1968). The fibrils embedded within the zona pellucida form parallel sheets but do not attain the flamboyant patterns seen in teleosts. The zona pellucida is perforated by radial pore canals that contain microvilli extending through its entire thickness from the surface of the oocyte; although short microvilli extend toward the zona pellucida from the follicular cells, they do not appear to enter the pore canals. A complete sheath of squamous follicular cells encloses the oocyte of *Petromyzon marinus* (Yorke and McMillan, 1980) but, in *Lampetra planeri,* they form a cup that envelops only the basal portion of the oocyte (Busson-Mabillot, 1967b).

Resting oocytes, 1 to 2 mm in diameter, of the hagfish *Myxine glutinosa* appear to secrete a primary envelope, rich in polysaccharides, similar to the zona pellucida of other fish (Patzner, 1974, 1975). It is penetrated by microvilli extending from both the oocyte and the follicular cell. It attains its maximum thickness of about 6 μm in oocytes 5 to 8 mm in length and then becomes thinner. A unique feature of the hagfish follicle is its ability to secrete a "shell" around the oocyte: not merely a simple investment but one with a micropyle for sperm entry and, at each pole, a fan-like array of hooks (Dodd and Dodd, 1985).

2.3.2 SECONDARY ENVELOPES

The secondary envelope formed by the follicular cells before ovulation may consist of a simple jelly coat. In the perch *Perca fluviatilis* this layer becomes five times thicker than the zona pellucida and is traversed by cytoplasmic processes that extend from the follicular cells to penetrate the pore canals (Figure 2.67) (Flügel 1967a). Columnar follicular cells, containing electron-dense droplets, form a jelly coat and attachment disc surrounding the zona pellucida at the animal pole of maturing follicles of the African catfish *Clarias gariepinus* while cuboidal cells containing moderately electron-dense droplets form a jelly coat over the rest of the surface (Figure 2.68) (van den Hurk and Peute, 1985). All of these follicular cells contain abundant granular endoplasmic reticulum and a few small mitochondria with lamellar cristae.

In many species of teleosts, especially oviparous species, follicular cells may produce a secondary envelope that is often highly ornamented (Figure 2.69). The follicular cells may retain an unspecialized appearance during the early stages of primary envelope formation, lacking the features characteristic of cells engaged in protein synthesis and secretion but, as the oocyte grows, the number of follicular cells increases and their shape transforms from squamous to cuboidal (Wourms and Sheldon, 1976; Busson-Mabillot, 1977; Thiaw and Mattei, 1991). When deposition of the primary envelope is complete, the follicular cells become columnar, evince increasing amounts of granular endoplasmic reticulum, and begin to lay down a secondary envelope outside the primary envelope (Figure 2.70). Extensive intercellular spaces that become filled with fibrillar matrix develop between the follicular cells (Figure 2.71).

Ornamentation of the secondary envelope may take many forms and often appears to be shaped within the intercellular spaces of the follicular cells much as a mould imposes its design on a waffle. The ultrastructure of the material of this ornamentation has been described in several species as resembling masses of closely packed microtubules, 15 to 20 nm in diameter, often coated with an electron-dense gelatinous material (Tsukahara, 1971; Wourms and Sheldon, 1976;

Busson-Mabillot, 1977; Dumont and Brummett, 1980; Hart, Pietri, and Donovan, 1984). Vesicles of electron-dense material of a tubular nature appear in the follicular cells; the tubules resemble microtubules, being about 25 nm in diameter, and have been termed "microtubule mimics" (Wourms, 1976). The presence of these characteristic tubules has been used to establish the probable route of their intracellular transport (Figure 2.72) and it is concluded that they are synthesized in the granular endoplasmic reticulum of the follicular cells and transported, in vesicles, directly to the surface of the oocyte; the Golgi complex appears to play no part in this process (Wourms and Sheldon, 1976) (Figure 2.73).

The Golgi complex of follicular cells is involved, however, in the formation of the secondary envelope of the cyprinodont *Aphyosemion splendopleure* (Thiaw and Mattei, 1991). The secondary envelope in this species consists of two-layers: a thin homogeneous inner layer which adheres to the zona pellucida and a superficial layer formed of parallel microtubule-like elements, 25 nm in diameter, embedded in a homogeneous matrix (Figure 2.74). The superficial layer is studded with large swellings, 9 μm high, interspersed with greater numbers of smaller swellings (Figure 2.75). Amorphous material forms in the cisternae of the abundant basal granular endoplasmic reticulum whose elements fragment into vesicles limited by a membrane covered with ribosomes (Figure 2.76). At the end of vitellogenesis, large intercellular spaces form between adjacent columnar follicular cells (Figure 2.77) and vesicles, originating in the apical Golgi complex, release their contents onto the surface by exocytosis (Figure 2.78). The respective contributions of the granular endoplasmic reticulum and apical Golgi complex to the various components of the secondary envelope are not clear; perhaps the amorphous material from the granular endoplasmic reticulum is processed in the Golgi complex and released by exocytosis onto the surfaces of the follicular cells where it is moulded by the intercellular spaces to ornament the secondary envelope.

In the cichlid *Cichlasoma fasciata* and other teleost fish, the adhesive apparatus that fixes spawned eggs to the substrate is composed of two distinct elements: an amorphous mucous jelly coat that is permeated by filaments connected to the surface of the zona pellucida (Figure 2.79) (Busson-Mabillot, 1977). The filaments consist of bundles of microtubule mimics (Figure 2.80) and are the first component of the adhesive coat to be elaborated, forming outside the zona pellucida at the first signs of secretory activity in the follicular cells (Figures 2.81 to 2.83). The granular endoplasmic reticulum of the follicular cells appears to be active in the production of the filaments. The adhesive filaments elongate at the beginning of vitellogenesis when intercellular spaces open between the follicular cells. Production of the jelly coat is described as an apocrine secretion of the follicular cells, where the mucous material, packed within cisternae of the granular endoplasmic reticulum, is released by rupture of the apical portion of the cell. Only a small portion of the cytoplasm is released, however, and most organelles, especially the empty cisternae of the endoplasmic reticulum and mitochondria, are retained within the cell after the expulsion of the secretory products. The Golgi complex appears to play no role in the secretion of either component of the mucous coat.

The developing secondary envelope of *Fundulus heteroclitus* is seen as bundles of electron-dense fibres that weave their way over the surface of the zona pellucida, coursing through the wide intercellular spaces between the follicular cells (Kuchnow and Scott, 1977; Dumont and Brummett, 1980). In *Cynolebias* spp., the follicular cells mould the microtubule mimics into a thistle-like secondary envelope of projecting spikes (Figure 2.69) (Wourms and Sheldon, 1976). These cells sculpt an elaborate arrangement of polygonal compartments over the zona pellucida of eggs of the sole *Pleuronichthys coenosus* (Figure 2.84) (Stehr and Hawkes, 1983). Since the follicular cells are polygonal, it is suggested that deposition of envelope material at their lateral margins produces this pattern (Figure 2.85). During formation of the envelope, the chambers enclosed by these partitions contain masses of oocyte microvilli extending across a large subfollicular space to touch the stubby microvilli of the follicular cells and even the follicular cells themselves. As the partitions become well developed, "floors", with a subpattern of hexagonal ridges, are laid down between them, covering the primary envelope (Figure 2.86), each hexagon encircling an oocyte microvillus (Figure 2.87B). These hexagonal patterns appear sporadically on eggs of other species in the subfamily Pleuronectinae (Hirai, 1993) and have been noted on eggs in such diverse families as Synodontidae, Callionymidae, and Uranoscopidae (Mito, 1963; Ikeda and Mito, 1988, cited by Hirai, 1993). Their functional significance is obscure.

Follicular cells produce two types of secondary en-

velope on the surface of the lamprey egg (Figure 2.88). Columnar follicular cells at the animal pole mould a gelatinous APICAL TUFT (Lewis and McMillan, 1965; Yorke and McMillan, 1980) that attracts spermatozoa during spawning (Kille, 1960). A radical breakdown of follicular cells over the basal two-thirds of the egg leaves an elaborate cup-shaped ADHESIVE COAT that serves to affix the egg to the substrate in an appropriate position to present its apical tuft for the attentions of passing spermatozoa.

The leathery CAPSULE of the egg of the hagfish *Myxine glutinosa* is presumably secreted by the follicular epithelium. Formation begins at the end of the growth period and the first accumulations occur at the poles (Patzner, 1975). Later these caps grow until they have surrounded the entire egg and, when the egg is enclosed, tufts of ANCHOR FILAMENTS, bearing hooks at their ends (Figure 2.89), are said to be secreted and moulded by sleeve-like extensions of the follicular epithelium (Lyngnes, 1930; Walvig, 1963; Koch et al., 1993). The animal pole always displays more anchor filaments than the vegetal pole (Figure 2.90). The upper side of the anchor filaments appears rough and grooved in scanning electron micrographs while the underside is smooth. A cluster of about eight anchor filaments, radiating from the distal ridge of a MICROPYLAR FUNNEL, surrounds the micropyle of *Eptatretus burgeri* (Figure 2.91) (Fernholm, 1975; Koch et al., 1993). The floor of this funnel forms a honeycomb pattern of which a single "honeycomb cell" at the centre opens to the interior. The capsule of *Myxine glutinosa* attains a thickness of 150 μm and appears homogeneous in electron micrographs (Walvig, 1963). An intercellular space of about 15 μm intervenes between the capsule and the follicular epithelium. This epithelium is simple squamous at first but, as development continues, the cells become taller, eventually becoming columnar. Encircling the egg, about one-fifth of the distance from the animal pole, the follicular epithelium forms a ring of stratified cells in the position to be occupied in the mature egg by a suture, the OPERCULAR RING (this suture later splits, providing escape for the young hagfish of 4 to 5 cm) (Figure 2.90).

2.4 Follicular Epithelium

As the oogonium begins meiotic division and transforms into an oocyte, it becomes enveloped by a thin epithelium of squamous cells and a new follicle is produced. The earliest stages of this investment have been demonstrated in the germinal ridge of the pipefish where PREFOLLICULAR CELLS (presumably derived from the luminal epithelium) extend processes between contiguous meiotic oocytes, eventually forming a simple squamous epithelium of FOLLICULAR CELLS around each oocyte (Figure 2.92) (Begovac and Wallace, 1987). The follicular cells, enclosed within their own basal laminae, form a continuous epithelium that isolates the oocytes from one another. Desmosomes, already established between the processes of the prefollicular cells, persist in the follicular epithelium.

Oogonia and oocytes of the common snook *Centropomus undecimalis* are dispersed among the somatic cells of the gonadal (germinal) epithelium that lines the ovarian lumen (Figure 1.3) (Grier, 2000). At the outset of folliculogenesis, some oogonia begin to divide by meiosis to produce oocytes. These oocytes descend into the deeper, basal regions of the epithelium where they become enveloped by processes from some of the epithelial cells (Figure 1.28). The oocyte, surrounded by its simple layer of these prefollicular cells, presses on the basement membrane of the gonadal epithelium, evaginating it and eventually causing the pinching off of a discrete follicle consisting of the oocyte surrounded by its layer of epithelial cells and enclosed in a basement membrane derived from the basement membrane of the gonadal epithelium. Folliculogenesis is concluded when the basement membrane completely encloses the epithelium; at this time this is referred to as the follicular epithelium.

Several functions have been ascribed to follicular cells; these vary from species to species, reflecting the spectrum of reproductive strategies exploited by fish. It has been suggested that follicular cells are nutritive, assisting in the uptake of materials by the oocyte, that they produce the secondary envelope, that they are steroidogenic, and that they assist in the expulsion of the egg during ovulation. Since these functions occur at different times during follicular development and, since not all may be represented in some species, there is temporal and interspecific variation in their ultrastructural expression. Follicular cells of fish are often referred to as "granulosa cells", implying a homology with the oestrogen-secreting cells surrounding the oocytes of mammals; this term has been avoided in the present work in favour of the non-committal designation "follicular cells".

In the earliest stages of oocyte development in teleosts, the follicular epithelium is still simple squamous (Flügel, 1964b; Hirose, 1972; Nicholls and Maple,

1972; Patzner, 1974; Busson-Mabillot, 1977; Caporiccio and Connes, 1977; Tsuneki and Gorbman, 1977; Bruslé, 1980; Nakashima and Iwamatsu, 1989). The cells contain a flattened nucleus and little cytoplasm (Figure 2.58); interdigitating junctions between them are reinforced by desmosomes anchored securely in the cytoplasm by bundles of tonofilaments (Figure 2.93). The epithelium is surrounded by its BASEMENT MEMBRANE which separates it from the vascular connective tissue of the theca. Few organelles are present within the follicular cells: occasional mitochondria, a small Golgi complex of two to four lamellae, polyribosomes, and small, isolated cisternae of granular endoplasmic reticulum.

The follicular epithelium of small follicles of elasmobranchs is a single squamous or cuboidal layer surrounded by its basement membrane (Figures 2.94 and 2.95) (Callard et al., 1989; Andreuccetti et al., 1999; Hamlett, Jezior, and Spieler, 1999). Interspersed among the squamous follicular cells of some species are enlarged, lipid-like cells of uncertain function (Figures 2.96 and 2.97). As the oocyte grows, the squamous follicular cells become cuboidal or columnar; mitotic proliferation increases their numbers and the layer becomes stratified (Figure 2.98). The large, round cells increase greatly in size during early development of the follicle and display a round nucleus and essentially "empty" cytoplasm; as folliculogenesis continues, they decrease in size and number and disappear prior to ovulation. Microvilli from the oocyte extend toward, and may touch, the follicular cells across the intervening space; these intermingle with a smaller number of microvilli from the follicular cells. Subsequently the amorphous, gel-like ZONA PELLUCIDA forms between the oocyte and follicular cells, embedding the microvilli within PORE CANALS. In the stingray, no processes extend from the oocyte although long processes from the follicular cells penetrate the zona pellucida to produce the typical striated appearance seen in sections (Hamlett, Jezior, and Spieler, 1999).

Three types of cells have been identified in the stratified follicular epithelium of *Raya asterias:* small, large, and pyriform (Andreuccetti et al., 1999). The small cells divide rapidly by mitosis, giving rise to pyriform cells by way of the large cells. The large cells have a large nucleus with dispersed chromatin and a prominent nucleolus; their abundant cytoplasm contains vesicles, mitochondria, lipid droplets, and masses of glycogen (Figure 2.99). The numbers of these organelles, especially mitochondria, increase as the cells transform into pyriform cells (Figure 2.100). The pyriform cells span the follicular epithelium from the basal lamina to the surface of the oocyte. Early in folliculogenesis, small surface protrusions from the follicular cells fuse with the oolemma at desmosome-like junctions (Figure 2.95B). As the perivitelline space enlarges, these junctions persist, thereby drawing out protrusions from the follicular cells (Figure 2.98). Eventually cytoplasmic continuity is established between the follicular cells and oocyte and true intercellular bridges are formed (Figure 2.101). These bridges may be 1 μm wide and up to 25 μm long. They contain mitochondria, ribosomes, whorls of membranes, and vesicles. The intercellular bridges disappear with the thickening and completion of the zona pellucida, leaving a few slender microvilli within this electron-dense layer. At the onset of viteollogenesis the cytoplasmic bridges are lost, the follicular epithelium undergoes regression and is once again composed of a few layers of small cells and scattered large cells.

"Rudimentary desmosomes" are described between follicular cells and the oocyte of the sea bass *Dicentrarchus labrax* before the homogeneous, electron-dense material of the zona pellucida is laid down (Figure 2.102A) (Caporiccio and Connes, 1977). As the zona pellucida thickens, these desmosomes maintain their contact between the microvilli within the pore canals (Figures 2.62 and 2.102B). In addition, well developed desmosomes link adjacent cells of the follicular epithelium (Figure 2.102C). Desmosomes have been reported between adjacent follicular cells of some species (Flügel, 1964b; Iwamatsu et al, 1988). Early in vitellogenesis, follicular cells of the medaka *Oryzias latipes* are joined by desmosomes to which bundles of tonofilaments are anchored (Figure 2.93) (Nakashima and Iwamatsu, 1989).

Other junctional types have also been reported in the follicular epithelium. Tight junctions between follicular cells of the ayu *Plecoglossus altivelus* constitute a moderately leaky blood-follicular barrier preventing access by many materials to the oocyte (Toshimori and Yasuzumi, 1979a). Tight junctions between follicular cells of the zebrafish *Brachydanio rerio* become less elaborate and "leakier" as oogenesis proceeds (Kessel, Roberts, and Tung, 1988). They appear to become dismantled during active vitellogenesis permitting the passage of yolk proteins derived from the blood vessels and their uptake by the oocyte by micropinocytosis (Figure 2.103).

There is extensive amplification of contacts between

oocyte microvilli and follicular cells of the zebrafish *Brachydanio rerio,* enhancing conditions for the establishment of gap junctions (Kessel et al., 1985). Processes from the follicular cells are usually wider and sparser than those from the oocyte but often do not reach the surface of the oocyte whereas microvilli from the oocyte make ample contact with follicular microvilli as well as with the surfaces of the follicular cells, often flattening themselves against the plasmalemma and growing for some distance along the surface (Figure 2.104). There is an intimate relationship between microvilli from the oocyte and follicular cells as they extend in opposite directions through the pore canals of the zona pellucida (Figure 2.105). Oocyte microvilli contain ample bundles of microfilaments (Figure 2.106) which may assist in their elongation through the pore canals. Gap junctions form between the oocyte microvilli and the surfaces of the follicular cells, often occurring near the bases of follicular cell processes (Figures 2.107 to 2.109). The oocyte microvilli may branch as they approach the surface of the follicular cells, thereby increasing membrane contact and augmenting the formation of gap junctions. Moreover, the branches continue to parallel the plasma membranes of the follicular cells for varying distances. Distal ends of the microvilli may invaginate the surface of the follicular cells and often insinuate themselves into the interstices between them. Some gap junctions also occur between the tips of oocyte microvilli and the bases of the follicular microvilli. No gap junctions were observed between the distal regions of follicular cell microvilli and more proximal regions of the oocyte microvilli.

Gap junctions between follicular cells and microvilli from the oocyte have also been reported in *Plecoglossus altivelus,* the chum salmon *Oncorhynchus keta,* and *Oryzias latipes* (Figure 2.110) (Toshimori and Yasuzumi, 1979b; Kobayashi, 1985b; Iwamatsu et al., 1988). Fluctuating numbers of gap junctional contacts occur between oocyte microvilli and follicular cells (heterocellular contacts) as well as between adjacent follicular cells (homocellular contacts) during follicular development and maturation in the Atlantic croaker *Micropogonias undulatus* (York, Patiño, and Thomas, 1993). There are high levels of these associations during vitellogenesis, low levels after completion of vitellogenesis, and a return to high levels during early maturation and hydration of the oocytes. These variations seem to result from alterations in the length of the oocyte microvilli and their surface contact with follicular cells rather than to changes in the numbers of microvilli. Numbers of contacts decline again as maturation is completed and ovulation approaches. It is suggested that this intercellular association and gap junctional communication may facilitate the transfer of maturation inducing steroid (MIS) from follicular cells to the oocytes, as well as factors necessary for normal embryonic development, and of ions, such as potassium, that support oocyte hydration.

Two types of associations are described between processes from follicular cells and the surface of the oocyte (Kobayashi, 1985b). In the commoner type, the expanded end of a process terminates in a slight depression of the oolemma (Figure 2.111). The apposing plasma membranes are separated by a space of 10 to 20 nm which diminishes to less than 5 nm in places where the occurrence of gap junctions is suspected (Figure 2.111B). The expanded ends of these processes show endocytotic activity (Figure 2.111C). The formation of coated vesicles in the oolemma in these regions (Figure 2.111D) hints at the transfer of materials from the follicular cells to the oocyte. In rarer associations, follicular cell processes fit deeply into indentations of the oolemma; the interspace is about 20 nm and desmosomes (or desmosome-like junctions) occur in some areas while, in others, coated invaginations of the oolemma are seen (Figure 2.112). In these junctions, no exocytotic activity is seen in the processes from the follicular cells.

As the oocyte enlarges, new follicular cells are produced and the follicular epithelium thickens so that, in late vitellogenesis, it may appear cuboidal or columnar. Although a multilayered follicular epithelium has been described in the ovary of the hagfish *Myxine glutinosa* (Patzner, 1975) and in immature follicles of the dogfish *Scyliorhinus canicula,* it forms a single layer in maturing follicles of the dogfish (Figure 2.96) (Dodd, 1983), and is a simple epithelium in lampreys and teleosts throughout development (Figures 2.61 and 2.70). Mitochondria and ribosomes increase in numbers and the Golgi complex proliferates from a simple stack of lamellae into a complex system of tubules and spherical vesicles, both smooth and coated (Nicholls and Maple, 1972; Wourms, 1976; Wourms and Sheldon, 1976; Nagahama, Chan, and Hoar, 1976; Nagahama, Clarke, and Hoar, 1978). Occasional centrioles appear between the Golgi complex and the nucleus. As the Golgi complex develops, the amount of granular endoplasmic reticulum increases greatly in amount. Near

the time of ovulation, the microvilli withdraw from the zona pellucida and the follicular cells shrink.

Follicular cells may assist in the passage of materials into the oocyte. The question is often asked as to whether materials pass to the oocyte by way of spaces between the follicular cells or are transported through the follicular cells themselves. This uptake would find its maximal expression during vitellogenesis when most rapid enlargement of the oocyte is occurring. Occluding junctions, of five to seven strands, demonstrated between the follicular cells of the ayu *Plecoglossus altivelis,* imply the presence of a blood-follicular barrier of "intermediate leakiness" that would prevent extensive intercellular passage of materials, thereby causing them to pass through the follicular cells (Toshimori and Yasuzumi, 1979a) (Figure 2.113). The presence of gap junctions between microvilli of vitellogenic oocytes and follicular cells of the ayu (Figure 2.114) (Toshimori and Yasuzumi, 1979b) suggests the passage of small molecules through channels connecting these cells. In red seabream *Pagrus major* there is a positive association between the acquisition of maturational competence and increased levels of gap junctions, not only between oocyte microvilli and follicular cells but also between adjacent follicular cells themselves (Patiño and Kagawa, 1999). Coated invaginations of the oolemma, about 150 nm in diameter, may indicate the uptake of exogenous nutrients by endocytosis in the preovulatory oocyte of the chum salmon *Oncorhynchus keta* (Figures 2.111D and 2.112B) (Kobayashi, 1985b).

On the other hand, evidence of intercellular passage at various stages of folliculogenesis was obtained by injecting the electron-opaque tracer horseradish peroxidase into the bloodstream of several species of fish (Abraham et al., 1984; Parmentier, van den Boogaart, and Timmermans, 1985). The marker was first detected in the pericapillary spaces of the ovarian stroma and from there, successively, in the collagen spaces surrounding the follicular epithelium, between the follicular cells, alongside the microvilli within the pore canals of the zona pellucida, on the surface of the oocyte beneath the zona pellucida and, finally, within pinocytotic vesicles in the oocyte (Figure 2.115) (Abraham et al., 1984). Although the molecules of horseradish peroxidase and the yolk precursor, vitellogenin, differ in many respects, it is suggested that this represents the pathway of vitellogenin uptake by oocytes. It also appears that microvilli penetrating the zona pellucida do not transmit the tracer but are bathed by it as it passes alongside them through the glycocalyx to the oocyte surface. The fact that the tracer bypassed the follicular cells suggests that vitellogenins are not taken up by them, belying the long-held belief that these cells are nutritive. It cannot be ruled out, however, that follicular cells synthesize some proteins that are taken up by the oocyte.

During early vitellogenesis in the stingray, transfer of materials between follicular cells and the oocyte is probably enhanced by increases in the surface area provided by indentations of the oolemma by large folds of the zona pellucida and follicular epithelium that enclose richly vascular connective tissue and thecal cells (Figure 2.116) (Hamlett, Jezior, and Spieler, 1999). The large, round, lipid-like cells of the follicular epithelium are carried in with these folds and, since they disappear before ovulation, it has been speculated that they fulfill a nutritive function. As vitellogenesis proceeds, the columnar follicular cells become engorged with transport vesicles and lipid droplets (Figures 2.97 and 2.117). At this time, processes from the follicular cells extend through the zona pellucida, invaginate the oolemma (Figure 2.118), and become pinched off within the ooplasm as discrete vesicles called TRANSOSOMES (Figure 2.66). The processes develop a thickened plaque of ribosomal nature where they invaginate the oolemma and these plaques persist within the transosomes. The production of transosomes appears to be related to the accumulation of large amounts of yolk in telolecithal eggs but the mechanisms by which follicles sequester yolk are still unclear.

A nutritive function has been ascribed to the intercellular bridges that are established between the follicular cells and oocyte of previtellogenic follicles of the elasmobranch *Raya asterias* (Figures 2.101 and 2.119) (Andreuccetti et al., 1999). The bridges may be 1 μm wide and up to 25 μm long. They contain mitochondria, ribosomes, whorls of membranes, and vesicles. It is suggested that the follicular cells act as "nurse cells" during the previtellogenic phase, transferring cytoplasmic components, such as RNAs and cytoplasmic organelles, to the oocyte by way of these bridges. The intercellular bridges disappear with the thickening and completion of the zona pellucida, leaving a few slender microvilli within this electron-dense layer.

In the lamprey *Petromyzon marinus,* the follicular epithelium surrounding the oocyte forms a complete and continuous layer within the follicle (Figure 2.120) (Yorke and McMillan, 1980). Prior to events leading

to ovulation, this is a simple squamous epithelium of stellate cells with wide gaps between; these spaces are spanned by cytoplasmic processes from neighbouring follicular cells. The follicular cells contain abundant granular and agranular endoplasmic reticulum, Golgi complexes, and free ribosomes; lipids may also be present. Follicular cells make an unusual contribution to the formation of yolk in the lamprey *Petromyzon marinus* (Lewis and McMillan, 1965). During vitellogenesis, while yolk is being formed within the oocyte, additional yolk is accumulated within the cytoplasm of some follicular cells. These "nurse cells" are subsequently incorporated into the oocyte, thereby increasing its mass and content of yolk (Figures 2.121A,B). In this fusion, the nurse cell loses its nucleus. The outer plasmalemma of the nurse cell becomes a portion of the oolemma; remnants of the intervening membranes of the two cells persist for some time within the newly constituted oocyte (Figure 2.121C).

The role of follicular cells in the formation of a secondary envelope around the zona pellucia of the egg has been established in several species (Wourms and Sheldon, 1976; Busson-Mabillot, 1977; Hart, Pietri, and Donovan, 1984). After vitellogenesis is complete, the follicular cells may give evidence of their involvement by assuming the characteristics of active protein production: abundant granular endoplasmic reticulum and electron-dense secretory vesicles. As the oocyte grows, the number of follicular cells increases and they transform from squamous to cuboidal. When deposition of the primary envelope is complete, the follicular cells become columnar and may begin to secrete a secondary envelope outside the primary envelope. The secondary envelope of many species is formed of closely packed microtubule-like material, the "microtubule mimics" (Wourms, 1976), that can be exploited as a naturally occurring marker to trace its route of transport from vesicles in the follicular cells (Figure 2.72), to the intercellular spaces, and to the secondary envelope (Wourms and Sheldon, 1976). It is concluded that the tubules making up the secondary envelope are synthesized and assembled in the granular endoplasmic reticulum of the follicular cells and extruded by exocytosis (Figure 2.73). The Golgi complex does not appear to take part in this process in some species; in the cyprinodont *Aphysemion splendopleure,* however, large vesicles originating in the apical Golgi complex are released by exocytosis onto the surface of the zona pellucida to form the secondary envelope (Thiaw and Mattei, 1991). Since not all eggs are enclosed by a secondary envelope and since there are great variations in its intricacy, there is a wide range, from species to species, in the participation of follicular cells in the production of the secondary envelope and a wide range in their morphological expression of protein production.

An unusual method of formation of the secondary envelope is seen in the sheatfish *Silurus glanis.* During early vitellogenesis, the follicular cells proliferate to form an irregular mass of cells around the zona pellucida (Figure 2.122A) (Abraham et al., 1993). These cells contain abundant granular endoplasmic reticulum and Golgi complexes and, as development proceeds, they synthesize large numbers of membrane-bound mucous droplets in their interior (Figure 2.122B). During vitellogenesis their epithelial organization is disrupted, the organelles fragment, and the cells are transformed into an irregular mass of "mucosomes" which, on contact with water following oviposition, swells to form an adhesive coat of mucopolysaccharides and mucoproteins that causes the eggs to adhere to the nest wall and to each other.

Follicular cells of lampreys produce a secondary envelope that consists of two parts: a fluffy, fibrous APICAL TUFT and, embellishing the basal two-thirds of the oocyte, a cup-shaped ADHESIVE COAT consisting of broken-down remnants of enlarged follicular cells (Figure 2.88) (Larsen, 1970; Yorke and McMillan, 1979). These areas are separated by an expanse of naked chorion. A few months before ovulation, there is a dramatic enlargement of some of the follicular cells surrounding the basal two-thirds of the oocyte (Larsen, 1970). These huge, cuboidal ADHESIVE CELLS become packed with irregular, swollen interconnected saccules containing flocculent material of varying electron density that may be derived from the Golgi complex or agranular endoplasmic reticulum (Figure 2.123) (Busson-Mabillot, 1967b; Yorke and McMillan, 1979). The adhesive cells also contain abundant granular endoplasmic reticulum and mitochondria; the nucleus is basal while Golgi complexes and smooth endoplasmic reticulum are apical, lying under the plasmalemma that is adjacent to the zona pellucida. Just before ovulation, as vacuoles appear within them, the adhesive cells begin to break down; their distended saccules, however, retain their integrity. As the egg is expelled from the follicle during ovulation, these adhesive saccules remain firmly affixed to the zona pellucida of the basal two-thirds of the egg, forming a secondary coat that will adhere to just about any surface, holding aloft the apical pole for the attentions

of passing spermatozoa (Figure 2.124). It is suggested that adhesion of ovulated eggs within the coelom is inhibited by the presence of proteins in the coelomic fluid that are rinsed off immediately after oviposition.

Cells synthesizing steroids may be identified by histochemical tests for the presence of enzymes involved in steroid biosynthesis, such as Δ^5-3β-hydroxysteroid dehydrogenase (3β-HSD), a key enzyme that catalyses the conversion of pregnenolone to progesterone and dehydroepiandrosterone to androstendione (Smith and Haley, 1987). Activity of this enzyme has been shown in follicular cells of many species, usually during vitellogenesis (Lambert, 1970a; Livni, 1971; Yaron, 1971; Iwasaki, 1973; Bara, 1974; Tang, Lofts, and Chan, 1974; van den Hurk and Peute, 1979). Follicular cells of the loach *Misgurnus fossilis* reacted weakly from vitellogenesis to spawning, but the micropylar cells (which are highly specialized follicular cells) displayed a strong reaction throughout the year (Ohta and Teranishi, 1982). In the goldfish, *Carassius auratus,* the enzyme was detected during follicular development but disappeared during vitellogenesis (Khoo, 1975). No 3β-HSD activity was noted in preovulatory follicular cells of several salmonids or the goldfish (Hoar and Nagahama, 1978; Nagahama, Clarke, and Hoar, 1978; Kagawa, Takano, and Nagahama, 1981). In another sort of histochemical test, labelled antisera have demonstrated the presence of 17β-oestradiol in preovulatory follicular cells of *Salmo gairdneri* (Schulz, 1986).

In the face of evidence that follicular cells are steroidogenic, at least in some species, it is a paradox that they reveal little ultrastructural evidence of this activity, such as abundant agranular endoplasmic reticulum, tubular mitochondrial cristae, or lipid droplets, but appear to be engaged in active protein production (Tsuneki and Gorbman, 1977; Hoar and Nagahama, 1978; van den Hurk and Peute, 1979; Kagawa et al, 1982; Ohta and Teranishi, 1982; Nagahama, Kagawa, and Young, 1982; Nakamura, Specker, and Nagahama, 1993). For example, in two species of salmon, *Oncorhynchus kisutch* and *O. gorbuscha,* the follicular cells of preovulatory follicles demonstrated extensive granular endoplasmic reticulum containing amorphous material of variable electron density (Figure 2.125A) (Nagahama, Clarke, and Hoar, 1978). However, since a small amount of tubular agranular endoplasmic reticulum *was* present, especially within the well-developed Golgi fields, and tubular cristae occurred in *some* mitochondria, the possible involvement of the follicular cells in steroid production cannot be excluded. During vitellogenesis, follicular cells of the medaka *Oryzias latipes* contain abundant granular endoplasmic reticulum and mitochondria with lamellar cristae; just before ovulation, the cisternae of the endoplasmic reticulum become dilated and tubular cristae appear within the mitochondria (Figure 2.126) (Kagawa and Takano, 1979; Iwamatsu et al., 1988; Nakashima and Iwamatsu, 1989). Similar observations were recorded during oocyte maturation in *Fundulus heteroclitus* where the proliferation of enormous Golgi complexes was accompanied by an increase in agranular endoplasmic reticulum and a decrease in both free ribosomes and granular endoplasmic reticulum (Wallace and Selman, 1980).

Follicular cells of some species have been shown to have a mechanical function during ovulation, applying a gentle, steady constriction that extrudes the egg from the follicle (Figure 2.127) (Yorke and McMillan, 1980). This topic will be considered more fully in the section on *Ovulation* (page 209).

2.5 Theca and the Ovarian Stroma

Peritoneal cells, continuous with those lining the coelom, form a simple squamous mesothelium that covers the ovary and, in hollow ovaries, lines the lumen. In the salmon *Oncorhynchus* spp., the lateral plasma membranes of these cells are heavily convoluted and joined by tight junctions and desmosomes (Nagahama, Clarke, and Hoar, 1978). Both granular and agranular endoplasmic reticulum are present within the mesothelial cells as well as small mitochondria, microfilaments, and free ribosomes. Micropinocytotic vesicles occur frequently at both apical and basal surfaces. Tight junctions and gap (communicating) junctions are described between the mesothelial cells of the ovary of the zebrafish *Brachydanio rerio* (Figure 2.128A) (Kessel, Roberts, and Tung, 1988). The tight junctions exhibit many discontinuities indicating that they may reinforce the epithelium as well as serving their occluding function. Freeze fracture shows the presence of many micropinocytic pits in these squamous cells (Figures 2.128B,C), perhaps indicating that micropinocytosis occurs under certain conditions.

Below this visceral peritoneum, there may be a capsule, the TUNICA ALBUGINEA, consisting of connective tissue, smooth muscle, and occasional non-myelinated nerve fibres (Figure 2.129). In the tubular ovary of the pipefish *Syngnathus scovelli,* several circumferential

smooth muscle layers, separated by loose fibrous connective tissue, lie internal to the coelomic epithelium, perpendicular to the longitudinal axis of the ovary (Figure 1.41C) (Begovac and Wallace, 1987). It is suggested that egg release may be controlled by a contraction wave of the ovarian wall, coordinated by large bundles of non-myelinated nerves coursing between the muscle fibres, that begins cranially and proceeds in a caudal direction, squeezing the eggs from the ovarian lumen.

The capsule encloses a STROMA of richly vascular loose fibrous connective tissue that invests the developing follicles (Figure 2.130). Some stromal fibroblasts flatten themselves around the basement membrane of the follicular epithelium to form a thin layer of cells, the FOLLICULAR THECA. As the follicles grow and distend the surface of the ovary, the stroma separating the theca and mesothelium may become extremely attenuated (Figure 2.131A) and, where two follicles abut, the stroma may be excluded so that a single theca is shared between them (Figure 2.131B) (Begovac and Wallace, 1987).

In the ovary of the pipefish, arterioles arising near the ovarian wall carry blood to capillaries and veins near the luminal epithelium, bathing the follicles with blood nutrients and plasma proteins (most notably vitellogenin) (Begovac and Wallace, 1987). A significant portion of the stroma of the pipefish ovary contains an extensive lymphatic compartment lined by attenuated endothelial cells loosely linked by desmosomes (Figure 2.132). This lymphatic network is described as a "sea" in which developing follicles reside; its significance is unclear.

Each follicle in the ovary of *Fundulus heteroclitus* is vascularized by an arteriole that arrives within a stalklike structure of stromal elements (Figure 1.33) (Brummett, Dumont, and Larkin, 1982). Abundant collagen, irregularly arranged smooth muscle cells, and occasional nerve fibres constitute the remainder of the stalk. The stalk is enveloped by an epithelioid layer of stromal cells. Branches of the arteriole penetrate deeply into the investing layers of the follicle, bringing blood to a capillary bed that is drained by more superficial venules; these flow into a ring-like vessel surrounding the presumed ovulation site of the follicle. This system of vessels terminates in a single collecting vein that leaves the follicle and courses toward the outer surface of the ovary. Endothelial cells of the follicular capillaries of the zebrafish *Brachydanio rerio* are connected by tight junctions and active micropinocytosis riddles their surfaces (Figure 2.133) (Kessel, Roberts, and Tung, 1988). The tight junctions are not extensively developed and their particles adhere preferentially to the E face; they are closely associated with gap (communicating) junctions. It is assumed that there is a selective channeling of materials across the endothelial cells by way of microvesicles.

The theca first appears during previtellogenesis when a few thin cells resembling fibroblasts surround the basement membrane of the follicular epithelium (Figure 2.134) (Busson-Mabillot, 1967b; Ulrich, 1969; Caporiccio and Connes, 1977; Bruslé, 1985; Begovac and Wallace, 1987; Grier, 2000). The thecal cells multiply and increase in thickness during vitellogenesis; collagenous fibres, continuous with fibres in the basement membrane, course between them (Figure 2.135) (Caporiccio and Connes, 1977). In some species, a single layer of squamous cells may persist throughout oogenesis but, in others, several layers of cells appear, sometimes forming two distinct layers, the theca interna and theca externa.

In addition to forming a protective capsule around the follicle, various other functions have been ascribed to the theca. It is the first barrier between the extravascular spaces and the follicular epithelium and may exert some level of selectivity on the materials permitted to enter and leave the follicle. In some species, thecal cells give evidence of being steroidogenic, assuming an endocrine role. As well, the theca may contain smooth muscle and is presumed to assist in the expulsion of the egg during ovulation.

The theca of small follicles of *Myxine glutinosa* consists of poorly differentiated cells, probably fibroblasts, in a connective tissue matrix (Figure 2.136) (Patzner, 1975; Tsuneki and Gorbman, 1977). At later stages, however, two thecal layers can be distinguished consisting of poorly differentiated fibroblast-like cells and cells that are possibly secretory (Figure 2.137). The fibroblasts have a conspicuous granular endoplasmic reticulum and large lipid-like inclusions (Fernholm, 1972). No cells of an apparently steroidogenic nature were found.

In early stages of thecal development in the lamprey *Lampetra planeri,* loose fibrous connective tissue of the stroma encloses the follicles; it contains occasional nerve fibres and blood vessels applied to the basal laminae of the follicular epithelium (Busson-Mabillot, 1967b). During previtellogenesis this simple connective tissue layer differentiates into a theca externa and

theca interna. The connective tissue of the early follicle perisists throughout follicular development as the theca externa. Granular endoplasmic reticulum, Golgi complexes, and large lipid droplets appear in the cells of the theca interna during previtellogenesis but, as vitellogenesis gains momentum, the thecal cells enlarge and these organelles diminish as the cells become packed with granular endoplasmic reticulum (Figures 2.138 and 2.139). Large spaces appear between the cells of the theca interna across which the cells extend slender processes. It is suggested that the cells of the theca interna secrete steroids.

In some elasmobranchs (e.g., *Scyliorhinus sorrakowah)* the theca externa is made up of fibroblasts embedded in vascular fibrous connective tissue while the theca interna consists of polyhedral cells containing lipid droplets (Callard et al., 1989). The reverse is true in other species (e.g., *Scyliorhinus canicula)* where the theca interna is fibroblastic and the theca externa contains cuboidal cells manifesting agranular endoplasmic reticulum, mitochondria with tubular cristae, and lipid droplets (Dodd and Dodd, 1980); these cells appear to be steroidogenic.

The theca of immature follicles of two cichlids, *Cichlasoma nigrofasciatum* and *Haplochromis multicolor,* is poorly vascularized; as the follicle develops, the vascularization of the theca increases (Nicholls and Maple, 1972). Endothelial cells of the capillaries demonstrate active pinocytosis, indicating transfer to or from the blood stream. The thecal cells are apparently derived from fibroblasts. During primary oocyte growth, they form a simple squamous layer of cells around the basement membrane of the follicular epithelium. These cells are extremely thin and contain few organelles. As development proceeds, their height increases but their organelles are little changed: isolated cisternae of granular endoplasmic reticulum, occasional mitochondria, and free polyribosomes. During vitellogenesis, however, a few thecal cells, usually those lying close to capillaries, transform into typical steroidogenic elements. The cytoplasm of these large, rounded cells is filled with agranular endoplasmic reticulum and the mitochondria appear to have tubular cristae.

Evidence of steroidogenesis may appear in thecal cells of teleosts during development of the follicle of some species. Activity of the enzyme 3β-hydroxysteroid dehydrogenase (3β-HSD) has often been detected and the cells may manifest the familiar appearance of steroidogenic cells: abundant agranular endoplasmic reticulum and mitochondria packed with tubular cristae. These observations are far from consistent so that, in some species, the thecal cells give no hint of steroidogenic activity while, in others, the evidence is clear. In a study of three species, 3β-HSD activity was noted in thecal cells of maturing oocytes of the carp *Cyprinus carpio,* but none in follicular cells (Livni, 1971). In *Mugil capito* and *Tilapia aurea,* however, this activity was demonstrated in follicular cells. Enzyme activity disappeared in all species before spawning.

Steroidogenesis may be detected within ordinary thecal cells but sometimes clumps of SPECIAL THECAL CELLS appear to have taken over this function (Yamamoto and Onozato, 1968; Nicholls and Maple, 1972; Nagahama, Chan, and Hoar, 1976; Nagahama, Clarke, and Hoar, 1978; Kagawa, Takano, and Nagahama, 1981; Bruslé, 1985; Matsuyama, Nagahama, and Matsuura, 1991; Nakamura, Specker, and Nagahama, 1993). Special thecal cells occur in the theca externa of some species (e.g., rainbow trout, *Salmo gairdneri:* van den Hurk and Peute, 1979) and theca interna of others (e.g., zebrafish, *Brachydanio rerio:* Yamamoto and Onozato, 1968). They are larger than ordinary thecal cells and are often found near blood vessels. They react positively for the presence 3β-HSD and contain abundant agranular endoplasmic reticulum as well as large mitochondria with dense matrix and tubular cristae; granular endoplasmic reticulum appears to be absent (Figures 2.125 and 2.140). They appear to arise from interstitial cells of fibroblastic origin (Yamamoto and Onozato, 1968; van den Hurk and Peute, 1979).

Cells displaying the ultrastructural characteristics of steroidogenesis are also found in the interstitial tissue between small oocytes, forming clumps with other types of cells such as fibroblasts (Figure 2.141C) (Yamamoto and Onozato, 1968; Nakamura, Specker, and Nagahama, 1993). In tilapia *Oreochromis niloticus,* it is concluded that these steroid producing cells are derived from tissues near the ovarian artery and vein (Figures 2.141A,B) and migrate to the interstitial areas during posthatching development, coincident with vascularization of the interstitial tissue. They finally enclose oocytes during early vitellogenesis, at a time when production of oestradiol-17β increases (Figures 2.141D to F).

In the rainbow trout *Salmo gairdneri,* the peripheral thecal layer gradually merges into the interstitial tissue (van den Hurk and Peute, 1979). Interstitial cells and special thecal cells contain agranular endoplasmic reticulum and mitochondria with tubular cristae

throughout the annual cycle. In addition, these cells contain free ribosomes, granular endoplasmic reticulum, polyribosomes, Golgi cisternae, a few lysosome-like bodies, and lipid droplets. Histochemical tests indicate that the interstitial cells and special thecal cells are the sites of most intense steroidogenesis, especially during the period when maturation of oocytes and ovulation takes place. At this time the numbers of these steroidogenic cells increase. The localization and nature of the special thecal cells in the trout ovary indicate that they are interstitial cells, found in the outer part of the theca of pre- and postovulatory follicles.

Bundles of nerve fibres, presumably autonomic, course among the yolky follicles and steroid producing cells of tilapia *Oreochromis niloticus* (Figure 2.142E) (Nakamura, Specker, and Nagahama, 1996). Thick nerve bundles enter the ovary in association with the ovarian artery and vein (Figures 1.34A to C) and send out branches that invade the central parts of the ovigerous lamellae. Groups of axons ramify from these bundles to penetrate the spaces between clusters of steroid producing cells (Figure 1.34D), forming slightly swollen terminals near these cells (Figures 2.142A to D). The nerve endings contain many clear synaptic vesicles (30 to 50 nm in diameter), a few dense-cored vesicles (30 to 80 nm), and some mitochondria; no synaptic structures were noted, such as a cleft with electron-dense material or pre- and postsynaptic membrane specializations. It is suggested that these terminals play a role in the regulation and production of steroid hormones in the ovary by releasing transmitter substances non synaptically.

Smooth muscle may be included in the theca of some species. The theca of the preovulatory follicle of the trout *Salmo gairdneri* consists of alternating layers of flattened smooth muscle and collagenous fibres enclosing the basement membrane of the follicle (Figure 2.143) (Szöllösi, Jalabert, and Breton, 1978). The muscle fibres display the active pinocytosis typical of smooth muscle cells and contain abundant microfilaments 7 to 8 nm in diameter. It is suggested that contraction of these fibres assists in the expulsion of the egg at ovulation.

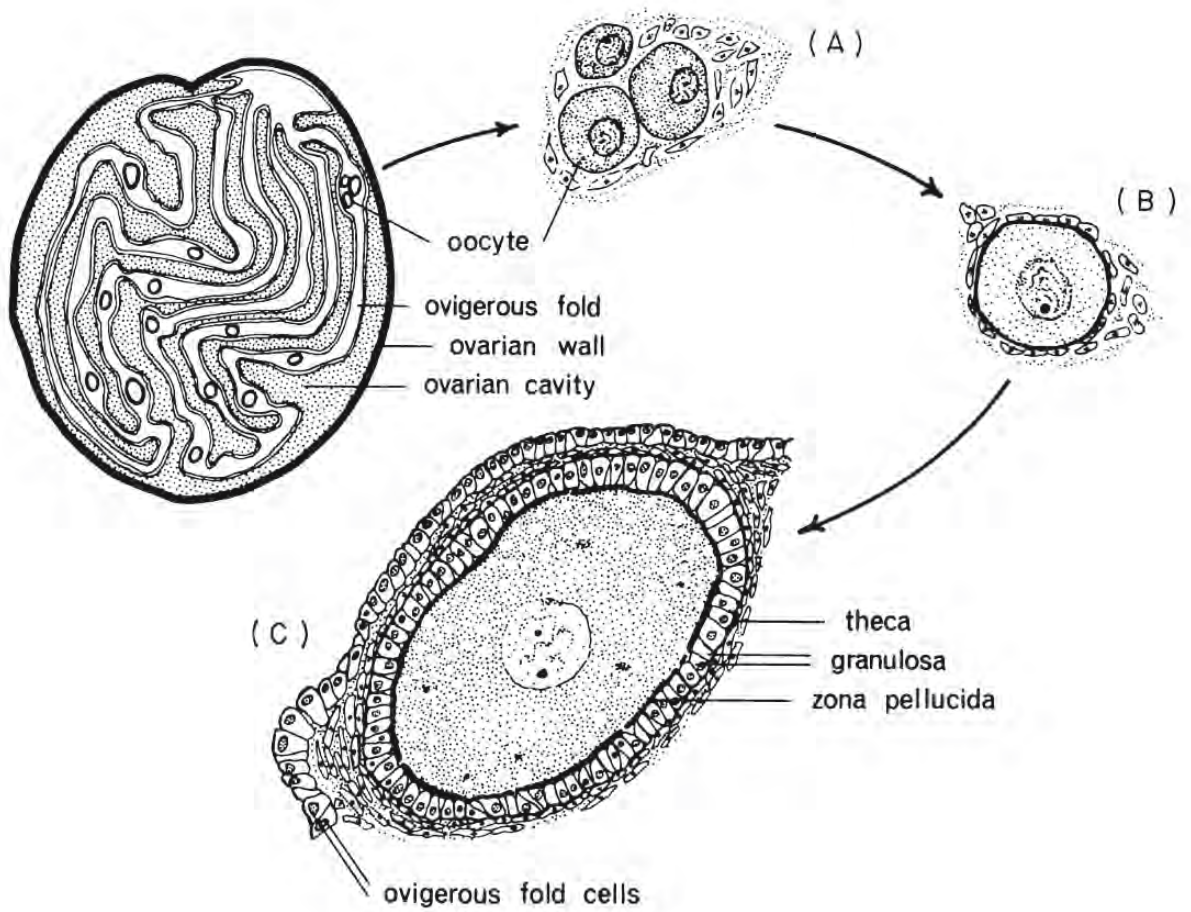

Figure 2.1: Drawings illustrating follicular development in the ovary of the surfperch *Cymatogaster*. Oocytes develop in ovigerous folds (upper left). (From Hoar, 1969; reproduced with permission from Elsevier Science and J.P. Wiebe).

A. A nest of oocytes in early stages of development.

B. As they grow and mature, various intracellular and extracellular changes occur. Initially follicular cells form a simple squamous epithelium around each oocyte.

C. As development proceeds, the follicular cells enlarge and may become cuboidal and even columnar. The follicular epithelium is surrounded by its own basal lamina which separates it from a sheath of condensed vascular connective tissue, the theca folliculi. The theca contains fibroblasts, collagenous fibres and capillaries and, in some species, special thecal steroid-producing cells.

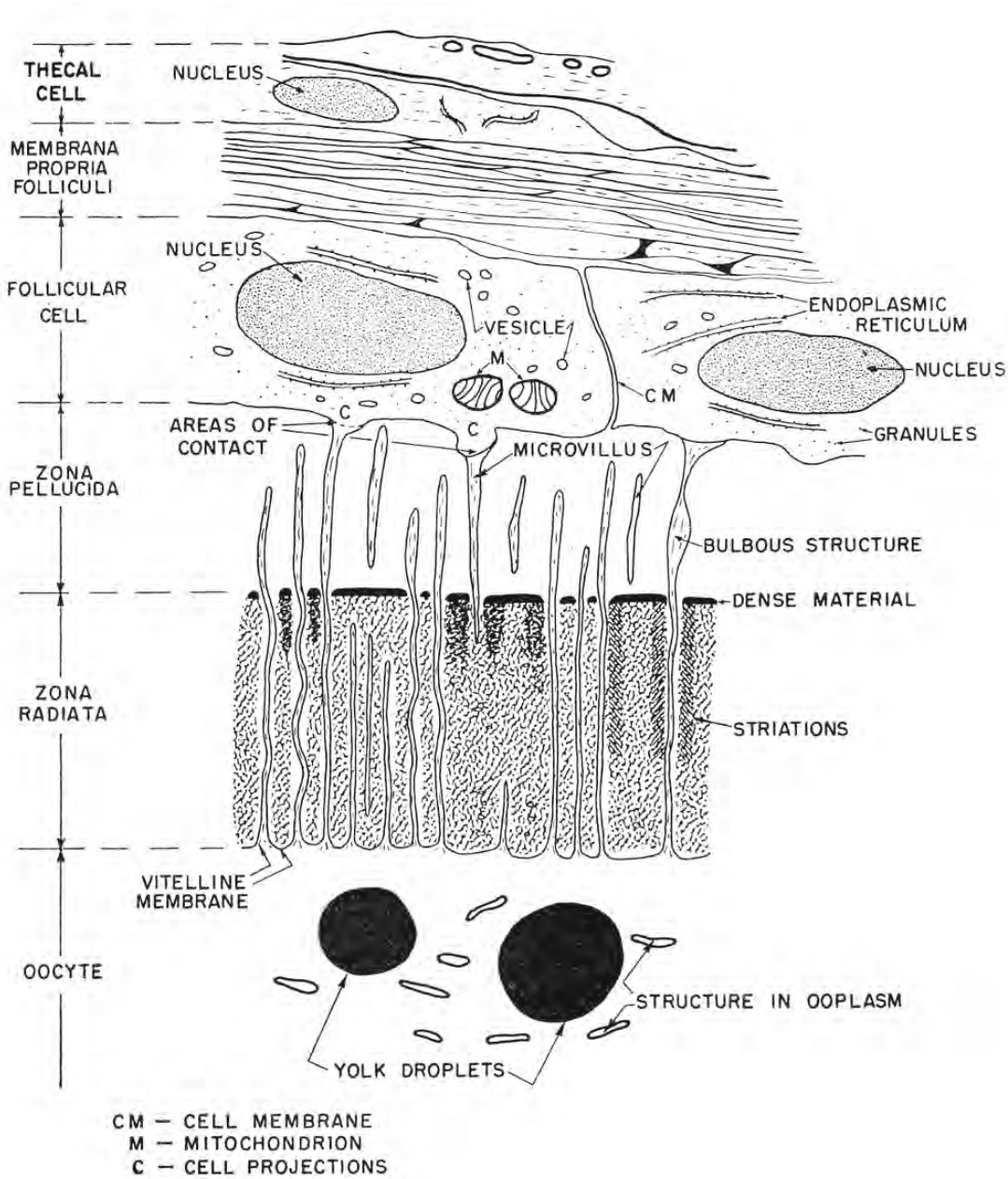

Figure 2.2: During oogenesis, a thick, translucent, acellular zona pellucida, or vitelline envelope, develops between the oocyte and follicular cells. (It is shown here as two layers: zona pellucida and zona radiata.) This diagram shows a portion of the peripheral region of a trout oocyte with its enveloping membranes. As the oocyte grows, the zona pellucida becomes perforated by pore canals, enabling an exchange of materials between the oocyte and follicular cells; these channels contain microvilli that extend from both the oocyte surface and the follicular cells. X 5,000 (From Hurley and Fisher, 1966; reproduced with permission of the NRC Press).

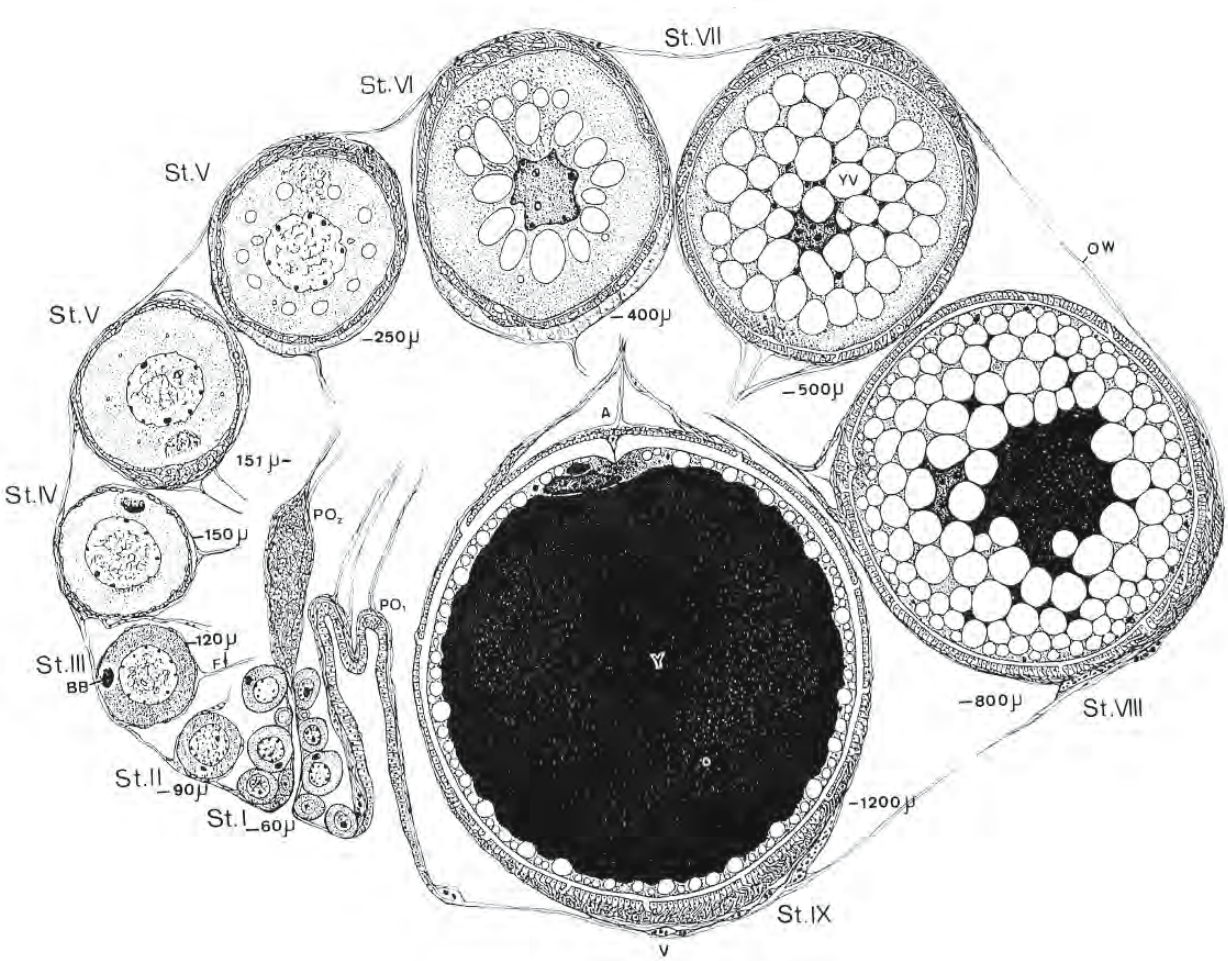

Figure 2.3: Diagram illustrating growing oocytes of the medaka *Oryzias latipes* at various stages of oogenesis. (From Iwamatsu et al., 1988; reproduced with permission from the Zoological Society of Japan).

Abbreviations: A, animal pole; BB, juxtanuclear complex, yolk nucleus, or Balbiani body; OW, ovarian wall; PO_1, postovulatory follicle just after ovulation; PO_2, postovulatory follicle 24 hours after ovulation; V, vegetal pole; Y, yolk mass; YV, yolk vesicle.

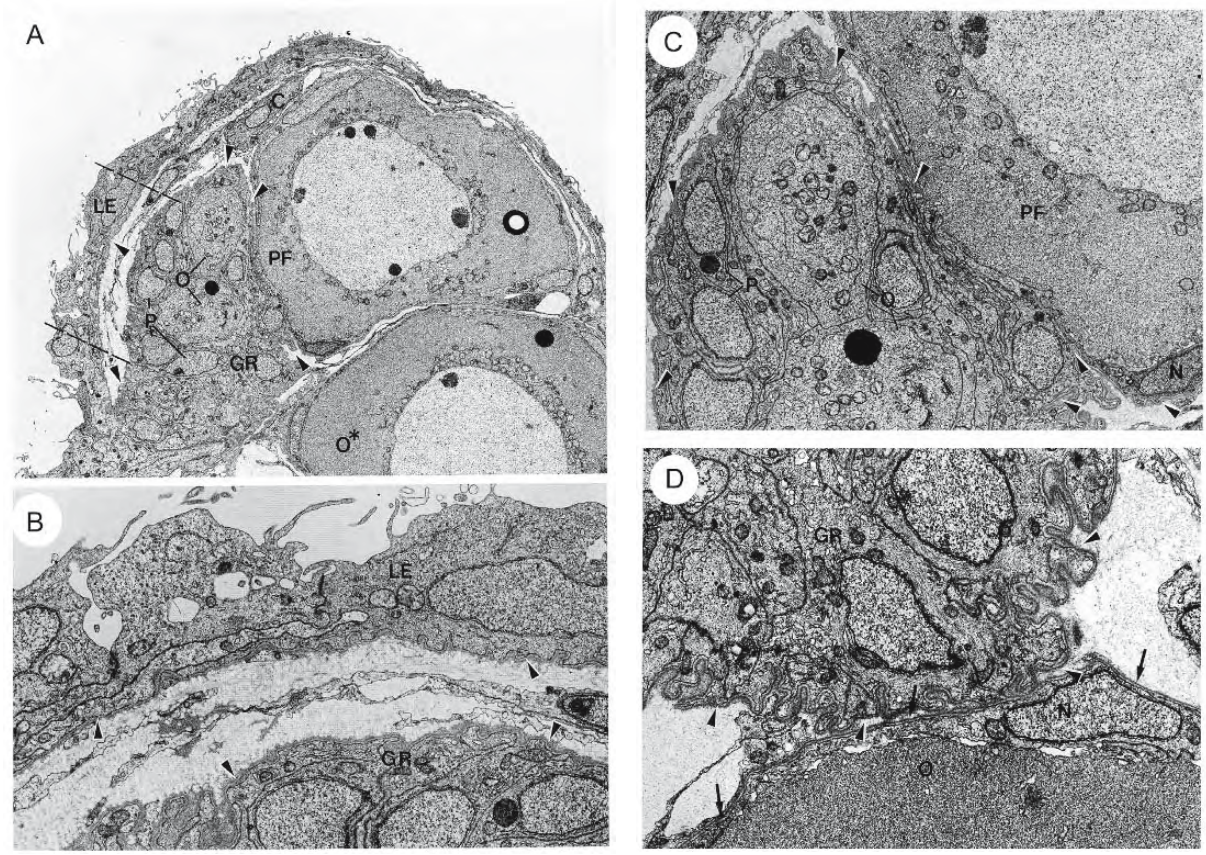

Figure 2.4: Electron micrographs of the germinal ridge (GR) and early follicular progression in the seahorse *Hippocampus erectus.* (From Selman, Wallace, and Player, 1991; © reproduced with permission of John Wiley & Sons, Inc.).

A. An overview showing the relationship of the luminal epithelium (LE), germinal ridge, and developing follicles. The germinal ridge, containing two adjacent oocytes (O) and several prefollicular cells (P), is an outfolding of the luminal epithelium. The basal lamina (arrowheads) underlying the luminal epithelium is continuous with the basal lamina surrounding the germinal ridge. A primordial follicle (PF), surrounded by flattened follicular cells, is "pinching" away from the germinal ridge (see C). The area between the dashed lines is magnified in B. O*, oocyte in a definitive follicle of the early follicular progression; C, connective tissue cells. X 2,800.

B. Part of the germinal ridge and overlying luminal epithelium (LE). Arrowheads indicate the basal lamina that underlies the luminal epithelium and surrounds the germinal ridge. X 10,400.

C. Higher magnification of the primordial follicle (PF from A) that is separating from the germinal ridge. The basal lamina (arrowheads) surrounding the germinal ridge has not yet completely separated this primordial follicle from the germinal ridge. N, follicular cell nucleus; O, contiguous oocytes in the germinal ridge; PF, prefollicular cells. X 7,640.

D. Oocyte (O) in a definitive follicle that has separated from the germinal ridge (GR). The basal lamina (arrowheads) surrounding the germinal ridge is separate from the basal lamina (arrows) that surrounds the primordial follicle. Cytoplasmic filaments are visible in the prefollicular cells. N, nucleus of the follicular cell. X 10,050.

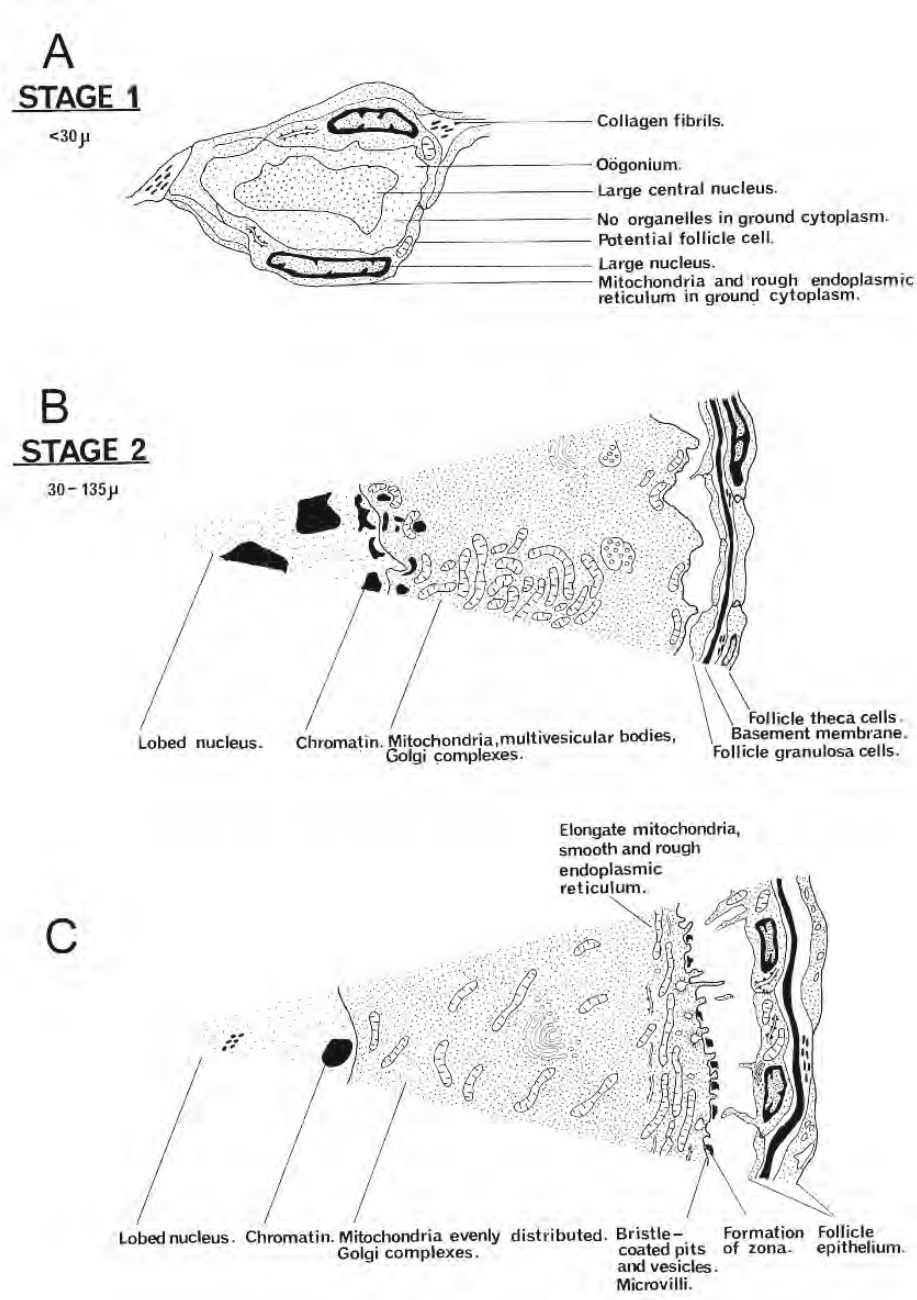

Figure 2.5: Diagrammatic representation of the eleven stages arbitrarily assigned to oogenesis in *Blennius pholis.* (From Shackley and King, 1977; reproduced with permission of the authors).

A. Stage 1 follicle consisting of an oogonium surrounded by squamous follicular cells. The follicular cells contain cytoplasmic filaments.

B. Early stage 2 oocyte and squamous follicular epithelium.

C. Late stage 2 oocyte and squamous follicular epithelium.

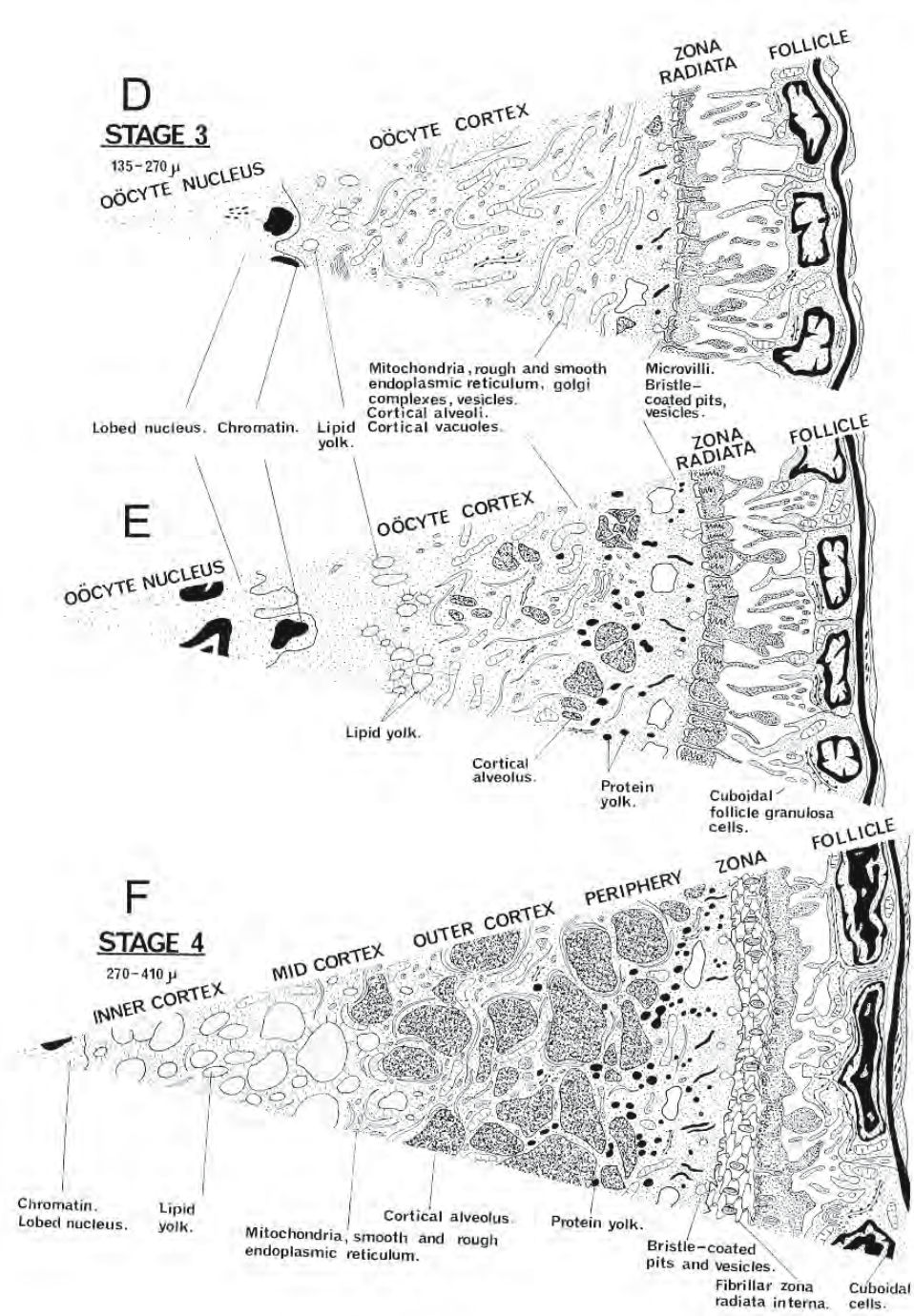

Figure 2.5: Continued.

D. Early stage 3 oocyte with columnar follicular epithelium.

E. Late stage 3 oocyte with columnar follicular epithelium.

F. Stage 4 oocyte surrounded by a cuboidal follicular epithelium. The cortex of the oocyte is divisible into regions: inner cortex, mid cortex, outer cortex, and periphery.

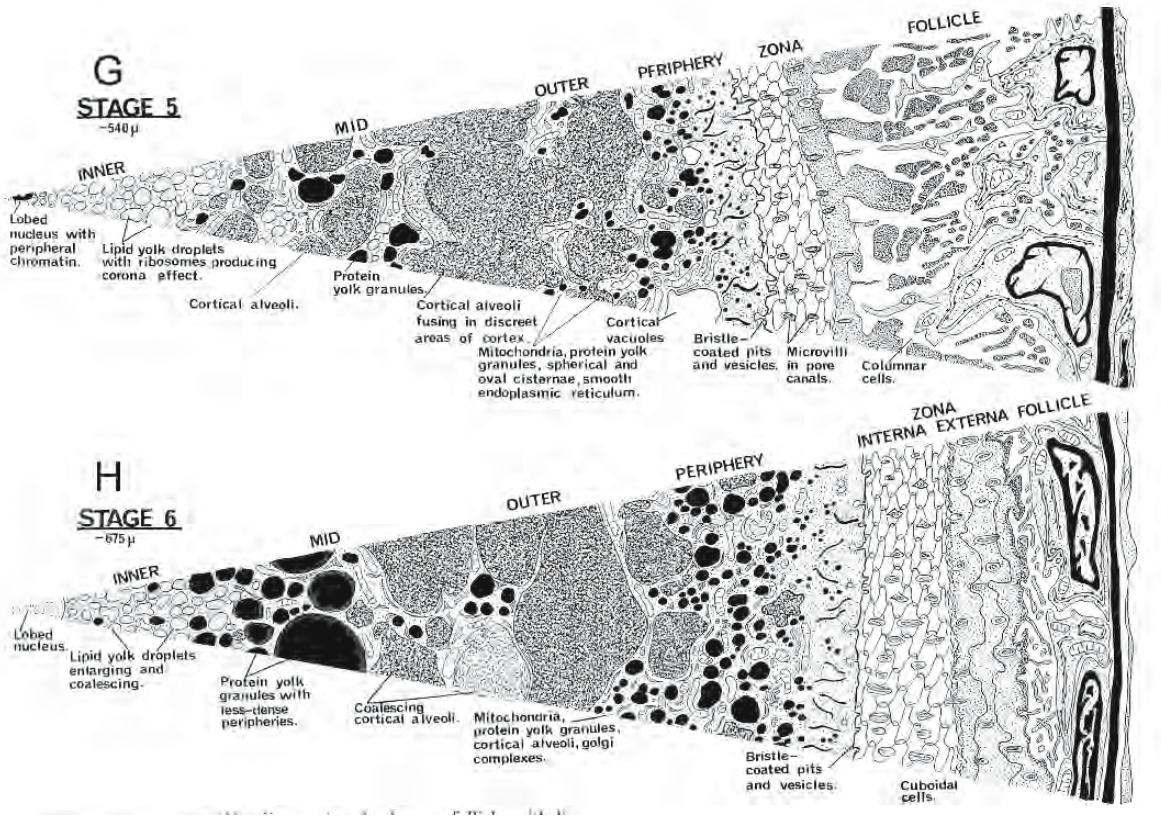

Figure 2.5: Continued.
G. Stage 5 oocyte with columnar follicular epithelium.
H. Stage 6 oocyte with cuboidal follicular epithelium.

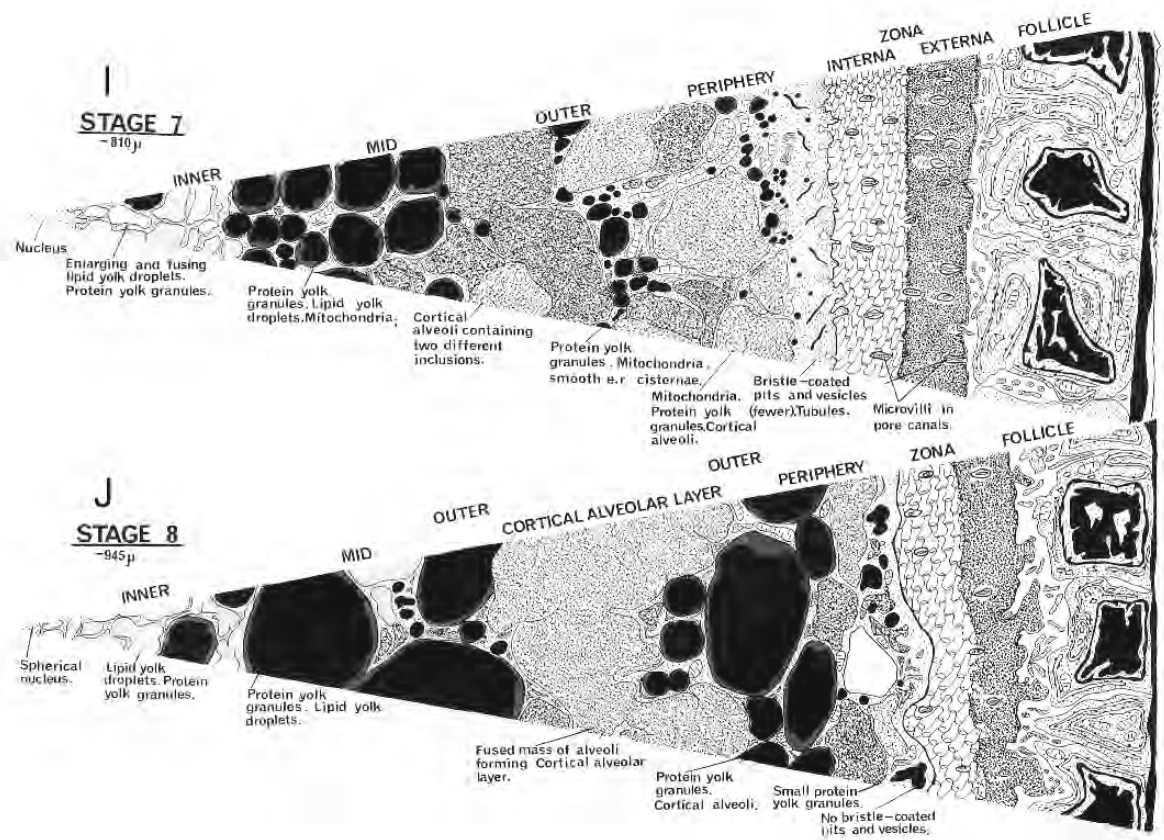

Figure 2.5: Continued.

I. Stage 7 oocyte with cuboidal follicular epithelium.

J. Stage 8 oocyte with cuboidal follicular epithelium.

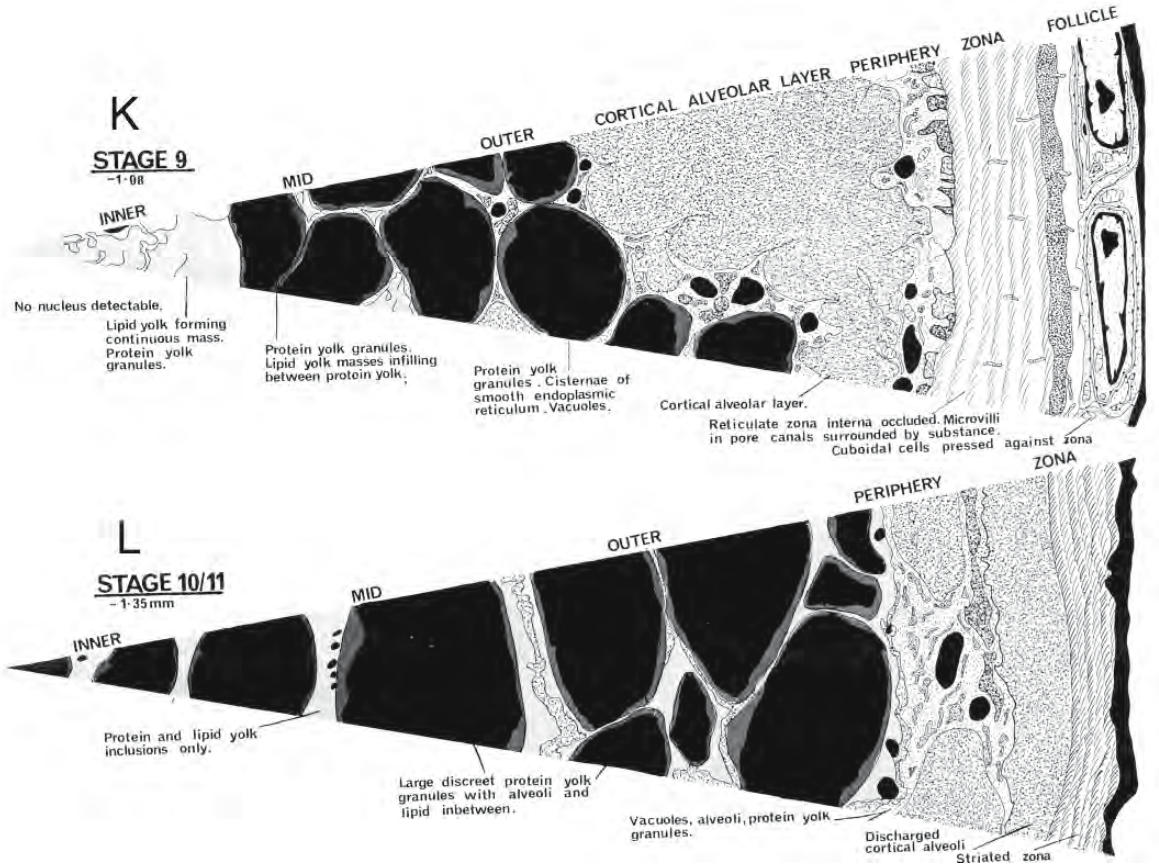

Figure 2.5: Continued.
K. Stage 9 oocyte with cuboidal follicular epithelium.
L. Stages 10/11, preovulation/ovulation oocyte. The oocyte is released from the follicle at ovulation.

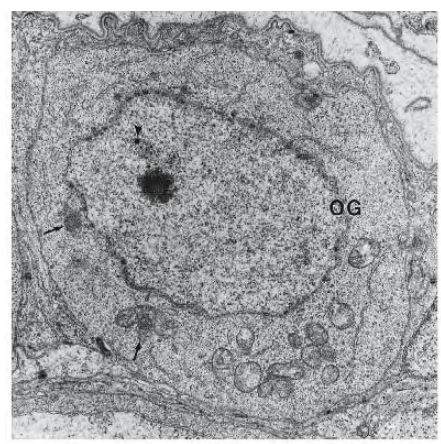

Figure 2.6: Electron micrograph of an oogonium (OG) within the germinal ridge of the pipefish, *Syngnathus scovelli.* There is a single nucleolus within the oval nucleus. Mitochondria, nuage material (arrows), and endoplasmic reticulum are present within the cytoplasm. Some dense-cored granules are seen above the nucleolus (arrowhead). X 14,000 (From Begovac and Wallace, 1988; © reproduced with permission of John Wiley & Sons, Inc.).

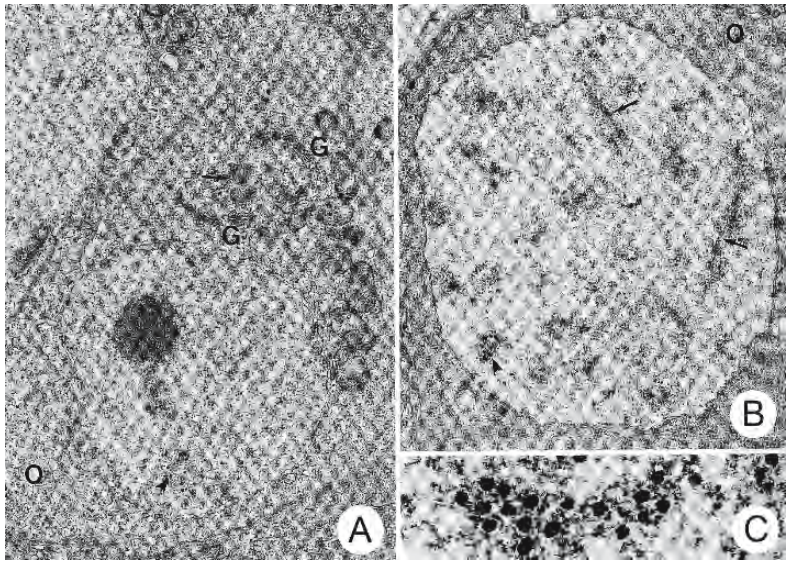

Figure 2.7: Electron micrographs of oocytes (O) of the pipefish *Syngnathus scovelli.* (From Begovac and Wallace, 1988; © reproduced with permission of John Wiley & Sons, Inc.).

A. Cellular organelles occur around the centrioles (arrow) at one side of the nucleus. Golgi complexes (G) have appeared. The spherical nucleus contains dense-cored granules (arrowhead). Leptotene chromatin is electron-dense. X 12,640.

B. Chromatin is pachytene. Long synaptonemal complexes (arrows) are present in the nucleus. The nucleus is less electron-dense than in Figure 57A. Dense-cored granules (arrowhead) can be seen in the nucleus. X 8,080.

C. Dense-cored granules specific to germ cell nuclei. X 65,200.

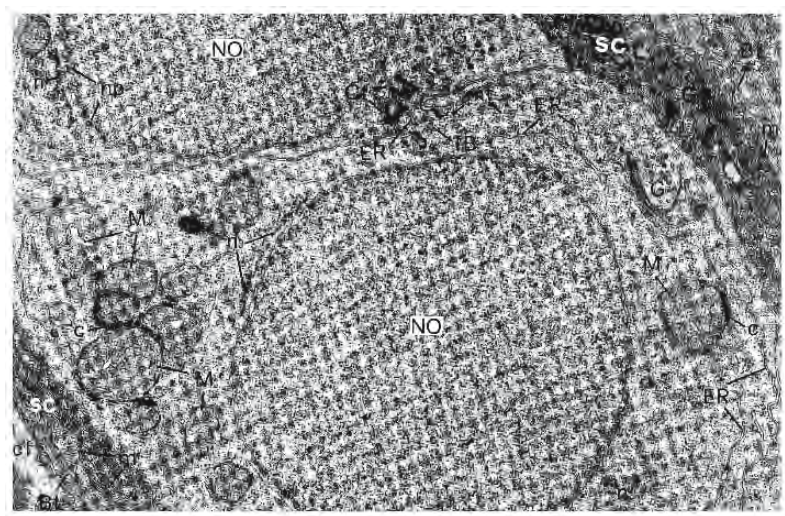

Figure 2.8: Electron micrograph showing a cytoplasmic bridge (IB) between two oogonia from the eel *Anguilla anguilla.* Electron-dense material outlines the cytoplasmic side of the bridge which appears to be traversed by cisternae of endoplasmic reticulum (ER) and microtubules (mt). A pair of centrioles (Ct) and vesicles of a Golgi complex (G) lie near the bridge. The oogonia are enveloped by somatic cells (SC) that are rich in microfilaments and separated by a basal lamina (BL) from the connective tissue stroma. c, "cement", cf, collagen fibres of the stroma; M, mitochondria; n, "nuage"; NO, nuclei of the oogonia. X 11,400. (From Grandi and Colombo, 1997; © reproduced with permission of John Wiley & Sons, Inc.).

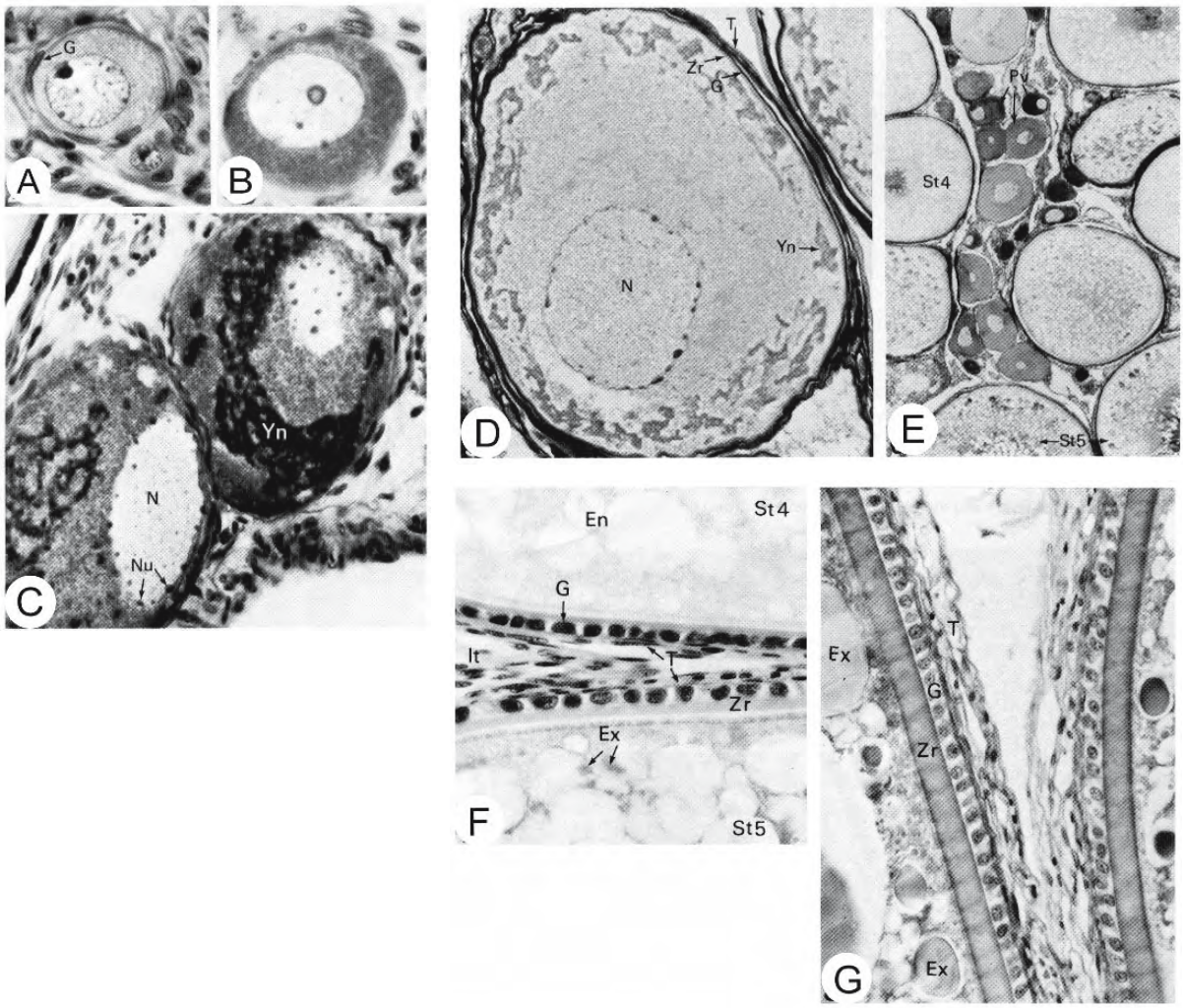

Figure 2.9: An increase in size is the most obvious manifestation of oocyte development. The oocyte grows both by an enlargement of the nucleus and the addition of cytoplasm. Later, most growth is due to an increase in the amount of cytoplasm and, in the final stages of maturation, the oocyte has its full complement of yolk and is ready to be ovulated. Seven principal stages of oocyte development in the rainbow trout *Salmo gairdneri* are shown in these photomicrographs. (From van den Hurk and Peute, 1979; reproduced with permission of the author).

A. Previtellogenic follicle, stage 1. G, follicular layer. X 560.

B,C. Previtellogenic follicles, stage 2. N, nucleus; Nu, nucleolus; Yn, yolk nucleus. X 560 and X 350.

D. Previtellogenic follicle, Stage 3. G, follicular layer; N, nucleus; T, theca; Yn, yolk nuclei; Zr, zona pellucida. X 350.

E. Portion of an ovary with vitellogenic follicles at stages 4 and 5. Pv, previtellogenic follicles. X 88.

F. Detail of vitellogenic follicles at stages 4 and 5. En, endogenous yolk; Ex, exogenous yolk; G, follicular layer; It, interstitial tissue; T, theca; Zr, zona pellucida. X 350.

G. Portions of two vitellogenic follicles at stage 6 showing aggregated exogenous yolk granules (Ex). G, follicular layer; T, theca; Zr, zona pellucida. X 350.

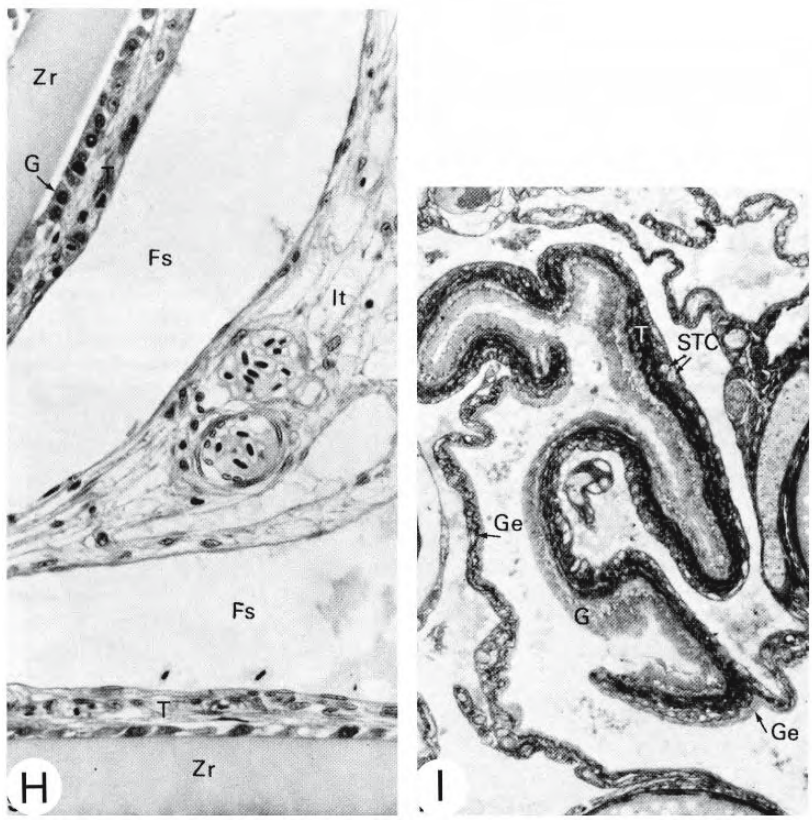

Figure 2.9: Continued.

H. Portions of mature follicles at stage 7. Fluid fills the space (Fs) between the theca (T) and the interstitial tissue (It). G, follicular layer; Zr, zona pellucida. X 350.

I. Postovulatory follicles. The follicular layer (G) is continuous with the germinal epithelium (Ge). STC, special thecal cells. X 88.

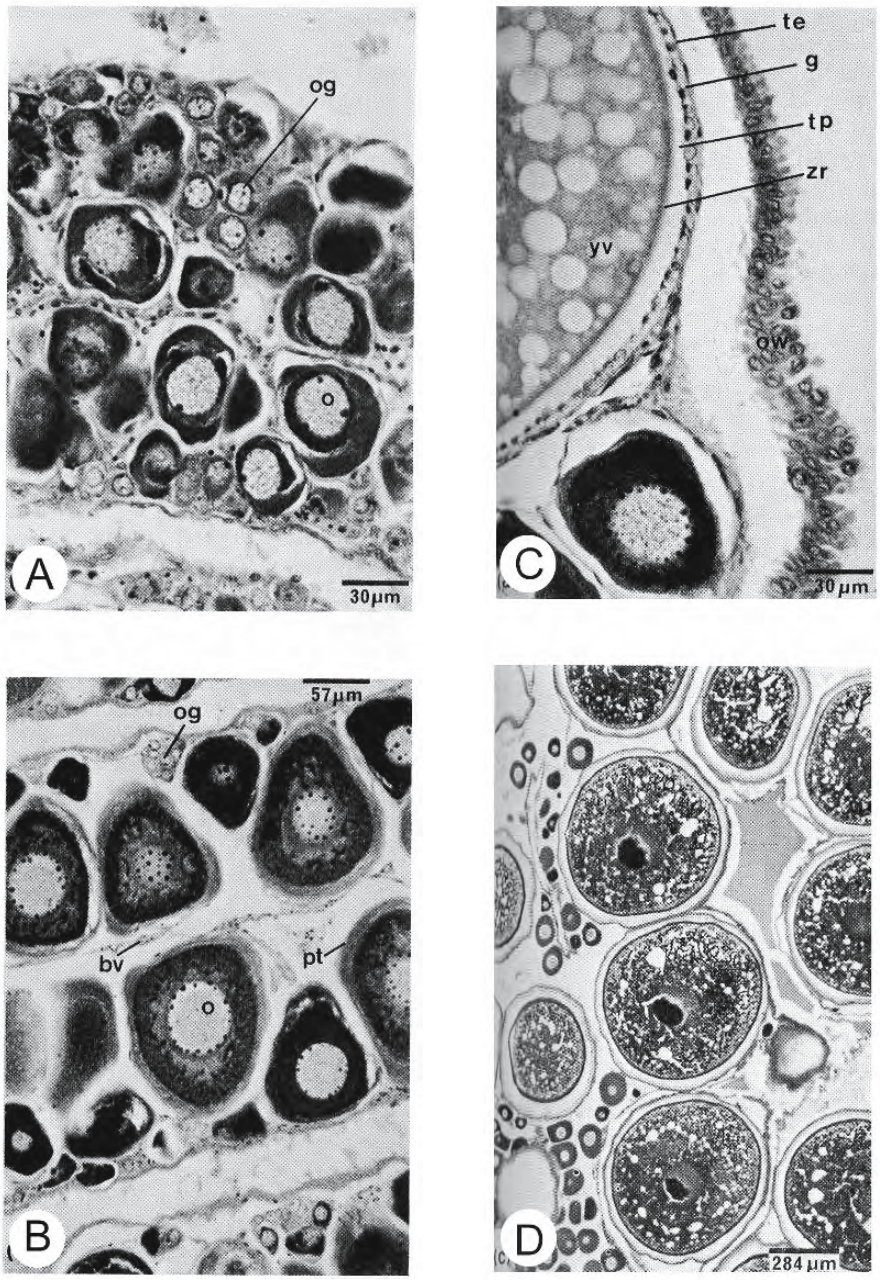

Figure 2.10: Classification of stages of ovarian maturity by macroscopic observation are useful in fecundity studies. These have been adapted, using histological criteria, for the pike *Esox lucius.* (From Treasurer and Holliday, 1981; reproduced with permission from Elsevier Science).

A. Stage I. Photomicrograph of a transverse section of an immature ovary showing three stages in oocyte development.

B. Stage IID. The internal organization of a lamella.

C. Stage III. Follicle and chorion of developing ovary.

D. Stage IV. The oocytes are greatly enlarged in the maturing ovary.

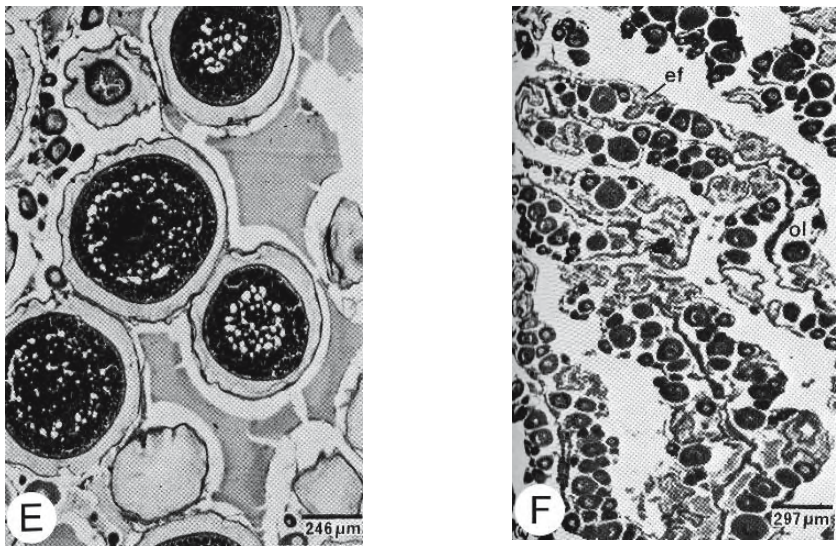

Figure 2.10: Continued.

E. Stage V. Gravid ovary with hyaline oocytes.

F. Stage VIII. Spent ovary showing disorganized ovigerous lamellae with empty follicles.

Abbreviations: bv, blood vessels; ef; empty follicle; g, follicular cells; o, oocyte; og, oogonium; ol, ovigerous lamella; ow, wall of oviduct; pt, primary theca; te, theca externa; tp, outer region of zona pellucida; yv, yolk vesicle; zr, zona pellucida.

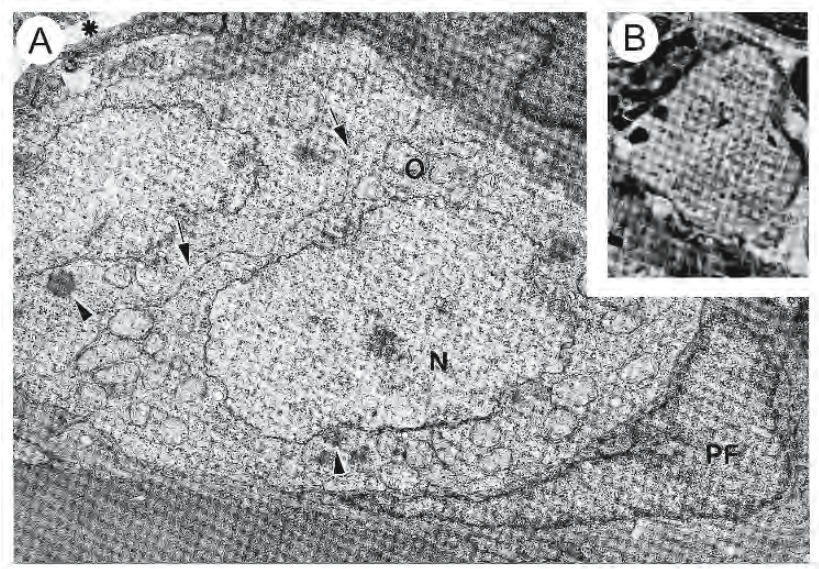

Figure 2.11: Nests of oocytes in the ovary of *Brachydanio rerio.* (From Selman et al., 1993; © reproduced with permission of John Wiley & Sons, Inc.).

A. Electron micrograph of a nest of meiotic oocytes. Pre-follicular cells (PF) envelop the nest of germ cells but do not surround individual oocytes which, therefore, abut on each other (arrows). Each oocyte has a large nucleus (N) and contains nuage (arrowheads) in the ooplasm. The asterisk indicates the ovarian lumen. X 11,300.

B. Photomicrograph of a nest of chromatin-nucleolus stage oocytes showing distinct chromosomes. X 605.

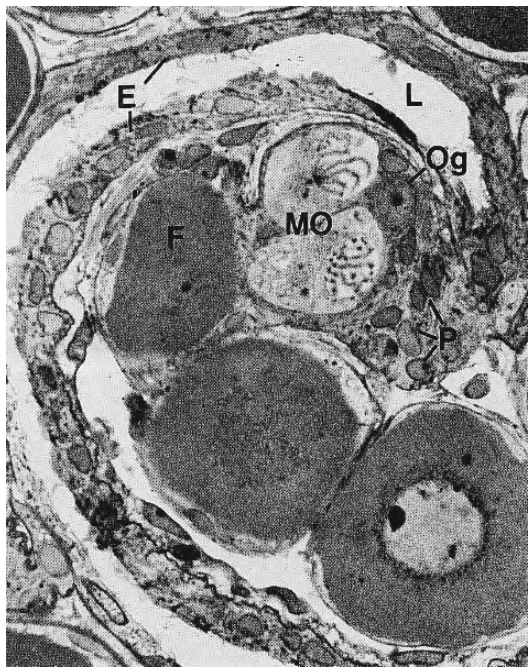

Figure 2.12: Photomicrograph of a section through the ovary of the seahorse *Hippocampus erectus.* Prefollicular cells (P), an oogonium (Og), and meiotic oocytes (MO) with visible chromosomes are present within the germinal ridge. A developing follicle (F) has separated from the germinal ridge. E, luminal epithelium; L, ovarian lumen. X 950 (From Selman and Wallace, 1989; reproduced with permission from the Zoological Society of Japan).

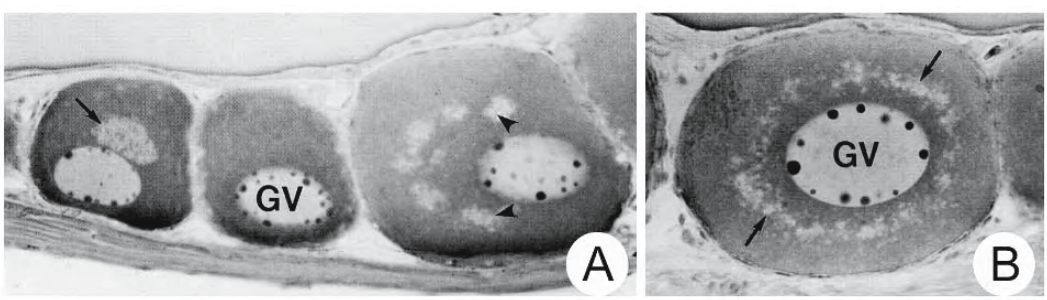

Figure 2.13: Micrographs of perinucleolar oocytes (O) of the pipefish *Syngnathus scovelli.* (From Begovac and Wallace, 1988; © reproduced with permission of John Wiley & Sons, Inc.).

A. Photomicrograph of oocytes in the primary growth phase. The germinal vesicle (GV) contains several nucleoli near its periphery. Juxtanuclear complexes are visible in two oocytes: in the left oocyte it forms an ovoid mass (arrow) and, at the right, a more diffuse, crescentic mass (arrowheads). X 330.

B. Photomicrograph showing the juxtanuclear complex as a perinuclear ring (arrows) around the germinal vesicle (GV). X 310.

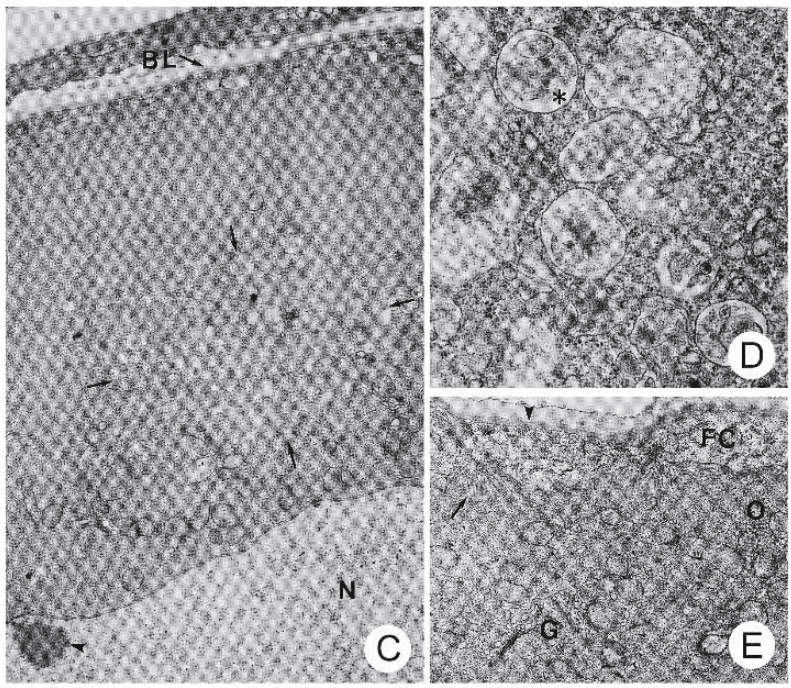

Figure 2.13: Continued.

C. In this electron micrograph, the arrows designate a juxtanuclear complex of organelles (Balbiani vitelline body) containing mitochondria and an aggregate of multivesicular bodies in the peripheral ooplasm. The nucleus (N) of the oocyte contains a perinuclear nucleolus (arrowhead). BL, basal lamina. X 7,500.

D. Electron micrograph at a higher magnification showing the multivesicular bodies (*) of the juxtanuclear complex of organelles. X 27,300.

E. Electron micrograph of the peripheral ooplasm showing abundant mitochondria and Golgi complexes (G). A basal lamina (arrowhead) overlies the squamous follicular cells (FC). The oocyte has begun to elaborate numerous microvillar processes (arrow) that extend toward the follicular cells. X 7,800.

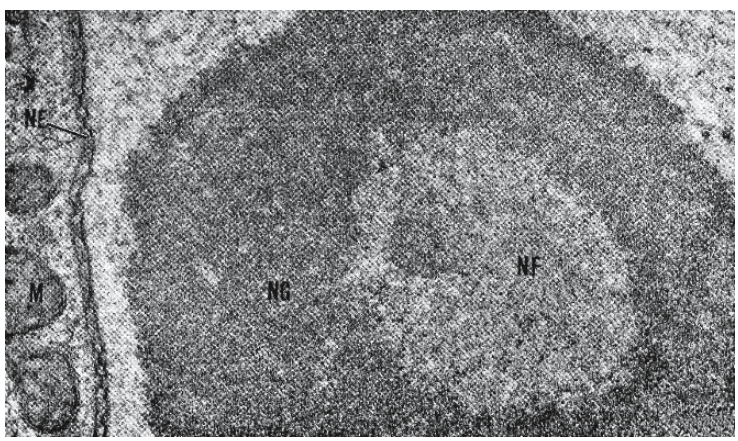

Figure 2.14: Electron micrograph of the nucleolus of a stage II oocyte of the pipefish *Syngnathus scovelli* showing the granular cortical region of tightly packed ribosomes (NG) and the filamentous central area (NF). X 40,000 (From Anderson, 1968; © reproduced with permission of John Wiley & Sons, Inc.).

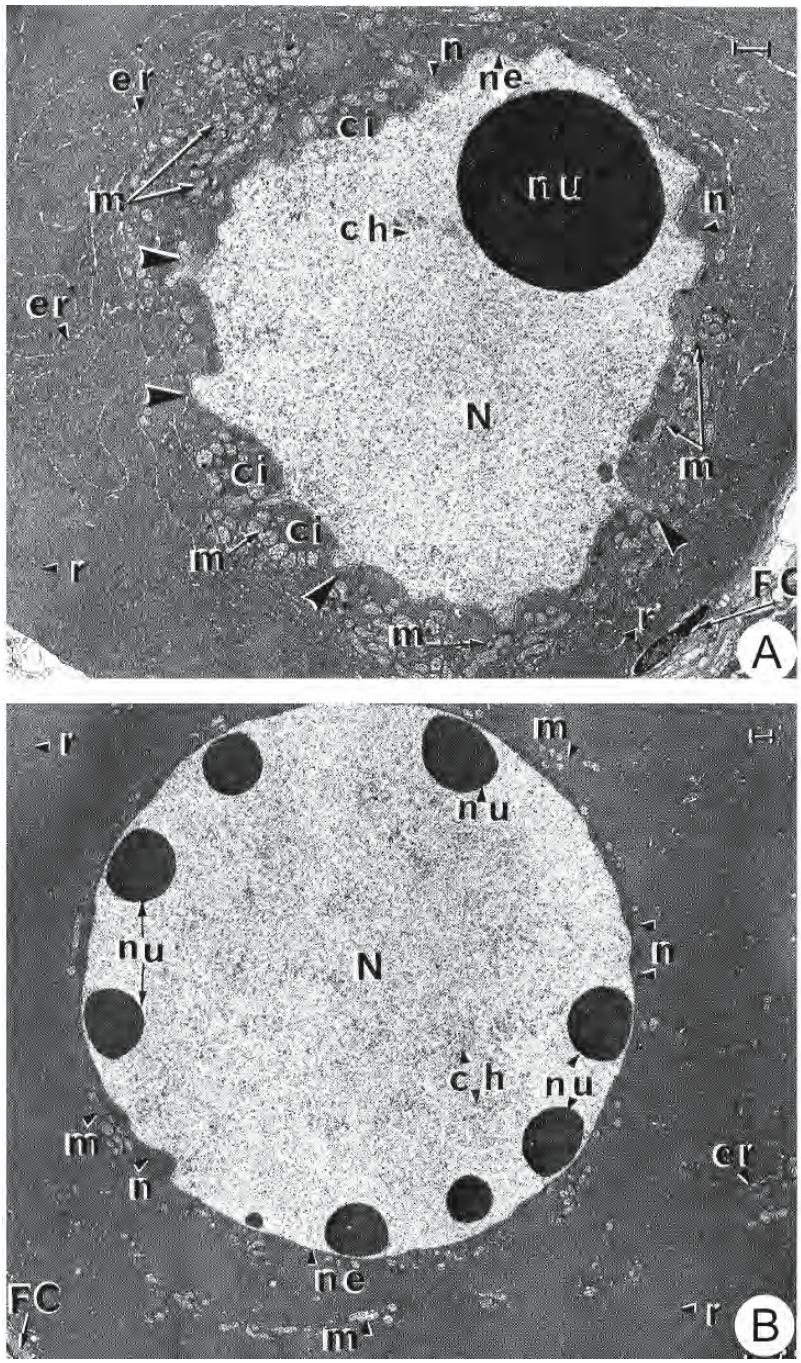

Figure 2.15: Electron micrographs of previtellogenic oocytes of the mullet *Mugil auratus.* The bars represent 1 μm. (From Bruslé, 1980; reproduced with permission of the author).

A. Depressions in the undulating nuclear envelope (arrowheads, ne) display several juxtanuclear complexes (ci) enclosed by aggregations of mitochondria (m). The nucleoplasm (N), without evident chromosomes, contains a large nucleolus (nu).

B. Later, the nucleus (N) becomes spherical with an almost smooth outline. Several dense, homogeneous nucleoli (nu) lie close to the inner nuclear membrane. Mitochondria become scattered peripherally.

Abbreviations: ch, chromatin; er, endoplasmic reticulum; FC, follicular cell; r, ribosomes.

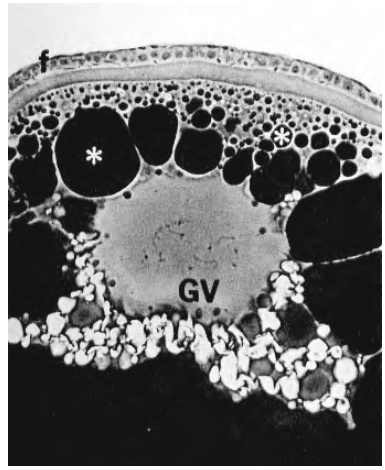

Figure 2.16: Phase-contrast micrograph of a vitellogenic follicle from *Cyprinodon variegatus* showing yolk spheres (*) of various sizes within the ooplasm. There are several lampbrush chromosomes within the germinal vesicle (GV). Follicular cells (f) overlie the zona pellucida. X 150 (From Wallace and Selman, 1981; reproduced with kind permission from the Society for Integrative and Comparative Biology).

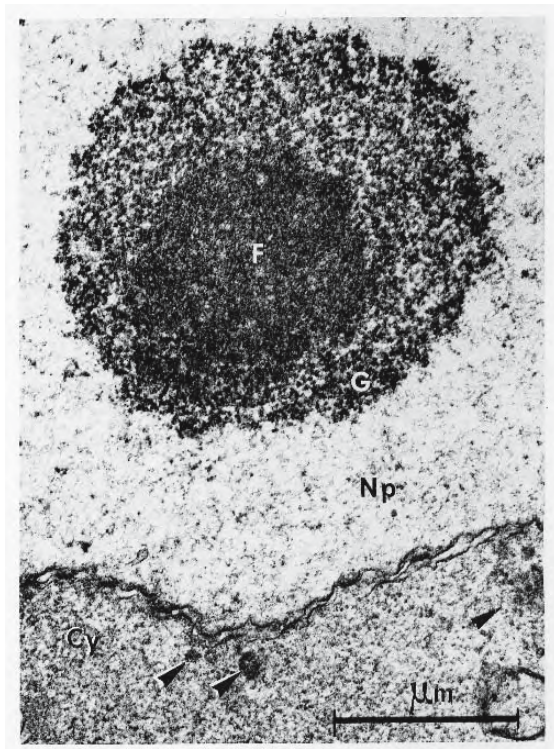

Figure 2.17: Electron micrograph of a portion of an oogonium of the viviparous teleost *Xiphophorus helleri.* The compact nucleolus has a fibrillar core (F) and a granular periphery (G). There are minute peripheral dense masses (arrows) in the ooplasm (Cy). Np, nucleoplasm X 31,000 (From Azevado and Coimbra, 1980, *Biologie Cellulaire*; reproduced with permission).

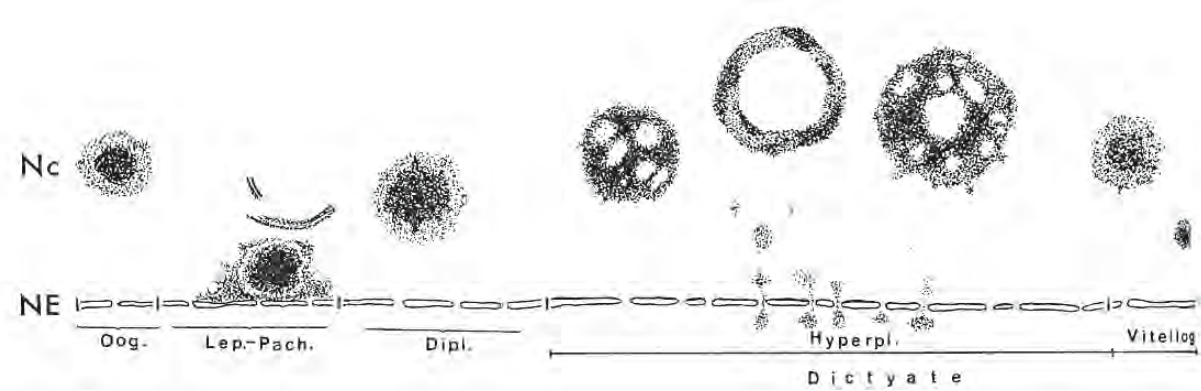

Figure 2.18: Drawings of the evolution of the nucleolus (Nc) of the viviparous teleost *Xiphophorus helleri* during oogenesis. Following the diplotene stage, when mitotic activity is suspended, the nucleoli enlarge from about 6 to 18 μm and become increasingly vacuolated. NE, nuclear envelope. (From Azevado and Coimbra, 1980, *Biologie Cellulaire*; reproduced with permission).

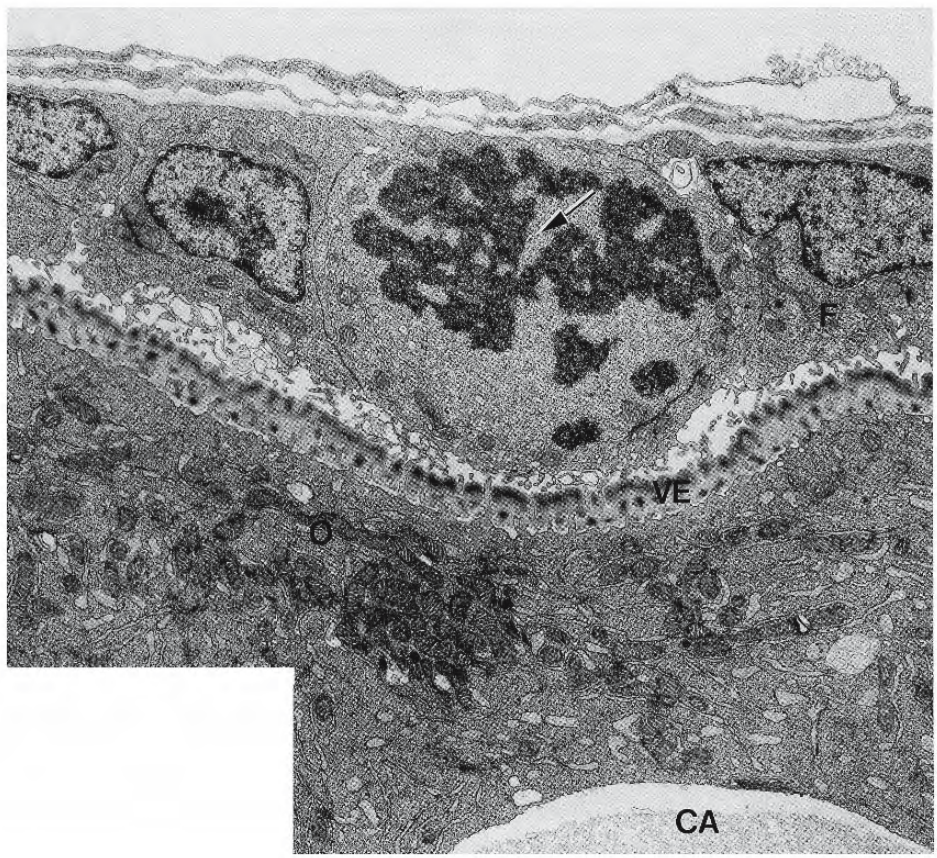

Figure 2.19: Electron micrograph of an ovarian follicle of *Brachydanio rerio*. One of the cells of the follicular epithelium (F) is dividing by mitosis (arrow indicates chromatin) in this cortical-alveolus stage. Mitochondria are closely associated with cisternae of granular endoplasmic reticulum in the cortical ooplasm (O). CA, cortical alveolus; VE, zona pellucida. X 8,400 (From Selman et al., 1993; © reproduced with permission of John Wiley & Sons, Inc.).

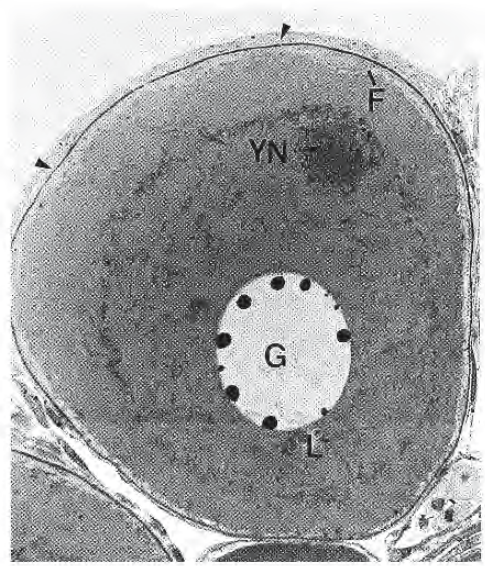

Figure 2.20: Photomicrograph of a section through a follicle of the seahorse *Hippocampus erectus.* The primary oocyte is in the perinucleolus stage. The ooplasm contains a distinct yolk nucleus (YN) or juxtanuclear complex of organelles. Several nucleoli lie within the periphery of the germinal vesicle (G). A darkly stained basement membrane (arrowheads) separates the follicular cells (F) from the theca. L, lipid droplets. X 565 (From Selman and Wallace, 1989; reproduced with permission from the Zoological Society of Japan).

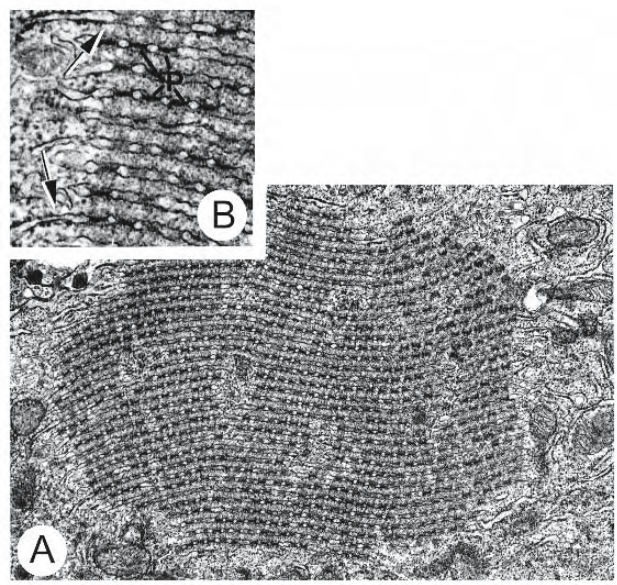

Figure 2.21: Electron micrographs of annulate lamellae in the ooplasm of a stage II oocyte of *Brachydanio rerio.* (From Selman et al., 1993; © reproduced with permission of John Wiley & Sons, Inc.).

A. X 14,400.

B. These annulate lamellae are continuous with the granular endoplasmic reticulum (arrows); nuclear pores are shown in side view. P, electron-dense pore complex. X 37,300.

Figure 2.22: Electron micrograph of annulate lamellae in a maturing oocyte of the medaka *Oryzias latipes.* The ends of the annulate lamellae (AL) are continuous with lamellae of the granular endoplasmic reticulum (ER). X 55,200 (From Iwamatsu et al., 1988; reproduced with permission from the Zoological Society of Japan).

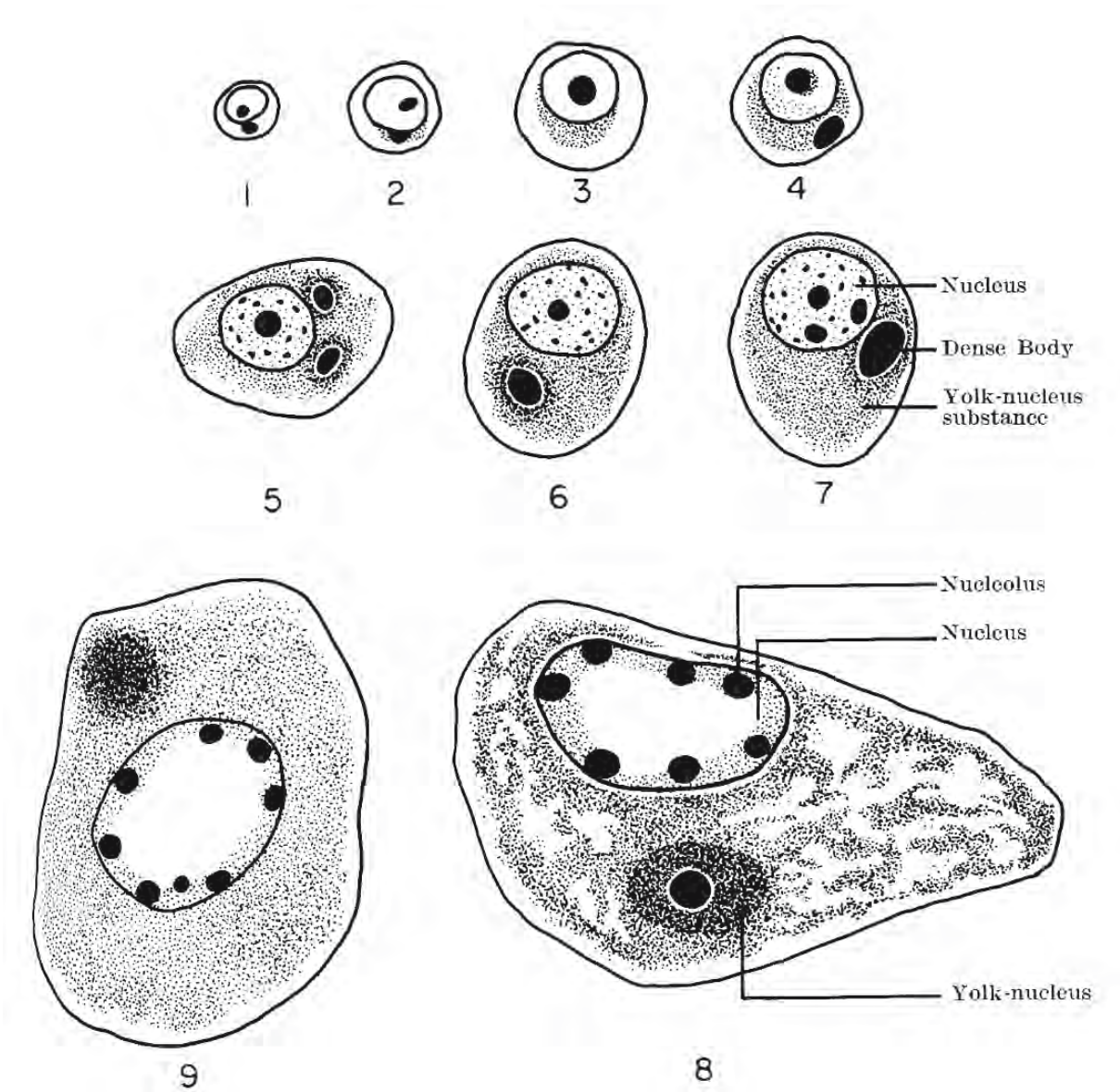

Figure 2.23: Drawings of sections of teleostean oocytes to show the development of the juxtanuclear complex of organelles. The drawings are taken from oocytes of *Channa* sp. except for nos. 3 and 10, which are of *Heteropneustes* sp. (From Guraya, 1963; reproduced with permission of the author).

1. Young oocyte showing dense body in the ooplasm.

2. Young oocyte showing basophilic yolk-nucleus substance and dense body adjacent to the nuclear membrane.

3. Young oocyte showing yolk-nucleus substance adjacent to the nuclear membrane.

4 - 7. Young oocytes showing the growth of the yolk nucleus and dense body.

8. Oocyte showing the proliferation of basophilic masses from the yolk nucleus.

9. Oocyte showing homogeneous yolk nucleus and uniformly distributed basophilic substance proliferated from the yolk nucleus.

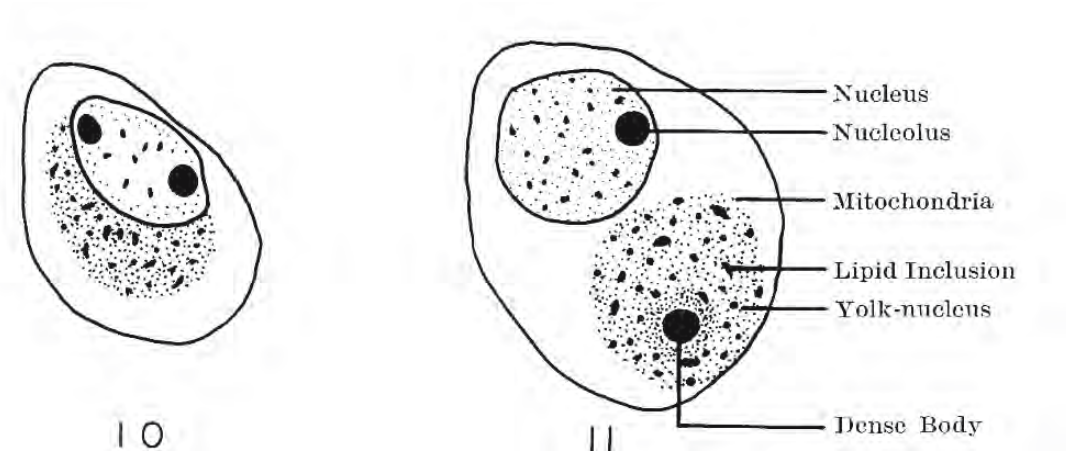

Figure 2.23: Continued.

10. Oocyte illustrating the various components of the juxtanuclear complex: yolk nucleus substance, lipid inclusions, and mitochondria.

11. Oocyte showing the various components of the juxtanuclear complex.

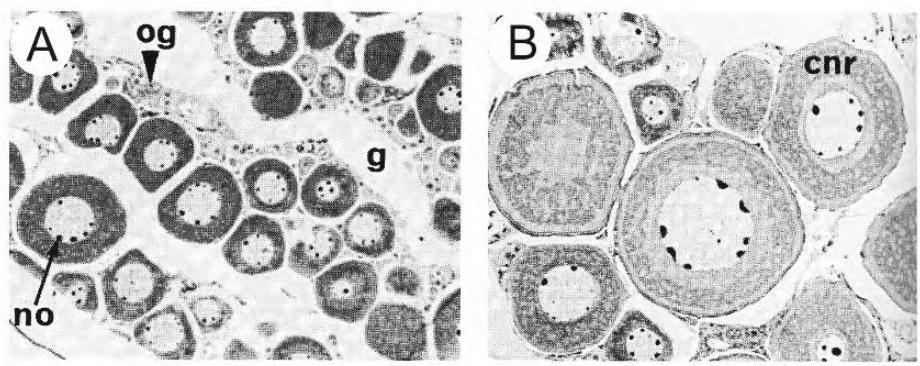

Figure 2.24: Photomicrographs of oocytes of the cod *Gadus morhua.* X 195 (From Kjesbu and Kryvi, 1989; reproduced with permission from Elsevier Science).

A. Oocytes in various stages of development. Oogonia (og) are situated at the lining of each ovigerous fold. g, interlamellar space; no, nucleolus.

B. Larger oocytes have acquired a circumnuclear ring (cnr) in their ooplasm.

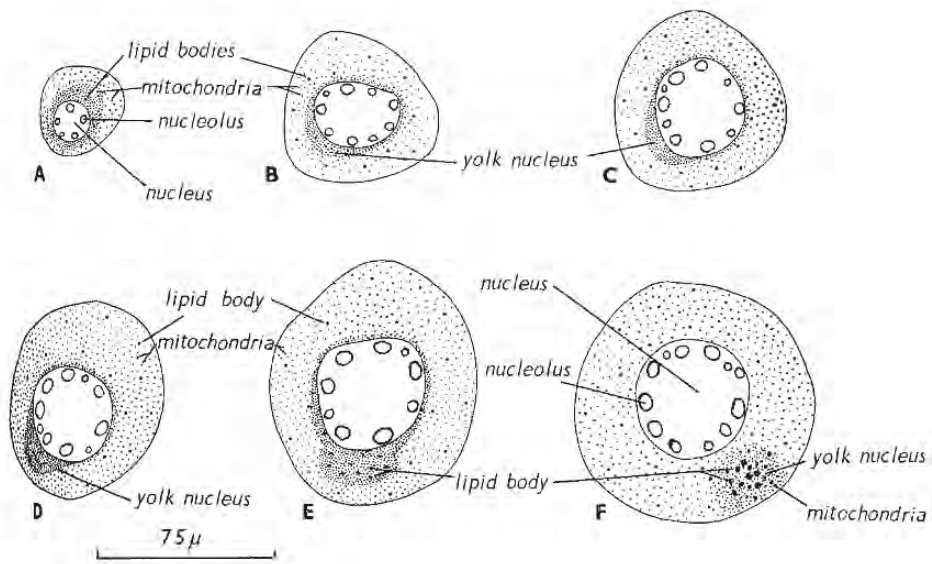

Figure 2.25: Camera lucida drawings of growing oocytes of *Heteropneustes fossilis.* (From Nayyar, 1964; reproduced with permission from the Company of Biologists, Ltd.).

A. Early oocyte with lipid granules and mitochondria concentrated around the nucleus.

B. The yolk nucleus has appeared beside the nucleus in the form of a mass of lipid bodies and mitochondria.

C, D. The yolk nucleus has increased in size and formed a conical cap on one side of the nucleus.

E. The yolk nucleus has become oval and still lies beside the nucleus.

F. The yolk nucleus is migrating toward the periphery of the oocyte.

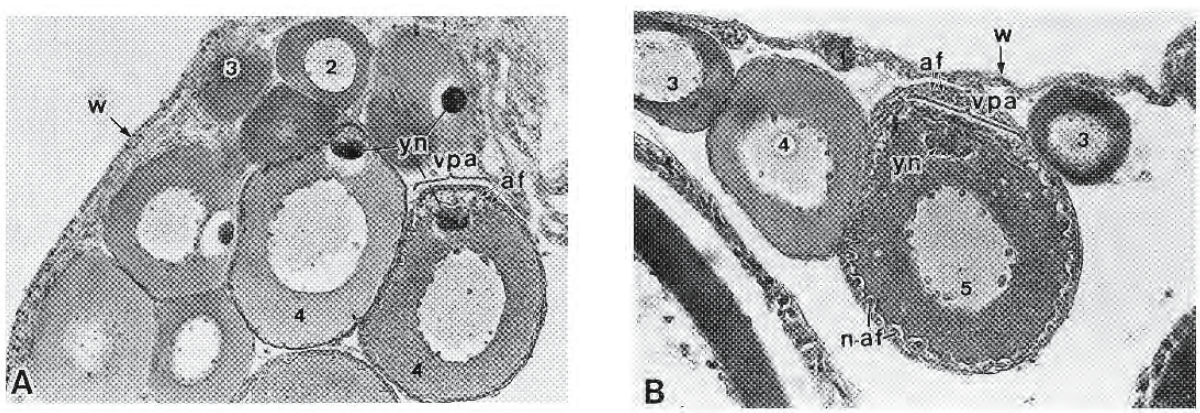

Figure 2.26: Sections from the ovary of the medaka *Oryzias latipes.* (From Iwamatsu and Nakashima, 1996; reproduced with permission from the Zoological Society of Japan).

A, B. Photomicrographs of sections through the ovary showing follicles containing oocytes in various stages of oogenesis. The vegetal pole area (vpa) is located at the side of the yolk nuclei (yn). Follicular cells are thick in this area and attaching filaments (af) are present. n-af, non-attaching filaments The numerals indicate stages of oogenesis. X 260.

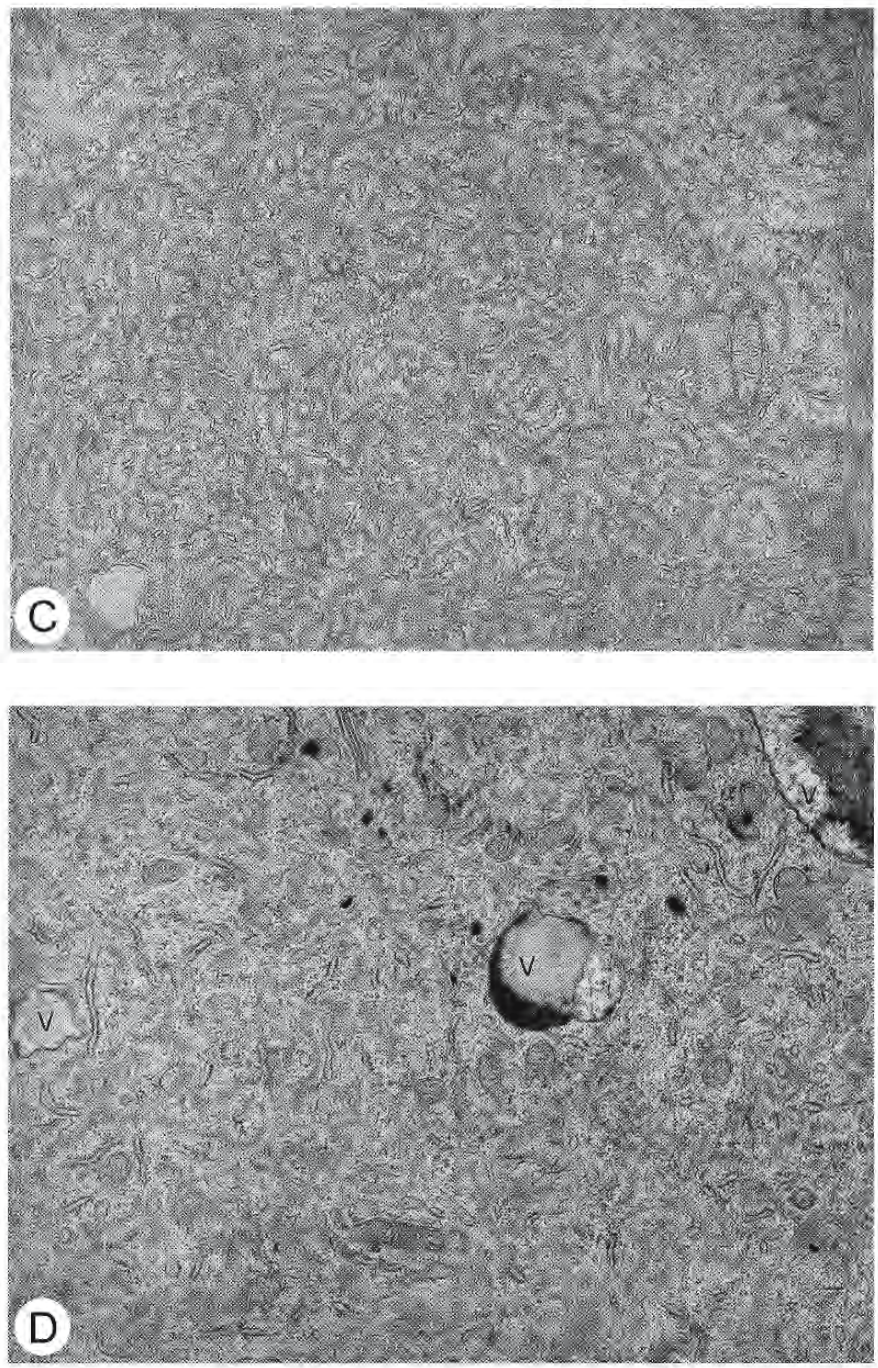

Figure 2.26: Continued.

C, D. Electron micrographs of yolk nuclei of previtellogenic oocytes.

C. The yolk nucleus of a stage III oocyte (3 above) is composed of aggregates of cytoplasmic organelles: filaments, agranular endoplasmic reticulum, and mitochondria. X 11,900.

D. The yolk nucleus of a stage IV oocyte (4 above) contains vesicles (V) of various sizes, Golgi complexes, and granular endoplasmic reticulum. X 17,000.

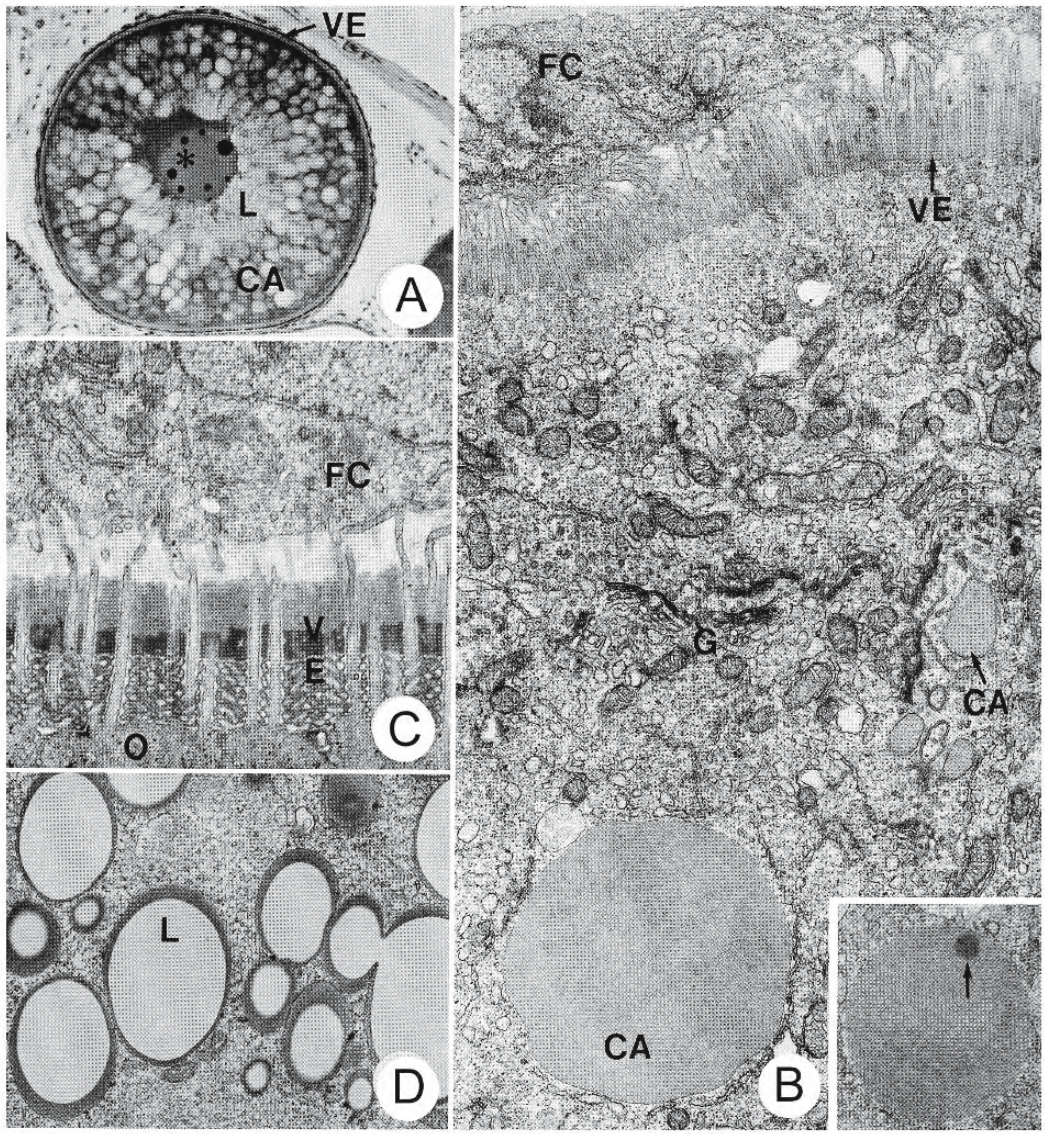

Figure 2.27: Micrographs of oocytes in the cortical alveolus stage from the pipefish *Sygnathus scovelli.* (From Begovac and Wallace, 1988; © reproduced with permission of John Wiley & Sons, Inc.).

A. Photomicrograph of an oocyte filled with large cortical alveoli (CA). The zona pellucida (VE) is present between the oocyte and its overlying follicular cells. Lipid (L) surrounds the nucleus. Several nucleoli are present within the germinal vesicle (*). X 140.

B. Electron micrograph of the cortex of an oocyte in an early cortical alveolus stage. The zona pellucida (VE) has appeared between the microvillar processes and cortical alveoli (CA) are present. Golgi complexes (G) intermingle with mitochondria. FC, follicular cell. X 10,700 The inset shows a cortical alveolus with an electron-dense inclusion (arrow). X 19,200.

C. Electron micrograph of an oocyte (O) in a later cortical alveolus stage. The zona pellucida (VE) has assumed a trilaminar appearance. FC, follicular cell. X 12,240.

D. Electron micrograph of lipid droplets (L) within an oocyte. The centre of each droplet appears empty as the result of partial extraction of lipid during processing. X 13,920.

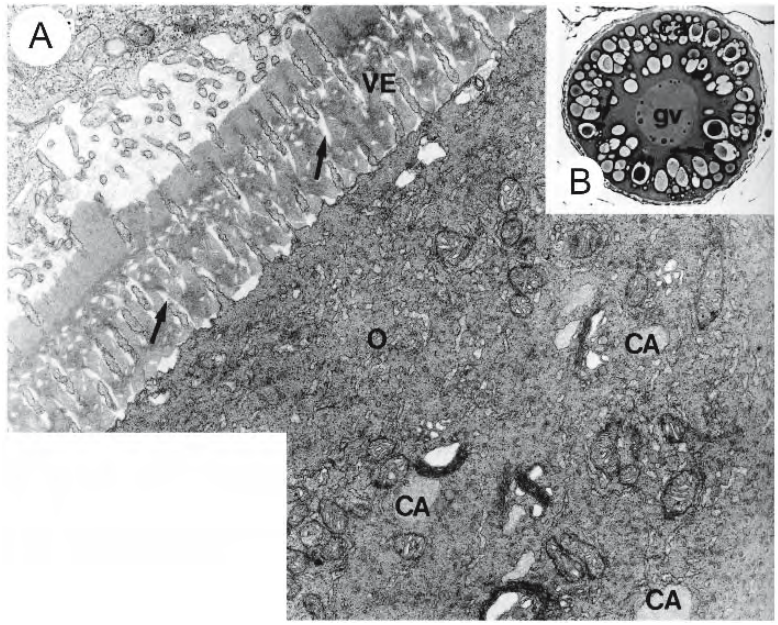

Figure 2.28: Micrographs of follicles in the cortical alveolus stage from the killifish *Fundulus heteroclitus.* (From Selman and Wallace, 1986; reproduced with kind permission from the Society for Integrative and Comparative Biology).

A. Electron micrograph showing microvilli extending through pore canals (arrows) in the zona pellucida (VE) of an oocyte (O). The ooplasm contains nascent cortical alveoli (CA). X 12,200.

B. Photomicrograph of an oocyte with cortical alveoli (CA) and lipid droplets (arrows) in the ooplasm. gv, germinal vesicle. X 96.

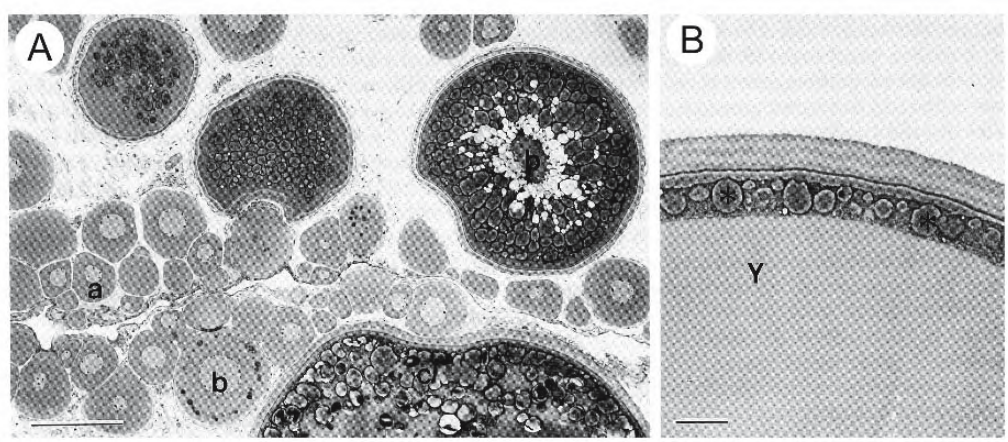

Figure 2.29: Photomicrographs of sections through ovigerous folds of the killifish *Fundulus heteroclitus.* (From Selman, Wallace, and Barr, 1988; © reproduced with permission of John Wiley & Sons, Inc.).

A. Follicles are at different stages of development: (a) primary growth stage, (b) yolk vesicle stage, and (c) vitellogenic follicle. Cortical alveoli increase in size and number as the follicle develops and move peripherally in the ooplasm. Bar = 0.2 mm.

B. Cortex of an egg showing cortical alveoli (*) in a layer of cortical ooplasm that surrounds a central mass of fluid yolk (Y). Bar = 0.05 mm.

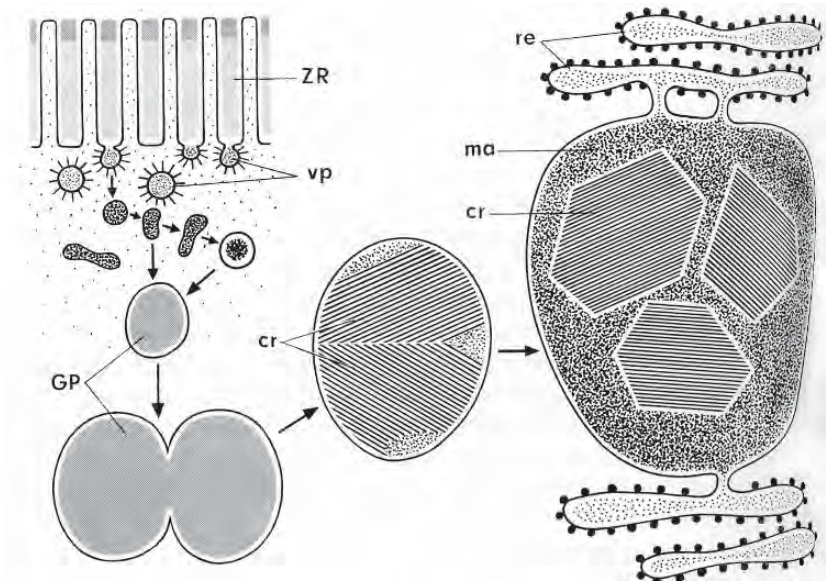

Figure 2.30: Diagrams illustrating the formation of protein yolk in *Brachydanio rerio.* Pinocytotic vesicles (vp) form on the surface of the oocyte (upper left). These fuse to form yolk bodies (GP) with homogeneous contents. The content of these yolk bodies may assume a crystalline structure (cr) (centre). Older yolk bodies continue to increase in size (right) by incorporating amorphous material (ma) from the granular endoplasmic reticulum (re) by a fusion of membranes. ZR, zona pellucida. (From Ulrich, 1969, *Journal de Microscopie*; reproduced with permission).

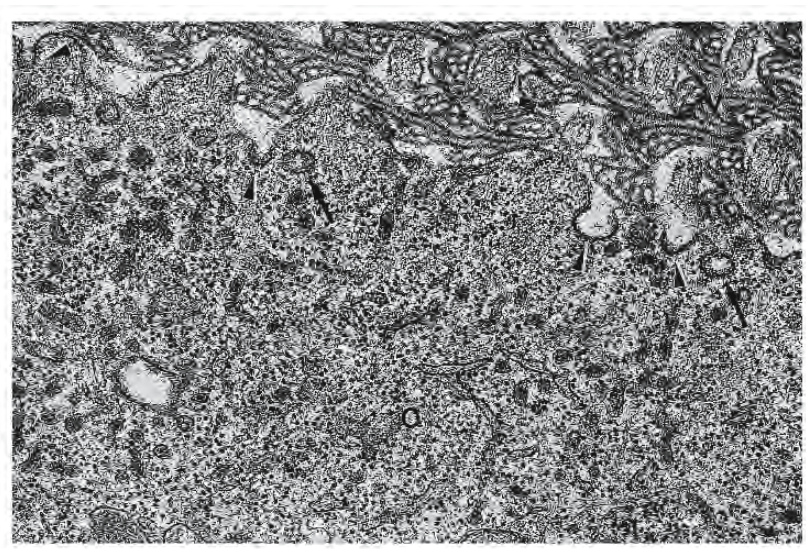

Figure 2.31: Electron micrograph showing abundant micropinocytotic activity at the surface of an oocyte (O) from an early vitellogenic follicle of the sheepshead minnow *Cyprinodon variegatus.* Coated pits (arrowheads), coated vesicles (arrows), and smooth-surfaced tubules are abundant. V, zona pellucida. X 35,280 (From Selman and Wallace, 1989; reproduced with permission from the Zoological Society of Japan).

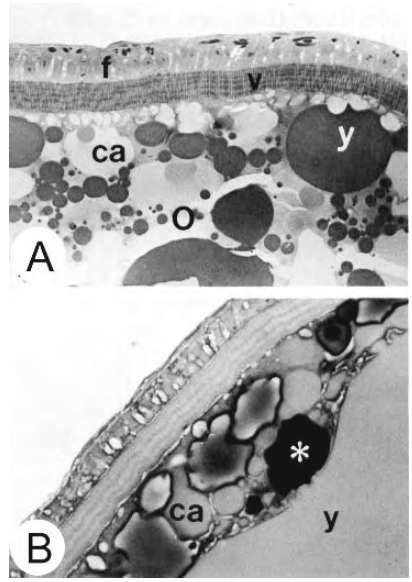

Figure 2.32: Photomicrographs of sections through follicles of the killifish *Fundulus heteroclitus.* (From Selman and Wallace, 1986; reproduced with kind permission from the Society for Integrative and Comparative Biology).

A. Vitellogenic follicle. The most obvious event marking the initiation of vitellogenesis is the appearance of membrane-bound, fluid-filled yolk spheres (y) lying between cortical alveoli (ca) in the peripheral ooplasm (O). f, follicular epithelium; v, zona pellucida. X 368.

B. Follicle in early maturation. The oocyte contains a central mass of fluid yolk (y) surrounded by peripheral yolk spheres, cortical alveoli (ca), and a lipid droplet (*). X 416.

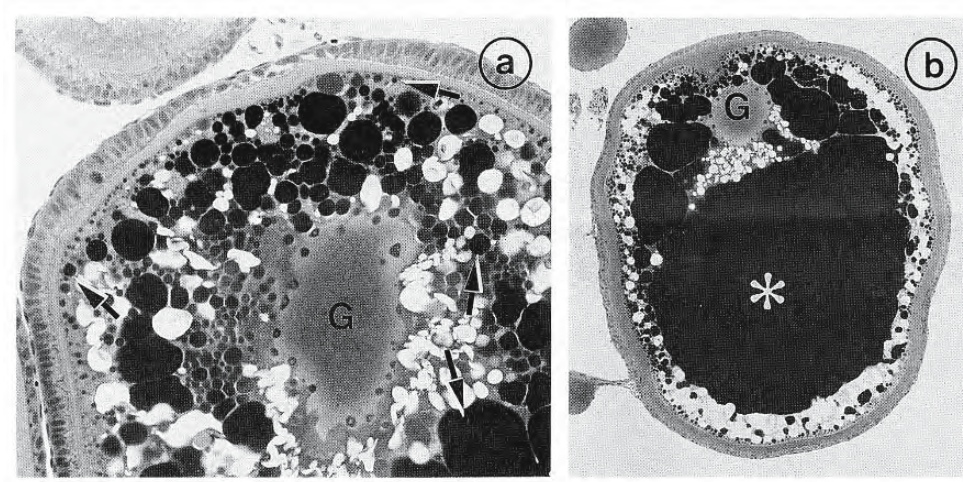

Figure 2.33: Photomicrographs through vitellogenic follicles of the sheepshead minnow *Cyprinodon variegatus*. Yolk accumulates within yolk spheres that coalesce to form a continuous mass of yolk. G, germinal vesicle (From Selman and Wallace, 1989; reproduced with permission from the Zoological Society of Japan).

A. Fluid-filled yolk bodies (arrows) in this mid-vitellogenic follicle are in various stages of fusion. X 215.

B. The central mass of fluid yolk (*) occupies much of the ooplasm in this late vitellogenic follicle. X 62.

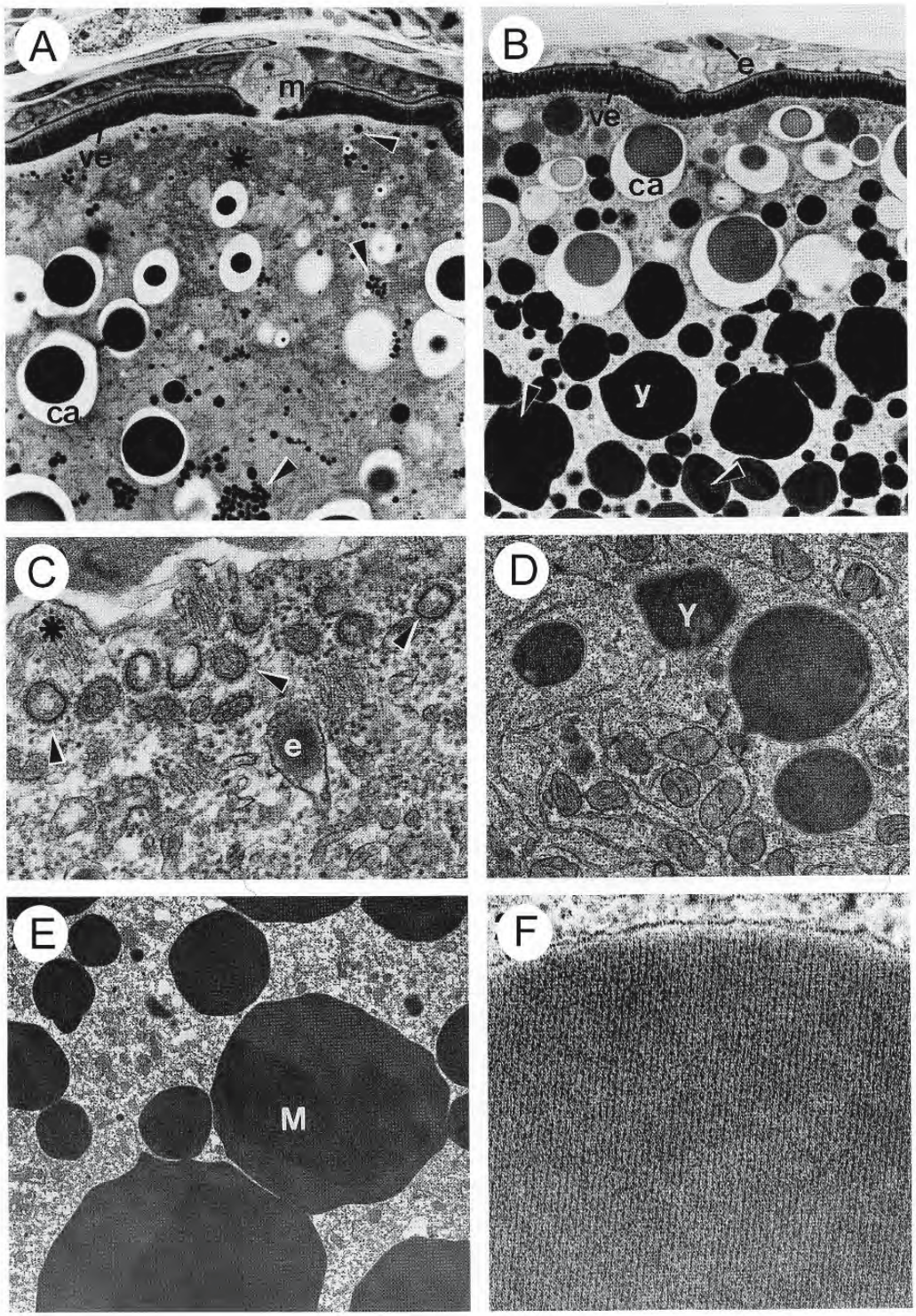

←——

Figure 2.34: Micrographs of sections through follicles of the zebrafish *Brachydanio rerio.* (From Selman et al., 1993; © reproduced with permission of John Wiley & Sons, Inc.).

A. Photomicrograph of an early vitellogenic follicle showing the follicular wall and numerous small yolk bodies (arrowheads) and cortical alveoli (ca) within the oocyte. The micropylar cell (m) within the follicular epithelium projects through the zona pellucida (ve) toward the oocyte. The darkly stained masses (*) in the cortical ooplasm represent aggregations of mitochondria and endoplasmic reticulum. The pore canals appear as light striations crossing the zona pellucida. X 815.

B. Photomicrograph of a midvitellogenic follicle. Yolk bodies (y) within the oocyte are of variable size and some display dark staining masses (arrowheads) or "main bodies" within them. Erythrocytes (e) are visible in a thecal capillary. ca, cortical alveolus; ve, zona pellucida. X 815.

C. Electron micrograph of the outer surface of a vitellogenic oocyte displaying endocytotic activity. Coated vesicles (arrowheads) and smooth-surfaced endosomes are abundant. e, endosome containing electron-dense material; *, bundle of actin filaments beneath the oolemma. X 44,100.

D. Electron micrograph of membrane-limited yolk bodies (Y) in an early vitellogenic oocyte. These small yolk bodies reveal no internal crystalline component. X 16,000.

E. Electron micrograph of crystalline yolk. The crystalline nature of the main bodies (M) is not apparent at this low magnification. X 3,240.

F. Electron micrograph of a yolk body showing a crystalline component next to the membrane. X 64,800.

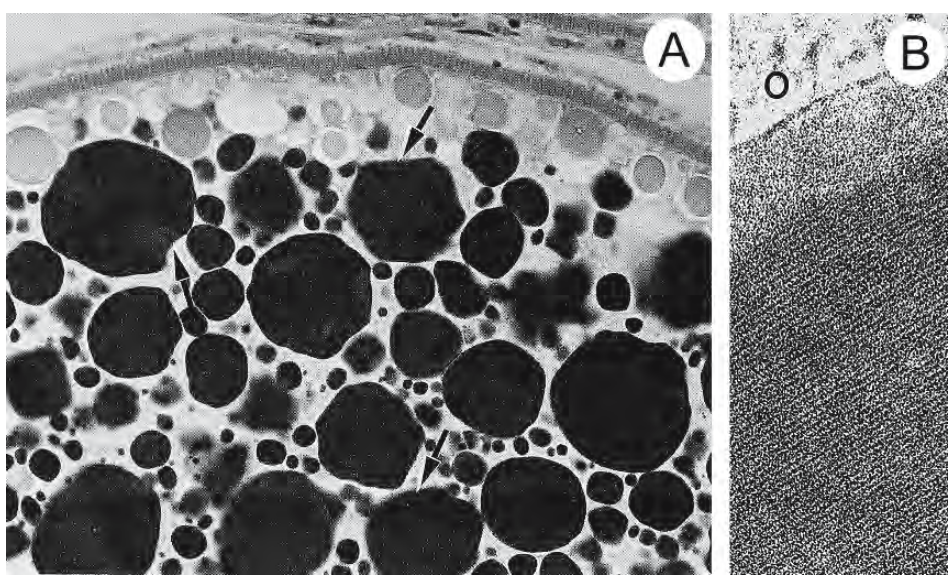

Figure 2.35: Yolk protein may be sequestered in platelets comprised of an orthorhombic crystalline structure. (From Selman and Wallace, 1989; reproduced with permission from the Zoological Society of Japan).

A. Photomicrograph of a section through a mid-vitellogenic follicle of the zebrafish *Brachydanio rerio* showing numerous yolk platelets of variable size (arrows) X 572.

B. Electron micrograph showing the crystalline core of a yolk platelet from a mullet *Mugil cephalus*. O, ooplasm. X 108,000.

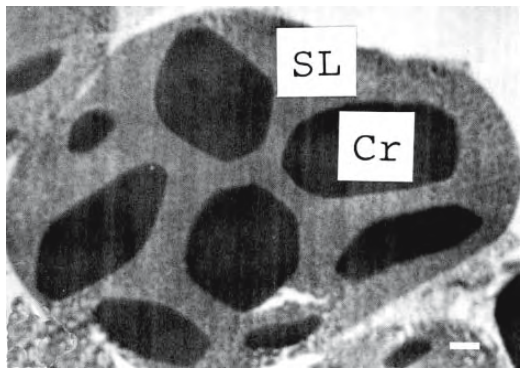

Figure 2.36: Scanning transmission electron micrograph of an ultrathin cryosection of a yolk platelet from *Pelvicachromis pulcher* (Cichlidae) showing the composition of crystals (Cr) and the non-crystalline matrix or superficial layer (SL). Bar = 1 μm (From Lange et al., 1983; reproduced with permission from Elsevier Science).

Figure 2.37: Micrographs of oocytes of the pipefish *Syngnathus scovelli* during vitellogenesis. (From Begovac and Wallace, 1988; © reproduced with permission of John Wiley & Sons, Inc.).

A. Photomicrograph of early vitellogenic oocyte with many small yolk spheres (Y) within the ooplasm. Cortical alveoli (CA) are displaced to the periphery. Lipid (L) is present centrally near the germinal vesicle and among the yolk spheres. X 120.

B. Photomicrograph of an oocyte in midvitellogenesis. The yolk spheres (Y) have become larger. Peripheral displacement of cortical alveoli (CA) and lipid has continued. X 255.

C. Photomicrograph of an oocyte during late vitellogenesis. Most of the yolk spheres have coalesced to form a central fluid mass (Y). Cortical alveoli (CA) and lipid droplets (*) remain in the peripheral part of the yolk mass. Arrowhead: zona pellucida. X 150.

D. Electron micrograph of an early vitellogenic oocyte in which yolk spheres are forming. The primary yolk spheres (Y1) contain condensed yolk and vesicular structures. Fully formed yolk spheres (Y3) contain electron-dense, yolk-specific inclusions (arrow). X 17,400.

E. Electron micrograph of an early vitellogenic oocyte with transitional yolk spheres (Y2) that are characterized by condensing yolk material and vesicular structures. One of the yolk spheres contains the electron-dense yolk-specific marker (arrow) in addition to vesicular elements. L, lipid. X 20,300.

F. Electron micrograph of midvitellogenic oocyte showing a heterogeneous collection of yolk-specific inclusions (arrowheads) within a large, mature yolk sphere (Y3). The yolk spheres are membrane bound (arrows). Smaller yolk spheres are also present. X 12,800.

G. Electron micrograph showing endocytotic activity at the periphery of a vitellogenic oocyte. The endocytotic vesicles are clathrin coated (arrows). VE, zona pellucida. X 36,600.

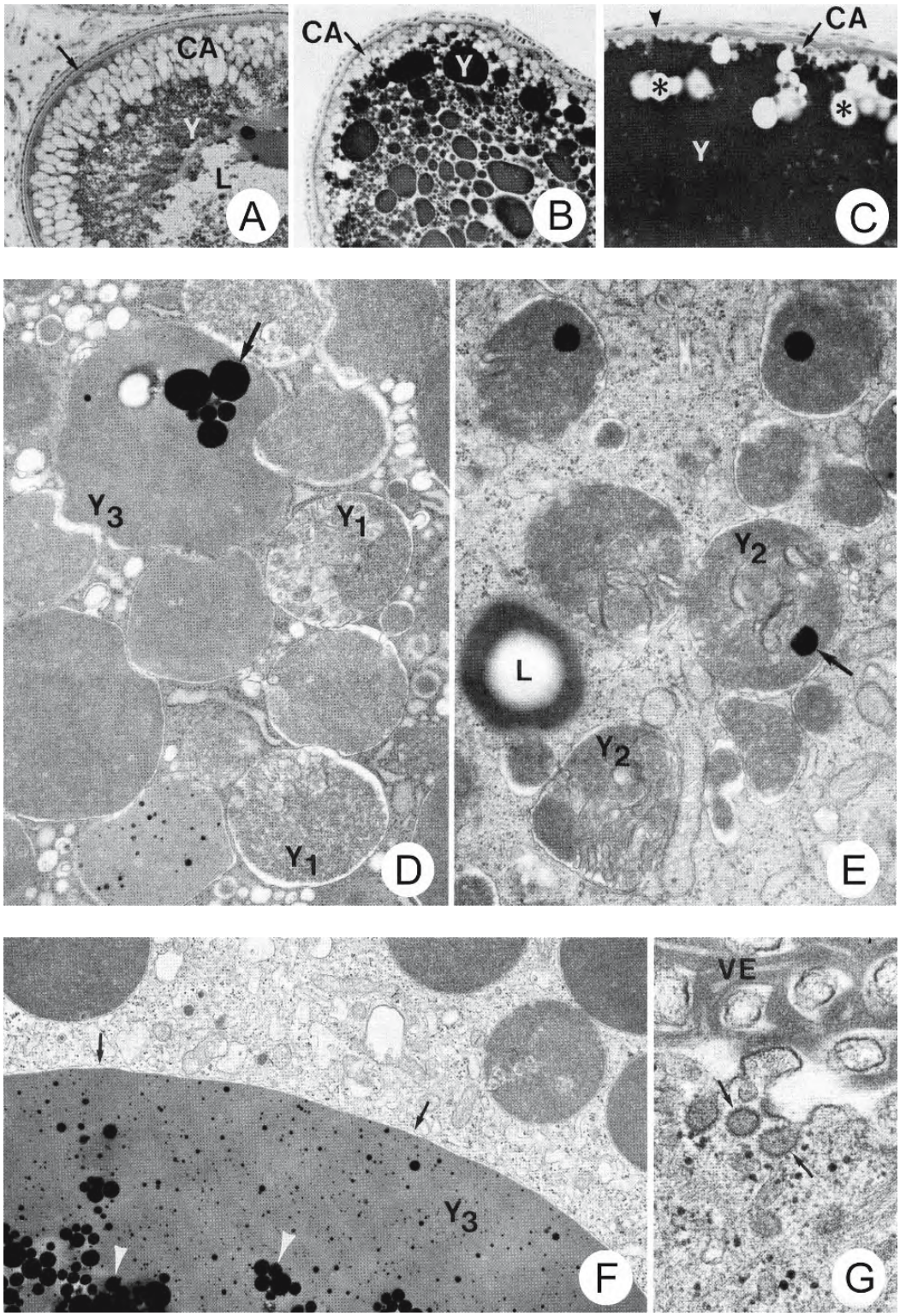

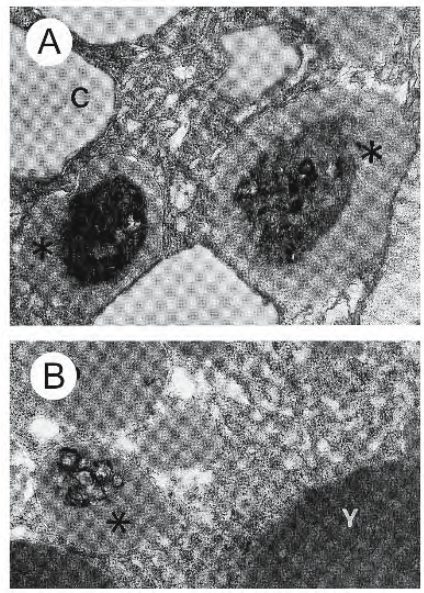

Figure 2.38: Electron micrographs of lysosome-like bodies (*) within oocytes of the seahorse *Hippocampus erectus.* (From Selman, Wallace, and Player, 1991; © reproduced with permission of John Wiley & Sons, Inc.).
A. Lysosome bodies lie next to cortical alveoli (C) in oocytes in the late cortical alveolus stage. X17,480.
B. Yolk spheres (Y) within a vitellogenic oocyte. Some still contain remnants of lysosome-like bodies within them. X 14,600.

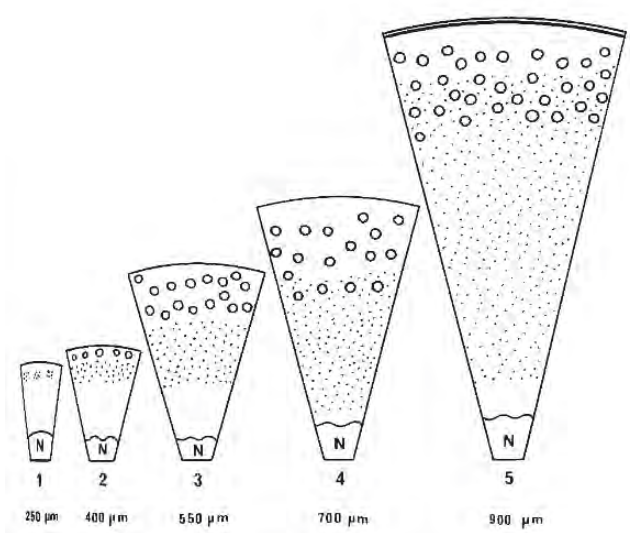

Figure 2.39: Diagrams illustrating the accumulation of multivesicular bodies during primary growth of the oocyte of the trout *Salmo trutta fario.* Multivesicular bodies (dots) appear at the periphery of an oocyte about 250 µm in diameter (1), accumulate to form a continuous layer (2), subsequently spreading toward the centre and later to the periphery of the oocyte (3-5). The circles represent cortical alveoli. N, nucleus. Lipid droplets are not shown. (From Busson-Mabillot, 1984, *Biologie Cellulaire*; reproduced with permission).

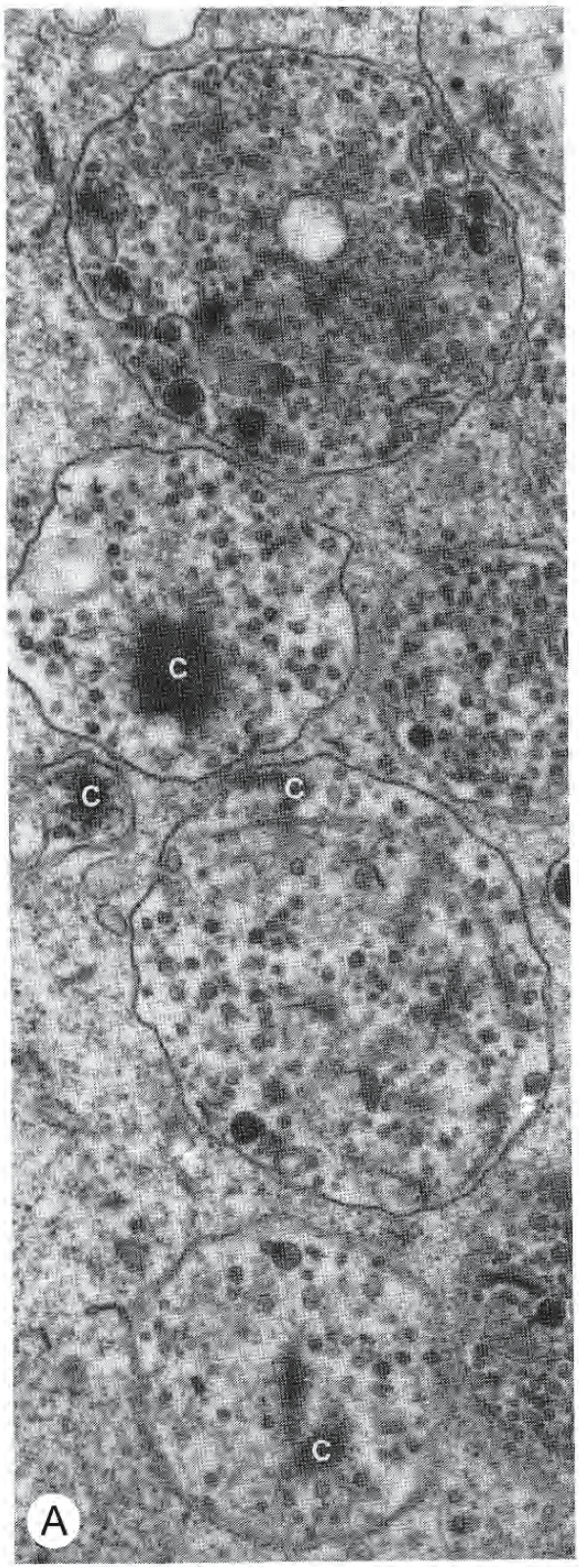

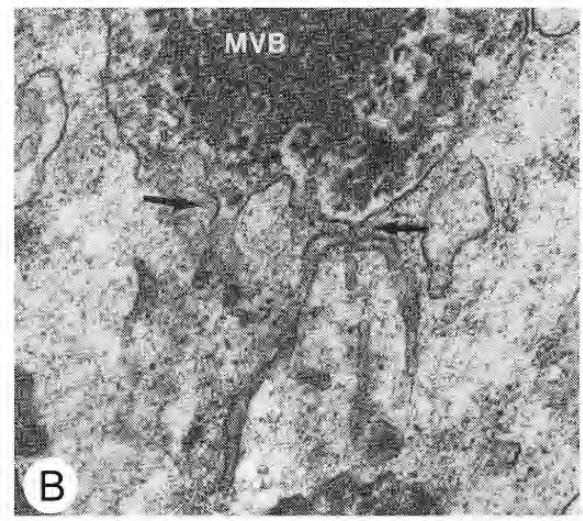

Figure 2.40: Electron micrographs showing multivesicular bodies in oocytes of the trout *Salmo trutta fario.* (From Busson-Mabillot, 1984, *Biologie Cellulaire*; reproduced with permission).

A. Multivesicular bodies from an oocyte of 300 μm, showing limiting membranes, inner vesicles, and finely granular clumps (c) within the matrix. X 50,000.

B. Continuity (arrows) between a multivesicular body (MVB) and cisternae of the agranular endoplasmic reticulum.

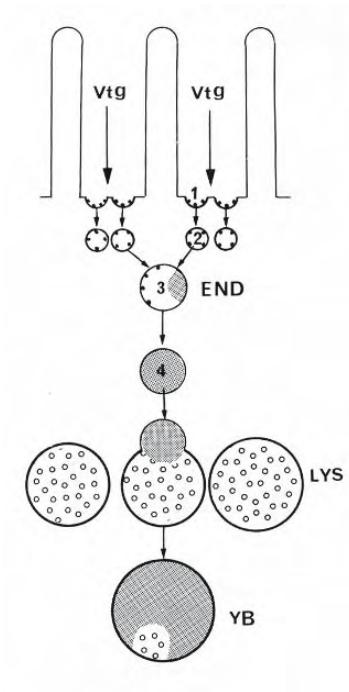

Figure 2.41: Diagram summarizing the sequence of vitellogenesis in the trout *Salmo trutta fario.* (From Busson-Mabillot, 1984, *Biologie Cellulaire*; reproduced with permission) Endocytotic vesicles (1,2) sequester vitellogenin (vtg). These coalesce (3,4) to form larger vesicles which eventually fuse with preexisting lysosomes (LYS) to form yolk bodies (YB).

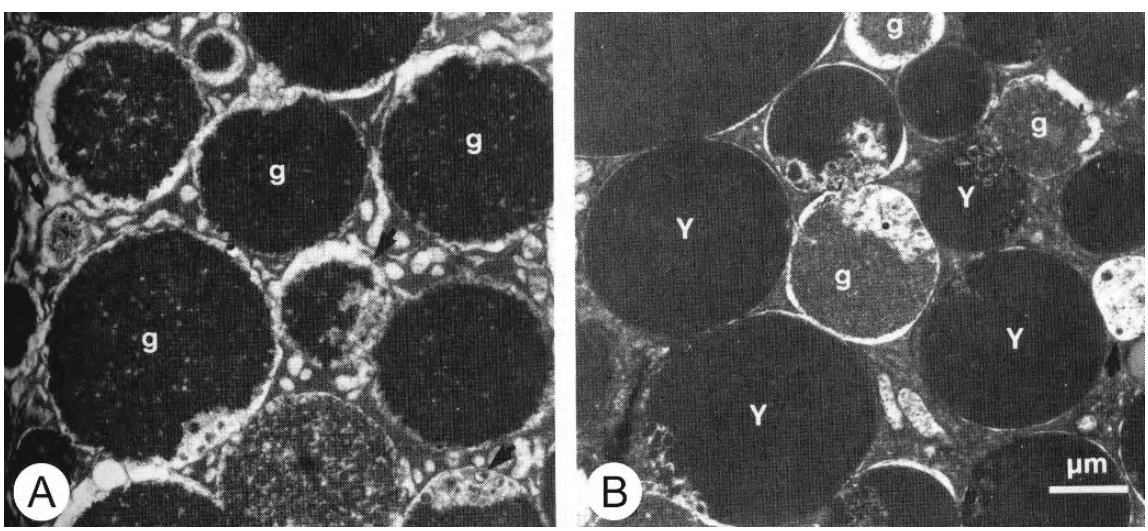

Figure 2.42: Electron micrographs of lysosomes during vitellogenesis in oocytes of the trout *Salmo trutta fario.* (From Busson-Mabillot, 1984, *Biologie Cellulaire*; reproduced with permission).

A. At the onset of vitellogenesis, most lysosomes of this region are packed with a coarse granular material (g). X 11,250.

B. Later, most lysosomes contain homogeneous yolk (Y), although some granular lysosomes (g) and plain multivesicular bodies (arrows) may be seen. X 11,250.

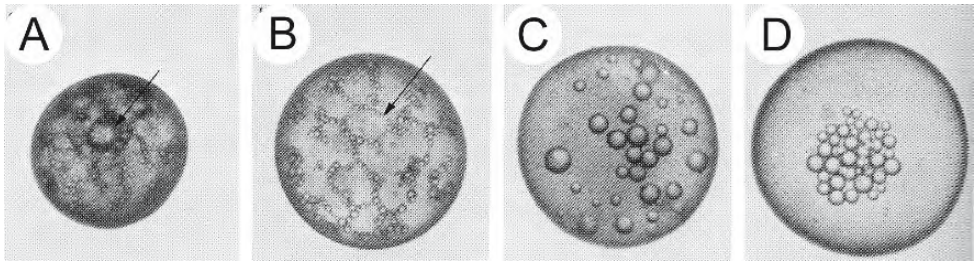

Figure 2.43: Photomicrographs of individual follicles *in vitro* of the killifish *Fundulus heteroclitus*. X 16 (From Wallace and Selman, 1978; reproduced with permission from Elsevier Science).

A. 1.6-mm follicle containing an oocyte with a germinal vesicle (arrow) near the upper surface.

B. 1.6-mm follicle containing an oocyte in which the germinal vesicle has migrated to the surface (arrow).

C. 1.7-mm follicle containing an oocyte in which there is no germinal vesicle. The oil droplets have begun to coalesce but are still peripherally attached.

D. 1.9-mm follicle containing an oocyte in which the oil droplets, no longer peripherally attached, collect at the upper surface.

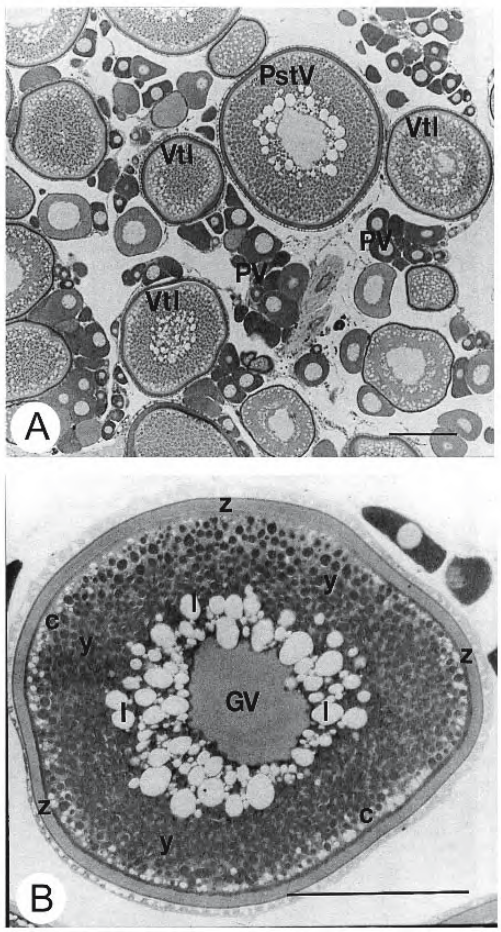

←

Figure 2.44: Photomicrographs of sections of the ovary of the gilthead seabream during the spawning season. Scale bars = 200 μm (From Gothilf et al., 1997; reproduced with permission from the Society for the Study of Reproduction, Inc.).

A. An overview showing several stages of oocyte development.

B. Follicle containing postvitellogenic oocyte.

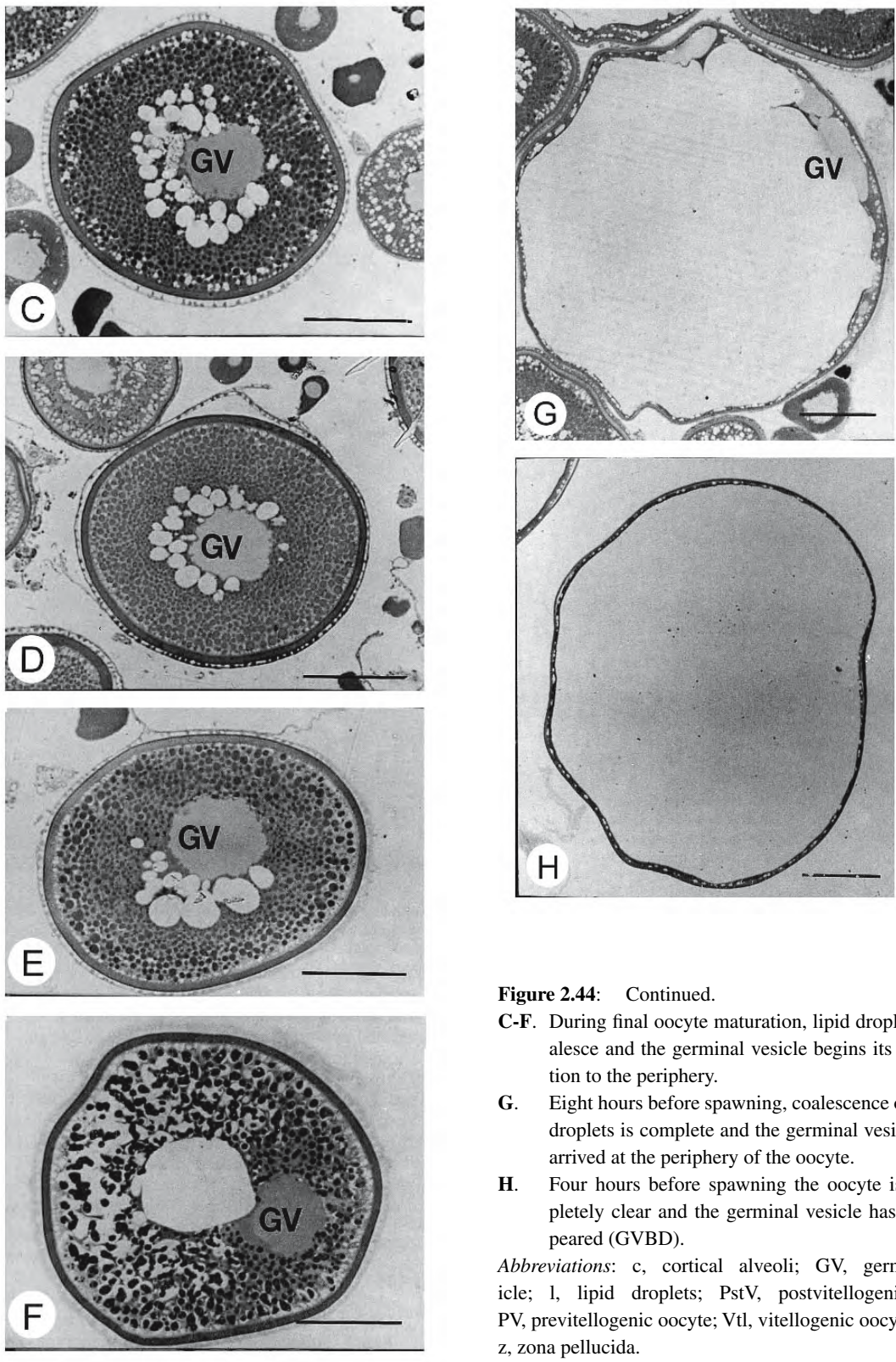

Figure 2.44: Continued.

C-F. During final oocyte maturation, lipid droplets coalesce and the germinal vesicle begins its migration to the periphery.

G. Eight hours before spawning, coalescence of lipid droplets is complete and the germinal vesicle has arrived at the periphery of the oocyte.

H. Four hours before spawning the oocyte is completely clear and the germinal vesicle has disappeared (GVBD).

Abbreviations: c, cortical alveoli; GV, germinal vesicle; l, lipid droplets; PstV, postvitellogenic oocyte; PV, previtellogenic oocyte; Vtl, vitellogenic oocyte; y, yolk; z, zona pellucida.

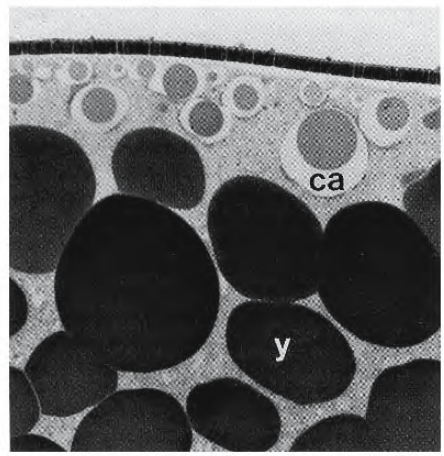

Figure 2.45: Photomicrograph of a section through the cortex of a mature egg of the zebrafish *Brachydanio rerio*. Yolk bodies (y) have smooth contours, homogeneous interiors, and lie subjacent to cortical alveoli (ca). X 78 (From Selman et al., 1993; © reproduced with permission of John Wiley & Sons, Inc.).

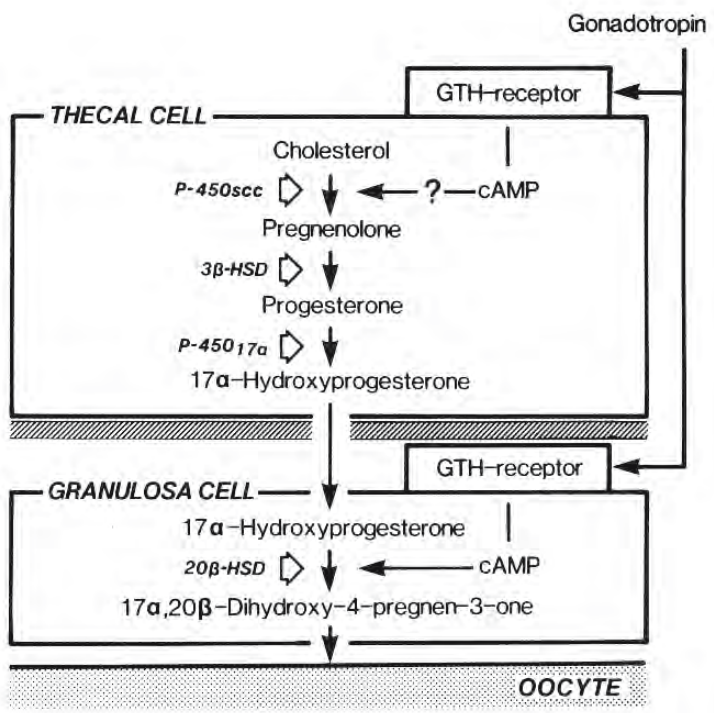

Figure 2.46: Two-cell model for the production of 17α,20β-dihydroxy-4-pregnen-3-one by salmonid postvitellogenic follicles. (From Nagahama et al., 1994; reproduced with permission from Elsevier Science).
Abbreviations: P-450scc, cholesterol side-chain cleavage cytochrome P-450; 3β-HSD, 3β-hydroxysteroid dehydrogenase-isomerase; P-450 17α, P450 17α -hydroxylase, 20β-hydroxysteroid dehydrogenase.

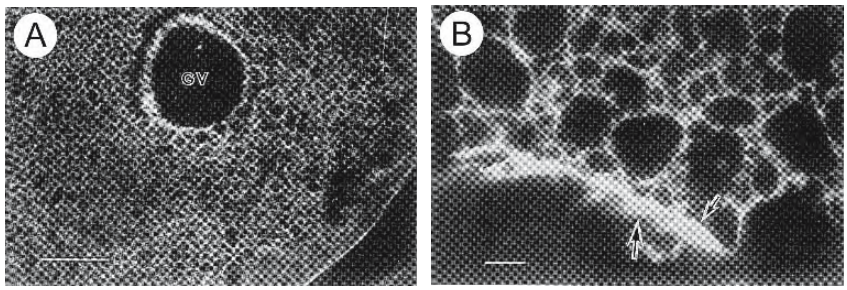

Figure 2.47: Photomicrographs showing the microtubular network in fully grown oocytes of the goldfish *Carassius auratus* by confocal immunofluorescence microscopy using tubulin antibody. Yolk granules appear as dark masses suspended within the meshes of the microtubular network. (From Jiang et al., 1996; reproduced with permission from the Zoological Society of Japan).

A. A condensed band of microtubules surrounds the germinal vesicle (GV). Bar = 100 μm.

B. Bright band of microtubules (small arrow) surrounding the germinal vesicle. Bar = 10 μm.

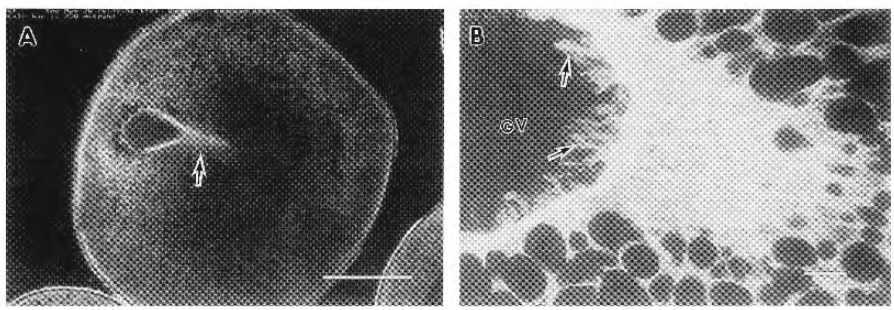

Figure 2.48: Photomicrographs showing the reorganization of the microtubular network during migration of the germinal vesicle to the animal pole in oocytes of the goldfish *Carassius auratus;* confocal immunofluorescence microscopy using tubulin antibody. (From Jiang et al., 1996; reproduced with permission from the Zoological Society of Japan).

A. Migrating germinal vesicle with a long perinuclear tail (arrow). Bar = 250 μm.

B. The perinuclear tail consists of condensed microtubular arrays and short microtubules in clefts (arrows). Bar = 10 μm GV, germinal vesicle.

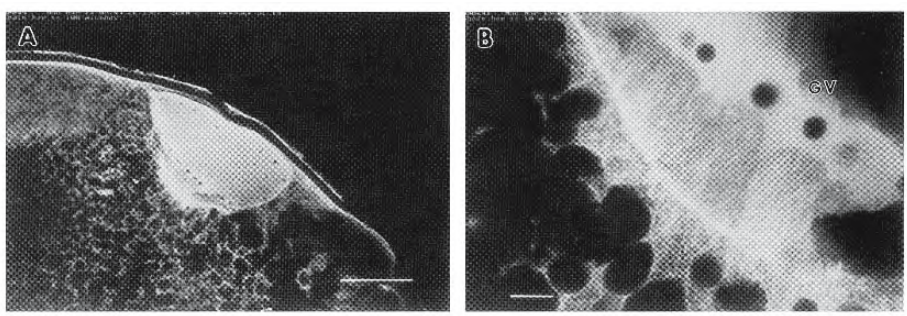

Figure 2.49: Photomicrographs showing the relationship of microtubules and the germinal vesicle at the animal pole in oocytes of the goldfish *Carassius auratus* at the time of germinal vesicle breakdown; confocal immunofluorescence microscopy using tubulin antibody. (From Jiang et al., 1996; reproduced with permission from the Zoological Society of Japan).

A. Numerous microtubules form a bright band at the vegetal surface of the germinal vesicle. Bar = 100 μm.

B. Microtubules penetrate the germinal vesicle (GV) from the bright band at its vegetal surface. Bar = 10 μm.

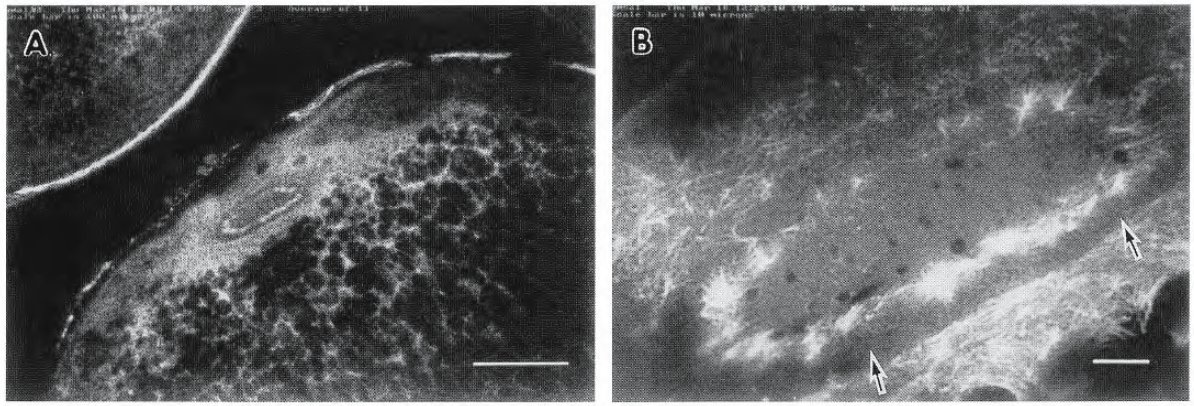

Figure 2.50: Photomicrographs showing the organization the microtubular network in the animal pole region of oocytes of the goldfish *Carassius auratus* following germinal vesicle breakdown; confocal immunofluorescence microscopy using tubulin antibody. (From Jiang et al., 1996; reproduced with permission from the Zoological Society of Japan).
A. A disc-shaped ring of condensed microtubules appears in the animal pole region. Bar = 100 μm.
B. Microtubular asters in the disc-shaped structure are surrounded by a microtubule-free area (arrows). Bar = 10 μm.

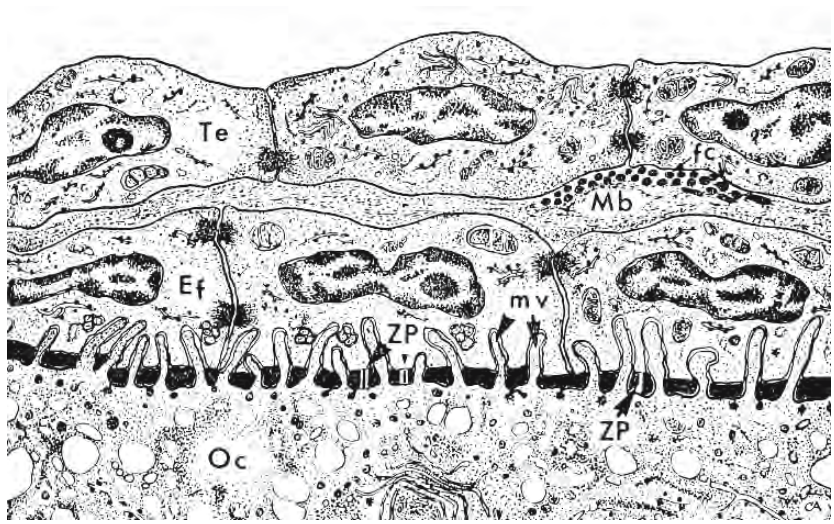

Figure 2.51: Diagram of the follicular wall of the poeciliid *Xiphophorus helleri* during the initial formation of the zona pellucida (ZP). This layer is secreted by exocytosis around the bases of microvilli (mv) that extend from the surface of the oocyte. (From Azevedo, 1974, *Journal de Microscopie*; reproduced with permission).
Abbreviations: Ef, follicular epithelial cell; fc, collagenous fibres; Mb, basement membrane of the follicular epithelium; Oc, cortical cytoplasm of the oocyte; Te, theca.

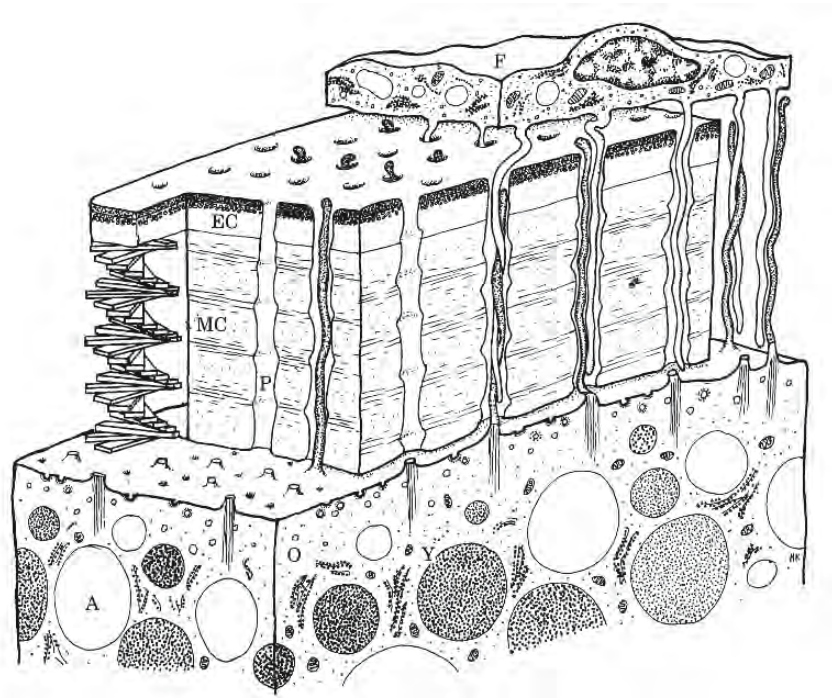

Figure 2.52: Diagram illustrating the elements of the follicular wall in spawning Atlantic cod *Gadus morhua.* Two sets of microvilli entwine within the pore canals (P): those from the oocyte (O) extend outward and those from the follicular cell (F) extend inward. Three layers are visible in the zona pellucida: the outer layer, Z1 (stippled), a middle layer Z2 (EC), and the thickest later, the architecturally complex Z3 (MC). (From Kjesbu, Kryvi, and Norberg, 1996; reproduced with permission from Elsevier Science).
Abbreviations: A, cortical alveolus; Y, yolk granule.

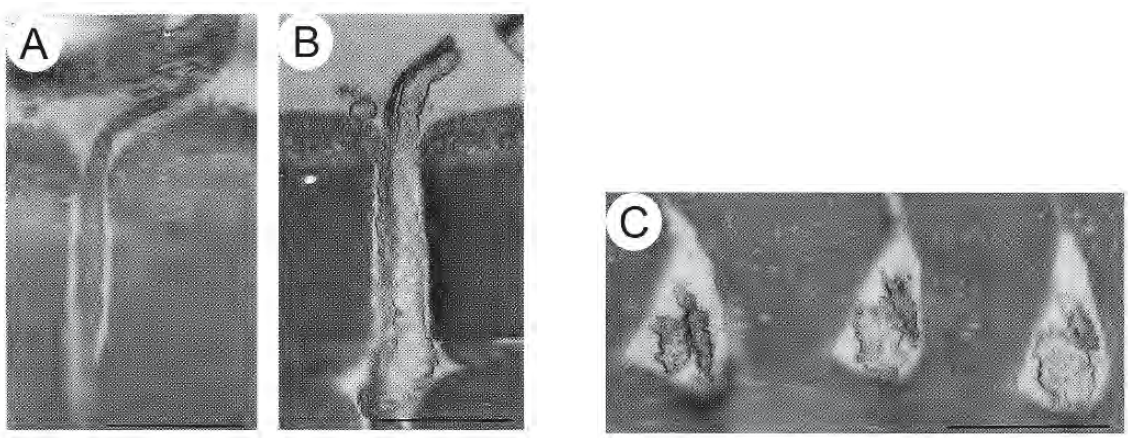

Figure 2.53: Transmission electron micrographs of the zona pellucida of spawning Atlantic cod *Gadus morhua.* Bar = 1 μm (From Kjesbu, Kryvi, and Norberg, 1996; reproduced with permission from Elsevier Science).
A. A microvillus from a follicular cell extends into a pore canal.
B. A microvillus from a follicular cell is closely associated within the pore canal with a microvillus from the oocyte.
C. This oblique section of the zona pellucida illustrates the relationship between the two microvilli within pore canals.

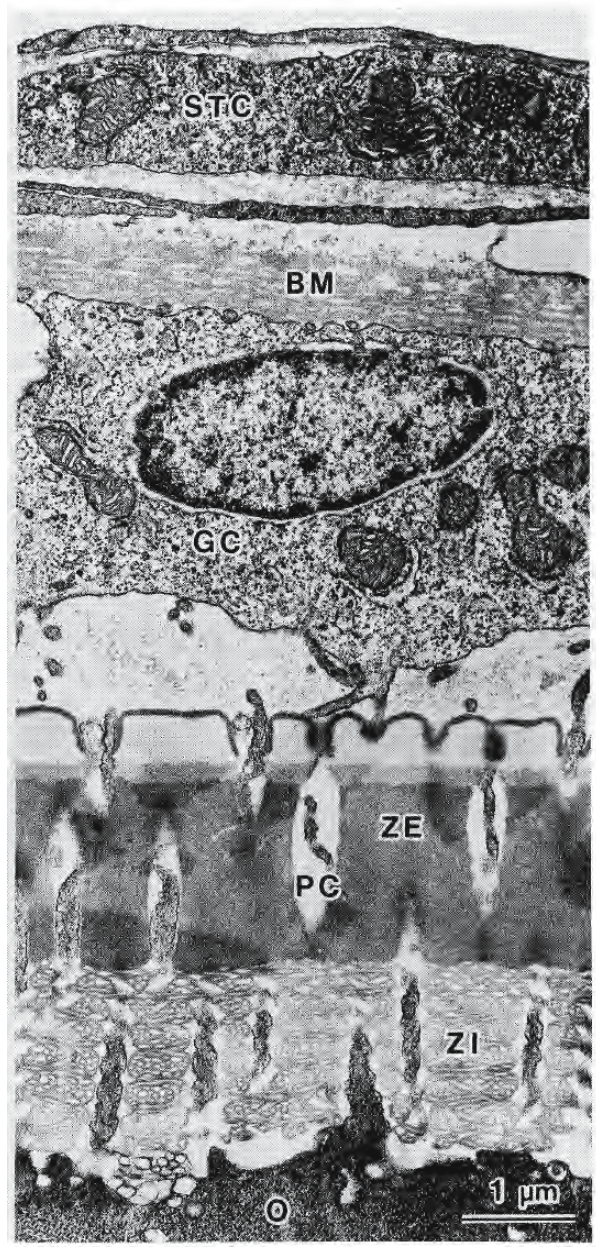

Figure 2.54: Electron micrograph of a section through the periphery of a follicle of the marine teleost *Pagrus major*. Only the peripheral ooplasm (O) of a vitellogenic oocyte is shown,. The internal part of the zona pellucida (ZI) consists of seven lamellae. A special thecal cell (STC) is present in the thecal layer. Bar = 1µ (From Matsuyama, Nagahama, and Matsuura, 1991; reproduced with permission from Elsevier Science).
Abbreviations: BM, basal lamina; GC, follicular cell; PC, pore canal; ZE, zona pellucida externa.

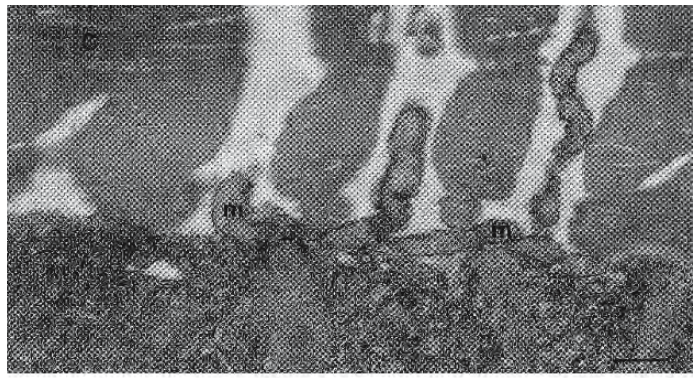

Figure 2.55: Transmission electron micrograph of the zona pellucida (c) of spawning Atlantic cod *Gadus morhua.* Microvilli (m) extending through a pore canal from a follicular cell have flattened themselves on the surface of the oocyte. Bar = 0.5 μm (From Kjesbu, Kryvi, and Norberg, 1996; reproduced with permission from Elsevier Science).

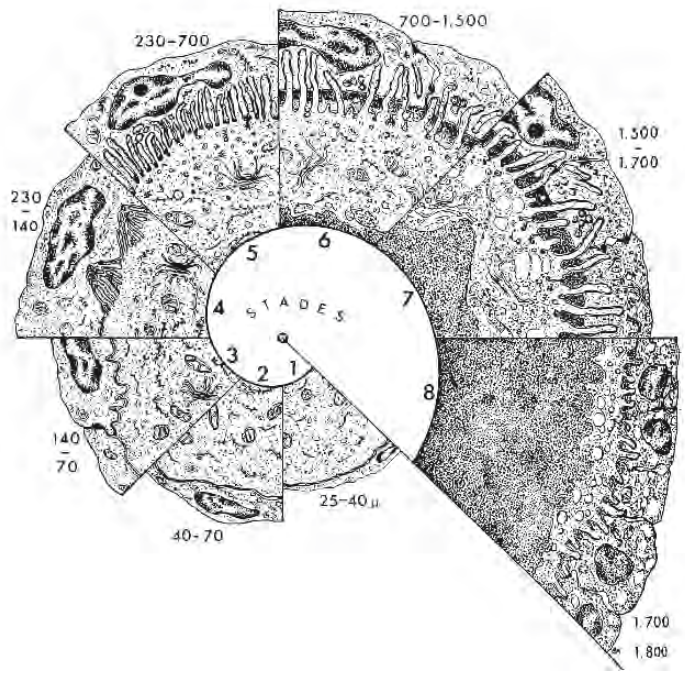

Figure 2.56: Scheme illustrating the development of the zona pellucida in the poeciliid *Xiphophorus helleri* during oogenesis. (The stages are based primarily on the diameter of the oocyte.) In stages 1, 2, and 3 the oocyte is closely surrounded by the follicular epithelium and the theca (not shown). At stage 4, microvilli extend from the oocyte toward the follicular epithelium. By stage 5, the beginnings of the zona pellucida are seen where an extracellular coat appears in the space separating the oocyte and follicular cells. In stages 6 and 7, this coat, which is perforated by microvilli extending both from the oocyte and from the follicular cells, thickens as oogenesis proceeds. Microvilli from the oocyte actually invaginate the follicular cells. The follicular cells become thicker and develop a more active appearance. In stage 8 of this viviparous teleost, the microvilli regress and their contact with the follicular cells becomes more tenuous; the zona pellucida becomes thinner and almost disappears. (From Azevedo, 1974, *Journal de Microscopie*; reproduced with permission).

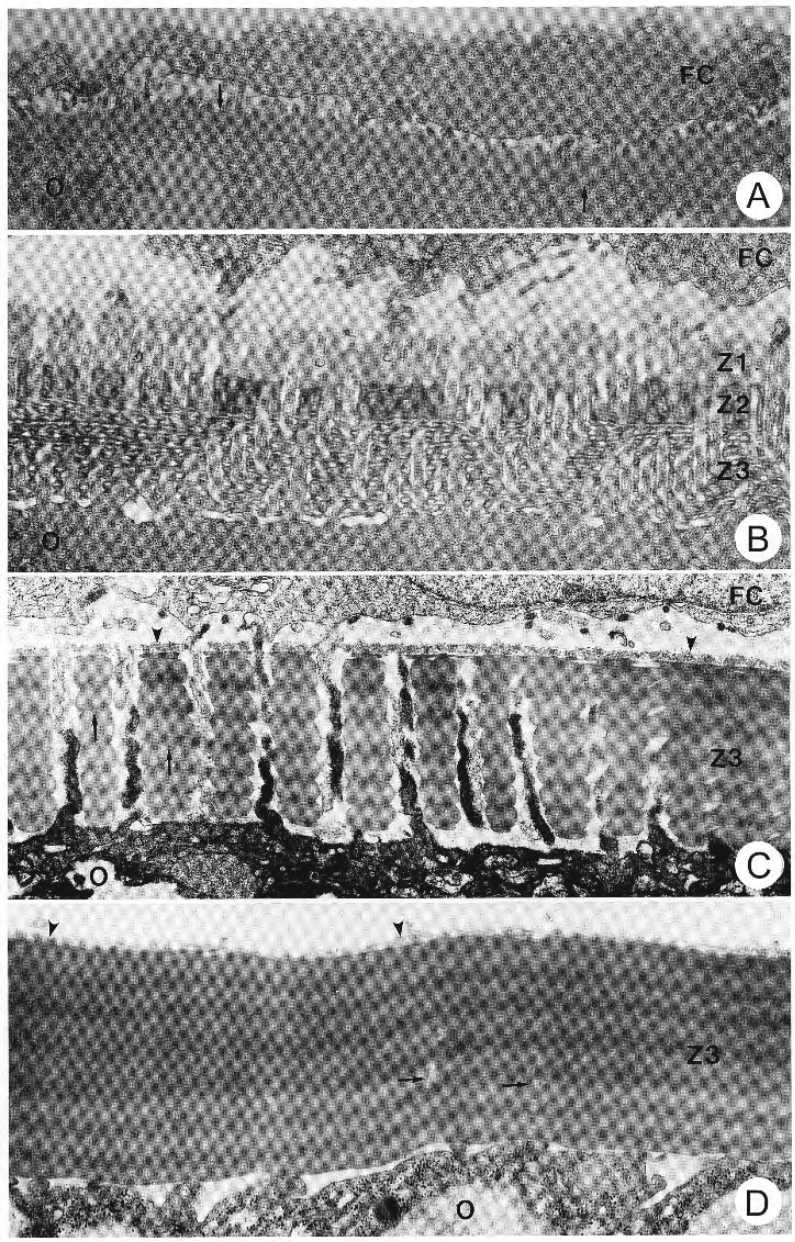

Figure 2.57: Transmission electron micrographs showing the development of the zona pellucida in the pipefish *Syngnathus scovelli.* (From Begovac and Wallace, 1989; © reproduced with permission of John Wiley & Sons, Inc.).

A. An early cortical alveoli-stage oocyte (O) showing the initial formation of Zone 1 (Z1) (arrows) of the zona pellucida. FC, follicular cell. X 16,900.

B. The zona pellucida in an oocyte (O) at a later cortical alveoli-stage. The Zones 2 and 3 (Z2, Z3) have formed beneath Zone 1. FC, follicular cell. X 16,900.

C. Zone 3 is compacted and prominent in a mid-vitellogenic oocyte (O) while the Zone 2 appears to have disappeared. Zone 1 (arrows) remains but is much thinner than in previous stages. Horizontal lamellae (arrows) are prominent within Zone 3. Microvilli from the oocyte and a follicular cell are present within the pore canals of the zona pellucida. X 16,900.

D. The outer Zone 1 (arrowheads) is retained in the zona pellucida of a mature egg Zone 3 is fully compacted; the horizontal lamellae are prominent. Only remnants of the pore canals (arrows) remain. X 16,300.

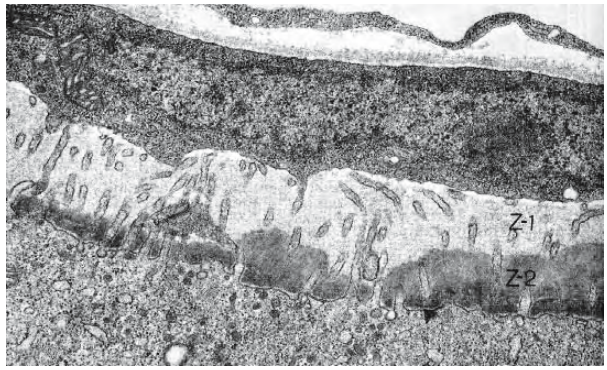

Figure 2.58: Transmission electron micrograph of a follicular cell and an oocyte in early vitellogenesis of a South American annual fish *Cynolebias* sp. Microvilli extend from the periphery of the oocyte and pass through the zona pellucida within pore canals. The periphery of the oocyte contains many dense vesicles and regions of continuity between the vesicles and the oolemma. The density of material within the vesicles is similar to that of Zone 2 (Z2) of the primary envelope. Zones 1 and 2 (Z1, Z2) lie between the oocyte and follicular cell. The follicular cell extends microvilli toward the oocyte; it contains a flattened nucleus, free ribosomes, and mitochondria. The basement lamina of the follicular epithelium, collagenous fibres, and the theca interna subtend the follicular cell. X 23,000 (From Wourms, 1976; reproduced with permission from Elsevier Science).

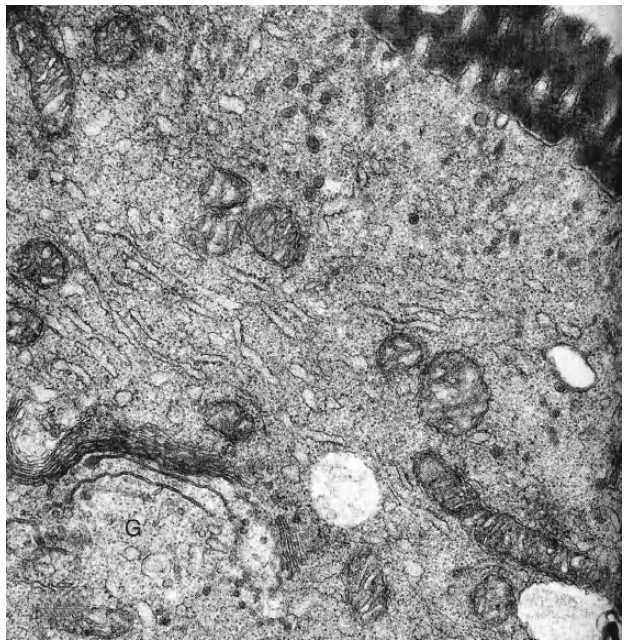

Figure 2.59: Transmission electron micrograph of the periphery and interior of an oocyte of the "annual fish" *Cynolebias melatotaenia* before the appearance of Zone 3 of the zona pellucida. The peripheral ooplasm displays enhanced apparatus for protein synthesis and secretion: free ribosomes, granular endoplasmic reticulum, and well developed Golgi complexes. Zones 1 and 2 of the zona pellucida are at the upper right. Microvilli, vesicles with dense contents, and sites of continuity between the vesicles and oolemma are seen. There is dense material in the vesicles of the large Golgi complex (G) at the lower left. Cisternae of the well-developed granular endoplasmic reticulum contain fibrillar material of low electron density. Many mitochondria are present. X 32,500 (From Wourms, 1976; reproduced with permission from Elsevier Science).

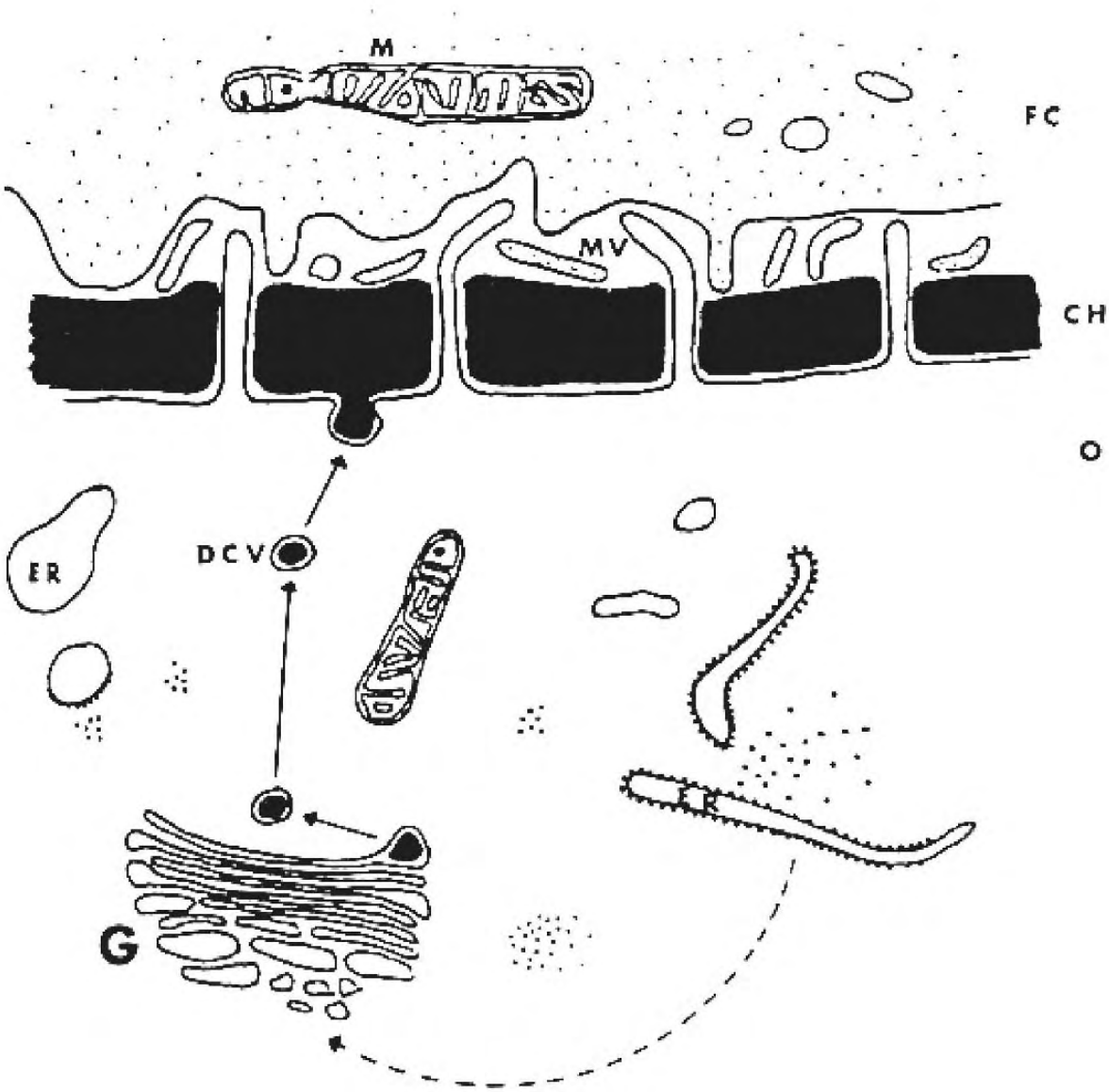

Figure 2.60: Schematic drawing summarizing the proposed steps in the formation of the zona pellucida in medaka *Oryzias latipes*. Precursor is synthesized in the ooplasm (O) and appears to be concentrated in the Golgi complexes (G). It is released into smooth-surfaced, dense-cored vesicles (DCV) which migrate to the oolemma and discharge their contents by exocytosis into the space between the oocyte and the follicular cell (FC). This material coalesces to form the zona pellucida (CH). (From Tesoriero, 1978; reproduced with permission from Elsevier Science).
Abbreviations: ER, endoplasmic reticulum; M, mitochondrion.

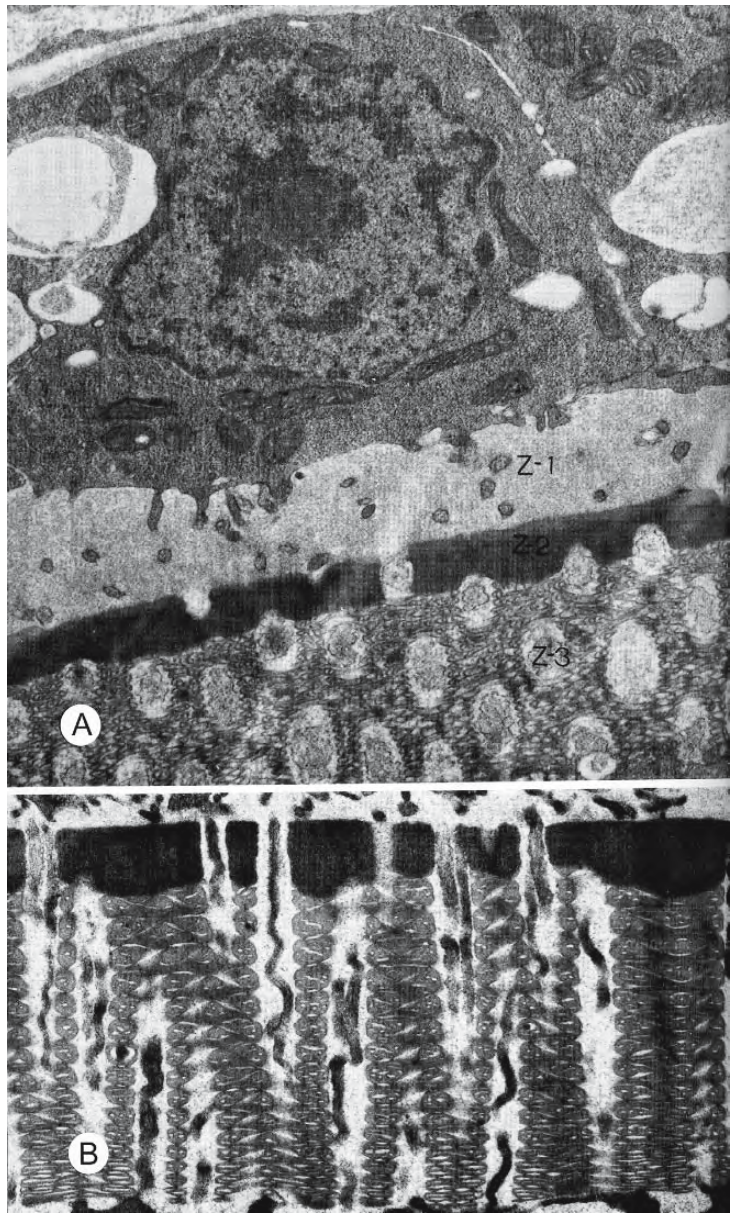

Figure 2.61: Transmission electron micrographs illustrating the primary envelopes of oocytes of two species of "annual fish" following the appearance of Zone 3 of the zona pellucida. (From Wourms, 1976; reproduced with permission from Elsevier Science).

A. Slightly tangential section of an oocyte of *Cynolebias melanotaenia*. A large cuboidal follicular cell dominates this figure; it contains many free ribosomes and mitochondria, but little granular endoplasmic reticulum. Three zones of the zona pellucida are present: Zone 1 (Z1), a low density fibrillar region; Zone 2 (Z2), a dense region; and Zone 3 (Z3), the major component consisting of interwoven fibrils. X 21,250.

B. Primary envelope of a stage 4 oocyte of *Austrofundulus transilis.* Zone 1 is uppermost and appears to be continuous with the material within the fenestrations; Zone 2 is electron dense; Zone 3, the thickest layer, is adjacent to the oocyte and consists of fine fibrils. Progressing outward, the fibrils are compressed into more massive units. Microvilli of the oocyte and follicular cells are contained within the pore canals. X 18,750.

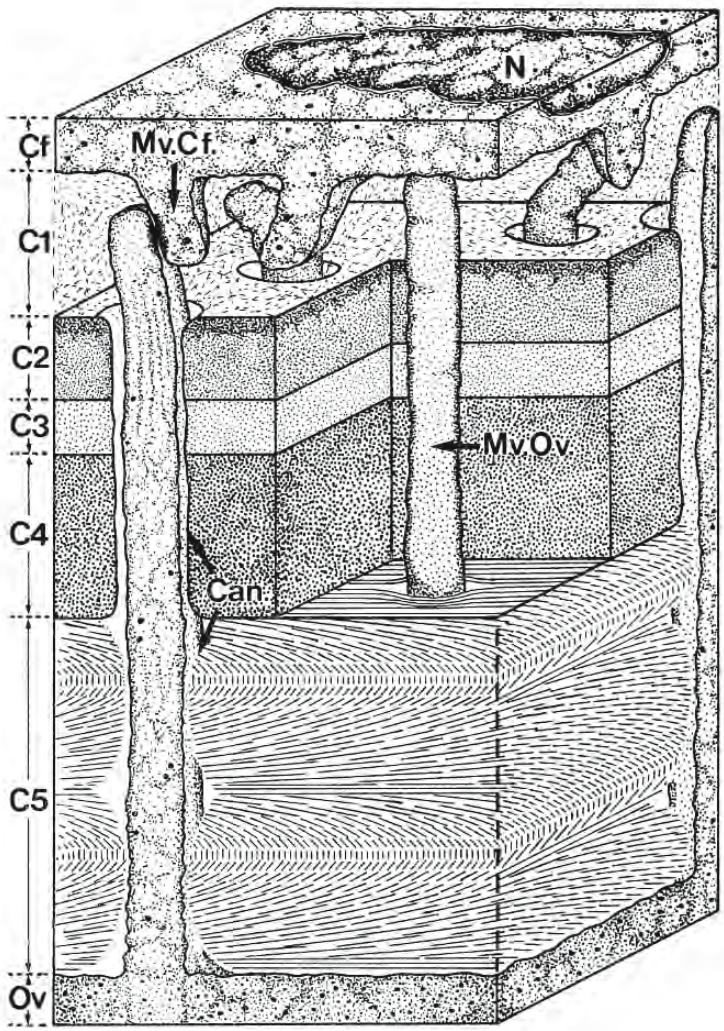

Figure 2.62: Diagram through the follicular wall of the sea bass *Dicentrarchus labrax.* The arching arrangement of fibrils in the major zone of the zona pellucida (C5) may provide flexibility. A portion of a follicular cell (Cf) is shown at the top; the periphery of an oocyte (Ov) appears at the bottom. The zona pellucida is shown in four layers (C2, C3, C4, C5). A desmosome is shown connecting microvilli within a pore canal. (From Caporiccio and Connes, 1977; reproduced with permission, © Masson Editeur).

Abbreviations: C1, subepithelial space; Can, pore canal; MvCf, microvillus of follicular cell; MvOv, microvillus of oocyte; N, nucleus of follicular cell.

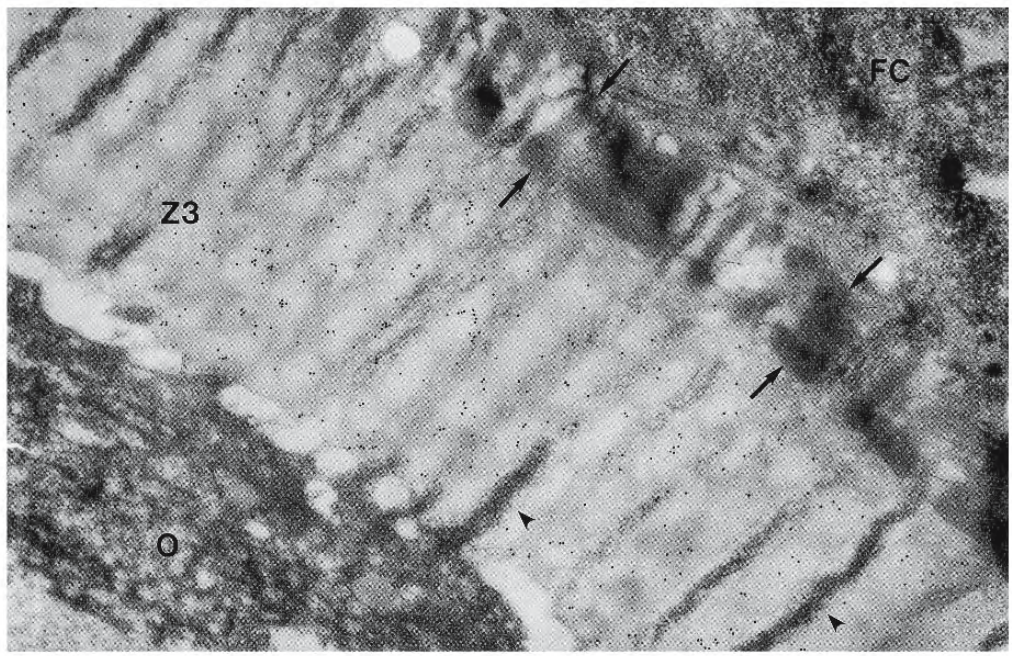

Figure 2.63: Immunogold staining was used to demonstrate that principal proteins of the zona pellucida originate within the follicle. A monoclonal antibody, raised against proteins of the zona pellucida, recognized no other component of the oocyte, plasma, or liver. In this transmission electron micrograph of the zona pellucida of the pipefish *Syngnathus scovelli,* the labelling is restricted to the Zone 3 (Z3) layer while the outer Zone 1 (Z1) and Zone 2 (Z2) layers (arrows) lack immunoreactivity. The oocyte (O), follicular cells (FC), and microvilli (arrowheads) within the pore canals also lack immunoreactivity. X 22,150 (From Begovac and Wallace, 1989; © reproduced with permission of John Wiley & Sons, Inc.).

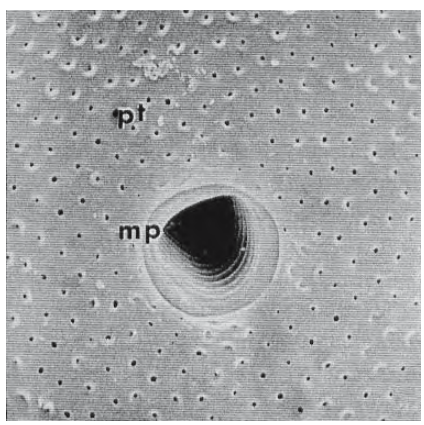

Figure 2.64: There is no degeneration of the outermost layer of the zona pellucida in the porgy *Pagras major* prior to maturation and the surface pits (pt) of the pore canals remain open. This is a scanning electron micrograph of the animal pole region of an ovum with the micropyle (mp) at the centre. X 2,000 (From Hosokawa, 1983; reproduced with permission from the Zoological Society of Japan).

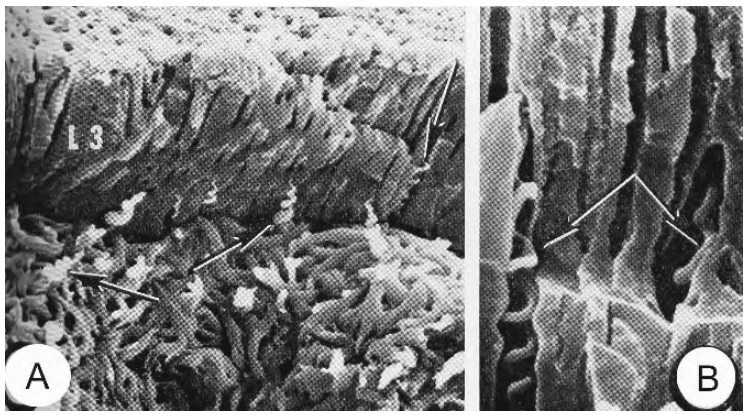

Figure 2.65: Scanning electron micrographs of the fractured zona pellucida of the white sturgeon *Acipenser transmontanus.* The outer layers are anchored to the second layer by screwlike projections. (From Cherr and Clark, 1982; reproduced with permission from Blackwell Publishing).

A. Screwlike projections (arrows) connect the second and third (L3) layers. X 3,300.

B. Screwlike projections (arrows) in the pits of the third layer. The pits conform to the shape of the screws. X 10,000.

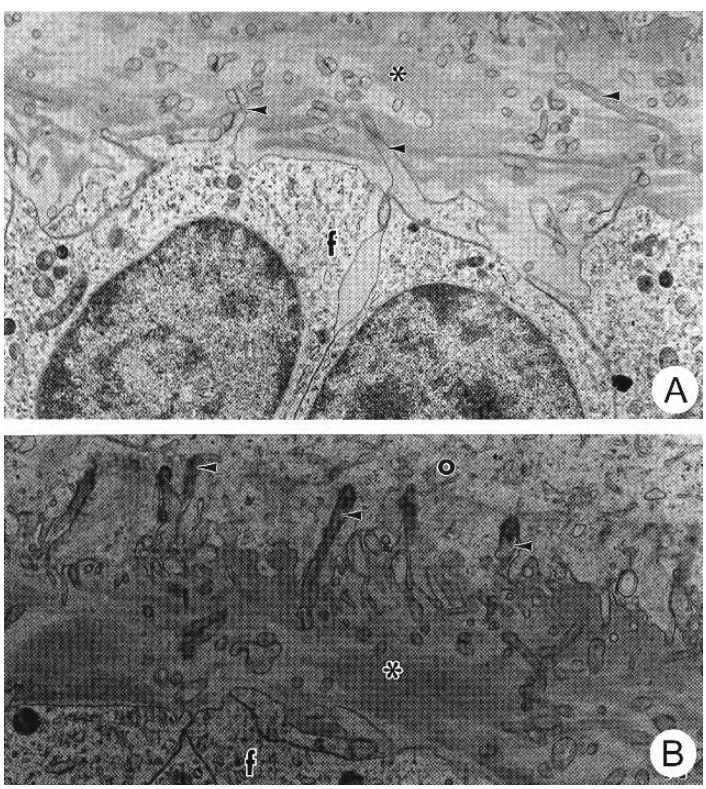

←

Figure 2.66: Transmission electron micrographs of the peripheral region of ovarian follicles of a viviparous elasmobranch, the yellow spotted stingray *Urolophus jamaicensis.* Pores in the delicate zona pellucida (*) contain processes (arrowheads) from the follicular cells (f). Tips of the processes invaginate the oocyte as transosomes and become incorporated in the cytoplasm. There are no processes extending from the oocyte. (From Hamlett, Jezior, and Spieler, 1999; reproduced with permission of Urban & Fischer Verlag).

A. Forming processes from follicular cells (f) extend through the zona pellucida (*), invaginate the oolemma, and become pinched off within the ooplasm as discrete vesicles, the transosomes (arrowheads). X 10,000.

B. Definitive transosomes (arrowheads) from follicular cells (f) cross the zona pellucida (*) to impinge on an oocyte (o). X 15,000.

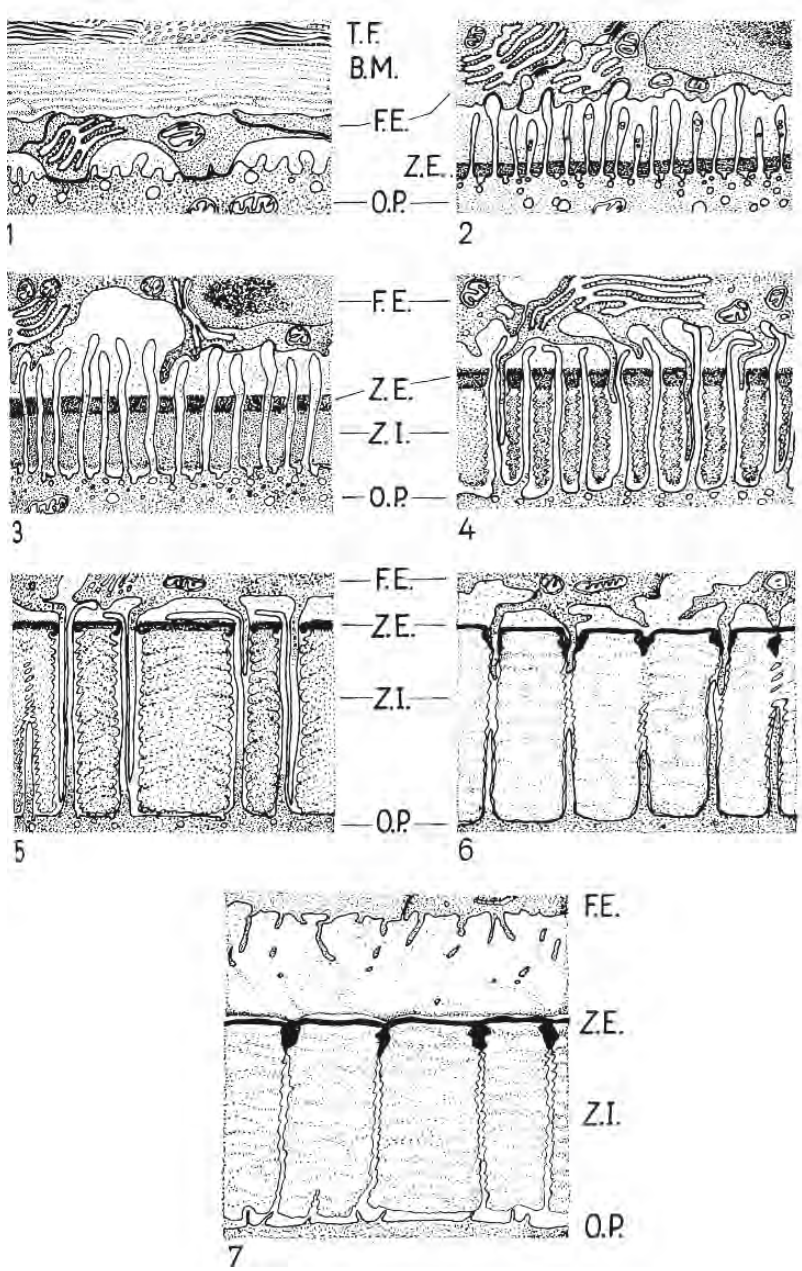

Figure 2.67: Schematic diagrams illustrating the involvement of follicular cells in the formation of a secondary envelope around the zona pellucida of the oocyte of the brook trout *Salvelinus fontinalis*. Processes from the oocyte extend through pore canals in the zona pellucida to indent the surface of the follicular cells. Meanwhile, processes from the follicular cells pass through the pore canals in the opposite direction. The follicular cells are pushed farther and farther away from the zona pellucida as they secrete the jelly-like material of the secondary envelope. Microvilli from follicular cells and oocyte withdraw from the zona pellucida near the time of ovulation. (From Flügel, 1967b; reproduced with permission of the author).
Abbreviations: BM, basement membrane of the follicular epithelium; FE, follicular epithelium; OP, ooplasm; TF, theca; ZE and ZI, outer and inner regions of the zona pellucida.

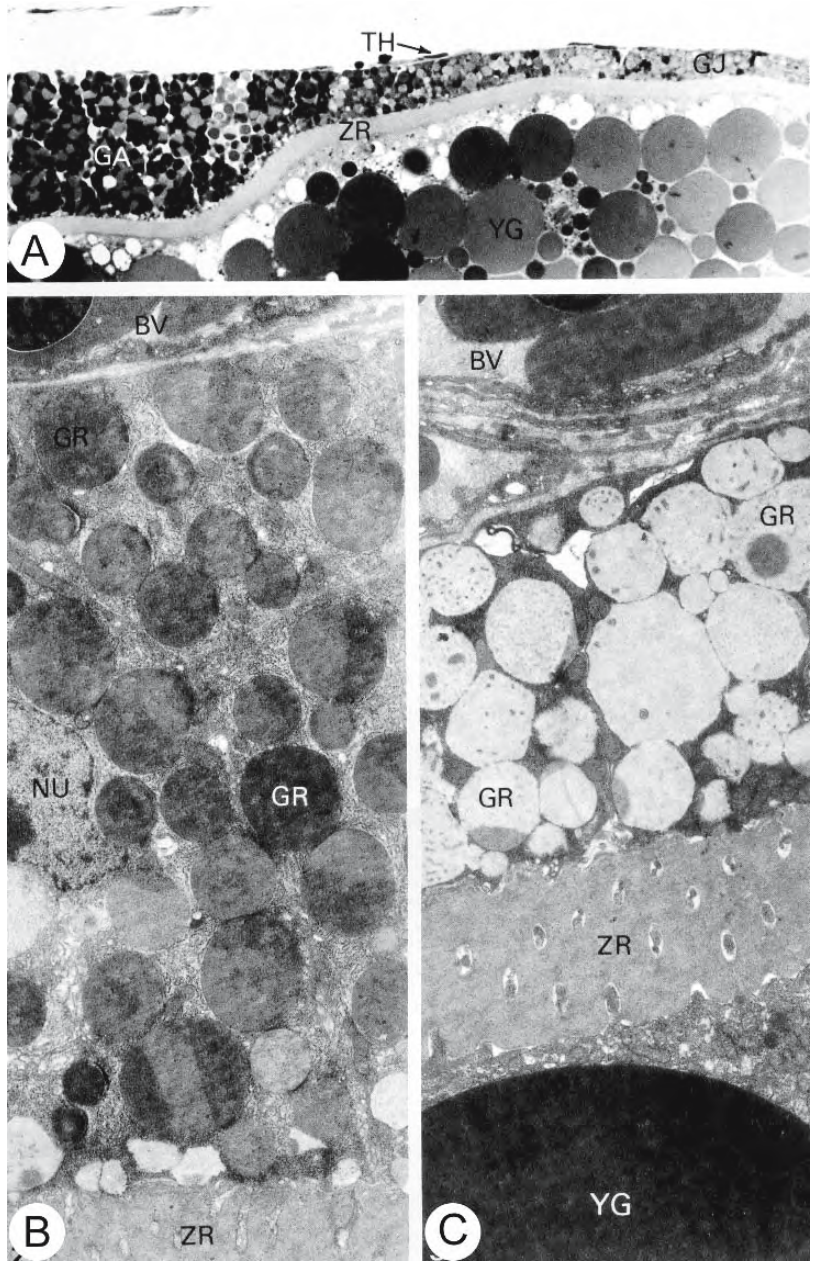

Figure 2.68: Transmission micrographs of postvitellogenic follicles of the African catfish Clarias *gariepinus.* (From van den Hurk and Peute, 1985; reproduced with permission of the authors).

A. Light micrograph showing two types of follicular cells: the columnar cells (GA) that form the attachment disc and cuboidal cells (GJ) that form the jelly coat. X 560.

B. Electron micrograph of a columnar follicular cell containing electron-dense granules (GR); these cells form the attachment disc. X 5,400.

C. Electron micrograph of a cuboidal follicular cell containing electron-lucent granules (GR). These cells form the jelly coat. X 5,400.

Abbreviations: BV, blood vessel; NU, nucleus; TH, theca; YG, yolk granule; ZR, zona pellucida.

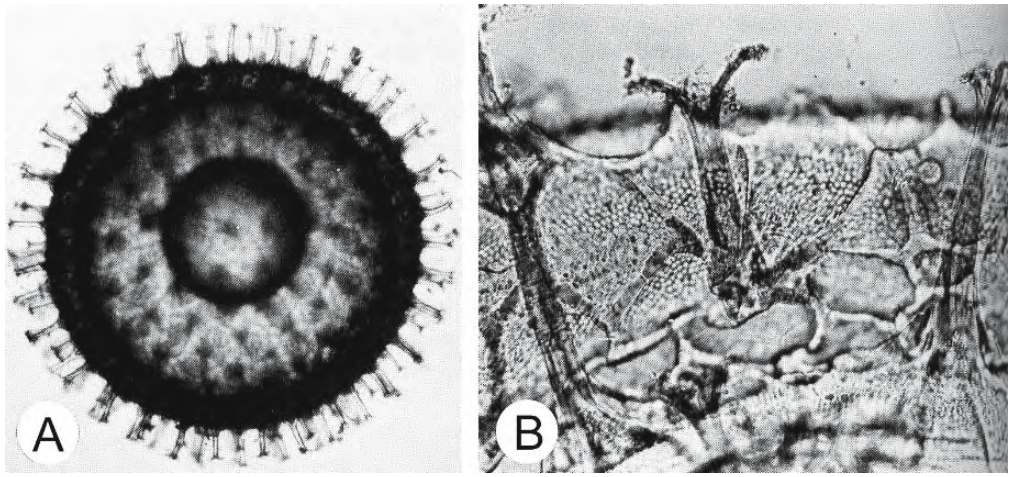

Figure 2.69: Light micrographs of whole fertilized eggs of the annual fish *Cynolebius melanotaenia* showing the elaborate ornamentation of the chorion. (From Wourms, 1976; reproduced with permission from Elsevier Science).

A. The surface of the egg is covered with spike-like projections. Note the large lipid droplet within the yolk mass. X ca 20.

B. Profile view of the chorion showing three spikes extending above the elaborate sculpting of the surface. The material of the secondary envelope is nearly transparent. X ca 385.

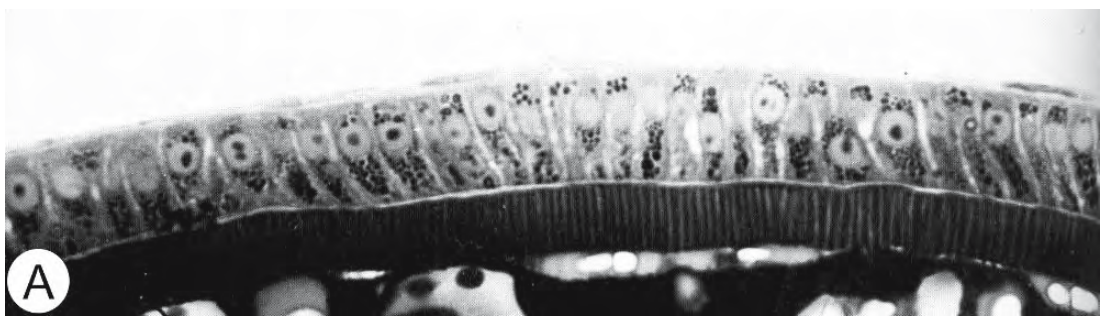

Figure 2.70: Micrographs of sections of the simple columnar follicular epithelium and oocyte of the annual fish *Cynolebius melanotaenia* when deposition of the primary envelope is complete. (From Wourms, 1976; reproduced with permission from Elsevier Science).

A. Photomicrograph showing the follicular epithelium resting upon the primary envelope (the light striations within represent pore canals). The follicular cells are packed with dark granules. X 725.

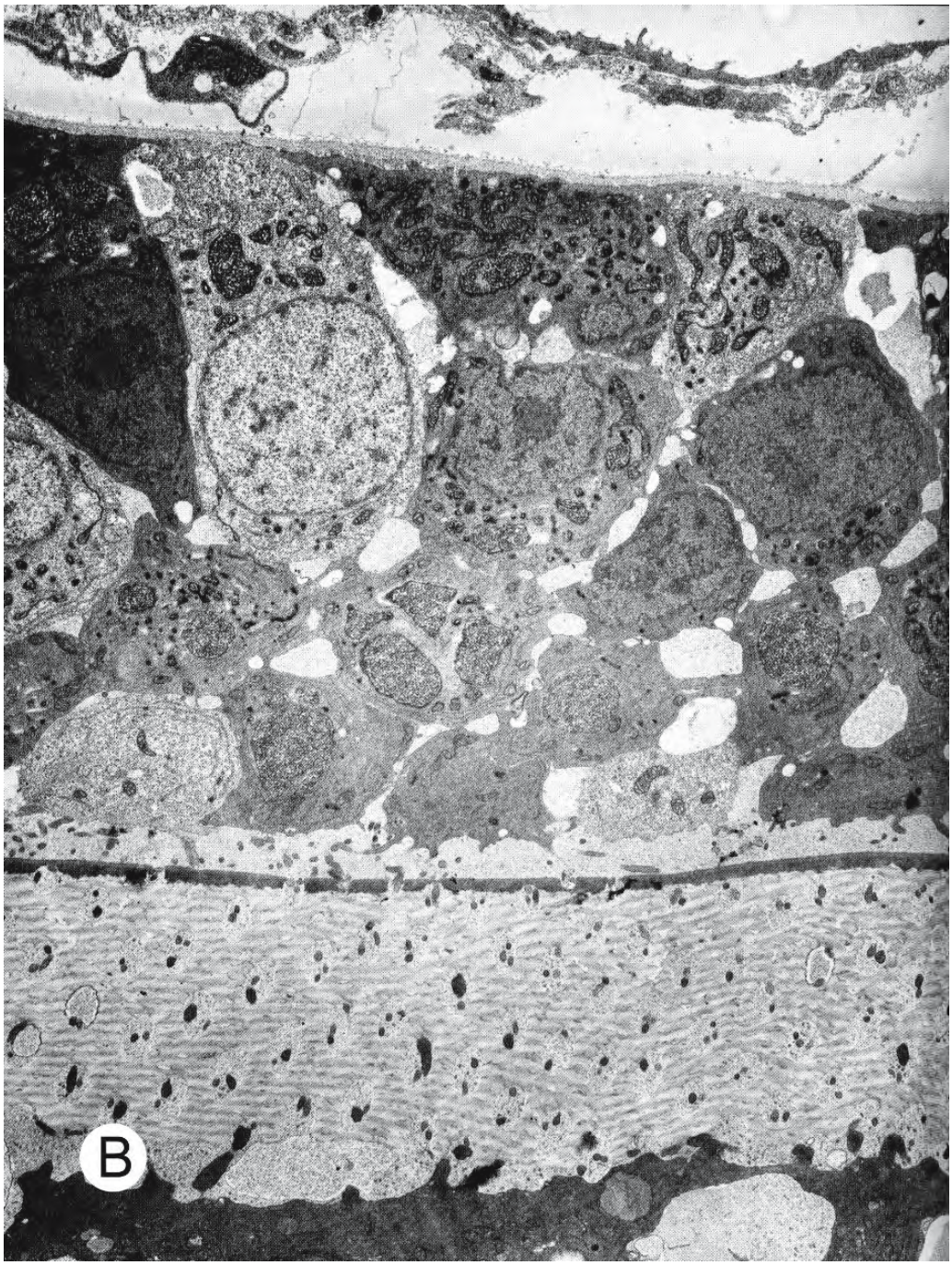

Figure 2.70: Continued.

B. Transmission electron micrograph of a tangential section through the follicular epithelium. The epithelial cells contain extensive granular endoplasmic reticulum and a number of large and small vesicles filled with dense material. Sections of fenestrations in the primary envelope contain microvilli from the oocyte and follicular cells. Extensive intercellular spaces have developed between the follicular cells. X 5,500.

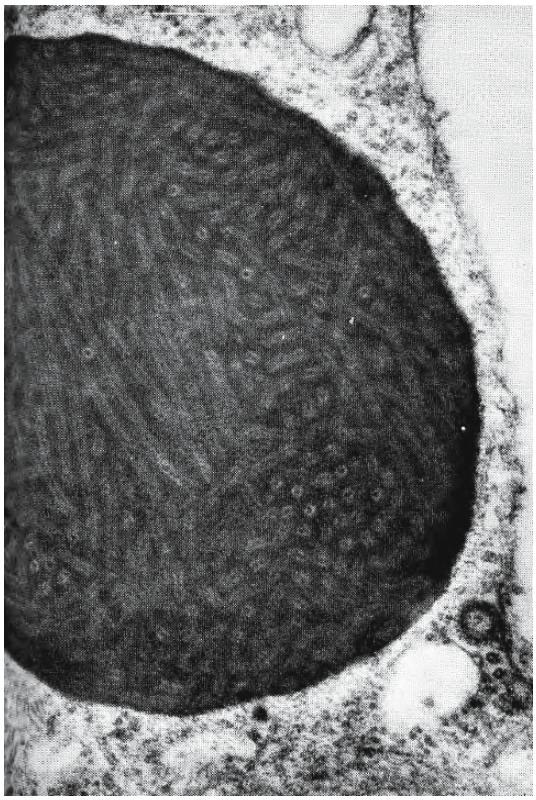

Figure 2.72: Transmission electron micrograph through a large, membrane-bound presecretion granule within a follicular cell of the annual fish *Cynolebius melanotaenia* at the outset of formation of the secondary envelope. The contents of the vesicle have fused to form a homogeneous mass containing tubular components in both transverse and longitudinal orientation. X 57,275 (From Wourms and Sheldon, 1976; reproduced with permission from Elsevier Science).

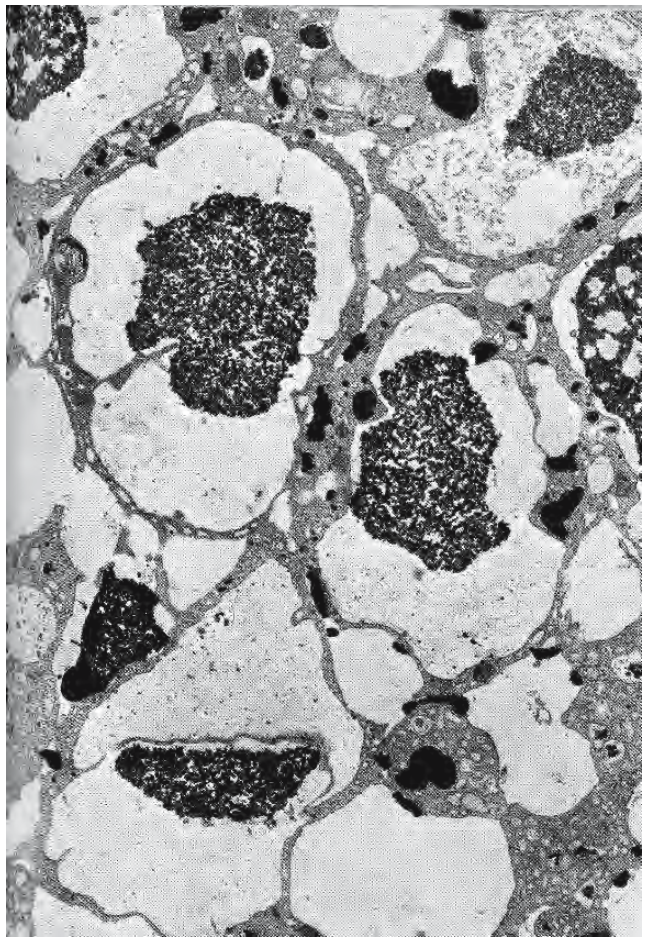

Figure 2.71: Transmission electron micrograph of a tangential section of the simple columnar follicular epithelium of the annual fish *Cynolebius melanotaenia* at the outset of formation of the secondary envelope. Large compartments filled with fibrillar matrix have developed between the follicular cells. X 5,000 (From Wourms and Sheldon, 1976; reproduced with permission from Elsevier Science).

→

Figure 2.73: Schematic diagram illustrating the synthesis and secretion of the tubular components of the secondary envelope by a follicular cell in the annual fish *Cynolebius melanotaenia.* At the outset of formation, flocculent material appears within cisternae of the granular endoplasmic reticulum, portions of which become dilated and seem to bud off to form vesicles. These vesicles grow by continued synthesis and by fusion with other vesicles; their membranes are studded with ribosomes. Larger vesicles contain partly assembled tubules. The vesicles continue to fuse, forming compact presecretion granules containing 25-nm tubular components. These vesicles transport the tubular components directly from the site of synthesis in the granular

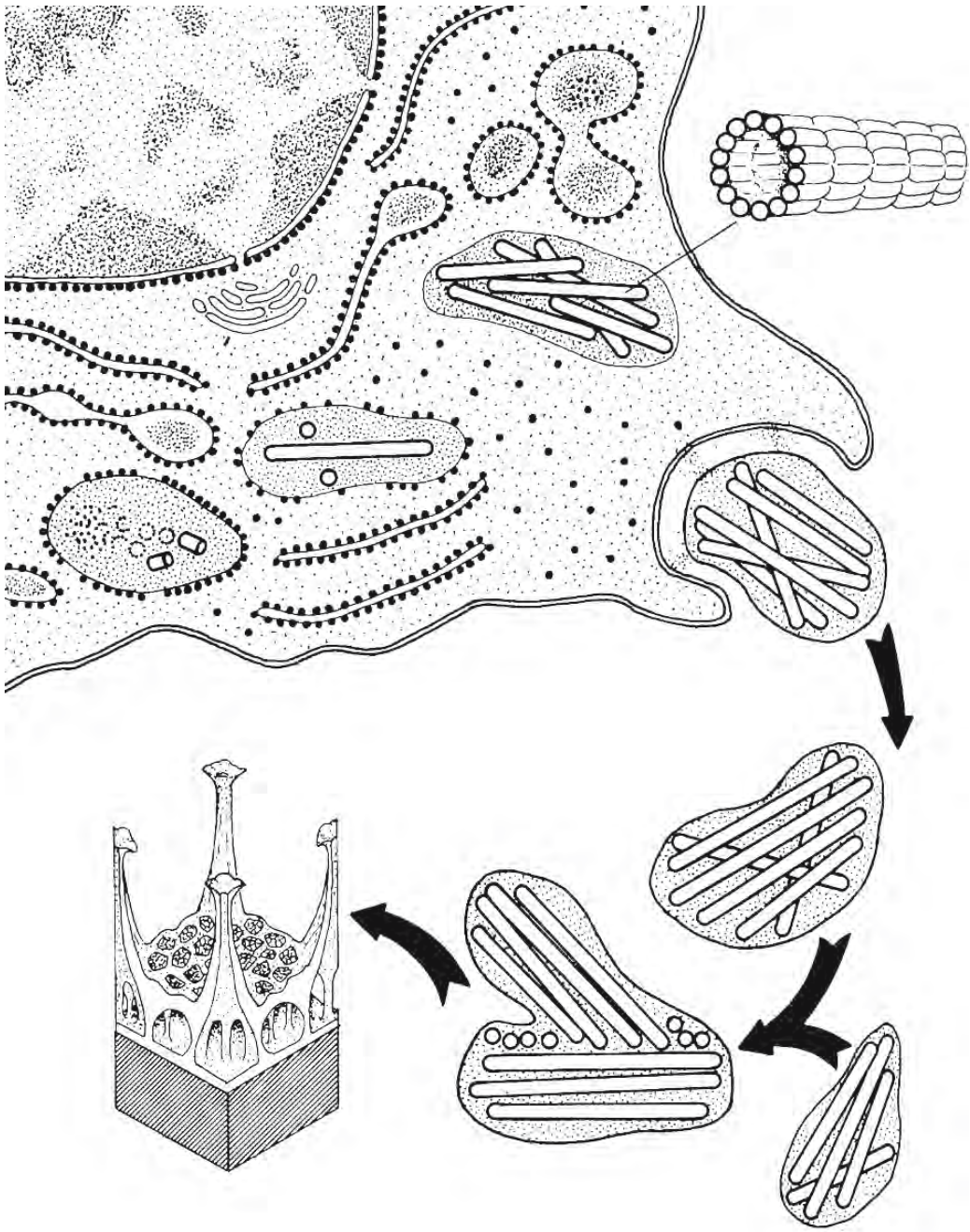

endoplasmic reticulum to the exterior of the cell; they appear to shed their ribosomes shortly before fusing with the plasma membrane. The vesicles discharge their contents in the form of a discrete granules. Several granules may fuse outside the cell. Follicular cells appear to play an active role in the selective deposition of tubular material in the secondary envelope and in the generation of its elaborate pattern. Although a Golgi complex is present, it does not appear to participate in the secretion of the tubular components. (From Wourms and Sheldon, 1976; reproduced with permission from Elsevier Science).

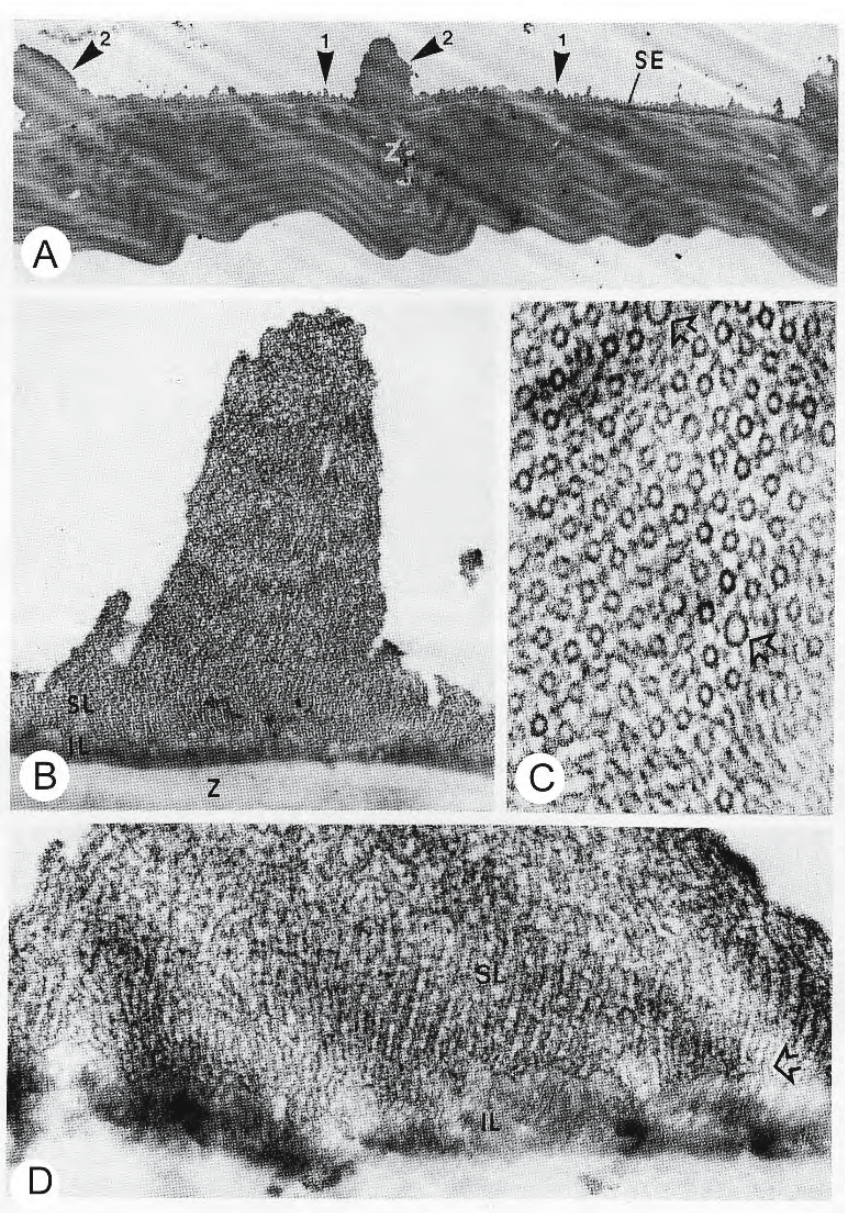

Figure 2.74: Transmission electron micrographs of sections through the egg envelopes of the cyprinodont *Aphyosemion splendopleure.* (From Thiaw and Mattei, 1991; reproduced with permission from Nuova Immagine Editrice).

A. The inner zone (Z) of the primary envelope is lamellar. Swellings of various sizes adorn the secondary envelope (SE); some are 2 μm in height (1), others are 9 μm (2). X 2,500.

B. The secondary envelope comprises two layers. The inner layer (IL) is made up of membranous elements lying directly on the lamellar zone (Z); the superficial layer (SL) consists of parallel structures separated by a lucent matrix. X 17,000.

C. Tangential section of the superficial layer of the secondary envelope. It consists of parallel tubular elements cut transversely. Most of the tubules are about 25 nm in diameter; a few are larger (arrow). Some of the tubules are joined by links. X 80,000.

D. Section of the secondary envelope. The parallel tubular elements are opened at the base (arrow). IL, inner layer; SL, superficial layer. X 45,000.

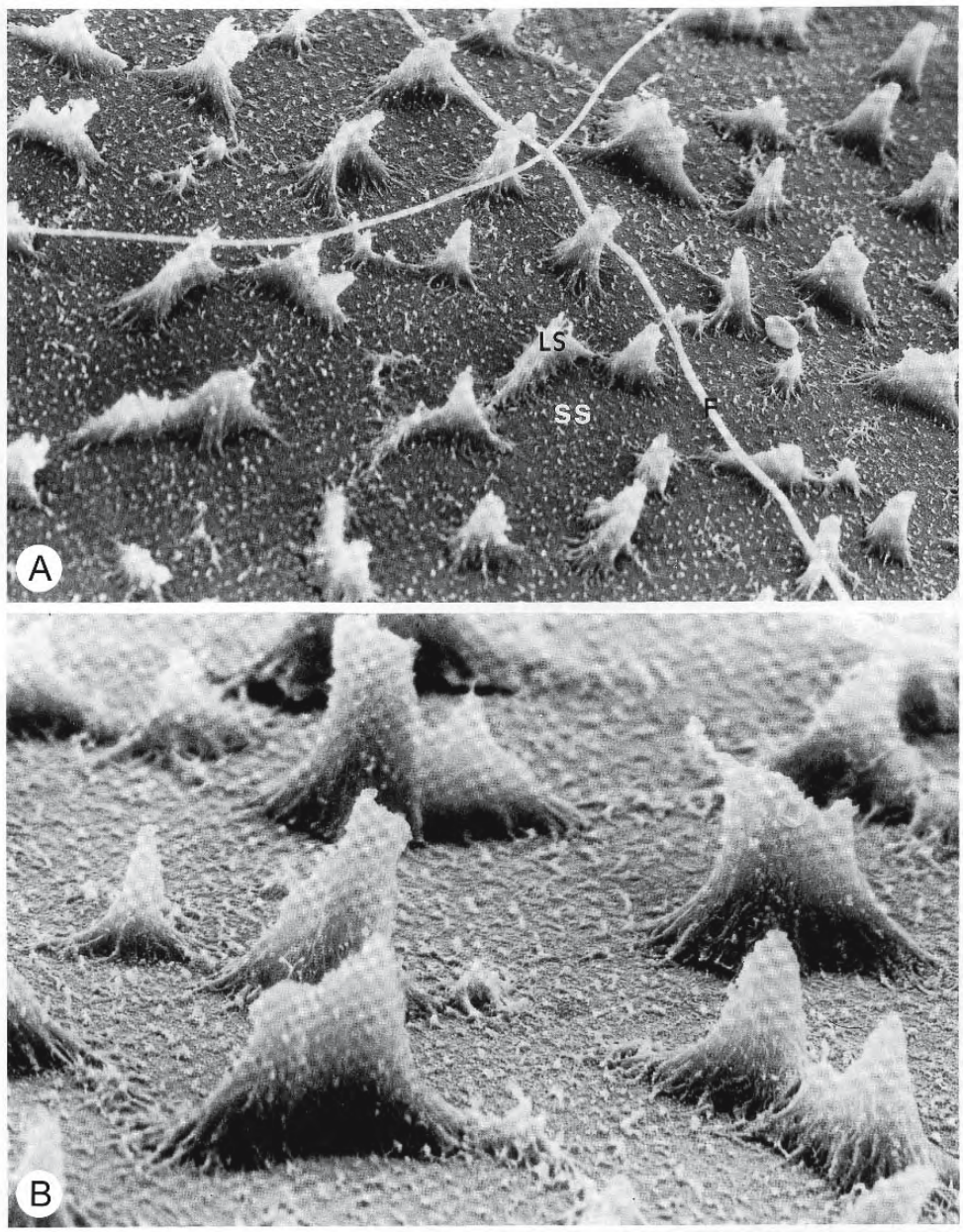

Figure 2.75: Scanning electron micrographs of the superficial layer of the secondary egg envelope of the cyprinodont *Aphyosemion splendopleure.* (From Thiaw and Mattei, 1991; reproduced with permission from Nuova Immagine Editrice).
A. Small swellings (SS) are scattered among large swellings 9 µm high (LS). F, filament. X 1,650.
B. Swellings of the superficial layer. X 3,850.

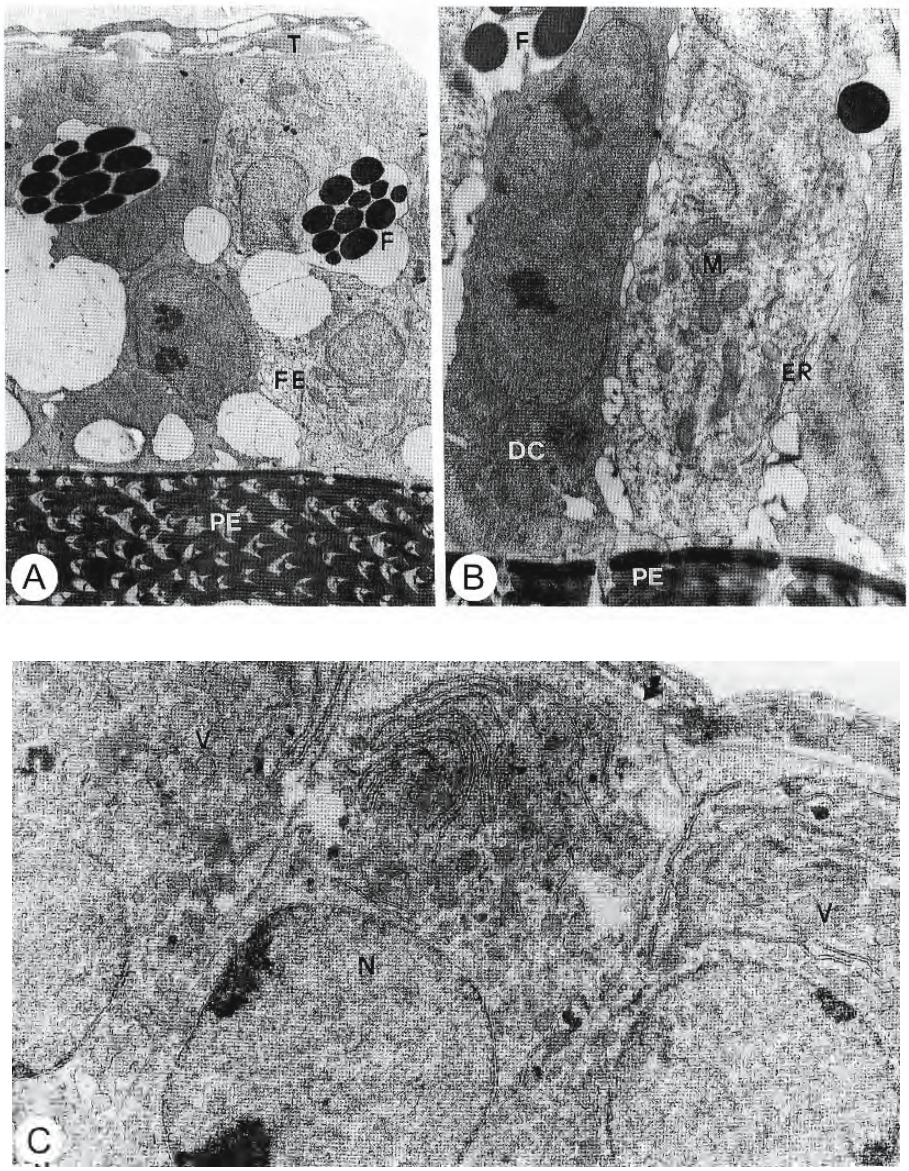

Figure 2.76: Transmission electron micrographs of sections through the ovarian follicles of the cyprinodont *Aphyosemion splendopleure* during vitellogenesis. (From Thiaw and Mattei, 1991; reproduced with permission from Nuova Immagine Editrice).

A. Oblique section showing the primary envelope (PE), follicular epithelium (FE), and theca (T). There is a difference in the electron density of the cytoplasm of the follicular cells. The intercellular spaces contain sections of filaments (F). X 5,000.

B. Cisternae of the endoplasmic reticulum (ER) and mitochondria (M) are visible in follicular cells with electron-lucent cytoplasm; they are difficult to identify in electron-dense cells (DC). F, sections of filaments; PE, primary envelope. X 11,000.

C. At the end of vitellogenesis, cisternae of the endoplasmic reticulum gather in the basal region of the follicular cells and pinch off vesicles (V). Arrow, basal lamina; N, nucleus. X 11,000.

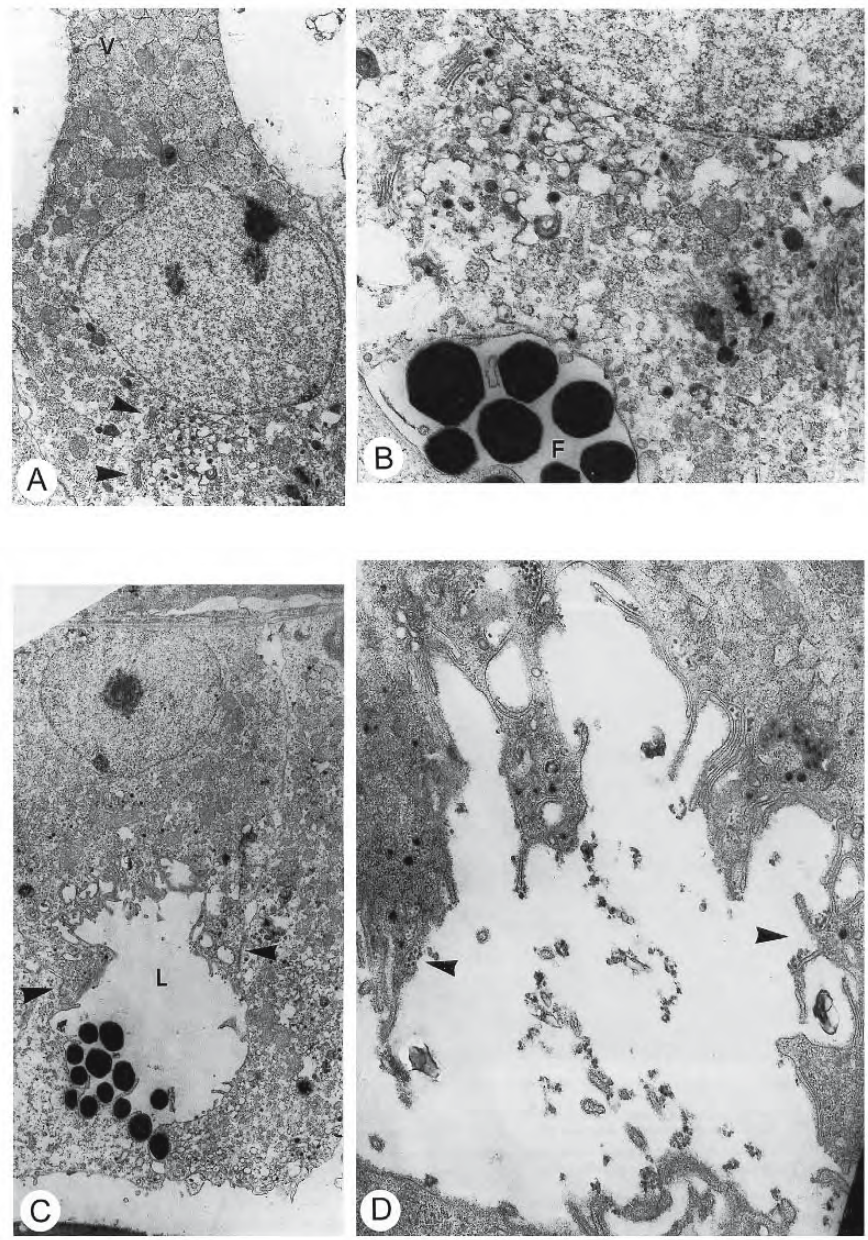

Figure 2.77: Transmission electron micrographs of sections through the ovarian follicles of the cyprinodont *Aphyosemion splendopleure* at the end of vitellogenesis. (From Thiaw and Mattei, 1991; reproduced with permission from Nuova Immagine Editrice).

A. At the end of vitellogenesis, the Golgi complex (arrowheads) becomes active in the cytoplasm between the nucleus and the surface of the oocyte. The endoplasmic reticulum has formed vesicles (V) in the opposite region. X 8,000.

B. Vesicles and secretory granules appear at the trans face of the Golgi complex. F, filaments. X 19,400.

C. Large intercellular spaces (L) form between follicular cells. Tight junctions (arrowheads) link the follicular cells around the spaces. X 5,700.

D. Granules are released (arrowheads) from the follicular cells into the intercellular spaces. X 20,500.

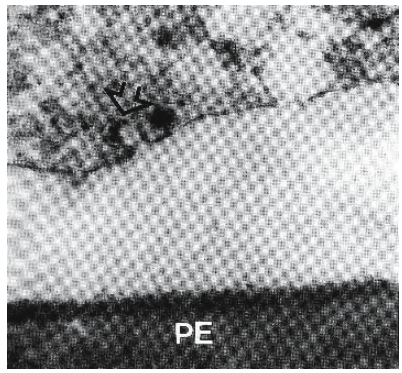

Figure 2.78: Transmission electron micrograph of a section through the ovarian follicle of the cyprinodont *Aphyosemion splendopleure* at the end of vitellogenesis. A dense granule (arrow) is liberated onto the surface of the primary envelope (PE). X 33,500 (From Thiaw and Mattei, 1991; reproduced with permission from Nuova Immagine Editrice).

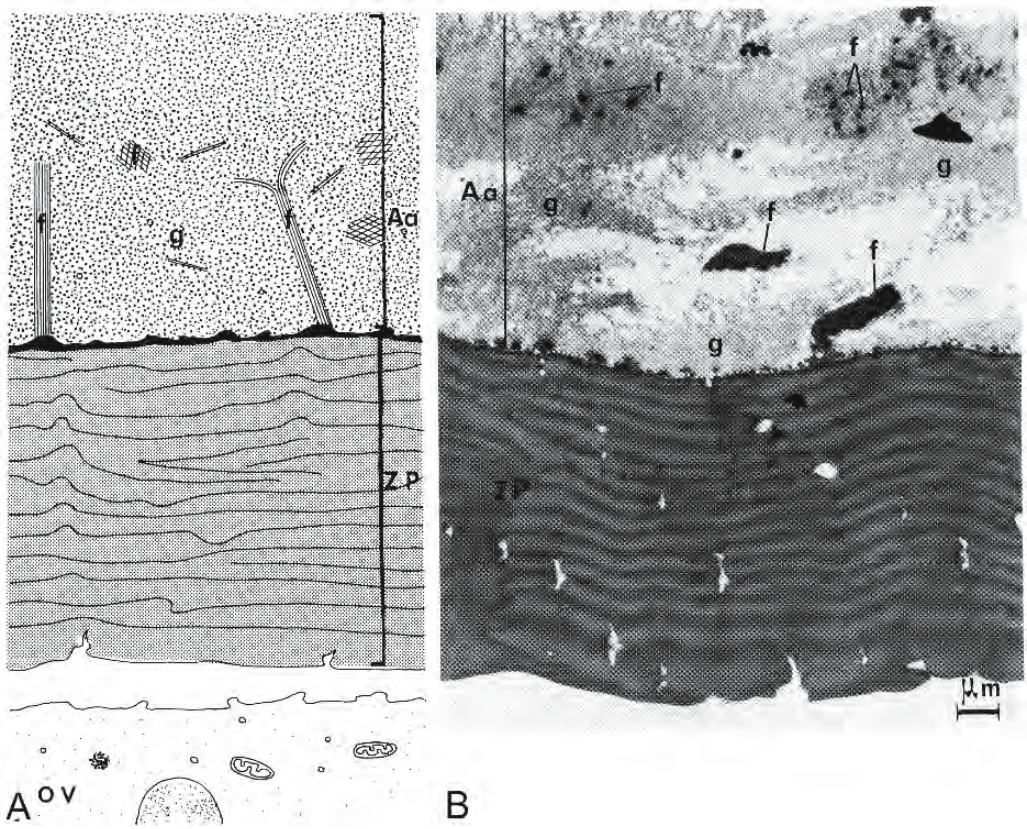

Figure 2.79: Section through the ovarian follicle of the cichlid *Cichlasoma fasciata* showing the adhesive apparatus. The adhesive layer (Aa) covers the zona pellucida (ZP) of the oocyte (OV). The amorphous mucous jelly coat (g) is penetrated by dense filaments (f) attached to the zona pellucida. (From Busson-Mabillot, 1977, *Biologie Cellulaire*; reproduced with permission).

A. Schematic drawing.

B. Transmission electron micrograph. X 7,000.

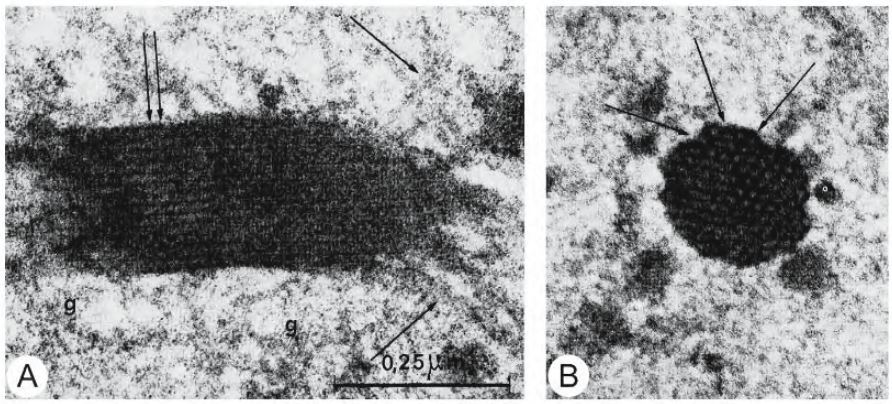

Figure 2.80: Transmission electron micrographs of sections through the ovarian follicle of the cichlid *Cichlasoma fasciata* showing the adhesive filamens. X 140,000 (From Busson-Mabillot, 1977, *Biologie Cellulaire*; reproduced with permission).
A. Longitudinal section showing the parallel elements (double arrow) that constitute a filament; g, glycoprotein.
B. Cross section of a filament composed of microtubule mimics (arrows) packed in hexagonal arrays.

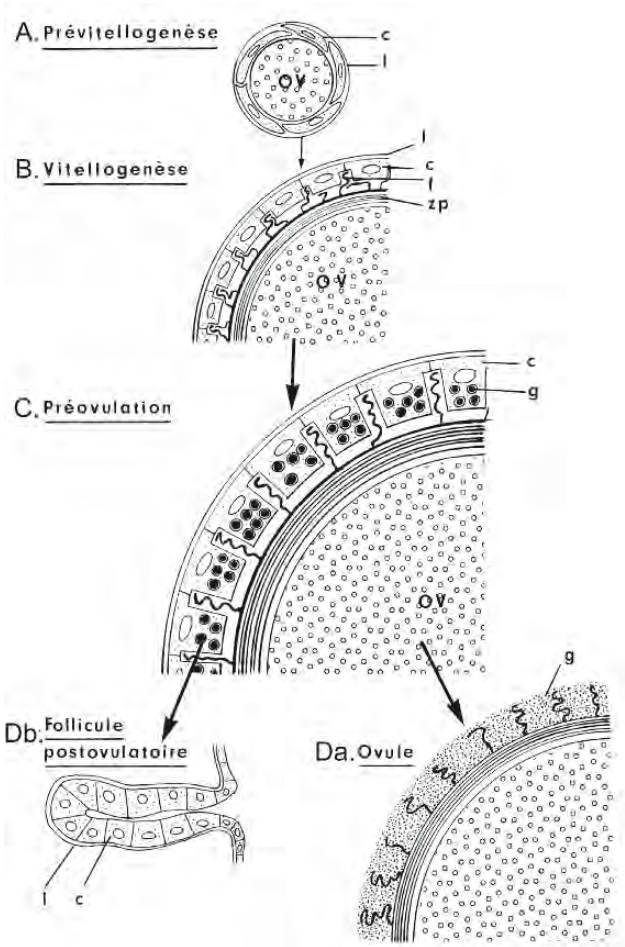

←

Figure 2.81: Schematic drawings of sections through the follicular epithelium of the ovarian follicle of the cichlid *Cichlasoma fasciata* to show the development of the adhesive apparatus during various stages in oogenesis. (From Busson-Mabillot, 1977, *Biologie Cellulaire*; reproduced with permission).

A. During previtellogenesis, the oocyte is in direct contact with the follicular epithelium which rests on its basement membrane.

B. The zona pellucida surrounds the oocyte at the onset of vitellogenesis. Adhesive filaments, attached to the zona pellucida, appear between the follicular cells.

C. At the end of vitellogenesis, the follicular cells are distended with glycoproteins.

Da. At ovulation, the glycoproteins surround the oocyte, forming the adhesive layer.

Db. The follicular epithelium and its basement membrane retract following expulsion of the oocyte, forming the postovulatory follicle.

Abbreviations: c, follicular cells; e, follicular epithelium; f, adhesive filaments; g, glycoproteins; l, basement membrane of follicular epithelium; ov, oocyte; zp, zona pellucida.

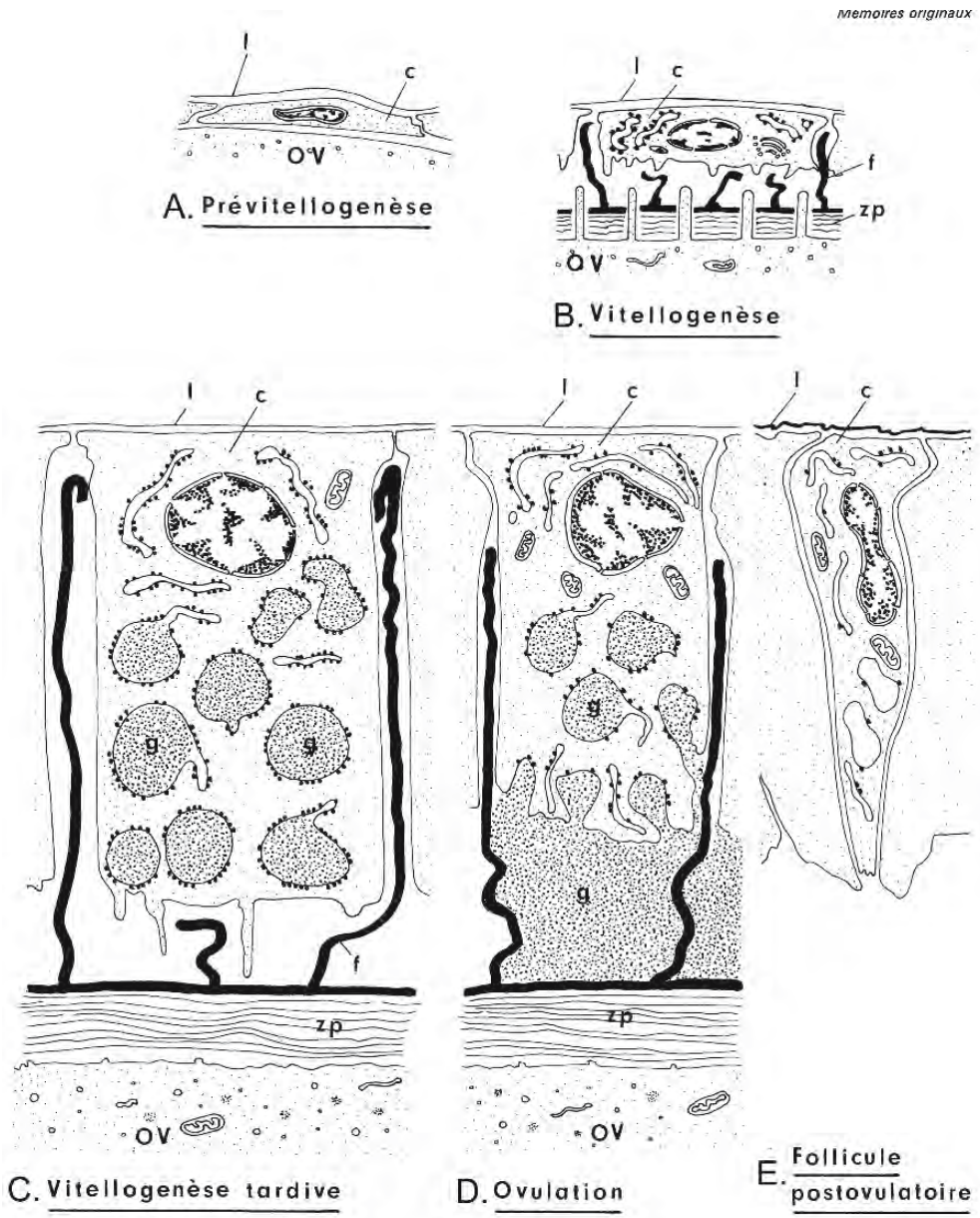

Figure 2.82: Schematic drawings of sections through the follicular epithelium of the ovarian follicle of the cichlid *Cichlasoma fasciata* to show changes in the follicular epithelium during various stages in oogenesis. (From Busson-Mabillot, 1977, *Biologie Cellulaire*; reproduced with permission).

A. The follicular cells are squamous during previtellogenesis; organelles are sparse.

B. Follicular cells enlarge at the beginning of vitellogenesis and show signs of secretory activity. Adhesive filaments appear.

C. At the end of vitellogenesis, the follicular cells become distended with glycoproteins within the granular endoplasmic reticulum.

D. During ovulation, the apical plasma membrane of the follicular cells ruptures to release glycoproteins which will constitute the adhesive layer.

E. In the retracted postovulatory follicle the follicular cells, emptied of their glycoproteins, become disorganized.

Abbreviations: c, follicular cells; e, follicular epithelium; f, adhesive filaments; g, glycoproteins; l, basement membrane of follicular epithelium; ov, oocyte; zp, zona pellucida.

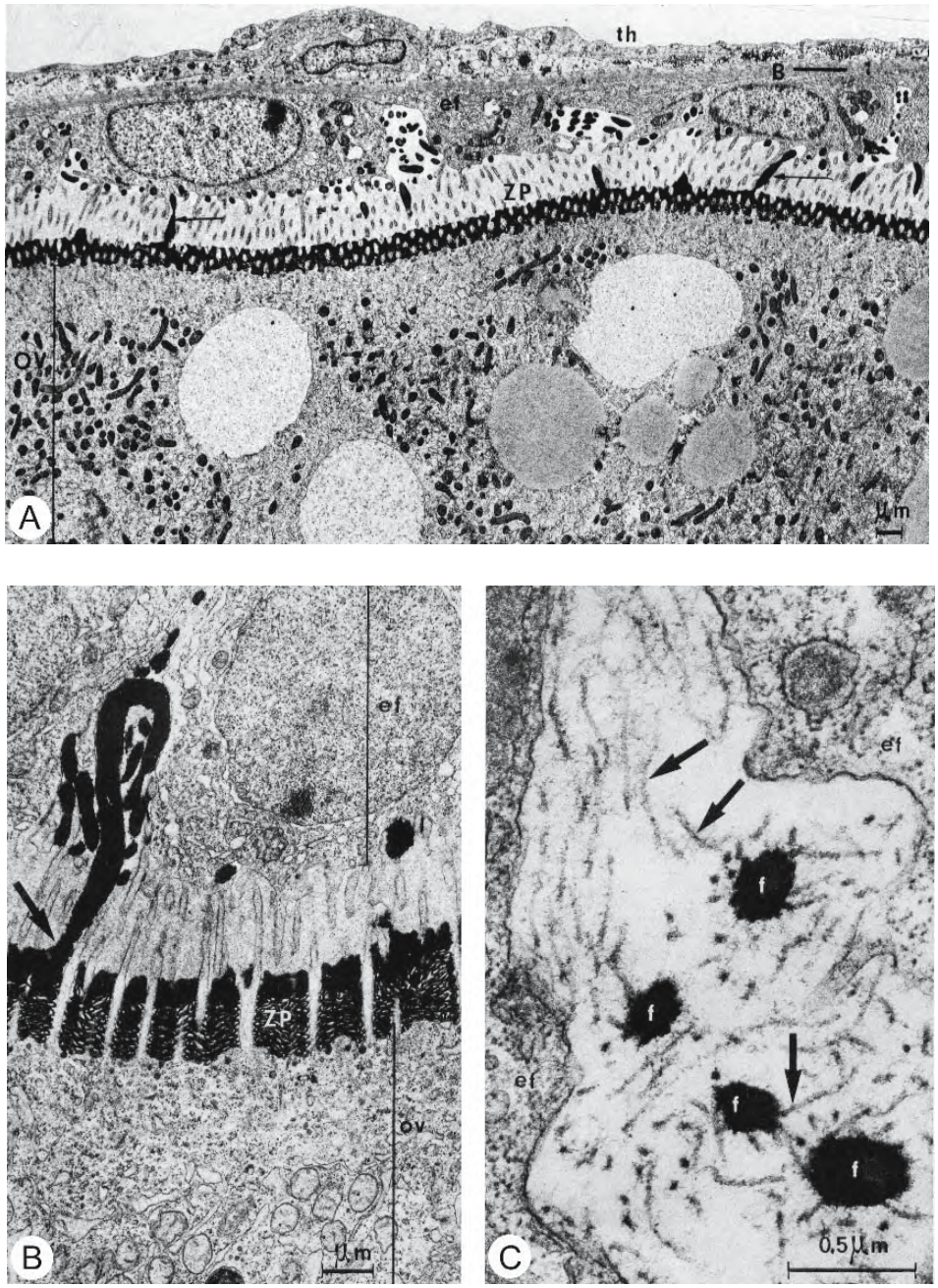

Figure 2.83: Transmission electron micrographs of sections through the periphery of ovarian follicles of the cichlid *Cichlasoma fasciata.* (From Busson-Mabillot, 1977, *Biologie Cellulaire*; reproduced with permission).

A, **B**. Distribution of filaments in the follicle at the beginning of vitellogenesis. Filaments (arrow), attached to the zona pellucida (zp) penetrate deep into the intercellular spaces of the follicular epithelium (ef). B, basal lamina of the follicular epithelium; ov, oocyte; th, theca. **A**: X 5,000; **B**: X 10,000.

C. Structure of the filaments (f) at the end of vitellogenesis. At this stage, the filaments become frayed temporarily, thereby displaying their microtubular nature (arrows). ef, follicular epithelium. X 50,000.

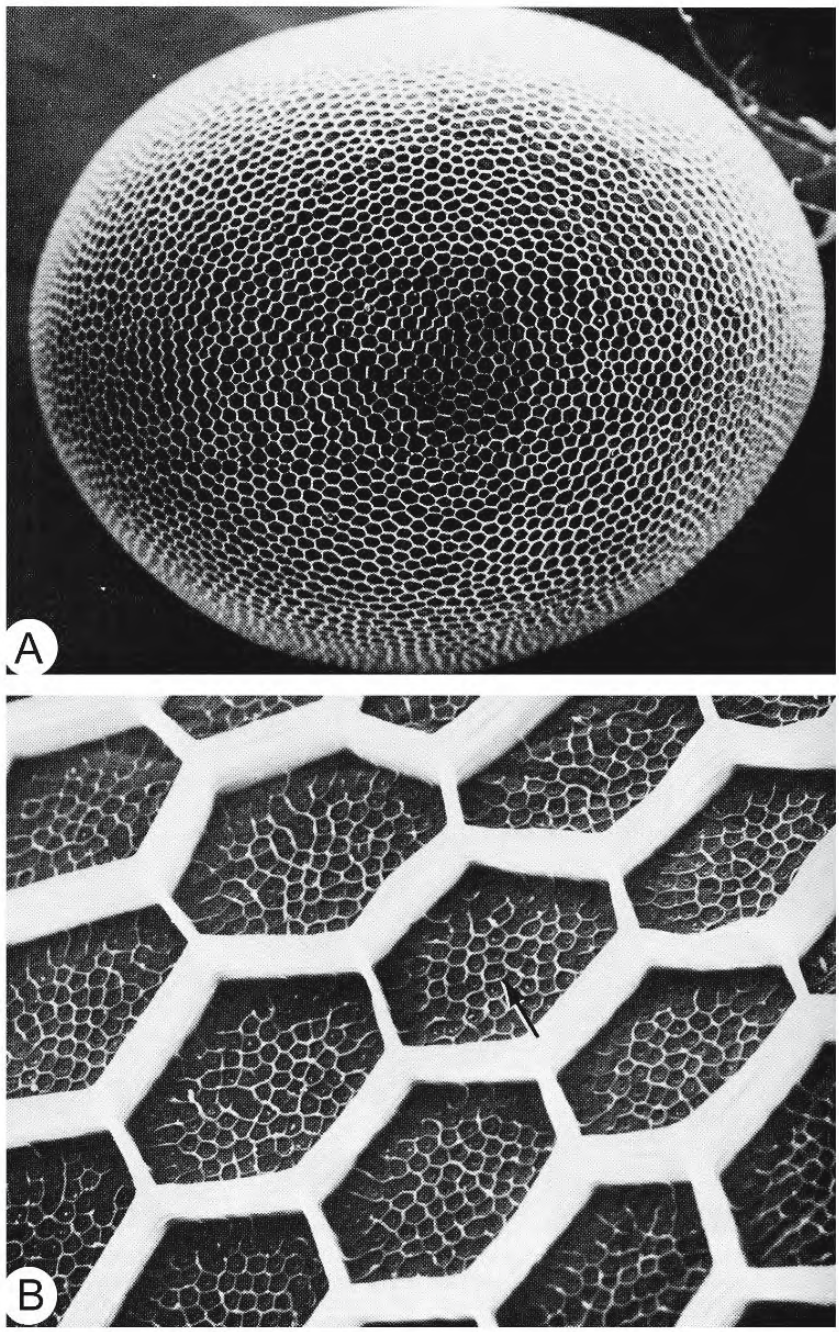

Figure 2.84: Scanning electron micrographs of ovulated eggs of the sole *Pleuronichthys coenosus* showing the elaborate arrangement of hexagonal surface compartments formed over the zona pellucida by the secondary envelope. (From Stehr and Hawkes, 1983; © reproduced with permission of John Wiley & Sons, Inc.).

A. An entire egg. X 96.

B. Inside each hexagonal chamber are regularly spaced pore canals, each of which is surrounded by a polygonal subpattern (arrow). X 1,500.

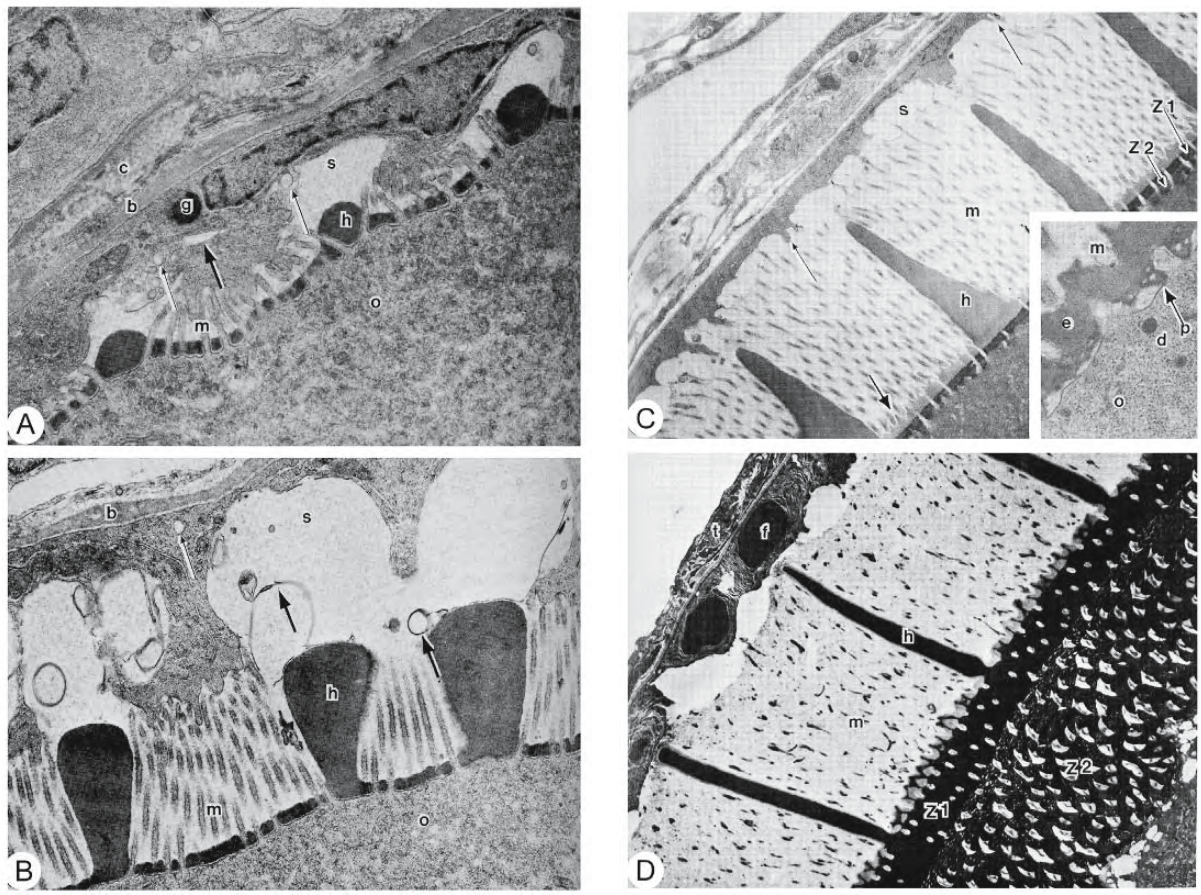

Figure 2.85: Transmission electron micrographs of the periphery of ovarian follicles of the sole *Pleuronichthys coenosus* to demonstrate stages in the formation of the compartmentalized secondary envelope. (From Stehr and Hawkes, 1983; © reproduced with permission of John Wiley & Sons, Inc.).

A. An oocyte in the late primary growth stage. Hexagonal partitions (h) are beginning to form in the secondary envelope. Flocculent material fills the subfollicular space (s). Microvilli (m) from the oocyte extend across this space to reach bulbous extensions of the follicular cells. Several electron-lucent vesicles containing flocculent material are present in a follicular cell (small arrow) as well as a vesicle of electron-dense material (g). The large arrow may indicate swollen granular endoplasmic reticulum. X 20,500.

B. An oocyte at the cortical alveolus stage. The hexagonal partitions (h) are larger and the subfollicular space has expanded. A few membranous fragments (arrows) are scattered in the subfollicular space. X 13,000.

C. An oocyte in a late cortical alveolus stage. Well defined hexagonal partitions (h) extend into the subfollicular space (s). Microvilli (m) from the oocyte extend toward the follicular cell while a few stubby microvilli (small arrow) are seen reaching out from the follicular cell. The hexagonal subpattern (large arrow) is beginning to appear in the floors of the compartments. The zona pellucida (Z1, Z2) is forming. X 6,800.

The **inset** is of an earlier oocyte where the zona pellucida (p) is just beginning to appear. Dense-cored vesicles (d) are present in the peripheral ooplasm.

D. An oocyte during vitellogenesis. The zona pellucida (Z1,Z2) of the primary envelope is well defined, partitions (h) of the secondary envelope enclose the hexagonal compartments, and microvilli (m) from the oocyte span the subfollicular space (s). X 4,500.

Abbreviations: b, basal lamina; c, collagenous fibres; f, follicular cells; fb, fibroblasts; g, granular material; h, hexagonal partitions; m, oocyte microvilli; o, ooplasm; p, pore canal; s, subfollicular space; t, thecal cells, Z1 and Z2, zona pellucida.

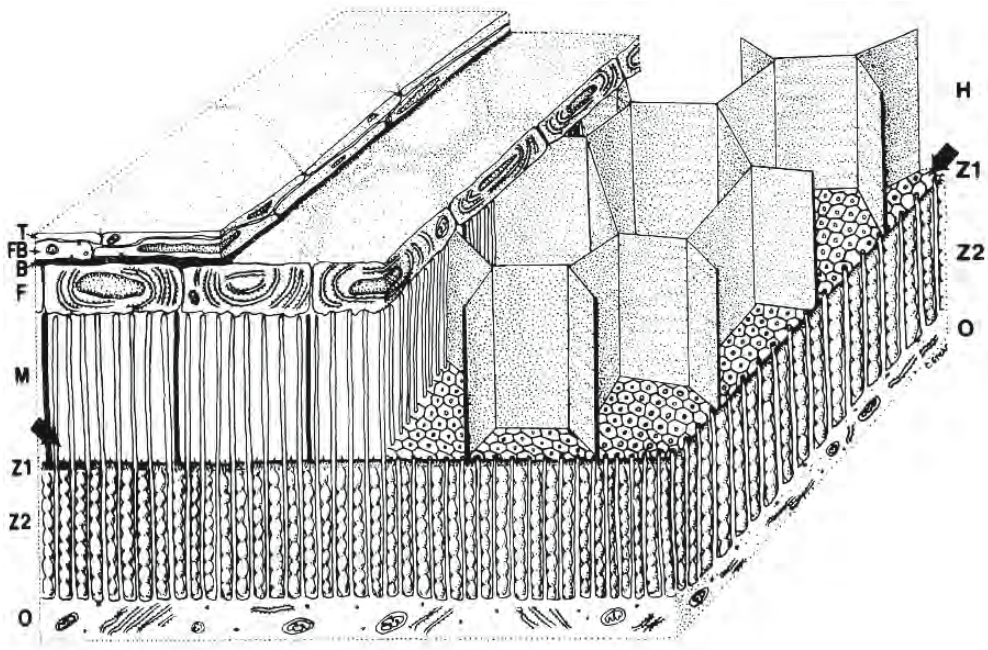

Figure 2.86: Schematic diagram to illustrate the elements of the follicular wall in the sole *Pleuronichthys coenosus* during late vitellogenesis. The floors of the hexagonal compartments display a subpattern of hexagonal ridges (arrows), each hexagon encircling an oocyte microvillus. (From Stehr and Hawkes, 1983; © reproduced with permission of John Wiley & Sons, Inc.) *Abbreviations*: B, basal lamina; F, follicular cells; FB, fibroblasts; H, hexagonal partitions; M, oocyte microvilli; O, ooplasm; T, theca; Z1 and Z2, zona pellucida.

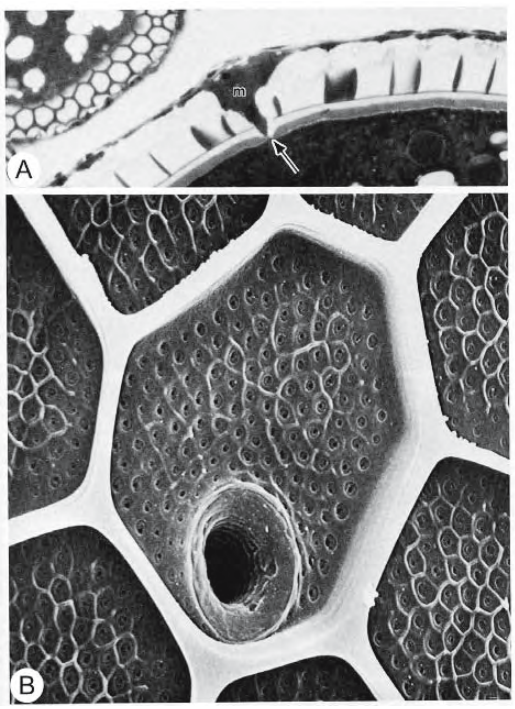

←

Figure 2.87: Micrographs of the envelope of the sole *Pleuronichthys coenosus.* (From Stehr and Hawkes, 1983; © reproduced with permission of John Wiley & Sons, Inc.).

A. Transmission electron micrograph of a section showing a micropylar cell (m) that penetrates both envelope layers and makes direct contact with the oocyte. The micropyle forms around the extension of this cell (arrow). X 940.

B. Scanning electron micrograph of the floors of the hexagonal compartments of the secondary envelope. The compartment at the centre of the figure encloses the single micropyle of the oocyte. The floors of the hexagonal compartments display a subpattern of hexagonal ridges, each hexagon encircling an oocyte microvillus. X 2,500.

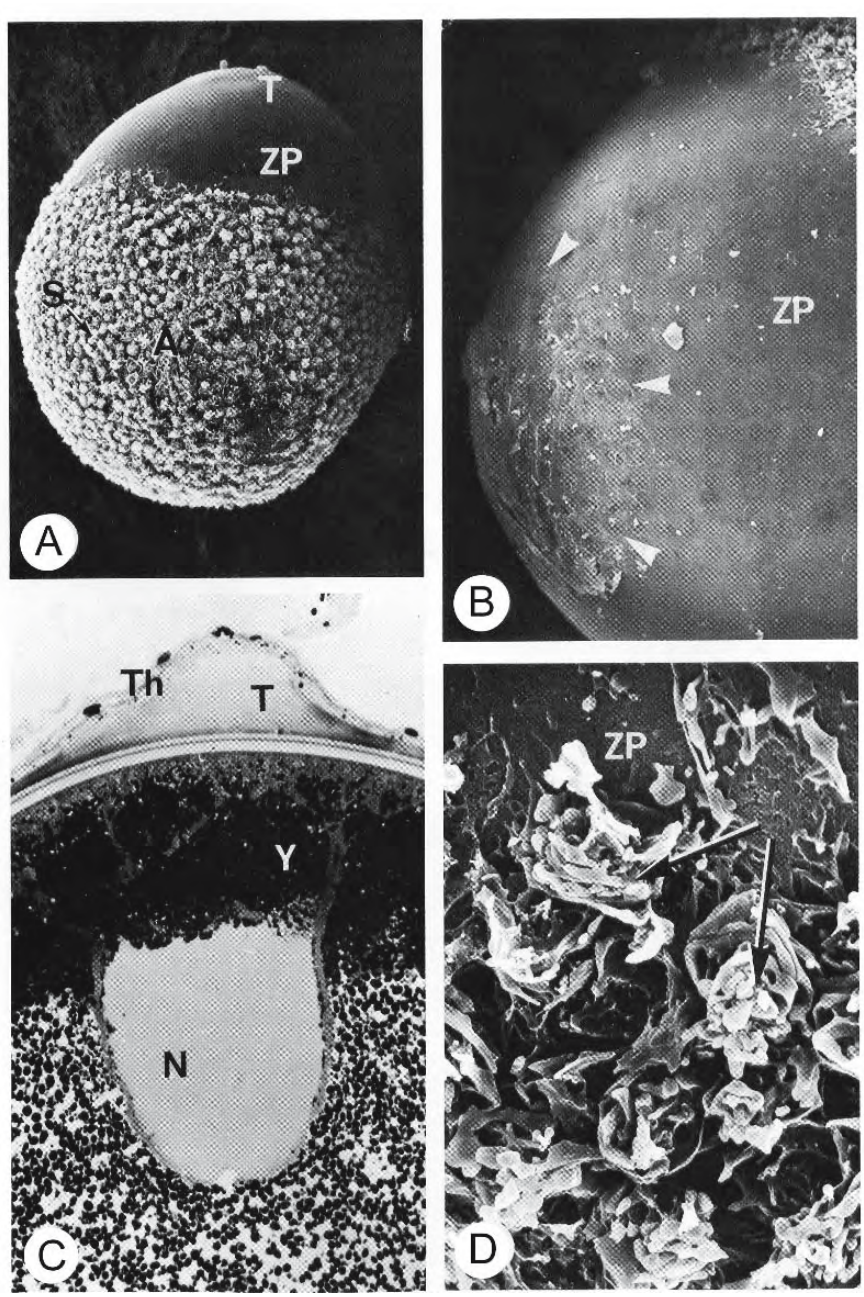

Figure 2.88: **A**, **B**, and **D** are scanning electron micrographs of the surface of a recently ovulated egg of the lamprey *Petromyzon marinus*. **C**. is a photomicrograph of a section of an unovulated lamprey egg. (From Yorke and McMillan, 1979; © reproduced with permission of John Wiley & Sons, Inc.).

A. Entire egg showing the adhesive coat (A), apical tuft (T) and, between these, the exposed surface of the zona pellucida (ZP). The adhesive coat is covered with clusters of adhesive saccules (S). X 70.

B. The irregular apical tuft (arrowheads) caps the apical pole and is surrounded by the more featureless exposed surface of the zona pellucida (ZP). X 145.

C. The section passes through the acellular apical tuft (T). N, nucleus, Th, theca, Y, yolk. X 260.

D. The adhesive coat consists of clusters of adhesive saccules (arrows) and is bordered by the exposed surface of the zona pellucida (ZP). X 720.

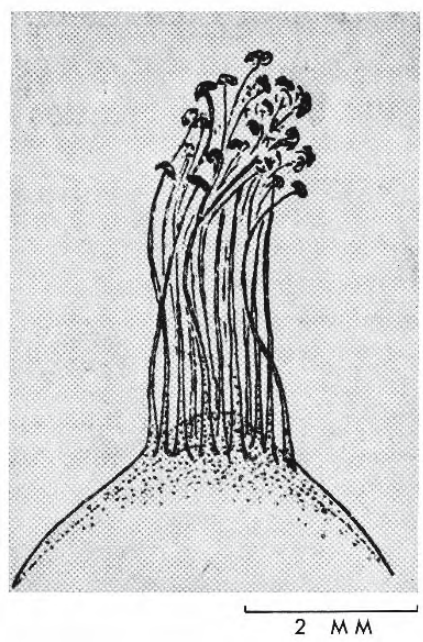

Figure 2.89: Sketch of the vegetal pole of an ovulated egg of *Myxine glutinosa* showing filaments with anchor-like terminals. (From Lyngnes, 1930, reproduced by Walvig, 1963; reproduced with permission).

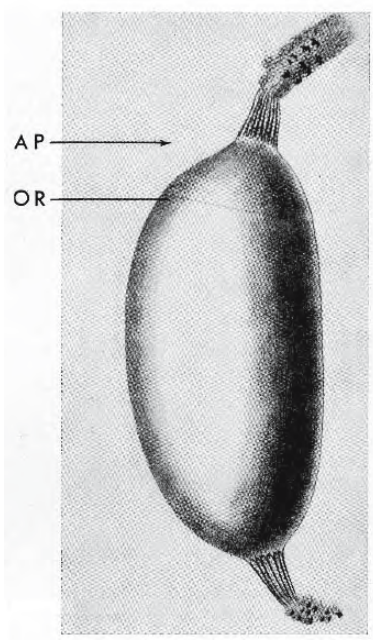

Figure 2.90: Mature egg of *Myxine glutinosa;* length (excluding anchor filaments): 17 mm. AP, animal pole; OR, opercular ring. (From Jensen, 1901, reproduced by Walvig, 1963; reproduced with permission).

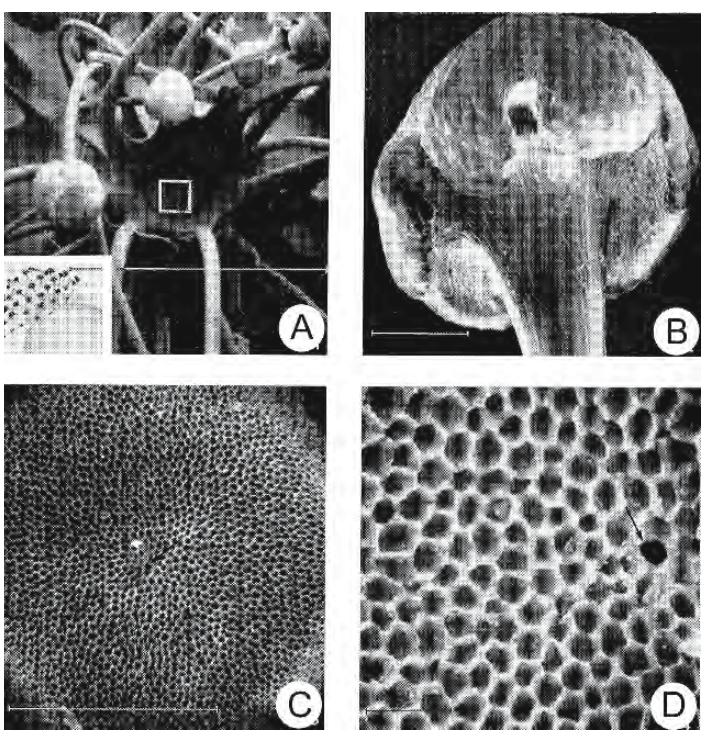

←

Figure 2.91: Photographs of intact eggs of the hagfish *Eptatretus burgeri.* (From Fernholm, 1975; reproduced with kind permission of Blackwell Publishing).

A. *Inset:* The animal pole of a fresh egg showing anchor filaments. Scale = 2 mm.

A. Scanning electron micrograph of the apical pole showing the micropylar funnel surrounded by eight anchor filaments. The square is enlarged in **C**. Scale = 1 mm.

B. Tip of an anchor filament. Scale = 100 μm.

C,D. Pattern of hexagonal ridges at the bottom of the micropylar funnel. Only one of the cells is open at the bottom (arrow in **D**). Scale = 100 μm in C, 10 μm in D.

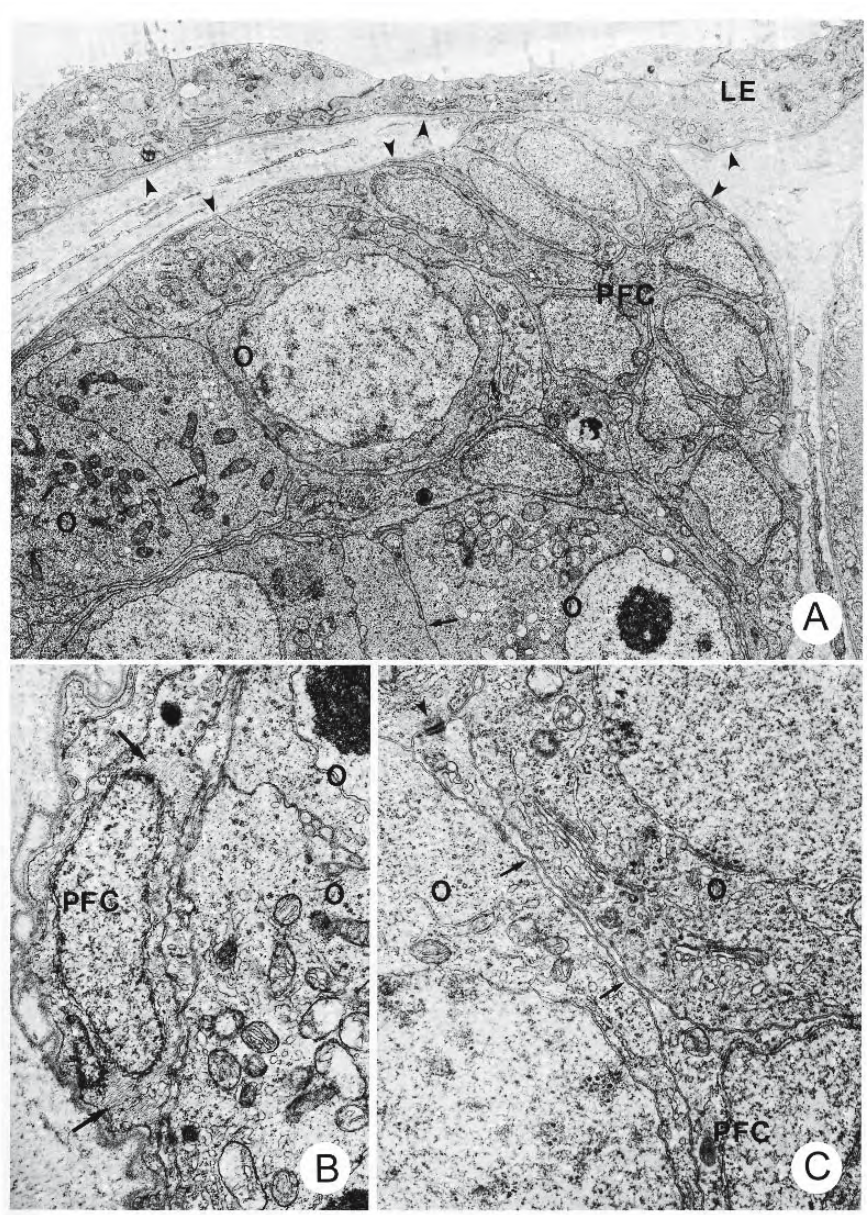

Figure 2.92: Transmission electron micrographs of sections through the germinal ridge of the pipefish *Syngnathus scovelli.* (For orientation, see Figure 1.39). (From Begovac and Wallace, 1987; © reproduced with permission of John Wiley & Sons, Inc.).

A. Groups of prefollicular cells (PFC) and oocytes (O) lie in the ridge. Borders of adjacent oocytes are contiguous (arrows). The basal lamina (arrowheads) of the luminal epithelium (LE) diverges from the luminal epithelial cells to envelop the germinal ridge. X 5,720.

B. The basal lamina surrounding the germinal ridge covers the left side of this prefollicular cell (PFC). Meiotic oocytes (O) with shared borders are indicated. Intracellular filaments (arrows) are apparent in the prefollicular cell. X 13,380.

C. A process (arrows) from a prefollicular cell (PFC) has extended between the borders of two meiotic oocytes (O) and has formed a desmosomal contact (arrowhead) with an adjacent prefollicular cell. X 16,200.

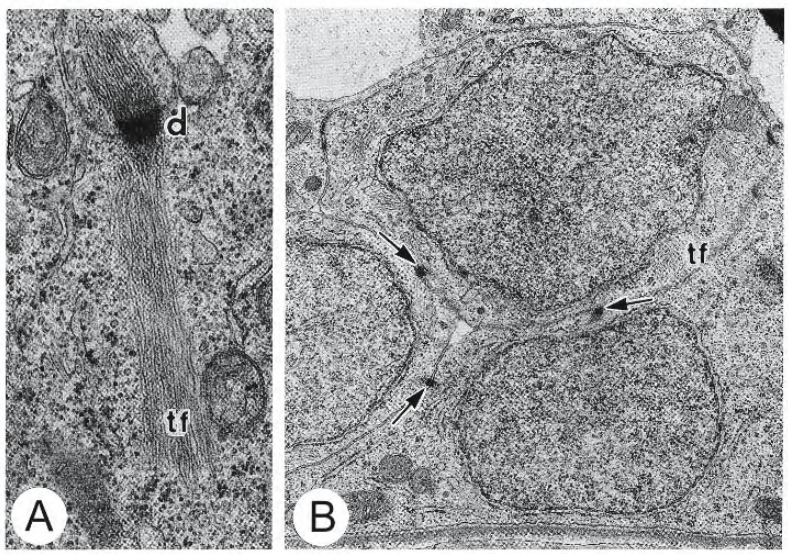

Figure 2.93: Transmission electron micrographs of sections through the follicular epithelium of the medaka *Oryzias latipes* during early vitellogenesis. (From Nakashima and Iwamatsu, 1989; © reproduced with permission of John Wiley & Sons, Inc.).

A. Portion of two follicular cells anchored by a desmosome (d) and tonofilaments (tf). X 31,000.

B. Tangential section through the follicular epithelium showing desmosomes (arrows) between adjacent cells. The cells contain bundles of tonofilaments (tf) as well as sparse mitochondria and granular endoplasmic reticulum. X 12,000.

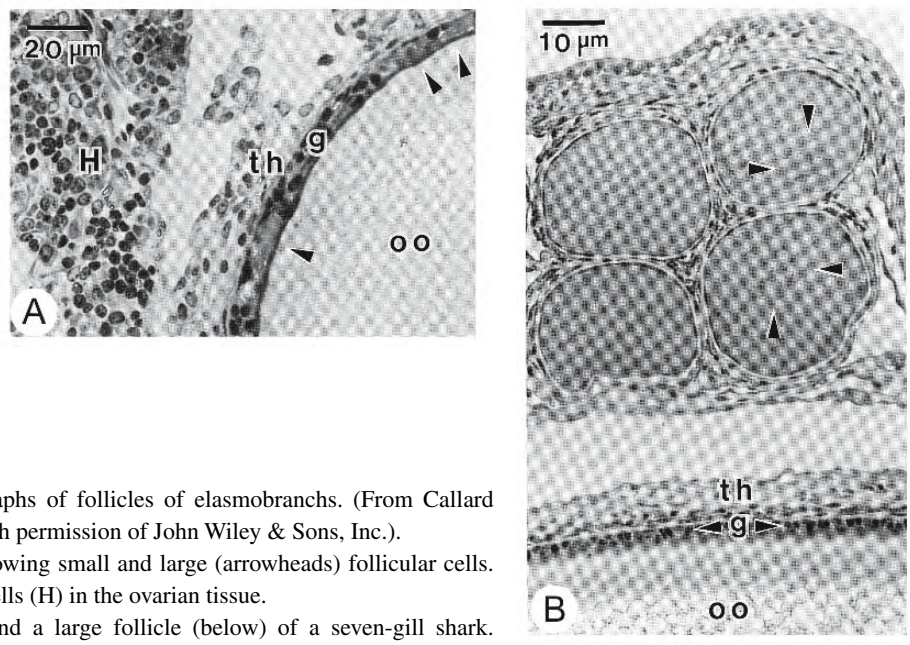

Figure 2.94: Photomicrographs of follicles of elasmobranchs. (From Callard et al., 1989; © reproduced with permission of John Wiley & Sons, Inc.).

A. Follicle of *Raja nevus* showing small and large (arrowheads) follicular cells. There are haemopoietic cells (H) in the ovarian tissue.

B. Small follicles (above) and a large follicle (below) of a seven-gill shark. Arrowheads indicate nuclei containing lampbrush chromosomes.

Abbreviations: g, follicular epithelium; oo, oocyte; th, theca.

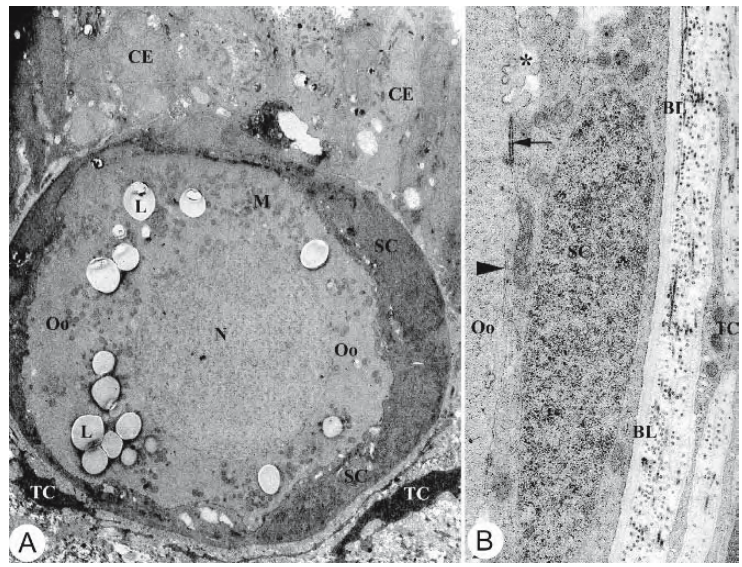

Figure 2.95: Transmission electron micrographs of primary follicles of the elasmobranch *Raya asterias.* (From Andreuccetti et al., 1999; reproduced with permission).

A. The follicular epithelium consists simple squamous cells. X 2,200.

B. The plasma membranes of a follicular cell and the oocyte run parallel and are separated by a space of 20 nm (arrowhead); at the arrow the membranes are connected by desmosome-like junctions. The perivitelline space (*) is beginning to appear. X 18,100.

Abbreviations: BL, basal lamina; CE, coelomic epithelium; L, lipid droplets; M, mitochondria; N, nucleus; Oo, oocyte; SC, squamous cell of the follicular epithelium; TC, thecal cell.

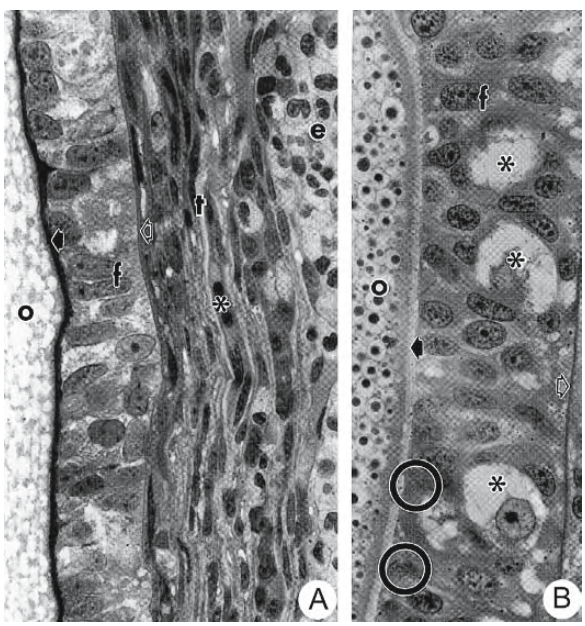

←

Figure 2.96: Light micrographs of sections through the follicular epithelium in the ovary of the yellow spotted stingray *Urolophus jamaicensis.* (From Hamlett, Jezior, and Spieler, 1999; reproduced with permission of Urban & Fischer Verlag).

A. In a follicle of 1 mm diameter, the oocyte (o) is separated from the columnar follicular epithelium (f) by the zona pellucida (dark arrow). The follicular cells rest on a basal lamina (open arrow) adjacent to the theca (t). Red blood cells (*) are visible in the thecal vessels. e, epigonal gland. X 600.

B. Large lipid containing cells (*) are interspersed among the columnar follicular cells (f) in a follicle 3 mm in diameter. Follicular cells contain yolk precursor vesicles (circles). X 600.

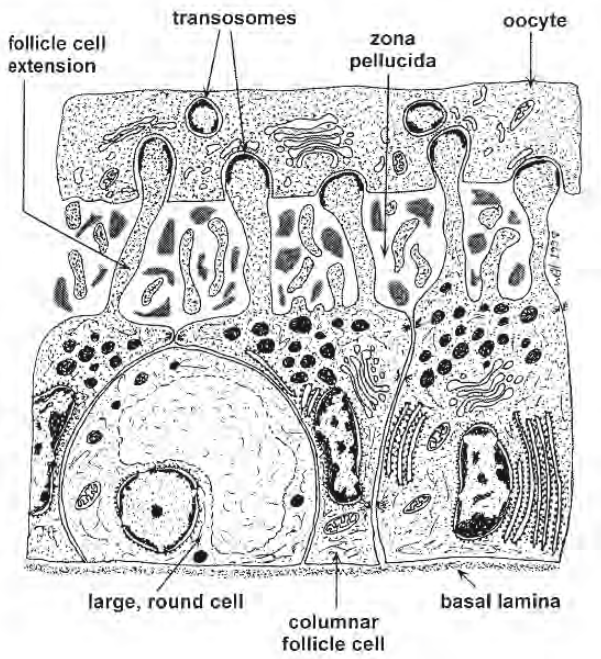

Figure 2.97: Composite drawing showing the relationship between follicular cells, the zona pellucida, and the oocyte in the follicle of the yellow spotted stingray *Urolophus jamaicensis.* (From Hamlett, Jezior, and Spieler, 1999; reproduced with permission of Urban & Fischer Verlag).

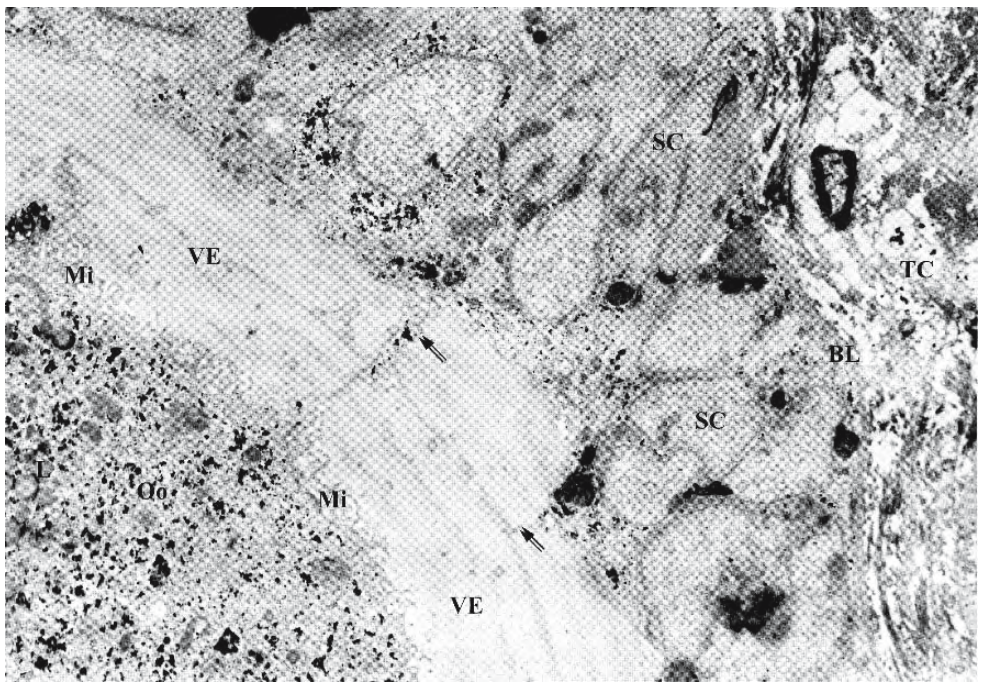

Figure 2.98: Transmission electron micrographs of a follicle 100 μm in diameter of the elasmobranch *Raya asterias.* Follicular cells form a double layer. Processes (double arrows) extend from the follicular cells into the zona pellucida. X 6,100 (From Andreuccetti et al., 1999; reproduced with permission).
Abbreviations: BL, basal lamina; L, lipid droplets; Mi, microvilli; Oo, oocyte; SC, small follicular cells; VE, zona pellucida; TC, thecal cell.

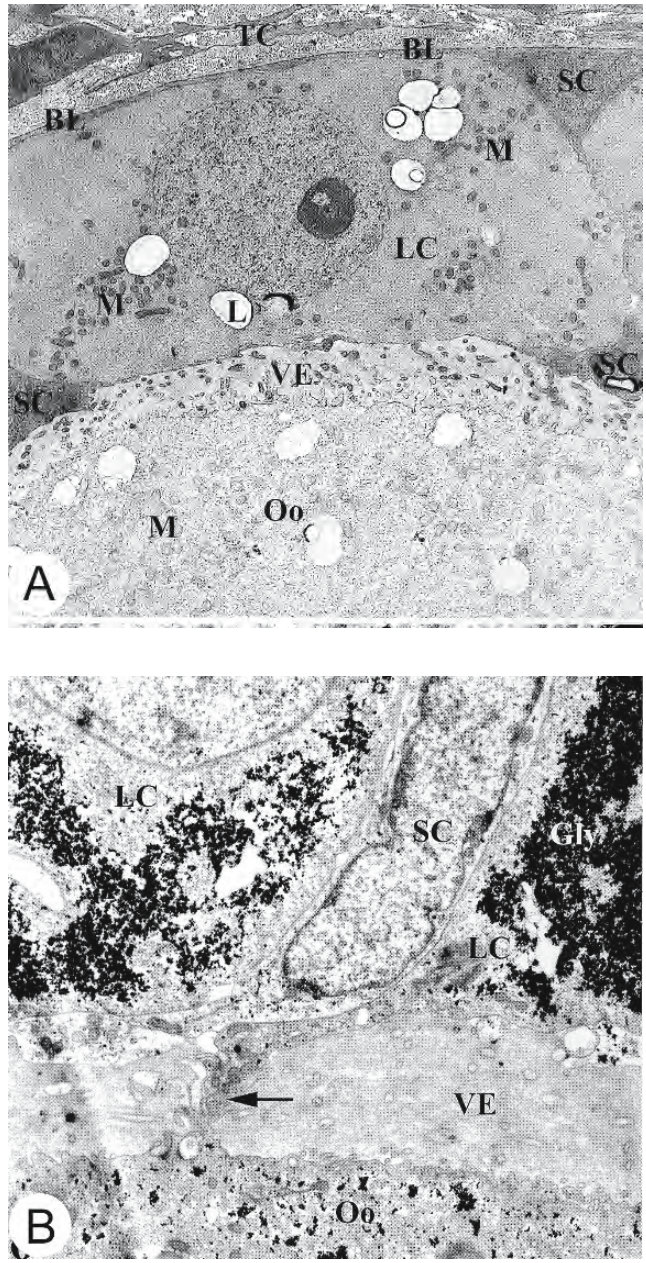

Figure 2.99: Transmission electron micrographs of follicles of the elasmobranch *Raya asterias.* (From Andreuccetti et al., 1999; reproduced with permission).

A. Follicle 150 μm in diameter. Small and large cells constitute the follicular epithelium. The small cells are located beneath the basal lamina and along the perivitelline space. X 3,800.

B. Follicle 200 μm in diameter. An intercellular bridge (arrow) connects a large cell with the oocyte. X 22,000.

Abbreviations: BL, basal lamina; Gly, glycogen; L, lipid droplets; LC, large follicular cell; M, mitochondria; Oo, oocyte; SC, small follicular cell; TC, thecal cell; VE, zona pellucida.

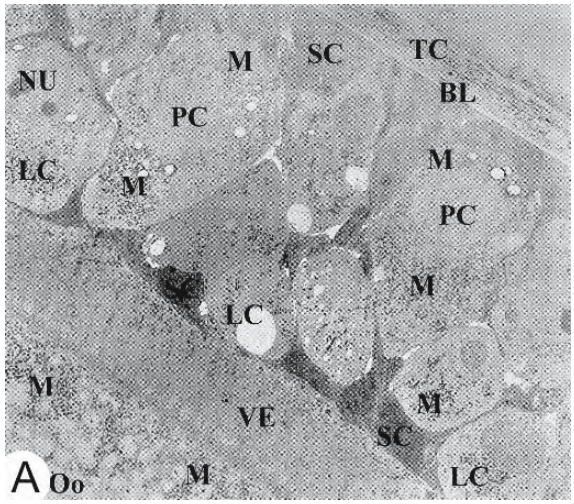

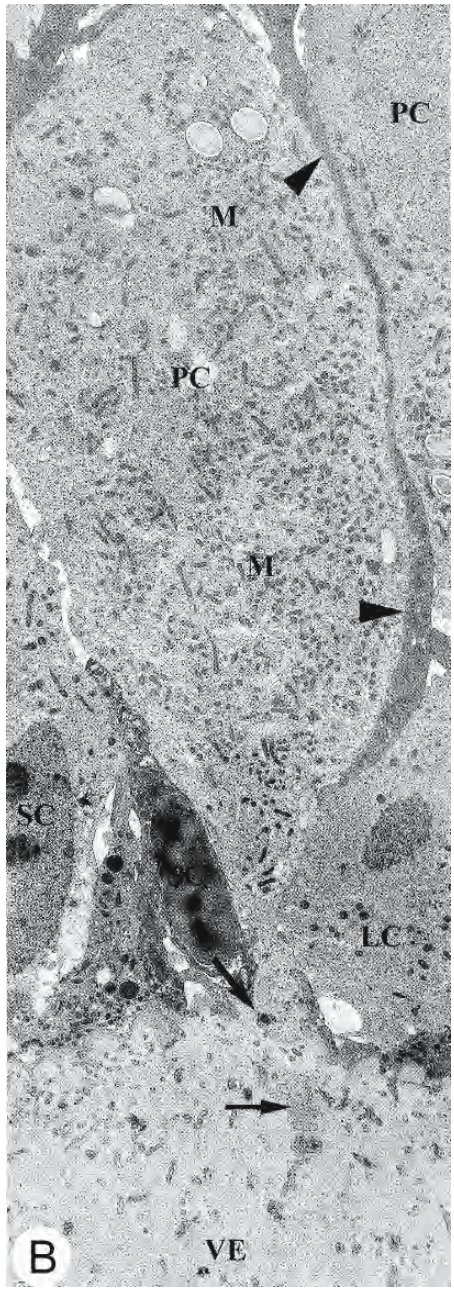

Figure 2.100: Transmission electron micrographs of follicles 1,400 μm in diameter of the elasmobranch *Raya asterias.* (From Andreuccetti et al., 1999; reproduced with permission).

A. The follicular epithelium is polymorphic, multilayered, and consists of small, large, and pyriform cells. The pyriform cells span the follicular epithelium from the basal lamina to the surface of the oocyte. X 1,800.

B. The cytoplasm of this pyriform cell is rich in mitochondria and ribosomes. The apex of the pyriform cell continues into an intercellular bridge (arrows). A long protrusion (arrowheads) of a small cell is interposed between two pyriform cells. X 3,800.

Abbreviations: BL, basal lamina; LC, large cell; M, mitochondria; NU, nucleolus; Oo, oocyte; PC, pyriform cell; SC, small cell; TC, thecal cell; VE zona pellucida.

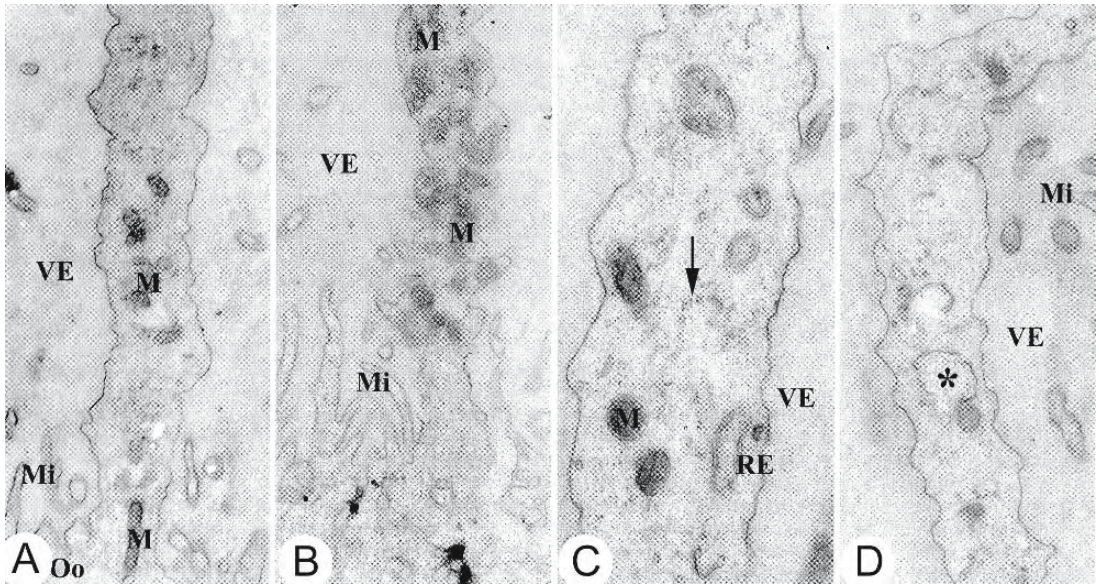

Figure 2.101: A series of transmission electron micrographs of follicles of the elasmobranch *Raya asterias* to illustrate intercellular bridges connecting pyriform cells to the oocyte. The bridges contain organelles. The arrow in **C** indicates ribosomes and the asterisk in D a membranous whorl. (From Andreuccetti et al., 1999; reproduced with permission).
A, X 15,000; **B**, X 18,200; **C**, X 10,000; **D**, X 21,800.
Abbreviations: M, mitochondria; Mi, microvilli; Oo, oocyte; RE, endoplasmic reticulum; VE, zona pellucida.

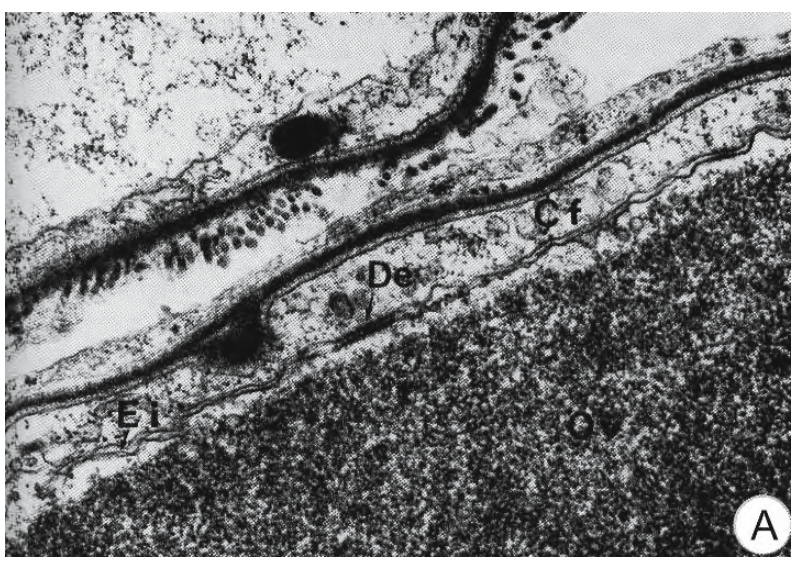

Figure 2.102: Transmission electron micrographs of the follicular periphery in the ovary of the sea bass *Dicentrarchus labrax.* (From Caporiccio and Connes, 1977; reproduced with permission, © Masson Editeur).
A. During previtellogenesis, desmosomal contacts (De) link the oocyte (Ov) and follicular cell (Cf) before the appearance of the zona pellucida. Ei, intercellular space. X 22,500.

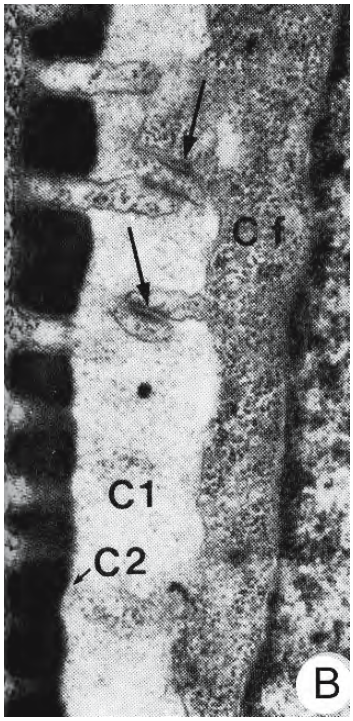

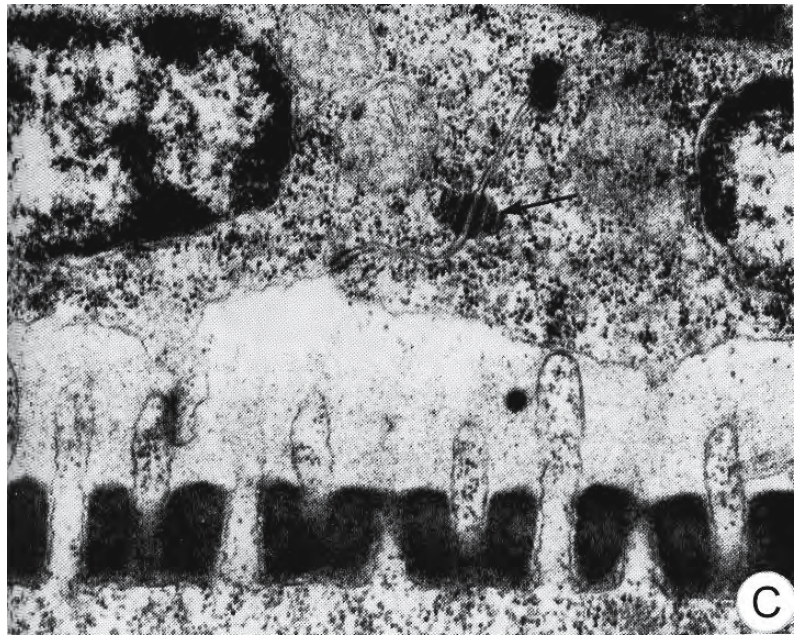

Figure 2.102: Continued.

B. Microvilli from the oocyte are connected by desmosomes (arrows) with microvilli from the follicular cells within pore canals of the developing zona pellucida (C1,C2). X 30,000.

C. Well developed desmosomes (arrow) link adjacent cells of the follicular epithelium. X 31,000.

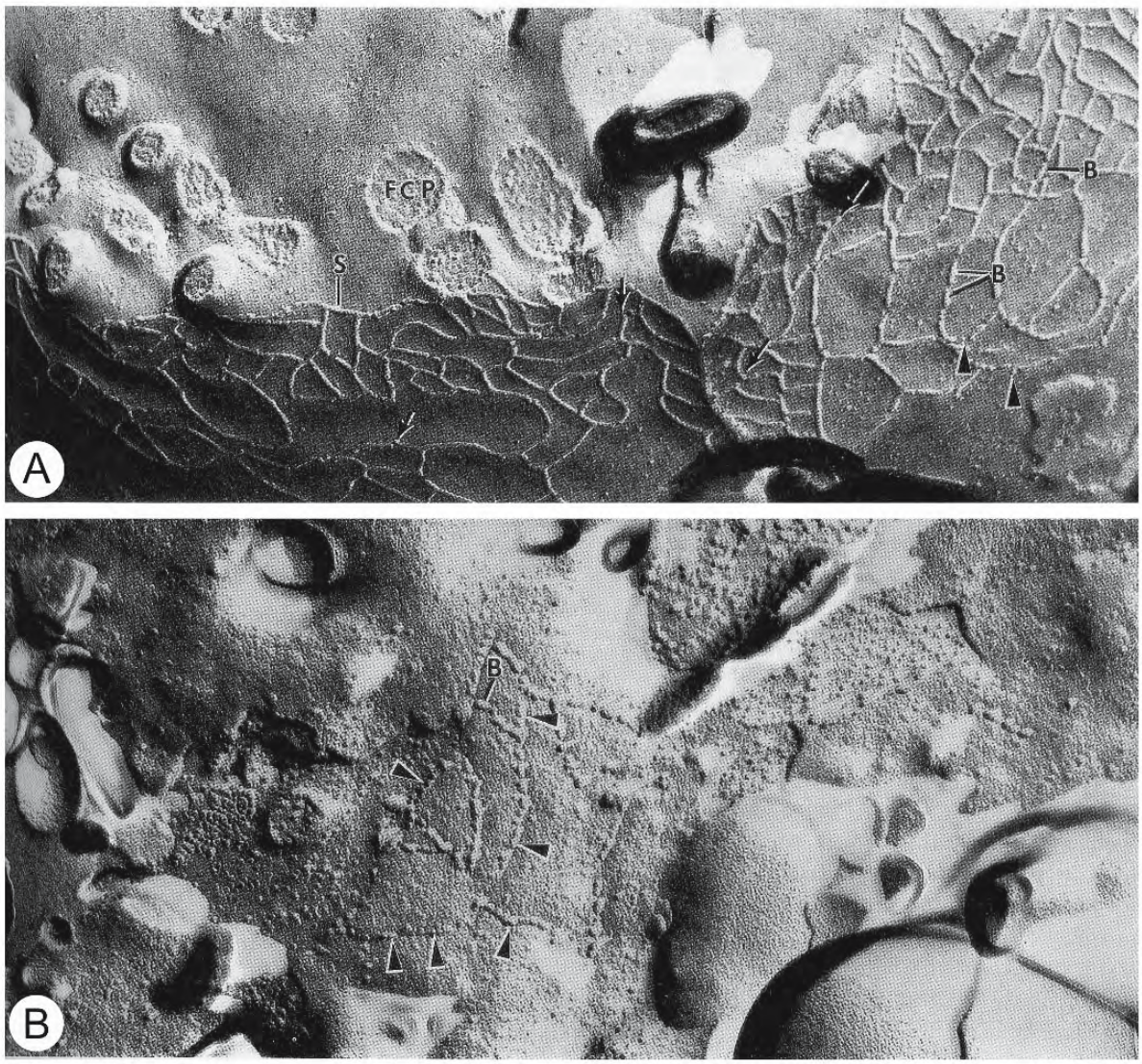

Figure 2.103: Electron micrographs of freeze-fracture replicas of the junctions between adjacent cells in the follicular epithelium in the ovary of the zebrafish *Brachydanio rerio.* (From Kessel, Roberts, and Tung, 1988; reproduced with permission from Nuova Immagine Editrice).

A. Multiple strands in tight junctions between follicular cells of a previtellogenic oocyte. An irregular network of strands (S) is formed in places by bars (B) of different lengths and occasionally by intercalated particles (arrowheads). FCP, process of a follicular cell. X 85,500.

B. The junctional complex from the follicular epithelium of a vitellogenic oocyte is not as extensive and has a more particulate appearance (arrowheads) than that shown above. Only short bars (B) are present in this replica. X 87,000.

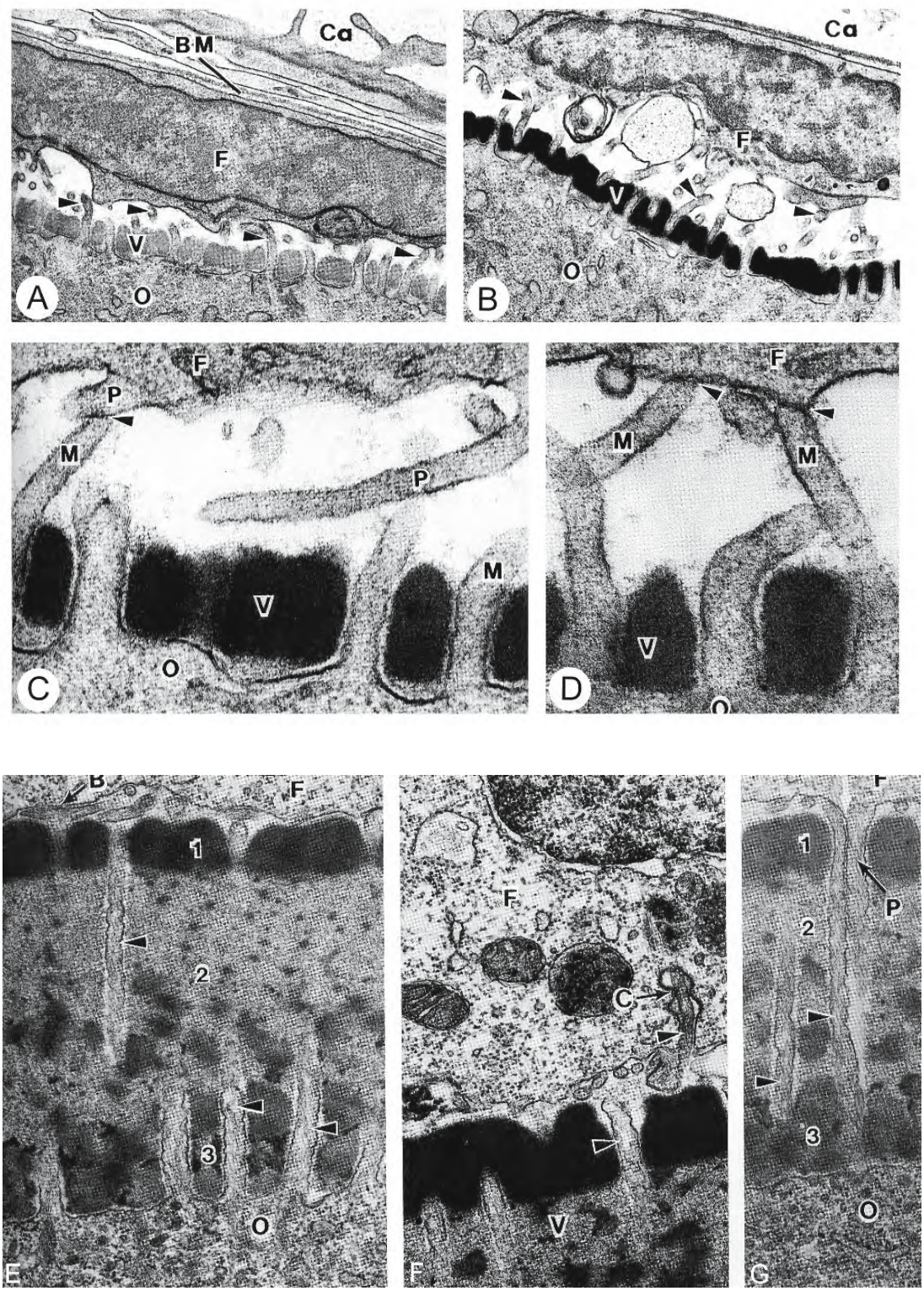

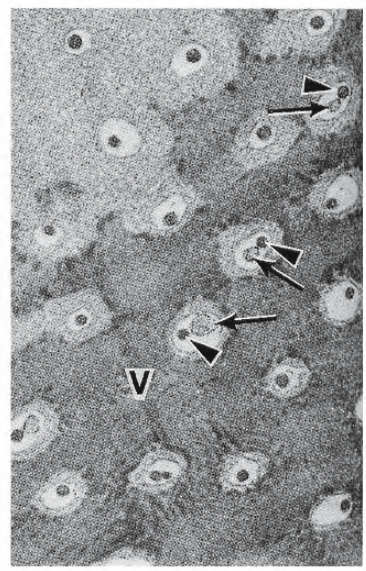

Figure 2.105: Transmission electron micrograph of a section of the periphery of an ovarian follicle of the zebrafish *Brachydanio rerio.* The pore canals within the zona pellucida (V) are cut transversely, thereby demonstrating the intimate relationship between microvilli from the oocyte (arrowheads) and processes from a follicular cell (arrows). X 18,600 (From Kessel et al., 1985; reproduced with permission from Nuova Immagine Editrice).

←

Figure 2.104: Transmission electron micrographs of sections of the periphery of ovarian follicles of zebrafish *Brachydanio rerio.* (From Kessel et al., 1985; reproduced with permission from Nuova Immagine Editrice).

A,B. The zona pellucida is forming in the perivitelline space. Microvilli (arrowheads) from the oocyte extend through their individual pore canals to make contact with squamous follicular cells. Sparser, stubbier microvilli extend from the follicular cells in the opposite direction. The follicular epithelium is surrounded by a prominent basal lamina. **A** X 17,000; **B** X 16,400.

C,D. There is close contact (arrowheads) between processes of follicular cells and microvilli of the oocyte. X 68,500.

E. At a later stage in its development, the zona pellucida exhibits three layers (1,2,3). Microvilli (arrowheads) from the oocyte extend through pore canals toward a follicular cell. Note the terminal branching (B) of one of these microvilli as it presses against the plasmalemma of a follicular cell. X 25,000.

F. An oocyte microvillus (arrowhead) has invaginated a follicular cell (C). X 27,300.

G. A process from a follicular cell lies parallel to an oocyte microvillus (arrowhead) within a single pore canal. X 27,300.

Abbreviations: BM, basal lamina; Ca, capillary; F, follicular cells; M, microvilli; O, oocyte; P, processes; V, zona pellucida.

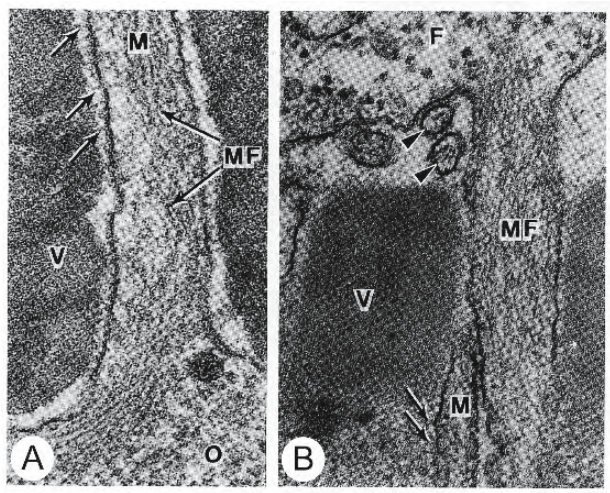

Figure 2.106: Transmission electron micrographs of a section through the periphery of an ovarian follicle of the zebrafish *Brachydanio rerio.* X 82,000 (From Kessel et al., 1985; reproduced with permission from Nuova Immagine Editrice).

A. Microfilaments (MF) abound in this longitudinal section of an oocyte microvillus (M) as well as in the cortical ooplasm (O). The arrows indicate transverse connections between the microvillus and the zona pellucida (V) of the wall of the pore canal.

B. Microfilaments (MF) are abundant within the process of a follicular cell (F). The arrowheads indicate cross sections of oocyte microvilli; a single microvillus from the oocyte (M) approaches the follicular cell process at the bottom of the picture. The arrows indicate transverse connections between the microvillus and the zona pellucida (V).

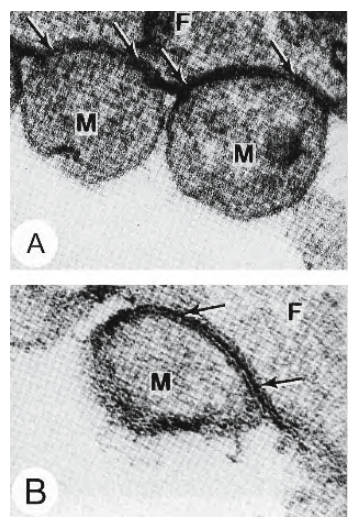

Figure 2.107A,B: Transmission electron micrographs of cross sections through oocyte microvilli (M) from ovarian follicles of the zebrafish *Brachydanio rerio.* The arrows indicate gap junctions between the microvilli and the surface of follicular cells (F). (From Kessel et al., 1985; reproduced with permission from Nuova Immagine Editrice).

A. X 120,000.

B. X 173,200.

Figure 2.108: Electron micrograph of freeze-fracture replica the periphery of an ovarian follicle of the zebrafish *Brachydanio rerio*. Arrowheads indicate several gap junctional arrays on the surface of a follicular cell. (From Kessel et al., 1985; reproduced with permission from Nuova Immagine Editrice).
Abbreviations: F, follicular cell; M, oocyte microvilli; P, processes from a follicular cell; V, zona pellucida.

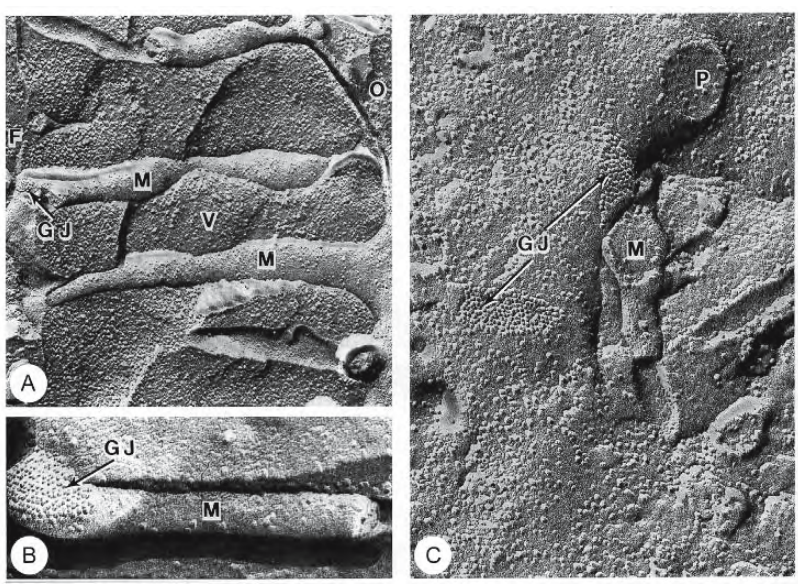

←

Figure 2.109: Electron micrographs of freeze-fracture replicas the periphery of ovarian follicles of the zebrafish *Brachydanio rerio* to illustrate gap junctional arrays on microvilli from oocytes and on nearby plasma membranes of follicular cells. (From Kessel et al., 1985; reproduced with permission from Nuova Immagine Editrice).
A. X 52,800.
B. X 134,000.
C. X 100,000.
Abbreviations: F, follicular cell; GJ, gap junctional array; M, oocyte microvilli; O, oocyte; P, process from a follicular cell; V, zona pellucida.

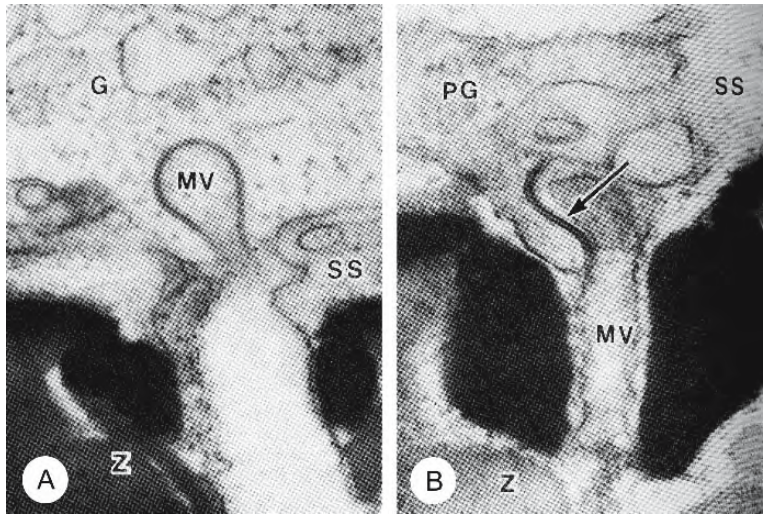

Figure 2.110: Transmission electron micrographs of a section through the periphery of an ovarian follicle of the chum salmon *Oncorhynchus keta.* Tips of oocyte microvilli protrude beyond the zona pellucida to invaginate a follicular cell (**A**), or attach itself to a process from a follicular cell (**B**). The arrow indicates a narrow space between the apposing plasma membranes of the microvillus and the process. (From Kobayashi, 1985b; reproduced with permission from Blackwell Publishing).
A. X 60,000. **B**. X 70,000.
Abbreviations: G, follicular cell; MV, oocyte microvillus; PG, process from a follicular cell; SS, subfollicular space; Z, zona pellucida.

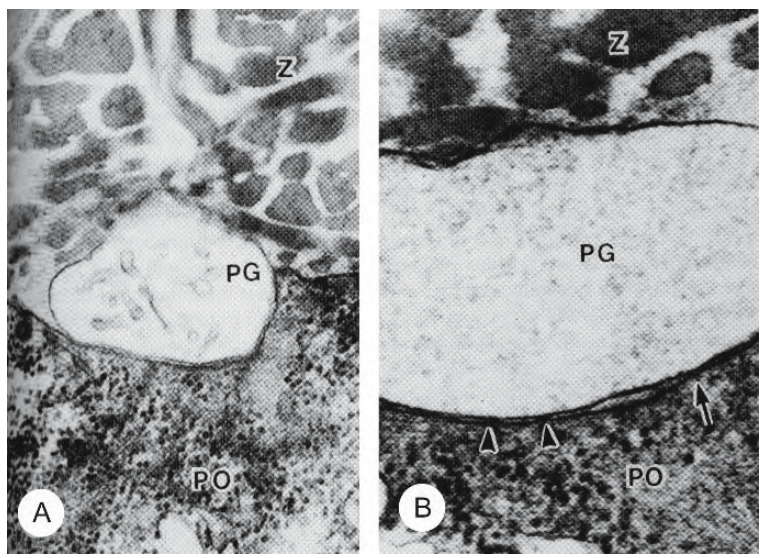

Figure 2.111: Transmission electron micrographs of a section through the periphery of an ovarian follicle of the chum salmon *Oncorhynchus keta* showing the association between processes from follicular cells (PG) with the oolemma. PO, peripheral ooplasm. (From Kobayashi, 1985b; reproduced with permission from Blackwell Publishing).
A. The expanded end of the process terminates in a slight depression of the oolemma. There is a small amount of filamentous material and agranular endoplasmic reticulum in the tip of the process. X 37,500.
B. A tight junction (arrow) and gap junctions (arrowheads) span the space between the tip of the process and the oolemma. X 75,000.

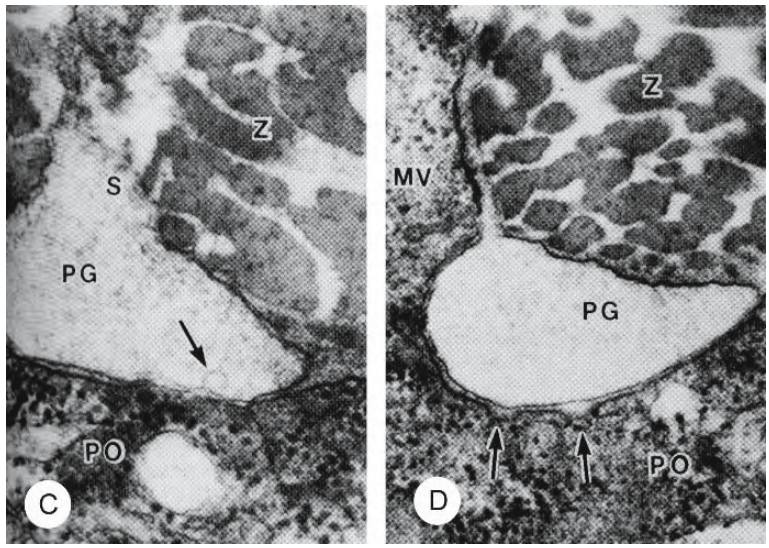

Figure 2.111: Continued.
C. Endocytotic activity (arrow) occurs in the expanded end of a process. X 66,000.
D. The oolemma in these regions forms coated vesicles (arrows). X 50,000.
Abbreviations: MV, oocyte microvillus; PG, process from a follicular cell; PO, peripheral ooplasm; Z, zona pellucida.

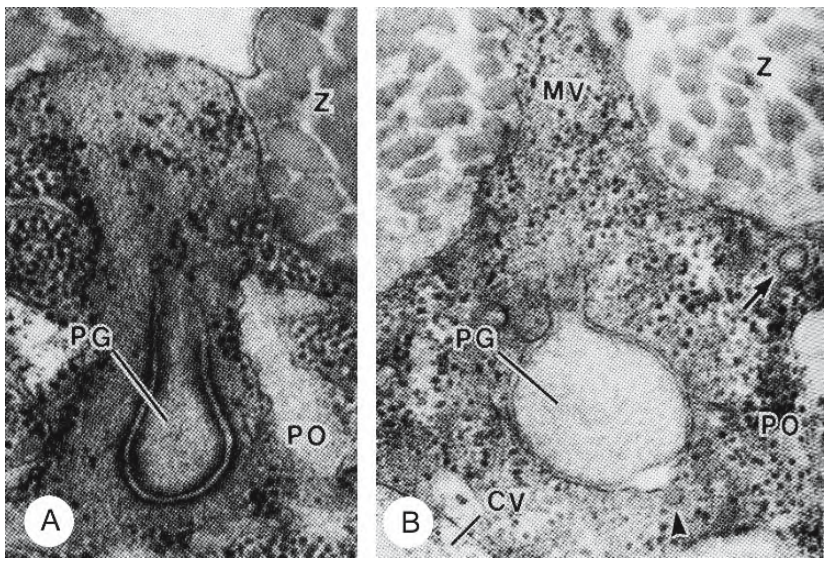

Figure 2.112: Transmission electron micrographs of a section through the periphery of an ovarian follicle of the chum salmon *Oncorhynchus keta* showing the association whereby the expanded ends of processes from follicular cells fit deeply into indentations of the oolemma. (From Kobayashi, 1985b; reproduced with permission from Blackwell Publishing).
A. Desmosomes or desmosome-like junctions occur between the plasmalemma of the process and the oolemma. X 56,000.
B. The arrow indicates a large, coated vesicle in the peripheral ooplasm. X 44,800.
Abbreviations: CV, cortical vesicle; MV, oocyte microvillus; PG, process from a follicular cell; PO, peripheral ooplasm; Z, zona pellucida.

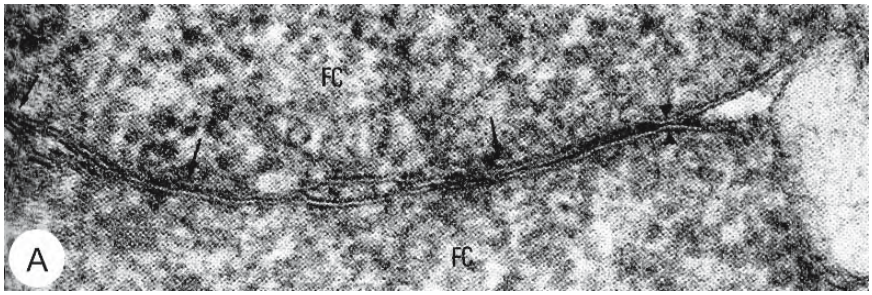

Figure 2.113: Electron micrographs of the junctions between adjacent cells in the follicular epithelium of the ayu *Plecoglossus altivelis.* (From Toshimori and Yasuzumi, 1979a; reproduced with permission from Elsevier Science).

A. Transmission electron micrograph showing regions of close proximity (arrows) and focal fusion (arrowhead) of the outer leaflets of membranes of follicular cells. X 100,000.

→

B. Electron micrograph of a freeze-fractured replica of the follicular epithelium. Five to seven strands consisting of ridges and grooves on the PF- and EF- fracture faces respectively, are displayed on the surface of a follicular cell (upper centre). X 24,000 *Inset*: A few strands terminate freely, without rejoining the network (arrowheads). The spaces between the strands are wide. X 46,000.

Abbreviations: A, PF (plasmatic) fracture face; B, EF (extraplasmatic) fracture face; BL, basal lamina; C, zona pellucida; FC, follicular cell; N, nucleus; O, oocyte.

←

Figure 2.114: Electron micrograph of a freeze-fractured replica of the follicular epithelium from a vitellogenic follicle of the ayu *Plecoglossus altivelis.* Gap junctions, consisting of clusters of 10 to 80 intramembranous particles (arrows), abound between microvilli of the oocyte and follicular cells. X 42,000 (From Toshimori and Yasuzumi, 1979b; reproduced with permission).

Abbreviations: A, PF fracture face; C, zona pellucida; F, EF face of plasma membrane of follicular cell; M, microvillus in a pore canal; P, process from follicular cell.

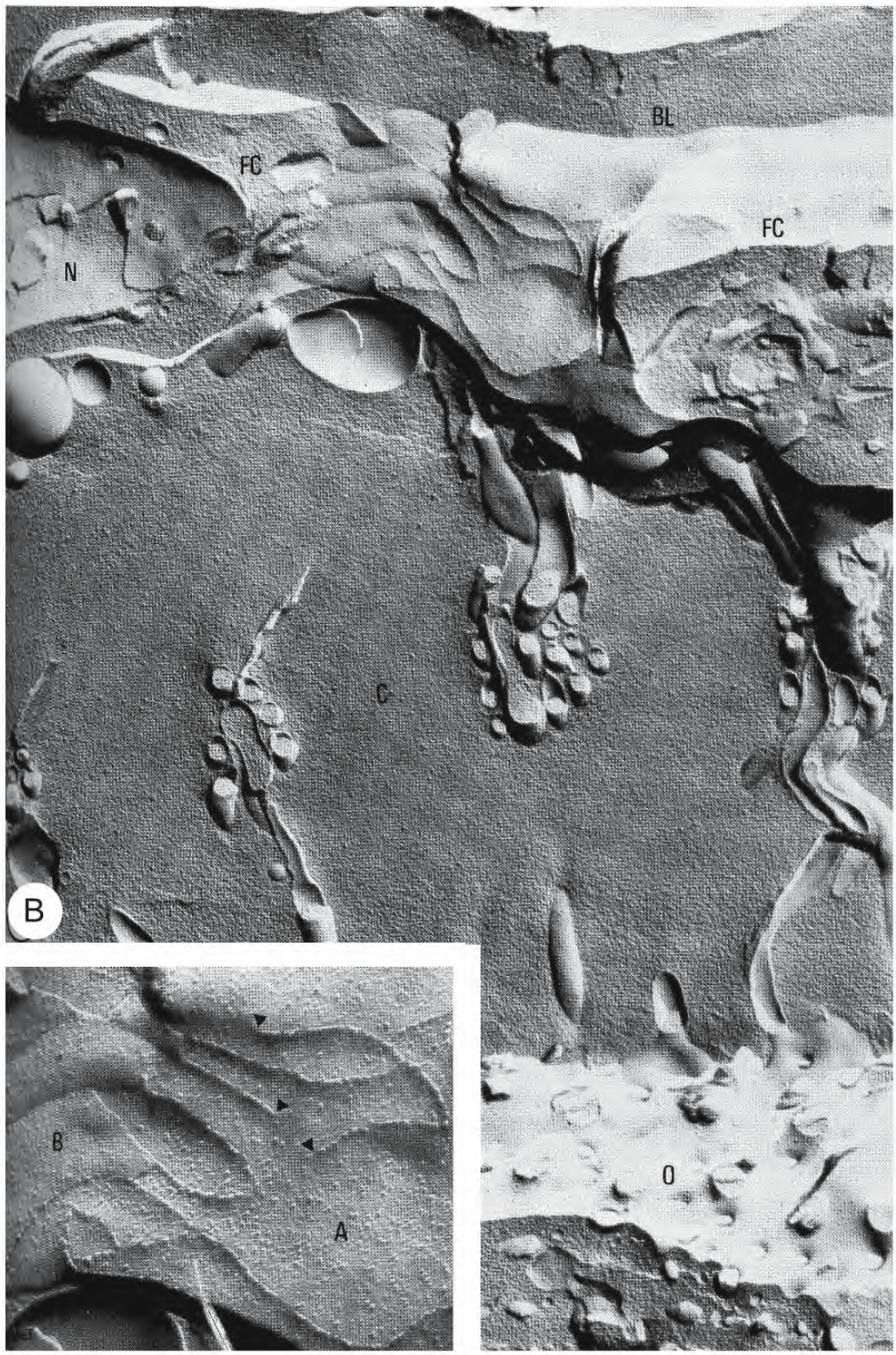

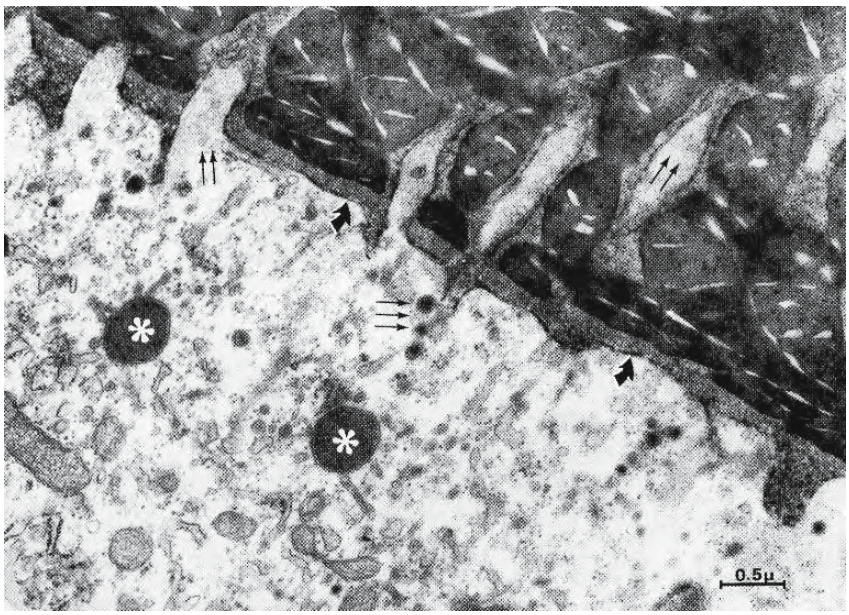

Figure 2.115: Transmission electron micrograph of a section through the periphery of an ovarian follicle in late vitellogenesis. This specimen was taken from a cyprinodont *Aphanius mento* that had been injected with horseradish peroxidase. The zona pellucida is shown at the upper right. Peroxidase has been deposited between the zona pellucida and the oolemma (curved arrows) and is located within pinocytotic vesicles (triple arrows). Oocyte microvilli within pore canals (double arrows) are surrounded by the tracer. The asterisks indicate cortical granules. X 18,450 (From Abraham et al., 1984; reproduced with permission of the author).

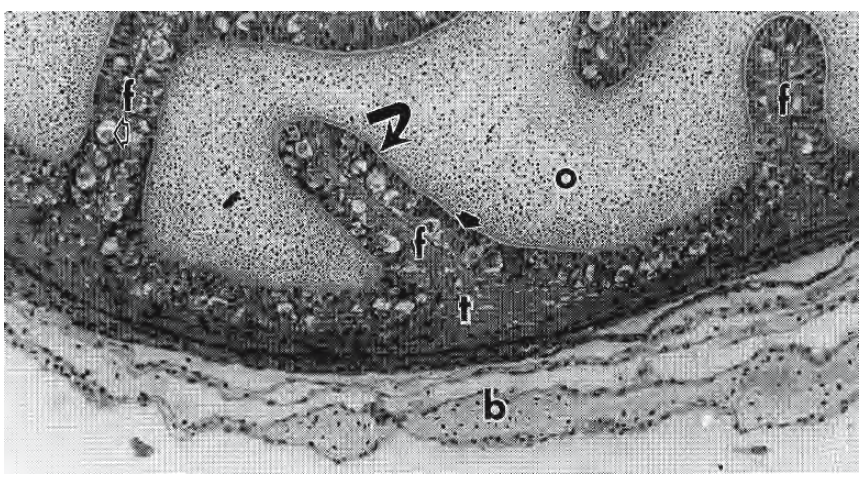

Figure 2.116: Photomicrograph of the periphery of an vitellogenic follicle of a viviparous elasmobranch, the yellow spotted stingray *Urolophus jamaicensis.* Inward folds (f) of the follicular wall, covered by the zona pellucida (curved arrow) and carrying thecal cells (t) and blood vessels, indent the surface of an oocyte (o). The follicular epithelium consists of large (open arrow) and small (closed arrow) cells. The follicle is surrounded by vascular connective tissue (b). (From Hamlett, Jezior, and Spieler, 1999; reproduced with permission of Urban & Fischer Verlag).

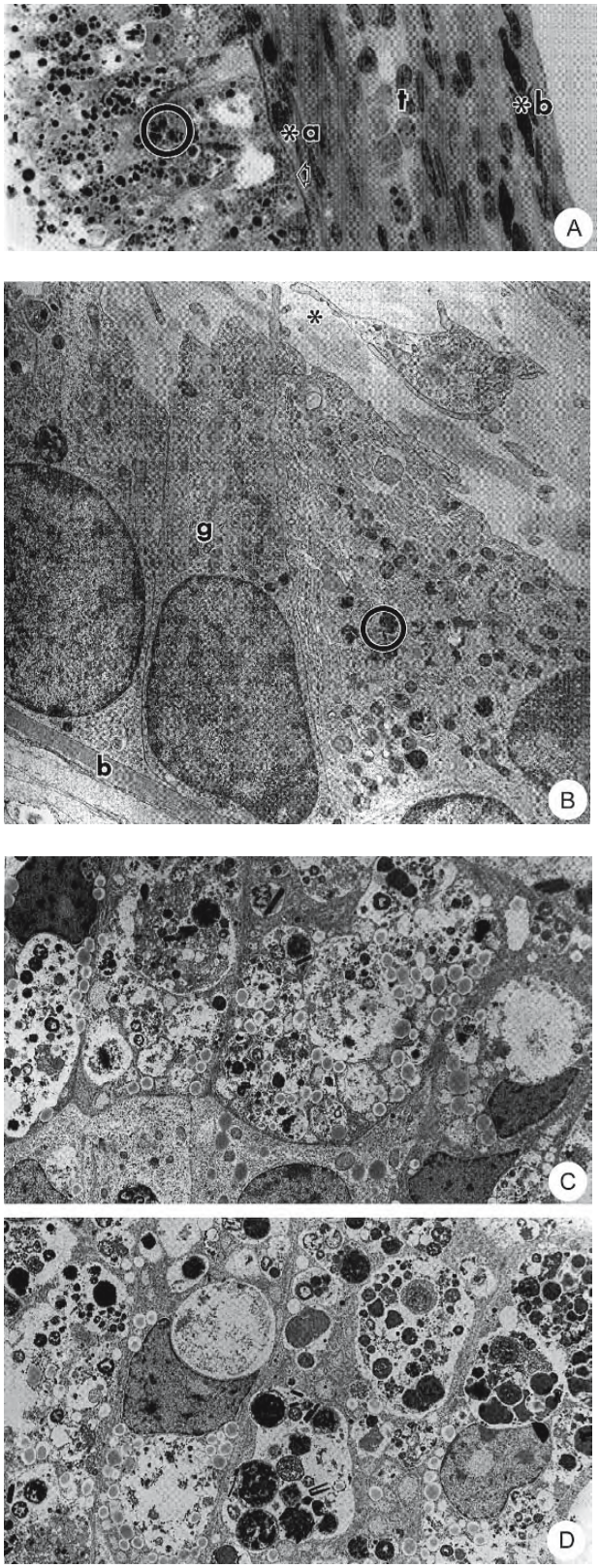

Figure 2.117: Micrographs of the periphery of follicles of a viviparous elasmobranch, the yellow spotted stingray *Urolophus jamaicensis.* (From Hamlett, Jezior, and Spieler, 1999; reproduced with permission of Urban & Fischer Verlag).

A. Photomicrograph of a vitellogenic follicle. Follicular cells contain prominent yolk precursor vesicles (circle). The open arrow indicates the basal lamina of the follicular epithelium. The theca (t) contains blood vessels (*a,*b) X 600.

B. Transmission electron micrograph of vitellogenic follicular cells containing heterogeneous transport vesicles (circle). The asterisk indicates the zona pellucida; b, basal lamina; g, Golgi complex. X 7,000.

C,D. Transmission electron micrographs of actively vitellogenic follicular cells containing heterogeneous transport vesicles. X 4,500.

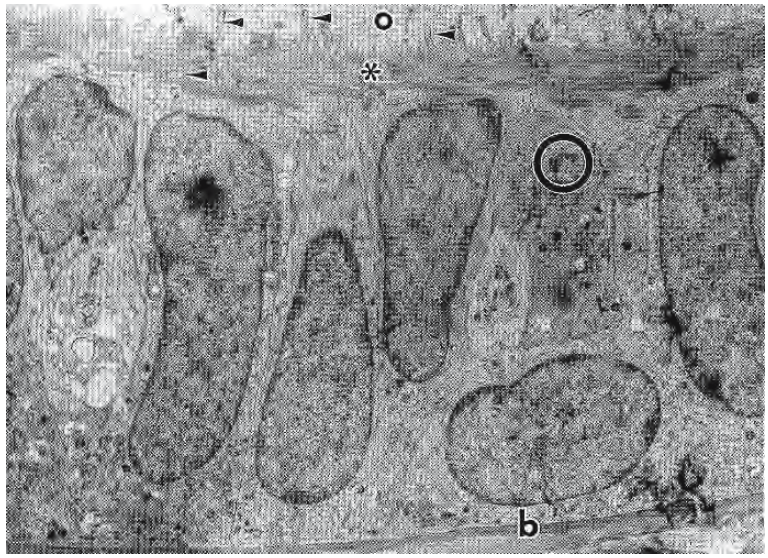

Figure 2.118: Electron micrograph of the follicular epithelium of a vitellogenic follicle of a viviparous elasmobranch, the yellow spotted stingray *Urolophus jamaicensis.* Follicular cells, containing yolk precursor vesicles (circle), extend processes or transosomes (arrowheads) into the zona pellucida (*) to invaginate the oolemma of the oocyte (o). b, basal lamina. X 5,000 (From Hamlett, Jezior, and Spieler, 1999; reproduced with permission of Urban & Fischer Verlag).

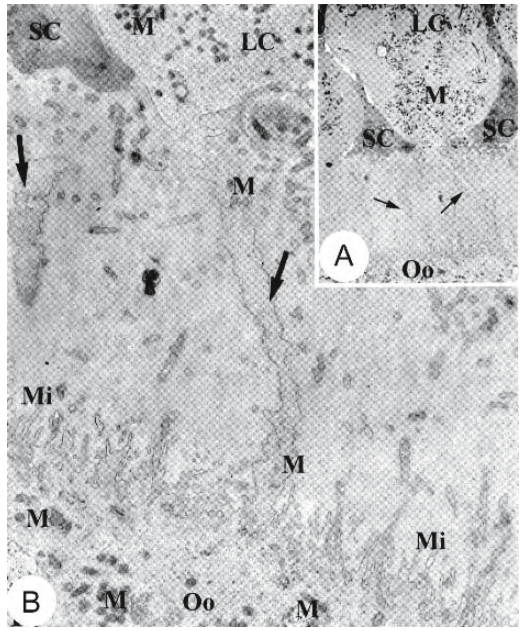

Figure 2.119: Transmission electron micrographs from a follicle of the elasmobranch *Raya asterias* to illustrate intercellular bridges (arrows) connecting a large follicular cell to the oocyte. (From Andreuccetti et al., 1999; reproduced with permission).
A. X 1,200.
B. Higher magnification of the same cell at the level of the intercellular bridges. X 3,400.
Abbreviations: LC, large follicular cell; M, mitochondria; Mi, microvilli; Oo, oocyte; SC, small follicular cell.

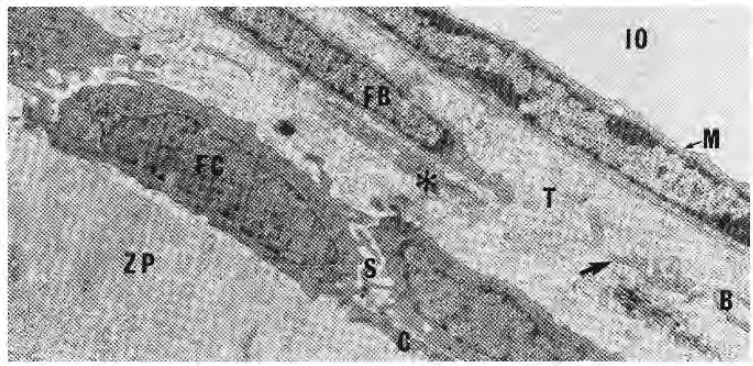

Figure 2.120: Electron micrograph of the mesothelium (M), theca (T), and its adjacent layers, and follicular cells (FC), of an early follicle of the lamprey *Petromyzon marinus*. Fibrocytes (FB) send long cytoplasmic processes (arrow) throughout the matrix to adjacent fibrocytes. The process from a cell not in this section borders on the cell body of the cell shown (*). Blood vessels (B) run within the theca. (From Yorke and McMillan, 1980; reproduced with permission from the Society for the Study of Reproduction, Inc.).
Abbreviations: C, cytoplasmic process; IO, intraovarian space; S, intercellular space; ZP, zona pellucida. X 13,400.

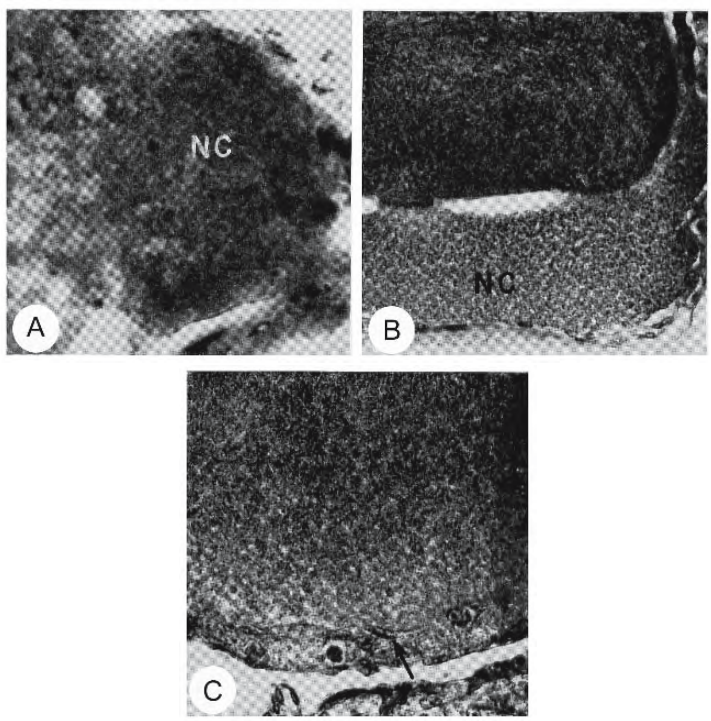

Figure 2.121: Photomicrographs of ovarian follicles of the lamprey *Petromyzon marinus* during vitellogenesis showing the merger of a yolk-laden "nurse cell" with a vitellogenic oocyte. (From Lewis and McMillan, 1965; © reproduced with permission of John Wiley & Sons, Inc.).

A. Nurse cell (NC) packed with yolk granules. X 950.

B. A large nurse cell (NC) has partially merged with an oocyte; at the points where they are not joined, the cells have been separated by shrinkage during processing. X 500.

C. Following the merger, membranous remnants (arrow) of the nurse cell persist in the cytoplasm of the oocyte. X 350.

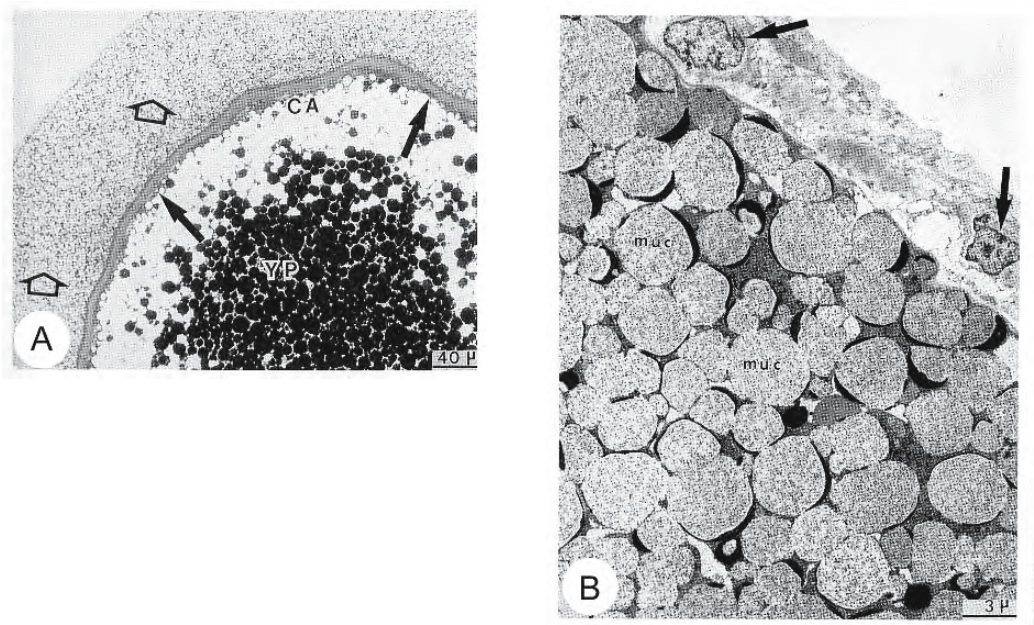

Figure 2.122: An unusual method of formation of the secondary envelope seen in vitellogenic oocytes of the sheatfish *Silurus glanis.* (From Abraham et al., 1993; © reproduced with permission of John Wiley & Sons, Inc.).

A. Photomicrograph. During early vitellogenesis the follicular cells proliferate to form an irregular mass of cells (open arrows) around the zona pellucida (dark arrows).

Abbreviations: CA, cortical alveoli; YP, yolk platelets.

B. Electron micrograph of these irregular cells or "mucosomes" (muc) adjacent to the theca (arrows).

Figure 2.123: Electron micrograph of a section of the basal region of an early follicle of the lamprey *Petromyzon marinus.* Squamous follicular cells (F) are lifted from the surface of the zona pellucida (ZP) by a large adhesive cell. Microvilli (MV) from the lateral borders of the adhesive cells extend into wide intercellular spaces. The surface of the zona pellucida is slightly depressed beneath the adhesive cell (arrows). The cytoplasm of the adhesive cell is packed with interconnected saccules (I) which show great variation in staining and contains a small amount of agranular endoplasmic reticulum (R). Th, theca. X 13,200 (From Yorke and McMillan, 1979; © reproduced with permission of John Wiley & Sons, Inc.).

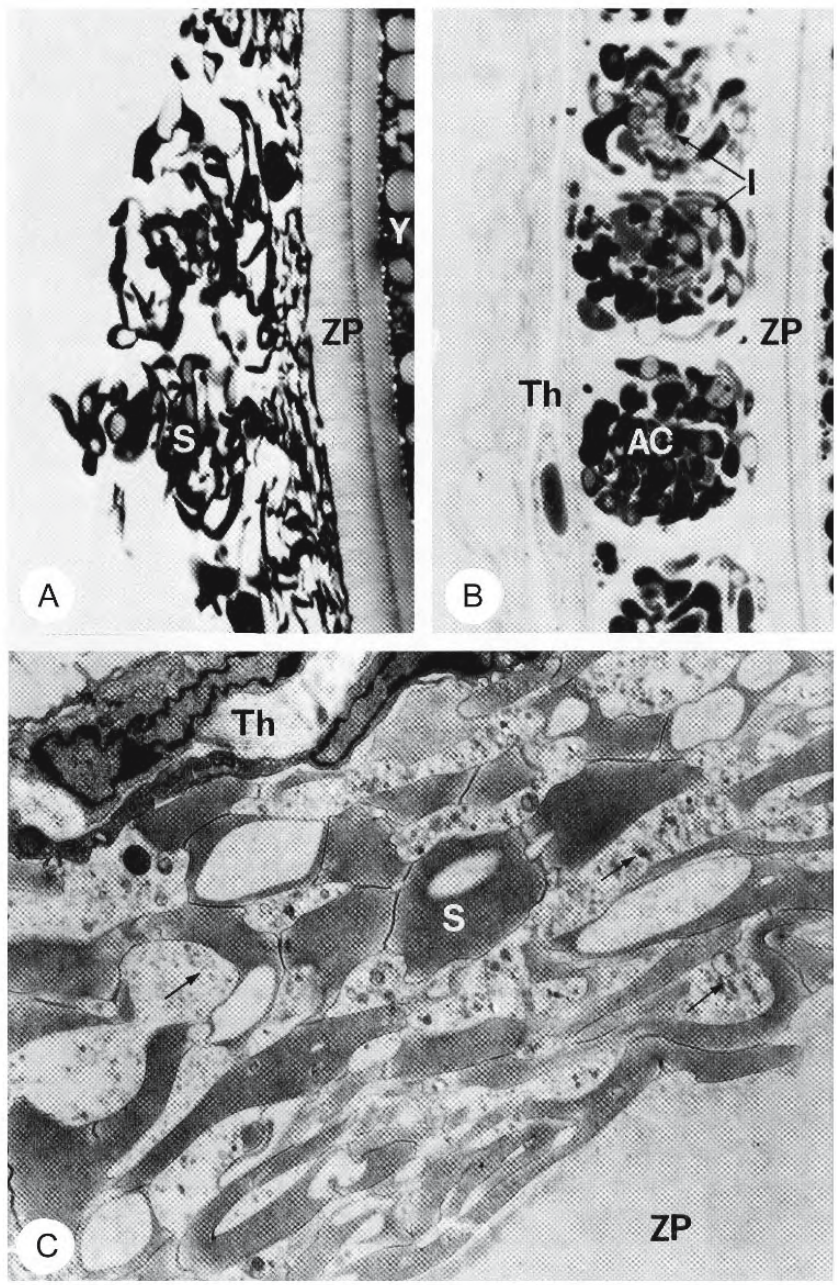

Figure 2.124: Micrographs of the adhesive layer of oocytes of the lamprey *Petromyzon marinus* around the time of ovulation. (From Yorke and McMillan, 1979; © reproduced with permission of John Wiley & Sons, Inc.).

A. Photomicrograph of a section through the surface of a recently ovulated egg showing the pleiomorphic adhesive saccules of the adhesive coat. X 1,050.

B. Photomicrograph of a similar region of an unovulated egg, just before spawning. X1,050.

C. Electron micrograph of an egg during spawning. Débris (arrows) from the follicular adhesive cells, especially in the form of adhesive saccules, adheres to the zona pellucida. The theca persists over this portion of the egg. X 7,200.

Abbreviations: AC, adhesive cells; S, adhesive saccules; Th, theca; Y, yolk; ZP, zona pellucida.

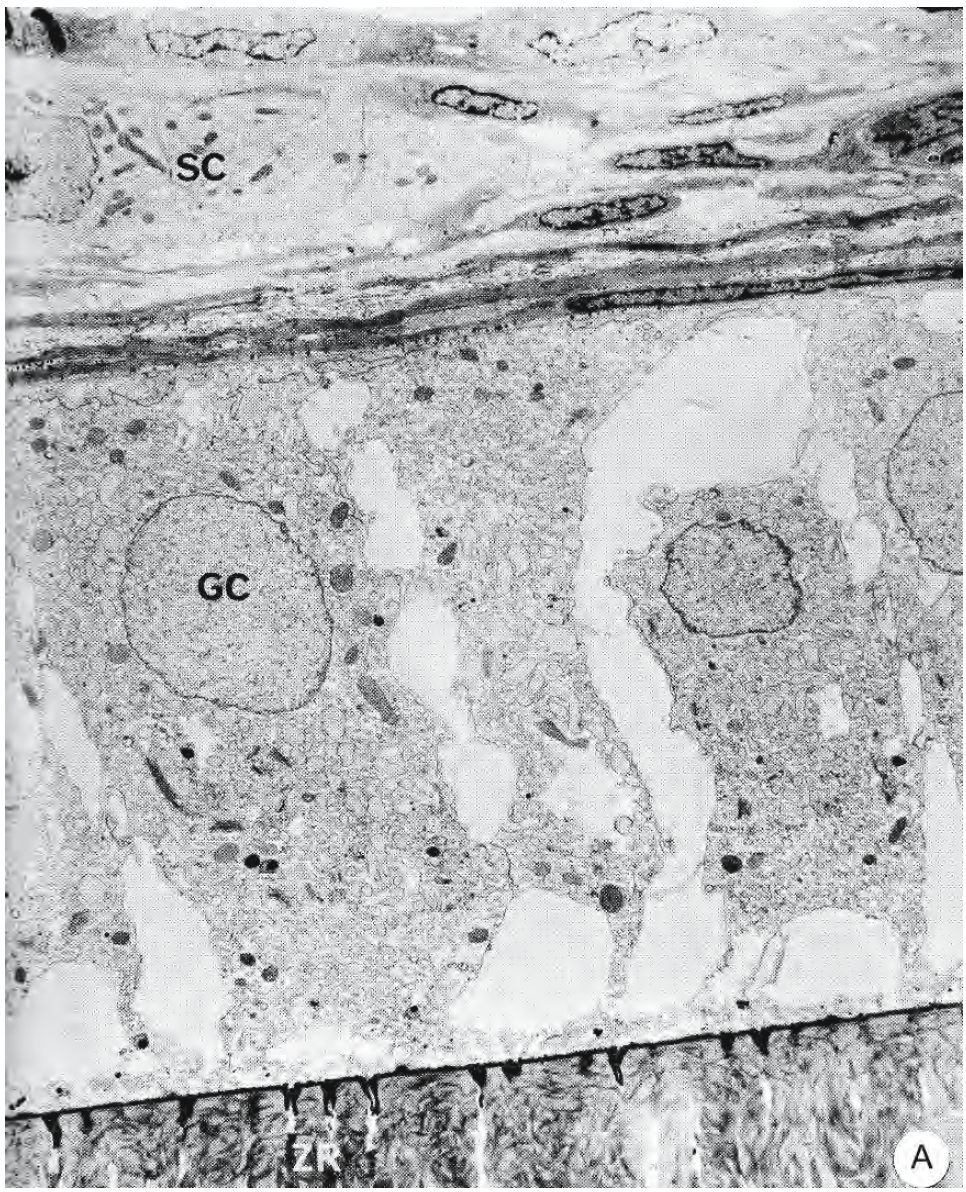

Figure 2.125: Electron micrographs of sections of the preovulatory follicle of a mature coho *Oncorhynchus kisutch.* (From Nagahama, Clarke, and Hoar, 1978; reproduced with permission of the NRC Press).

A. Extensive granular endoplasmic reticulum in the follicular cells (GC) contains amorphous material of variable electron density. Special thecal cells (SC) are seen in the theca. ZR, zona pellucida. X 3,750.

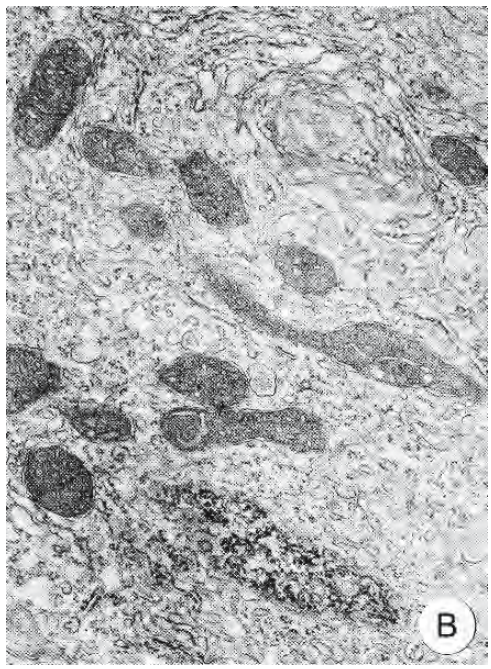

Figure 2.125: Continued.
B. The cytoplasm of a special thecal cell is packed with agranular endoplasmic reticulum and mitochondria with tubular cristae. X 20,000.

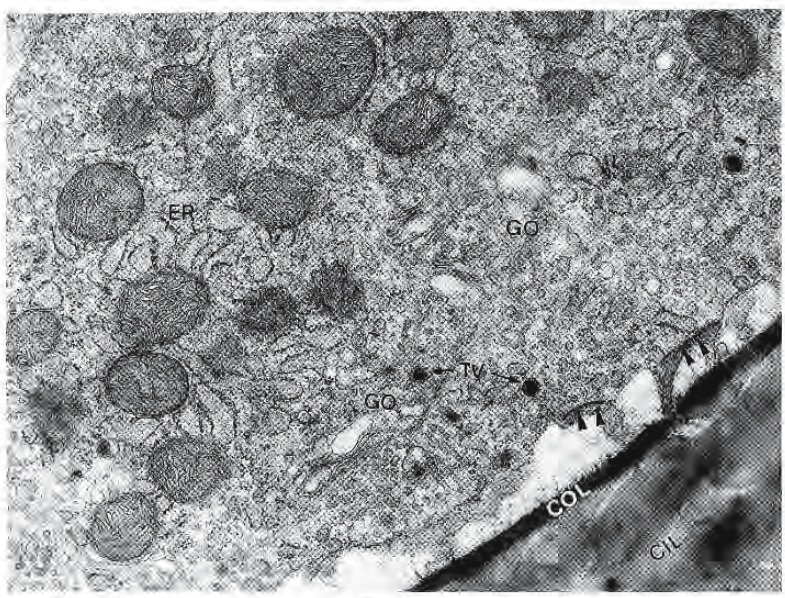

Figure 2.126: Electron micrograph of a section of a postovulatory follicle of the medaka *Oryzias latipes* showing a portion of a follicular cell packed with dilated Golgi lamellae (GO), granular endoplasmic reticulum (ER), and mitochondria with tubular cristae. The arrowheads indicate gap junctions between the follicular cell and processes from the oocyte. X 21,000 (From Iwamatsu et al., 1988; reproduced with permission from the Zoological Society of Japan).
Abbreviations: CIL, COL, inner and outer layers of the zona pellucida; TV, transport vesicles.

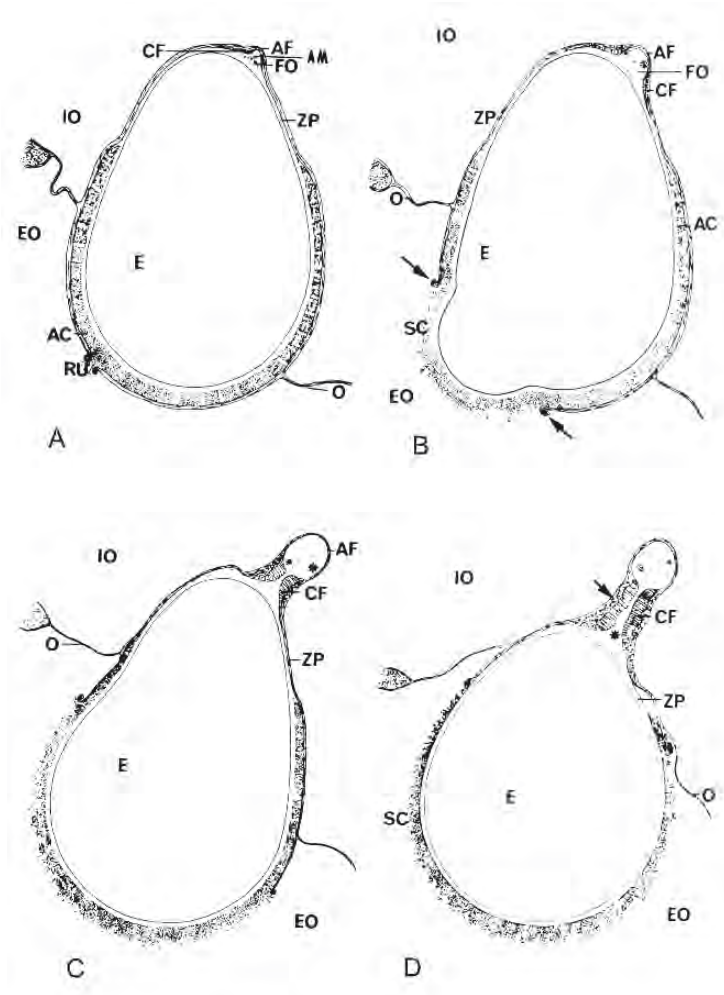

Figure 2.127: Drawings illustrating the mechanical function of follicular cells during ovulation in the lamprey *Petromyzon marinus* where a gentle, steady constriction extrudes the egg from the follicle. X 65 (From Yorke and McMillan, 1980; reproduced with permission from the Society for the Study of Reproduction, Inc.).

A. Shortly after the rupture of the follicular and thecal layers, the oocyte nucleus has become indistinguishable and adhesive cells near the site of rupture are breaking down in a wave that progresses rapidly away from this centre. A deeply staining, amorphous material has accumulated in the fluid of ovulation and apical follicular cells have a well developed secretory appearance. Follicular cells surrounding the apical follicular cells are becoming columnar.

B. There is a continued increase in the height of the columnar follicular cells during early stages of emergence of the egg. As the egg enters the extraovarian space, it is covered with the remnants of the adhesive cells which form the adhesive coat. The follicular cells and theca are pulled back from the rupture (arrows).

C. At a mid stage in egg emergence, follicular cells near the apical end of the follicle become columnar and create a constriction that pinches off the apical follicular cells, forming a sphere (*).

D. The wave of elongation continues to transform the follicular cells and they become successively more columnar. The constricted portion of the follicle (arrow) elongates, pushing the egg ahead. Strands of material (*), derived from the fluid of ovulation, trail from the apical end of the egg.

Abbreviations: AC, adhesive cells; AF, apical follicular cells; AM, amorphous material; CF, columnar follicular cells; E, egg; EO, extraovarian space; FO, fluid of ovulation; IO, intraovarian space; O, ovarian wall; SC, adhesive coat. RU, site of rupture; ZP, zona pellucida.

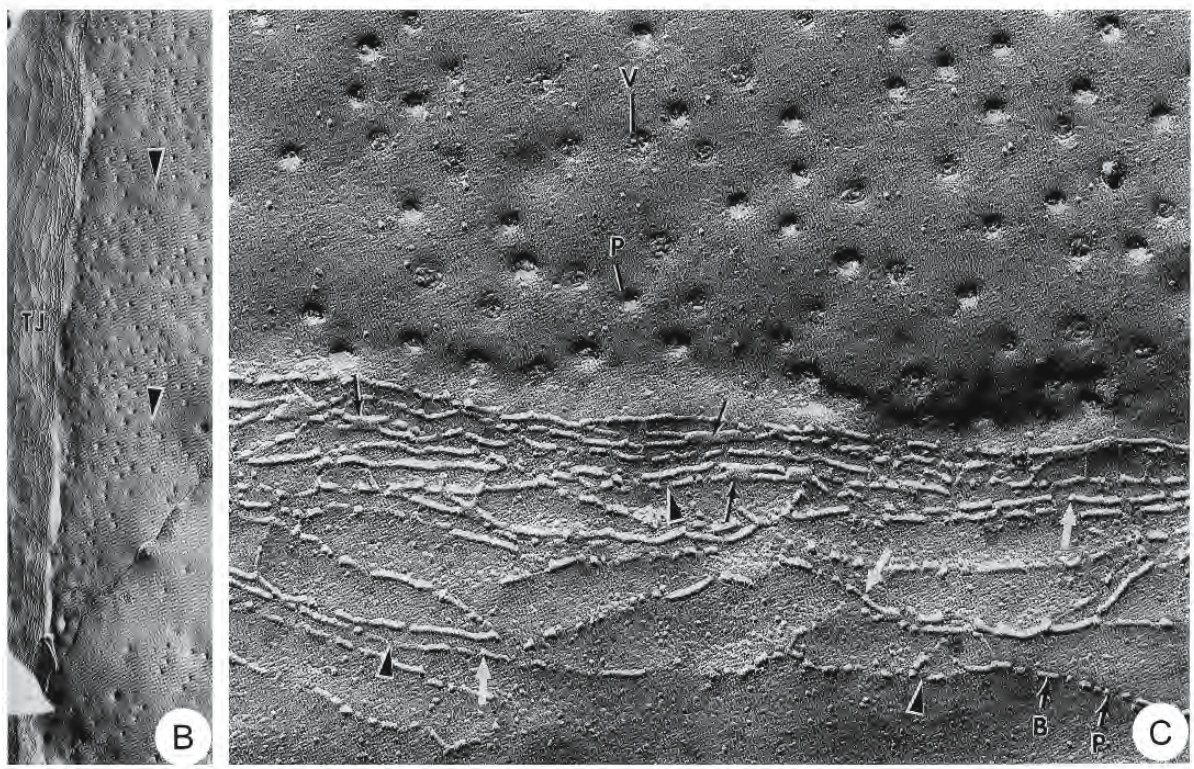

Figure 2.128: Electron micrographs of freeze-fracture replicas of junctions between mesothelial cells from the ovary of the zebrafish *Brachydanio rerio.* (From Kessel, Roberts, and Tung, 1988; reproduced with permission from Nuova Immagine Editrice).

A. Lattice of tight junctional strands (TJ) with intercalated communicating junctions (CJ). X 110,200.

B. There is an almost linear arrangement of the tight junctional strands (TJ). The arrowheads indicate micropinocytotic pits and vesicles. X 49,000.

C. An enlargement of **B** to illustrate short bars (B), particles (P) and particle free regions (arrowheads). The black arrows indicate apparent fusion of some of the strands. A slight enlargement (white arrows) occurs at the ends of some bars. The upper P and V indicate micropinocytotic pits and vesicles. X 87,000.

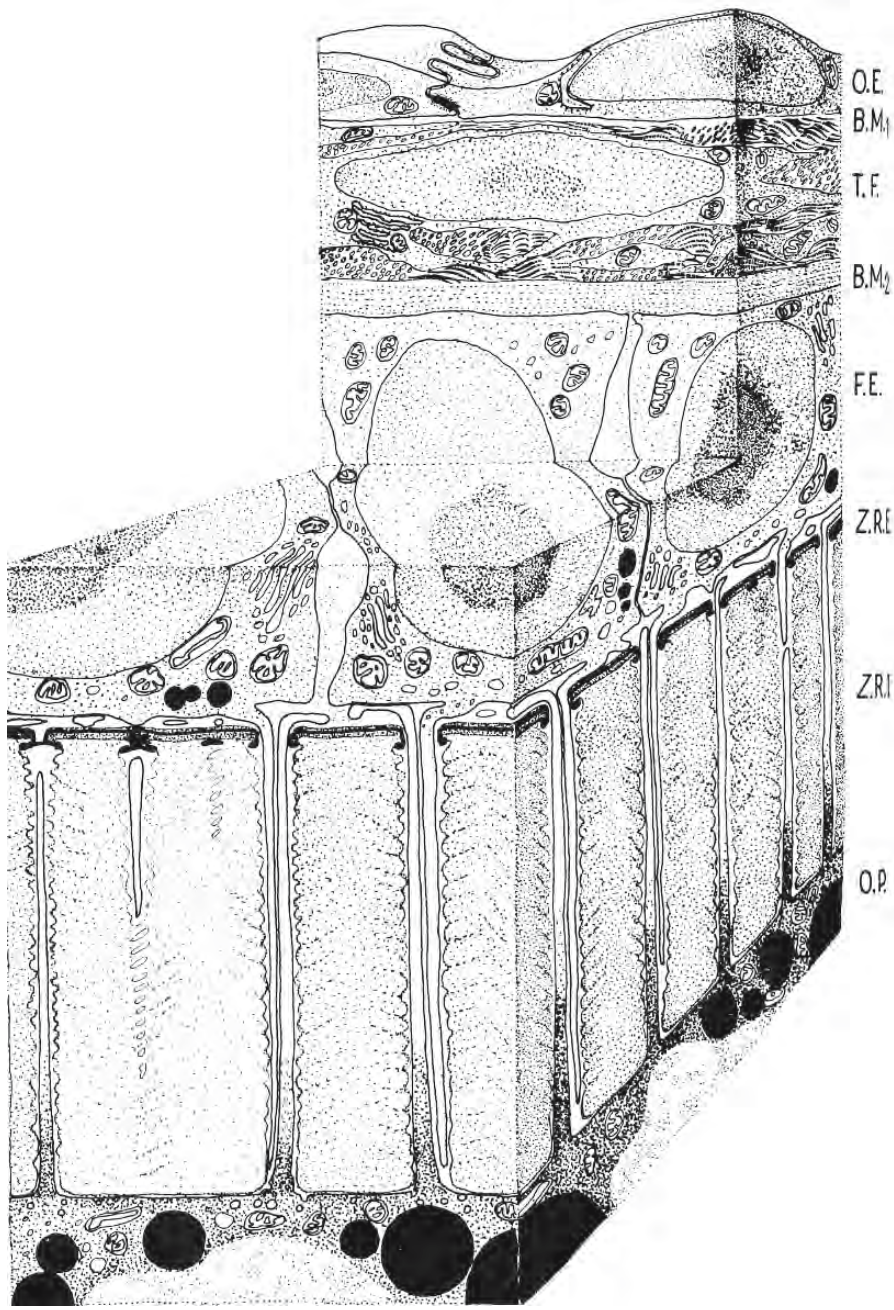

Figure 2.129: Schematic diagram of the follicular wall of the eastern brook trout *Salvelinus fontinalis.* (Egg diameter about 3.0 mm) (From Flügel, 1967b; reproduced with permission of the author).
Abbreviations: BM_1, mesothelial basal lamina; BM_2, basal lamina of the follicular epithelium; FE, follicular epithelium; OE, ovarian mesothelium; OP, ooplasm; TF, theca; ZRE, external region of zona pellucida; ZRI, internal region of zona pellucida.

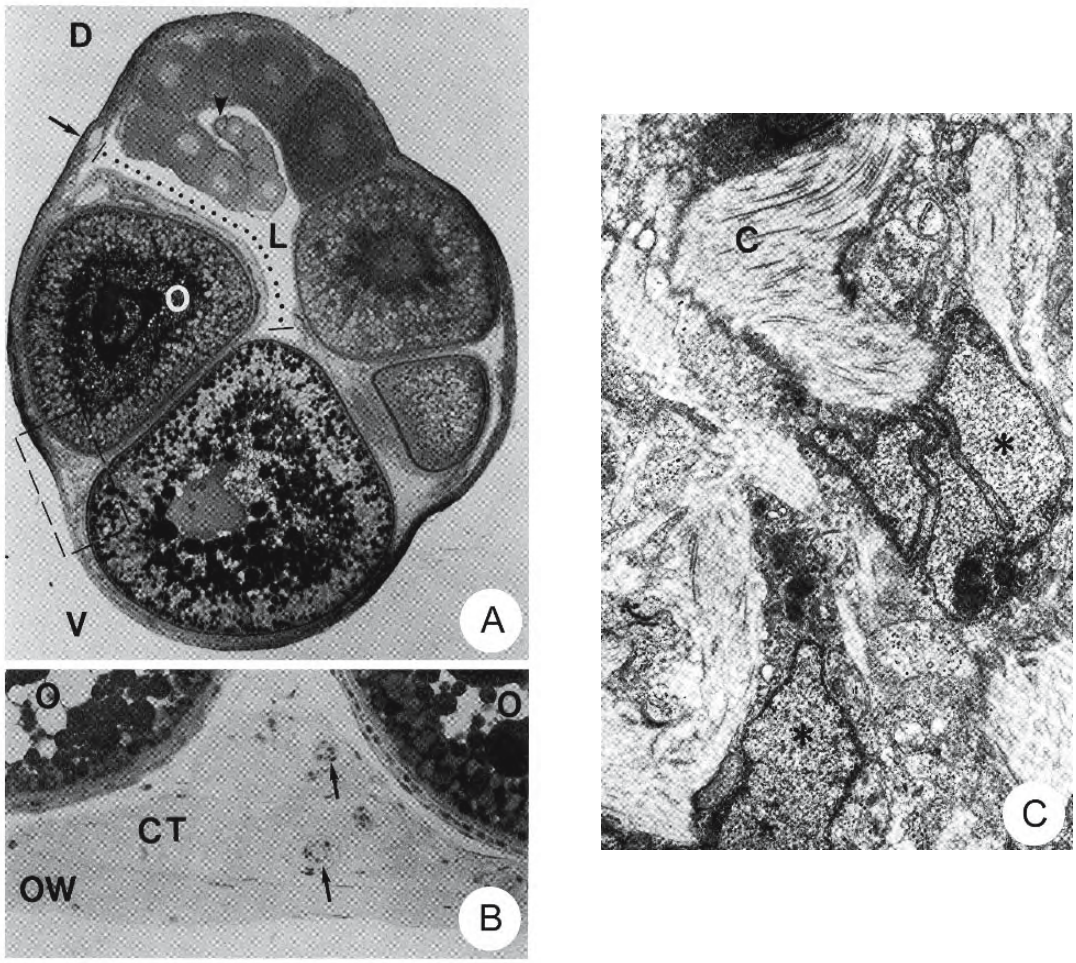

Figure 2.130: Micrographs of sections of the ovary of the pipefish *Syngnathus scovelli.* (From Begovac and Wallace, 1987; © reproduced with permission of John Wiley & Sons, Inc.).

A. Photomicrograph of a transverse section of an entire ovary depicting various stages of oocyte development. The germinal ridge (arrowhead) and young developing follicles have curled to protrude into the ovarian lumen. The mature edge is indicated by the dotted line overlying the largest oocytes. The boxed area is enlarged in **B**. D, dorsal; V, ventral. X 100.

B. Enlargement of boxed region in **A**. A vascular connective tissue stroma fills the space between adjacent follicles. The arrows indicate arterioles dispersed within the connective tissue. X 270.

C. Electron micrograph of the connective tissue stroma consisting of collagen and connective tissue cells (*). X 8,690.

Abbreviations: C, collagen; CT, connective tissue; L, ovarian lumen; O, oocyte; OW, ovarian wall.

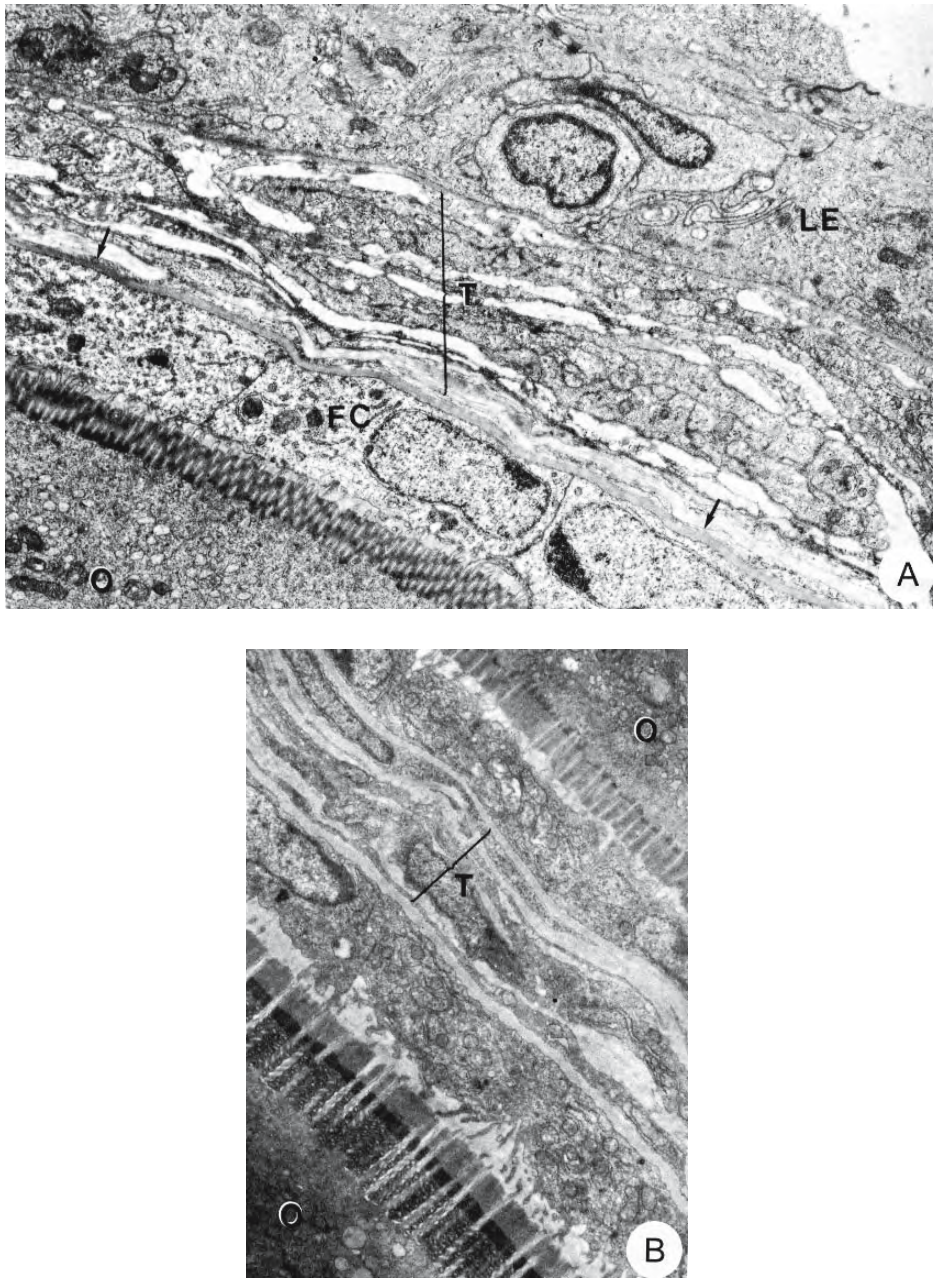

Figure 2.131: Electron micrographs of sections of the follicular periphery in the ovary of the pipefish *Syngnathus scovelli.* (From Begovac and Wallace, 1987; © reproduced with permission of John Wiley & Sons, Inc.).

A. This micrograph illustrates the layers interposed between the oocyte and the luminal epithelium. The thecal layer consists of attenuated fibroblasts and is well developed. The follicular epithelium consists of a simple layer of cuboidal cells resting on a thick basal lamina (arrows). X 7,650.

B. Where two follicles abut, the stroma may be extruded so that a single theca sandwiched between two basal laminae of the follicular epithelia, is shared between them. X 5,550.

Abbreviations: FC, follicular cells; LE, luminal epithelium; O, oocyte; T, theca.

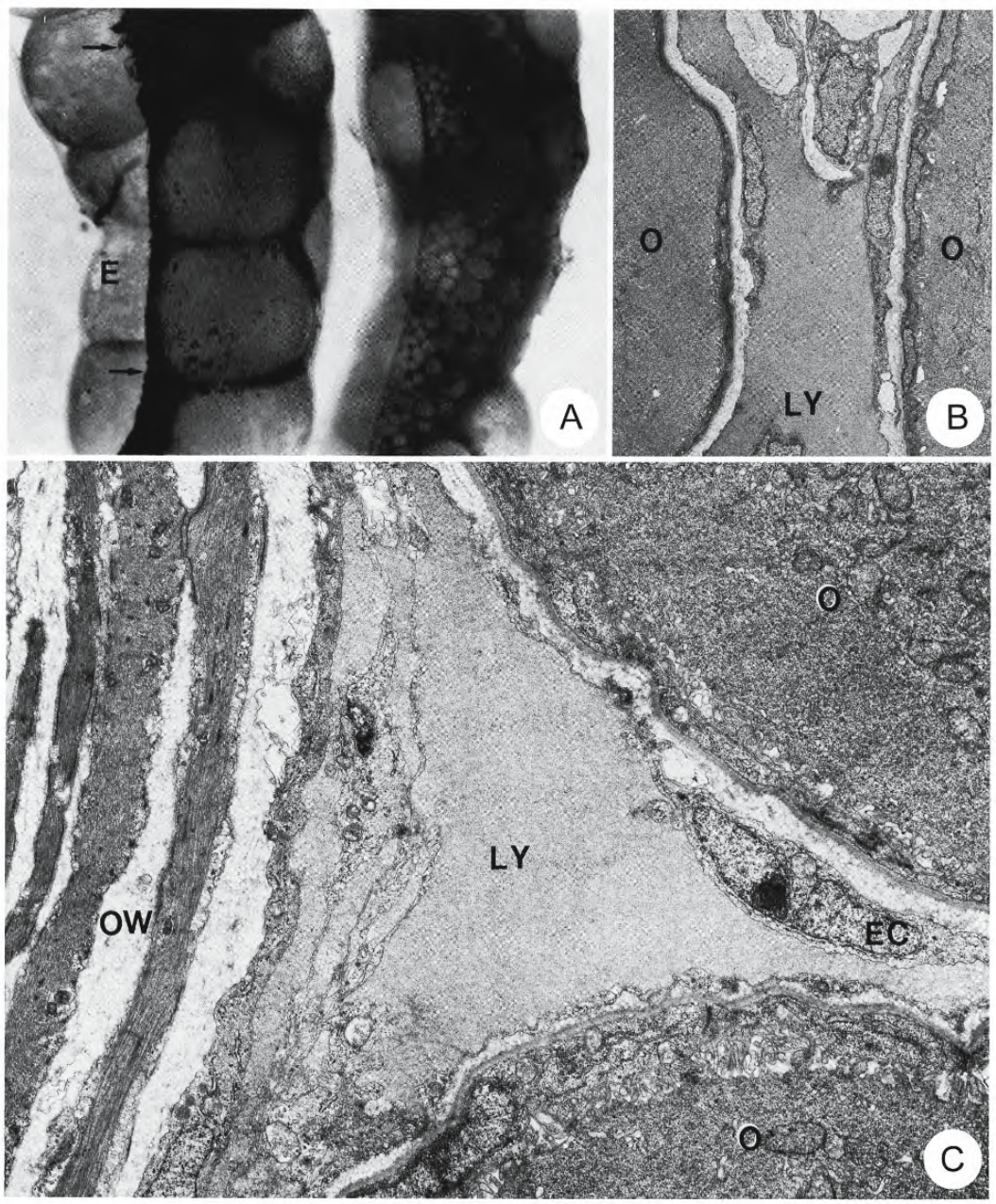

Figure 2.132: Micrographs of the ovary of the pipefish *Syngnathus scovelli.* (From Begovac and Wallace, 1987; © reproduced with permission of John Wiley & Sons, Inc.).

A. India ink preparations of fresh intact ovaries demonstrating the extent of the lymphatic network in the spaces between follicles. The lymphatics end abruptly at the extreme mature edges (arrows) as eggs (E) are visible in the ovarian lumen. The ovary on the right demonstrates the extent of lymphatics among early follicles. X 27.

B. Transmission electron micrograph of a section showing the lymphatic space (LY) extending between the lateral borders of adjacent young oocytes. X 3,300.

C. Transmission electron micrograph of a section showing a triangular lymphatic space (LY) between adjacent early developing oocytes (O) and the ovarian wall (OW). A distinct endothelial cell (EC) lines the lymphatic space. X 7,850.

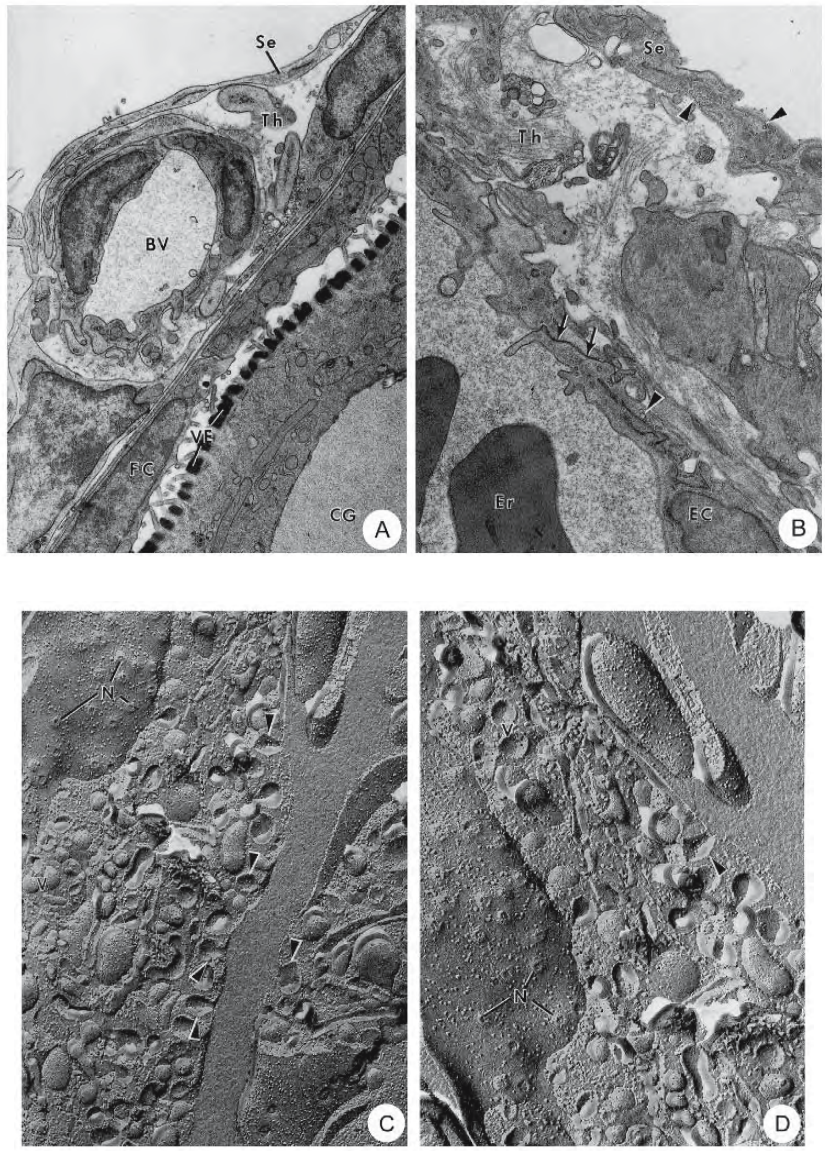

Figure 2.133: Electron micrographs from the ovary of the zebrafish *Brachydanio rerio* to illustrate follicular circulation. (From Kessel, Roberts, and Tung, 1988; reproduced with permission from Nuova Immagine Editrice).

A. Transmission electron micrograph of the follicular envelope and oocyte cortex early in oogenesis. A blood vessel of the theca is interposed beneath the serosa. X 9,800.

B. Transmission electron micrograph showing a junction (arrows) between two endothelial cells. Micropinocytotic pits and vesicles are identified by arrowheads in both serosal and endothelial cells. X 12,400.

Abbreviations: BV, blood vessel; CG, cortical granule in oocyte; Er, erythrocyte; FC, follicular cell; Se, mesothelial or serosal cell; Th, theca; VE, zona pellucida.

C, **D**. Electron micrographs of freeze-fracture replicas of many micropinocytotic pits and vesicles. Fractures through necks (N) of open vesicles (V) appear as craters on the P face. Fracture planes that include both open pits and connected vesicles are identified at arrowheads. These figures may be replicas of either serosal cells or endothelial cells; it is difficult to distinguish these cells in freeze fracture preparations but pinocytosis is similarly active in both. **C** X 38,400; **D** X 85,000.

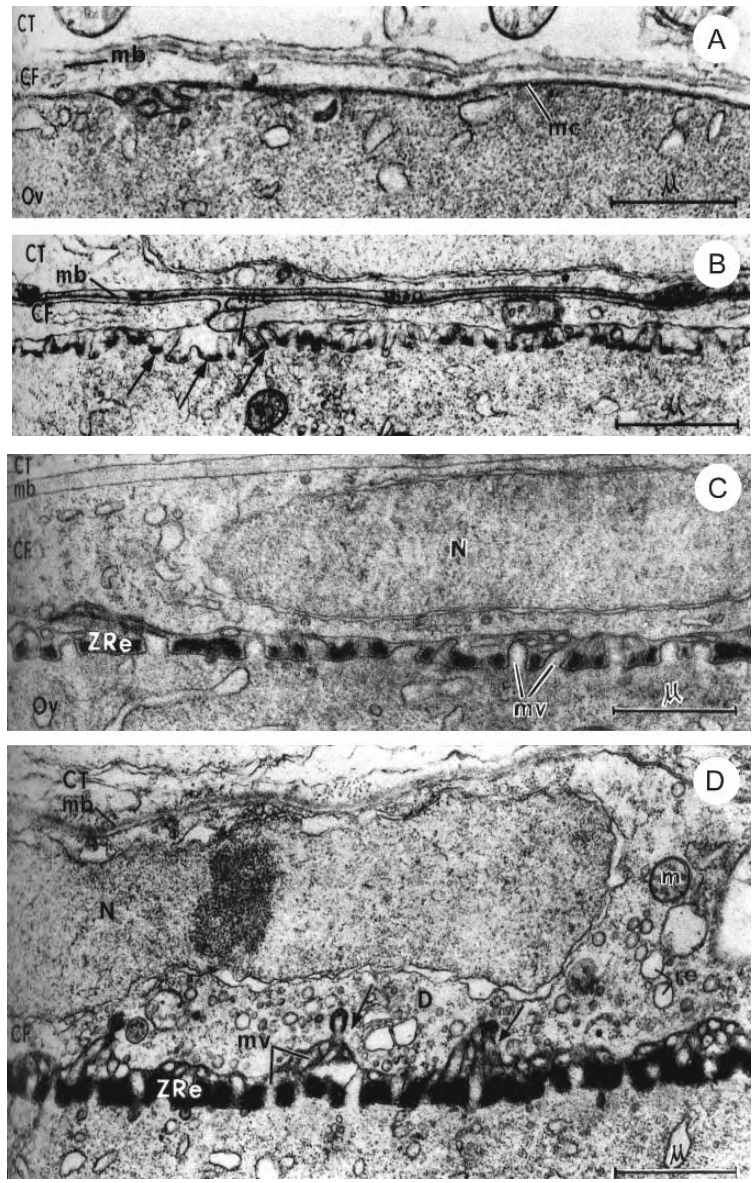

Figure 2.134: Electron micrographs showing the development of the theca during previtellogenesis in the zebrafish *Brachydanio rerio.* X 22,200 (From Ulrich, 1969, *Journal de Microscopie*; reproduced with permission).

A. Young oocyte, 30 µm in diameter. Thecal cells (CT) are separated from the squamous follicular epithelium (CF) by a basal lamina (mb). The follicular cells are closely applied to the oocyte (Ov). The oolemma (mc) shows few indentations.

B. An oocyte 80 µm in diameter has produced microvilli (mv) 0.1 µm in length which press against the follicular cells. Osmiophilic material (arrows) has appeared between the microvilli.

C. In an oocyte 100 µm in diameter, the microvilli have elongated and extended beneath the follicular epithelium. The follicular cells have become thicker and their cytoplasm is rich in ribosomes. Osmiophilic material constitutes the external layer of the zona pellucida.

D. Microvilli continue to elongate in an oocyte 130 µm in diameter; they form bundles (arrows) beneath the follicular epithelium. The follicular cells, containing several organelles, continue to thicken.

Abbreviations: CF, follicular epithelium; CT, thecal cells; D, Golgi complex; m, mitochondrion; mb, basal lamina; mc, oolemma; mv, microvilli; N, nucleus; Ov, oocyte; Zre external layer of zona pellucida.

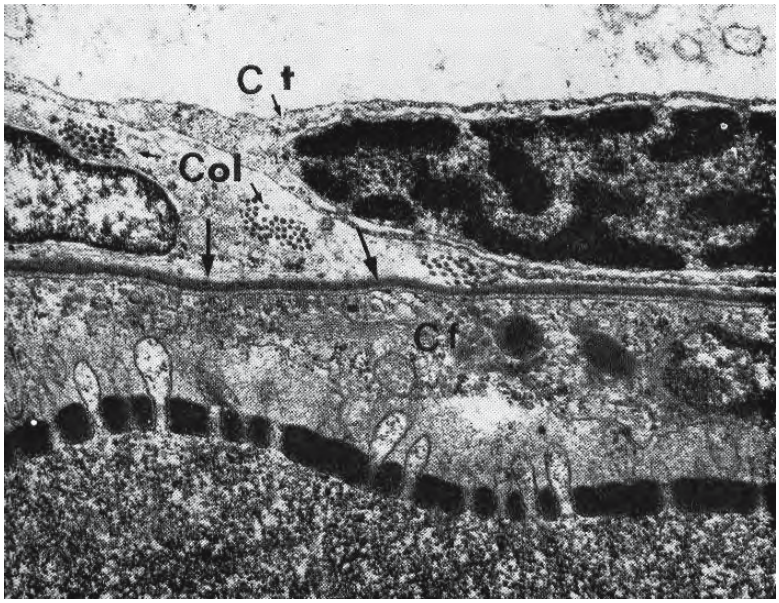

Figure 2.135: Transmission electron micrograph of the periphery of an ovarian follicle of the sea bass *Dicentrarchus labrax*. Thecal cells (Ct) are separated from the follicular epithelium (Cf) by a double basal lamina (arrows) and collagenous fibres (Col). X 20,000 (From Caporiccio and Connes, 1977; reproduced with permission, © Masson Editeur).

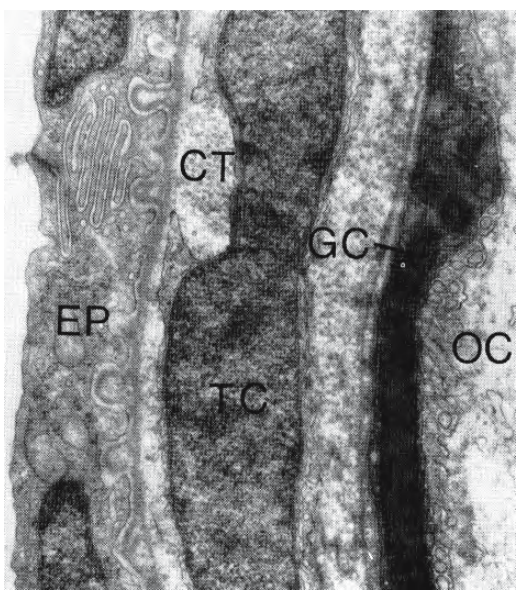

Figure 2.136: Transmission electron micrograph of a section of the ovary of the hagfish *Eptatretus stouti* showing the follicular wall during early oogenesis. The oocyte (OC) is surrounded by a deeply staining follicular layer (GC). The theca consists of poorly differentiated cells (TC), probably fibroblasts, in a connective tissue matrix (CT). Squamous mesothelial cells (EP) abut the coelomic cavity. X 16,800 (From Tsuneki and Gorbman, 1977; reproduced with kind permission of Blackwell Publishing).

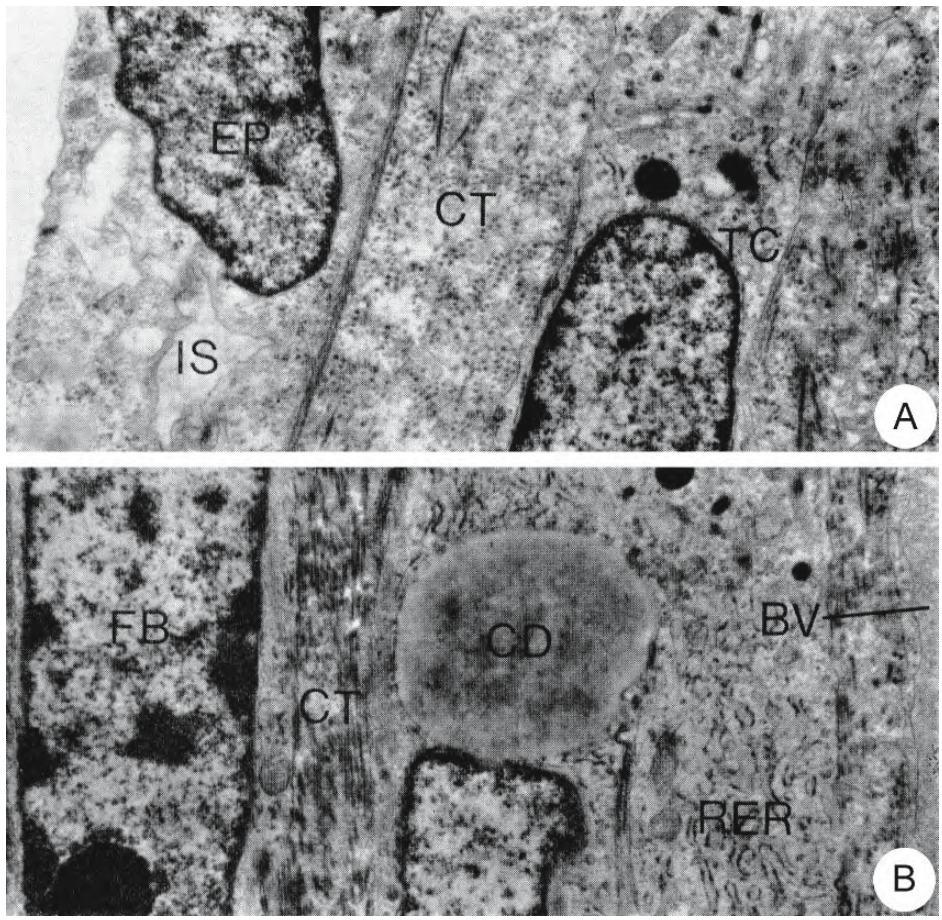

Figure 2.137: Transmission electron micrographs of sections of the ovary of the hagfish *Eptatretus stouti* showing the follicular wall during an "intermediate" stage of oogenesis. Two layers can be distinguished in the theca: the theca externa (Figure **A**) and the theca interna (Figure **B**). X 12,200 (From Tsuneki and Gorbman, 1977; reproduced with kind permission of Blackwell Publishing).

A. Granules are forming within the Golgi complex of a thecal cell.

B. A fibroblast in the theca interna displays conspicuous granular endoplasmic reticulum and a large, lipid-like inclusion.

Abbreviations: BV, blood vessel; CD, colloid droplet; CT, connective tissue; EP, peritoneal epithelium or mesothelial layer; FB, fibroblast; IS, intercellular space; RER, granular endoplasmic reticulum; TC, thecal cell.

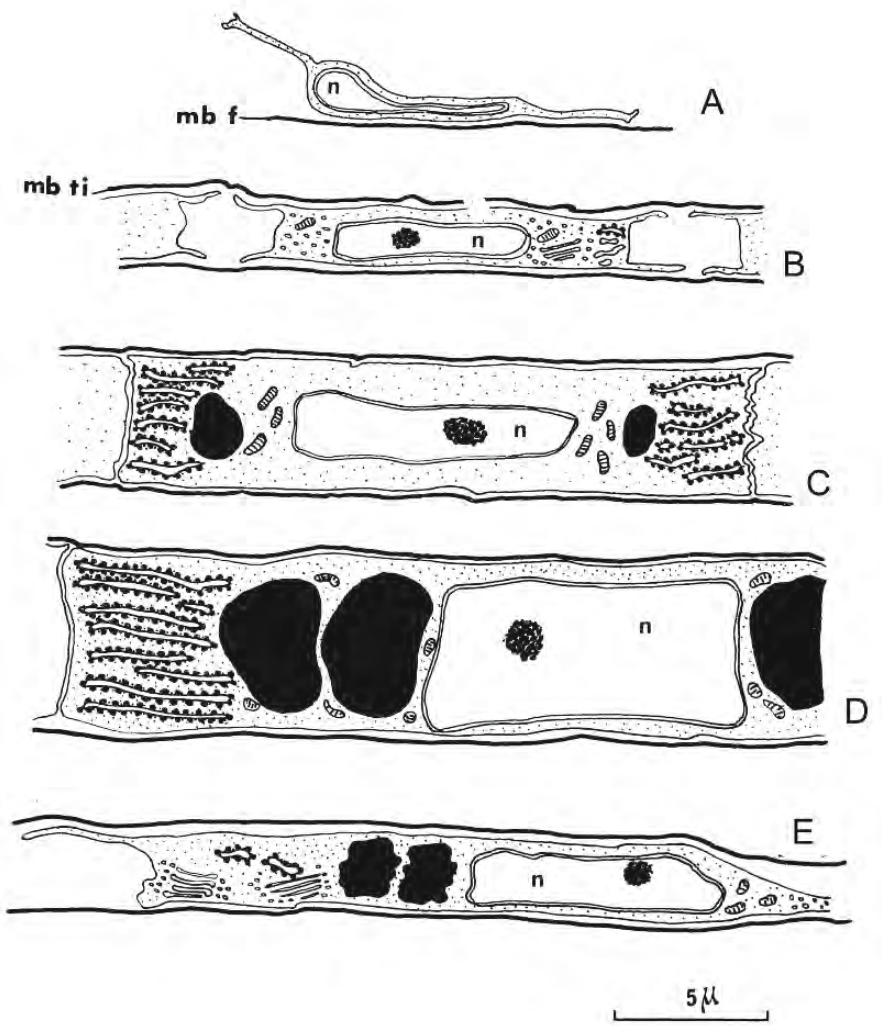

Figure 2.138: Schematic diagrams illustrating changes in the theca interna during vitellogenesis in the ovary of the lamprey *Lampetra planeri.* (From Busson-Mabillot, 1967b, *Journal de Microscopie*; reproduced with permission).

A. During previtellogenesis, some fibroblasts become flattened against the basement membrane of the follicular epithelium.

B. These cells shorten and thicken; granular endoplasmic reticulum develops within their cytoplasm. Large spaces appear between the cells of the theca interna across which the cells extend slender processes. An external basement membrane appears.

C. At the onset of vitellogenesis, stacks of granular endoplasmic reticulum appear at the ends of the cells and lipid droplets appear next to the nucleus.

D. The granular endoplasmic reticulum and the lipid droplets continue to increase during vitellogenesis.

E. The thecal cells once again become flat during late vitellogenesis and at the close of vitellogenesis. The lipid droplets become diminished and the endoplasmic reticulum assumes an agranular appearance. Large, apparently empty, intercellular spaces separate the thecal cells.

Abbreviations: mbf, basement membrane of the follicular epithelium; mbti, external basement membrane; n, nucleus.

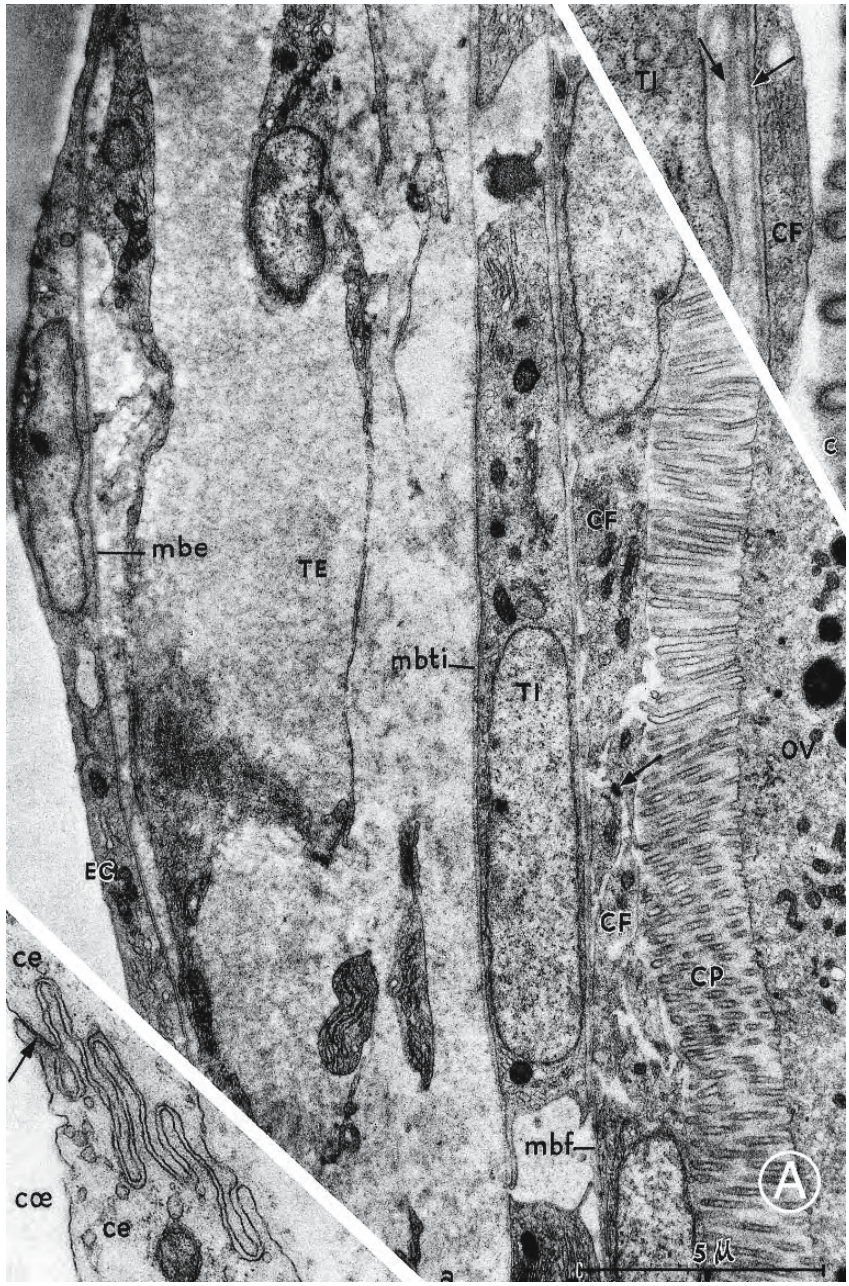

Figure 2.139: Transmission electron micrographs of sections of the peripheral regions of the ovarian follicle of the lamprey *Lampetra planeri.* (From Busson-Mabillot, 1967b, *Journal de Microscopie*; reproduced with permission).

A. Vegetal pole of the follicle at the beginning of vitellogenesis. The zona pellucida consists of a single layer. It is covered by the follicular epithelium whose cells are joined by desmosomes (arrow). The basal lamina of the follicular epithelium separates the follicle from the stroma. A basal lamina separates the single layer of the theca interna from the vascular connective tissue of the theca externa. Another basal lamina separates the theca from the coelomic epithelium (mesothelium) covering the ovarian lobe. X 8,000.

Inset upper: Two basal membranes (arrows) separate the theca interna and the follicular epithelium. X 28,000.

Inset lower: Detail of the peritoneal epithelium. The border between two epithelial cells is deeply interdigitated; it is sealed apically by a tight junction (arrow).

Figure 2.139: Continued.

B. At the beginning of vitellogenesis, the cytoplasm of cells of the theca interna (cut perpendicular to their long axis) is varied; in some there is only agranular endoplasmic reticulum (arrow) and Golgi complexes while others contain large lipid droplets (L) near parallel cisternae of granular endoplasmic reticulum. The theca interna is separated from the follicle by the follicular basal membrane while its own basal lamina (bti) separates it from the theca externa. Thin extensions of follicular cells (F) are interposed between the zona pellucida and the follicular basal lamina. X 18,000.

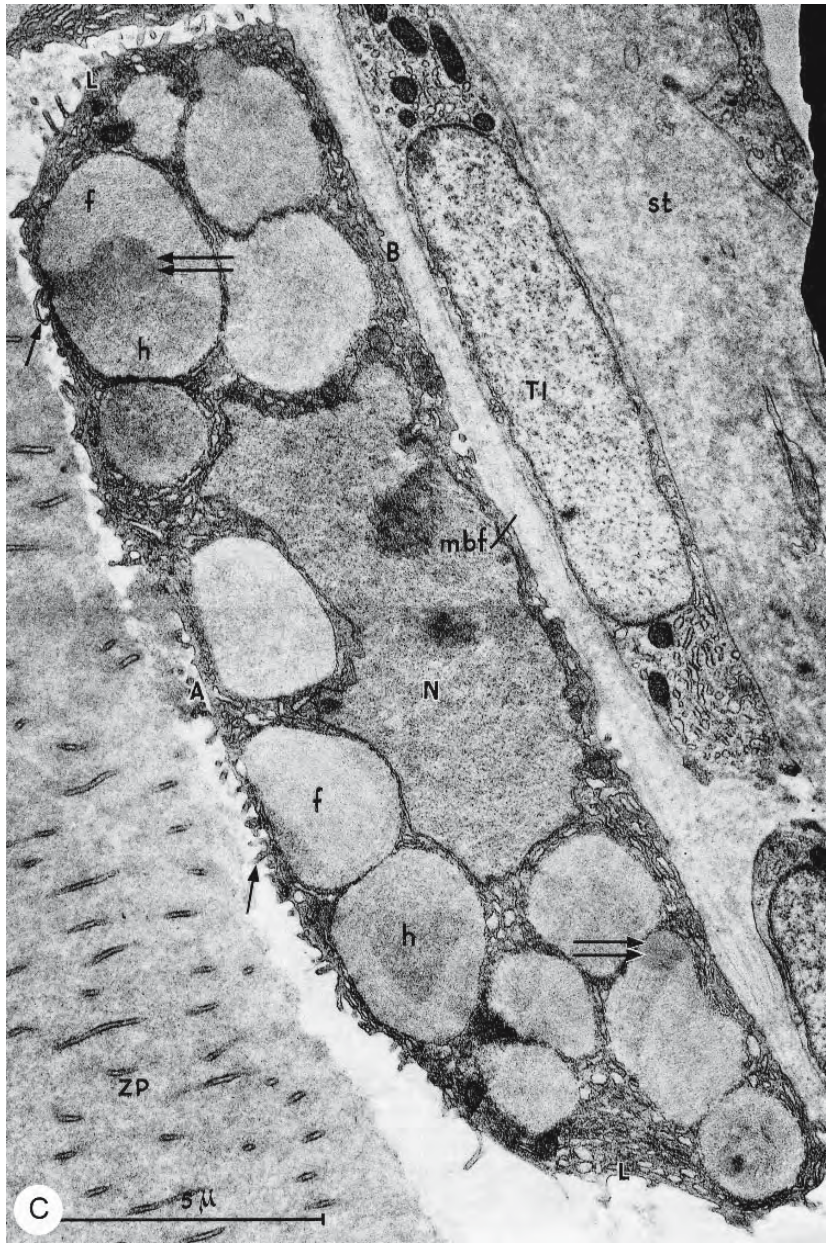

Figure 2.139: Continued.

C. During intense vitellogenesis, this follicular cell contains a heterogeneous collection of secretion granules: fibrous (f), granular (h), and one with dense globules (double arrow). The basal membrane (B) of the follicular cell is fairly smooth and is separated from its basal lamina by a uniform space. Many microvilli extend from the lateral (L) and apical (A) borders; these do not penetrate the zona pellucida. The theca interna, consisting of a single layer of squamous cells, separates the follicle from the rest of the stroma. X 9,000.

Abbreviations: ce, peritoneal epithelium; cœ, coelom; CF, follicular cell; CP, zona pellucida; D, Golgi complex; EC, coelomic epithelium (mesothelium); ER, endoplasmic reticulum; mbe, basal lamina of the theca externa; mbf, basal lamina of the follicular epithelium; mbti, basal lamina of the theca interna; N, nucleus; OV, oocyte; st, stroma; TE, theca externa; TI, theca interna; ZP, zona pellucida.

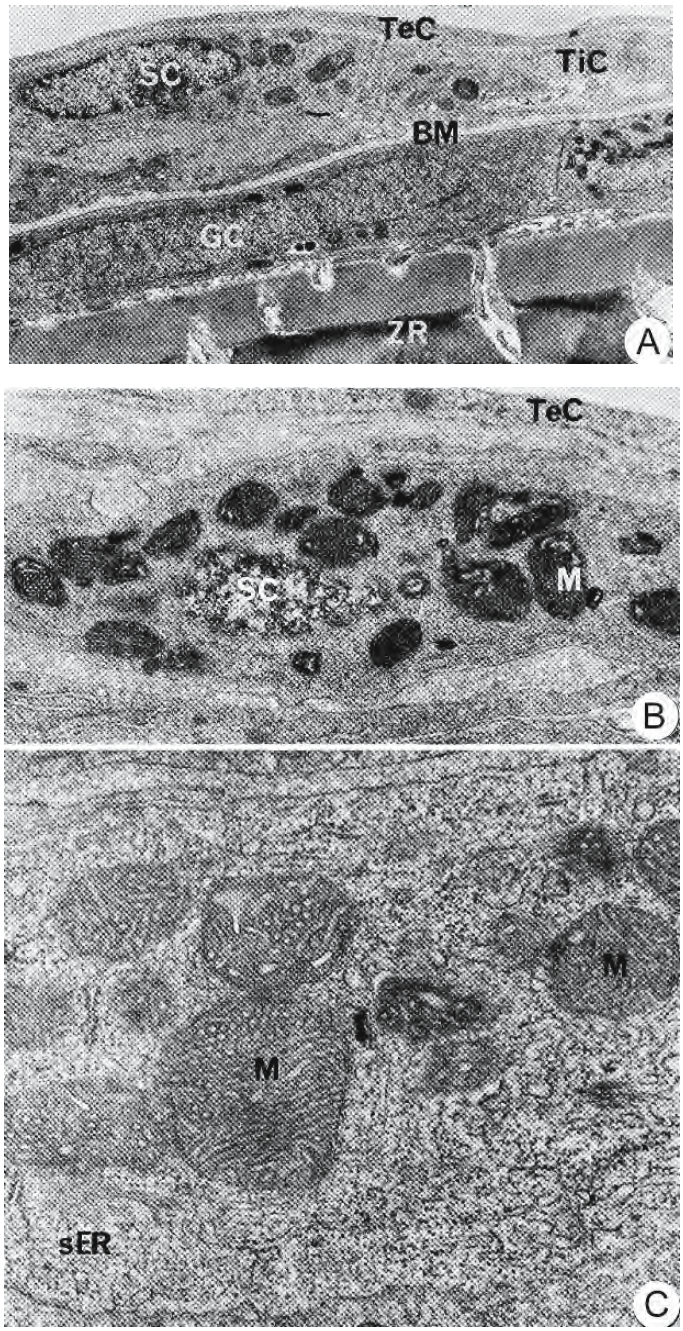

Figure 2.140: Transmission electron micrographs of sections of preovulatory follicles of the goldfish *Carassius auratus.* (From Nagahama, Chan, and Hoar, 1976; reproduced with permission of the NRC Press).

A. The contrast is obvious between a special thecal (SC) cell and an ordinary cell of the theca interna (TiC). Squamous cells of the theca externa (TeC) enclose the follicle. The follicular basal lamina (BM) separates the theca from the follicular epithelium (GC). ZR, zona pellucida. X 10,000.

B. This section shows a cell of the theca externa (TeC) and a special thecal cell (SC) containing a moderate amount of agranular endoplasmic reticulum and many electron-dense mitochondria (M) with tubular cristae. X 20,000.

C. The cytoplasm of a special thecal cell (SC) is characterized by large mitochondria (M) with tubular cristae and the presence of agranular endoplasmic reticulum (sER). X 45,000.

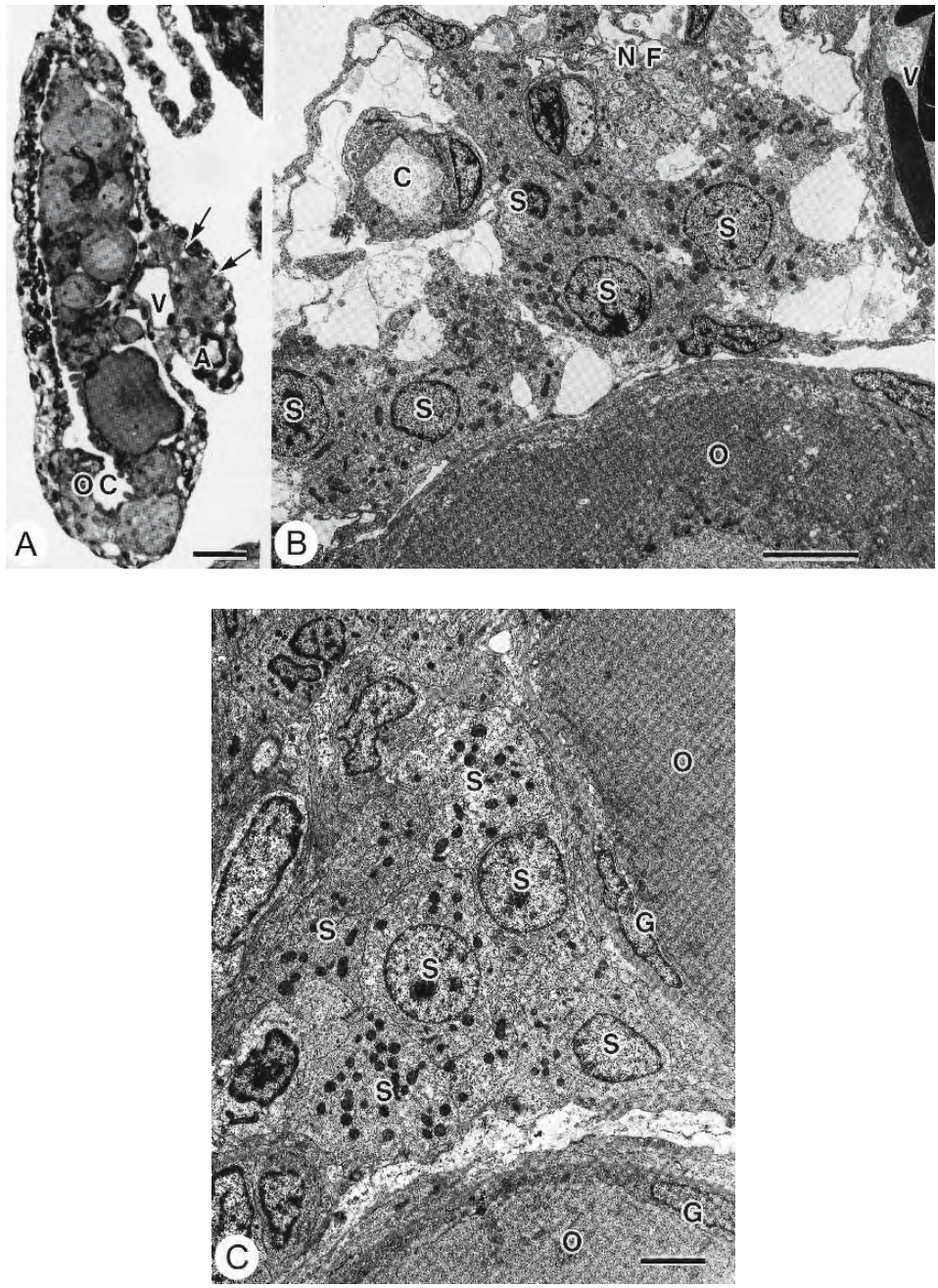

Figure 2.141: Photomicrographs (**A,D**) and transmission electron micrographs (**B,C,E,F**) of sections of the developing follicle during early vitellogenesis in tilapia *Oreochromis niloticus.* (From Nakamura, Specker, and Nagahama, 1993; reproduced with permission from Springer-Verlag).

A. Clusters of steroid producing cells (arrows) are seen near the ovarian artery and vein in this section of the ovary 50 days after hatching. X 410 Bar = 25 μm.

B. Clusters of steroid producing cells in an ovary 50 days after hatching. X 3,600 Bar = 5 μm.

C. Clusters of steroid producing cells in the interstitial region between oocytes in an ovary 70 days after hatching. X 4,100 Bar = 2.5 μm.

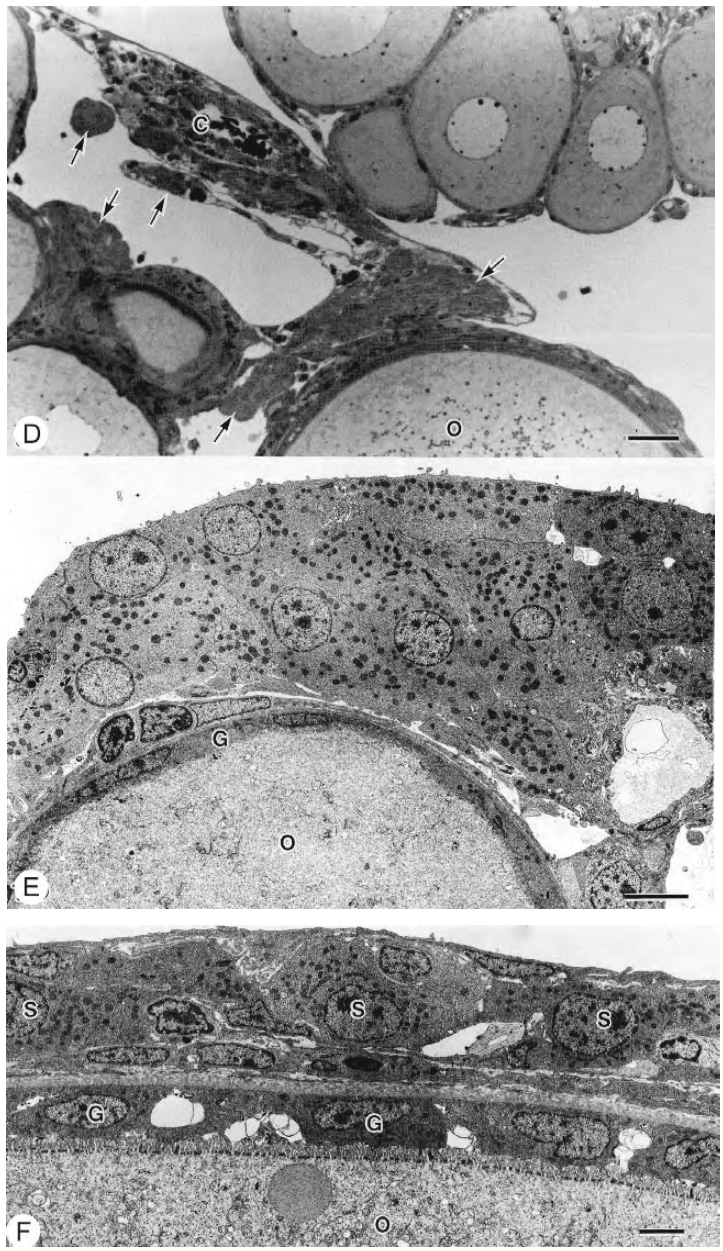

Figure 2.141: Continued.

D. Clusters of steroid producing cells (arrows) are distributed among oocytes at the early vitellogenic and perinucleolus stages 100 days after hatching. X 520 Bar = 25 µm.

E. A cluster of steroid producing cells encapsulates an oocyte during early vitellogenesis in an ovary 100 days after hatching. X 3,100 Bar = 5 µm.

F. The follicular epithelium and steroid producing cells in the theca of a vitellogenic oocyte 11 days after hatching. X 4,500 Bar = 2.5 µm.

Abbreviations: A, artery; C, capillary; G, follicular epithelial cell; NF, nerve fibre; O, oocyte; OC, ovarian cavity; S, steroid producing cell; V, vein.

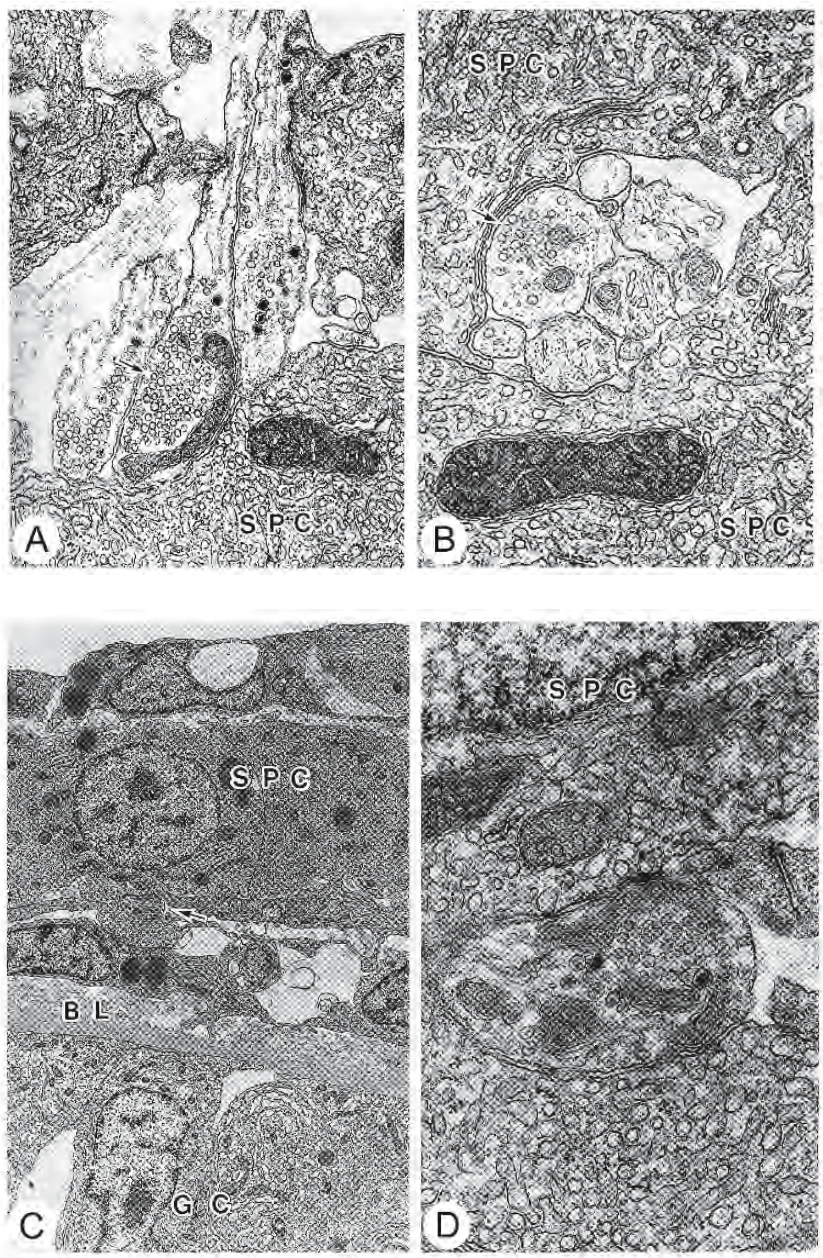

Figure 2.142: Bundles of nerve fibres, presumably autonomic, course among the yolky follicles and steroid producing cells of tilapia *Oreochromis nilotica.* (From Nakamura, Specker, and Nagahama, 1996; reproduced with permission from the Zoological Society of Japan).

A-D. Transmission electron micrographs showing the distribution of nerve terminals within the ovary.

A. Axon terminals, packed with synaptic vesicles (arrow), rest on the surface of steroid producing cells. X 27,000.

B. Axons invade the narrow space between steroid producing cells and terminate (arrow) on the surface of one of these. X 41,600.

C. An axon terminal (arrow) is seen near a steroid producing cell in the theca. X 5,700.

D. Detail of the axon terminal shown at the arrow in Figure **C**. It contains many synaptic vesicles and dense-cored vesicles. X 42,700.

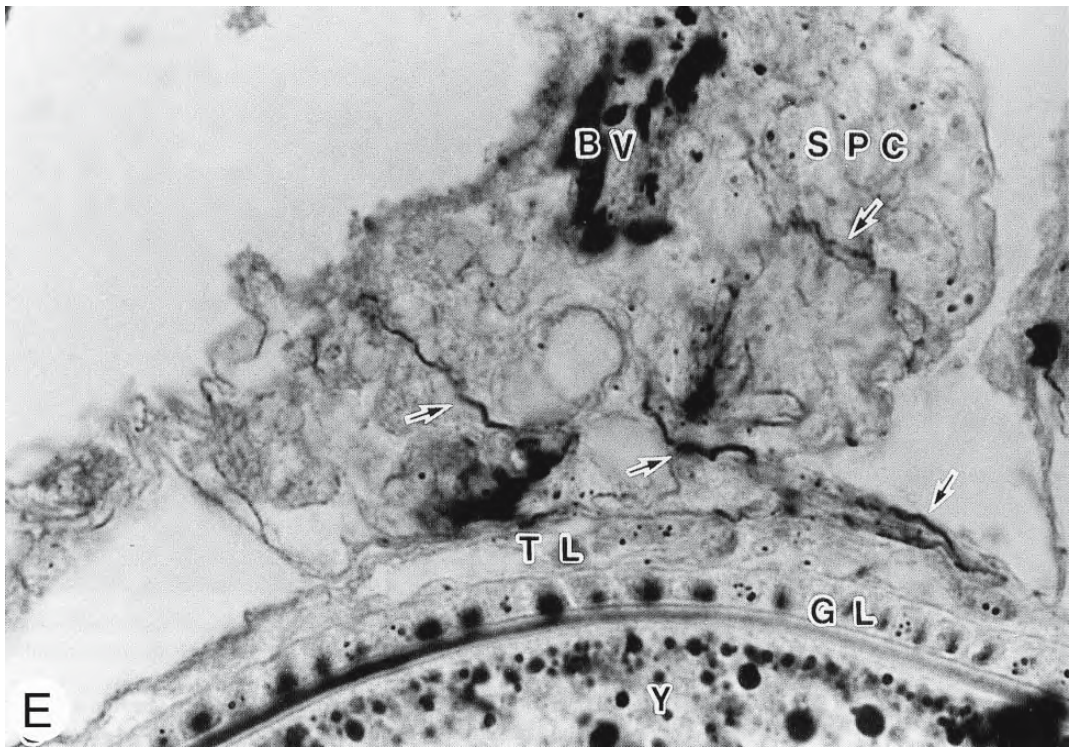

Figure 2.142: Continued.

E. Photomicrograph of axon terminals (arrows), stained with silver, distributed within a cluster of steroid producing cells. X 1,000.

Abbreviations: BL, basal lamina; BV, blood vessel; GC, follicular cell; GL, follicular epithelium; SPC, steroid producing cell; TL, thecal layer; Y, yolk.

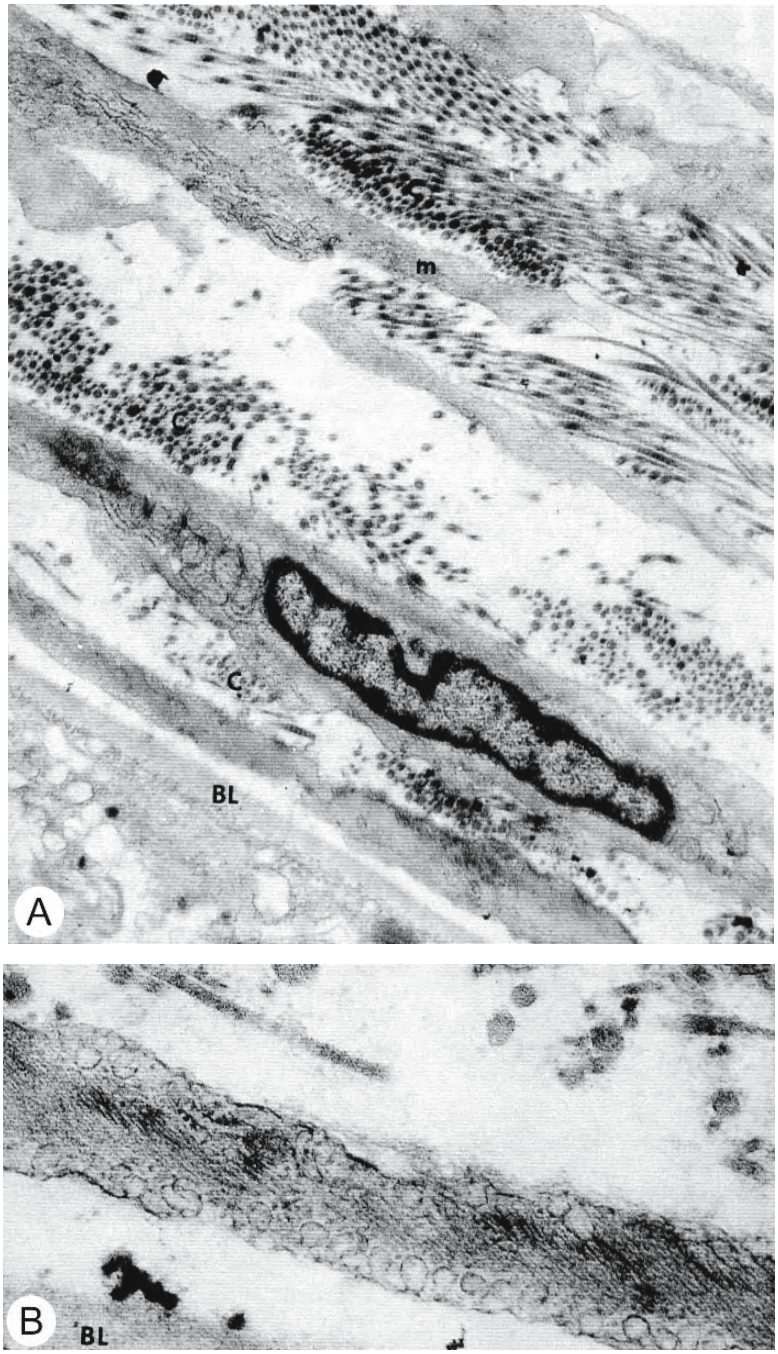

Figure 2.143: Transmission electron micrographs of sections through the thecal layers in the postovulatory ovary of the trout *Salmo gairdneri.* (From Szöllösi, Jalabert, and Breton, 1978; reproduced with permission of INRA, Paris).

A. Layers of smooth muscle-like cells (m) of the theca alternate with layers of collagen fibres (c). Small groupings of organelles congregate near the nuclear poles of the muscle cells; the rest of the cytoplasm is occupied by thin filaments. The follicular basal lamina (BL) separates the theca from the follicular epithelium. X 15,000.

B. The putative muscle fibre contains filaments 7 to 8 nm in diameter and displays active pinocytosis, typical of smooth muscle. X 60,000.

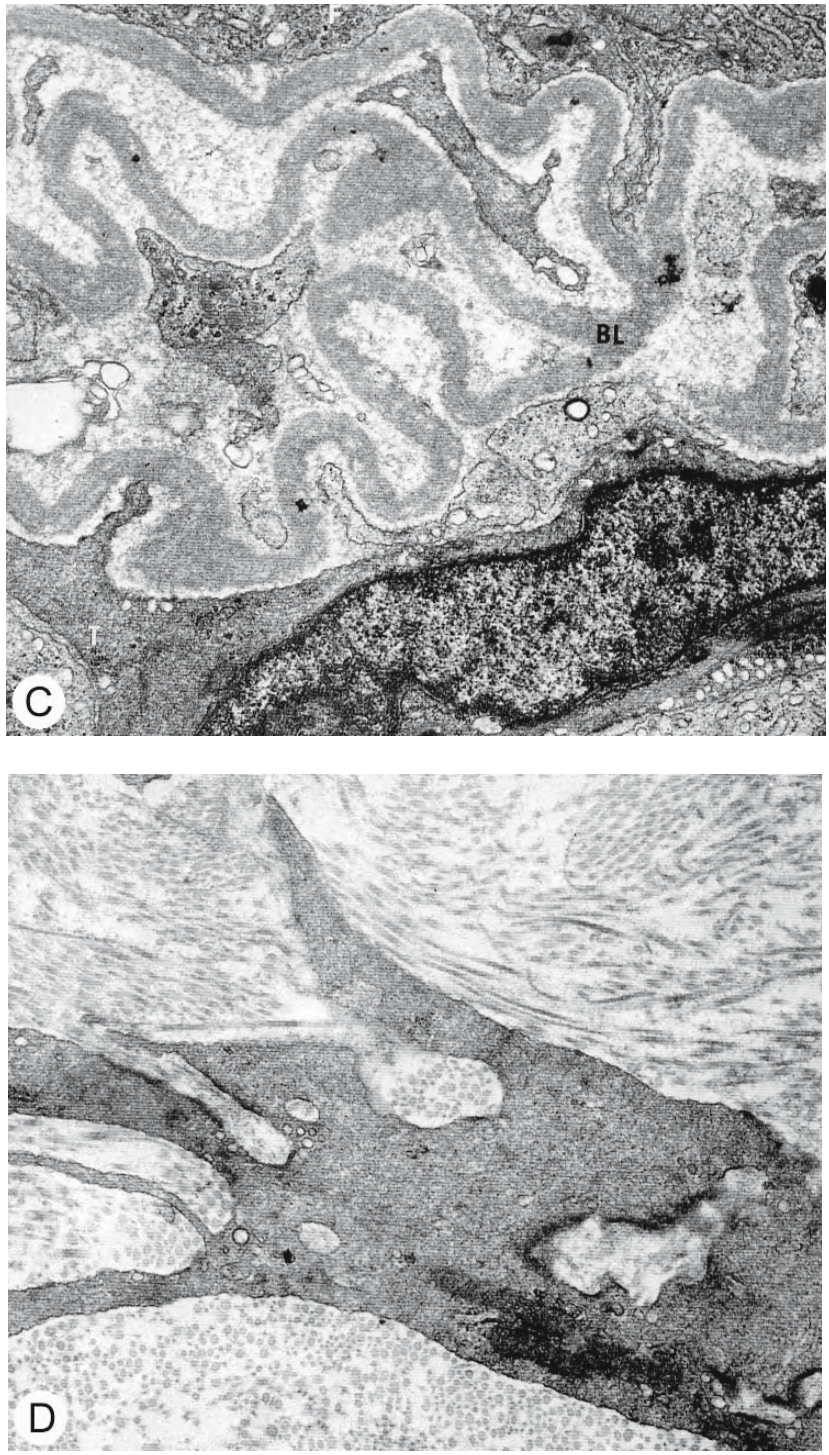

Figure 2.143: Continued.

C. The thick basal lamina (BL) between the follicular cells (centre) and the theca is extensively folded. X 14,000.

D. Within a few hours of ovulation, stellate thecal cells isolate large bundles of collagen fibrils. Two small, internalized, isolated phagocytic vesicles containing a few collagen fibrils are seen. X 30,000.

CHAPTER 3

OVULATION

3.1 Introduction

After completion of the first meiotic division, a rupture (the STIGMA) develops in a specific area of the follicular wall and the mature oocytes are released into the coelom or ovarian cavity by the process of ovulation (Nagahama, 1983). Meiosis continues up to the second meiotic metaphase and, at this time, the eggs are ready for fertilization. Several steps are involved in this release: separation of the vitelline envelope and follicular epithelium as microvilli from both sides become detached; enzymatic degradation and rupture of the follicle; and expulsion of the oocyte. The motive force expelling the oocyte has been attributed variously to the formation of fluids within the follicle, to swelling of the oocyte, and to contractions of the follicular wall. In some viviparous species, fertilization and embryological development take place within the follicle so that no ovulation occurs. Subsequent release of the embryos from their follicular sanctuary is sometimes referred to as "ovulation" (e.g., Venkatesh, Tan, and Lam, 1992a,b) but this usage seems inappropriate and will not be used in this text.

Various aspects of ovulation have been studied during its normal occurrence in the reproductive cycle of intact fish *(Carassius auratus:* Nagahama, Chan, and Hoar, 1976; *Petromyzon marinus*: Yorke and McMillan, 1980; *Salvelinus leucomaenis:* Kagawa, Takano, and Nagahama, 1981). However, since this event occurs over a brief period of time, it has often proved convenient to induce ovulation in females by manipulations of day length *(Oryzias latipes:* Hirose, 1972; Kagawa and Takano, 1979; Iwamatsu and Ohta, 1981a) or by injections of hormones such as human chorionic gonadotropin (HCG) *(Plecoglossus altivelis*: Hirose and Ishida, 1974; *Limanda yokohomae:* Oshiro and Hibiya, 1981). In follicles isolated from gravid females, ovulation has been induced by additions of prostaglandin $F_{2\alpha}$ *(Salmo gairdneri:* Jalabert and Szöllösi, 1975; Szöllösi, Jalabert, and Breton, 1978; *Carassius auratus,* Kagawa and Nagahama, 1981), hydrocortisone *(Oryzias latipes:* Pendergrass and Schroeder, 1976), or the maturation-inducing steroids 17,20β,21-trihydroxy-4-pregnene-3-one (20β-S) and 17,20β-dihydroxy-4-pregnene-3-one (17,20β-P) *(Cynoscion nebulosus,* Pinter and Thomas, 1999) to the medium.[10]

Some time prior to ovulation in *Fundulus heteroclitus,* each follicle establishes a close relationship with the luminal surface of the ovary in a localized, nearly circular spot (Brummett, Dumont, and Larkin, 1982). A fusion between the basement membranes of the follicular cells and luminal epithelium appears to occur, excluding blood vessels from the area (Figure 3.1). The squamous luminal mesothelial cells covering this area become increasingly flat as the follicle matures and it is presumed that ovulation occurs at this site. This avascular area is surrounded by a raised lip of cells containing a ring-shaped vessel that collects blood from capillaries in the follicular theca (Figures 1.33A,C). The mature egg of *Fundulus* is ovulated into the lumen of the ovary and passes from there to the posterior nongerminal portion of the ovary, the OVISAC.

Ultrastructural studies have revealed that microvilli from both follicular cells and the oocyte withdraw from the zona pellucida near the time of ovulation and that a wide space forms between the zona pellucida and the follicular cells (Figure 2.67) (Flügel, 1967b; Hirose, 1972; Iwamatsu and Ohta, 1977). The mechanism directing this interruption of follicle-oocyte communication prior to ovulation is unknown.

The presence of "ovulation-inducing enzymes" has been postulated for several fish. These are thought to break down collagen, thereby weakening the follicular wall in preparation for its rupture. Isolated follicles of

[10] Peter and Yu (1997) have presented an extensive review summarizing the major environmental and hormonal factors controlling ovulation in teleosts.

the loach *Misgurnus anguillicaudatus* produce proteases immediately before induced ovulation (Oshiro and Hibiya, 1975, 1982). Several lytic enzymes (chymotrypsin, aminopeptidases, acid and alkaline phosphatases, various esterases, and glycosidases) were found in the coelomic fluid of the trout *Salmo gairdneri* within 24 hr of ovulation but no collagenase could be detected (Szöllösi, Jalabert, and Breton, 1978). In addition, collagenase was sought without success in extracts of pre- and postovulatory ovaries. Actinomycin D and cyclohexamide induced blockage of steroid-induced ovulation in isolated follicles of yellow perch *Perca flavescens,* presumably by inhibiting production of the proteolytic enzymes needed to detach the oocyte from the follicle and weaken the follicular wall (Theofan and Goetz, 1981). More recently, collagenolytic metallo-proteases have been demonstrated in follicular walls of yellow perch and brook trout *Salvelinus fontinalis* around the time of ovulation (Berndtson and Goetz, 1988, 1990). Increases in the numbers of lysosomes within follicular cells near the time of ovulation have provided morphological evidence for the presence of hydrolytic enzymes in these cells (Yamamoto and Yamazaki, 1966; Kagawa and Takano, 1979; Kagawa, Takano, and Nagahama, 1981). An increase in lysosome-like bodies was also observed in follicular cells of cultured follicles of the medaka just before ovulation was expected to occur (Figure 3.2) (Iwamatsu and Ohta, 1981a).

It has been suggested that the accumulation of fluid within the follicle could apply gentle pressure to expel the oocyte as well as lubricating its passage. As the time of ovulation approaches in the lamprey *Petromyzon marinus,* there is an accumulation of FLUID OF OVULATION between the vitelline envelope and the follicular epithelium in the apical regions of the follicle (Figure 3.3) (Lewis and McMillan, 1965; Yorke and McMillan, 1980). Acid and neutral mucoplysaccharides, present in the follicular cells that distintegrate at ovulation, may participate in this process and it is suggested that enzymatic breakdown of acid mucopolysaccharides may cause the osmotic uptake of water, causing swelling of the neutral mucopolysaccharides (Larsen, 1970). There was a great influx of water into ovaries of ayu *Plecoglossus altivelis* and plaice *Limanda yokohomae* just prior to ovulation that was induced by injections of hormones (Hirose and Ishida, 1974; Oshiro and Hibiya, 1981). Most of the water was absorbed by fully-grown yolky oocytes that ovulated soon after and it was suggested that abrupt absorption of water causes rupture of the ripening oocytes.

The expulsion of the egg during ovulation, at least in the lamprey *Petromyzon marinus,* appears to result from gentle contractions produced by changes in shape of the follicular cells (Figure 3.4) (Yorke and McMillan, 1980). At the first sign of imminent ovulation, a few apical follicular cells enlarge and assume a secretory appearance (Figures 2.127A,B and 3.3A). These cells produce the fluid of ovulation that accumulates between the zona pellucida and follicular cells, forming a hollow mound near the apical pole (Lewis and McMillan, 1965; Yorke and McMillan, 1980). Microvilli from the oocyte withdraw from their canaliculi and a PERIVITELLINE SPACE appears between the oolemma and the vitelline envelope (Figure 3.5A). As ovulation begins, the follicular cells change shape, starting at this fluid-filled end of the follicle, forming a hollow sleeve of columnar cells surmounted by a hollow ball of flatter follicular cells at its distal end (Figures 2.127C,D and 3.4). This change in shape constricts the follicle at one end, thereby pushing the oocyte through an apical rupture which appears at about the same time. Indicative of the reduction in area of the follicular epithelium is the progressive appearance of convolutions in its basement membrane where the cells become taller (Figure 3.5B). The presence of a well-developed fibrous cytoskeleton within the apical follicular cells and adhaerens junctions between them enhances the concept of gentle pressure produced by these cells. The expulsion of the egg is lubricated by slippery fluids derived from the fluid of ovulation and from the autolysis of adhesive cells. The gelatinous fluid of ovulation, moulded by this stocking cap of follicular cells, persists on the egg after ovulation and constitutes the sticky, fluffy, APICAL TUFT that appears to orient the spermatozoon for its penetration of the chorion (there is no micropyle in eggs of the lamprey) (Kille, 1960). This tuft shrinks considerably with the fixatives used for microscopy (Yorke and McMillan, 1979).

The preovulatory changes in the follicular epithelium of the lamprey are accompanied by degenerative changes in the theca overlying the adhesive cells, adjacent to the coelom (Yorke and McMillan, 1980). Areas of disruption appear in the collagenous matrix, often in association with vacuolated cytoplasmic extensions of a fibroblast. This degeneration is accompanied by an invasion of macrophages from blood vessels in the area. Autolysis of the theca results in the rupture of the follicle in an area overlying the débris of the adhe-

sive cells and bordering directly on the coelom (Figure 2.127A). Thus freed, the egg emerges into the coelom.

Contractions of the theca assist ovulation in several teleosts. The theca behaves physiologically like smooth muscle whose contractions can be evoked *in vitro* by the addition of prostaglandin $F_{2\alpha}$ (Szöllösi, Jalabert, and Breton, 1978). Thecal cells of several species resemble smooth muscle cells, displaying abundant microfilaments (5 to 7 nm) and pinocytotic vesicles prior to ovulation (Figures 2.143A,B) (Szöllösi and Jalabert, 1974; Pendergrass and Schroeder, 1976; Nagahama, Chan, and Hoar, 1976; Szöllösi, Jalabert, and Breton, 1978). In some species, however, the dense bodies and pinocytotic vesicles characteristic of smooth muscle have not been seen. Physiological evidence for contractility of the microfilaments of the thecal cells has been provided: cytochalasin B, which blocks polymerization of actin filaments, thereby paralysing many kinds of cellular movement, completely and reversibly inhibits *in vitro* ovulation of medaka and trout oocytes (Jalabert and Szöllösi, 1975; Schroeder and Pendergrass, 1976); and agents that block Ca^{2+} influx, necessary for muscular contraction, inhibit ovulation of trout oocytes *in vitro* (Jalabert and Szöllösi, 1975).

The PROSTAGLANDINS are a group of 20-carbon fatty acids containing a 5-carbon ring; they are short-lived and affect a wide variety of physiological processes by acting as local hormones. They appear to play a significant role in ovulation in oviparous teleosts although the effective prostaglandins vary from species to species (Jalabert, 1976; Goetz and Theofan, 1979; Goetz et al, 1987; Berndtson, Goetz, and Duman, 1989; Goetz et al., 1989a,b). In oviparous teleosts, where ovulation immediately follows oocyte maturation, follicles synthesize large amounts of prostaglandins during oocyte maturation and ovulation (Berndtson and Goetz, 1986; Berndtson et al., 1989a; Goetz et al., 1989b). By contrast, in the viviparous guppy *Poecilia reticulata,* where the foetus develops within the follicle and is released a considerable time later, production of prostaglandins by follicles is low during oocyte growth, maturation and gestation; it increases significantly in mid and late gestation. This delay in synthesis may arrest ovulation, thereby facilitating intrafollicular fertilization and gestation (Venkatesh, Tan, and Lam, 1992b). Several tissue components within the ovary of the brook trout *Salvelinus fontinalis* synthesize primary prostaglandins but differ in their capacity to produce E and F prostaglandins (Goetz et al., 1987, 1989b). Although follicular walls synthesize small amounts of PGE_2 and $PGF_{2\alpha}$, especially in postovulatory tissue, the greatest synthesis occurs in tissues outside the mature follicles, predominantly of PGE_2. This extrafollicular tissue consists of immature follicles and stromal tissue; incubated separately, the stromal tissue synthesizes PGE_2 while the immature follicles synthesize $PGF_{2\alpha}$.

3.2 Atretic Follicles, Postovulatory Follicles, and Corpora Lutea

Eggless follicles are often seen within the ovary of fish. They may arise either by atresia (degeneration) of a developing follicle or by the expulsion of the egg during ovulation. ATRETIC and POSTOVULATORY FOLLICLES have long attracted the attention of endocrinologists who have suspected them as a possible source of hormones associated with reproduction (Ball, 1960; Hoar, 1969; Browning, 1973; Kosmath, Patzner, and Adam, 1983b). This interest has been reflected in the literature by frequent use of the term "corpus luteum", implying the presence of an endocrine gland that secretes steroid hormones and plays a role in reproduction. In the present work, the term ATRETIC FOLLICLE will be used for follicles in which the egg is obviously undergoing degeneration, POSTOVULATORY FOLLICLE for empty follicles produced by the expulsion of an egg, and CORPUS LUTEUM for the richly vascular follicular remnant whose origins, whether by atresia or ovulation, cannot be determined.

3.2.1 ATRETIC FOLLICLES

ATRETIC FOLLICLES, or CORPORA ATRETICA, result from degeneration of an oocyte and its resorption by phagocytosis; this process is ATRESIA. Follicular atresia occurs widely in the ovaries of vertebrates and may occur at any stage in follicular development (Hisaw and Hisaw, 1959; Dodd, 1977). Indeed, atresia has been described in the primordial germ cells of the indifferent gonad of the medaka, *Oryzias latipes* (Figure 3.6) (Hogan, 1978). It is not known why some follicles are able to develop to ovulation while their neighbours undergo degeneration.

The onset of atresia has been said to be unrelated to age, stage of the reproductive cycle, environmental conditions (season, temperature, light, availability of food, etc.), and the general health of the individual animal (Saidapur, 1978) although experiments with captive Atlantic cod *Gadus morhua* show an increase

in the incidence of atresia in vitellogenic oocytes with decreased feeding levels (Kjesbu et al., 1991). Mass atresia of maturing oocytes in wild stocks of Atlantic cod has been attributed to severe malnutrition during some critical period for ovarian growth, resulting in a failure to spawn or "skipped spawning" in most females during 1999 (Rideout, Burton, and Rose, 2000). It is suggested that this failure may have contributed to the current lack of recruitment in north Atlantic cod stocks.

Although atresia may affect the oocyte at any stage of development, it is described more frequently in maturing and unovulated mature oocytes (Rastogi, 1969). The apparent rarity of small atretic follicles may be due to two factors: small follicles take a shorter time than mature follicles to disappear and, being smaller, appear in fewer microscopic sections. Atresia of small follicles is described in several species of elasmobranchs (Hisaw and Hisaw, 1959). Ova containing no yolk apparently undergo simple absorption. The clear fluid content of the ovum decreases, the walls of the follicle collapse, and the follicular layer atrophies and disintegrates. In slightly larger follicles, in which small amounts of yolk have been deposited, secretion of yolk ceases and the follicular epithelium increases in thickness by elongation and swelling of cells which may remain attached to their basement membrane. Follicular cells fill with vacuoles and the vitelline envelope disappears. Yolk granules, liberated by disintegration of the ovum, as well as débris from the degenerating ovum, are removed by follicular cells which become phagocytic.

The first sign of atresia in small, yolk-free oocytes of the freshwater mud eel, *Amphipnous cuchia,* is the disappearance of the nuclear membrane and disintegration of chromatin (Rastogi, 1969). The oolemma is thrown into folds, invading the decomposed ooplasm. The follicular epithelium remains single-layered and shows no hyperplasia. The theca thickens and becomes more vascular. Follicular cells invade the oocyte, functioning as phagocytes; this invasion is followed by that of vascular thecal tissue. Eventually the oolemma and ooplasm are removed. The phagocytes become pycnotic and are suspended in a meshwork of fibrous thecal material. This mass shows no sign of secretory activity.

In follicular atresia of yolky follicles, the sequence of events is similar in most fish (CYCLOSOMES: Lewis and McMillan, 1965; ELASMOBRANCHS: Hisaw and Hisaw, 1959; Chieffi, 1962; Lance and Callard, 1969; Te Winkel, 1972; Fasano, Pierantoni, and Chieffi, 1989; Chieffi Baccari et al., 1992; TELEOSTS: Bretschneider and Duyvené de Wit, 1947; Rai, 1966; Chan, Wright, and Phillips, 1967; Pant, 1968; Wiebe, 1968; Rastogi, 1969; Shrivastava, 1969; Lambert, 1970b; van den Hurk and Peute, 1979; Babu and Nair, 1983; Miranda et al., 1999). In early stages, the follicular cells proliferate, aggressively fragment the vitelline envelope, and invade the oocyte, removing its contents by phagocytosis (Figure 3.7). As the oocyte disintegrates, there is a folding and collapse of the follicular wall (Figure 3.8). In several species of fish, the follicular layer of larger follicles becomes deeply folded during atresia, greatly increasing the absorptive surface exposed to the yolk (Figure 3.9) (Hisaw and Hisaw, 1969; Rastogi, 1969; Dodd and Sumpter, 1984). The basement membrane remains intact and connective tissue of the tunica intima is carried into the folds along with branches of blood vessels. Ultrastructural observations on the phagocytic removal of the oocyte in the perch *Perca fluviatilis* and the electric ray *Torpedo marmorata* indicate dissolution of the oocyte nucleus, disintegration of the yolk mass, breakdown of cortical alveoli, and degeneration of mitochondria and other cytoplasmic constituents (Figures 3.10A and 3.11A to D) (Lang, 1981b; Chieffi Baccari et al., 1992). Increasing numbers of small cytoplasmic vacuoles appear in the follicular cells during the early stages of atresia and granular endoplasmic reticulum increases at the same time (Figures 3.10B to G). Several Golgi complexes shed small vesicles that coalesce into smooth-surfaced tubules. Thecal cells and leucocytes, which invade the follicle from surrounding capillaries, appear to take no part in digesting or transforming oocytic material. Agranular endoplasmic reticulum as well as mitochondria with tubular cristae arise in follicular cells of the electric ray *Torpedo marmorata* suggesting a steroidogenic role for these cells (Figures 3.11E,F) (Chieffi Baccari et al., 1992). Indeed, the nuclei of these cells migrate from the basal to apical poles at this time, indicating the change in the role of these cells from phagocytosis of yolk to the release of secretions into the richly vascularized stroma. In addition, the presence of 3β-HSD activity in the follicular cells implies steroidogenic activity (Lupo Di Prisco, 1968, *cited by* Chieffi Baccari et al., 1992). On the other hand, teleosts have revealed no evidence of glandular function in the postovulatory corpus luteum.

As the amount of yolk in the follicle decreases, phagocytosis by the follicular cells decreases and,

when the yolk is completely removed, adjacent folds of the follicular epithelium fuse to produce a richly vascular CORPUS LUTEUM that may almost fill the cavity (Figure 3.7D). The theca increases in thickness and granules appear in its cells which now invade the follicular tissue and become the dominant cell type, follicular cells becoming rare and isolated in small clumps (Figure 3.12). Eventually, the follicular and thecal cells degenerate (Figures 3.10H to J) to be resorbed by the ovarian stroma and the follicle shrinks. A yellow-brown pigment, the so-called age pigment LIPOFUSCIN (Lang, 1981b; Besseau and Faliex, 1994), is formed during the regression of the follicular cells (Figure 3.13). These shrunken follicles may persist for a long period. Some follicular cells still contain discernible elements of the oocyte, but most contain membranous whorls, heterophagic lysosomes, and electron-dense bodies (Figure 3.11G) (Lang, 1981b; Chieffi Baccari et al., 1992).

"Open" and "closed" forms of atresia have been described in the hagfish, *Myxine glutinosa* (Walvig, 1963; Kosmath, Patzner, and Adam, 1983a,b). The OPEN TYPE occurs in eggs larger than 3 mm where follicular cells and yolk platelets are discharged into the coelom through a perforation in the follicular wall. Vascular connective tissue and wandering phagocytic cells from the theca then invade the follicular lumen and remove the débris remaining from the follicular cells. No perforation of the follicular wall appears in the CLOSED TYPE of atresia that occurs in oocytes of preovulatory follicles not yet 3 mm in diameter. These cease development and lipid droplets, often surrounded by small, electron-dense granules, accumulate in the peripheral ooplasm. The thecal layer thickens and becomes richly vascular (Tsuneki and Gorbman, 1977). Thecal cells, containing lysosomes, become phagocytic and invade the oocyte (Figure 3.14). Follicular cells are sometimes present but often they disappear, especially as atresia progresses. The invading phagocytes remove residual yolk platelets and the remnants of follicular cells from the follicular lumen. Production of hormones was not detected in either type of atretic follicle (Kosmath, Patzner, and Adam, 1983b).

A rarer type of atresia, involving no marked phagocytosis or follicular hypertrophy, has been described in the brook stickleback *Eucalia inconstans* and in the Indian knifefish *Notopterus notopterus* (Braekevelt and McMillan, 1967; Shrivastava, 1969). The oocyte is removed by liquifaction and nothing resembling a corpus luteum is formed.

In spite of high hopes, no 3β-HSD activity has been found in atretic follicles of several species (Lambert and van Oordt, 1965; Lance and Callard, 1969; Lambert, 1970b; Yaron, 1971; Livni, 1971; Lang, 1981b; Kosmath, Patzner, and Adam, 1983b) although activity was noted in follicular cells of the goldfish *Carassius auratus* following phagocytic removal of the atretic oocyte (Khoo, 1975). No 3β-HSD reaction was obtained in atretic follicles of the perch *Perca fluviatilis* although the presence of smooth-surfaced tubules, formed by the coalescence of small vesicles that arose from the Golgi complex, gave the appearance of steroidogenesis (Lang, 1981b).

INTERSTITIAL GLAND CELLS have been described in the ovary of the dogfish, *Scoliodon sorrakowah* (Guraya, 1972), and in a teleost, *Mystus cavasius* (Saidapur and Nadkarni, 1976) as vascularized masses of cells remaining from atresia of large previtellogenic and early vitellogenic follicles (Figure 3.15). In these species they are said to arise from the transformation of the theca interna and surrounding stromal elements after the ova and follicular cells have been removed. In the carp, *Cyprinus carpio,* some interstitial cells appear to arise from persisting thecal gland cells of postovulatory follicles and from residual follicular epithelial cells (Guraya and Kaur, 1982). They contain sudanophilic lipid droplets and display activity for 3β-HSD (as well as other enzymes involved in steroidogenesis) suggesting that they may participate in the production of steroid hormones. In the guppy *Poecilia reticulata* these cells demonstrate agranular endoplasmic reticulum and mitochondria with tubular cristae and have been shown to play a role in steroidogenesis (Venkatesh et al., 1992). It is unclear what relationship these cells bear to the steroidogenic interstitial cells of tilapia *Oreochromis niloticus* that arise near the ovarian blood vessels and eventually migrate to the theca around vitellogenic oocytes (Nakamura, Specker, and Nagahama, 1993).

3.2.2 POSTOVULATORY FOLLICLES

After expulsion of the egg during ovulation, the follicular epithelium may hypertrophy and become phagocytic in much the same manner as seen in atretic follicles, clearing away any débris remaining in the lumen. As with atresia, the follicular epithelium becomes folded and invaded by richly vascular thecal tissue. The resulting mass of cells eventu-

ally becomes indistinguishable from that remaining from an atretic follicle.

Postovulatory follicles of the Brazilian characin *Astyanax bimaculatus lacustris* have been used as a model for APOPTOSIS or genetically programmed cell death[11], a normal physiological process of self destruction (Drummond et al., 2000). Apoptosis is the major mechanism responsible for the elimination of follicular cells in the postovulatory follicles during ovarian recovery after spawning. Postovulatory follicles are rapidly reabsorbed as the follicular cells develop phagocytic activity. The follicular cells undergo hypertrophy a few hours after spawning, showing the well developed organelles characteristic of protein synthesis: basal granular endoplasmic reticulum, mitochondria, and Golgi complexes (Figures 3.16A,B); these are requirements of programmed cell death since apoptosis is dependent on the expression of new genes being encoded in the DNA of the target cell. In specimens fixed with tannic acid, the presence of darkly stained follicular cells scattered among clear cells may indicate the presence of damaged cells, heralding their eventual disintegration (Figure 3.16C). Follicular cells destined for destruction release large, organelle-filled blebs and protrusions, the APOPTOTIC BODIES, into the lumen of the follicle (Figure 3.16D). These are phagocytosed either by adjacent healthy follicular cells or by mononuclear phagocytes (Figures 3.16E,F). Four days after spawning, the bulk of postovulatory follicles are reduced but not completely reabsorbed.

Because of a suspected role in hormonal production, the fate of postovulatory follicles of fish has received considerable attention (CYCLOSTOMES: Lygnes, 1931; Lewis and McMillan, 1965; Patzner, 1978; Kosmath, Patzner, and Adam, 1984a,b; ELASMOBRANCHS: Hisaw and Hisaw, 1959; Lance and Callard, 1969; TeWinkel, 1972; Fasano, Pierantoni, and Chieffi, 1989); TELEOSTS: Rai, 1966; Lehri, 1968; Pant, 1968; Shrivastava, 1969; Nicholls and Maple, 1972; Khoo, 1975; Nagahama, Chan and Hoar, 1976; Nagahama, Clarke, and Hoar, 1978; Szöllösi, Jalabert, and Breton, 1978; van den Hurk and Peute, 1979, 1985; Kagawa and Takano, 1979; Kagawa, Takano, and Nagahama, 1981; Lang, 1981a). There is great similarity in the descriptions. In many species there is a proliferation of follicular cells which become phagocytic, much in the same manner as those of atretic follicles, and remove débris left in the hollow follicle (Figure 3.17). The follicular wall collapses into its empty lumen and folds of the follicular epithelium become invaded by richly vascular thecal elements. Proliferation of the follicular cells continues and, in a few species, proliferation of thecal cells is also described. In *Squalus acanthias,* a corpus luteum develops from postovulatory follicles by hypertrophy of the follicular cells surrounded by a separate thecal sheet but, in *Scyliorhinus stellaris* and several species of *Raja,* it is formed by hypertrophy of both thecal and follicular cells (Fasano, Pierantoni, and Chieffi, 1989). Since there appears to be continuous secretion of yolk by the follicular epithelium long after the ovum has been discharged, at least in some elasmbobranchs, care must be exercised in distinguishing the corpora lutea of atresia from those resulting from ovulation (Hisaw and Hisaw, 1959).

Thecal cells appear to participate in the phagocytic cleanup of postovulatory follicles of the trout *Salmo gairdneri* (Szöllösi, Jalabert, and Breton, 1978). Within 12 to 24 hours of ovulation, stellate thecal cells begin phagocytosis of adjacent collagen, their slender processes penetrating the surrounding connective tissue space (Figure 2.143D). The number of phagocytic vesicles within the thecal cells increases with time. Within a few hours of ovulation, flattened smooth muscle cells of the theca transform into stellate cells with many amoeboid processes that isolate and phagocytose bundles of collagen.

When the débris has been removed from the lumen, the corpus luteum may become organized into a compact structure of irregular shape. At this stage it is impossible to distinguish postovulatory corpora lutea from those derived from atresia of large follicles. Luteal bodies remaining from the atresia of small follicles also resemble postovulatory follicles, differing only in their smaller size. Eventually the follicular cells degenerate, leaving a solid, compact mass that finally disappears. The surrounding thecal elements and blood vessels also disappear. Postovulatory corpora lutea are not found in the mud eel, *Amphipnous cuchia,* since the evacuated follicles disappear in the stroma with "bewildering rapidity" (Rastogi, 1969). In the viviparous guppy *Poecilia reticulata,* fertilization and gestation take place within the follicular wall and postovulatory corpora lutea are not found (Lambert, 1966).

Steroidogenesis has been detected in postovulatory follicles of several species of fish, both oviparous (Nicholls and Maple, 1972; Khoo, 1975; Nagahama,

[11] The literature on the morphology of apoptosis has been reviewed by Hacker (2000).

Chan, and Hoar, 1976) and viviparous (Lance and Callard, 1969). In some, special thecal cells react positively for 3β-HSD and show the ultrastructural characteristics of steroidogenesis (Bara, 1965; Kagawa, Takano, and Nagahama, 1981); in others, it is the follicular cells (Lambert, 1970a; Kagawa and Takano, 1979). In some fish, both cell types appear to contribute actively to steroidogenesis, with the special thecal cells sometimes appearing to be most active (Yaron, 1971; Nicholls and Maple, 1972; Khoo, 1975; Nagahama, Chan, and Hoar, 1976; van den Hurk and Peute, 1979, 1985; Smith and Haley, 1987). In the few fish in which the postovulatory follicles have been studied at an extended interval following ovulation, steroidogenesis appears to subside with time (Lance and Callard, 1969). No evidence was found for steroidogenesis in postovulatory follicles of the viviparous smooth dogfish *Mustelus canis* (TeWinkel, 1972).

Four stages in the life of a postovulatory follicle have been described in *Perca fluviatilis* (Figures 3.18 and 3.19) (Lang, 1981a).

STAGE 1, REORGANIZATION PHASE: For two days following ovulation there is a reorganization of the disorganized follicular epithelium. Some of its cells become phagocytic; they contain lysosomes and resorb follicular cells that have lost contact with the basement membrane or have been damaged during ovulation (Figure 3.20). Other cells of the follicular epithelium transform into synthetically active cells.

STAGE 2, VACUOLAR PHASE: From days 2 to 6 following ovulation, the follicle prepares itself for secretion.

STAGE 3, GLOBULAR PHASE: From about 8 to 14 days following ovulation, the presence of agranular endoplasmic reticulum, mitochondria with tubular cristae, and 3β-HSD activity are consistent with the concept that the follicular cells are steroidogenic. They enlarge and form vacuoles, up to 15 μm in diameter, containing proteinaceous and cholesterol-related material. These vacuoles appear to be shed as a holocrine secretion into the follicular lumen. The lumen may appear as a red spot due to the presence of erythrocytes. Thecal cells do not exhibit any structural evidence of secretion and show no 3β-HSD activity.

STAGE 4, REGRESSION PHASE: The follicular cells remaining after secretion degenerate; no yellow pigments are formed.

The formation of a postovulatory corpus luteum has been described in the cichlid *Cichlasoma nigrofasciatum* (Nicholls and Maple, 1972). In this species, the manifestations of steroidogenesis are apparent in both the follicular epithelium and theca. The basic organization of the preovulatory follicles remains after ovulation and the thecal layers with their capillaries remain intact for at least 7 days, still separated from the follicular epithelium by its basement membrane. The ultrastructure of presumed steroidogenic cells of the theca remains unchanged during this time and penetration of thecal elements into the follicular layer apparently does not occur. Follicular cells proliferate rapidly attaining a thickness of up to four layers of cells by one hour after oviposition (presumably only a few hours after ovulation). The innermost cells, in particular, tend to become columnar and to bulge into the region vacated by the oocyte. This proliferation throws the basement membrane into folds. The endoplasmic reticulum of the follicular cells dissociates itself from ribosomes and by 24 hours after oviposition the follicular cells are packed with large quantities of smooth membrane, largely tubular agranular endoplasmic reticulum. Mitochondria lie between the membranes. Also present are free polyribosomes, occasional lipid droplets, and inclusions tentatively identified as lipofuscin. Some cells contain a large Golgi complex consisting of several individual lamellar stacks and associated vesicles. A few days after spawning, degenerative processes appear within these postovulatory follicles although comparable degeneration of the theca was not observed, even 10 days following oviposition when the presumed steroid-secreting thecal cells are still clustered close to capillaries and may continue secreting steroid hormones during this time. The follicular cells, however, seem to be actively secretory for only a few days; their large amounts of smooth membrane then seem to become disorganized and gradually disappear while quantities of deposited lipids apparently increase.

Postovulatory follicles of tilapia *Oreochromis mossambicus* are the most prominent structures in the ovary for 5 to 7 days after spawning when the next clutch of eggs begins to grow (Figure 3.21A) (Smith and Haley, 1987). On the first day after spawning occasional capillaries are scattered throughout the theca. About eight percent of the cells of the theca interna appear steroidogenic, displaying agranular endoplasmic reticulum (usually tubular) and mitochondria with tubular cristae (Figures 3.21C,D and 3.22A). Also present in these cells are granular endoplasmic reticulum, free ribosomes, microfilaments, and occasional lipid droplets. The cells of the theca externa as well as the non-steroidogenic cells cells of the theca interna

are fibroblastic with cytoplasm containing granular endoplasmic reticulum, free polyribosomes, and microfilaments. Cells of the theca externa are widely separated from one another; each is attached to a cell of the theca interna by a few desmosomes and large intercellular spaces open between the points of attachment (Figure 3.21B). Follicular cells are cuboidal with lobed nuclei (Figure 3.22B). The cells are packed with abundant agranular endoplasmic reticulum that appears vesicular. Some granular endoplasmic reticulum occurs basally and free ribosomes are scattered throughout. Mitochondrial cristae are largely lamellar (Figure 3.22C). The apical surface of these cells bulges into the lumen; prominent desmosomes attach the apicolateral surfaces. The apical surface is regular with few microvilli; many vesicles are fused with its inner plasmalemma. Occasional blood cells appear in the lumen. By 5 to 7 days after spawning, the follicular cells are usually columnar with apical microvilli; vesicles appear fused to the inner surface of the apical plasmalemma (Figure 3.23). Each cell contains several moderately developed Golgi complexes and a small amount of tubular agranular endoplasmic reticulum. Some microtubules are found and the number of microfilaments is increased. A few multivesicular bodies are seen. Most mitochondria contain lamellar cristae but a few tubular cristae are occasionally present. It is possible that a steroid hormone produced in the thecal cells may be further converted to other steroids by enzymes in the agranular endoplasmic reticulum of the follicular cells. The primary site of steroidogenesis, however, appears to be in the special thecal cells.

Postovulatory follicles of various salmonids have a folded follicular epithelium that is continuous with the coelomic epithelium of the lamellae (Figures 2.9I and 2.143C) (Nagahama, Clarke, and Hoar, 1978; Szöllösi, Jalabert, and Breton, 1978; van den Hurk and Peute, 1979; Kagawa, Takano, and Nagahama, 1981). Strong 3β-HSD activity is present in the large numbers of special thecal cells arranged around the young postovulatory folicle, but only weak activity in the follicular cells (Figures 3.24A and 3.25A,B). Electron micrographs of these special thecal cells show the presence of abundant agranular endoplasmic reticulum and tubular mitochondrial cristae (Figures 3.24B,C, 3.25C,D). These features also appear, to some extent, in the follicular cells of young postovulatory follicles of the rainbow trout, *Salmo gairdneri,* which also appear to be steroidogenic (Figures 3.24D,E) (van den Hurk and Peute, 1979). In addition, the follicular cells exhibit well-developed Golgi complexes, many lysosome-like structures, coated vesicles, and electron-dense vesicles. Later, these manifestations of steroidogenesis are reduced. Both special thecal and follicular cells of postovulatory follicles synthesize steroids that may be related to the development of new follicles. The special thecal cells of two species of salmon *(Oncorhynchus* spp.) are described as steroidogenic while the follicular cells appear degenerate (Nagahama, Clarke, and Hoar, 1978). By one month after ovulation, special thecal cells of the white-spotted char *Salvelinus leucomaenis* still posssess the cellular organelles typical of steroidogenesis but appear to be undergoing degeneration (Kagawa, Takano, and Nagahama, 1981).

In the African catfish *Clarias gariepinus,* where ovaries of unstripped fish may contain overripe eggs within the ovarian cavity, hypertrophied follicular cells contain heterophagic lysosomes and are actively phagocytic, removing material of the disintegrating ovulated eggs (Figure 3.17) (van den Hurk and Peute, 1985). Eventually autophagic lysosomes take part in the degradation of the contents of the follicular cells and are ultimately responsible for the disintegration of the postovulatory follicle. It is suggested that disintegrating, overripe eggs release compounds that inhibit the production of steroids by follicular cells of the postovulatory follicles, thereby stopping the production of sex pheromones and avoiding a potential spawning, since fertilization of overripe eggs might lead to birth of deformed fry.

True corpora lutea develop in both viviparous and oviparous elasmobranchs (Chieffi, 1962; Chieffi Baccari et al., 1992). They develop from atretic follicles in *Torpedo marmorata* and *T. ocellata* (ovoviviparous) and from postovulatory follicles in *Scyliorhinus stellaris* and *S. canicula* (oviparous). After phagocytosis of the yolk in *Torpedo,* the follicular cells undergo hypertrophy and show clear signs of lipid and steroid metabolism. Thus the atretic follicle assumes the structure of a true epithelial gland which persists during several months of gestation. In *T. marmorata,* an increase in the number of fully developed corpora lutea coincident with the lengthening of the uterine folds during the reproductive cycle suggests an influence of these structures on pregnancy. Possible effects of the corpora lutea on the genital tract of the oviparous *Scyliorhinus* is left for speculation.

The organization of corpora lutea is similar in oviparous and viviparous elasmobranchs and consists

of lipid-filled cells (derived from the follicular epithelium arranged around a central lumen; in early stages of luteal formation, hypertrophy of the cells may obscure the lumen (Figure 3.26) (Koob and Callard, 1991). The cells contain large nuclei with conspicuous nucleoli and abundant lipid droplets; in addition they manifest the agranular endoplasmic reticulum and mitochondria with tubular cristae characteristic of steroid-producing cells. A vascular connective tissue stroma is provided by ingrowths from the theca. The corpora lutea of oviparous forms decline within a few weeks but, in viviparous species, they persist throughout gestation. Degeneration of corpora lutea involves a reduction in size of the structure, increased disorganization of the lobules, a decrease in the lipid content of individual cells, death of cells, and an accumulation of cellular débris in the lumen.

There is no morphological indication of steroidogenesis in postovulatory follicles of *Myxine glutinosa* (Kosmath, Patzner, and Adam, 1984a). A period of reorganization, where the cellular débris remaining after ovulation is removed by phagocytosis, is soon followed by regression and disappearance of the follicle; in this phase the follicular cells and theca degenerate and are removed by blood-borne phagocytes. No cholesterol nor 3β-HSD activity was detected in the cells of the postovulatory follicle (Kosmath, Patzner, and Adam, 1984b).

3.3 Follicular Steroidogenesis

Two important hormones are secreted by the ovarian follicles of many fish. Vitellogenic follicles secrete predominantly OESTRADIOL-17β and postvitellogenic follicles mainly 17α,20β-DIHYDROXY-4-PREGNEN-3-ONE (17α,20β-DP) (Vankatesh, Tan, and Lam, 1992a; Pankhurst, 1997); the pathway of their biosynthesis is shown in Figure 3.27. Oestradiol-17β, under the influence of gonadotropin, promotes vitellogenesis by stimulating the synthesis and secretion of yolk protein in the liver (Wallace and Selman, 1981; Nagahama, 1987; Kanamori, Adachi, and Nagahama, 1988). Production of the hormone 17α,20β-DP, stimulated by a gonadotropin surge during postvitellogenesis, initiates germinal vesicle breakdown (GVBD), the beginning of the processes that culminate in oocyte maturation (Goetz, 1983; Nagahama and Adachi, 1985; Nagahama, 1987).

Three sources of these hormones have been proposed: the follicular epithelium, the thecal layers (including "special thecal cells"), and interstitial cells of the ovary. Evidence has been gathered for a large number of fish using histochemical tests for the presence of steroidogenic enzymes such as 3β-hydroxysteroid dehydrogenase (3β-HSD); more recently immunocytochemical methods have been used. Although ultrastructural evidence for steroidogenesis has often been recorded, it is equivocal. Varying patterns of steroidogenesis, therefore, have been proposed for the follicles of different groups of fish. Bearing in mind the vast range of reproductive strategies found in fish, however, this is not surprising.

An explanation for some of the dilemma, at least for salmonids, is provided by the TWO-CELL-TYPE MODEL that proposes a synergism between the thecal and follicular cells, where thecal cells synthesize the precursors testosterone and 17α-hydroxyprogesterone for conversion by follicular cells to the hormones oestradiol-17β and 17α,20β-DP respectively (Figure 3.28) (Kagawa et al., 1982; Nagahama, Kagawa, and Young, 1982; Nagahama, 1984, 1987; Kanamori, Adachi, and Nagahama, 1988). It is suggested that the two-cell-type model, at least for the production of oestradiol-17β, also applies to the ovary of tilapia, *Oreochromis niloticus* (Nakamura, Specker, and Nagahama, 1993).

According to the two-cell-type model, during vitellogenesis the thecal layers produce aromatizable androgens, mainly testosterone, in response to gonadotropin; these are converted to oestradiol-17β by aromatase enzyme systems present in the follicular layer (Kagawa et al., 1982; Nagahama, 1984; Young, Kagawa, and Naghama, 1982, 1983). Just prior to oocyte maturation, gonadotropin stimulates thecal layers to produce 17α-hydroxyprogesterone; this is converted to 17α,20β-DP by follicular layers where gonadotropin has induced the activity of 20β-hydroxysteroid dehydrogenase, the enzyme involved in this conversion (Nagahama, 1984; Young, Adachi, and Nagahama, 1986). A single population of receptors for gonadotropin on both thecal and follicular cells of the amago salmon, *Oncorhynchus rhodurus* (Kanamori and Nagahama, 1988a), stimulate steroidogenesis by mechanisms involving adenylate cyclase—cyclic AMP (cAMP) (Figure 3.29) (Kanamori and Nagahama, 1988b). The shift in steroidogenic responsiveness of these cells to gonadotropin appears to result from a change in cellular events at a step(s) subsequent to cAMP production.

The two-cell-type model provides an explanation for the sparse ultrastructural and histochemical

evidence of steroidogenesis by preovulatory follicular cells which often manifest organelles typical of protein-secreting cells (Nagahama, Chan, and Hoar, 1976; Hoar and Nagahama, 1978; Matsuyama, Nagahama, and Matsuura, 1991). Since several biochemical steps are involved in the production of testosterone by thecal cells, this is reflected in their ultrastructural appearance of steroidogenesis (Figure 3.30) (Selman et al., 1993); aromatization of testosterone to oestradiol-17β, however, involves only a few steps and the organelles typical of steroidogenesis are masked by those carrying out other activities within the follicular epithelium (Kagawa et al., 1982). It may be noted in this regard, that follicular cells of coho salmon, *Oncorhynchus kisutch,* contain small amounts of agranular endoplasmic reticulum and mitochondria with tubular cristae distributed throughout their abundant protein-producing organelles (Nagahama, Clarke, and Hoar, 1978).

The generalization cannot be made, however, that the two-cell-type model operates in the ovaries of all fish. For example, in the killifish, *Fundulus heteroclitus,* follicular cells are the primary source of follicular steroids in response to pituitary stimulation so that synthesis of oestradiol-17β and 17α,20β-DP does not require the involvement of thecal cells (Petrino et al., 1989). Thecal cells appear to be steroidogenic, however, in spite of their nonsteroidogenic appearance; it is suggested that they synthesize testosterone, providing a second source of aromatizable substrate for the synthesis of oestradiol-17β by follicular cells.

There is a common steroidogenic pathway for much of the synthesis of the two hormones which play such an important role in vitellogenesis and maturation of ovarian follicles in teleosts (Figure 3.31) (Kobayashi et al., 1996). Prior to oocyte maturation, a distinct shift occurs from the production of oestradiol-17β to 17α,20β-DP, probably the result of a decrease in the activity of the enzyme C17,20-lyase (cytochrome P-450 17α-hydroxylase/C17,20-lyase). It is presumed that the decrease in oestradiol-17β production would lead to an accumulation of 17α-hydroxy progesterone, the immediate precursor of 17α,20β-DP.

Three steroid hormones play a significant role in regulating the wide range of reproductive strategies seen in female elasmobranchs: oestradiol-17β, testosterone, and progesterone (Tsang and Callard, 1983, 1992; Callard et al., 1989; Koob and Callard, 1991,1999; Callard, Fileti, and Koob, 1993)[12]. Oestradiol-17β and testosterone are associated with follicular development while progesterone plays a role in egg retention and pregnancy. As would be expected, the amounts of these steroids in the circulation fluctuate with the stage in the reproductive cycle. Isolated follicular epithelial cells of several species synthesize significant quantities of testosterone, oestradiol-17β, and progesterone without requiring thecal elements. Thecal tissue alone, in the presence of testosterone, is able to synthesize oestradiol-17β and an interaction between follicular and thecal layers *in vivo* is suggested. Testosterone is the predominant product of thecal cells and is also produced by the corpora lutea. The corpora lutea are the principal source of progesterone in both viviparous and oviparous species.

Conflicting pictures of ovarian steroidogenesis are seen within the cyclostomes. No 3β-HSD was detected in the ovary of *Myxine glutinosa* nor did the cells of its follicle reveal any ultrastructural features indicative of steroid production (Fernholm, 1972; Tsuneki and Gorbman, 1977). The mature ovary of *Eptatretus burgeri,* however, is capable of a range of steroid bioconversions when incubated *in vitro* with various precursors (Hirose et al., 1975). It is not clear whether this is a real difference between the two species or difference in the sensitivities of the techniques used. The theca interna of the primary follicle of *Lampetra planeri* differentiates during metamorphosis. Its cells manifest the characteristic appearance of steroidogenesis some time before vitellogenesis, containing abundant agranular endoplasmic reticulum and lipid droplets (Busson-Mabillot, 1966); tentative histochemical and spectrophotometric evidence of hydroxysteroid dehydrogenase activity has been noted in these cells (Seiler, Seiler, and Claus, 1981). In the ovary of the sea lamprey *Petromyzon marinus,* however, no clearly defined steroidogenic cell types were found and no 3β-HSD was detected (Weisbart, Youson, and Wiebe, 1978). The cells of the theca interna often contained large lipid droplets in their cytoplasm (Figure 3.32), but these cells did not possess other characteristics of steroid-producing cells.

[12] Koob and Callard (1999) have provided an overview of the spectrum of reproductive modes together with speculation on their hormonal regulation as seen in female elasmobranchs.

3.4 Chorion

As vitellogenesis ends and the oocyte is ready for ovulation, the zona pellucida changes ultrastructurally and perhaps chemically. The primary envelope becomes thinner and the outermost zone is often lost; the elaborate fibrillar patterns fade into a homogeneous, translucent zone. The "arabesque" patterns are transformed at ovulation and the chorion assumes the woven appearance (Dumont and Brummett, 1980) of a fibrous laminate that strengthens the layer by acting equally in all directions to accommodate tensile stresses (Figure 3.33A) (Grierson and Neville, 1981). This transformed primary envelope is sometimes covered by the secondary envelope that may be elaborately ornamented (Figure 3.33B). The outer covering of the egg is now a CHORION.

Although the term "chorion" has been used in several ways, it may be defined as the acellular, highly structured envelope enclosing an ovulated egg or developing embryo, separating it from the external environment (Hart, Pietri, and Donovan,1984). The chorion is usually perforated by a passage, the MICROPYLE, through which a spermatozoon gains access to the ooplasmic surface and effects fertilization. The outer surface is often adorned with specializations in the form of threads, filaments, fibrils, or spikes.

The chorion is soft within the ovary but it begins to harden following ovulation. After fertilization, it separates from the surface of the oocyte and hardening continues. Penetration by the spermatozoon brings about an increase in calcium content of the peripheral ooplasm, causing the cortical alveoli to fuse with the oolemma — the "cortical reaction" — beginning at the site of sperm entry and proceeding as a wave over the surface of the egg. Upon fusion, the vescles discharge their contents into the space between the plasma membrane and the chorion: the PERIVITELLINE SPACE. An acidic glycosaminoglycan that is too large to penetrate the chorion is released, thereby causing an increase in the osmolarity of the perivitelline fluid relative to the surroundings. Since the chorion is permeable to water and small electrolytes, there is an influx of water, increasing the hydrostatic pressure in the perivitelline space and forcing the elastic chorion to expand away from the plasma membrane. Subsequently, the chorion loses its elasticity and becomes tough and rigid in the process of hardening. The hardened chorion serves to protect the egg from mechanical damage and microbial attack.

In some species, the microvilli from both oocyte and follicular cells withdraw from the pore canals and the outer openings may become blocked with "plugs" (Figures 3.34B,C) (Flügel, 1964a, 1967b; Stehr and Hawkes, 1967; Dumont and Brummet, 1980; Hart and Donovan, 1983). In some salmonids, however, the microvilli do not withdraw and have been observed in the pore canals of ovulated eggs (Schmehl and Graham, 1987). In the zebra danio *Brachydanio rerio,* most of each pore canal remains open except for the plug, presumably deposited on the withdrawal of the microvilli by a mechanism not understood (Hart and Donovan, 1983).

Remnants of the primary envelope persist as a fibrous, lamellar coat in the chorion of a wide range of species. This may be surrounded by jelly coats, filaments, and ornamentation provided by the secondary envelope. A simple chorion, said to be derived solely from the primary envelope is found on the egg of the zebra danio (Hart and Donovan, 1983). It is 1.5 to 2.0 μm thick and consists of three zones: pore canals penetrate the inner two zones only (Figure 3.34A). The OUTER LAYER is about 0.1 μm thick, homogeneous, electron dense, and evenly dispersed over the surface; it is adorned with prominent projections (Figure 3.34C). Distinct plugs of osmiophilic material block the outer opening of each pore canal at this level (Figure 3.34B). The MIDDLE LAYER, about 0.15 μm thick, is of medium electron density and has a compact, fibrillar appearance. The fibres, about 0.05 to 0.06 μm in diameter, are organized in crisscrossing bundles around the pore canals. The INNER LAYER comprises most of the chorion and consists of 16 horizontal electron-dense lamellae of about equal thickness alternating with 15 interlamellar portions of lower density. The centre-to-centre spacing of the pore canals is 1.7 μm. Their diameter just below the plug is about 0.2 μm, widening to 0.3 or 0.4 μm at the inside. There are about 7.2×10^5 pore canals per egg.

The inner layers of the chorion of the medaka *Oryzias latipes* are similar to the chorion of the zebra danio, except that these are enclosed in a filamentous coat derived from the secondary envelope (Hart, Pietri, and Donovan, 1984; Iwamatsu, 1992). The chorion is about 12 to 15 μm thick and consists of three distinct zones: an OUTER ZONE, fuzzy, electron-lucent, about 0.12 μm thick; a MIDDLE ZONE, homogeneous, electron-dense, about 0.06 μm thick, with an irregular inner border; and an INNER ZONE formed of 10 to 12 electron-dense lamellae alternating with interlamellae

of lower electron density (Figures 3.35A,B). The outer surface of the chorion is raised into a uniform interconnecting system of ridges in a pattern of hexagons and pentagons; presumably this pattern is an impression of the follicular epithelium, representing an outline of the cells and their intercellular spaces (Figures 3.35C,I). The chorion is adorned with two types of filaments produced by the follicular epithelium. About 25 to 35 ATTACHING FILAMENTS originate from the vegetal pole area of the chorion, intertwining tightly to form a ropelike cord (Figure 3.35I) that joins with cords from neighbouring eggs to form a cluster suspended within the gonoduct. The remainder of the chorion is covered by NONATTACHING FILAMENTS of variable length: some are short and stubby while others taper into long threadlike processes that intertwine with filaments on adjacent eggs, producing a gossamer netting that serves to maintain the integrity of the egg cluster. Both types of filaments are formed of densely packed tubules (microtubules or "microtubule mimics") with an average outside diameter of approximately 19.5 and 18.8 nm respectively (Figures 3.35E to H) (Hart, Pietri, and Donovan, 1984). The wall of each microtubule is cylindrical and is composed of globular subunits arrayed in longitudinal rows. Fourteen of these structural subunits are ranged around the wall of each tubule. In mature oocytes of the medaka *Oryzias latipes,* the long attaching filaments are wound spirally on the axis between the animal and vegetal poles (Figure 3.36) (Iwamatsu 1992). The short non-attaching filaments, distributed on the rest of the chorionic surface, are also bent in a unilateral direction on the egg axis. This spiraling can be either right-handed or left-handed and is established early in oogenesis. It appears not to be an inherited pattern but is imposed during oogenesis by rotation of the oocyte and its follicular epithelium within the basement membrane.

Cross-fractures through the glutaraldehyde-fixed chorion of *Oryzias* indicate that the lamellae are sheets of tightly packed, interwoven fibres, often enclosing teardrop-shaped cavities measuring about 0.3 by 0.7 μm (Hart, Pietri, and Donovan, 1984). The layering of these fibrous sheets is presumably the structural and physical basis for mechanical stability and toughness. The fibres appear to be formed of a heterogeneous family of high molecular weight glycoproteins. The small teardrop-shaped holes may represent remnants of the pore canals. The lamellae of the inner zone of *Oryzias* are continuous and uninterrupted by patent pore canals. The inner surface of the chorion is pebbled with regularly spaced bulges formed by the bulblike bases of both types of filaments which are firmly rooted within the lamellae of the inner zone of the chorion (Figure 3.35D).

Analyses of the proteins of the chorion have utilized the HATCHING ENZYME, a proteolytic endoprotease that breaks down the chorion during hatching (Schoots et al., 1982). In the annual fish *Nothobranchius korthausae,* which has a relatively thick envelope, the inner zone of the chorion is entirely digested but, in the pike *Esox lucius* and the zebra-fish *Brachydanio rerio,* which have thin envelopes, a decrease in thickness of only 30% and 15% respectively is observed. The inner layer of the chorion appears to be the natural substrate for this enzyme. Histochemical and biochemical investigations utilizing this enzyme have shown that the inner layer consists of proteins and glycoproteins (Hagenmeier, 1973; Iuchi and Yamagami, 1976). On the basis of biochemical analyses of the proteolytic products of the inner layer of the medaka, Yamagami (1981) speculates that six glycoproteins, ranging in molecular weight from 86 to 214 kDa, with a repeating polypeptide unit of about 26 kDa, are linked to form the lamellae, while the interlamellar portion may be an interlinking of 70-kDa proteins. In another study, the chorion of unfertilized medaka eggs was shown to consist of two major proteins of 77 to 73 and 49 kDa as well as a minor 150-kDa protein (Iwamatsu, Shibata, and Kanie, 1995). Upon fertilization, the major proteins are polymerized to insoluble, high molecular weight proteins by the temporary formation of several new proteins (132, 114, 62, and 61 kDa), thereby increasing toughness of the chorion.

Analysis of homogenates of isolated chorions from mature ovarian and ovulated eggs of *Carassius auratus* by SDS-polyacrylamide gel electrophoresis shows the presence of at least 20 bands (Cotelli et al., 1988). Five principal classes were recognized, A° to E° in order of decreasing sizes. Of these, the D° class, ranging from 40 to 60 kDa, was the most prominent and represented about 70% of the total chorion components. The principal glycoproteins found in the chorions of unfertilized eggs of the whitefish *Coregonus lavaretus* have a molecular mass ranging from 17 to 105 kDa (Scapigliati et al., 1995). Analysis of purified chorion of *Oncorhynchus mykiss* showed a pattern of four major components (129, 62, 54, and 47 kD) representing about 80% of the total proteins (Brivio, Bassi, and Cotelli, 1991). The 129 and 47 kD polypeptides are glycosylated and belong to the "aspargine-linked' gly-

coprotein family. This "simple" pattern of the chorion of *O. mykiss* may reflect its apparent homogeneity as observed with the electron microscope compared to other species (Cotelli et al., 1986).

The secondary envelope may produce fantastic ornamentation. On the pelagic eggs of the C-O sole *Pleuronichthys coenosus* it forms roughly hexagonal compartments about 30 μm across with walls about 10 μm high and 1 to 2 μm thick (Figure 2.84) (Stehr and Hawkes, 1983). The floor of each compartment is perforated by remnants of the pore canals, each pore being surrounded by a subpattern of polygonal ridges. It is suggested that this complex chorion may influence buoyancy of the egg; it may also strengthen the egg surface and act as a resilent bumper. Perhaps the most elaborate secondary envelope of any species so far described is that of the "annual" cyprinodonts *Cynolebias melanotaenia* and *C. ladigesi* where the eggs must survive in damp soil during South American dry seasons when their aquatic habitat dries (Wourms, 1976; Wourms and Sheldon, 1976). The surface of the egg bristles with uniformly spaced, hollow, conical projections, about 0.25 mm long, that terminate as a crown of recurved spikes (Figure 2.69). This ornamentation of elaborate chorionic extensions may function as "gills" for the long periods spent in damp soil. They may also provide an anchor for periods of flooding and be shock absorbers to protect the egg from sharp particles in the soil.

Sometimes the secondary envelope is coated with a gelatinous material that probably contributes to the adhesiveness of the egg. The demersal eggs of the blenny *Blennius pavo* are attached to the substratum by an adhesive disc that covers about one-third of its surface (Patzner, 1984). This disc consists of a tangled mesh of "anchoring filaments" (Figures 3.37A,B) attached to the remainder of the chorion by branching root-like structures. The micropyle is located at a naked area at the centre of this adhesive disc (Figures 3.37E,F); presumably the spermatozoon makes its entrance before attachment of the egg. Electron micrographs of cross sections of these filaments show a pattern of subfilaments similar to the "microtubule mimics" that constitute the filaments seen in *Fundulus* (Figure 3.37D).

The thickness and complexity of the chorion of fishes show wide variation (Stehr and Hawkes, 1979; Lønning, Kjørsvik, and Falk-Petersen,1988). Generally, chorions of marine teleost eggs that are pelagic and float free in open water are thin with a homogeneous, lamellated structure (Figure 3.38). Chorions of demersal eggs are usually thicker, with a more complex appearance, thereby resisting the mechanical stresses of development on the bottom of a body of water. In labrids, values recorded in freshly stripped mature eggs ranged from a thickness of 1.8 μm with five to six lamellae in pelagic eggs of *Ctenolabrus rupestris* to a thickness of 18.5 μm with about 18 lamellae in the demersal eggs of *Centrolabrus exoletus* (Lønning, 1972). It should be noted, however, that the chorion of several pleuronectids with pelagic eggs ranges from 2.5 μm with six to nine lamellae in *Limanda limanda, Platichthys flesus,* and *Hippoglossoides platessoides* to 15.5 μm with five lamellae in *Pleuronectes platessa.* The chorion of the pelagic eggs of the cod *Gadus morhua* has five lamellae and is 4.5 μm thick.

Distinctive features of the chorion have been used to differentiate the eggs of several species by means of transmission and scanning electron microscopy (Figure 3.39) (Johnson and Werner, 1986; Schmehl and Graham, 1987; Mooi, 1990; Mooi, Winterbottom, and Burridge, 1990; Loureiro and de Sá, 1996; Thiaw and Mattei, 1996). These include patterns on the fibrous inner surface of the chorion as well as differences in filaments, hooks, the adhesive layer, and plugs in pore canal openings. Little relationship was observed, however, between the ultrastructure of the chorions of several species of teleosts and their taxonomic position (Lønning, 1972). Rather, the structure appears to be determined by the reproductive strategy of the species, with demersal eggs tending to have more resistant chorions. Variations were also found in the chorions of the same species from different geographical areas; this may have a genetic basis (Morin and Able, 1983) or be related to differences in salinity, temperature, and viscosity of the seawater (Lønning, 1972).

The chorions of viviparous fish, where the eggs are protected within the body of the female, are thin and simple (Flegler, 1977). The chorion separates from the egg at ovulation and encloses the embryo until hatching. In *Dermogenys pusillus* (Hemiramphidae), the chorion may be produced by the oocyte itself comprising only a primary envelope of two layers perforated by fenestrations containing microvilli from both the oocyte and follicular cells. The thicker inner layer is fibrillar and its structure, although less elaborate, is reminiscent of the "arabesques" noted in the primary envelope of oviparous species. As the egg matures, the pore canals disappear, the external layer becomes thin and irregular, and the thicker, inner layer flattens and becomes almost homogeneous, consisting appar-

ently of fine fibrils; the chorion persists during embryogenesis.

There are two distinctive secondary envelopes on the surface of the lamprey egg: an APICAL TUFT on the animal pole and an elaborately textured ADHESIVE COAT that cups the vegetal two-thirds of the egg (Figures 2.88A and 3.40) (Kille, 1960; Yorke and McMillan, 1979). The apical tuft consists of transparent, nonsticky gelatinous material that appears to be secreted and moulded by a cap of follicular cells in the apical region; under phase contrast or polarized light, it is seen to contain many fine fibrils (Figures 2.88C and 2.127A). The adhesive coat is an unusual secondary envelope in that it consists of remnants of specialized follicular cells, the ADHESIVE CELLS, that break down during ovulation (Yorke and McMillan, 1979, 1980). During maturation, these follicular cells enlarge and become packed with huge saccules (Figure 2.123). In addition, their cytoplasm contains abundant granular endoplasmic reticulum and mitochondria; Golgi complexes and agranular endoplasmic reticulum are limited to the cytoplasm adjacent to the zona pellucida. The nucleus is located in an extreme basal position, toward the overlying theca, and the entire surface of the cell is covered with microvilli, which on one side are in contact with the zona pellucida. The saccules are formed by the coalescence of two types of membrane-bound vesicles that are produced by the Golgi complex and granular endoplasmic reticulum respectively (Figure 3.41) (Busson-Mabillot, 1967b). During ovulation, the adhesive cells break down, beginning in regions adjacent to the zona pellucida (Figures 2.127A,B) (Yorke and McMillan, 1979, 1980). The intracellular saccules become attached to the zona pellucida, forming the elaborate adhesive coat (Figure 2.88D). A similar sort of adhesive coat is described on the eggs of the clupeid *Dorosoma petenense* where the follicular cells are retained on the surface of the zona pellucida after ovulation (Shelton, 1978). This epithelium is said to transform directly into a functional, sticky egg membrane.

A brief description of the chorion of the hagfish *Eptatretus stouti* indicates a similar sort of complex, lamellar chorion in this distantly related species (Koch et al., 1993). It is variable in thickness but about 200 μm thick in the figure shown (Figure 3.42). It consists of three layers, an outer columnar/globular region, a middle region of 11 to 12 horizontal lamellae, and an inner dense layer.

3.5 Micropyle

The tough chorion of teleost eggs is impenetrable to spermatozoa and the only passageway for a spermatozoon to fertilize the egg is by way of a pore that penetrates the chorion at the animal pole, the MICROPYLE. Since teleostean spermatozoa lack acrosomes and need not dissolve the egg membrane to reach the egg surface, they do not require capacitation before they can attach and fuse with the oolemma (Iwamatsu, Ishijima, and Nakashima, 1993). The first spermatozoon reaches the micropyle within seconds of insemination and enters to interact with microvilli of the SPERM ENTRY SITE on the oolemma (Figures 3.43 and 3.44) (Ohta and Iwamatsu, 1983; Wolenski and Hart, 1987a; Bern and Avtalion, 1990). The micropyle, therefore, orients the position of sperm entry to a region on the animal pole near the egg nucleus. The speed of spermatozoa of the medaka *Oryzias latipes* decreases as they move down the micropylar canal toward the oolemma (Figure 3.45) (Iwamatsu, Ishijima, and Nakashima, 1993; Ishijima, Hamaguchi, and Iwamatsu, 1993). Following attachment of the spermatozoon to the egg microvilli, the sperm head is rapidly engulfed by fusion of the plasma membranes of the interacting gametes. Immediately after this rapid response, the egg plasma membrane elevates to form the nipple-shaped FERTILIZATION CONE into which the entire sperm head, midpiece, and a portion of the flagellum are absorbed. In eggs of the zebra danio, *Brachydanio rerio,* this occurs between one and two minutes after insemination (Wolenski and Hart, 1987a).

The micropylar areas of salmonid and herring eggs possess some "sperm guidance factors" which facilitate entry of homologous spermatozoa into the micropyle (Yanagimachi et al., 1992). A substance in unfertilized eggs of the medaka *Oryzias latipes* guides spermatozoa into the micropyle (Iwamatsu, Ishijima, and Nakashima, 1993). This guidance factor may exist in the micropylar apparatus rather than in the perivitelline space or cortex; it loses its activity following fertilization. Glycoproteins occurring in a "diluted mucus area" in the outermost layer of the chorion of unfertilized eggs of the medaka play an important role in guiding spermatozoa into the micropyle (Iwamatsu, Yoshizaki, and Shibata, 1997). The reduced incidence of sperm entry into micropyles of fertilized eggs seems to result from inactivation of these glycoproteins as they are rendered insoluble by polymerization following fertilization.

In the grass goby *Zosterisessor ophiocephalus,* follicular cells produce a forest of attachment filaments up to 600 μm in length surrounding the micropyle (Figure 3.46) (Giulianini and Ferrero, 2000). These specializations of the secondary envelope form a crown about 76 μm in diameter that would appear to present a barrier to sperm entry (Giulianini et al., 2001). The sperm, however, are able to pass through perforations between the filament insertions on the chorion — even when the egg adheres strongly to its substrate — to reach the micropyle (Figure 3.47).

Scanning electron micrographs show that entry to the micropylar canal of many species is attained through a funnel-shaped VESTIBULE on the outer surface of the chorion (Figure 3.48) (Szöllösi and Billard, 1974; Stehr and Hawkes, 1979; Kobayashi and Yamamoto, 1981; Iwamatsu and Ohta, 1981b; Ohta and Iwamatsu, 1983; Hart, Pietri, and Donovan, 1984; Wolenski and Hart, 1987a; Iwamatsu, Ishijima, and Nakashima, 1993; Iwamatsu, et al., 1997). In some species the vestibule is surrounded by small pores and/or protrusions that may produce pheromones, attracting spermatozoa to the micropyle (Stehr and Hawkes, 1979). Spermatozoa of the cypriniform *Barbus conchonius* and the perciform *Luciocephalus* sp. may be guided to the micropyle by an elaborate pattern of spiral ridges that emboss the chorion of the animal pole once some form of species-specific chemoattractant brings them close to the egg. (Figures 3.49 and 3.50) (Amanze and Iyengar, 1990; Riehl and Kokoscha, 1993). In *Fundulus heteroclitus,* where fibres of the secondary envelope could impede access by spermatozoa, a fibril-free zone, 50 to 100 μm in diameter, surrounds the micropyle (Kuchnow and Scott, 1977). On the contrary, the perimicropylar region of several species of cyprinodonts is surrounded by adhesive filaments while the rest of the chorion exhibits simple ornamentations of varying shape (Figure 3.51) (Thiaw and Mattei, 1992). The walls of the vestibule in *Fundulus* are studded with small, tapered projections (Figure 3.52A) (Dumont and Brummett, 1980); in *Brachydanio rerio,* radial folds adorn the funnel (Hart and Donovan, 1983). Eggs of the leaffish *Nandus nandus* (Nandidae, Perciformes) are attached to plants and other substrates by a dense carpet of short filaments arrayed in a circular area around the micropyle (Figure 3.53) (Britz, 1997). The micropyle of the blenny *Blennius pavo* is at the centre of an adhesive disc that consists of an elaborate mesh of anchoring filaments (secondary envelope) attached to the chorion (Figures 3.37E,F) (Patzner, 1984). It is a conundrum how spermatozoa penetrate this jungle of filaments to reach the micropyle of an attached egg.

The walls of the micropylar canal may be sculpted, reflecting the laminar structure of the chorion "giving the appearance of leaflets of an iris diaphragm" (Figure 3.52B). Annular or spiral rib-like thickenings are often observed within the channel (Kobayashi and Yamamoto, 1981; Patzner, 1984; Nakashima and Iwamatsu, 1989). In several species, the micropylar opening at the bottom of the micropylar canal terminates on the inner surface of the chorion as a crater in the centre of a bulge that nestles snugly against the oolemma (Stehr and Hawkes, 1979; Kobayashi and Yamamoto, 1981; Ohta and Iwamatsu, 1983; Yamamoto and Kobayashi, 1992). In *Fundulus* this opening is 2.5 to 3.0 μm in diameter and is surrounded by a small, smooth lip (Dumont and Brummett, 1980).

Differences in the appearance, with the scanning electron microscope, of the micropyle and surface patterns of the chorion (knobs, pits, etc.) have been used to identify the eggs of several species of salmonids and a classification of three categories of micropyles has been suggested (Riehl, 1980). TYPE I has a deep pit and short canal, TYPE II a flat pit and long canal, and TYPE III a canal but no pit. The sides of the canals are often reinforced by annular or helicoid thickenings. The eggs of 11 salmonids studied fit into categories II or III. It is interesting to note, however, that eggs of some species of *Salmo* are classified as Type II *(salar, alpinus),* and others as Type III *(gairdneri, trutta).* No pit or vestibule is seen in the Type III micropyle of the eel *Anguilla japonica* (Ohta et al., 1983). A species-specific micropyle may present the initial isolating mechanism in sympatric speciation and/or is an important feature of sperm selection (Riehl, 1980). Hirai (1988) has distinguished nine species of pelagic eggs by means of a simplified technique for scanning electron microscopy.

A taxonomic key, based on characteristics of the micropyle of unfertilized eggs, as seen with the scanning electron microscope, has been prepared for four species of Sparidae (Figure 3.54) (Chen, Shao, and Yang, 1999). Cladistic analyses of the structure of the micropyles were used to suggest generic interrelationships between the species; the results agree with conclusions obtained using morphological, biochemical, and molecular data. This study was extended to four species in three other families of Perciformes (Li, Wu, and Yang, 2000); although the ultrastructure of the

surface of the zona pellucida, the density of distribution of pores, and the size of the eggs were useful characters for distinguishing the species, the ultrastructure of the micropyles was the most important feature for identifying the eggs. Micropyles in both of these studies were of Type III.

Elaborate surface arrays of parallel ridges on the zona pellucida suggest phylogenetic relationships among certain anabantoid genera (Britz, Kokoscha, and Riehl, 1995). These ridges spiral from the Type I micropyle and are presumed to assist in sperm guidance (Figure 3.55). Three of the genera, *Ctenops, Parasphaerichthys*, and *Sphaerichthys,* are considered to be members of the family Belontiidae. A fourth genus, *Luciocephalus,* is often grouped alone as a separate suborder, Luciocephaloidei (Nelson, 1984). Similarities in the spiral arrays have been used as evidence for inclusion of all four genera in the Anabantoidei or, perhaps, in a separate suborder.

The oolemma below the micropyle is the SPERM ENTRY SITE (Figure 3.56) (Brummett and Dumont, 1979; Hart and Donovan, 1983; Ohta and Iwamatsu, 1983; Wolenski and Hart, 1987a; Ohta, 1991). This region of the egg of *Brachydanio* conforms to the shape of the inner surface of the micropyle, resulting in a deep depression of its surface (Figure 3.44A). The plasmalemma of this region differs from the rest of the egg surface, often displaying a distinct cluster of 15 to 20 microvilli (Figures 3.44B and 3.57A). The remainder of the oolemma surrounding this area may be contoured by interconnecting small folds or microplicae. The first polar body, or a scar which marks its former position, can usually be found about 100 μm from the centre of the sperm entry site in the eggs of *Fundulus heteroclitus* (Brummett and Dumont, 1979). A band of compact, homogeneous, electron-dense material spreads out for some distance in the ooplasm beneath the sperm entry site (Figure 3.44B) (Ohta and Iwamatsu, 1983; Wolenski and Hart, 1987a). Cortical granules are absent from the cytoplasm in this region, but many elongate mitochondria and a number of free ribosomes have been described (Figures 3.43A,B). Elsewhere granular cortical cytoplasm forms a uniformly thick band below the oolemma.

Although sperm entry sites have been less extensively studied in nonteleostean fish, several interesting examples have been recorded in Acipenseriformes. In Acipenseridae, the number of micropyles varies in different females of a species and also in the eggs of one female (Linhart and Kudo, 1997). The sturgeon *Acipenser stellatus* has from one to 13; there may be up to 33 in beluga *Huso huso,* and 55 in the Russian sturgeon *Acipenser gueldenstaedti.* There are three to 15 micropyles within two lightly-pigmented rings in an area of 0.1 to 0.2 mm at the animal pole of the eggs of *Acipenser transmontanus* (Figure 3.58) (Cherr and Clark, 1982; Ginsburg and Dettlaff, 1991). Each micropyle has a funnel-shaped entrance and their number and arrangement seem to be characteristic of a particular female. Mature eggs of the closely related family Polyodontidae, the paddlefish *Polyodon spathula,* possess from four to 12 micropyles in the animal pole region (Figure 3.59). As in micropyles of other fish, the sperm entry site at the bottom of the micropyle is elaborated to form a tuft of microvilli. Although there have been denials of the presence of a micropyle in eggs of Polypteriformes, a single micropyle was demonstrated at the animal pole of eggs of *Polypterus ornatipinnis* (Figure 3.60) (Bartsch and Britz, 1997).

In many teleosts the micropyle is formed during vitellogenesis by a single follicular cell that enlarges and differentiates to become the highly specialized MICROPYLAR CELL (Figures 2.87A and 3.61) (Iwamatsu et al., 1988). The micropylar cell remains attached by tight junctions to the oolemma by a thick cytoplasmic extension (Iwamatsu, Nakashima, and Onitake, 1993) and, as the zona pellucida is being laid down around it, moulds the channel of the micropyle through this layer so that folds in the wall of the vestibule and micropylar canal form a replica of the surface of the micropylar cell (Figures 2.34A and 3.62A,B) (Aravindan and Padmanabhan, 1972; Stehr and Hawkes, 1983; Kobayashi and Yamamoto, 1985). In the medaka *Oryzias latipes*it is suggested that these patterns are carved by the micropylar cell during oogenesis as a result of movements of the follicular cells (Iwamatsu, Nakashima, and Onitake, 1993). The folds form left-handed spiral patterns in most eggs but a few show no spiralling (Figures 3.62C,D). After ovulation, the micropylar cell is lost and the micropyle becomes the pore that admits a spermatozoon to the egg at the time of fertilization.

With the light microscope, the micropylar cell of the loach *Misgurnus anguillicaudatus* and smelt *Hypomesus transpacificus nipponensis* can easily be distinguished from other follicular cells as early as the yolk vesicle stage of oocyte development by its enormous size and low affinity for dyes (Ohta and Teranishi, 1982; Takano and Ohta, 1982); in the medaka *Oryzias latipes,* however, it stains more intensely than

the other follicular cells (Nakashima and Iwamatsu, 1989). The micropylar cell is conical with its tapered apex facing the oolemma and wide, basal surface abutting partly on the follicular cells overlying it and partly on the basement membrane of the follicular epithelium.

The ultrastructure of the micropylar cell has been described in detail in follicles of several species (Riehl, 1977; Ohta and Teranishi, 1982; Kobayashi and Yamamoto, 1985; Nakashima and Iwamatsu, 1989). A micropylar cell is not detectable in previtellogenic ovarian follicles but, in the early vitellogenic phase, it becomes differentiated from neighbouring follicular cells by its slightly larger size and electron-dense cytoplasm (Figure 3.63). As vitellogenesis proceeds, it assumes the shape of a mushroom, with a large cell body, resting in an indentation of the zona pellucida (Figure 3.64). Eventually a thick protoplasmic process from this cell penetrates the zona pellucida and extends toward the oolemma within the MICROPYLAR CANAL. The surface of the micropylar cell facing the oolemma bears several short microvilli whereas its outer surface, surrounded by polygonal follicular cells, is smooth (Kobayashi and Yamamoto, 1985).

Well developed granular endoplasmic reticulum fills most of the micropylar cell body, and other organelles are present in moderate amounts: mitochondria, Golgi complex, agranular endoplasmic reticulum, vesicles, and lysosome-like bodies. Its size and electron density increase with vitellogenesis and the granular endoplasmic reticulum and Golgi complexes increase in abundance in the cytoplasm adjacent to the zona pellucida. In some species, cisternae of the granular endoplasmic reticulum are extremely dilated and contain flocculent material giving the cell a vacuolated appearance (Takano and Ohta, 1982; Kobayashi and Yamamoto, 1985). Bundles of tonofilaments occupy the perinuclear cytoplasm on the opposite side of the cell (Figure 3.65A).

By late vitellogenesis, the enlarged micropylar cell extends a broad cytoplasmic process through the zona pellucida to reach the oocyte surface (Figure 3.65B). The process contains a conspicuous central core of parallel bundles of microtubules surrounded by a few 10-nm intermediate filaments and microfilaments. A constriction around the process, a short distance from the tip, forms a spherical END BULB, containing few organelles, that extends beyond the micropylar canal to indent the surface of the oolemma. Adhaerens junctions develop between the plasma membranes of the end bulb and oocyte of the salmon *Oncorhynchus keta* (Kobayashi and Yamamoto, 1985) (Figures 3.66A,B). There is the appearance of the transfer of materials from the end bulb to the specialized cytoplasm of the oocyte in the micropylar region (Figure 3.66C).

It is unclear whether the micropylar canal is produced as the growing zona pellucida is formed around the micropylar process or whether the process actually bores its way through this layer. Presumably the cell body and adjacent stratified follicular cells hollow out the vestibule. The spiral pattern of ridges on the inside of the micropylar canal of *Oryzias* may be carved by the micropylar process acting like a screw as it it extends through the zona pellucida toward the oolemma (Nakashima and Iwamatsu, 1989). The fact that the outer reaches of the channel are lined by the inturned outermost layer of the zona pellucida argues in favour of the boring action of the micropylar process. This explanation is enhanced by the screw-like appearance of the cytoplasmic process that contains a twisted bundle of microtubules with a bundle of tonofilaments at its core (Figure 3.65C).

As the time of ovulation draws near, the follicular cells over the entire oocyte show signs of degeneration as do the micropylar cell and the stratified follicular cells of the micropylar region (Kobayashi and Yamamoto, 1985). The micropylar cell shrinks and withdraws its process, partially or completely, from the micropylar canal. A blunt extension from the oocyte invades the inner opening of the micropylar canal; this may simply be a response to increased internal pressure of the oocyte resulting from hydration.

Much information for the establishment of the animal pole/vegetal pole axis in postvitellogenic oocytes — and thereby the ultimate positioning of the micropyle — has been derived from investigations of the medaka *Oryzias latipes* (Iwamatsu, 1992, 1994; Iwamatsu, Nakashima, and Onitake, 1993; Iwamatsu and Nakashima, 1996). The first indication of a future axis is the apparently random positioning of the electron-dense, fibrillar yolk nucleus during the latter part of primary growth (Figures 2.26 and 3.67). Presumably the yolk nucleus produces some diffusible substance which reaches adjacent follicular cells, causing them to elongate and become anchored to the basement membrane in the VEGETAL POLE AREA. Elsewhere, the follicular cells become dislocated from the basement membrane, permitting the oocyte and its jacket of follicular cells to rotate within a chamber formed of the basement membrane surrounded by thecal cells.

Isolated follicles are translucent so that filaments on the surface of the chorion provide visual evidence of this motion (Figure 3.68) (Iwamatsu, 1992). A forest of filaments extends from the chorion: long ATTACHING FILAMENTS that form a tangled mat in the vegetal pole area and shorter NON ATTACHING FILAMENTS elsewhere on the surface (Figures 3.36 and 3.62C). These filaments extend between the follicular cells (Figure 3.69) and, as the oocyte rotates, the non-attaching filaments line up like reeds in a stream indicating that some oocytes rotate in a clockwise direction, others counterclockwise, around the centre of the vegetal pole area. It is suggested that the position of the micropylar cell, and hence the location of the animal pole, is determined by this movement. This rotation enables the large cytoplasmic extension of the micropylar cell to scour its spiral pattern within the micropylar vestibule and canal (Figures 3.62A,B and 3.70).

The micropylar apparatus of the hagfishes *Myxine glutinosa* and *Eptatretus burgeri* are surrounded by 60 to 80 anchoring filaments at the animal pole of the egg (Figures 2.91A, 3.71A, and 3.72C) (Walvig, 1963; Fernholm, 1975; Patzner, 1975; Kosmath, Patzner, and Adam, 1981; Koch et al., 1993). During development of the folicle, the micropyle is formed by a stalk of follicular cells that perforates the chorion, continuing its inward progression to form an indentation of the oolemma at the animal pole (Figures 3.72B and 3.73) (Lyngnes, 1930). The outer opening is surrounded by a honeycomb pattern of partitions at the base of the funnel (Figures 2.91C,D and 3.72A). With a diameter of about 4 μm, the micropyle of *Eptatretus* is large enough to admit a single spermatozoon but sufficiently restrictive to prevent polyspermy (Koch et al., 1993). The function of a chamber hollowed out partway along the canal is unexplained (Figure 3.71B) (Kosmath, Patzner, and Adam, 1981).

There is no micropyle in the eggs of the lampreys, *Lampetra fluviatilis* and *L. planeri* (Kille, 1960). The entry of spermatozoa is restricted to the region of the apical fibrous tuft which appears to orient the sperm head so that it strikes the chorion at an angle of about 90°. Spermatozoa of lampreys, unlike those of other fish, possess an acrosome and it is presumed that enzymes are released that digest a path through the chorion, perhaps by way of the pore canals (Afzelius, Nicander, and Sjödén, 1968).

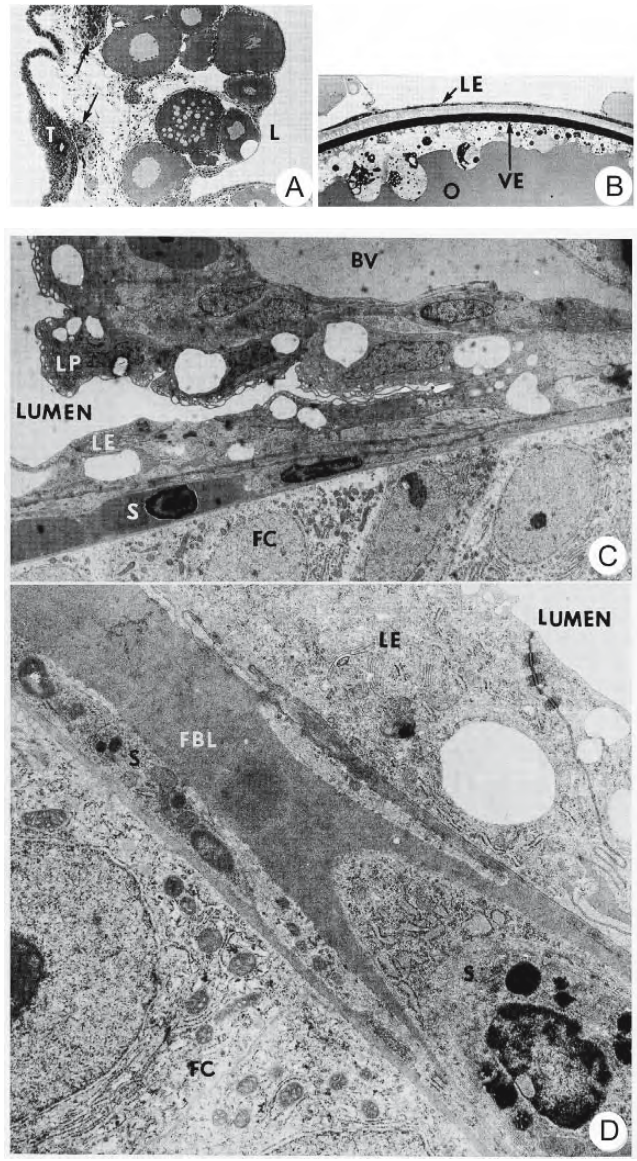

Figure 3.1: Micrographs of sections of the ovary of the killifish *Fundulus heteroclitus*. (From Brummett, Dumont, and Larkin, 1982; © reproduced with permission of John Wiley & Sons, Inc.).

A. Photomicrograph of an Epon section through the wall and ovigerous lamella of a nongravid ovary. Most follicles are closely apposed to the layer defining the lumen (L) of the ovary. A loose stroma fills the space between the follicles and the outer muscular tunic (T). The arrows indicate atretic or degenerating postovulatory follicles. X 450.

B. Photomicrograph of an Epon section through the presumed site of ovulation. The luminal epithelium (LE) is stretched flat and is closely applied to underlying connective tissue and follicular elements. O, oocyte; VE, zona pellucida. There is a young oocyte at each side of the site. X 450.

C. Transmission electron micrograph of a section through the future ovulation site and surrounding lip. Blood vessels (BV) course beneath the rounded cells of the lip (LP). Flattened luminal epithelial cells (LE) over the site are underlain by their basal lamina, vascular and stromal elements (S), the follicular basal lamina, and the follicular epithelium (FC). X 3,900.

D. Transmission electron micrograph of a section through the future ovulation site. There has been a partial fusion of the basal laminae (FBL) of the flattened luminal epithelial cells (LE) and follicular epithelium (FC). Some stromal elements (S) are visible in the intervening layer. X 12,200.

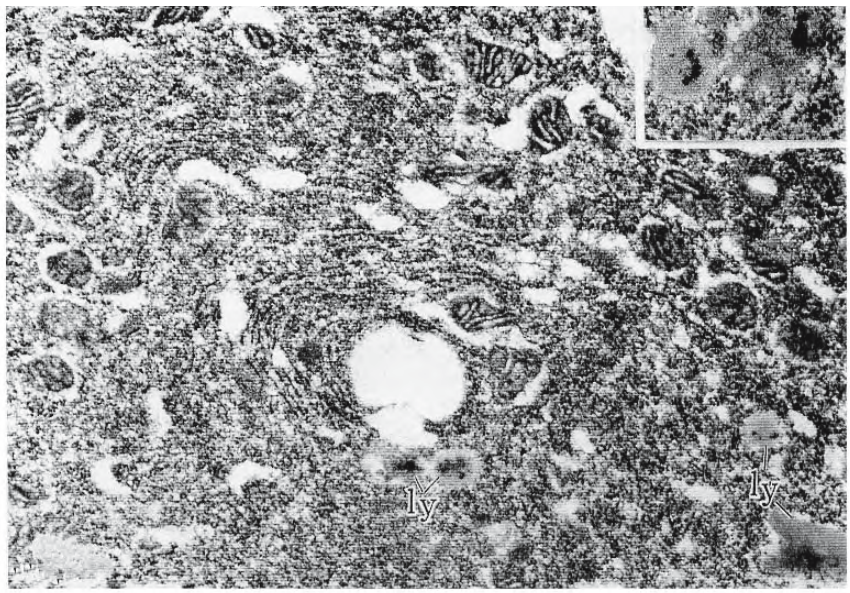

Figure 3.2: Transmission electron micrograph of the cytoplasm of a cultured follicular cell of the medaka *Oryzias latipes* showing the presence of lysosome-like bodies (ly) just before ovulation was expected to occur. X 16,800 (From Iwamatsu and Ohta, 1981a; reproduced with permission from the Zoological Society of Japan).

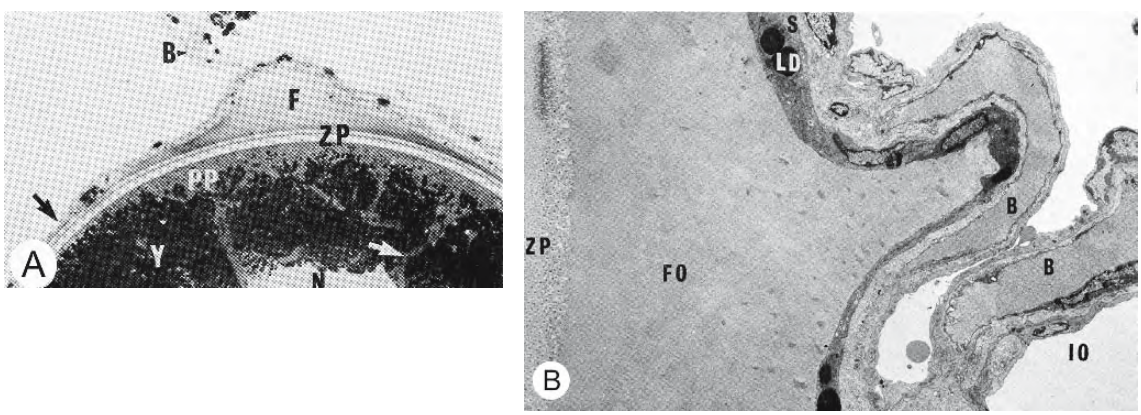

Figure 3.3: "Fluid of ovulation" in the follicle of the lamprey *Petromyzon marinus.* (From Yorke and McMillan, 1980; reproduced with permission from the Society for the Study of Reproduction, Inc.).

A. Photomicrograph of the apical area of the follicle after the formation of the fluid of ovulation (F) at a site near the point of entry of a blood vessel (B). The zona pellucida (ZP) is enclosed by the follicular layers (arrow). Cords of yolk-free cytoplasm (white arrow) extend from the eccentric nucleus (N) to the surface and form the polar plasm (PP). X 700.

B. Transmission electron micrograph of the apical region of a follicle showing the follicular cells enclosing the fluid of ovulation (FO) several days prior to the events leading to the rupture of the follicle. There is a greater accumulation of lipid in this region than in follicular cells elsewhere in the follicle.

Abbreviations: B, blood vessel; IO, intraovarian space; LD, lipid; ZP, zona pellucida; Y, yolk.

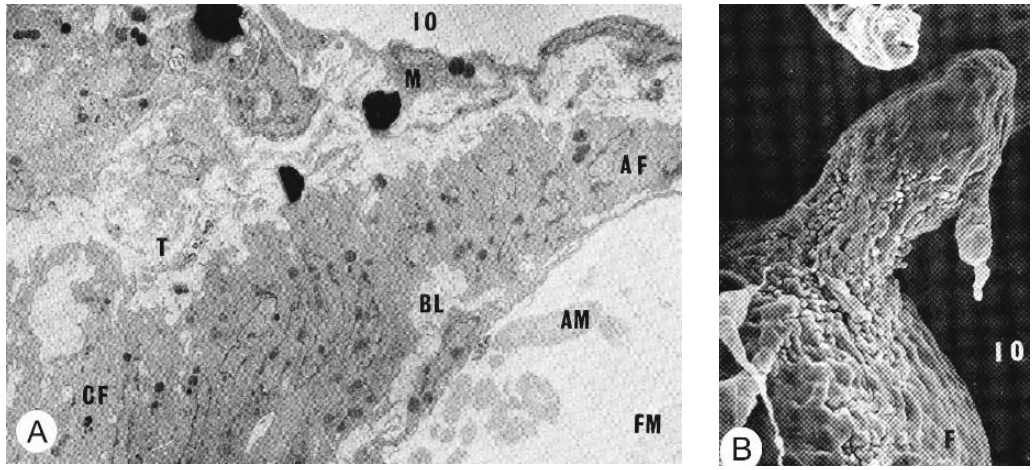

Figure 3.4: Micrographs of sections of the follicle of the lamprey *Petromyzon marinus* during ovulation. Follicular cells change shape, beginning at the fluid-filled end of the follicle; as they become columnar, they form a sleeve-like constriction that gently extrudes the egg from the follicle. (From Yorke and McMillan, 1980; reproduced with permission from the Society for the Study of Reproduction, Inc.).

A. Transmission electron micrograph. Follicular cells in the constricted apical region of the follicle are much taller than the adjacent follicular cells which form a sphere containing filamentous material and the amorphous remains of the fluid of ovulation. The theca is thicker and more convoluted over the columnar cells. X 3,200.

B. Scanning electron micrograph of the apical end of the follicle during ovulation. The egg is extruded ahead of the lengthening constriction of the follicle. X 185.

Abbreviations: AF, apical follicular cells; AM, amorphous material; BL, basal lamina; CF, columnar follicular cells; F, apical end of follicle; FM, filamentous material; IO, intraovarian space; M, mesothelium; T, theca.

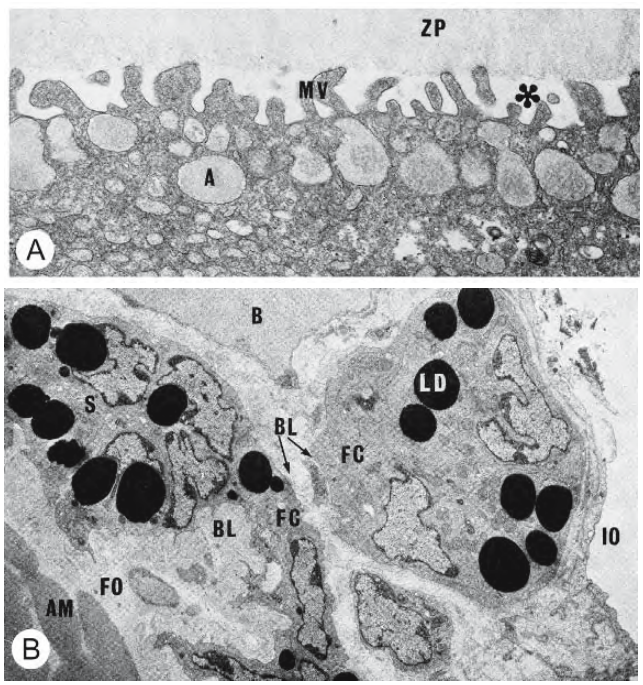

Figure 3.5: Electron micrographs of sections of follicles of the lamprey *Petrozyzon marinus* just prior to its rupture. (From Yorke and McMillan, 1980; reproduced with permission from the Society for the Study of Reproduction, Inc.).

A. Microvilli (MV) from the oocyte are retracted from canaliculi in the zona pellucida (ZP); faint traces of these canaliculi may be seen. Withdrawal of the microvilli creates the perivitelline space (*) between the oolemma and the zona pellucida. A, cortical alveolus. X 24,250.

B. Two follicular cells (FC) bestride the entrance of a blood vessel (B). The fluid of ovulation (FO) contains amorphous material (AM). The follicular layer is folded and thrown into projections enclosing remnants of the intercellular spaces (S); its basal lamina (BL) is highly convoluted. These follicular cells have accumulated many lipid droplets (LD); follicular cells farther from this centre of activity do not show these characteristics. IO, intraovarian space. X 5,810.

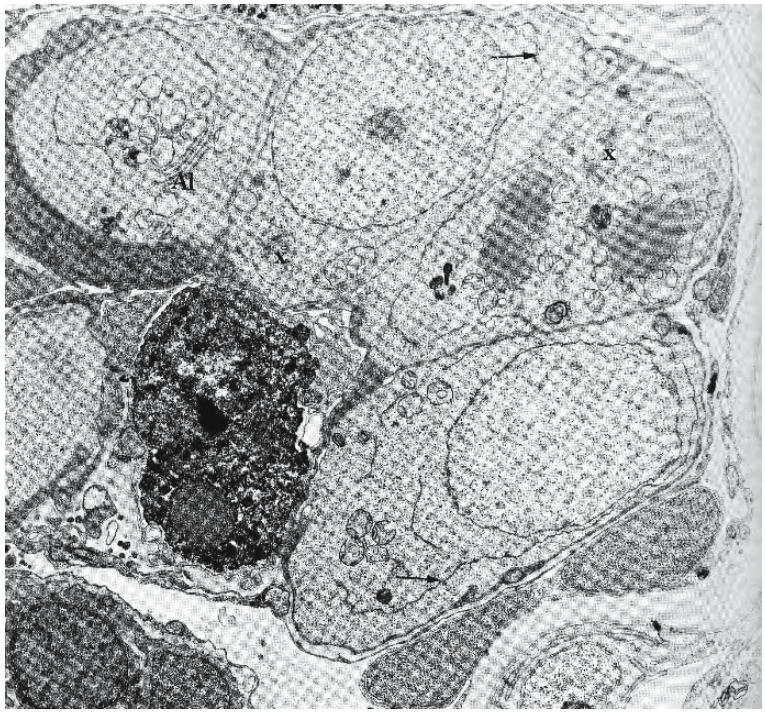

Figure 3.6: Transmission electron micrograph showing an atretic germ cell within a cluster of indifferent germ cells in a section of the ovary of the medaka *Oryzias latipes*. A1, annulate lamellae; X, Golgi complex. (From Hogan, 1978; reproduced with permission from Elsevier Science).

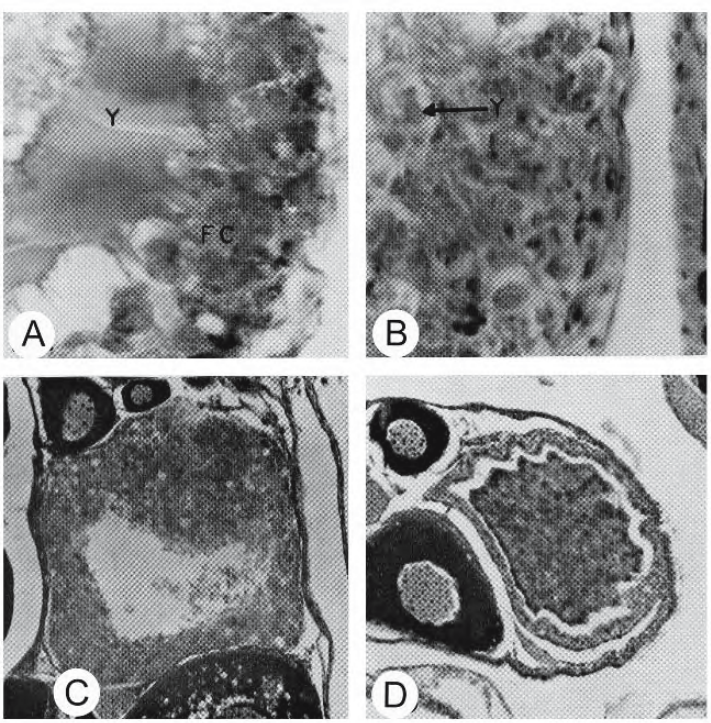

←

Figure 3.7: Light micrographs of sections of the ovary of the brook stickleback *Eucalia inconstans* showing stages in follicular atresia. (From Braekevelt and McMillan, 1967; © reproduced with permission of John Wiley & Sons, Inc.).

A. The edge of an unspawned, mature oocyte at an early stage of atresia. The zona pellucida has disappeared but yolk (Y) is still plentiful. Follicular cells (FC) are hypertrophied. X 650.

B. Phagocytosis is well advanced at a later stage of atresia; little yolk (Y) remains. X 650.

C. A collapsing follicle during advanced atresia. X 155.

D. A ball of cells, the corpus luteum, remains at the end of the atretic process. X 155.

Figure 3.8: Light micrograph of a section of an ovarian follicle of the sea lamprey *Petromyzon marinus.* Atresia is well advanced and much of the oocyte has been removed as a result of extensive phagocytic invasion. The zona pellucida is collapsed but the follicular layers remain distended. Phagocytes can be seen inside and outside the zona pellucida. X 160 (From Lewis and McMillan, 1965; © reproduced with permission of John Wiley & Sons, Inc.).

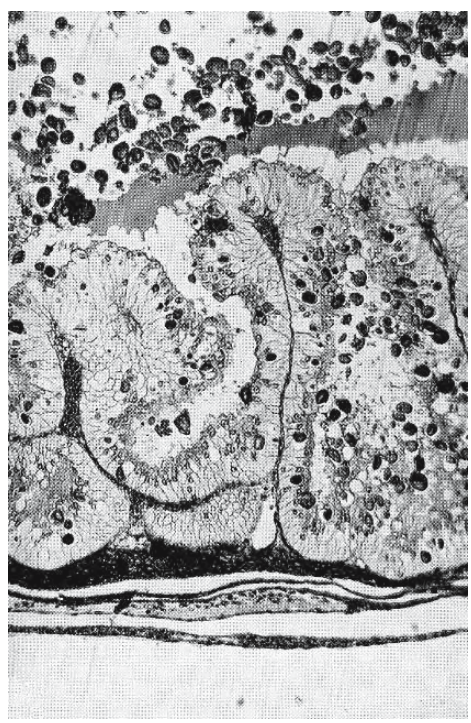

Figure 3.9: Light micrograph of a section of the ovary of the spiny dogfish *Squalus suckleyi* showing extensive folding of the follicular epithelium in a large atretic follicle. The folds enhance absorption of yolk by the follicular cells. (From Hisaw and Hisaw, 1959; reproduced with permission).

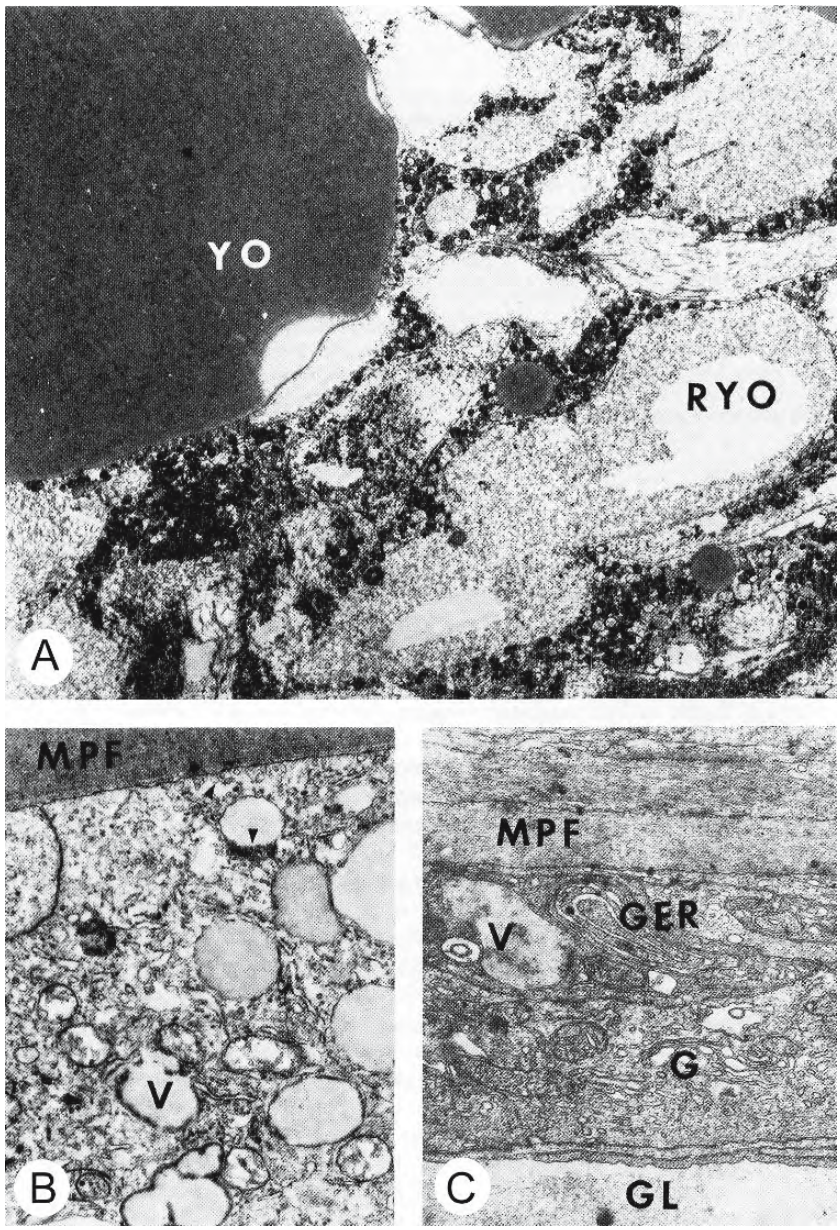

Figure 3.10: Micrographs of sections through atretic follicles of the perch *Perca fluviatilis.* All are electron micrographs except for **D** which is a photomicrograph. (From Lang, 1981b; reproduced with permission of the author).

A. Empty, membrane bordered vesicles (RYO) remain in the oocyte after the resorption of proteinaceous yolk platelets (YO). The ooplasm between these remnants is filled with degenerative mitochondria. X 4,000.

B. The cytoplasm of a follicular cell contains numerous carbohydrate vacuoles (V) whose contents are being resorbed (lower arrowhead) and numerous smooth-surfaced vesicles and pinocytotic elements (upper arrowhead). MPF, basal lamina of the follicular epithelium X 12,400.

C. The cytoplasm of a follicular cell contains a Golgi complex (G), granular endoplasmic reticulum (GER), and carbohydrate vacuoles (V). A temporary gelatinous layer (GL) forms between the zona pellucida and the follicular cells. MPF, basal lamina of the follicular epithelium. X 10,300.

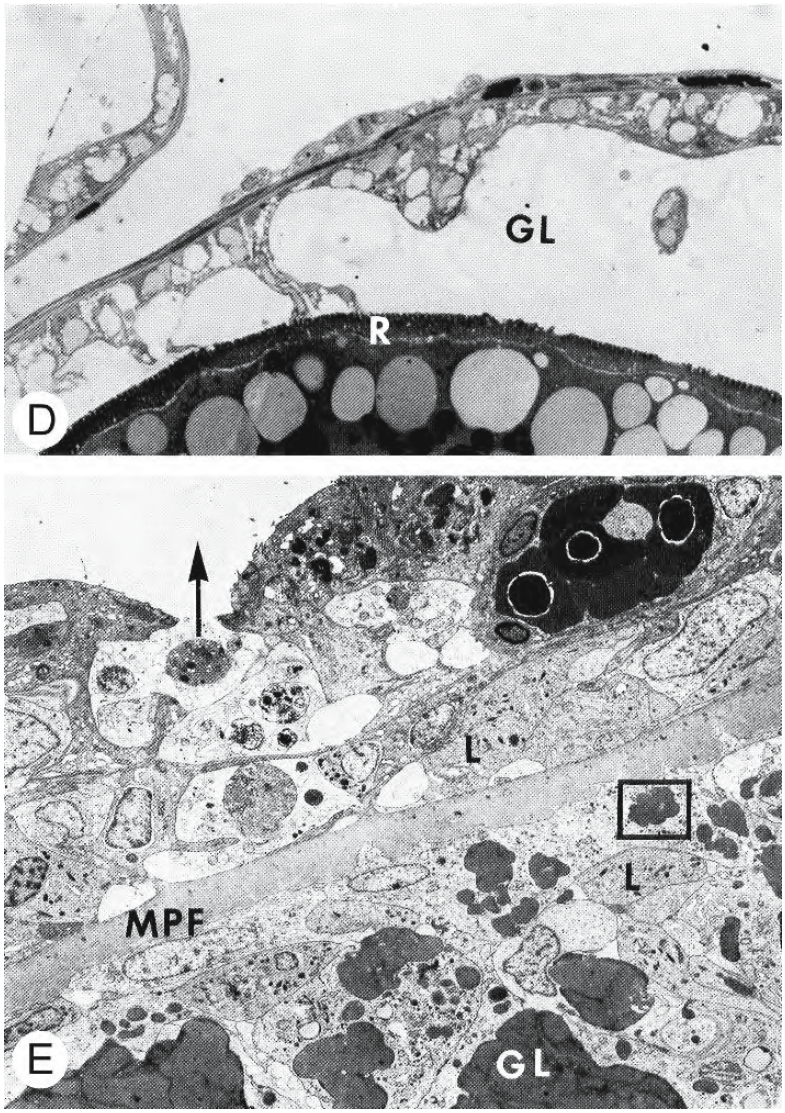

Figure 3.10: Continued.

D. Photomicrograph of the follicular envelope of an atretic oocyte. The follicular cells have invaded the gelatinous layer (GL) and contain large polysaccharide granules. R, zona pellucida. X 280.

E. Section of the follicular envelope of an atretic oocyte. The gelatinous layer (GL) has been fragmented into islets which are being phagocytosed by the follicular cells. Both the theca and follicular epithelium contain leucocytes (L) and wandering cells which discharge their contents into the ovarian lumen (arrow). MPF, basal lamina of the follicular epithelium X 2,600.

F. Atretic oocyte showing remnants of proteinaceous yolk platelets (YO) with lysosomes. X 3,500.

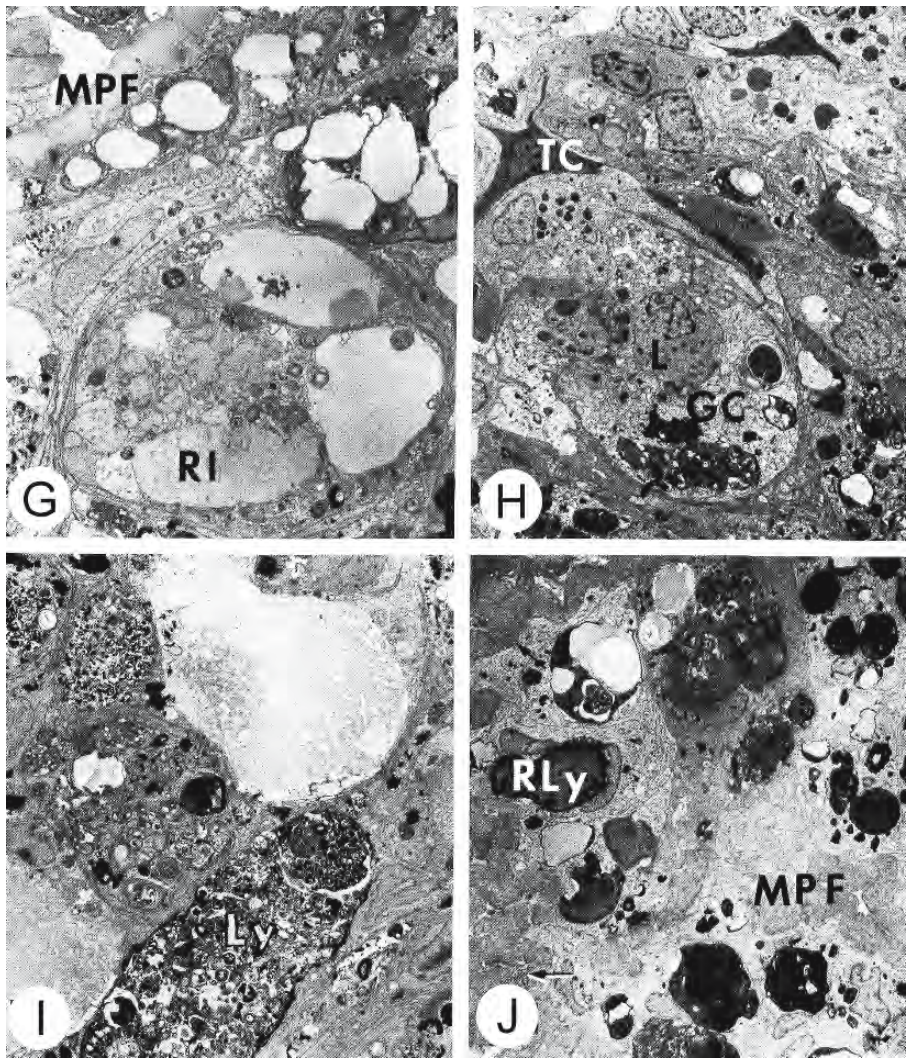

Figure 3.10: Continued.

G - J. These micrographs illustrate degeneration of follicular and thecal cells at a later stage in atresia.

G. Large fragments of the zona pellucida (RI) and other lytic vacuoles are enclosed within "oval bodies". MPF, basal lamina of the follicular epithelium. X 2,300.

H. The interior of the oocyte has been invaded by phagocytic follicular cells (GC), some leucocytes (L), and thecal cells (TC). X 2,300.

I. The contents of the "oval bodies" disintegrate into an accumulation of membranous whorls and myelin figures characteristic of residual bodies of lysosomal breakdown (Ly). X 2,300.

J. Large, lipid-rich residual bodies (RLy) within the granulosa cells are enclosed in disintegrating strands of the of the basal lamina of the follicular epithelium (MPF and arrows). X 1,900.

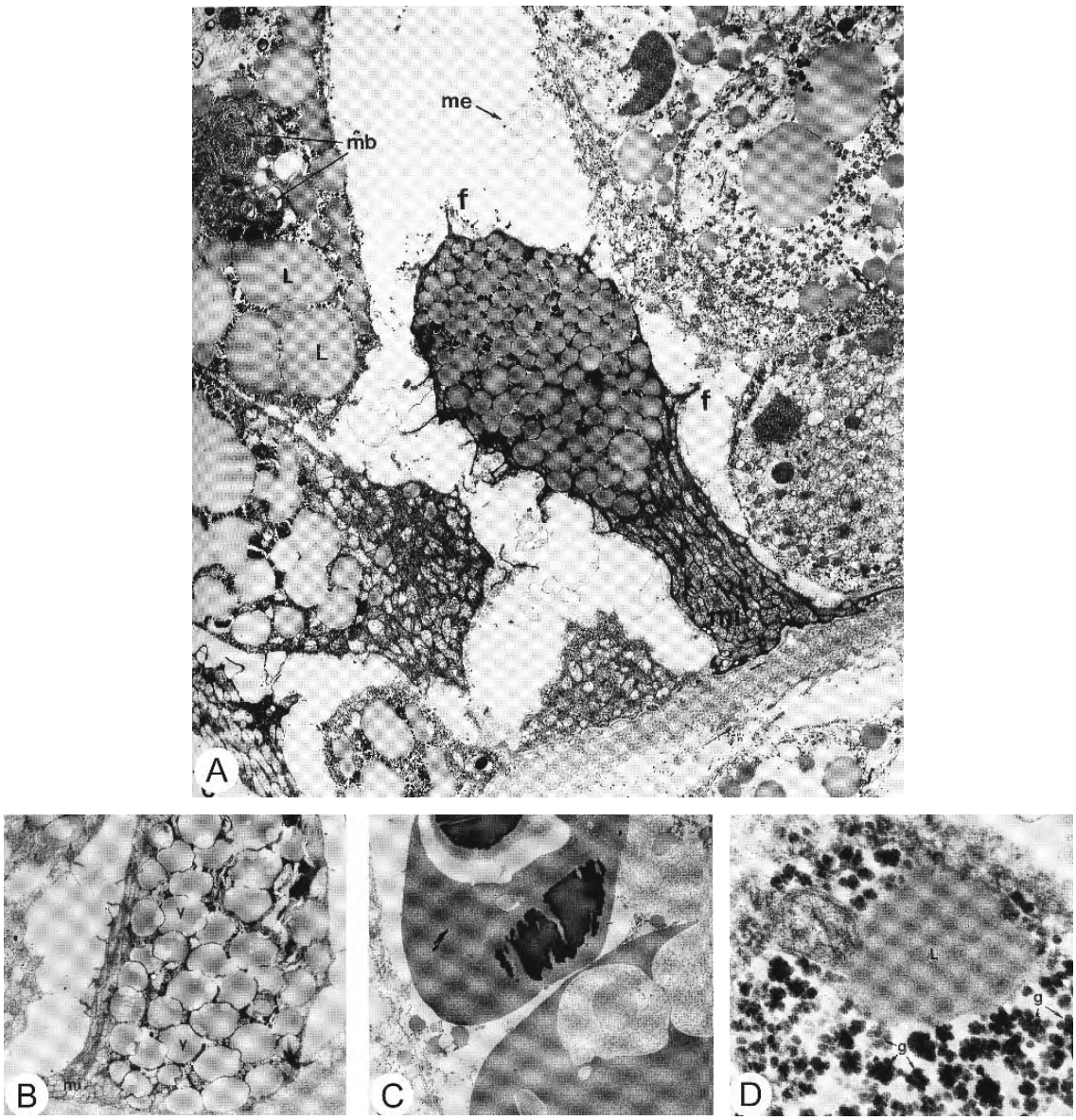

Figure 3.11: Electron micrographs of sections through atretic follicles of the electric ray *Torpedo marmorata.* (From Chieffi Baccari et al., 1992; reproduced with permission from Elsevier Science).

A. In this micrograph, the zona pellucida has disappeared and several follicular cells have invaded the ooplasm. The follicular cells are packed with yolk platelets and their plasma membranes have developed numerous undulating folds (f) which are indicative of their phagocytic activity. Mitochondria (mi) have accumulated in the apical and basal regions. A follicular cell at the upper left is packed with lipid droplets (L) and myelin figures (mb); the lipid droplets are surrounded by rosettes of glycogen. Membranous envelopes (me), remaining from phagocytosed yolk platelets, are scattered throughout the follicular cavity. X 2,520.

B. A follicular cell is packed with phagocytosed yolk platelets (y) enclosed by concentric membranous lamellae. mi, mitochondria X 2,448.

C. Large yolk platelets are undergoing digestion. X 2,448.

D. A final stage in the digestion of a yolk droplet. The lipid (L) and carbohydrate components (glycogen rosettes, g) have become segregated. X 40,800.

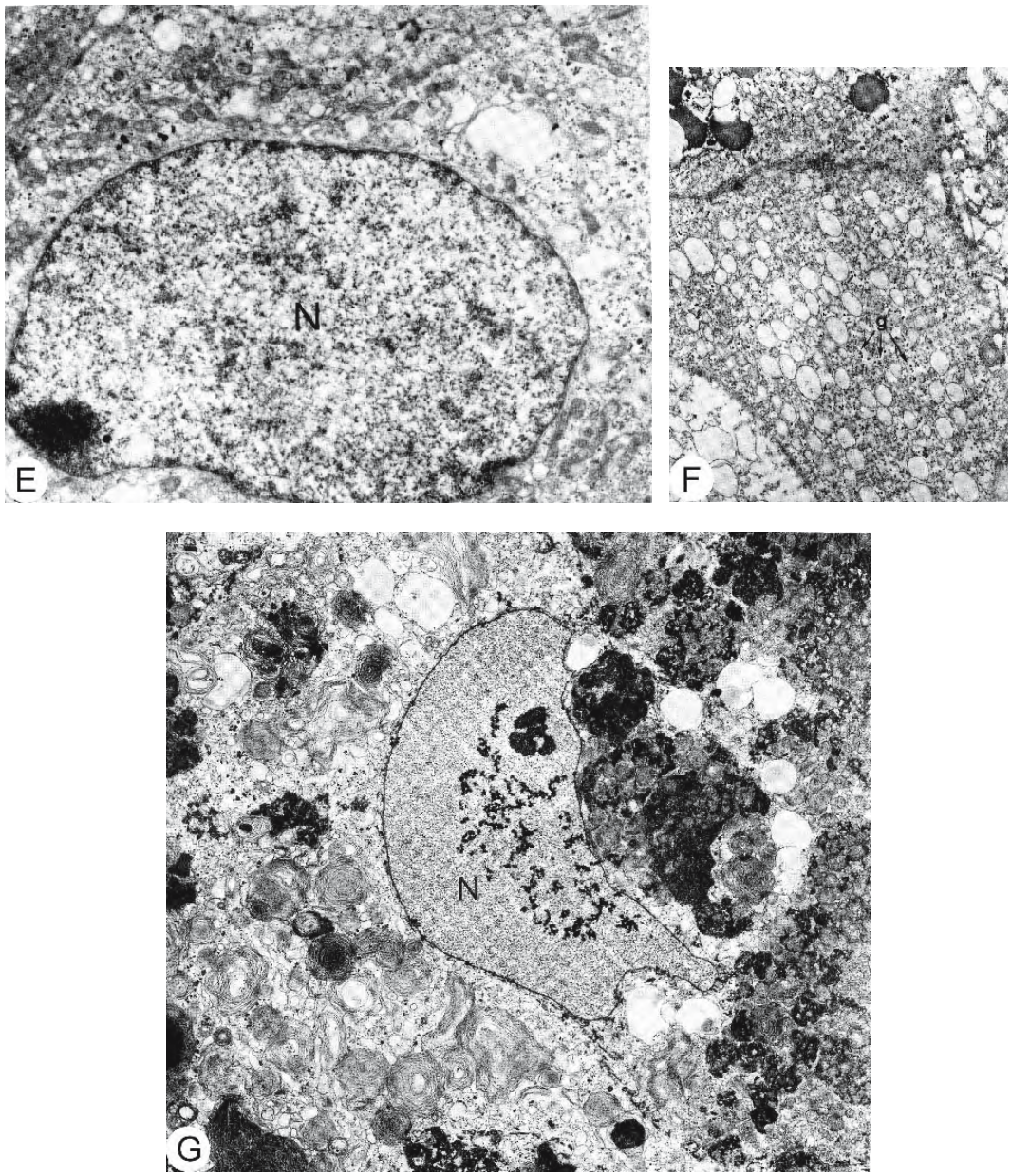

Figure 3.11: Continued.

E. A glandular cell from a late stage atretic follicle contains a euchromatic nucleus (N) and numerous mitochondria with tubular cristae. X 3,600.

F. The cytoplasm of a glandular cell from a late stage atretic follicle is packed with agranular endoplasmic reticulum. g, residual glycogen granules. X 8,500.

G. A degenerating glandular cell from a late stage atretic follicle; note the thickening of the nuclear membrane and the accumulation of membranous whorls and myelin figures in the cytoplasm. N, nucleus. X 2,880.

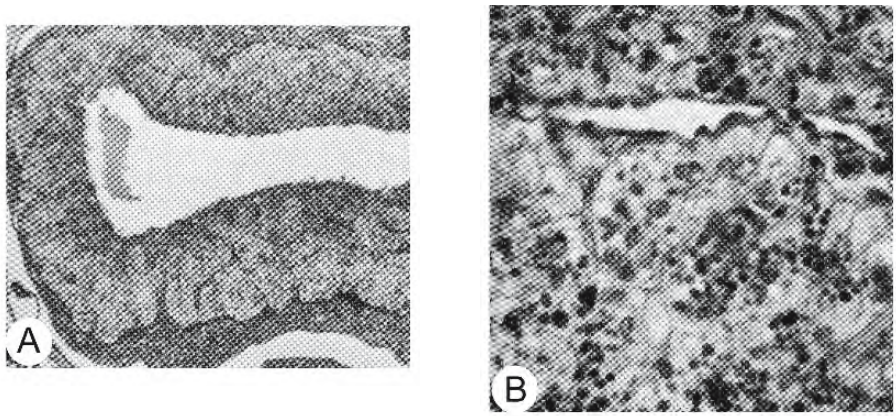

Figure 3.12: Photomicrographs from a section of a preovulatory atretic follicle of the dogfish *Mustelus canis*. When yolk has been removed by phagocytic activity of the follicular cells, adjacent folds of the follicular epithelium fuse. The theca increases in thickness and invades the follicular tissue, becoming the dominant tissue. (From TeWinkel, 1972; © reproduced with permission of John Wiley & Sons, Inc.).

A. Fusion of the folds of the follicular epithelium and thickening of the theca has occurred. X 40.

B. The same section at higher magnification shows pale follicular cells at the bottom and darker thecal cells, packed with granules, above. X 450.

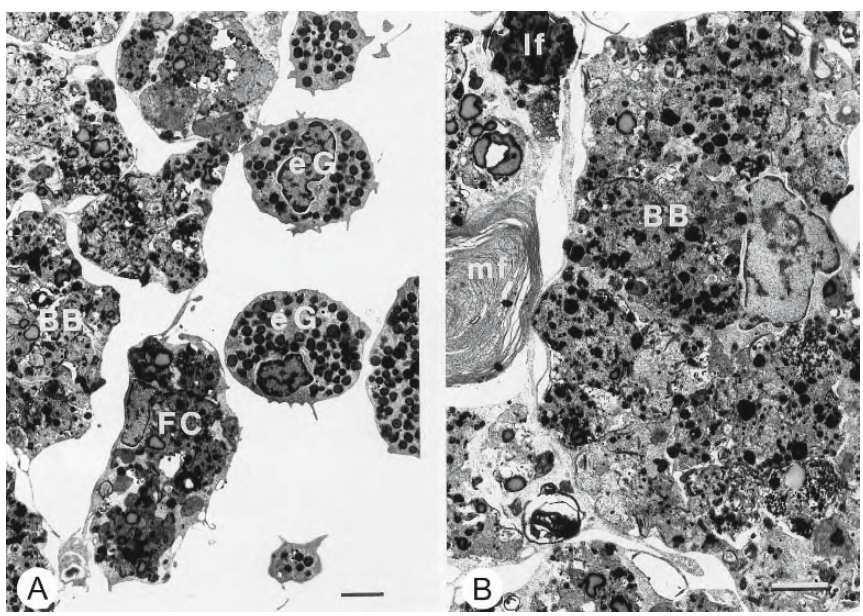

Figure 3.13: Electron micrographs of lipofuscin pigment in bodies remaining from follicular breakdown in the ovary of the striped bream *Lithognathus mormyrus*. Bars = 2 μm (From Besseau and Faliex, 1994; reproduced with permission from Springer-Verlag).

A. Eosinophilic granulocytes (eG) and follicular cells (FC) are seen in the region of follicular breakdown. Lipofuscin pigment is seen within a degenerative body (BB). X 4,300.

B. Myelin figures (mf) and degenerative bodies (BB) containing lipofuscin pigment (lf) remain after follicular breakdown. X 5,700.

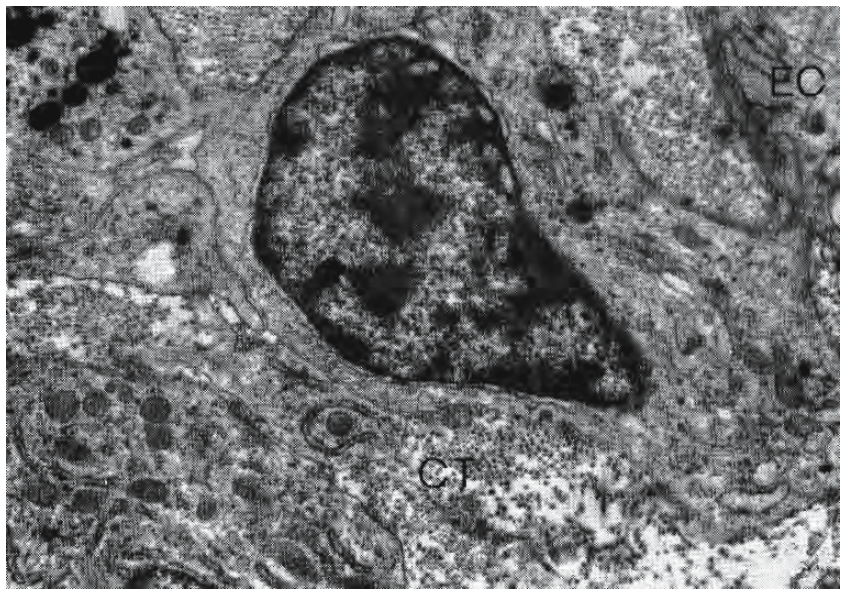

Figure 3.14: Electron micrograph of a section of an atretic follicle in the ovary of the hagfish *Eptatretus stouti.* Thecal cells contain lysosomes, colloid droplets, granular endoplasmic reticulum, Golgi complex, and mitochondria. X 12,200 (From Tsuneki and Gorbman, 1977; reproduced with kind permission of Blackwell Publishing).
Abbreviations: CT, connective tissue; EC, endothelial cell.

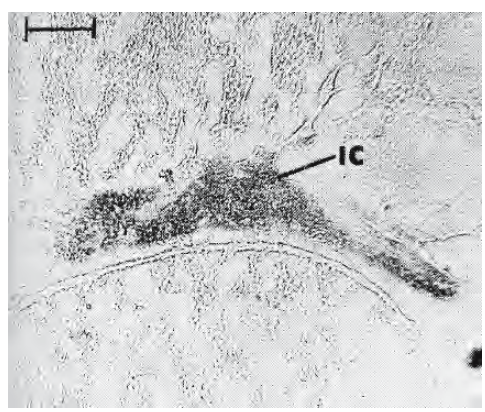

Figure 3.15: Photomicrograph of a cryostat section of the ovary of the catfish *Mystus cavasius* stained to show 11β-HSD (11β-hydroxysteroid dehydrogenase) activity in the interstitial gland cells (IC). Bar = 100 μm (From Saidapur and Nadkarni, 1976; reproduced with permission from Elsevier Science).

Figure 3.16: Micrographs of sections of postovulatory follicles of the teleost *Astyanax bimaculatus lacustris* illustrating programmed cell death or apoptosis. (From Drummond et al., 2000; © reproduced with permission of John Wiley & Sons, Inc.).
A. Photomicrograph of a section taken a few hours after spawning; the follicular cells (F) have undergone hypertrophy. The arrow indicates a micropylar cell. X 590.

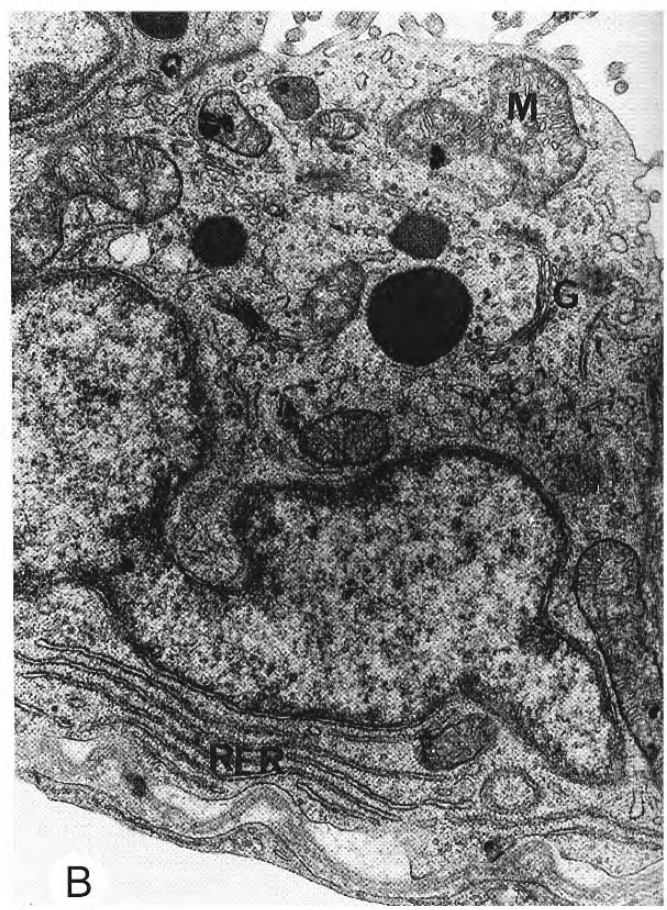

Figure 3.16: Continued.
B. Electron micrograph of a hypertrophied follicular cell showing the organelles characteristic of protein synthesis: well developed granular endoplasmic reticulum (RER), Golgi complex (G), and mitochondria (M). X 18,740.

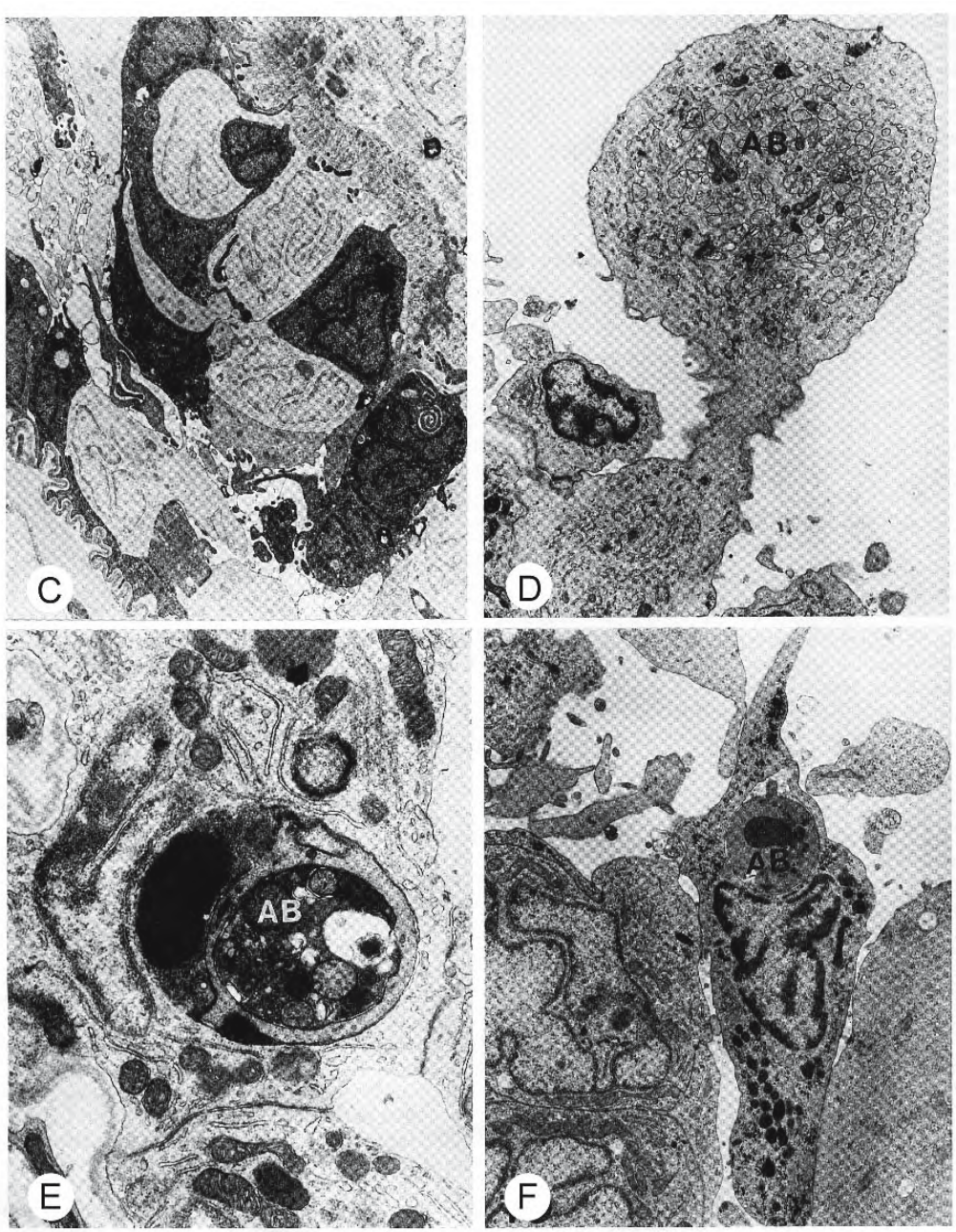

Figure 3.16: Continued.

C. Electron micrograph of follicular cells fixed with tannic acid. Dark cells with electron dense cytoplasm may be slated for disintegration. X 5,060.

D. Electron micrograph of a follicular cell destined for destruction. The cell releases large, organelle-filled blebs, the apoptopic bodies (AB), into the lumen of the follicle. 7,900.

E. Electron micrograph of the final stage of apoptosis where an apoptopic body (AB) is being phagocytosed by a normal follicular cell. X 22,500.

F. Electron micrograph of a granular macrophage in the lumen of a postovulatory follicle during involution. A possible phagocytosed apoptopic body (AB) is contained within the cytoplasm. X 7,900.

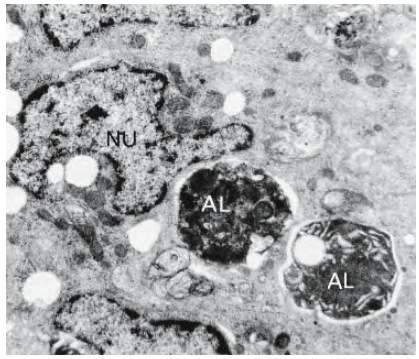

Figure 3.17: Electron micrograph of a part of a phagocytic follicular cell from a postovulatory follicle of the African catfish *Clarias gariepinus.* The cell contains autophagic vacuoles (AL). NU, nucleus. X 6,200 (From van den Hurk and Peute, 1985; reproduced with permission of the authors).

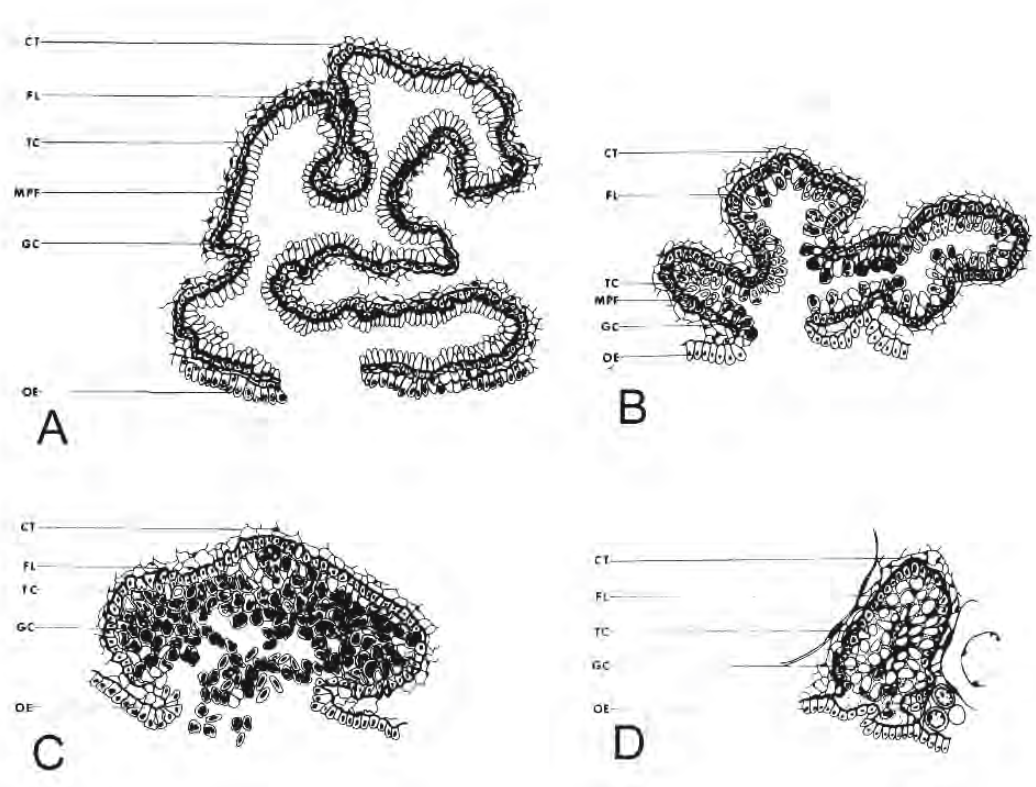

Figure 3.18: Schematic drawings illustrating four stages in the transformation of a postovulatory follicle of the perch *Perca fluviatilis.* (From Lang, 1981a; reproduced with permission from Elsevier Science).

A. Reorganization phase following ovulation.

B. Vacuolar phase where the follicle prepares itself for secretion.

C. Globular phase where follicular cells assume the appearance of steroidogenesis.

D. Regression phase: degeneration of the follicular cells remaining after secretion.

Abbreviations: CT, connective tissue; FL, fibrillar layer; GC, follicular cell; MPF, basement membrane of the follicular epithelium; OE, ovarian epithelium; TC, thecal cell.

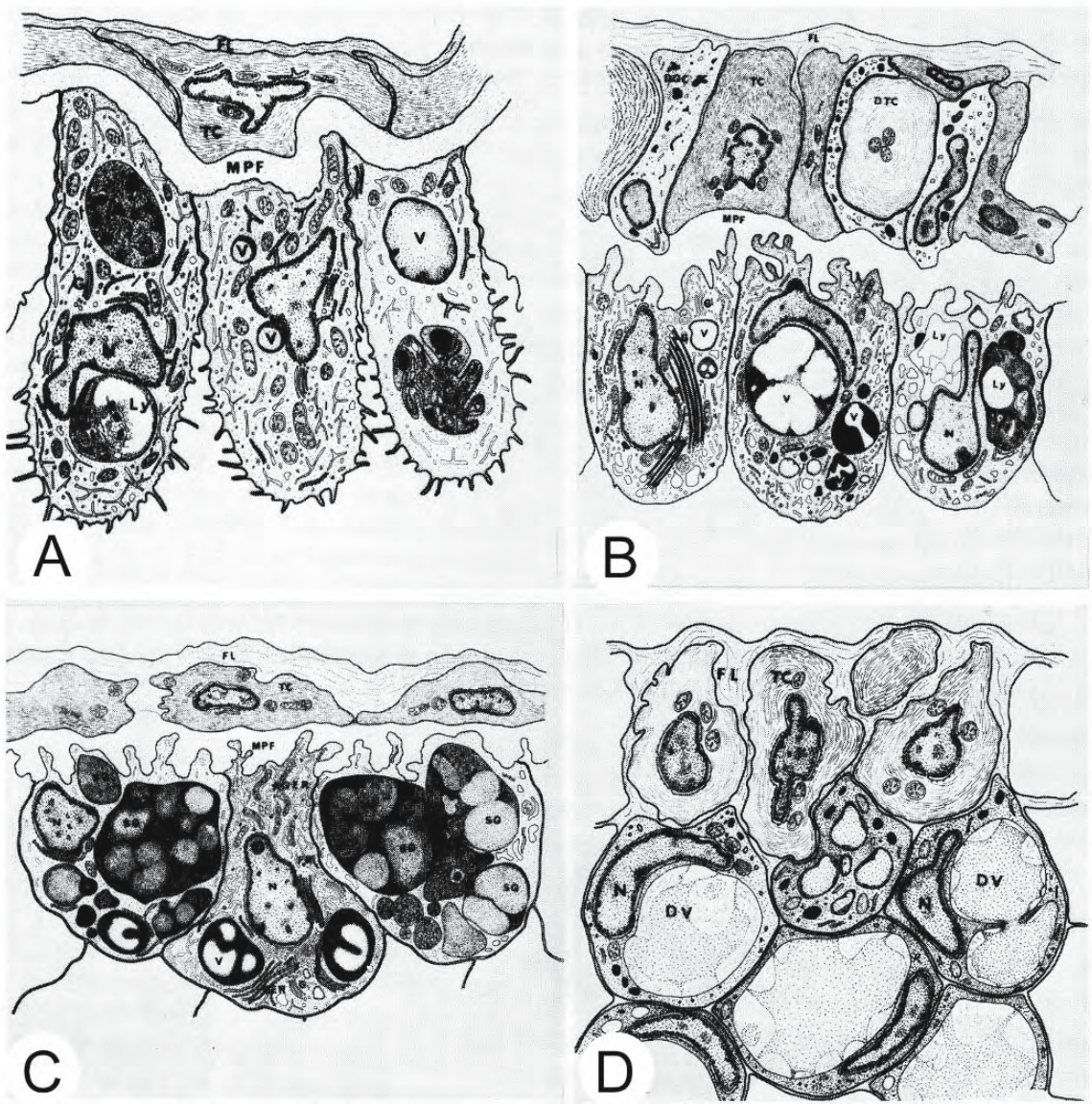

Figure 3.19: Schematic drawings illustrating the follicular envelopes at four stages in the transformation of a postovulatory follicle of the perch *Perca fluviatilis.* (From Lang, 1981a; reproduced with permission from Elsevier Science).

A. Reorganization phase. The follicular cells contain large autophagic vesicles (LY).

B. Vacuolar phase. Some follicular cells still contain lysosomes (LY) and degenerative cytoplasm but most cells contain well-differentiated cytoplasm with agranular endoplasmic reticulum.

C. Globular phase. Some granular and agranular endoplasmic reticulum is present within the follicular cells. Most of these cells contain vacuoles of proteinaceous and cholesterol-related material.

D. Regression phase. The remaining follicular cells contain large vacuoles of acid mucopolysaccharides (DV). The follicular basement membrane has disappeared.

Abbreviations: AGER, agranular endoplasmic reticulum; DGC, degenerative follicular cell; DTC, degenerative thecal cell; FL, fibrillar layer; FR, free ribosomes; G, Golgi complex; GER, granular endoplasmic reticulum; MPF, follicular basement membrane; N, nucleus; SG, vacuoles of proteinaceous and cholesterol-related material; TC, thecal cell; V, acid mucopolysaccharide vacuoles.

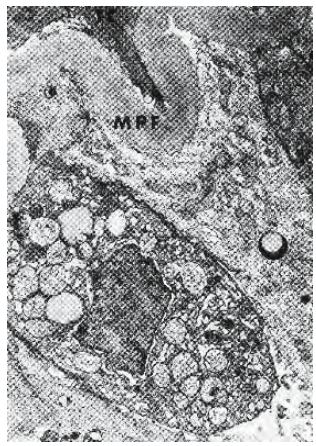

Figure 3.20: Electron micrograph of a section of a postovulatory follicle of the perch *Perca fluviatilis* showing two types of follicular cells one hour after ovulation. The lower cell is phagocytic and contains lysosomes. The upper, lighter cell contains mitochondria and agranular endoplasmic reticulum. MPF, follicular basement membrane. X 4,420. (From Lang, 1981a; reproduced with permission from Elsevier Science).

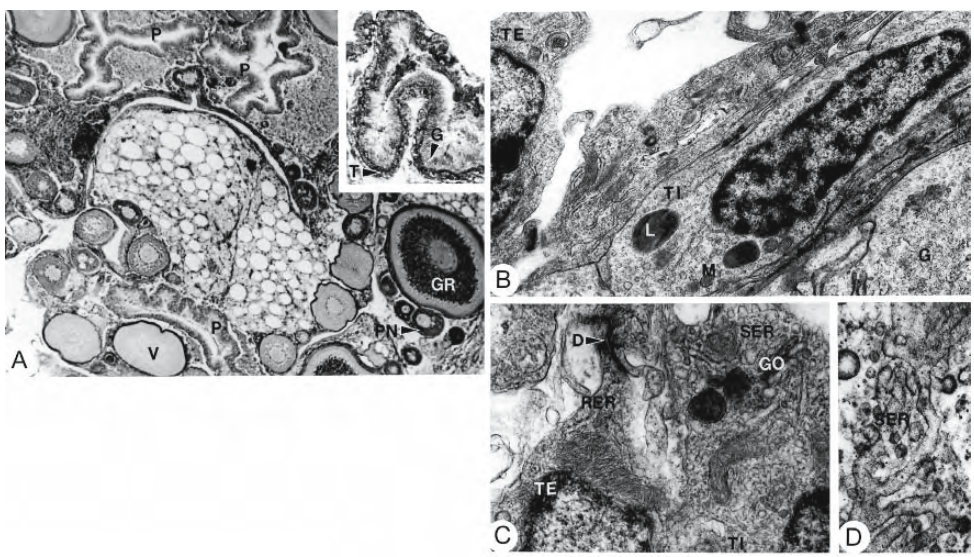

Figure 3.21: Micrographs of sections of postovulatory follicles of tilapia *Oreochromis mossambicus* one day after spawning. **A** is a photomicrograph; **B**, **C**, and **D** are electron micrographs. (From Smith and Haley, 1987; reproduced with permission of the authors).

A. Several postovulatory follicles (P), previtellogenic oocytes of the perinucleolar stage (PN), oocytes at the yolk vesicle stage (V), and an oocyte at the yolk granule stage (GR) can be seen. X 68. The inset shows a postovulatory follicle at a higher magnification with its outer thecal layer (T) and inner follicular layer (G). X 190.

B. Wide spaces exist between cells of the theca externa (TE). Although a cell of the theca interna (TI) contains lipid droplets (L), it has a fibroblastic, not steroidogenic, appearance. G, follicular cell; M, mitochondria with lamellar cristae. X 15,000.

C. Cell of the theca externa (TE) attached by a desmosome (D) to a cell of the theca interna (TI) containing agranular endoplasmic reticulum (SER). GO, Golgi complex; RER, granular endoplasmic reticulum. X 30,000.

D. Tubular agranular endoplasmic reticulum (SER) from a special thecal cell. X 90,000.

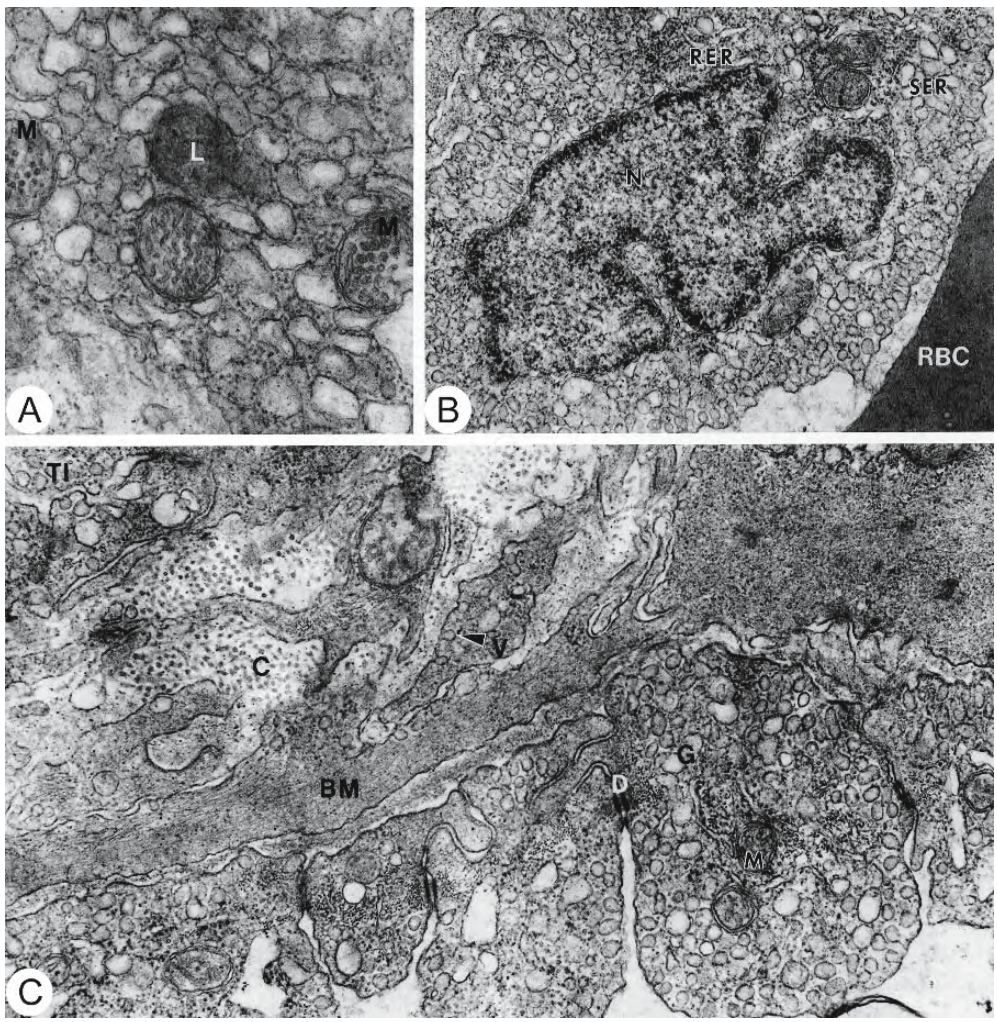

Figure 3.22: Electron micrographs of sections of postovulatory follicles of tilapia *Oreochromis mossambicus* one day after spawning. (From Smith and Haley, 1987; reproduced with permission of the authors).

A. Mitochondria (M) with tubular cristae in a cell of the theca interna. L, lipid droplet. X 80,000.

B. Follicular cell with basal granular endoplasmic reticulum (RER) and subapical agranular endoplasmic reticulum (SER). RBC, a red blood cell in the follicular lumen. X 45,000.

C. Collagenous fibres (C) course between the theca interna (TI) and the follicular basal lamina (BM). The follicular cells (G) contain agranular endoplasmic reticulum. D, desmosomes; M, mitochondria with lamellar cristae; V, vesicle. X 40,000.

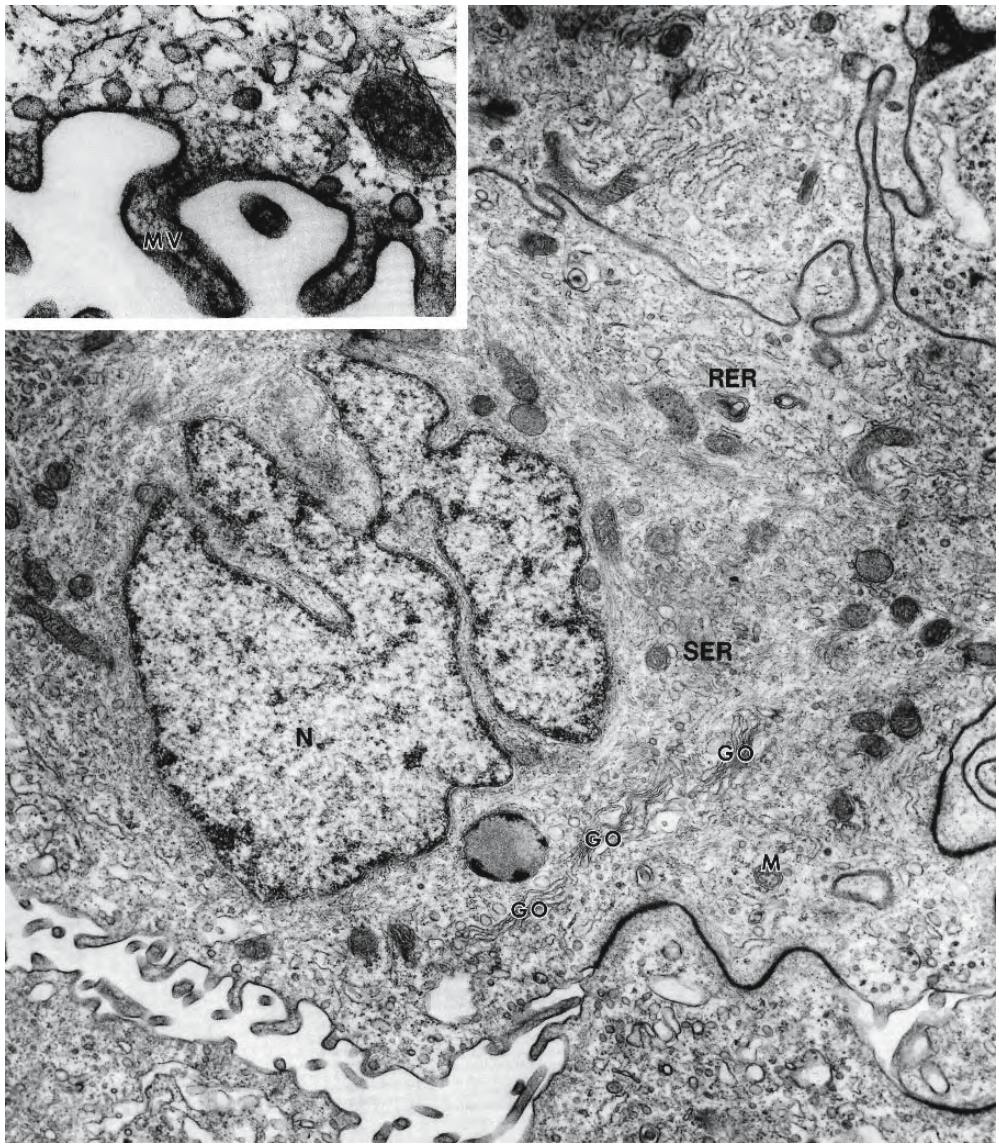

Figure 3.23: Electron micrographs of a section of a follicular cell from a postovulatory follicle of tilapia *Oreochromis mossambicus* six days after spawning. The cell contains basal granular endoplasmic reticulum (RER), tubular agranular endoplasmic reticulum (SER), and three Golgi complexes (GO) near the nucleus (N). M, mitochondrion with tubular cristae. X 18,500 The inset shows microvilli (MV) and vesicles at the apical plasma membrane. X 60,000 (From Smith and Haley, 1987; reproduced with permission of the authors).

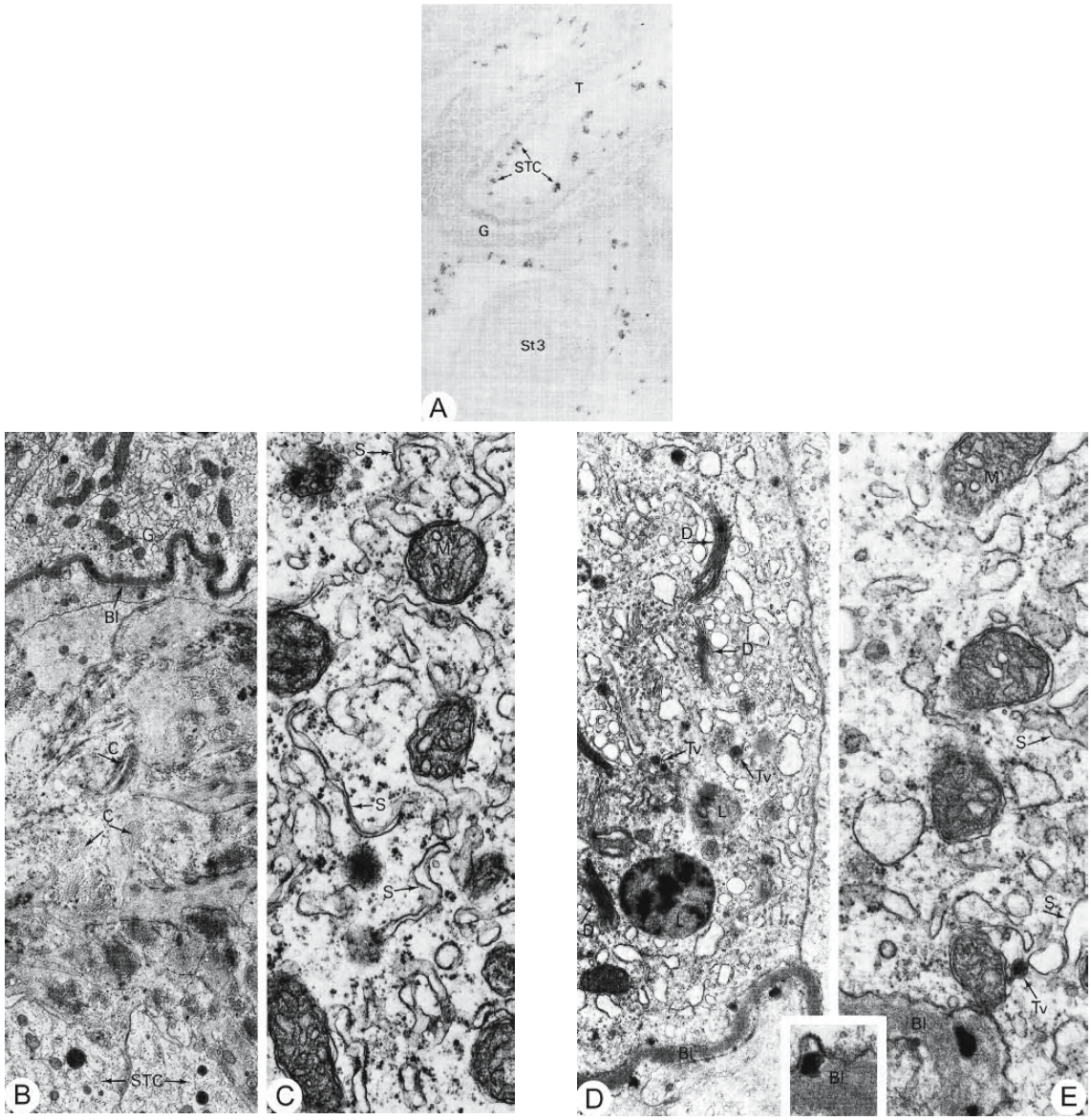

Figure 3.24: Micrographs of sections of postovulatory ovaries of the rainbow trout *Salmo gairdneri.* (From van den Hurk and Peute, 1979; reproduced with permission of the author).

A. Photomicrograph of a section stained to show 3β-hydroxysteroid dehydrogenase (3β-HSD) activity. Strong activity is present in large numbers of special thecal cells (STC) arranged around a young postovulatory follicle but only weak activity in the follicular cells (G). St3, previtellogenic follicle; T, theca. X 560.

Figures **B** to **E** are transmission electron micrographs.

B. Follicular wall of a young postovulatory follicle. A follicular cell (G) at the top is separated from a special thecal cell (STC) by the follicular basal lamina (Bl) and fibrous connective tissue (C) of the thecal layer. X 5,500.

C. The cytoplasm of a special thecal cell contains abundant agranular endoplasmic reticulum (S) and mitochondria (M) with tubular cristae. X 34,000.

D. A follicular cell of a young postovulatory follicle contains Golgi complexes (D), transport vesicles (Tv), and lysosomes (L). Bl, basal lamina X 13,000.

E. This follicular cell from a young postovulatory follicle contains agranular endoplasmic reticulum (S) and mitochondria (M) with tubular cristae and appears to be steroidogenic. The inset shows exocytotic activity next to the basal lamina of the follicular cell. Tv, transport vesicle. X 34,000.

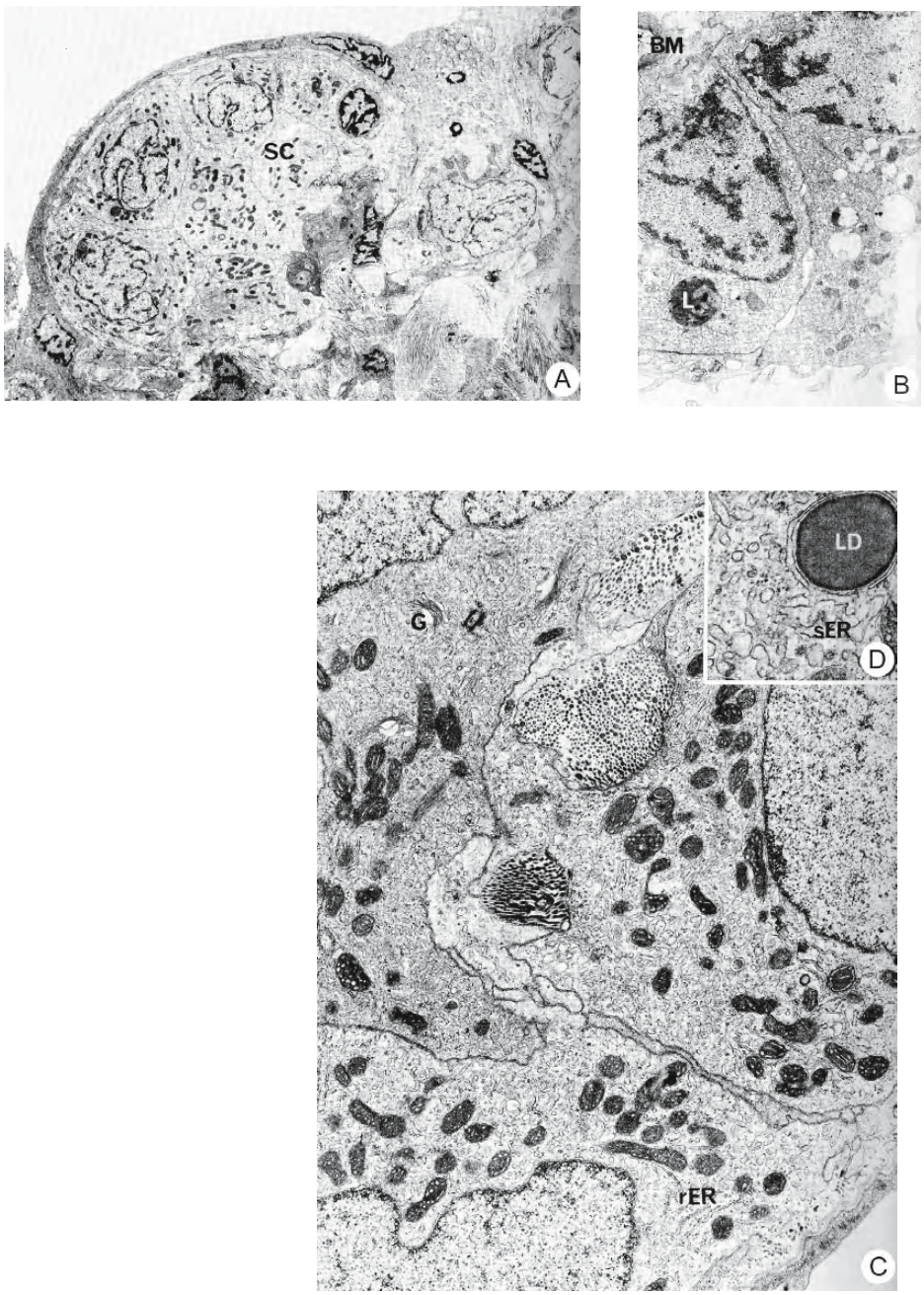

Figure 3.25: Transmission electron micrographs of sections from postovulatory follicles of mature coho *Oncorhynchus kisutch.* (From Nagahama, Clarke, and Hoar, 1978; reproduced with permission of the NRC Press).

A. Special thecal cells (SC) form a cluster close to the serosal epithelium. X 3,200.

B. Degenerate follicular cells. BM, follicular basal lamina; L, lysosome. X 8,000.

C. Special thecal cell showing extensive agranular endoplasmic reticulum and large mitochondria with tubular cristae. G, Golgi complex, rER, granular endoplasmic reticulum. X 12,000.

D. Portion of a special thecal cell containing extensive agranular endoplasmic reticulum (sER) and a lipid droplet (LD). X 40,000.

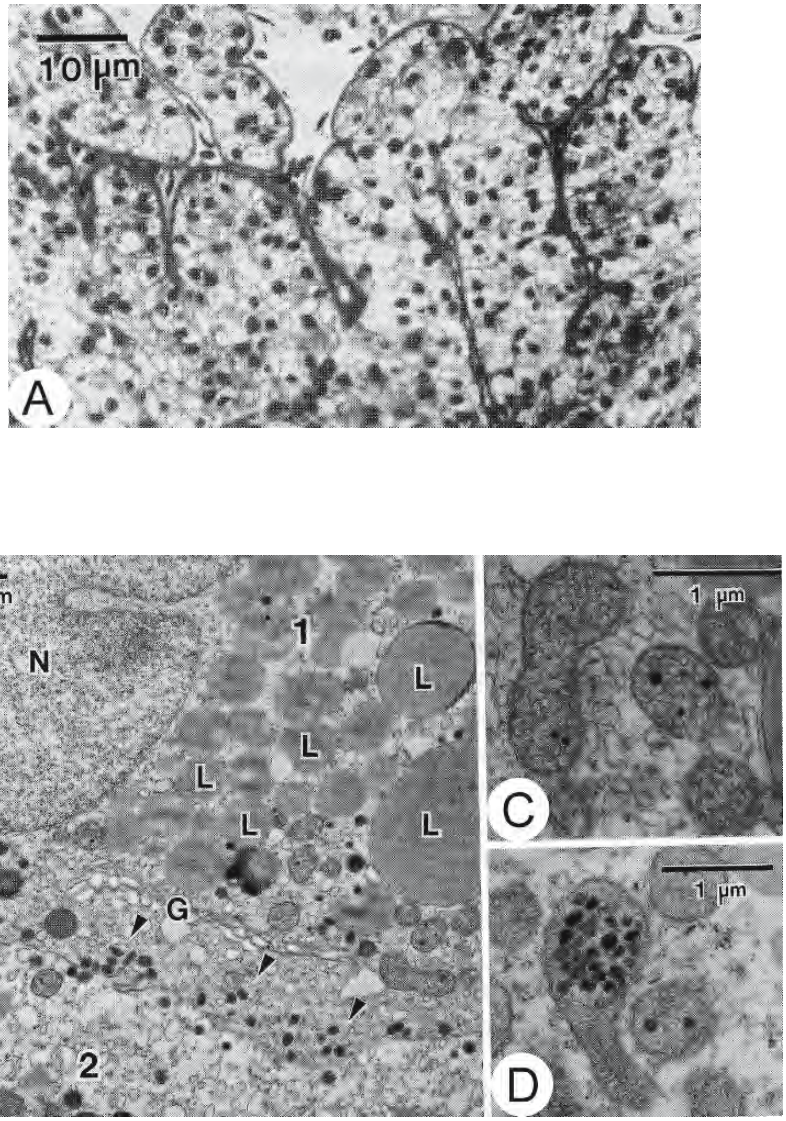

Figure 3.26: Micrographs of sections of corpora lutea of the spiny dogfish *Squalus acanthias.* (From Koob and Callard, 1991; with permission S. Karger AG, Basel).

A. Photomicrograph of cells filled with lipid droplets forming the bulk of the corpus luteum. The cells are derived from the follicular epithelium and have large nuclei with conspicuous nucleoli. Partitions between these cells are derived from the follicular basal lamina and thecal connective tissue. Bar = 10 µm.

B. Electron micrograph of two luteal cells (1,2) from **A**. Abundant lipid droplets (L) and small granules (arrowheads) pack the cytoplasm. G, Golgi complex; N. nucleus. Bar = 1 µm.

C,**D**. Mitochondria from corpus luteum shown in **B**. Bar = 1 µm.

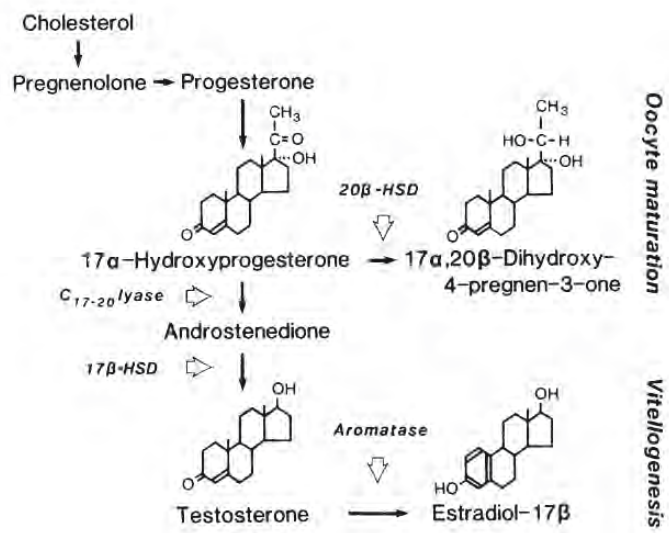

Figure 3.27: Pathway of steroid biosynthesis in the ovary of salmonids. 17β-HSD = 17β-hydroxysteroid dehydrogenase; 20β-HSD = 20β-hydroxysteroid dehydrogenase. (From Nagahama, 1987; reproduced with permission from the Zoological Society of Japan).

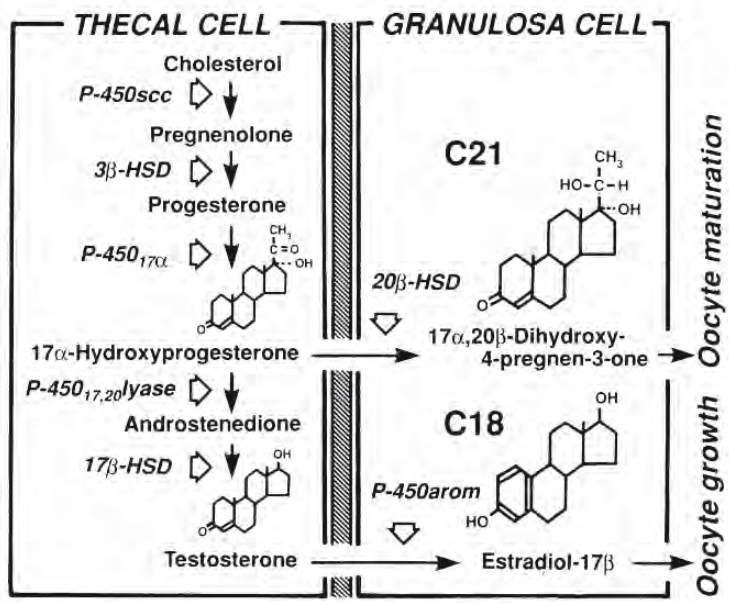

Figure 3.28: A two-cell model for the pathway of steroid biosynthesis in the ovarian follicle of salmonids during oocyte growth and maturation, showing the relative contribution of thecal and follicular (granulosa) cell layers in the production of oestradiol-17β and 17α,20β-dihydroxy-4-pregnen-3-one (17α,20β-DP). (From Nagahama et al., 1994; reproduced with permission from Elsevier Science).

Abbreviations: P-450scc, cholesterol side-chain cleavage cytochrome P-450; 3β-HSD, 3β-hydroxysteroid dehydrogenase-isomerase; P-450$_{17\alpha}$, P-450 17α-hydroxylase; 17β-HSD, 17β-hydroxysteroid dehydrogenase; P-450arom, aromatase cytochrome P-450; 20β-HSD, 20β-hydroxysteroid dehydrogenase.

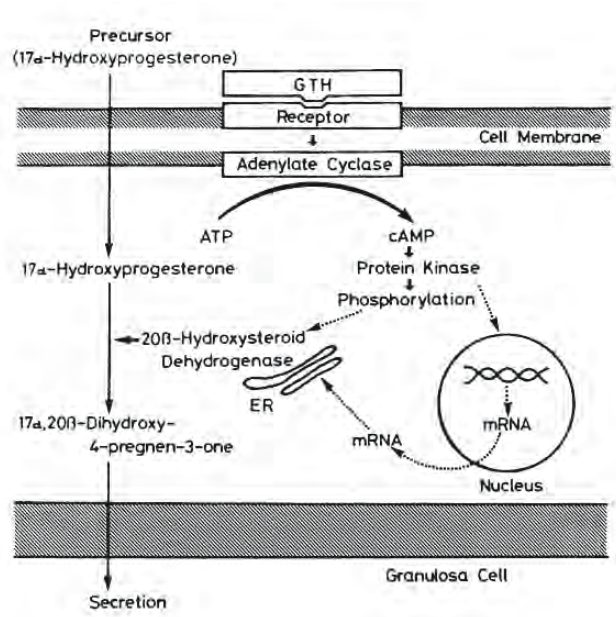

Figure 3.29: A diagram to illustrate the receptor-adenylate cyclase-cyclic AMP mechanism for activation of a follicular (granulosa) cell in the amago salmon by 20β-HSD (20β-hydroxysteroid dehydrogenase). (From Nagahama, 1984; reproduced with permission of the author).

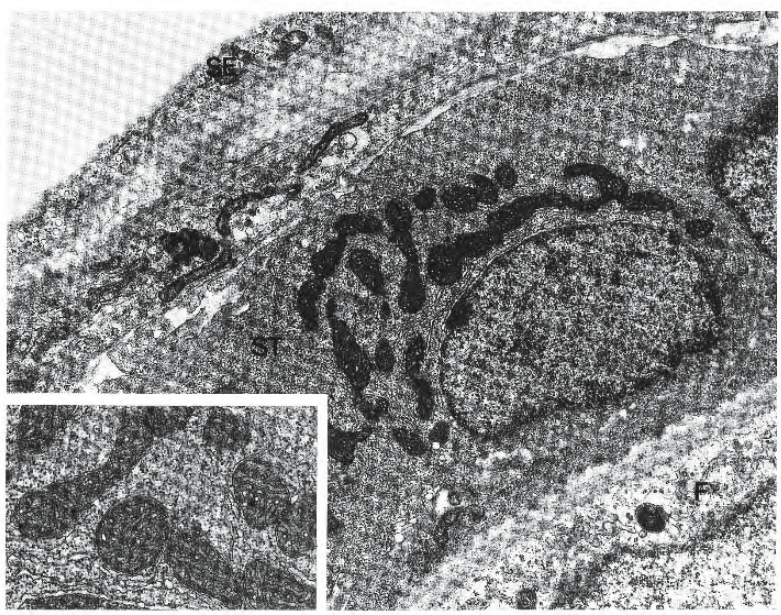

Figure 3.30: Electron micrograph of a special thecal cell (ST) within the theca of a late cortical alveolus-stage follicle of *Brachydanio rerio*. The cell contains profiles of agranular endoplasmic reticulum and abundant mitochondria. X 11,600 The **inset** shows that some mitochondria are packed with tubular cristae in a dense matrix. X 23,200 (From Selman et al., 1993; © reproduced with permission of John Wiley & Sons, Inc.).

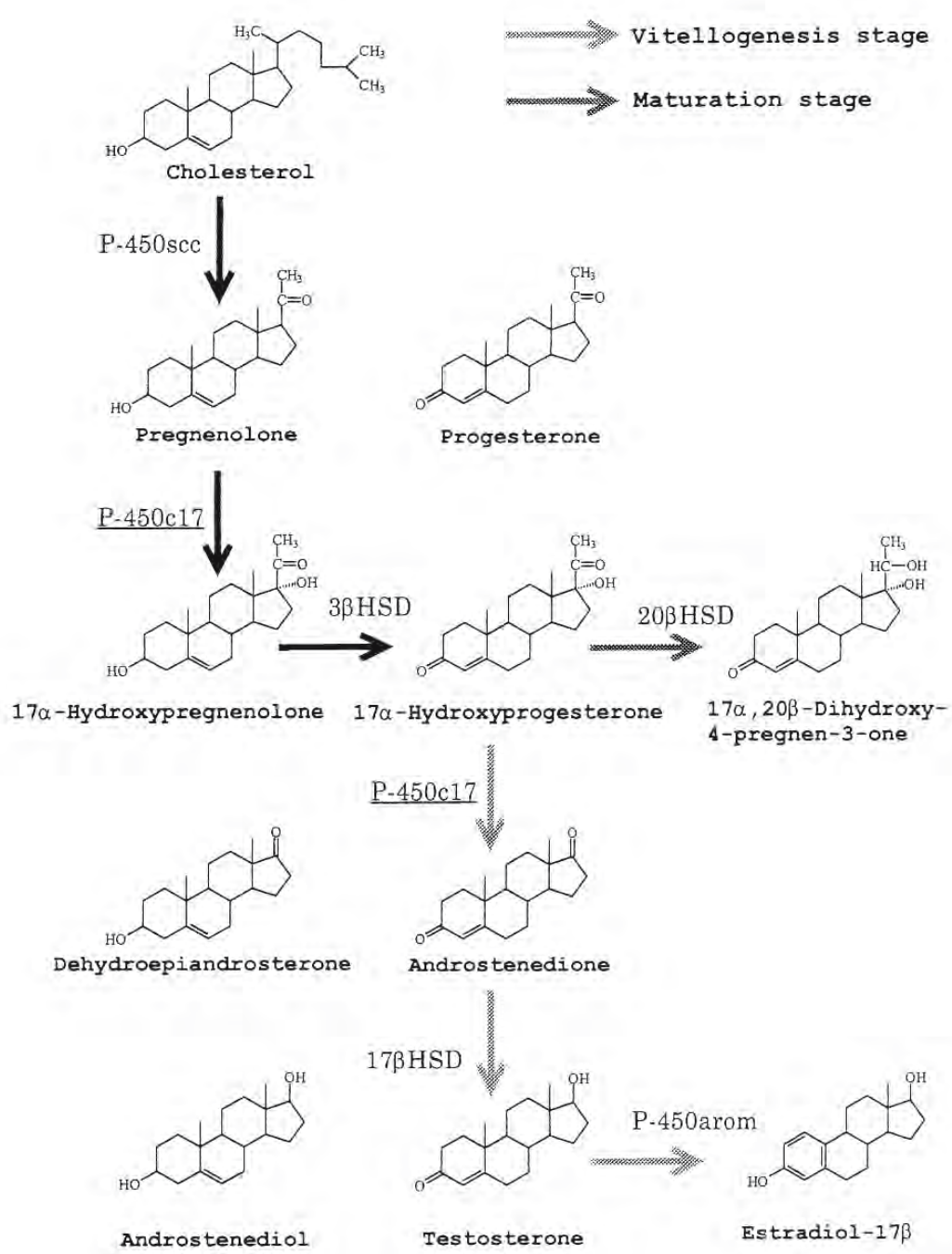

Figure 3.31: Steroidogenic pathways of ovarian oestradiol-17β and biosynthesis of 17α,20β-dihydroxy-4-pregnen-3-one in ovarian follicles of the medaka during vitellogenesis and oocyte maturation. (From Kobayashi et al., 1996; reproduced with permission from the Zoological Society of Japan).

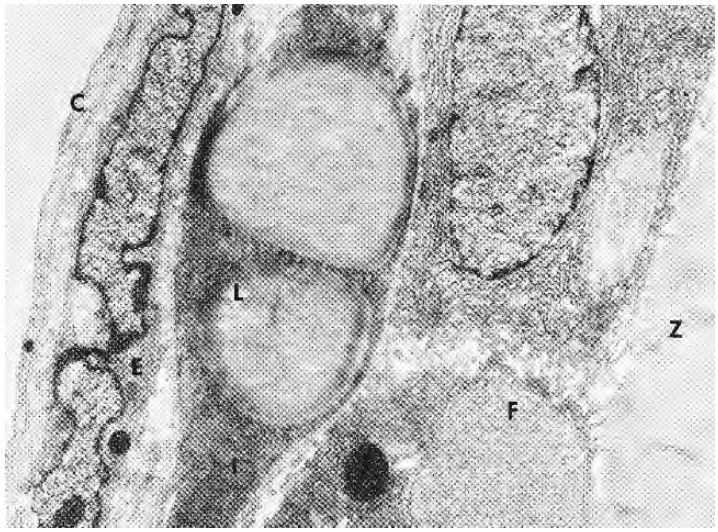

Figure 3.32: Electron micrograph of a section through the follicular wall from the ovary of the lamprey *Peteromyzon marinus*. The section includes the zona pellucida (Z) at the right, follicular cells (F), theca interna (I), theca externa (E), and the coelomic epithelium (C). Large lipid droplets (L) distend a cell of the theca interna. X 9,600 (From Weisbart, Youson, and Wiebe, 1978; reproduced with permission from Elsevier Science).

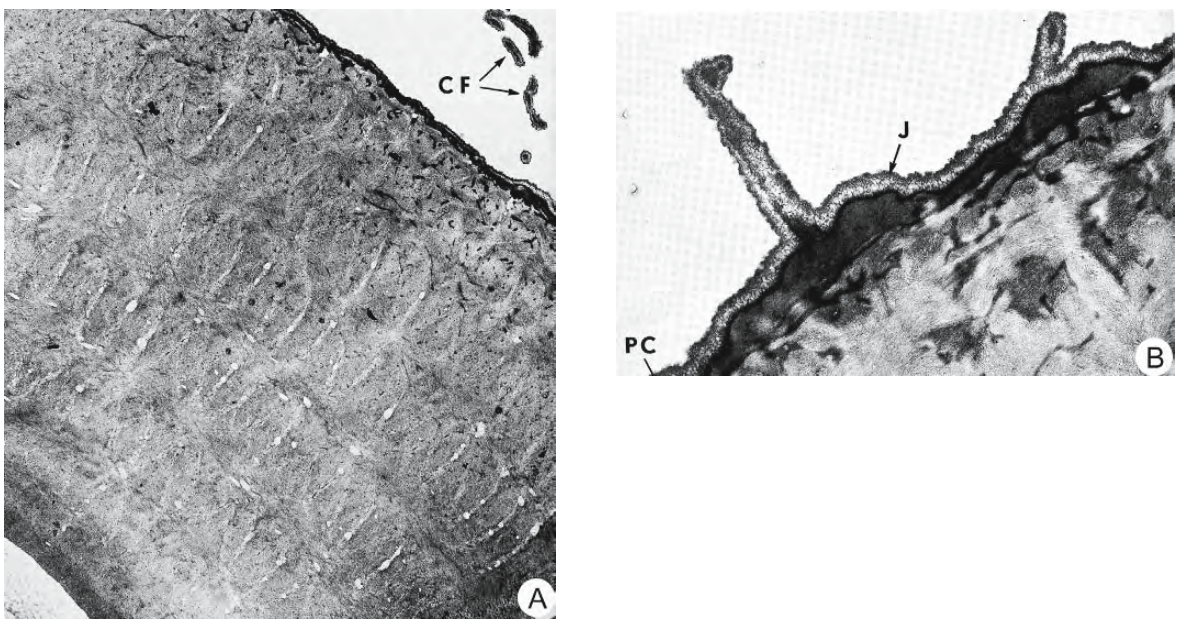

Figure 3.33: Electron micrographs of sections through the chorion of an ovulated egg of *Fundulus heteroclitus*. (From Dumont and Brummett, 1980; reproduced with permission of Wiley-Liss, Inc., a subsidiary of John Wiley & Sons, Inc.).

A. As vitellogenesis ends and the oocyte is ready for ovulation, the zona pellucida changes to become the chorion. The elaborate fibrillar patterns of this primary envelope have largely disappeared and the pore canals are almost totally obliterated. The envelope is more compact and has assumed a woven appearance. At the lower left corner, the envelope is lined by a film of less dense material; it is covered by a thin layer of electron-dense jelly. CF, chorionic fibrils. X 5,100.

B. The transformed primary envelope is covered by a spongy appearing jelly-like secondary envelope (J) that is elaborately ornamented. The external opening of a pore canal (PC) is plugged. X 14,500.

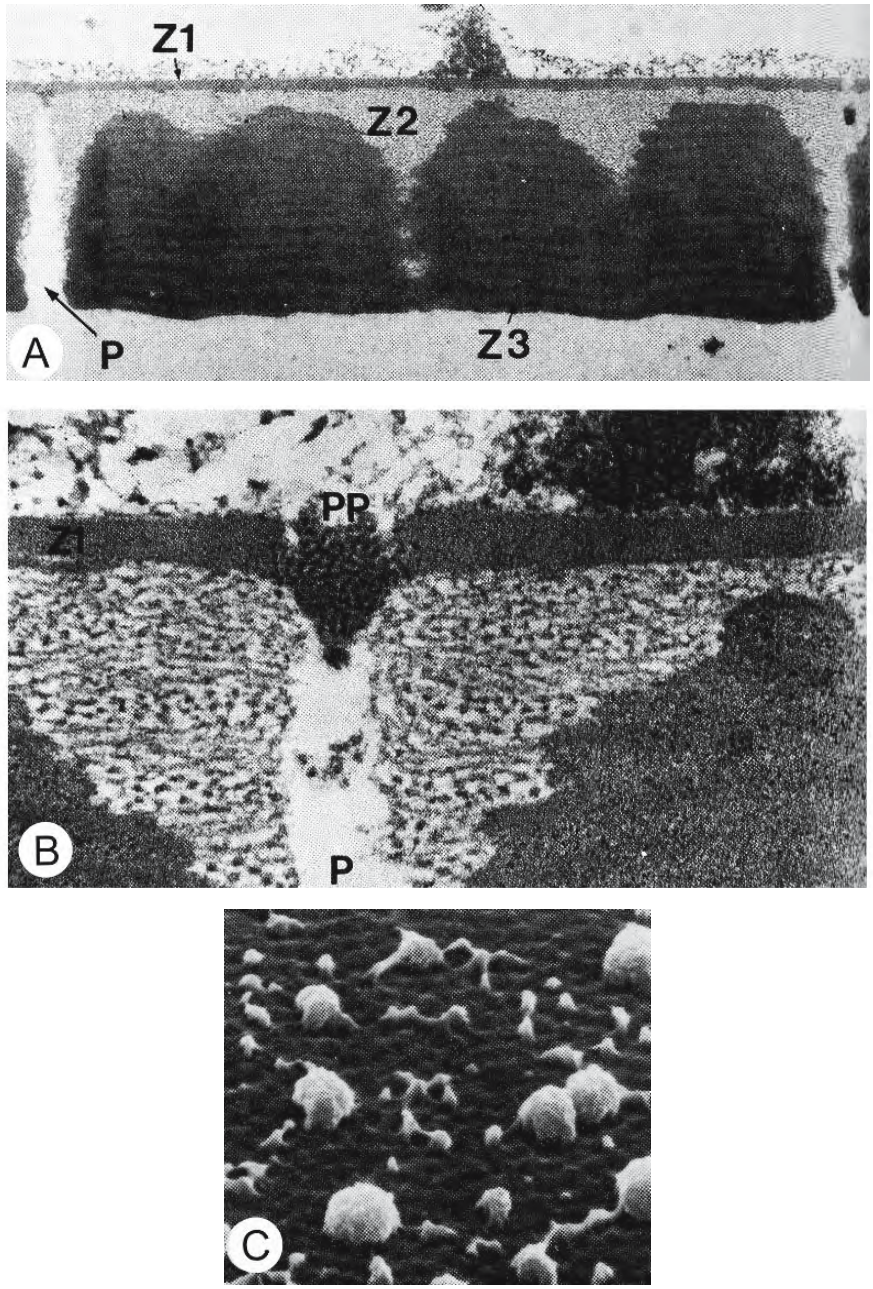

Figure 3.34: Electron micrographs of the chorion of the egg of *Brachydanio rerio.* (From Hart and Donovan, 1983; © reproduced with permission of John Wiley & Sons, Inc.).

A. Transmission electron micrograph of a section through the chorion of an unfertilized egg showing the outer, electron-dense zone (Z1), middle fibrillar zone (Z2), and inner lamellar zone (Z3). The surface of the chorion is covered by a thin layer of granular material and dome-shaped electron-dense bodies. P, pore canal. X 17,660.

B. Transmission electron micrograph of a section through a pore canal (P) with its pore plug (PP) in the outer, electron-dense zone (Z1). The fibres of the middle layer are arranged in crisscrossing bundles around the outer portion of the pore canal. X 89,000.

C. Scanning electron micrograph of the outer surface of the chorion showing hemispherical, dome-like projections. X 4,700.

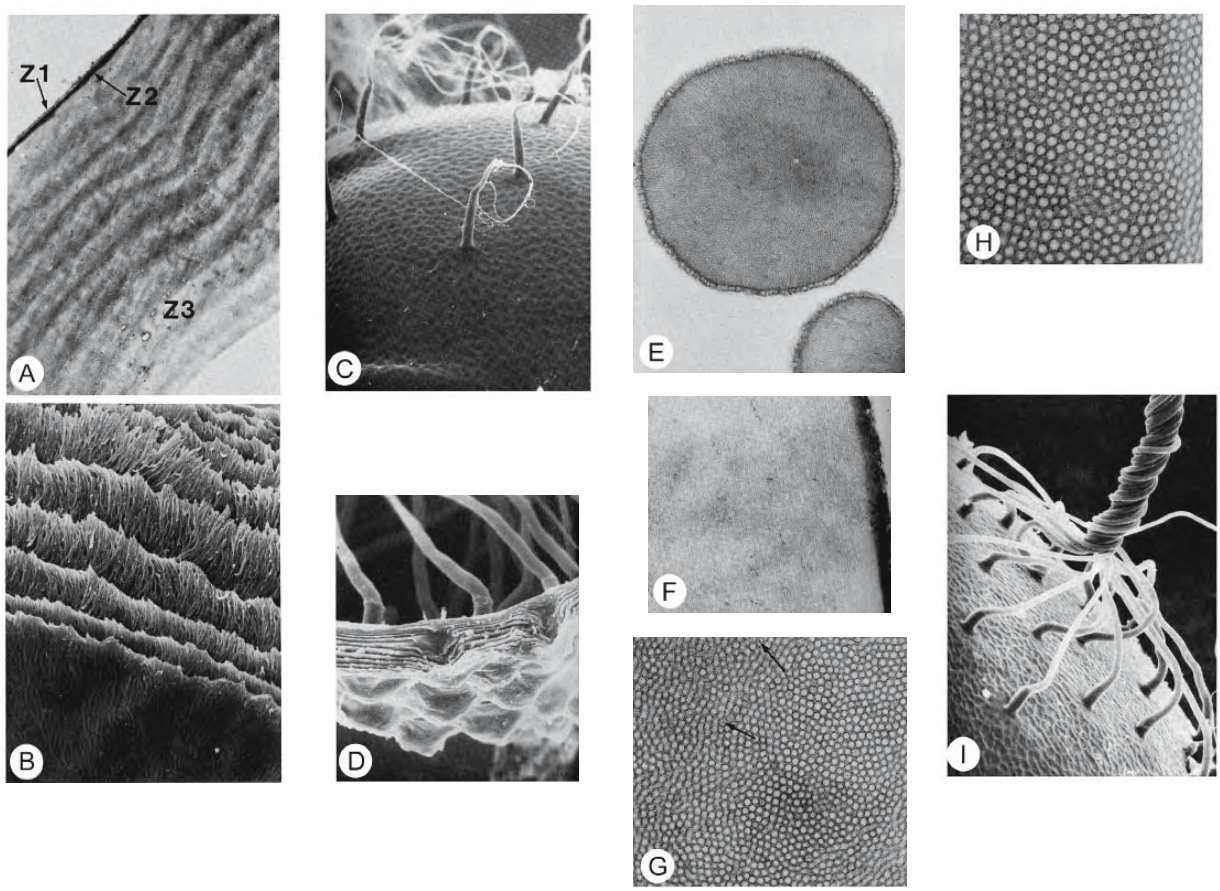

Figure 3.35: Electron micrographs of the chorion of the egg of *Oryzias latipes.* (From Hart, Pietri, and Donovan, 1984; © reproduced with permission of John Wiley & Sons, Inc.).

A. Transmission electron micrograph of a section through the chorion. It is composed of an outer electron-lucent zone (Z1), a middle electron-dense zone (Z2), and an inner zone (Z3) of ten to twelve electron-dense lamellae alternating with interlamellae of lower electron density. X 12,500.

B. Scanning electron micrograph of a fracture surface across the chorion showing the feather-like, fibrous appearance of the inner zone. X 1,500.

C. Scanning electron micrograph of the honeycomb surface of the chorion with nonattaching filaments. X 300.

D. Scanning electron micrograph of a cross-fracture of the chorion through the region bearing attachment filaments. The bases of the filaments are reflected as hemispherical protrusions along the inner surface. (Two filaments were lost in preparation.) The arrangement of the lamellae indicates that they normally wrap around the base of the filament. X 4,150.

E. Transmission electron micrograph through a cross section of the distal segment of a nonattaching filament. X 27,800.

F. Transmission electron micrograph of a longitudinal section of the distal segment of a nonattaching filament showing the orderly arrangement of straight, unbranched tubules. X 24,000.

G. Transmission electron micrograph through a cross section of a nonattaching filament showing electron-dense tubules with an electron-lucent core. Some electron-dense particles were seen within the tubules (arrows). X 100,000.

H. Transmission electron micrograph of the tubules of the distal segment of a nonattaching filament as seen in cross section. X 160,000.

I. Scanning electron micrograph af an array of attachment filaments originating from a localized portion of the chorion and uniting to form a rope-like cord. X 350.

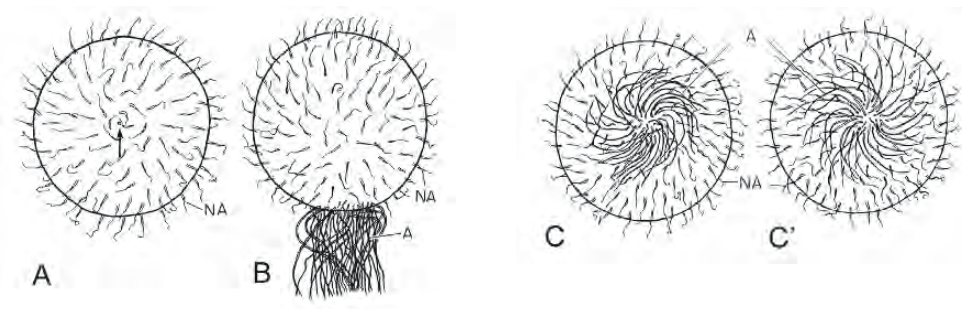

Figure 3.36: Diagrams illustrating the patterns of attaching and nonattaching filaments on the chorion of mature eggs of the medaka *Oryzias latipes*. (From Iwamatsu, 1992; reproduced with permission from the Zoological Society of Japan).

A. Animal pole. The arrow indicates the micropyle. Right handed pattern.

B. Lateral view of equator.

C, **C**[1]. In these views of the vegetal pole, the attaching filaments exhibit either the left-handed (**C**) or right-handed (**C**[1]) spiral pattern.

Abbreviations: A, attaching filaments; NA, nonattaching filaments.

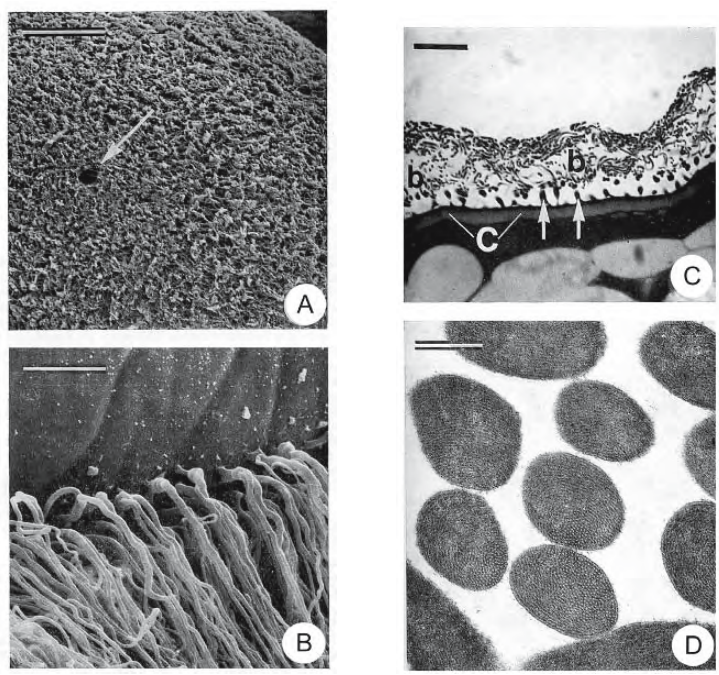

Figure 3.37: Micrographs of the egg of the blenny *Blennius pavo.* (From Patzner, 1984; reproduced with permission from Urban & Fischer Verlag).

A. Scanning electron micrograph of the micropylar region showing the adhesive disc surrounding the entrance to the micropyle (arrow). Bar = 100 μm.

B. Scanning electron micrograph of the transition zone between the adhesive disc with its anchoring filaments and the naked surface of the egg. Bar = 20 μm.

C. Photomicrograph of a section through the adhesive disc showing branched (b) and unbranched (arrows) parts of the anchoring filaments. C, chorion. Bar = 20 μm.

D. Transmission electron micrograph of cross sections through several anchoring filaments. A pattern of subfilaments resembles the "microtubule mimics" seen in Figure **3.35E**.

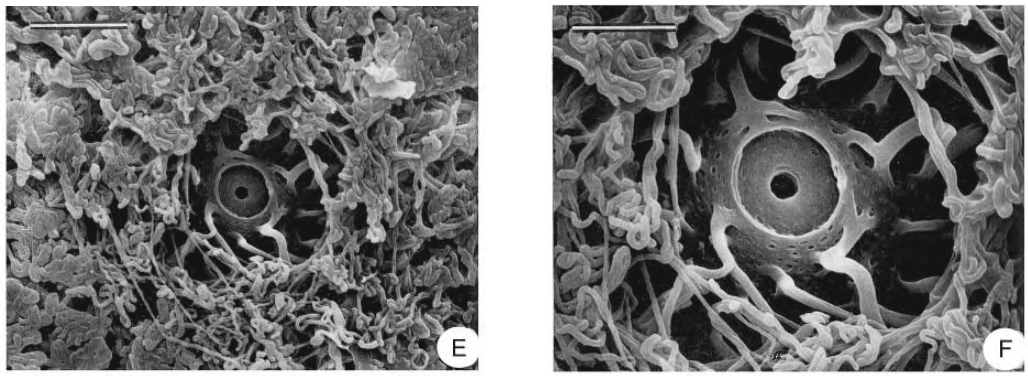

Figure 3.37: Continued.
E,**F**. Scanning electron micrographs of the micropylar region. Bar in **E** = 20 μm; in **F** = 10 μm.

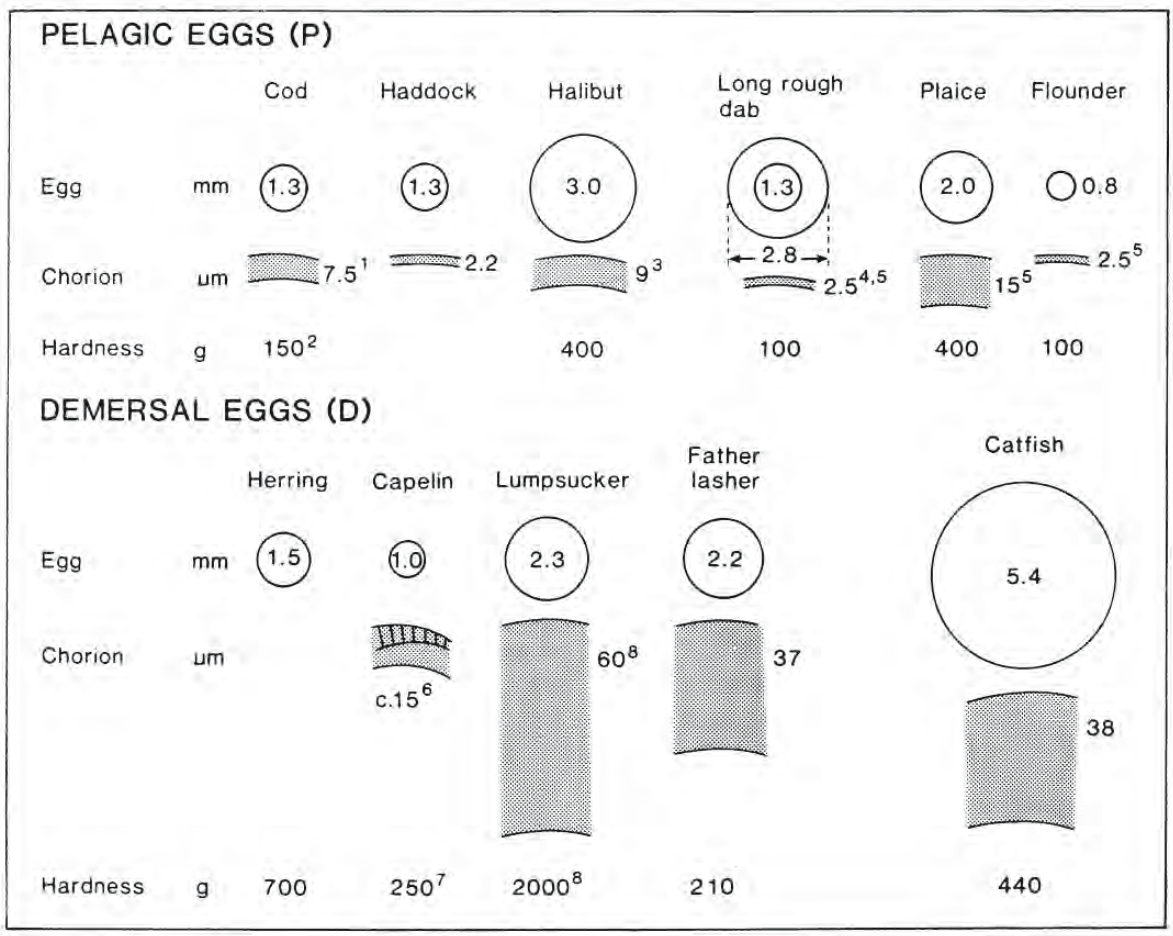

Figure 3.38: A comparison of the eggs of several species of fish to demonstrate that the chorions of demersal eggs are usually thicker and harder than those of pelagic species. (From Lønning, Kjørsvik, and Falk-Petersen, 1988; reproduced by permission of Taylor & Francis AS).

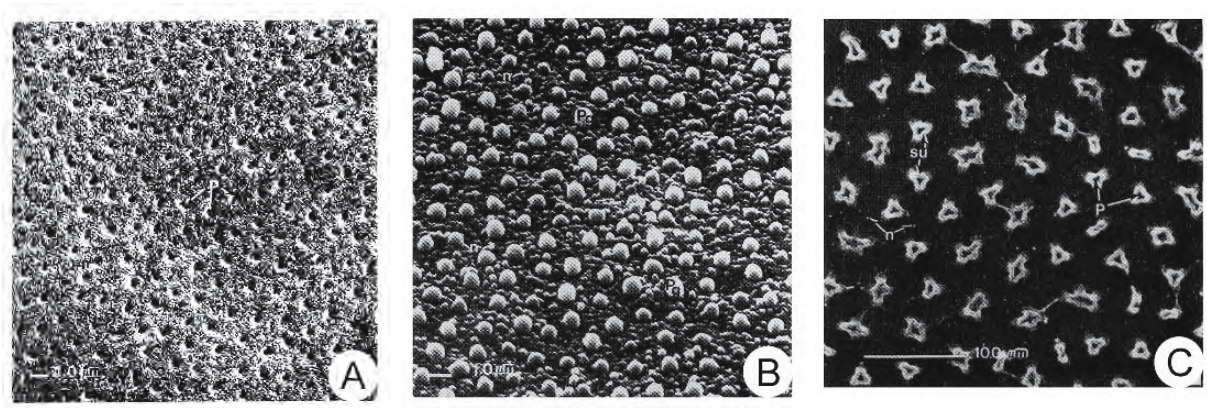

Figure 3.39: Scanning electron micrographs of the surface of the chorion of three species of freshwater fish. (From Johnson and Werner, 1986; reproduced with permission from Elsevier Science).
A. *Alosa pseudoharengus*
B. *Oncorhynchus kisutch*
C. *Osmerus mordax*
Abbreviations: n, nodule; p, pore; Pg, plug; su, subunit.

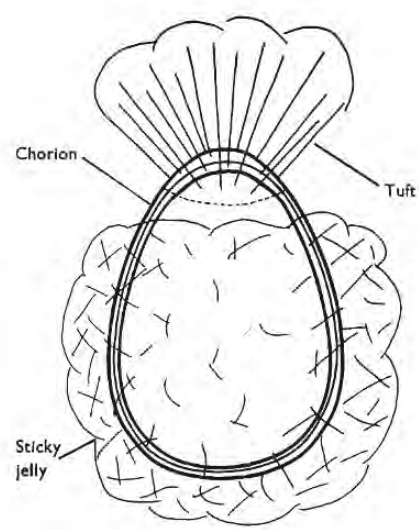

Figure 3.40: Diagram of the egg of the lamprey *Lampetra* sp. showing the apical tuft on the animal pole and the adhesive coat ("sticky jelly") that cups the vegetal two-thirds of the egg. (From Kille, 1960; reproduced with permission from Elsevier Science).

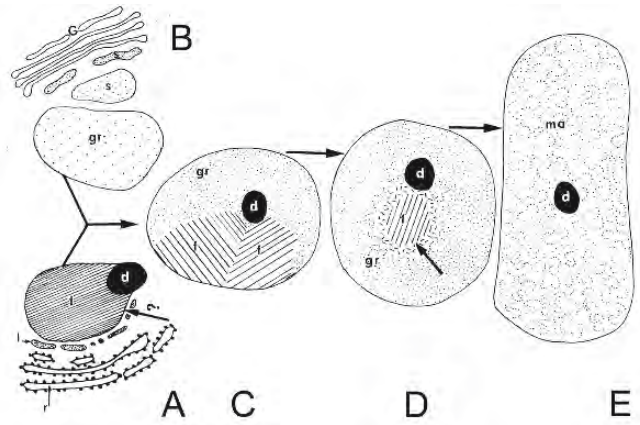

Figure 3.41: Diagrams to illustrate the origin and development of follicular secretory granules in the ovary of the lamprey *Lampetra planeri.* (From Busson-Mabillot, 1967b, *Journal de Microscopie*; reproduced with permission).

A. Membrane-bound secretory granules appear in the follicular cells at the beginning of intensive vitellogenesis. The granules contain a paracrystalline, fibrillar substance (f), often accompanied by a dense globule (d). Granular endoplasmic reticulum (r) is abundant near the granules. Tubules of smooth endoplasmic reticulum (l) appear to be continuous with the fibrillar granule.

B. At about the same time, saccules (s) of the Golgi complex (G) are distended by a homogeneous, electron-lucent, granular substance. Membrane-bound secretion granules, containing a substance structurally identical to the material in the Golgi saccules (gr), appear nearby.

C. Heterogeneous granules form quickly by coalescence of the granules shown in Figures **A** and **B**. They contain two or three masses of fibrillar material (f), a large mass of the granular substance (gr), as well as one or two dense globules (d).

D. The fibrillar masses (f) diminish in volume during development of the heterogeneous granules and become surrounded by a meshwork of short fibrils (arrow).

E. The fibrillar masses have disappeared in the mature granule and the granular material has assumed a characteristic marbled appearance (ma). Only the dense globule (d) retains its earlier appearance.

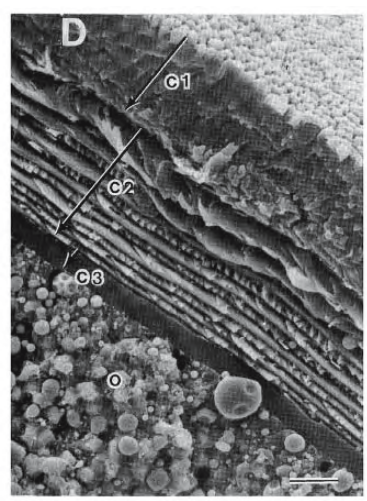

Figure 3.42: Scanning electron micrograph of the chorion and ooplasm (o) from an ovulated egg of the hagfish *Eptatretus stouti* fractured near the micropylar canal (not seen). The chorion is organized into three main zones, C1, C2, and C3. X 500 Bar = 20 μm (From Koch et al., 1993; reproduced with permission from Elsevier Science).

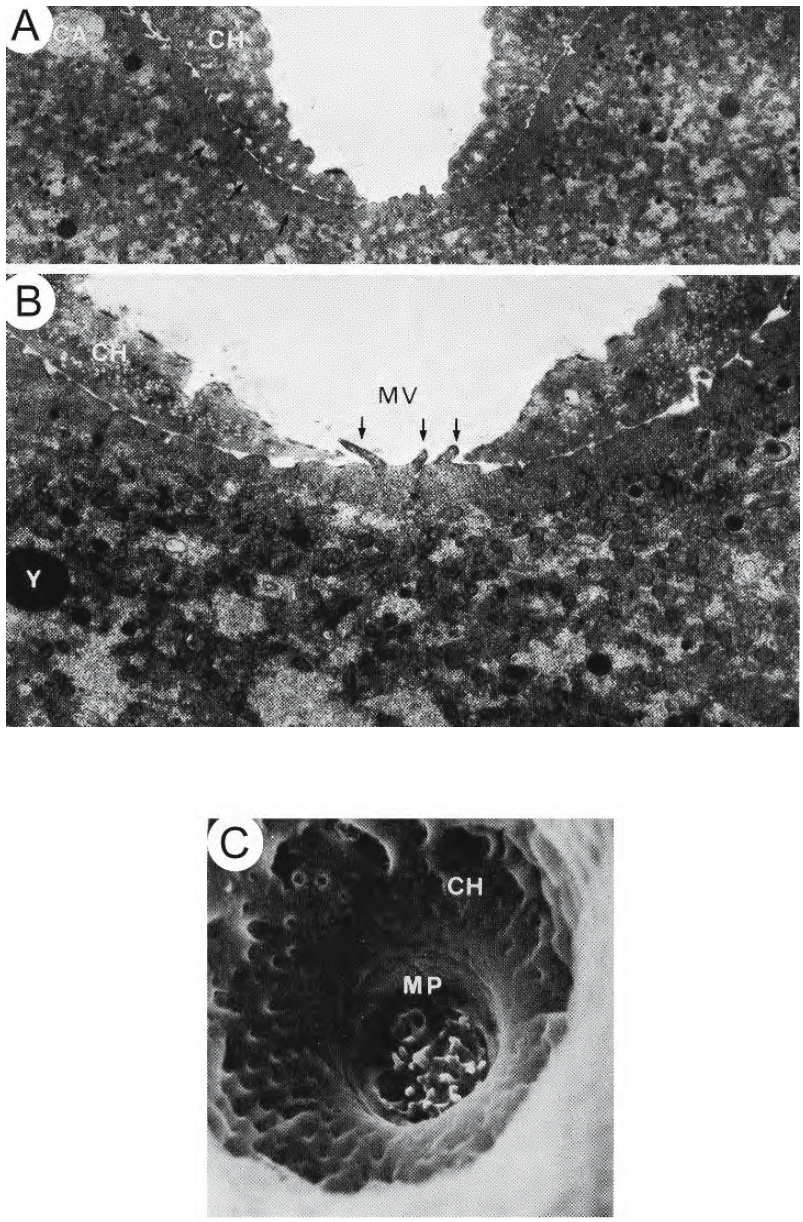

Figure 3.43: Electron micrographs of sperm entry sites on eggs of the rose bitterling *Rhodeus ocellatus.* (From Ohta and Iwamatsu, 1983; © reproduced with permission of John Wiley & Sons, Inc.).

A,**B**. Transmission electron micrographs of sections through the egg surface beneath the micropyle. Microvilli (MV) are seen in **B** on the egg surface just beneath the micropyle. **A**: X 2,800; **B**: X 7,280.

C. Scanning electron micrograph of the micropylar apparatus and egg surface beneath the micropyle of unfertilized eggs with chorion intact. There are microvilli at the bottom of the funnel-shaped micropyle. X 7,000.

Abbreviations: CA, cortical alveolus; CH, chorion; MP, micropyle; Y, yolk granule.

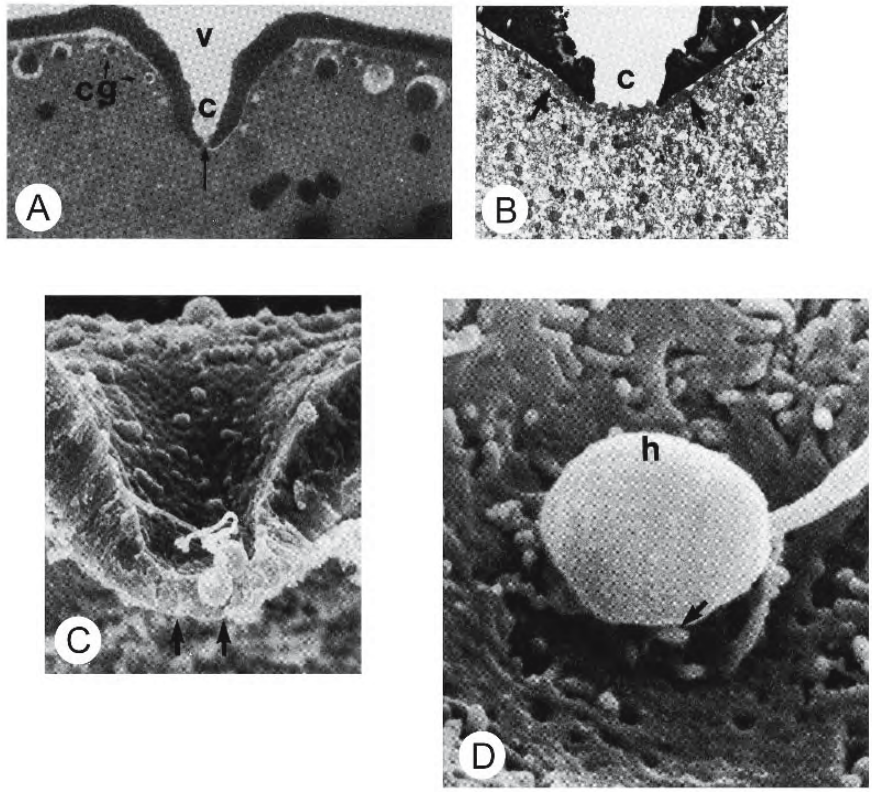

Figure 3.44: Micrographs of sperm entry sites on eggs of the zebrafish *Brachydanio rerio.* (From Wolenski and Hart, 1987a; © reproduced with permission of John Wiley & Sons, Inc.).

A. Photomicrograph of a section through the micropylar region of an unactivated egg. The micropyle, consisting of the outer vestibule (v) and the inner micropylar canal (c), produces a cone-shaped depression in the egg surface. A single layer of small cortical granules (cg) lies beneath the oolemma except in the region of the inner micropylar aperture (arrow). X 4,000.

B. Transmission electron micrograph of a section through the sperm entry site showing microvilli projecting through the inner micropylar aperture into the micropylar canal (c). An electron-dense layer (arrows) beneath the sperm entry site spreads outward for some distance below the oolemma. X 8,500.

C. Scanning electron micrograph of a cross fracture through the micropyle five seconds after insemination. The inner micropylar aperture (arrows) accommodates a single spermatozoon. X 4,000.

D. Scanning electron micrograph of a fertilizing sperm attached to the microvilli of the sperm entry site five seconds after insemination. Binding occurs (arrow) between the microvilli and the equatorial surface of the spherical sperm head (h). X 17,000.

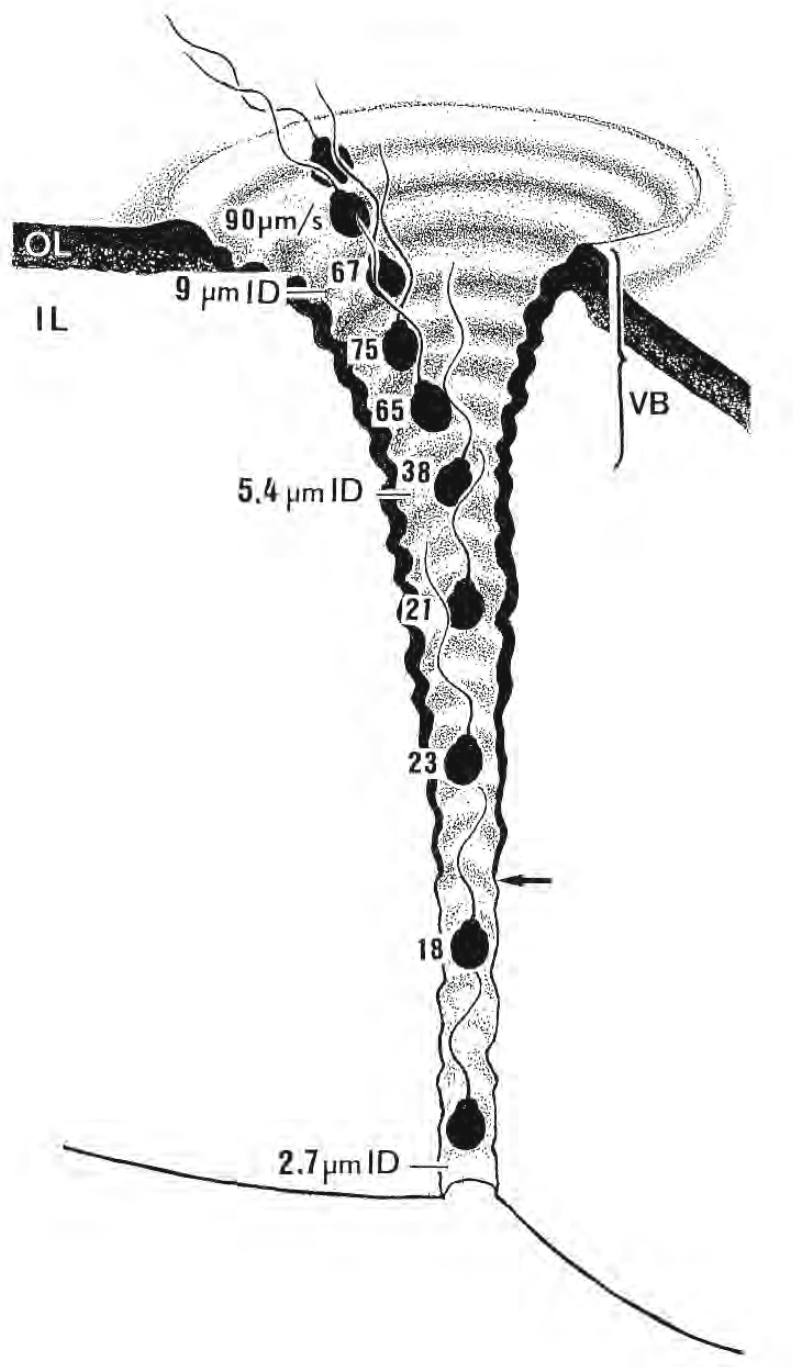

Figure 3.45: Diagram of the structure of the micropyle of the medaka *Oryzias latipes*. The speed of a swimming spermatozoon decreases as it moves down the micropylar canal toward the oolemma. The inner diameter (ID) at the vestibule (9.0 μm), the outer aperture (5.4 μm), and the end of the canal (2.7 μm) are indicated. The inner wall of the micropyle consists of the outermost layer (OL) of the chorion in the outer two thirds, including the vestibule (VB), and the inner layers of the chorion in the inner one third (arrow) of the micropyle. (From Iwamatsu, Ishijima, and Nakashima, 1993; © reproduced with permission of John Wiley & Sons, Inc.).

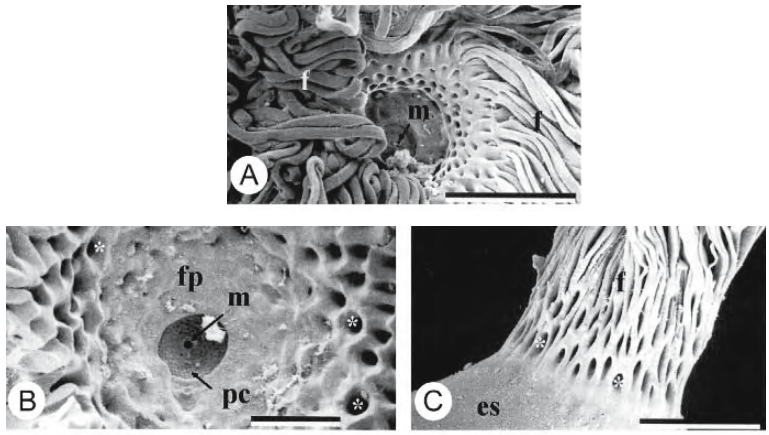

Figure 3.46: Scanning electron micrographs of the micropylar area of mature eggs of the grass goby *Zosterisessor ophiocephalus.* (From Giulianini and Ferrero, 2000; reproduced with permission from Unione Zoologica Italiana).

A. A forest of attachment filaments up to 600 μm in length forms a crown about 76 μm in diameter around the micropyle. Bar = 50 μm.

B. The micropylar pit is surrounded by perforations (asterisks) formed by merged basal filaments. Bar = 20 μm.

C. Lateral view of the oocyte showing a cribiform column of netted filaments rising from the basal plate surrounding the micropylar area. The filaments divide and fray distally. Bar = 50 μm.

Abbreviations: es, egg surface; f, filaments; fp, filament plate; m, micropyle; pc, pore canal.

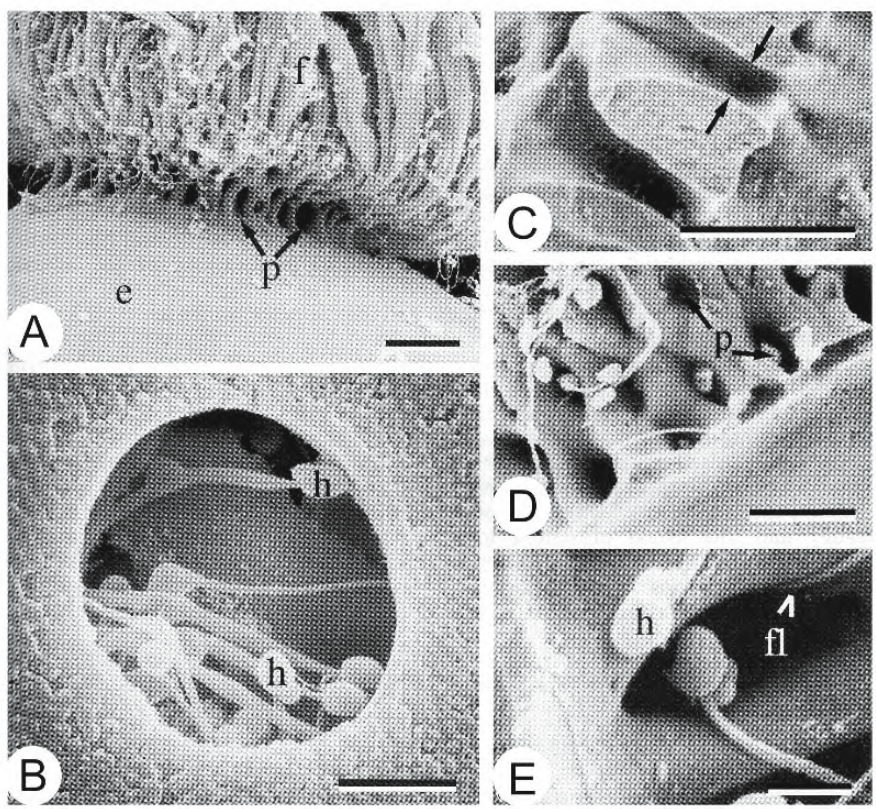

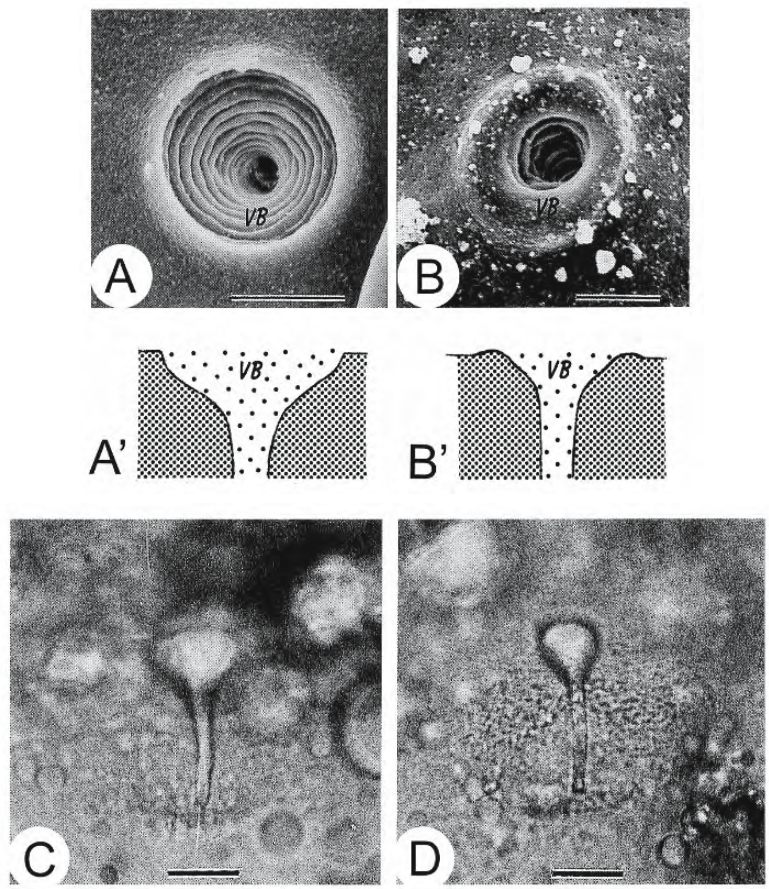

Figure 3.48: Entry into the micropylar canal of many species is attained through a funnel-shaped vestibule on the outer surface of the chorion. (From Iwamatsu et al., 1997; reproduced with permission from the Zoological Society of Japan).

A,**B**. Scanning electron micrographs of the micropyles from eggs of medaka *Oryzias latipes* (**A**) and *O. melastigma* (**B**). Longitudinal sections through the micropyles are shown in the diagrams below. VB, vestibule. Bars = 5 μm.

C,**D**. Photomicrographs of unfertilized eggs of *O. latipes* showing a micropyle with a large vestibule (**C**) and one with a small vestibule (**D**). Bars = 20 μm.

←

Figure 3.47: Scanning electron micrographs of artificially fertilized eggs of the grass goby *Zosterisessor ophiocephalus.* (From Giulianini et al., 2001; reproduced with permission from Elsevier Science).

A. Side view of filament adhesion apparatus (f) with basal perforations (p) adjacent to the egg surface (e). Bar = 20 μm.

B. Basal plate viewed from the inner micropylar face with heads of spermatozoa (h) inside the adhesion apparatus. Bar = 5 μm.

C. Basal filaments fractured to show tapered perforations. The arrows indicate the minimum width. Bar = 10 μm.

D. Perforations (p) viewed from the outer side showing rhomboid bottleneck. Bar = 10 μm.

E. Spermatozoon (h) entering a perforation from the outer side. Note the flagellum (fl) of a spermatozoon that has just entered. Bar = 2 μm.

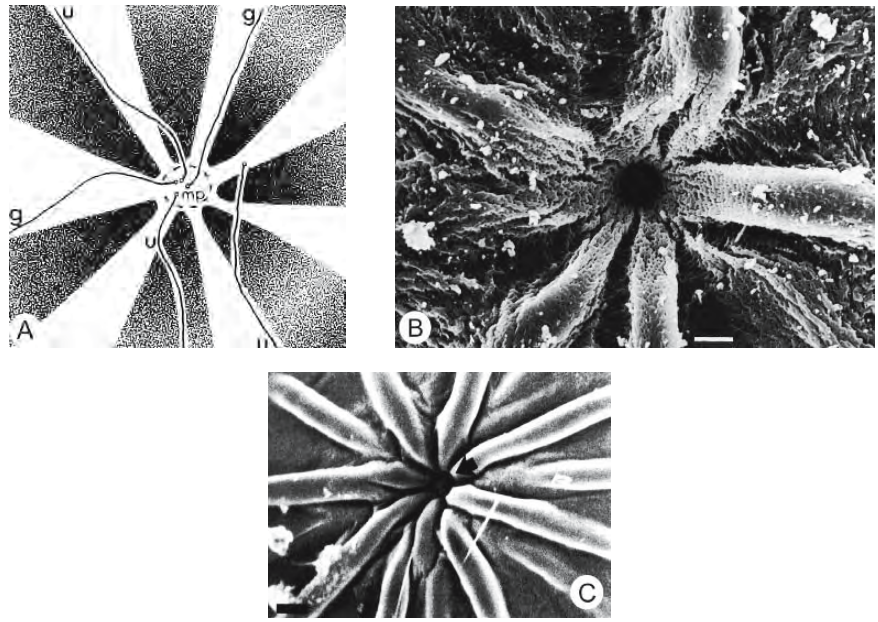

Figure 3.49: Spermatozoa may be guided to the micropylar region of the egg of the rosy barb *Barbus conchionus* by spiral ridges that emboss the chorion of the animal pole. (From Amanze and Iyengar, 1990; reproduced with permission of the Company of Biologists Ltd., Cambridge).

A. Diagram showing the trajectories of "guided" (g) and "unguided" (u) sperm in the micropylar region. The stippled regions indicate ridges; mp, micropylar pit.

B. Scanning electron micrograph of the micropylar region of an unfertilized egg showing micropylar ridges and grooves. Bar = 4 μm.

C. Scanning electron micrograph of a fertilized egg showing micropylar pit plugged by three late-arriving sperm (arrow). Bar = 1 μm.

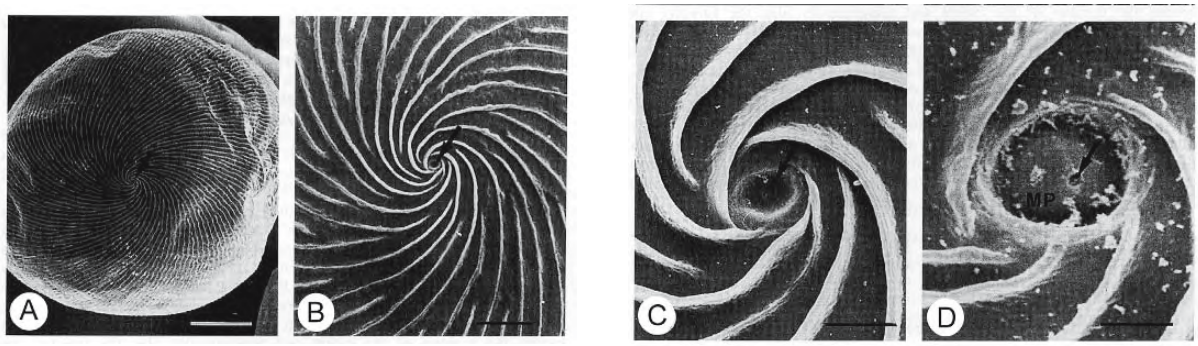

Figure 3.50: Scanning electron micrographs of the egg of the perciform *Luciocephalus* sp. to show an elaborate pattern of spiral ridges surrounding the micropylar pit (indicated by an arrow in each micrograph). (From Riehl and Kokoscha, 1993; reproduced with permission from Elsevier Science).

A. View of the entire egg. Bar = 500 μm.

B. Some of the spiral ridges enter the micropylar pit. Bar = 100 μm.

C. The micropyle consists of the micropylar pit (arrow) and the micropylar canal at the centre. Bar = 25 μm.

D. The micropylar canal (arrow) is at the centre of the micropylar pit (MP). Bar = 10 μm.

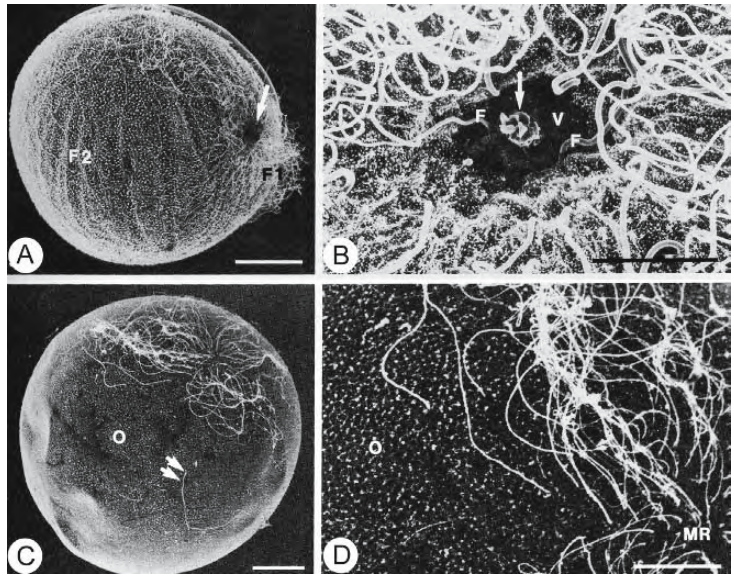

Figure 3.51: Scanning electron micrographs of the egg of two cyprinodonts. The micropylar region is surrounded by adhesive filaments while the rest of the chorion exhibits simple ornamentations of varying shape. (From Thiaw and Mattei, 1992; reproduced with permission of the NRC Press).

A. *Fundulusoma thierryi.* The micropyle opens through a vestibule (arrow). There are many filaments in the region of the micropyle (F1), but some are implanted in other regions (F2). Bar = 200 µm.

B. The micropylar apparatus of the egg shown in **A**. The micropylar canal is blocked by a plug (arrow). Some filaments (F) are implanted in the vestibule (V). Bar = 50 µm.

C. *Epiplatys fasciolatus.* The surface of the egg is ornamented (O); filaments are concentrated in a region without ornamentation. The double arrow indicates a filament that is implanted in the median region of the egg. Bar = 200 µm.

D. Enlargement of the micropylar region of the egg shown in **C**. Ornamentations (o), visible on the left, are absent in the micropylar region (MR). Bar = 100 µm.

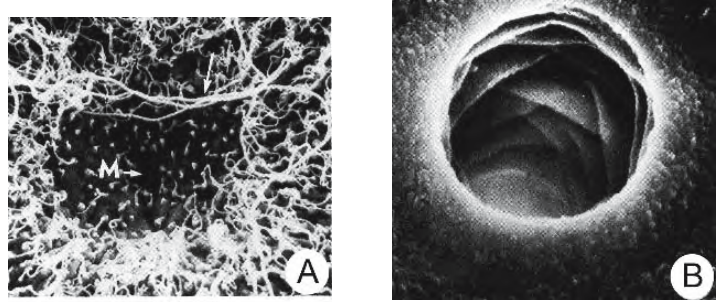

Figure 3.52: Scanning electron micrographs of the micropylar region of the egg of *Fundulus heteroclitus.* (From Dumont and Brummett, 1980; reproduced with permission of Wiley-Liss, Inc., a subsidiary of John Wiley & Sons, Inc.).

A. The micropyle (M) is situated at the base of a conical depression. The walls of the depression are adorned with small, tapered filaments. Surrounding the micropylar depression are several short and a few long (arrow) chorionic filaments. X 830.

B. The micropyle is surrounded by a raised lip. The walls of the micropylar canal appear like a series of iris diaphragms reflecting the laminar nature of the chorion. X 34,000.

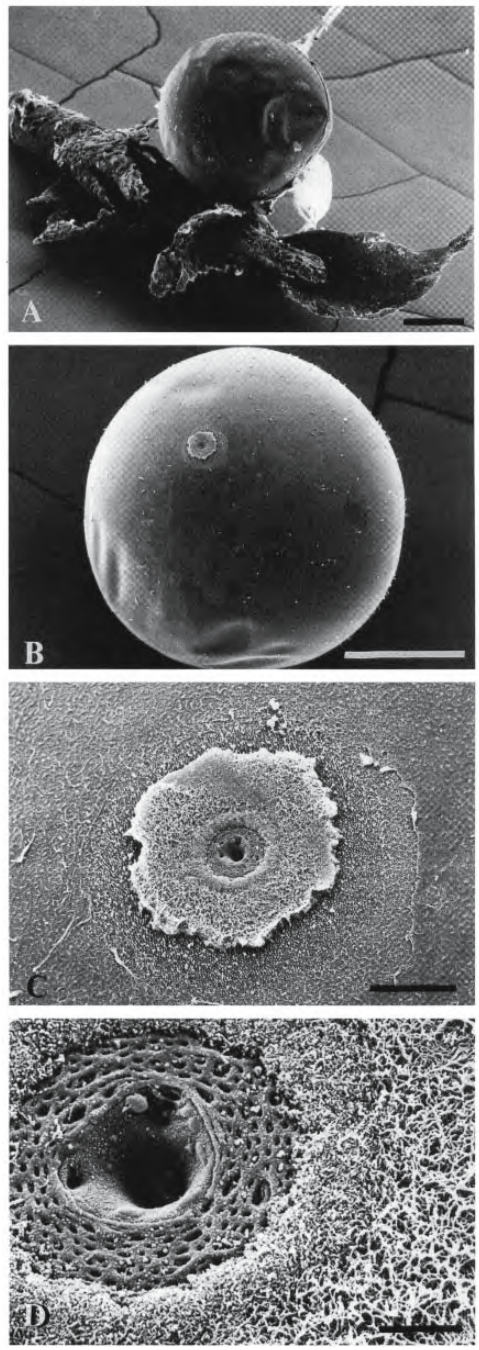

Figure 3.53: Scanning electron micrographs of a freshly spawned egg of the leaffish *Nandus nandus*. These eggs are attached to various substrates by a dense carpet of short filaments arrayed around the micropyle. (Britz, 1997; courtesy of the American Museum of Natural History).

A. Egg attached to moss. Bar = 400 μm.

B. Animal pole. Bar = 200 μm.

C. Micropylar region. Bar = 20 μm.

D. Micropyle. Bar = 4 μm.

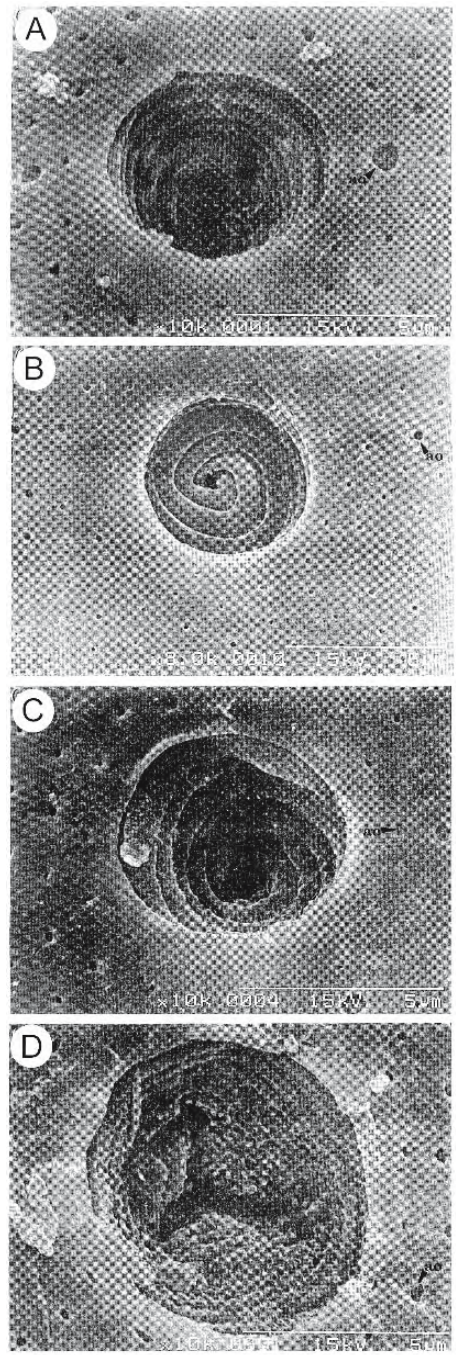

Figure 3.54: These scanning electron micrographs of the micropyles of unfertilized eggs of four species of Sparidae were used as the basis of a taxonomic key. ao, accessory openings Bar = 5 μm (From Chen, Shao, and Yang, 1999; reproduced with permission from Elsevier Science).

A. *Sparus sarba* X 10,000.

B. *Acanthopagrus latus* X 8,000.

C. *A. schlegeli* X 10,000.

D. *Pagrus major* X 10,000.

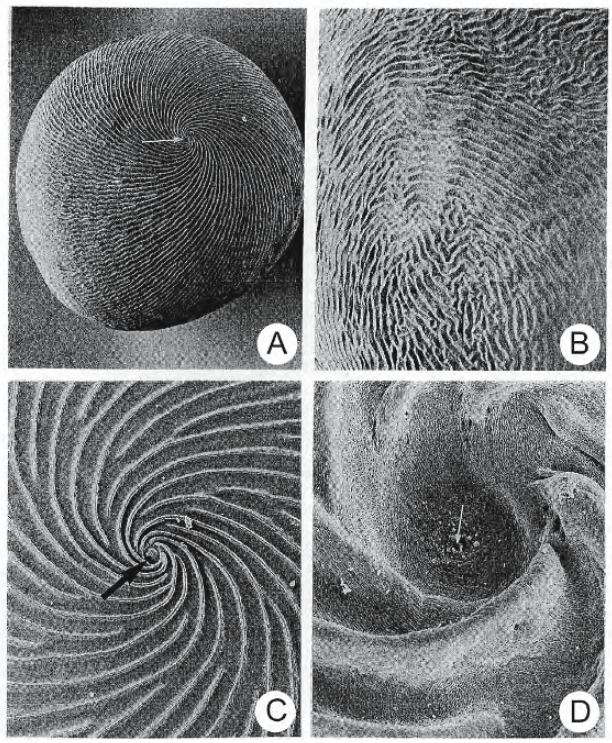

Figure 3.55: Scanning electron micrographs of the egg of *Luciocephalus pulcher.* Elaborate arrays of parallel ridges on the zona pellucida suggest phylogenetic relationships. These ridges spiral from the Type I micropyle and are presumed to assist in sperm guidance. (From Britz, Kokoscha, and Riehl, 1995; reproduced with permission from the Ichthyological Society of Japan).

A. View of the animal pole of the egg. The arrow indicates the micropyle. X 27.8.

B. An irregular pattern of ridges near the vegetal pole. X 60.

C. The micropyle (arrow) at the centre of the spiraling ridges at the animal pole. X 232.

D. Micropylar pit with the micropylar canal (arrow). X 1,920.

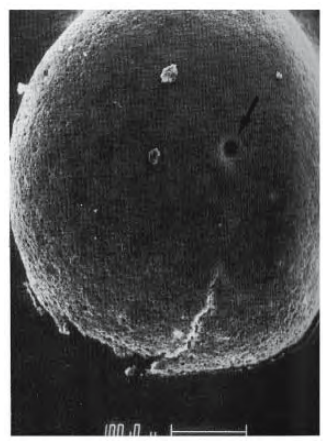

Figure 3.56: Scanning electron micrograph of the dechorionated egg of *Brachydanio rerio.* (From Hart and Donovan, 1983; © reproduced with permission of John Wiley & Sons, Inc.) The egg surface immediately beneath the micropylar apparatus appears as a cone-shaped depression (arrow). X 150.

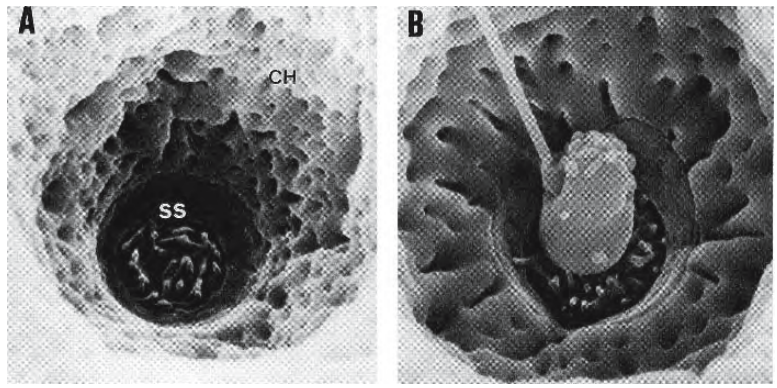

Figure 3.57: Scanning electron micrographs of the micropylar region of eggs of the rose bitterling *Rhodeus ocellatus.* X 8,800 (From Ohta, 1991; reproduced with permission).

A. Sperm-entry site (SS) of an unfertilized egg. CH, chorion.

B. A fertilizing spermatozoon appears to attach to the microvilli of the sperm-entry site.

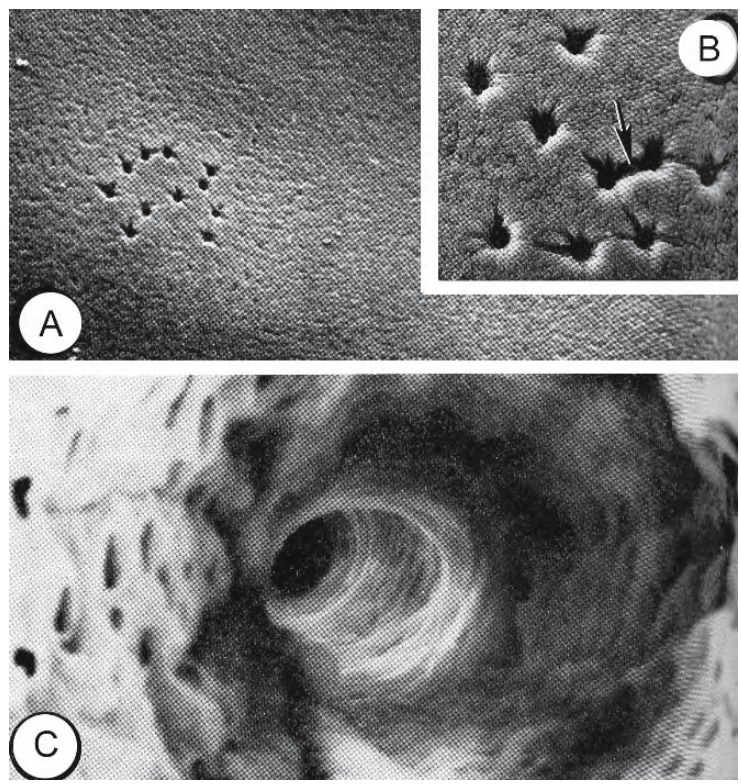

Figure 3.58: Scanning electron micrographs of the micropylar region of the mature egg of the white sturgeon *Acipenser transmontanus.* (From Cherr and Clark, 1982; reproduced with permission from Blackwell Publishing).

A. A group of micropyles at the animal pole of the egg. X 120.

B. Some micropyles are superficially connected by shallow channels (arrow). X 320.

C. The funnel shaped entrance to one of the micropyles viewed from the outside. The lining of the micropylar canal is ridged. X 7,400.

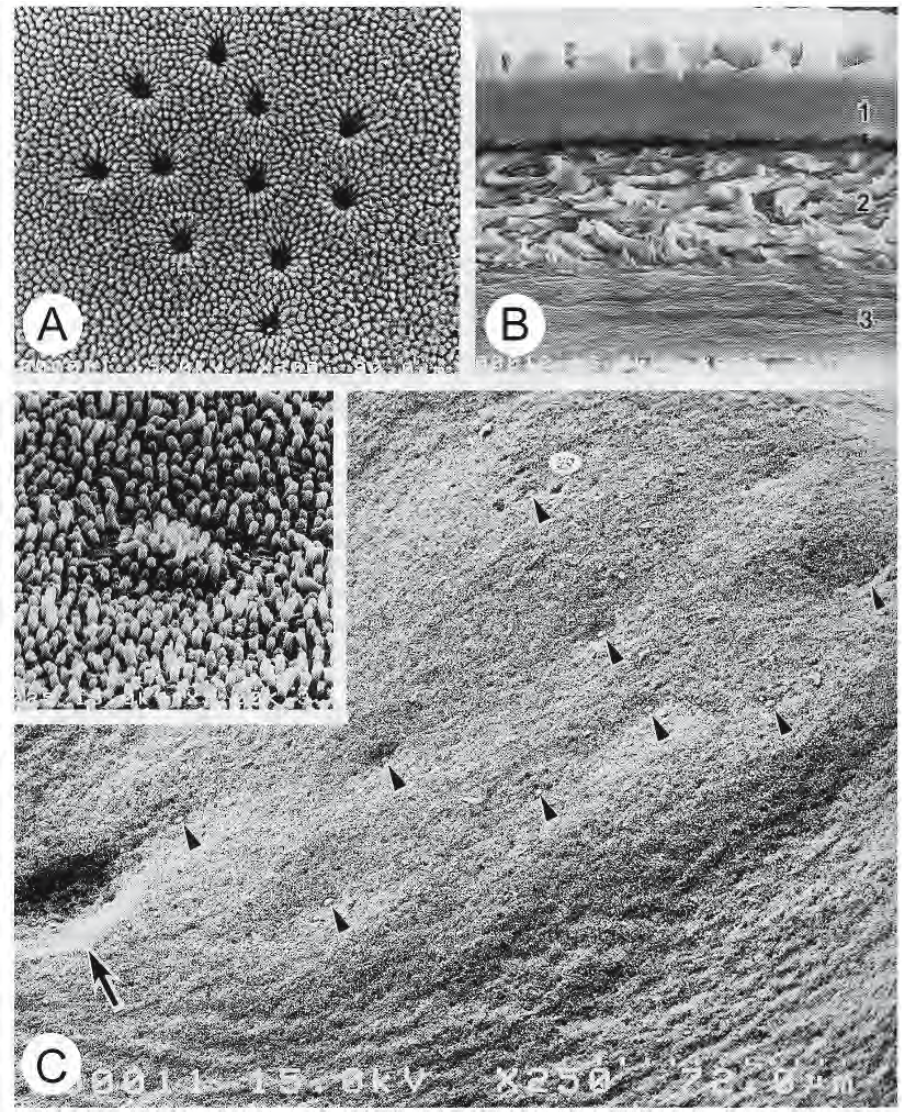

Figure 3.59: Scanning electron micrographs of mature eggs of the paddlefish *Polyodon spathula,* an egg with multiple micropyles. (From Linhart and Kudo, 1997; reproduced with permission from Elsevier Science).

A. A group of 11 micropyles at the animal pole. The external apertures are lined with cylindrical structures formed by differentiation of the outermost layer of the chorion. X 220.

B. The broken surface of the chorion showing three layers (1, 2, and 3). The outermost layer differentiates to form cylindrical structures. X 980.

C. The surface of an egg in the micropylar region with the chorion removed. The round impression of the first polar body (arrow) is located near a group of sperm entry sites (arrowheads). X 530.

Inset: tuft of microvilli of a sperm entry site on the surface of the oolemma under a micropyle. X 5,400.

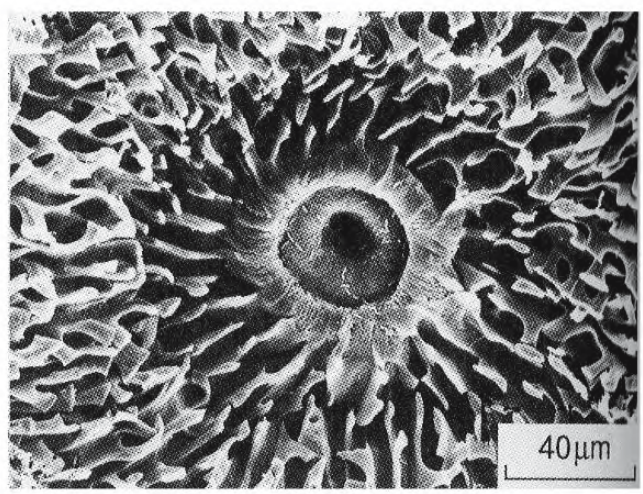

Figure 3.60: Scanning electron micrograph of the micropylar region of a fertilized egg of the actinopterygian fish *Polypterus ornatipinnis*. The chorionic surface is covered with glutinous tufts except for a small area at the animal pole. A narrow ring-like wall surrounds the micropylar area with the micropylar canal at the centre. A number of ridges, originating from the circular wall, transform centrifugally into the glutinous tufts. (From Bartsch and Britz, 1997; reproduced with permission of the Cambridge University Press).

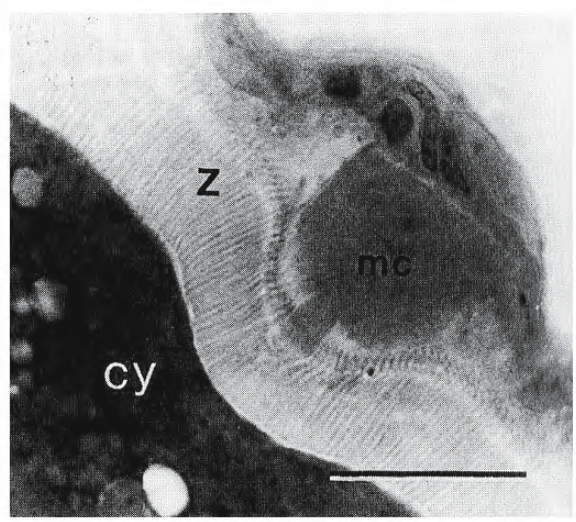

Figure 3.61: Photomicrograph of a section through a vitellogenic oocyte of the white bass *Morone chrysops* showing the zona pellucida (z) at the site where the micropylar cell (mc) penetrates the micropyle. The cytoplasm (cy) beneath is relatively free of yolk globules. Bar = 25 µm (From Mylonas et al., 1997; reproduced with permission from Elsevier Science).

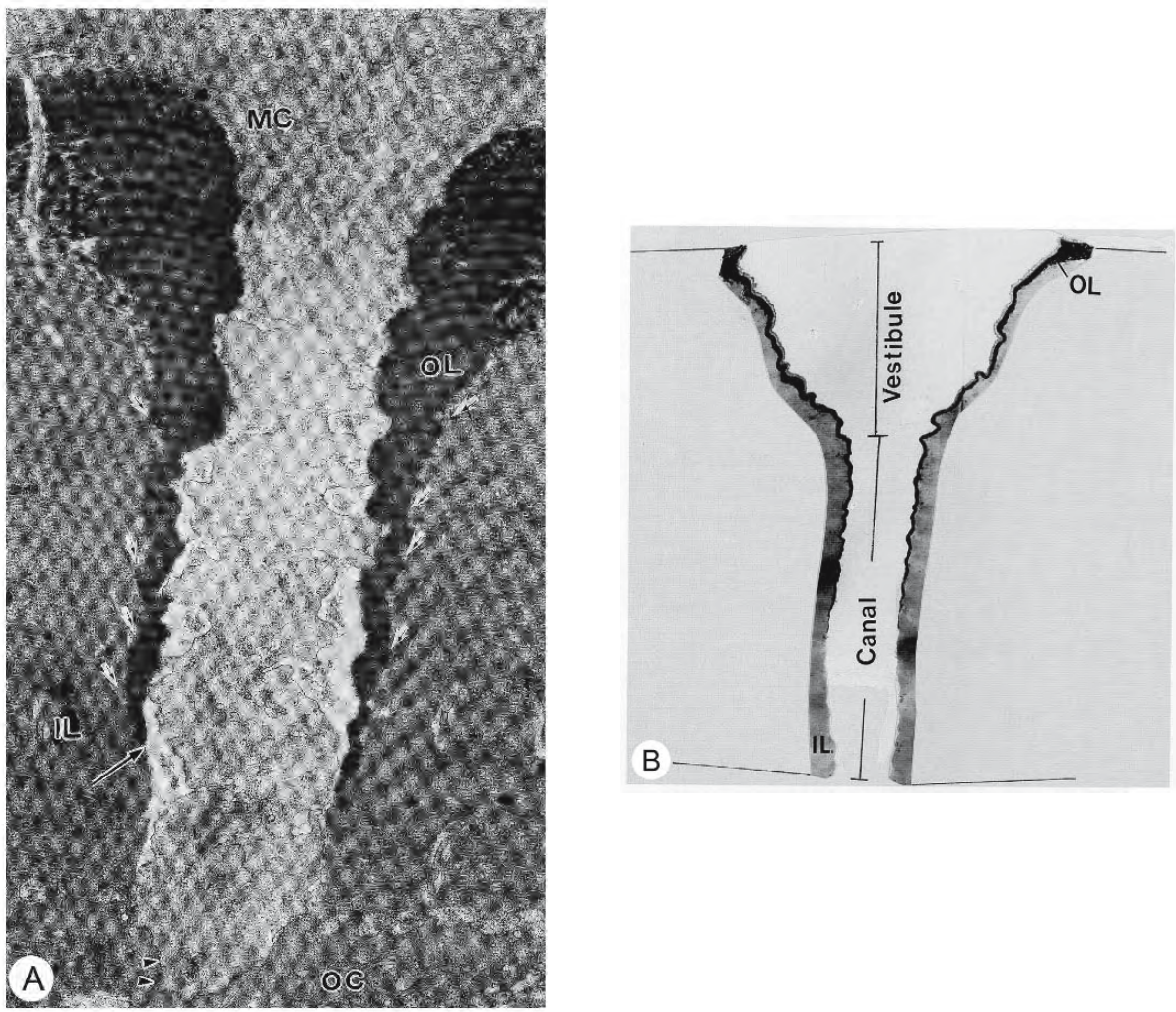

Figure 3.62: The micropyle of the medaka *Oryzias latipes* is formed during vitellogenesis by a single micropylar cell. It moulds the micropylar channel as the zona pellucida is laid down around it. (From Iwamatsu, Nakashima, and Onitake, 1993; © reproduced with permission of John Wiley & Sons, Inc.).

A. Transmission electron micrograph of a section through the cytoplasmic extension of the micropylar cell (MC) and micropyle of a fully-grown oocyte. The outer layer of the chorion (OL) extends inward, over the inner layer (IL), to line the micropylar canal as far as the large arrow. The cytoplasmic extension contains a bundle of microtubules. Folds in the surface of the cytoplasmic extension mould indentations in the wall of the micropylar canal. The micropylar cell is attached to the indented oolemma by tight junctions (arrowheads). OC, oocyte. X 60,000.

B. Transmission electron micrograph of a longitudinal section of the micropyle of a mature egg. The outer layer (OL) of the chorion is electron dense and overlies the inner layer (IL) around the outer two-thirds of the micropylar canal. X 36,000.

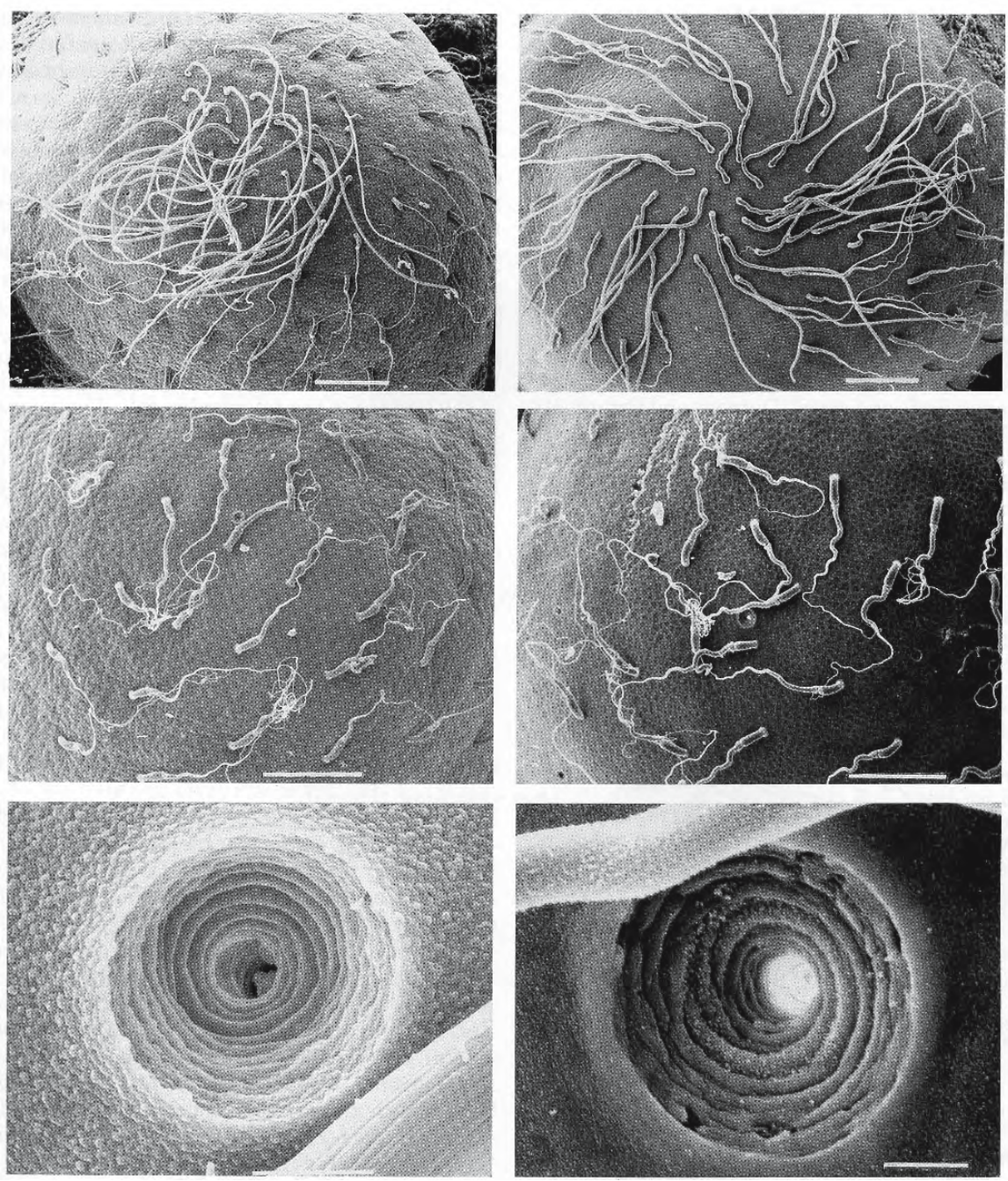

Figure 3.62: Continued.

C. Scanning electron micrographs of non-attaching filaments and micropyles at the animal pole (middle, bottom) and attaching filaments at the vegetal pole (top). Bar = 5 μm.

The three pictures on the left are from an egg with a left-handed spiral arragement of the attaching filaments and non-attaching filaments. *Bottom*: the spiral in the wall of the micropyle is left-handed.

The three pictures on the right are from an egg with a right-handed spiral arrangement of the attaching filaments and non-attaching filaments. *Bottom*: the spiral in the wall of the micropyle is left-handed.

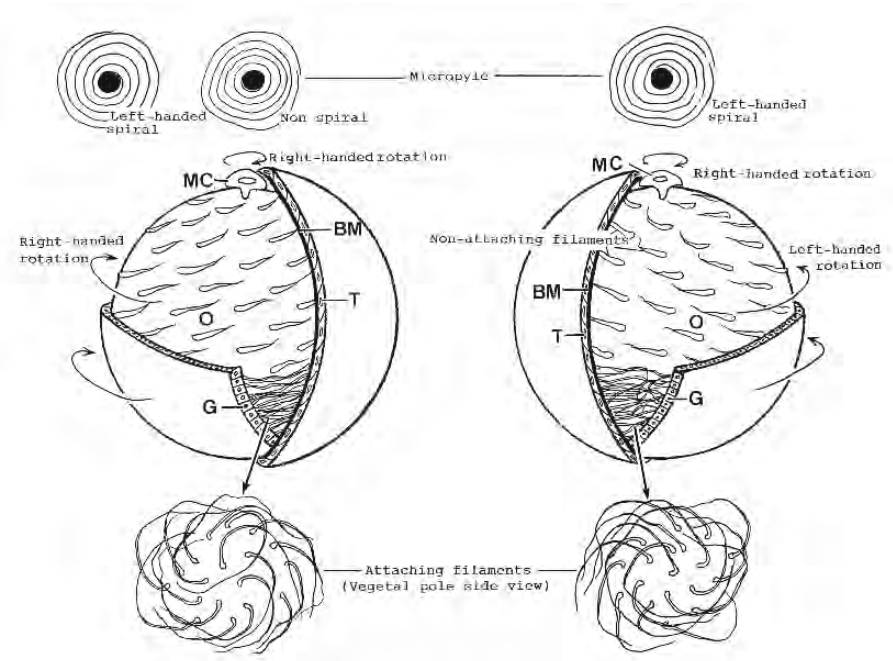

Figure 3.62: Continued.

D. Schematic diagram showing two patterns of attaching and non-attaching filaments and micropyles in intrafollicular oocytes of the medaka. The thecal cell layer (T) and basement membrane (BM) are immobile. The micropylar cell (MC) rotates in a right-handed direction. On the left, the oocyte (O) with its follicular layer (G) moves in a right-handed direction; on the right, it rotates in a left-handed direction.

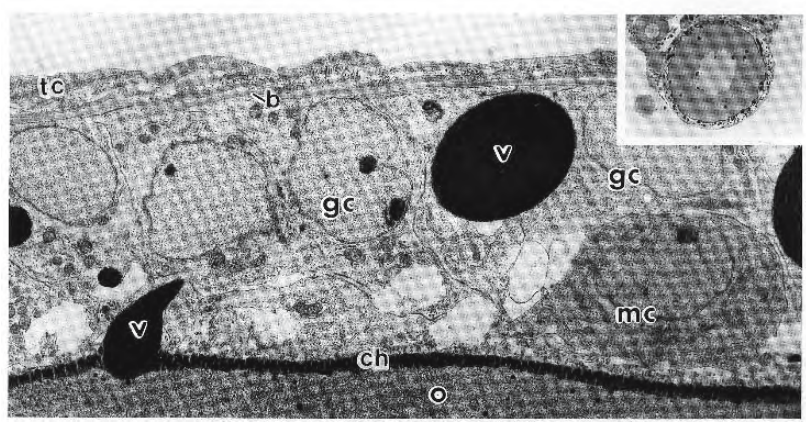

Figure 3.63: Transmission electron micrograph of the follicular layer in the animal pole region of an oocyte of the medaka *Oryzias latipes.* A micropylar cell (mc) with electron-dense cytoplasm and nucleoplasm is surrounded by follicular cell (gc) and abuts the zona pellucida (ch). X 4,700 (From Nakashima and Iwamatsu, 1989; © reproduced with permission of John Wiley & Sons, Inc.).

Inset: photomicrograph of the whole follicle. X 140.

Abbreviations: b, follicular basal lamina; o, ooplasm; tc, thecal cell; v, short villi penetrating the zona pellucida.

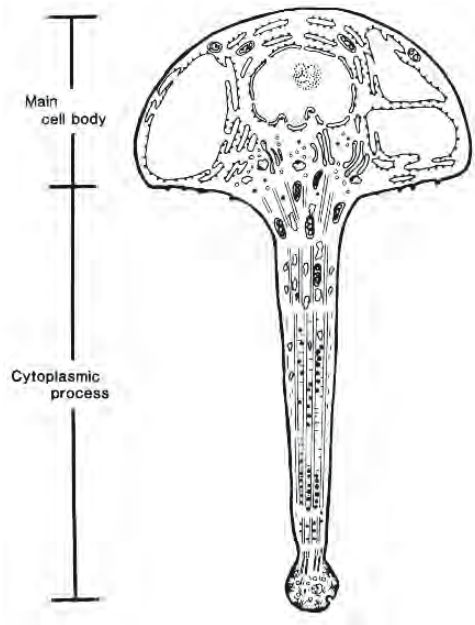

Figure 3.64: Diagram of a micropylar cell from the chum salmon *Oncorhynchus keta* during vitellogenesis. The main cell body is about 25 μm high and 40 μm wide and fits into the micropylar vestibule. Its inner surface bears a few short microvilli whereas the outer surface, abutting polygonal follicular cells, is smooth. The central nucleus contains finely dispersed chromatin and a prominent nucleolus. Granular endoplasmic reticulum and other organelles occupy the cytoplasm of the main cell body. The thick cytoplasmic process extends through the micropylar canal; a bundle of microtubules forms its central core. The bulbous end of the process indents the surface of the oocyte, forming desmosomal junctions with the oolemma. (From Kobayashi and Yamamoto, 1985; © reproduced with permission of John Wiley & Sons, Inc.).

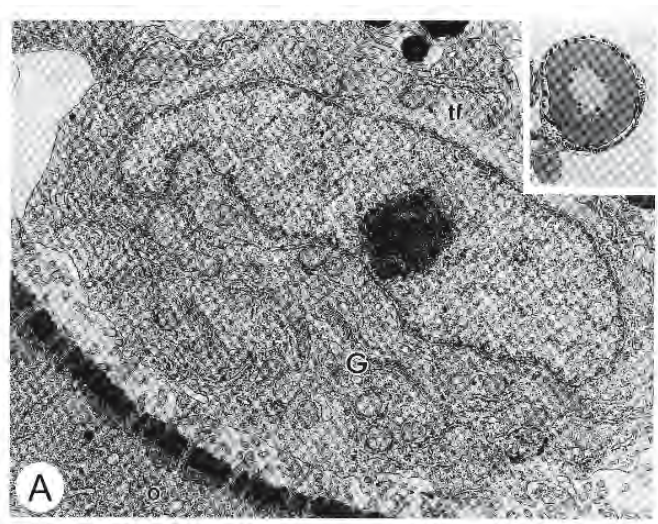

Figure 3.65: Transmission electron micrographs of sections of micropylar cells of the medaka *Oryzias latipes.* (From Nakashima and Iwamatsu, 1989; © reproduced with permission of John Wiley & Sons, Inc.).

A. Micropylar cell during early vitellogenesis. The cell is large with a flattened nucleus. Cytoplasmic organelles are abundant. Golgi complexes are well developed on the oocyte side of the cell; bundles of tonofilaments are apparent on the opposite side. X 14,000.

Inset: Photomicrograph of the entire follicle. X 110.

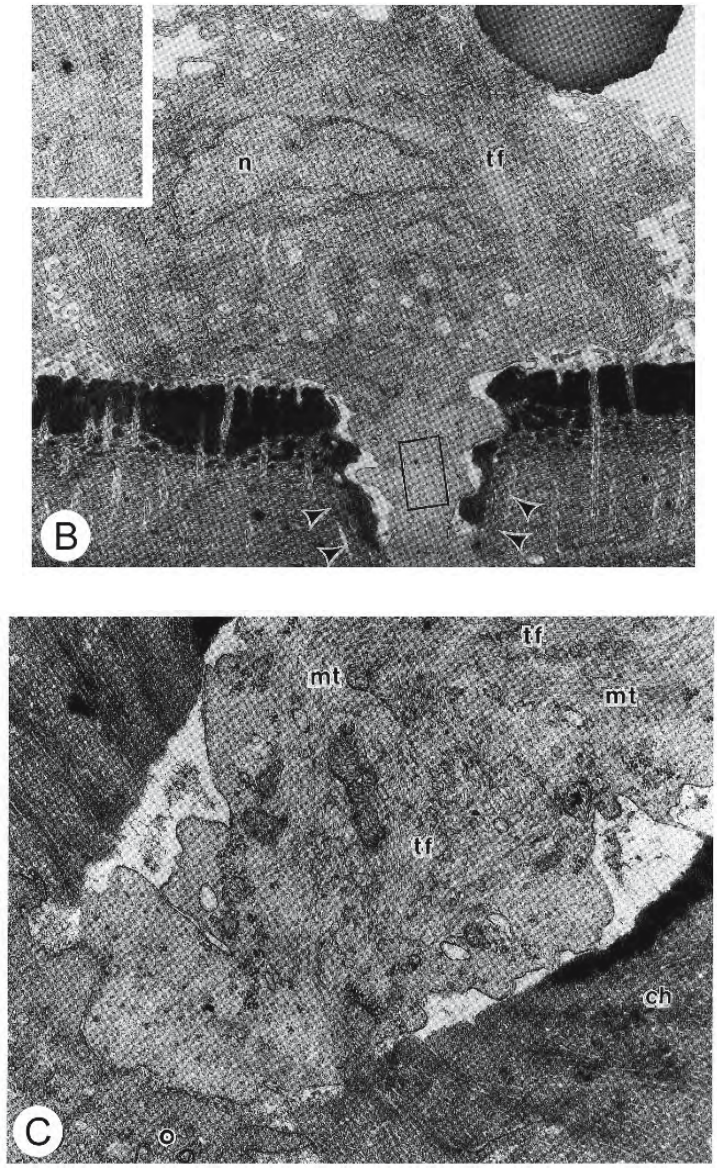

Figure 3.65: Continued.

B. Later in vitellogenesis the micropylar cell has assumed a mushroom shape and its cytoplasmic process has penetrated the zona pellucida. Arrowheads indicate structural distortion of the inner layer of the zona pellucida. X 23,400.

Inset: The rectangle on the process has been enlarged to show a bundle of microtubules but no tonofilaments. X 51,500.

C. The tip of the micropylar cell process abutting the oolemma of an oocyte in late vitellogenesis. Bundles of microtubules and tonofilaments, with their associated mitochondria, become spirally twisted as the process elongates.

Abbreviations: ch, zona pellucida; G, Golgi complex; mt, microtubules; n, nucleus; o, oocyte; tf, tonofilaments.

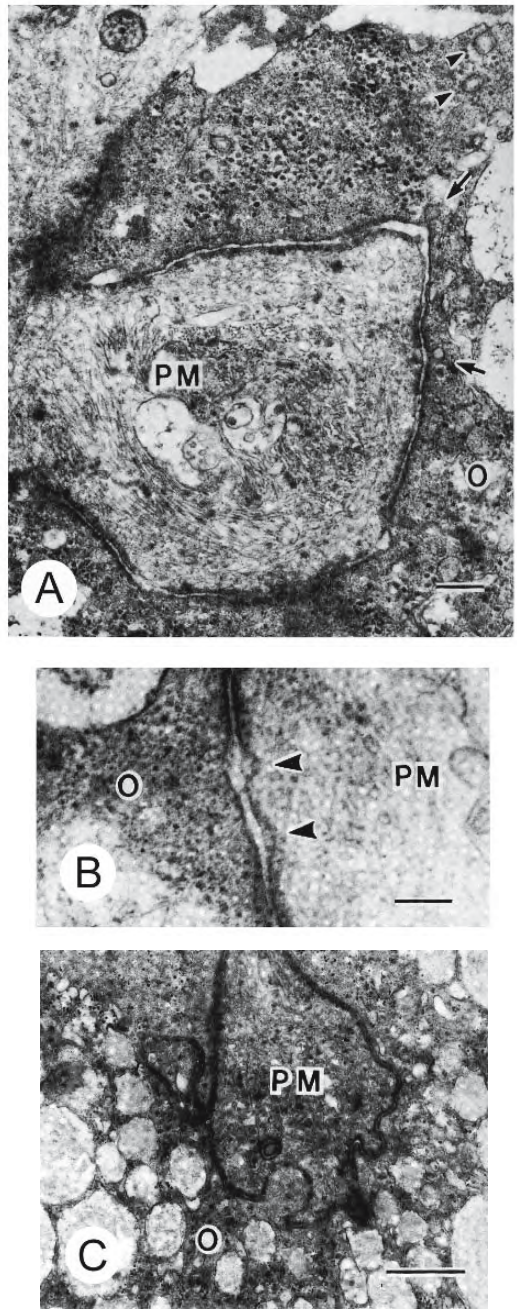

Figure 3.66: Transmission electron micrographs of end bulbs of micropylar cells from the chum salmon *Oncorhynchus keta* during late vitellogenesis. (From Kobayashi and Yamamoto, 1985; © reproduced with permission of John Wiley & Sons, Inc.).

A. The bulbous end of a micropylar cell (PM) has invaginated the surface of the oocyte (O). Adhaerens junctions are abundant between the membranes of the two cells. Vesicular bodies and 10-nm filaments are abundant in the bulb. There are large (arrowheads) and small (arrows) coated vesicles in the ooplasm. Bar = 0.5 μm.

B. Adhaerens junctions have developed between the membrane of the process and the oolemma. There is a suggestion of exocytotic activity (arrowheads) on the membrane of the micropylar cell (PM) where it lies adjacent to the oolemma. Bar = 0.2 μm.

C. Ellipsoidal vesicles are abundant in the ooplasm (O) adjacent to the lobulated end of the process (PM). Bar = 1 μm.

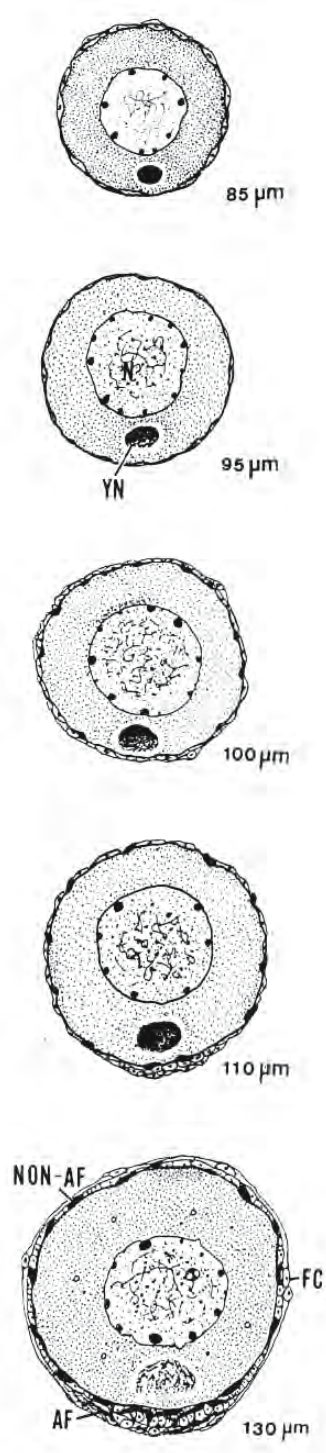

Figure 3.67: Diagrams summarizing changes in the morphology and distribution of the yolk nucleus and the nuclei of follicular cells in sectioned oocytes of the medaka *Oryzias latipes*. (From Iwamatsu and Nakashima, 1996; reproduced with permission from the Zoological Society of Japan).
Abbreviations: AF, attaching filaments; FC, follicular cell; NON-AF, non-attaching filaments; YN, yolk nucleus.

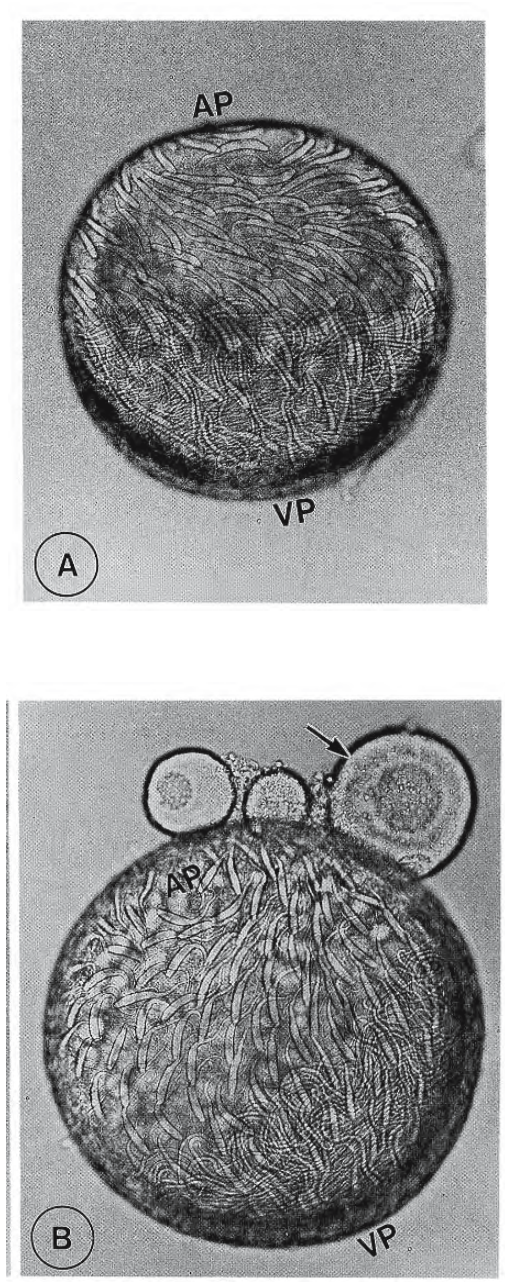

Figure 3.68: Photomicrographs of living vitellogenic oocytes of the medaka *Oryzias latipes* showing chorionic filaments; the filaments assume either a right- or left -handed spiral pattern. **A** is an early stage of vitellogenesis and the filaments demonstrate the right-handed pattern. **B** represents a later stage and its filaments spiral in a left-handed direction. Long, attaching filaments wind on the vegetal hemisphere; the shorter non-attaching filaments adorn the chorion over the remainder of the oocyte. The proximal part of the attaching filaments bends in the direction of the animal pole. Early previtellogenic oocytes, about 115 μm in diameter (arrow), are shown in **B**. These display primordial filaments. X 210 (From Iwamatsu, 1992; reproduced with permission from the Zoological Society of Japan).
Abbreviations: AP, animal pole; VP, vegetal pole.

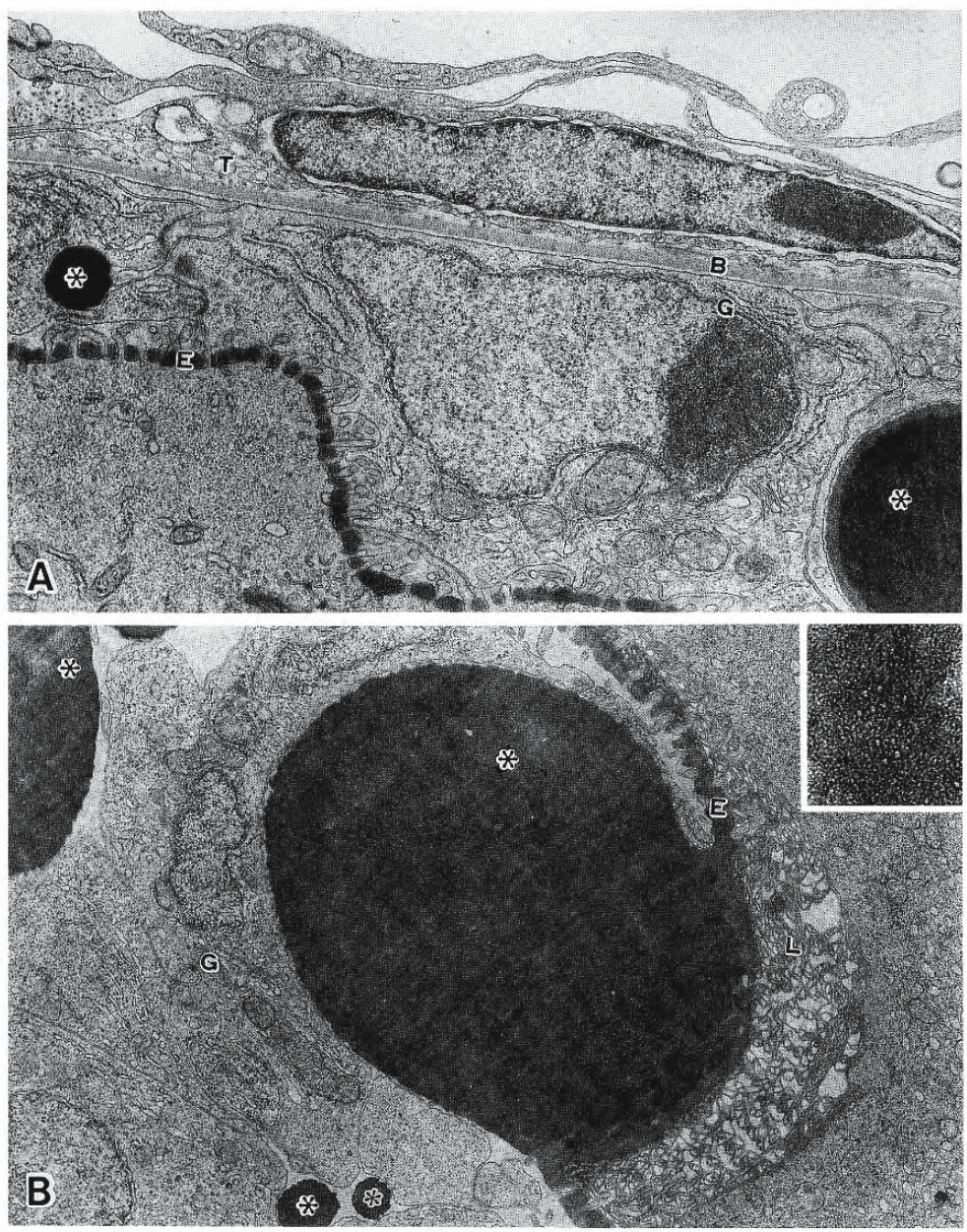

Figure 3.69: Transmission electron micrographs of sections of previtellogenic oocytes of the medaka *Oryzias latipes* showing non-attaching filaments among the follicular cells (G). (From Iwamatsu, 1992; reproduced with permission from the Zoological Society of Japan).

A. Non-attaching filaments (*) between follicular cells during late previtellogenesis. The follicular epithelium (G) lies between its basement membrane (B) and the zona pellucida (E). A thecal cell (T) overlies the basement membrane. X 13,000.

B. A non-attaching filament at the centre (*) originates from the zona pellucida which consists of an outer layer (E) and an inner layer (L). X 9,700.

The *inset* shows the outer layer of the zona pellucida composed of electron-dense amorphous and tubular structures. X 92,000.

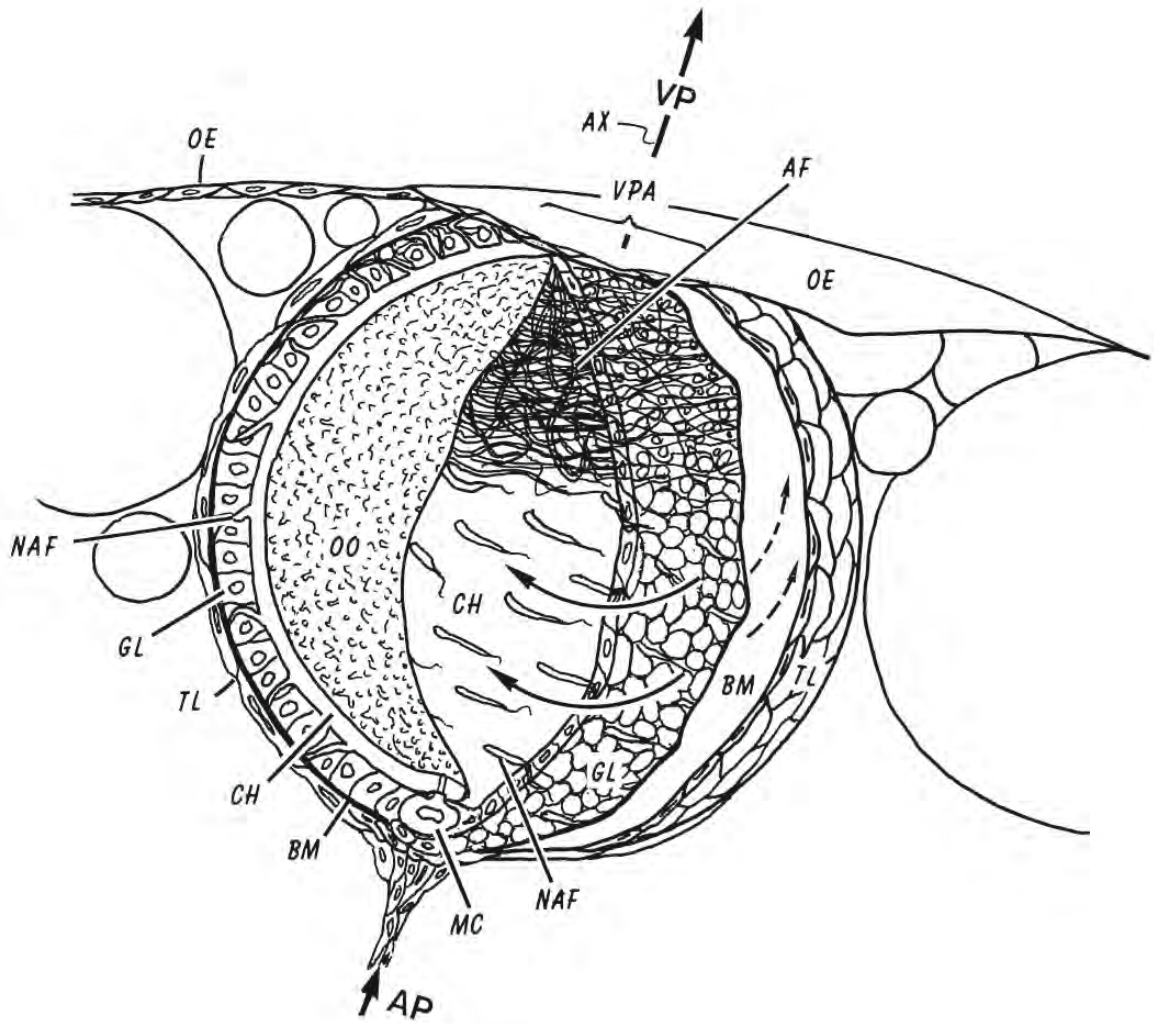

Figure 3.70: Hypothetical diagram to illustrate the rotation of an oocyte around an axis in the follicle of the medaka *Oryzias latipes.* (From Iwamatsu, 1994; reproduced with permission from Blackwell Publishing) The oocyte, with its follicular layer (GL) rotates within the basement membrane (BM) and the thecal layer (TL) prior to the differentiation of the micropylar cell (MC) at the animal pole (AP), the antipode of the vegetal pole (VP) at the centre of the vegetal pole area (VPA). The direction of rotation (arrows) around the oocyte axis is opposite to the direction of bending of the attaching (AF) and non-attaching (NAF) filaments on the chorion (CH). An oocyte could rotate in either direction within the follicle. OE, ovarian epithelium.

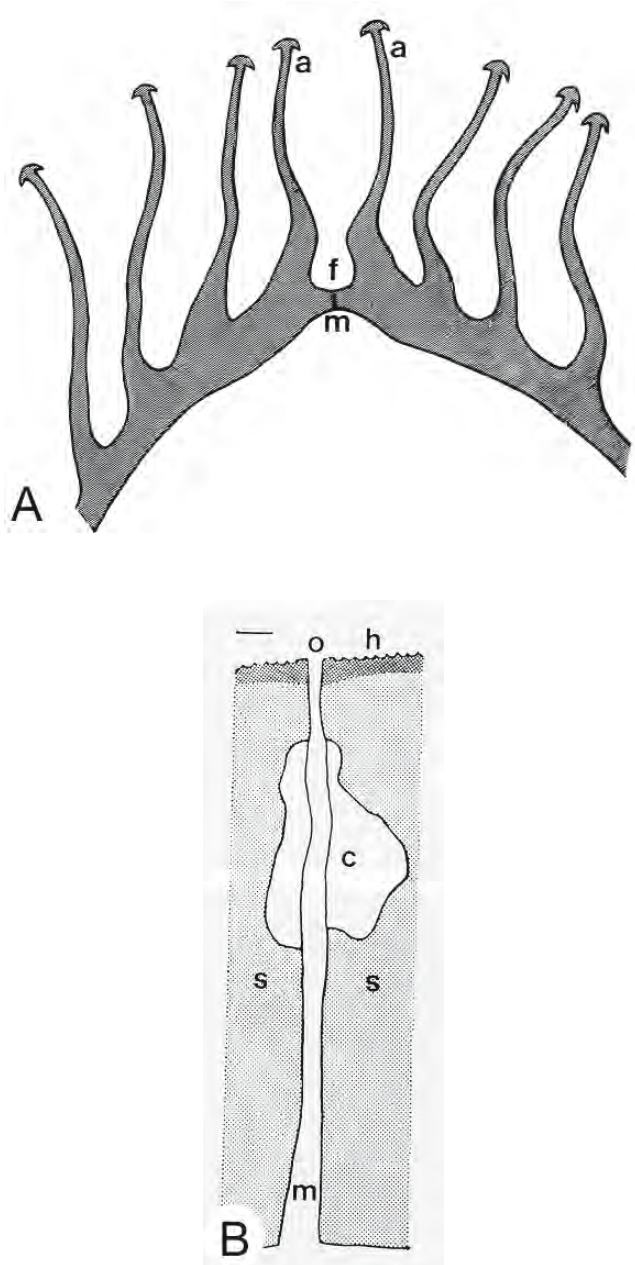

Figure 3.71: Schematic diagrams from an ovum of the hagfish *Myxine glutinosa.* (From Kosmath, Patzner, and Adam, 1981; reproduced with permission from Urban & Fischer Verlag).

A. The micropylar area showing anchoring filaments (a) rooted in the chorion, micropylar funnel (f), and the micropylar canal (m).

B. The micropylar canal (m) penetrates the chorion (s) passing through an enlarged cavity (c). It is entered by way of the micropylar opening (o).

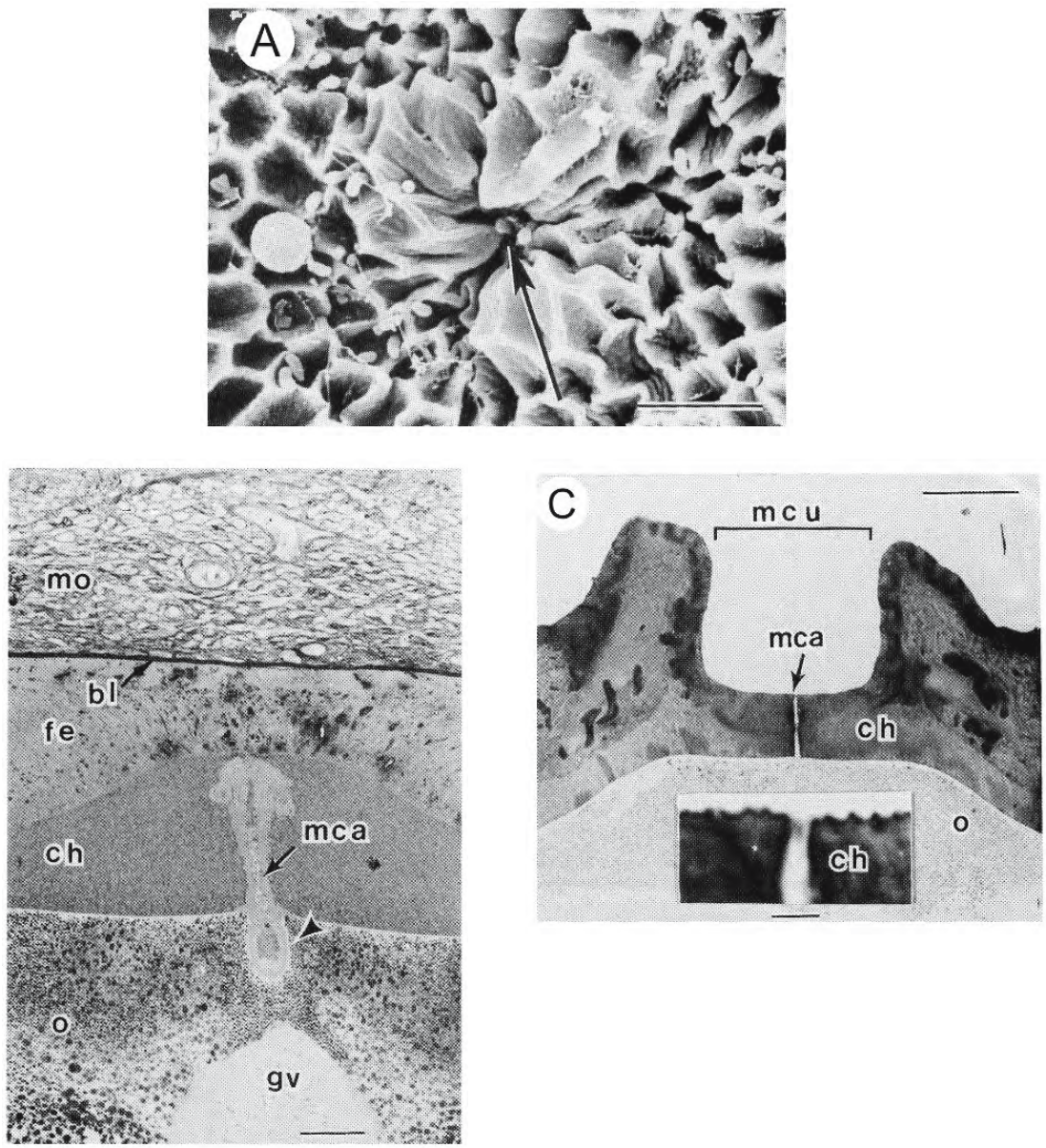

Figure 3.72: Micrographs illustrating the micropylar apparatus of the hagfish *Eptatretus stouti.* (From Koch et al., 1993; reproduced with permission from Elsevier Science).

A. Scanning electron micrograph of the surface of the micropylar base with possible entrance to the micropylar canal (arrow). X 1,700.

B. Photomicrograph of a section of an oocyte showing early development of the micropylar canal (mca) in the zona pellucida (ch) with anchor filaments not yet evident. A region of the canal (arrowhead) has penetrated into the ooplasm (o) near the germinal vesicle (gv). X 190 Bar = 50 µm.

Abbreviations: bl, basal lamina; fe, follicular epithelium; mo, mesovarium..

C. Photomicrograph of a section through the micropylar canal (mca) opening from the micropylar cup (mcu) in the chorion (ch) of an ovulated egg. X 75 Bar = 200 µm.
Inset: higher magnification of the honeycomb base of the micropylar cup adjacent to the canal. X 690 Bar = 10 µm.

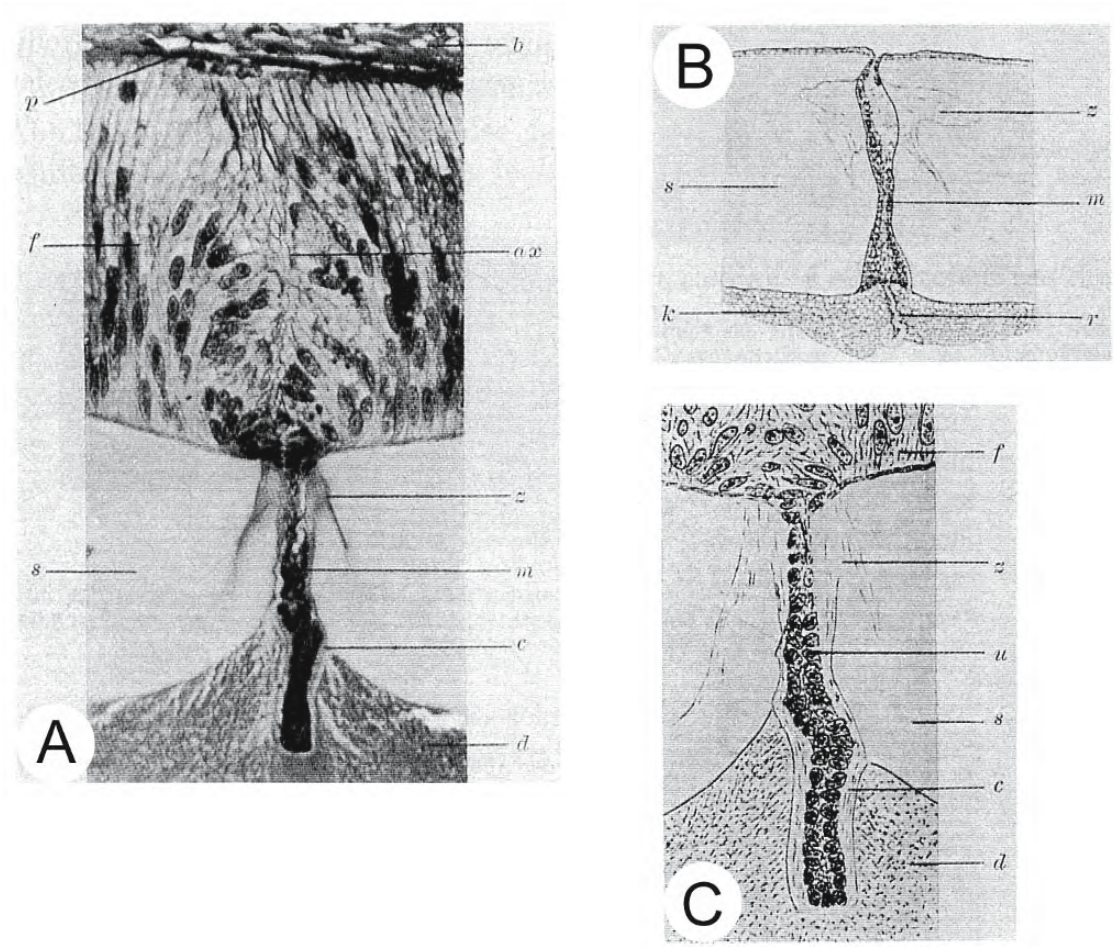

Figure 3.73: The micropylar apparatus of an oocyte of the hagfish *Myxine glutinosa* immediately before spawning. (From Lyngnes, 1930; reproduced with permission from Springer-Verlag).

A. Photomicrograph of a section through the micropylar canal. The thick follicular epithelium (f) consists of columnar cells and is separated from the connective tissue (b) of the theca by the follicular basement membrane (p). The zona pellucida (s) is perforated by the micropylar canal (m). Follicular cells along the axis of the micropylar canal assume a spindle formation (ax) that continues as a cord of cells through the micropylar canal to form a cylindrical extension (c) that invaginates the germinal disc of the oocyte. The yolky cytoplasm of the oocyte (d) is shown at the bottom. Some of the follicular cells forming the micropylar canal appear to have hollowed out a space (z) alongside. X 160.

B. Sketch of the micropylar apparatus based on Fig. **A**. There is a hyaline streak (r) in the germinal disc (k) at the base of the micropylar canal. X 260.

C. A sketch of the micropylar apparatus at a higher magnification. An outgrowth (u) of follicular cells (f) forms a cylinder of cells (c) that invaginates the germinal disc (d). X 260.

CHAPTER 4

EVENTS ASSOCIATED WITH FERTILIZATION

4.1 Introduction

Within seconds of fertilization in teleosts there is an explosive breakdown of the cortical vesicles over the entire surface of the egg[13]. The chorion is lifted away from the oolemma and the PERIVITELLINE SPACE is created. Although this "cortical reaction" is induced by the penetration of the oolemma by a spermatozoon, some freshwater eggs may be activated "parthenogenetically" by their passage from the isotonic body fluids into fresh water during spawning (Hart, Yu, and Greenhut, 1977; Hart and Yu, 1980; Kobayashi, 1985a; Ohta et al., 1990; Hart and Collins, 1991). Activation of unfertilized marine eggs of the long rough dab *Hippoglossoides platessoides limandoides* can be induced by transferring them to sea water (Lønning and Davenport, 1980).

4.2 Oolemma and the Cortical Ooplasm

Before fertilization, the surface of an egg from which the chorion has been removed is cobbled with hemispherical bulges, revealing the location of cortical alveoli below (Figure 4.1) (Brummett and Dumont, 1981; Kobayashi, 1985a; Ohta et al., 1990; Hart and Collins, 1991). The oolemma is decorated by numerous microvilli and microplicae which are sparser over the elevations than in the regions between. In sections, the microplicae appear as electron-dense, finger-shaped projections (Figure 4.2B). The apposition of the cortical vesicles to the inside of the oolemma is accompanied by an apparent clearing of membrane particles from the site of contact between the apposed membranes; a dimple in the particle-free zone appears to mark the site of contact (Hart and Collins, 1991) (Figures 4.2D,E). The oolemma is closely associated with the chorion in intact eggs and the folds and microvilli either invade the lumina of the pore canals or are sandwiched between the chorion and the oolemma.

Beneath the oolemma is the CORTICAL LAYER OF OOPLASM (Kobayashi, 1985a; Hart and Collins, 1991). It is thickest at the animal pole and gradually becomes thinner toward the antipode. The electron-dense PERIPHERAL REGION of cortical ooplasm lacks most of the organelles found in the rest of the cortex although profiles of endoplasmic reticulum and an occasional coated vesicle may be detected. The ooplasm is less compact in the INNER REGION which contains the most conspicuous organelles of the cortex: the spherical, membrane-bound CORTICAL ALVEOLI (Figures 4.2A to C). Other organelles of the inner region are mitochondria, circular and tubular profiles of agranular endoplasmic reticulum, annulate lamellae, lysosomes, and Golgi complexes (Figure 4.2B). An elaborate anastomosing network of smooth cisternae throughout the cortical cytoplasm constitutes the CORTICAL ENDOPLASMIC RETICULUM (Figure 4.3A). It consists of isolated circular vesicles and tubular profiles and forms close associations with both the cortical alveolar membranes and oolemma (Figures 4.3B to D).

Except below the micropyle, the membrane-bound cortical alveoli are arranged within the cortical ooplasm, always separated from the oolemma by cytoplasm (Figure 4.4). They are variable in size, attaining diameters of 2 to 25 μm in chum salmon *Oncorhynchus keta* (Kobayashi, 1985a), 10 to 40 μm in medaka *Oryzias latipes* (Gilkey et al, 1978), and up to 50 μm in *Fundulus heteroclitus* (Selman, Wallace, and Barr, 1988). (An apparent fusion during fixation has artifactually produced vesicles greater than 100 μm in sections of *Fundulus* eggs.) In these three species the cortical alveoli form a single layer within the cortical ooplasm but, in the rose bitterling *Rhodeus ocellatus,* they occur in several layers (Ohta et al., 1990). In the zebra danio *Brachydanio rerio,* a single layer surrounding the sperm entry site contrasts with multi-

[13] Hart (1990) has presented an exhaustive review of this literature. Little information is available on eggs of other fishes.

layered rows throughout the remainder of the ooplasm (Hart and Donovan, 1983). Near the sperm entry site of *Brachydanio,* the alveoli are 2.7 to 2.8 μm in diameter and are densely packed; from this region to the vegetal pole, they progressively increase in size and become sparser so that a gradient is established in the structural organization of the egg cortex from the site of sperm entry to the vegetal pole.

There is indirect evidence for the presence of actin and actin-containing filaments within the cortical ooplasm (Hart and Wolenski, 1988; Wolenski and Hart, 1987b, 1988a). Microfilaments 6 to 7 nm in diameter have been described in the cores of microplicae and in the cortical layer near the sperm entry site of *Brachydanio* (Wolenski and Hart, 1987a). The presence of actin was demonstrated just beneath the oolemma of unactivated eggs using rhodamine phalloidin and fluorescence microscopy (Wolenski and Hart, 1987b). It is suggested that bundles of actin filaments displace membranous organelles from the cortex and may be important in maintaining the overall shape of the egg and plicae. In eggs of the chum salmon, they may assist in expulsion of the cortical alveoli during the cortical reaction (Kobayashi, 1985a).

4.3 Cortical Alveoli

An electron-dense core surrounded by an electron-lucent halo has been described in cortical alveoli of several species (Figure 4.2B) (Iwamatsu and Ohta, 1976; Kudo, 1976, 1983; Hart and Yu, 1980; Hart and Donovan, 1983; Kobayashi, 1985a). In eggs of *Brachydanio,* the core consists of tightly-packed particles 6 to 12 nm in diameter; these are surrounded by less compact, circular fibrillo-granular aggregates 25 to 50 nm in diameter (Figures 4.5A to C) (Hart and Collins, 1991). Sometimes cortical alveoli are observed lacking the halo; in the zebrafish the perigranular membrane encloses a mass of small particles of a similar size to those of the central mass of the cored particles (Figure 4.5D). Cortical granules of *Salmo gairdneri* show an electron-lucent core surrounded by electron-dense material (Figure 4.6) (Inoue et al., 1987). There are two types of cortical alveoli in eggs of the rose bitterling (Ohta et al., 1990): alveoli of the animal pole contain electron-lucent droplets suspended within an electron-dense matrix (Figure 4.7A) whereas, at the vegetal pole, the contents are homogeneous and electron dense (Figure 4.7B). In addition to cortical alveoli, membrane-bound granules, packed with finely granular or homogeneous material, have been described in the cortical ooplasm of unfertilized eggs of carp *Cyprinus carpio* and goldfish *Carassius auratus* (Figure 4.8) (Kudo, 1976). Designated as CA GRANULES, they are much smaller than cortical alveoli and scattered around them. They are more plentiful in the animal than the vegetal hemisphere.

Cortical alveoli contain glycoproteins. They stain with periodic acid-Schiff reagent, alcian blue at low pH, colloidal iron, and bromphenol blue, and are often metachromatic with toluidine blue suggesting that they contain an acidic glycoconjugate consisting of a polysaccharide and protein, that is, acid mucopolysaccharide and/or mucoprotein (reviewed by Hart, 1990). A unique class of glycoproteins sharing characteristic biochemical and biological features has been designated HYOSOPHORIN and is associated with cortical alveoli of several species (Kitajima, Inoue, and Inoue, 1989). In fact, it has been suggested that these glycoproteins, not sulphated mucopolysaccharides, are the major water-soluble components of cortical alveoli (Inoue et al., 1987). H-HYOSOPHORIN has been defined as the major glycoprotein of the cortical alveoli (and therefore derived from the Golgi complex) with a high carbohydrate content (85 to 90% w/w), whose protein core comprises tandem repetitions of identical protein sequences; it is completely cleaved into repeating units (L-HYOSOPHORIN) following the cortical reaction (Kitajima, Inoue, and Inoue, 1989). Although the first hyosophorins described were polysialoglycoproteins, not all belong to this category (Taguchi et al., 1993). Despite differences in sequence, however, hyosophorins from different species of fish are characterized by the presence of either polyanionic and/or bulky multiantennary structures (Figure 4.9). A polysialoglycoprotein of 200 kDa was isolated from unfertilized eggs of the rainbow trout *Salmo gairdneri* (Inoue and Inoue, 1986; Kitajima, Inoue, and Inoue, 1986; Inoue et al., 1987). It is composed of a small protein core of 30 kDa to which are covalently bound multiply branched, variably elongated, oligo- and polysialylglycan chains. The core consists of a complete tandem repeat of about 25 tridecapeptide units. Similar polysialoglycoproteins have been reported in eggs of other salmonids and show a high degree of homology (Kitajima et al., 1988). In the kokanee salmon *Oncorhynchus nerka,* however, the hyosophorin of the unfertilized egg is unique in that two polysialylglycan chains are characterized: one contains 13 amino acids, the other 12 and, in the opinion of

Song, Kitajima, and Inoue (1990), these differences are sufficient to cast doubt on the placement of the kokanee in the Genus *Oncorhynchus.* The hyosophorin of the flounder *Paralichthys olivaceus* differs from that of other fish in possessing a novel pentaantennary carbohydrate structure with a five-tined carbohydrate fork attached to the repeating decapeptide of the protein core (Figure 4.10) (Seko et al., 1989).

Attempts to locate hyosophorin within cortical alveoli by morphological methods have been disappointing (Inoue et al., 1987). It is difficult to raise antibodies to hyosophorin, perhaps because of the unusual chemical structure of both the carbohydrate prosthetic groups and the apoprotein so that immunocytochemical methods have been of little help. In addition, the large amounts of yolk within the mature egg have hindered studies of the cortex. Hyosophorin has been identified, however, in a fraction rich in cortical alveoli obtained from homogenized salmon eggs by low-speed centrifugation.

LECTINS, specific carbohydrate-binding proteins commonly found in plants, have been described in the eggs of various fish (Krajhanzl, Horejsi, and Kokourek, 1978a,b). All known lectins contain two or more binding sites for carbohydrate units and can agglutinate, or cross link, cells. Lectins have been localized by immunological methods within the cortical alveoli of previtellogenic oocytes (Krajhanzl et al., 1984a,b; Nosek, 1984) and in the thin layer of cortical alveoli of mature eggs that have not undergone activation (Nosek, Krajhanzl, and Kocourek, 1983, 1984). Lectins are synthesized during previtellogenesis in the Golgi complex (Nosek, 1984) and increase in amount during later stages when cortical alveoli fill the entire ooplasm before moving to the periphery as the oocyte accumulates yolk (Nosek, Krajhanzl, and Kocourek, 1983). The lectins are discharged into the perivitelline space following the cortical reaction and it is suggested that they contribute to the physiological mechanisms preventing polyspermy by agglutinating supernumerary spermatozoa (Nosek, Krajhanzl, and Kocourek, 1983; Kudo and Inoue, 1989). They may also agglutinate pathogenic bacteria that penetrate the outer envelopes of the egg, thereby preventing them from attacking the egg.

4.4 Fertilization[14]

Spermatozoa of most teleostean fishes have no acrosomal apparatus and gain access to the surface of the egg through the micropyle that perforates the chorion (Iwamatsu and Ohta, 1978, 1981b; Kudo, 1980, 1983b; Brummett and Dumont, 1981; Gilkey, 1981; Kobayashi and Yamamoto, 1981, 1987; Ohta and Iwamatsu, 1983; Ohta, 1985; Wolenski and Hart, 1987a; Bern and Avtalion, 1990; Ohta, 1991; Ohta and Nashirozawa, 1996). The first spermatozoon arriving at the micropyle navigates the canal to reach the oolemmal microvilli at the SPERM ENTRY SITE (Figures 3.43A,B, 3.57A,B, 4.11, and 4.12). It attaches to these microvilli and, in some species, is rapidly engulfed before the oolemma elevates to form the FERTILIZATION CONE (Figures 4.13 to 4.16) (Iwamatsu and Ohta, 1981b; Ohta and Iwamatsu, 1983; Iwamatsu, 1998). In other species, however, the fertilization cone may develop either before or at the same time as the spermatozoon is incorporated (Kudo, 1980, 1983b; Kudo and Sato, 1985; Kobayashi and Yamamoto, 1987; Wolenski and Hart, 1987a). Following penetration of the sperm in the rose bitterling *Rhodeus ocellatus ocellatus,* the sperm entry site transforms into a SWOLLEN MASS that plugs the micropyle and prevents penetration of excess spermatozoa (Figure 4.17) (Ohta and Nashirozawa, 1996). The swollen mass may be a type of fertilization cone; it appears identical in form and function except that fertilization cones recede quickly after fusion of the membranes of the gametes but the swollen mass persists and appears to function as a micropylar plug.

The expanded surface area afforded by the cluster of microvilli at the sperm entry site may expedite the binding-fusion process (Wolenski and Hart, 1987a). There have been suggestions that the interaction between the spermatozoon and the sperm binding site results from specific receptors in the membrane of the microvilli that recognize and/or bind with the plasma membrane of the spermatozoon (Ohta and Iwamatsu, 1983; Wolenski and Hart, 1987a; Ohta, 1991). However, since spermatozoa can fertilize a dechorionated egg at any point on its surface (Sakai, 1961; Iwamatsu and Ohta, 1978), receptors for spermatozoa, if they exist, must be present over the entire oolemma (Gilkey, 1981).

[14] An exhaustive review of the recent literature on fertilization in teleosts has been presented by Iwamatsu (2000).

Spermatozoa of tilapia *Oreochromis niloticus* reach the micropyle in less than 1 second and attain the sperm binding site on the oolemma within 3 to 5 seconds after insemination (Bern and Avtalion, 1990). Engulfment of the head in this species is always followed by an indentation of the oolemma: the CLEFT OF PENETRATION (Figure 4.18). The sperm tail is still visible protruding from the oolemma 1 to 2 minutes after insemination. The microvilli of the sperm binding site gradually disappear following penetration of the spermatozoon, perhaps depriving other spermatozoa of receptors, thereby playing a role in the prevention of polyspermy.

Formation of a two-tiered fertilization cone has been described in some species. In fertilized eggs of the ayu fish *Plecoglossus altivelis,* the first fertilization cone is a cylindrical structure, about 7 μm long and 1.1 to 1.5 μm in diameter, that rises from the sperm entry site within 10 to 15 seconds of immersion in fresh water (Figure 4.19) (Kudo 1983b). At about 20 seconds, a second tier forms a pedestal about 3.2 μm high elevating the first cone from its apex. After about 60 seconds this structure recedes to form a mound on the surface of the egg with the sperm tail extending from it. A less elaborate two-tiered fertilization cone appears in the carp *Cyprinus carpio.* It reaches a height of more than 10 μm and a breadth of 3 to 4 μm within 40 seconds of immersion of fertilized eggs in fresh water, resulting in a transient plugging of the micropyle (Figure 4.20) (Kudo and Sato, 1985). Within 1.5 to 2 minutes the second tier appears at its base. The earlier cone shortens, a volcano-like structure rises in the micropylar region and, extending from the centre of its crater, is the two-tiered fertilization cone brandishing the sperm tail from its apex (Figure 4.21).

The elkhorn sculpin *Alcichthys alcicornis* provides a convenient model for studying the early stages of fertilization (Munehara, Takano, and Koya, 1989; Koya, Takano, and Takahashi, 1993). This cottid demonstrates "internal gametic association" where sperm, introduced into the ovarian cavity by copulation, enter the micropylar canals of ovulated eggs but there is no sperm/egg fusion until the eggs are released into sea water (Figure 4.22). During experimental manipulations, sperm remain attached to the ooplasmic surfaces of eggs freshly stripped from copulated females and fertilization is initiated when the eggs are immersed in sea water. By 10 seconds after immersion, a fertilizing spermatozoon penetrates the ooplasm for about half its head length and several vesicles appear in the area of penetration (Figure 4.23A). As vesiculation advances, the plasma membrane of the sperm disappears, thereby exposing the nuclear membrane of the sperm to the ooplasm. A fertilization cone forms around the unpenetrated portion of the sperm head and an electron-dense triangular region, containing no organelles other than ribosomes, appears in the ooplasm surrounding the penetrating sperm head (Figures 4.23B,C). The microtubules of the sperm tail degenerate by 30 seconds and there is a loss of motility (Figure 4.23D). The mitochondria of the sperm remain outside the oolemma. By 2 to 3 minutes the sperm has penetrated up to its midpiece. By 3 minutes after immersion, the nuclear membrane of the sperm separates from the chromatin, beginning at the anterior region of the sperm head (Figures 4.23E,F). By 5 minutes, no trace of the sperm can be detected and a separating polar body is noticable ultrastructurally (Figure 4.23G).

Although insemination takes place in two species of South American catfishes of the family Auchenipteridae, it is not clear that fertilization is internal (Meisner et al., 2000). The male has a GONOPODIUM or intromittent organ formed from an elongated genital papilla and modified anal fin (Figures 4.24A,B). The presence of sperm within the tortuous folds and narrow depressions of the ovarian cavity shows that insemination has occurred (Figures 4.24C,D) but no fertilized eggs or early embryos have been demonstrated in either species. There appear to be no distinct storage structures and, in many cases, the sperm seem to be embedded within the epithelium lining the cavity. Since the time and place of fertilization are not known, it may be that, as in the case of the sculpin, fertilization does not occur until the eggs reach seawater.

Unlike the situation in most fish, spermatozoa of the white sturgeon *Acipenser transmontanus* possess an ACROSOME at the anterior end (Cherr and Clark, 1984, 1985). This caplike, membrane-bound sac contains enzymes that are released during the ACROSOMAL REACTION and are believed to facilitate entry of the sperm into the ovum (Figure 4.25). (It is a mystery why an acrosome is needed in the sturgeon when the sperm is able to gain access to the ovum by way of multiple micropyles.) An insoluble 70 kDa glycoprotein from layer (L3), located immediately inside the insoluble jelly coat (L4) of the egg envelope, undergoes proteolysis to produce a soluble 66 kDa glycoprotein which induces the acrosomal reaction in homologous sperm but fails to do so in sperm of the Great Lakes sturgeon *A. fulvescens.*

There is no micropyle in the lampreys *Lampetra fluviatilis* and *L. planeri* and it is unclear how fertilization is accomplished (Kille, 1960; Afzelius, Nicander, and Sjödén, 1968; Nicander, and Sjödén, 1971). The spermatozoon has an acrosome and is oriented at right angles to the animal pole of the egg by the apical FIBROUS TUFT (Figure 3.40) whose fibrils appear continuous with those in the pore canals of the outer chorion (Figure 4.26). It is suggested that proteolytic enzymes from the spermatozoon dissolve a passage through the chorion by way of the pore canals. Within 2.5 minutes of striking the chorion, tail movements cease and the spermatozoon slips passively through the inner layer of the chorion and crosses the perivitelline space. When the spermatozoon embeds itself in the chorion, a HEAD FILAMENT is thrust forward from its head and becomes attached to the egg cortex (Figure 4.27), activating the egg. A "thin thread" of ooplasm rises to meet it and the spermatozoon, perhaps drawn by elasticity of the cortical ooplasmic strand, penetrates the oolemma. No supernumerary spermatozoa are seen in the perivitelline space.

4.5 Cortical Reaction

Upon activation of the egg, a wave of massive exocytosis passes over the surface of many teleost eggs and the cortical alveoli release their contents beneath the chorion into the perivitelline space (Figures 4.28 and 4.29) (Ohta et al., 1990). Cortical alveolar breakdown may easily be observed in living eggs by means of a dissecting microscope as a clearing of the somewhat opaque egg (Brummett and Dumont, 1981). The wave begins near the site of sperm penetration and proceeds to the antipode of the egg (Iwamatsu and Ohta, 1976; Gilkey et al., 1978; Iwamatsu and Keino, 1978; Brummett and Dumont, 1981; Gilkey, 1981; Kobayashi, 1985a; Ohta et al., 1990; Iwamatsu et al., 1991). This wave of exocytosis is preceded by about 17 seconds by a transient increase in cytoplasmic Ca^{2+} which is released from cytoplasmic stores, and also passes as a wave over the surface of the oocyte (Ridgway, Gilkey, and Jaffe, 1977; Gilkey et al., 1978; Yoshimoto et al., 1986; Iwamatsu, Yoshimoto, and Hiramoto, 1988). This wave has been followed in eggs of the medaka *Oryzias latipes* by means of the photoprotein AEQUORIN[15] which reacts specifically with Ca^{2+} by emitting light (Figure 4.30) (Ridgway, Gilkey, and Jaffe, 1977; Gilkey et al., 1978; Yoshimoto et al., 1986; Iwamatsu et al., 1991). Free cytoplasmic Ca^{2+} rises about 300 fold following sperm entry and then returns to its resting level. This release and removal of Ca^{2+} passes as a wave in the cortical ooplasm from the point of sperm entry to the antipode in 2 to 3 minutes. Both the Ca^{2+} wave and the cortical reaction are propagated at the same constant speed of about 10 μm per second with about 17 seconds between the two waves. By contrast, the cortical reaction is slow in the marine eggs of the long rough dab *Hippoglossoides platessoides limandoides* and a few intact cortical alveoli may be found 30 minutes after insemination (Lønning and Davenport, 1980).

No such wave of exocytosis has been observed in activated eggs of the zebra danio *Brachydanio rerio,* where the cortical reaction is initiated randomly shortly after sperm penetration and occurs, more or less simultaneously, over the entire egg surface (Hart and Yu, 1980; Hart and Collins, 1991). Breakdown is somewhat delayed around the micropyle, perhaps facilitating incorporation of the spermatozoon (Wolenski and Hart, 1987a).

A scheme for the release of the calcium from intracellular stores suggests involvement of the PHOSPHOINOSITIDE CASCADE, a common pathway in many types of cells (Figure 4.31) (Iwamatsu, Yoshimoto, and Hiramoto, 1988b). In this scheme, binding of a spermatozoon to its receptor in the oolemma leads to activation of phospholipase C (PLC), mediated by guanine nucleotide-dependent regulatory protein (Gp). PLC catalyses the breakdown of phosphatidylinositol 4,5-biphosphate (PIP_2) into diacylglycerol (DG) and inositol 1,4,5-triphosphate (IP_3). IP_3, functioning as an intracellular messenger, interacts with a specific receptor on the cytoplasmic calcium stores which release Ca^{2+} into the cytosol. This cytosolic Ca^{2+} then activates more PLC, thereby forming more IP_3 and DG, and the calcium wave continues over the egg. It is presumed that the elaborate cortical endoplasmic reticulum is the storage site of this Ca^{2+} (Figure 4.3A) (Hart and Collins, 1991).

Fertilization also triggers an abrupt depolarization of the oolemma (Figure 4.32) (Nuccitelli, 1980a,b).

[15] Concentrations of Ca^{2+} in cells can be monitored with the fluorescent probe AEQUORIN, a protein produced by the luminous jellyfish *Aequorea forskalea.* This bioluminescent protein contains a fluorescent photophore that emits light on binding Ca^{2+}; the rate of emission depends upon the concentration of Ca^{2+}.

The average resting potential of unfertilized medaka eggs in Ringer's solution is –39 ± 9 mV. Following fertilization in dilute Ringer's solution, the membrane depolarizes over a period of 20 ± 10 sec by a few millivolts, presumably by the influx of Ca^{2+} and Na^{+} ions and efflux of K^{+}. Depolarization is followed by a long hyperpolarizing phase with an average amplitude of 31 ± 12 mV. It is suggested that two changes in the oolemma bring about an increase in its permeability to K^{+} during hyperpolarization and K^{+} flows back into the ooplasm. First, the rise in internal free Ca^{2+} may cause an opening of K^{+} channels and, secondly, new K^{+} channels may be added to the surface by the incorporation of new membrane as a result of the exocytosis of the cortical vesicles. Recovery from hyperpolarization has a fast phase lasting 155 ± 18 sec followed by a slower rate of change which reaches a steady post-fertilization resting potential of –19 ± 15 mV by 9.4 ± 1 min after fertilization.

During the cortical reaction, the membranes of the cortical vesicles fuse with the oolemma and there occurs a sudden massive exocytosis (Figures 4.4, 2.5J,K, 4.33, 4.34, and 4.35) (Iwamatsu and Ohta, 1976; Hart, Yu, and Greenhut, 1977; Shackley and King, 1977; Iwamatsu and Keino, 1978; Hart and Yu, 1980; Brummett and Dumont, 1981; Kobayashi, 1985a; Schalkoff and Hart, 1986; Hart and Collins, 1991). One or more openings appear in the oolemma and the contents of the alveoli are released into the perivitelline space (Figure 4.36). Just before expulsion, a coating of compact ooplasm envelops the cortical alveoli of some species; this coat eventually coalesces with the dense peripheral ooplasm as exocytosis continues (Figures 4.37 and 4.38) (Iwamatsu and Ohta, 1976; Kobayashi, 1985a). A wide, transient CRATER or CRYPT, lined with membrane of low particle density, remains on the surface at the site of the expulsion (Figure 4.39A) and the differences in particle density are maintained between the domains of the former cortical vesicle and the oolemma, even after most evidence of exocytosis has disappeared from the surface, suggesting that constituents of the two membrane domains remain distinct and do not readily interact (Figure 4.39B) (Hart and Collins, 1991). Large numbers of microvilli sprout within the craters of some species, beginning at the opening and spreading throughout; eventually these microvilli disappear as the craters shrink (Figure 4.40) (Iwamatsu and Ohta, 1976; Iwamatsu and Keino, 1978; Brummett and Dumont, 1981; Kobayashi, 1985a).

4.6 Fate of Alveolar Membrane

As a result of cortical alveolar breakdown and exocytosis, the smooth inner surface of the alveolar membrane becomes part of the oolemma (Ohta et al., 1990). This new mosaic surface consists of two domains: the original oolemma and the membrane formerly delimiting the cortical alveoli. The mosaic is visible with the scanning electron microscope in the eggs of some species (Hart, Yu, and Greenhut, 1977; Hart and Yu, 1980; Kobayashi, 1985a; Donovan and Hart, 1986) but not in others (Iwamatsu and Keino, 1978). In the zebra danio, for example, the former alveolar membrane has a pebbled surface while the oolemmal surface appears folded (Figure 4.41A). Microvilli appear in the craters within two minutes of activation in the chum salmon *Oncorhynchus keta* and obscure the distinction between domains (Kobayashi, 1985a). The magnitude of the incorporation of membrane can be appreciated from estimates of the areas of the domains in the zebra danio whose egg is 500 μm in diameter and contains about 3300 alveoli with an average diameter of 13 μm (Hart, Yu, and Greenhut, 1977). The surface area of the unfertilized egg would be 785,400 μm^2 and the area of alveolar membrane added to this surface during the cortical reaction is estimated to be as great as 1,776,000 μm^2. How is this excess membrane accommodated?

The mosaic resulting from exocytosis appears to be temporary and the alveolar membranes likely have limited existence on the surface of the egg (Hart and Yu, 1980; Hart and Collins, 1991). Several suggestions have been made for the uptake of the alveolar membrane. Some membrane is incorporated into new microvilli that sprout on the surface, especially within the craters (Iwamatsu and Ohta, 1976; Iwamatsu and Keino, 1978; Brummett and Dumont, 1981; Kobayashi, 1985a); some is strung out into threads and lost into the perivitelline space (Figure 4.42) (Brummett and Dumont, 1981); and some is taken up by endocytosis (Hart and Yu, 1980; Kobayashi, 1985a; Donovan and Hart, 1982, 1986; Hart and Collins, 1991). It appears that this endocytosis is selective, with the vesicular membrane being taken up from the vacated craters in coated vesicles and passed to the lysosomal compartment (Figures 4.41B,C and 4.43). Degradation in the lysosomal compartment would yield important protein and lipid precursors for the construction of the new membrane that will be required for cleavage of the fertilized egg. Localized folds of the oolemma

then overgrow and replace any alveolar membrane remaining at the surface. No evidence for membrane uptake by endocytosis was found, however, in eggs of *Fundulus heteroclitus* (Brummett and Dumont, 1981).

4.7 Perivitelline Space

Simultaneous with the cortical reaction the chorion separates from the oolemma, creating the PERIVITELLINE SPACE (Figures 4.44 and 4.45) (Iwamatsu and Ohta, 1976; Hart and Yu, 1980; Brummett and Dumont, 1981; Kobayashi, 1985a). A short time after fertilization, the chorion is completely lifted away from the oolemma and the narrow perivitelline space is clearly demarcated. As exocytosis continues, the space continues to widen as the extruded contents of the cortical alveoli become organized as a conspicuous layer of gelatinous material under the chorion. There are two factors involved in creating the perivitelline space: not only is there a decrease in the volume of ooplasm as a result of the loss of the cortical alveoli, but there may also be an expansion in the diameter of the egg itself caused by the osmotic influx of water (Iwamatsu and Ohta, 1976). Indeed, because of this expansion, the chorion becomes thinner. A soft, elastic chorion is found, for example, in eggs of the long rough dab *Hippoglossoides platessoides limandoides* and a large perivitelline space is produced that constitutes as much as 85% of the total volume of the egg (Lønning and Davenport, 1980). In eggs of the cod *Gadus morhua,* on the other hand, the chorion is inextensible and the small perivitelline space, which occupies up to 20% of the volume of the egg, is created mainly at the expense of the ooplasm (Davenport, Lønning, and Kjørsvik, 1981).

The chorion acts as a semipermeable membrane, being impermeable to many of the large molecules of the alveolar exudate but permeable to water, small electrolytes, sugars, and dyes (Alderdice, Jensen, and Velsen, 1984). Therefore the alveolar exudate sets up a concentration gradient across the chorion, drawing water and solutes into the perivitelline space from the bathing medium, the so-called "colloid osmotic pressure" (Yamamoto, 1961). Presumably the net influx ceases when internal hydrostatic pressure resists further inflow. At equilibrium, however, there would still be diffusion in both directions of water and small electrolytes (Potts and Rudy, 1969). The high affinity for water of "hydrophilic sols" in the alveolar exudate may also contribute to the influx of water (Lønning and Davenport, 1980).

Transparent SPHERICAL BODIES are visible within the perivitelline space shortly after the cortical reaction begins. These are remnants of the electron-dense cores of the cortical alveoli that swell and, in the living egg, become more transparent; in the medaka *Oryzias latipes,* they attain diameters of 5 to 63 μm. With the scanning electron microscope they appear as dense spherules on the inside of the chorion (Figure 4.46). Spherical bodies remain visible for some time during development. It is suggested that the oolemma and chorion are held apart, at least in part, by the physical presence of these bodies (Iwamatsu and Ohta, 1976).

With the release of the alveolar contents into the perivitelline space, a special protease appears that cleaves the large H-hyosophorin molecules into their least repeating units, L-hyosophorin, and these become a major consituent of the perivitelline fluid (Inoue and Inoue, 1986; Inoue et al., 1987). The depolymerization appears to be complete within 5 minutes of fertilization. The enzyme is a unique proteinase, HYOSOPHORINASE (Kitajima, Inoue, and Inoue, 1989), that is probably present in an inactive form, together with H-hyosophorin, within the cortical alveoli (Kitajima and Inoue, 1988). Presumbly its activity is inhibited in the dormant egg by the high ionic strength within the alveoli and, following exocytosis, it becomes active in the low ionic concentrations of salt within the perivitelline fluid. It has been suggested that one of the functions of L-hyosophorin may be as an osmoregulator in the perivitelline space (Kitajima, Inoue, and Inoue, 1989). L-hyosophorin molecules have been reported in the fluids surrounding salmonid embryos until hatching.

4.8 Formation of the Chorion

Following the cortical reaction, the eggs of most species become turgid as the result of two processes: not only is there an influx of water, creating increased turgor pressure on the chorion, there are also chemical and structural changes within the chorion itself that increase its "hardness", thereby making it tougher and more rigid. The zona pellucida is catalytically converted into a highly cross-linked and insoluble chorion (Oppen-Berntsen, Helvik, and Walther, 1990). Peroxidase in the chorion of the fish *Trilobon hakonensis* may help toughen the chorion by crosslinking tyrosine residues; in the presence of NaI and H_2O_2,

it may also assist in the defence of the egg against bacteria, fungi, and viruses (Kudo, Sato, and Inoue, 1988). This transformation contributes to the protection of the embryo, both mechanically and functionally. It is achieved through the action of exudates released from the cortical alveoli that reach the perivitelline space by way of the pore canals. The cortical alveoli appear to supply not only the structural components for the formation of the chorion but also may build an active defense mechanism for the protection of the embryo (Kudo and Yazawa, 1995). Its outer layer is digested enzymatically and replaced with these exudates which cover the surface with finely filamentous material and endow it with bactericidal and fungicidal properties, lodged largely in the outermost layers; the zona pellucida possessed no such properties (Kudo, 1982. 1992; Kudo and Inoue, 1986, 1989, 1991; Kudo, Sato, and Inoue, 1988; Kudo and Teshima, 1991). The outer layer gradually becomes five times thicker and loses its distinction into two layers (Figures 4.47 and 4.48). The transformed chorion develops increased chemical and mechanical resistance, including resistance to enzymatic degradation. Enzymes produced by the chorion (but not the zona pellucida) are able to digest several substrates and are presumed to protect the embryo from invaders or pathogens present in the ambient water (Kudo and Inoue, 1991; Kudo, 1992). Chorionic extracts, unlike those from the zona pellucida, have been shown to agglutinate fish sperm, thereby providing a deterrant to polyspermy (Kudo and Inoue, 1989). Several biochemical modifications resulting from the actions of the cortical alveolar exudates at the time of transformation have been recorded (Kudo, 1998b, 1998c).

Hardening is dependent upon the presence of Ca^{2+} ions (Zotin, 1958; Davenport, Lønning, and Kjørsvik, 1986; Kudo and Teshima, 1998). That hardening is accompanied by a change in the proteins of the chorion was demonstrated by sodium dodecyl sulphate — polyacrylamide gel electrophoresis (SDS-PAGE) where chorions of unfertilized eggs of the medaka *Oryzias latipes* gave four major protein bands of 150, 83, 78, and 51 kDa whereas, after hardening, bands were obtained of 135, 61, and 51 kDa (Masuda, Iuchi, and Yamagami, 1991). Similar changes in the constituent proteins were detected following hardening of the chorions of rainbow trout *Oncorhynchus mykiss* (Iuchi, Masuda, and Yamagami, 1991).

Hardening of chorions does not occur to the same extent in eggs of all species (Davenport, Lønning, and Kjørsvik, 1986). For example, chorions of the demersal eggs of the lumpsucker *Cyclopterus lumpus,* which must withstand contact and abrasion with the substrate, become ten times harder than those of pelagic eggs of the cod *Gadus morhua* (Lønning, Kjørsvik, and Davenport, 1984). There appears to be a structural manifestation of hardening in some species (Lønning, Kjørsvik, and Davenport, 1984; Davenport, Lønning, and Kjørsvik, 1986). Hard chorions have a surface with large characteristic papillae and the pores are filled with the same adhesive substance that covers the surface of the eggs and binds them into masses; soft chorions still retain the regular pattern of pores of the unfertilized egg (Figure 4.49).

4.9 Block to Polyspermy

Several mechanisms operate in teleosts to prevent penetration of the oolemma by more than one spermatozoon. No recent literature is available on other groups of fish but it is known that in cyclostomes, acipenserids, as well as teleosts, a single spermatozoon enters the egg at fertilization (Hart, 1990). In sharks and chimaeras, however, more than one spermatozoon may penetrate the oolemma, although only one spermatozoon nucleus fuses with the egg nucleus. Although sturgeon eggs have several micropyles, these are located in a small area on the egg surface and the cortical reaction passes over them in such a short time that polyspermy seldom occurs (Ginsburg, 1961).

In many animals, where the eggs lack a chorion, there are two blocks to polyspermy: a FAST BLOCK brought about by a change in membrane potential, and a SLOW BLOCK induced by exocytosis of the contents of the cortical alveoli (Jaffe, 1980). In fish, where the chorion restricts sperm access, there is no need for the fast electrical block and polyspermy is prevented by an array of mechanical means (Hagiwara and Jaffe, 1979; Nuccitelli, 1980b). The micropyle of many species is a passage so narrow that it restricts access to the oolemma to only one spermatozoan (Figures 4.50 and 4.51) (Ginsburg, 1961; Sakai, 1961; Brummett and Dumont, 1979; Iwamatsu and Ohta, 1981b; Kobayashi and Yamamoto, 1981; Hart and Donovan, 1983; Kudo, 1983b; Ohta and Iwamatsu, 1983; Ishijima, Hamaguchi, and Iwamatsu, 1993). In addition, a narrowing of the micropylar canal is reported following fertilization in some species, thereby excluding supernumerary spermatozoa (Figures 3.45, 4.15, and 4.52) (Kobayashi and Yamamoto 1981, 1993;

Hirai and Yamamoto, 1986; Yamamoto and Kobayashi, 1992; Iwamatsu, Ishijima, and Nakashima, 1993; Iwamatsu, 1998). Extracts of the chorion (but not of the zona pellucida) have the ability nonspecifically to agglutinate fish spermatozoa (Kudo and Inoue, 1989); this would tend to inhibit polyspermy.

When the head of the first spermatozoon penetrates the oolemma, the cortical reaction is triggered and the supernumerary spermatozoa lined up behind it are forcibly ejected from the micopylar canal by a jet stream of perivitelline fluid (Figure 4.53) and, a few seconds after activation, a plug of amorphous and granular material may block the micropylar canal (Figures 4.54 and 4.55) (Kobayashi and Yamamoto, 1981; Wolenski and Hart, 1987a; Iwamatsu et al., 1991; Iwamatsu, Ishijima, and Nakashima, 1993). In addition, a FERTILIZATION CONE may rise from the oolemma, forming a plug at the inner opening of the micropylar canal (Figure 4.56). After fertilization in the rosy barb *Barbus conchionus* the entrance to the micropylar canal is blocked by non-fertilizing sperm following elevation of the fertilization membrane (Figure 3.49C) (Amanze and Iyengar, 1990). Although the micropylar canal of the carp *Cyprinus carpio* is broad enough to accommodate several spermatozoa abreast, a conspicuous fertilization cone forms a plug that penetrates the canal and excludes supernumerary invaders (Figure 4.56) (Kudo, 1980). In some species the fertilization cone is formed by a tuft of microvilli that surround the fertilizing spermatozoon on the egg surface (Figures 4.20A,B) (Iwamatsu and Ohta, 1978; Ohta and Iwamatsu, 1983; Kudo and Sato, 1985; Ohta, 1985) but, in others, it is formed without the apparent involvement of microvilli (Figure 4.57) (Kobayashi and Yamamoto, 1981; Brummett, Dumont, and Richter, 1985; Wolenski and Hart, 1987a). The plasma membrane, shed by the fertilizing spermatozoon as it enters the ooplasm, may be incorporated into the oolemma of the fertilization cone and, since this membrane has no affinity with the membrane of other spermatozoa, may deter penetration by them (Kobayashi and Yamamoto, 1981). In spite of various mechanical blocks to polyspermy, however, a few spermatozoa may penetrate into the perivitelline space only to be inactivated by an "agglutinating factor", presumably lectins, released by rupture of the cortical alveoli (Brummett and Dumont, 1981; Nosek, Krajhanzl, and Kocourek, 1983; Kudo and Inoue, 1989).

With as many as 50 or more micropyles in Acipenseriformes, there would seem to be ample opportunity for polyspermy. It appears that this is prevented, at least in the paddlefish *Polyodon spathula,* by the formation of cytoplasmic processes, probably fertilization cones, within one minute after activation, that seal the micropylar canals (Figure 4.58) (Linhart and Kudo, 1997).

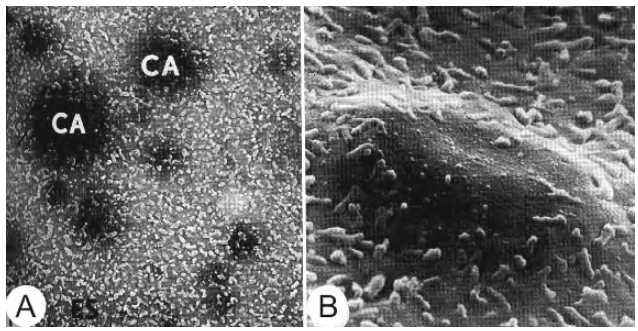

Figure 4.1: Scanning electron micrographs of the surface of unfertilized, unactivated eggs of *Fundulus heteroclitus* from which the chorion has been removed. (From Brummett and Dumont, 1981; © reproduced with permission of John Wiley & Sons, Inc.).

A. The hemispherical bulges reveal the locations of cortical alveoli (CA) beneath the surface of the egg (ES). A dense mat of microvilli invests the surface except over the cortical alveoli. X 1,800.

B. A cortical alveolus lies in the ooplasm immediately beneath the smooth bulge on the surface of the egg; microvilli are abundant elsewhere. X 8,800.

Figure 4.2: Images of the egg cortex of the zebrafish *Brachydanio rerio.* (From Hart and Collins, 1991; reproduced with permission from Springer-Verlag).

A. Scanning electron micrograph of a cross-fractured cortex of an unactivated egg showing the plasma membrane (P) decorated with a reticulum of small folds and cortical granules (CG). X 5,175.

B. Transmission electron micrograph of a section through the cortex of an unactivated egg. The outer layer of the cortical cytoplasm (small arrowheads) is more electron dense than the deeper less compact layer with cortical granules (CG). The large arrowheads point to profiles of smooth cisternae of the cortical endoplasmic reticulum. X 25,000.

Abbreviations: CV, coated vesicle; L, lysosome; M, mitochondrion.

C. Freeze-fracture replica of the cortical ooplasm of an unactivated egg with P-face (P) and E-face (E) surfaces of the fractured membranes of cortical granules. The large arrow indicates the direction of shadowing. X 29,450.

D,**E**. Freeze-fracture images of an egg two minutes after activation. P-face replicas of elevated cortical granules show an absence of membrane particles from the site of contact between the apposed membrane of the cortical alveolus and the oolemma. The inward dimple (arrowhead) in **E** in the replica of the elevated cortical granule appears to mark the site of fusion between the membrane of the cortical granule and the oolemma. **D** X 84,800; **E** X 59,000.

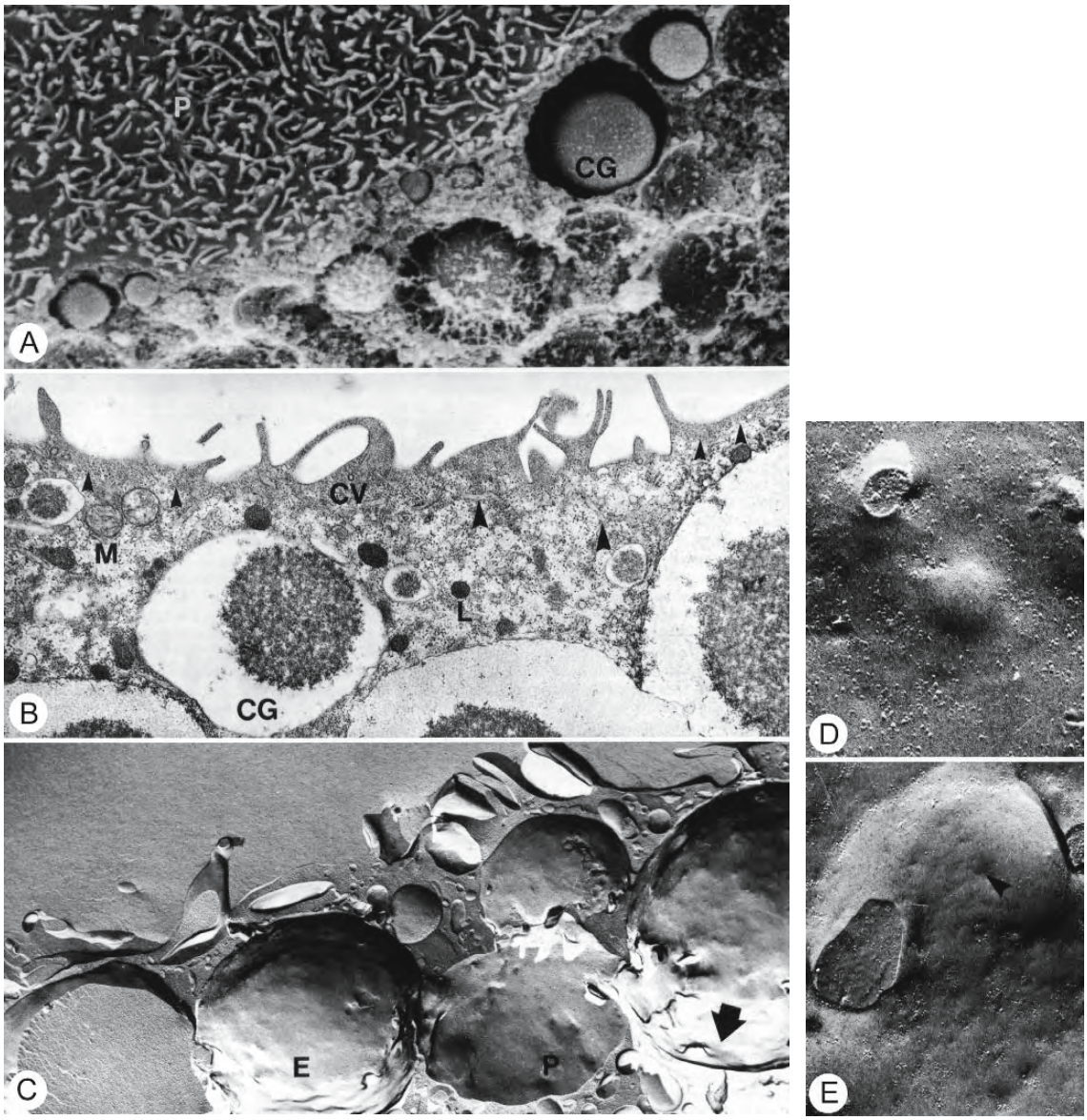

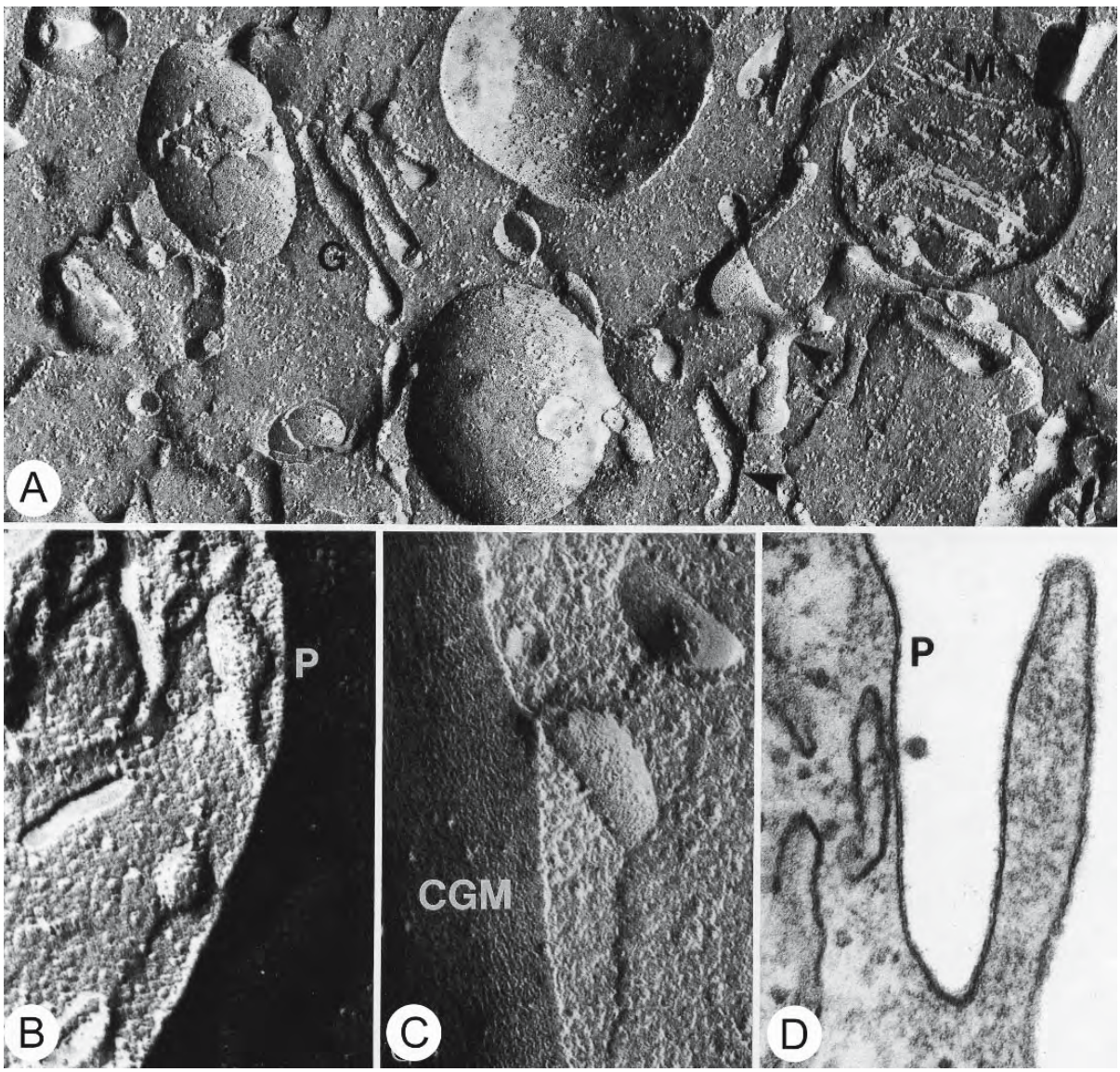

Figure 4.3: Electron micrographs of the unactivated egg of the zebrafish *Brachydanio rerio* to illustrate the cortical endoplasmic reticulum. (From Hart and Collins, 1991; reproduced with permission from Springer-Verlag).

A. Freeze-fracture replica showing the cortical endoplasmic reticulum (arrowheads) branching in the cortical cytoplasm. X 50,500.

Abbreviations: G, Golgi complex; M, mitochondrion.

B,**C**. Replicas showing the close apposition between the cortical endoplasmic reticulum and the oolemma (P) in **B** and the membrane of a cortical granule (CGM) in **C**. **B** X 36,000; **C** X 58,000.

D. Transmission electron micrograph to illustrate the narrow gap separating the cortical endoplasmic reticulum and oolemma (P). X 123,000.

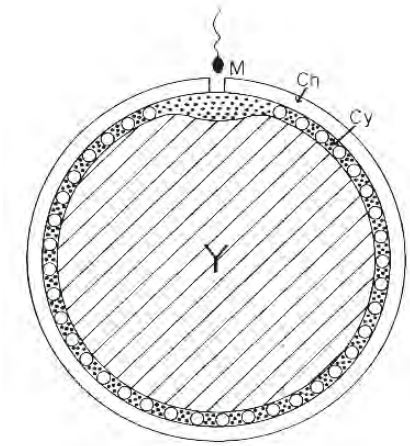

Figure 4.4: Diagram of an unfertilized egg of the medaka *Oryzias latipes* (1.2 mm in diameter). (From Gilkey, 1981; reproduced with kind permission from the Society for Integrative and Comparative Biology) A sperm will cross the chorion (Ch) via the micropyle (M), enter the cytoplasm (Cy) and initiate a wave of cortical vesicle secretion. Vesicles are indicated by small circles. Most of the egg is occupied by the membrane-bound yolk compartment (Y). The cytoplasmic thickness (0.03 mm) is exaggerated and oil droplets are omitted for clarity.

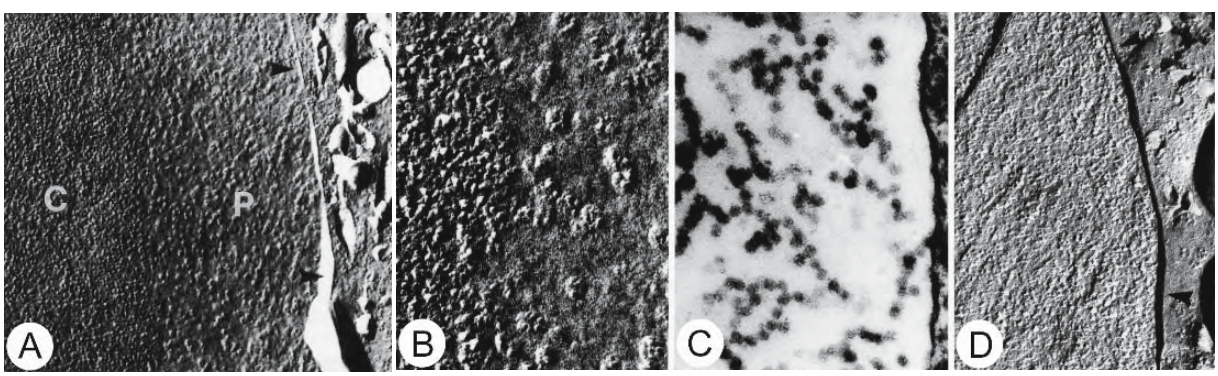

Figure 4.5: Cortical granules from unactivated eggs of the zebrafish *Brachydanio rerio.* (From Hart and Collins, 1991; reproduced with permission from Springer-Verlag).

A. Electron micrograph of a replica of a freeze-fractured cortical granule showing central (C) and peripheral (P) contents within membrane (arrowheads). X 17,000.

B. A higher magnification of the replica showing contents of the central region on the left, peripheral contents on the right. X 77,000.

C. Transmission electron micrograph of a section of a cortical granule showing the fibrillo-granular meshwork of the peripheral contents. X 77,000.

D. Some cortical granules lack the peripheral halo. This electron micrograph of a replica of a freeze-fractured cortical granule shows only small particles within the limiting membrane (arrowheads). X 77,000.

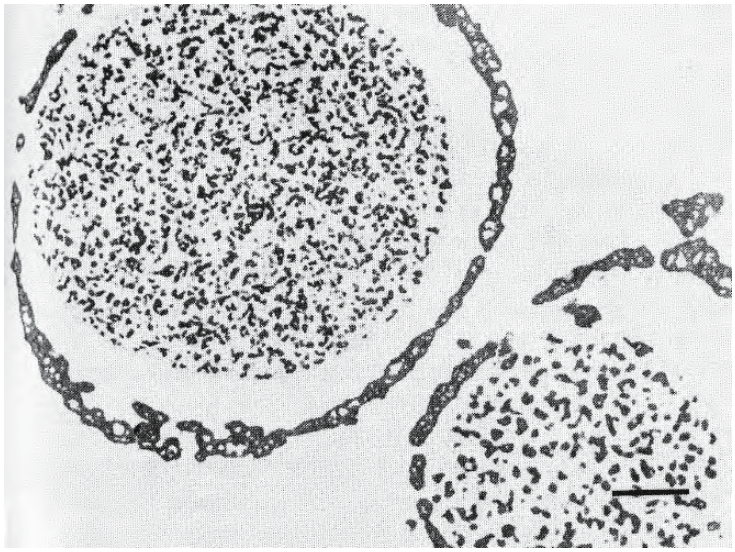

Figure 4.6: Transmission electron micrograph of a section of cortical granules of rainbow trout *Salmo gairdneri.* The granule consists of an electron-lucent spherical core and an electron-dense peripheral region. Bar = 2 μm (From Inoue at al., 1987; reproduced with permission from Elsevier Science).

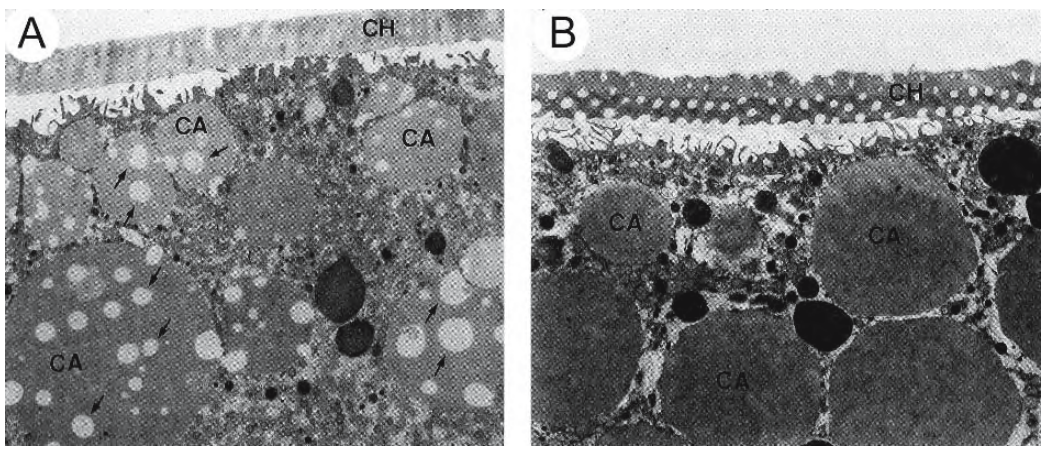

Figure 4.7: Transmission electron micrographs of sections of the cortical cytoplasm of unactivated eggs of the rose bitterling *Rhodeus ocellatus ocellatus* showing two types of cortical alveoli. (From Ohta et al., 1990; reproduced with permission).

A. Cortical alveoli (CA) of the animal pole area contain electron-lucent droplets (arrows) within an electron-dense matrix. X 3,360.

B. Contents of cortical alveoli at the vegetal pole are homogeneous and electron-dense. X 3,640.

Abbreviation: CH, chorion.

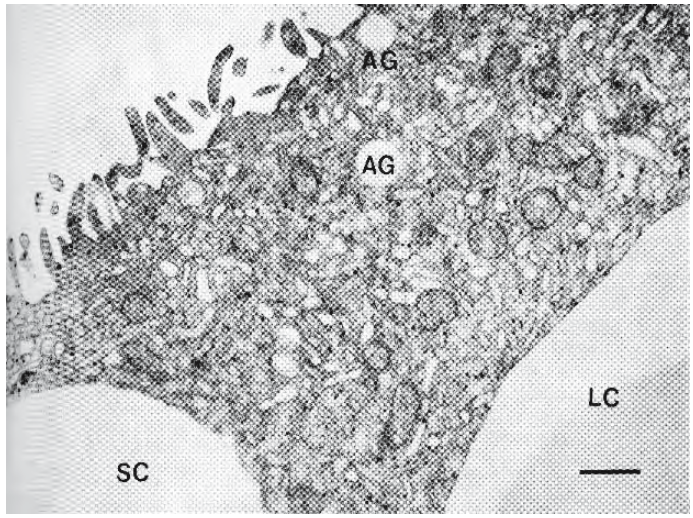

Figure 4.8: Transmission electron micrograph of a section of the cortical cytoplasm of a mature egg of the common carp *Cyprinus carpio.* Deposits of the reaction product for cholinesterase activity are localized on the plasmalemma, in the cytoplasmic matrix, in mitochondria, and on a few cisternal membranes of the granular endoplasmic reticulum, but not in the cortical alveoli or CA-granules (AG). (From Kudo, 1978; reproduced with permission from Blackwell Publishing).
Abbreviations: LC, large cortical alveolus; SC, small cortical alveolus. Bar = 1 μm. X 11,500.

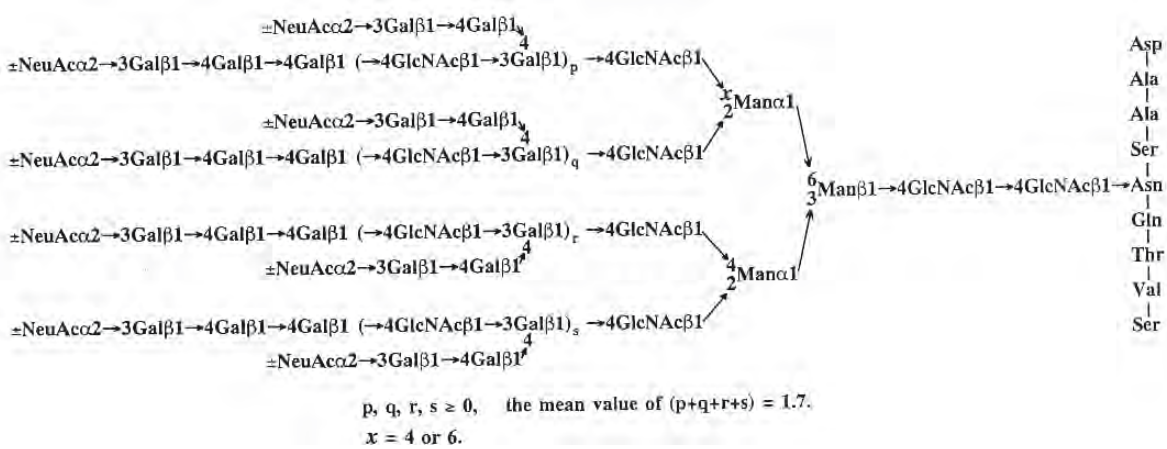

Figure 4.9: The overall structure of the L-hyosophorin from the medaka *Oryzias melastigma.* (From Taguchi et al., 1993; reproduced with permission from the American Society for Biochemistry and Molecular Biology).

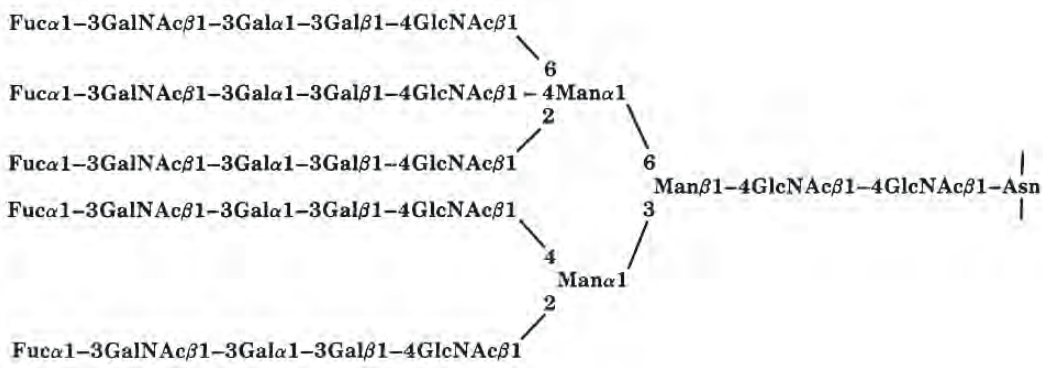

Figure 4.10: The L-hyosophorin of the flounder *Paralichthys olivaceus* differs from that of other fish in possessing a pentaantennary carbohydrate structure. (From Seko et al., 1989; reproduced with permission from the American Society for Biochemistry and Molecular Biology).

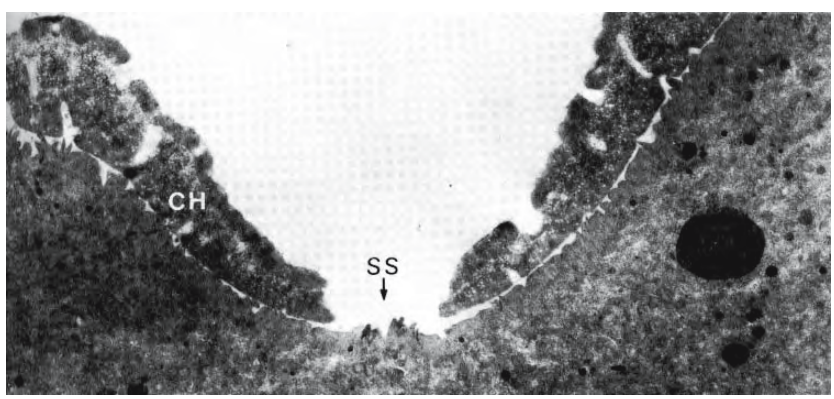

Figure 4.11: Transmission electron micrograph of a section through the micropylar region of an unfertilized egg of the bitterling *Rhodeus ocellatus.* (From Ohta, 1985; © reproduced with permission of John Wiley & Sons, Inc.) There are well-developed microvilli (or microplicae) at the sperm entry site (SS) on the egg surface beneath the micropyle. CH, chorion. X 4,200.

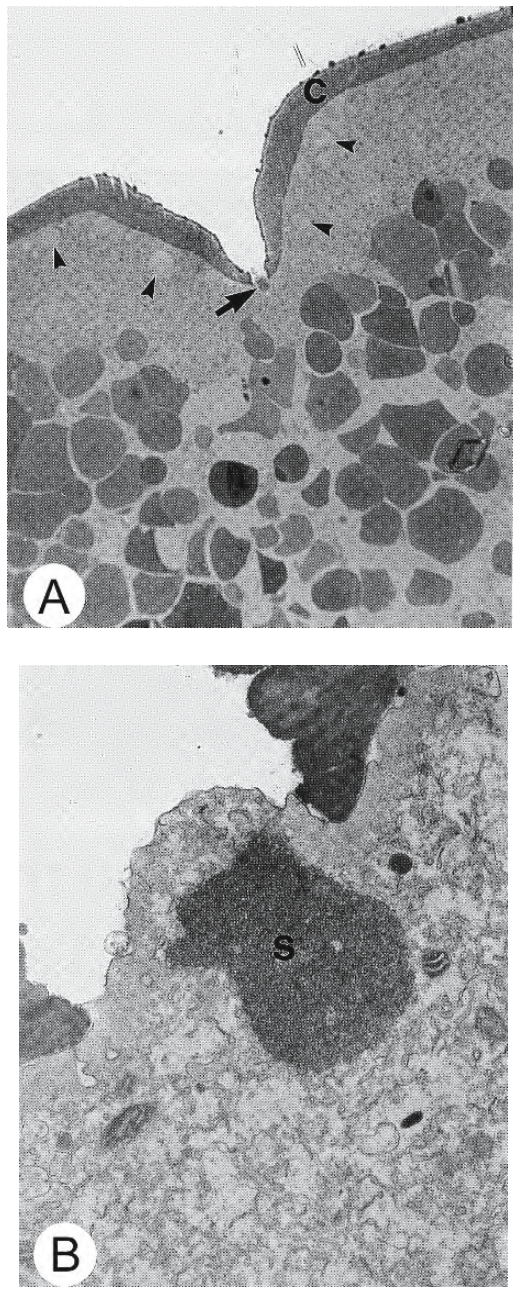

Figure 4.12: Micrographs of sections of eggs of the zebrafish *Brachydanio rerio* in the region of the micropyle taken 90 seconds after insemination. (From Wolenski and Hart, 1988b; reproduced with permission from Blackwell Publishing).

A. Photomicrograph of an egg which has completely incorporated the sperm head (arrow). There is no evidence of a fertilization cone. The cortical granules (arrowheads) have not broken down and the chorion (C) has not raised from the oolemma. X 1,200.

B. Transmission electron micrograph of the same egg showing the sperm nucleus (S) beneath the oolemma. The cytoplasm at the sperm entry site is raised slightly. X 15,000.

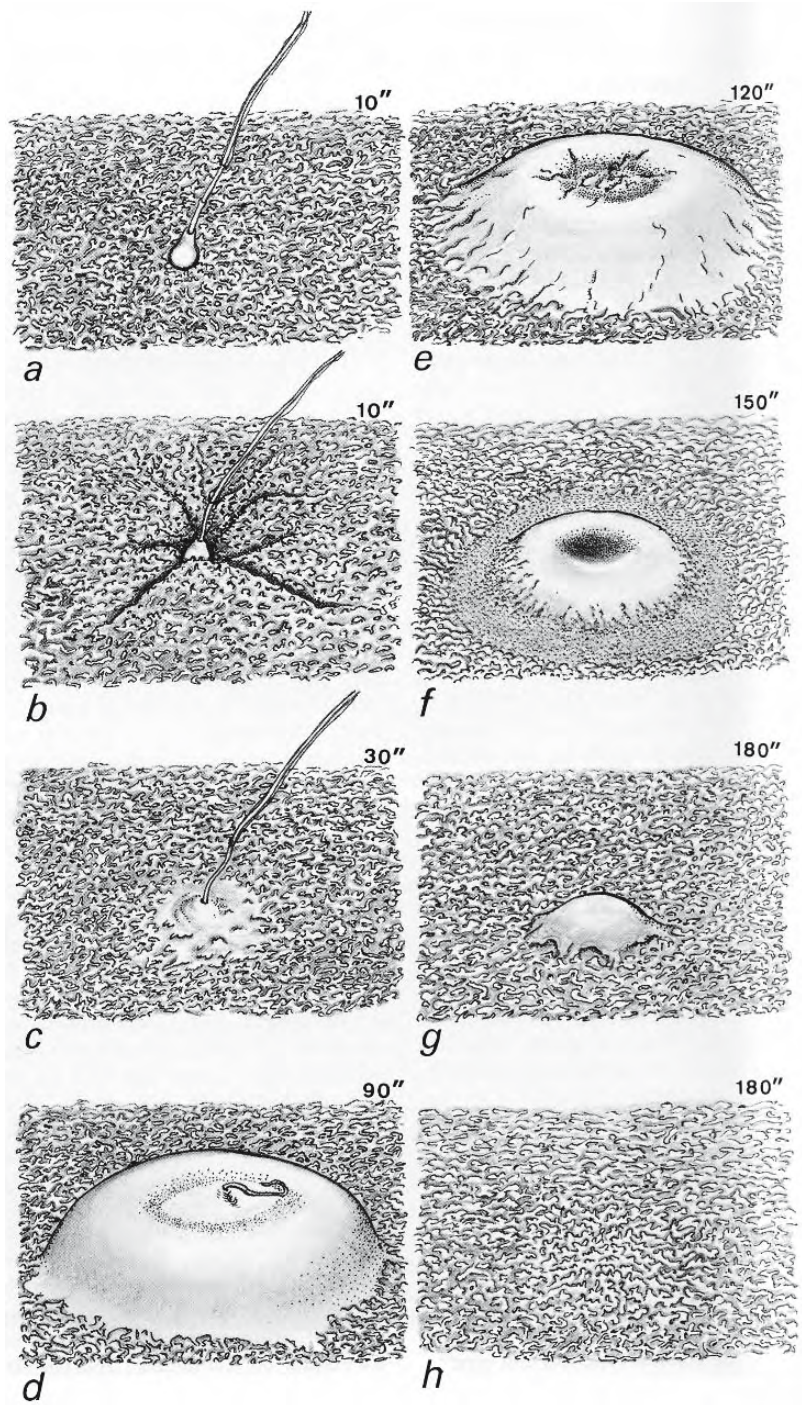

Figure 4.13: Diagrammatic representation of the events associated with sperm penetration in eggs of the medaka *Oryzias latipes* as seen with the scanning electron microscope following fixation and removal of the chorion. Times after insemination are indicated in seconds. Rapid engulfment of the sperm head is followed by formation of the fertilization cone. The forest of microvilli covering the surface of the oolemma is absent from the fertilization cone. After incorporation of the sperm, the cone retracts and disappears. (From Iwamatsu and Ohta, 1981b; © reproduced with permission of John Wiley & Sons, Inc.).

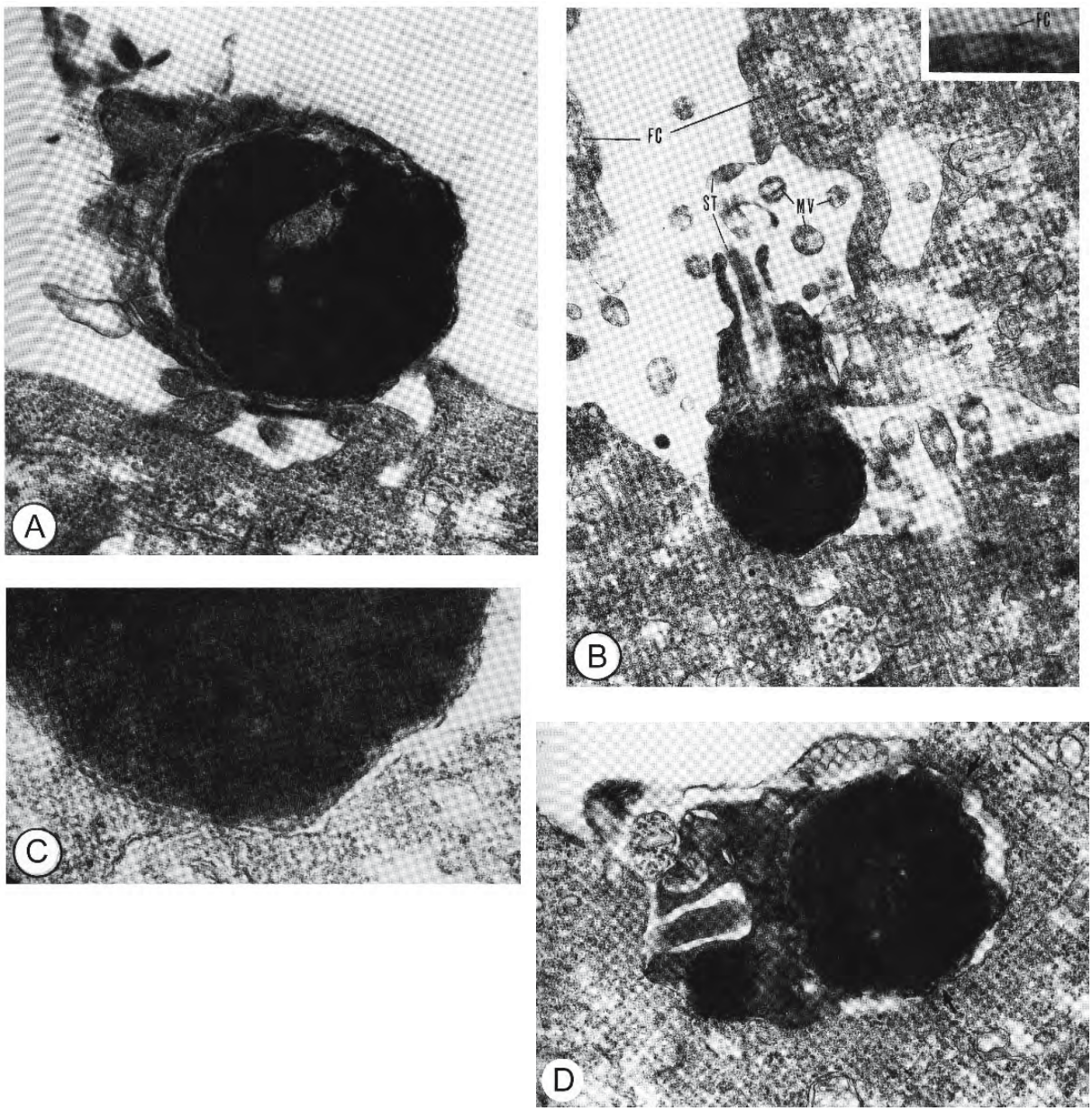

Figure 4.14: Transmission electron micrographs of the sperm attachment site in the egg of the medaka *Oryzias latipes* shortly after insemination. (From Iwamatsu and Ohta, 1978, © reproduced with permission of John Wiley & Sons, Inc.).

A. A spermatozoon on the vitelline surface. The sperm head has been caught by microvilli of the egg 10 seconds after insemination. There has been no fusion between the plasma membranes of the sperm and egg. X 28,000.

B. A spermatozoon surrounded by microvilli (MV) and the fertilization cone (FC: see inset) of the egg 10 seconds after insemination. The sperm tail (ST) is trapped by microvilli. X 16,800. **T**here has been no fusion between their plasma membranes. X 56,000.

C. A higher magnification of the point of contact between sperm and egg shown in **B**. There has been no fusion between their plasma membranes. X 56,000.

D. A spermatozoon enclosed by cytoplasmic protrusions of the egg 1 minute after insemination. There has been partial fusion (arrow) of the plasma membranes of the sperm and egg. X 28,000.

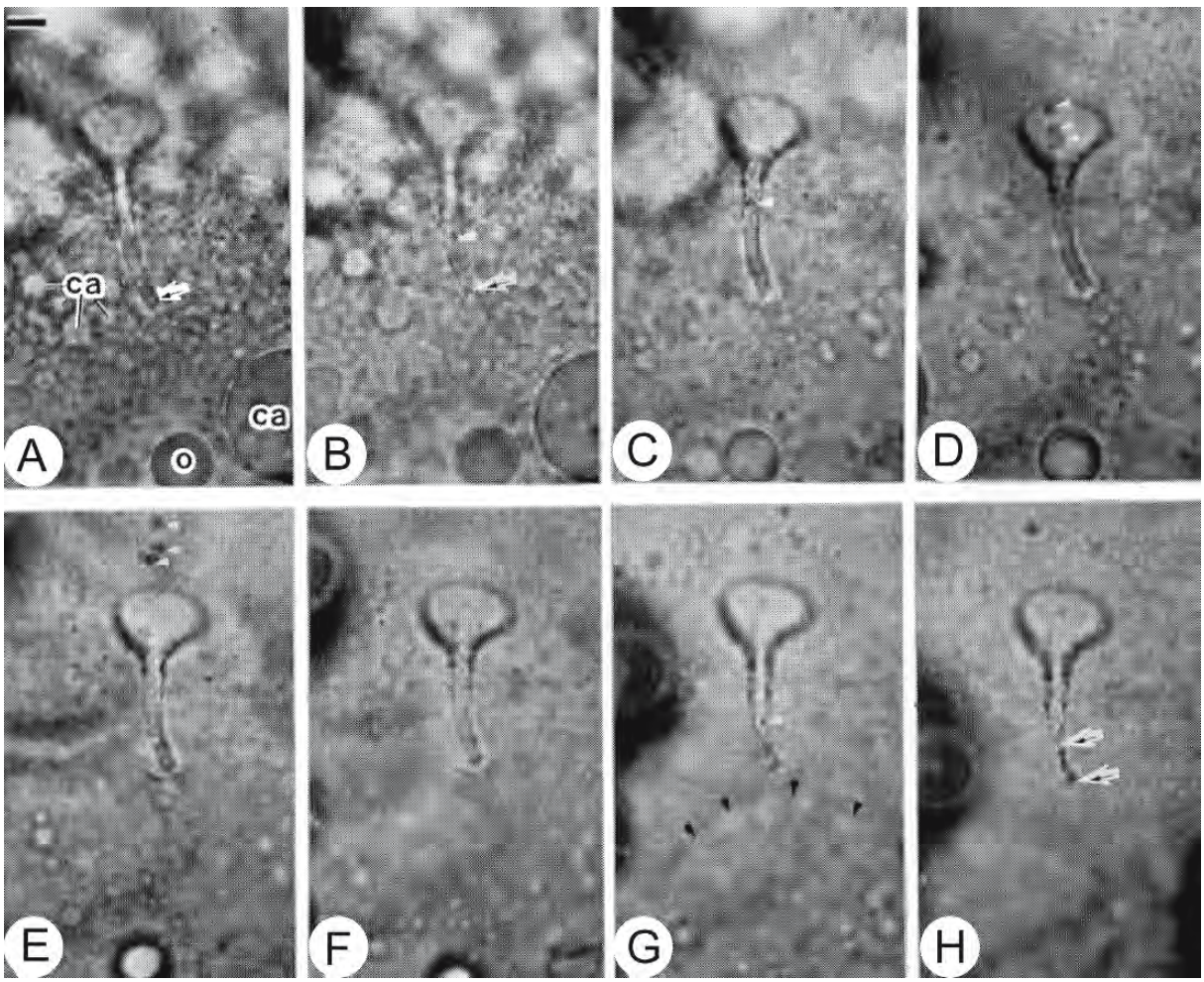

Figure 4.15: Photomicrographs of a living egg of the medaka *Oryzias latipes* showing the early response of the animal pole region to sperm entry. In these figures, about five minutes has elapsed following attachment of the spermatozoon to the oolemma. Bar = 10 μm (From Iwamatsu, 1998; reproduced with permission from Blackwell Publishing).

A. An egg with two spermatozoa in the micropyle has responded by exocytosis of cortical alveoli (ca) around the inner end (arrow) of the micropylar canal. o, oil droplet.

B,**C**. The second spermatozoon (white arrowhead) has been pushed toward the micropylar vestibule by the fertilization cone surrounding the first spermatozoon.

D-**F**. Supernumerary spermatozoa (white arrowheads) have been squeezed out of the micropyle.

G,**H**. The lower third (between arrows) of the micropylar canal has closed. Black arrowheads indicate the large blister-like fertilization cone.

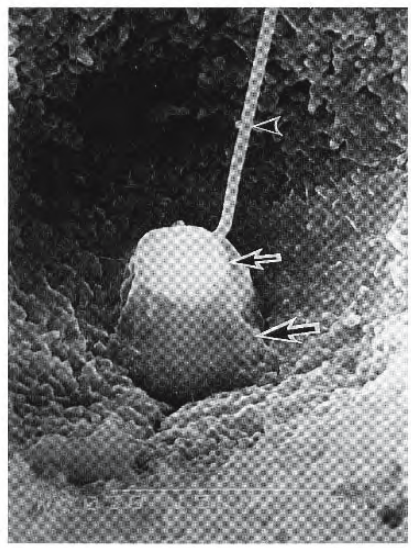

Figure 4.16: Scanning electron micrograph of an egg fused with a sperm head (small arrow) at the sperm entry site on the egg surface immediately under the micropyle in eggs of *Tribolodon hakonensis.* The fertilization cone (large arrow) has risen from the region of the site beneath the fused sperm head. The arrowhead indicates the sperm tail. X 7,900 (From Kudo, 1998a; © reproduced with permission of John Wiley & Sons, Inc.).

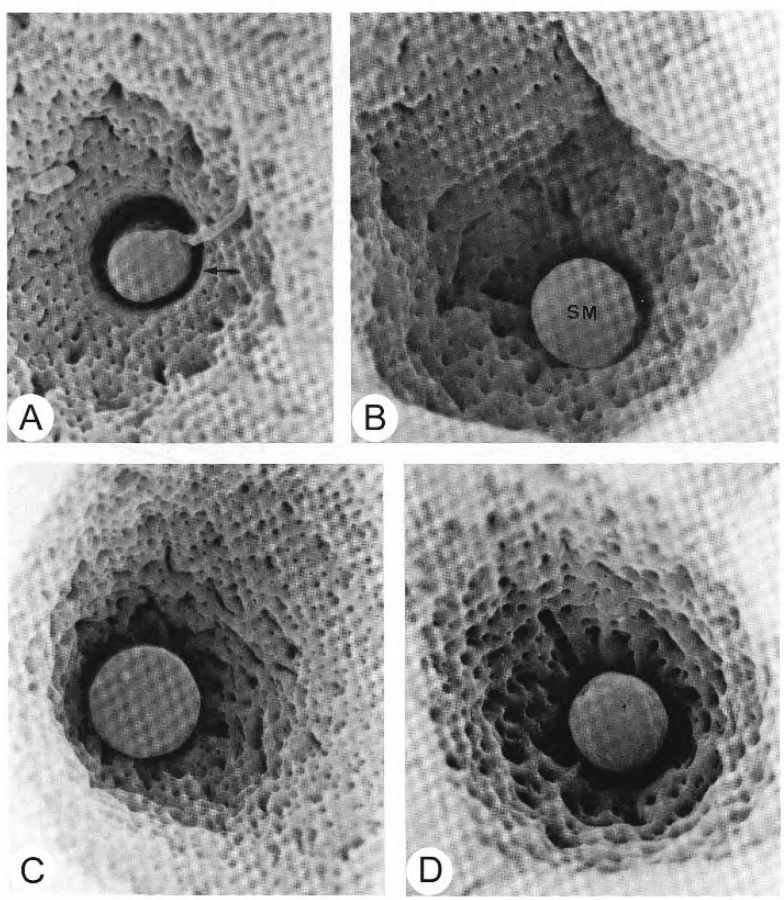

Figure 4.17: Scanning electron micrographs showing the process of sperm entry through the micropyles of inseminated eggs of the rose bitterling *Rhodeus ocellatus ocellatus.* (From Ohta and Nashirozawa, 1996; © reproduced with permission of John Wiley & Sons, Inc.).

A. One minute after insemination. A fertilizing spermatozoon (arrow) is visible at the sperm entry site. X 5,800.

B. Three minutes after insemination. The fertilizing spermatozoon is no longer visible and a swollen mass (SM) has formed and plugs the micropyle. X 5,800.

C. Five minutes after insemination. X 4,900.

D. Twenty minutes after insemination. A swollen mass remains plugging the micropyle. X 4,900.

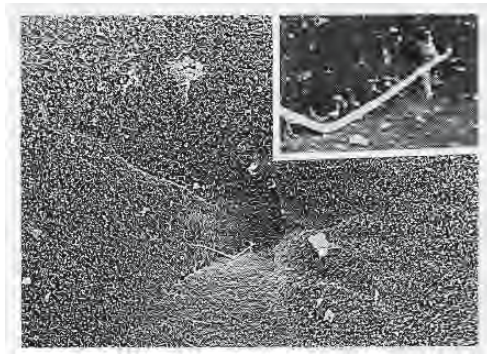

Figure 4.18: Engulfment of the sperm head in eggs of tilapia *Oreochromis niloticus* is followed by an indentation of the oolemma, the cleft of penetration. This is a scanning electron micrograph of the cleft of penetration in a dechorionated egg following penetration of the sperm head one minute after insemination. X 1,105 The sperm tail remains outside (inset X 6,460). (From Bern and Avtalion, 1990; reproduced with permission from Elsevier Science).

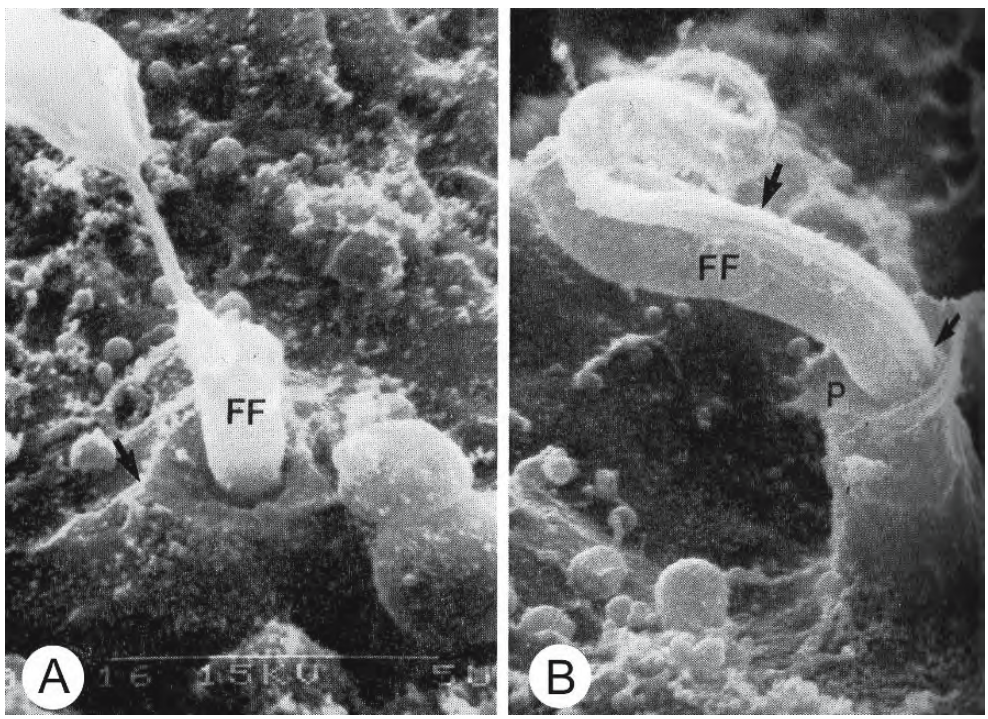

Figure 4.19: Scanning electron micrographs showing the two-tiered fertilization cone that is formed in the ayu fish *Plecoglossus altivelis.* The chorion was dissected away after fixation. (From Kudo, 1983b; reproduced with permission from Blackwell Publishing).

A. The first fertilization cone (FF) is a cylindrical structure that rises from the sperm entry site within 15 seconds of immersion in fresh water. X 15,000.

B. At about 20 seconds, a second tier forms a pedestal (P) elevating the first cone (FF) from its apex. The sperm tail is in close contact with the first fertilization cone (arrows). X 15,000.

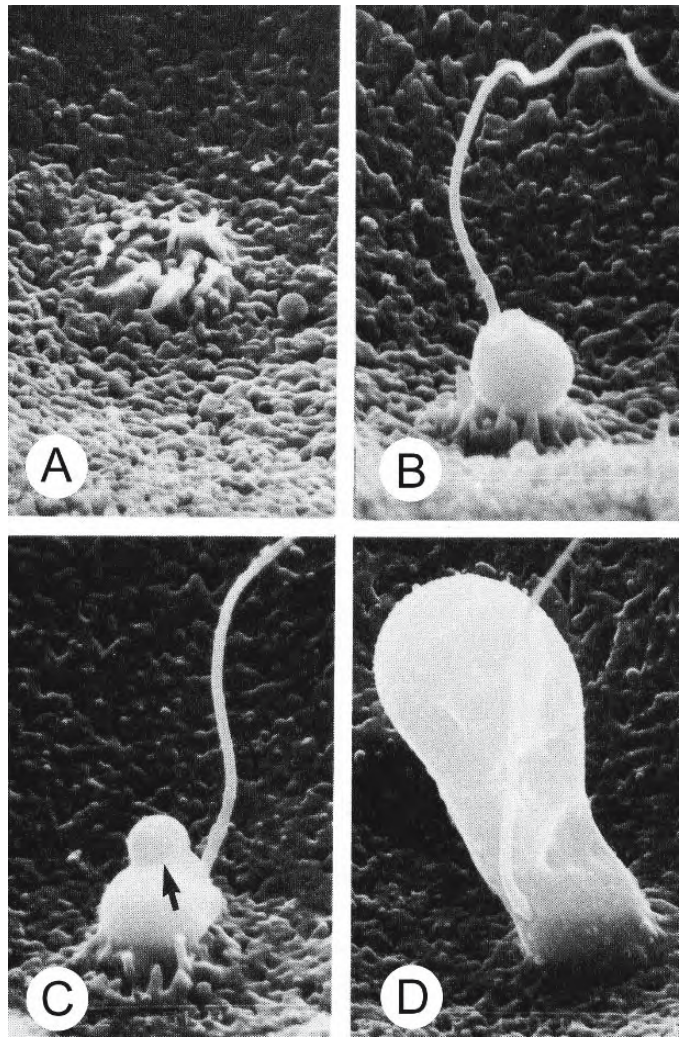

Figure 4.20: Scanning electron micrographs of fertilization cones in eggs of the carp *Cyprinus carpio*. In these preparations, the egg envelopes were removed mechanically after fixation. X 6,000 (From Kudo and Sato, 1985; reproduced with permission from Blackwell Publishing).

A. The sperm entry site in an unfertilized egg consists of a tuft of microvilli.

B. Fusion of sperm and egg at 10 seconds after activation by immersion in fresh water. A few microvilli of the sperm entry site surround the fused sperm head.

C. Formation of an early fertilization cone at 20 seconds. The cone (arrow) is a dome-like eminence atop the fused sperm head.

D. The early fertilization cone at 40 seconds.

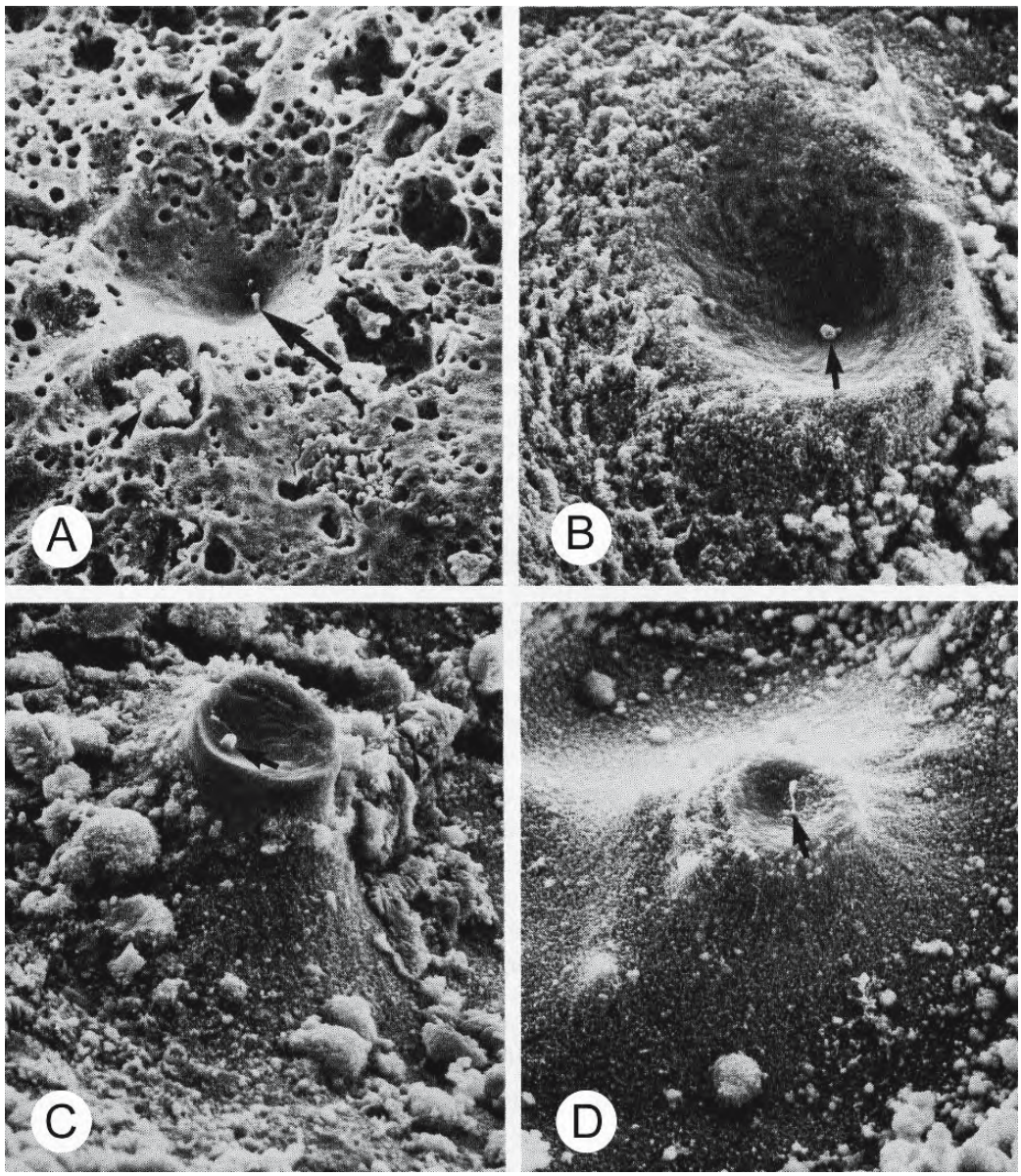

Figure 4.21: Scanning electron micrographs of the micropylar region of fertilized eggs of the carp *Cyprinus carpio.* In these preparations, the egg envelopes were removed mechanically after fixation. X 6,000 (From Kudo and Sato, 1985; reproduced with permission from Blackwell Publishing).

A. Some large pits surrounding the micropylar region contain cortical alveolar material (small arrow) at 60 seconds after activation by immersion in fresh water. The large arrow indicates an early fertilization cone. X 250.

B. The late fertilization cone has formed in the micropylar region by 90 seconds. It consists of an eminence resembling a wide-mouthed volcano containing the early fertilization cone within its crater (arrow) X 4,100.

C. A late fertilization cone at 120 seconds with the shortened early cone and a sperm tail at its apex. X 4,100.

D. A late fertilization cone at 120 seconds. The early fertilization cone has retracted and only a sperm tail remains (arrow). X 4,100.

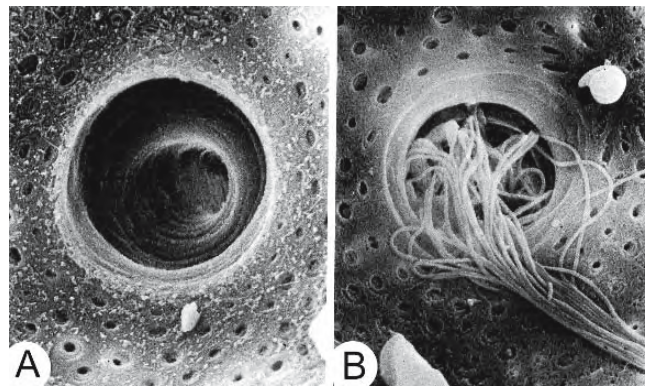

Figure 4.22: Scanning electron micrographs of the external orifice of the micropylar canal of an unimpregnated (**A**) and impregnated (**B**) female elkhorn sculpin *Alcichthys alcicornis* to demonstrate internal gametic association. Sperm, introduced into the ovarian cavity by copulation, enter the micropylar canals of ovulated eggs but there is no sperm/egg fusion until the eggs are released into seawater. X 4,500 (From Munehara, Takano, and Koya, 1989; reproduced with permission of the American Society of Ichthyologists and Herpetologists).

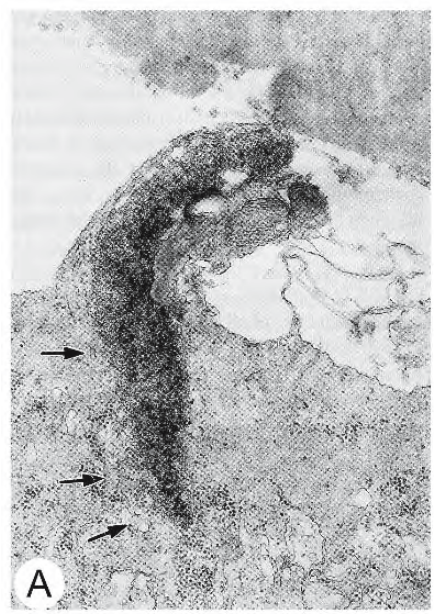

Figure 4.23: Transmission electron micrographs of sections of eggs of the elkhorn sculpin *Alcichthys alcicornis* after immersion in seawater. (From Koya, Takano, and Takahashi, 1993; reproduced with permission from the Zoological Society of Japan).

A. By ten seconds after immersion in seawater a fertilizing spermatozoon has penetrated the ooplasm and fusion of the membranes of the sperm and egg has begun. Several vesicles are seen near the sperm head (arrows). X 20,000.

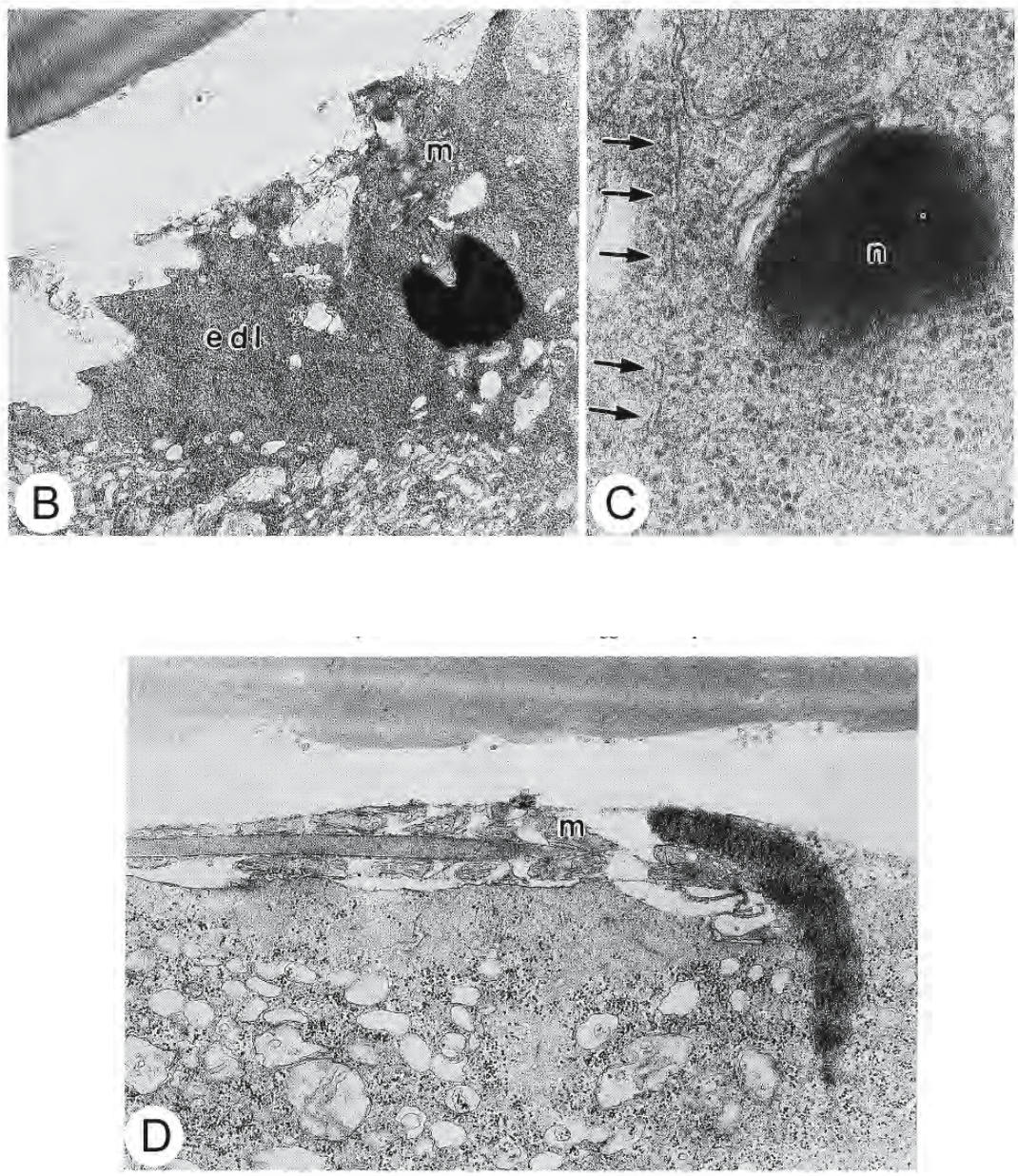

Figure 4.23: Continued.

B. By two minutes after immersion in sea water, the sperm head and mitochondria (m) have penetrated the ooplasm. The ooplasm around the sperm forms an electron-dense zone (edl) containing lysosomes. X 12,000.

C. At two minutes, the vesicles (arrows) are arranged in a row near the sperm nucleus (n). X 45,000.

D. The microtubules of the sperm tail have degenerated by 30 seconds after immersion in seawater. The sperm mitochondria (m) remain outside the oolemma. X 15,000.

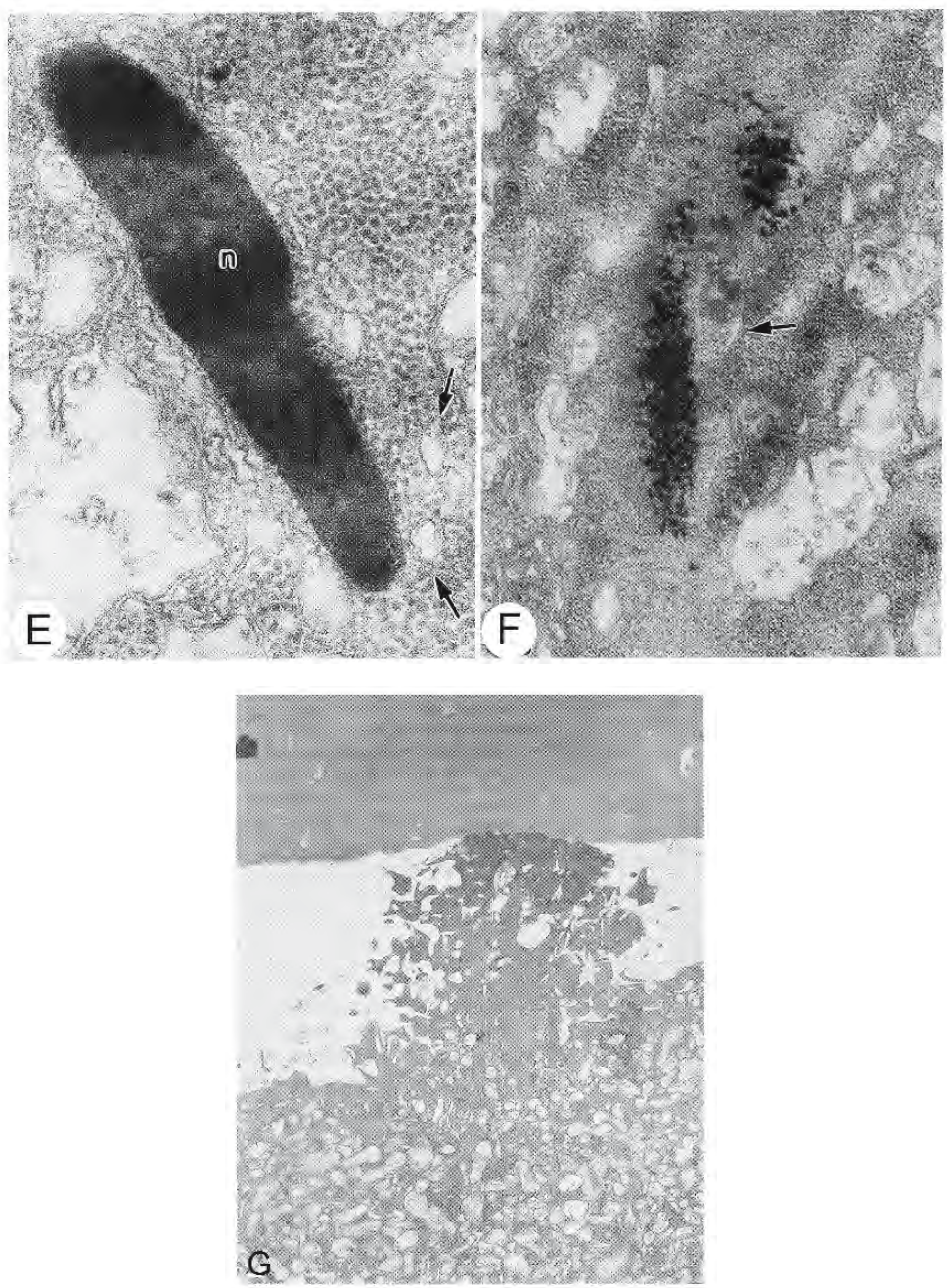

Figure 4.23: Continued.

E. The penetrated sperm nucleus (n) in the ooplasm three minutes after immersion. The nuclear membrane becomes vesiculated, beginning at the anterior region of the sperm head (arrows). X 60,000.

F. At three minutes chromatin of the penetrated sperm disperses; a fragment of the nuclear membrane is visible near the centriole (arrow). X 60,000.

G. By five minutes after immersion, the second polar body is undergoing its second meiotic division within the perivitelline space. X 4,000.

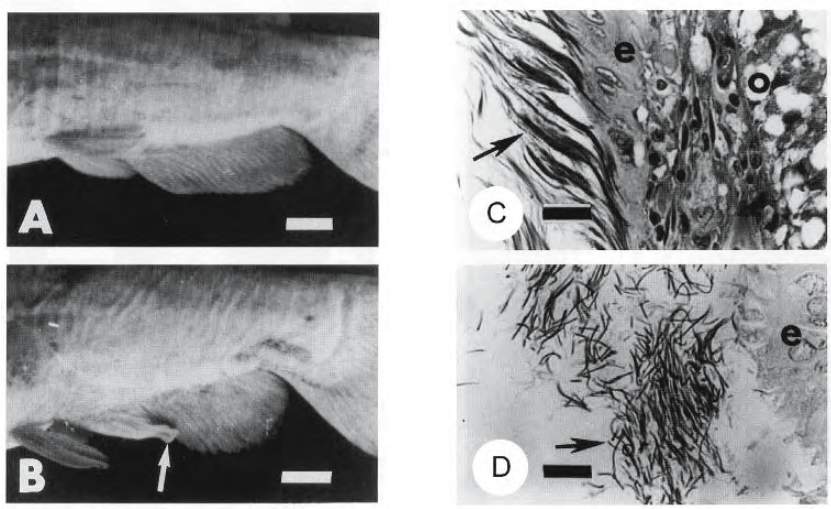

Figure 4.24: Internal fertilization may take place in South American catfish *Trachelyopterus* spp. (From Meisner et al., 2000; © reproduced with permission of John Wiley & Sons, Inc.).

A. Photograph (negative reversed) of the unmodified anal fin of a mature female *T. lucenai.* Bar = 10 mm.

B. Photograph (negative reversed) of the modified anal fin of a mature male *T. lucenai.* Bar = 10 mm.

C. Photomicrograph of a section through the ovary of a mature female *T. lucenai* with spermatozoa (arrow) closely associated with the epithelium (e) lining the ovarian lumen. o, oocyte. Bar = 10 μm.

D. Photomicrograph of a section through the ovary of a mature female of *T. galeatus* showing spermatozoa (arrow) in the ovarian lumen. e, ovarian epithelium. Bar = 10 μm.

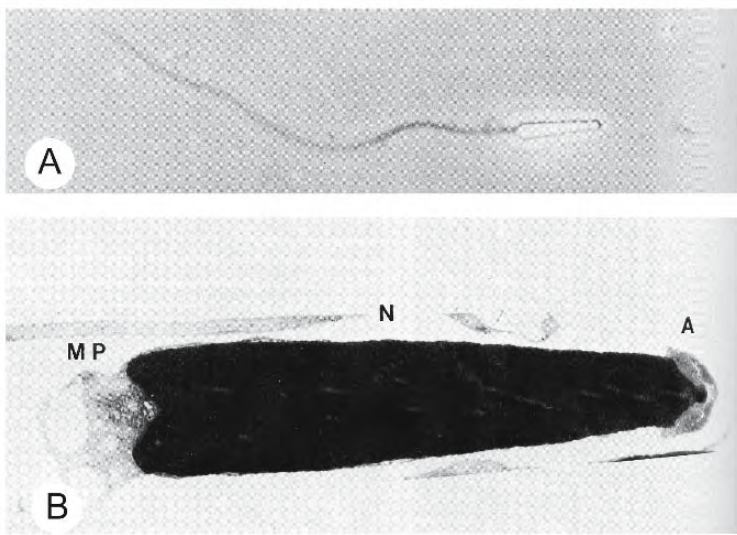

Figure 4.25: Spermatozoa of the white sturgeon *Acipenser transmontanus* possess a cap-like, membrane-bound sac, the acrosome. (From Cherr and Clark, 1984; © reproduced with permission of John Wiley & Sons, Inc.).

A. By phase contrast microscopy, the acrosome can been seen at the anterior end of the sperm head. X 485.

B. This transmission electron micrograph of a longitudinal section through the body of a sperm shows the acrosomal region (A), nucleus (N), and midpiece (MP). X 18,200.

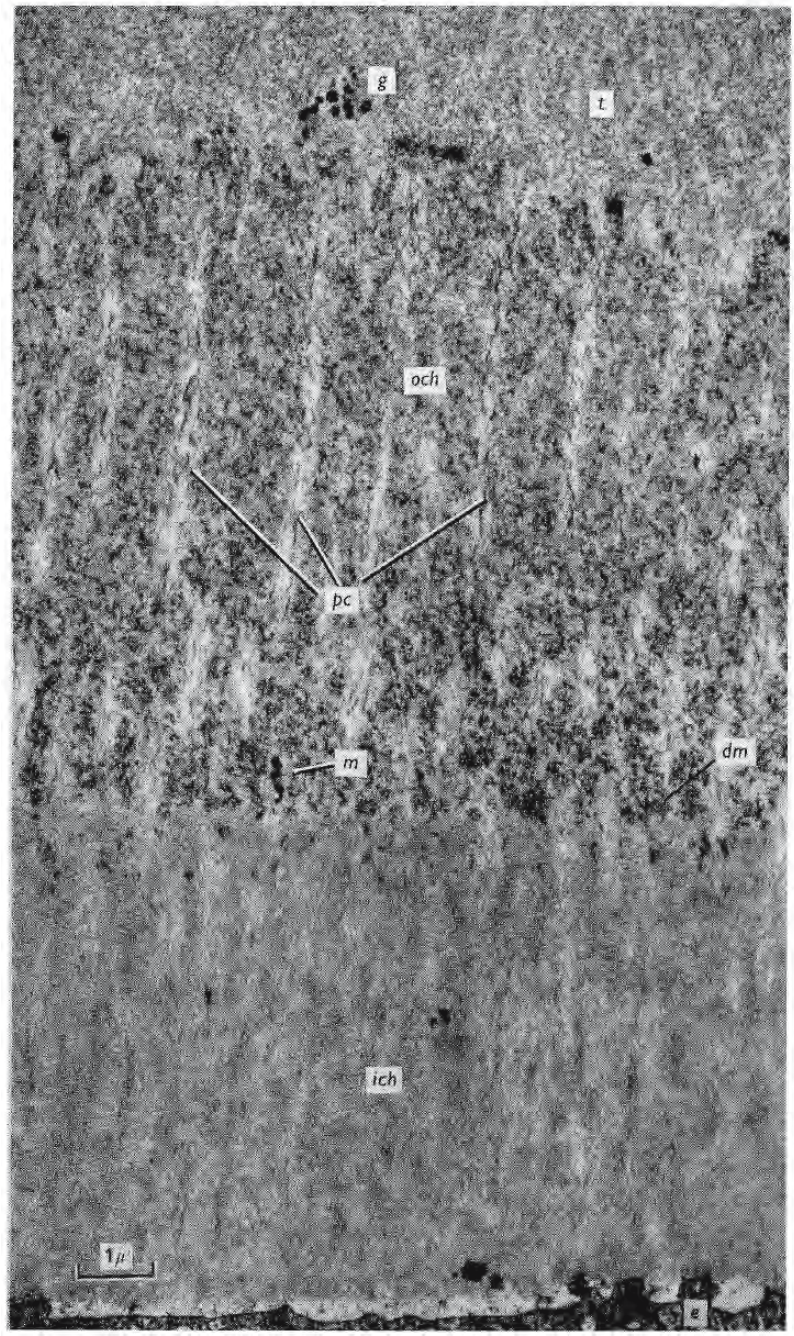

Figure 4.26: Transmission electron micrograph of a section through the chorion and tuft at the animal pole of a recently spawned egg of a river lamprey *Lampetra fluviatilis.* The inner chorion (ich) shows only faint radial striations produced by indistinct pore canals leading to the surface of the egg (e). Many slightly oblique sections of pore canals (pc) penetrate the outer chorion (och). The outer chorion contains large numbers of electron dense particles (dm) scattered among fine, radial fibres and an occasional membranous remnant (m). Only the innermost layer of the tuft (t), with some granules (g), is visible. Bar = 1μm (From Afzelius, Nicander, and Sjödén, 1968; reproduced with permission from the Company of Biologists, Ltd.).

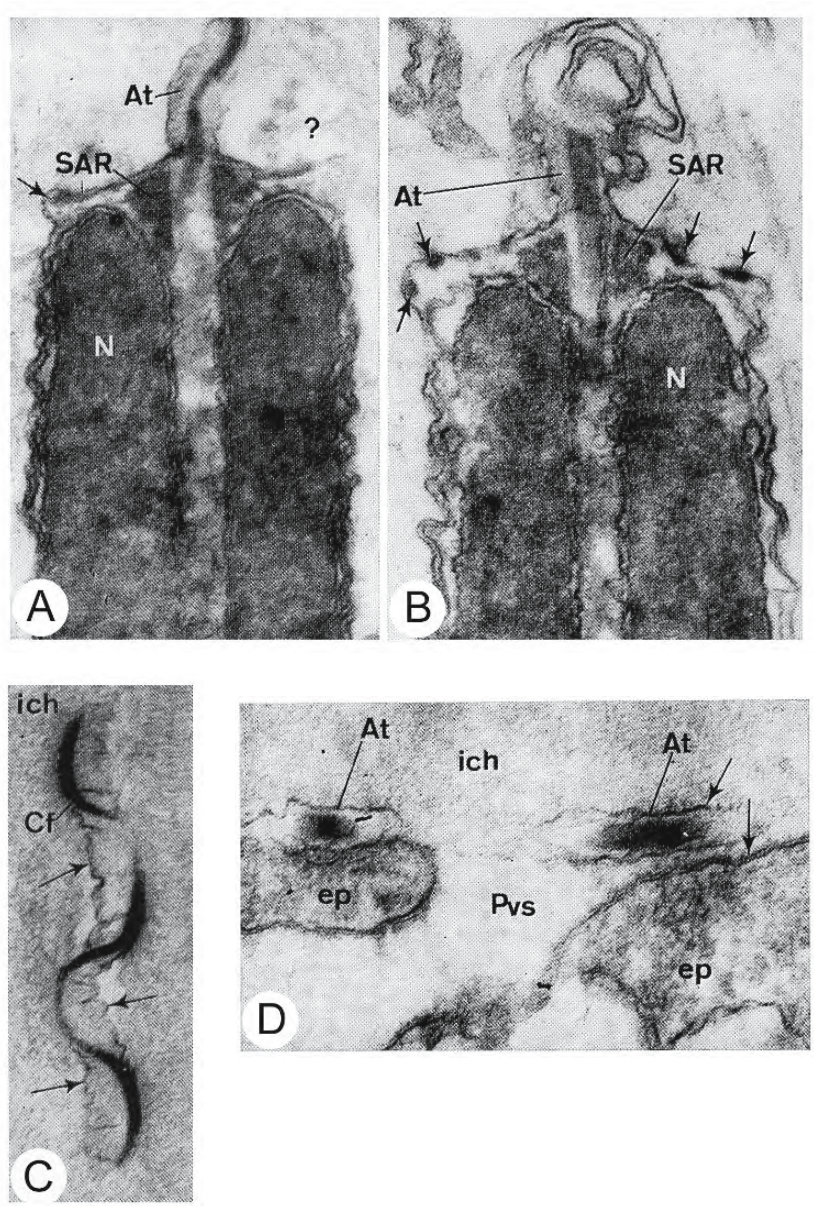

Figure 4.27: Transmission electron micrographs of sections of the heads of sperm of the river lamprey, *Lampetra fluviatilis.* (From Nicander and Sjödén, 1971; reproduced with permission from Nuova Immagine Editrice).

A,**B**. Apex of sperm heads embedded within the chorion of an egg following the formation of the acrosomal tubule (At) containing its head filament within. The subacrosomal ring (SAR) has partly emerged from a depression in the nuclear apex (N). The basal acrosomal membrane has fused with the plasma membrane of the sperm head in **A** (arrow); it retains spotlike thickenings in **B** (arrows). X 70,000.

C. Longitudinal section of the acrosomal tubule within a pore of the inner chorion (ich). Its head filament assumed (Cf) a helical form and the membrane of the acrosomal tubule is wrinkled (arrows). X 60,000.

D. An acrosomal tubule (At) and head filament lying within the narrow perivitelline space of an inseminated egg (Pvs) between the inner chorion (ich) and projections of the egg surface (ep). X 100,000.

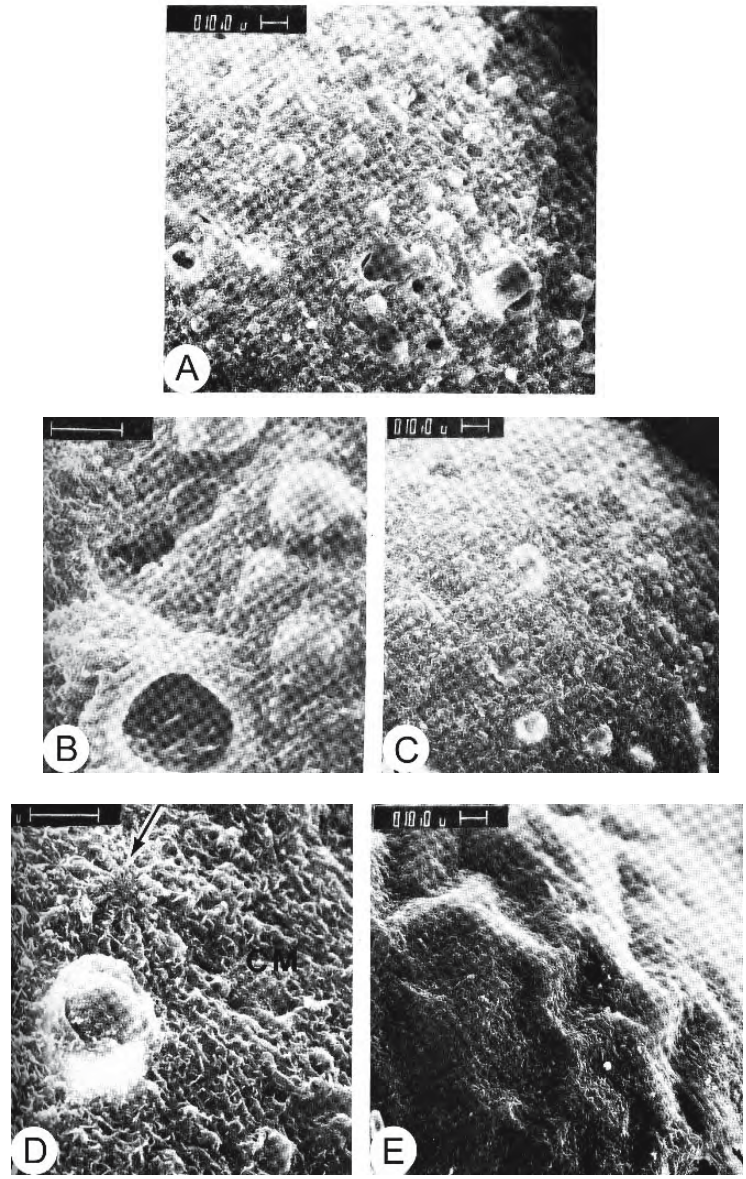

Figure 4.28: Scanning electron micrographs of the surfaces of dechorionated, ripe eggs of the zebrafish *Brachydanio rerio* fixed at intervals after activation by immersion in fresh water. (From Hart, Yu, and Greenhut, 1977; © reproduced with permission of John Wiley & Sons, Inc.).

A. The surface of an egg two minutes after activation. Cortical granules are in various stages of elevation and extrusion. X 400.

B. The egg surface shown in **A**. Note the limiting membrane of the evacuated cortical granule. X 1,200.

C. The surface of an egg four minutes after activation. X 400.

D. A cortical granule, with dense core and surrounding granular material, being extruded. Envelopment of the limiting membrane (CM) of a cortical granule within several folds of the oolemma (arrow) suggests its retrieval by the egg cell. X 1,200.

E. The surface of the oolemma seven minutes after activation. X 400.

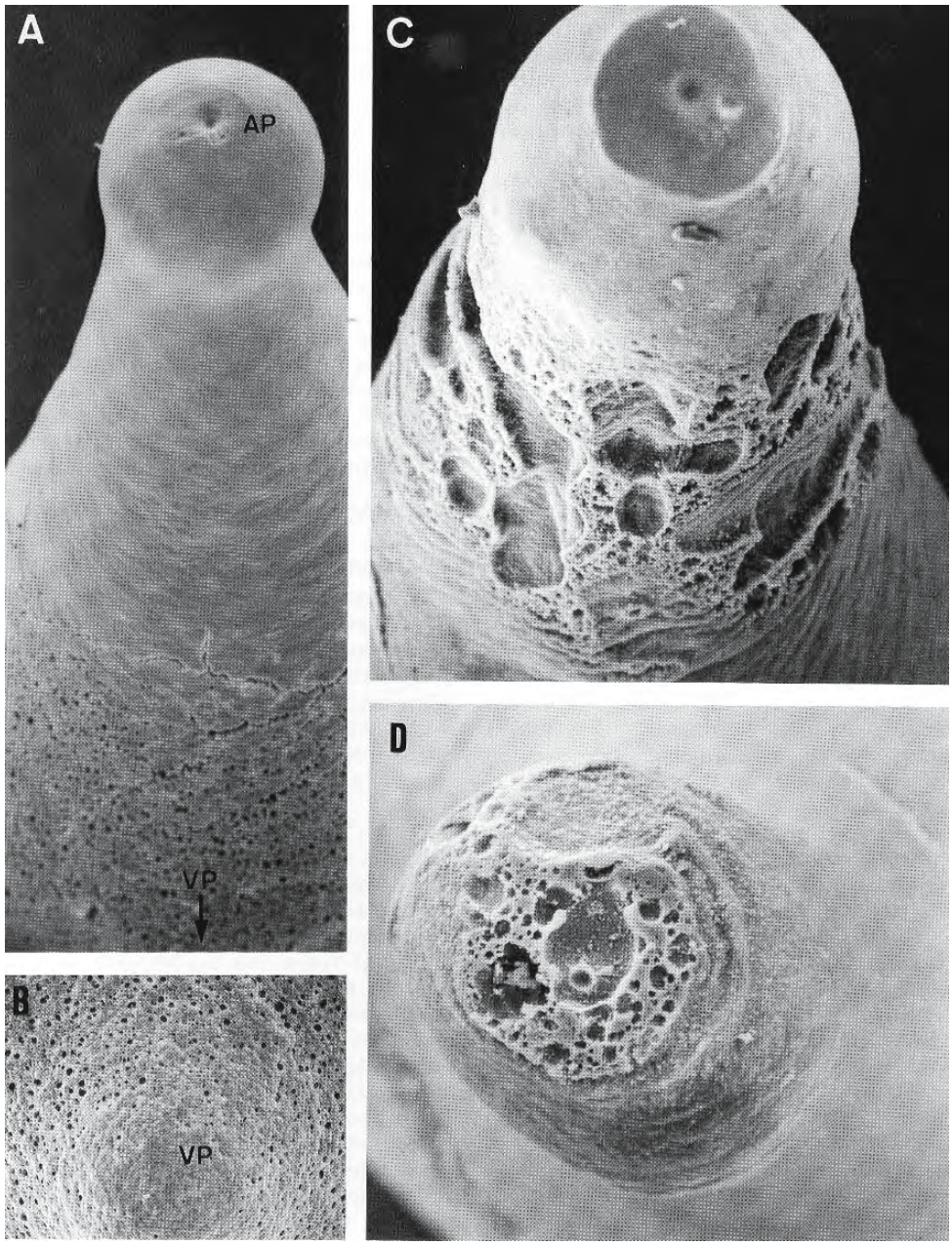

Figure 4.29: Scanning electron micrographs of mature eggs of the rose bitterling *Rhodeus ocellatus ocellatus* activated by immersion in fresh water. (From Ohta et al., 1990; reproduced with permission) The micrographs **A** to **D** show that the breakdown of cortical alveoli progressed from the vegetal pole (VP) to the animal pole (AP).

A. At five minutes after immersion in fresh water, breakdown has begun at the vegetal pole but has not yet occurred at the animal pole. X 110.

B. Breakdown has occurred at the vegetal pole. X 190.

C. By ten minutes after immersion in fresh water, an area around the sperm entry site at the animal pole remains unchanged. X 170.

D. By twenty minutes after activation, breakdown is proceeding at the animal pole. X 170.

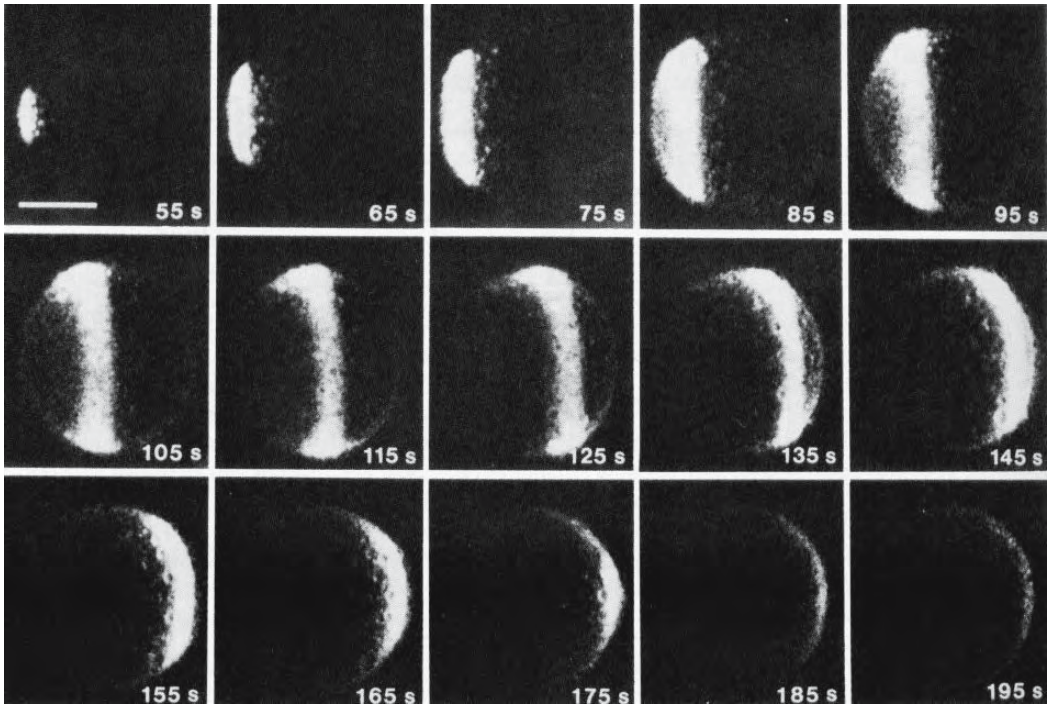

Figure 4.30: A series of photomicrographs of an egg of the medaka *Oryzias latipes* at intervals following insemination. A wave of intracellular Ca^{2+}, released by fertilization, passes down the egg from the micropyle at the left; it is visualized by the luminenscence of aequorin microinjected into the egg. Bar = 500 μm (From Yoshimoto et al., 1986; reproduced with permission from Blackwell Publishing).

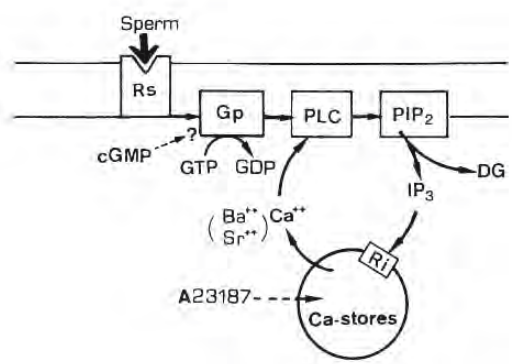

Figure 4.31: The release of calcium from intracellular stores precedes the cortical reaction in oocytes of fish. This scheme suggests the involvement of the phosphoinositide cascade, a common pathway in many cells. Binding of a spermatozoon to its receptor (Rs) leads to the activation of phospholipase C (PLC) mediated by a guanine nucleotide-dependent regulatory protein (Gp). PLC catalyses breakdown of phosphatidylinositol 4,5-biphosphate (PIP_2) into diacylglycerol (DG) and inositol 1,4,5-triphosphate (IP_3). IP_3 interacts with a specific receptor (Ri) on cytoplasmic calcium stores which releases Ca^{2+} to the cytosol. The cytosolic Ca^{2+} activates PLC, in turn forming IP_3 and DG. (From Iwamatsu, Yoshimoto, and Iwamatsu, 1988b; reproduced with permission from Elsevier Science).

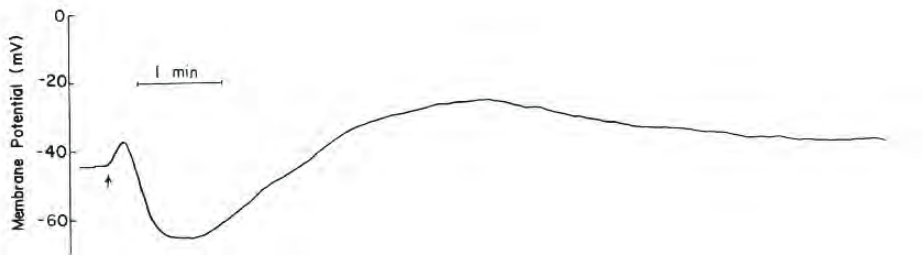

Figure 4.32: Electrical changes accompanying fertilization and cortical vesicle breakdown in the egg of the medaka *Oryzias latipes.* The average resting potential across the oolemma of unfertilized eggs in 10 % Ringer's solution is –39 ±9 mV. Following fertilization (arrow), the membrane depolarizes over a period of 20 ±10 sec by a few millivolts. This is followed by a longer phase of hyperpolarization. A steady resting potential of –19 ±15 mV is reached by 9.4 ±1 min after fertilization. (From Nuccitelli, 1980b; reproduced with permission from Elsevier Science).

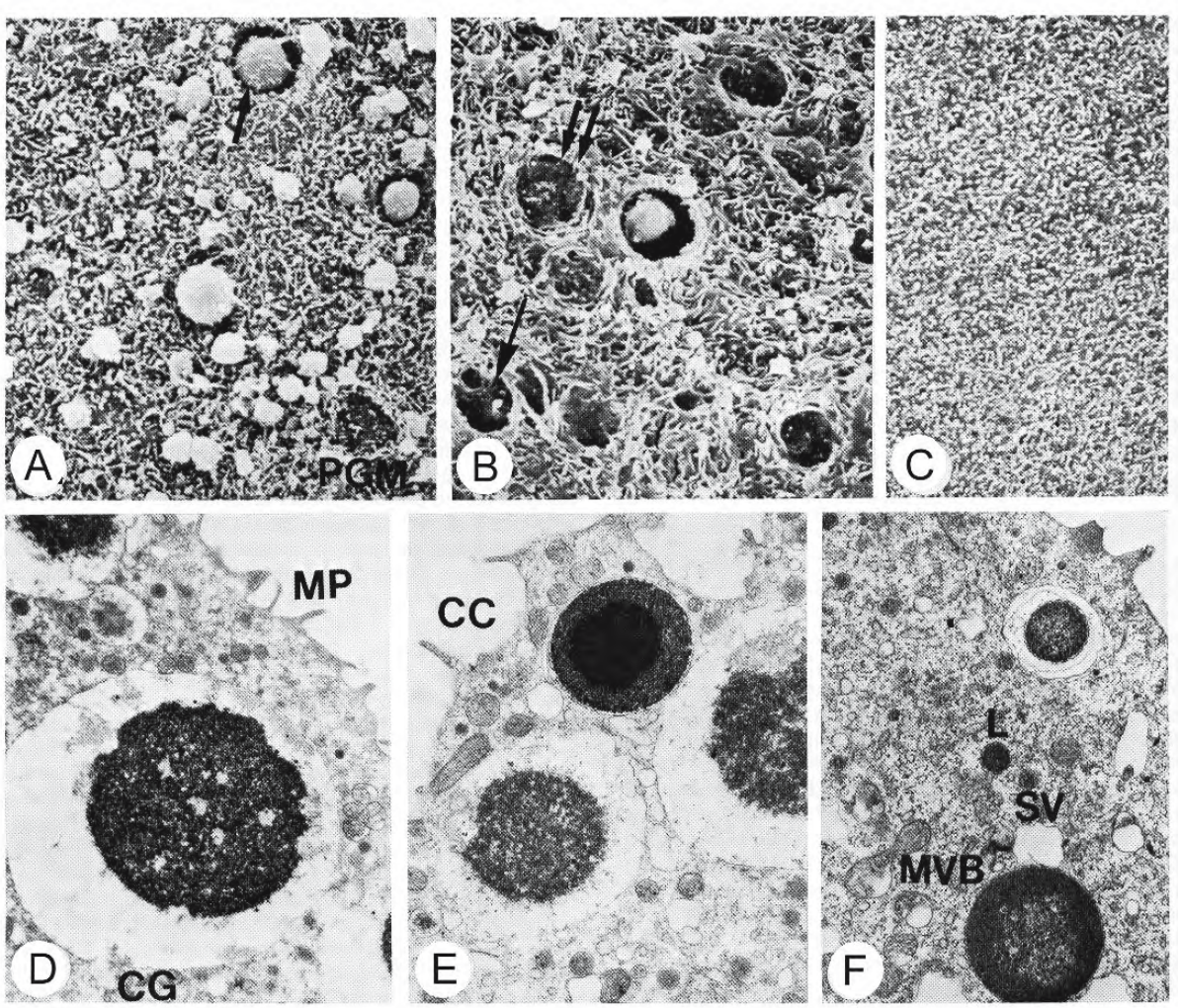

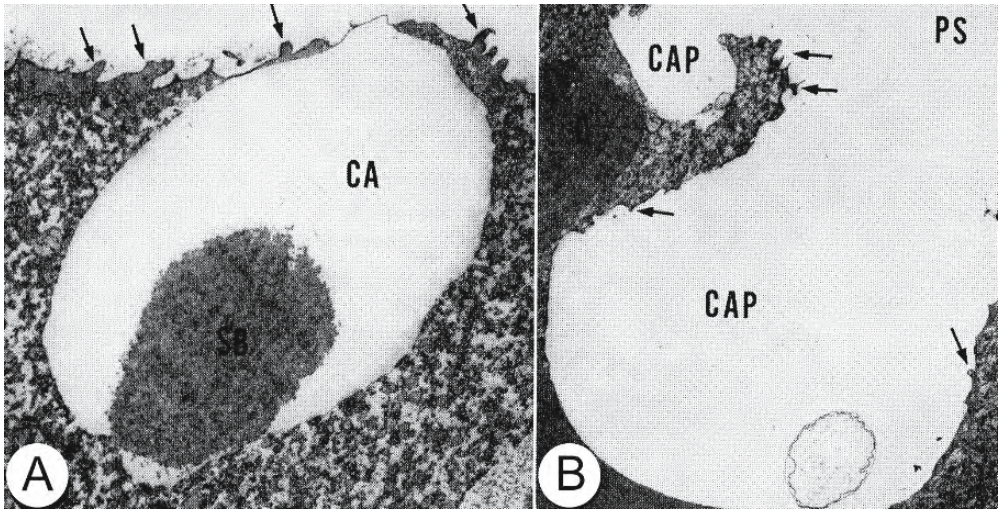

Figure 4.34: Transmission electron micrographs of sections of the cortex of eggs of the medaka *Oryzias latipes.* (From Iwamatsu and Keino, 1978; reproduced with permission from Blackwell Publishing).

A. A cortical alveolus (CA) and its contents, including a spherical body (SB) before breakdown. Microvilli (arrows) decorate the oolemma. X 2,800.

B. By 45 seconds after insemination, only empty pockets (CAP), opening into the perivitelline space (PS), remain from the cortical alveoli. X 1,890.

←———

Figure 4.33: Scanning (**A**,**B**,**C**) and transmission (**D**,**E**,**F**) electron micrographs illustrating exocytosis of cortical granules induced in eggs of the zebrafish *Brachydanio rerio* by immersion in fresh water. (From Schalkoff and Hart, 1986; reproduced with permission from Springer-Verlag).

A. The surface of an egg one minute after activation. It displays a complex mosaic consisting of the original oolemma, cortical granules in the process of discharging their contents (arrow), and evacuated cortical granules represented by patches of perigranular membrane (PGM). X 1,200.

B. By two minutes after activation, the surface is dominated by crypts (arrow) and patches of membrane (double arrows) remaining from cortical granules. X 1,200.

C. The surface at five minutes is adorned with microplicae, indicating that the cortical reaction is complete. X 1,200.

D. At one minute after activation, the cortex contains intact, membrane-bound cortical granules (CG). Microplicae (MP) dominate the surface of the oolemma. X 2,130.

E. By two minutes after activation, evacuation of cortical granule crypts (CC) has occurred. X 10,000.

F. Cortical granules are absent from the cortex by five minutes after activation. Organelles in the cortical ooplasm include multivesicular bodies (MVB), lysosomes (L), and smooth vesicles (SV). X 10,800.

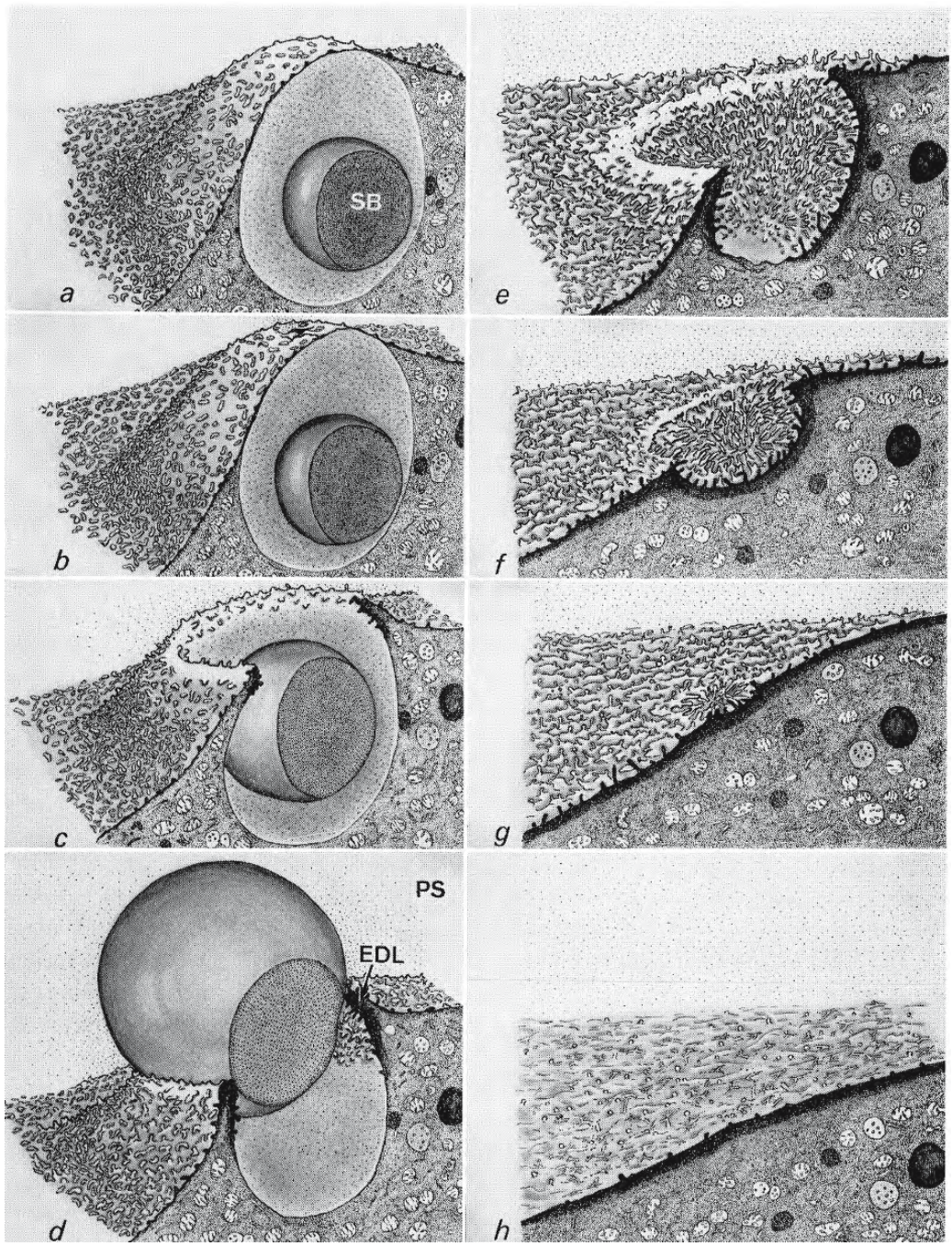

Figure 4.35: Diagrams illustrating breakdown of the cortical alveolus in the egg of the medaka *Oryzias latipes*. Breakdown begins with the formation of holes and gaps (b) at the apex of the cortical alveolus. This is followed by the formation of a large aperture (c) into the perivitelline space (PS) and the release (d) of colloidal material and a spherical body (SB). An electron-dense layer (EDL) forms beneath the alveolar pocket. The envelope shrinks (e,f,g) and disappears (h). Microvilli are abundant on the surface of the oolemma and within the alveolar pocket. (From Iwamatsu and Keino, 1978; reproduced with permission from Blackwell Publishing).

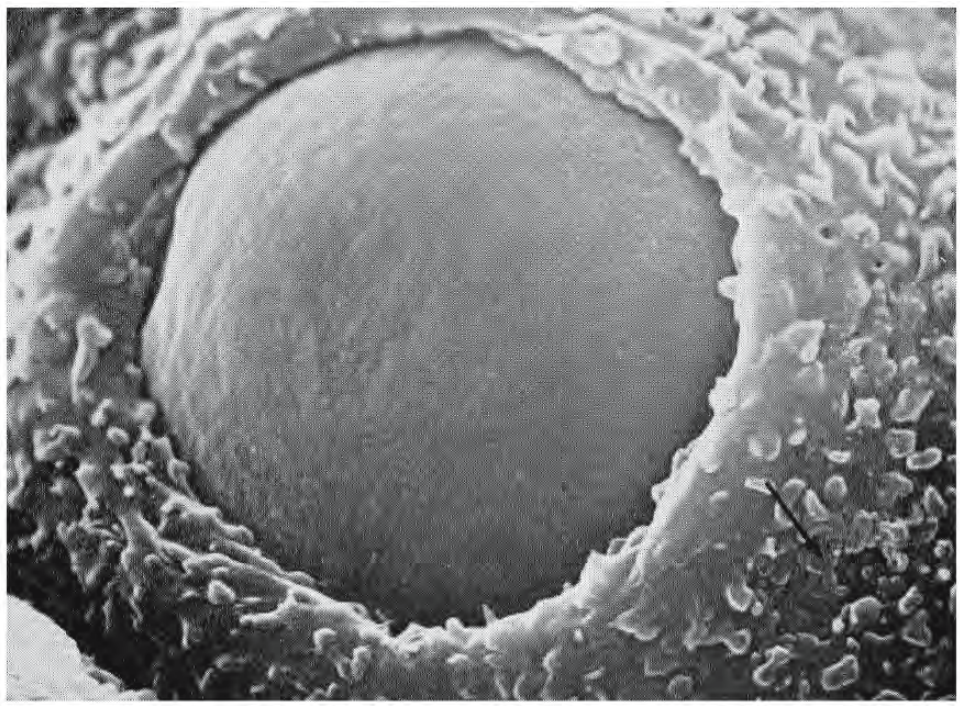

Figure 4.36: Scanning electron micrograph of the surface of an egg of the medaka *Oryzias latipes* 60 seconds after insemination. Just before its release, a spherical body peeps through a large aperture in a cortical alveolus. X 4,380 (From Iwamatsu and Keino, 1978; reproduced with permission from Blackwell Publishing).

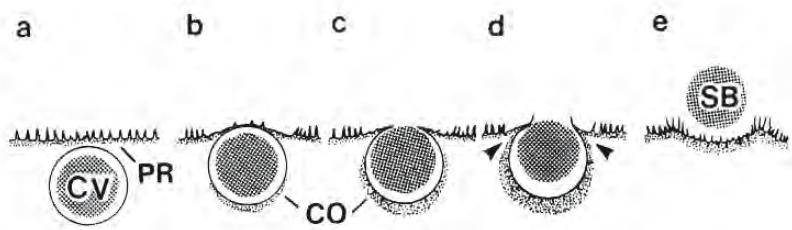

Figure 4.37: Schematic drawings showing the distribution of compact ooplasm in the cortical layer of the egg of the chum salmon *Oncorhynchus keta* during the breakdown of cortical alveoli. In the intact egg (a) a cortical alveolus (CV) approaches the oolemma. As it approaches (b), a small area of its membrane becomes decorated with compact ooplasm (CO). As the alveolus opens to the perivitelline space (c), the alveolar membrane, with this compact ooplasm, increases in area. The compact ooplasm unites (d) with the cortical layer (arrowheads). The alveolar contents (SB) are finally discharged (e). (From Kobayashi, 1985a; reproduced with permission of the Faculty of Science, Hokkaido University).

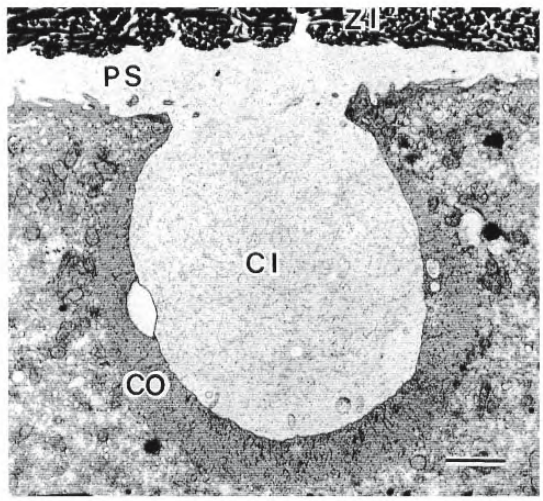

Figure 4.38: Transmission electron micrograph of a section through the cortical layer of the animal pole layer of the egg of the chum salmon *Oncorhynchus keta* during the breakdown of a cortical alveolus. A coating of dense ooplasm (CO) envelops the cortical alveolus just before expulsion of its contents (CI) into the perivitelline space (PS). Bar = 2 μm (From Kobayashi, 1985a; reproduced with permission of the Faculty of Science, Hokkaido University).

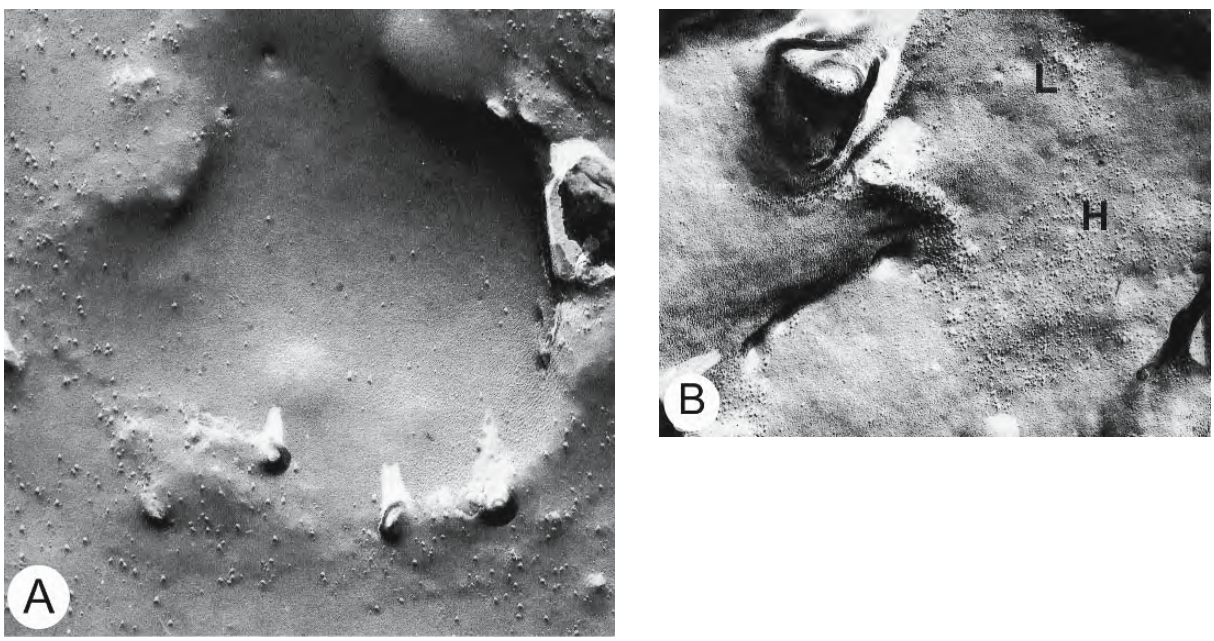

Figure 4.39: Electron micrographs of freeze fracture replicas of activated eggs of the zebrafish *Brachydanio rerio* to illustrate later stages of cortical granular exocytosis. (From Hart and Collins, 1991; reproduced with permission from Springer-Verlag).

A. En face view of a wide, transient crater, lined with a membrane of low particle density, remains on the surface of the site of expulsion. The difference in particle density is maintained between the domains of the former cortical vesicle and the oolemma. X 41,000.

B. P-face replica of the surface of an egg 4 minutes after activation showing distinct membrane domains of high (H) and low (L) particle density. X 49,248.

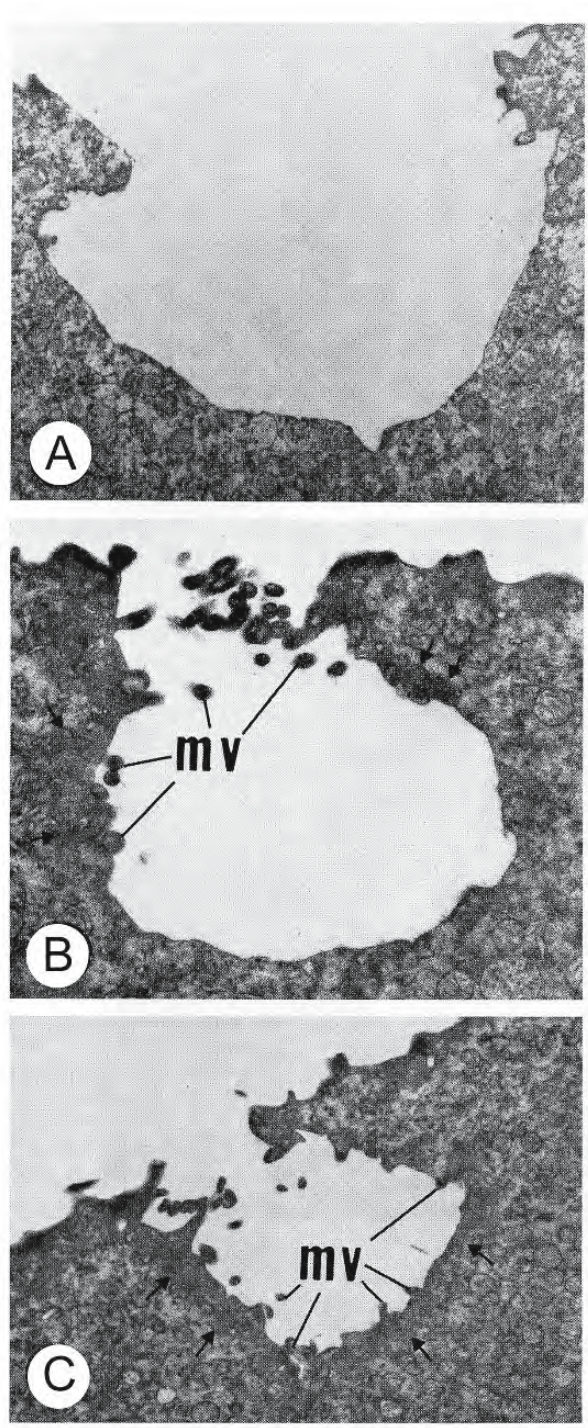

Figure 4.40: Transmission electron micrographs of eggs of the medaka *Oryzias latipes* showing shrinkage of the pockets left from the release of the contents of cortical alveoli. Large numbers of microvilli (mv) sprout within the crater, beginning near the aperture (**A**,**B**). An electron-dense layer of ooplasm (arrows) surrounds the crater. **A** X 4,700; **B** X 9,300; **C** X 4,870 (From Iwamatsu and Ohta, 1976; reproduced with permission from Springer-Verlag).

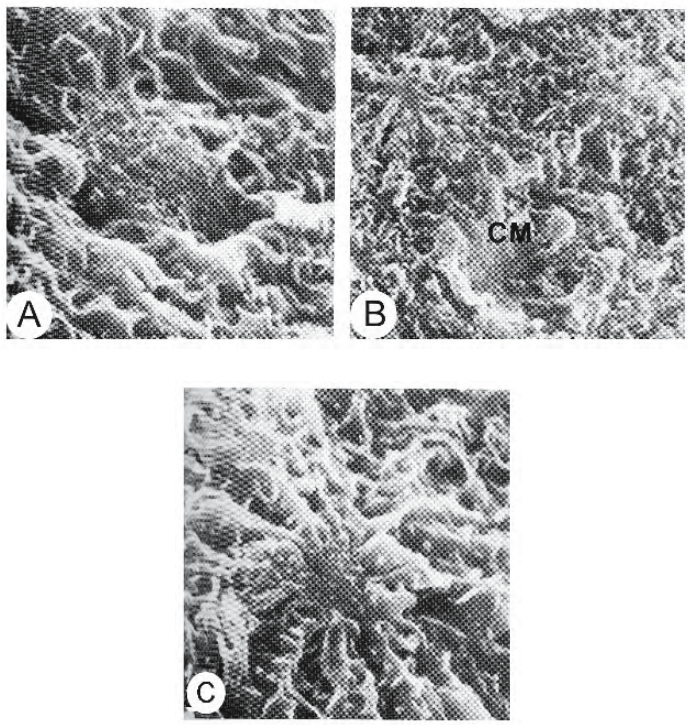

Figure 4.41: Scanning electron micrographs of the surface of the egg of the zebrafish *Brachydanio rerio* following cortical alveolar breakdown. (From Hart and Yu, 1980; © reproduced with permission of John Wiley & Sons, Inc.).

A. Although most evidence of exocytosis has disappeared from the surface, two membrane domains remain distinct: the "pebbled" surface left from the perigranular membrane is surrounded by the "folded" membrane derived from the oolemma. X 3,000.

B. Membranous folds of the oolemma surround the perigranular membrane patch (CM) as it is being enveloped. X 2,400.

C. The perigranular membrane patch is almost completely enveloped by converging, radiating folds of the oolemma. X 3,500.

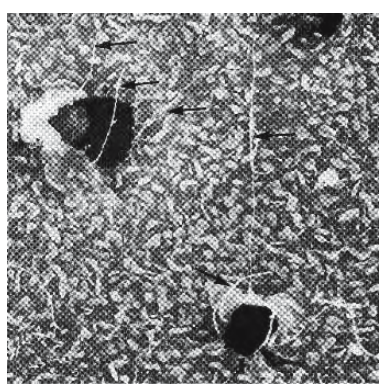

Figure 4.42: Scanning electron micrograph of the surface of an egg of *Fundulus heteroclitus* at 50 seconds after insemination, following the cortical reaction. Threads of excess membrane (arrows) are expelled from the empty crater of a cortical vesicle. X 1,400 (From Brummett and Dumont, 1981; © reproduced with permission of John Wiley & Sons, Inc.).

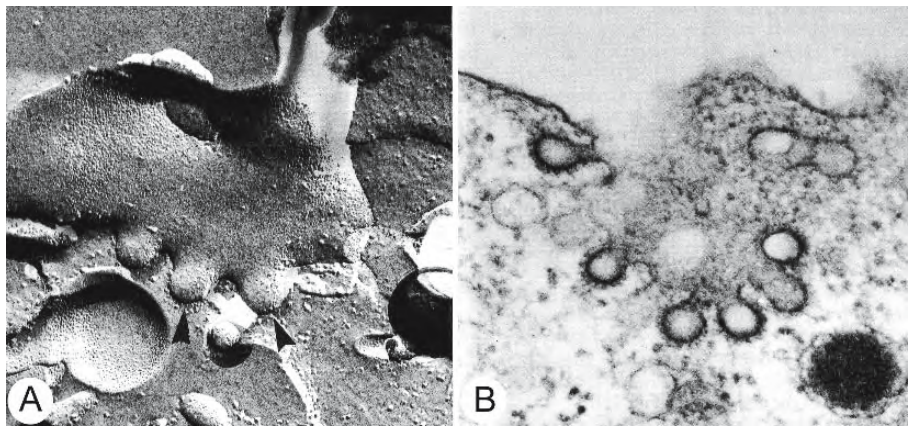

Figure 4.43: Images of the egg cortex of the zebrafish *Brachydanio rerio.* (From Hart and Collins, 1991; reproduced with permission from Springer-Verlag).

A. Profile view of a freeze-fractured vacated crypt of a cortical alveolus showing attached coated vesicles (arrowheads). X 102,600.

B. Transmission electron micrograph of a grazing section through a vacated crypt of a cortical alveolus showing several forming coated vesicles. X 80,770.

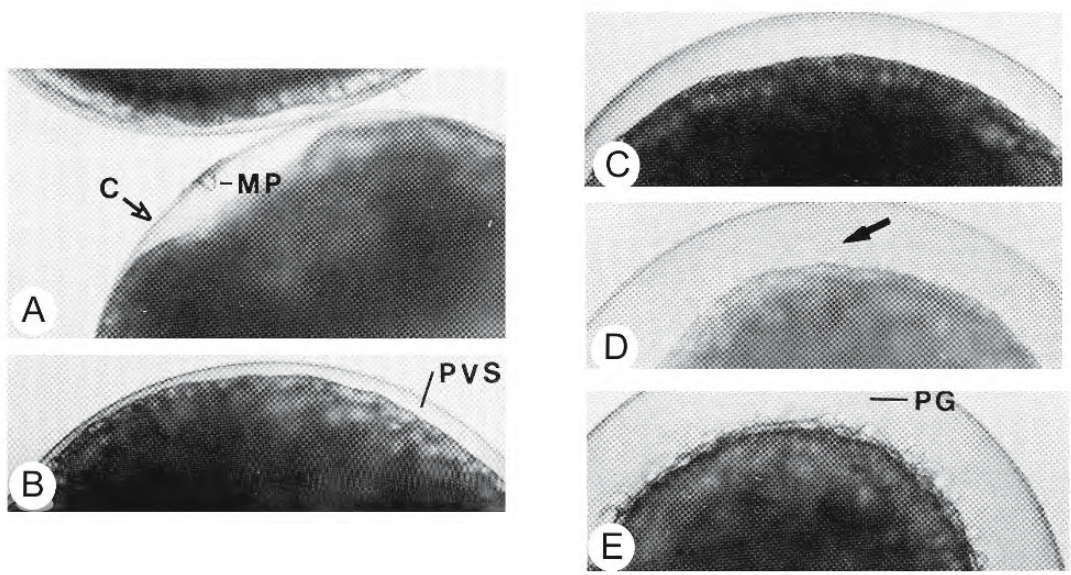

Figure 4.44: Photomicrographs of sections through the cortex of eggs of the zebra danio *Brachydanio rerio* to show the formation of the perivitelline space following the cortical reaction. X 160 (From Hart and Yu, 1980; © reproduced with permission of John Wiley & Sons, Inc.).

A. A fertilized egg during initial elevation of the chorion (C) in the vicinity of the micropyle (MP).

B. A fertilized egg 30 seconds after activation showing elevation of the chorion and the definition of a perivitelline space (PVS). No exocytosis of cortical granules is visible.

C. A fertilized egg 60 seconds after activation. Many cortical granules appear as blister-like elevations at the surface of the egg.

D,**E**. Eggs two to three minutes after activation showing intense exocytosis of cortical granules at the surface. Newly released central cores (arrow) become hydrated and transformed into perivitelline globules (PG).

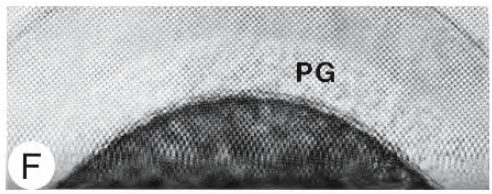

Figure 4.44: Continued.
F. A fertilized egg six to seven minutes after activation. The discharged material from the cortical granules together with the perivitelline globules (PG) forms a colloid-like hyaline layer around the egg.

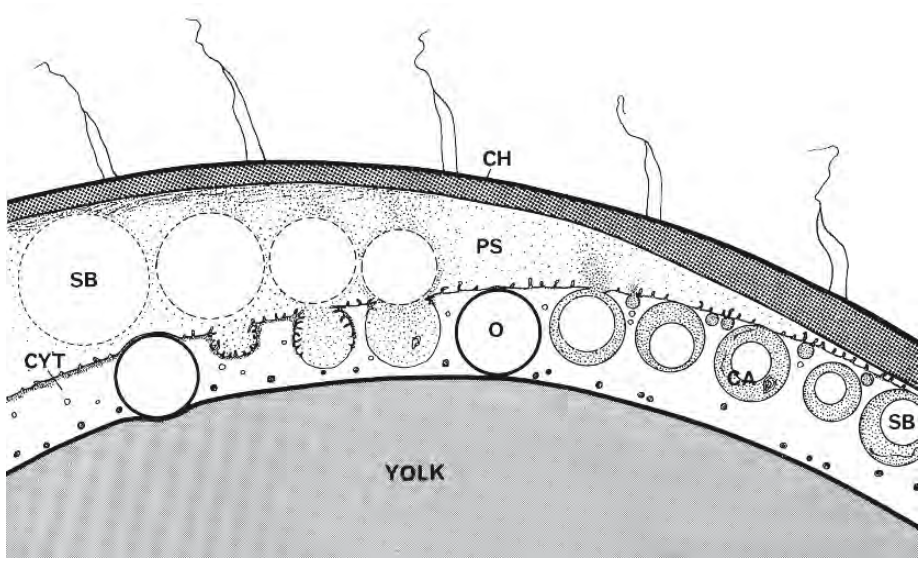

Figure 4.45: This diagram shows the development of the perivitelline space in the egg of the medaka *Oryzias latipes* as a result of the cortical reaction. (From Iwamatsu and Ohta, 1976; reproduced with permission from Springer-Verlag) Breakdown of cortical alveoli (CA) begins with the formation of a large aperture into the perivitelline space (PS) and the release of colloidal material and spherical bodies (SB). The alveolar envelope then shrinks as its smooth surface becomes covered by many microvilli. Elevation of the chorion is accompanied by a reduction in thickness of the chorion (CH) and the layer of cytoplasm (CYT) between the yolk and oolemma. O = oil droplet.

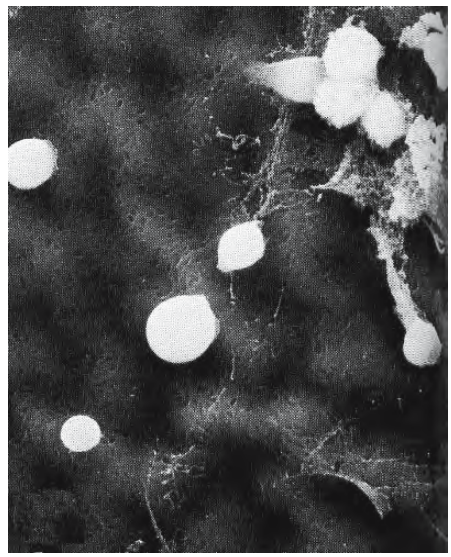

Figure 4.46: A scanning electron micrograph of the inside of the chorion removed from an egg of *Fundulus heteroclitus* fixed three seconds after insemination. Dense granules and particulate material, presumably released by cortical alveoli, adhere to the inner surface. X 1,000 (From Brummett and Dumont, 1981; © reproduced with permission of John Wiley & Sons, Inc.).

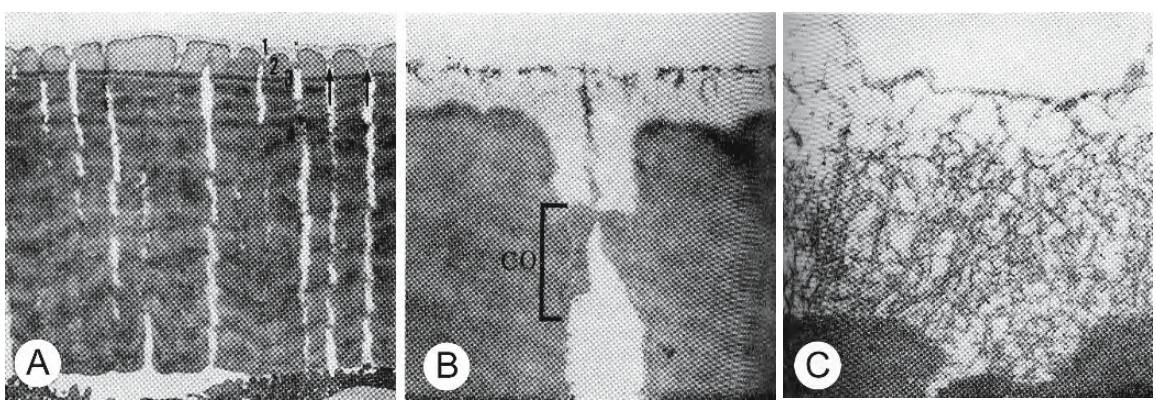

Figure 4.47: Transmission electron micrographs of sections through the chorion of the carp *Cyprinus carpio.* (From Kudo, 1982; reproduced with permission from Blackwell Publishing).

A. At the time of fertilization, the chorion is perforated by pore canals and consists of four layers, 1, 2, 3, and 4. The perivitelline space is seen at the bottom of the micrograph. X 2,600.

B. At this time, the first layer of the chorion consists of an inner electron-dense region and an outer electron-lucent portion that is formed from material oozing through the pore canals. A columnar barrier (CO) constricts the pore canal, providing an anchor point for the outer layer. X 28,000.

C. After 40 minutes, the filamentous outer layer of the chorion has increased in thickness by five fold. X 28,000.

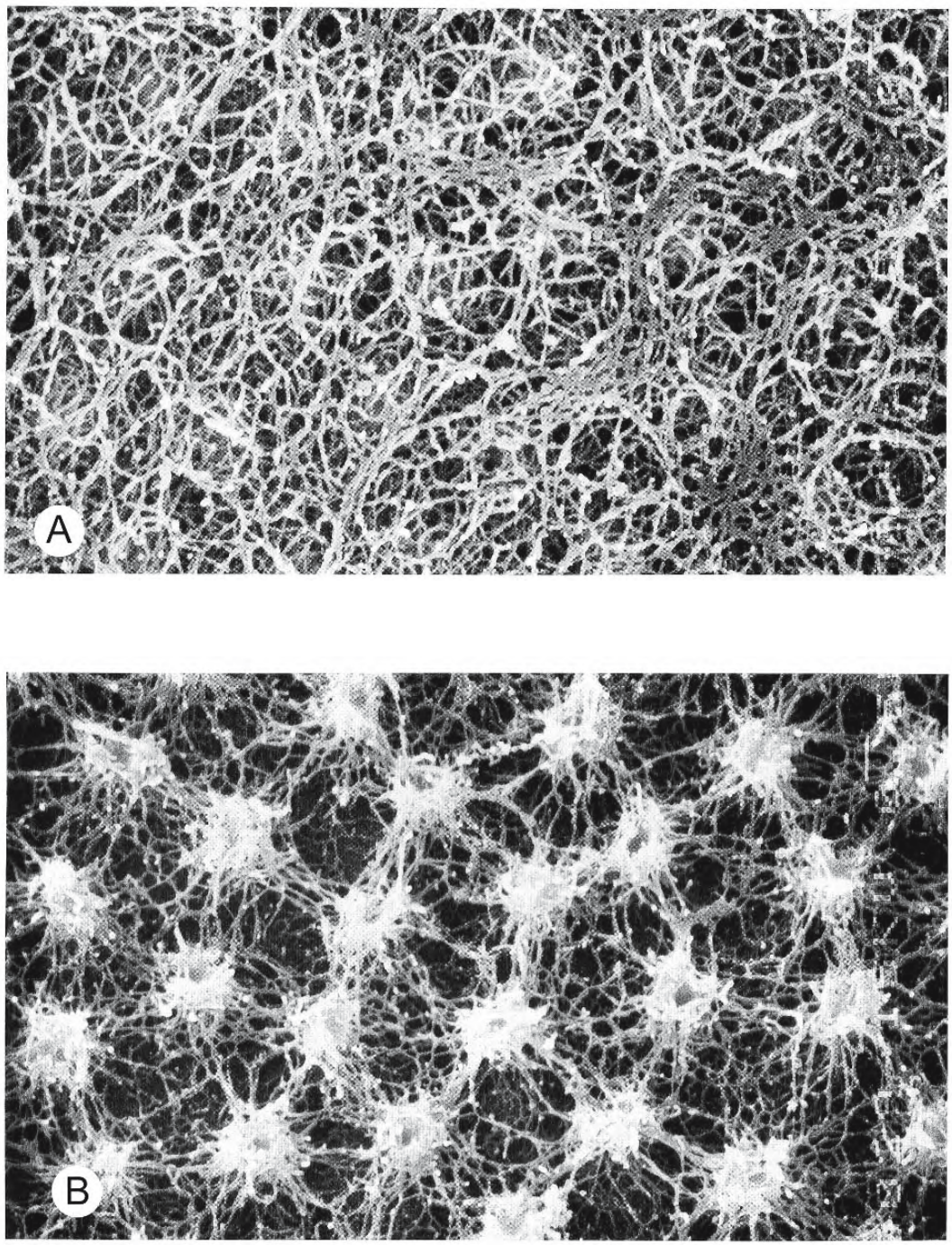

Figure 4.48: Scanning electron micrographs of the surface of the chorion of eggs of the ayu fish *Plecoglossus altivelis.* (From Kudo and Inoue, 1989; © reproduced with permission of John Wiley & Sons, Inc.).

A. At the time of fertilization, the surface is covered with a fairly uniform meshwork of filamentous material extending in all directions. X 17,000.

B. Some time later, the filaments have aggregated into regularly spaced round masses. X 17,000.

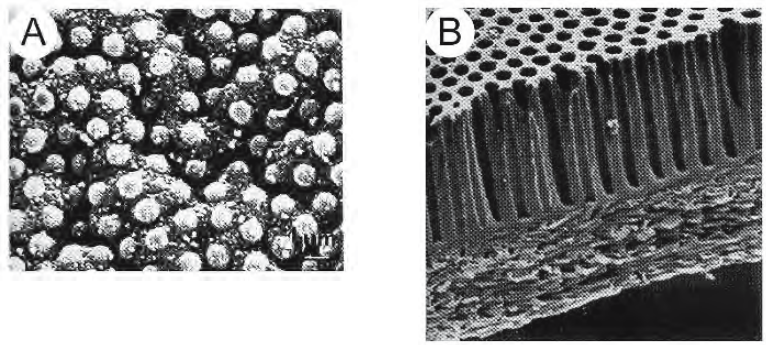

Figure 4.49: Scanning electron micrographs of chorions of fertilized eggs. (From Davenport, Lønning, and Kjørsvik, 1986; reproduced with permission from Elsevier Science).

A. The hard chorion of the demersal egg of the lumpsucker *Cyclopterus lumpus* four hours after fertilization. The chorion is reinforced when its pores become plugged after activation. These eggs must withstand contact with the sea bottom.

B. The broken edge and surface of the soft chorion in the vegetal region of the demersal egg of the capelin *Mallotus villosus* three days after fertilization. The regular pattern of pore canals of the unfertilized egg is retained. Although the chorion remains soft and pliable during development, it resists the shrinkage and swelling caused by severe changes in temperature of the intertidal region. It withstands, however, the bursting stresses of wave action.

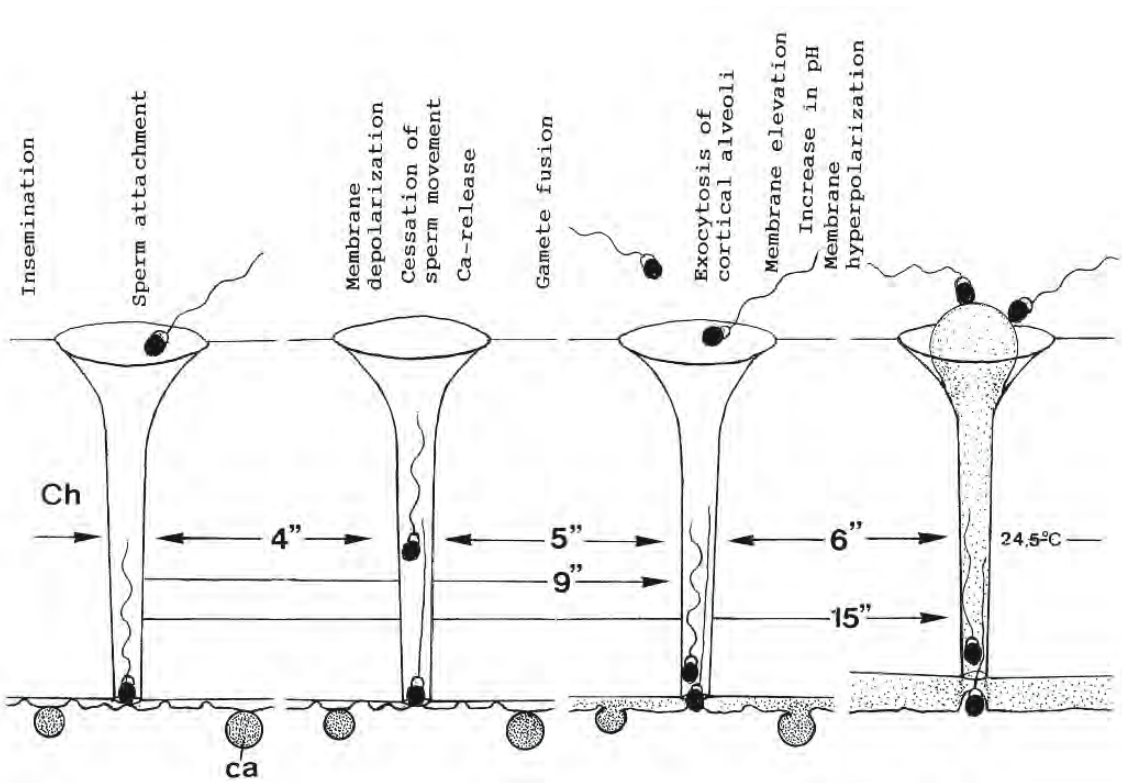

Figure 4.50: Diagram showing the sequence of events in fertilization of the egg of the medaka *Oryzias latipes.* (From Iwamatsu et al., 1991; reproduced with permission from Blackwell Publishing) The time from insemination to sperm attachment through the micropyle depends on the concentration of sperm surrounding the egg.

Abbreviations: Ca, cortical alveolus; Ch, chorion.

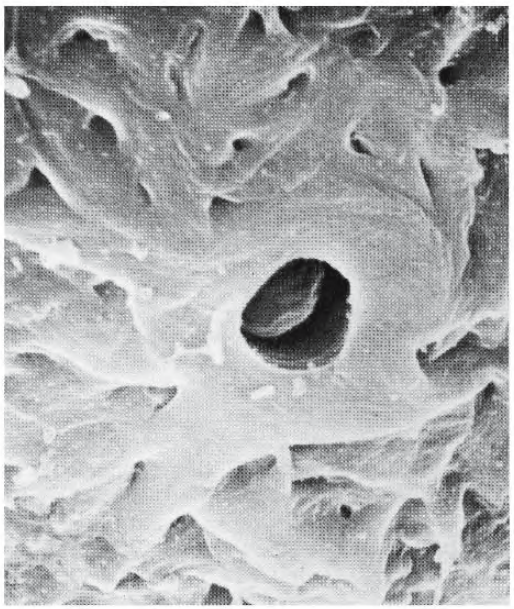

Figure 4.51: Scanning electron micrograph of the inner opening of the micropyle in the egg of *Fundulus heteroclitus.* (From Brummett and Dumont, 1979; © reproduced with permission of John Wiley & Sons, Inc.) The diameter of the canal precludes the admission of more than the single sperm which can be seen about to emerge. X 14,400.

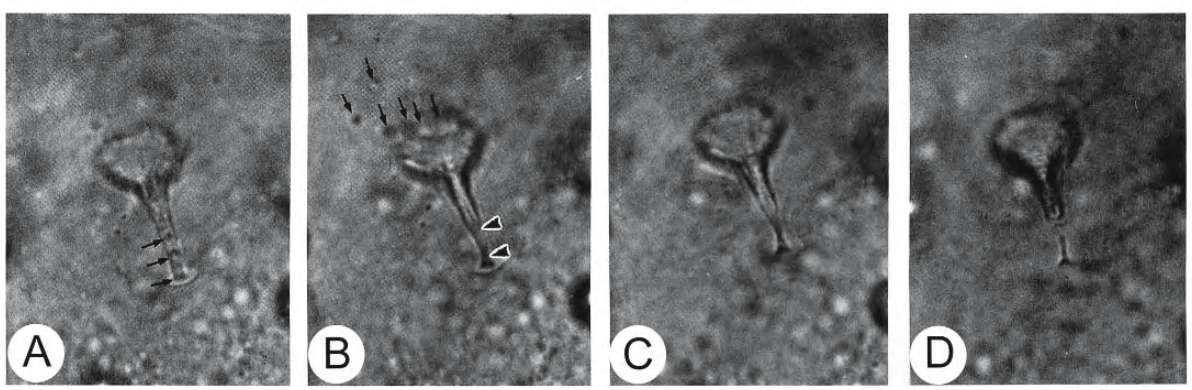

Figure 4.52: Photomicrographs by phase contrast of a living egg of the medaka *Oryzias latipes* showing changes in the micropyle following insemination at 23° C. Arrows indicate spermatozoa. X 940 (From Iwamatsu, Ishijima, and Nakashima, 1993; © reproduced with permission of John Wiley & Sons, Inc.).

A. Before insemination.

B. 125 seconds after attachment of sperm to the oolemma. Contraction (arrowheads) of the inner layer of the chorion following discharge of the alveolar contents results in the closure of the inner third of the micropylar canal.

C. 180 seconds.

D. 300 seconds.

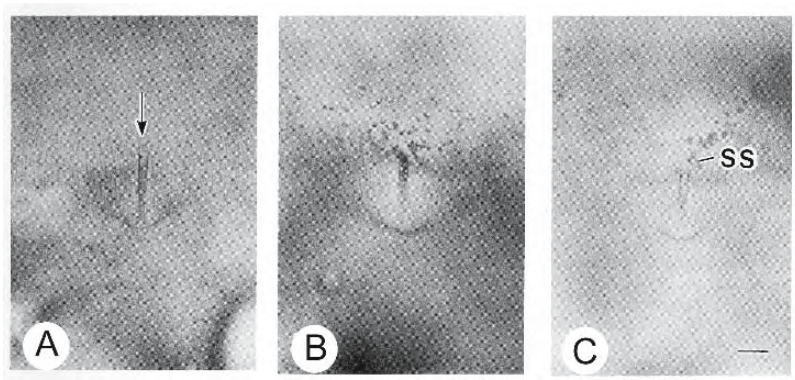

Figure 4.53: Photomicrographs of the micropyle in a living egg of the chum salmon *Oncorhynchus keta.* Bar = 20 μm (From Kobayashi and Yamamoto, 1987; © reproduced with permission of John Wiley & Sons, Inc.).
A. The unfertilized egg. The micropyle is indicated by an arrow.
B. Immediately after insemination.
C. Seven minutes after insemination showing the discharge of supernumerary spermatozoa (SS) from the micropylar canal.

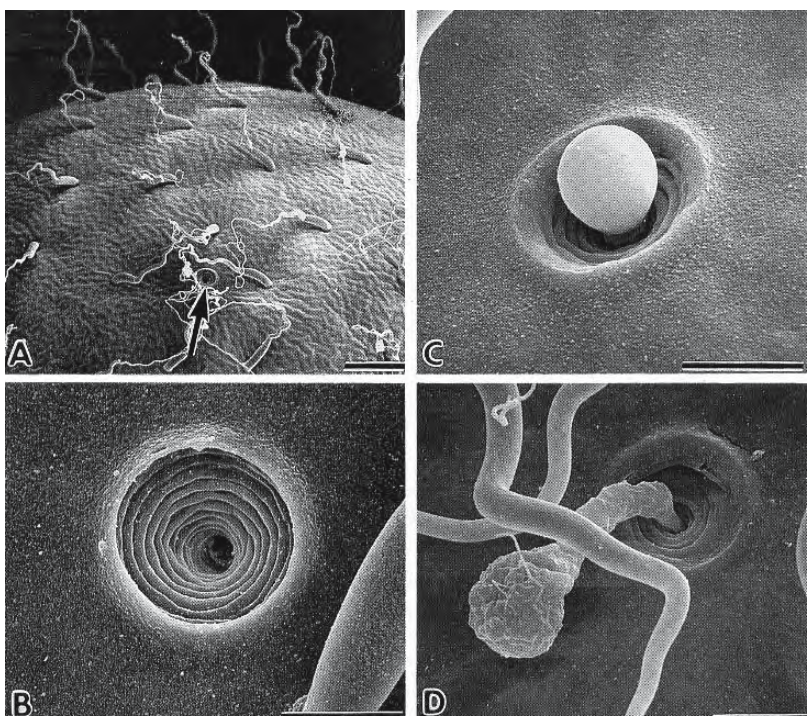

Figure 4.54: Scanning electron micrographs of the micropylar aperture in eggs of the medaka *Oryzias latipes* before and after insemination. (From Iwamatsu et al., 1991; reproduced with permission from Blackwell Publishing).
A. The arrow indicates the micropyle of an unfertilized egg. Bar = 100 μm.
B. This micropyle is shown at a higher magnification. Bar = 10 μm.
C, **D**. Vitelline fluid has exuded from the micropyle by 15 seconds after sperm attach to the egg. Bar = 10 μm.

Figure 4.55: Electron micrograph of a section through the micropylar canal of an egg of the chum salmon *Oncorhynchus keta* 240 seconds after activation. The lumen of the canal is filled with amorphous material blocking passage of a supernumerary spermatozoon (S). Bar = 2 μm (From Kobayashi and Yamamoto, 1981; © reproduced with permission of John Wiley & Sons, Inc.).

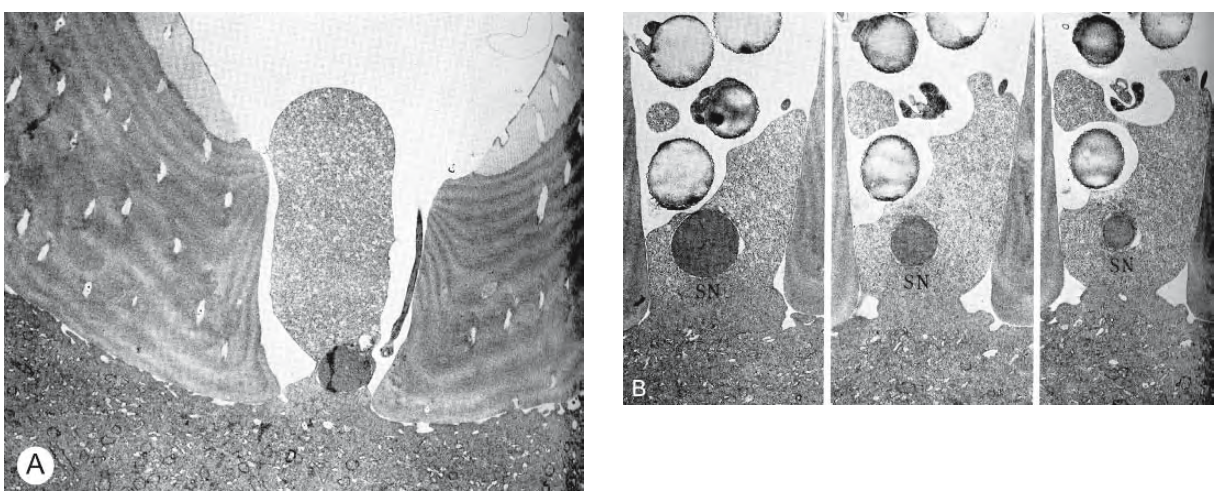

Figure 4.56: Transmission electron micrographs of sections through the micropyles of inseminated eggs of the common carp *Cyprinus carpio.* (From Kudo, 1980; reproduced with permission from Blackwell Publishing).

A. The fertilization cone has grown as far as the micropylar vestibule and plugs the micropylar canal. A sperm head is embedded at the base of the fertilization cone; its tail lies alongside the cone. X 4,600.

B. Three sections of a single fertilization cone containing the first sperm nucleus (SN). Several spermatozoa, denied access by the fertilization cone, are clustered in the micropylar canal. X 6,100.

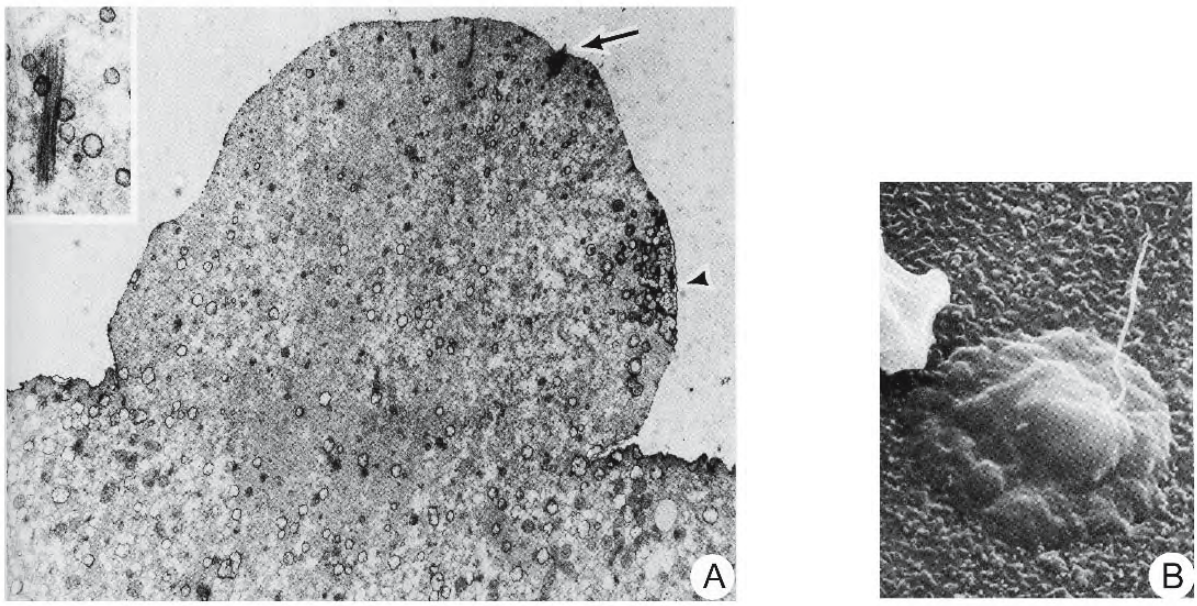

Figure 4.57: Electron micrographs showing the fertilization cones of eggs of *Fundulus heteroclitus* fixed three minutes after insemination. (The chorion was removed from fixed eggs.) (From Brummett, Dumont, and Richter, 1985; © reproduced with permission of John Wiley & Sons, Inc.).

A. Transmission electron micrograph of a section through the definitive fertilization cone. Several dark staining vesicles are seen in the cytoplasm of the cone, especially near its surface (arrowhead). A portion of a sperm tail protrudes from the surface of the cone (arrow) X 4,300.
Inset: Another section of this cone showing portion of the sperm tail within the ooplasm. X 15,800.

B. Scanning electron micrograph of the surface of the egg showing a sperm tail protruding from a fertilization cone. The surface of the cone is relatively smooth compared to the surface of the egg immediately surrounding it. X 2,500.

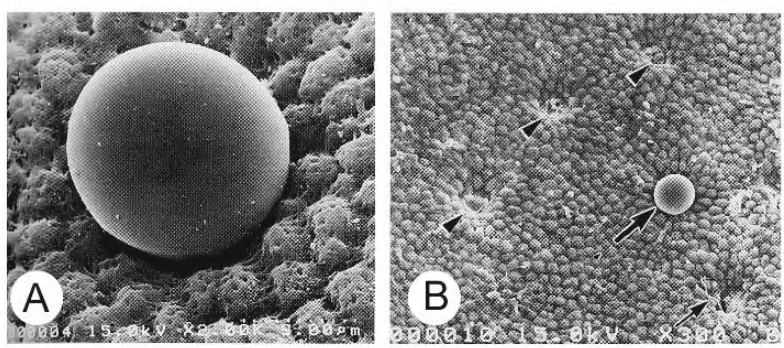

Figure 4.58: Scanning electron micrographs of the surface of inseminated eggs of the paddlefish *Polyodon spathula* one minute after fertilization. The paddlefish produces an egg with multiple micropyles. (From Linhart and Kudo, 1997; reproduced with permission from Elsevier Science).

A. The ball-shaped end of a fully developed fertilization cone extends from the external aperture of a micropyle. X 2,200.

B. One of the micropylar canals in the micropylar area of the chorion is sealed with a fully grown cone (large arrow); the others (arrowheads) appear to be blocked to various degrees with other materials, probably exudates from the cortical alveoli. A sperm tail extends from a pore of one of the micropylar canals (small arrow). X 440.

CHAPTER 5

OVIDUCTS AND OVIPARITY

5.1 Oviducts

Oviducts of many vertebrates are derived from the Müllerian duct. Eggs released into the coelom at ovulation are gathered up by a funnel at the end of the oviduct and conveyed to the outside. *En route,* the oviduct often provides a protective coating and, in some viviparous species, it becomes a haven for developing embryos. In the AGNATHA, however, no oviducts develop and eggs are shed directly into the coelom, escaping from the body via gential pores that perforate the body wall just before spawning. Any protective coating on these eggs, therefore, must be provided by the ovary before ovulation.

The so-called oviducts of TELEOSTS are not derived from Müllerian ducts but, in most species, are formed from the peritoneal folds that enclose the ovary (Henderson, 1967). These membranous envelopes extend posteriorly, guiding the mature eggs to a single median genital pore that opens, at the time of reproduction, between the anus and urinary papilla. This arrangement has an advantage in animals where the enormous numbers of eggs produced could choke the coelom. In salmonids, however, the ova are discharged directly into the coelom and pass through a constriction in the posterior abdominal wall into the genital cavity; they leave the body by way of an orifice in the urinogenital papilla (Figure 5.1).

A simple columnar epithelium lines both the ovarian cavity and the oviduct of the bleak *Alburnus alburnus* (Lahnsteiner, Weismann, and Patzner, 1997). CILIATED CELLS, interconnected by junctional complexes, constitute most of the epithelium of the oviduct (Figure 5.2) and assist in the transport of eggs. Below the ciliary rootlets of these epithelial cells, the cytoplasm contains abundant tubular granular endoplasmic reticulum, mitochondria, and a nucleus with a single nucleolus. The cytoplasm also contains coated vesicles, numerous ribosomes, and some lipid vacuoles; the absence of a Golgi complex and secretory vesicles indicates that these cells are neither secretory nor steroidogenic. Small clusters of MICROVILLOUS CELLS, similar to those lining the ovarian cavity (see page 7), are also found in the epithelium lining the oviduct of the bleak (Figure 5.3). Within the ovarian lumen, they secrete components of the ovarian fluid which maintain its ionic gradient, thereby preventing activation of the eggs: closure of the micropyle, swelling of the eggs, and shell hardening. Presumably, they continue this function in the oviduct and contribute their secretions to the ovarian fluid. Table 1.1 records analysis of the composition of the ovarian fluid in the bleak[16].

The peritoneal oviducts of viviparous teleosts are inadequate to the task of sheltering and nourishing developing embryos and these duties are carried out, perforce, by the ovary itself.

Viable sperm are stored for periods up to several months within the ovary and oviduct of the oviparous poeciliid platyfish *Xiphophorus maculatus*. The oviduct or GONODUCT is a convoluted, posterior extension of the peritoneum covering this cystovarian ovary; it is lined by simple to pseudostratified mesothelium derived from the lining of the lumen (Figure 5.4A) (Potter and Kramer, 2000). Lying between the two mesothelial layers are the typical loose vascular connective tissue and scattered smooth muscle cells that underlie all peritoneum (Figure 5.4B). The duct extends posteriorly to exit at a urogenital opening associated with a papilla just posterior to the anus. An elaborate array of surface modifications decorate the mesothelial cells of the lining: scallops, lobular extensions, microvilli and microvillous appendages, and deep intracellular pits and pockets (Figure 5.5). The sperm become associated with special epithelial cells, SPERM-ASSOCIATED CELLS, that lack extensive surface microvilli but contain an array of deep sur-

[16] Similar values for four species of salmonids are recorded in an earlier paper by these authors (Lahnsteiner, Weismann, and Patzner, 1995).

face pits and pockets. The cytoplasm of these cells is moderately electron-dense and contains an abundance of free ribosomes as well as a few mitochondria and small vesicles; endoplasmic reticulum is sparse. Microtubules, intermediate filaments, and microfilaments constitute the cytoskeleton of the sperm-associated cells; the microtubules reinforce intercellular junctions and the microfilaments support the microvillous extensions of the surface. The sperm lie either within the invaginations or are taken up and incorporated within the cytoplasm of these cells (Figures 5.5D and 5.6). Intact sperm nuclei, neck, mitochondria, and flagella can be seen within the pits and pockets while sperm nuclei, without flagella or other organelles, occur deep within the cytoplasm of the sperm-associated cells. There is no indication of lysosomal activity or sperm breakdown. Rejection of sperm by the immune system of the female is probably averted by the barrier provided by apical junctional complexes between the epithelial cells (Figure 5.6).

The oviducts of CHONDRICHTHYES are derived from Müllerian ducts and demonstrate many homologies to the oviducts of other vertebrates (Figure 5.7). At ovulation, eggs are cast into the coelom from the ovary and swept into a ciliated funnel, the OSTIUM, at the upper end of the oviduct, to begin their journey to the exterior. Fertilization is internal in elasmobranchs: sperm, received in the cloaca during copulation, make their way to the upper reaches of the oviduct and fertilize the eggs. Often the sperm are stored within the oviduct for long periods of time before fertilization occurs (Figure 5.8) (Pratt, 1993). If the sperm are contained within a SPERMATOPHORE, the oviduct secretes enzymes that break down this package to free the sperm contained within. The oviducts of oviparous forms secrete jelly coats and tough, collagenous egg capsules that protect developing eggs from predators and other rigours of the outside world. An egg capsule usually contains only one egg but, in some cases, three or four eggs may be present. In viviparous forms, the oviducts may be enlarged into uteri which provide a hospitable environment for gestation, often of several months' duration; oxygen must be supplied during this period and wastes must be removed; nutrients are often provided from the mother's circulation.

The basic plan of this remarkable oviduct is similar throughout the elasmobranchs. It is lined with a highly variable TUNICA MUCOSA whose epithelium reflects the function of the region (Figure 5.9). In glandular regions, the epithelium is invaginated to form a thick layer of tubular glands that pour their secretions at the bases of blunt folds that are covered with ciliated, stratified cuboidal epithelium. Elsewhere, the epithelium forms rounded folds that may be covered with stratified squamous to cuboidal epithelium which may or may not bear cilia. The tunica mucosa is subtended by a richly vascular TELA SUBMUCOSA of loose fibrous connective tissue that may contain a few scattered smooth muscle fibres. This layer merges imperceptibly into the smooth muscle of the TUNICA MUSCULARIS which consists of a loose inner layer of circular fibres and a denser outer layer of longitudinal fibres. The oviduct is enclosed by a TUNICA SEROSA of loose fibrous connective tissue covered by simple squamous or cuboidal mesothelial cells.

The oviduct of Chondrichthyes may be divided into several functional regions: ostium, oviduct, oviductal (nidamental) gland, isthmus, uterus, and cervix (Figures 1.52, 5.10, and 5.11) (Stanley, 1963; Koob and Callard, 1991; Hamlett et al., 1998b; Hamlett and Koob, 1999). In nearly all elasmobranchs, regardless of reproductive mode, ovulated eggs are initially encapsulated in a shell produced by a specialized gland that is unique among vertebrates: the NIDAMENTAL GLAND, SHELL GLAND, or OVIDUCTAL GLAND[17] (Koob and Callard, 1991). In oviparous species, the egg is oviposited soon after formation and development occurs entirely within the capsule; at hatching, the young have internalized all their yolk and are fully developed. In many viviparous species, the egg capsule functions transiently during the initial stages of development and embryos may emerge from it to complete development within the fluids of the uterus. In some live-bearing species, however, the egg capsule remains intact throughout gestation and becomes integrated into a placenta.

Little has been written about the ostium and upper reaches of the oviduct of elasmobranchs. These are common oviductal structures in most vertebrates and presumably function similarly in all elasmobranchs to transport ovulated eggs by means of ciliary currents (Hamlett and Koob, 1999). Longidtudinal folds, covered with a simple columnar ciliated epithelium, protrude into the lumen of the anterior oviduct of the Atlantic guitarfish *Rhinobatos lentiginosus;* basal bodies of the ciliary rootlets form a distinct line

[17] Since the gland does not always produce a shell and, since no "nidus" or nest is produced in some species of elasmobranchs, Hamlett et al. (1998a) recommend that the term "oviducal gland" be used to describe this structure.

line extending across the apical regions of the cells (Figure 5.12) (Hamlett et al., 1998b). Secretory cells, located between adjacent folds and, in smaller numbers among the ciliated cells of the surface, probably provide a lubricant that assists the cilia in moving ovulated eggs into the oviductal gland. The connective tissue stroma of the folds is poorly vascularized. There is no smooth muscle in this region.

Development, structure, and activity of the other regions of the female reproductive tract of elasmobranchs vary with the reproductive mode. The oviductal gland is the predominant organ in the oviduct of oviparous forms (Figures 5.11 and 5.13) and the uterus is relatively inconspicuous, simply providing a conduit for the large egg capsule. The situation is reversed, however, in viviparous species and the oviductal gland plays a relatively minor role, sometimes encapsulating the eggs in diaphanous membranes, while the uterus often manifests various types of structural modifications as it envelops the embryos during their development to term. In some species, elaborate, richly vascular extensions of the uterine wall, the TROPHOTAENIAE, serve to nourish the developing young.

In at least two live-bearing species, a short segment of the oviduct, the ISTHMUS, connects the oviductal gland with the uterus (Koob and Callard, 1991; Callard and Koob, 1993; Hamlett and Koob, 1999). In *Squalus acanthias,* the isthmus coils before entering the uterus, forming a stricture that is postulated to be a closing mechanism (Verschlußvorrichtung) that prevents the backflow of urine and seawater into the coelom but becomes compliant and extensible when eggs are being transported to the uterus (Figure 5.14) (Widakowich, 1907, cited by Callard and Koob, 1993). How the isthmus functions is not known.

The oviducts of both egg-laying and live-bearing elasmobranchs enter the common urogenital sinus by way of a constricted CERVIX (Koob and Callard, 1991). The cervix closes the uterus of oviparous species, preventing the premature entry of the forming egg capsule into the urogenital sinus. In live-bearing forms, it presents the final barrier through which the foetuses emerge at parturition. It must be capable of changing size or properties at different times during the reproductive cycle in order to accommodate the passage of eggs or term foetuses. The common UROGENITAL SINUS in adult female oviparous elasmobranchs is an enlarged sac into which the oviducts enter separately; it may house the egg capsule for several hours before oviposition.

5.2 Oviductal Gland and Egg Capsule

In general, oviparous chondrichthyes produce two kinds of egg capsules (Figure 5.15). The capsule of the dogfish *Scyliorhinus,* for example, is rectangular with tendrils extending from each corner: the familiar "mermaid's purse" of the seacoast. The second type is seen in the Port Jackson shark, *Heterodontus,* and is helical with long, coiled, filamentous tendrils extending from the apex. The tendrils anchor the egg in position by coiling around upright masses of seaweed (Figure 5.16). A much simpler capsule encloses the eggs of viviparous species. For example, in the spiny dogfish, *Squalus acanthias,* a clear, amber capsule surrounds several developing eggs within the uterus. This shell breaks down about the time of absorption of the external gills and the embryos float freely in the uterine fluid. Most studies have been carried out on the elaborate egg capsule of an oviparous species, the dogfish *Scyliorhinus canicula.*

The ovum of *Scyliorhinus canicula* is about 13 mm in diameter when spherical and is protected by a tough, roughly rectangular capsule, about 22 x 53 mm, consisting of two convex walls firmly sealed at all four edges (Figures 5.17 and 5.18) (Rusaouën-Innocent, 1990a; Knight and Feng, 1992). Two lateral ridges that form along the suture are prolonged into long, tapering tentacles. The posterior margin of the capsule (the part extruded first) is deeply incurved and forms a seal similar to a crimped weld (Figure 5.19). The anterior border is straight and is joined by a sophisticated seal which separates to permit hatching when development of the embryo is complete.

Two capsules are produced simultaneously within the two oviductal glands of *Scyliorhinus canicula,* at a maximum rate of two every 60 hours during a protracted breeding season (Koob and Callard, 1991; Knight and Feng, 1992). Formation of the capsule begins before ovulation so that the capsule is one-third to one-half formed before the egg enters the lumen of the oviductal gland (Figure 5.20). The capsule protects the embryo from predation, mechanical injury, fouling, and infection throughout an extended period of development of at least five months. Its wall is extremely tough and resistant to chemical and enzymic attack though freely permeable to small molecules and ions (Knight and Feng, 1992, 1994a; Feng and Knight, 1992). This envelope is resistant to bursting and is filled with a viscous, jelly-like material that functions as an efficient shock absorber.

The capsule wall is a composite material constructed largely of collagen fibrils with a highly ordered, kinked molecular arrangement set in a matrix containing spherical filler particles, 2 μm in diameter, composed of hydrophobic proteins with an exceptionally high tyrosine content (Figure 5.21) (Knight and Hunt, 1974, 1976, 1986; Rusaouën et al., 1976; Rusaouën-Innocent, 1990a; Knight and Feng, 1992, 1994a; Feng and Knight, 1992; Knight, Feng, and Stewart, 1996). The wall is made up of four layers: L_1 on the outside, then L_2 and L_3, and, on the inside, L_4 (Figure 5.22). The outer layer (L_1) is about 25 μm thick in dehydrated, tanned specimens[18]; it consists of fine fibrils above densely packed, amorphous granules, rich in tyrosine (Figure 5.23). Layer L_2 is about 225 μm thick and constitutes the bulk of the capsule wall; it is similar to plywood and consists of about 30 sheet-like LAMELLAE held together with a phenolic resin. The outer lamellae are better ordered than the inner ones and each lamella appears to consist of five LAMINAE. Each lamina contains parallel collagen-containing fibrils that show a periodicity of about 37 nm (Figure 5.24) (Knight and Hunt, 1974; Rusaouën-Innocent, 1990b; Knight and Feng, 1994b). The laminae are stacked with an angle of 45° between fibrils in successive laminae, to give an orthogonal arrangement (Figure 5.25). Although finely striated, L_3 appears more homogeneous than the other layers and is about 30 μm thick; its striations are orthogonal to the laminae of L_2. The inner layer, L_4, is only 4 to 5 μm thick and, with the light microscope, appears homogeneous.

The layers of the selachian capsule, as well as the tendrils and jelly, are extruded successively by an amazing coordination of the secretions of a large number of simple tubular glands arrayed in transverse zones of the oviductal gland (Figure 5.22). The inner layer, L_4, is formed first by the most anterior zone; more posteriorly, L_3 is added, followed by the thickest layer, L_2, and finally the outer layer L_1, which is produced in the most posterior zone (Figure 5.26) (Knight and Feng, 1994a; Knight, Feng, and Stewart, 1996). Each lamella is produced from a separate transverse groove in the lining of the gland; each transverse groove, in turn, contains a single row of geometrically placed SPINNERETS which define the orientation of molecules in the extruded material (Knight et al., 1996). After the material has flowed for some distance from the spinnerets, the molecules aggregate into fibrils which become laminated at three hierarchical levels and helically twisted at five to six levels. This linear secretory pathway permits the study of the secretion, orientation, fibrillogenesis, and assembly of a complex collagenous structure of great strength. Layers L_1, L_2, and L_3 are coiled around each other in the tendrils.

The oviductal gland is a compound tubular gland. It is a dilation of the anterior oviduct about 20 mm posterior to the ostium and is surrounded by a thin, tough connective tissue sac (Figures 5.10 and 5.27) (Stanley, 1963; Knight and Feng, 1992; Knight, Feng, and Stewart, 1996; Hamlett et al., 1998a). Each female has two oviductal glands which appear to function in synchrony so that egg capsules or tendrils are at the same stage of formation in each of the two oviducts. Similar dorsal and ventral mirror-image halves of the gland enclose a dorsoventrally flattened LUMEN into which the egg case is extruded (Figure 5.28A). Most of the wall consists of long, simple tubular glands, about 60 μm in diameter, which are packed in a fairly hexagonal pattern and open into this lumen (Figures 5.28B and 5.29). Each half of the gland produces one of the two walls of the capsule, while the thickened marginal rib arises within grooves at the left and right limits of the flattened lumen; the tendrils are formed within two shallow pits located one on each side of the gland. The gland changes in size during the sexual cycle: in sexually mature females of *Scyliorhinus canicula* it may be 3.5 cm long and 2 cm in diameter but is only a slight thickening of the oviduct in sexually immature females.

The tubular glands are arranged in six transverse ZONES, zones A to F, which form the capsule and its jelly as a coextrusion (Figure 5.27) (Feng and Knight, 1992; Knight and Feng, 1992; Knight, Feng, and Stewart, 1996). Zone A secretes the jelly; zones B to E produce layers L_4 to L_1 respectively. Histochemical studies on the oviductal glands of *Scyliorhinus canciula* (and other species) have shown that the zones have differing functions. Zone A, the most anterior, constitutes about one quarter of the length of the gland and appears to secrete a neutral mucopolysaccharide with small quantities of collagen. Zone B consists of a single row of tubules secreting a sulphated mucopolysaccharide and may contribute to a thin layer on the inner surface of the capsule, probably L_4. Zone C has three or four rows of tubules and, together with the first few rows of tubules in zone D, it appears to form

[18] It is suggested that these values of thickness have been reduced by about 15% by dehydration; in addition, tanned shells appear to be thinner than those removed from the oviducts.

layer L_3. In addition, it secretes the components of an oxidative phenolic tanning system which strongly stabilize the inner layer, L_3, and the outer layer, L_1; these include protein rich in tyrosine residues, free DOPA, an orthodihydroxyphenol oxidase, and a peroxidase. Zone D consists of about 30 rows of tubules that form the bulk of the thickness of the capsule, layer L_2, secreting collagen and possibly accessory proteins; the storage granules in zone D appear to contain small quantities of peroxidase. Zone E also secretes components of a phenolic tanning system as well as some collagen. Zone F, which has been subdivided on the basis of histochemical observations, consists of short tubules lying perpendicular to the tubules of zone E. Zone F_1 secretes a phenolic protein together with peroxidase and orthodihydroxyphenol oxidases; zone F_2 secretes neutral mucopolysaccharides and peroxidases; and zones F_3 and F_4 secrete sulphated mucopolysaccharides and peroxidase. Tubules of the F zone appear to contribute a thin, electron-dense layer on the surface of L_1. Alternatively, a morphological basis has been used to differentiate four regions of the oviductal gland where the CLUB and PAPILLARY ZONES correspond to zone A, the BAFFLE ZONE to zones B, C, D, and E, and the TERMINAL ZONE to zone F (Figure 5.29) (Hamlett. et al., 1998a).

The tubular glands consist of a simple columnar epithelium of granular secretory cells lying between ciliated columnar cells (Figures 5.30A,B) (Knight and Feng, 1992; Knight, Feng, and Stewart, 1996). Each tubule is surrounded by a basement membrane and richly vascular collagenous connective tissue; there are no smooth muscle or myoepithelial cells in the wall of the tubule. The tubules of zone D are shortest, about 6 mm, in the most anterior row and increase progressively in length, reaching approximately 12 mm in the most posterior row; this correlates with the thickness of the lamellae derived from each row.

The secretory cells of zone D have the characteristic appearance of cells specialized for protein secretion: their nucleus contains a large nucleolus and little heterochromatin; there is extensive granular endoplasmic reticulum; a large Golgi stack and apical microvilli; and the cytoplasm is packed with numerous approximately spherical secretory granules about 2 μm in diameter (Figure 5.31) (Rusaouën, 1978; Feng and Knight, 1992; Knight et al., 1993; Knight, Feng, and Stewart, 1996). The marked junctional complexes and extensive interdigitations of the lateral membranes probably indicate that this epithelium is also actively secreting ions. Within cisternae of the endoplasmic reticulum, the collagen appears anisotropic but, as the granules make their way to the apical border of the cell, it becomes dehydrated and undergoes a series of liquid crystal transformations, thereby providing a compact way of storing collagen (Figures 5.32 and 5.33). The granules appear to be released into the lumen by merocrine secretion. As it passes along the tubules, presumably by ciliary action, the collagen appears to rehydrate, reverting to the earlier phases of the liquid crystal. Coalescence of the secreted granules into a thread within the lumen is thought to occur by hydrophobic interactions. It is suggested that the changes in the molecular arrangement of the collagen are brought about by a dramatic increase in pH encountered in passing from the secretory cell, through the secretory tubule and secretory duct, into the lumen of the oviductal gland (Figure 5.34) (Feng and Knight, 1994a).

Zone D, the largest zone of the oviductal gland, produces the lamellae of the thickest region of the capsule, L_2. Each lamella originates within a deep transverse fold which runs around the circumference of the lumen and rarely branches (Figures 5.26 and 5.35). Each of the lamellae constituting layer L_2 is formed within a transverse groove which receives secretion from a single row of D-zone tubules. There is an exact numerical correspondence in the number of lamellae of L_2, the number of D-zone transverse grooves, and the number of rows of D-zone tubules. The depth of the transverse grooves increases continuously from the first (375 μm) to the last (1030 μm). During the formation of the capsule wall, the lamellae bend through approximately 90° as they leave the transverse groove and move posteriorly, adhering together to form a single sheet that is closely applied to the lumen of the gland (Figure 5.28).

The functional unit in all parts of the gland consists of a SECRETORY TUBULE composed of columnar secretory cells interspersed with some columnar ciliated cells, a short DUCT lined with columnar ciliated cells but lacking secretory cells, and a SPINNERET (Figure 5.29) (Knight and Feng, 1992; Knight, Feng, and Stewart, 1996; Hamlett et al., 1998a,b). A single row of spinnerets opens into the base of each transverse groove in zones B to E (Figure 5.36). (Tubular glands in zone A secrete their mucopolysaccharides directly into the lumen of the gland.) These grooves run around the entire width of the gland with little branching. Each spinneret is formed of two half-overlapping, flattened

BAFFLE PLATES which project into the base of the transverse groove on each side of the opening of the secretory duct (Figure 5.37). The baffle plates are supported by a thin core of loose vascular connective tissue and are covered on both sides by a ciliated, low columnar epithelium. They are arranged at an angle of approximately 45° to the longest axis of each transverse groove (Figures 5.38A,B). The baffle plates divide the base of the groove into three compartments: the ANTERIOR and POSTERIOR CRYPTS between the baffle plates and the walls of the transverse groove, and the oblique slit (CENTRAL CRYPT) between each pair of baffle plates. The baffle plates divide the secreted material into three flows: anterior, central/oblique, and posterior, that join to form a single sheet (Figure 5.35). The material is probably still plastic in the transverse grooves.

Both surfaces of the transverse groove and both surfaces of each baffle plate are densely ciliated (Knight and Feng, 1992). The axis of ciliary beat seems to be vertical on both faces of the transverse groove and approximately -45° and +45° to the vertical axis on the anterior and posterior faces of the baffle plates respectively (Figure 5.38C). Ciliary rootlets are oriented in line with the direction of beat. Observations on capsule formation in *Raja erinacea* indicate that material within the lumen of the tubular gland is roughly circular in cross section and 15 μm in diameter; as it passes through the spinneret, it diverges smoothly and emerges as a flattened ribbon, about 10 x 425 μm (Figure 5.39A) (Knight et al., 1996). Each spinneret extrudes a single flattened ribbon. As the secreted material diverges from the secretory tubule, a curved pattern of molecular orientations is set up and, after the material has flowed some distance from the spinnerets, the molecules aggregate into fibrils. This material is largely collagenous. Overlapping rows of ribbons fuse together to form a single lamella (Figure 5.39B). The overlapping of five ribbons at each point in the lamella gives rise to a construction that is similar to plywood except that there are curved fibres in each ply. A z-series of confocal images cut parallel to the plane of a single lamella confirms this pattern of stepped rotation of the molecular axis in successive ribbons (Figure 5.39C). This arrangement provides great toughness and resiliency to the egg capsule.

Before the ovum enters the oviductal gland, the POSTERIOR TENDRILS are formed in marginal TENDRIL FORMING REGIONS of the E zone (Figure 5.40) (Feng and Knight, 1994b; Knight, Feng, and Stewart, 1996). The tendrils are moved along the channels by cilia and rotate during formation so that, in cross section, the lamellae exhibit a Swiss-roll construction of alternating narrow and broad laminae which entrap fluid-filled CANALICULI between them (Figure 5.41). In contrast to the orthogonal arrangement in adjacent laminae of the capsule wall, collagenous fibres are oriented approximately at right angles in adjacent laminae of the tendrils: circumferentially in the narrow laminae and longitudinally in the broad laminae. When the posterior tendrils are fully formed, all of the tubular glands are activated in the CAPSULE-WALL FORMING REGION between the tubular forming regions and production begins on the posterior margin of the capsule: the POSTERIOR MARGINAL SEAL with its crimped construction. This is followed by formation of the walls of the POUCH whose dorsal and ventral halves are held apart by the jelly secreted by the A zone (Figure 5.26). Extrusion of the jelly, which will come to surround the ovum, appears to provide much of the force for the expulsion of the capsule. When about one-third of the capsule has been formed, the ovum enters the lumen of the gland from the anterior oviduct and assists in the propulsion of the egg case (Figure 5.20). The ovum becomes enveloped by the layers of the capsule wall which are extruded in sequence until finally the pouch is complete and the ANTERIOR SEAL is formed. The MARGINAL RIBS of the pouch are formed by the tendril forming regions and these extend beyond the anterior seal to become the ANTERIOR TENDRILS. Innervation of the oviductal gland by two sympathetic nerve branches which enter near each tendril forming region suggests that sympathetic activity may activate secretion of the posterior tendrils, the first event of the secretory cycle.

A consistent feature of elasmobranch oviductal glands that produce an egg envelope is the baffle zone. The viviparous yellow spotted stingray *Urolophus jamaicensis,* however, is an exception in that it does not produce an egg envelope; a typical baffle zone is lacking but a modified "baffle equivalent zone" persists (Hamlett et al., 1998b). The oviductal glands actively synthesize and assemble fibrils to produce a transitory egg covering (Hamlett et al, 1996b).

In addition to the production of egg capsules, the oviductal gland of female elasmobranchs is a principal site of sperm storage, thereby enhancing the chances of successful insemination (Pratt, 1993). The gland, with its long, narrow tubules, provides a favourable environment for the maintenance of sperm for periods of months or even more than a year in some species (Figure 5.8). Some of the tubules seem to be special-

ized for sperm retention and, in some species such as *Sphyrna lewini,* may constitute a true seminal vesicle.

5.3 Uterus in Elasmobranchs

In many species of elasmobranchs, the dilated posterior region of the female genital tract may be modified as a uterus, cervix, and common urogenital sinus (Figures 5.11 and 5.42A,B) (Koob and Hamlett, 1998; Hamlett and Hysell, 1998). The uterus harbours the egg capsule of oviparous forms during the completion of sclerotization and it secretes materials that may contribute to this process. In aplacental viviparous species, the uterus functions as a respiratory membrane and regulator of the ionic and osmotic environment; it provides no supplemental nutrients and the embryos subsist on their own yolk stores or by feeding on ovulated eggs. In placental viviparous species, the uterus provides nutrients for the developing embryos after their yolk stores have been depleted.

The uterus is lined by a TUNICA MUCOSA consisting of an epithelium, with its basal lamina, resting on loose, vascular connective tissue that may be so richly hydrated that it sometimes appears mesenchymal (Figure 5.43) (Hamlett et al., 1998b; Hamlett and Hysell, 1998). The connective tissue is subtended by two layers of smooth muscle: an inner circular layer and outer longitudinal layer. The muscle is enclosed by a TUNICA ADVENTITIA consisting of delicate fibrous connective tissue and the simple squamous mesothelium of the peritoneum. Each of the layers of the uterus is modified to reflect the reproductive mode of the various species.

The lining of the gravid uterus of the oviparous little skate *Raja erinacea* is thrown up into richly vascularized longitudinal folds with branching tubular glands in the intervening grooves (Figure 5.44) (Koob and Hamlett, 1998; Hamlett and Hysell, 1998). The simple columnar epithelial cells on the surfaces of the folds bristle with cilia and microvilli while at the sides of the folds the epithelial cells are lower and contain apical secretory vesicles. The loose subepithelial connective tissue of each ridge is richly vascular and its capillaries press against the epithelial basal lamina (Figure 5.44C). In electron micrographs there is a strong appearance of a transporting epithelium: elaborate intercellular channels with extensive lateral cell processes penetrating between the epithelial cells and apical junctional complexes sealing these channels from the lumen (Figure 5.45). The cytoplasm of the epithelial cells contains mitochondria, granular endoplasmic reticulum, Golgi complexes, free ribosomes, polysomes, and occasional lysosomes. The secretory cells from the sides of the folds are cuboidal with surface microvilli and elaborate apical vesicles containing frothy, moderately electron dense secretory material (Figure 5.44D). The cytoplasm contains abundant granular endoplasmic reticulum and Golgi complexes. Lateral folds create extensive intercellular channels between the cells. The structure of the uterine wall is consistent with its role in "finishing" the egg capsule. Ciliary action and smooth muscle move the egg through the lumen, uterine secretions assist in tanning the capsular matrix, the rich vascularization provides the oxygen necessary for tanning to occur, and the elaborate intercellular spaces evince a transporting epithelium that removes excess water from the lumen.

The egg capsule is white when it leaves the oviductal gland and contains no catecholic substance although an inactive form of the enzyme, catechol oxidase, is incorporated into the matrix during secretion (Koob, 1991; Koob and Cox, 1988, 1990, 1993; Koob and Callard, 1991). Tanning occurs as the egg passes into the uterus where catechols begin to accumulate in the capsular material and are oxidized, under the influence of catechol oxidase, to quinones (Figure 5.46). The oxygen required for this tanning is transported from the maternal circulation by the uterus. Calcium and, to a lesser extent magnesium, are incorporated into the capsule during its formation in the oviductal gland; subsequent binding of these minerals is concomitant with the tanning process in the uterus (Figure 5.47).

The oviparous uterus of elasmobranchs shares many structural features with that of viviparous species (Hamlett and Hysell, 1998). Initially, all elasmobranch embryos rely on their yolk reserves contained within the foetal yolk sac. As development continues, various sources of nutrients are tapped and viviparity manifests itself in many ways from species to species. Modifications in the uterine lining provide for the prolonged support of developing embryos. Included are increased vascularization, bringing greater oxygen supplies to the lumen, elaborate extensions of the tunica mucosa that enhance its surface area for metabolic exchange, and thinning of the tissues between the capillaries and the surface, thereby reducing the diffusion distance for gas exchange. Four types of viviparity have been categorized: aplacental yolk sac

viviparity, where the developing embryo relies solely on its own yolk reserves for nourishment; aplacental oophagous viviparity, where the embryo nourishes itself within the uterus by grazing on its siblings; aplacental viviparity with uterine villi or TROPHONEMATA, where vascularized finger-like processes secrete a nutrient "uterine milk" called HISTOTROPH; and placental viviparity.

The uterus of the spiny dogfish *Squalus acanthias* provides no nutrients for the developing embryos but it maintains osmotic and ionic levels, thereby giving them a safe haven for their development (Hamlett and Hysell, 1998). This is an example of APLACENTAL YOLK SAC VIVIPARITY. The lining of the gravid uterus is thrown up in longitudinal flaps whose rims are expanded by a large artery that sends capillaries into the core of loose connective tissue, supplying nutrients to the epithelium and the smooth muscle of the wall (Figures 5.42A to C). The folds are covered by a stratified cuboidal epithelium with a microvillous border (Figures 5.42D,E).

The sandtiger shark *Carcharias taurus* exemplifies APLACENTAL OOPHAGOUS VIVIPARITY (Hamlett and Hysell, 1998). In addition to feeding on ovulated eggs, the foetus practices intrauterine cannibalism, feeding on its hapless siblings that had the misfortune to be ovulated at a later time. The smooth wall of the nongravid uterus is lined by a layer of cuboidal epithelial cells with a microvillous border (Figure 5.48A). Immediately below are three to five layers of flattened cells containing fibres and lipid droplets, and deeper still is a thicker layer of cells containing frothy, Schiff-positive vesicles. Longitudinal folds develop in the uterus of gravid females, thereby increasing the surface area of the lining (Figure 5.48B). The surface epithelial cells have become cuboidal and vascularization of the connective tissue has increased.

In another form of APLACENTAL VIVIPARITY, seen in the yellow spotted stingray *Urolophus jamaicensis,* vascularized villi or trophonemata increase the surface area for the secretion of nutrient "uterine milk" or histotroph that is ingested by the developing embryo and/or absorbed by external gill filaments (Hamlett and Hysell, 1998). The gravid uterus is lined by a dense mat of trophonemata. A large blood vessel in the core of each trophonema sends capillaries throughout the connective tissue of the finger-like organ (Figure 5.49A). The surface of the trophonema is thrown up into ridges with cores of delicate vascularized connective tissue. As the foetus develops, the cuboidal epithelium on the surface of the ridges becomes attenuated simple squamous (Figure 5.49B). A single basal lamina and sparse connective tissue separate this epithelium from the endothelial cells of the capillaries below. Abundant micropinocytotic vesicles in the endothelial cells indicate brisk exchange of materials. Secretory crypts between the ridges are lined by simple cuboidal epithelial cells containing large numbers of apical secretory vesicles (Figure 5.49C). These cells contain abundant granular endoplasmic reticulum, numerous Golgi complexes, and several types of secretion vesicles (Figures 5.49D,E). There are a few microvilli on the surface of these cells; the borders between adjacent cells are straight and are joined apically by tight junctions.

PLACENTAL VIVIPARITY is seen in Atlantic sharpnosed sharks *Rhizoprionodon terraenovae* (Hamlett and Hysell, 1998). Placental sharks usually develop in separate uterine compartments, with each embryo surrounded by its own egg envelope. After its yolk stores are exhausted, the empty yolk sac develops into a HAEMATROPHIC PLACENTA. The uterine compartment is smooth before implantation and composed of a simple columnar secretory epithelium overlying richly vascular loose connective tissue (Figures 5.50A to C). The usual MEROCRINE SECRETION takes place from these epithelial cells where droplets of secretion are released with no loss of cytoplasm or membrane. In addition, however, these cells release membrane-bound cytoplasmic masses, or "blebs" into the lumen; this is APOCRINE SECRETION where cytoplasm and membrane are lost from the apex of a secretory cell while the basal portion survives to produce more secretion. The surface of the uterus at term is a modified simple cuboidal epithelium with few secretory vesicles and sparse microvilli; it rests on a dense vascular bed (Figures 5.50C,D). The uterus is separated from the richly vascular foetal portion of the placenta (the distal portion of the former yolk sac) by the egg envelope.

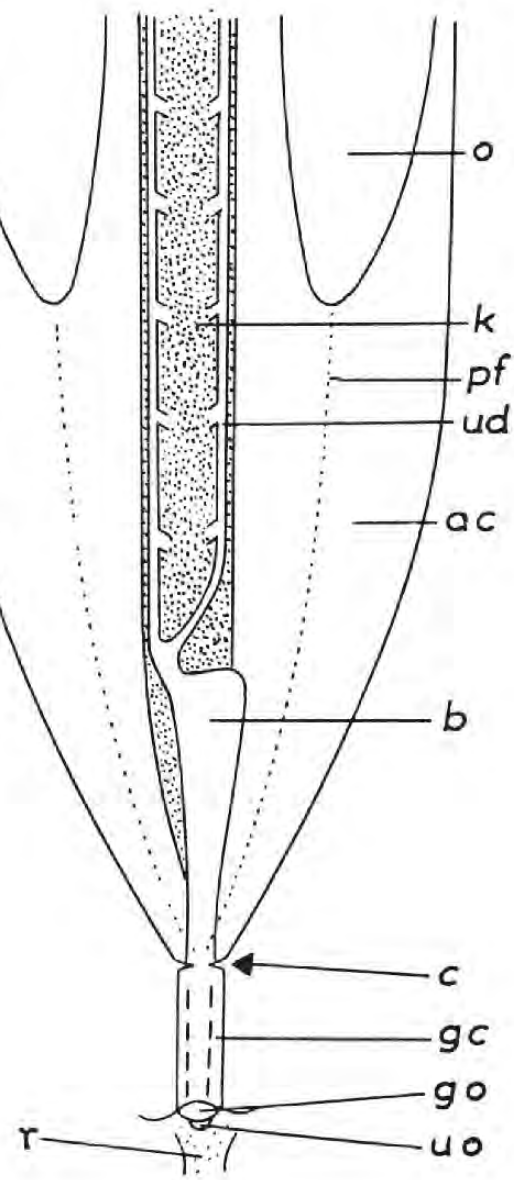

Figure 5.1: The urinary and genital system of a female trout. Ova are discharged directly into the coelom (ac) and pass through a constriction (c) in the posterior abdominal wall into the genital cavity (gc). They leave the body by way of an orifice (go) in the urinogenital papilla. (From Henderson, 1967; Fisheries and Oceans, Canada. Reproduced with the permission of the Minister of Public Works and Government Services, 2002).
Abbreviations: b, bladder; k, kidneys; o, ovary; pf, peritoneal fold; ud, urinary duct; uo, urinary orifice.

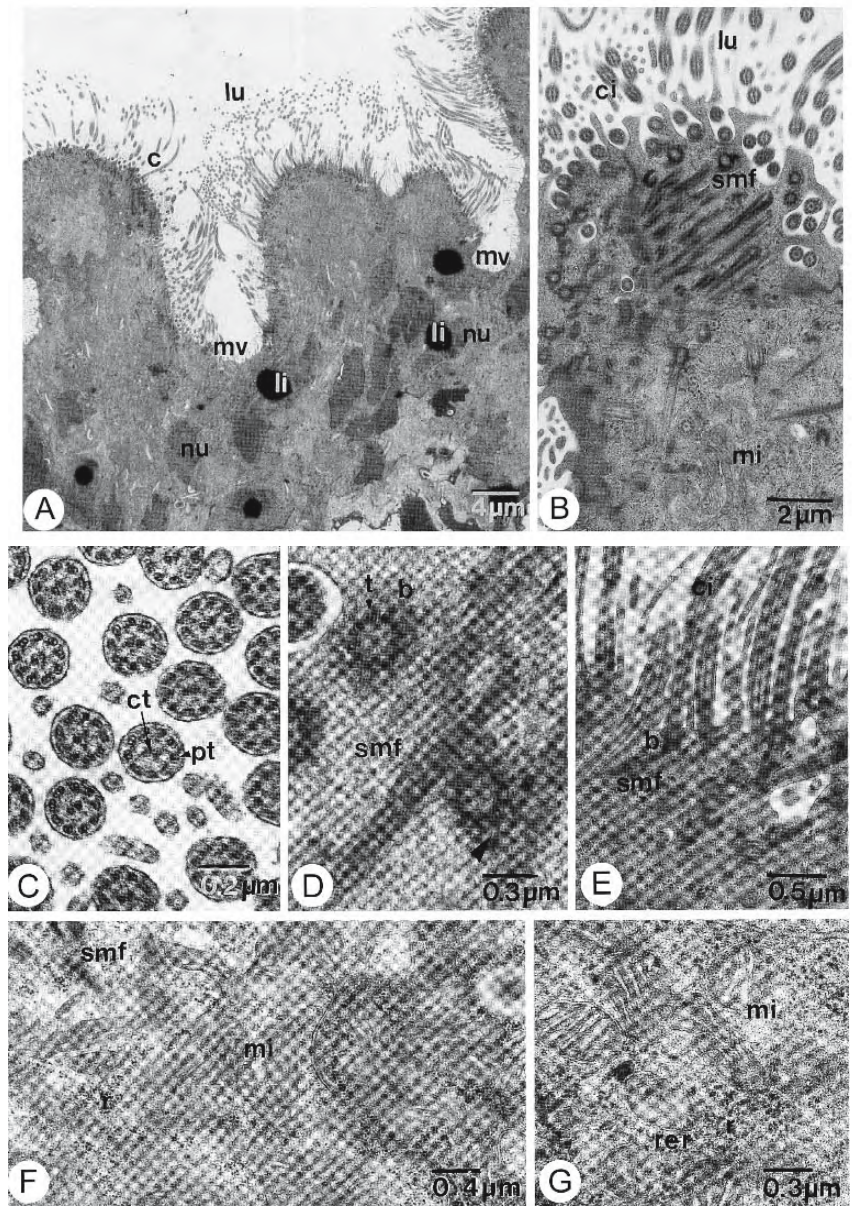

Figure 5.2: Transmission electron micrographs of sections of the oviduct of the bleak *Alburnus alburnus.* (From Lahnsteiner, Weismann, and Patzner, 1997; reproduced with permission from Elsevier Science).

A. Ciliated cells constitute most of the epithelium lining the oviduct; these are interspersed with small clusters of microvillous cells containing large lipid vacuoles.

B. Apical region of a ciliated cell.

C. Cross sections of cilia from a ciliated cell.

D. Sections through ciliary basal bodies. Microfilaments insert (arrowhead) at the tubule triplets of the basal body.

E. Longitudinal sections of basal bodies and cilia.

F. The mid region of a ciliated cell contains mitochondria and accumulations of free ribosomes.

G. The cytoplasm of a ciliated cell contains abundant mitochondria and granular endoplasmic reticulum.

Abbreviations: b, basal body; c, ciliated cell; ci, cilium; ct, central microtubules of cilium; li, lipid vacuole; lu, lumen; mi, mitochondrion; mv, microvillous cell; nu, nucleus; pt, peripheral microtubules of cilium; r, ribosomes; rer, granular endoplasmic reticulum; smf, striated ciliary rootlets; t, microtubule triplet.

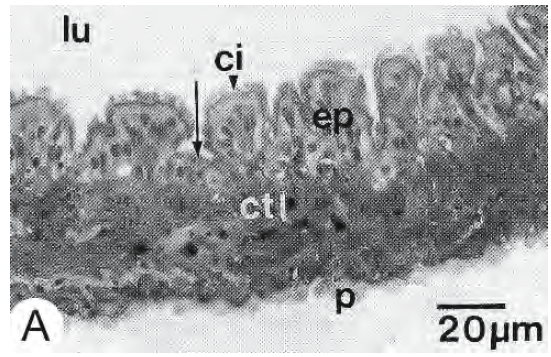

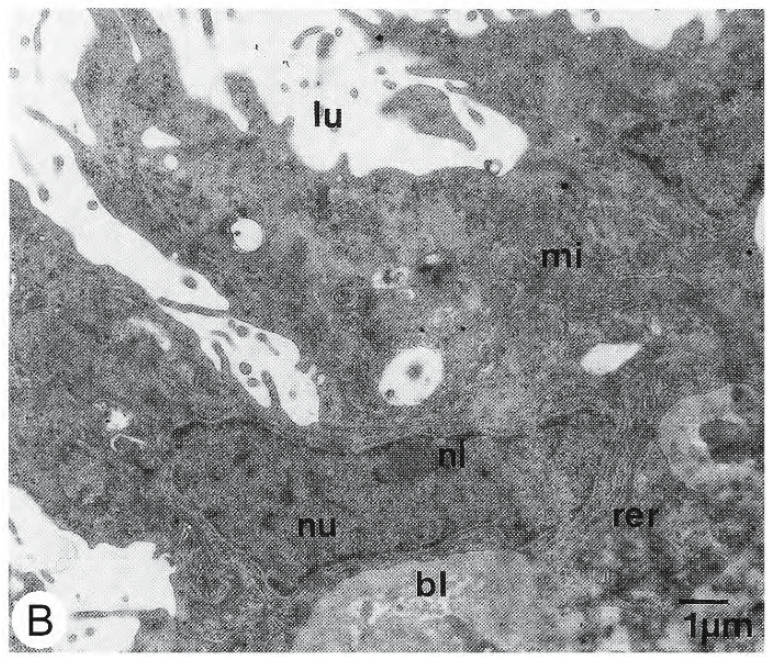

Figure 5.3: Micrographs of sections from the bleak *Alburnus alburnus.* (From Lahnsteiner, Weismann, and Patzner, 1997; reproduced with permission from Elsevier Science).

A. Photomicrograph of an oviduct showing the location of a cluster of microvillous cells (arrow) in the crevice between mucosal folds covered with ciliated cells.

B. Transmission electron micrograph of microvillous epithelial cells of the ovarian cavity.

Abbreviations: bl, basal lamina; ci, cilia; ctl, submucosal connective tissue; ep, epithelium; lu, lumen; mi, mitochondria; nl, nucleolus; nu, nucleus; p, peritoneum; rer, granular endoplasmic reticulum.

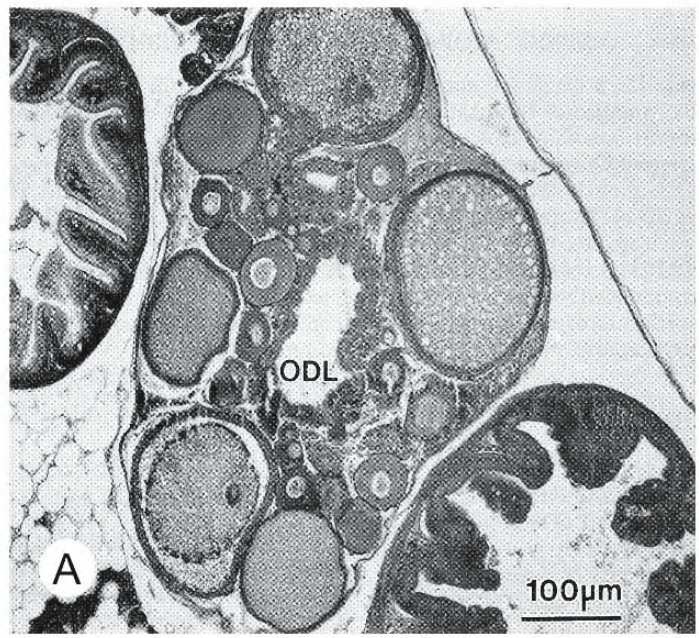

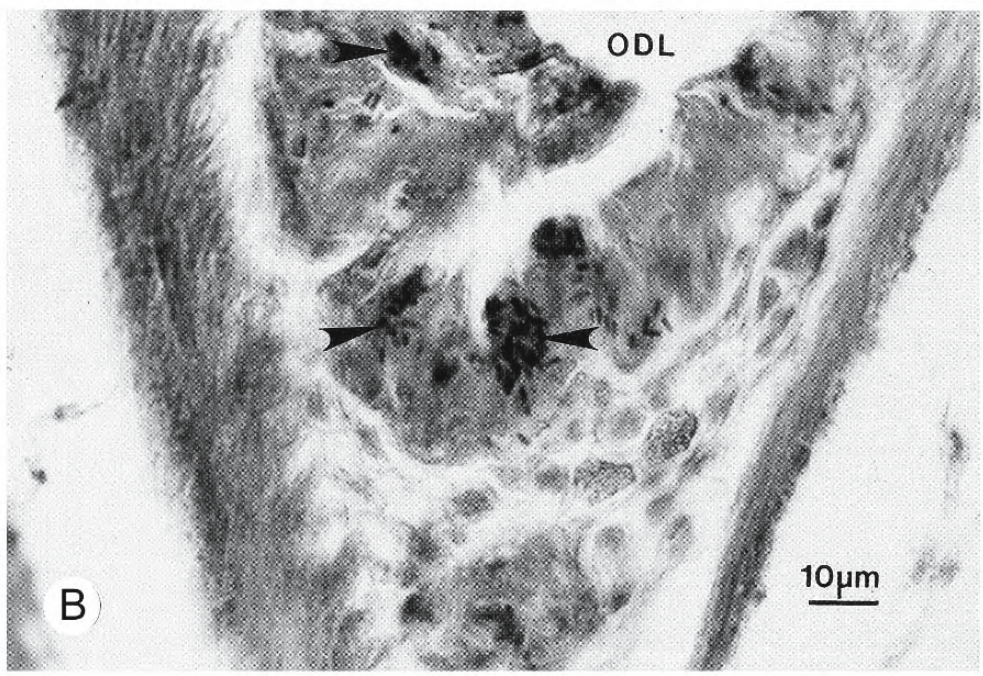

Figure 5.4: Photomicrographs of sections through the ovary and ovarian ducts of the platyfish *Xiphophorus maculatus.* (From Potter and Kramer, 2000; © reproduced with permission of John Wiley & Sons, Inc.).

A. Cross section through the mature ovary showing oocytes at different stages of development surrounding the ovarian duct and lumen (ODL). X 150.

B. Section through the ovarian duct of an inseminated fish showing sperm heads (arrowheads) incorporated within the cytoplasm of epithelial cells lining the lumen of the ovarian duct (ODL). X 1,000.

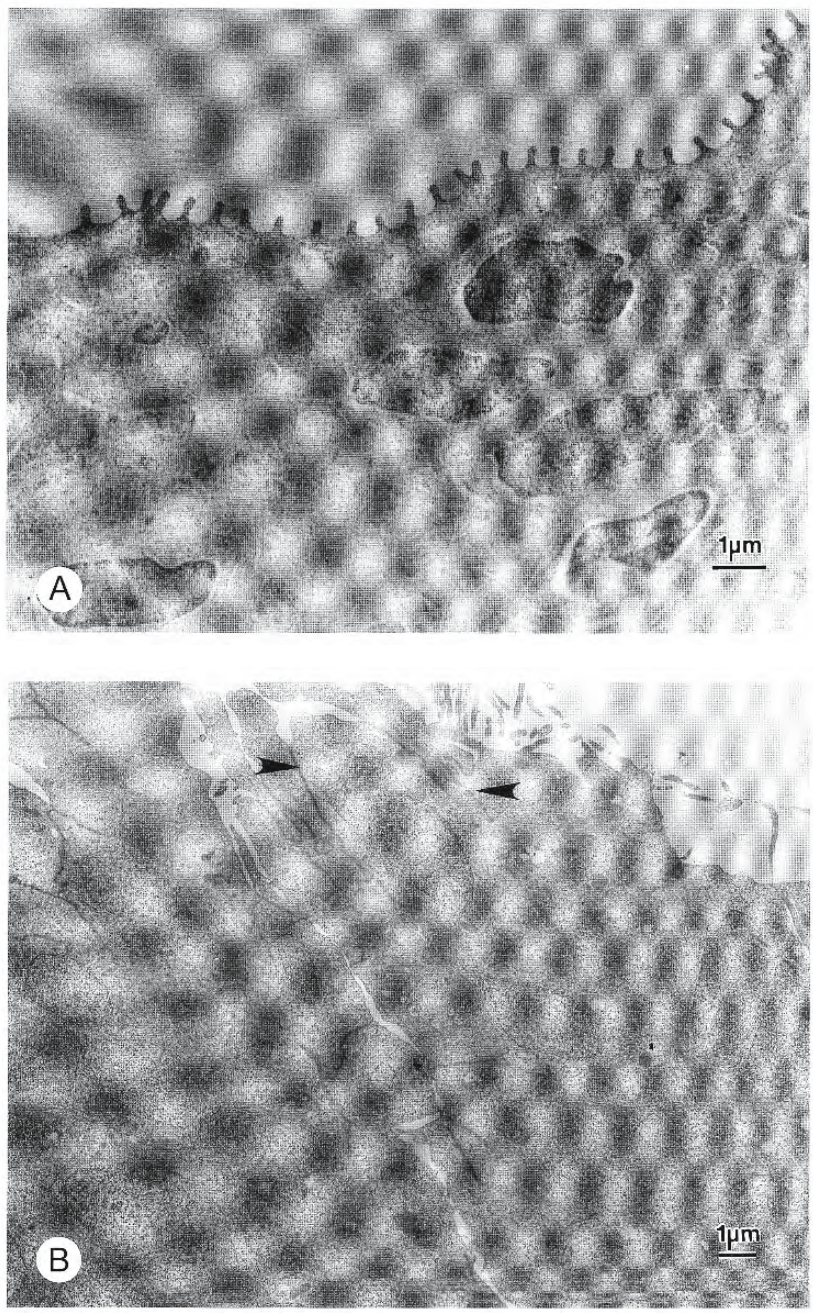

Figure 5.5: Transmission electron micrographs of sections through the epithelium of ovarian ducts of the platyfish *Xiphophorus maculatus.* (From Potter and Kramer, 2000; © reproduced with permission of John Wiley & Sons, Inc.).

A. Some epithelial cells exhibit a uniformly scalloped apical membrane. X 10,730.

B. The surface membranes of some epithelial cells exhibit broad lobular extensions. Apical junctional complexes (arrowheads) are apparent. X 5,870.

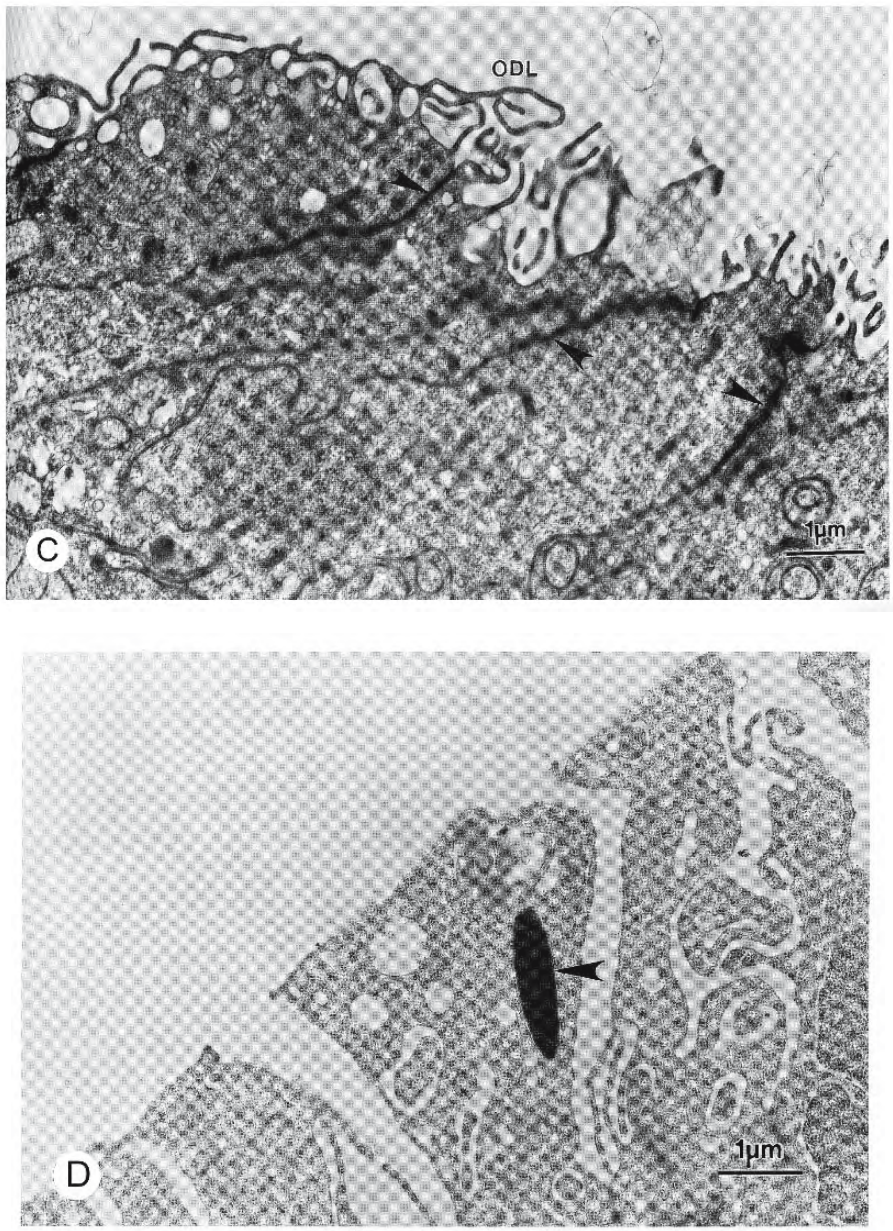

Figure 5.5: Continued.

C. In some regions, the surface epithelium contains extensive microvilli and branched microvillus-like appendages projecting into the lumen (ODL). Junctional complexes (arrowheads) are conspicuous. X 16,700.

D. A sperm nucleus (arrowhead) is incorporated within a specialized epithelial cell of the duct, the sperm-associated cell. This epithelium has deep surface folds and pockets. X 15,170.

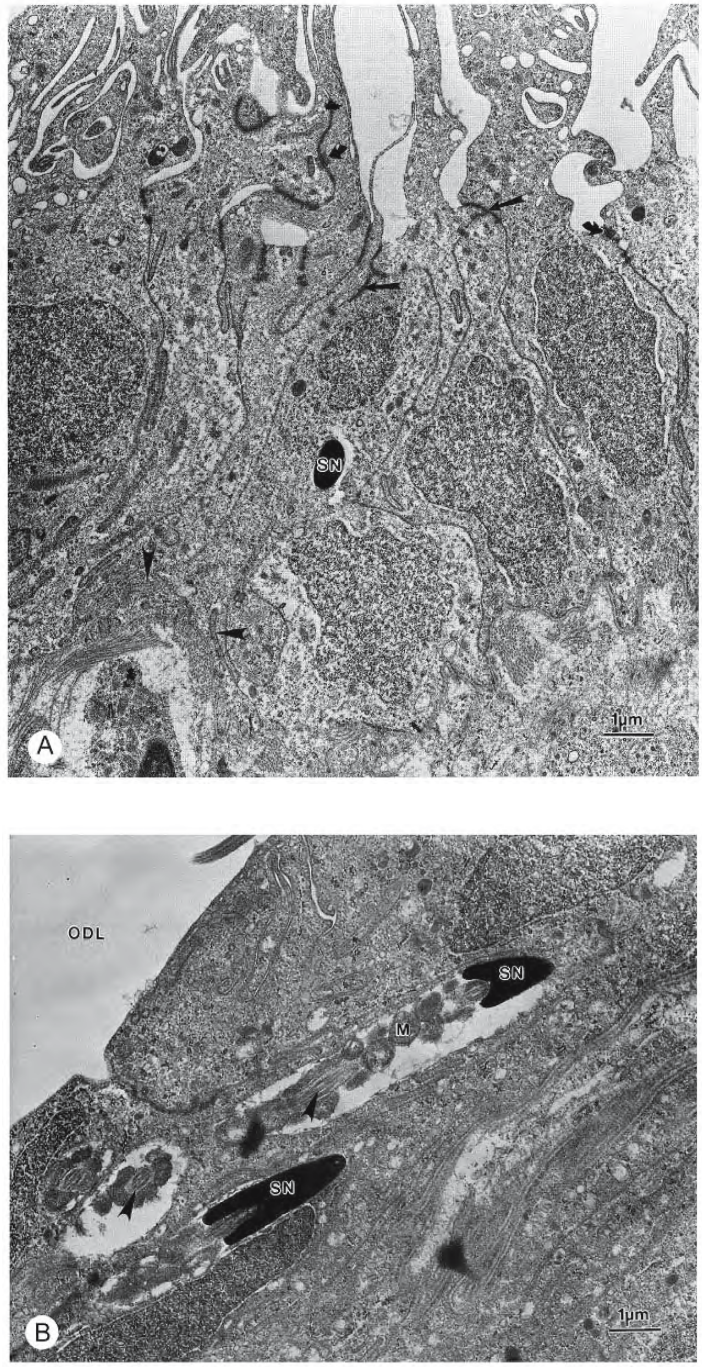

Figure 5.6: Transmission electron micrographs of sections through the epithelium of ovarian ducts of the platyfish *Xiphophorus maculatus.* (From Potter and Kramer, 2000; © reproduced with permission of John Wiley & Sons, Inc.)

A. Complex infoldings (arrowheads) penetrate deep between these epithelial cells of the ovarian duct. Apical tight junctions (arrows) and desmosomes (curved arrows) are apparent. A sperm nucleus (SN) is incorporated within a sperm-associated cell. X 13,960.

B. These sperm-associated cells exhibit deep surface pits and pockets. Intact sperm nuclei (SN) with midpiece mitochondria (M) and flagella (arrowheads) are seen within the pockets. ODL, lumen of the ovarian duct. X 13,350.

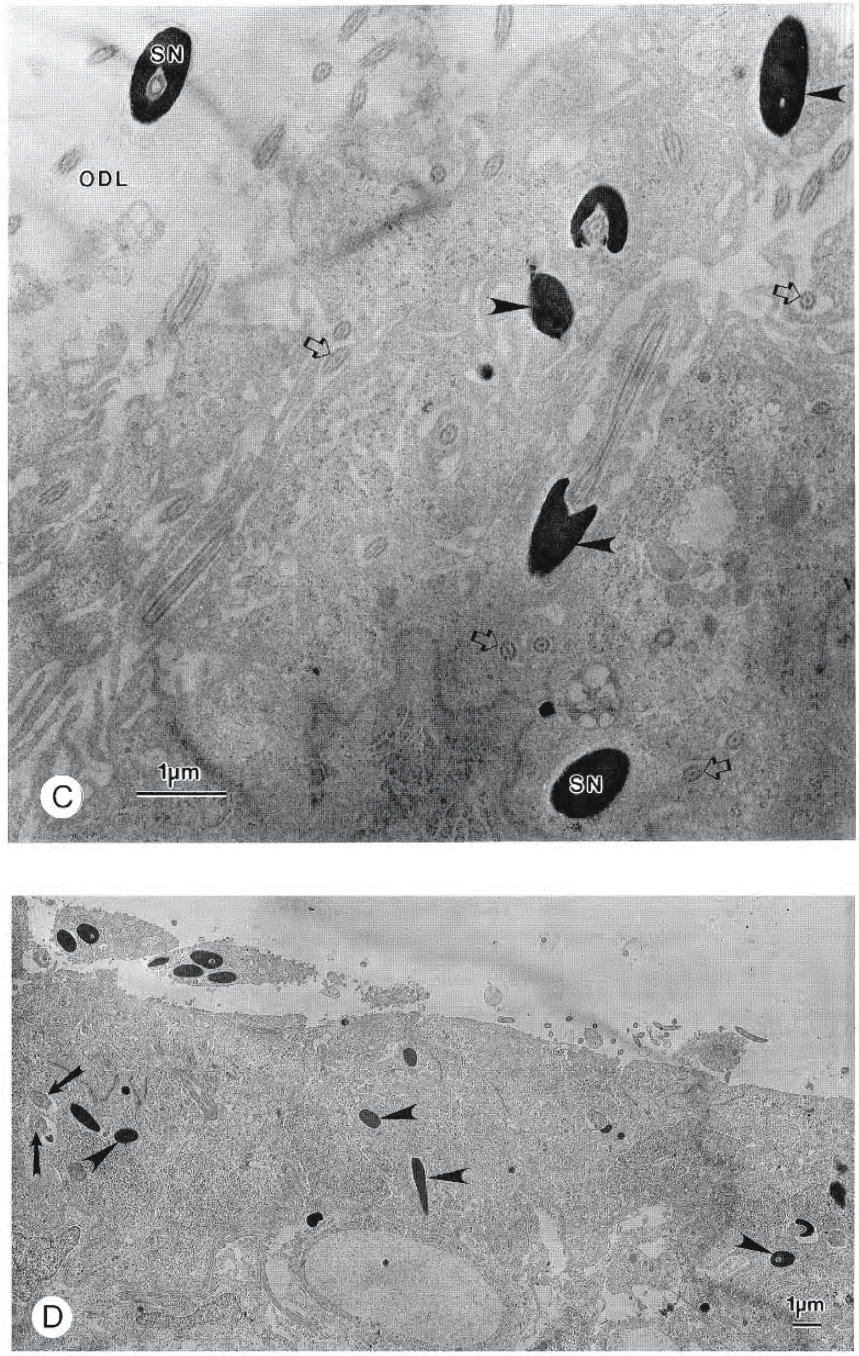

Figure 5.6: Continued.

C. Numerous sperm (arrowheads) are contained within the surface pockets and pits of sperm-associated cells. Sperm nuclei (SN) are also seen within the lumen of the ovarian duct (ODL) and deep within the cytoplasm of a sperm-associated cell. The open arrows indicate sperm tails at the surface within pits and incorporated within the cytoplasm. X 16,300.

D. Sperm-associated cells contain sperm nuclei (arrowheads) in their basal regions. Many sperm tails (arrows) are embedded within the cytoplasm. X 5,410.

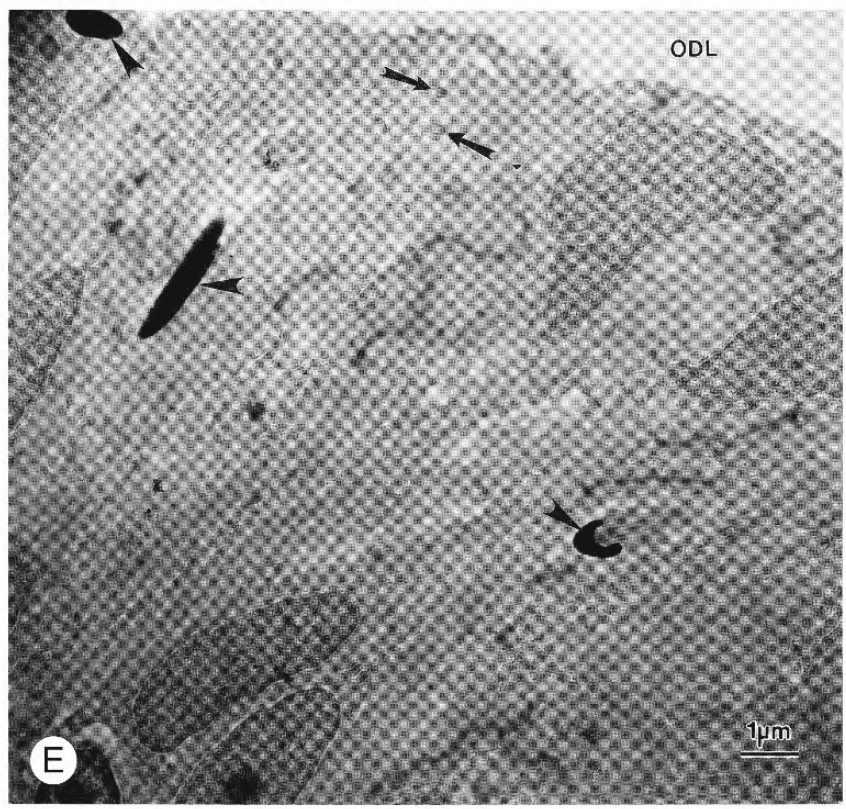

Figure 5.6: Continued.

E. Several sperm nuclei (arrowheads) and flagella (arrows) are incorporated within the sperm-associated cells. ODL, lumen of ovarian duct. X 9,970.

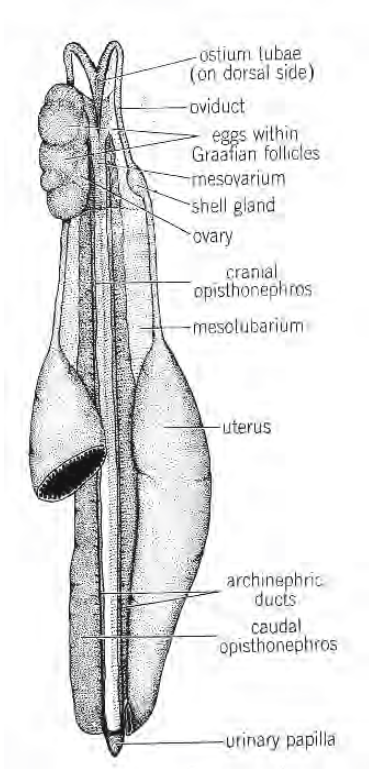

Figure 5.7: Drawing of a ventral view of the urogenital organs of a mature, pregnant female dogfish. One ovary is shown only in outline and part of one uterus has been removed in order to expose structures lying dorsal to them. (From Weichert, 1970; reproduced with permission of the McGraw-Hill Companies).

Figure 5.9: Photomicrograph of a cross section of the oviduct of a dogfish *Squalus acanthias*. X 85 The wall is thrown up into rounded folds covered by a tunica mucosa of stratified cuboidal epithelium. The tunica submusosa, forming the core of the folds and subtending them, is made up of loose fibrous connective tissue containing several blood vessels and scattered smooth muscle cells. This layer merges imperceptibly into the smooth muscle of the tunica mucularis consisting of a loose inner layer of circular fibres and a denser outer layer of longitudinal fibres. The oviduct is enclosed by a tunica serosa of loose fibrous connective tissue covered by simple cuboidal to low columnar cells.

←

Figure 5.8: Photomicrographs to illustrate sperm storage in the oviductal gland of a recently inseminated blue shark *Prionace glauca.* (From Pratt, 1993; reproduced with kind permission of Kluwer Academic Publishers).

A. Cross section of the oviductal gland. Sperm appear as dark masses in the shell secreting tubules surrounding the S-shaped central lumen. SZ = sperm storage zone.

B. Sections of oviductal tubules showing sperm (S) storage within the lumina (arrow).

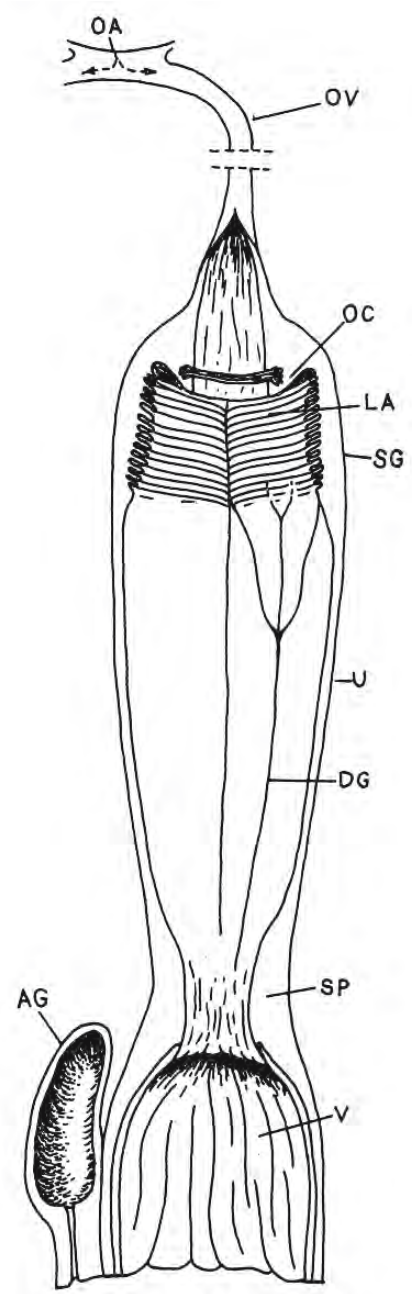

Figure 5.10: Diagram of the adult female reproductive tract of the chimaeroid *Hydrolagus colliei.* About life size. The lower region is split along one side and laid open so that the dorsal half lies to the right. (From Stanley, 1963; © reproduced with permission of John Wiley & Sons, Inc.).
Abbreviations: AG, accessory genital gland; DG, dorsal median groove of the uterus; LA, lamellae; OA, ostium; OC, oviductal cone; OV, oviduct; SG, shell gland; SP, utero-vaginal sphincter; U, uterus; V, vagina.

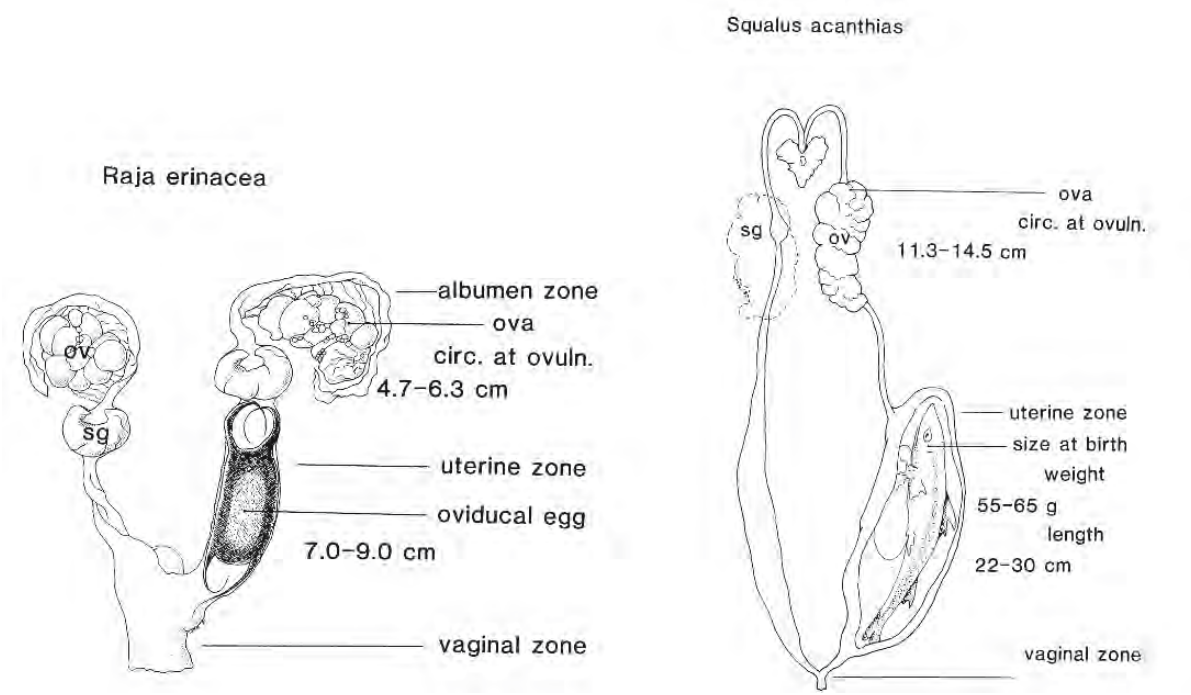

Figure 5.11: Female reproductive tracts of *Raja erinacea* (oviparous) and *Squalus acanthias* (viviparous) to show the relative sizes of ovulated and encapsulated eggs and embryos. Follicular circumference at ovulation is indicated. (From Callard and Koob, 1993; © reproduced with permission of John Wiley & Sons, Inc.).
Abbreviations: ov, ovary; sg, shell gland.

Figure 5.12: Photomicrograph of a section of the simple ciliated columnar epithelium (c) of the oviduct of the Atlantic guitarfish *Rhinobatos lentiginosus.* Arrows indicate secretory cells in the crypt region. Basal bodies of the ciliary rootlets form a distinct line extending across the apical regions of the cells. X 600 (From Hamlett et al., 1998b; reproduced with permission of the North Carolina Academy of Science).

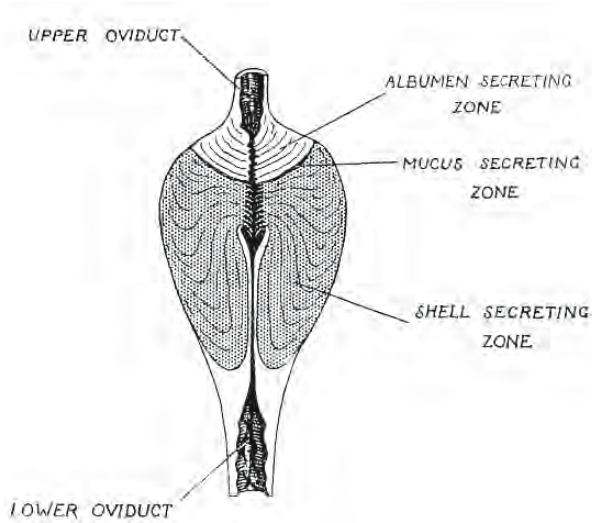

Figure 5.13: Drawing of a vertical section through a non-secreting oviductal gland of *Scylliorhinus canicula.* X 1.3 (From Metten, 1939; reproduced with permission from the Royal Society).

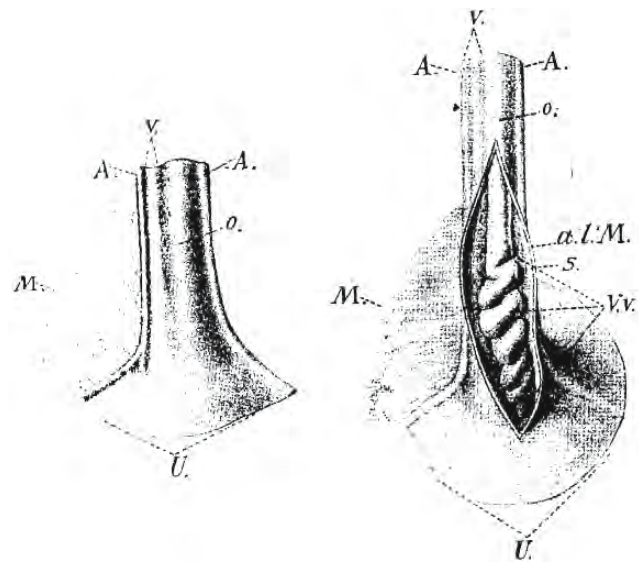

Figure 5.14: Drawings to illustrate the isthmus (Verschlußvorrichtung), a short, constricted section of the oviduct connecting the oviductal gland with the uterus in *Squalus acanthias.* (From Widakowich, 1907; reproduced with permission from Urban & Fischer Verlag).
Abbreviations: A, uterine artery; alM, outer longitudinal muscle of the oviduct; M, mesentery; o, oviduct; S, serosa; V, venous space; U, uterus; Vv, isthmus.

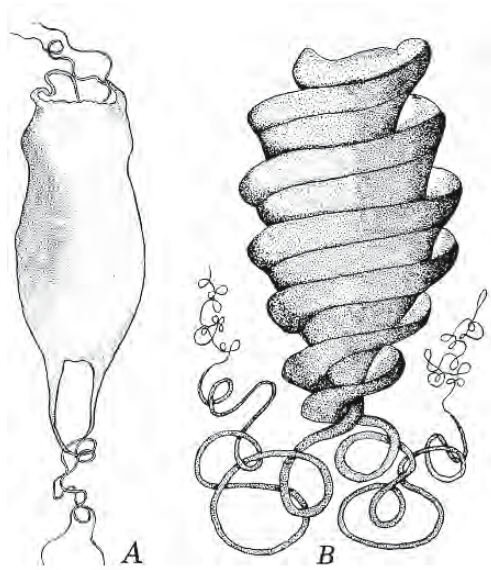

Figure 5.15: Elasmobranch egg cases. (From Weichert, 1970; reproduced with permission of the McGraw-Hill Companies).
A. The dogfish *Scyllium.*
B. The bullhead shark *Heterdontus galeatus.*

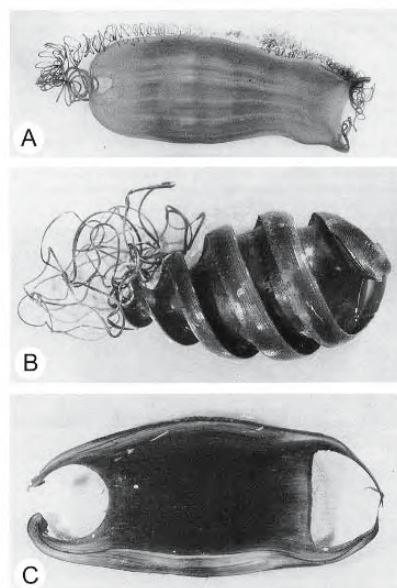

Figure 5.16: Representative egg capsules of oviparous sharks and skates. (From Hamlett and Koob, 1999; © reproduced with permission of the Johns Hopkins University Press).
A. *Cephaloscyllium ventriosum.*
B. *Heterodontus mexicanus.*
C. *Bathyraja interrupta.*

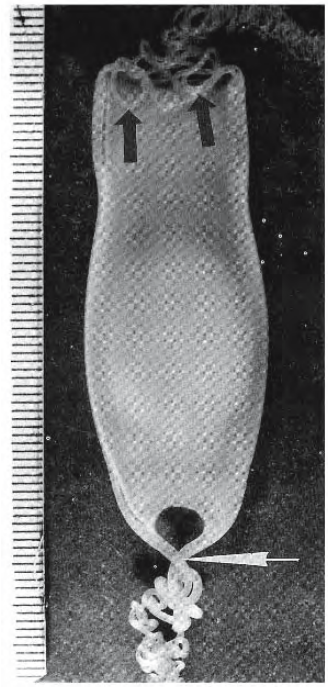

Figure 5.17: Photograph of the ventral surface of a whole egg capsule of the dogfish *Scyliorhinus canicula.* Anterior tendrils form two hook-like structures where they join the egg capsule (black arrows); the posterior tendrils cross at approximately 90° (white arrow). Scale in millimetres (From Feng and Knight, 1994b; reproduced with permission from the Royal Society).

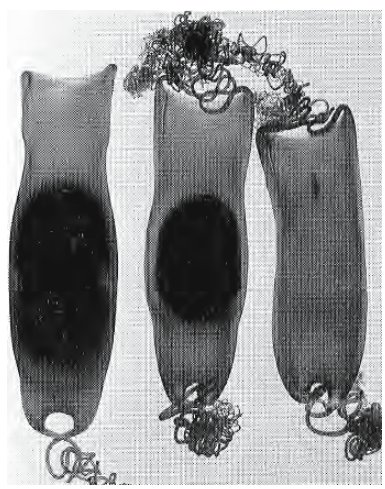

Figure 5.18: Photograph of whole egg capsules of the dogfish *Scyliorhinus canicula.* (From Knight, Feng, and Stewart, 1996; reproduced with permission of Cambridge University Press) A rare double-yolker is shown at the left. A single-yolked capsule is shown at the centre and a rare anovular capsule at the right.

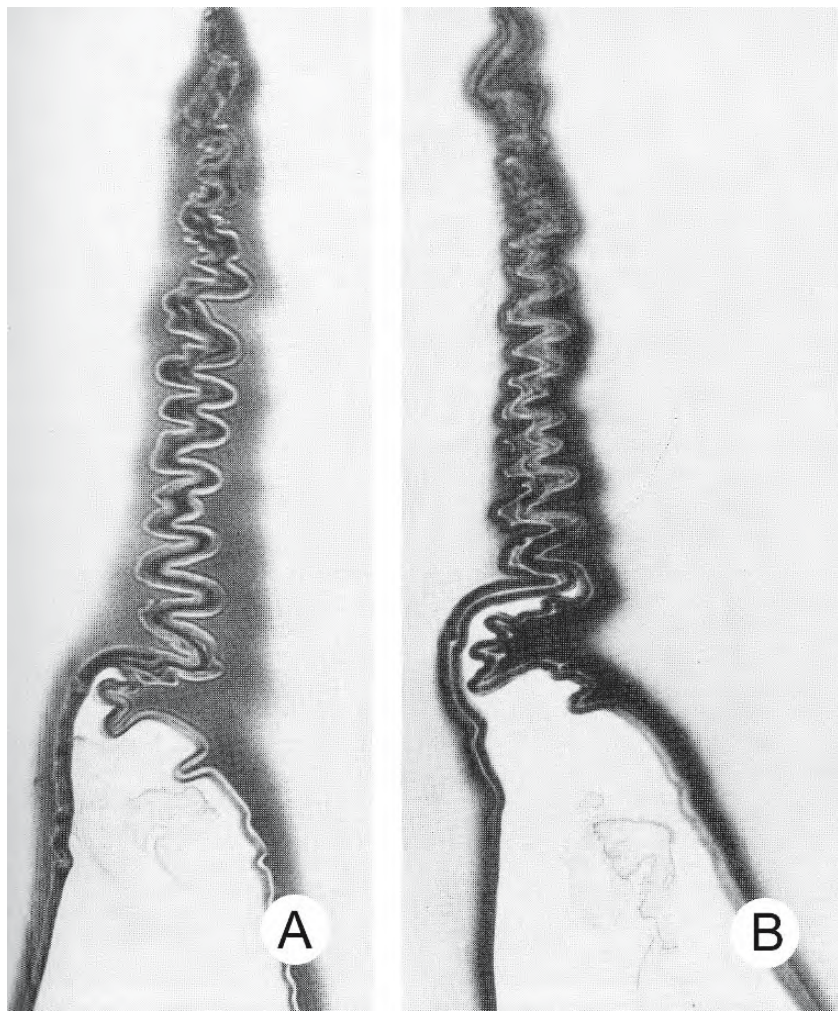

Figure 5.19: Photomicrographs of adjacent cryostat sections showing the folded structure of the posterior marginal seal of the egg capsule of the dogfish *Scyliorhinus canicula* (**A**. Peroxidase reaction, **B**. DOPA-oxidase). The capsule from which these sections were taken was approximately half formed within the oviductal gland. The seal has a similar structure and function to a crimped weld and is probably extensively cross-linked. (From Feng and Knight, 1992; reproduced with permission from Elsevier Science).

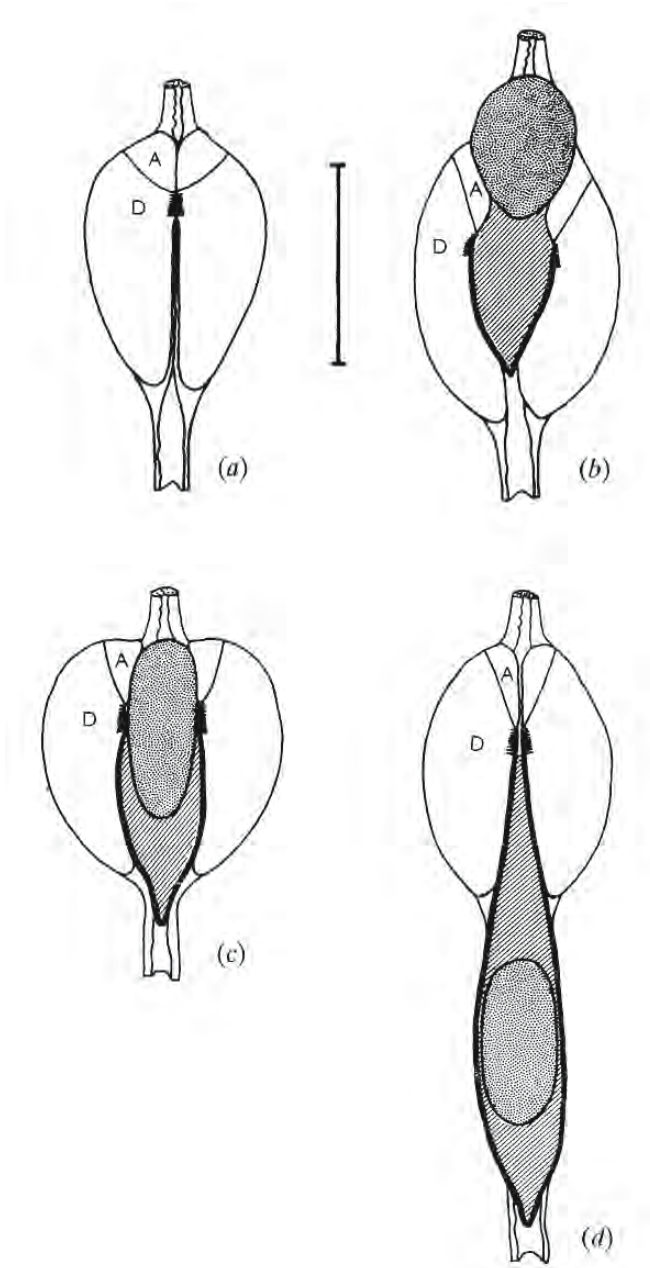

Figure 5.20: Semidiagrammatic drawings of halved, actively secreting oviductal glands showing stages in the formation of the egg capsule of the dogfish *Scyliorhinus canicula.* (From Feng and Knight, 1994b; reproduced with permission from the Royal Society).

A. Resting gland. A and D indicate zones of glandular tubules.

B. Formation of the posterior third of the capsular wall. The ovum has yet to enter the lumen of the gland.

C. Pressure of the ovum on the openings of the A-zone tubules is thought to prevent secretion of the jelly, allowing the ovum to be encapsulated while moving posteriorly relative to the gland.

D. Secretion of the jelly restarts after the ovum has passed the A-zone openings but gradually reduces to produce the tapering posterior two thirds of the capsular wall. Scale bar = 20 mm.

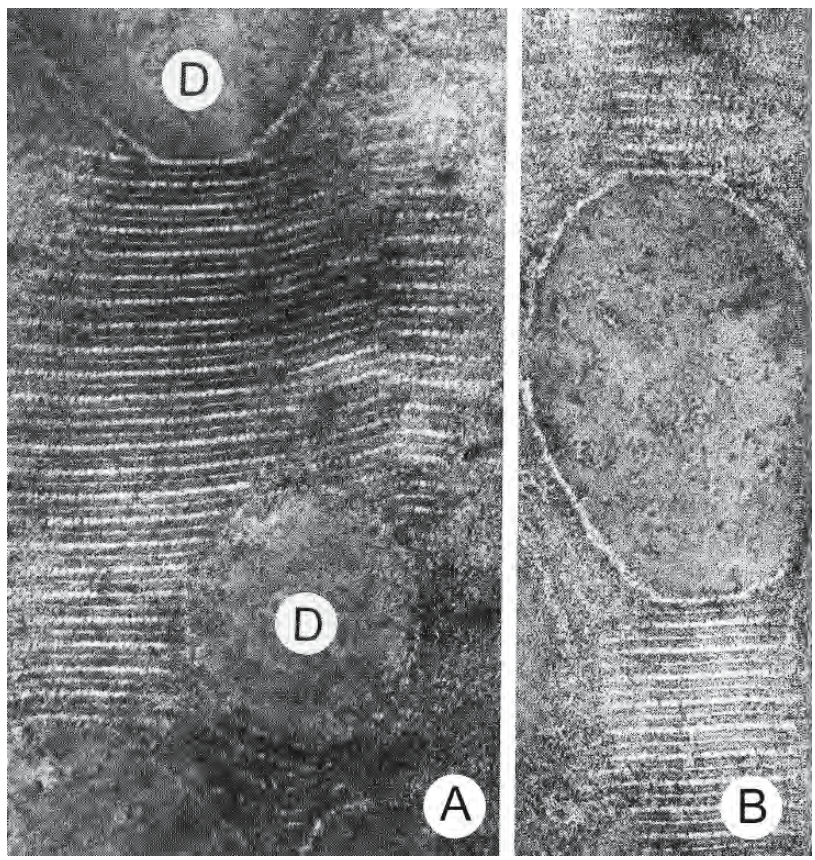

Figure 5.21: Transmission electron micrographs of sections of the wall of the egg capsule of the dogfish *Scyliorhinus canicula.* The wall is a composite material constructed largely of collagen fibres with a highly ordered, kinked molecular arragement set in a matrix containing hydrophobic spherical filler particles 2 μm in diameter. X 104,000 (From Knight and Feng, 1994a; reproduced with permission from Elsevier Science).

A. The outermost layer (L_1) of the egg capsule showing hydrophobic granules (D). Some 23 repeats of the axial period of the fine fibrillar phase of the collagen can be seen between the two granules.

B. As in **A**. A hydrophobic granule appears to lie between two segments of the final fibrillar phase. The broad lucent band of the banding pattern appears to run all the way around the granule, suggesting that it is coated with a complete layer of collagen molecules.

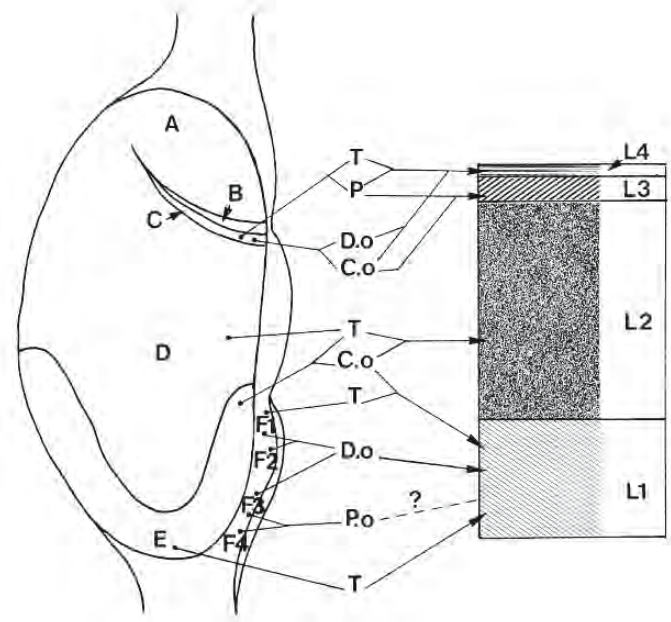

Figure 5.22: Diagram of a longitudinal section of the oviductal gland of the dogfish *Scyliorhinus canicula* indicating the source of the various substances involved in tanning of the egg capsule. The layers of the capsule are shown on the right, from the exterior (L_1) to the interior (L_4). The zones of the gland from A to F_4 are indicated. (From Rusaouën-Innocent, 1990a; reproduced with permission of the NRC Press).
Abbreviations: C.o, catechol oxidase; D.o, DOPA-oxidase; P, polyphenol; P.o, peroxidase; T, tyrosine.

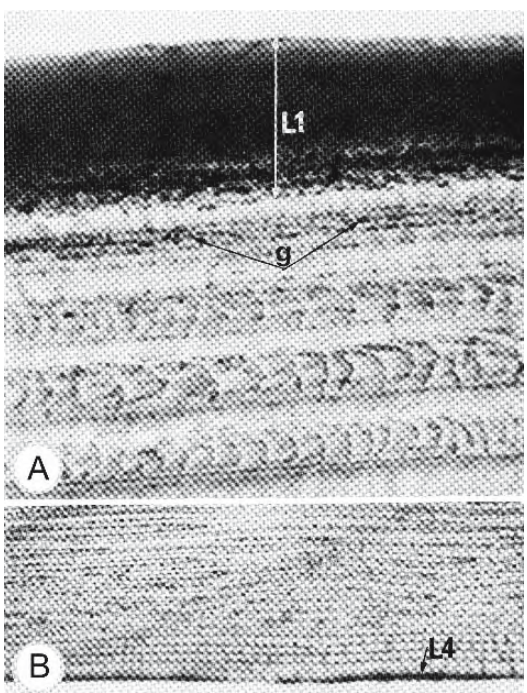

←

Figure 5.23: Photomicrographs of sections of the egg capsule of the dogfish *Scyliorhinus canicula.* (From Rusaouën-Innocent, 1990a; reproduced with permission of the NRC Press) The outer layer, L_1, is about 25 µm thick in dehydrated, tanned specimens; it consists of fine fibrils above densely packed, amorphous granules rich in tyrosine. Layer L_2 constitutes the bulk of the wall and is about 225 µm thick; it is similar to plywood and consists of about 30 lamellae. Although finely striated, L_3 appears more homogeneous than the other layers and is about 30 µm thick. The inner layer, L_4, is only 4 to 5 µm thick and appears homogeneous.

A. Layer L_1 and a portion of L_2 stained to show tyrosine. g, granules X 825.

B. Layers L_3 and L_4 stained to show tyrosine. X 250.

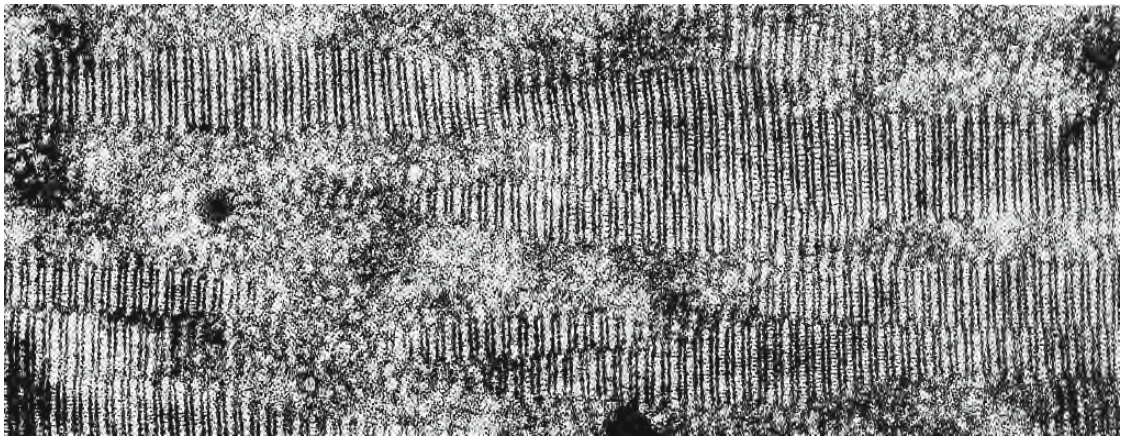

Figure 5.24: Transmission electron micrograph of a section through layer L_2 of the newly formed egg capsule of the dogfish *Scyliorhinus canicula.* The longitudinally sectioned spindle-shaped, collagen-containing fibrils show a periodicity of about 37 nm. (From Knight and Feng, 1994b; reproduced with permission from Elsevier Science).

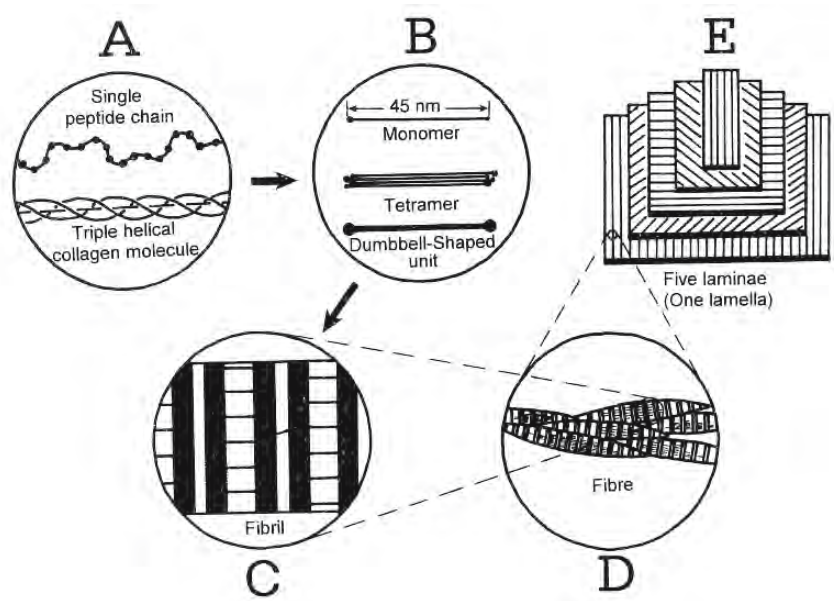

Figure 5.25: Diagrams illustrating structural hierarchies in layer L_2 of the egg capsule of the dogfish *Scyliorhinus canicula.* (From Knight and Feng, 1994b; reproduced with permission from Elsevier Science).

A. The coiled collagen molecule is formed of three helical peptide chains twisted together.

B. It is suggested that the collagen molecule is 45 nm long with a relatively large "head" formed from hydrophobic, non-helical peptides and a smaller "tail" formed in the same way. The chains may be associated head-to-tail to form a tetramer with a dumbbell shape.

C. The dumbbell shaped units are cross-linked and aligned in such a way as to form cross striations.

D. Fibrils twist together to form a fibre.

E. The fibres are arranged at 45° in adjacent laminae to form a structure similar to plywood.

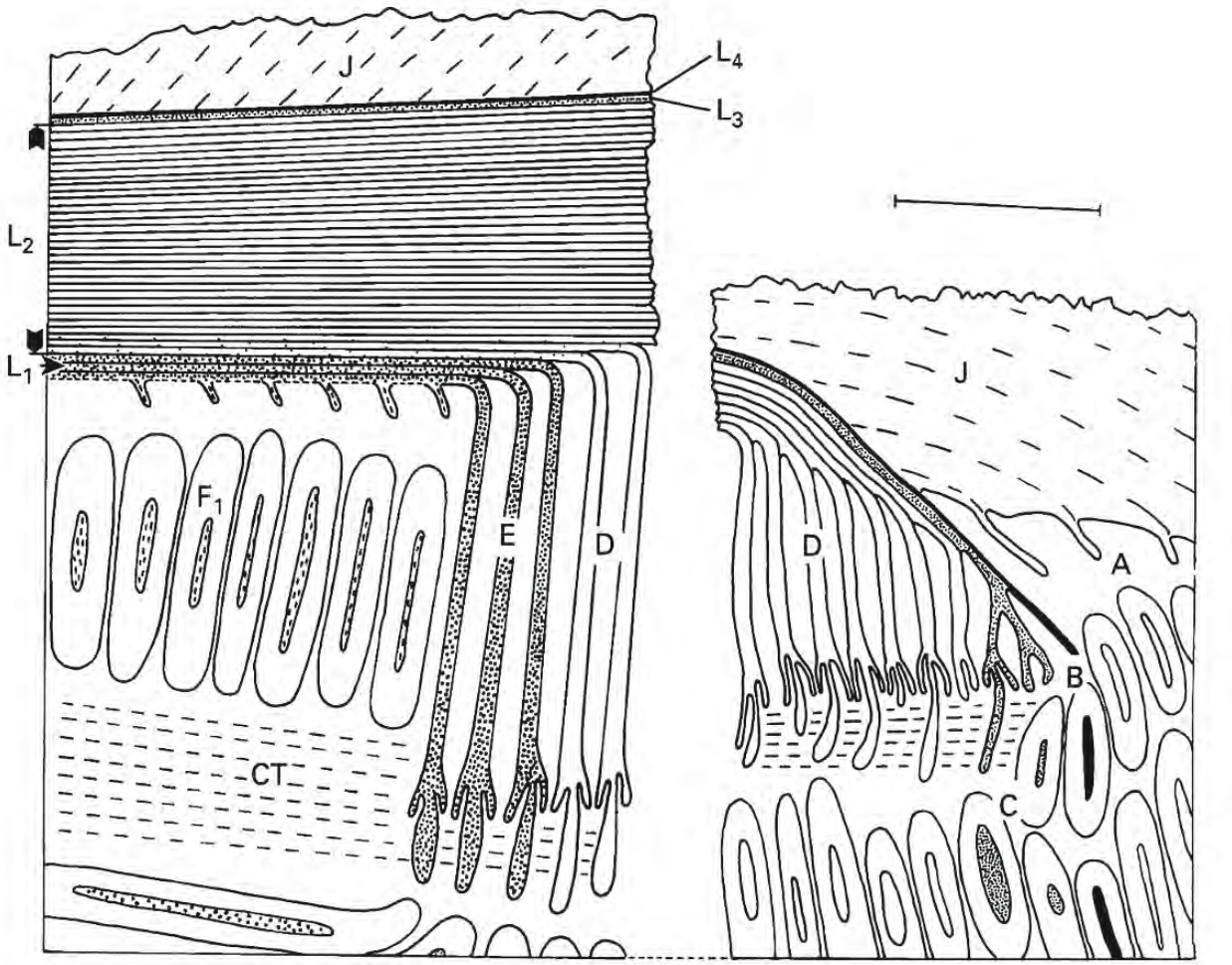

Figure 5.26: Diagram of a vertical longitudinal section of part of the actively secreting oviductal gland of the dogfish *Scyliorhinus canicula.* (From Knight, Feng, and Stewart 1996; reproduced with permission of Cambridge University Press) Jelly (J) is secreted from the A zone; layers L_4 to L_1 of the capsular wall are secreted from zones B to E respectively. The outermost layer of the capsule (L_1) is lowest in the drawing. Zone F_1 contributes little to the outer surface of the egg capsule. For the sake of clarity, only the epithelium surrounding the tubular glands (lowest parts of the drawing) has been drawn. CT, connective tissue. Scale bar = 500 μm.

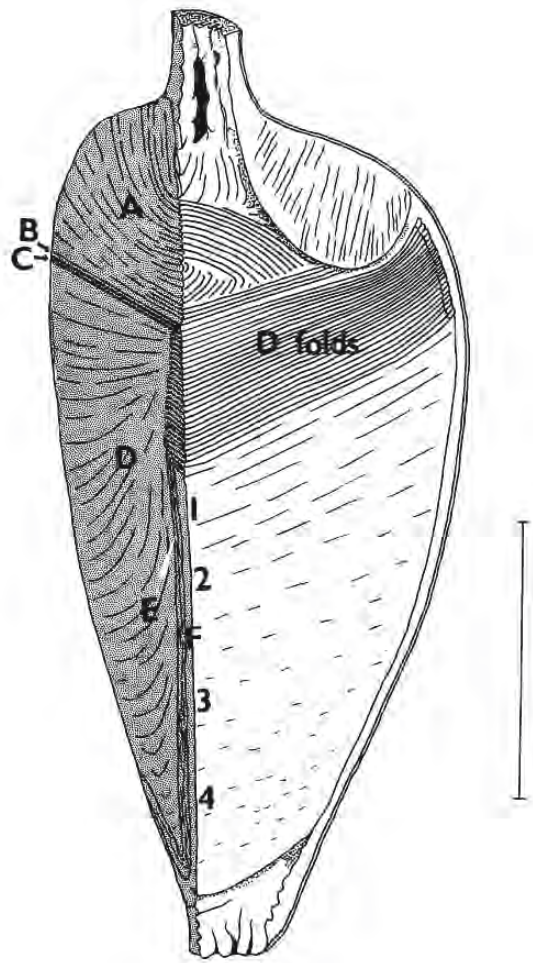

Figure 5.27: Semidiagrammatic view of a quarter of the oviductal gland of the dogfish *Scyliorhinus canicula.* The longitudinal surface at the left is shaded and shows the distribution of glands A to E. The lumen of the gland is shown to the right with the more superficial zones of glands F_1 to F_4. D zone grooves lie between the D folds which encircle the entire gland. Scale bar = 20 mm. (From Knight et al., 1993; reproduced with permission from the Royal Society).

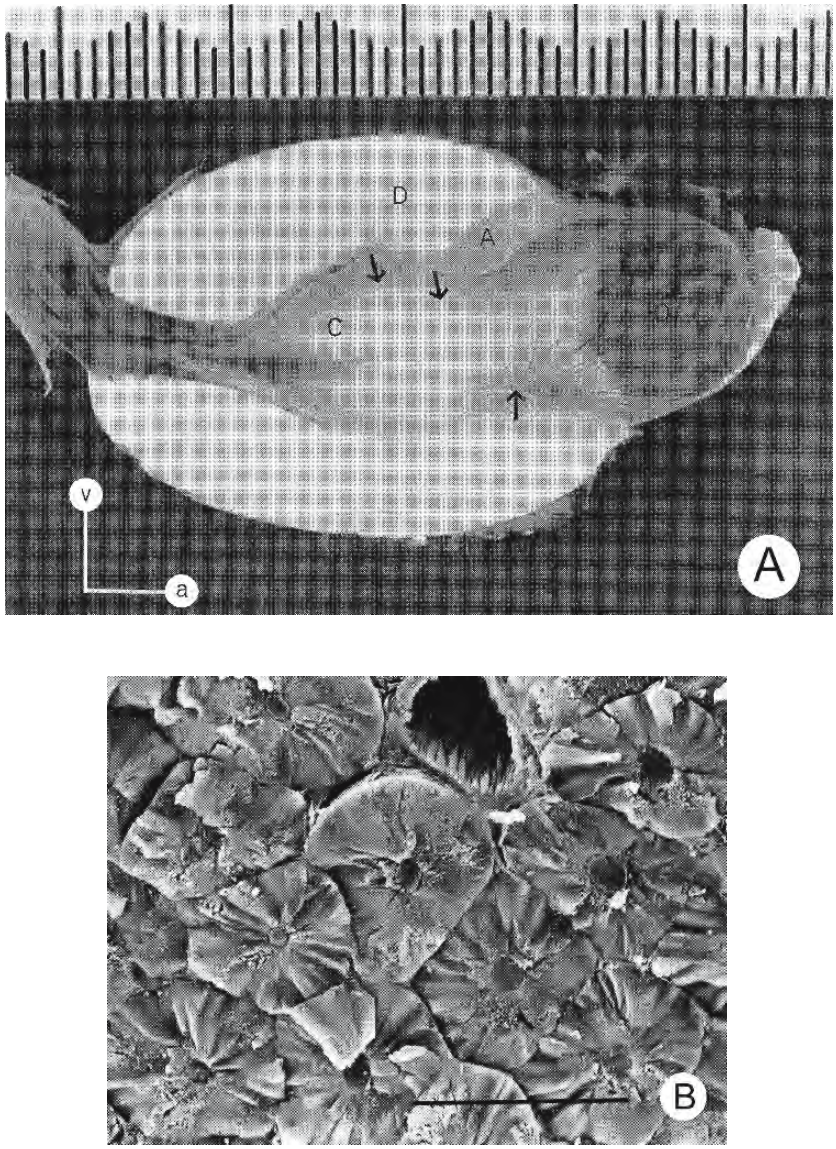

Figure 5.28:

A. Photograph of a fixed, actively secreting oviductal gland of the dogfish *Scyliorhinus canicula.* The gland has been cut in half and the jelly and ovum have been removed. The position of the ovum (O) can be seen as an oval dilation of the lumen of the anterior oviduct and anterior part of the oviductal gland. Zones A and D of the tubular glands are labelled. Less than one-third of the capsule wall (C) has been formed. The limits of the D-zone folds (downward pointing arrows) and A-zone gland openings (upward pointing arrow) can be distinguished in the lumen of the gland. a, anterior axis; v, vertical axis. Scale: short gradations = 1 mm.

B. Scanning electron micrograph of a transverse fracture of D-zone tubules. Secretion (narrow arrow) is seen in the lumina of the tubules. Spherical secretory granules (broad arrow), thought to contain collagen, are seen in the columnar epithelial cells. Bar = 100 μm.

(From Knight and Feng, 1992; reproduced with permission from Kluwer Academic/Plenum Publisher)

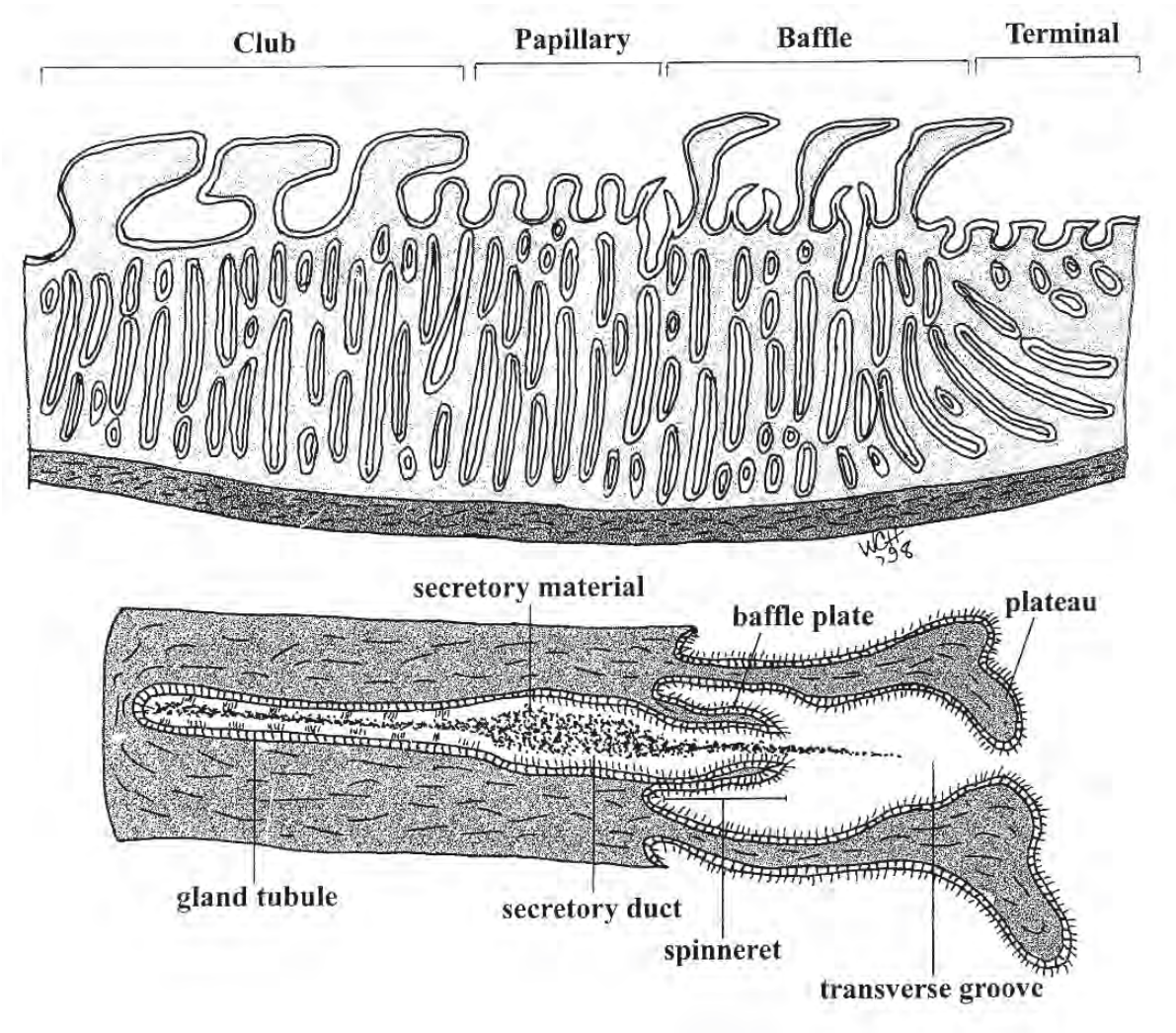

Figure 5.29: A morphological basis has been used to differentiate four regions of the oviductal gland of elasmobranchs. At the top is a composite line diagram of a "generic" oviductal gland consisting of four zones: club, papillary, baffle, and terminal. The lower illustration shows a unit of the baffle zone comprising a glandular tubule, secretory duct, spinneret with baffle plates, and a transverse groove between plateau projections. (From Hamlett et al., 1998a; © reproduced with permission of John Wiley & Sons, Inc.).

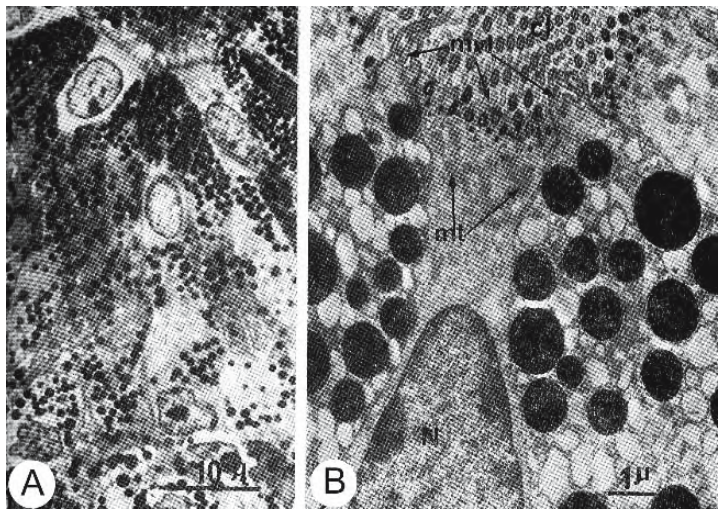

Figure 5.30: Micrographs of sections through the tubular glands of Zone D in the oviductal gland of a dogfish. (From Rusaouën, 1978; reproduced with permission of Masson, Paris).

A. Photomicrograph. Granular secretory cells, interspersed with columnar ciliated cells, are abundant. X 1,800.

B. Transmission electron micrograph. The apical regions of the secretory cells. Ciliated columnar cells (cl) lie between secretory cells with large microvilli (mvl). X 7,800.

Abbreviations: mt, mitochondria; N, nucleus.

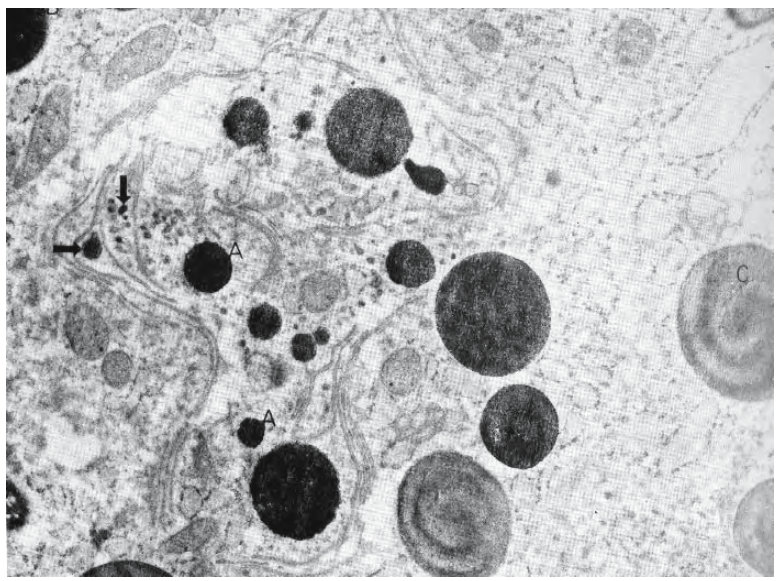

Figure 5.31: Transmission electron micrograph of a section through a secretory cell in Zone D of the oviductal gland of the dogfish *Scyliorhinus canicula.* This cell displays the characteristic specializations for protein secretion: extensive granular endoplasmic reticulum, well developed Golgi complex, and numerous secretory granules (arrows). Small granules near the maturing face (arrows) of the Golgi complex react to the peroxidase reagent. The letters A, B, and C indicate a transition in the granules as they move away from the Golgi complex. X 17,000 (From Feng and Knight, 1992; reproduced with permission from Elsevier Science).

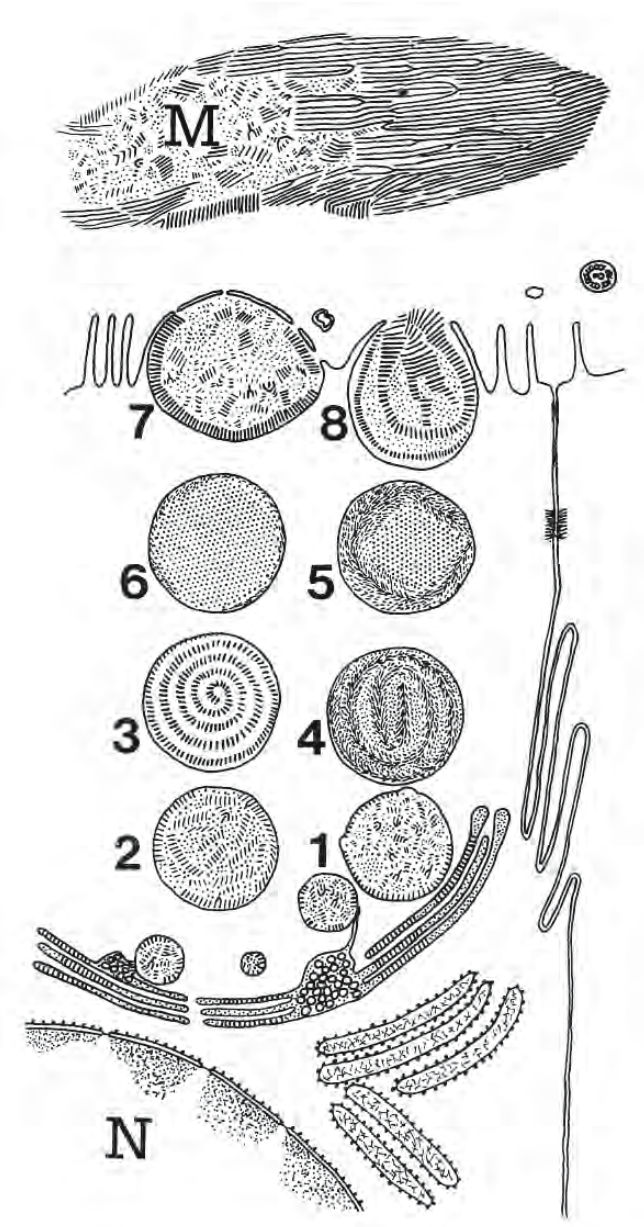

Figure 5.32: Diagram showing a part of a secretory cell in the proximal part of a D-zone secretory tubule of the oviductal gland of the dogfish *Scyliorhinus canicula.* A tentative scheme is illustrated for the sequence of changes thought to occur during storage and secretion of (pro)collagen. Within the cisternae of the endoplasmic reticulum the collagen appears anisotropic but, as the granules make their way to the apical border of the cell, it becomes dehydrated and undergoes a series of liquid crystal transformations (1 to 8), thereby providing a compact way of storing collagen. The granules appear to be released into the tubule by merocrine secretion (7,8). The junctional complex (upper right) and extensive interdigitations of the lateral membranes probably indicate that this epithelium is also actively secreting ions. (From Knight et al., 1993; reproduced with permission from the Royal Society).
Abbreviations: M, secreted material that forms a coalesced strand; N, nucleus.

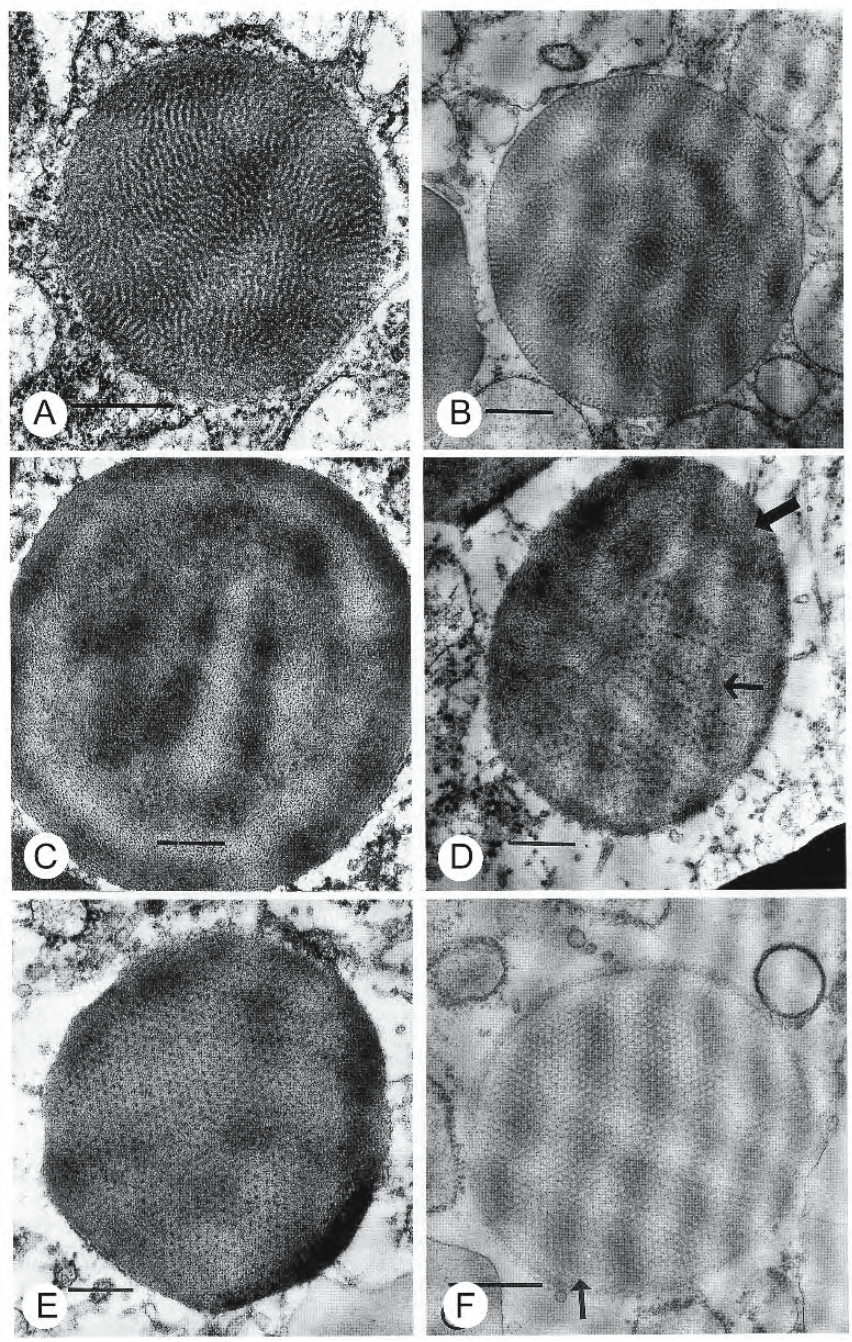

Figure 5.33: Electron micrographs from secretory cells in the proximal part of a D-zone tubule of the oviductal gland of the dogfish *Scyliorhinus canicula.* These micrographs are arranged, from least (**A**) to most mature (**F**), to illustrate a tentative scheme for the sequence of changes in granules thought to occur during storage and secretion of (pro)collagen. During this transformation, the material in the granules becomes arranged to give rise to a concentric or spiral pattern. Compare these figures with Figure 5.32. (From Knight et al., 1993; reproduced with permission from the Royal Society).
A,**B**,**E**,**F**. Bar = 0.5 μm, **C**,**D**. Bar = 250 nm.

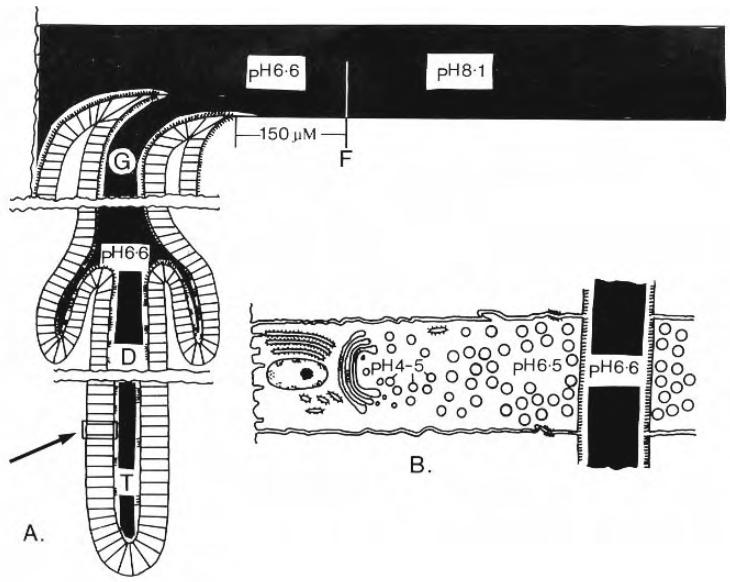

Figure 5.34: Diagram illustrating the suggested pH values in different parts of the oviductal gland and forming egg capsule of the dogfish *Scyliorhinus canicula.* **B** represents an enlargement of the rectangular box in **A** (arrow). The secreted material is shaded. Final fibrils first appear (F) after the secreted material has moved approximately 150 μm in a posterior direction from the transverse groove of origin. (From Feng and Knight, 1994a; reproduced with permission from Elsevier Science).
Abbreviations: D, lumen of secretory duct; G, transverse groove; T, lumen of secretory tubule.

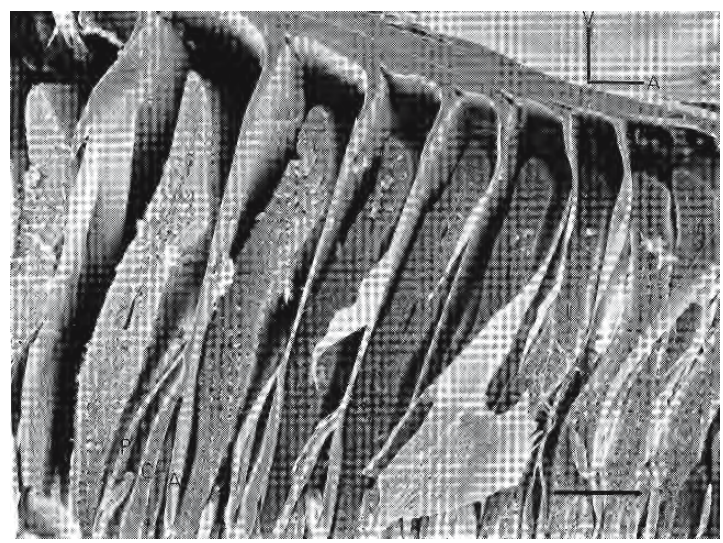

Figure 5.35: Scanning electron micrograph of D-zone folds in a fractured surface of the oviductal gland of the dogfish *Scyliorhinus canicula.* Lamellae, which give rise to part of layer L_2 of the capsular wall, are being extruded from the transverse grooves of the D-zone. A lamella can be seen to arise from the confluence of three flows: anterior (A), central (C), and posterior (P) separated by two baffle plates. A, anterior axis; V, vertical axis. Scale bar = 100 μm (From Knight and Feng, 1992; reproduced with permission from Kluwer Academic/Plenum Publisher).

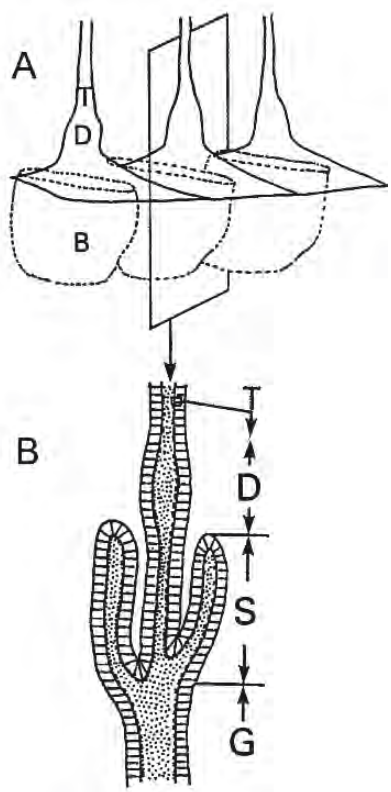

Figure 5.36: The functional unit in all parts of the oviductal gland of the dogfish *Scyliorhinus canicula* consists of a secretory tubule of columnar secretory cells interspersed with some columnar ciliated cells, a short duct lined with columnar ciliated cells but lacking secretory cells, and a spinneret. A single row of spinnerets opens into the base of each transverse groove in zones B to E. (From Knight, Feng, and Stewart, 1996; reproduced with permission of Cambridge University Press).

A. A simplified drawing of an internal cast of part of a single D-zone transverse groove, viewed from the posterior side to show the structure of the spinnerets which secrete the bulk of the thickness of the capsular wall. The secretory tubule (T) opens via a short secretory duct (D) into the space between two oblique baffle plates (B; shown dotted).

B. A diagrammatic section of the plane outlined in **A**. Two baffle plates, which separate the secretory material into three flows, are shown. These flows coalesce in the transverse groove. The secreted material in the lumen of the gland tubule (T), secretory duct (D), spinneret (S), and the transverse groove (G) is stippled.

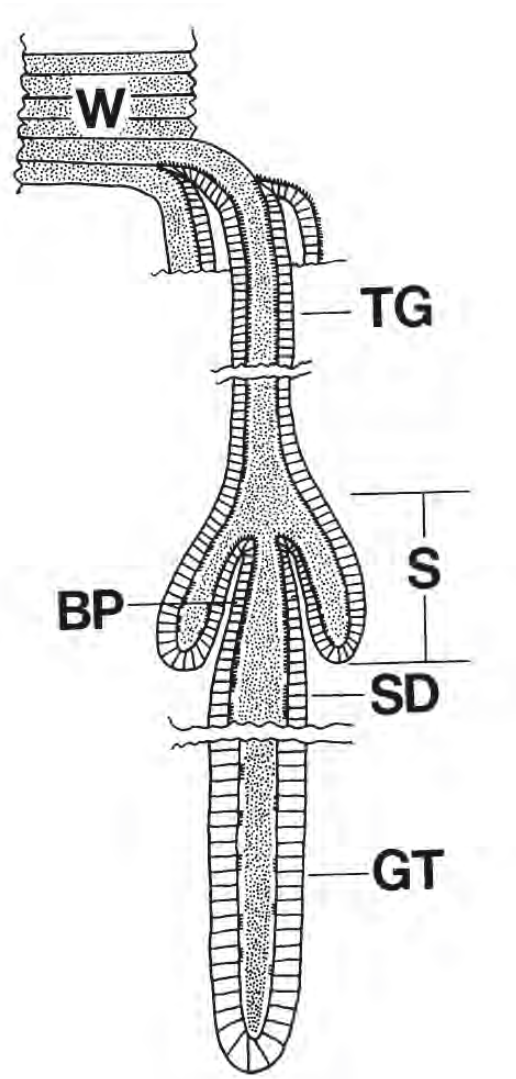

Figure 5.37: Diagram illustrating the functional unit of the D-zone gland of the oviductal gland of the dogfish *Scyliorhinus canicula.* A long, noncoiled glandular tubule (GT) passes its secretion to a secretory duct (SD). From this the secretion passes between two baffle plates (BP) which lie at an angle to form the spinneret (S). From here the secretion passes apically through the transverse groove (TG) to give rise to a single lamella of the white egg case (W). The glandular tubule is approximately 60 μm in diameter. (From Knight et al., 1993; reproduced with permission from the Royal Society).

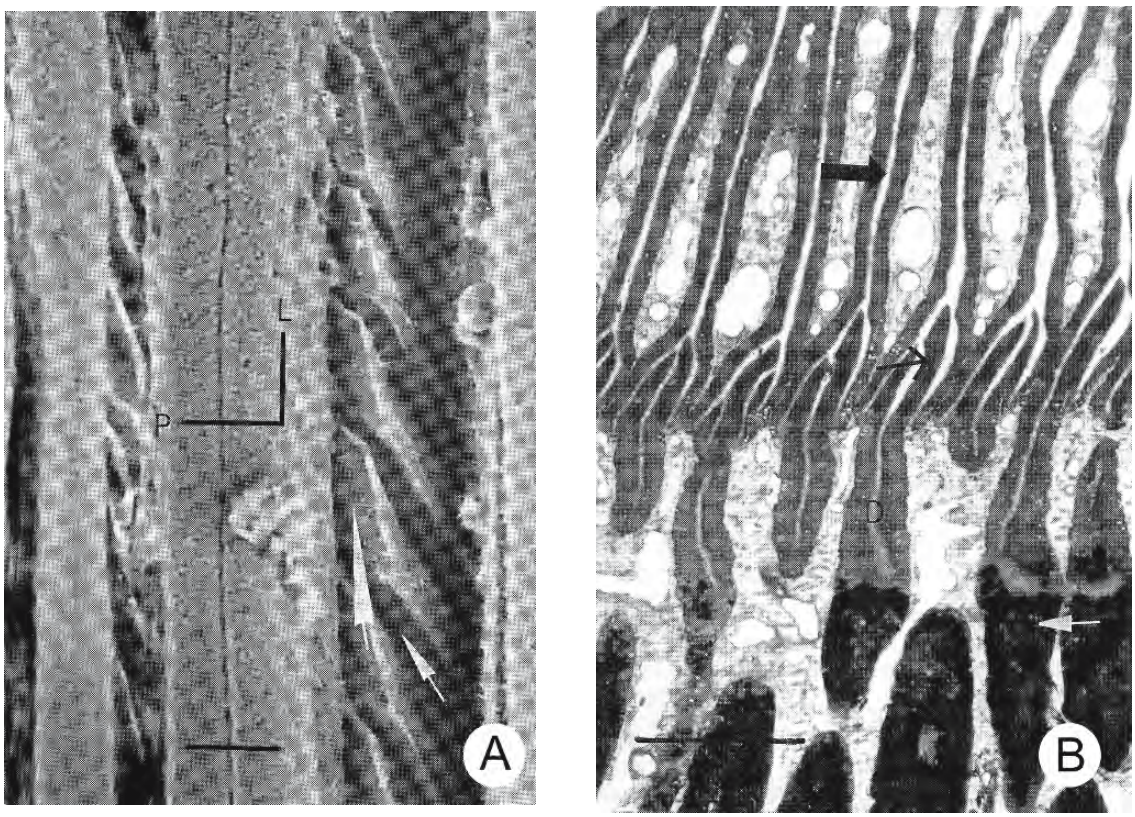

Figure 5.38: Micrographs of the oviductal gland of the dogfish *Scyliorhinus canicula.* (From Knight and Feng, 1992; reproduced with permission from Kluwer Academic/Plenum Publisher).

A. Scanning electron micrograph looking down into two E-zone transverse grooves which run vertically up this figure. The spinnerets in the bottom of the groove consist of a regular arrangement of baffle plates. The small arrow indicates the oblique space between two baffle plates; the large arrow points to the space between the posterior surface of the baffle plate and the wall of the transverse groove. Scale bar = 100 μm.

B. Photomicrograph of a section of the oviductal gland showing the D-zone grooves (broad arrow), baffle plates (narrow arrow), secretory ducts, and gland tubules (white arrow). Scale bar = 200 μm.

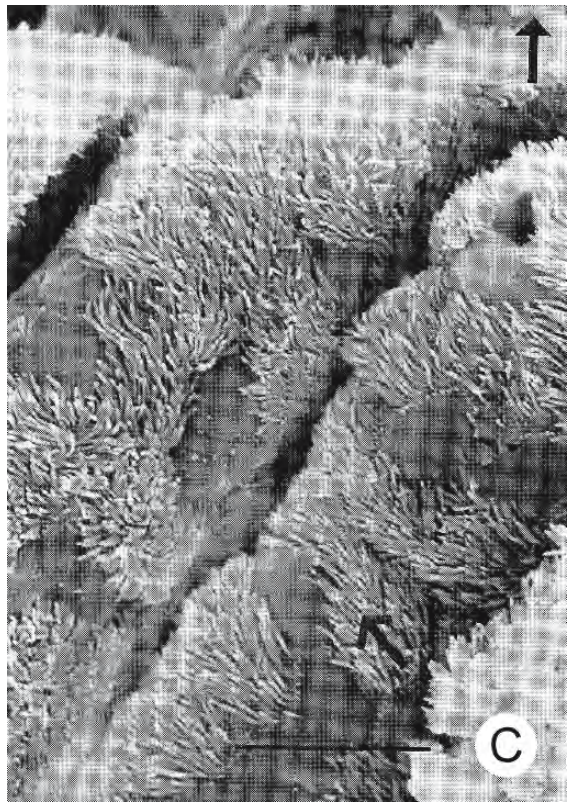

Figure 5.38: Continued.

C. Scanning electron micrograph of the surface of the apical parts of the baffle plates. Viscous secretion is thought to flow vertically (vertical arrow) from the apex of the spinnerets and obliquely across the anterior (and posterior) surfaces (oblique arrow). Cilia are oriented in these directions and may help to direct the flows. Scale bar = 10 μm.

⟶

Figure 5.39: Micrographs from the oviductal gland of the ray *Raja erinacea.* (From Knight et al., 1996; reproduced with permission from Kluwer Academic/Plenum Publisher).

A. Scanning electron micrograph of a natural cast of three D-zone spinnerets. The arrowhead indicates the direction of flow of material. Material within the lumen of the tubular gland is roughly circular in cross section; as it passes through the spinneret it diverges smoothly and emerges as a flattened ribbon. Scale bar = 50 μm.

B. Nomarski micrograph of a single row of D-zone spinnerets. An overlapping row of ribbons fused together to form a single lamella. The overlapping of five ribbons at each point of the lamella gives rise to a plywood-like construction. Ribbons fuse along curved lines to form a lamella (arrows). The arrowhead indicates the direction of flow of material through the spinnerets. Scale bar = 50 μm.

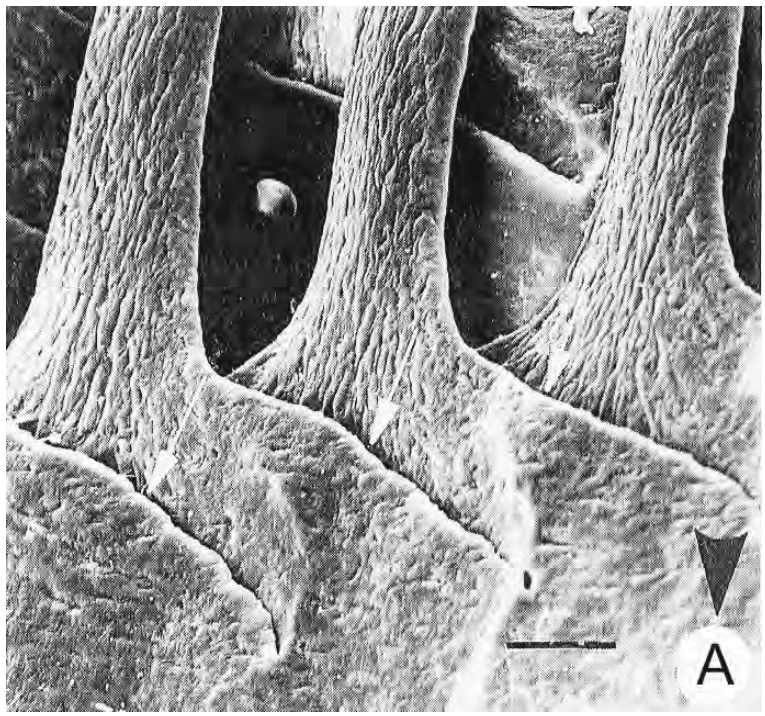

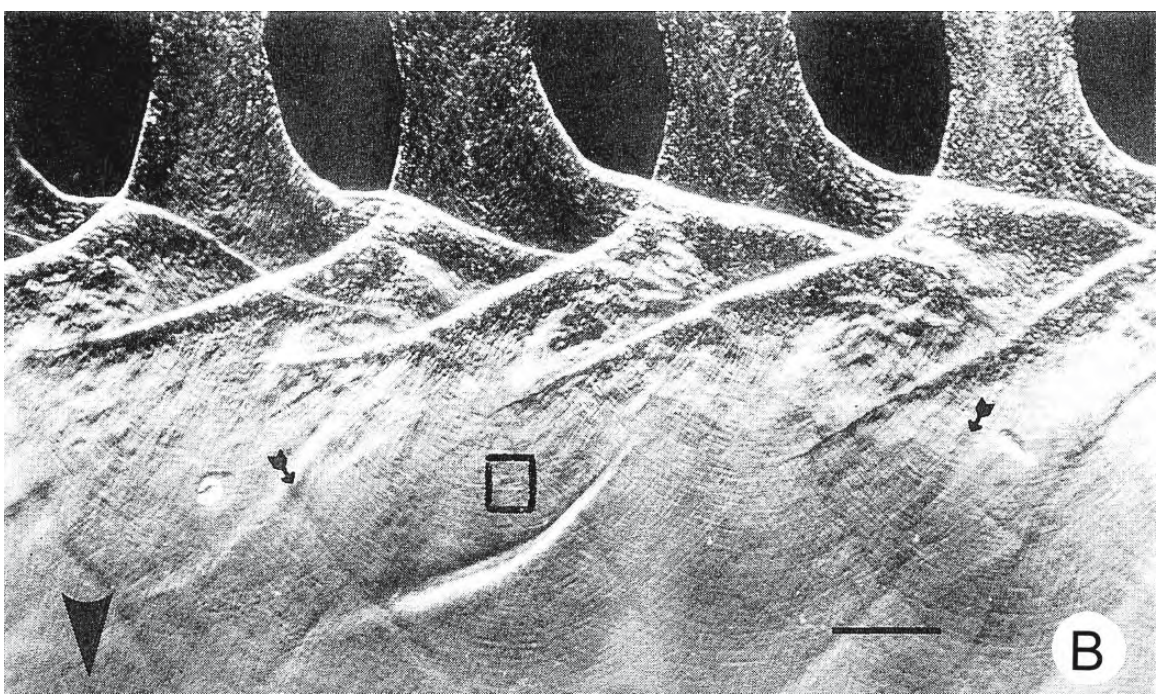

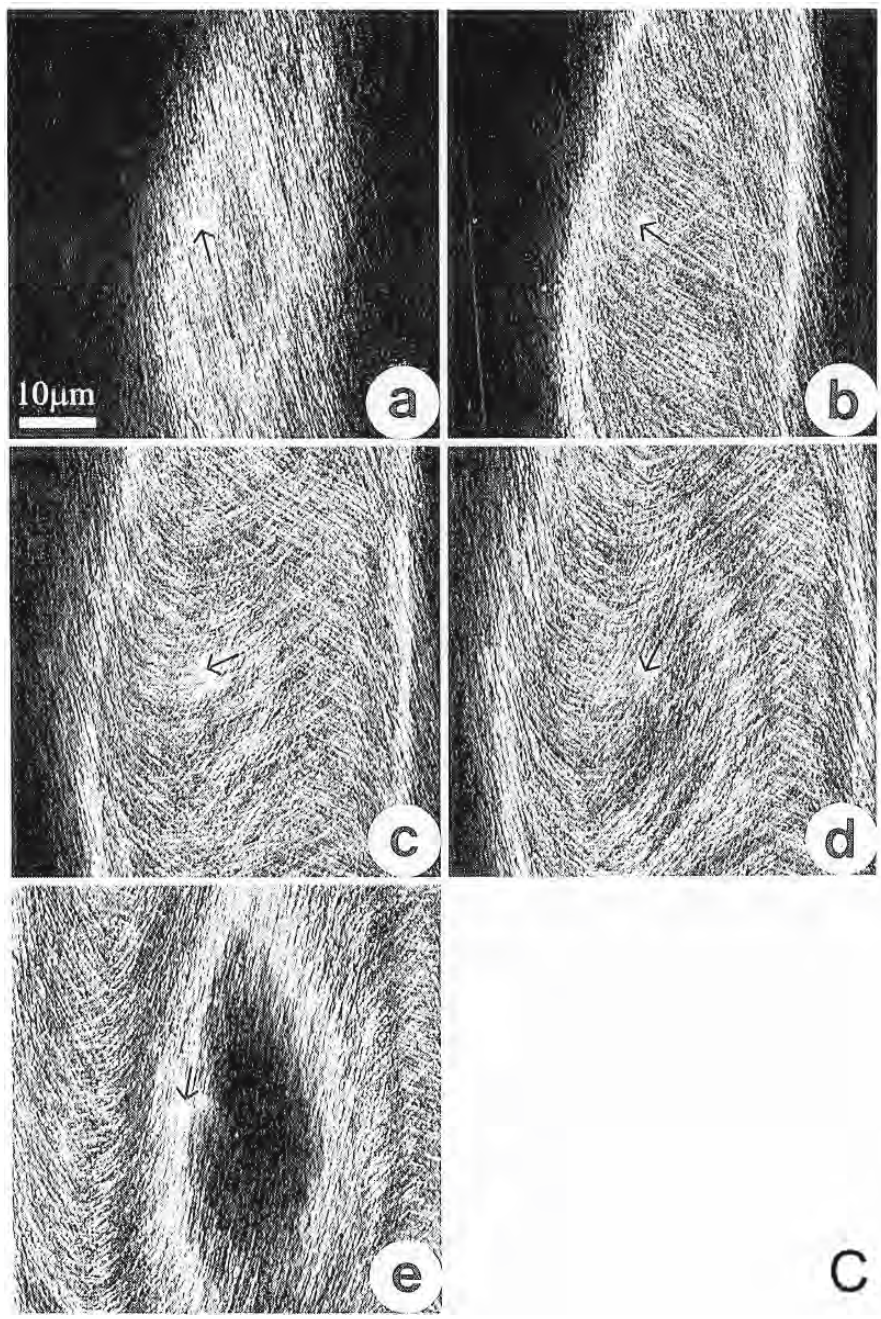

Figure 5.39: Continued.

C. Selected images from a confocal z-series of optical sections cut parallel to the plane of a single lamella in an area similar to that boxed in **B**. The fibre axis at any point, e.g., the tip of the arrow, can be seen to pass through five stepped, anti-clockwise rotations from the inner lamella (a) to the outer (e), confirming the plywood-like construction inferred from **B**. The curvature of the fibres can be seen in c and e (arrows).

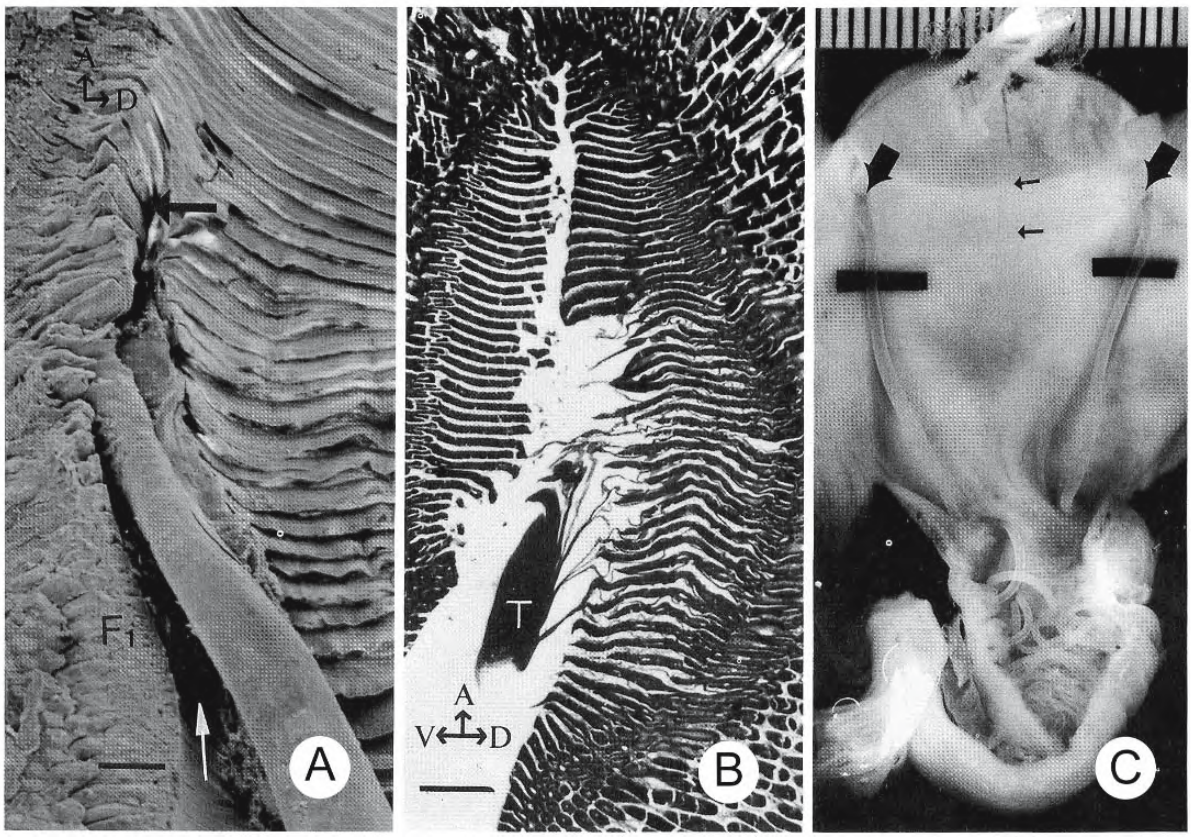

Figure 5.40: Photographs to illustrate formation of posterior tendrils in the marginal trendril forming regions of the E zone of the nidamental gland of the dogfish *Scyliorhinus canicula.* (From Feng and Knight, 1994b; reproduced with permission from the Royal Society).

A. Scanning electron micrograph of a tendril forming in an active, right tendril forming region. A separate duct joins the main lumen at the point indicated by the black arrow and continues as the marginal channel (white arrow) which receives opening of the glands of the F_1 zone. Scale bar = 300 μm.

B. Paraffin section of an active, right tendril forming region forming the proximal part of an anterior tendril (T). Only the posterior 30 or so transverse grooves on the dorsal side of the marginal channel are active at this stage. No secretion is seen in the anterior grooves or the grooves on the ventral side. Scale bar = 500 μm.

C. Photograph of a whole oviductal gland and the anterior part of the posterior oviduct opened with a ventral midline incision. The forming tendrils emerge from the tendril forming regions (broad arrows) and remain uncoiled until they reach the posterior oviduct. The tendril appears to hang randomly in the posterior oviduct. The small arrows indicate the first and last transverse grooves of the D-zone of the capsular wall forming region. Scale in millimetres.

Abbreviations: A, anterior; D, dorsal; V, ventral.

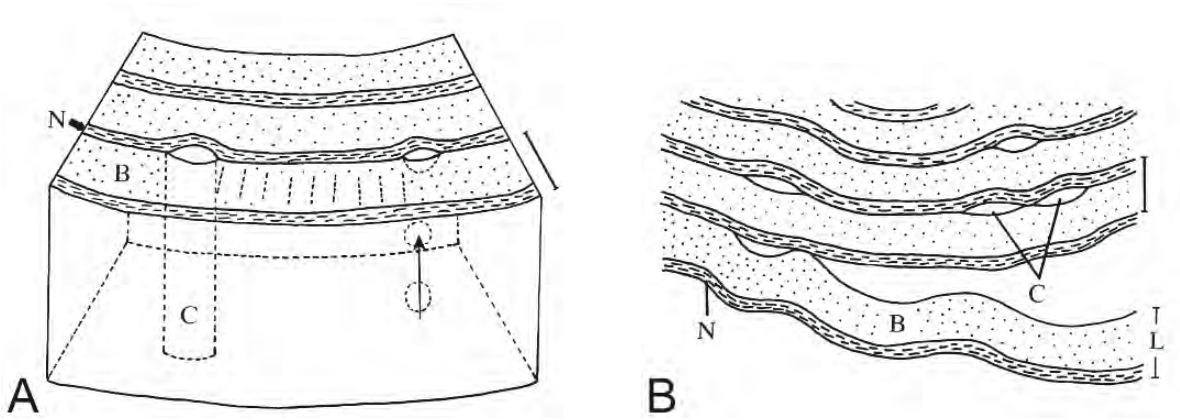

Figure 5.41: Diagrams illustrating the formation and structure of tendrils of the egg case of the dogfish *Scyliorhinus canicula.* (From Feng and Knight, 1994b; reproduced with permission from the Royal Society).

A. Transverse section of a portion of a tendril showing its lamellar nature. The fibril orientation is longitudinal in the broad lamina (B) and circumferential in the narrow lamina (N). The slight, progressive change of orientation of the fibrils within the broad lamina is indicated (dotted lines). Fluid-filled canaliculi (C) and lines of small voids (arrow) are entrapped between the laminae. Scale bar = 6 μm.

B. Transverse section of a part of a forming tendril suggesting that canaliculi (C) are formed by the incomplete adhesion of a pleated lamella (L) secreted from a transverse groove of the D-zone. B is a broad lamina; N is a narrow lamina. Scale bar = 6 μm.

→

Figure 5.42: The gravid uterus of the spiny dogfish *Squalus acanthias.* (From Hamlett and Hysell, 1998; © reproduced with permission of John Wiley & Sons, Inc.).

A. Photograph of the uterus opened to show longitudinal rows of flap-like appendages (arrows). The oviduct (o) is shown at the right. Embryo sacs ("candles"), 3 cm in total length, have been removed. Scale in cm.

B. Scanning electron micrograph of a uterine flap, consisting of a thin fold (f) and a rounded free edge (*), on the inner surface of the uterus shown above. X 60.

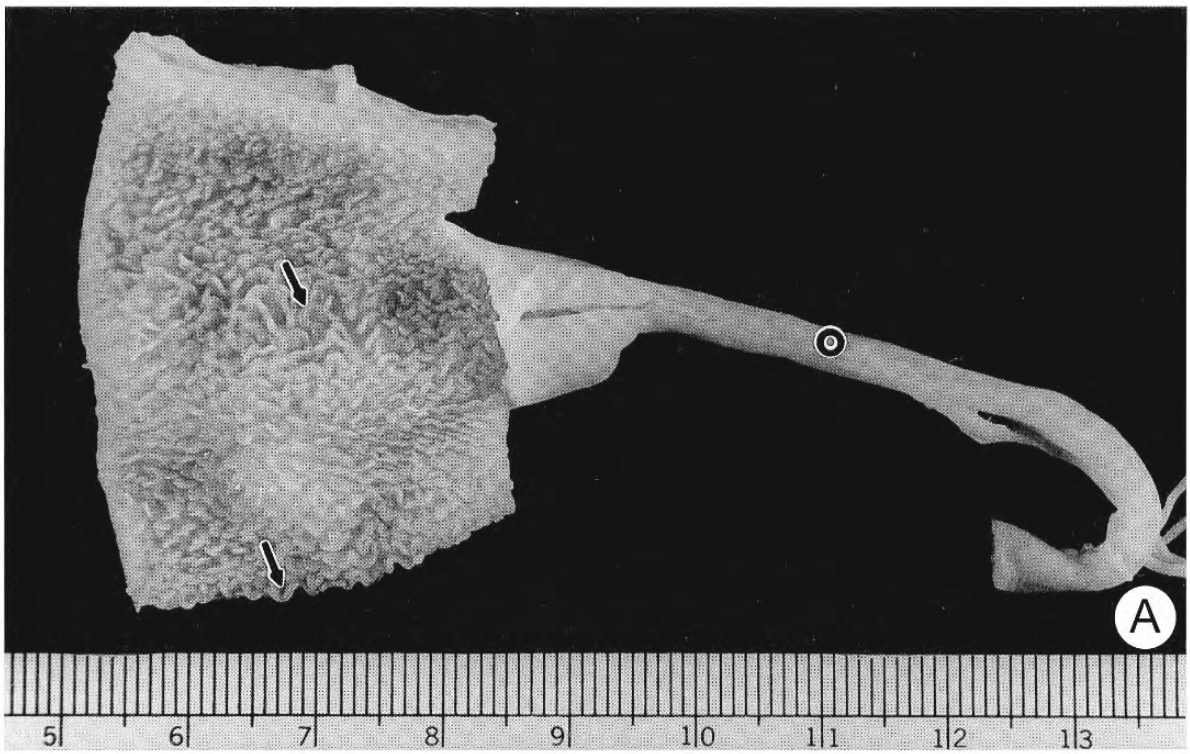

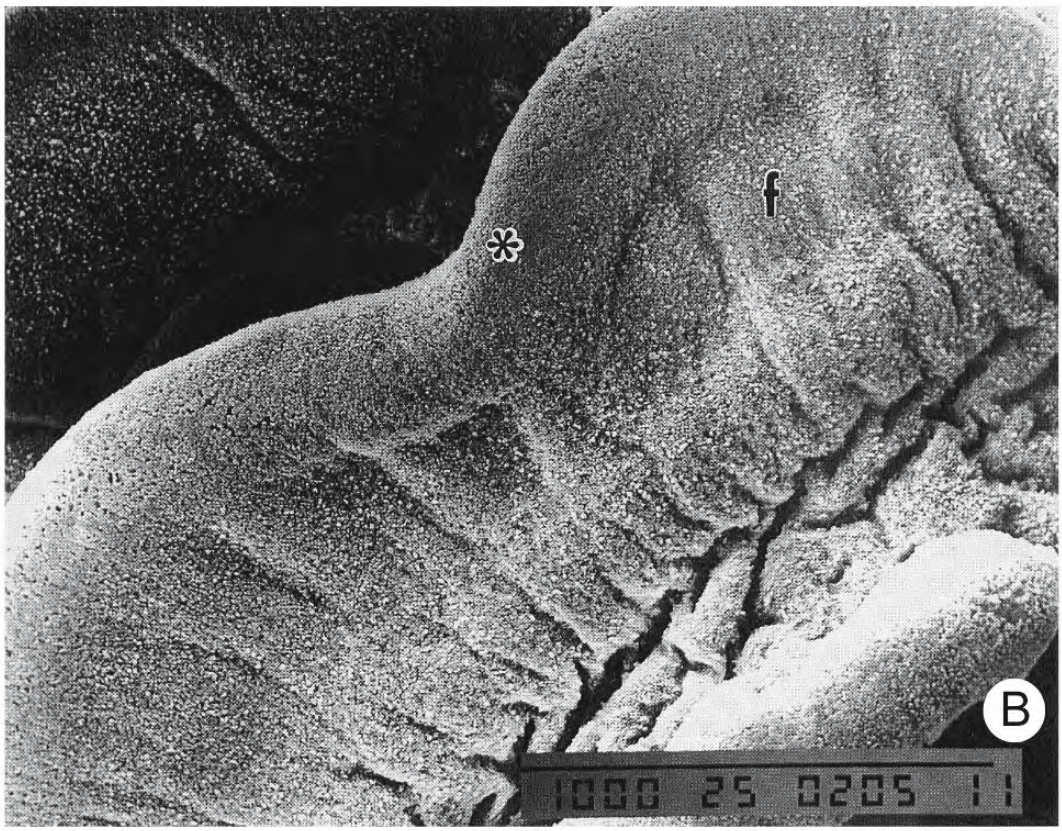

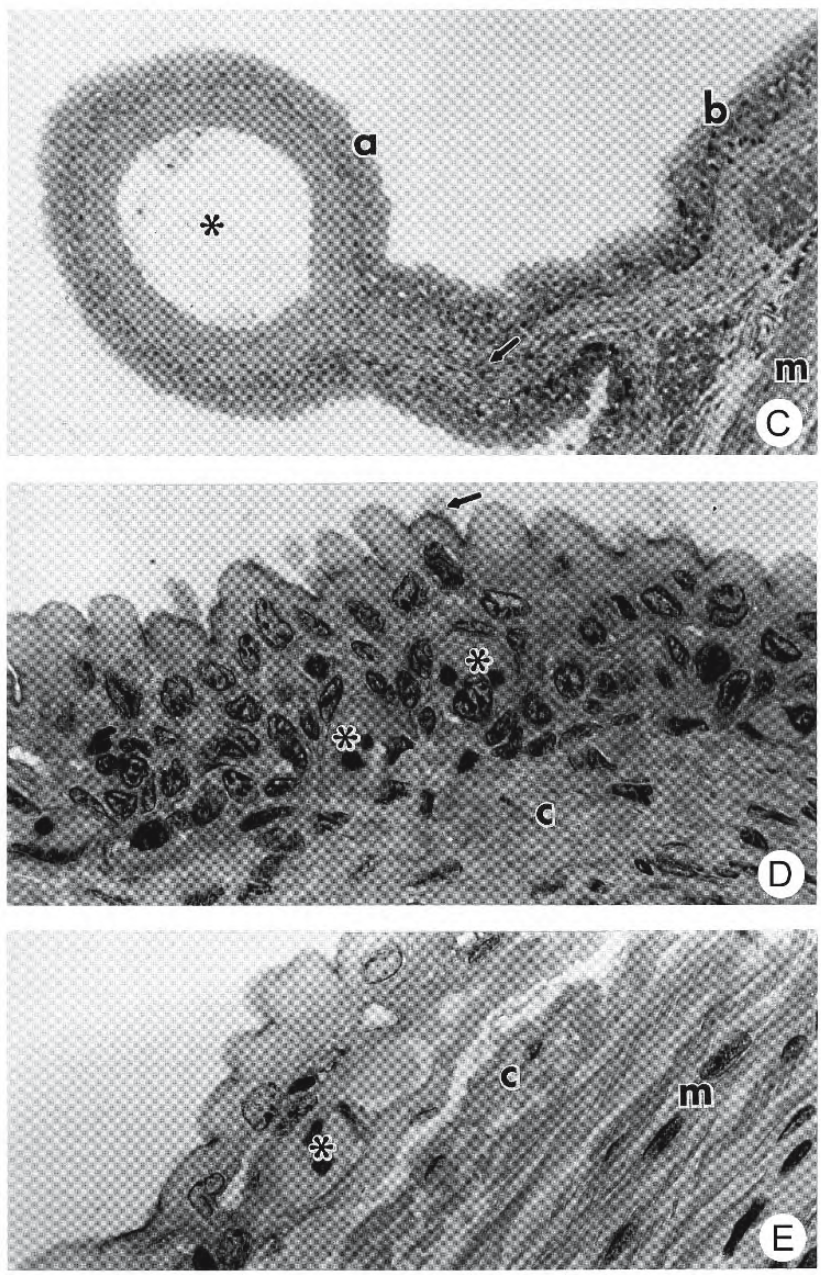

Figure 5.42: Continued.

C. Photomicrograph of a section through a uterine flap. The flap contains a core of connective tissue (arrow) and its rounded edge is created by an artery (*). The epithelia of the fold, its rounded edge (a), and the uterine lining (b) are identical. Smooth muscle (m) of the uterine wall is seen at the lower right. X 200.

D. Equivalent section to "a" in figure **C**. The epithelium has microvilli (arrow), is vascularized (*), and rests on a core of collagenous connective tissue predominantly composed of collagen (c). X 600.

E. Equivalent section to "b" in figure **C**. The epithelium is vascularized (*), rests on a layer of collagenous connective tissue (c), and is surrounded by smooth muscle (m). X 600.

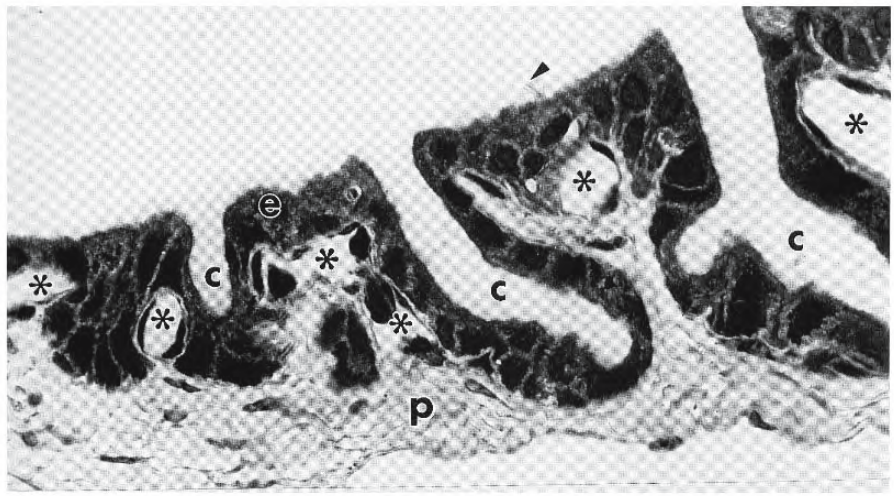

Figure 5.43: Photomicrograph of a section through the wall of the gravid uterus of the skate *Raja erinacea.* The folds of the lining are covered with a simple columnar ciliated epithelium (e) and have a core of richly vascular loose connective tissue. The arrowhead points to a few cilia on the epithelial cells. Asterisks indicate abundant blood vessels in the submucous connective tissue. X 600 (From Hamlett and Hysell, 1998; © reproduced with permission of John Wiley & Sons, Inc.).
Abbreviations: c, secretory crypts between the folds; p, submucous connective tissue.

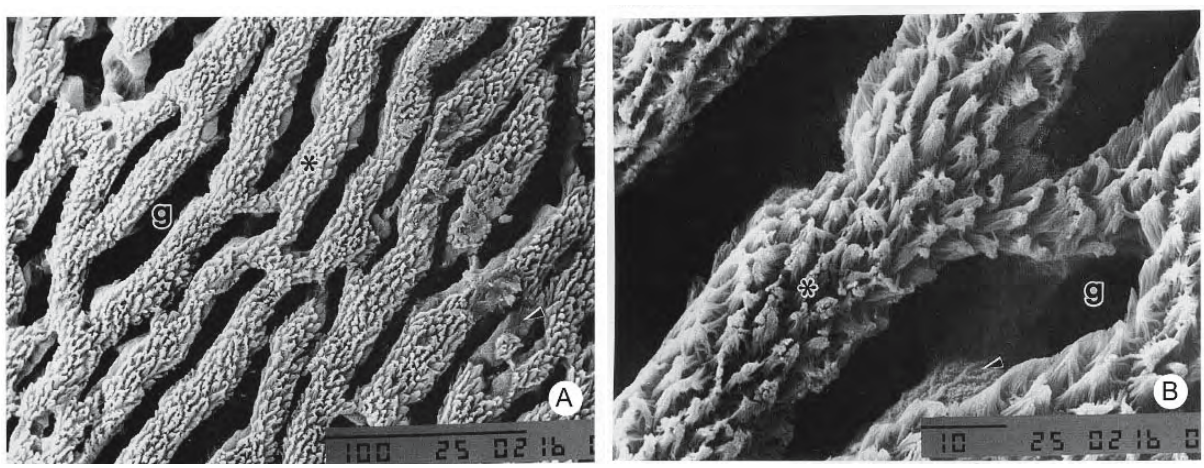

Figure 5.44: Micrographs of the uterine lining of the little skate *Raja erinacea.* (From Koob and Hamlett, 1998; © reproduced with permission of John Wiley & Sons, Inc.).
A,**B**. Scanning electron micrographs showing the richly vascular, branching longitudinal folds (*) in the lining of the uterus. Glands (g) open into the uterine slits. The arrowhead indicates secretory gland cells.

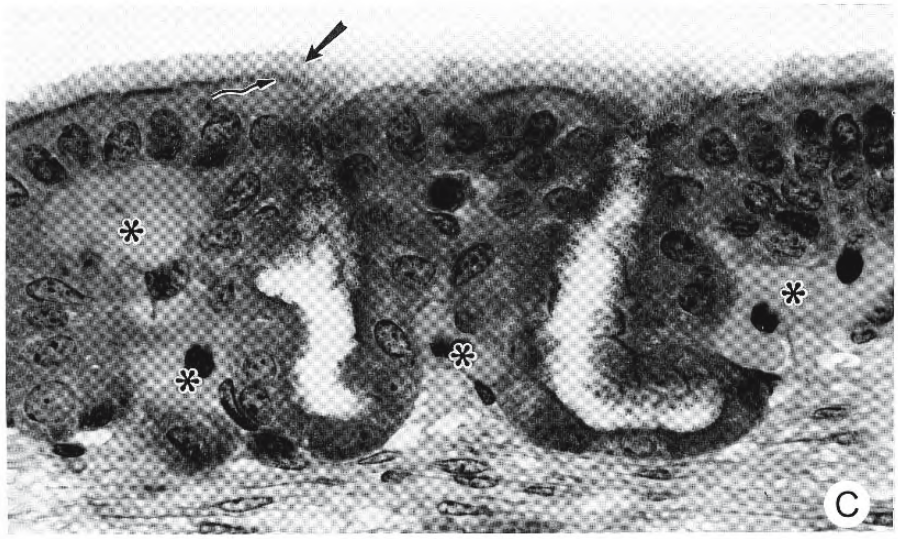

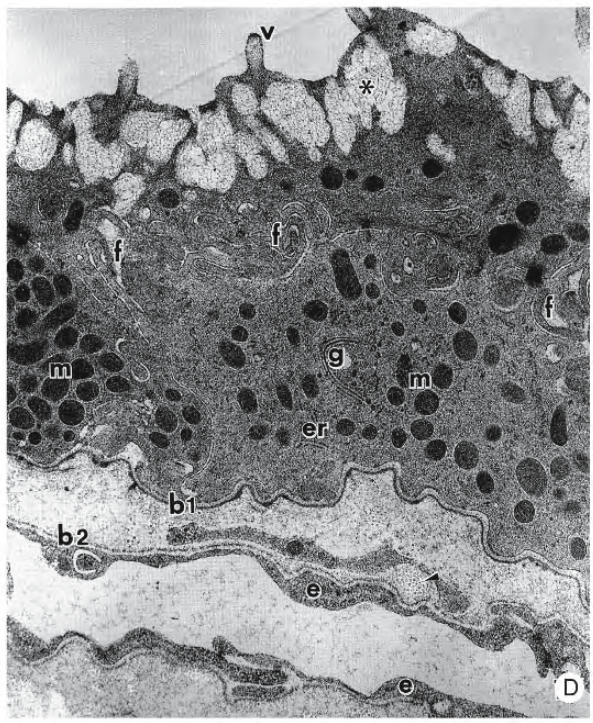

Figure 5.44: Continued.

C. Light micrograph of a section through the richly vascular (*) uterine wall. The dense covering of cilia (arrow) subtends well defined basal bodies beneath (undulating arrow). X 600.

D. Transmission electron micrograph of a section through secretory cells in the epithelium lining the uterus. The characteristics of active secretion are evident in these cells: microvilli (v), secretory vesicles (*), mitochondria (m), granular endoplasmic reticulum (er), Golgi complex (g), and lateral membrane folds (f) enclosing intercellular channels. A capillary, lined by endothelial cells (e) and enclosed by its basal lamina (b2) courses through the bottom of the micrograph. The capillary is separated from the epithelium by a delicate layer of loose connective tissue and the epithelial basal lamina (b1). The arrowhead indicates a cross section of a collagen bundle. X 8,000.

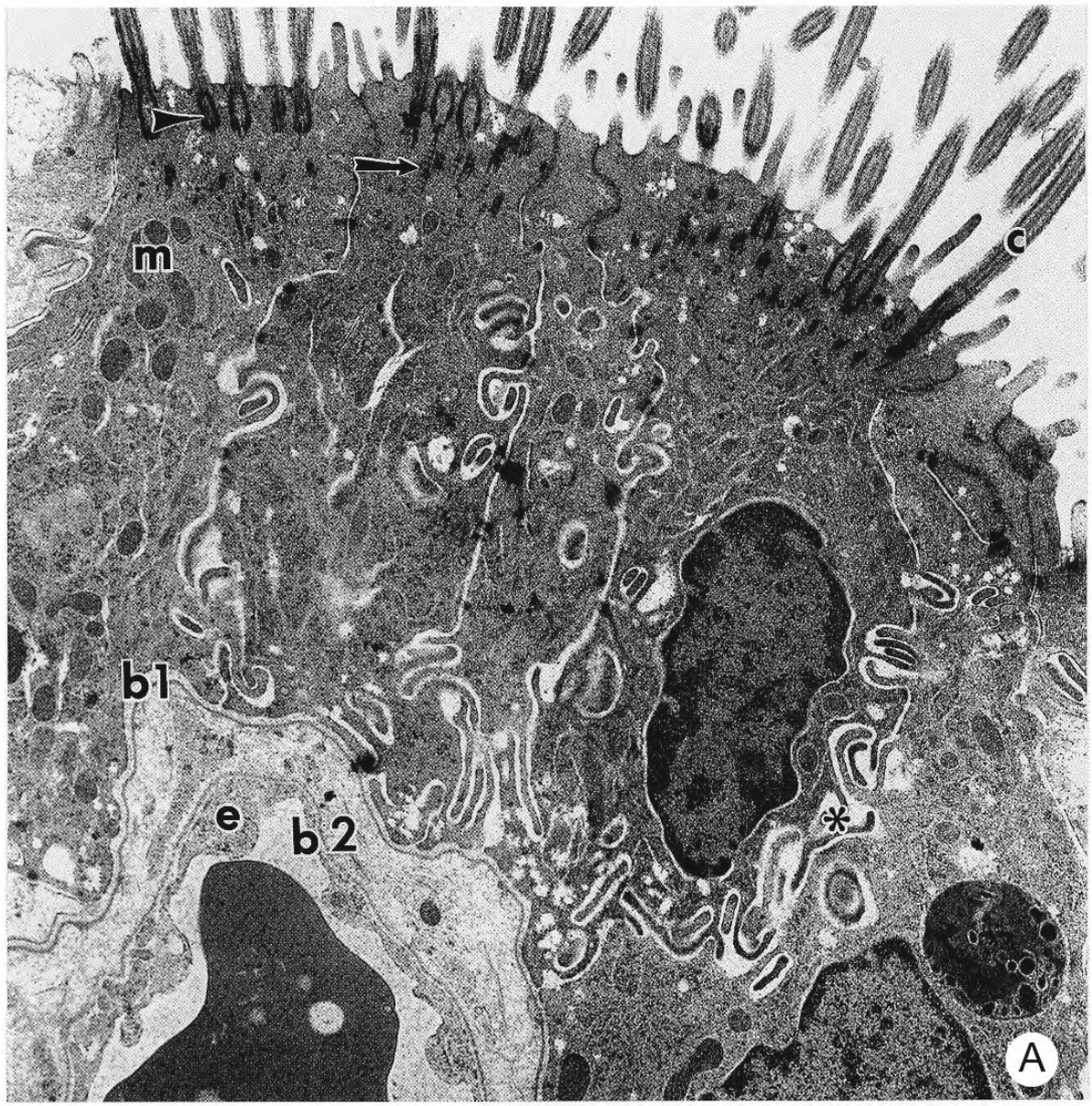

Figure 5.45: Transmission electron micrographs of sections through the epithelium of the uterine lining of the little skate *Raja erinacea.* (From Koob and Hamlett, 1998; © reproduced with permission of John Wiley & Sons, Inc.).

A. Section through columnar surface cells showing cilia (c), basal bodies (arrowhead), striated rootlet fibres (arrow), and elaborate intercellular folds (*). The basal lamina of the epithelium (b1) and the basal lamina of the endothelium (b2) enclose a delicate layer of loose connective tissue. e, endothelium; m, mitochondria X 6,000.

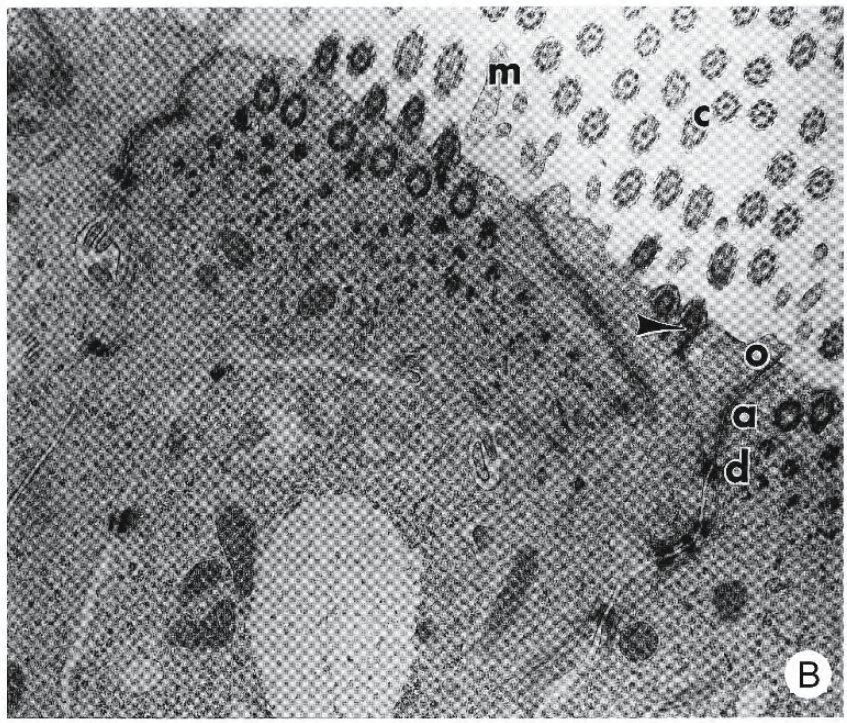

Figure 5.45: Continued.

B. This section shows well developed junctional complexes sealing the intercellular channels in the uterine epithelium from the lumen. The junctions comprise a zonula occludens (o), zonula adhaerens (a), and a macula adhaerens or desmosome (d). Also shown are microvilli (m) and cilia (c) with their basal bodies (arrowhead). X 16,000.

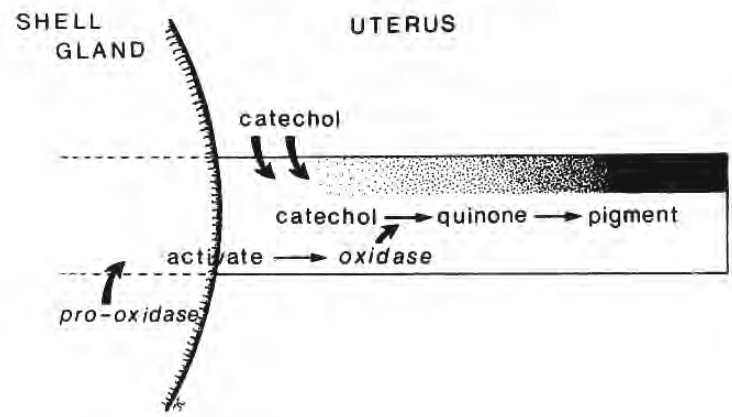

Figure 5.46: Diagram to illustrate the mechanism of tanning in the egg capsule of the little skate *Raja erinacea.* The egg capsule is white when it leaves the oviductal gland and contains no catecholic substance although an inactive form of the enzyme, catechol oxidase, is incorporated into the matrix during secretion. Tanning occurs as the egg passes into the uterus where catechols begin to accumulate in the capsular material and are oxidized, under the influence of catechol oxidase, to quinones. The oxygen required for this tanning is transported from the maternal circulation by the uterus. (From Koob and Cox, 1990; reproduced with permission of the Cambridge University Press).

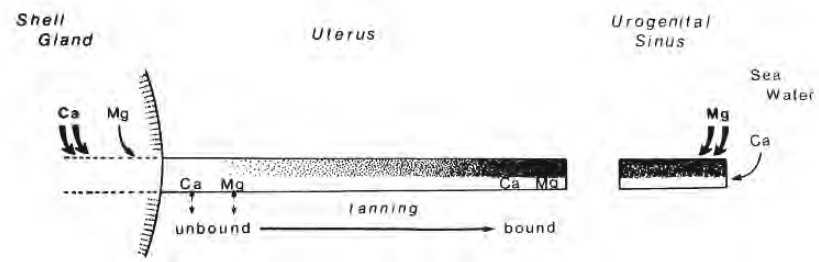

Figure 5.47: Diagram to illustrate the sequence of deposition and binding of calcium and magnesium during formation and tanning in the egg capsule of the little skate *Raja erinacea.* (From Koob, 1991; reproduced with permission of the American Society of Ichthyologists and Herpetologists).

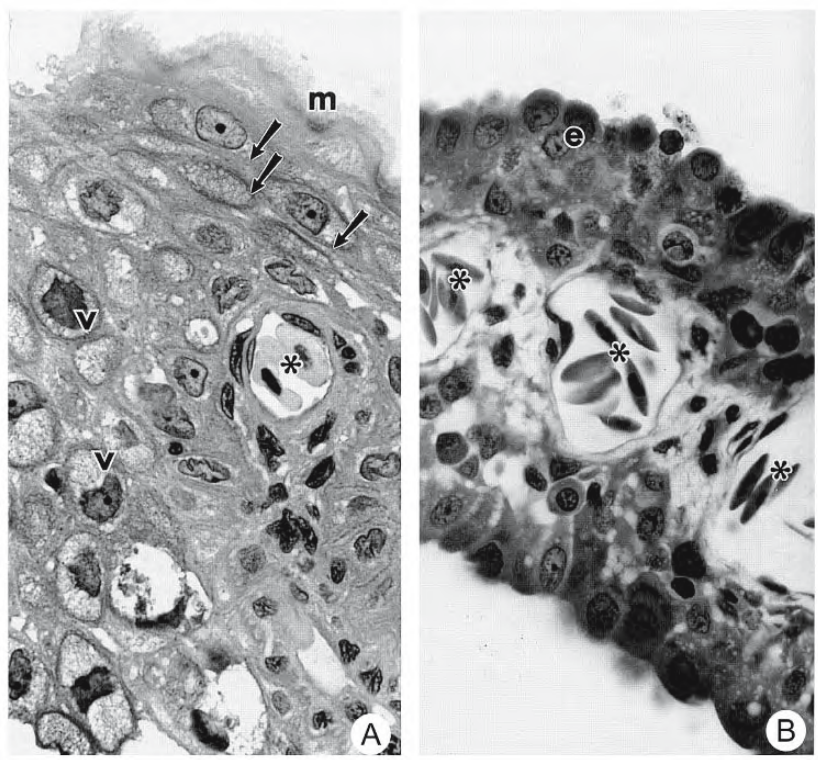

Figure 5.48: Photomicrographs of sections of the uterine wall of the sandtiger shark *Carcharias taurus.* (From Hamlett and Hysell, 1998; © reproduced with permission of John Wiley & Sons, Inc.).

A. Nongravid uterus. The surface epithelium has microvilli (m) and is supported by several layers of flattened cells containing prominent cytoplasmic filaments (arrows). Below this layer is a zone of rounded cells containing frothy vesicles. (v) and a blood vessel (*). X 600.

B. Gravid uterus. This fold is from a uterus that contained eggs and embryos. The development of longitudinal folds has increased the epithelial surface area over that shown in **A**. Blood vessels (*) have enlarged. X 600.

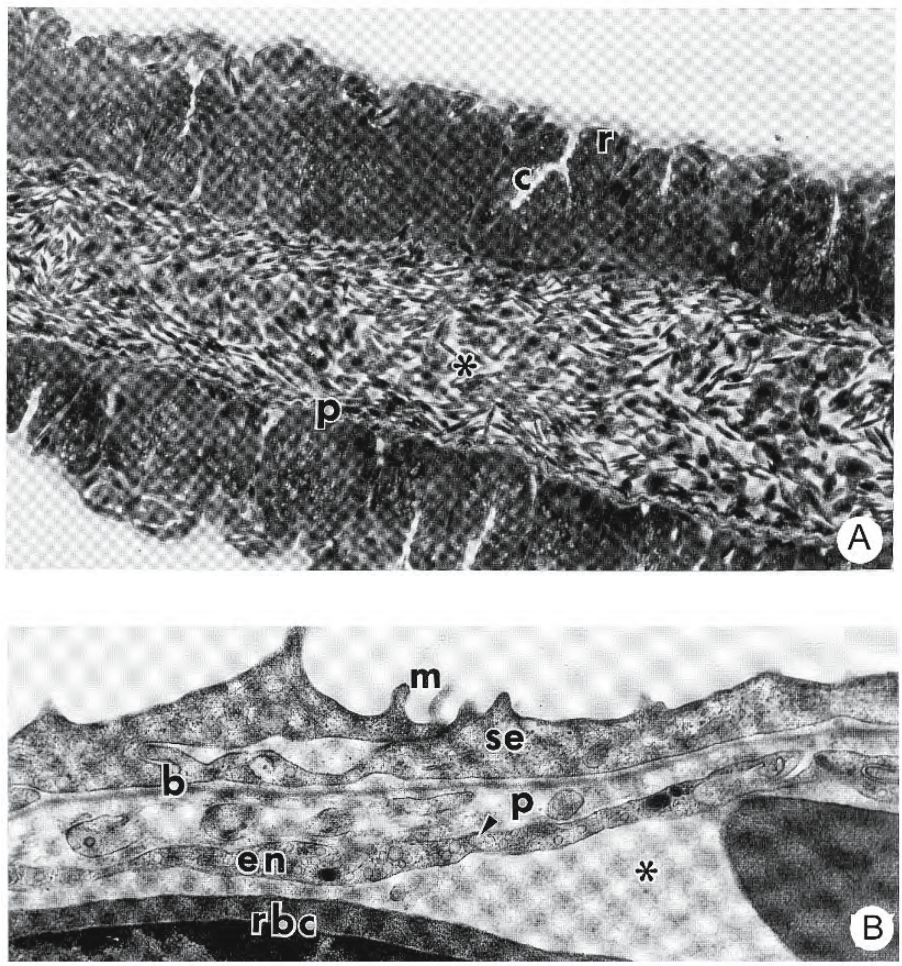

Figure 5.49: Micrographs of sections through the uterine wall of gravid yellow spotted stingrays *Urolophus jamaicensis.* (From Hamlett and Hysell, 1998; © reproduced with permission of John Wiley & Sons, Inc.).

A. Photomicrograph of a longitudinal section of a trophonema from a gravid female. Secretory crypts (c) alternate with epithelial ridges (r). A thin lamina propria mucosae (p) separates the epithelium from the core blood vessel (*). X 200.

B. Transmission electron micrograph of an epithelial ridge of a trophonema. The simple squamous epithelial cells (se) display a few microvilli (m) and rest on a thin basal lamina (b) which is separated from a blood vessel (*) by a lamina propria mucosae of delicate loose connective tissue (p). Pinocytotic vesicles (arrowhead) are abundant within the endothelial cell. An erythrocyte (rbc) is indicated in the blood vessel. X 18,500.

C. Photomicrograph of a longitudinal section of a trophonema from a gravid female. Each surface ridge contains a vascular branch (*) below a simple squamous epithelium (arrowheads). The simple columnar epithelial cells of the crypts (c) contain apical secretory vesicles (s) and are separated from the subjacent blood supply (*) by the delicate connective tissue of the lamina propria mucosae (p). X 600.

D. Transmission electron micrograph of a trophonema from a gravid female. Secretory cells contain granular endoplasmic reticulum (er), Golgi complexes (g), and secretory vesicles (s). A blood vessel (*) is shown at the lower left. X 2,000.

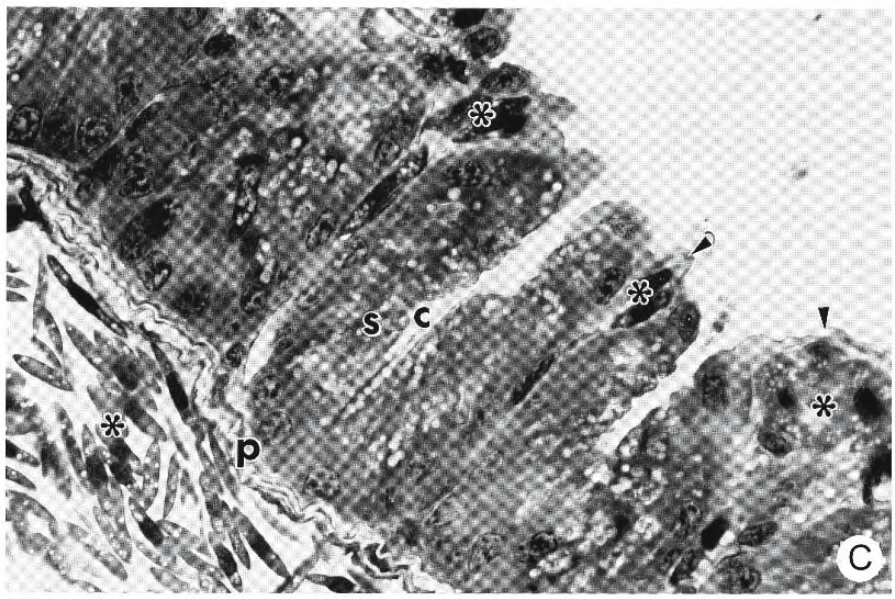

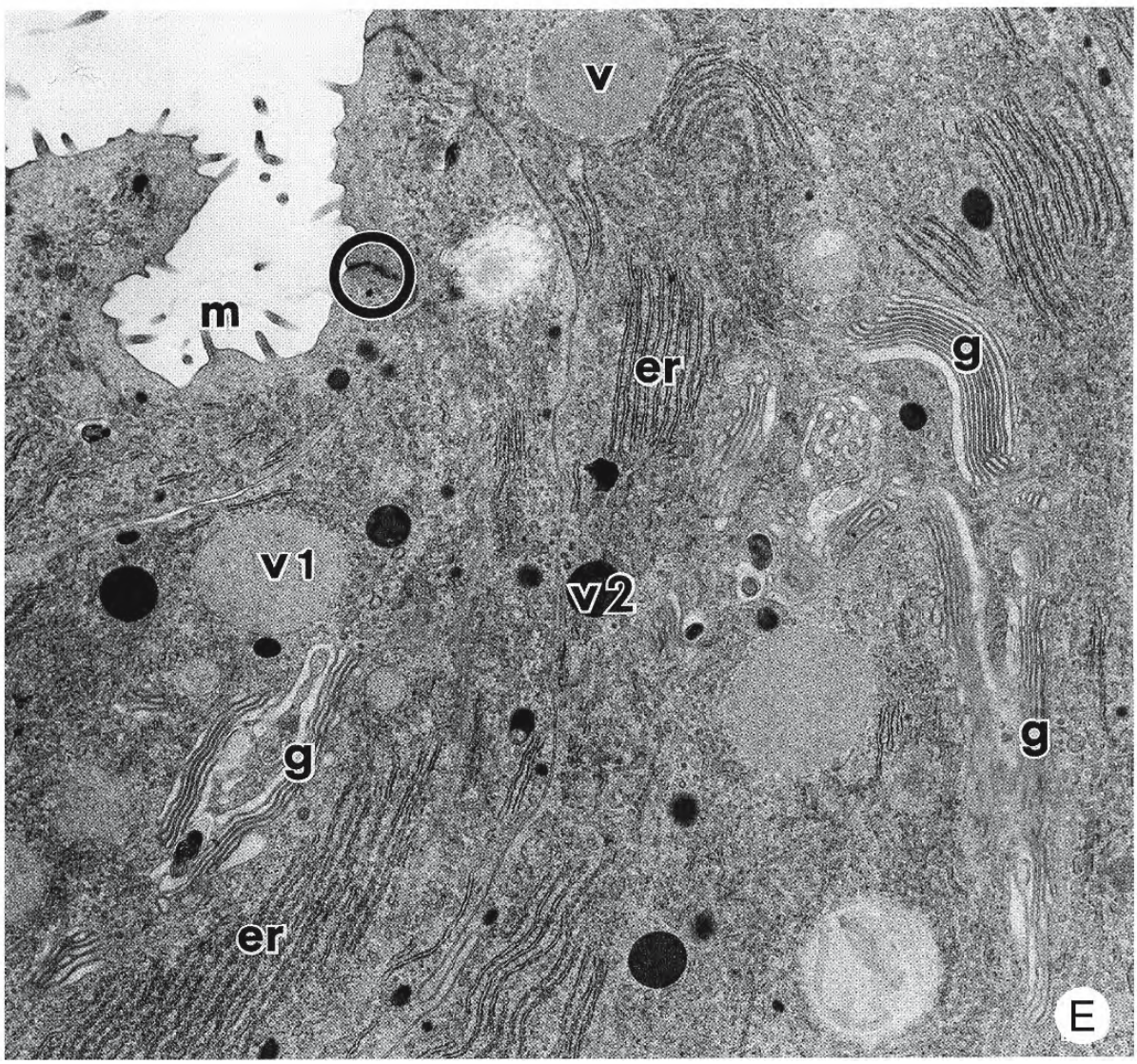

Figure 5.49: Continued.

E. Transmission electron micrograph of epithelial cells from the surface of a trophonema. The cells are joined apically by tight junctions (circle) and display microvilli (m). They contain the organelles indicative of active secretion: granular endoplasmic reticulum (er) and Golgi complexes (g). Two types of secretory vesicles are present: large vesicles with flocculent contents (v1) and smaller vesicles with electron-dense contents (v2). X 8,000.

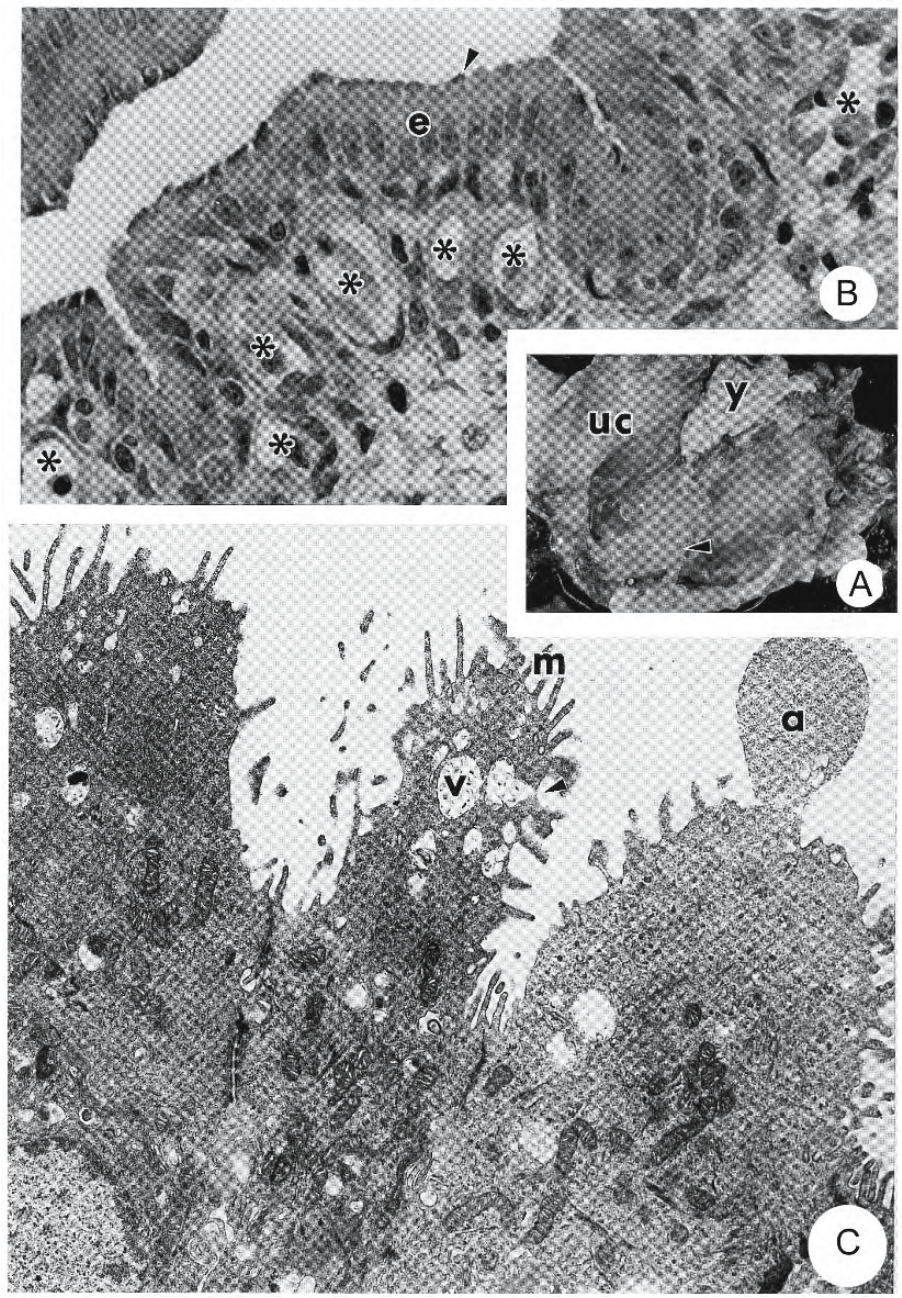

Figure 5.50: Micrographs of sections of the uterine wall of the Atlantic sharpnosed shark *Rhizoprionodon terraenovae.* (From Hamlett and Hysell, 1998; © reproduced with permission of John Wiley & Sons, Inc.).

A. Before implantation, an embryo resides in its own uterine compartment (uc). It is nourished by the contents of its yolk sac (y) that are conveyed to the embryo by way of the yolk stalk (arrowhead).

B. Photomicrograph of a section through the wall of the uterine compartment showing its smooth lining of simple columnar epithelium (e) resting on a rich vascular bed (*). Note the secretory blebs (arrowhead) on the epithelial cells. X 400.

C. This transmission electron micrograph through the epithelium of a uterine compartment illustrates microvilli (m), merocrine secretory vesicles (v), merocrine secretion (arrowhead), and apocrine secretory blebs (a). X 8,000.

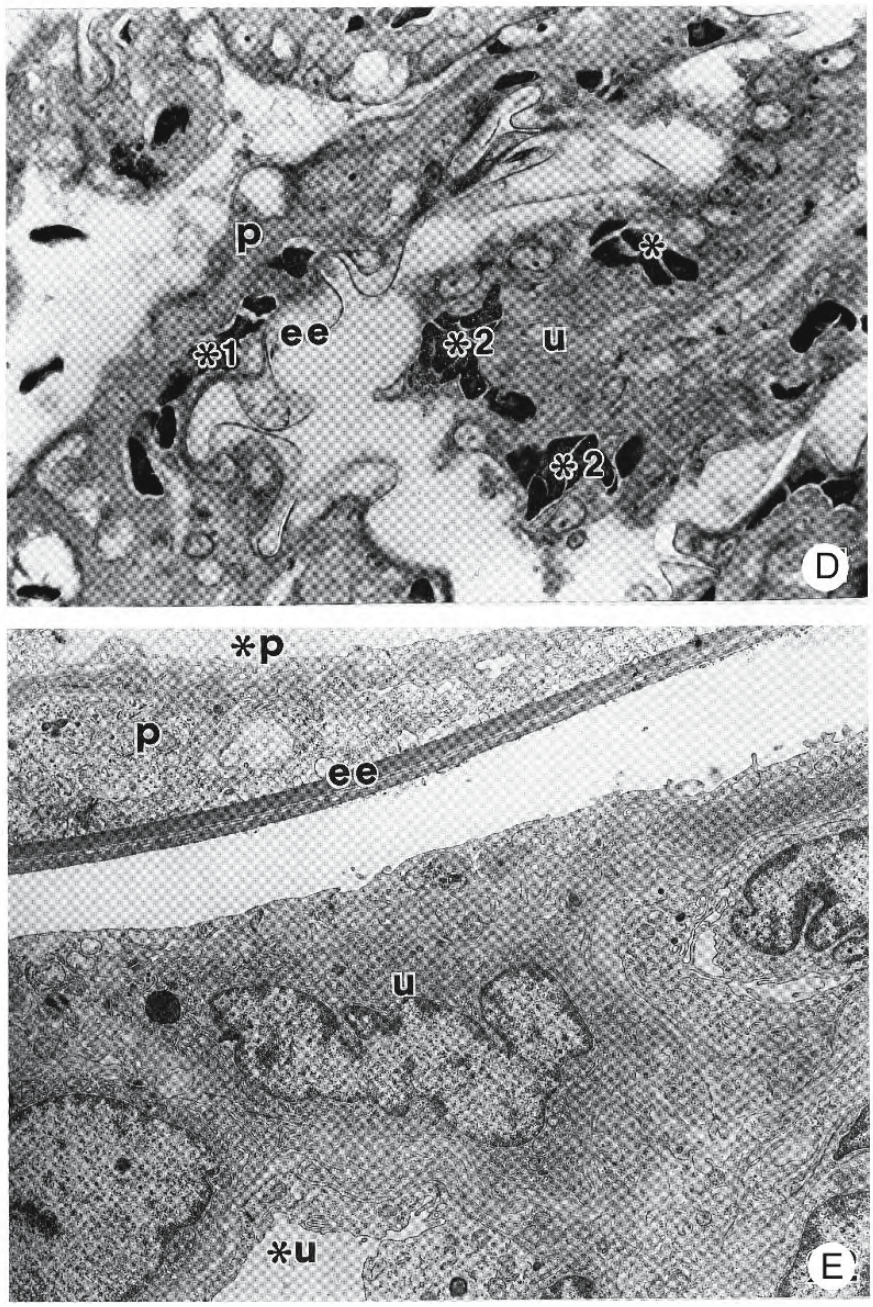

Figure 5.50: Continued.

D. Photomicrograph of a term uterus and foetal portion of the placenta. The foetal placenta (p) has a dense vascular bed (*1) and is separated by the egg envelope (ee) from the uterus (u) which also has a dense vascular bed (*2). X 600.

E. Transmission electron micrograph showing the foetal portion of the placenta (p) with its placental vascular bed (*p) abutting the egg envelope (ee) and the uterus (u) with its vascular bed (*u) separated from the egg envelope. X 10,000.

CHAPTER 6

VIVIPARITY

6.1 Introduction

Viviparity is a process in which eggs are fertilized internally and undergo development within the maternal reproductive system (Wourms, Grove, and Lombardi, 1988)[19]. Although most fishes are oviparous, 54 families of living fishes have species that bear living young; these include 40 families of chondrichthyans, the single coelacanth, *Latimeria chalumnae,* and 14 families of teleosts. While as many as 420 of 600 to 800 species of chondrichthyans practice viviparity, only 510 of an estimated 18,000 species of teleosts do so. One explanation for this disparity may be that teleosts lack Müllerian ducts which are used as brood chambers in other viviparous vertebrates (Wake, 1985; Schindler and Hamlett, 1993). The teleosts, however, have shown great resourcefulness in making other arrangements for the internal care of their young and gestation occurs within the ovary itself.

In the evolution of viviparity, there has been a tendency away from a dependency of the embryo on its own yolk reserves to a greater reliance on nutrients supplied by the mother, thereby establishing the distinction between LECITHOTROPHY and MATROTROPHY. In lecithotrophy, little or no nutrient material crosses to the embryo from the maternal circulation and all, or nearly all, of the substrates for growth and metabolism are obtained from yolk reserves stored in the egg prior to fertilization (Grove and Wourms, 1991, 1994; Hollenberg and Wourms, 1994). During gestation, lecithotrophic embryos undergo a loss in weight of organic material similar to that which takes place during the development of oviparous fishes. In matrotrophy, however, yolk reserves are supplemented during gestation by materials provided by the mother: not only has the mother laid down yolk during vitellogenesis but she supplies additional nutrients during embryonic development. With the establishment of matrotrophy, various elaborate structures have evolved, always from preexisting structures, that facilitate nutrient transfer during gestation (Grove and Wourms, 1991).

This transfer of nutrients is achieved in several ways (Wourms, Grove, and Lombardi, 1988). In the simplest, termed either OOPHAGY or ADELPHOPHAGY, some embryos of the brood prey on their siblings, either as eggs or as embryos. More advanced transfer is by way of TROPHODERMY, where richly vascularized elaborations of maternal and embryonic epithelia, although not in intimate association, facilitate exchange across intertissue spaces. In a third type of matroprophic adaptation, PLACENTOTROPHY, maternal nutrients are transferred to the embryo by way of a PLACENTA which may be defined as the intimate apposition or fusion of maternal and foetal organs for physiological exchange. One type of placentotrophy is found only in sharks: the YOLK SAC PLACENTA, which consists of a modified yolk sac closely apposed to the uterine epithelium. This structure functions in the absorption of yolk during early gestation; later it becomes modified as the foetal portion of the placenta. Other placental relationships have been cited, including the FOLLICULAR PLACENTA, an intimate association between the follicular wall and embryonic surfaces; BUCCAL AND BRANCHIAL PLACENTAS where richly vascular extensions of maternal tissue grow into the foregut of the foetus; and the TROPHOTAENIAL PLACENTA where elaborate outgrowths of the hindgut of the foetus, the TROPHOTAENIAE, absorb nutrients provided by the ovarian luminal epithelium.

It is often difficult not to overstep the line separating the realms of histology and embryology; this distinction becomes especially tenuous in a discussion of viviparity. For the most part, developmental considerations have been omitted from the present work except where they may cast light on the nature of a mature

[19] A classic series of papers on viviparity in fishes was published between 1933 and 1952 by C.L. Turner and is listed in the *Literature Cited;* this work formed a solid basis for the later research that is cited in this section.

organ. Foetal structures (such as gills, the gut, and skin) have been included only where they combine with maternal tissues to form a more-or-less discrete organ, the PLACENTA.

6.2 Viviparity in Elasmobranchs

Viviparity is the dominant form of reproduction among elasmobranchs, especially the sharks and rays where an evolutionary transition shows increasing dependence on the mother during development (Wourms, 1981; Hamlett, 1987; Wourms, Grove, and Lombardi, 1988; Hamlett and Koob, 1999). Oviparous species develop independently of the mother; they are lecithotrophic and are completely dependent on the yolk reserves contained within their yolk sacs. Some viviparous species are also lecithotrophic and, although they develop within the uterus, they also depend on their own yolk reserves; the mother simply provides physical protection for her brood and permits the necessary respiratory exchanges (Figure 6.1). The most efficient route for nutrient transfer occurs in foetal sharks and rays by way of HISTOTROPH, a nutrient fluid provided by the tissues of the mother (Wourms, 1981). With the establishment of the yolk sac placenta in Carcharhinidae and Sphyrnidae, haematrophic exchange provides nutrients directly from the maternal to foetal circulation. Viviparous development in elasmobranchs is either APLACENTAL, where no morphologically definitive vascular exchange organ is formed, or PLACENTAL, where a maternal-foetal exchange organ is formed (Hamlett and Hysell, 1998).

Although the ovaries and oviducts begin development as paired structures, they often become asymmetrical in adults and, in some viviparous sharks, the right ovary is functional and the left atrophies (Wourms, 1981). Nevertheless, both oviducts are present. Among viviparous rays, the right ovary and oviduct undergo varying degrees of reduction or loss. The oviduct of elasmobranchs originates as a simple tubular Müllerian duct which then undergoes regional differentiation.

During ovulation, an ovum is expelled from the ovary into the coelom, drawn into the OSTIUM TUBAE, and transmitted down one of the two oviducts (Figure 6.2). As it passes the OVIDUCTAL or SHELL GLAND, it is fertilized and enveloped in an oversized, amber-coloured EGG CAPSULE that it will eventually "grow into" as it develops. The egg capsule is a tertiary membrane of stout construction in oviparous forms, able to withstand the rigours of life outside the mother (Wourms, Grove, and Lombardi, 1988; Hamlett, 1993). A more delicate egg capsule surrounds viviparous embryos and appears to contain a unique form of collagen or a collagen-like protein where the banding pattern characteristic of collagen may be absent. The capsule establishes two subcompartments: the UTERINE COMPARTMENT and PERIFOETAL COMPARTMENT (Figures 6.3 and 6.4) and may be retained throughout gestation, even being incorporated into the placenta; alternatively the embryo may emerge from it to complete development unconfined within the uterine lumen. In only one species, *Prionace glauca,* has the absence of an egg capsule been noted (Otake and Mizue, 1985).

The viviparous embryo, enclosed in its oversized egg capsule, passes into the enlarged lower region of the oviduct that is modified to form a UTERUS (Figure 6.5) (Hamlett, 1987; Castro and Wourms, 1993; Hamlett and Hysell, 1998). Excess egg capsule is folded into a neat package and stored in a diverticulum of the uterine wall, the MEMBRANE RESERVOIR (Figures 6.6 and 6.7) (Teshima and Mizue, 1972; Hamlett, Wourms, and Hudson, 1985c; Lombardi and Files, 1993). As the foetus grows, its increasing size is accommodated by membrane paid out from the reservoir. At term, all of the membrane will have been withdrawn to enclose the full-sized foetus and the lumen of the reservoir becomes confluent with that of the uterus.

Several embryos may be accommodated within the uteri of some sharks. During the initial months of gestation, each embryo, enclosed in its own egg capsule, may be surrounded by dorsolateral and ventromedial folds of the uterine wall that span the lumen to form UTERINE COMPARTMENTS, each of which contains one embryo within its surrounding egg capsule (Figures 6.8 and 6.9) (Schlernitzauer and Gilbert, 1966; Hamlett, 1987; Wourms, Grove, and Lombardi, 1988; Castro and Wourms, 1993; Hamlett et al., 1993a). Only a few aplacental sharks develop uterine compartments (e.g., *Galeus canis, Mustelus vulgaris).*

6.2.1 APLACENTAL VIVIPARITY IN ELASMOBRANCHS

Depending upon the amount of yolk contained within the ova of viviparous embryos, there is a variable period of dependence on the mother for sustenance (Wourms, 1981; Wourms, Grove, and Lombardi,

1988; Hamlett and Hysell, 1998). The foetus may be wholly LECITHOTROPHIC and retain its independence by utilizing its own yolk resources throughout gestation, undergoing considerable net loss in dry weight during development. Alternatively, embryos may obtain nutrients by preying on their siblings within the uterus, either consuming ovulated eggs (OOPHAGY), or cannibalizing developing embryos (ADELPHOPHAGY). In contrast to other viviparous sharks, ovulation continues throughout gestation in most oophagous species, providing a steady food supply for the developing foetuses (Wourms, Grove, and Lombardi, 1988).

In aplacental yolk sac viviparity, the mother provides for respiratory exchange and the regulation of water and electrolytes; she does not necessarily provide nutrients directly but may simply create a felicitous environment for gestation. Hypertrophy of smooth muscle of the wall as well as increases in its connective tissue layers adapt the uterus for its burden of a long gestation. Respiratory exchange is accommodated by an increase in vascularization of the uterus and a reduction in the tissue barriers between the maternal blood and the uterine lumen. In the spiny dogfish, *Squalus acanthias,* where development is lecithotrophic, the eggs and their jelly are encapsulated within a thin membrane, the CANDLE, which is closely apposed to the uterine wall. The candle ruptures about halfway through gestation and the embryos complete development in the uterine fluids. The area of the uterine respiratory surface is increased both by the dilation necessary to accommodate the embryos and also by the development of longitudinal folds, or RUGAE (Figures 5.42A,B) (Jollie and Jollie, 1967b; Hamlett and Hysell, 1998). These have a core of loose, richly vascular connective tissue whose capillaries radiate from a central arteriole (Figures 5.42C to E, and 6.10A,C). The capillaries insinuate themselves between the bases of the epithelial cells, thereby reducing the barrier to gaseous exchange. Although they appear to be intraepithelial, the capillaries are separated from the epithelial cells by a delicate basal lamina, presumably derived from both the endothelium and epithelium; no other stromal elements intervene (Figures 6.10B,D). The luminal epithelium, simple columnar in the non-pregnant uterus, becomes stratified cuboidal; its microvillous border suggests an osmoregulatory function. Conspicuous extracellular compartments separating the layers and junctional complexes between the apical borders of adjacent juxtaluminal epithelial cells may indicate active transport (Figures 6.10C,F,G,H). The apical cytoplasm of the juxtaluminal cells is packed with smooth-surfaced, electron-lucent vacuoles (Figure 6.10H). Since these are confined to the apical regions of the epithelium, they do not appear to be involved in transport across the barrier. Respiratory exchange occurs across the ectoderm of the yolk sac for only a brief period in early development, before the development of external gills (Jollie and Jollie, 1967a). Only a thin layer of one or two non-keratinized squamous ectodermal cells, sparse underlying connective tissue, and thin endothelial cells resist respiratory exchange between the uterine lumen and the vitelline capillaries; both the epithelial and endothelial cells display active pinocytosis (Figure 6.11). When the gills assume their function of respiratory exchange, the outer layers of the yolk sac take on the appearance of a protective epidermis and the squamous epithelial cells become keratinized and conjoined by desmosomes. Collagenous fibres, fibroblasts, and scattered smooth muscle fibres thicken and strengthen the subepithelial connective tissue.

Embryos of many sharks and rays are nourished by a viscous nutrient fluid, the HISTOTROPH, secreted by the uterine epithelium (Wourms, 1981; Wourms, Grove, and Lombardi, 1988). This fluid provides both a source of energy as well as the molecular constituents required for synthesis during cell replication and tissue growth and, in some species (e.g., *Mustelus laevis, Dasyatis violacea),* its organic content exceeds that of cow's milk. The presence of maternal blood serum proteins, especially immunoglobulin M (IgM), suggests that histotroph plays an immunological role in addition to its specialized nutrient functions. (Histotroph of placental sharks may contain oestrogens, indicating that it may also have an endocrine function.)

In many elasmobranchs, most of the uterine lining secretes histotroph but, in more advanced species, this production is enhanced by specialized projections of the uterine wall, the TROPHONEMATA, which may closely envelop the embryo; in some rays, the entire lining of the uterus undergoes hypertrophy (Figure 6.12) (Hamlett, Wourms, and Smith, 1985; Wourms, Grove, and Lombardi, 1988; Hamlett et al., 1993a, 1996). During early gestation, trophonemata form from the luminal epithelium as beds of richly vascular connective tissue covered by a simple epithelium. Trophonemata are spatulate, villiform processes embossed with a pattern of anastomosing, cable-like ridges (Figure 6.13).

A simple squamous epithelium invests a massive capillary network that extends between two arteries that run along the internal margin of the trophonema and a large, central, axial vein (Figures 6.14 and 6.15). The capillaries, with their investing epithelium, are probably the site of transport of amino acids, lipids, and proteins from the maternal blood to the histotroph. In addition, the capillary bed likely functions in gas exchange and waste absorption. A dense stroma of reticular connective tissue supports each trophonema. The efficiency of trophonemata may be enhanced in some species where they are said to enter the foetus by way of the spiracles, pass into the oesophagus, and secrete histotroph directly into the gut.

During mid to late gestation, trophonemata enter their second differentiative phase when some of the epithelial cells form acini among the extensive capillary beds; these synthesize and secrete proteins into the histotroph by way of pits lying between the surface ridges. Thus, the components of histotroph have two origins: transport directly from the maternal blood and synthesis and secretion by trophonemal cells. Simple cuboidal to low columnar epithelial cells cover the cable-like ridges and extend into the crypts (Figures 6.16 and 6.17A) (Hamlett, Wourms, and Smith, 1985; Hamlett et al., 1993a, 1996a). Huge lipid droplets distend these cells but less conspicuous protein secretory granules and mucous droplets are also present (Figures 6.17B,C). Nuclei are round to oval and contain a dispersed pattern of heterochromatin. Scant apical microvilli are present. The epithelium is reinforced by an apical terminal web associated with junctional complexes between adjacent cells (Figure 6.16D and 6.17C). The organelles indicative of protein production are present: well developed granular endoplasmic reticulum, polyribosomes, and an extensive supranuclear Golgi complex (Figure 6.17E). Uncoated vesicles are given off by the Golgi complex and there is a progressive increase apically in the electron density of material contained within vacuoles and presecretory granules.

It is assumed that transport, gas exchange, and waste removal continue during mid to late gestation. As term approaches, the trophonemata become increasingly efficient for respiratory exchange (Hamlett et al., 1993a, 1996a). The surface epithelium at the flattened edges of the trophonemata becomes attenuated and the underlying capillaries become dilated, forming irregular sinusoids that bulge close beneath the surface (Figures 6.18A,B, 6.19A to D). The endothelial cells contain micropinocytotic vesicles and mitochondria. A few reticular fibres separate the basal laminae of the endothelium and epithelium, offering scant resistance to the exchange of gases. Stellate pericytes, common to the microcirculation of many parts of the body, embrace the sinusoids (Figures 6.19D, and 6.20); it has been variously suggested that pericytes are contractile and control the flow of blood through small vessels or that they constitute a mesenchymal reserve of undifferentiated cells.

6.2.2 YOLK SAC PLACENTA OF ELASMOBRANCHS

The most advanced form of viviparity in elasmobranchs is seen in Carcharhinidae and Sphyrnidae where there is haemotrophic exchange of materials between the uterine wall and the YOLK SAC PLACENTA of the foetus (Wourms, Grove, and Lombardi, 1988). Among fishes (with the possible exception of the coelacanth *Latimeria),* the yolk-sac placenta occurs only in sharks; of 253 species of viviparous sharks, about 27% are known to be placental. The yolk sac forms a vascular pad that flattens itself against the uterine wall and nutrients are passed from the maternal blood into the blood of the foetus (Figure 6.21). In most of these sharks, the embryo is lecithotrophic for the first few months of gestation. When yolk reserves are exhausted, usually in mid gestation, the yolk sac placenta becomes functional (Hamlett and Wourms, 1984; Hamlett, Wourms, and Hudson, 1985a; Wourms, Grove, and Lombardi, 1988; Hamlett, 1989; Castro and Wourms, 1993). Haematrophic exchange is augmented, in some placental species, by nutrients provided by histotroph secreted by the uterine wall and absorbed by the foetus, either by way of the gut or other routes.

During gestation, dorsal and ventral folds of the uterine wall may form, creating individual compartments for each developing foetus (Schlernitzauer and Gilbert, 1966). They consist of a simple columnar epithelium enclosing a core of vascular connective tissue and a few smooth muscle cells. Fusion of the folds takes place in the bonnethead shark *Sphyrna tiburo* just after the placentas are established. The orientation of the partitions gradually changes to accommodate the growing foetuses, becoming progressively more longitudinally placed (Figure 6.22). The compartments increase the surface area of the uterine lining both for the secretion of histotroph and also for meta-

bolic exchange between mother and foetus (Hamlett, 1989). The partitions isolate each foetus from its siblings, thereby preventing entanglement of the umbilical stalks and abrasion from developing scales when the egg capsules rupture.

In both aplacental and placental sharks, the yolk sac arises as a ventral outpouching of the embryonic gut and contains the yolk mass enclosed within endodermal epithelium (Hamlett and Wourms, 1984; Wourms, Grove, and Lombardi, 1988). As this endodermal evagination distends, it remains enclosed by the mesoderm and ectoderm of the body wall and is attached to the embryo by the YOLK STALK (Figure 6.23). A split subsequently forms within the mesoderm, creating the EXTRAEMBRYONIC COELOM, a space enclosed by SOMATIC MESODERM on the outside and SPLANCHNIC MESODERM inside.

The wall of the yolk sac consists of six concentric regions: ectoderm, somatic mesoderm, extraembryonic coelom, splanchnic mesoderm, endoderm, and yolk syncytium (Figure 6.24) (Hamlett and Wourms, 1984). The extraembryonic coelom is lined by MESOTHELIUM, a simple squamous epithelium whose flattened cells are pinocytotically active with numerous smooth-walled vesicles associated with their upper and lower cell surfaces (Figure 6.25); dense, membrane-bound, homogeneous granules and longitudinally oriented fibrils occupy the cytoplasm. The mesoderm is invaded by abundant blood vessels that extend from the vitelline artery and vitelline vein of the embryo. Vitelline capillaries, delimited by a basal lamina, are closely apposed to the basal surface of the splanchnic mesoderm. Smooth-walled pinocytotic vesicles occur in both the inner and outer surfaces of the continuous capillary endothelium and the cytoplasm contains dense membrane-bound granules and transport vesicles.

The yolk sac is covered with ectodermal epithelium that is continuous, by way of the yolk stalk, with the ectoderm that encloses the embryo itself (Figure 6.26) (Hamlett and Wourms, 1984; Wourms, Grove, and Lombardi, 1988). The cavity containing the yolk is surrounded by the YOLK SYNCYTIUM[20] and ENDODERMAL EPITHELIUM (Figures 6.27 and 6.28A) and is continuous with the lumen of the gut by way of a passage within the yolk stalk, the DUCTUS VITELLO-INTESTINALIS. During the period of vitellogenic development, yolk platelets from the yolk mass are passed up the ductus by ciliary action of its epithelial cells and are digested and absorbed in the intestine (Figure 6.29) (Hamlett, 1989; Hamlett, Schwartz, and DiDio, 1987). In addition, some enzymatic breakdown of yolk occurs within the yolk syncytium and nutrient macromolecules are transported to the embryo by the abundant blood vessels of the yolk sac (Figure 6.28). The presence of microvilli on some of the simple columnar epithelial cells of the ductus raises the possibility that yolk metabolites are also absorbed within the ductus itself (Figures 6.30 and 6.31). Scattered between the epithelial cells of the ductus are granular ENTEROENDOCRINE CELLS which do not attain the surface and whose secretions appear to be directed basally into the surrounding connective tissue. Enteroendocrine cells constitute part of the PARACRINE SYSTEM; their secretions may have a regulatory effect on adjacent cells[21].

Preimplantation embryos possess transitory EXTERNAL GILL FILAMENTS that originate on the posterior surface of the gill arch and emerge through the gill slits (Figure 6.32) (Hamlett et al., 1985; Hamlett, 1989). These aid in respiration but may also absorb nutrients from the histotroph before the establishment of the yolk sac placenta. Each filament contains a single capillary loop connecting afferent and efferent branchial arteries. During later embryonic life, the filaments are retracted and resorbed when definitive gill lamellae develop at the base of the filaments. At this time, the yolk sac placenta assumes the functions of both respiration and haematrophic nutrition.

Before implantation in placental sharks, the ectoderm covering the yolk sac is a simple, low cuboidal epithelium and, although it appears to be impervious to macromolecules, it may accommodate some respiratory and excretory exchange (Hamlett and Wourms, 1984; Wourms, Grove, and Lombardi, 1988). Interlocking microplicae extend over the epithelial surface except at the periphery where there are ridge-like boundaries between adjacent cells (Figure 6.33A). The cytoplasm of this epithelium is characteristic of cells that are synthesizing and secreting proteins and contains granular endoplasmic reticulum with dilated, vesicular cisternae, many polysomes, mitochondria,

[20] A SYNCYTIUM is a multinucleate mass of protoplasm.

[21] Secretory cells, occurring singly in epithelia of many parts of the body, may release peptides which regulate the activity of neighbouring cells. As a rule these cells do not extend to the surface of the epithelium. They constitute the PARACRINE SYSTEM and may be contrasted with the more familiar endocrine system which releases hormones that act on a target tissue, usually at some distance from the point of release.

a Golgi complex with associated populations of coated and uncoated vesicles, and conspicuous lipid-like inclusions (Figures 6.33B,C). There is no evidence of pinocytotic activity. This epithelium rests on a basal lamina below which is a collagenous stroma containing dense spherical inclusions (Figure 6.33D).

The inner regions of the yolk sac comprise the somatic mesoderm, an intervening narrow extraembryonic coelom, and the splanchnic mesoderm-vitelline capillary region (Figure 6.25) (Wourms, Grove, and Lombardi, 1988). The structure of the somatic and splanchnic mesoderm is similar to that of classic mesothelium, consisting of a single layer of squamous cells lying on vascular, areolar connective tissue. Mesothelial cells have flattened nuclei, longitudinal cytoplasmic fibrils, smooth-walled and coated vesicles, and dense, membrane-bound granules. Surfaces of adjacent cells interdigitate but show few desmosomes. Yolk-sac capillaries, lined by continuous endothelium, are adjacent to the inner surface of the splanchnic mesodermal layer. Abundant endocytotic activity in mesothelial and endothelial epithelia indicates the occurrence of vesicular transport, presumably of materials derived from yolk breakdown. The endoderm is in close contact with the basal lamina of the capillary endothelium. Its cells contain many mitochondria and polyribosomes, heterogeneous smooth-walled vesicles, and many yolk degradation vesicles (Figure 6.34A). The innermost layer, the yolk syncytial layer, contains many heterogeneous yolk granules in various stages of degeneration (Figures 6.34B,C).

As yolk reserves are depleted, the uterine epithelium secretes histotroph that bathes the embryo (Hamlett, 1989). In most sharks, the embryo is still contained within its egg capsule (Figure 6.3). The capsule is 4.7 μm thick in the shark *Mustelus canis* and consists of four or more orthogonally-arranged laminae of fibrous material (Figure 6.35) (Lombardi and Files, 1993). The outer lamina is tightly constructed with no visible pores greater than 250 nm in diameter. The capsule is permeable to materials below a molecular weight of 5 kDa so that urea and glucose cross readily. It is suggested that the egg capsule assists in the establishment and maintenance of the placental attachment by acting as a semipermeable membrane between the intracapsular and extracapsular compartments. In this scheme, the foetus releases solutes of high molecular weight, drawing water from the extracapsular fluids, across the egg capsule, into the capsular compartment (Figure 6.36). The resulting distention of the egg capsule eventually obliterates the extracapsular space, apposing the yolk sac/egg capsule complex against the uterine lining, thereby permitting the subsequent interdigitation of maternal and embryonic tissues in the formation of the yolk sac placenta (Figure 6.37).

Around the time of implantation, when the yolk is consumed, the yolk sac, especially the proximal portion, becomes a hollow, spherical bag supported by richly vascular connective tissue linked to the vitelline artery and vein (Wourms, Grove, and Lombardi, 1988; Castro and Wourms, 1993). Increased ramification of these vessels in the distal rugose placenta combined with surface folding and connective tissue hyperplasia give this region its spongy texture. Initially, the maternal portion of the placenta contains all of the cell layers that are present at nonattachment sites. Although varying degrees of interdigitation and fusion of maternal and foetal tissues enhance the exchange of materials, the selachian placenta is considered to be NON-INVASIVE and NON-DECIDUATE so that maternal and foetal tissues can be separated without detaching uterine tissue (Hamlett, Wourms, and Hudson, 1985c; Hamlett, 1987). There is no bleeding nor shedding of maternal tissue at parturition.

As the foetus implants, the yolk stalk elongates (Gilbert and Schlernitzauer, 1966; Hamlett, Wourms, and Hudson, 1985a; Wourms, Grove, and Lombardi, 1988; Hamlett, 1993; Hamlett, Miglino, and Didio, 1993). When the yolk sac flattens itself against the uterine wall to form the foetal portion of the placenta, the yolk stalk is designated the UMBILICAL STALK; it contains the muscular umbilical artery, umbilical vein, the ductus vitello-intestinalis, and, in most species, a remnant of the extraembryonic coelom (Figure 6.38). The yolk sac becomes regionally modified into two distinct regions: the diaphanous PROXIMAL SMOOTH SEGMENT is confluent with the umbilical stalk and drapes over the richly vascular DISTAL RUGOSE PORTION that abuts the uterine attachment site (Figures 6.39 and 6.40). Increased vascularization of the yolk sac is reflected at the point of contact by enhanced vascularization of the uterine wall. Adjacent regions of the uterus differentiate into PARAPLACENTAL SITES that produce mucus (Figure 6.41). The junction of the vascularized yolk sac and uterine wall is the site at which the embryo will implant and the PLACENTA will be formed. The placenta consists of the ATTACHMENT SITE on the uterine wall, the egg capsule in most species, and the flattened, vascular pad of the foetal yolk sac.

The foetal portion of the placenta includes the umbilical cord, the smooth proximal portion, the richly vascular rugose distal portion, and the egg capsule (Figures 6.42 and 6.43). There are no noticeable differences in the structure from region to region of the yolk sac placenta prior to implantation (Hamlett and Wourms, 1984; Hamlett, 1989; Hamlett et al., 1993a).

In the HAEMATROPHIC nutrition of placental sharks, materials are transferred from the blood in maternal capillaries of the uterine wall to foetal capillaries in the rugose distal portion of the placenta (Schlernitzauer and Gilbert, 1966; Teshima, 1975; Hamlett, Wourms, and Hudson, 1985a,c; Wourms, Grove, and Lombardi, 1988; Hamlett et al., 1993a). Foetal capillaries are better developed than maternal ones in *Mustelus griseus,* thereby facilitating the exchange of materials (Teshima, 1975). In addition, foetal haemoglobin of *Squalus suckleyi* has a greater affinity for oxygen than adult haemoglobin, thereby optimizing the transfer of oxygen from maternal to foetal circulation (Manwell, 1963).

The barriers to the exchange of materials are: maternal endothelium, maternal epithelium, egg capsule, foetal epithelium, and foetal endothelium (Figure 6.44). In different classes of placentas, there may be a reduction in these barriers and an increase in the area of tissue contact by means of interdigitation (Figure 6.45). In some sharks, the number and thickness of layers of cells and extracellular matrix may be diminished. The maternal and foetal epithelia may degenerate, permitting each of the capillary networks to abut its own side of the egg capsule at the maternal-foetal placental junction. The embryonic coelom within the placenta may be obliterated by fusion. The role of the egg capsule as a possible barrier to placental transport is enigmatic since little is known of its permeability (Wourms, Grove, and Lombardi, 1988; Lombardi and Files, 1993). It is presumed that its permeability in viviparous species is enhanced by a reduction in thickness and the possible loss or macromolecular rearrangement of collagen. Although it is a potential permeability barrier, the egg capsule appears to permit the ready passage of small molecules but may hinder passage of macromolecules. In some species, there may be no egg capsule.

During early gestation in the Atlantic sharpnose shark *Rhizoprionodon terraenovae* the uterine wall consists of a simple cuboidal epithelium resting on a layer of vascular loose areolar tissue containing strands of longitudinal smooth muscle (Figure 6.46) (Castro and Wourms, 1993; Hamlett, Miglino, and Didio, 1993). Below is a continuous layer of inner circular and outer longitudinal smooth muscle covered by a closely applied tunica serosa. As gestation continues, vascularization increases in the distal yolk sac as well as in adjacent regions of the uterine wall. The uterine wall increases in thickness and becomes soft and spongy. Its epithelial cells proliferate and become closely packed. When the yolk supply is exhausted, the distal yolk sac implants and becomes enveloped by the uterine wall. At this time, there are two sources of nutrients for the foetus: haematrophic exchange takes place by way of the yolk sac placenta while aplacental regions of the uterine wall produce histotroph. At the implantation site, the uterine wall bears numerous ridges, folds, and protruberances (Figure 6.47) covered with either a pseudostratified epithelium or a layer of short, columnar epithelial cells two cells thick. These projections interdigitate with ridges of the yolk sac, incorporating pleats of the egg capsule between them (Figure 6.48). Extensive capillary beds are embedded in loose areolar connective tissue beneath both the maternal and foetal epithelia; the capillaries may be fenestrated (Figure 6.49). The paraplacental region of the luminal lining of the uterus is also thrown up into elaborate folds whose simple columnar epithelial cells elaborate mucus (Figure 6.50). These folds appear shortly after implantation when the uterine wall begins to produce histotroph, filling the compartment. The epithelial cells of the uterine attachment site are cuboidal to squamous (Hamlett, 1989). Their cytoplasm has a rich array of endoplasmic reticulum and prominent secretion vesicles filled with flocculent material that resembles the substance seen in the space between the uterine epithelium and the egg capsule (Figures 6.51 and 6.52). The appearance of steroid production in these cells may be indicative of an endocrine function in the shark placenta. The aplacental folds continue to grow and increase in complexity until parturition.

ATTACHMENT SITES in the uterine lining incorporate highly vascular folds that interdigitate with deep grooves in the rugose distal portion of the foetal yolk sac (Figure 6.53B) (Hamlett, Wourms, and Hudson, 1985c; Hamlett, 1993). The egg capsule lies between the maternal and foetal epithelia and is closely apposed to both (Figure 6.54). Attachment sites in the sandbar shark *Carcharhinus plumbeus* consist of a simple, low columnar epithelium underlain by an extensive vascular network (Figures 6.53A,E). The ultrastruc-

ture of the uterine epithelium indicates great activity in the transport of materials between the rich blood supply and luminal surface, including features such as the tight junctions sealing the luminal borders, elaborate folding and interdigitation of lateral cell boundaries, branched microvilli, and saccular invaginations of the apical surface; the presence of apical coated pits and numerous coated vesicles probably indicates the transfer of serum proteins to the embryo (Figures 6.53C,D). The uterine epithelial cells also contain lipid-like inclusions, a prominent granular endoplasmic reticulum, and many free ribosomes. The endothelium of the uterine capillaries is pinocytotically active and there is little distance to impede flow between the epithelial cells and the capillaries nor is a significant barrier presented by their thin basal laminas and sparse intervening connective tissue. In addition to the transport of maternal serum proteins, gases, wastes, and possibly immunoglobulins, the attachment sites probably regulate water, electrolytes, and osmoregulatory factors.

The RUGOSE, DISTAL PORTION of the placenta of *C. plumbeus* consists of a simple columnar SURFACE EPITHELIUM of peg-like cells derived from the ectoderm (Figures 6.55A,B), a collagenous STROMA containing vitelline capillaries, and an innermost BOUNDARY CELL LAYER (Figure 6.55K) (Hamlett, Wourms, and Hudson, 1985a). The egg capsule fits closely around the surface epithelium (Figure 6.55C). The ultrastructure of this region bears witness to its haemotrophic function: the surface epithelial cells are closely apposed to the abundant capillaries of the vitelline circulation and give the appearance of active absorption with their extensive apical system of smooth-walled, membranous, anastomosing canaliculi and tubules (Figures 6.55D,E). Active endocytotic uptake of the tracer horseradish peroxidase has been demonstrated in the epithelial cells of the distal placenta but not by the epithelium of the smooth portion nor by the umbilical cord. Whorl-like inclusions in the basal cytoplasm of the surface epithelial cells lie adjacent to the pinocytotically active endothelium of the capillaries and are assumed to be yolk proteins being transferred from the mother to the embryo throughout gestation (Figures 6.55F to I); presumably the same yolk protein precursors that are involved in oocyte growth continue to be produced by the maternal liver and are used as nutrients for the developing embryo after it has exhausted its original supply of yolk. All absorptive activity of the yolk sac appears to have been assumed by the epithelial cells of the ectodermal surface while the formerly active endodermal cells form a supportive BOUNDARY LAYER with scant microvilli and sparse organelles except for a few mitochondria (Figure 6.55J). A well developed collagenous stroma separates the two epithelia.

The SMOOTH PROXIMAL SEGMENT of the shark placenta does not come into contact with the uterine lining but isolates the attachment site by draping over the distal portion of the placenta so that little of it is exposed to the perifoetal compartment contained within the egg capsule (Hamlett, Wourms and Hudson, 1985b). The proximal segment of *C. plumbeus,* consists of outer ECTODERMAL EPITHELIUM, an intervening collagenous STROMA, and the inner MESOTHELIUM (Figure 6.56J). Presumably, with the disappearance of the yolk, the endodermal epithelium has withdrawn from the yolk sac. Capillaries are sparse in the stroma. The surface epithelium bears a prominent glycocalyx. It may be one to three cells thick and contains two cell types (Figures 6.56A,B,C,D,F). Golgi complexes and elements of endoplasmic reticulum are rare in both epithelial cell types and there are few of the organelles characteristic of cells engaged in synthetic activity. Cuboidal cells predominate; these have a dome-like apical surface covered with microvilli and an ovoid nucleus. The second type has a convoluted nucleus and a flattened apex with microvill and cilia (Figures 6.56C,D,G). Microplicae occur on the surfaces of a few cells. Both types contain lipid inclusions, many cytoplasmic filaments, and are joined by desmosomes (Figure 6.56E). Epithelial cells of the middle layer are joined by desmosomes and are similar to those of the surface except that they lack microvilli and cilia. The innermost epithelial cells possess an undulating basal contour and rest on a conspicuous basal lamina. Mesothelial cells are squamous with a fusiform nucleus, many smooth-walled pinocytotic pits, transport vesicles, mitochondria, free ribosomes, and a large number of cytoplasmic filaments (Figures 6.56H,I). The endoplasmic reticulum, except for a few patches of the granular type, and Golgi complexes are poorly developed. The mesothelial cells rest on a prominent basal lamina that separates them from the connective tissue stroma. The function of the proximal portion of the placenta is enigmatic but the presence of well developed collagenous tissue, as well as abundant desmosomes and cytoplasmic filaments within the epithelial and mesothelial cells, suggests that it may resist mechanical stress. The numerous pinocytotic pits and vesicles in the mesothelial cells may

indicate fluid exchange between the cavity of the placenta and the perifoetal compartment within the egg capsule. Structures characteristic of steroid secretion have been described in the simple cuboidal epithelium of the smooth proximal segment of the yolk sac of *Rhizoprionodon terraenovae:* mitochondria with tubular cristae, agranular endoplasmic reticulum, and extensive lamellar bodies (Figure 6.57) (Hamlett, 1993). It is suggested that these cells may be a source of oestradiol and testosterone.

Umbilical stalks of most species of *Carcharhinus* are smooth and their squamous epithelium appears not to be permeable to the fluids within the uterus. In many selachians, however, the stalk is festooned with arborescent, richly vascular, absorptive processes called APPENDICULAE (Figures 6.58 to 6.61) (Hamlett, 1986, 1987, 1989, 1993; Wourms, Grove, and Lombardi, 1988; Castro and Wourms, 1993; Hamlett et al., 1993a). These outgrowths may be of various shapes: flattened or cylindrical, finger-like or club-shaped, sometimes branching. After placentation has occurred, it has been suggested that the placental uterine wall continues to secrete histotroph until parturition although, perhaps, only in species that possess appendiculae (Hamlett, 1989).

Appendiculae of *R. terraenovae* form vascular, lobed protrusions from the umbilical cord (Hamlett, 1993; Hamlett et al., 1993a,b) (Figure 6.61A). They are covered with continuations of the surface epithelium of the stalk and enclose a core of richly vascular areolar connective tissue. The epithelium consists of MICROVILLAR and GRANULAR CELLS subtended by flattened BASAL CELLS (Figures 6.61C,D,G). Microvillar cells, bristling with long microvilli, form pyriform processes that are insinuated between adjacent cells; their cytoplasm contains lipid and micropinocytotic vesicles at the apex. Dilated intercellular spaces often occur between adjacent cells and may represent functional transport channels. Microvillar cells absorb nutrients produced by the uterus as well as exogenous material of the size of proteins. Granulated cells undergo cycles of synthesis so that different secretory phases may be observed within a single tissue section (Figures 6.61D to F). Cells seemingly devoid of most organelles have just undergone exocytosis; granular endoplasmic reticulum is active in other cells and the supranuclear Golgi complex is prominent. As synthesis proceeds, the apical cytoplasm becomes engorged with secretory droplets, displacing the mitochondria to the base of the cell; following exocytosis, the synthesis-secretion cycle repeats. The nature of the secretory material is unknown. In addition to absorption of nutrients from the histotroph, appendiculae are probably engaged in respiration and ion regulation of the periembryonic fluid. It is difficult to speculate on other functions until the nature of the secretory droplets is known. Beneath the surface layer is a layer of basal cells that rest on the basal lamina (Figure 6.61D) It is believed that these cells are generative and provide replacements for the surface epithelial cells.

The core of the umbilical cord contains an artery, vein, and the ductus vitello-intestinalis (Figure 6.60). These structures are invested by vascular fibrous connective tissue containing occasional smooth muscle fibres (Figure 6.62A). The ductus vitello-intestinalis is lined by a simple columnar epithelium of interspersed ciliated and microvillous cells (Figures 6.62B,C). The apical borders of these cells are sealed by tight junctions while desmosomes reinforce their lateral membranes. Mitochondria are abundant apically; a modest Golgi complex, scant granular endoplasmic reticulum, lipid droplets, and moderate glycogen deposits fill out the cytoplasm. A little agranular endoplasmic reticulum is observed. Deeply wedged between the bases of these surface epithelial cells are scattered fusiform enteroendocrine cells filled with membrane-bound electron-dense granules (Figures 6.62D,E). As is usual with these cells, the nucleus is apical and the granules are in the basal cytoplasm. The apparent inversion of these cells indicates that they do not deposit their secretions into the lumen but rather into connective tissue near capillaries. Their cytoplasm is rich in granular endoplasmic reticulum and free ribosomes. Presumably these cells have a paracrine function, modulating the activity of local areas of the placenta.

No egg capsule intervenes in the placenta of the blue shark *Prionace glauca* (Otake and Mizue, 1985). Cells of the simple columnar uterine epithelium present the classic appearance of protein secretion: abundant basal granular endoplasmic reticulum, supranuclear Golgi complexes, and apical secretory vesicles; they appear to secrete an electron-dense material that accumulates in the space between maternal and foetal tissues (Figures 6.63A to F). Abundant capillaries are closely applied to the epithelium and junctional complexes seal the apical borders between adjacent cells. Two layers of cells constitute the epithelium of the distal portion of the foetal yolk sac (Figures 6.63G to K). Huge, superficial cells, bristling with microvilli, appear active in the vesicular uptake of macromolec-

ular material. Their apical cytoplasm is packed with tubular structures and coated vesicles while most of the cytoplasm contains scattered granular and agranular endoplasmic reticulum. Desmosomes connect the cells laterally. The flattened basal cells contain mitochondria and endoplasmic reticulum. Their indented basal surface is separated by two thin basal laminas from the extremely thin, fenestrated endothelial cells of the underlying capillaries. This description presents a picture of ready uptake by vitelline capillaries of macromolecular material produced by the uterine epithelium. Since both maternal and foetal epithelia within the placenta are thick, however, they do not seem to be conducive to gaseous exchange between maternal blood and the uterine fluid and this exchange appears to take place in aplacental regions of the intrauterine lining where the epithelium is thin and closely applied to abundant underlying capillaries which may be fenestrated (Figure 6.64A) (Otake and Mizue, 1986). In addition, the uterine epithelium displays the characteristics of highly active fluid transport, suggesting its involvement in osmoregulation of the uterine fluid: its cells show abundant branching microvilli, elaborate intercellular spaces sealed by apical tight junctions, and elaborations of the basal plasmalemma. There is some evidence of secretion although scant endoplasmic reticulum or Golgi complexes are seen (Figures 6.64B to E); a few goblet cells are scattered here and there. Foetal involvement in gaseous exchange and water-solute transport probably takes place in the proximal region of the placenta.

An extreme example of placental efficiency is seen in *Scoliodon laticaudus (sorrakowah)* where there is virtually no lecithotrophic phase and the embryo implants immediately after ovulation; this is probably the most highly evolved example of viviparity in sharks (Teshima, Ahmad, and Mizue, 1978; Wourms, 1993). The oocyte is probably the smallest of all sharks, about 1 mm in diameter, and nutrition of the embryo is almost completely matrotrophic. Placentation commences soon after implantation and the foetus is dependent upon its mother until parturition. The uterine wall forms stalked, richly vascular, goblet-shaped TROPHONEMATOUS CUPS into which the foetal portion of each placenta fits (Figure 6.65). This placenta is highly vascular and the barriers to the exchange of nutrients are greatly reduced by the elimination of the egg capsule and possible degeneration of the uterine epithelium during late development. It is assumed that maternal nutrients are conveyed to the embryo both by haematrophic transfer across the placenta and by imbibition of uterine fluid into the gut; in the absence of physiological studies, it is not possible to determine the relative contribution from each source. As might be expected in the virtual absence of yolk, there is no ductus vitello-intestinalis (or else it is obliterated early in development) (Figures 6.66B,C). The umbilical stalk becomes extremely long and is adorned by abundant, long appendiculae whose dense capillary beds, closely underlying the thin epithelium, impose their embossed cable-like pattern on the surface (Figures 6.66A,D). It seems likely that the major function of the appendiculae is gas exchange but they may also participate in other activities such as excretion.

6.3 Viviparity in Coelacanths

Latimeria chalumnae is viviparous (Wourms, Atz, and Stribling, 1991). The eggs are remarkably large and contain massive amounts of yolk. Each foetus is contained within its own, well-vascularized compartment within the uterine region of the right oviduct (Figure 6.67). Embryos are lecithotrophic during the early and middle stages of development with oophagy (the ingestion of supernumerary eggs by developing young) as a probable source of additional nutrients. The yolk sac of late term foetuses is large, flaccid, heavily-vascularized and nearly devoid of yolk (Figure 6.68). A massive vascular plexus develops in the wall of the uterine compartment at its site of contact with the yolk sac and together these richly vascularized tissues form a yolk sac placenta. Since there is no interdigitation of maternal and foetal tissue, the yolk sac is free to move and the placenta is said to be non-adherent or transposable. Regions of the uterine wall that are adjacent to other parts of the foetus do not develop this rich vascularization nor is it seen in the non-gravid uterus.

The placental regions of the uterine lining are embossed by an anastomosing network of capillaries covered by a thin, simple squamous epithelium whose surface may be amplified, either by pleats, ridges, or branching processes (Figure 6.69A). Beneath the capillary network lies a subcortical sinus that appears to be lined by endothelium. Surrounding this are a well vascularized connective tissue stroma, alternating layers of transverse and longitudinal smooth muscle, and a simple squamous serosal epithelium (Figure 6.69B).

Most of the wall of the yolk sac consists of a dense stroma of fibrous connective tissue (Figure 6.69C).

Its external surface is convoluted and folded (Figures 669D,E) and consists a simple squamous epithelium adhering closely to an intercommunicating bed of cortical sinuses, presumably derived from the vitelline circulation. The internal surface is laced with blood vessels from the vitelline circulation and is lined by a layer of yolk-digesting endoderm and syncytial cells.

The primary function of the yolk sac placenta is presumed to be gas exchange and the exchange of materials of low molecular weight such as metabolites and metabolic wastes. There is little evidence that uterine histotroph plays a significant role in nutrition of the embryos and oophagy may well be the major source of supplemental nutrition.

6.4 Viviparity in Teleosts

Viviparity has evolved independently in several groups from two orders of teleosts: Cyprinodontiformes and Perciformes (Hoar, 1969; Wake, 1985). In the absence of Müllerian ducts, there are no uteri or true oviducts and a channel to the exterior is formed either from a sheath of peritoneal folds outlying the ovary or from the tissue of the ovary itself. Since these structures conduct genital products to the outside it is appropriate to designate them "oviducts" although they are not homologous with oviducts of other vertebrates. Because of their origins, however, they lack the competency for hypervascularization and secretion that is required of a nutritive chamber and, instead, the cystovarian ovary of all viviparous teleosts provides the hospitable environment required for gestation: the lumen is lined with peritoneum and the developing embryos are shed into this sanctuary instead of being released into the coelom as in other vertebrates (Figure 6.70).

Fertilization is internal in viviparous animals. As far as is known, in all teleosts, with the exception of *Zoarces,* it occurs within the ovarian follicles. Sperm are deposited in the oviducts and ovarian lumen where they may be stored for long periods, being nourished by cells of the luminal epithelium (Figures 6.71 and 6.72) (Jalabert and Billard, 1969; Nagahama, 1983; Pusey and Stewart, 1989; Burns et al., 1995; Muñoz, Casadevall, and Bonet, 1999). A diverticulum of the lumen may form a SEMINAL RECEPTACLE lined by a simple epithelium resting on a prominent basal lamina; sperm heads appear to be embedded within the epithelial cells (Figures 6.73 and 6.74) For the several months between copulation and fertilization in *Cymatogaster aggregata,* sperm are held within sperm pockets in the luminal epithelium, undergoing no morphological changes detectable with the electron microscope (Gardiner, 1978). The sperm heads maintain a close association with the unspecialized cells lining the pockets but the plasma membranes of each sperm and epithelial cell remain intact, separated by a space of several nanometers (Figure 6.75). About one month after fertilization, residual sperm are no longer housed within the pockets and have either been taken up by granulocytes or consumed by the developing embryos.

Similar retention of sperm occurs in the oviduct of the oviparous poeciliid platyfish *Xiphophorus maculatus* (Potter and Kramer, 2000). The oviduct or GONODUCT is lined by simple to pseudostratified mesothelium derived from the lining of the ovarian lumen (Figure 5.4). An elaborate array of surface modifications festoons the cells of the lining: scallops, lobular extensions, microvilli, microvillous appendages, and deep intracellular invaginations (Figure 5.5). The sperm become associated with special epithelial cells, SPERM-ASSOCIATED CELLS, that lack extensive surface microvilli but contain an array of deep surface pits and pockets. The sperm lie either within the invaginations or are taken up and incorporated within the cytoplasm of these cells (Figure 5.6). Intact sperm nuclei, neck, mitochondria, and flagella can be seen within the pits and pockets while sperm nuclei, without flagella or other organelles, occur deep within the cytoplasm of the sperm-associated cells. There is no indication of lysosomal activity or sperm breakdown. Rejection of sperm by the immune system of the female is probably averted by the barrier provided by apical junctional complexes between the epithelial cells (Figure 5.6A).

At the time of fertilization, ovarian follicles approach the inside of the luminal epithelium and a small depression or DELLE may form in the epithelium (Figure 6.73), creating a thin membrane between sperm and egg (Nagahama, 1983). Presumably a sperm penetrates this thin barrier and fertilization is effected in the absence of a micropyle. Small pockets of the luminal epithelium extend toward the mature follicles in *Heterandria formosa,* forming a thin epithelial disc pressed against the follicular epithelium (Figure 6.76A) (Fraser and Renton, 1940). When the ovum is ready for fertilization, it extends a spherical protruberance toward the luminal pocket (Figure 6.76B). Large numbers of sperm swarm toward the thin membrane separating them from the ovum and

one of them must penetrate to effect fertilization. After entrance of the sperm, the protruberance is withdrawn and the epithelium of the follicle and that of the pocket form a plug of cells that projects into the ovarian lumen (Figure 6.76C).

Cleavage commences and development begins within the follicle. At some point, the egg is expelled into the ovarian lumen and development is completed (Wourms, 1981). In some species, most development occurs within the follicle so that gestation is FOLLICULAR and a highly advanced embryo is released[22] into the lumen. In LUMINAL gestation, the embryo is released into the lumen at an early stage and most development occurs within the ovarian lumen. *Jenynsia* is an intermediate form where the first half of development occurs within the follicle and the latter half within the ovarian lumen. In all situations, the embryo is enveloped by a richly vascularized nutritive epithelium that has been provided by the ovary. Depending on whether gestation is follicular or luminal, the embryos undergo a longer or shorter sojourn in the ovarian lumen before being released to the exterior in the process of parturition. Since there is no direct contact between maternal and foetal membranes, the transfer of nutrients, gases, electrolytes, and wastes in matrotrophic species is mediated through a viscous secretion of the follicular or luminal epithelia, the EMBRYOTROPH (Schindler and Hamlett, 1993). Indeed, richly vascular postovulatory follicles may continue to be active and contribute to the embryotroph during luminal gestation (Korsgaard, 1983). Viviparity in several species of two genera of halfbeaks (Hemiramphidae) has been divided into five categories depending on whether development is follicular or largely luminal as well as upon the degree of lecithotrophy/matrotrophy present (Meisner and Burns, 1997).

6.4.1 FOLLICULAR GESTATION

Follicular gestation, where the embryo develops within the ovarian follicle, is known to occur in two families of Perciformes (Labrisomidae and Clinidae) and three families of Cyprinodontiformes (Poeciliidae, Hemiramphidae, and Anablepidae) (Schindler and Hamlett, 1993). The evolution of follicular gestation has required the solution of several functional problems (Grove and Wourms, 1994): spermatozoa must cross the follicular wall for fertilization to occur, the site of gestation must be compartmentalized from other maternal tissues in order to maintain the appropriate environment for embryonic development and to protect the embryo from the maternal immune system, and there must be metabolic exchange between the mother and the embryo. In addition, in those species where embryonic nutrition is matrotrophic, nutrients must cross the follicular epithelium.

In some species, the follicle is little more than a passive holding chamber for the embryo while in others its wall becomes secretory and richly vascular, providing nutrients and carrying away wastes. Often the secretions of the follicular epithelium are enhanced by increases in its surface area provided by elaborations such as villi or ridges. These structures constitute the maternal contribution to the "follicular placenta"; the foetal component is a closely apposed, richly vascular and expanded pericardial sac and yolk sac (Wourms, 1981; Grove and Wourms, 1991). This maternal-embryonic association varies with the quantity of yolk in the egg (Hoar, 1955, 1957). If yolk is abundant, the follicular wall merely becomes fibrous and vascular and intimately associated with the expanded pericardial sac of the embryo (Poeciliidae). If the yolk mass is small, both the follicular wall and the embryo are modified to form a vascular, loose, placental type of interconnection (Anablepidae).

Although there seems to be little maternal-embryonic transfer of nutrients in the guppy, *Lebistes reticulatus* (Poeciliidae), there are structural responses to the presence of an embryo (Jollie and Jollie, 1964a,b); perhaps the follicular placenta provides for respiratory and osmoregulatory demands during gestation (Schindler and Hamlett, 1993). As the embryo develops, vascularity of the follicle increases and tonofilaments, apparently associated with desmosomes, accumulate within cells of the thecal layers, strengthening the follicle; there appears to be no increase in the number of collagenous fibres (Jollie and Jollie, 1964b). The maternal portion of the PLACENTA is the richly vascular portion of the follicular wall where maternal capillaries approximate embryonic capillaries of the yolk sac (Figure 6.77). In this region, the zona pellucida disappears about three to four weeks after fertilization. The follicular epithelium is composed of actively pinocytotic squamous cells that resemble

[22] The word "ovulation" is sometimes used for the release of a fertilized embryo of viviparous species from the follicle into the ovarian lumen. This usage seems inappropriate and the term "hatching" is preferred.

endothelial cells. No embryonic vascularity is evident in regions where the zona pellucida is still present in the space between the follicular wall and embryonic surface and the follicular wall is largely avascular and thinner. The PLACENTAL BARRIER, at the time of closest approximation of maternal and foetal blood, consists of six or seven layers: maternal capillary endothelium; maternal capillary basement membrane; inner follicular epithelium; fertilization membrane (if present); foetal yolk sac epithelium; foetal capillary basement membrane; and foetal capillary endothelium. Micropinocytosis appears to be the only mechanism by which transplacental exchange is effected and micropinocytotic vesicles are abundant in all cellular layers of the barrier. Although there are distinct changes in the steroidogenic potential of the follicles during the reproductive cycle of the guppy, no particular steroid seems to be involved in maintaining gestation (Venkatesh et al., 1992).

Grove and Wourms (1994) describe gestation in *Heterandria formosa,* a matrotrophic species where embryos increase in dry weight about 40 fold during development within the ovarian follicle. Nutrient transfer is presumed to occur across a follicular placenta that is formed by the close apposition of the embryonic surface to the follicular epithelium. ("Embryonic surface" includes the entire body surface during early gestation and the pericardial amnion-serosa during mid and late gestation.) The single hollow ovary occupies most of the body cavity in gravid females (Figure 6.78). Because *H. formosa* displays superfoetation, embryos at about five stages of development may be obtained from the same ovary. (Embryos at three stages of development are visible in the figure.) The ovary consists of an outer simple epithelium, an ovigerous stroma of connective tissue, and an inner simple epithelium that lines the lumen. The lumen is connected to the exterior by a short duct just posterior to the anus. Pockets of the lumen penetrate the stroma and extend between the follicles. Each follicle is supplied with blood from a median, dorsal blood vessel that branches extensively along the length of the ovary. The blood supply to individual follicles increases after fertilization by development of an extensive capillary network at the base of the follicular epithelium.

During vitellogenesis, the zona pellucida and follicular epithelum are typical of those of other teleosts (Figure 6.79). The zona pellucida is a dense matrix, penetrated by microvilli from the oocyte. The simple cuboidal epithelium of the follicle lacks the membrane specializations typical of transporting cells: apical microvilli, junctional complexes, and basal surface specializations. The numerous microvilli that extend through the egg envelope from the oocyte are closely associated with the follicular cells and extend into surface invaginations. Apical, lateral, and basal coated pits and coated vesicles are prominent. Follicular cells are closely applied to each other along their lateral surfaces but no junctional complexes, desmosomes, or lateral infoldings are present. The follicular epithelium rests on a well-developed basal lamina. Only a few capillaries are associated with the follicle. As in other teleosts, yolk proteins and other metabolites destined for the oocyte likely cross the follicular epithelium by an intracellular route. The presence of coated pits and vesicles as well as other vesicular structures indicates that follicular cells may also absorb and process exogenous proteins.

Follicular cells undergo a dramatic change in morphology after fertilization and acquire the ultrastructural features typical of transporting cells. Junctional complexes are seen at an early stage (Figure 6.80); apical microvilli and surface invaginations appear later. The zona pellucida, now called the egg envelope, is much thicker than that of vitellogenic oocytes and is not perforated by microvilli. Dense extracellular material lies between the egg envelope and the follicular cells. Capillaries of the follicular circulation lie beneath the well developed basal lamina (Figure 6.81). By the time embryos reach the early tailbud stage, the follicular placenta is fully differentiated and the ultrastructure of the follicular cells indicates, by displaying apical microvilli, apical junctional complexes, surface invaginations, and an extensively folded basal surface, that the follicular epithelium is specialized for maternal-embryonic transport (Figures 6.82 and 6.83). Apical and basal coated pits are present. The cytoplasm contains granular endoplasmic reticulum, Golgi complexes, and electron-dense vesicles that may be lysosomes. Numerous apical electron-lucent vesicles appear to be derived from the apical surface and may indicate that these follicular cells absorb and process follicular fluid. The well developed junctional complexes between the follicular cells form a barrier to the free movement of large molecules and ions and effectively isolate the embryo from the mother; this barrier may be important for immunological protection of the embryo, preventing its rejection by the mother. The egg envelope, which lacks perforations and remains intact throughout gestation, becomes progres-

sively thinner and less dense as gestation proceeds. Presumably nutrient molecules in the maternal circulation cross the capillary endothelium, either by diffusion or transcytosis, cross the basal laminae separating the capillaries and follicular epithelium, and then cross the follicular epithelium by a transcellular route. Nutrient molecules entering the intrafollicular space then cross the egg envelope to be absorbed by surface cells of the embryo. Extensive folding of the basal surface of the follicular cells and the possibility that the egg envelope may act as a molecular filter suggest that molecules of low molecular weight may constitute a significant part of the nutrient traffic across the follicular placenta. Morphological evidence of macromolecular uptake by follicular cells and the embryonic surface is provided by the endocytotic pits and vesicles at the base of the follicular epithelium and on the surface of absorptive cells on the embryo.

An extreme of matrotrophic nutrition is seen in the four-eyed fish *Anableps* spp., where embryos increase in dry weight by as much as 8,000 times during gestation (Turner, 1938a; Knight et al., 1985). Nutrient transfer is facilitated within the follicular placenta by increases in surface area provided by richly vascular, hemispherical projections, the VASCULAR BULBS, on the pericardial sac; in addition, microplicae on the surface of the bulbs further amplify their surface area for exchange (Figure 6.84). During mid to late gestation, the juxtaembryonic follicular epithelium differentiates into two regions: a region of shallow pits where the vascular bulbs come to interdigitate in a ball-and-socket fashion with the follicular wall (Figures 6.85A to F) and a region where the follicular epithelium forms long, vascular villous extensions (Figures 6.85G,H). The follicular cells of both regions appear to constitute a transporting rather than a secretory epithelium. No egg membrane inhibits the exchange of materials by intervening in the fluid-filled space between the maternal and embryonic epithelia (Figure 6.84, Pl. 3). In terms of percentage weight increase, the follicular placenta of *Anableps* appears to be the most efficient adaptation for maternal-embryonic nutrient transfer in teleost fishes and closely approximates the efficiency of oophagy and embryonic cannibalism of lamnoid sharks.

Clinus superciliosis is a matrotrophic clinid (Order Perciformes) that breeds all year round and exhibits extreme superfoetation: as many as 12 broods may be found within the ovary of a single female (Veith, 1979b). Autoradiographic studies reveal that nutrients, in the form of amino acids, are secreted by the follicular epithelium and absorbed by embryos of *C. superciliosus* and *C. dorsalis* within the follicle, especially by the epidermis (including that of the fins) and the gut (Veith, 1980; Cornish, 1985).

6.4.2 LUMINAL GESTATION

The ovarian epithelium plays the dominant role in the transfer of nutrients from the mother to the embryo during luminal gestation in matrotrophic species (Hoar, 1955; Schindler, 1990). In early stages of gestation, the epithelial cells of the ovigerious folds become hypertrophied and there is increased vascularization of the supporting connective tissue. Since there is no attachment between maternal and foetal tissues, the passage of all substances is mediated by way of EMBRYOTROPH (Schindler and Hamlett, 1993). Ovigerous folds may form compartments around the embryos, increasing surface area of contact and enhancing efficient nutrient transfer (Figures 6.86 and 6.87). Various organs have evolved into a range of structures for the transfer of nutrients (Table 6.1) (Wourms, 1981; Wake, 1985; Wourms, Grove, and Lombardi, 1988; Schindler and Hamlett, 1993). Leaf-like extensions from the luminal wall of the ovary may partly fill the gill cavities and mouth of the embryo (Figure 6.88) to provide a specialized organ for transfer of materials between adult and embryo. The yolk sac, pericardial sac, and coelomic sac play a major role in nutrient uptake in several species (Figure 6.89); flat vascular extensions of soft absorptive tissue grow between the rays of the vertical fins of Embiotocidae; in a few teleosts, finger-shaped or ribbon-like extensions of the proctodaeum, the TROPHOTAENIAE, take up materials from the embryotroph (Figure 6.90). Other nutritive devices have also been described but by far the greatest amount of morphological and physiological study has been directed to the trophotaeniae of goodeids.

Ovarian Luminal Epithelium

The wall of the cystovarian ovary of viviparous teleosts consists of four layers: the luminal epithelium, connective tissue stroma, a layer of smooth muscle, and peritoneum. The lumen may be partitioned by ovigerous folds whose epithelium and connective tissue core are continuous with those of the ovarian wall; some of the ovigerous folds enclose developing follicles (Figures 6.87 and 6.91). The connective tissue

TABLE 6.1. Trophic patterns in viviparous fishes (From Wourms, 1981)

- I. Facultative viviparity
- II. Obligate viviparity
  - A. Lecitrophy
  - B. Matrotrophy
    1. Oophagy and adelphophagy
    2. Placental analogues
       a. Epidermis and fin epithelium
       b. Gill epithelium
       c. Trophonemata
       d. Branchial placenta
       e. Yolk sac
       f. Pericardial amnion and chorion
       g. Follicular pseudoplacenta
       h. Hypertrophied gut
       i. Trophotaeniae
    3. Yolk sac placenta

stroma contains numerous stellate fibroblasts, bundles of collagenous fibres 1 to 3 μm in diameter, and large blood vessels; a well-developed capillary bed is apposed to the basal lamina of the epithelium (Figures 6.92A and 6.93C). The muscle consists of a thin outer sheet of longitudinal fibres and an inner circular layer (Figure 6.93A) (Lombardi and Wourms, 1985a).

The luminal epithelium of goodeids is simple squamous to cuboidal and is derived from the peritoneal epithelium (Lombardi and Wourms, 1985a; Schindler, Kujat, and de Vries, 1988; Schindler, 1990; Hollenberg and Wourms, 1995). It lines the lumen, covering the richly vascular ovigerous folds. The epithlial cells are often domed, reminiscent of a transitional epithelium (Figure 6.94). Fissures separate the epithelial cells, giving the surface a cobblestone appearance in scanning electron micrographs (Figures 6.93B,C); these MARGINAL CLEFTS may become deep and may contain leucocytes (Figure 6.95) (Hollenberg and Wourms, 1995). The surface cells become flattened in a gravid ovary as the epithelium stretches to accommodate the developing embryos; the subepithelial connective tissue swells, forcing the capillaries closer to the surface, thereby reducing the blood-embryotroph pathway (Figures 6.96A,B) (Schindler, Kujat, and de Vries, 1988).

The lateral membranes of the epithelial cells interdigitate and the cells are connected by large desmosomes with thick attachment plaques; intermediate filaments radiate into the cytoplasm from the plaques (Figures 6.92B and 6.97). Tight junctions are not conspicuous between the epithelial cells and the intercellular distances are the same in the adluminal position as elsewhere along the lateral membranes. Often desmosomes occur in positions where tight junctions would be expected. Many tonofilaments (intermediate filaments) permeate the epithelial cells; many are continuous with the filaments associated with the attachment plaques of the desmosomes (Figure 6.98). The resemblance of the luminal epithelium to a transitional epithelium and the reinforcement provided by desmosomes and intracellular tonofilaments would be expected in a membrane subjected to the distension brought about by its burden of growing embryos. The well developed collagenous layer below the epithelium, evident in several of the figures, is consistent with this explanation.

The apical surface of the epithelial cells is without extensions except for occasional cilia. Endocytotic activity may be observed on all surfaces of the cells, increasing greatly in gravid ovaries (Figures 6.96C,D and 6.99). The cytoplasm is criss-crossed by organized bundles of intermediate filaments and contains scant granular endoplasmic reticulum, several mitochondria, Golgi stacks, and a diversified vacuolar apparatus composed of numerous small vesicles, some

lysosome-like vesicles and multivesicular bodies, and a few short tubules (Figure 6.93D). The epithelial cells exhibit morphological features associated with the vesicular transport of macromolecules and appear inadequate for the synthesis of proteinaceous secretions; it is suggested that they pass along macromolecules derived from the serum (Schindler, Kujat, and de Vries, 1988; Schindler, 1990; Schindler and Kujat, 1990; Hollenberg and Wourms, 1995). The only recent dissenting voice in this general acceptance of vesicular transport by the luminal epithelium is that of Lombardi and Wourms (1985a) who describe the presence of granular endoplasmic reticulum, a Golgi complex, and spherical vesicles within the apical cytoplasm in the goodeid *Ameca splendens,* suggesting a secretory process similar to that of other protein secreting cells. A form of apocrine secretion by the luminal epithelium has been suggested in some species where apical blebs appear to be released into the luminal cavity, possibly contributing to the embryotroph (Figure 6.100) (Hollenberg and Wourms, 1995).

The thin layer of epithelial cells is separated from the attenuated endothelial cells of the capillaries by a delicate web of collagenous connective tissue and the thin basal laminae of both epithelia so that there is slight barrier to the passage of materials from the lumen of the capillaries to the lumen of the ovary (Figures 6.92A,C) (Lombardi and Wourms, 1985a; Schindler, 1990; Schindler and Kujat, 1990). Indeed, the large nuclei of the epithelial cells become recessed between the meshes of the capillary network, thereby reducing the blood-embryotroph pathway, in some places, to less than 1 μm (Figure 6.101).

In the jenynsiid, *Jenynsia lineata,* where no placenta forms and the embryos suckle on "nipples" formed from the luminal wall, the structure of the nutritive epithelium is remarkably similar to that of goodeids (Schindler and de Vries, 1988b). In *Jenynsia,* long, richly vascular, branching folds of the luminal wall form VILLI OVARIALES that grow into one opercular cleft of each embryo, establishing contact between the maternal nutritive tissue and the embryonic digestive tract (Figures 6.102 and 6.103) (Turner, 1940d). As in the goodeids, the luminal epithelial cells show evidence, both apically and basally, of vesicular transport of macromolecules, appearing to serve for the transcellular passage of maternally-derived substances (Figure 6.104A). Since there is little ultrastructural evidence of protein production, it is assumed that the epithelium is not a source of secretory products. The epithelium of both the lumen and villi is simple squamous. Zonulae occludentes are abundant between the apical borders of adjacent cells and the epithelium is continuous except for a few gaps at the tips of the villi that allow paracellular passage of particulate matter (Figure 6.104B). Most adjacent cells interdigitate (Figure 6.104C), presumably providing plasmalemmal reserves that accommodate variations in height of the epithelium. The luminal epithelium rests on a thin basal lamina. The epithelial cells contain abundant filaments, electron-dense granules, mitochondria, polysomes, a Golgi complex, and a variety of vacuoles (Figure 6.104A); granular endoplasmic reticulum is sparse.

Embryotroph

Embryotroph contains lipids, amino acids, glucose, and other sugars; its content of proteins is low. The mean osmolarity of embryotroph has been shown to be higher than that of the plasma so that there tends to be an influx of fluid into the gestational chamber (Veith, 1979a; Korsgaard, 1983; Cornish and Veith, 1987). Electrophoretic comparisons of maternal blood serum and the embryotroph indicate many similarities in the composition of these fluids (Kristofferson, Broberg, and Pekkarinen, 1973; Korsgaard, 1983; de Vlaming et al., 1983; Schindler and de Vries, 1988a; Schindler and Kujat, 1990; Schindler and Hamlett, 1993; Hollenberg and Wourms, 1995). Since most ultrastructural studies of the maternal epithelia present little evidence of protein production, it is suggested that embryotroph is elaborated by transcytosis, where materials are taken up by endocytosis at one surface of an epithelial cell, pass across the cell unchanged within pinocytotic vesicles, and are released at the other surface by exocytosis (Schindler and de Vries, 1988a; Schindler, 1990). In addition, sibling embryos, whose development has been arrested, atretic ova, and sloughings from the luminal epithelium, may provide another source of embryotrophic proteins (Hollenberg and Wourms, 1994).

Although urea was absent from the maternal serum of surfperches (Embiotocidae), large amounts were detected in the embryotroph suggesting that embryos, but not adults, produce urea as a nitrogenous waste and that the ovarian membranes are relatively impermeable to it (de Vlaming et al., 1983).

Embryonic Absorptive Epithelia: Trophotaeniae

Some embryos develop absorptive extensions of the proctodaeum, the TROPHOTAENIAE, which assist in the uptake of materials from the embryotroph (Figure 6.105). Although most descriptions have been from goodeids of the Order Cyprinodontiformes, the presence of trophotaeniae has also been noted in members of two other orders: the zoarcid, *Parabrotula dentiens* (Perciformes) (Figure 6.106) (Turner, 1936) and in the bythitid *Oligopus longhursti* (Ophidiiformes) (Wourms and Cohen, 1975). Trophotaeniae are closely applied to the wall of the ovarian lumen and, together, these two components constitute the TROPHOTAENIAL PLACENTA (Lombardi and Wourms, 1985b; Schindler and Kujat, 1990). Facilitating the exchange of materials are dense capillary beds lying beneath both the luminal and trophotaenial epithelia.

Trophotaeniae are rosette- or ribbon-like extraembryonic processes extending from the perianal region of most goodeid embryos (Figures 6.107A,B); during gestation, they are bathed in the embryotroph secreted by the internal luminal epithelium but do not appear to establish permanent relationships with this epithelium (Figures 6.107F and 6.108) (Lombardi and Wourms, 1985b; Hollenberg and Wourms, 1994). Individual trophotaeniae commonly contain two to three major blood vessels deeply embedded in a core of loose connective tissue that is surrounded by the closely apposed trophotaenial epithelium (Figures 6.107C,D,E). In the connective tissue, wavy collagenous fibres and stellate fibroblasts with long cytoplasmic processes are commonly oriented in successive transverse lamellae about 10 to 20 μm apart. Blood is supplied through a ventral ramification of the dorsal mesenteric artery. Within each trophotaenia, the arteries branch extensively giving rise to a capillary bed that extends throughout, immediately beneath the basal lamina of the epithelium. Blood is drained by trophotaenial veins situated on either side of the posterior hindgut; these join the subintestinal vein which carries blood to the hepatic portal vein.

At the base of each trophotaenia there is a confluence of the endodermal epithelium lining of the gut and the ectodermal epithelium of the integument. These epithelia merge as the trophotaenia elongates, forming a mosaic of ABSORPTIVE CELLS (derived from enterocytes) surrounding small islands of stratified squamous PAVEMENT CELLS (from the integument). These regions may be distinguished in scanning electron micrographs by the forests of microvilli on the surface of the absorptive cells and the fingerprint patterns of microridges on the pavement cells (Figure 6.109) (Schindler and de Vries, 1986a,b; 1987b). Capillaries, that are fenestrated in some species, nestle against the basal lamina of the epithelium (Figures 6.110 and 6.111A) and carry absorbed materials to the sinus-like blood vessels in the mesenchymatous core of the trophotaenia from whence they are drained into the foetal hepatic portal system.

Trophotaenial absorptive cells resemble intestinal absorptive cells and show an apical microvillous border, apicolateral junctional complexes, and desmosomes between adjacent cells; a cisternal complex may parallel the lateral plasma membranes and pinocytotic invaginations of the basolateral plasma membranes are common (Figures 6.112 and 6.113) (Mendoza, 1972; Lombardi and Wourms, 1985b; Schindler and de Vries, 1986a, 1987a,b, 1988a; Schindler and Kujat, 1990; Schindler and Hamlett, 1993; Hollenberg and Wourms, 1994; Kokkala and Wourms, 1994). The cytoplasm may be horizontally traversed by bundles of intermediate filaments and contains numerous mitochondria, some granular endoplasmic reticulum, polysomes, a Golgi complex, microtubules, irregular dense bodies, and a few membrane-bound bodies; the nucleus is basal. The epithelium is separated by a space of about 90 nm from a delicate basal lamina about 100 nm thick. Macromolecules from the embryotroph cannot penetrate the exposed cell membranes of this epithelium by way of intramembranous protein channels or pumps but must be taken up by micropinocytosis (Schindler and de Vries, 1987a).

There are two morphologically distinct, species-specific lines of trophotaenial absorptive cells based on the presence or absence of a typical endocytotic apparatus (Figure 6.114) (Schindler and de Vries, 1987a; Hollenberg and Wourms, 1994; Kokkala and Wourms, 1994). The endocytotic apparatus is well developed in most goodeids and ingestion of proteins is comparable to that of other absorptive epithelia. The cortical zone of the epithelial cells is crowded with membranous invaginations, vesicles, vacuoles, and dense apical tubules; mitochondria are located between this endocytotic apparatus and the nucleus (Figures 6.115A, 6.116A, 6.117, and 6.118) (Lombardi and Wourms, 1985b,c; Große Wichtrup, 1985, 1986; Schindler and de Vries, 1987b, 1988a, 1990). Internalized solutes accumulate in large, apical storage vacuoles and, after several hours, make their way

to a lamellar membranous complex that underlies the peripheral plasma membranes and communicates with the intercellular space; vesicles carry materials to the basolateral or basal cell surface where their contents are released by exocytosis (Figure 6.119). Figure 6.120 is a summary of the proposed pathway by which proteins are transferred across the trophotaenial placenta.

In species where there is a well-developed endocytotic apparatus in the trophotaenial absorptive cells, it is suggested that there is both opportunistic and selective uptake of proteins from the heterogeneous mixture in the embryotroph (Hollenberg and Wourms, 1994). The system of apical cytoplasmic tubules seems to provide for the non receptor-mediated uptake of proteins, targetting them to lysosomes for degradation to amino acids. Coated pits, on the other hand, are associated with receptor-mediated endocytosis and the targetting of endocytosed proteins to both lysosomal and non lysosomal compartments.

An endocytotic apparatus is lacking in two genera of goodeids, *Girardinichthys* and *Goodea,* and the supranuclear cytoplasm is dominated by a large number of mitochondria that are separated from the microvillous border by a narrow rim containing the terminal web; invaginations of the apical plasma membrane are rare and few multivesicular bodies are present (Schindler and de Vries, 1986a; Hollenberg and Wourms, 1994; Kokkala and Wourms, 1994) (Figures 6.111B and 6.115B). The brush border, abundant mitochondria, and basal coated vesicles suggest a transporting epithelium in which nutrients are absorbed, packaged, and exported without degradation. Presumably a hyperproteinaceous environment at the free surface stimulates micropinocytotic activity, giving rise to an internal apical canalicular system which subsequently develops into multivesicular bodies. This amplification of membranous material is likely more time-consuming than simply stepping up the activity of a pre-existing endocytotic apparatus so that protein uptake is slow. Some material is transferred to the basal and basolateral plasma membranes where it is released by exocytosis (Figure 6.111A). No mechanism has developed whereby the internalized membranes are recycled.

The stratified squamous pavement epithelium forms irregular islands of ridged cells between the absorptive cells (Figure 6.109). It proclaims its integumentary origins by its stratification in up to six layers, the mucopolysaccharide-coated microridges on the free surfaces, and the large numbers of desmosomes strengthening the interdigitating borders of adjacent cells. Tonofilaments converge on the desmosomes and junctional complexes seal the superficial layer of cells. There is a well developed Golgi complex and both granular and agranular endoplasmic reticulum evident in some places (Figure 6.111C). Often the squamous cells slide beneath the absorptive epithelium forming a BASAL LAYER (Figures 6.116B, and 6.121).

The two strains of trophotaenial epithelial cells appear to provide for the two basic necessities of life of the young: a supply of nutrients and respiratory exchange (Schindler and de Vries, 1986a). The absorptive epithelium, derived from the endodermal lining of the gut, resembles intestinal absorptive cells and may be regarded as fulfilling the absorptive function. The ridged, statified squamous epithelium is similar to the epithelium covering the secondary lamellae of fish gills and is presumed to be active in gaseous exchange.

A system of INTERCELLULAR SPACES, continuous with the infoldings of the basolateral membranes of the absorptive cells, extends between the absorptive and basal cells (Figures 6.121 and 6.122). As development proceeds, increasing distension of the intercellular spaces may cause progressive distortion of the absorptive epithelium (Figure 6.123) (Mendoza, 1972). These spaces may have an excretory role by storing wastes, a suggestion that is reinforced by the appearance of lamellar structures and membranous blebs released into these cavities (Figure 6.124A). The presence of leucocytes within the intercellular spaces and crowded into the connective tissue may indicate the acquisition of passive immunity (Figures 6.124B,C).

Other Embryonic Absorptive Structures

Of all the embryonic structures that contribute to the placentas of viviparous teleosts, the trophotaeniae have received most attention. Other structures include the pericardial, yolk and coelomic sacs; the skin of the body, fins, and fin folds; and the gills and buccopharyngeal tissues (Dépêche, 1973; Dobbs, 1975; Grove and Wourms, 1991; Schindler and Hamlett, 1993). These absorptive structures are often covered with a thin squamous epithelium closely applied to richly vascular loose connective tissue. Most of the epithelial cells show patterns of microridges that enhance their surface area, presumably facilitating the exchange of materials (Foscarini, 1989). Indeed, in *Clinus supercilosus,* the surface epidermis, especially that of the

pericardial and yolk sacs, gradually loses its microridges as the gut assumes more and more of the duties of nutrient uptake (Veith, 1980). In addition to these placental absorptive structures, embryotroph may be taken in by the mouth and its nutrients absorbed by a precociously developed gut (Dobbs, 1975; Veith, 1980).

The PERICARDIAL, YOLK, AND COELOMIC SACS play a major role in maternal-embryonic exchange in many viviparous teleosts, especially during early stages of gestation (Dépêche, 1973; Grove and Wourms, 1991; Schindler and Hamlett, 1993). Later, as in goodeids and jenynsiids, these organs may regress as their functions are taken over by other structures. In lecithotrophic species, such as the guppy *Poecilia reticulata,* which rely on nutrients stored in the egg, the functions of these sacs are restricted to gas exchange and osmoregulation; chloride cells have been described among the microridges and are presumed to contribute to osmoregulation (Dépêche, 1973).

In matrotrophic species, however, these sacs become greatly expanded and participate in nutrient absorption in addition to respiration and osmoregulation (Veith, 1980; Grove and Wourms, 1991). In the follicular placenta of *Heterandria formosa,* the pericardial sac expands to form a hood covering the head and, together with the yolk sac, is extensively vascularized by a portal plexus derived from the vitelline circulation (Figure 6.125) (Grove and Wourms, 1991). During early development, in addition to the absorptive epithelium that covers the surfaces of the pericardial and yolk sacs, the surface epithelium on other regions of the body also participates in the exchange of materials. This epidermal epithelium is a patchwork of both absorptive cells and cells that do not appear to be absorptive (Figure 6.126); during subsequent development, the areas covered by non-absorptive cells increase so that, eventually, there is little absorption through the skin and the pericardial and yolk sacs become the primary sites of uptake of exogenous nutrients. The absorptive epithelia are bilaminar, consisting of a layer of specialized superficial cells and a layer of extremely thin basal cells (Figure 6.127). Basal cells are connected to each other and to the superficial cells by desmosomes.

The thicker SUPERFICIAL LAYER of the absorptive epithelium ranges from 1 to 10 μm in thickness and is more conspicuous and complex than the basal layer (Grove and Wourms, 1991). Specializations between the superficial cells include the interdigitation of lateral plasma membranes, desmosomes, and apical junctional complexes (Figure 6.128). Numerous elongate, branching microvilli project from the apical surface. Superficial cells contain several Golgi complexes and extensive granular endoplasmic reticulum. Coated pits often occur between the bases of the microvilli and there are coated vesicles in the apical cytoplasm. Large electron-lucent vesicles, 0.5 to 1.5 μm in diameter, within the apical cytoplasm, contain flocculent material and are often associated with the Golgi complex. They appear to be endosomes: acidic prelysosomal compartments associated with receptor-mediated endocytosis. Myelin figures are also often present. A heterogeneous group of dense-staining vesicles and multivesicular bodies are scattered throughout the cytoplasm and may be lysosomes. Because microvilli increase surface area for transmembrane absorption, uptake of low molecular weight molecules, including nutrients such as monosaccharides and amino acids, may play an important role. The presence of the coated pits and vesicles indicates that specific proteins are absorbed through receptor-mediated endocytosis.

BASAL CELLS are 0.1 to 3 μm thick and contain few organelles, although some mitochondria, a limited amount of granular endoplasmic reticulum, an occasional Golgi complex, and some coated pits and vesicles are present (Figure 6.129) (Grove and Wourms, 1991). ENDOTHELIAL CELLS of the portal plexus are so closely applied to the basal cells that, at some points, their respective basal laminae cannot be distinguished (Figures 6.130C,D). The endothelial cells possess few organelles but small, smooth surfaced pits are prominent on their inner and outer surfaces. Presumably maternal nutrients from the embryotroph are passed into the foetal capillaries by transcytosis.

Cells resembling CHLORIDE CELLS occur singly or in pairs in the surface epithelium, indicating its probable role in osmoregulation (Grove and Wourms, 1991). They rest on the basal lamina and contain a basal nucleus, numerous mitochondria, and an extensive system of tubular, membrane-bound channels (Figures 6.130A,B). The channels appear swollen in places and communicate laterally and basally with the intercellular spaces. Coated vesicles, Golgi complexes, numerous microtubules, and, to a lesser extent, granular endoplasmic reticulum, are present as well. Apical junctional complexes are present between the chloride cells and adjacent superficial epithelial cells.

The absorptive epithelium continues to cover the pericardial and yolk sacs as development progresses,

but NON-MICROVILLOUS SUPERFICIAL CELLS appear in increasing numbers in other regions of the surface epithelium (Grove and Wourms, 1991). These cells are more squamous (0.5 to 2 μm thick) and less complex in ultrastructural organization than the microvillous cells (Figures 6.129C,D). They are covered with a glycocalyx and bear microplicae and lateral ridges that become more apparent as parturition approaches. Presumably these cells represent the initial stages of epidermal differentiation and play little role in nutrient uptake.

An especially intimate placental association between maternal and embryonic tissues is described in the extreme matrotroph *Anableps* where, as the embryo develops, "vascular bulbs" form on the richly vascular pericardial trophoderm and associate with pits in the follicular wall in a ball-and-socket fashion (Figures 6.84 and 6.85B,E) (Knight et al., 1985). The surface cells of the vascular bulbs are ridged by microplicae. Each vascular bulb contains a blood sinus and the sinuses of adjacent bulbs are continuous (Figure 6.85D). These sinuses drain into the portal system that drains into the sinus venosus. Adjacent regions of the follicular wall form rows of villi which come in contact with the lateral and dorsal surfaces of the embryo (Figures 6.85G,H). The surface of the villi is covered with short, stumpy microvilli; a well-defined brush border is absent. The villi embrace the vascular bulbs and may initiate the formation of pits in the follicular wall. In terms of percentage weight increase of the developing embryo, the follicular placenta of *Anableps* appears to be the most efficient adaptation for maternal-embryonic nutrient transfer in teleost fishes.

Exchange with the embryotroph also may occur through the SKIN covering the body, the fin-folds, and fins. Richly vascular FIN FOLDS are well developed in *Goodea luitpoldii* and, to a lesser extent, in other genera of goodeids (Mendoza, 1958; Geraudie and Chilmonczyk, 1976). These folds of richly vascular loose connective tissue are covered with a thin, squamous epithelium and probably augment the exchange occurring in the trophotaeniae and body surface (Figure 6.131). Vascularized spatulate expansions of the interradial fin web on the dorsal fin of some embiotocids are also presumed to function in maternal-foetal exchange (Figures 6.132 and 6.133) (Webb and Brett, 1972; Dobbs, 1975). In scanning electron micrographs, the epidermal cells of these fin flaps appear as flattened sheets patterned with numerous microridges; occasional mucous cells are interspersed among the squamous epithelial cells. The villous hindgut of this species probably functions primarily in the absorption of nutrients from the embryotroph while the vascular fin flaps facilitate the respiratory exchange of gases.

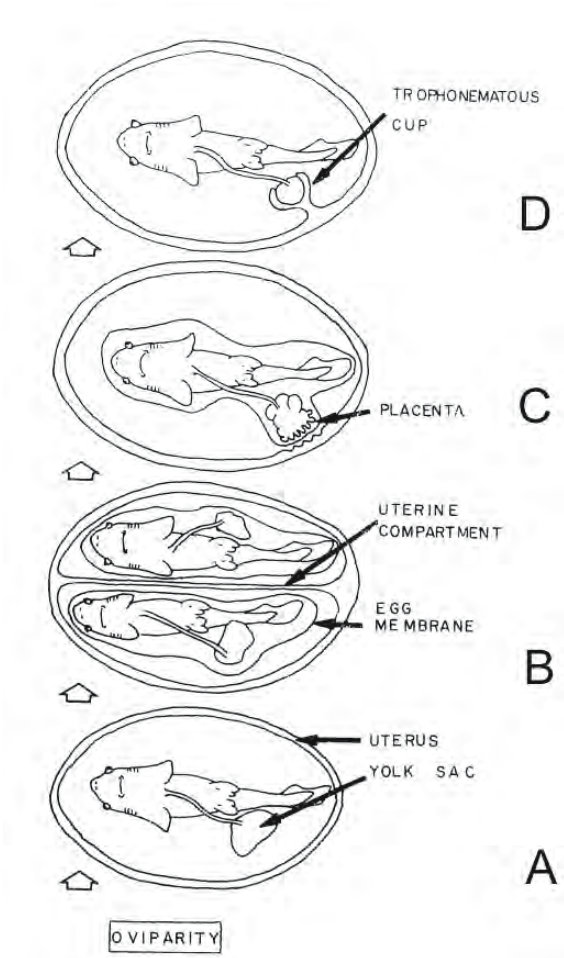

Figure 6.1: A scheme to illustrate the evolution of placentation in sharks. (From Hamlett, 1987; reproduced with permission of the author).

A. Uterine retention of lecithotrophic embryo.

B. Uterine compartments form; egg envelope thins and becomes pliable.

C. Yolk sac placenta established.

D. Purely matrotrophic development with functional placenta established at implantation. For simplicity, the presence of additional compartmentalized embryos is not indicated in **C** and **D**.

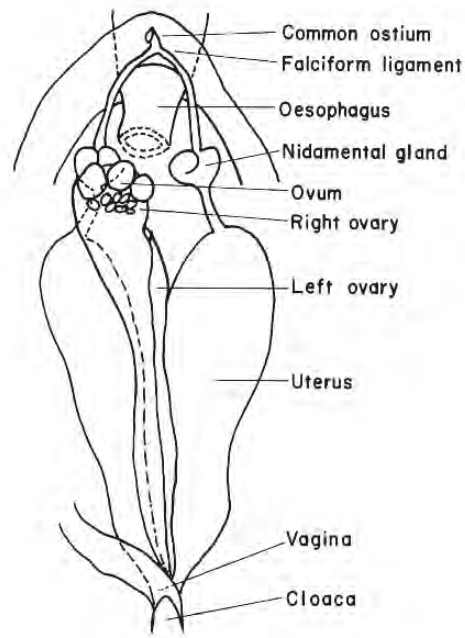

Figure 6.2: Sketch of the female reproductive organs of the sumitsuki shark *Carcharhinus dussumieri.* (From Teshima and Mizue, 1972; reproduced with permission of the authors).

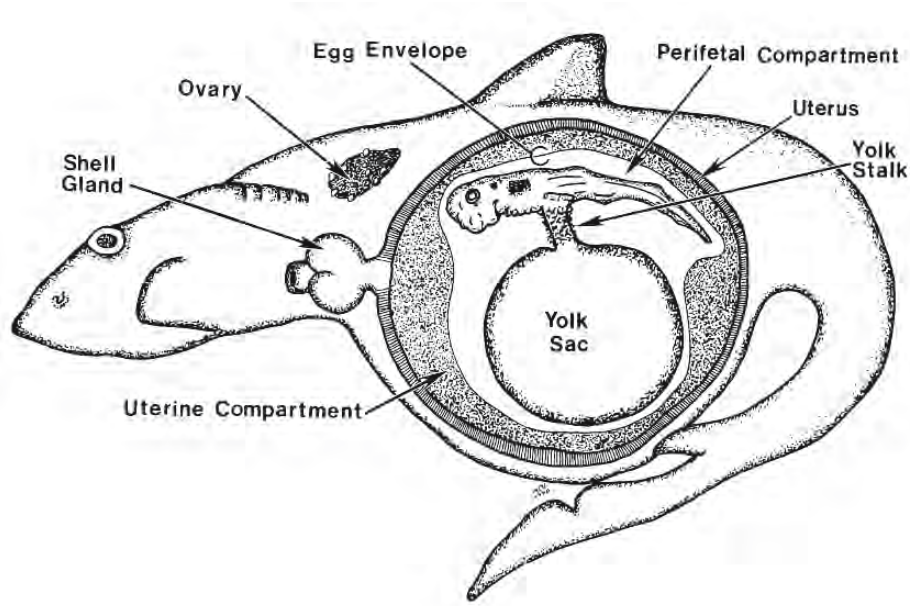

Figure 6.3: Interpretive drawing of an Atlantic sharpnose shark *Rhizoprionodon terraenovae* during an early stage of gestation. The ovary contains small, developing oocytes while the uterus harbours yolk-dependent, early-term embryos. A delicate egg capsule that surrounds the embryo establishes two subcompartments: the uterine compartment and the perifoetal compartment. (From Hamlett, 1993; reproduced with kind permission of Kluwer Academic Publishers).

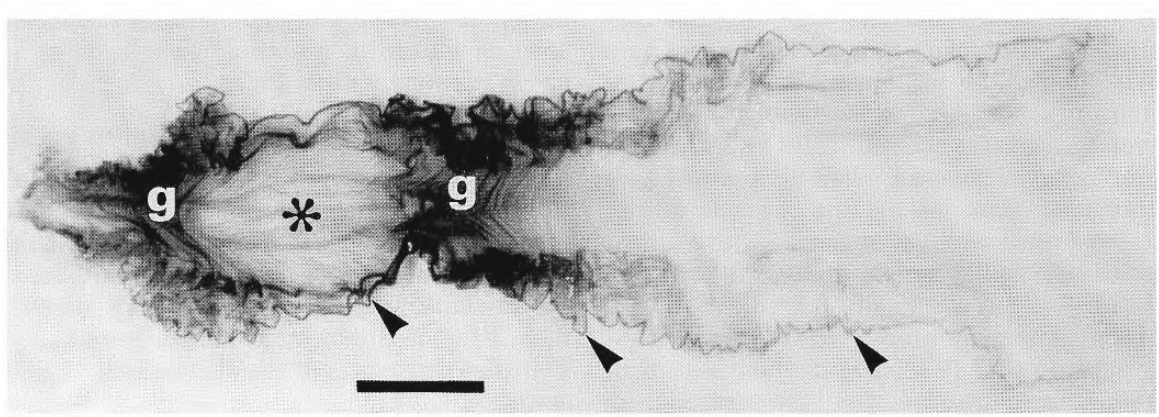

Figure 6.4: Photograph of an isolated egg capsule of an early term embryo of the smooth dogfish *Mustelus canis.* The asterisk indicates the former location of the embryo which has been removed. Gathered regions of the egg capsule (g) lie both anterior and posterior to the embryo's position. Darkened lateral bands (arrowheads) represent pleating of the egg capsule. Scale bar = 3 cm (From Lombardi and Files, 1993; © reproduced with permission of John Wiley & Sons, Inc.).

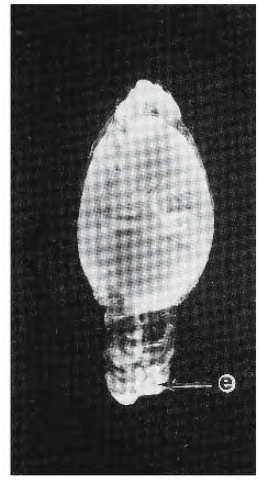

Figure 6.5: Photograph of a recently fertilized egg of the sharpnose shark *Rhizoprionon terraenovae.* Most of the egg envelope (e) is gathered together at one end of the egg. X 1/6 (From Castro and Wourms, 1993; © reproduced with permission of John Wiley & Sons, Inc.).

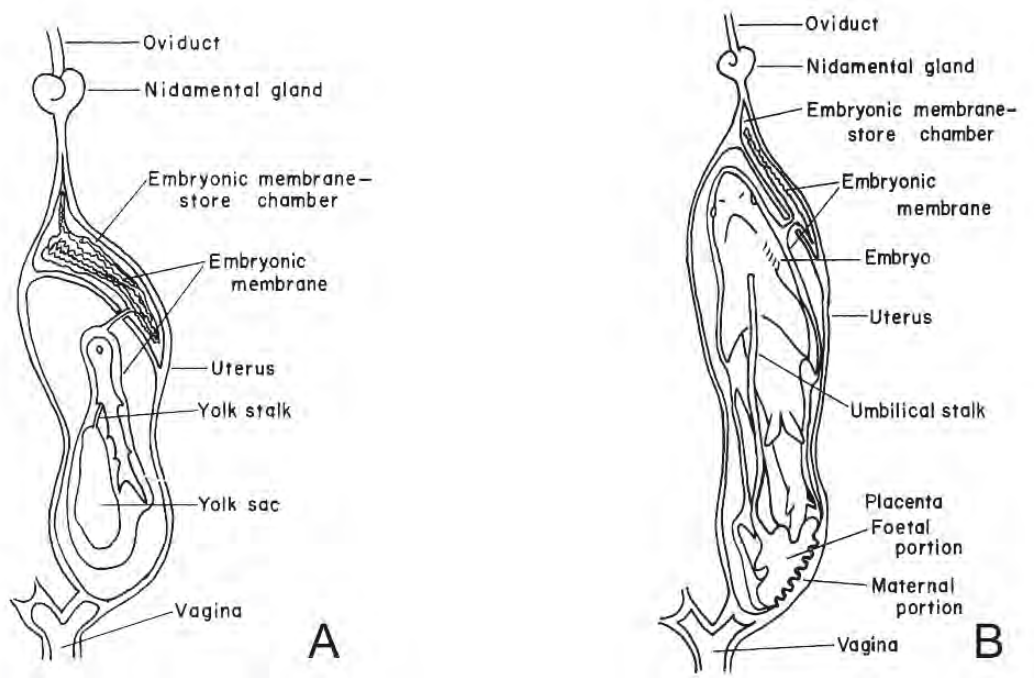

Figure 6.6: Sketches of the female reproductive organs of the sumitsuki shark *Carcharhinus dussumieri.* (From Teshima and Mizue, 1972; reproduced with permission of the authors).

A. Uterus with the membrane reservoir (embryonic membrane-store chamber) in the anterior region. The placenta has not yet been established.

B. The placenta has been established within the gravid uterus.

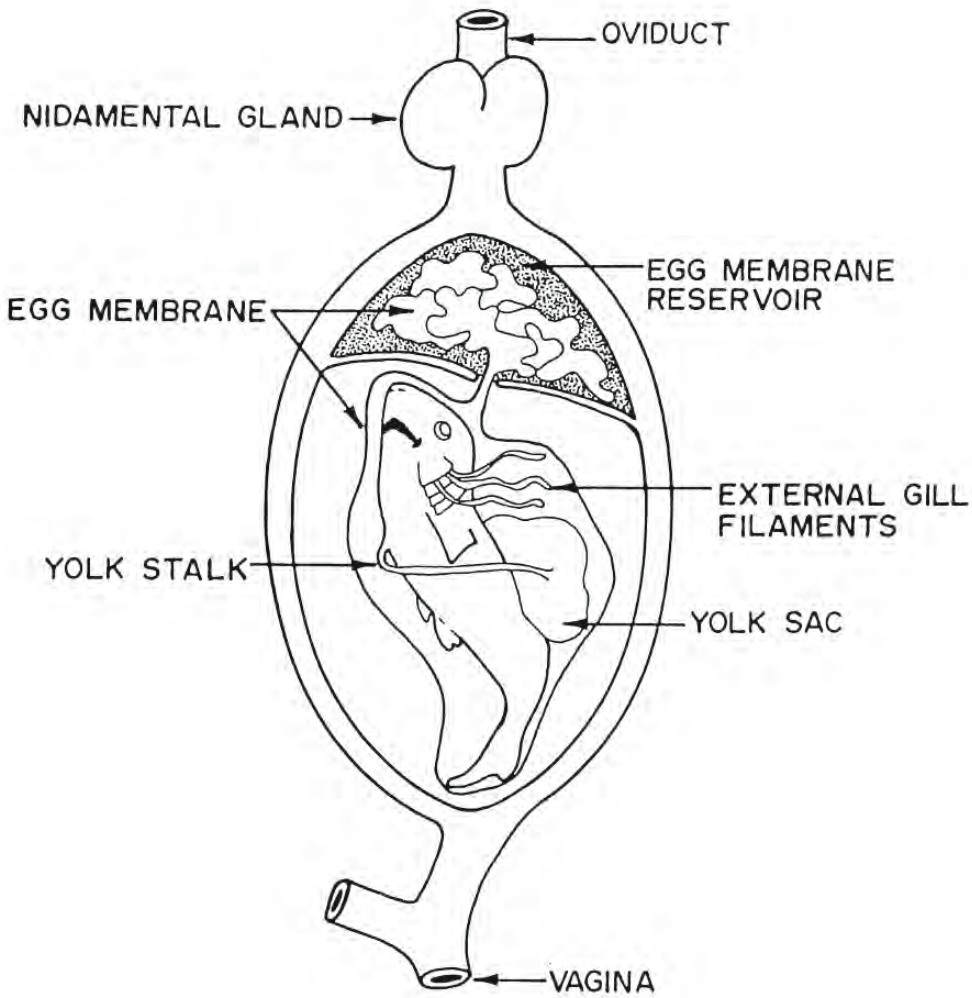

Figure 6.7: Diagram of a preimplantation stage of a carcharhinid embryo early in gestation. (From Hamlett, 1987; reproduced with permission of the author) The external gill filaments are conspicuous. The yolk sac contains yolk and is not attached to maternal tissues. Excess egg capsule is folded into a neat package and stored in the membrane reservoir.

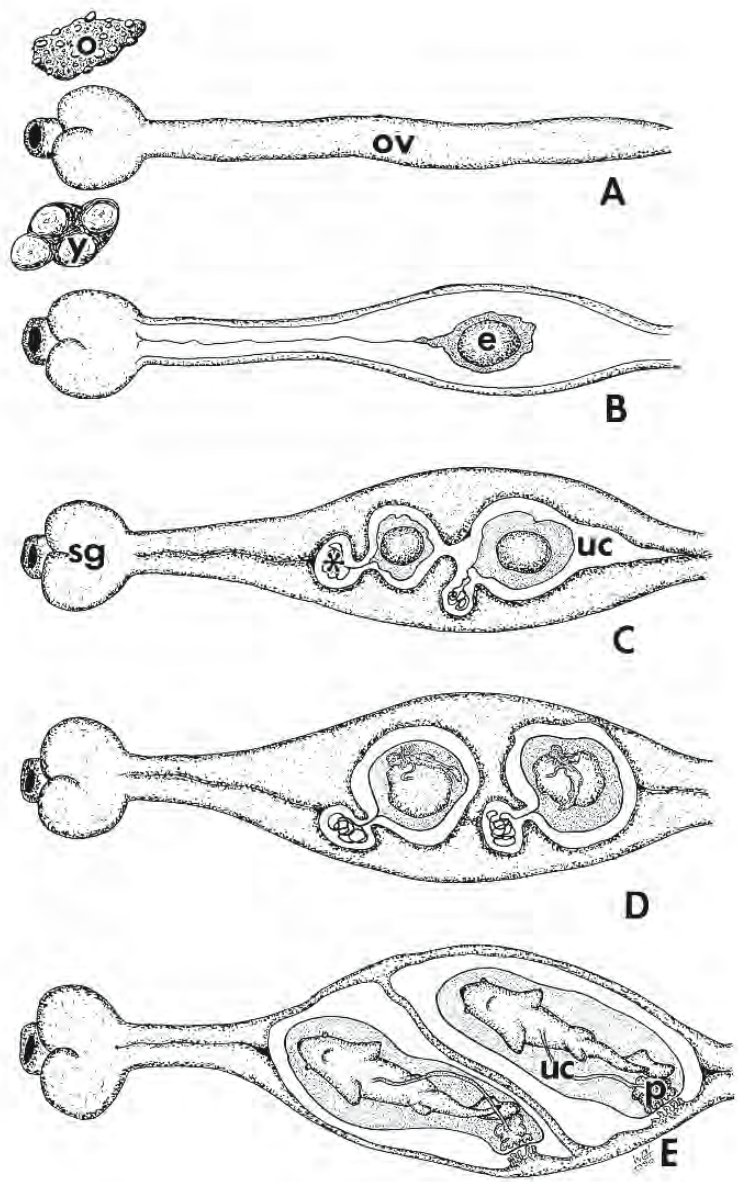

Figure 6.8: Several embryos may be accommodated within compartments in the uteri of some placental sharks; two compartments are shown in these diagrams of longitudinal sections of the reproductive system of a placental shark. Immature sharks possess an ovary (o) with developing eggs and a small oviduct (ov). Yolked eggs (y) are shed, fertilized, and enter the shell gland (sg). Fertilized eggs (e) reside in uterine compartments (uc) and the excess egg envelope is sequestered in a membrane reservoir (*). The yolk sac differentiates into an umbilical cord (uc) and the yolk sac becomes a functional placenta (p). (From Hamlett et al., 1993a; © reproduced with permission of John Wiley & Sons, Inc.).

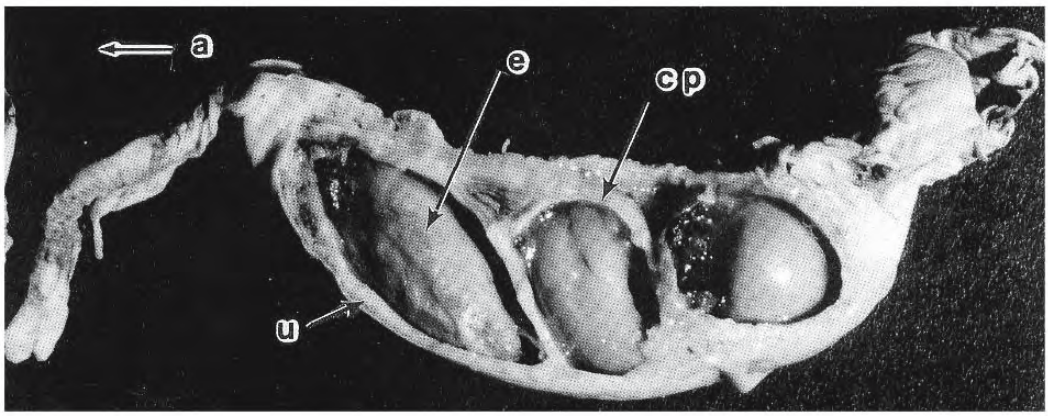

Figure 6.9: Photograph of the gravid uterus of the sharpnose shark *Rhizoprionodon terraenovae.* The uterus (u) has been dissected to reveal three uterine compartments (cp) that contain eggs (e) with small embryos. The anterior end (a) is to the left. X 1 (From Castro and Wourms, 1993; © reproduced with permission of John Wiley & Sons, Inc.).

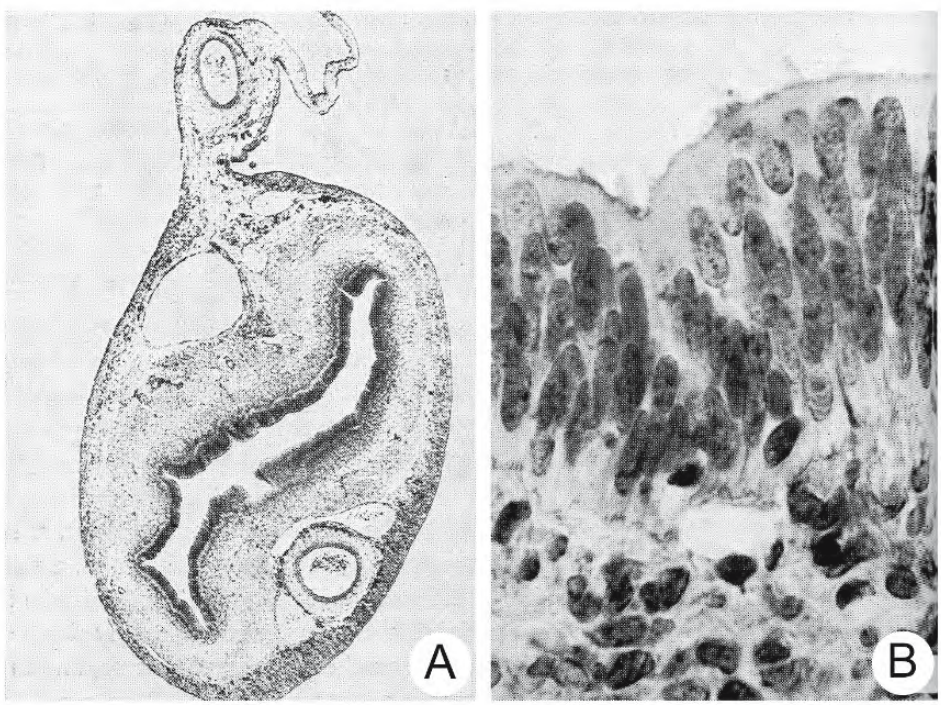

Figure 6.10: Micrographs of sections through the uterus of the spiny dogfish, *Squalus acanthias.* (From Jollie and Jollie, 1967b; reproduced with permission from Elsevier Science).

A. Photomicrograph of a cross section of the nonpregnant uterus. The vascular uterine "mesentery" is shown at the top. The lining of the uterine lumen is smooth and the connective tissue of the wall is thin but dense and largely avascular. Sections of the major blood vessels are seen in the mesentery and between the layers of smooth muscle. X 40.

B. Photomicrograph of a section of the simple columnar epithelium that lines the nonpregnant uterus. Apically some of these cells bear cilia; others appear to have a brush border. The subepithelial connective tissue is dense. A capillary lies immediately beneath the epithelium. X 440.

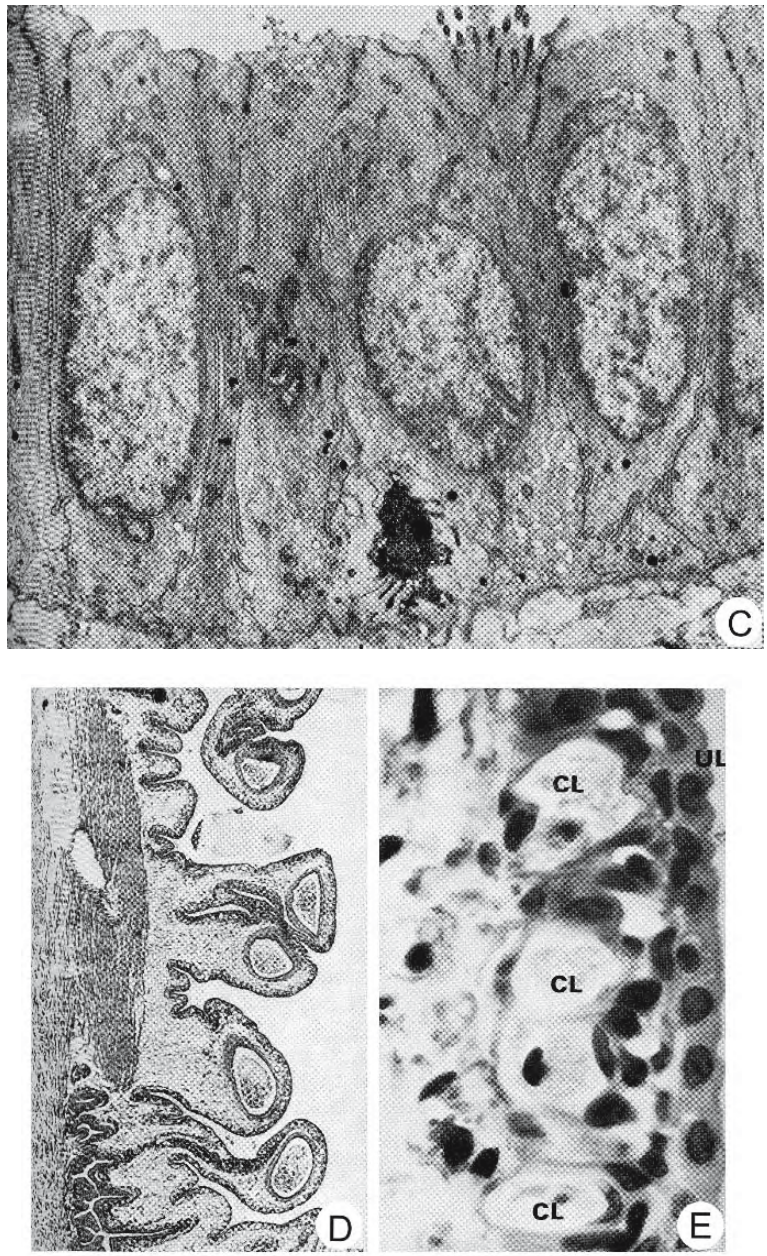

Figure 6.10: Continued.

C. Electron micrograph of a section through the epithelium of the nonpregnant uterus. Junctional complexes are well developed between the apical borders of the epithelial cells and lateral plasma membranes are closely interdigitated. One cell is ciliated. X 6,300.

D. Photomicrograph of a cross section of a portion of the wall of a pregnant uterus. Mucosal folds, or rugae, are longitudinally oriented. Arterioles are present in the cores of the rugae. Layers of smooth muscle of the tunica muscularis are located at the left. X 40 (Compare with **A**).

E. Photomicrograph of a section of pregnant uterus. The epithelium of the tunica mucosa is richly supplied with capillaries (CL); connective tissue is sparse. UL, uterine lumen. X 440 (Compare with **B**).

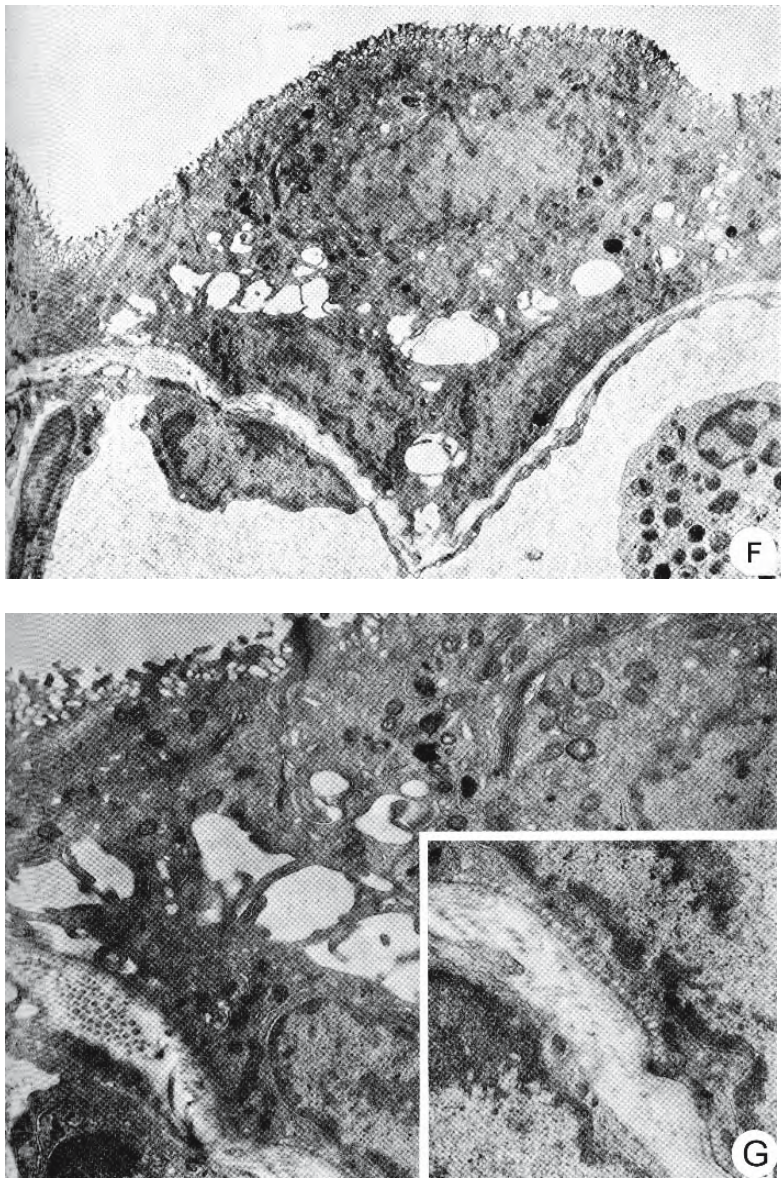

Figure 6.10: Continued.

F. Electron micrograph of a section of the pregnant uterus to demonstrate the "respiratory barrier". The epithelium consists of two layers of low cuboidal or squamous cells. The apical cytoplasm of the juxtaluminal epithelial cells is highly vacuolated and the intercellular spaces extensively dilated. A layer of connective tissue separates this epithelium from the endothelium of a uterine capillary. X 4,500.

G. An electron micrograph of the section shown in **F** at a greater magnification. Apical vesicles abound in the surface epithelial cells and distention of the intercellular spaces is apparent. A thin layer of connective tissue is interposed between the epithelium and the endothelial cell at the lower right. X 13,500 The inset shows this connective tissue. Abundant micropinocytotic vesicles line the basal plasmalemma of the juxtacapillary epithelial cells. X 19,000.

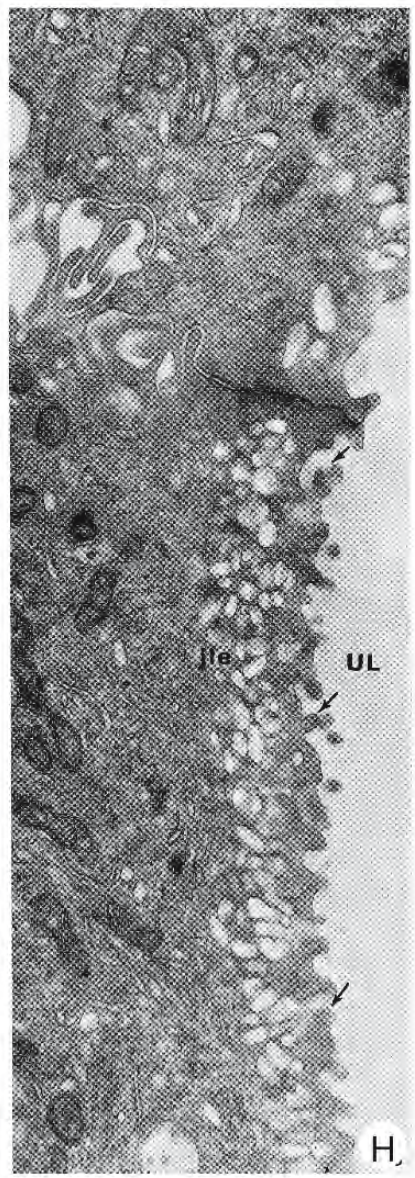

Figure 6.10: Continued.

H. Electron micrograph of a section of adjoining juxtanuclear epithelial cells (jle) from a pregnant uterus. The occluding zonule of a junctional complex seals the intercellular spaces from the lumen (UL). The apical cytoplasm of the juxtaluminal cells is packed with smooth-surfaced, electron-lucent vacuoles. At several points (arrows) the vacuoles appear to communicate with the apical plasmalemma and with each other. X 25,000.

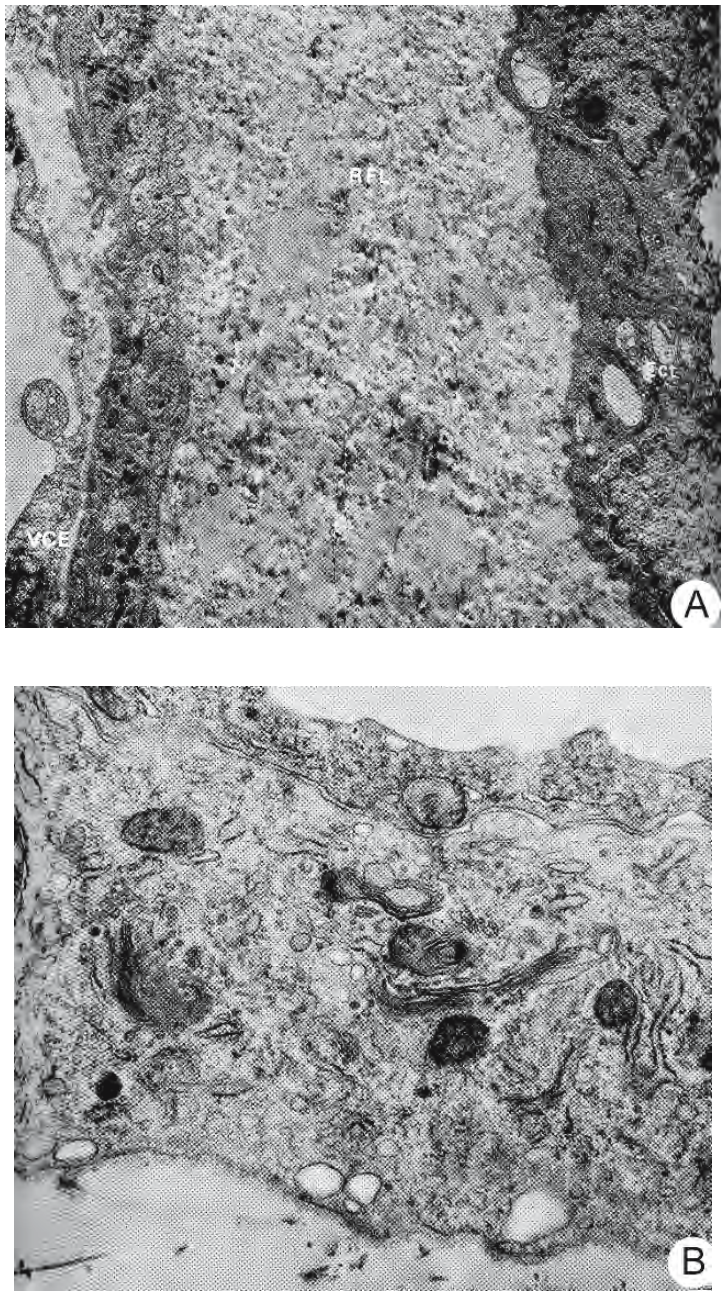

Figure 6.11: Electron micrographs of sections through the respiratory barrier of the yolk sac of the spiny dogfish *Squalus acanthias.* (From Jollie and Jollie, 1967a; reproduced with permission from Elsevier Science).

A. The respiratory barrier consists of non-keratinized squamous ectodermal cells (Ect), a layer of fine reticular fibres (RFL), and the endothelium of the vitelline capillary (VCE). X 5,200.

B. The ectodermal epithelium of the functioning respiratory barrier is non-keratinized. A few pinocytotic vesicles are seen. Note the large Golgi complexes and abundant endoplasmic reticulum. The basal lamina of the ectodermal epithelium is seen at the bottom of the micrograph. X 27,000.

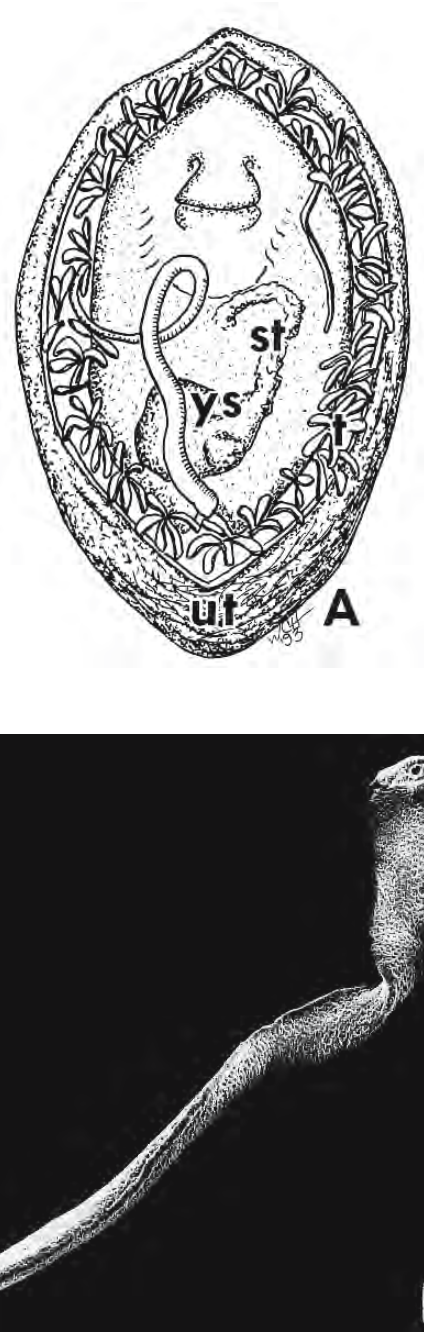

Figure 6.12: Trophonemata enhance the production of histotroph in the uterus of the southern stingray *Dasyatis americana.* (From Hamlett et al., 1993a; © reproduced with permission of John Wiley & Sons, Inc.).

A. An embryo, with its yolk stalk (st) and yolk sac (ys) still attached, resides in the uterus (ut) adorned with trophonemata (t).

B. Scanning electron micrograph of a single trophonema showing its central vessel, flattened nature, and cabled surface. X 24.

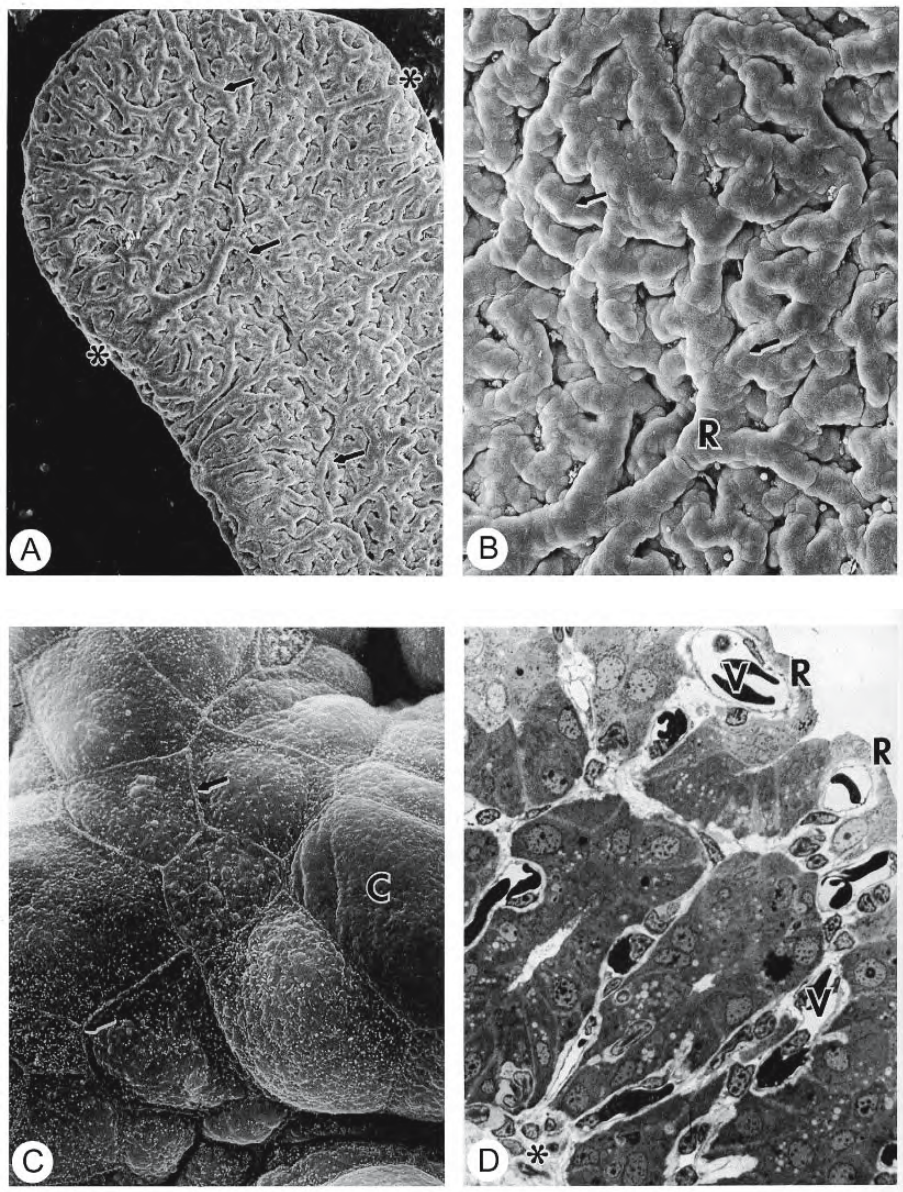

Figure 6.13: Trophonemata of the cownose ray *Rhinoptera bonasus* are richly vascularized, spatulate, villiform processes embossed with a pattern of anastomosing, cable-like ridges. **A**, **B**, and **C** are scanning electron micrographs of the surface of a trophonema. (From Hamlett, Wourms, and Smith, 1985; reproduced with permission from Nuova Immagine Editrice).

A. Asterisks mark the edges of the trophonema. The surface is ridged (arrows). X 60.

B. The surface is embossed with a series of interlocking ridges (R). The borders of adjacent cells are visible (arrows). X 225.

C. The surface epithelial cells are roughly polyhedral with sharply defined boundaries between adjacent cells and a relatively smooth and convex contour (C). X 2,625.

D. Photomicrograph of a section through a trophonema showing the rich vascularization (V) of the ridges (R). Loose connective tissue (*) forms the core of the trophonema. X 3,000<.

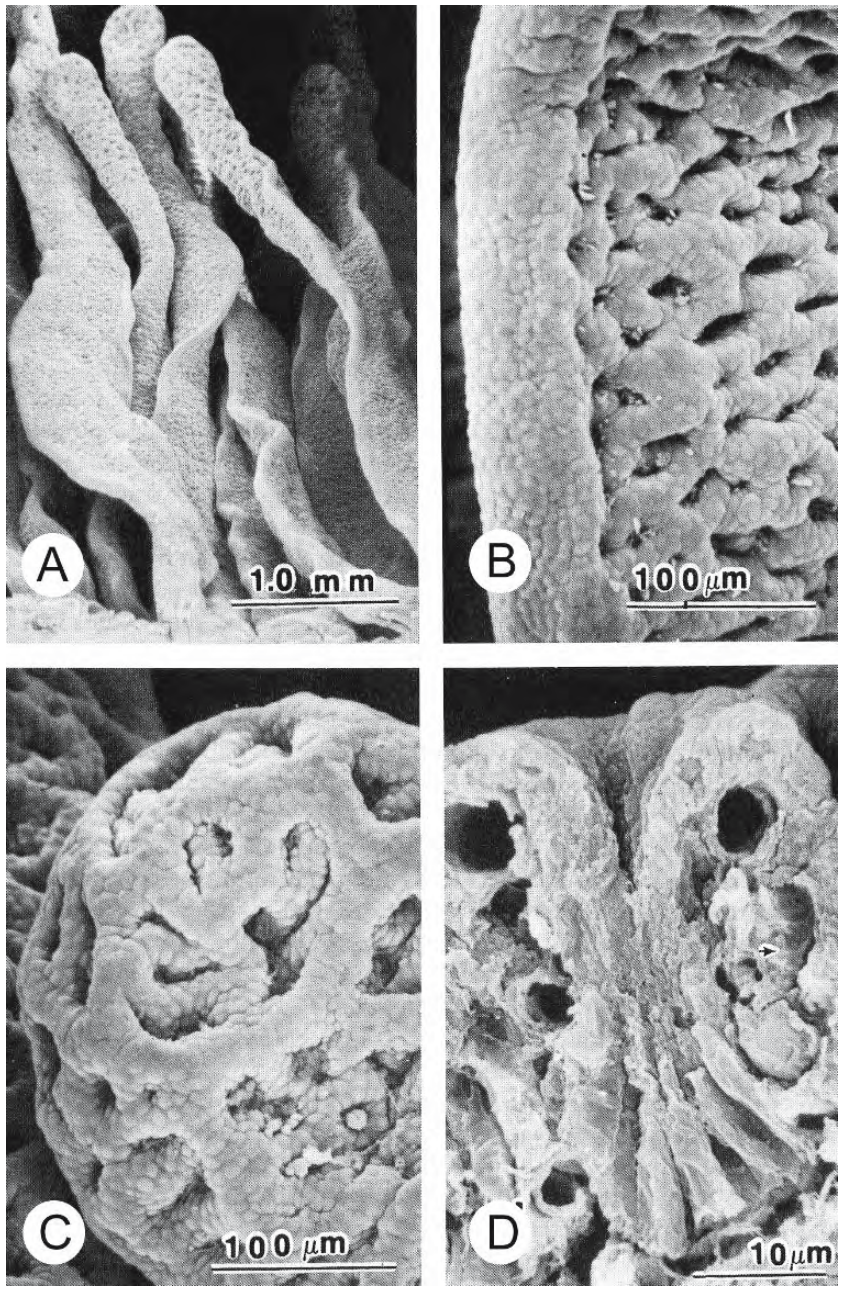

Figure 6.14: Scanning electron micrographs of trophonemata in the uterine wall of the butterfly ray *Gymnura micrura* during early gestation. (From Wourms, Grove, and Lombardi, 1988; reproduced with permission from Elsevier Science).

A. Trophonemata are spatulate, villiform processes.

B. The surface of the trophonema is embossed with a convoluted network of "cables" that enclose a capillary network. An artery is contained within the distended lateral margin on the left.

C. The basic organization of an anastomosing capillary bed predominates at the spatulate tip of a trophonema. Acinar glands (lower right) are occasionally observed.

D. Sections of the capillary bed, covered by the surface epithelium, are seen in this freeze-fracture preparation of a trophonema.

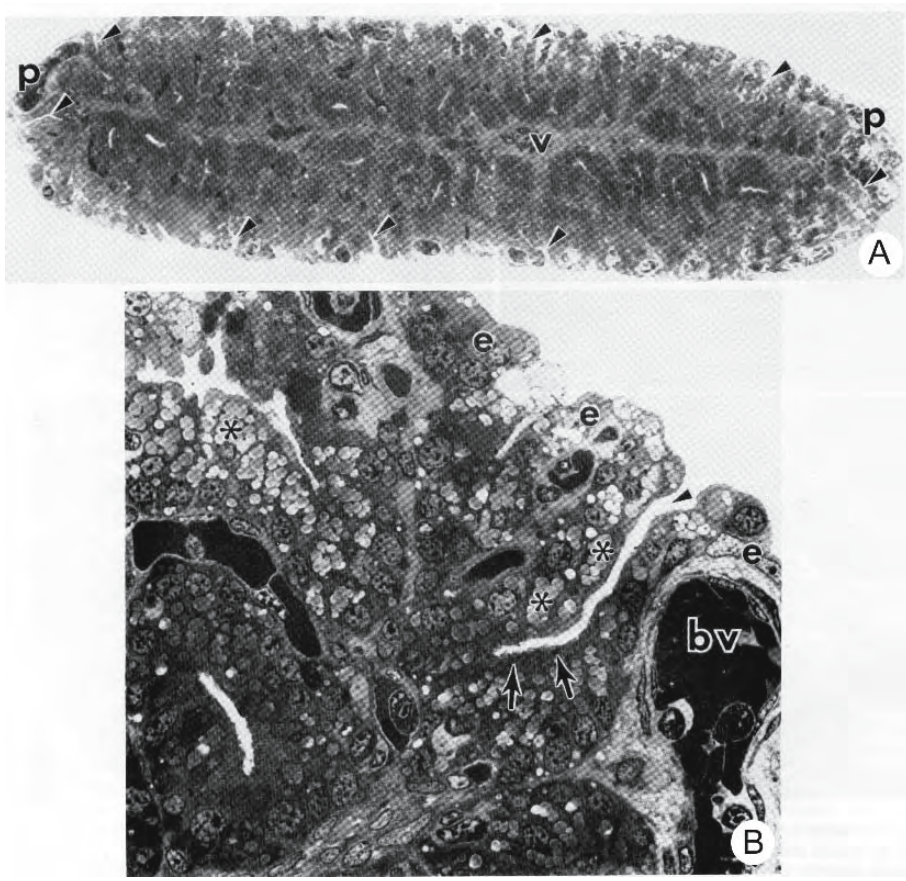

Figure 6.15: Photomicrographs of sections of an early trophonema of the southern stingray *Dasyatis americana.* (From Hamlett et al., 1996; reproduced with permission of the NRC Press).

A. This cross section through an entire trophonema shows the central blood vessel (v), smaller peripheral vessels (p), and many crypts (arrowheads). X 600.

B. The surface is covered with a simple cuboidal epithelium (e) overlying peripheral blood vessels (bv). At this magnification, the cells of the crypts are seen to be filled with small, dark secretion vesicles (arrows) and large lipid droplets (*). X 3,000.

⟶

Figure 6.16: Transmission electron micrographs of sections through the epithelial surface of trophonemata of the cownose ray *Rhinoptera bonasus.* (From Hamlett, Wourms, and Smith, 1985; reproduced with permission from Nuova Immagine Editrice).

A. The cytoplasm of an epithelial cell displays the characteristic array of organelles involved in protein synthesis and secretion: granular endoplasmic reticulum (R), Golgi complexes (G), and secretion granules (S) in varying stages of maturation. The nucleus (N) is at the lower left; its nuclear envelope is continuous with the dilated cisternae of the granular endoplasmic reticulum (arrow). A multivesicular body (M) and coated vesicles (circle) are also present. X 24,624.

B. Junction of two epithelial cells. The lateral boundaries are straight (arrows). The cytoplasm is dominated by granular endoplasmic reticulum (R) whose cisternae may become greatly distended (*). Presecretory granules (P) are more electron-dense than the material within the cisternae of the granular endoplasmic reticulum. Mitochondria (M) are abundant. X 23,940.

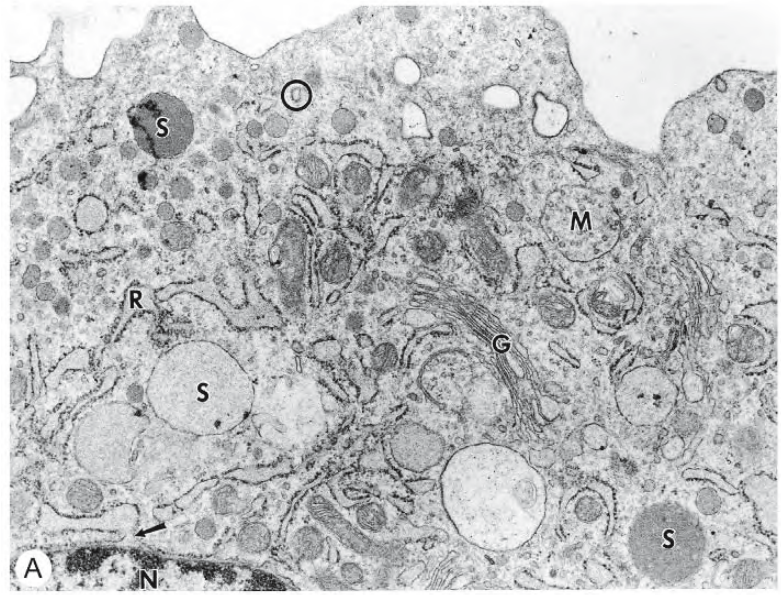

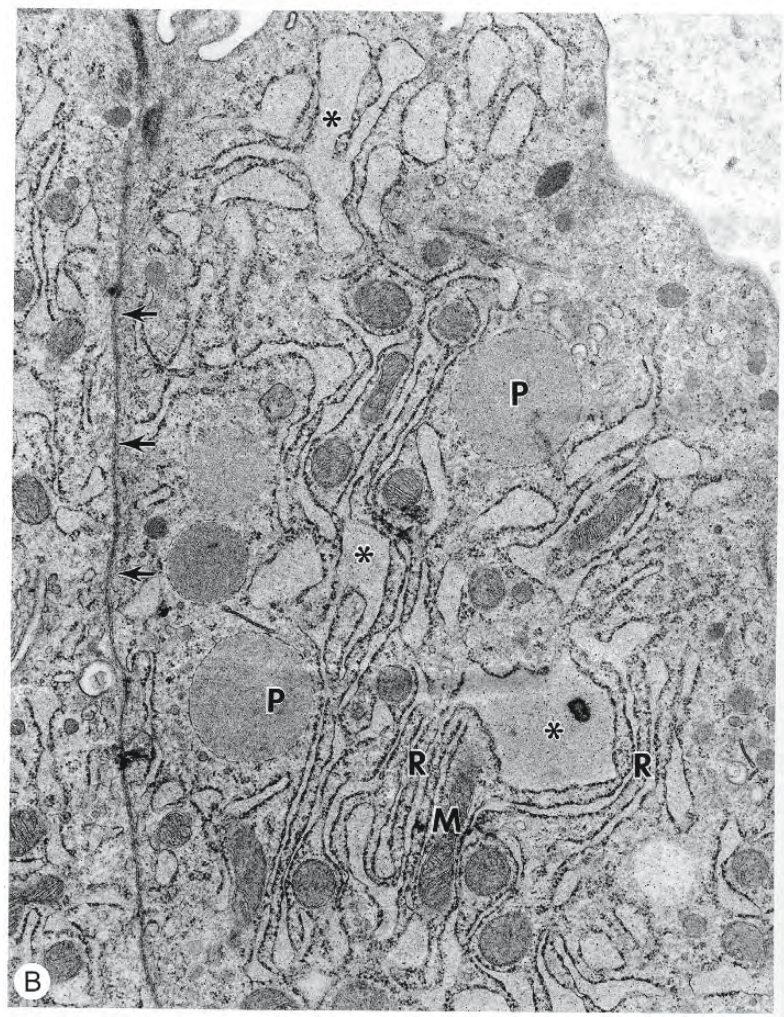

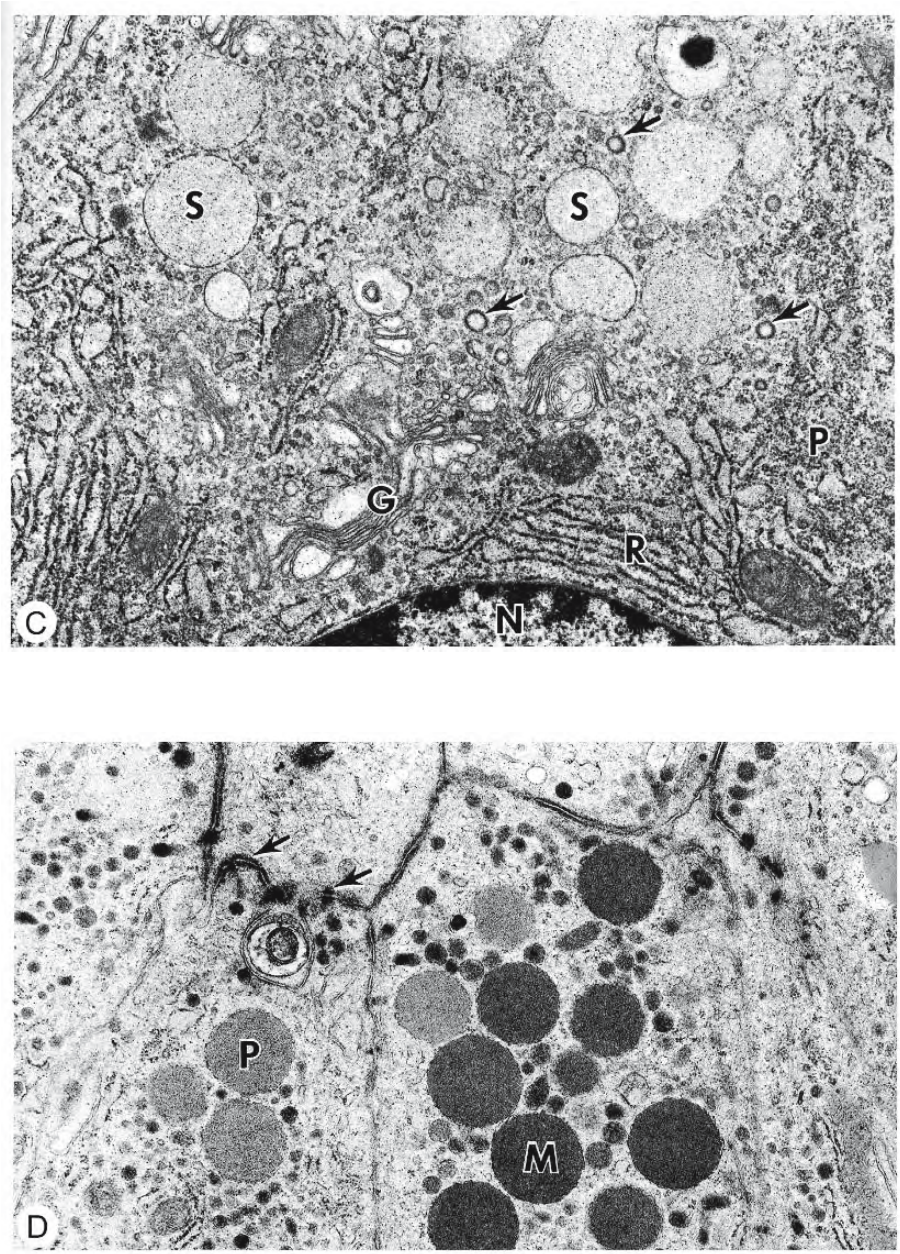

Figure 6.16: Continued.

C. The cytoplasm of a trophonemal epithelial cell. Coated vesicles (arrows) occur in the region of the Golgi complex (G) but are not seen to be directly associated with it. The nucleus (N), polyribosomes (P), presecretion granules (S), and granular endoplasmic reticulum (R) also occupy the cytoplasm. X 20,235.

D. This micrograph is a tangential section through the apices of several trophonemal cells. The arrows indicate an extensive array of junctional complexes between adjacent cells. Presecretory granules (P) are less electron-dense than mature membrane-limited secretory granules (M). X 31,350.

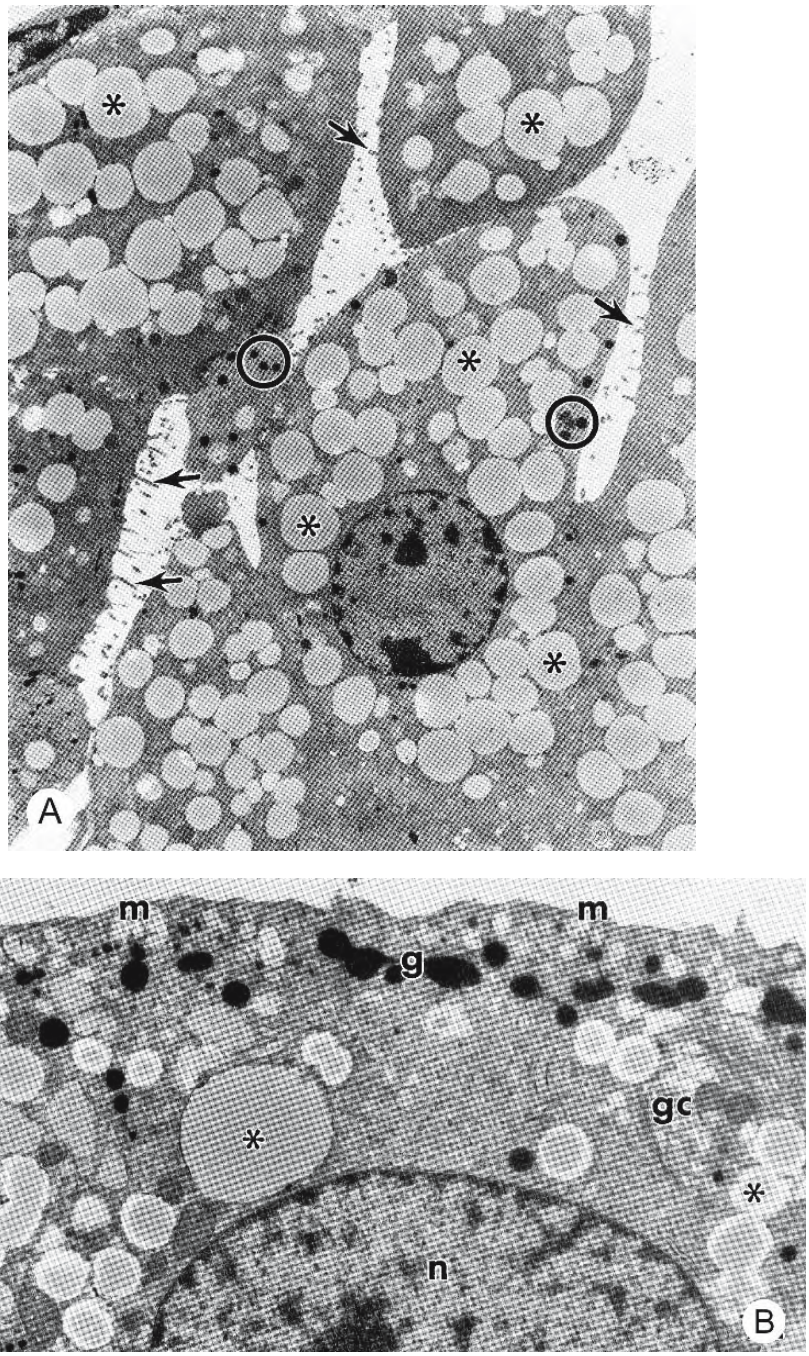

Figure 6.17: Transmission electron micrographs of sections through trophonemal epithelial cells of the southern stingray *Dasyatis americana.* (From Hamlett et al., 1996; reproduced with permission of the NRC Press).

A. Cells covering the "cables" on the surface of a trophonema display apical microvilli (arrows) which also extend into the crypts between the epithelial cells. The cells contain secretory granules (circles) and are packed with large lipid droplets (*). X 4,300.

B. Trophonemal epithelial cells may contain protein secretory granules (g), lipid (*), and mucus (m) at the same time. The Golgi complex (gc) and nucleus (n) are shown. X 8,700.

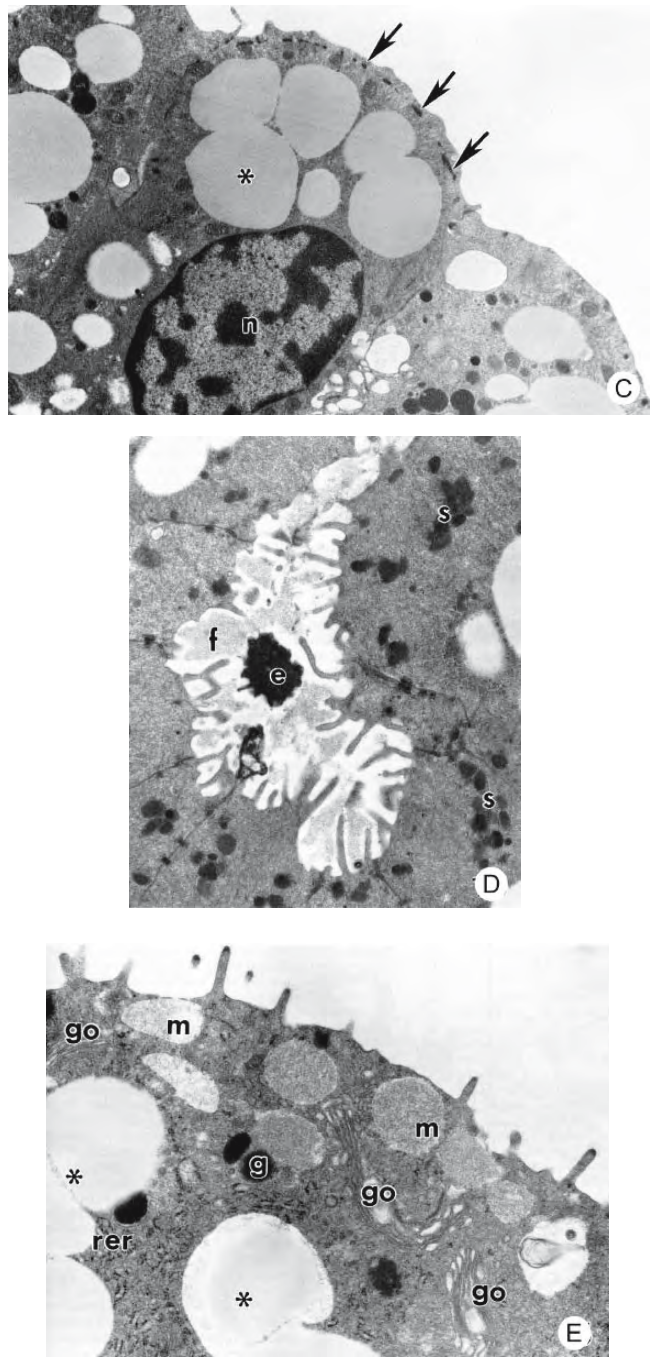

Figure 6.17: Continued.

C. Trophonematal epithelial cells containing lage lipid droplets (*). Arrows indicate the terminal web. n, nucleus X 7,500.

D. Cells from a secretory crypt contain proteinaceous secretory vesicles (s). Electron-dense (e) and flocculent (f) secretory material are present in the lumen. X 11,000.

E. This surface secretory cell contains lipid (*), granular endoplasmic reticulum (rer), Golgi complexes (go), proteinaceous secretory granules (g), and mucus (m). X 19,000.

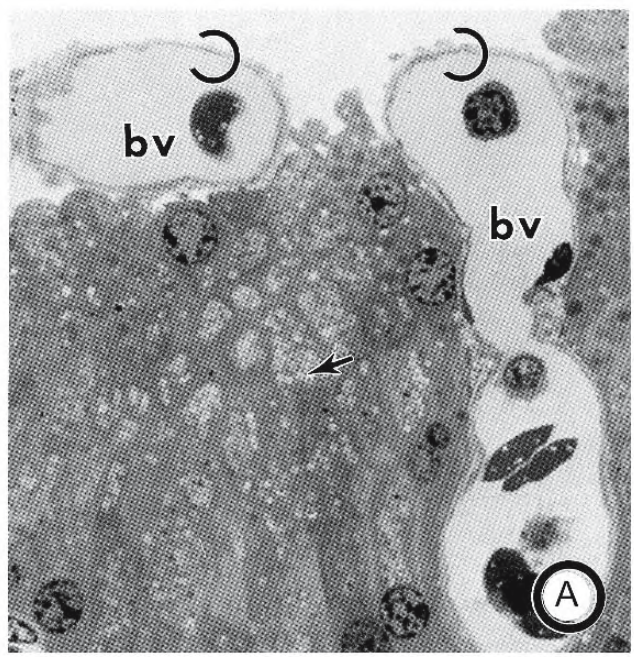

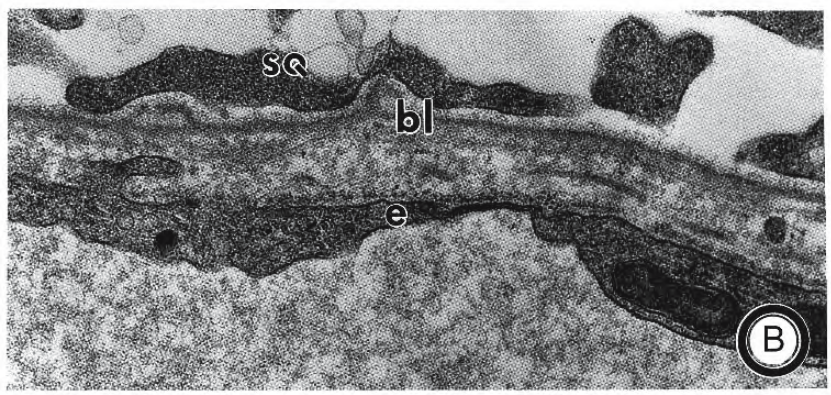

Figure 6.18: Transmission electron micrographs of sections through a trophonema of the southern stingray *Dasyatis americana* as term approaches. Increased efficiency for respiratory exchange is apparent. (From Hamlett et al., 1983a; © reproduced with permission of John Wiley & Sons, Inc.).

A. The surface epithelium becomes attenuated (half circles) and underlying capillaries (bv) become dilated, forming irregular sinusoids that bulge close beneath the surface. The arrow indicates lipid droplets. X 1,200.

B. Little resistance to respiratory exchange is presented by the squamous epithelial cell of the trophonema (sq) and the attenuated endothelial cell (e) of the capillary. These cells are separated by a thin layer of loose connective tissue and a basal lamina (bl). X 39,000.

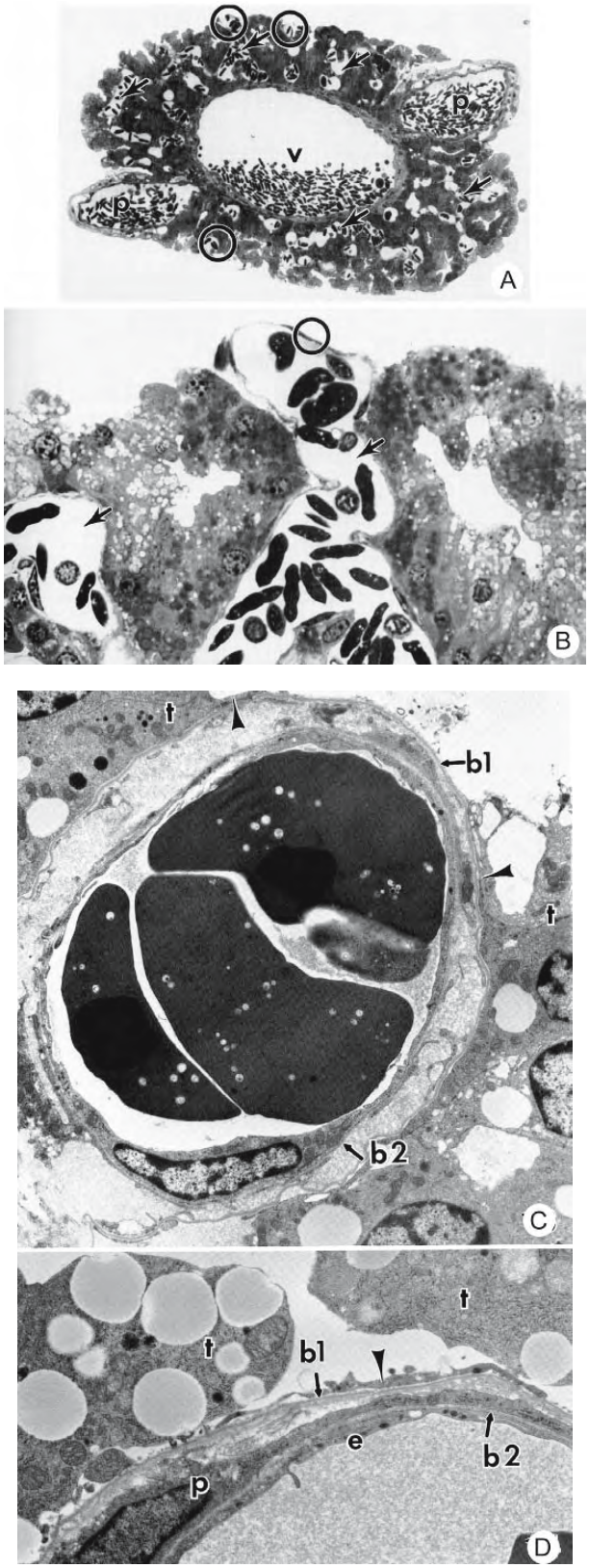

Figure 6.19: Micrographs of sections through trophonemata of the southern stingray *Dasyatis americana* at term. (From Hamlett et al., 1996; reproduced with permission of the NRC Press).

A. Photomicrograph of a cross section through an entire trophonema showing its large central blood vessel (v) and dilated peripheral vessels (p) at the flattened terminals. The epithelium over the peripheral vessels has become squamous (circles). Interstitial vessels have dilated to form sinusoids (arrows). X 600.

B. Simple squamous epithelium (circle) covers the peripheral vessel at the centre of this photomicrograph. Interstitial vessels have dilated to form sinusoids (arrows). X 3,500.

C. Transmission electron micrograph of a trophonema from a uterus containing near-term foetuses. Endothelial cells of the dilated peripheral vessel at the centre are separated from the thin squamous epithelial cells (arrowheads) by sparse loose connective tissue between the endothelial basal lamina (b2) and epithelial basal lamina (b1). Trophonemal secretory cells (t) are seen on each side of the vessel. X 6,200.

D. A pericyte (p), lying in loose connective tissue, clasps a peripheral blood vessel in this trophonema. The pericyte is separated from the endothelial cell (e) by the thin endothelial basal lamina (b2) and from the extremely thin surface epithelium (arrowhead) by the epithelial basal lamina (b1). X 8,700.

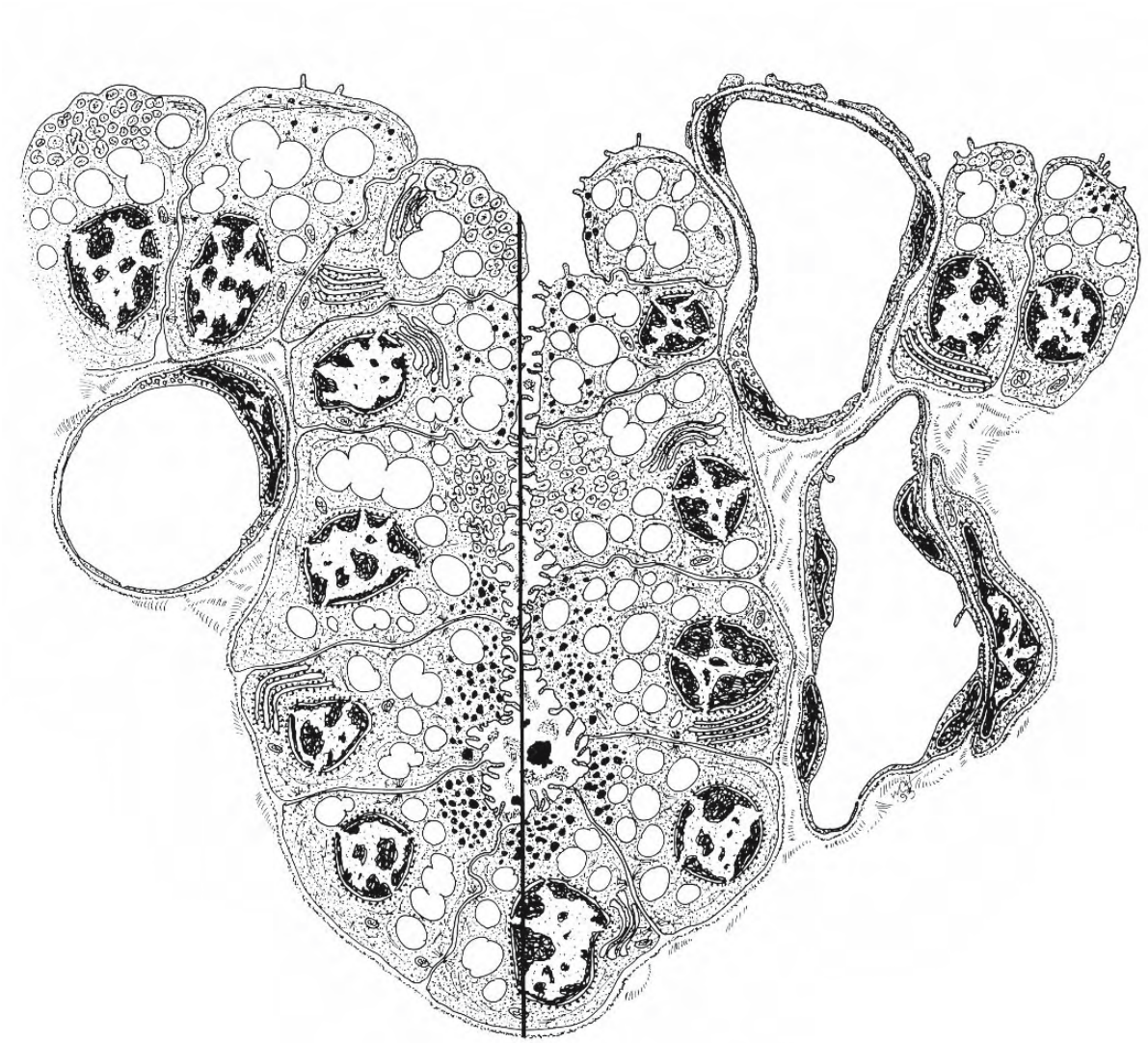

Figure 6.20: Composite line drawing, derived from transmission electron micrographs, of the uterus of the southern stingray *Dasyatis americana*. The situation in a uterus containing fertilized eggs is shown at the left; that of a uterus containing term foetuses on the right. Small vessels lie under a cuboidal epithelium in early gestation. In later gestational stages, the peripheral vasculature increases in size to form sinusoids and the epithelium over these is thinner. The remainder of the surface and crypt cells continue to function in secretion. (From Hamlett et al., 1996; reproduced with permission of the NRC Press).

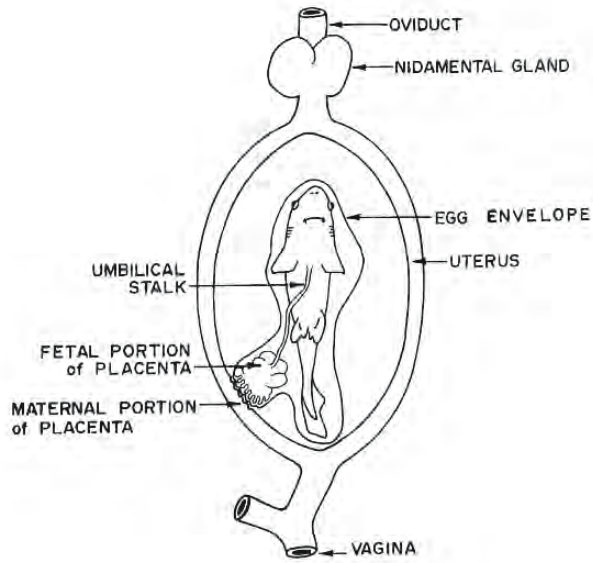

Figure 6.21: Diagram of a near-term carcharhinid embryo within the maternal uterus. The now empty yolk sac has become implanted in the maternal uterine wall. The egg envelope intervenes between embryonic and maternal tissues. Concomitant with growth and elongation of the embryo, the membrane reservoir has been obliterated and the embryo has enlarged to fill the envelope. (From Hamlett, 1987; reproduced with permission of the author).

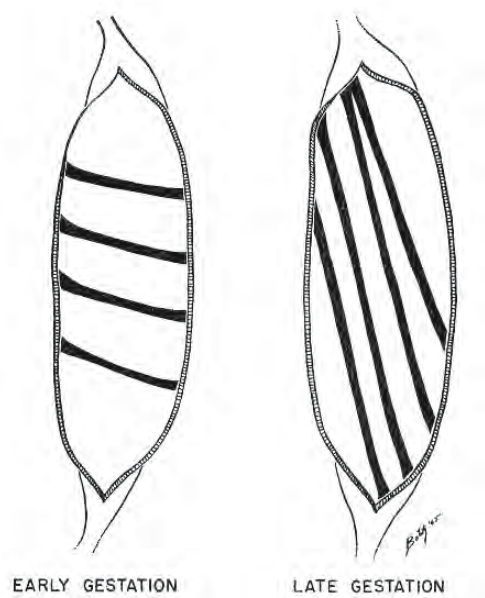

Figure 6.22: Diagrams showing the orientation of the uterine compartments in the bonnethead shark *Sphyrna tiburo* during early and late gestation. The change in the orientation of these compartments occurs gradually as the embryos grow. (From Schlernitzauer and Gilbert, 1966; © reproduced with permission of John Wiley & Sons, Inc.).

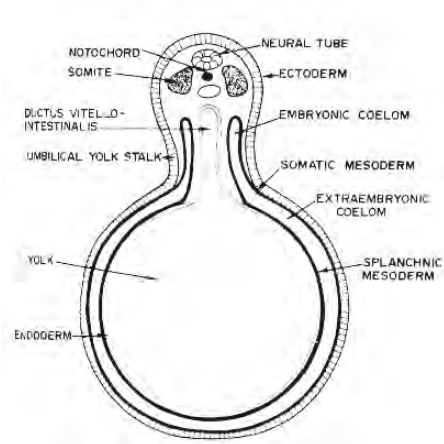

Figure 6.23: Diagram of an idealized transverse section of a preimplantation shark embryo at a level just anterior to the junctions of the ductus vitello-intestinalis and the gut. In both aplacental and placental sharks, the yolk sac arises as a ventral outpouching of the embryonic gut and contains the yolk mass enclosed within endodermal epithelium. As this endodermal evagination distends, the yolk sac remains enclosed by the mesoderm and ectoderm of the body wall and is attached to the embryo by the yolk stalk. A split subsequently forms within the mesoderm, creating the extraembryonic coelom, a space enclosed by somatic mesoderm on the outside and splanchnic mesoderm inside. The cavity containing the yolk is continuous with the lumen of the gut by the ductus vitello-intestinalis. (From Hamlett and Wourms, 1984; reproduced with permission from Elsevier Science).

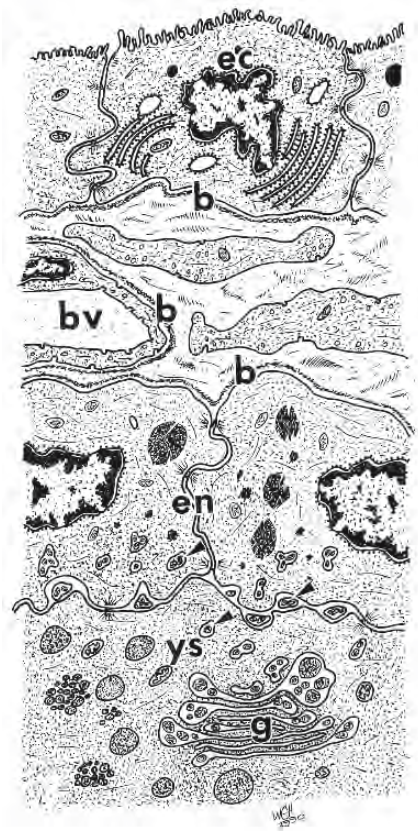

←

Figure 6.24: The wall of the preimplantation yolk sac consists of six concentric regions: ectoderm (ec), somatic mesoderm, extraembryonic coelom, splanchnic mesoderm, endoderm (en), and yolk syncytium (ys). The mesodermal layers and extraembryonic coelom lie between the basal laminae (b) of the ectoderm and endoderm in this stylized drawing. A blood vessel (bv) lies in the loose connective tissue of the mesoderm. Partially solubilized yolk is modulated through the Golgi complex (g) of the yolk syncytium and is transferred to the endoderm in membrane-limited vesicles (arrowheads). (From Hamlett. 1993; reproduced with kind permission of Kluwer Academic Publishers).

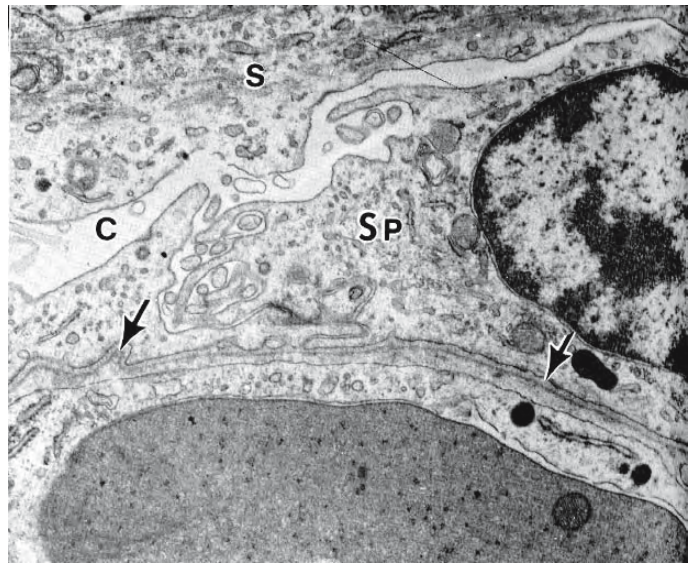

Figure 6.25: Transmission electron micrograph of a section through the wall of the yolk sac of a preimplantation embryo of the Atlantic sharpnose shark *Rhizoprionodon terraenovae.* The extraembryonic coelom (C) lies between the somatic mesoderm (S) and splanchnic mesoderm (Sp). The endothelial basal lamina (arrows) separates the splanchnic mesoderm from the endothelium of a yolk sac capillary containing an erythrocyte. X 19,000 (From Hamlett and Wourms, 1984; reproduced with permission from Elsevier Science).

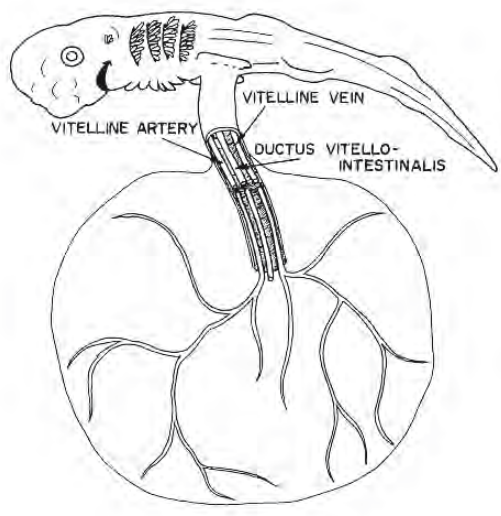

Figure 6.26: The yolk sac of a preimaplantation stage of a carcharhinid embryo is covered with ectodermal epithelium that is continuous, by way of the yolk stalk, with the ectoderm that encloses the embryo itself. The yolk stalk contains a vitelline artery, vein, and ciliated ductus vitello-intestinalis, confluent with the foetal gut. (From Hamlett, 1987; reproduced with permission of the author).

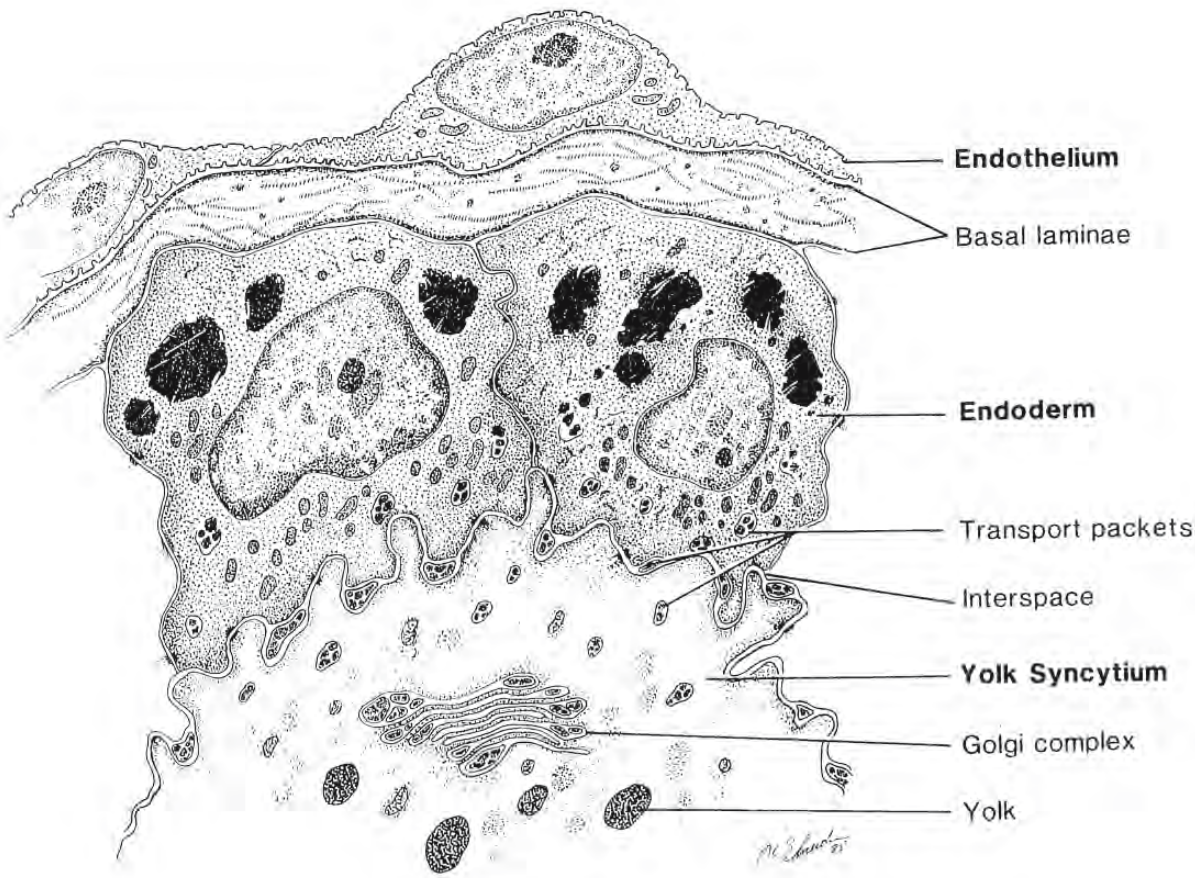

Figure 6.27: Drawing of a section of the yolk syncytial-endodermal complex in the yolk sac of a preimplantation shark embryo. Yolk platelets are partially digested within the yolk syncytium. The products are modified within the syncytial Golgi complex and transported to the endoderm in membrane-limited packets. Metabolites are then passed to the endothelium. (From Hamlett, 1987; reproduced with permission of the author).

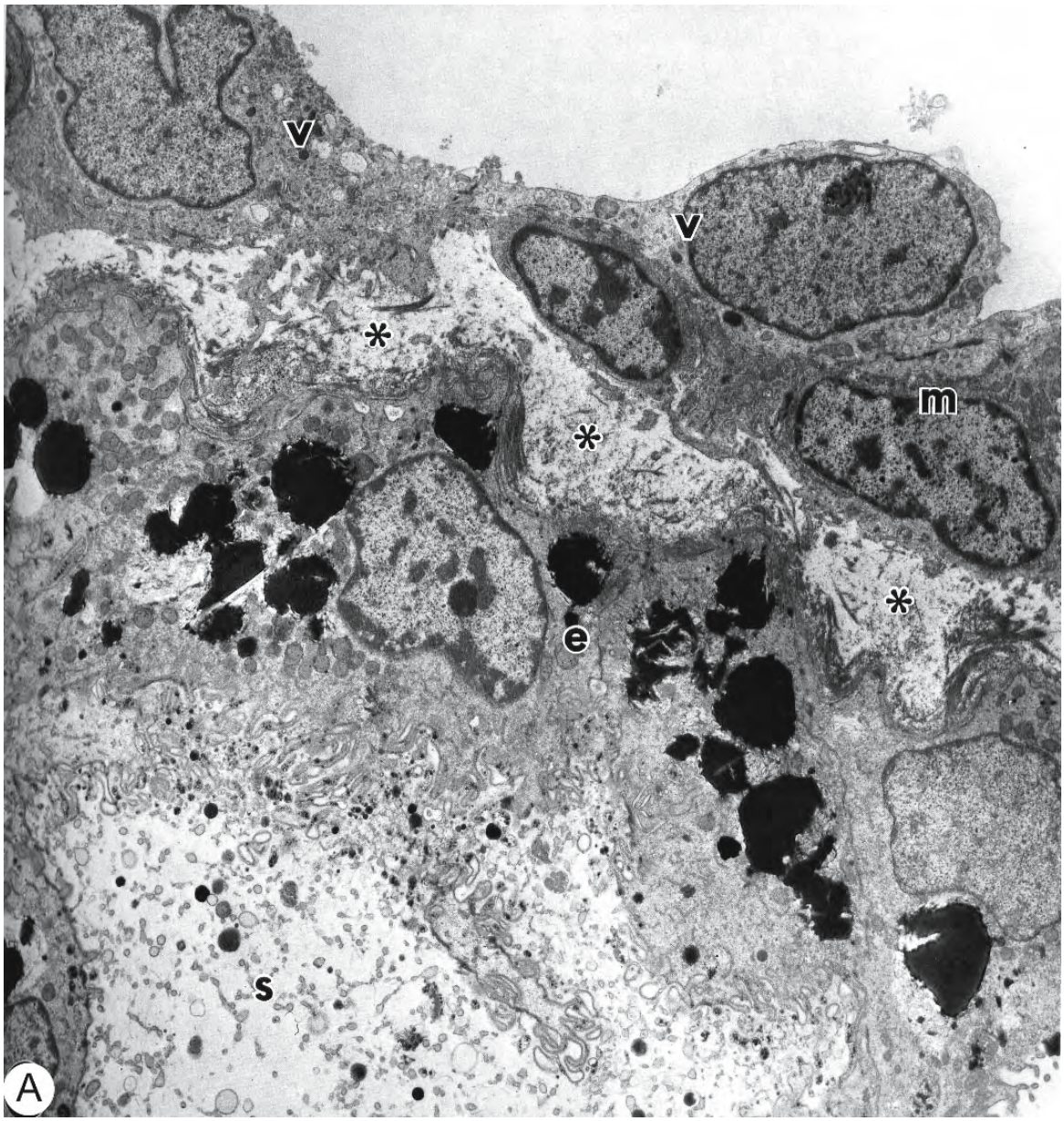

Figure 6.28: Transmission electron micrographs of sections of the preimplantation yolk sac of the shark *Rhizoprionodon terraenovae.* (From Hamlett, Schwartz, and DiDio, 1987; reproduced with permission of the authors).

A. The yolk syncytial-endodermal complex is composed of the central yolk syncytium (s), the endoderm (e), a connective tissue space (*) containing mesenchymal cells (m), and the endothelium of the vitelline vessels (v). The endoderm is a simple cuboidal layer abutting the yolk syncytium and is intensely amplified by folds that interdigitate with the membrane delimiting the yolk syncytium. X 5,412.

B. In this section through the yolk syncytium, vesicles containing yolk droplets fuse with the forming face of the Golgi complex open arrows). Yolk droplets bud off the ends of the dilated Golgi cisternae as well as from the maturing face in membrane-bound packets (solid arrows). The endoderm (e) is visible at the top. X 44,500 The inset shows several yolk droplets being modified within the Golgi complex. X 66,000.

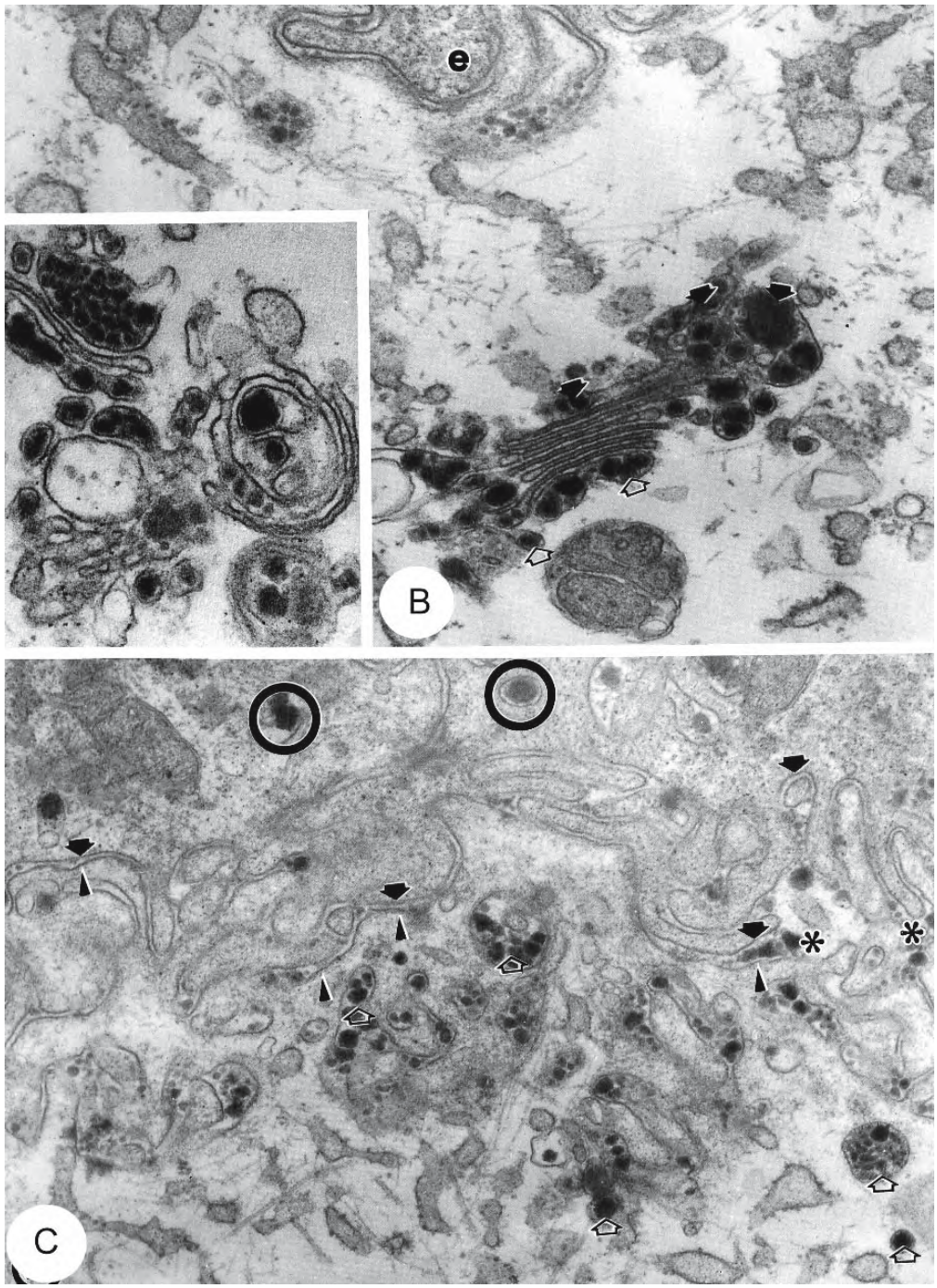

Figure 6.28: Continued.

C. Membrane-bound packets (open arrows) containing yolk droplets are visible within the yolk syncytium. The membranes of the yolk syncytium (arrowheads) and the adjacent endodermal cell (solid arrows) are closely apposed and enclose an interspace (*) containing yolk droplets. Yolk droplets are subsequently endocytosed by the endodermal cells and are initially surrounded by a membrane (circles). X 33,000.

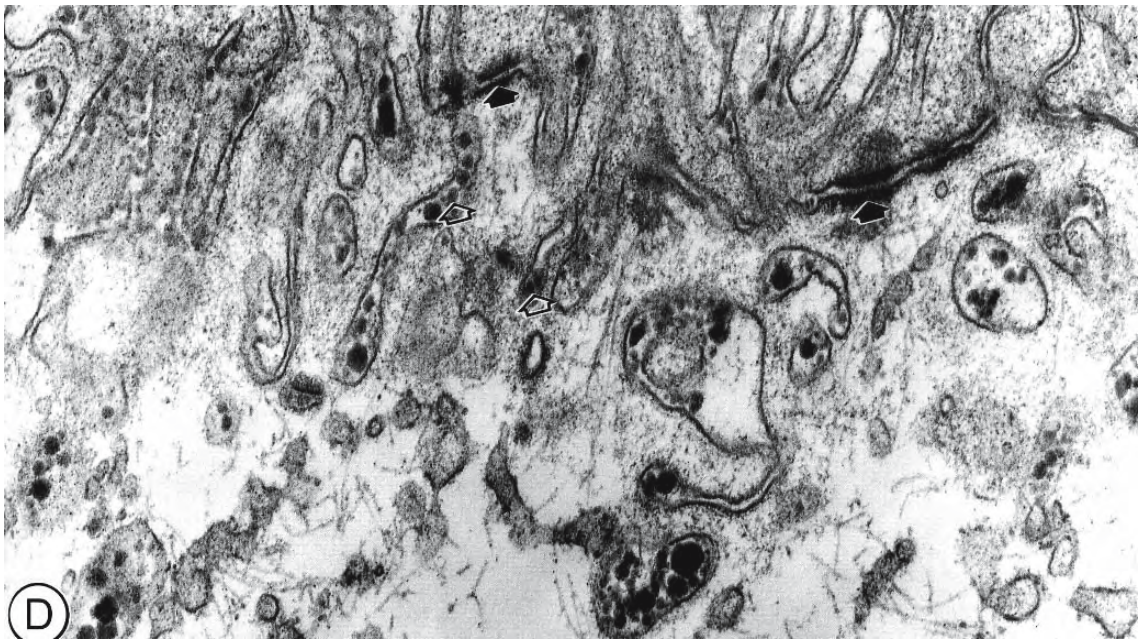

Figure 6.28: Continued.
D. The membranes of the yolk syncytium and the endodermal cells are closely apposed, elaborately interdigitated, and joined by desmosomes (solid arrows). Yolk droplets are seen in the interspace (open arrows). X 40,000.

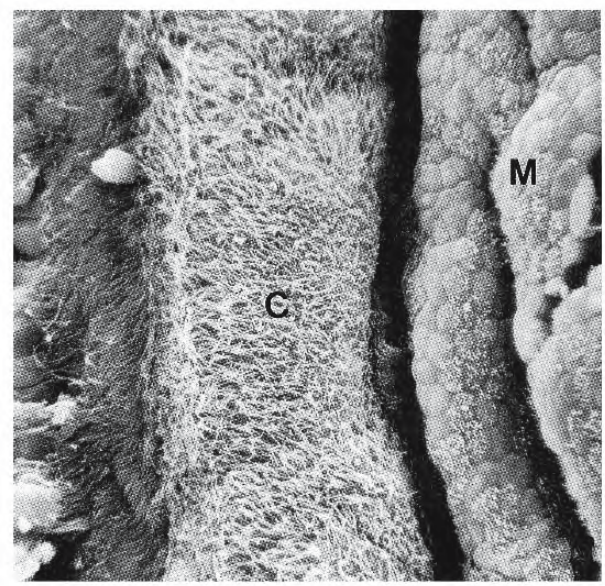

Figure 6.29: Scanning electron micrograph of the interior of the ductus vitello-intestinalis from the yolk stalk of an elasmobranch embryo. Linear rows of ciliated (C) and microvillar (M) cells line the wall. During vitellogenic development, yolk platelets from the yolk mass are passed up the ductus by ciliary action of the epithelial cells. (From Hamlett et al., 1993a; © reproduced with permission of John Wiley & Sons, Inc.).

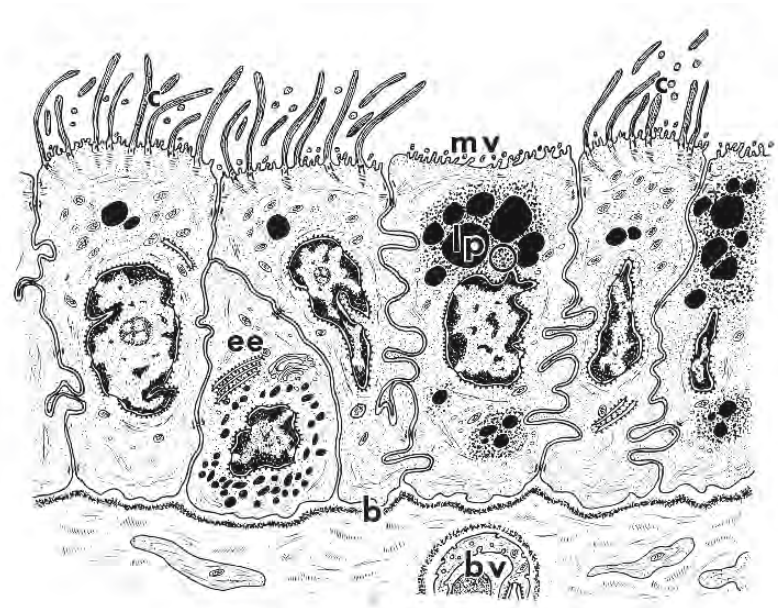

Figure 6.30: This drawing depicts the three cell types that make up the epithelial lining of the ductus vitello-intestinalis from the yolk stalk of an elasmobranch embryo. These include ciliated columnar cells (c), microvillar cells (mv) with prominent lipid inclusions (lp) and glycogen (circle), and enteroendocrine cells (ee). Note that the enteroendocrine cell does not attain the surface; its secretion granules appear to be directed basally into the vascular connective tissue lying below. A basal lamina (b) separates the epithelium from the connective tissue. bv, blood vessel. (From Hamlett. 1993; reproduced with kind permission of Kluwer Academic Publishers).

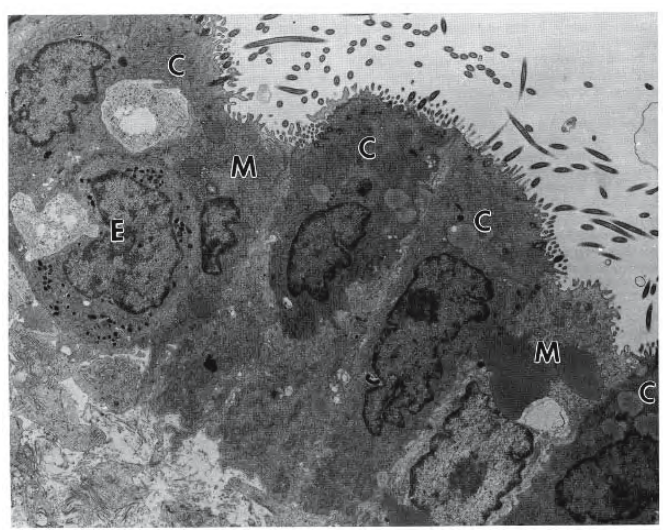

Figure 6.31: Transmission electron micrograph of a section of the epithelial lining of the ductus vitello-intestinalis from the umbilical cord of the Atlantic sharpnose shark *Rhizoprionodon terraenovae.* Three distinct cell types make up the epithelium. Columnar cells with cilia and microvilli (C) alternate with strictly microvillar cells (M) rich in lipid and glycogen. Enteroendocrine cells (E) do not attain the surface. X 6,600 (From Hamlett, 1989; © reproduced with permission of John Wiley & Sons, Inc.).

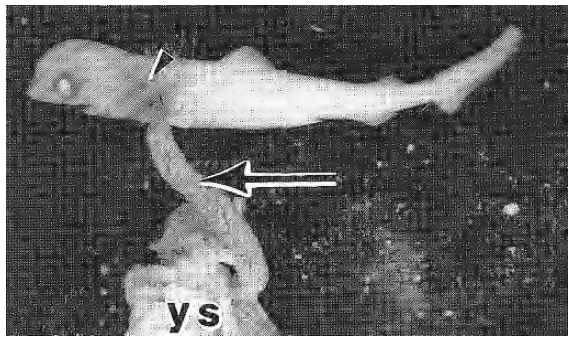

Figure 6.32: Photograph of a 6.0-cm embryo of the Atlantic sharpnose shark *Rhizoprionodon terraenovae.* Gill filaments (arrowhead) are prominent. The contents of the yolk sac (ys) are reduced and the yolk stalk is covered by bushy appendiculae (arrow). (From Hamlett., 1993; reproduced with kind permission of Kluwer Academic Publishers).

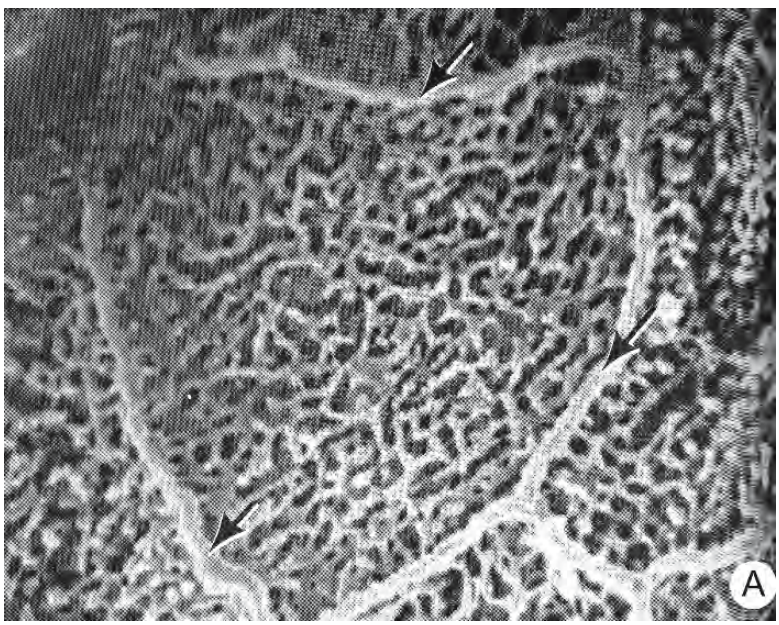

Figure 6.33: Micrographs of the ectoderm of the yolk sac from an embryo of the Atlantic sharpnose shark *Rhizoprionodon terraenovae.* (From Hamlett and Wourms, 1984; reproduced with permission from Elsevier Science).

A. This scanning electron micrograph shows the labyrinthine pattern of microplicae extending over the epithelial surface except at the periphery where ridge-like boundaries delineate adjacent cells (arrows). X 6,000.
B. Transmission electron micrograph of dilated cisternae of granular endoplasmic reticulum (R), lipid-like inclusions (L), coated vesicles (large arrows), uncoated vesicles (small arrows), and Golgi complexes (G) in the cytoplasm of a somatic ectodermal cell. X 22,000.
C. The nucleus (N) and parallel arrays of granular endoplasmic reticulum (R) in a somatic ectodermal cell. Cisternae of the endoplasmic reticulum are not dilated. X 29,000.
D. A collagenous stroma (C) lies between the somatic ectoderm (E) and the mesoderm of the yolk sac. A basal lamina (L) subtends the ectodermal cell. Circular profiles of inclusion bodies (arrows) occur within the stroma. X 63,000.

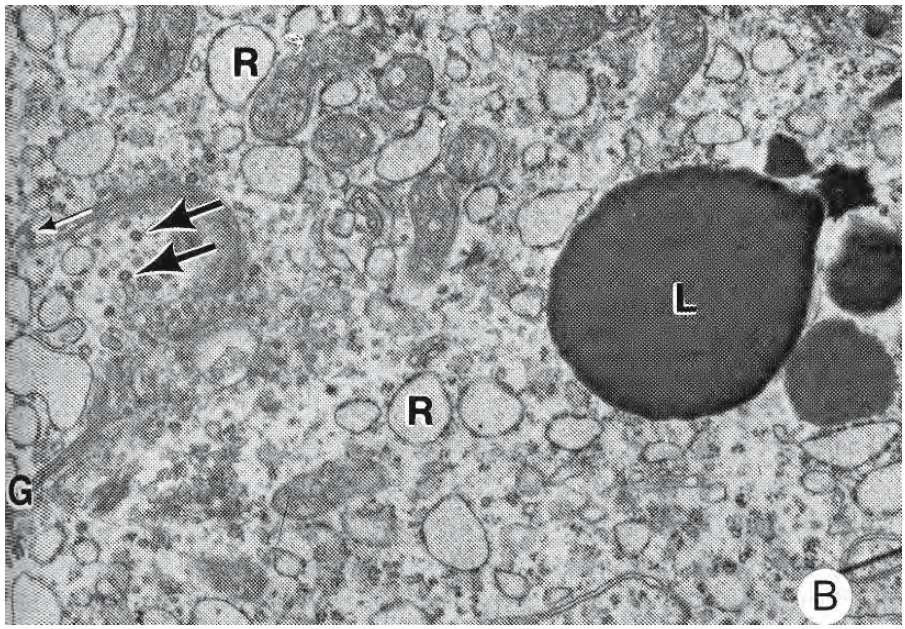

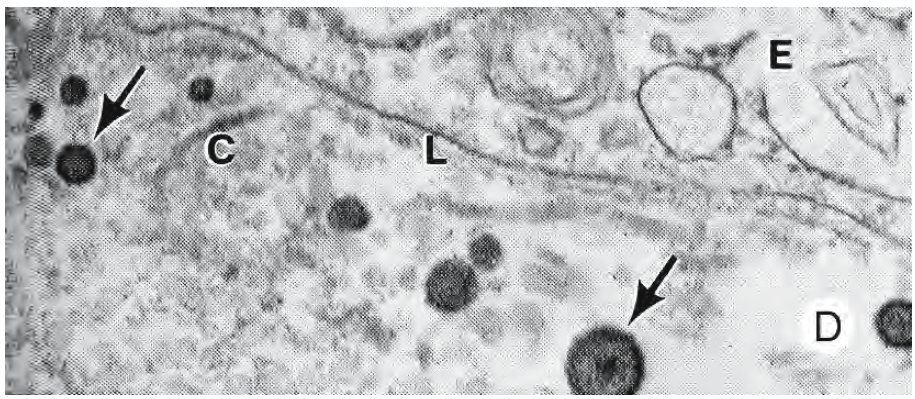

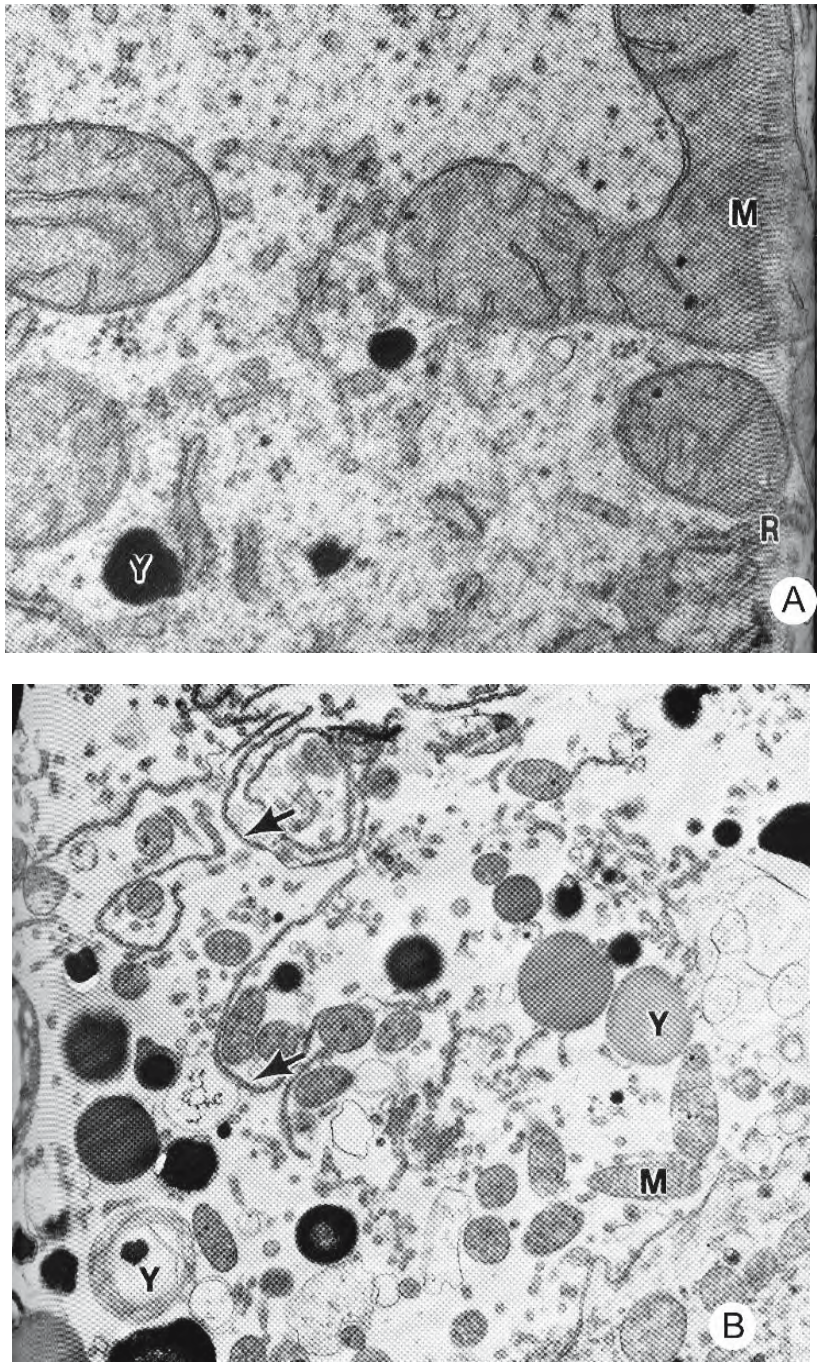

Figure 6.34: Transmission electron micrographs of sections of the yolk sac from an embryo of the Atlantic sharpnose shark *Rhizoprionodon terraenovae.* (From Hamlett and Wourms, 1984; reproduced with permission from Elsevier Science).

A. The cytoplasm of endodermal cells contains mitochondria (M), scattered elements of granular endoplasmic reticulum (R), and yolk degradation bodies (Y). X 92,000.

B. A heterogeneous collection of yolk granules (Y), mitochondria (M), and membranous lamellae (arrows) are seen in the yolk syncytium. X 14,000.

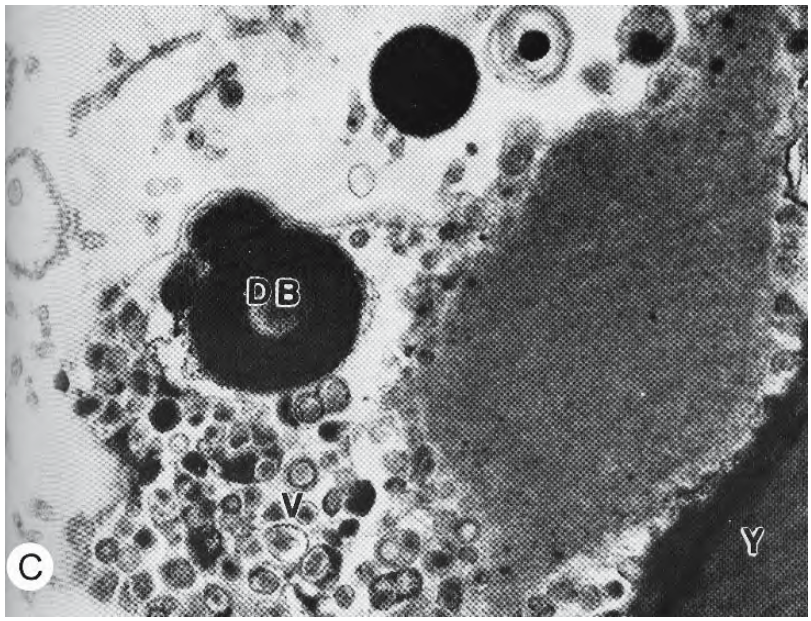

Figure 6.34: Continued
C. Numerous small yolk degradation vesicles (V) and larger yolk degradation bodies (DB) are associated with the periphery of yolk platelets (Y) within the yolk syncytium. X 29,000.

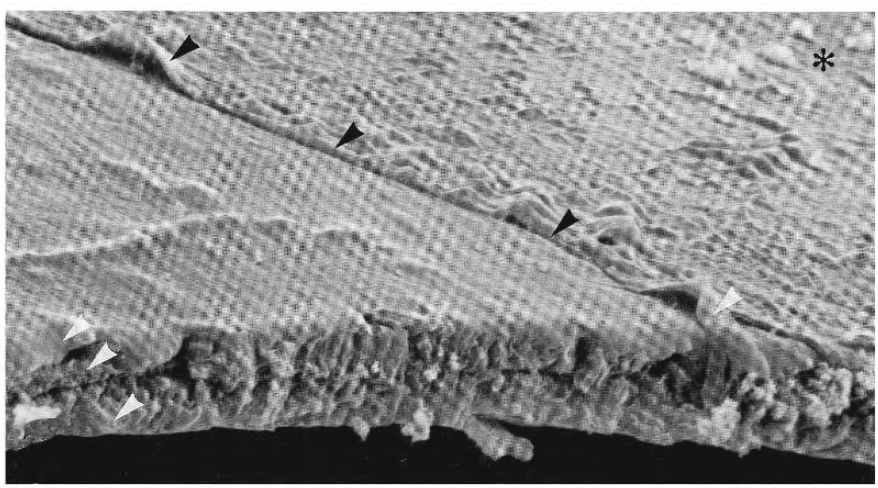

Figure 6.35: Scanning electron micrograph of the cut surface of an egg capsule of the viviparous shark *Mustelus canis* revealing multiple laminae (white arrowheads). Black arrowheads indicate the edge of the incomplete outer lamina. Granular calcium deposits are present on the capsular surface (*). X 4,067 (From Lombardi and Files, 1993; © reproduced with permission of John Wiley & Sons, Inc.).

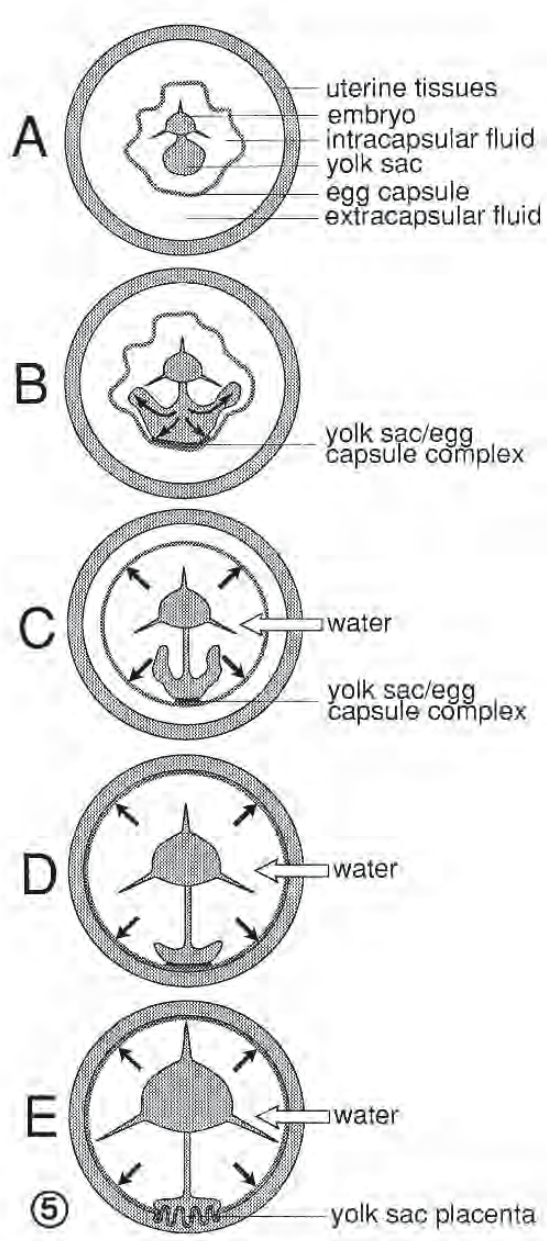

Figure 6.36: Diagrams to illustrate a hypothetical mechanism of placentation in *Mustelus canis.* (From Lombardi and Files, 1993; © reproduced with permission of John Wiley & Sons, Inc.).

A. Early term embryo enclosed within the egg capsule.
B. Hypertrophy of the surface of the yolk sac and formation of the yolk sac/egg capsule complex.
C. Release by the embryo of solute particles of high molecular weight causes movement of water into the intracapsular space from extracapsular and maternal tissue fluids (white arrow) thereby causing distention of the egg capsule (black arrows).
D. Distention of the egg capsule obliterates the extracapsular space resulting in the apposition of the yolk sac/egg capsule complex against the uterine lining.
E. The yolk sac placenta is formed by the interdigitation of maternal and embryonic tissues.

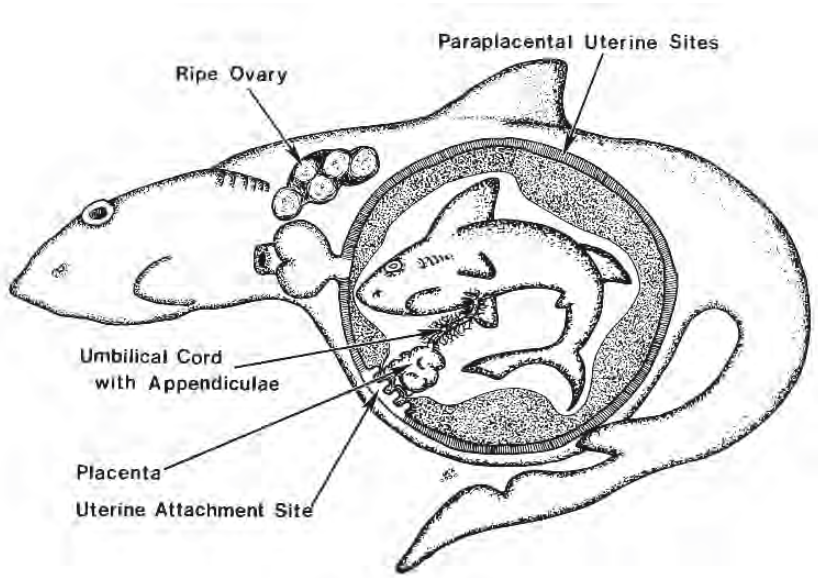

Figure 6.37: Schematic drawing of a female of the Atlantic sharpnose shark *Rhizoprionodon terraenovae* at term. The yolk stalk is transformed into an umbilical cord with appendiculae; the yolk sac contributes to a functional placenta. Specialized attachment sites for the distal portion of the placenta modulate metabolic exchange. (From Hamlett. 1993; reproduced with kind permission of Kluwer Academic Publishers).

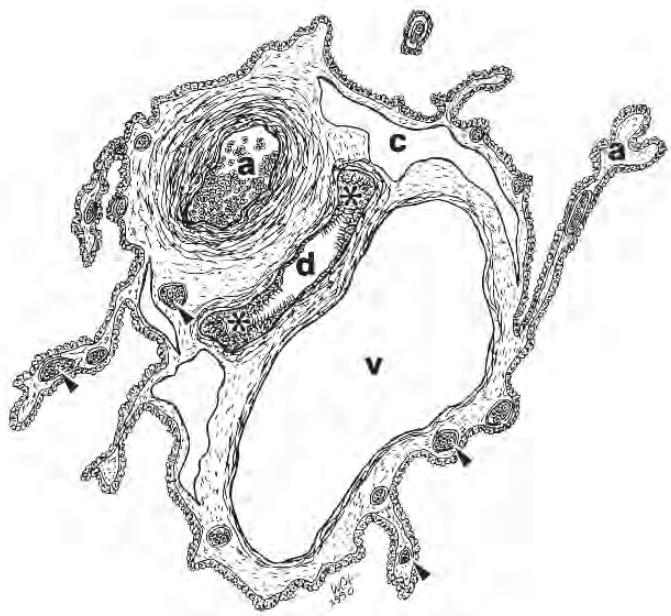

Figure 6.38: Sketch of a cross section of a mature umbilical cord of the Atlantic sharpnose shark *Rhizoprionodon terraenovae.* Shown are sections of the muscular umbilical artery (a), umbilical vein (v), ductus vitellointestinalis (d) with rows of cilia (*), and the extraembryonic coelom (c). Small blood vessels (arrowheads) occupy the connective tissue stroma of the appendiculae (a) as well as the body of the cord. (From Hamlett. 1993; reproduced with kind permission of Kluwer Academic Publishers).

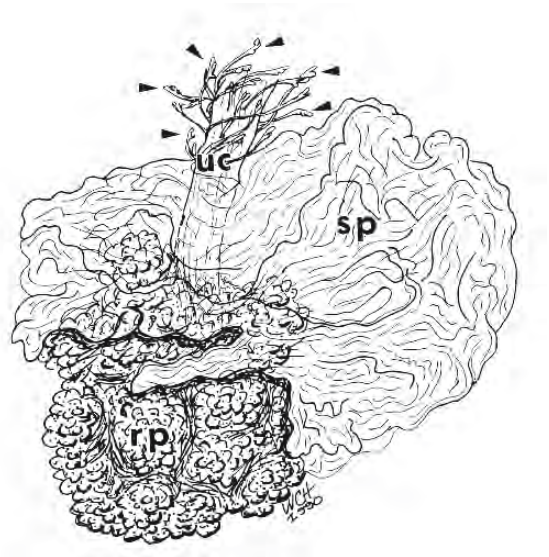

Figure 6.39: Sketch of the yolk sac of the Atlantic sharpnose shark *Rhizoprionodon terraenovae.* The yolk sac becomes regionally modified into two regions. The diaphanous proximal smooth segment (sp) is confluent with the umbilical cord (uc) and drapes over the richly vascular distal rugose portion (rp) that abuts the uterine attachment site. Appendiculae (arrowheads) emerge from the umbilical cord. (From Hamlett. 1993; reproduced with kind permission of Kluwer Academic Publishers).

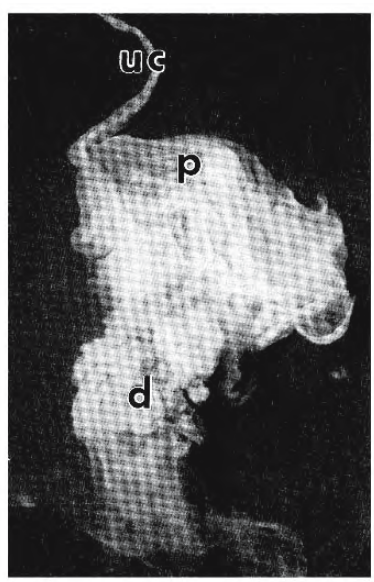

Figure 6.40: Photograph of the placenta of the blacknose shark *Carcharhinus plumbeus.* The placenta is differentiated into a proximal smooth portion (p) that is confluent with the umbilical cord (uc) and a distal rugose portion (d). (From Hamlett et al., 1983a; © reproduced with permission of John Wiley & Sons, Inc.).

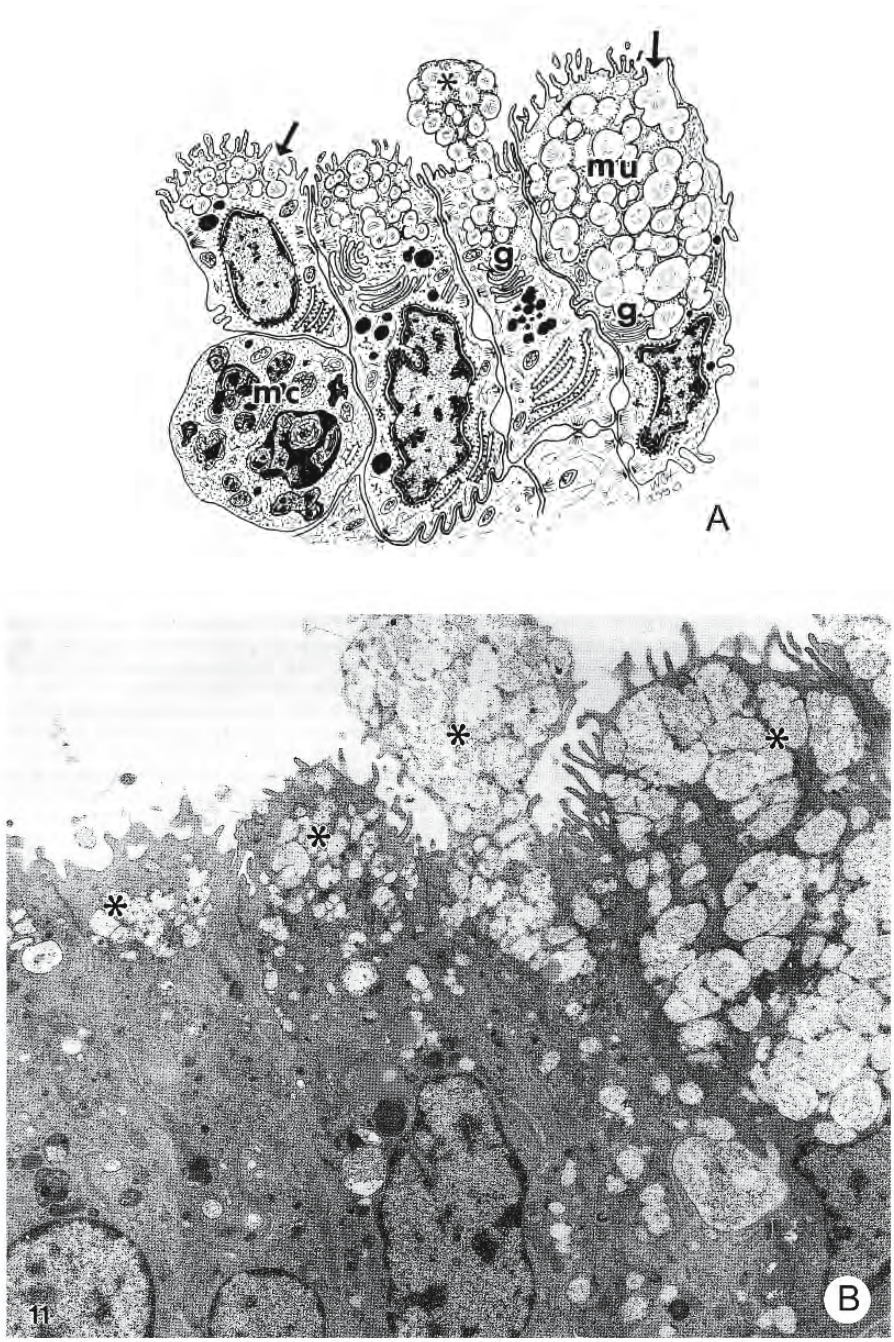

Figure 6.41: Representations of sections of the paraplacental area of the term uterus of the Atlantic sharpnose shark *Rhizoprionodon terraenovae.*

A. In this sketch, the columnar epithelial cells have prominent Golgi complexes (g) and apical mucous vesicles (*). Mucus (mu) is released by exocytosis (arrows). A macrophage (mc) is wandering between the epithelial cells. (From Hamlett, 1993; reproduced with kind permission of Kluwer Academic Publishers).

B. Transmission electron micrograph of a similar section as that shown above. The asterisks indicate mucous vesicles in the columnar epithelial cells. X 12,000 (From Hamlett, Miglino, and DiDio, 1993; reproduced with permission from Nuova Immagine Editrice).

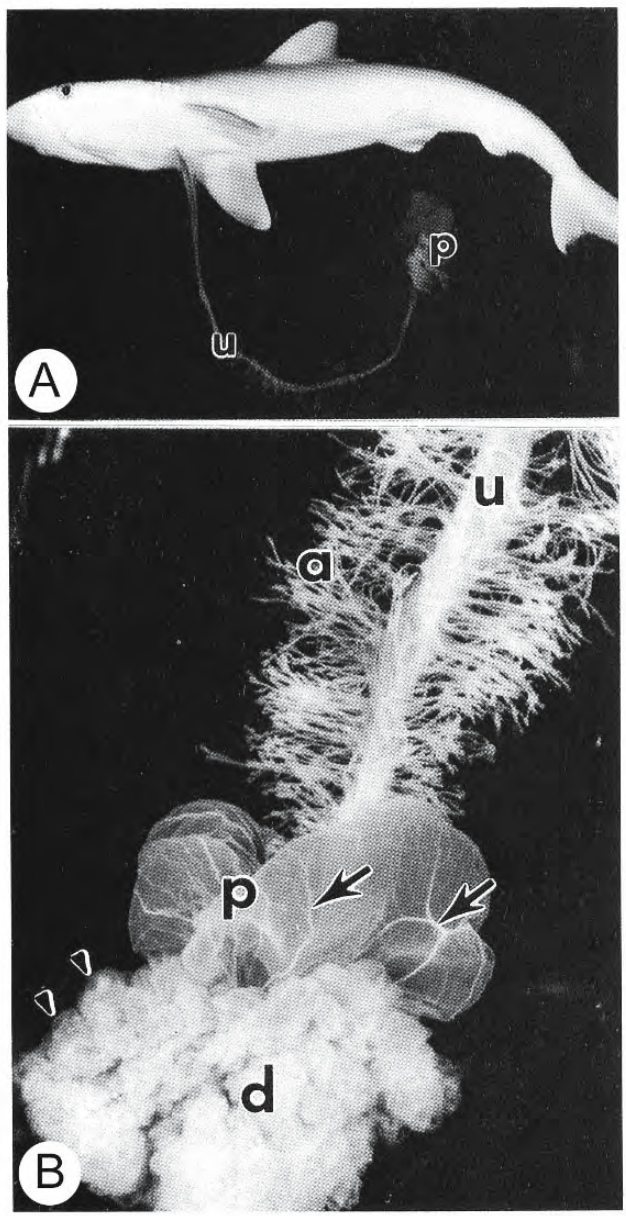

Figure 6.42: Aspects of the intact umbilical cord and placenta of the Atlantic sharpnose shark *Rhizoprionodon terraenovae.* (From Hamlett, Miglino, and DiDio, 1993; reproduced with permission from Nuova Immagine Editrice).

A. Photograph of a term foetus connected to the foetal yolk sac portion of the placenta (p) by the umbilical cord (u).

B. This close-up view shows appendiculae (a) extending from the umbilical cord (u). Vascular channels (arrows) are visible in the proximal portion (p) of the yolk sac. The distal portion of the yolk sac (d) has a lobulated, rugose surface (arrowheads).

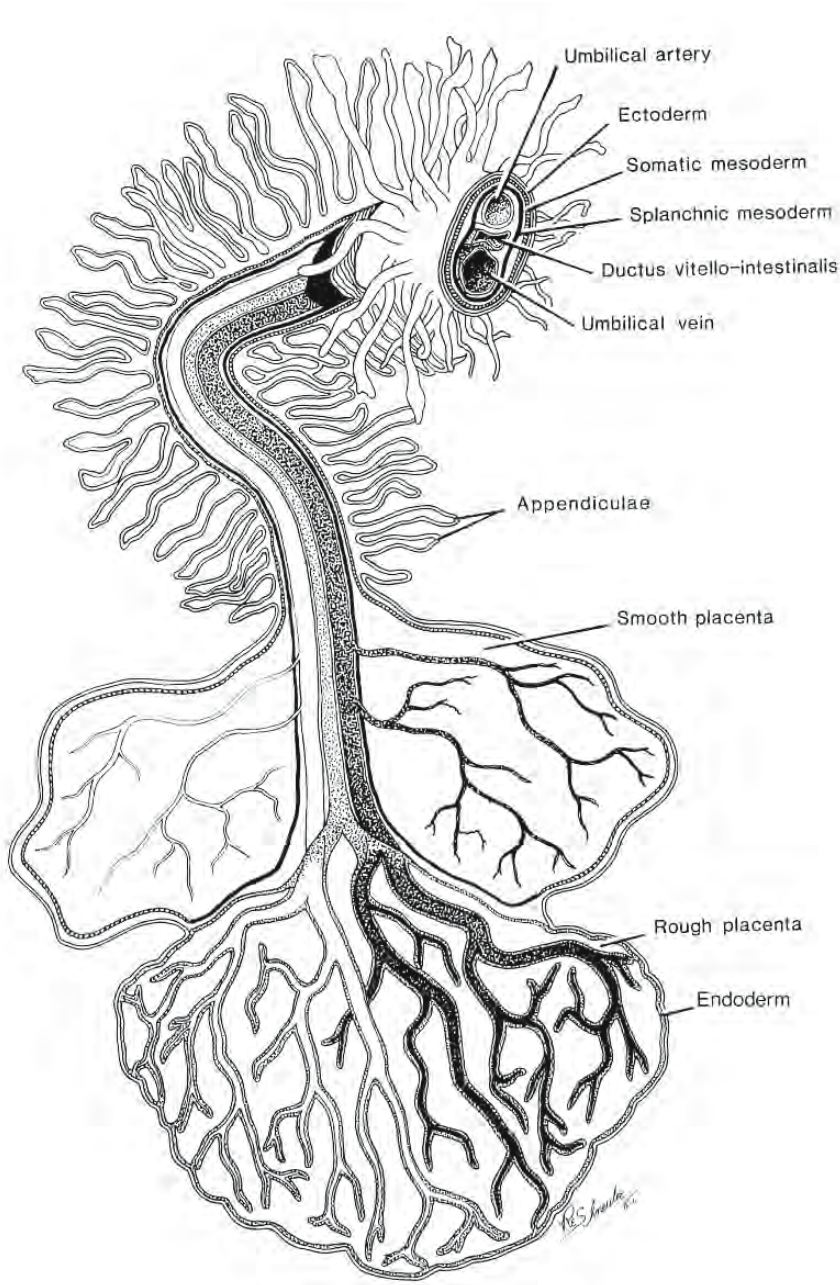

Figure 6.43: Stereodiagram of the germ layer contributions to the shark yolk sac placenta. The appendiculae are vascularized outpocketings of ectoderm that are filled with loose connective tissue. The smooth placenta has contributions from ectoderm and somatic mesoderm. The rugose (rough) placenta is richly supplied by mesodermally derived vasculature. Endodermal cells coat the blood vessels and the inner aspect of the ectoderm. (From Hamlett, 1987; reproduced with permission of the author).

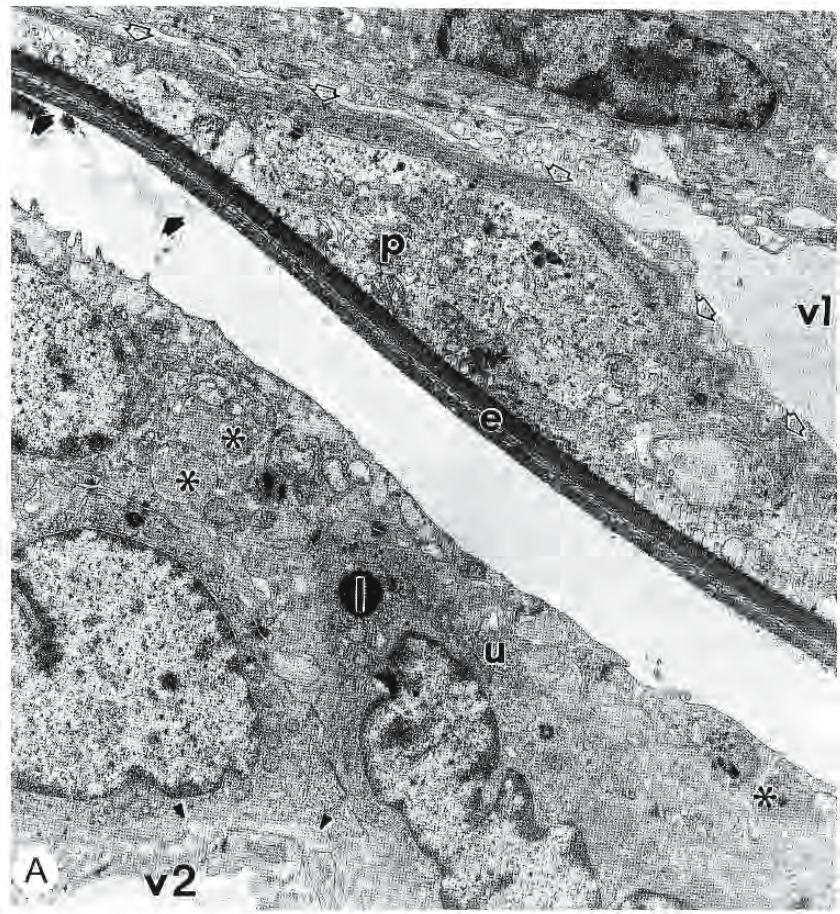

Figure 6.44: The site of placental-uterine exchange in the shark.

A,B. Electron micrographs of sections of the uterus of the Atlantic sharpnose shark *Rhizoprionodon terraenovae*. (From Hamlett, Miglino, and DiDio, 1993; reproduced with permission from Nuova Immagine Editrice).

A. The placental epithelium (p) is separated from the uterine epithelium (u) by the egg envelope (e) and an interspace. The uterine epithelial cells of the attachment site contain secretory vesicles (*) and lipid inclusions (l). Secretory material (black arrows) is present in the interspace. A basal lamina (arrowheads) separates the uterine epithelium from the continuous endothelium of the vascular bed (v2). The placental epithelium is separated from its subjacent blood supply (v1) by a prominent basal lamina (open arrows). X 10,000.

B. The uterine epithelium is a single layer of low cuboidal cells bearing a few microvilli (arrowheads). The plasmalemmas of adjacent cells are elaborately infolded (open arrow) and the intercellular spaces are sealed apically by junctional complexes (circle). The cytoplasm of the epithelial cells contains Golgi complexes (g), polysomes and free ribosomes (r). A basal lamina (black arrow) separates the epithelium from the continuous endothelium (e) of a vessel containing erythrocytes and white blood cells (w). X 9,000.

C. The uterine/placental association in the blacknose shark *Carcharhinus plumbeus* is shown in this drawing. The egg envelope (ee) is borne aloft by abundant microvilli of the epithelial cells of the term placenta (upper portion of illustration). This epithelium is separated from the fenestrated endothelium of its blood supply by a common basal lamina. On the uterine side, the fenestrated endothelium of the blood vessels is separated by a basal lamina from the simple cuboidal epithelium (lower portion of illustration). These epithelial cells display extensive granular endoplasmic reticulum and both coated and uncoated vesicles. (From Hamlett et al., 1983a; reproduced with permission of John Wiley & Sons, Inc.).

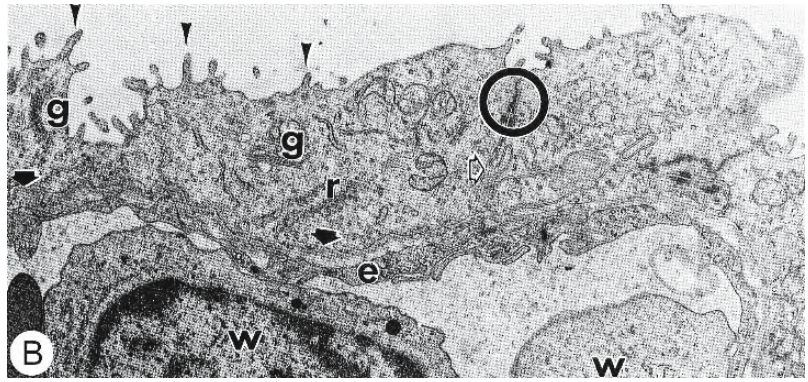

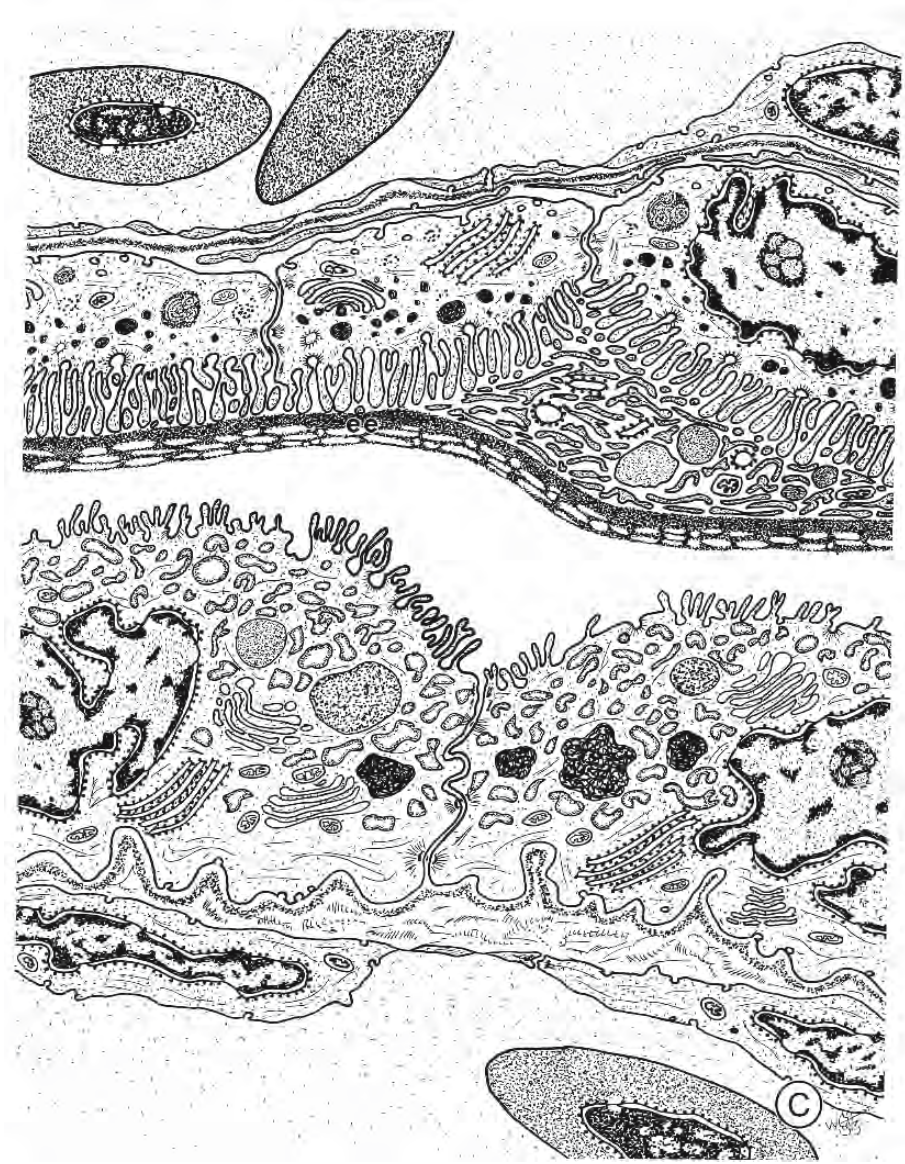

Figure 6.45: There may be a reduction in the barriers to the exchange of materials in the shark placenta and an increase in the area of tissue contact by means of interdigitation. This is a simplified drawing of the placenta of a 235-mm embryo of *Mustelus griseus.* The placenta consists of a maternal (solid black) and foetal portion (dotted area). Blood vessels are cross-hatched. (From Teshima, 1975; reproduced with permission from the Ichthyological Society of Japan).

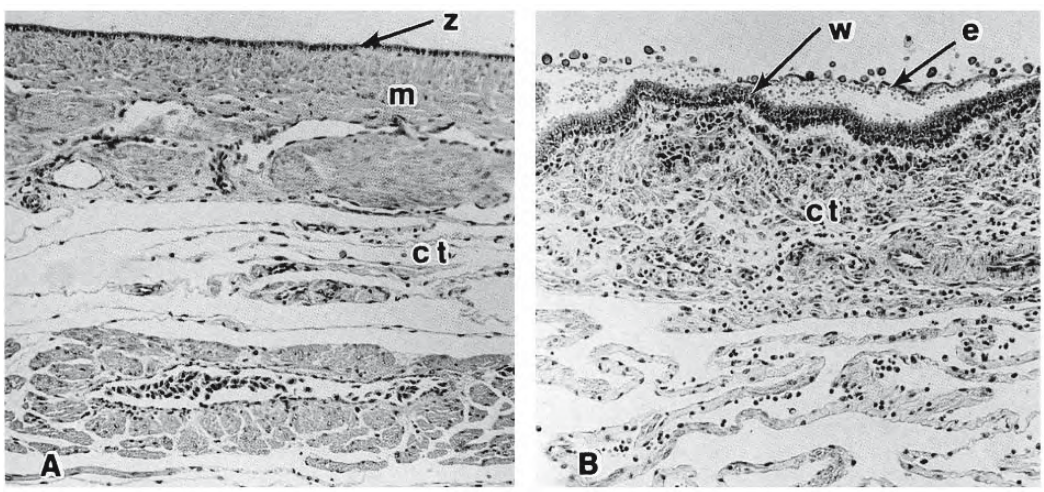

Figure 6.46: Photomicrographs of sections of the uterine wall of the Atlantic sharpnose shark *Rhizoprionodon terraenovae* during early gestation. (From Castro and Wourms, 1993; © reproduced with permission of John Wiley & Sons, Inc.).

A. Outer region of the uterine wall showing serosal epithelium (z), longitudinal and circular muscle layers (m), and a connective tissue layer (ct). X 35.

B. Inner region of the uterine wall showing the lumen, the egg envelope (e) overlying the luminal epithelium (w) and connective tissue (ct). X 100.

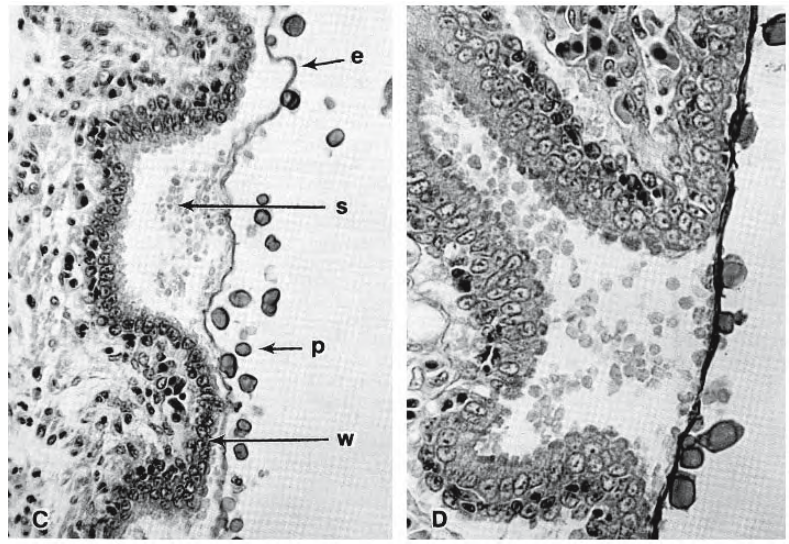

Figure 6.46: Continued.

C. Section of the inner part of the uterus showing the epithelium (w). A shallow luminal pit containing putative secretory products (s) lies on the on the epithelial side of the egg envelope (e); yolk platelets (p) are seen on the luminal side. X 200.

D. The egg envelope is closely applied to the luminal epithelium except in the region of the luminal pit. X 350.

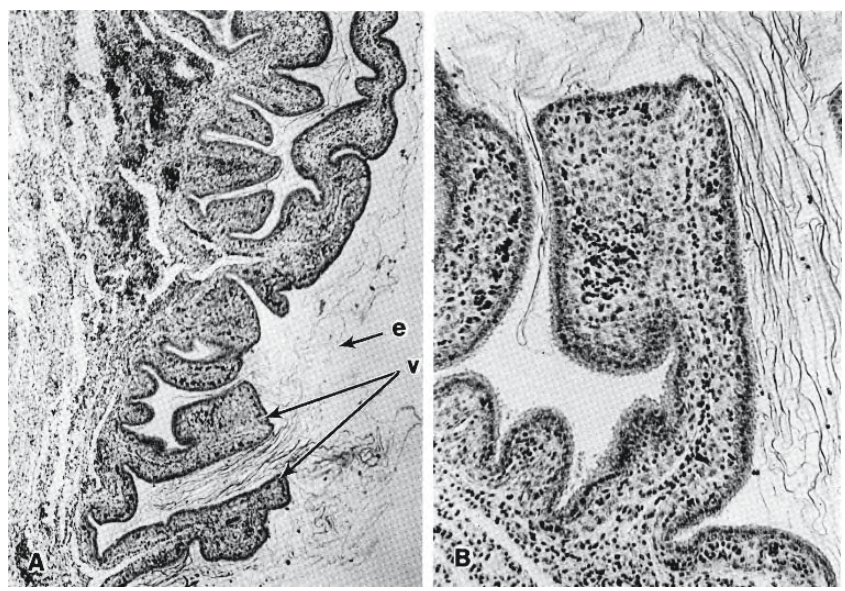

Figure 6.47: Photomicrographs of sections of the uterine wall of the Atlantic sharpnose shark *Rhizoprionodon terraenovae* at the time of implantation. (From Castro and Wourms, 1993; © reproduced with permission of John Wiley & Sons, Inc.).

A. At the implantation site, the uterine wall bears numerous ridges, folds, and protruberances covered with either a pseudostratified epithelium or a layer of short, columnar epithelial cells two cells thick. Placental villi (v) are covered by the egg envelope (e). X 35.

B. This placental villus is covered by the much-folded egg envelope. X 100.

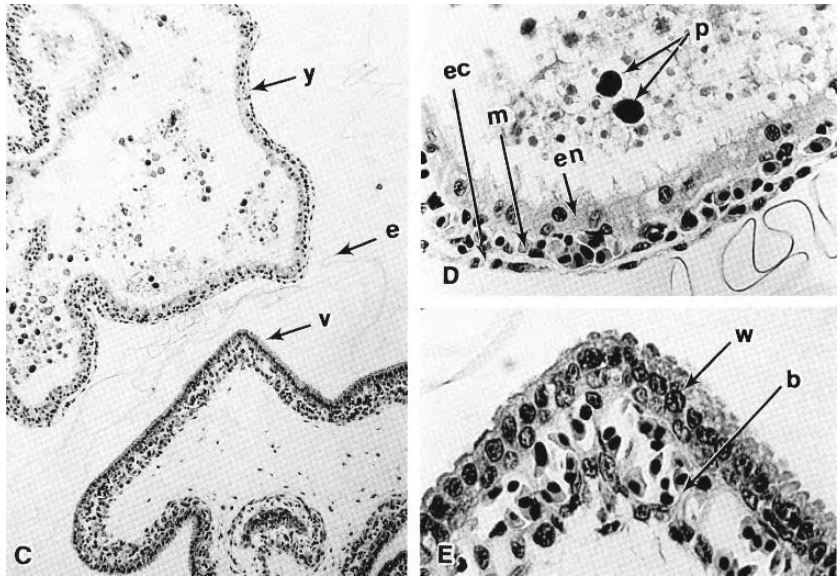

Figure 6.47: Continued.

C. The yolk sac (y) and a villus (v) at the implantation site are separated by the egg envelope (e). X 75.

D. The yolk sac is composed to three layers: ectoderm (ec), mesoderm (m), and endoderm (en). X 225.

E. The epithelium (w) of this placental villus is two cells thick and rests on loose connective tissue containing capillaries (b). X 350.

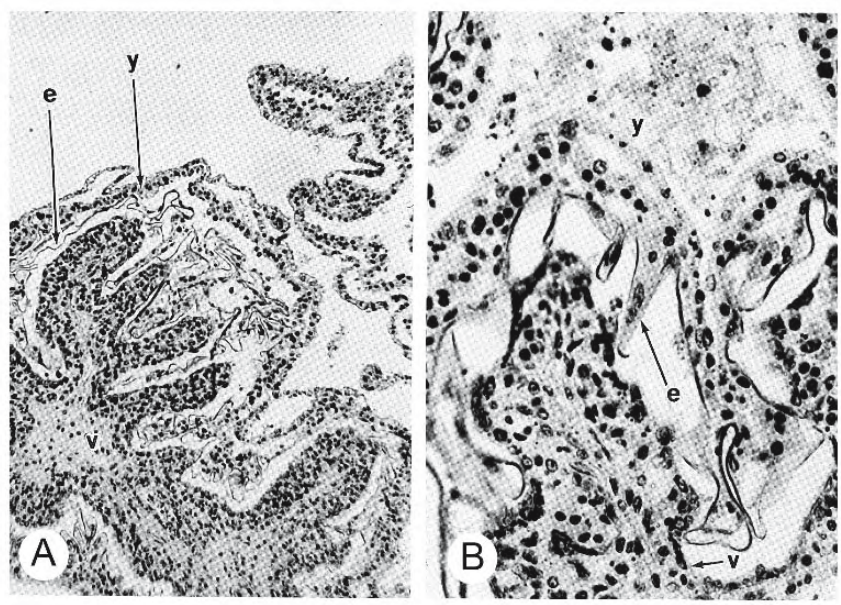

Figure 6.48: Photomicrographs of sections of the uterine wall of the Atlantic sharpnose shark *Rhizoprionodon terraenovae* during gestation. (From Castro and Wourms, 1993; © reproduced with permission of John Wiley & Sons, Inc.).

A. Placental villi (v) interdigitate with the yolk sac (y); the egg envelope (e) separates them. X 125.

B. Extensions of the yolk sac (y) are closely interdigitated with a placental villus (v). The egg envelope (e) adheres tightly to the yolk sac.

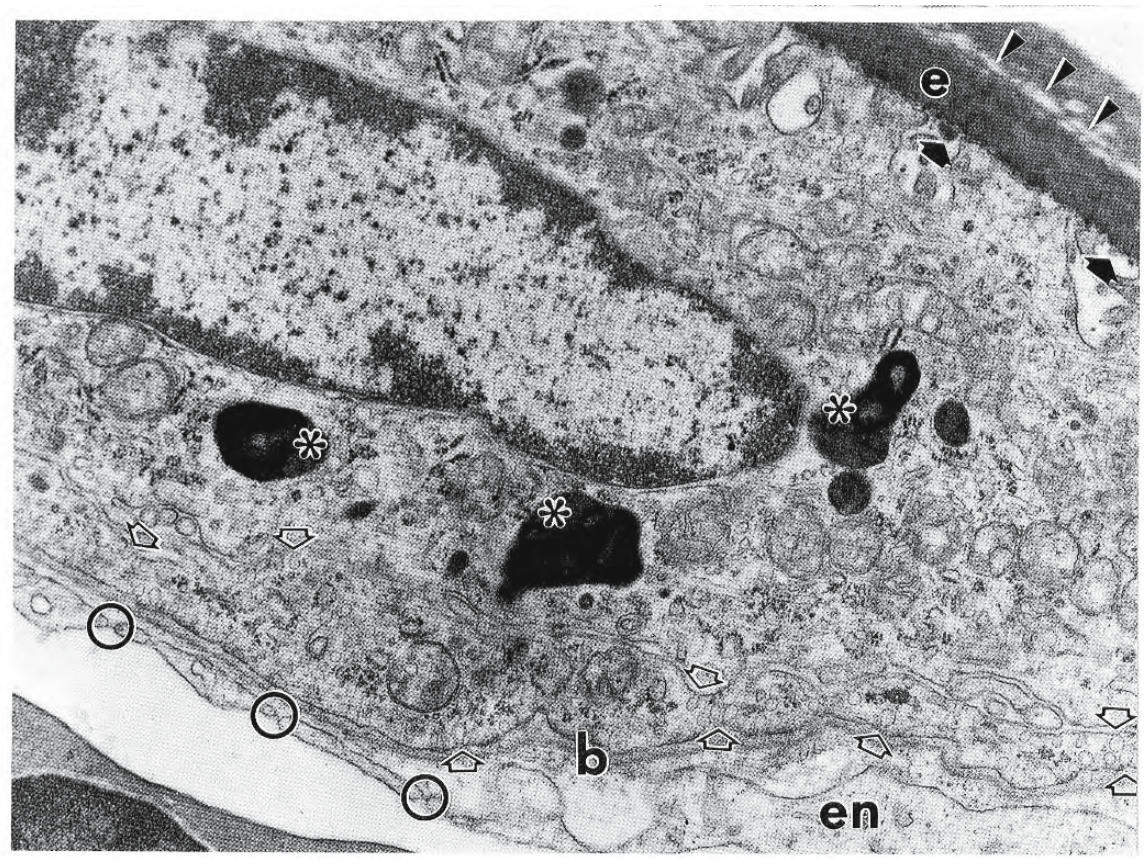

Figure 6.49: Transmission electron micrograph of a section through the placenta of the Atlantic sharpnose shark *Rhizoprionodon terraenovae.* A large surface cell of the uterine epithelium contains lysosomes (*); the egg envelope (e) is closely applied to its apical surface. Electron-dense material (black arrows), presumably of uterine origin, is present in the interspace between the egg envelope and the plasmalemma. Slits, or delaminations, occur in the egg envelope (arrowheads). Deeper epithelial cells have smooth-walled caveolae on both their abluminal and adluminal surfaces (open arrows). A basal lamina (b) separates the epithelium from the underlying fenestrated endothelium (en) of a capillary. Circles indicate fenestrations. X 20,000 (From Hamlett, Miglino, and DiDio, 1993; reproduced with permission from Nuova Immagine Editrice).

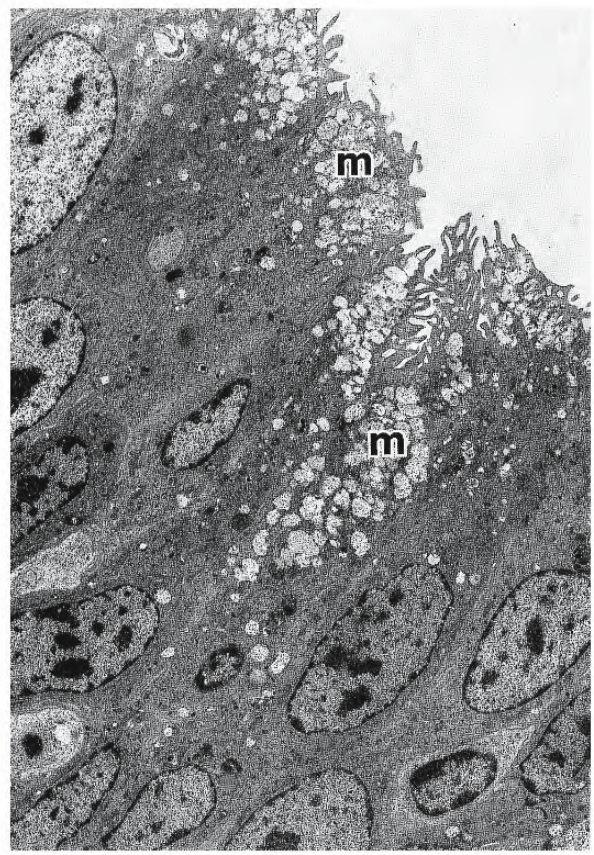

Figure 6.50: Transmission electron micrograph of a section of the epithelium of the paraplacental region of the shark uterus at term. The simple columnar epithelial cells are packed with mucous droplets (m). (From Hamlett et al., 1983a; © reproduced with permission of John Wiley & Sons, Inc.).

→

Figure 6.51: Transmission electron micrographs of sections of the uterus of the term Atlantic sharpnose shark *Rhizoprionodon terraenovae.* (From Hamlett, 1989; © reproduced with permission of John Wiley & Sons, Inc.).

A. The uterus (M) and distal placenta (P) are separated by the egg envelope (E). Leucocytes (L) occupy a blood vessel immediately beneath the epithelium. X 7,375.

B. A basal lamina (arrowheads) separates the vascular endothelium (V) from the uterine epithelium (M). Secretory vesicles (V) occupy the cytoplasm of the epithelial cells and secretory product (*) lies in the space beneath the egg envelope (E). X 8,850.

C. There is little separation between the blood channels of the uterus (BC1) and placenta (BC2). Uterine secretory vesicles (V) and extracellular secretory product (P) are evident. The egg envelope (E) is closely applied to the placental epithelial cells (PL). X 9,750.

D. On the uterine side, the egg envelope shows delaminations (arrowheads) that may represent transverse or tangential sections of laminated material adjacent to lamellae sectioned longitudinally (*). The placental plasmalemma (arrows) is in close contact with the egg envelope and may endocytose uterine secretions (S). X 31,000.

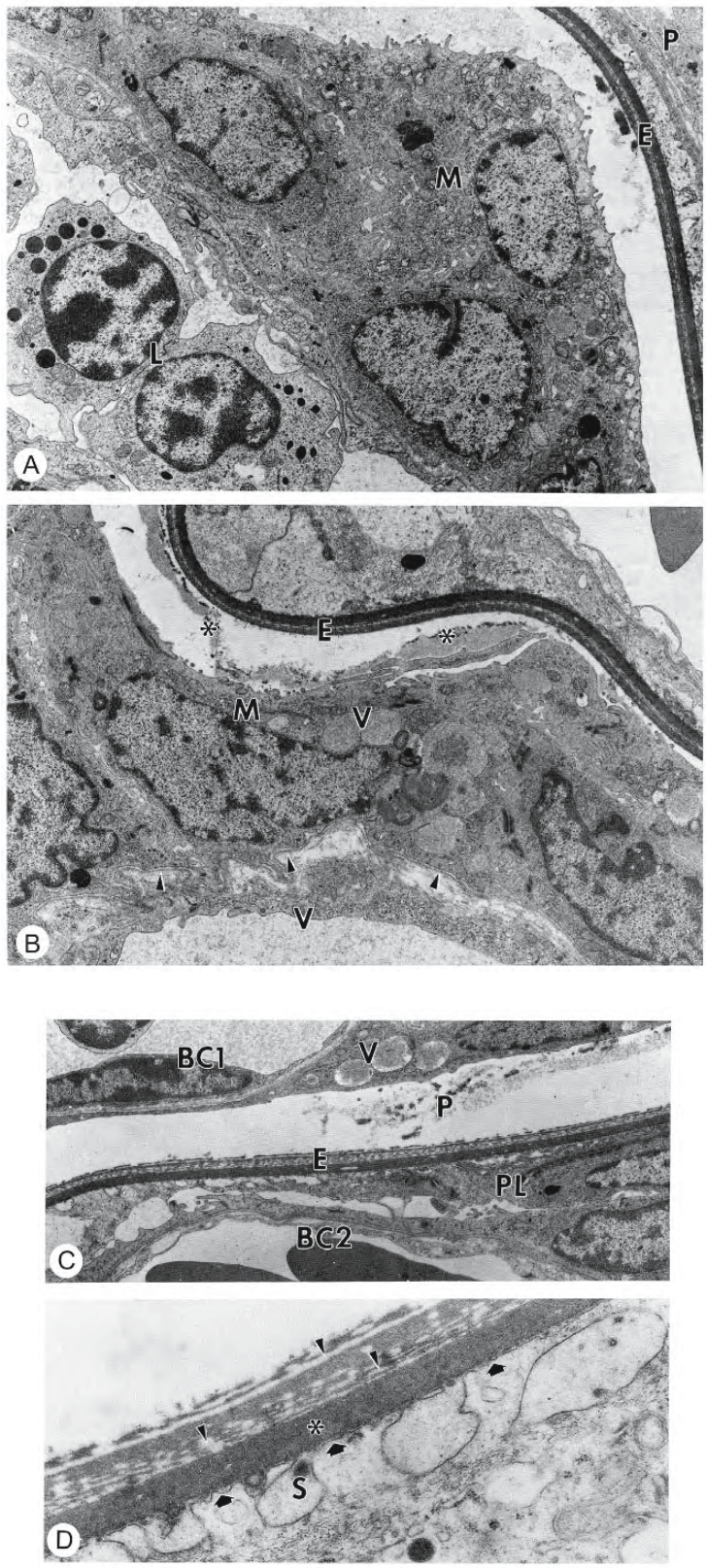

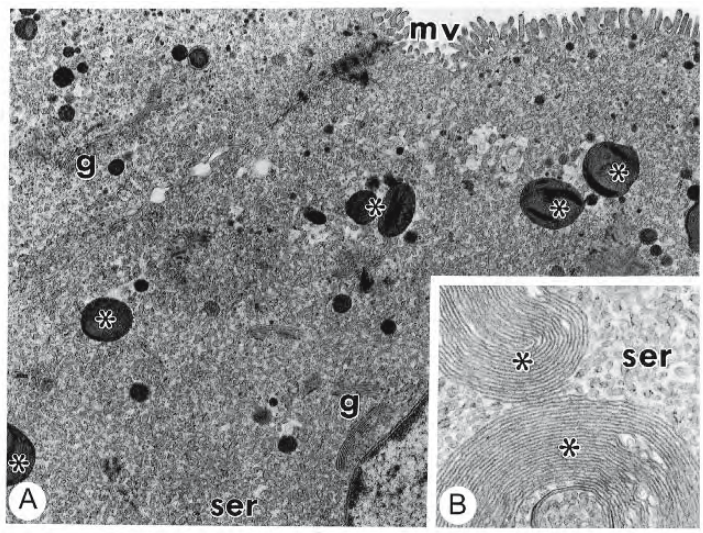

Figure 6.52: Transmission electron micrographs of sections of the yolk sac of the Atlantic sharpnose shark *Rhizoprionodon terraenovae.* (From Hamlett, Miglino, and DiDio, 1993; reproduced with permission from Nuova Immagine Editrice).

A. Two adjacent epithelial cells from the proximal portion of the yolk sac are packed with masses of agranular endoplasmic reticulum (ser). These cells have a border of stubby microvilli (mv); they contain Golgi complexes (g), and irregular inclusions (*). X 11,000.

B. The cytoplasm of an epithelial cell from the proximal portion of the yolk sac is packed with agranular endoplasmic reticulum (ser) and contains lamellar whorls of membrane (*). X 31,000.

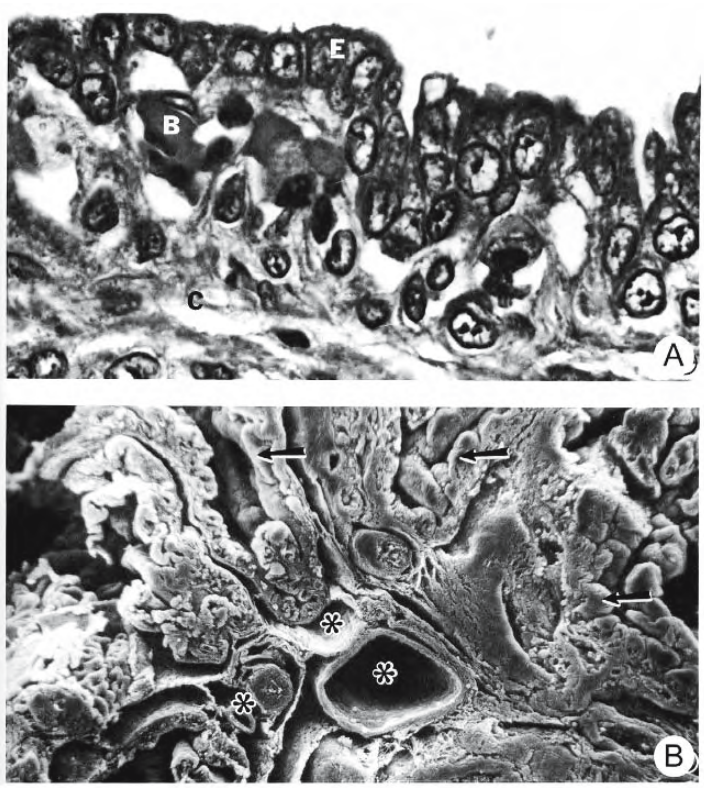

Figure 6.53: Representations of attachment sites in the gravid term uterus of the sandbar shark *Carcharhinus plumbeus.* (From Hamlett, Wourms, and Hudson, 1985c; reproduced with permission from Elsevier Science).

A. Photomicrograph of a section of the uterus showing its simple cuboidal to low columnar epithelium (E), blood vessels (B), and subepithelial connective tissue (C). X 400.

B. Scanning electron micrograph of a transverse section of the placental attachment site. Maternal blood vessels (*) lie beneath the folded epithelium. X 90.

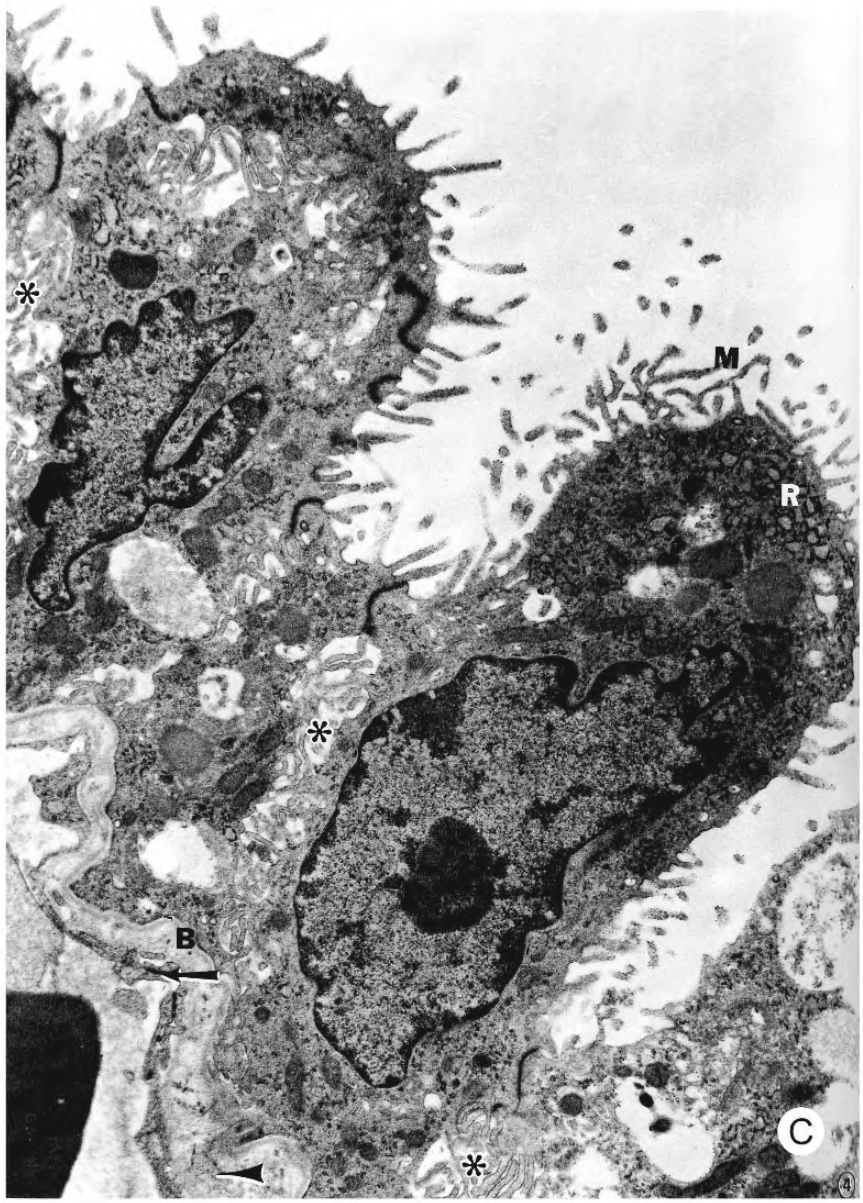

Figure 6.53: Continued.

C. Transmission electron micrograph of a section of the uterine wall. The epithelial cells have branching apical microvilli (M), highly folded and interdigitated lateral boundaries (*), and elements of granular endoplasmic reticulum (R). A basal lamina (B) separates the epithelium from the thin capillary endothelium (arrow) below; little connective tissue intervenes (arrowhead). X 11,491.

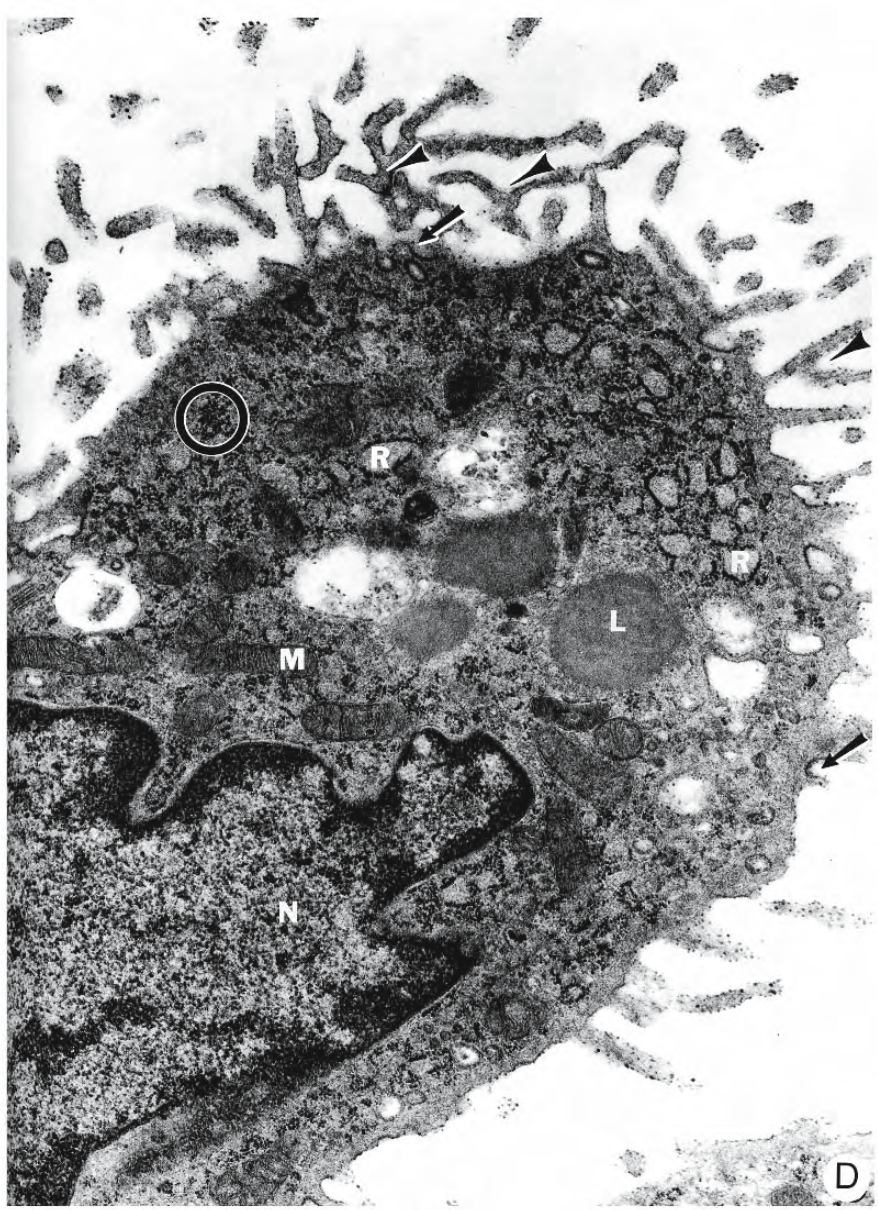

Figure 6.53: Continued.

D. Transmission electron micrograph of a section of a uterine epithelial cell. The cell has branched microvilli (arrowheads) and contains elements of granular endoplasmic reticulum (R) with dilated cisternae, coated pits (arrows), mitochondria (M), lipid-like inclusions (L), and prominent free ribosomes (circle). The large nucleus (N) is indicated. X 30,780.

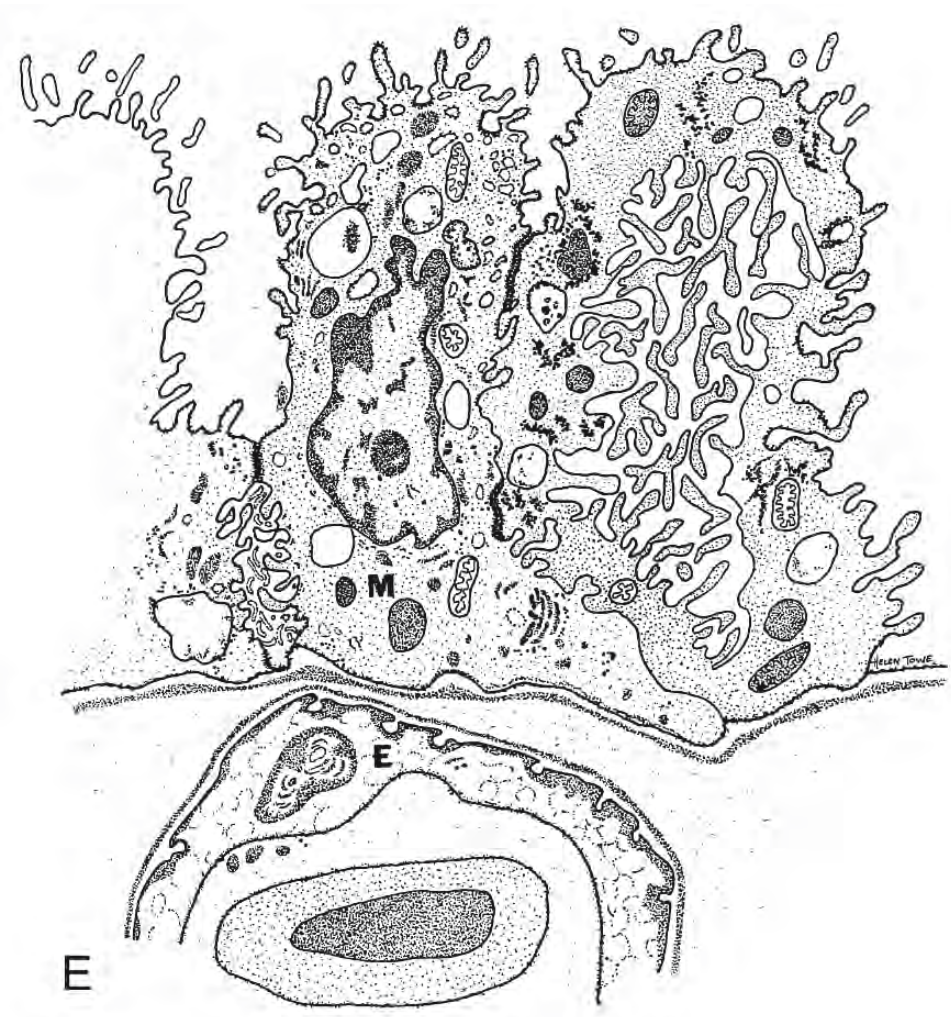

Figure 6.53: Continued.

E. Schematic drawing of the cellular organization of the uterine attachment site as seen with the transmission electron microscope. Little barrier intervenes between the simple maternal epithelium (M) from the endothelium (E) of a subjacent capillary.

Figure 6.54: Schematic drawing of a section of the term placenta of the Atlantic sharpnose *Rhizoprionodon terraenovae.* The egg envelope (ee) separates the foetal (above) and maternal (below) portions of the placenta. The squamous uterine epithelium (ut) has basal pinocytotic vesicles (large circles), lipid inclusions (lp), and secretory vesicles that release their contents into the uterine lumen (*). Subjacent capillaries (bv1) are continuous. Electron-dense vesicles (arrows) of uterine origin are endocytosed by the distal portion of the foetal placenta (pl). The placental epithelium has basal pinocytotic vesicles (large circles) and crystalline inclusions (c) that are interpreted as yolk precursors. Subjacent capillaries (bv2) are fenestrated (small circles). Basal laminae of the epithelia and endothelia are indicated (b). (From Hamlett. 1993; reproduced with kind permission of Kluwer Academic Publishers).

→

Figure 6.55: Representations of the rugose, distal portion of the placenta in the gravid term uterus of the sandbar shark *Carcharhinus plumbeus.* Unless otherwise indicated, the figures are transmission electron micrographs of sections. (Except for **I**, all figures are from Hamlett, Wourms, and Hudson, 1985a, and are reproduced with permission of Elsevier Science.).

A. Scanning electron micrograph of the elongate, peg-shaped surface epithelial cells (arrows). X 240.

B. Photomicrograph of a section reveals the egg envelope (arrow) above the surface epithelium (E). Capillaries (C) and boundary pavement cells (P) lie below. X 4,000.

C. The transversely sectioned egg envelope (E) abuts the apical canalicular system (C) in the epithelial cells of the distal placenta. X 44,352.

D. Ruthenium red (R) coats the uterine surface of the egg envelope (E) and its interstices (arrows). X 61,603.

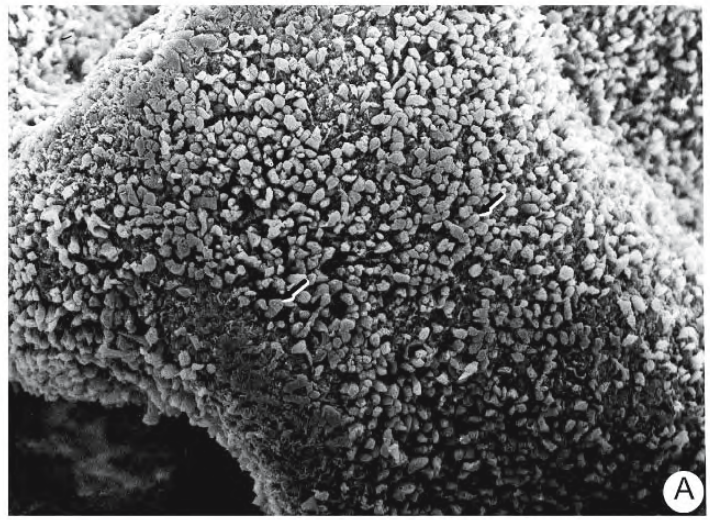

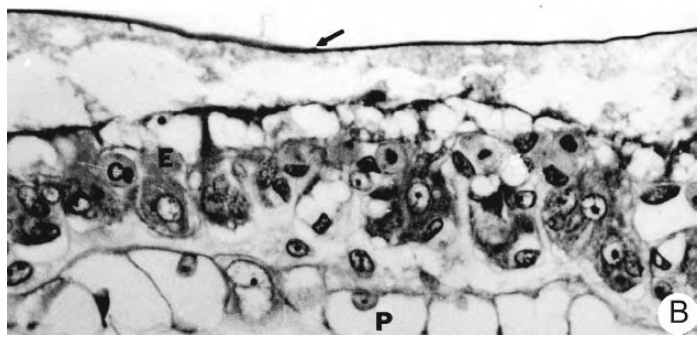

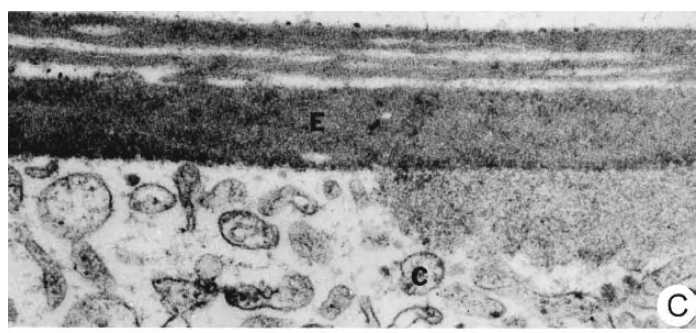

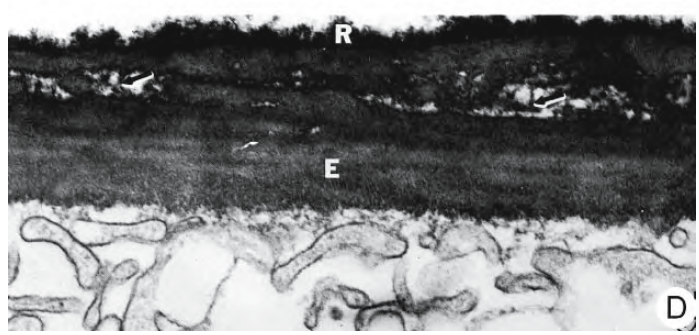

Figure 6.55: Continued.

E. A cell from the distal portion of the placenta incubated for 20 minutes in horseradish peroxidase. Reaction product (HRP) can be seen within the canalicular system (C). The base of the epithelial cell is closely apposed to the capillary endothelium (E). A common basal lamina (arrow) separates the two cell types. X 9,576 Inset: Smooth walled vesicles contain HRP reaction product (arrows) that has budded off from the canaliculi. X 13,680.

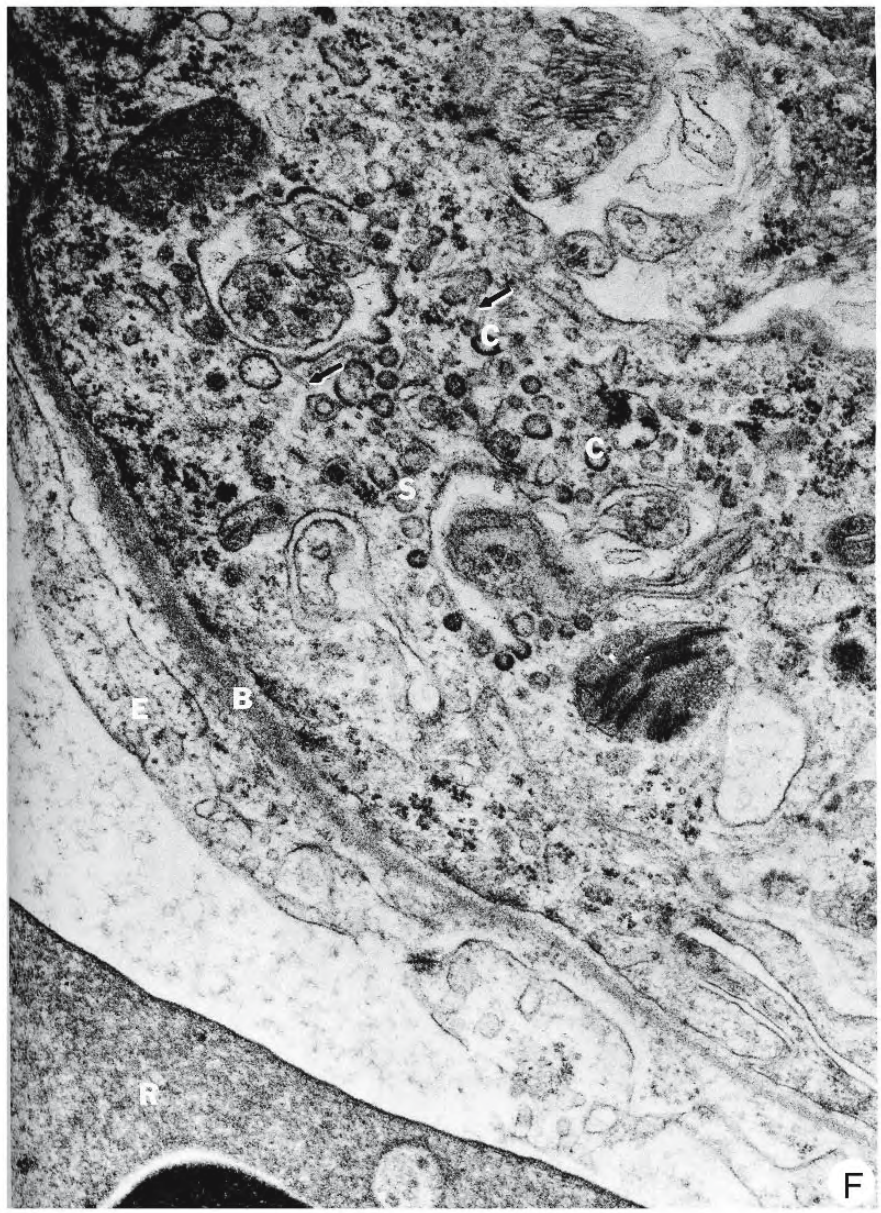

Figure 6.55: Continued.

F. Both coated (C) and uncoated (S) vesicles are closely associated with cytoplasmic microtubules (arrows) in an epithelial cell from the basal region of the distal portion of the placenta. A basal lamina (B) separates the epithelial cell from the endothelium (E) of a capillary containing a red blood cell (R). X 50,160.

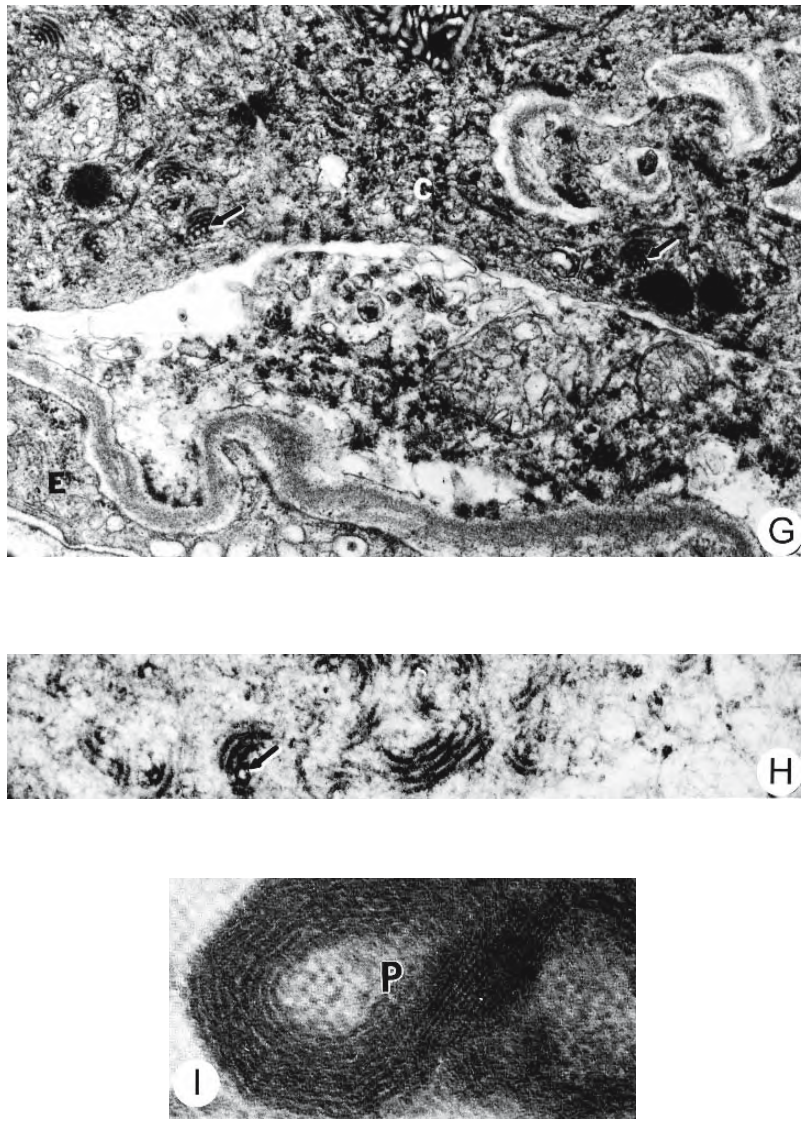

Figure 6.55: Continued.

G. A surface epithelial cell (C) of the distal portion of the placenta is closely apposed to the endothelium (E) of one of the abundant capillaries of the vitelline circulation. Whorl-like inclusions (arrows) occupy the basal cytoplasm of the epithelial cell. X 50,160.

H. The whorl-like inclusions in an epithelial cell are made up lamellar subunits (arrow) in various stages of aggregation. X 62,700.

I. Paracrystalline whorl-like inclusions (P) within the epithelial cells may represent vitellogenin or its precursors produced by the maternal liver and transferred across the uteroplacental complex. X 89,800 (From Hamlett, 1989; © reproduced with permission of John Wiley & Sons, Inc.).

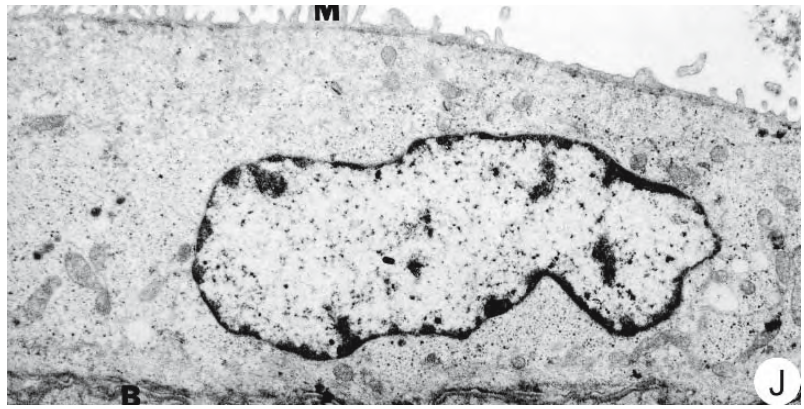

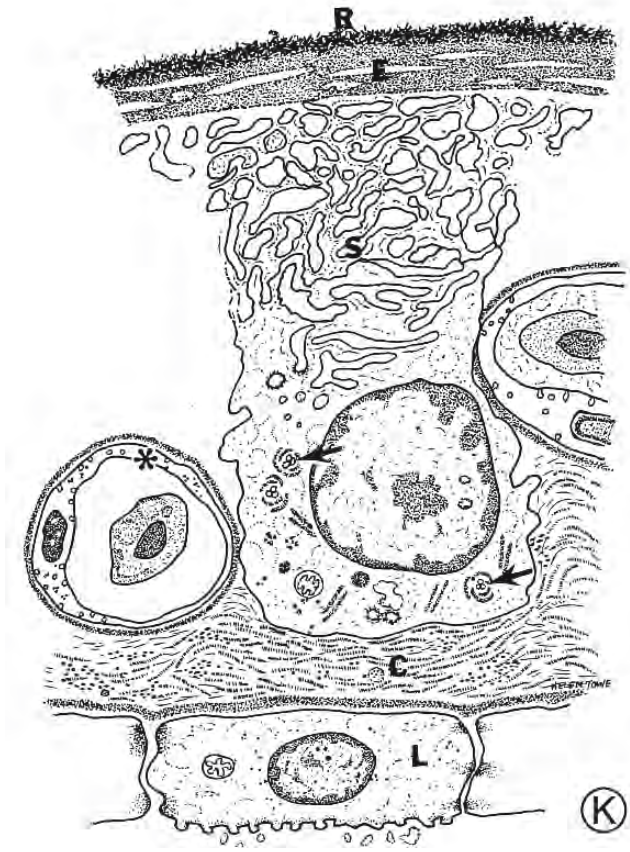

Figure 6.55: Continued.

J. Formerly active endodermal cells form a supportive boundary layer with scant microvilli (M) and sparse organelles except for a few mitochondria. The boundary pavement cells rest on a distinct basal lamina (B).

K. Schematic drawing showing the cellular organization in the rugose, distal portion of the yolk sac placenta. Ruthenium red (R) adheres to the maternal surface of the egg envelope (E). The cytoplasm of the epithelial cell contains an apical canalicular system (S) and whorl-like inclusions (arrows). A capillary (*), part of the vitelline circulation, is closely associated with the basal-lateral surface of the epithelial cell; its endothelial cells show active pinocytosis. A well developed collagenous stroma (C) separates the surface epithelium from the inner boundary layer (L).

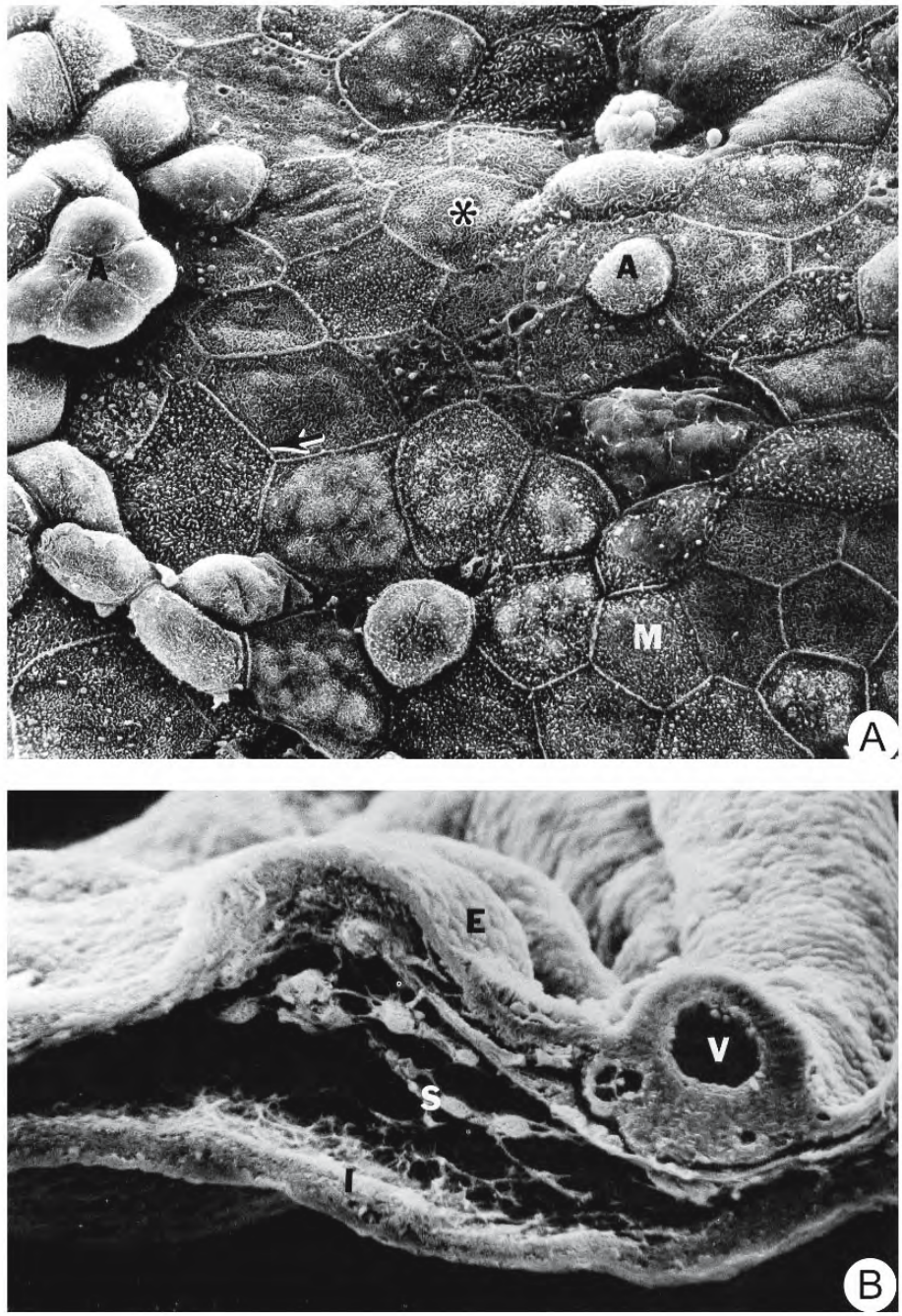

Figure 6.56: Representations of the smooth, proximal portion of the placenta in the gravid term uterus of the sandbar shark *Carcharhinus plumbeus.* Figures **A** to **E** are scanning electron micrographs while **F** to **I** are transmission electron micrographs of sections. (From Hamlett, Wourms, and Hudson, 1985b; reproduced with permission from Elsevier Science).

A. Peripheries of the cells on the surface of the smooth portion are marked by prominent elevations (arrow). Many microvilli (M) and microplicae (*) cover the bulging apical surfaces (A) of the epithelial cells. X 840.

B. The broken edge of a cross section of the placenta shows the epithelial cells (E) separated from the inner layer (I) by a collagenous stroma (S) containing a blood vessel (V). X 255.

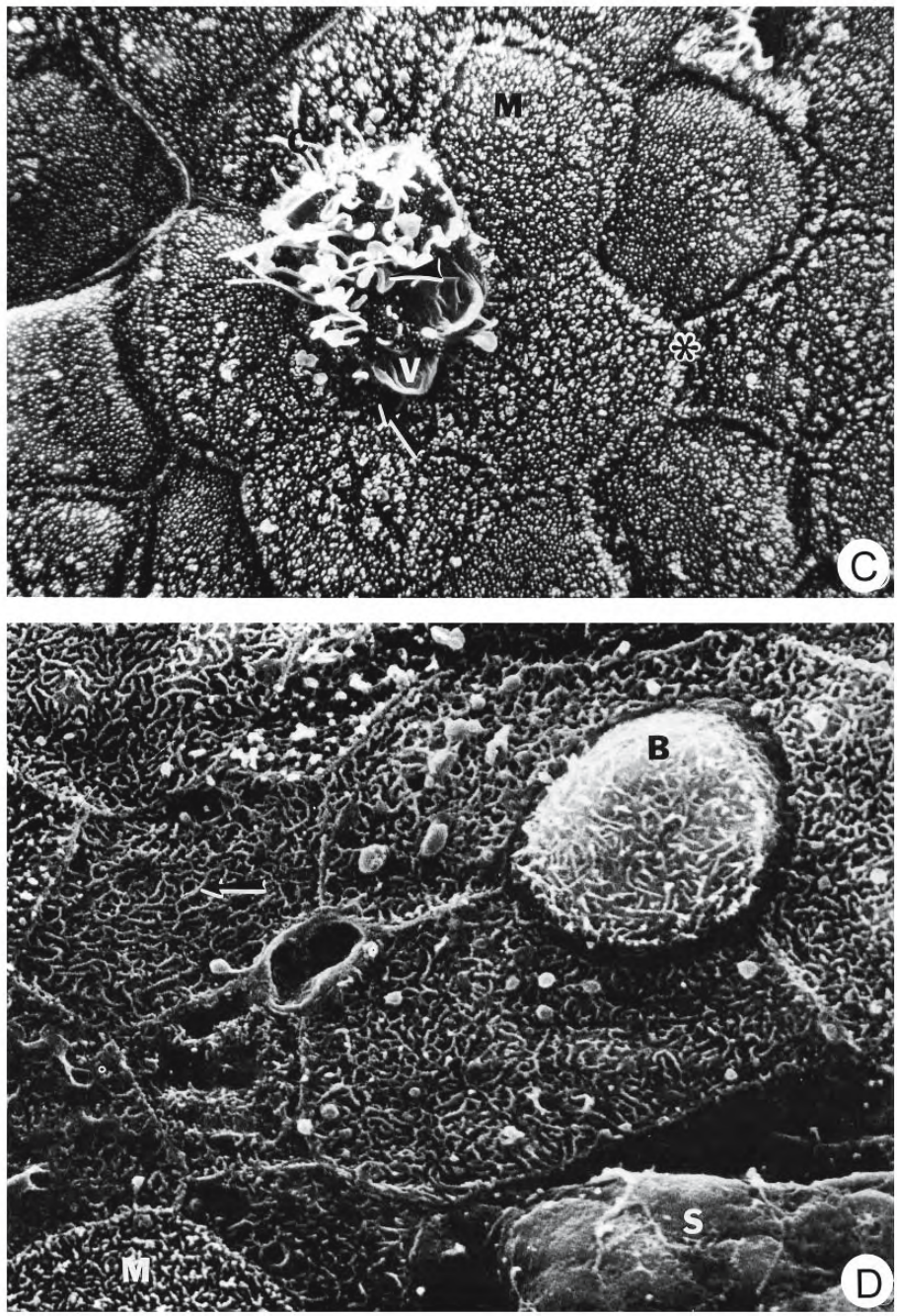

Figure 6.56: Continued.

C. Five adjacent cells on the surface of the smooth portion form a rosette around a central cell. The peripheral cells possess microvilli (M) that are most dense at the cell borders (*). The surface of the central cell shows microvilli (arrow), cilia (C), and vesiculations (V). X 3,000.

D. Some epithelial cells have microvilli (M), others have microplicae (arrow), while still others possess a smoother surface contour (S) and bulging cell apices (B). X 3,300.

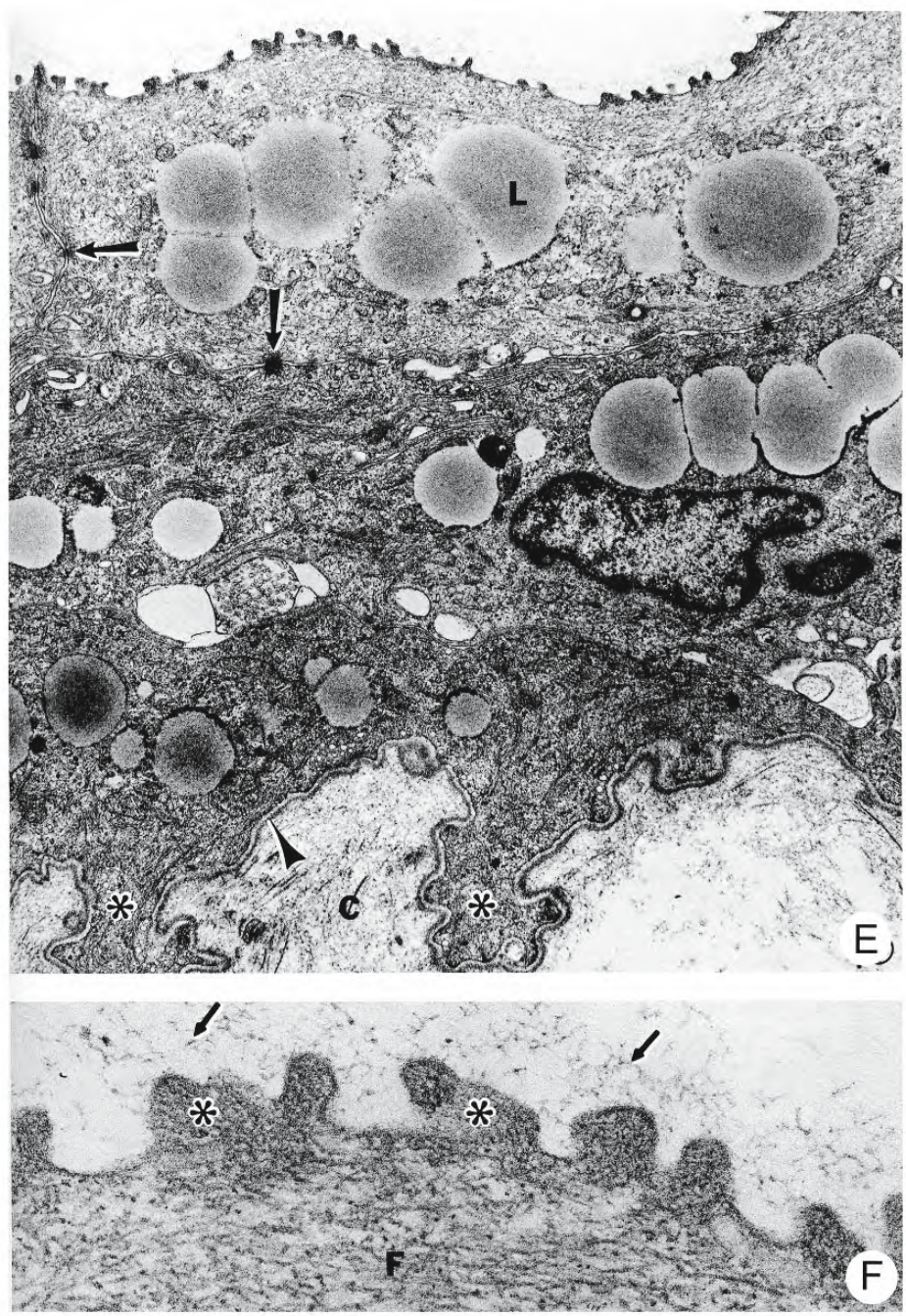

Figure 6.56: Continued.

E. Epithelial cells contain large lipid-like inclusions (L) and many cytoplasmic filaments. Desmosomes (arrows) join cells and the deepest cell layer possesses an undulating basal contour (*) and a prominent basal lamina (arrowhead) adjacent to a collagenous stroma (C). X 9,576.

F. A prominent glycocalyx (arrows) coats the surface of the microplicae (*). Fibrous elements (F) of the terminal web occur just beneath the apical plasmalemma. X 59,616.

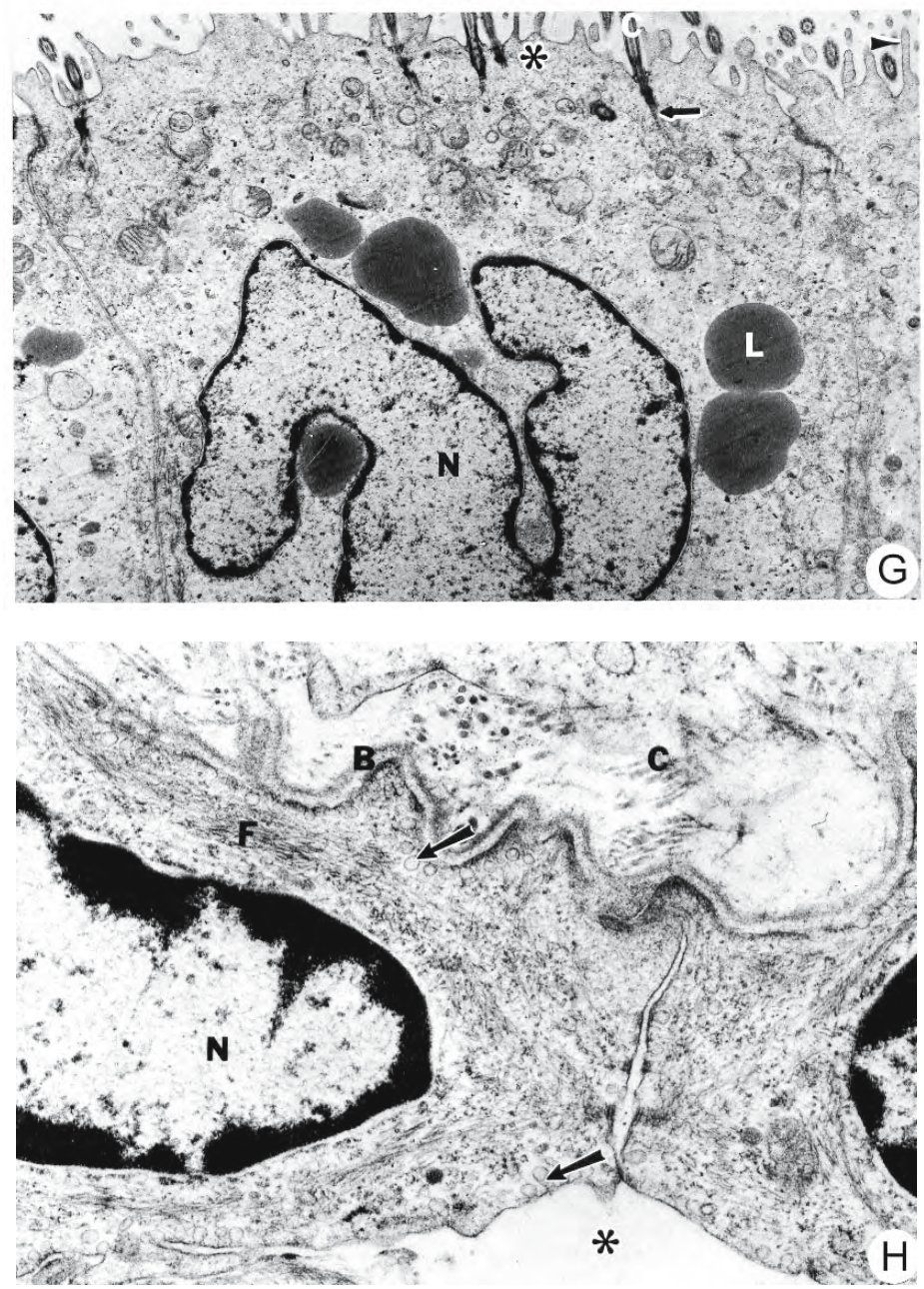

Figure 6.56: Continued.

G. This epithelial cell has a lobate nucleus (N), flat apical border (*), cilia (C) with associated rootlets, microvilli (arrowhead), and lipid-like inclusions (L). X 4,468.

H. The inner cell layer is much like a mesothelium. The flattened cells have a fusiform nucleus (N), a basal lamina (B) adjacent to a collagenous stroma (C), an abundance of cytoplasmic fibrils (F), and many pinocytotic pits and vesicles (arrows) on both the abluminal and adluminal surfaces. The inner surface of the cells is bounded by the cavity of the placenta (*). X 30,780.

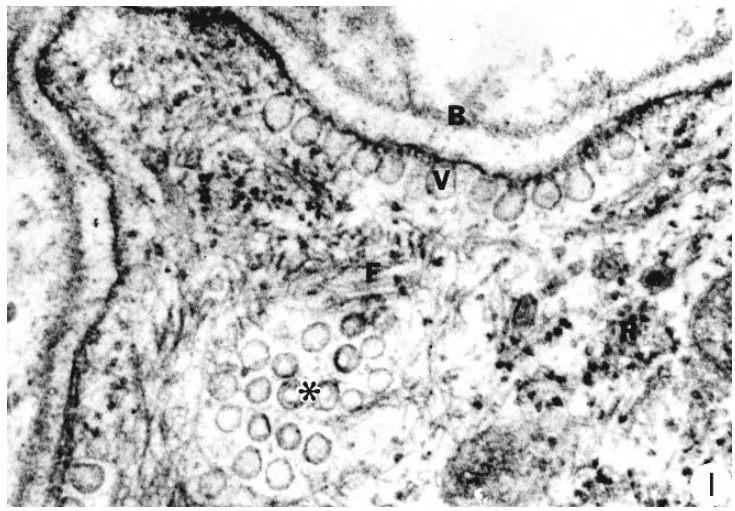

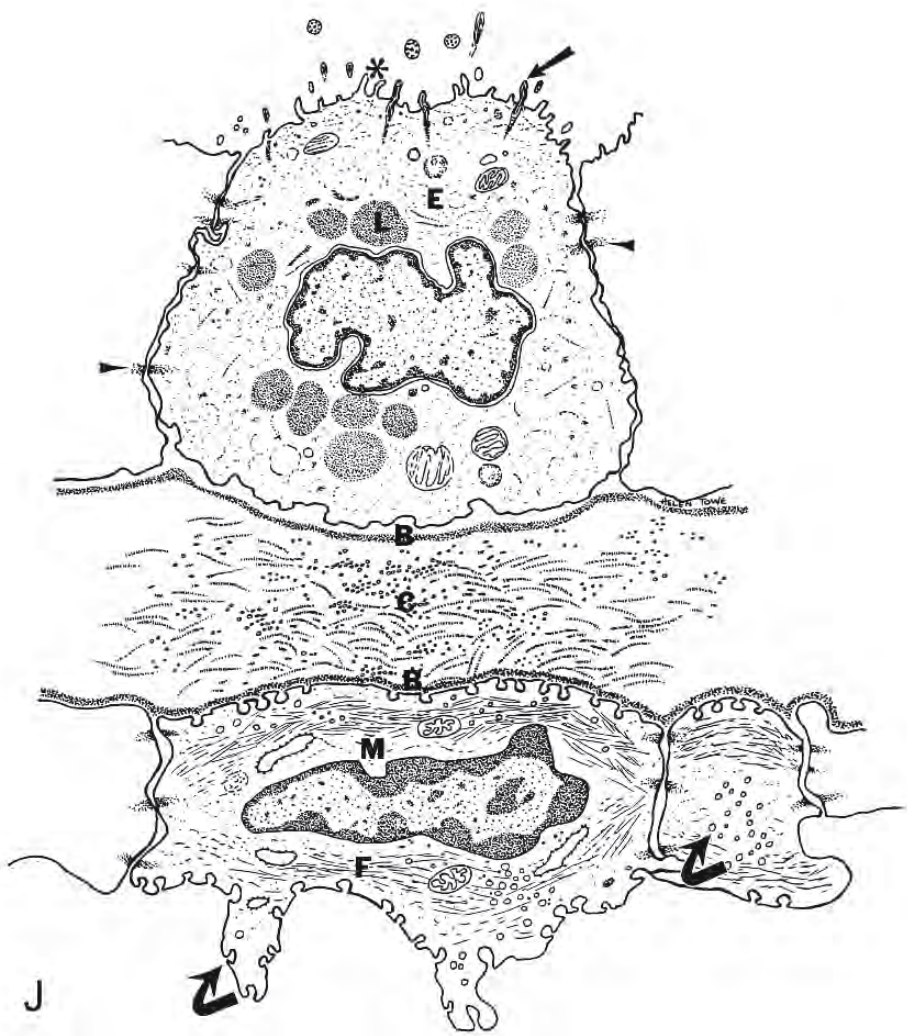

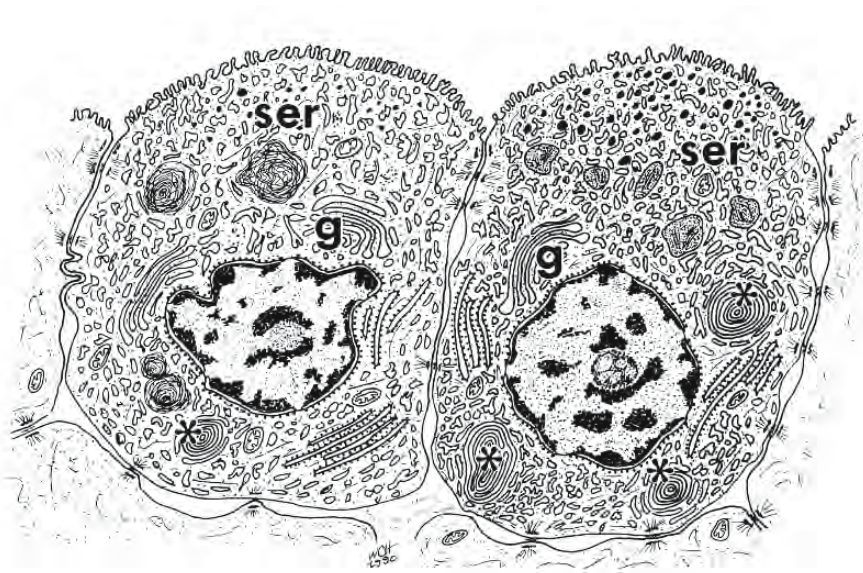

Figure 6.57: Schematic drawing of cuboidal epithelial cells from the smooth, proximal portion of the term placenta of the sandbar shark *Carcharhinus plumbeus.* Prominent Golgi complexes (g) and abundant agranular endoplasmic reticulum (ser), which may assume lamellar configurations (*), are characteristic of steroid production. (From Hamlett. 1993; reproduced with kind permission of Kluwer Academic Publishers).

←

Figure 6.56: Continued.

I. Pinocytotic vesicles (V) form a nearly continuous zone on the cell surface adjacent to the basal lamina (B). Numerous transport vesicles (*) occur in the cytoplasm as do free ribosomes (R) and filamentous elements (F). X 75,240.

J. Schematic drawing showing the cellular organization in the smooth, proximal portion of the yolk sac placenta. The surface epithelial cells (E) may possess microvilli (*) or cilia (arrow). Desmosomes (arrowheads) join adjacent cells and lipid (L) inclusions occur in the cytoplasm. The basal laminas (B) of both the surface epithelial cells and the deeper mesothelial cells (M) are separated by a collagenous stroma (C). Mesothelial cells are characterized by an abundance of cytoplasmic filaments (F) and numerous pinocytotic pits and vesicles (curved arrows).

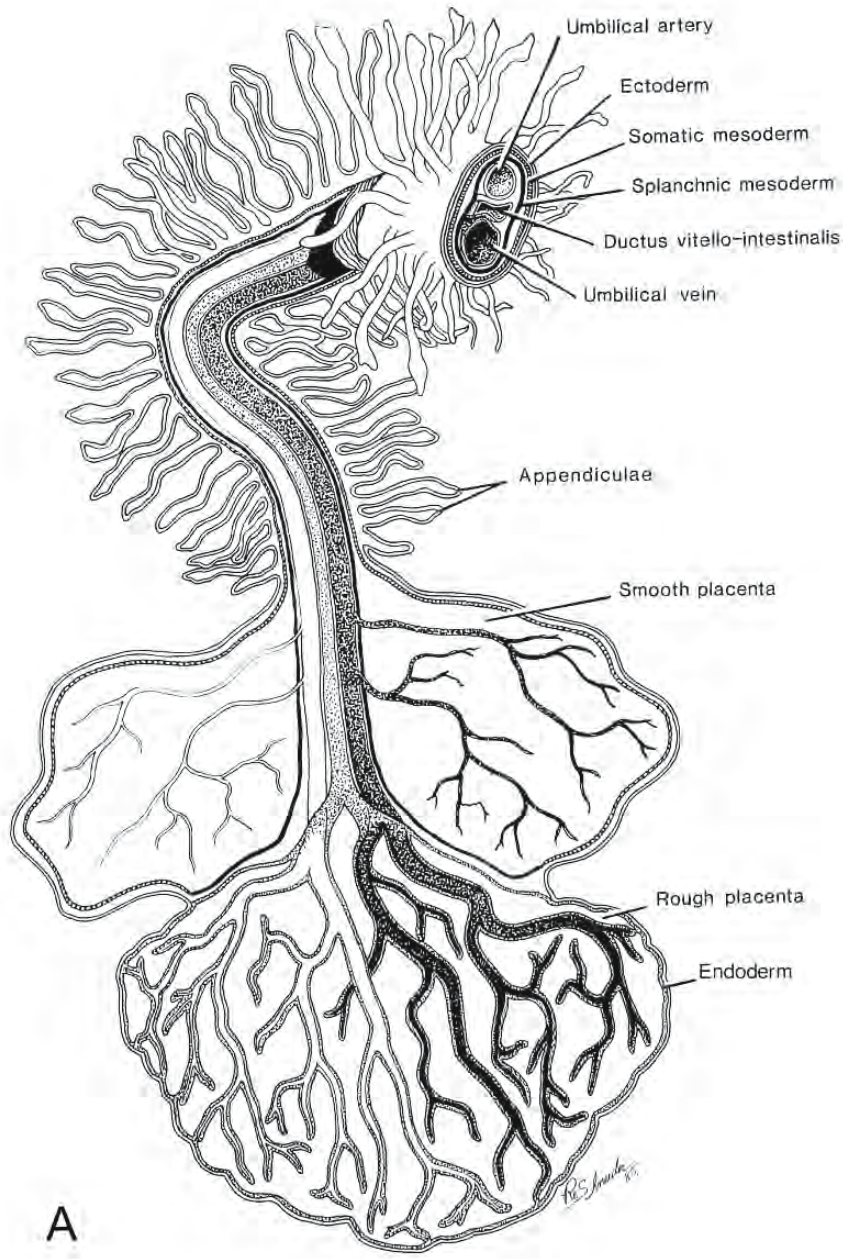

Figure 6.58: Schematic drawings to illustrate the structure of the yolk sac placenta of the shark. (From Hamlett, 1987; reproduced with permission of the author).

A. Stereogram of the umbilical cord and placenta. Appendiculae are vascularized outpocketings of ectoderm that are filled with loose connective tissue. The smooth, proximal portion of the placenta has contributions from ectoderm and somatic mesoderm. The rugose or rough distal portion is richly supplied by mesodermally-derived blood vessels. Endodermal cells coat the blood vessels and the inner aspect of the ectoderm.

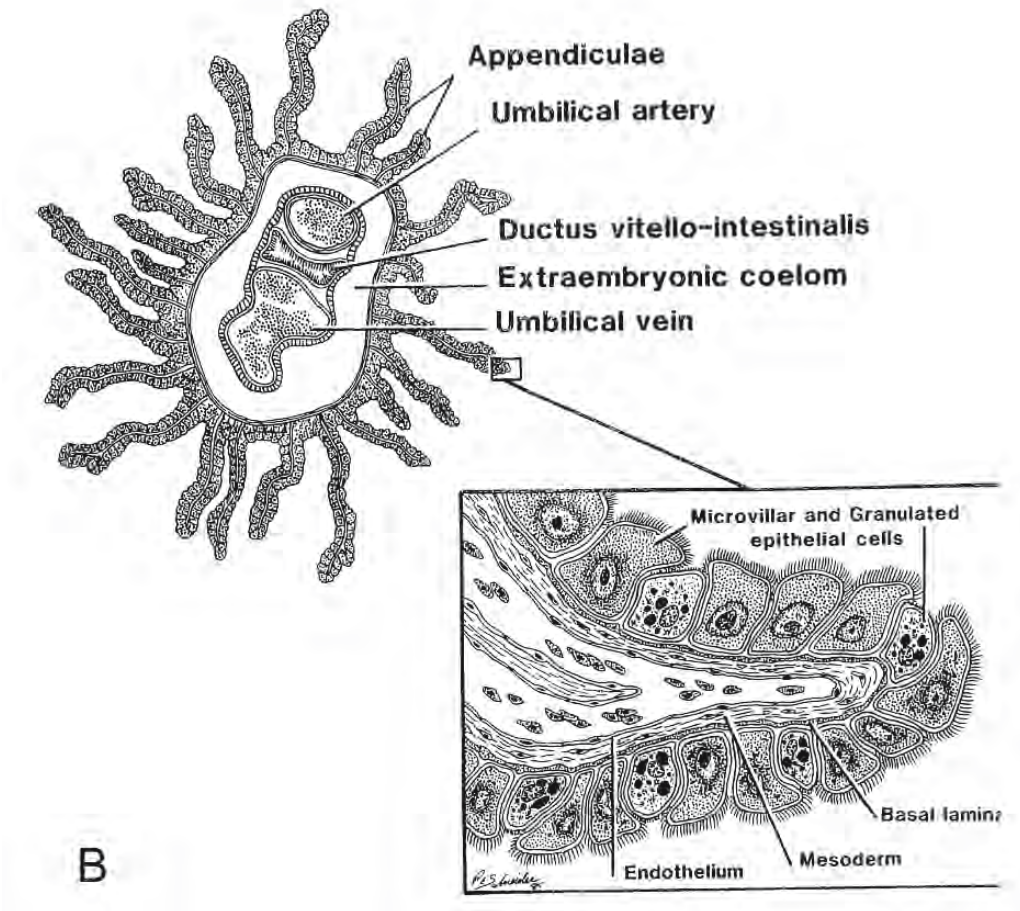

Figure 6.58: Continued.

B. Drawing of a cross section of the umbilical cord illustrating the umbilical artery and vein, ciliated ductus vitellointestinalis, extraembryonic coelom, and appendiculae. The enlargement demonstrates the histological features of an appendicula. The epithelium with microvillar and granulated cells rest on a basal lamina. The connective tissue elements and endothelium, with its basal lamina, are mesodermally derived.

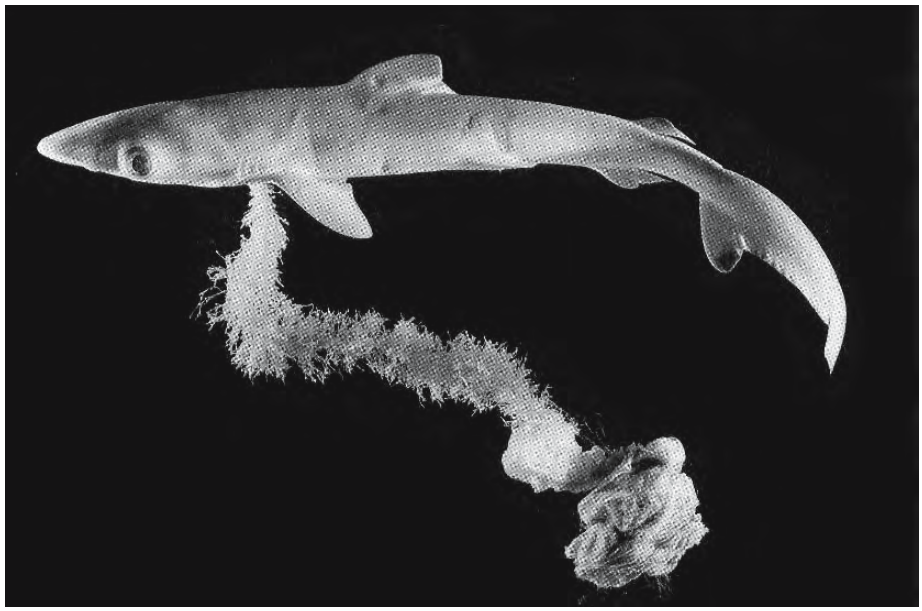

Figure 6.59: Photograph of a 250-mm embryo of the sharpnose shark *Rhizoprionodon terraenovae* at midterm. The appendiculae covering the umbilical cord have reached their maximum development and the yolk sac is reduced. X 0.5 (From Castro and Wourms, 1993; © reproduced with permission of John Wiley & Sons, Inc.).

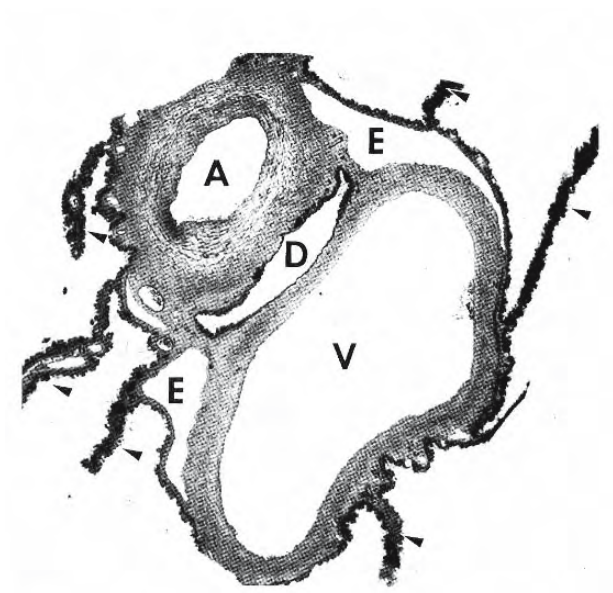

Figure 6.60: Photomicrograph of a cross section of the umbilical cord of the sharpnose shark *Rhizoprionodon terraenovae* showing the umbilical artery (A), umbilical vein (V), ductus vitellointestinalis (D), extraembryonic coelom (E), and appendiculae (arrowheads). (From Hamlett et al., 1993b; reproduced with permission from Nuova Immagine Editrice).

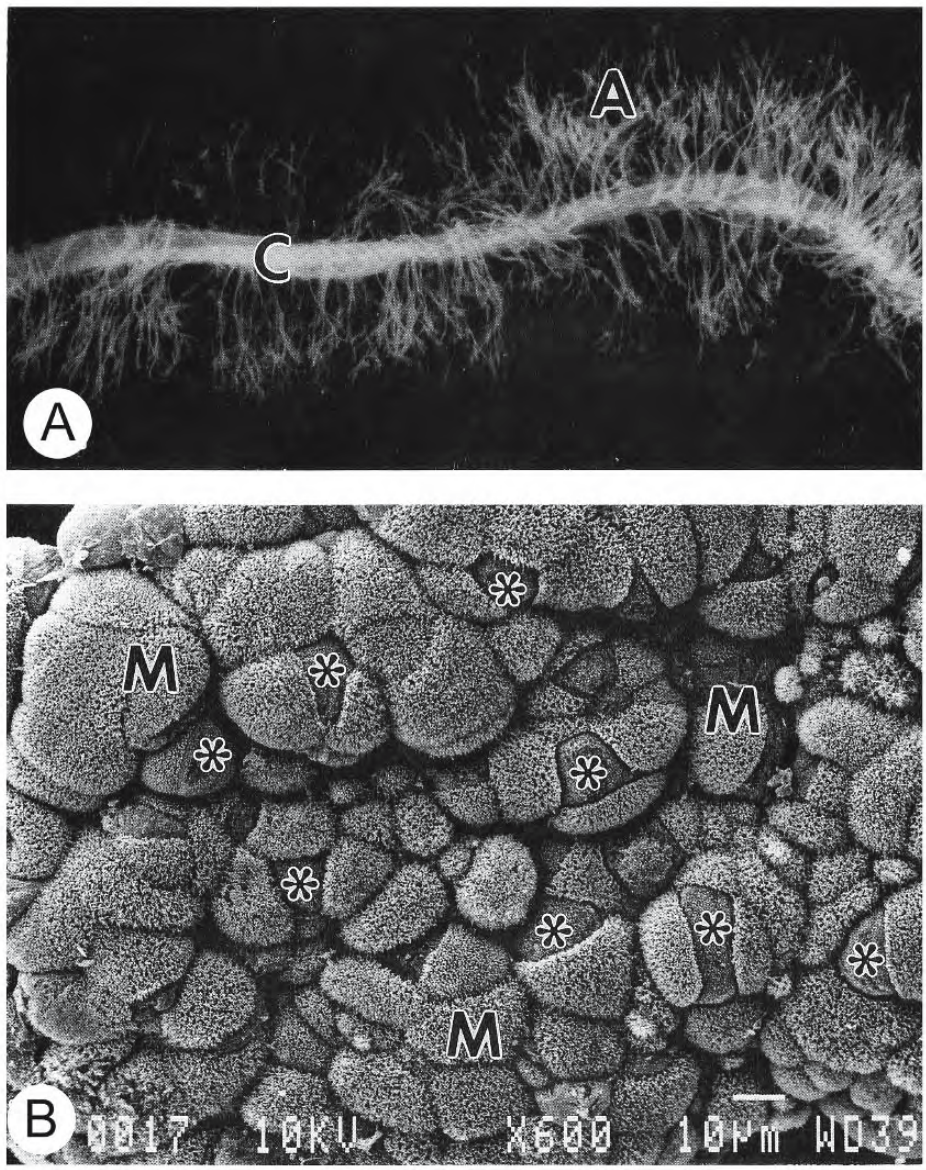

Figure 6.61: Representations demonstrating appendiculae on the umbilical cord of the sharpnose shark *Rhizoprionodon terraenovae.* (**A** to **F** are from Hamlett, 1989; © reproduced with permission of John Wiley & Sons, Inc.).

A. Photograph of the umbilical cord (C) festooned with prominent appendiculae (A).

B. Scanning electron micrograph of the surface of an appendicula reveals two cell types. Microvillar epithelial cells (M) outnumber the deeper granulated cells (*). X 600 [13].

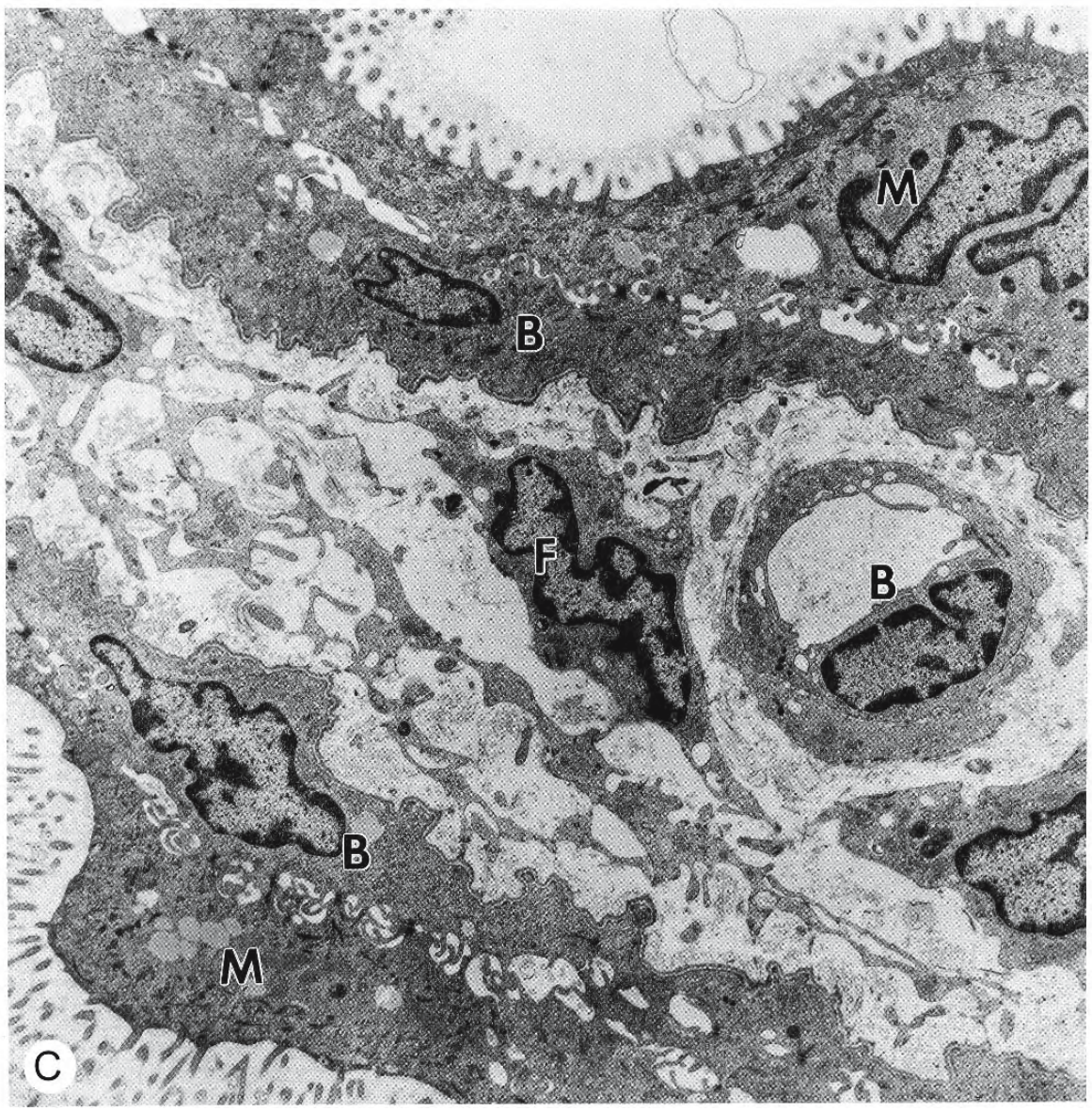

Figure 6.61: Continued.

Figures C to F are transmission electron micrographs of sections of appendiculae.

C. Cross section. The surface is covered with microvillar cells (M) bristling with long microvilli. The surface cells are separated by dilated intercellular spaces from the basal cells (B). Loose connective tissue with fibroblasts (F) and blood vessels (B) form the core of the appendicula. X 5,900.

Figure 6.61: Continued.

D. Cross section. Granular cells (G) are interposed between microvillar cells (M) on the surface of this appendicula. Exceptionally long and dense microvilli arise from the apical surface of the microvillar cells. Intercellular spaces are conspicuous. A layer of basal cells (B) abuts the core of vascular connective tissue. X 2,340.

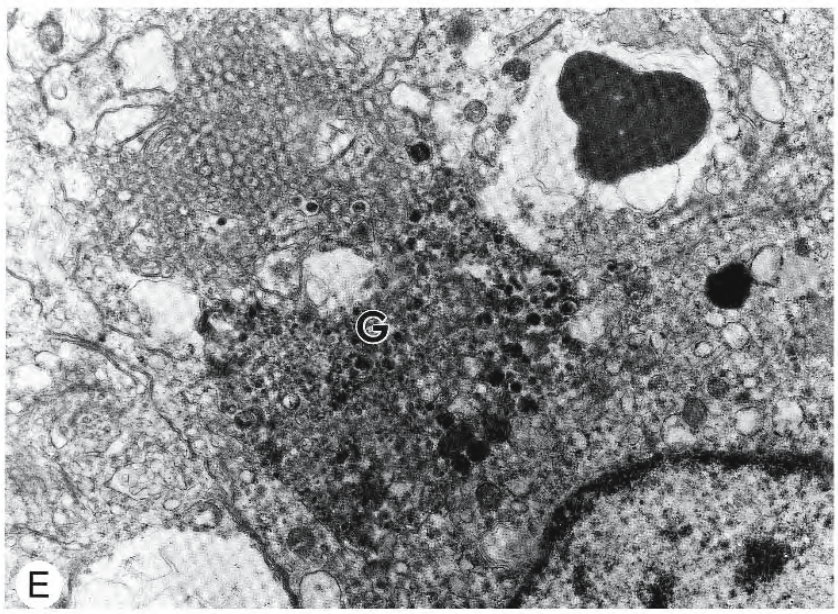

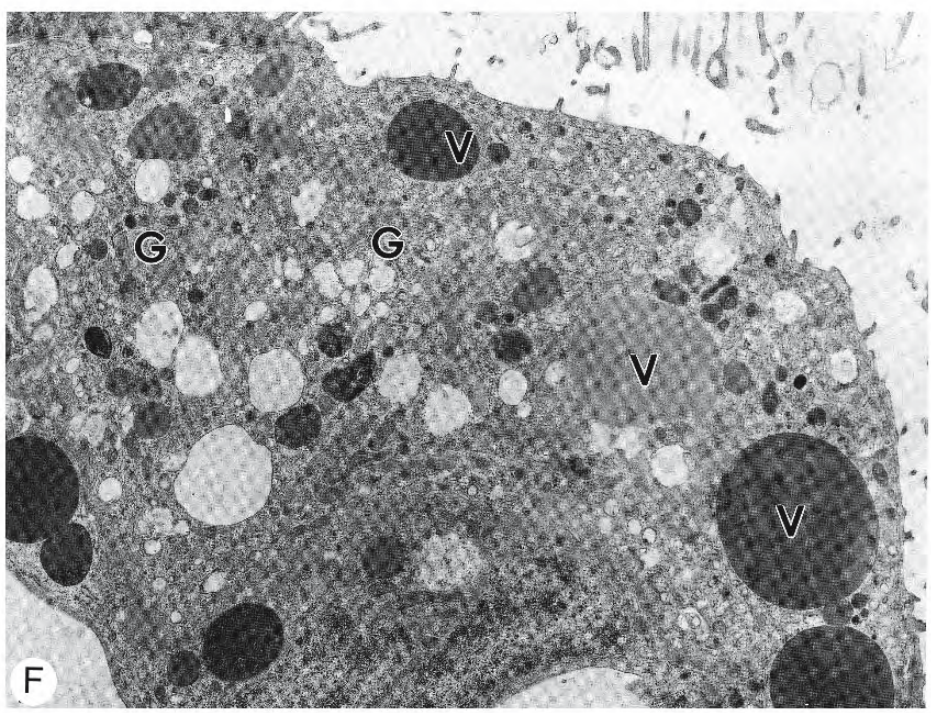

Figure 6.61: Continued.

E. The supranuclear Golgi complex (G) in an appendicular granulated cell is actively modulating presecretory material. X 15,840.

F. This appendicular granulated cell contains a profusion of secretory vesicles (V) and prominent Golgi complexes (G). X 10,140.

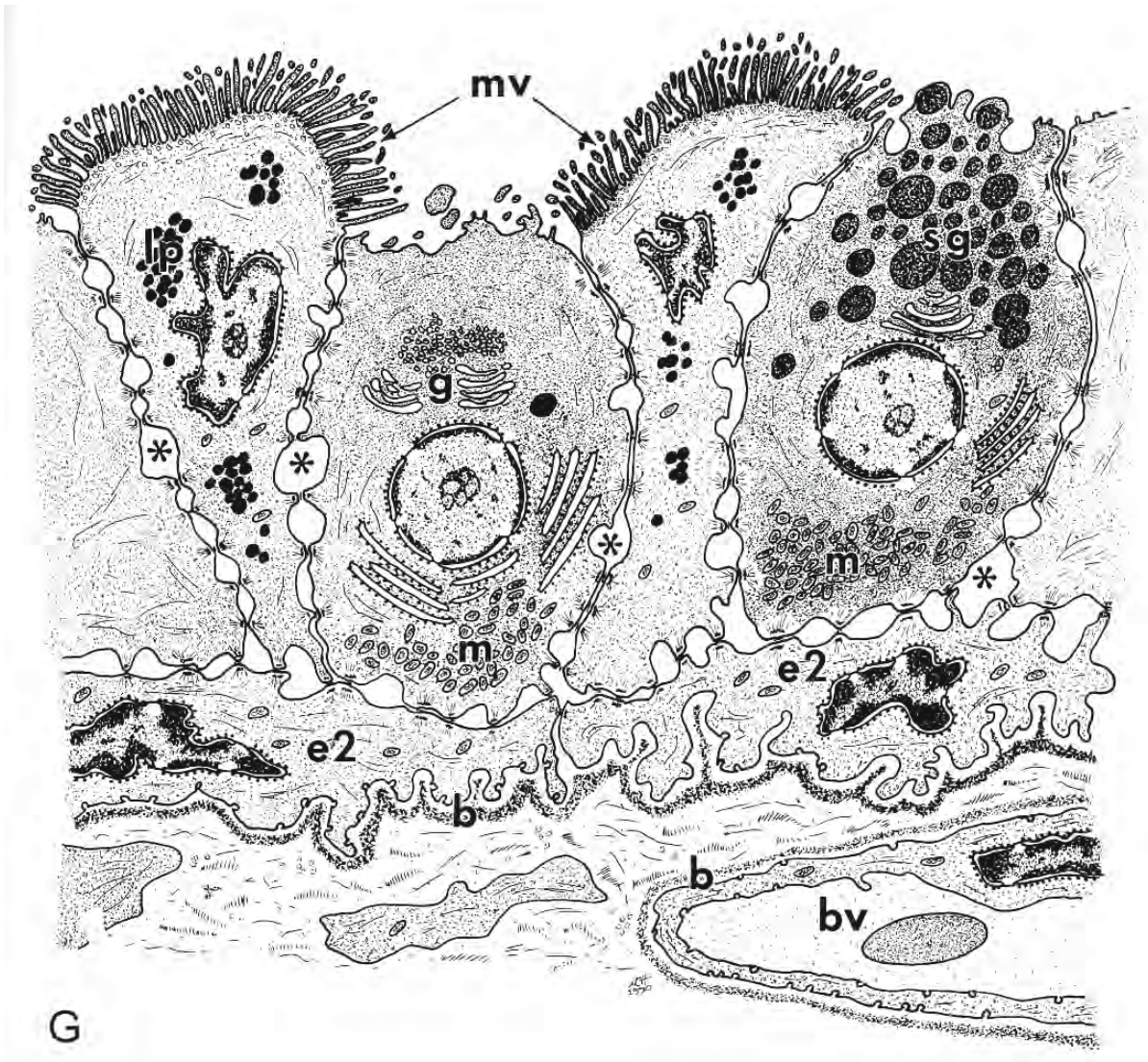

Figure 6.61: Continued.

G. Summary diagram illustrating the structure of the appendicular surface. Microvilli (mv) abound on the columnar microvillar cells; these cells contain lipid inclusions (lp). Wedged between the microvillar cells are granular cells containing Golgi complexes (g), mitochondria (m), and secretory granules (sg). Intercellular spaces (*) between adjacent surface cells and the underlying epithelial layer (e2) are often dilated. Apical tight junctions occur between adjacent surface cells. (From Hamlett. 1993; reproduced with kind permission of Kluwer Academic Publishers).

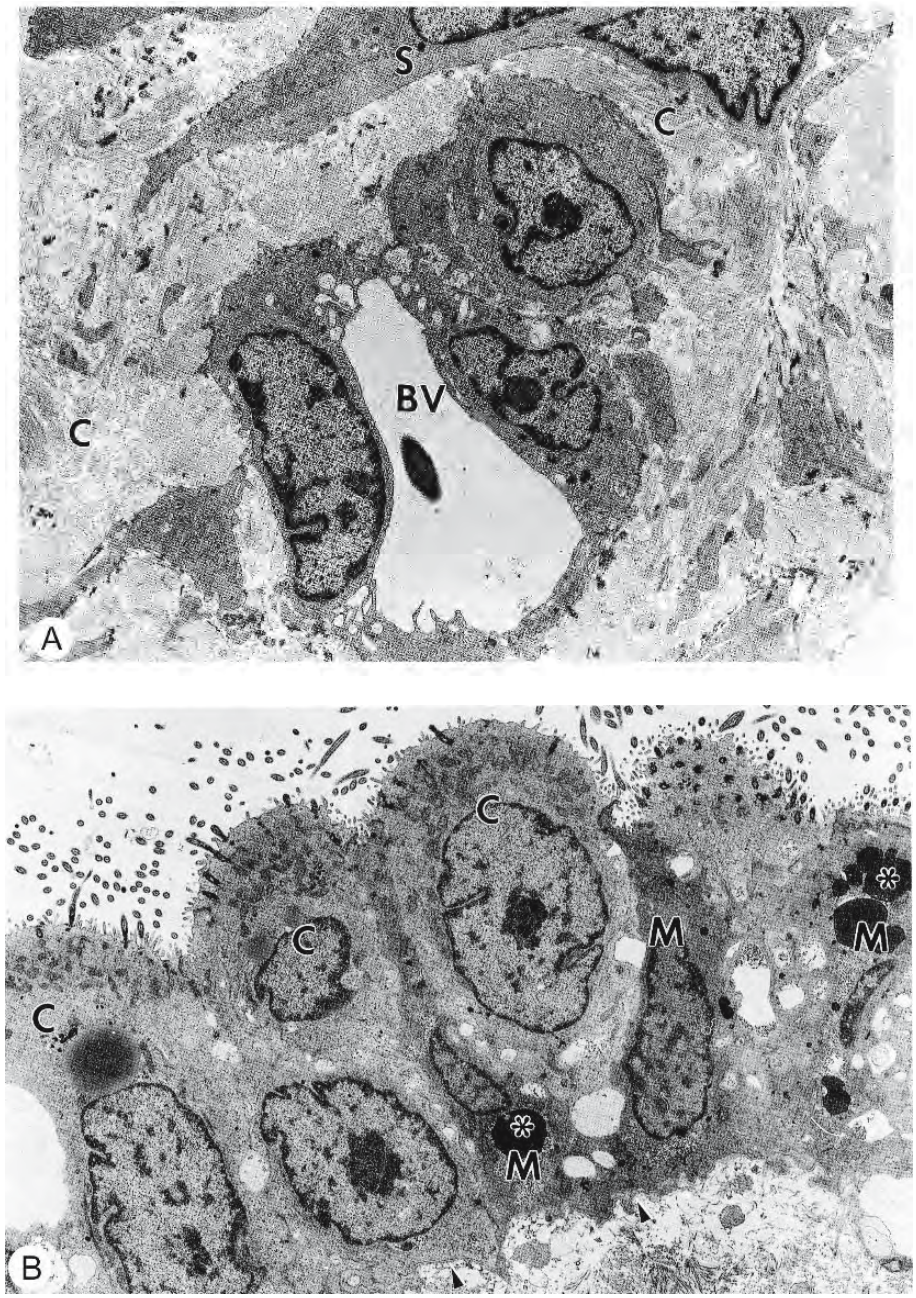

Figure 6.62: Transmission electron micrographs from sections of the ductus vitello-intestinalis in the umbilical cord of the sharpnose shark *Rhizoprionodon terraenovae.* (From Hamlett, 1993b; reproduced with permission from Nuova Immagine Editrice).

A. The connective tissue investment of the ductus contains blood vessels (BV), collagen (C), and smooth muscle cells (S). X 7,000.

B. Ciliated cells (C) are interspersed with microvillar cells (M) containing prominent lipid inclusions (*) and glycogen. A basal lamina (arrowheads) separates the epithelium from the surrounding connective tissue elements. X 4,500.

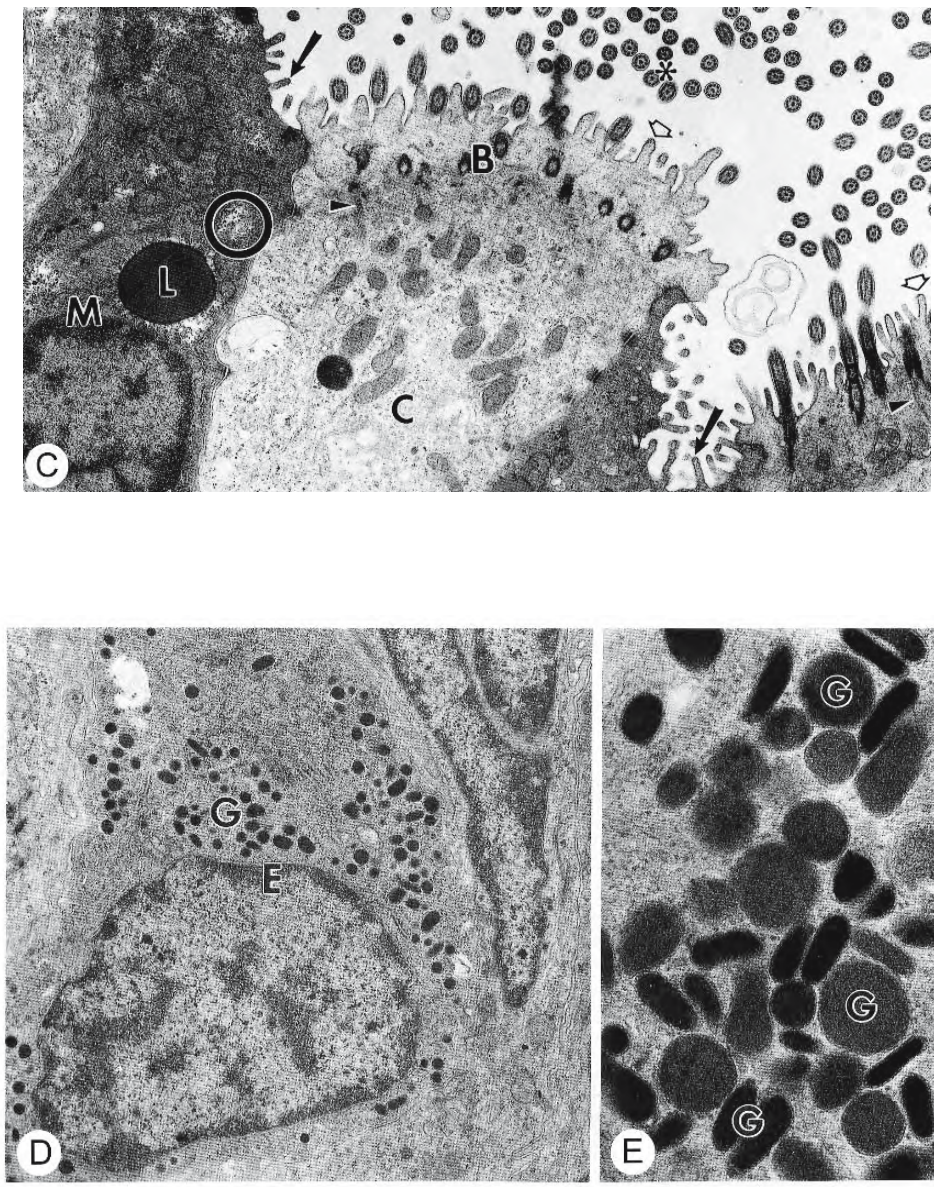

Figure 6.62: Continued.

C. A profusion of cilia (*) emerges from a row of basal bodies (B) anchored by striated rootlet fibres (arrowheads) within ciliated cells (C). Microvilli (open arrows) also occur on the ciliated cells. Microvillar cells (M) have unbranched microvilli (arrows), prominent lipid inclusions (L), and glycogen stores (circle). X 11,000.

D. Enteroendocrine cells (E) with secretion granules (G) are wedged between adjacent epithelial cells of the ductus. X 13,000.

E. Granules of the enteroendocrine cells (G) are membrane bound and of variable shape and electron density. X 45,500.

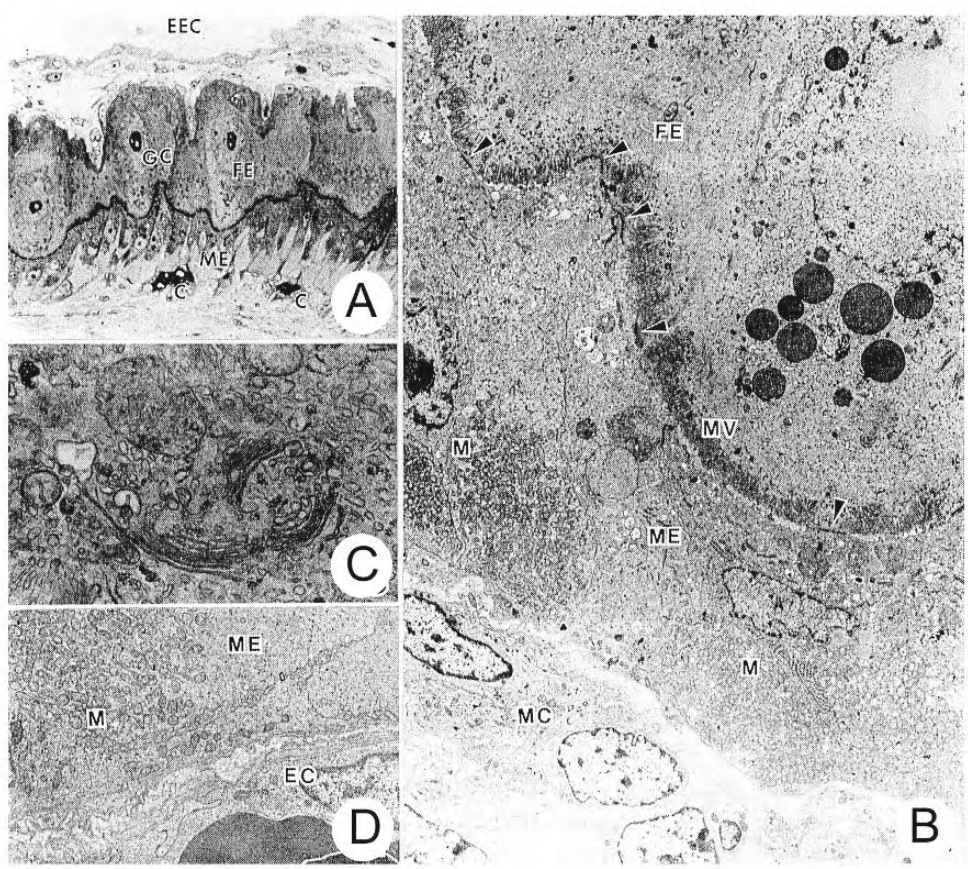

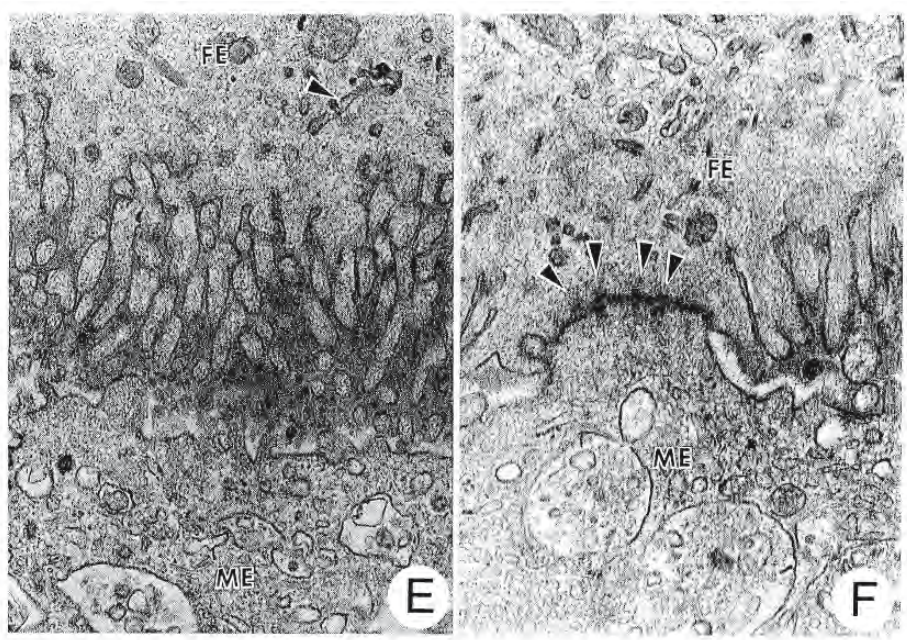

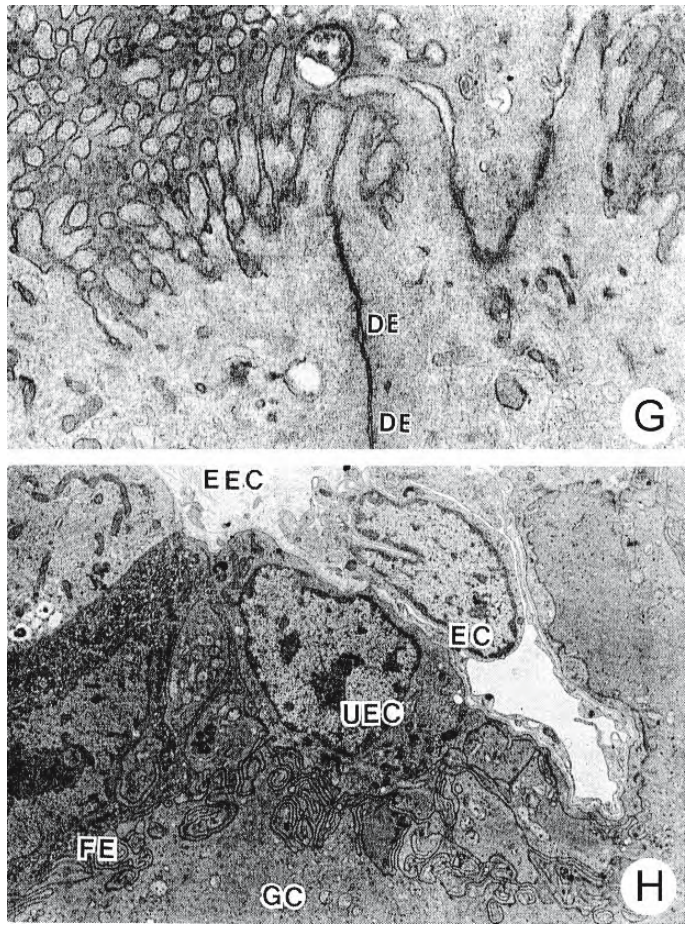

Figure 6.63: Micrographs of sections of the placenta of the blue shark *Prionace glauca.* No egg capsule intervenes between maternal and foetal tissues in this species. All figures are transmission electron micrographs except for **A** and **I** which are photomicrographs. (From Otake and Mizue, 1985; reproduced with permission from the Ichthyological Society of Japan)

A. Photomicrograph of the distal rugose portion of the placenta. X 210.

Abbreviations: C, capillary; EEC, extra-embryonic coelom; FE, foetal epithelium; GC, giant cell; ME, maternal epithelium.

B. Electron micrograph from the rugose distal portion of the placenta showing the foetal epithelium (FE) closely apposed (arrowheads) to the maternal epithelium (ME). There are numerous mitochondria (M) in the basal cytoplasm of the maternal epithelial cell. The foetal epithelium is covered by microvilli (MV). MC, maternal connective tissue. X 2,660

C. A Golgi complex in the cytoplasm of an epithelial cell of the maternal placenta. X 14,000.

D. The basal portion of a maternal epithelial cell (ME) is packed with mitochondria (M). An endothelial cell (EC) of a capillary is nearby. X 4,620.

E. Packed microvilli from foetal epithelial cells (FE) press against maternal epithelial cells (ME); no egg capsule intervenes. The arrowhead indicates a tubular structure in the foetal epithelial cell. X 1,800.

F. The arrowheads indicate electron-dense material in the region where maternal (ME) and foetal (FE) epithelia come in close contact. X 22,860.

G. Desmosomes (DE) connect adjacent cells in the apical portion of the foetal epithelium. The intercellular space contains material of high electron-density., X 20,500.

H. The basal portion of a foetal epithelial cell (FE) is separated by two thin basal laminas from the thin, fenestrated endothelial cell (EC) of an underlying capillary. An underlying degenerate basal cell (UEC) and a giant superficial cell (GC) crowd into this region. The extraembryonic coelom (EEC) is seen at the top. X 4,400.

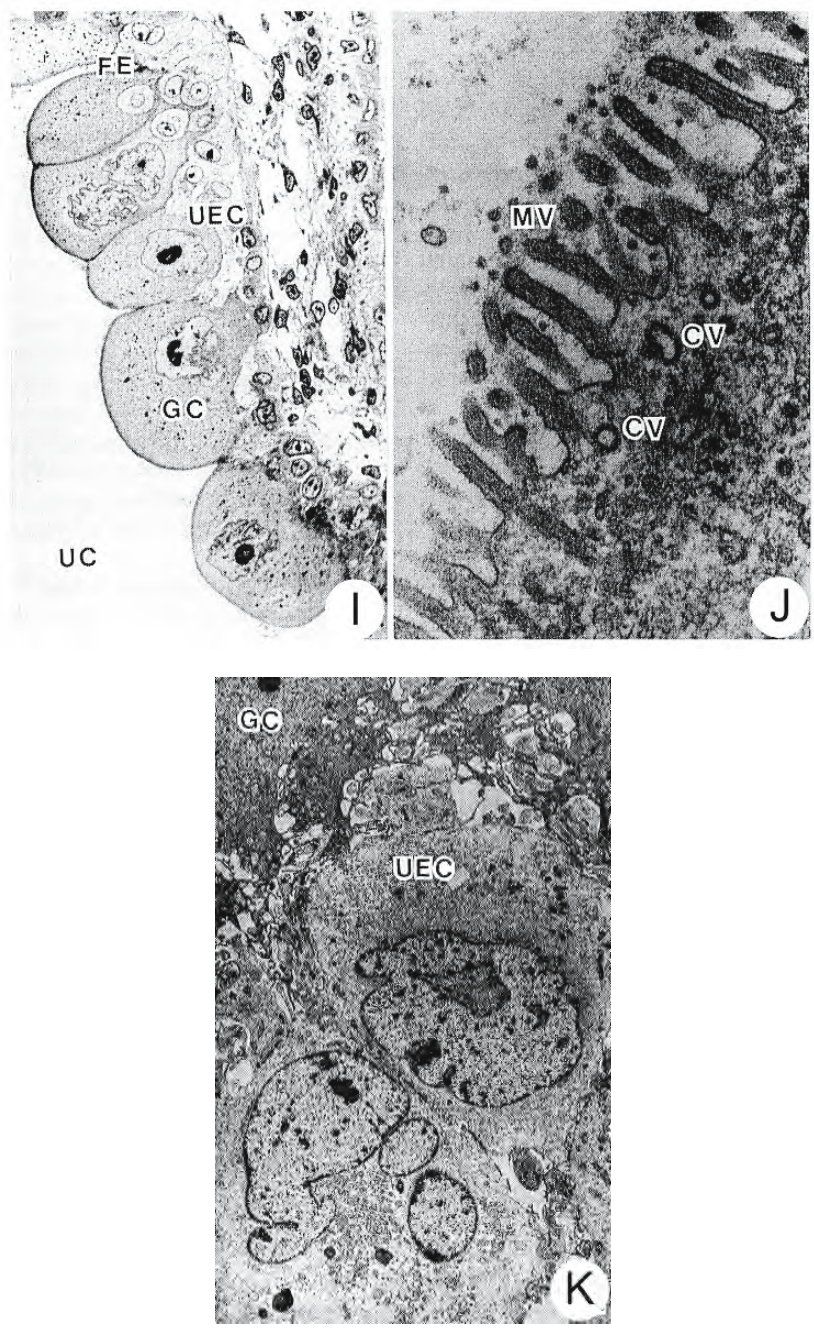

Figure 6.63: Continued.

I. Photomicrograph of the smooth proximal portion of the placenta abutting on the uterine cavity (UC). Giant superficial cells (GC) and underlying basal cells (UEC) constitute the foetal epithelium (FE). X 270.

J. Transmission electron micrograph showing microvilli (MV) on the free surface of a giant epithelial cell from the foetal yolk sac. There are coated vesicles (CV) in the apical cytoplasm. X 28,620.

K. Giant superficial cell (GC) and flattened basal cell (UEC) from smooth proximal portion of the placenta. X 2,430.

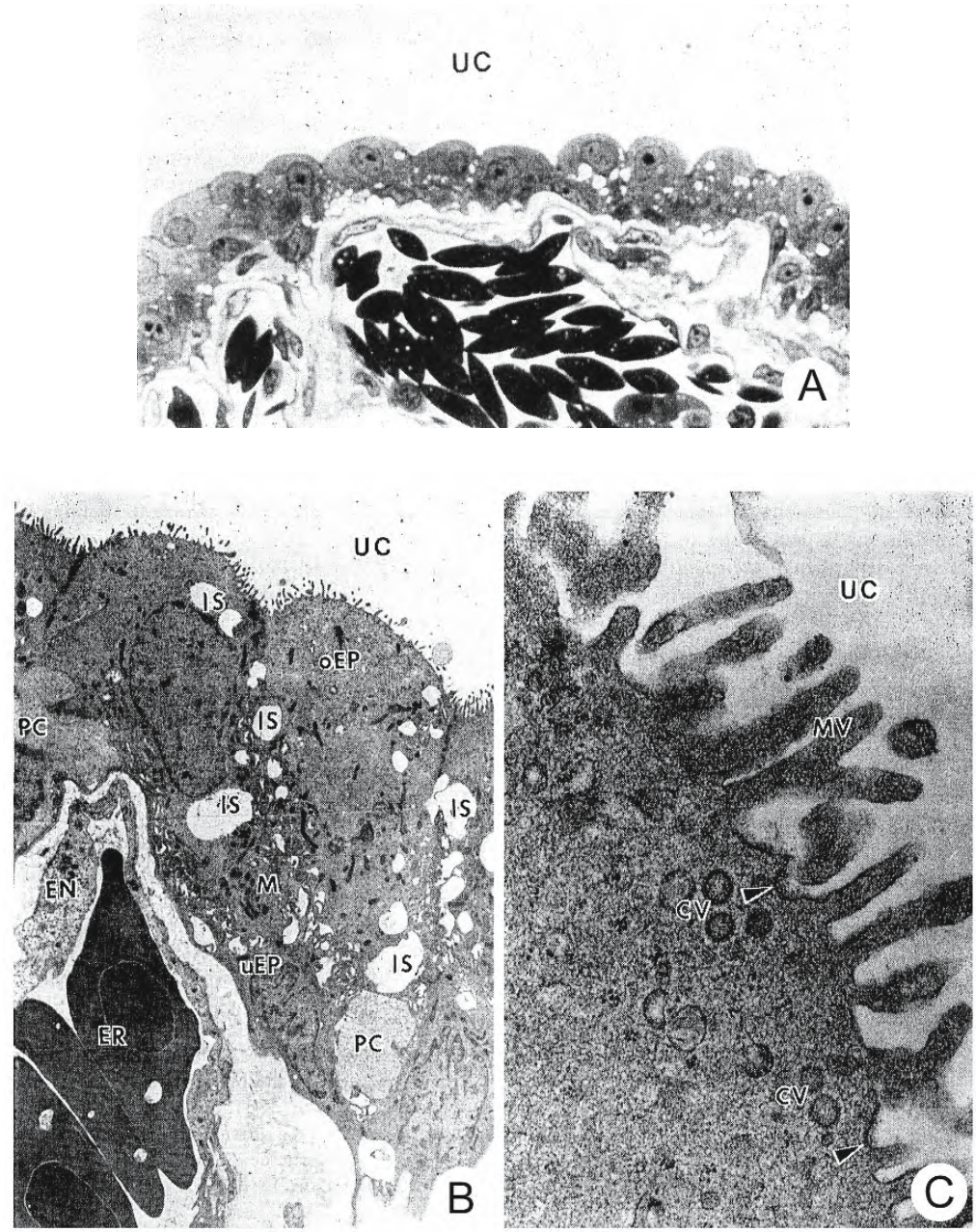

Figure 6.64: Micrographs of sections of the intrauterine epithelium of the blue shark *Prionace glauca* during late gestation. **A** is a photomicrograph; the other figures are transmission electron micrographs. (From Otake and Mizue, 1986; reproduced with permission from the Ichthyological Society of Japan).

A. The intrauterine epithelium presents a thin barrier between the uterine cavity and the endothelium of capillaries. X 500.

B. The intrauterine epithelium rests on loose vascular connective tissue. Intercellular spaces are abundant between the epithelial cells. Abundant mitochondria are distributed in the basal and lateral portions of the superficial epithelial cell. X 2,790.

C. The free surface of a superficial epithelial cell with branched microvilli. Invaginations (arrowheads) are seen between the bases of the microvilli. X 25,740.

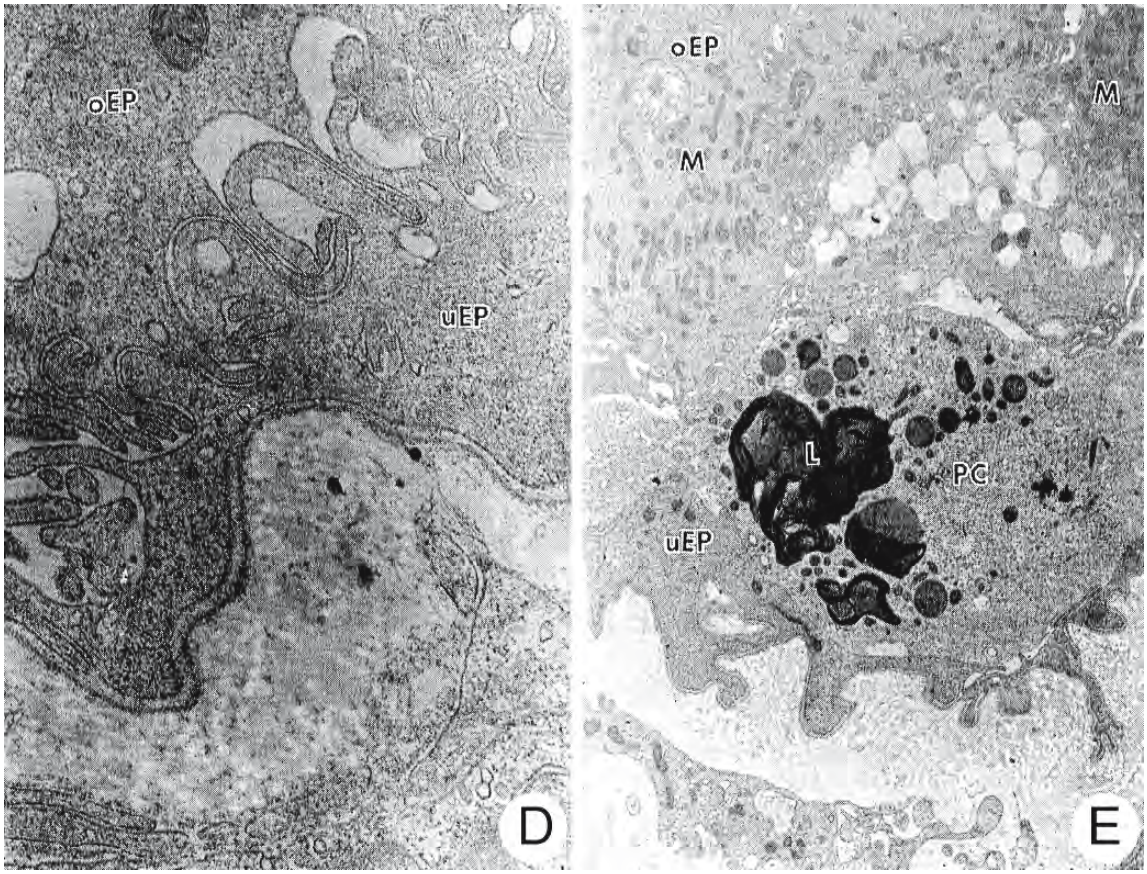

Figure 6.64: Continued.

D. The basal plasmalemmas of superficial and basal epithelial cells are elaborately folded. These cells rest on a distinct basal lamina. X 26,550.

E. A superficial epithelial cell contains abundant mitochondria. A wandering phagocyte contains large lysosome-like granules. X 4,230.

Abbreviations: CV, coated vesicle; EN, endothelial cell; ER, erythrocyte; IS, intercellular spaces; L, lysosome-like granules; M, mitochondria; MV, microvilli; oEP, superficial cell of the uterine epithelium; PC, phagocyte; UC, uterine cavity; uEP, basal cell of the uterine epithelium.

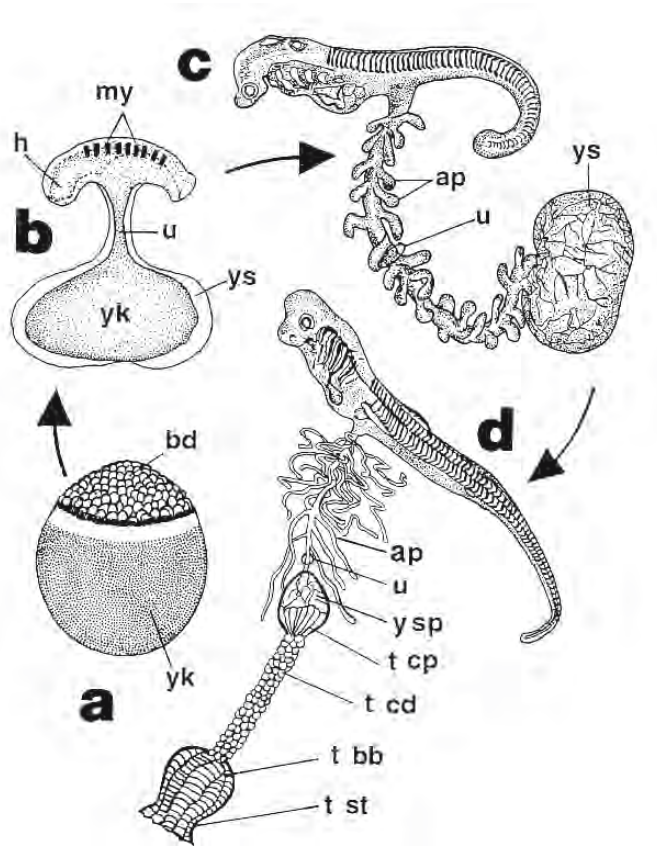

Figure 6.65: An extreme example of placental efficiency is seen in *Scoliodon laticaudus (sorrakowah)* where there is virtually no lecithotrophic phase and the embryo implants immediately after ovulation. Distinctive features of this development are summarized in this diagram. (From Hamlett. 1993; reproduced with kind permission of Kluwer Academic Publishers).

A. The minute (1 mm), nearly yolk-free egg undergoes a modified form of selachian development where the blastoderm appears to undergo complete epiboly over the yolk mass.

B. A 1-mm embryo shortly after hatching from the egg envelope. The head is to the left and there are about eight to nine somites. Development of the caudal region is incomplete. The embryo is connected to the yolk sac by an umbilical stalk. Yolk reserves are rapidly depleted.

C. By the 3-mm stage, although the embryo has developed only to a mid-somite condition, the yolk has disappeared. The yolk sac is undergoing growth and differentiation, the umbilical stalk has elongated, and appendiculae are beginning to develop. Implantation takes place shortly after this stage.

D. At 11 mm, the implanted embryo is still at a rudimentary stage of development and organogenesis. Fin folds and fins, eyes, buccal opening, gill arches, liver, heart, and intestine are forming. The umbilical stalk has lengthened and its appendiculae have begun do elongate. The yolk sac has differentiated into the embryonic portion of the yolk sac placenta and has implanted into the trophonematous cup, a specialized outgrowth of the uterine wall. The maternal portion of the placenta consists of the trophonematous cup, the trophonematous cord, the trophonematous bulb, and the trophonematous stalk.

Abbreviations: ap, appendiculae; bd, blastoderm; h, head; my, somites; t bb, trophonematous bulb; t cd, trophonematous cord; t cp, trophonematous cup; t st, trophonematous stalk; u, umbilical stalk; yk, yolk mass; ys, yolk sac; ysp, yolk sac placenta.

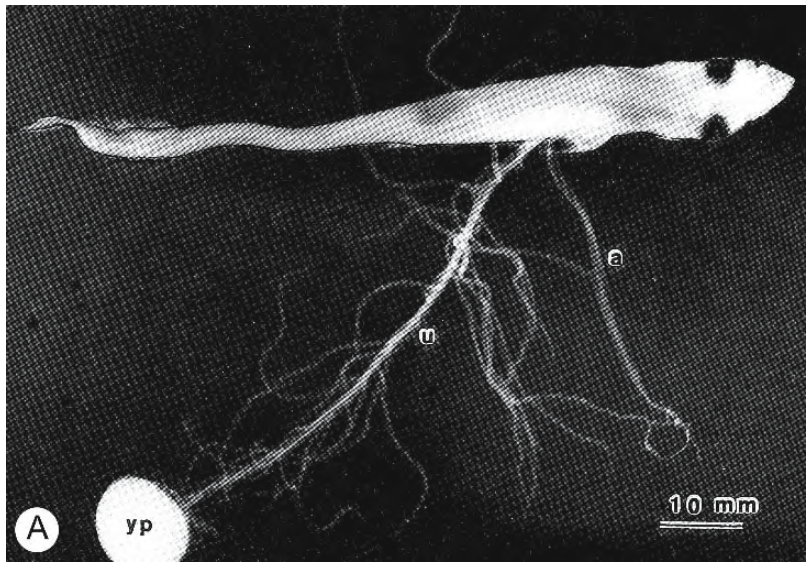

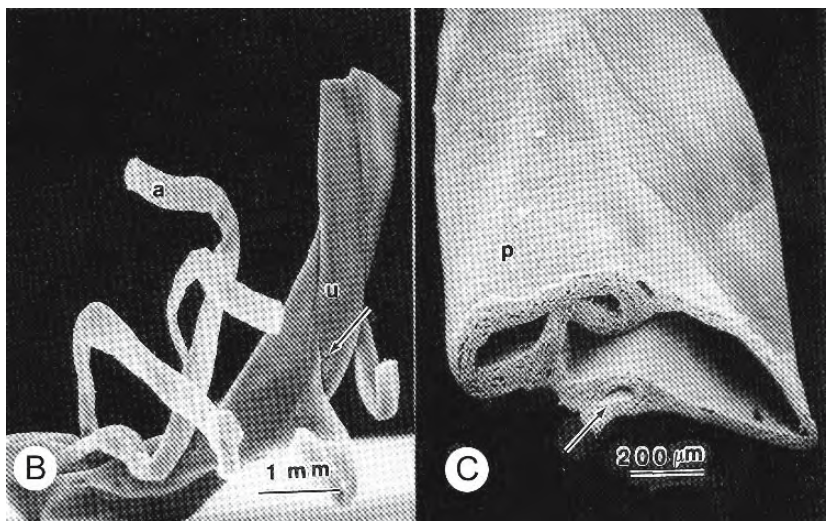

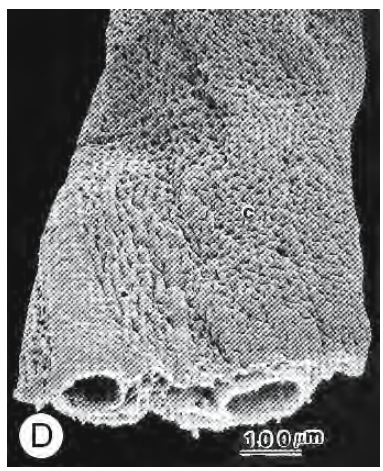

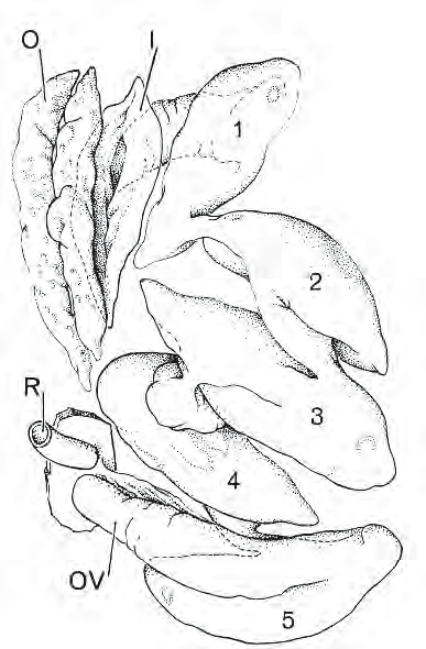

Figure 6.67: Sketch of the reproductive tract of a gravid female coelacanth *Latimeria chalumnae.* Each foetus (numbered 1 to 5) is contained within its own, well-vascularized compartment in expanded portions of the right oviduct. (From Smith et al., 1975; reproduced with permission from the American Association for the Advancement of Science).
Abbreviations: I, infundibulum of the oviduct; O, ovary; OV, distal part of the oviduct; R, rectum.

←

Figure 6.66: Features of the placental apparatus of *Scoliodon laticaudus (sorrakowah)*. (From Wourms. 1993; reproduced with kind permission of Kluwer Academic Publishers).

A. In this photograph of a mid late term pup about 90 mm long, the vascularized umbilical stalk (u) extends from the ventral region to an opaque spherical yolk sac placenta (yp) about 11 mm in diameter. Long, thin, flattened appendiculae (a) extend from the umbilical stalk. Scale bar = 10 mm.

B. Photograph of a part of the umbilical stalk (u) with appendiculae (a). The arrow indicates the origin of one appendicula. Because of their length and fragility, only the basal regions of the appendiculae are present. Scale = 1 mm.

C. This scanning electron micrograph of a cryofractured section through the umbilical stalk reveals a vein and an artery. A vascular branch (arrow) to an appendicula lies in the middle of the lower wall. What appears to be a third vessel in the upper middle portion of the section is actually the left hand vessel folded on itself. Small pits (p) occur on the left upper surface. A vitello-intestinal duct, common to most placental and non-placental sharks, is absent. Scale = 250 μm.

D. Overview of an appendicula by scanning electron microscope. The surface is a system of branching and anastomosing capillaries (c). The transverse section in the foreground reveals two major vessels lying parallel to each other with an intervening central lumen. Scale = 100 μm.

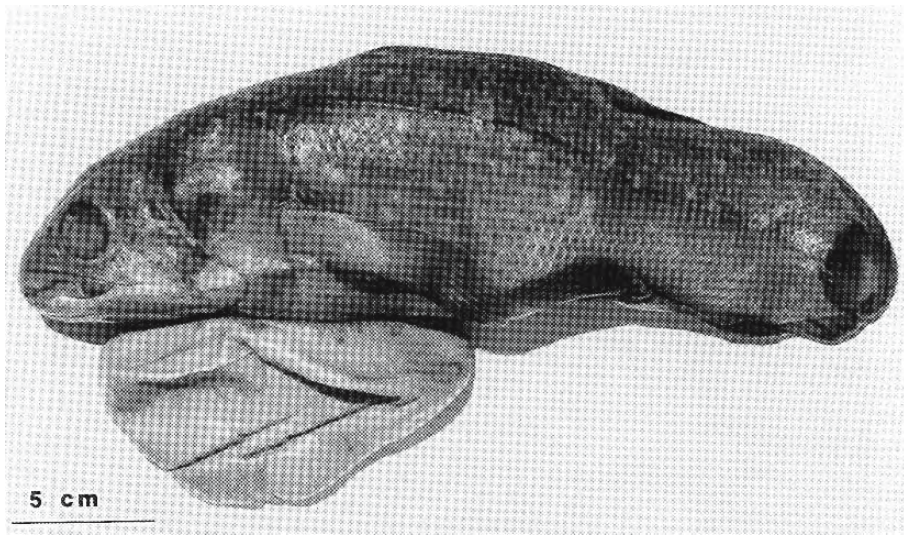

Figure 6.68: Coelacanth *Latimeria chalumnae.* Photograph of a pup lying on its right side after removal from its uterine compartment. The yolk sac is flaccid with a long junction between the ventral surface and the pup. (From Wourms, Atz, and Stribling, 1991; reproduced with kind permission of Kluwer Academic Publishers).

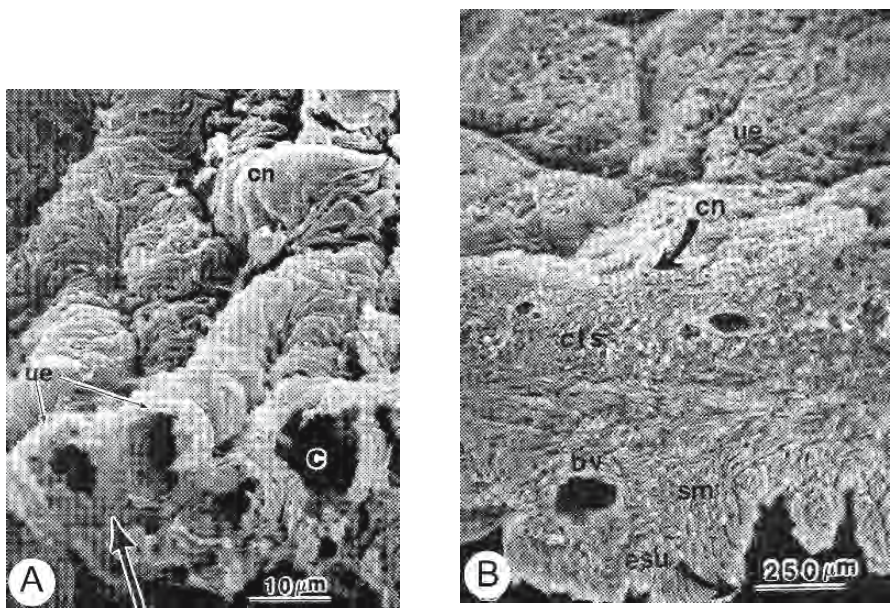

Figure 6.69: Scanning electron micrographs of the walls of the uterus and yolk sac of the coelacanth *Latimeria chalumnae.* (From Wourms, Atz, and Stribling, 1991; reproduced with kind permission of Kluwer Academic Publishers).

A. Placental regions of the uterine lining are embossed by an anastomosing network of capillaries (cn) covered by a simple squamous epithelium (ue) whose surface is amplified by pleats and ridges. Underlying capillaries (c) were exposed by cutting through the wall. The arrow indicates the cut surface.

B. In this section of the uterine wall, the luminal surface of the uterine epithelium (ue) is at the top. Circular profiles (cn) of the capillary network are exposed along the cut surface. Blood vessels (bv) lie within the connective tissue stroma (cts) and smooth muscle (sm) of the wall. The wall is enclosed within serosal epithelium (esu).

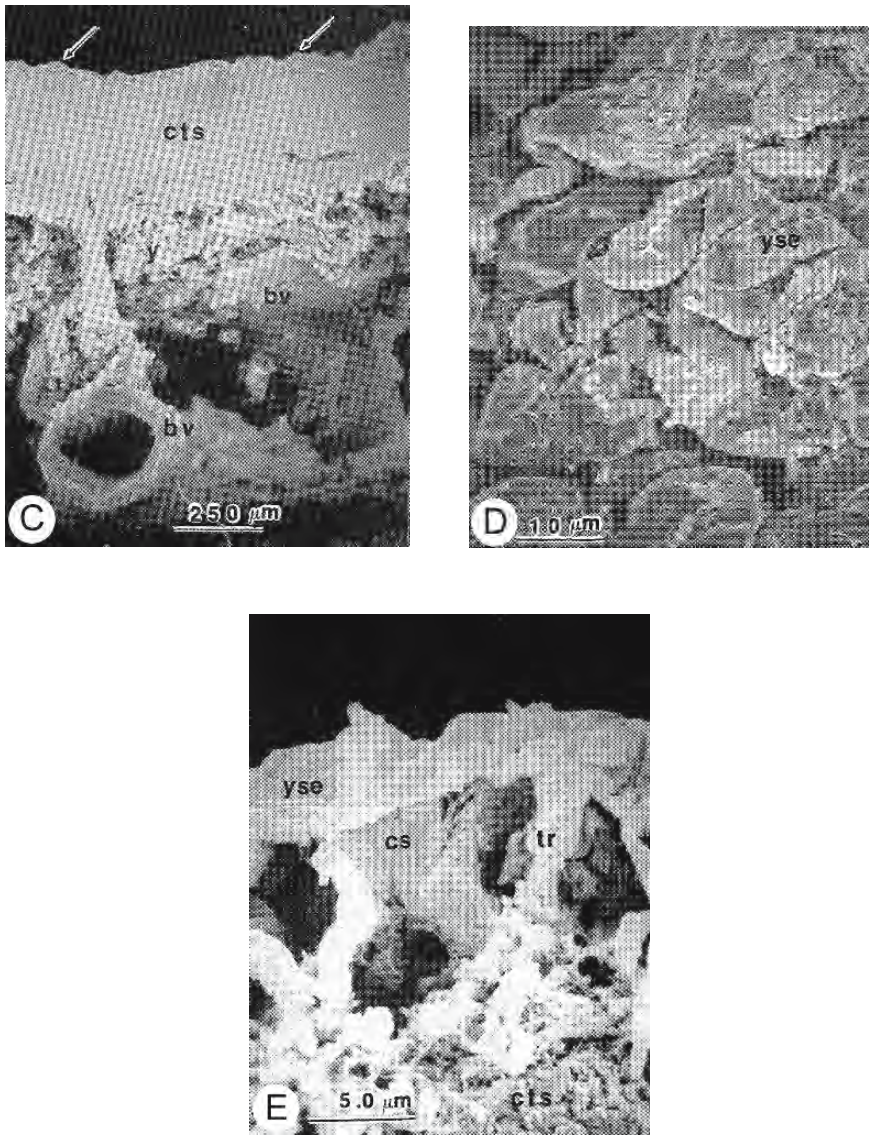

Figure 6.69: Continued.

C. This transverse section of the wall of the yolk sac shows that it is constituted largely of a dense stroma of fibrous connective tissue (cts). A thin epithelial layer (arrows) covers the external surface. Yolk (y) and blood vessels (bv) of the vitelline circulation lie beneath the cortex.

D. The external surface of the yolk sac is convoluted and folded and consists of a simple squamous epithelium (yse) adhering to an intercommunicating bed of cortical sinuses.

E. Transverse section of the cortex of the yolk sac. The squamous epithelium (yse) of the yolk sac encloses a well developed system of cortical sinuses (cs). Columnar trabeculae (tr) extend from the undersurface of the epithelium to a loosely organized boundary at the upper surface of the connective tissue stroma (cts).

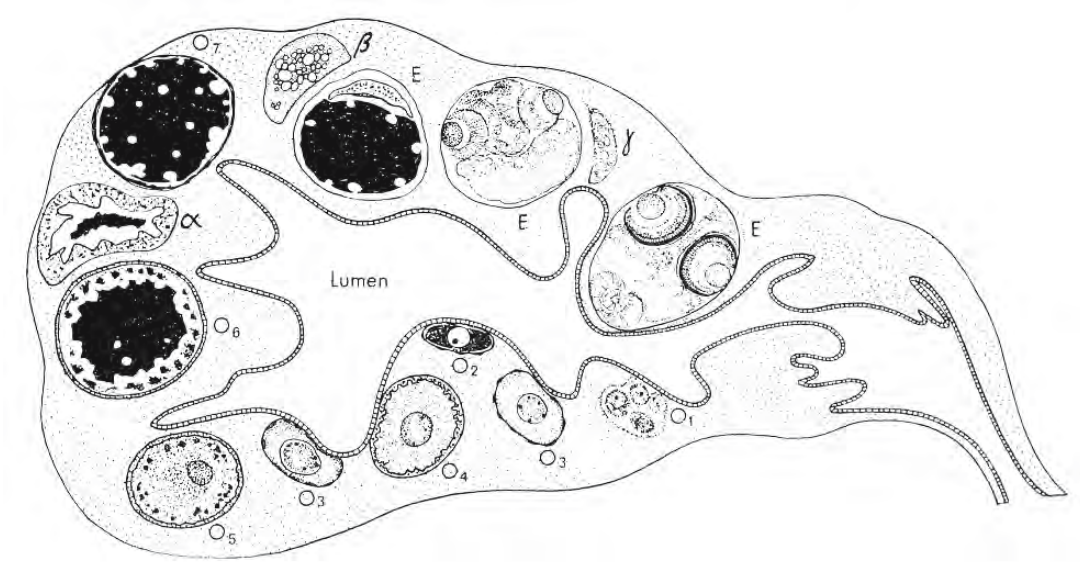

Figure 6.70: Schematic representation of a transverse section of the ovary of the guppy *Poecilia reticulata.* The ovary is a singular, saccular organ. Development of oocytes and embryos takes place within its wall. Various stages of follicular growth and follicular atresia have been combined into one picture; actually these stages do not occur simultaneously. O_1 to O_7 are oocytes in various stages of development; E indicates embryos; while α, β, and γ are stages of follicular atresia. (From Lambert, 1970a; reproduced with permission from Elsevier Science).

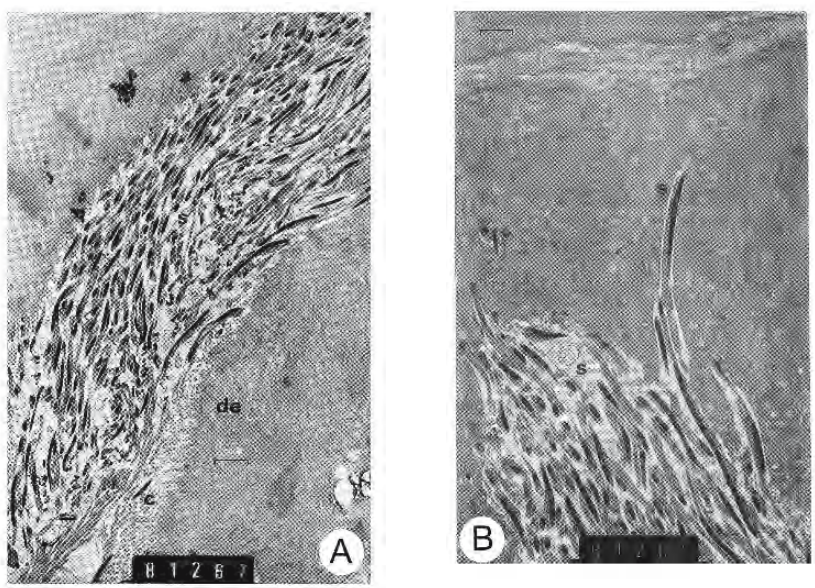

Figure 6.71: Electron micrographs of sections of the oviduct of *Lepidogalaxias salamandroides,* a small, freshwater fish (Family Lepidogalaxiidae, Order Salmoniformes) endemic to the southwest of Western Australia. (From Pusey and Stewart, 1989; reproduced with permission from Elsevier Science).

A. Free spermatozoa in the oviduct. Scale bar = 10 μm.

B. The crypt region of the oviduct showing embedded spermatozoa. Scale bar = 3 μm.

Abbreviations: c, cilia; de, duct epithelium; s, spermatozoa.

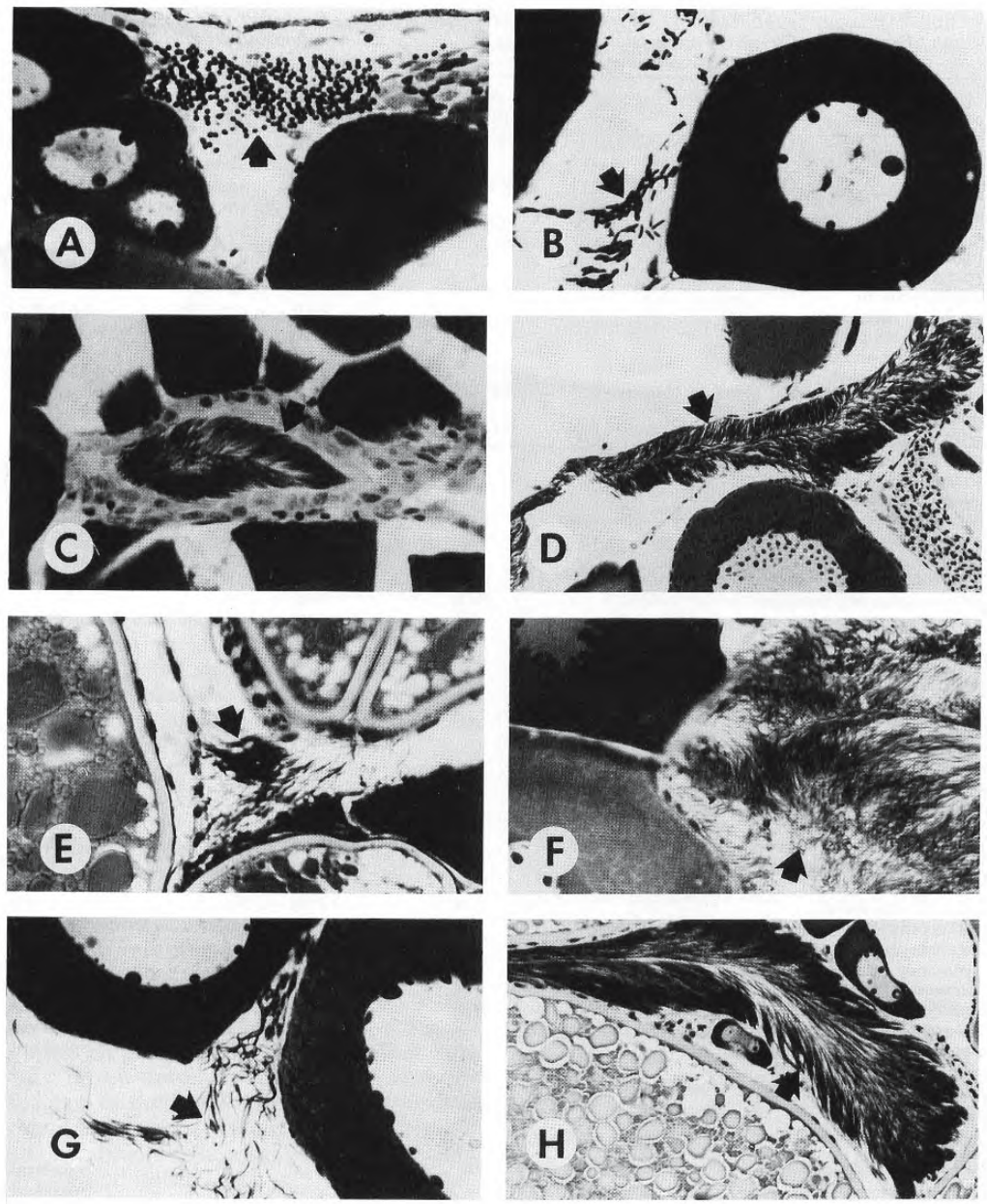

Figure 6.72: Photomicrographs of sections through mature ovaries of several species from the Subfamily Glandulocaudinae of the Family Characidae. Arrows indicate spermatozoa. (From Burns et al., 1995; © reproduced with permission of John Wiley & Sons, Inc.).

A. *Planaltina myersi*. X 438.
B. *Gephryocharax atricaudatus*. X 438.
C. *Xenurobrycon polyancistrus*. X 438.
D. *Tyttocharax* sp. X 219.
E. *Pseudocornyopoma heterandria*. X 438.
F. *Pseudocornyopoma doriae*. X 438.
G. *Mimagoniates sylvicola*. X 438.
H. *Mimagoniates microlepis*. X 219.

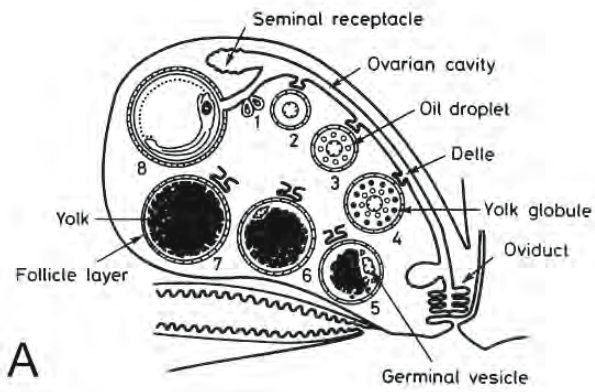

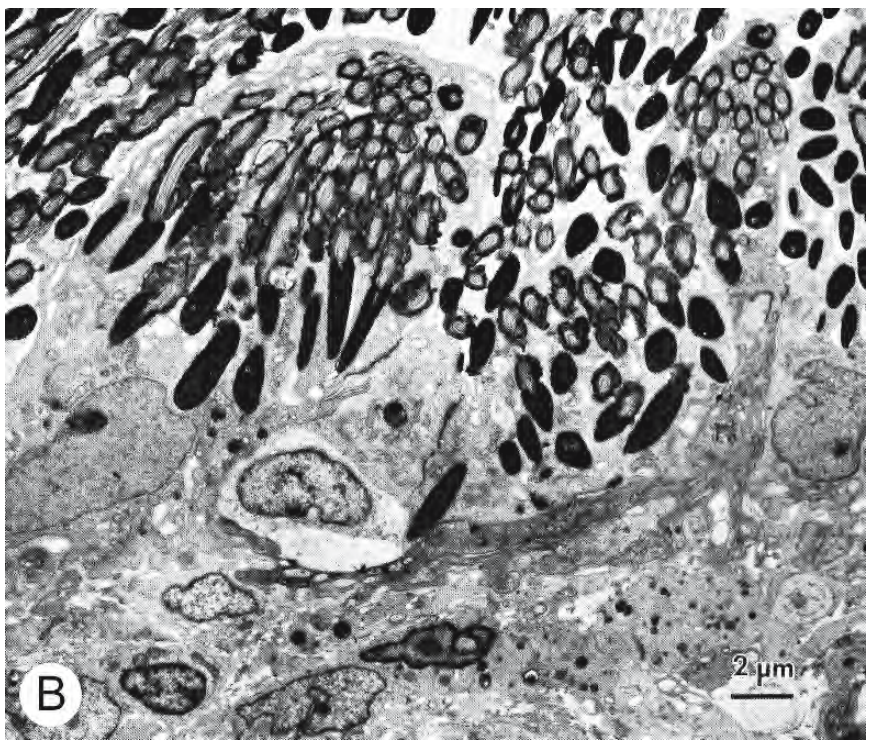

Figure 6.73: Sperm storage in the guppy *Poecilia reticulata*. (From Nagahama, 1983; reproduced with permission from Elsevier Science and K. Takano).

A. Diagrammatic representation of the ovary showing follicles at various stages of development (1 to 8) and the location of the specialized structures of internal fertilization: the delle and seminal receptacle.

B. Electron micrograph of a section of the seminal vesicle within the ovary. Spermatozoa are deeply embedded in the apical cytoplasm of the epithelial cells.

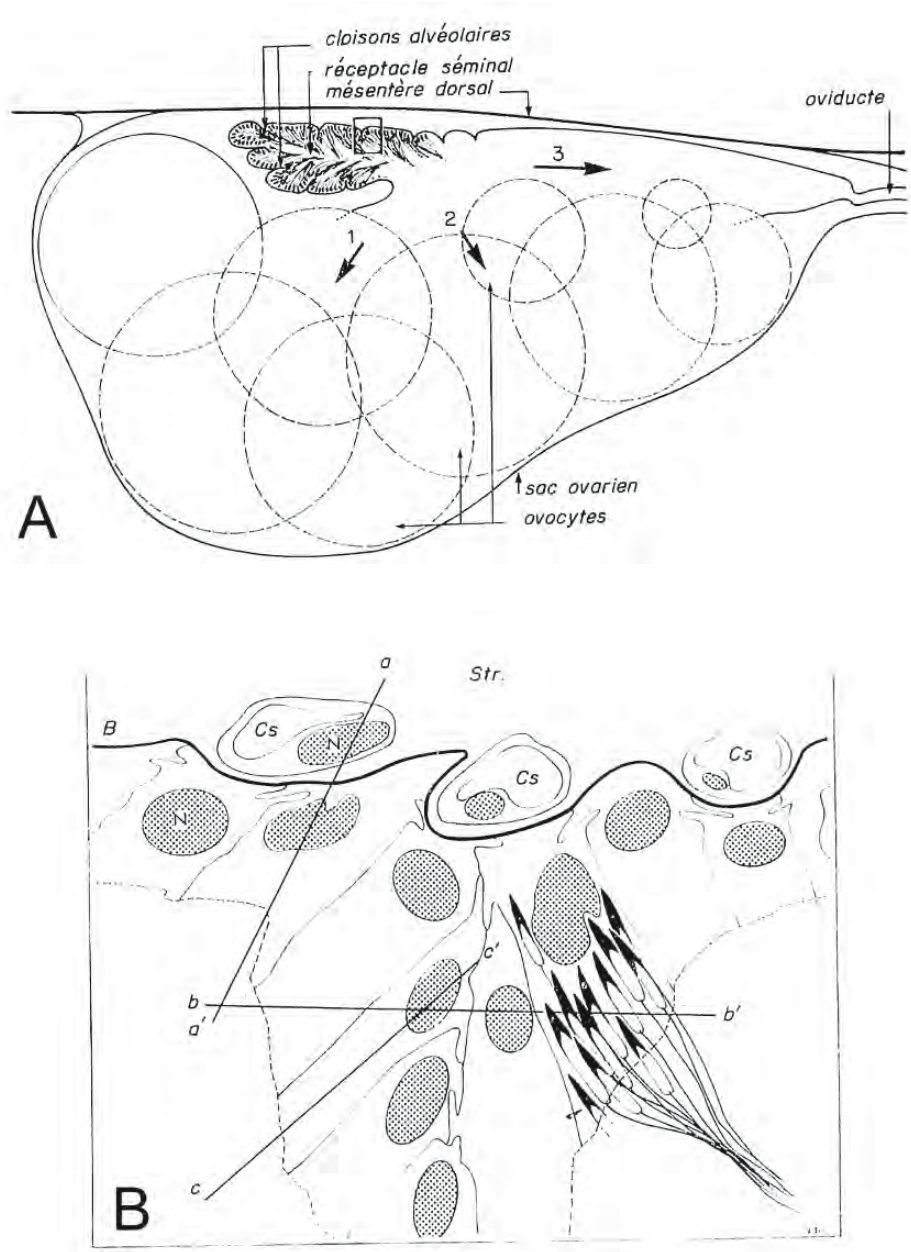

Figure 6.74: The seminal receptacle of the guppy *Poecilia reticulata.* (From Jalabert and Billard, 1969; reproduced with permission of INRA, Paris).

A. Schematic diagram of a sagittal section of an ovary showing the seminal receptacle at the top. The ovary is surrounded by visceral peritoneum. Oocytes at various stages of development are indicated by numbered circles. The seminal receptacle is incompletely divided into chambers.

B. An enlargement of the rectangle shown in A showing a portion of an alveolar chamber of the seminal receptacle. The section shown in the electron micrograph below (Figure 6.74C) was cut along the line b — b'. For simplicity, spermatozoa have been shown within only one cell.

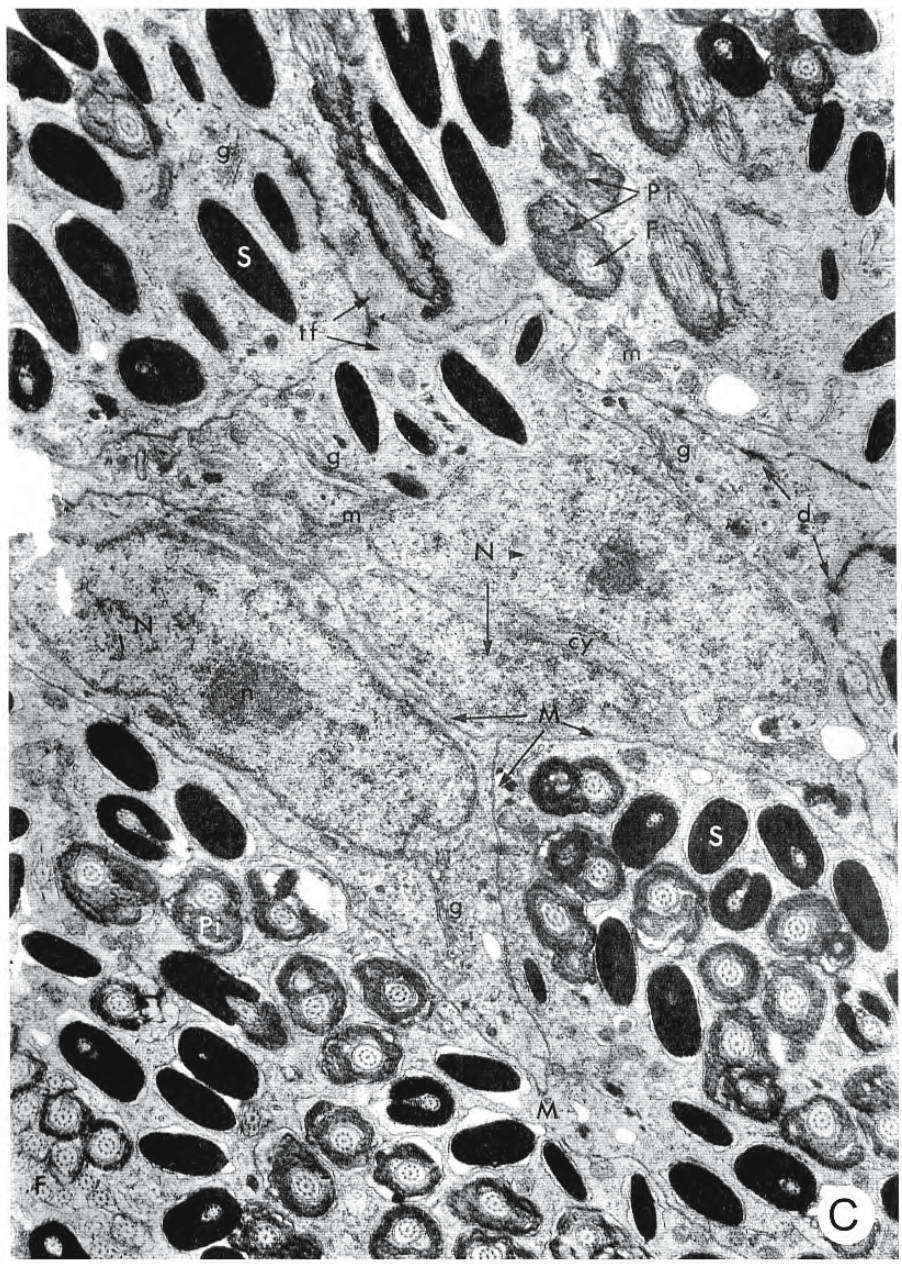

Figure 6.74: Continued.

C. Electron micrograph of a tangential section of the seminal receptacle (b — b' above) showing spermatozoa at various levels within host cells. Numerous desmosomes connect the cells and lateral borders are markedly interdigitated. The lobes of the nucleus at the centre are separated by a cytoplasmic bridge.

Abbreviations: B, basal lamina; Cs, blood capillary; cy, cytoplasm of host cell; d, desmosome; F, flagellum; g, Golgi complex; M, cell membrane; m, mitochondria; N, nucleus, Pi, mitochondrial midpiece of sperm; S, sperm head; Str, connective tissue stroma of the ovary; tf, tonofilaments. X 12,000.

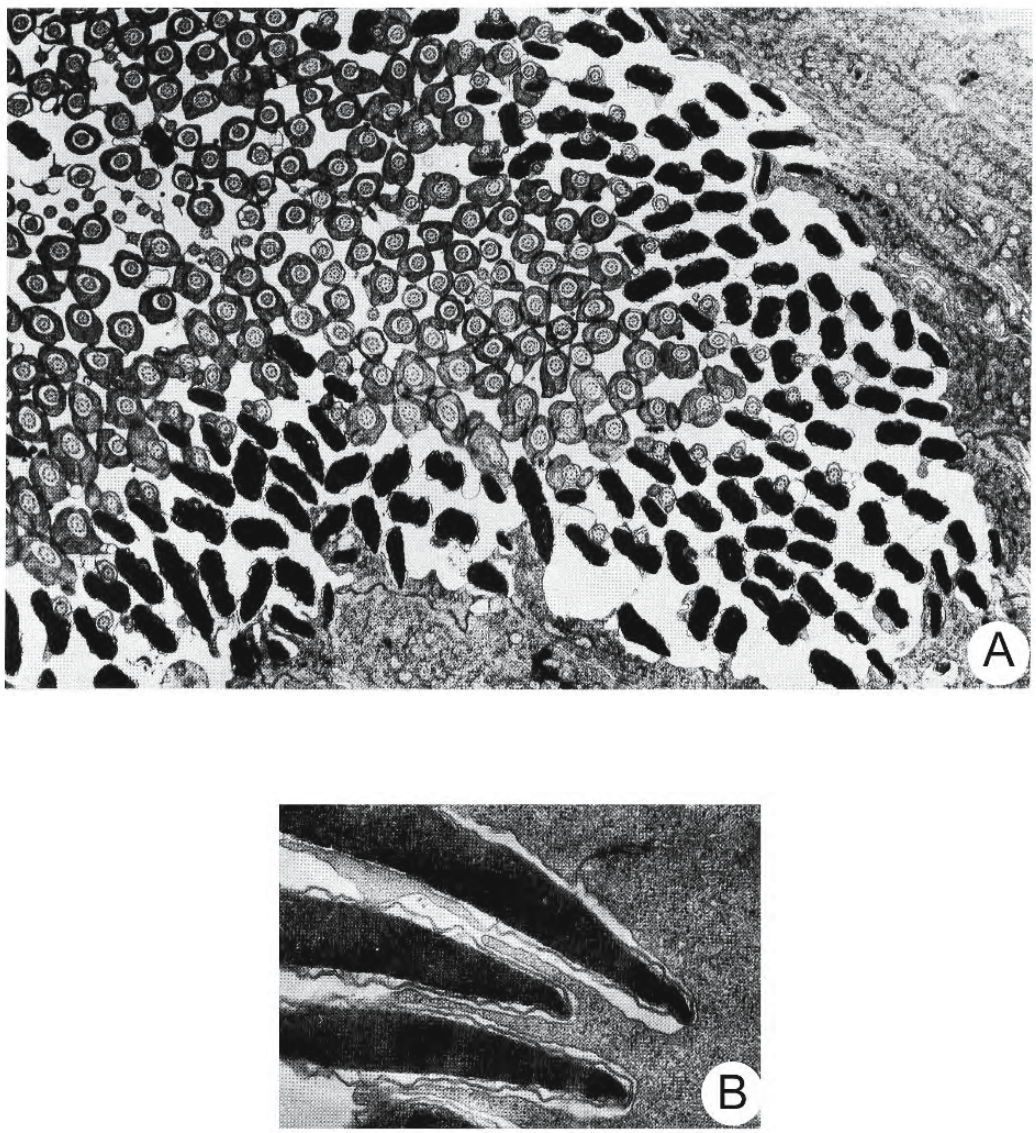

Figure 6.75: Transmission electron micrographs of sections of the ovary of *Cymatogaster aggregata* showing spermatozoa within pockets in the luminal epithelium. (From Gardiner, 1978; © reproduced with permission of John Wiley & Sons, Inc.).

A. The spermatozoa are oriented with their heads toward the epithelial cells and are sectioned transversely at various levels of the head and mitochondrial midpiece. X 6,300.

B. Sperm heads lodged within indentations of the ovarian epithelium. The membranes of the sperm and epithelia are separated by a space of several nanometers and remain intact. X 21,000.

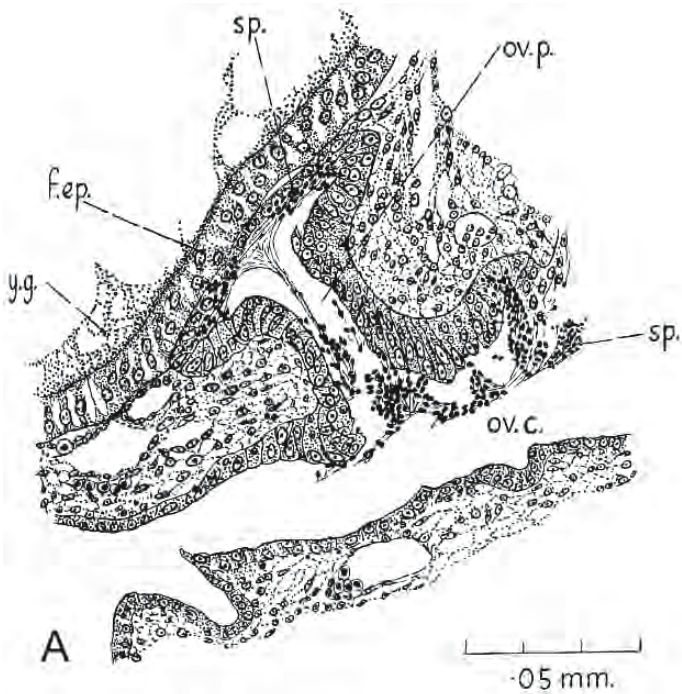

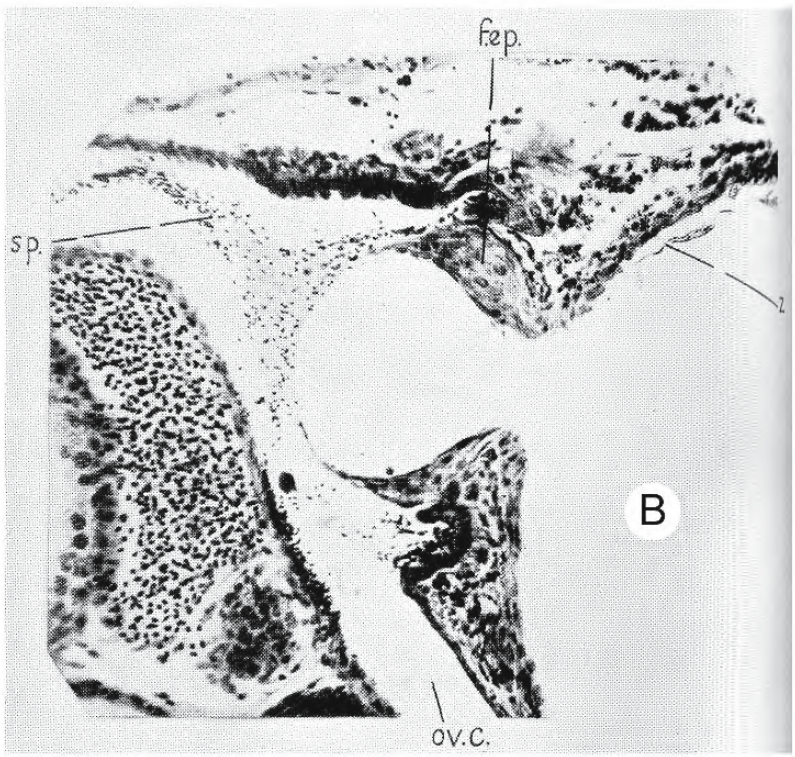

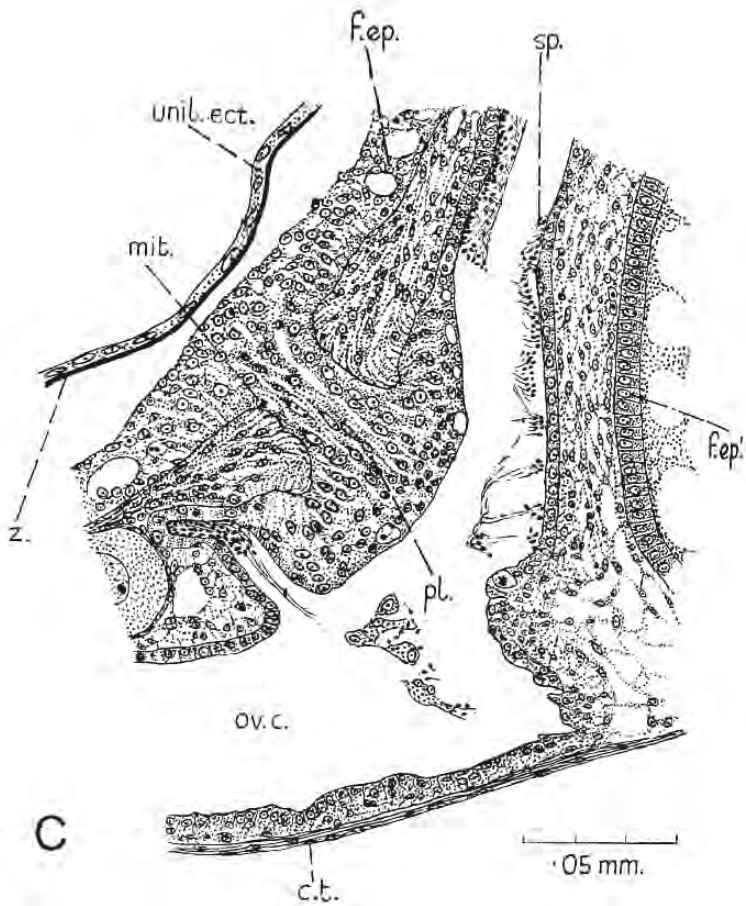

Figure 6.76: Illustrations showing sperm storage in the ovary of *Heterandria formosa.* (From Fraser and Renton, 1940; reproduced with permission from the Company of Biologists, Ltd.).

A. Drawing of a section through a pocket of the ovarian cavity, the expanded distal wall of which is pressed against the follicular epithelium. Masses of spermatozoa are seen both in the pocket and in the ovarian cavity. X 520.

B. Photomicrograph of a section through a special protruberance from an egg into the ovarian cavity at the time of fertilization. Crowds of spermatozoa are gathered over the thin membrane of the protruberance. The zona pellucida and follicular epithelium are absent beneath the protruberance. X 300.

C. Drawing of a section through the solid plug formed after fertilization from the union of the follicular epithelium and that of the ovarian pocket. The zona pellucida has separated from the follicle during fixation. Part of the wall of another ovum (f.ep1) is also seen. X 530.

Abbreviations: c.t, connective tissue sheath of the ovary; f.ep, follicular epithelium; mit, cell undergoing mitosis; ov.c, ovarian cavity; ov.p, pocket of the ovarian cavity; pl, plug; sp, spermatozoa; unil.ect, unilaminar ectoderm; yg, yolk granules; z, zona pellucida.

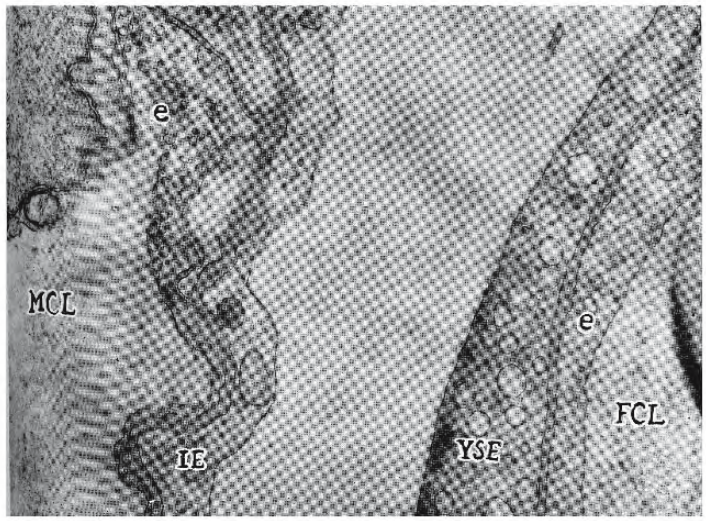

Figure 6.77: Transmission electron micrograph of a section of the ovary of the guppy *Lebistes reticulatus* showing the foetal-maternal barrier at four weeks of gestation. Several layers are interposed between the lumina of a maternal capillary (MCL) and a foetal capillary (FCL). These include both maternal and foetal endothelial cells (e), their basal laminas, the inner follicular epithelium (IE) and the yolk sac epithelium (YSE). There is extensive micropinocytosis in all cellular layers of the barrier. X 12,000 (From Jollie and Jollie, 1964b; © reproduced with permission of John Wiley & Sons, Inc.).

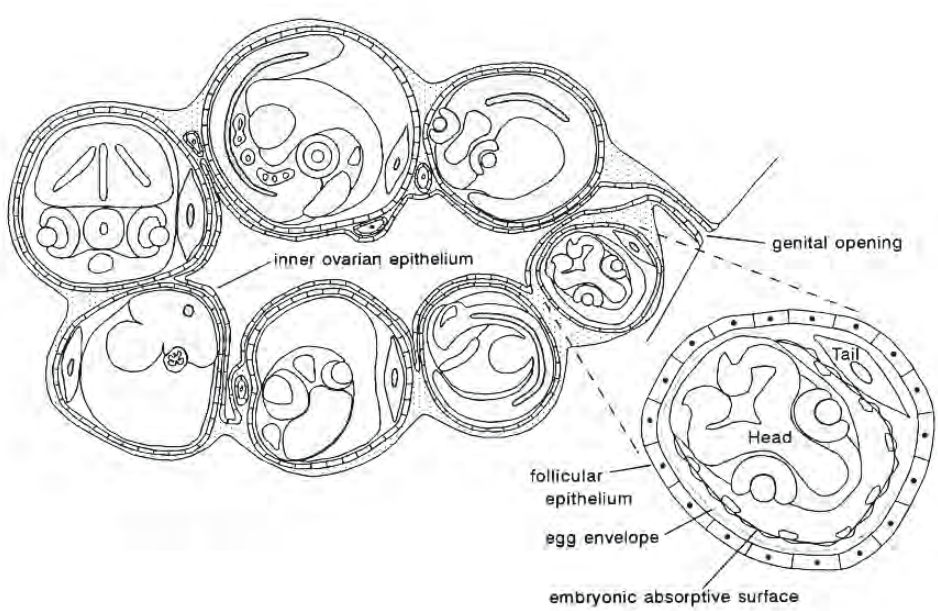

Figure 6.78: Diagram of a section through the ovary of the poeciliid *Heterandria formosa* to illustrate the relationship of the embryos to the ovarian tissues. One follicle has been enlarged to illustrate the presence of the egg envelope between the absorptive surface of the embryo and the follicular epithelium. This diagram demonstrates superfoetation where embryos at three stages of development are present in the same ovary. (From Grove and Wourms, 1994; © reproduced with permission of John Wiley & Sons, Inc.).

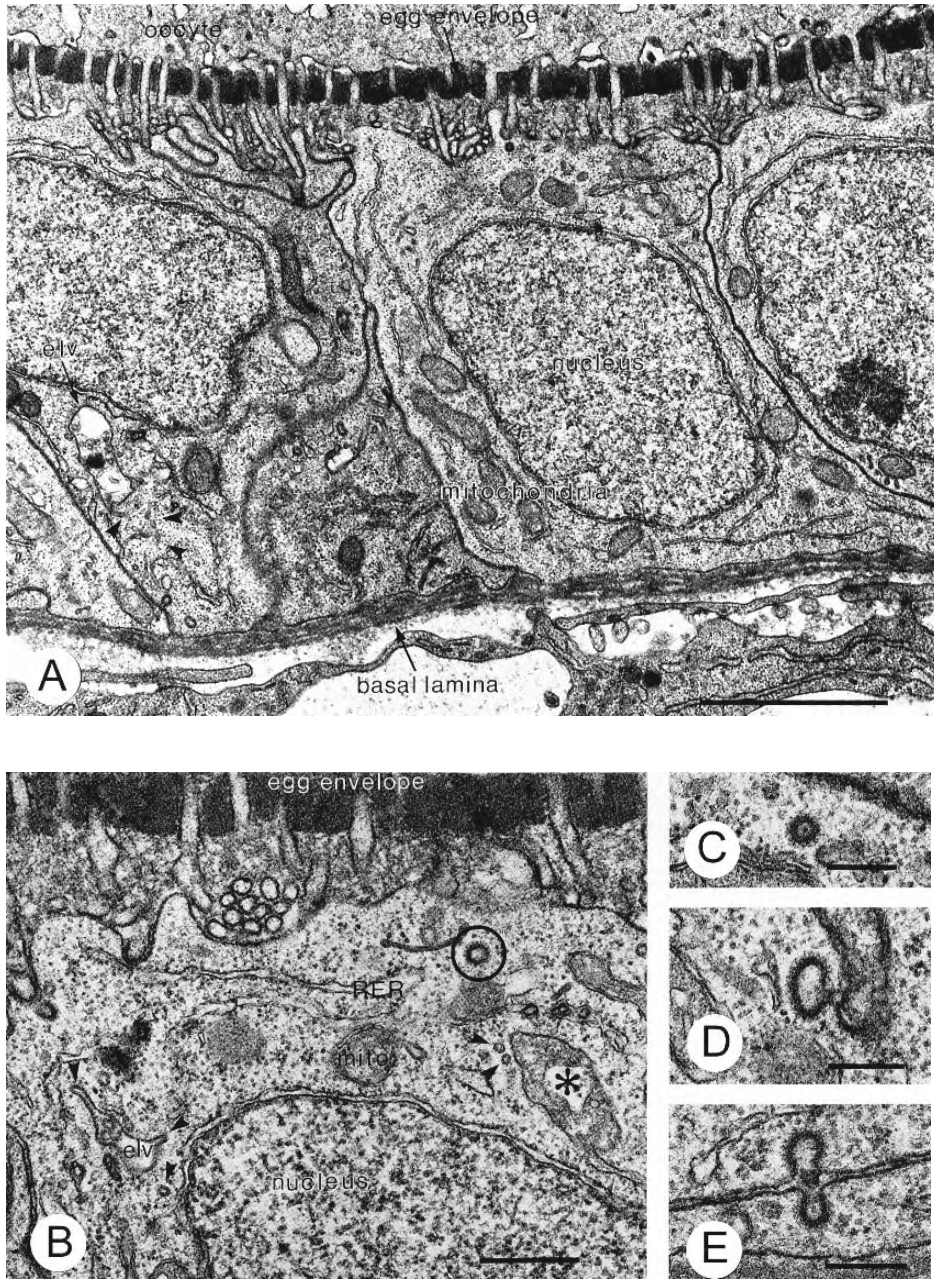

Figure 6.79: Transmission electron micrographs of sections of the follicular epithelium of an early vitellogenic oocyte of the poeciliid *Heterandria formosa.* (From Grove and Wourms, 1994; © reproduced with permission of John Wiley & Sons, Inc.).

A. Follicular epithelium. Note the irregular electron-lucent vesicle (elv) and associated tubular extensions (arrowheads). Bar = 2 μm.

B. Apical region of a follicular cell and oocyte. Mitochondria (mito), some granular endoplasmic reticulum (RER), vesicles containing flocculent material (*), coated vesicles (circle), irregular electron-lucent vesicles (elv), and cross-sectional profiles of their tubular extensions (arrowheads) occur in the cytoplasm. Bar = 500 nm.

C. A coated vesicle from the cell shown in **B.** Bar = 200 nm.

D,**E.** Coated pits on the lateral surfaces of follicular cells. Bar = 250 nm.

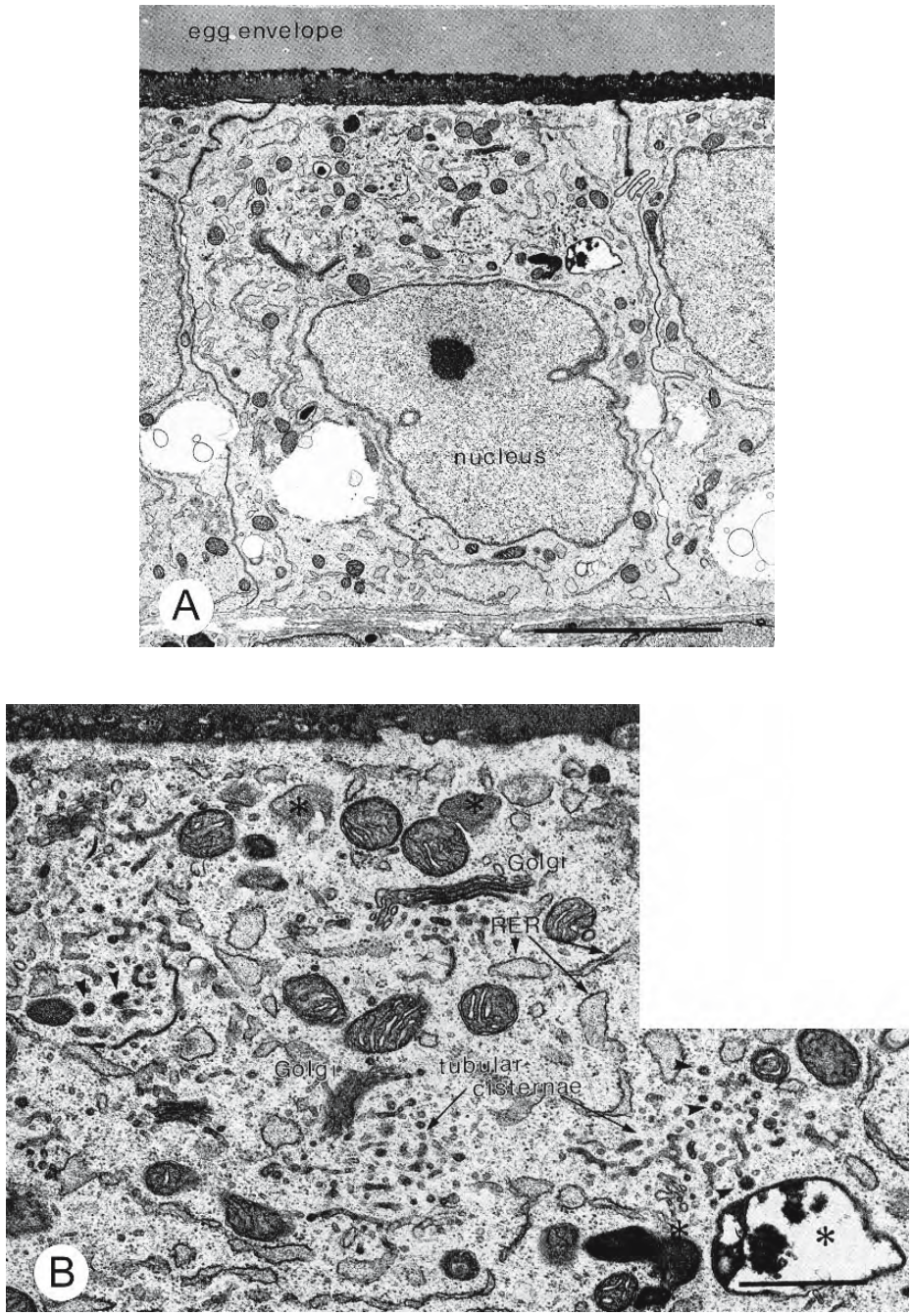

Figure 6.80: Transmission electron micrographs of sections of the follicular epithelium soon after fertilization in the poeciliid *Heterandria formosa.* (From Grove and Wourms, 1994; © reproduced with permission of John Wiley & Sons, Inc.).

A. The follicular cells have acquired the ultrastructural features of transporting cells. Bar = 5 μm.

B. The apical cytoplasm of the cell shown in A contains granular endoplasmic reticulum (RER), coated vesicles (arrowheads) and other vesicles (*). Bar = 1 μm.

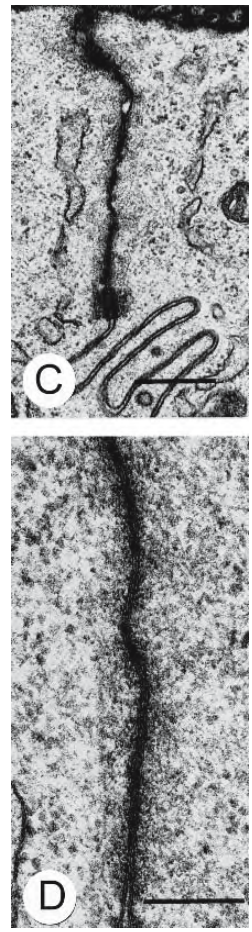

Figure 6.80: Continued.
C. An apical junctional complex from the cell shown in **A.** Bar = 500 nm.
D. Junctional complex illustrating a region with the characteristics of a tight junction. Bar = 250 nm.

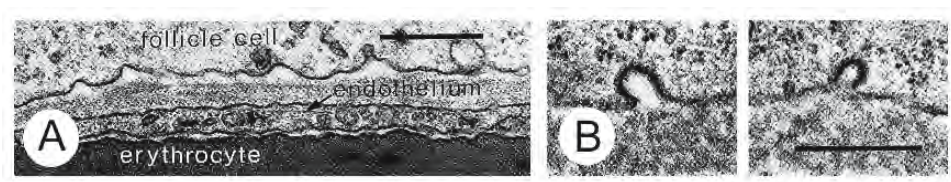

Figure 6.81: Transmission electron micrographs of a section through the basal region of the follicular epithelium soon after fertilization in the poeciliid *Heterandria formosa.* Bars = 500 nm (From Grove and Wourms, 1994; © reproduced with permission of John Wiley & Sons, Inc.).
A. A capillary is closely apposed to the follicular basal lamina. Its endothelial cell contains small vesicles.
B. Coated pits are seen in the basal plasmalemma of the follicular cell.

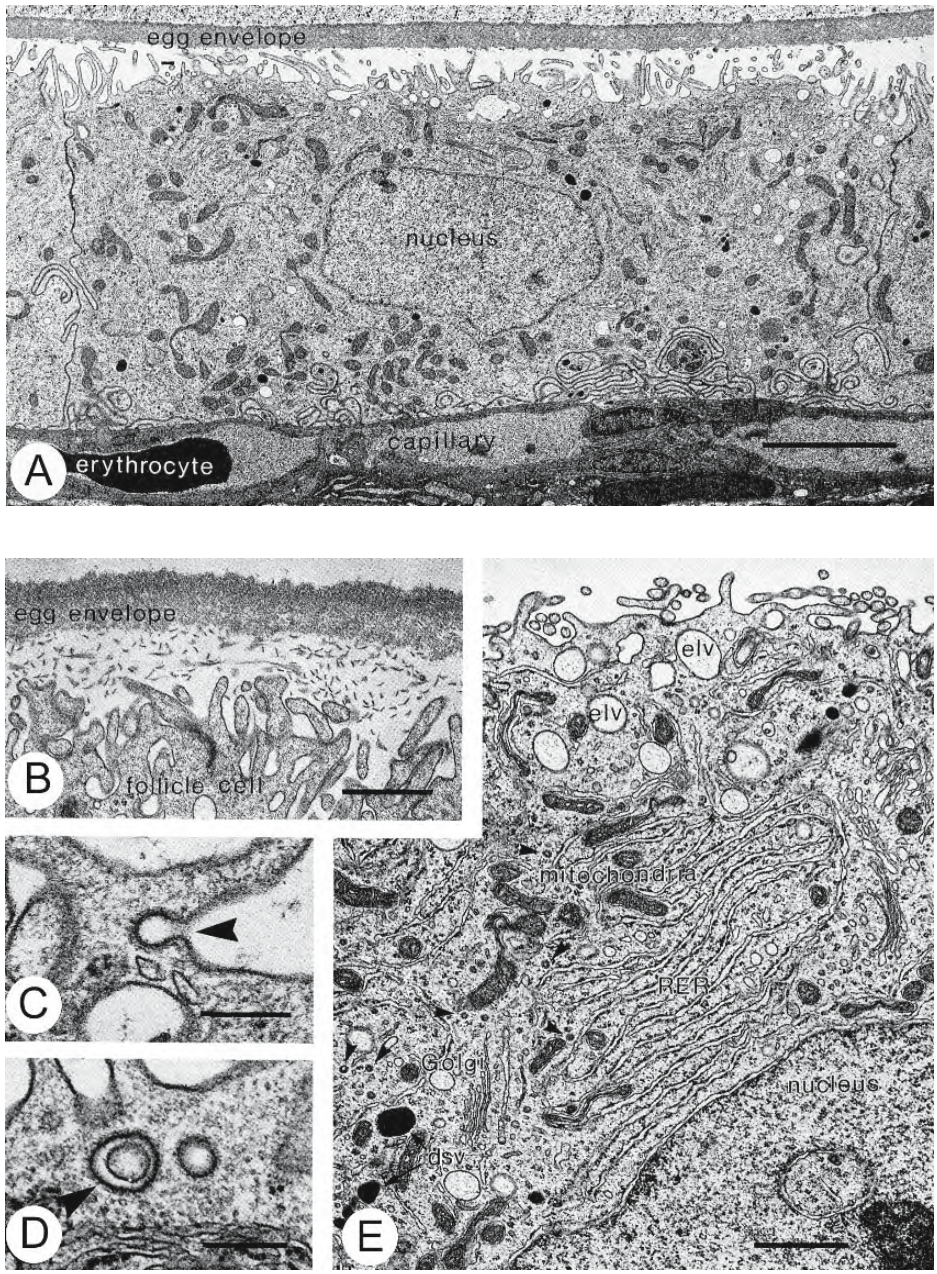

Figure 6.82: Transmission electron micrographs of sections of the follicular epithelium investing a midterm embryo of the poeciliid *Heterandria formosa.* (From Grove and Wourms, 1994; © reproduced with permission of John Wiley & Sons, Inc.).

A. The follicular cells form a low cuboidal epithelium, the egg envelope (zona pellucida) is intact, and capillaries are closely applied to its basal lamina. Bar = 5 μm.

B. Microvilli cover the apical surface of a follicular cell. Bar = 1 μm.

C. The arrowhead indicates a coated endocytotic pit at the base of a microvillus on the apical surface of a follicular cell. Bar = 250 nm.

D. An apical microvillus is surrounded by a coated pit (arrowhead). Bar = 250 nm.

E. The apical, supranuclear cytoplasm of a follicular epithelial cell contains electron-lucent vesicles (elv), mitochondria, granular endoplasmic reticulum (RER), Golgi complexes, and electron-dense vesicles (dsv). Bar = 1 μm.

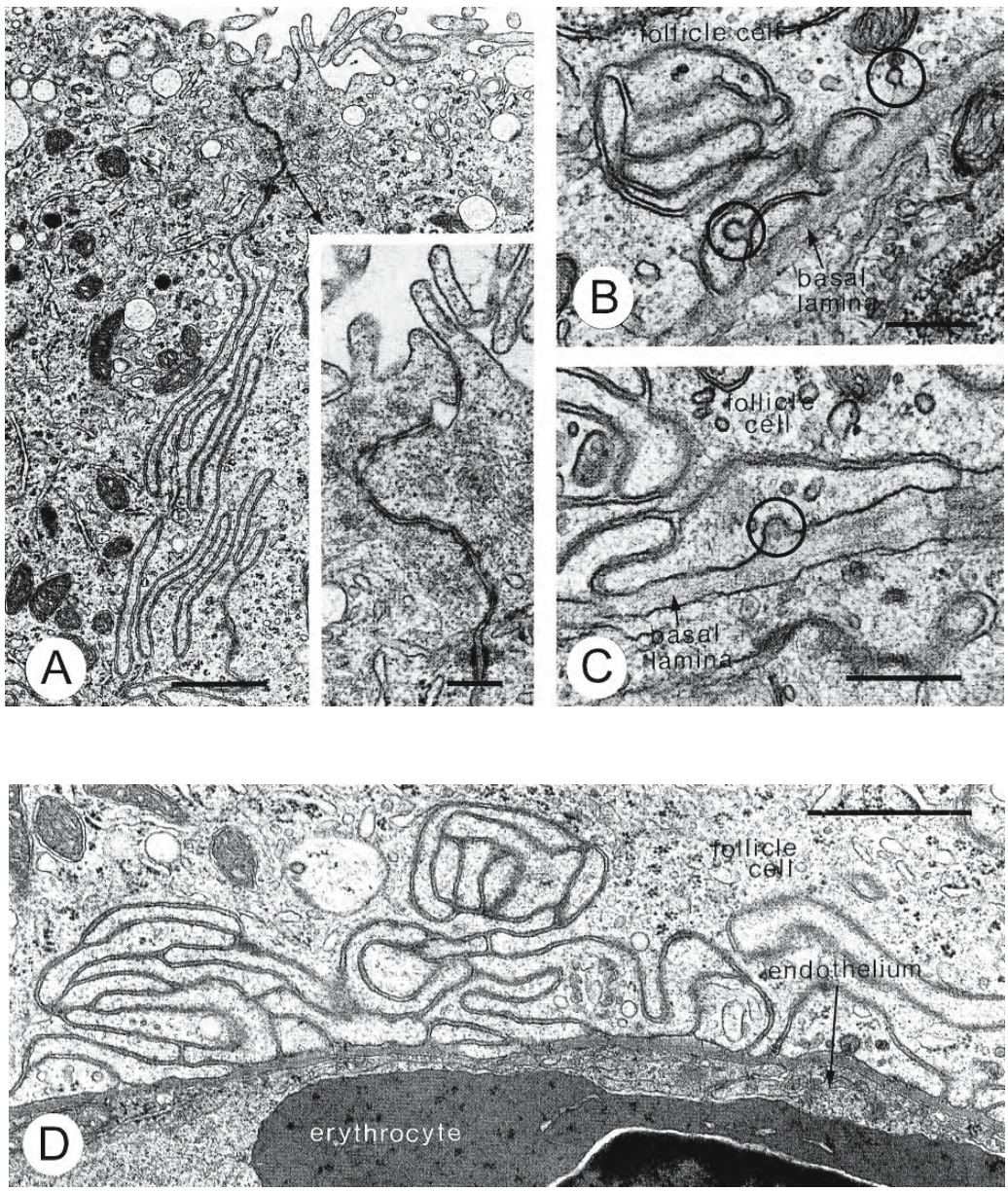

Figure 6.83: Transmission electron micrographs of sections of the follicular epithelium investing a midterm embryo of the poeciliid *Heterandria formosa.* (From Grove and Wourms, 1994; © reproduced with permission of John Wiley & Sons, Inc.).

A. Lateral membranes of adjacent cells interdigitate extensively with each other. Bar = 1 μm The inset shows apical junctional complexes. Bar = 250 nm.

B. The basal surface of a follicular cell shows coated pits (circles). Bar = 500 nm.

C. Smooth surfaced pits are also seen in the basal membrane. Bar = 400 nm.

D. The basal surface of this follicular cell is extensively folded. A capillary is closely apposed to its basal lamina. Bar = 1 μm.

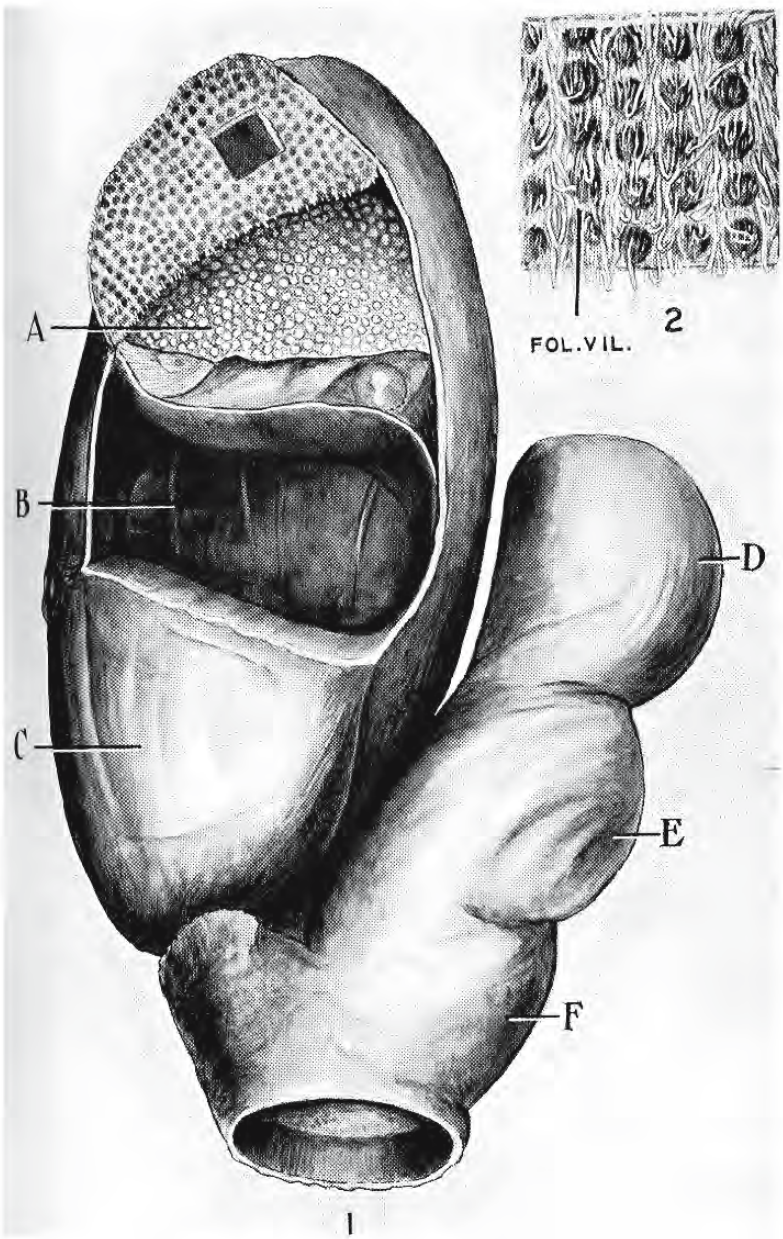

Figure 6.84: Drawings demonstrating adaptations for viviparity in embryos and the ovary of *Anableps anableps.* (From Turner, 1938a; © reproduced with permission of John Wiley & Sons, Inc.).

Plate 1. Ovary.

1. Ovary containing seven 21-mm embryos. A indicates a follicle with the ovarian wall dissected away and a flap of the follicular wall laid back to show the relation of the yolk sac and yolk sac bulbs to the follicular wall and follicular villi. B is a space from which an embryo and the follicle have been removed. C, D, E, and F represent embryos enclosed within intact follicles and the ovarian wall.

2. An enlargement of the internal surface of the follicle from the window depicted in **1** Shown are follicular villi and the depressions caused by contact with yolk sac bulbs.

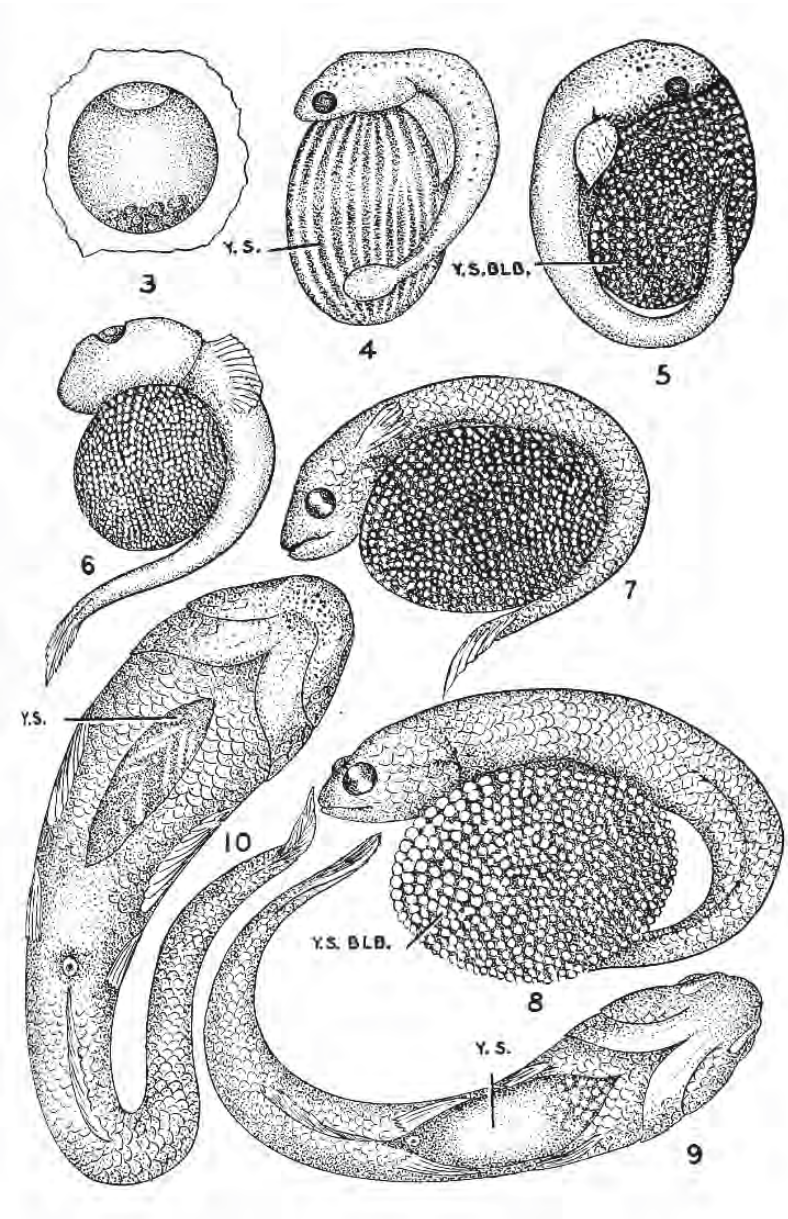

Figure 6.84: Continued.

Plate 2. Embryonic stages.

3. Blastula showing yolk, oil droplets, blastodisc, and vitelline membrane.

4. Embryo 7 mm, with expanded yolk sac. Blood vessels are indicated by light lines. The yolk sac is transparent and contains no yolk.

5. Embryo 14 mm with expanded yolk sac and early stages of yolk sac bulbs.

6. Embryo 17 mm with more advanced yolk sac bulbs.

7. Embryo 19 mm with yolk sac at maximal stage of expansion.

8. Embryo 21 mm. Yolk sac bulbs have reached their maximal size.

9. Embryo 41 mm. Yolk sac is being absorbed and yolk sac bulbs are disappearing.

10. Embryo 43 mm. Yolk sac has been withdrawn into the body cavity and ventral body wall is closing.

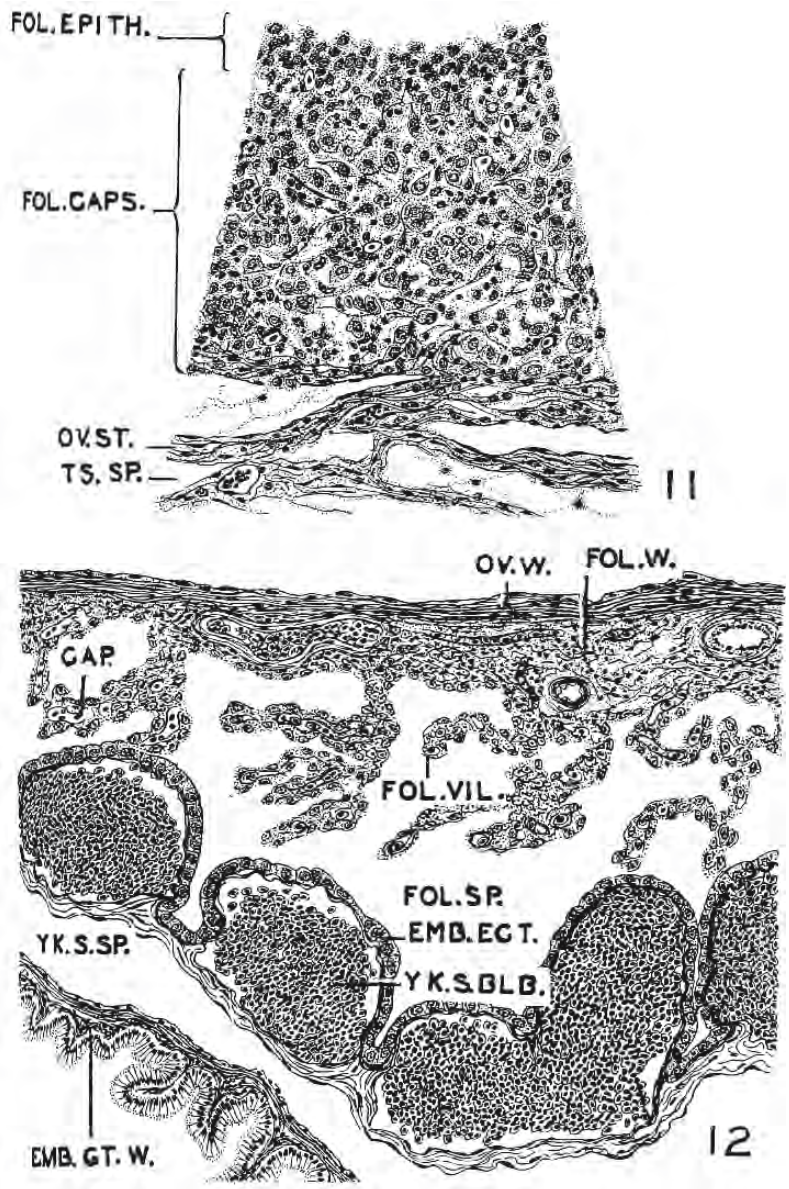

Figure 6.84: Continued.

Plate 3. Sections of the follicular wall.

11. The capsule surrounding a blastula as well as the underlying spongy connective tissue stroma. X 300.

12. The wall of a follicle containing a 21-mm embryo. The yolk sac of the embryo is covered with a cuboidal epithelium supported by a thin layer of connective tissue. Beneath this epithelium, blood vessels and bulbs have thin walls composed of endothelium lying upon delicate connective tissue. Many richly vascular follicular villi hang free in the follicular space. X170.

Abbreviations: CAP, capillary; EMB.ECT, embryonic ectoderm; EMB.GT.W, embryonic gut wall; FOL.CAPS., follicular capsule; FOL.EPITH., old follicular epithelium; FOL.SP, follicular space; FOL.VIL, follicular villus; FOL.W, follicular wall; OV.ST., ovarian stroma; OV.W, ovarian wall; TS.SP., tissue space; Y.S., yolk sac; YK.S.BLB, yolk sac bulb; YK.S.SP, yolk sac space.

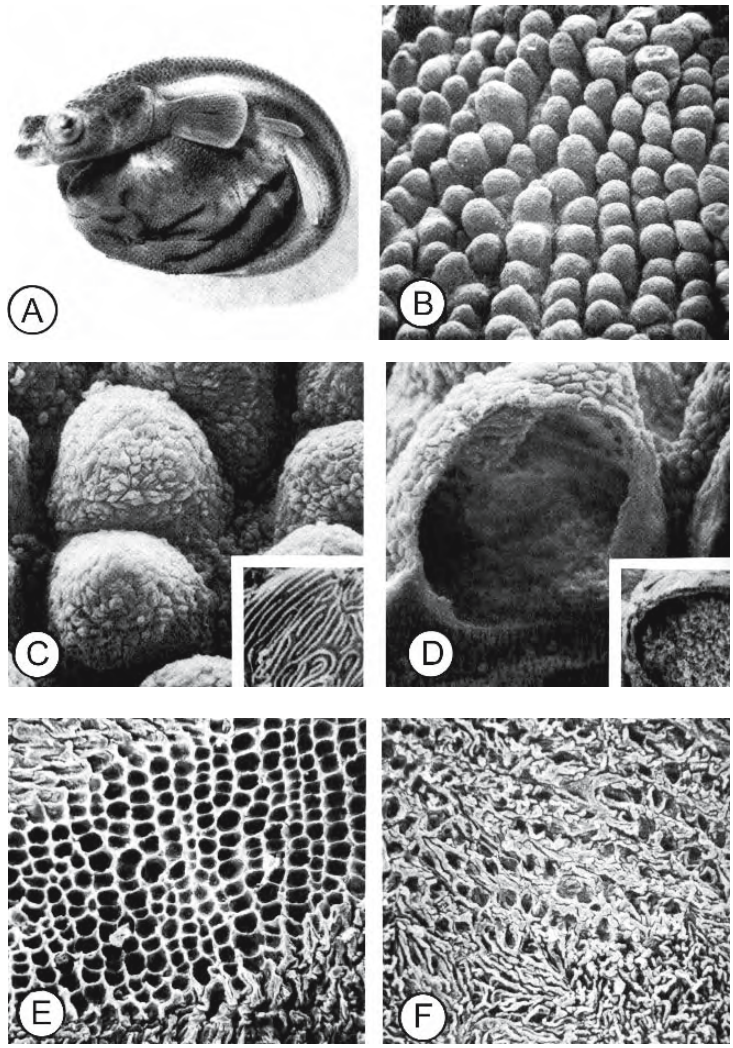

Figure 6.85: The four-eyed fish *Anableps dowi* demonstrates an extreme of matrotrophic nutrition where embryos increase in dry weight as much as 8,000 times during gestation and nutrient transfer is facilitated in the follicular placenta by increases in surface area for exchange. Figures **B** to **H** are scanning electron micrographs. (Knight et al., 1985; © reproduced with permission of John Wiley & Sons, Inc.).

A. Photograph of a 60-mm embryo removed from its follicle. The large, prominent pericardial trophoderm bears vascular bulbs on its surface and occupies the same position in which the yolk sac is found in most embryos. X 2.

B. Vascular buds studding the surface of the pericardial trophoderm increase the surface area for exchange. X 40.

C. Several vascular bulbs from the region shown in **B.** Individual epithelial cells on their surfaces are delineated by intercellular clefts. X 170 The inset shows the microplicae that further amplify the surface for exchange. X 4,000.

D. Vascular bulbs are hollow, domelike chambers. A portion of the wall of this vascular bulb has been broken away to reveal an empty blood sinus within. The blood sinuses are continuous from one vascular bulb to another. X 320 A fractured vascular bulb containing erythrocytes is shown in the inset. X 300.

E. Regions of the inner surface of the follicular wall are riddled with shallow pits that interdigitate with the vascular bulbs of the pericardial trophoderm. X 20.

F. An adjacent region of the same follicular wall shown in E is covered with villous processes, some of which have been deformed to accommodate vascular bulbs. X 20.

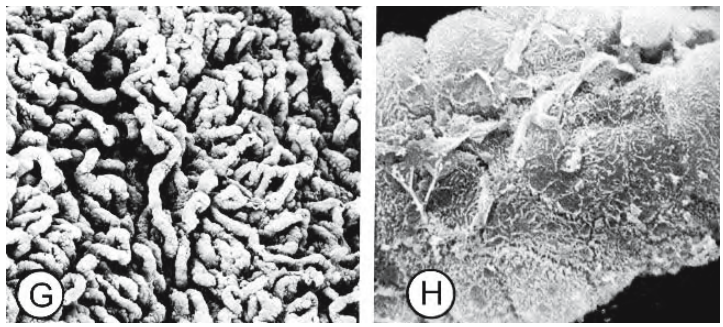

Figure 6.85: Continued.
G. In late gestation, the hypertrophied epithelium lining the follicular wall is comprised entirely of free villi. X 80.
H. On the surface of a follicular villus, the epithelial cells possess short stubby microvilli and irregular microplicae. X 1,140.

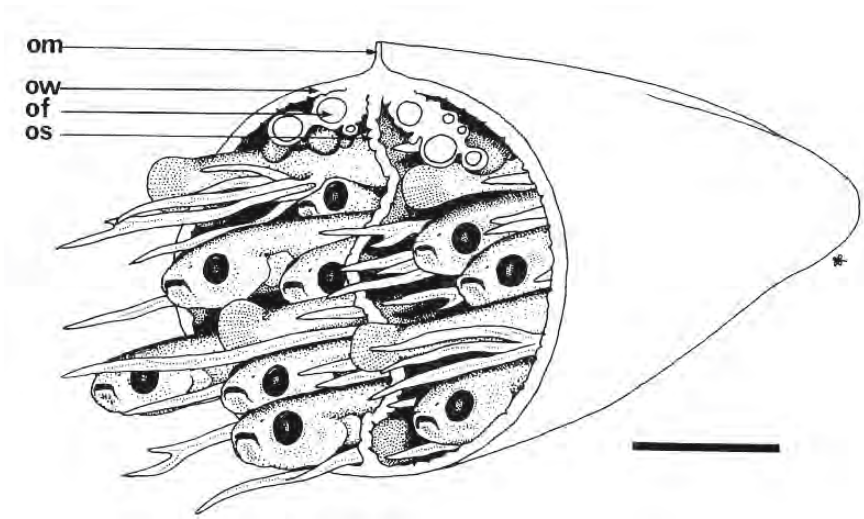

Figure 6.86: Schematic diagram of the near-term ovary of the goodeid *Ameca splendens* illustrating the relationships of embryos to the internal structures of the ovary. The anterior third of the ovary has been removed to illustrate the internal ovarian anatomy. Ribbon-like absorptive trophotaeniae, extending from the hindgut of the embryos, are bathed in the nutritive embryotrophe of the ovarian lumen. Bar = 1 cm (From Wourms, Grove, and Lombardi, 1988; reproduced with permission from Elsevier Science).
Abbreviations: of, oocyte; om, mesovarium; os, ovarian septum; ow, ovarian wall.

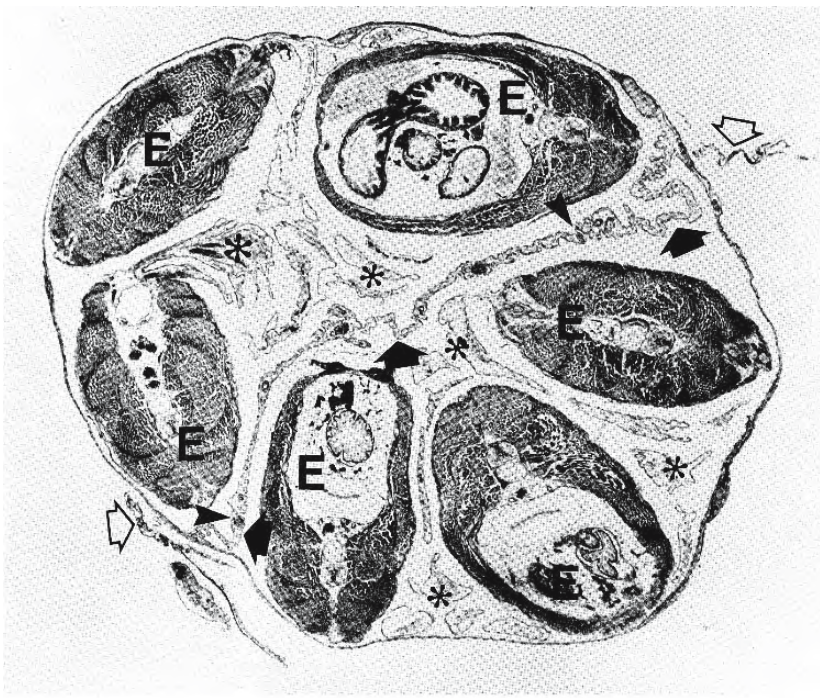

Figure 6.87: Photomicrograph of a cross section through the ovary, containing six embryos (E), of the goodeid *Xenotoca eiseni.* (From Schindler, 1990; reproduced with permission) The ovary is suspended by two mesovaria (open arrows). The ovarian cavity is incompletely (arrowheads) divided by a folded median septum (arrows). The internal ovarian epithelium covers the inner lining of the ovarian wall as well as both sides of the septum. The asterisks indicate sections through embryonic trophotaeniae. X 25.

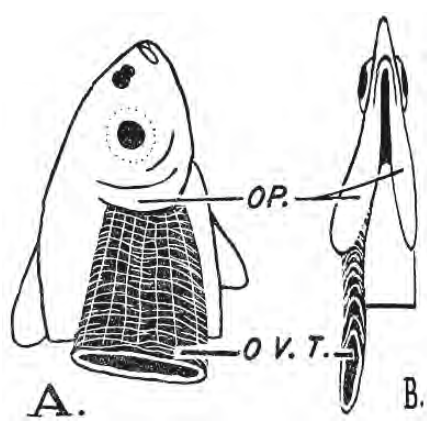

Figure 6.88: Drawings of the anterior end of an unborn, 37-mm embryo of the embiotocid fish *Cymatogaster aggregata* to show the relationship of a fold of ovarian tissue (OV.T) to the operculum (OP) of the embryo. (From Turner, 1952; reproduced with permission of the American Society of Ichthyologists and Herpetologists).

A. Intact embryo with a fold of maternal ovarian tissue inserted under the right operculum.

B. Ventral view of the same embryo.

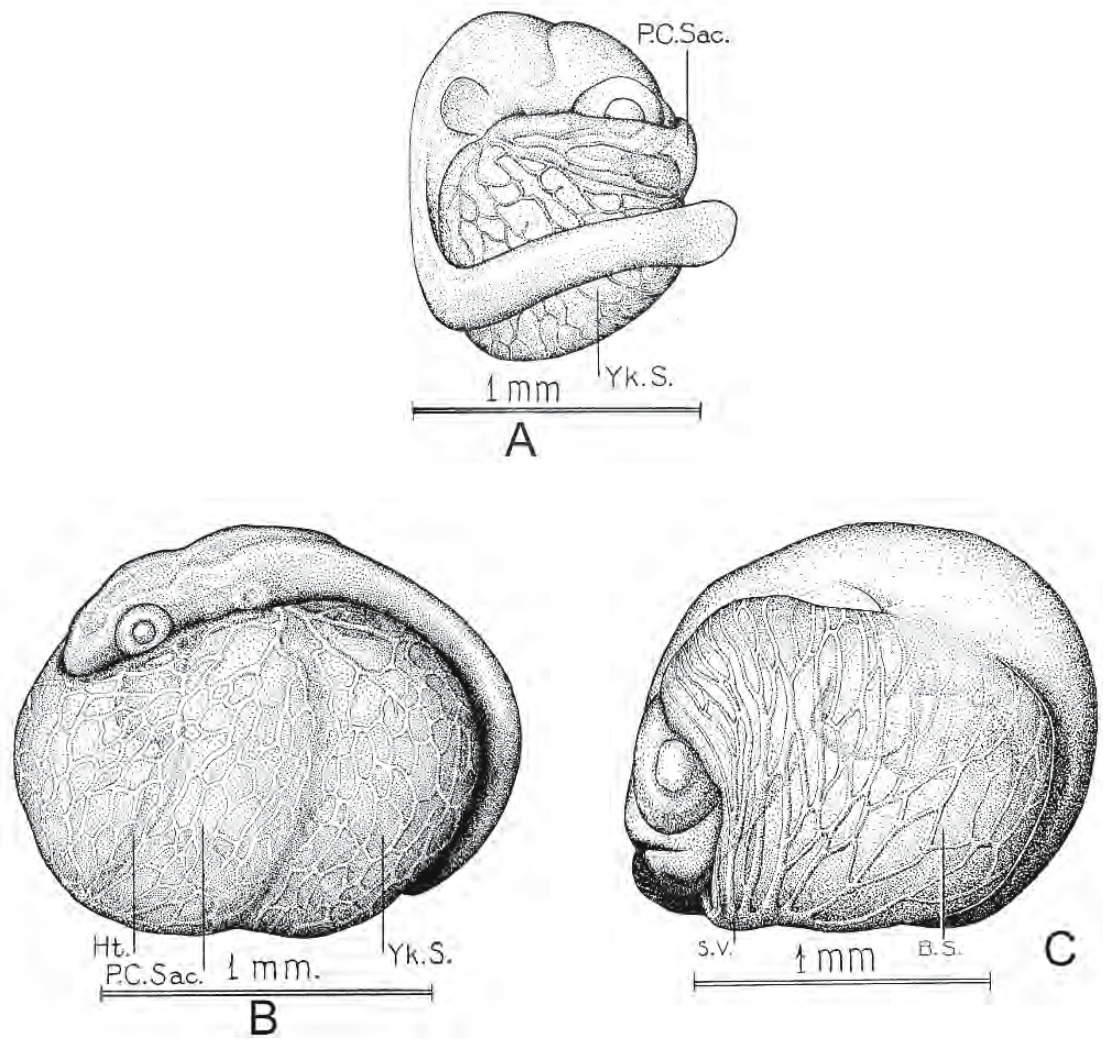

Figure 6.89: The yolk sac, pericardial sac, and coelomic sac play a major role in the uptake of nutrients in several species. (From Turner, 1940a,c; © reproduced with permission of John Wiley & Sons, Inc.).

A. In this drawing of an early stage of the goodeid *Ataenobius toweri*, the pericardial sac and yolk sac are covered by a portal vascular network.

B. This early stage of the goodeid *Goodea luitpoldii* illustrates the portal network in a relatively small yolk sac and an expanded pericardial sac.

C. The yolk sac has been almost completely absorbed in this embryo of the poeciliid *Poeciliopsis* sp. The "belly sac" is covered by a portal network and consists of the pericardial sac anteriorly and an expanded coelom posteriorly.

Abbreviations: BS, "belly sac"; HT, heart; P.C.Sac, pericardial sac; SV, sinus venosus; Yk.S., yolk sac.

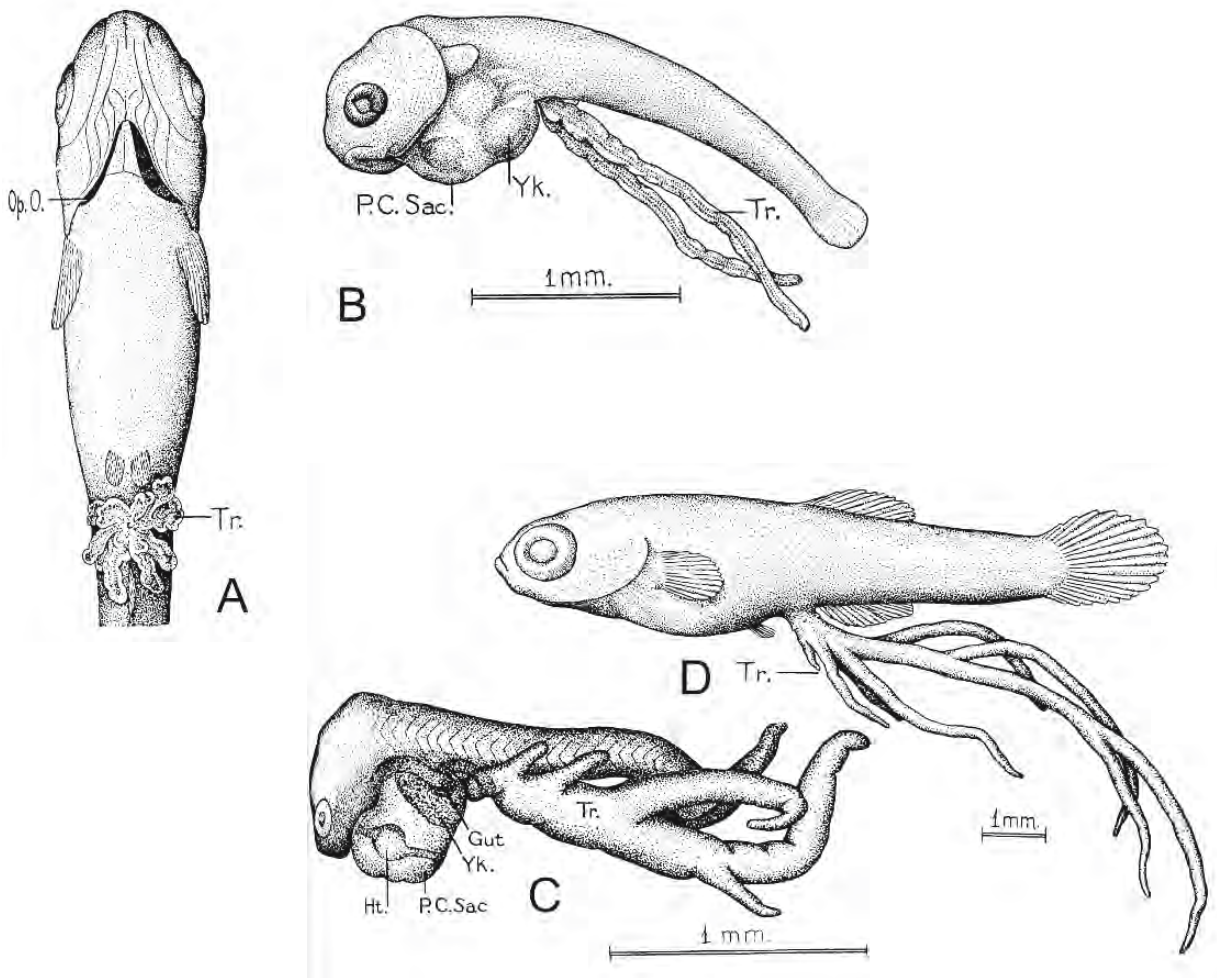

Figure 6.90: In a few teleosts, finger-shaped or ribbon-like extensions of the proctodaeum, the trophotaeniae, take up materials from the embryotroph; these drawings illustrate trophotaeniae in goodeids. (From Turner, 1940c; © reproduced with permission of John Wiley & Sons, Inc.).

A. Ventral view of an embryo of *Goodea luitpoldii* illustrating trophotaeniae clustered around the anal opening.

B. In this early embryo *Characodon lateralis*, the yolk sac is receding and the pericardial sac is at its maximal size. Trophotaeniae are growing rapidly and becoming vascularized. (The extensive portal network on the pericardial sac is not illustrated.).

C. The yolk is almost exhausted in this embryo of *Zoogoneticus quitzeoensis*. The vascular pericardial sac has begun to recede and is being replaced functionally by the rapidly developing trophotaeniae.

D. An embryo of *Zoogoneticus quitzeoensis* in late gestation. The trophotaeniae are highly vascular and serve for respiration and the absorption of nutrients.

Abbreviations: HT, heart; Op. O, opercular opening; P.C.Sac, pericardial sac; Tr, trophotaeniae; Yk, yolk.

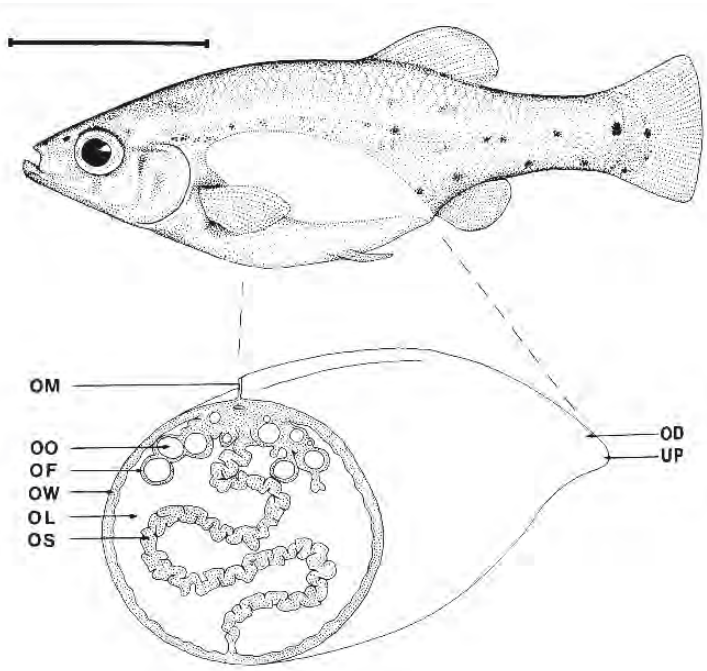

Figure 6.91: Schematic representation of an adult female of *Ameca splendens* illustrating the relative size and position of the ovary within the body cavity. Both the embryos and the anterior third of the ovary have been deleted to illustrate the internal ovarian anatomy. Bar = 2 cm (From Schindler and Wourms, 1985a; © reproduced with permission of John Wiley & Sons, Inc.).

Abbreviations: OD, oviduct; OF, ovarian fold; OL, ovarian lumen; OM, mesovarium; OO, oocyte; OS, ovarian septum; OW, ovarian wall; UP, urinogenital pore.

→

Figure 6.92: Transmission electron micrographs of sections of gravid ovaries of goodeids. (From Schindler, 1990; reproduced with permission).

A. Segments of the internal ovarian epithelium of *Xenotoca eiseni* cover opposite folds on the ovarian septum. Capillaries in a near-surface position are enclosed by attenuated cytoplasmic processes. The demarcation between the darker subepithelial zone and the multilocular core of the ovarian folds is marked by a series of arrowheads. X 7,360.

B. Three cells of the internal ovarian epithelium of *Xenotoca eiseni* are connected by apical junctional complexes and may be highly interdigitated. Bundles of intermediate filaments criss-cross the cytoplasm. Numerous electron-lucent vesicles and a few elements of the granular endoplasmic reticulum are distributed throughout the cytoplasm. X 24,300.

C. The flattened internal ovarian epithelium and the endothelium of a subjacent capillary in the ovary of *Girardinichthys viviparus* exhibit endocytotic or exocytotic activity (arrows). X 36,000.

Inset: The luminal surface of the internal ovarian epithelium shows a coated pit (arrow) and two small uncoated invaginations (arrowheads). The cytoplasm contains an inclusion of lipoid material. X 32,000.

Abbreviations: E, erythrocyte; En, endothelium; C, capillary; IOE, internal ovarian epithelium; OL, ovarian lumen.

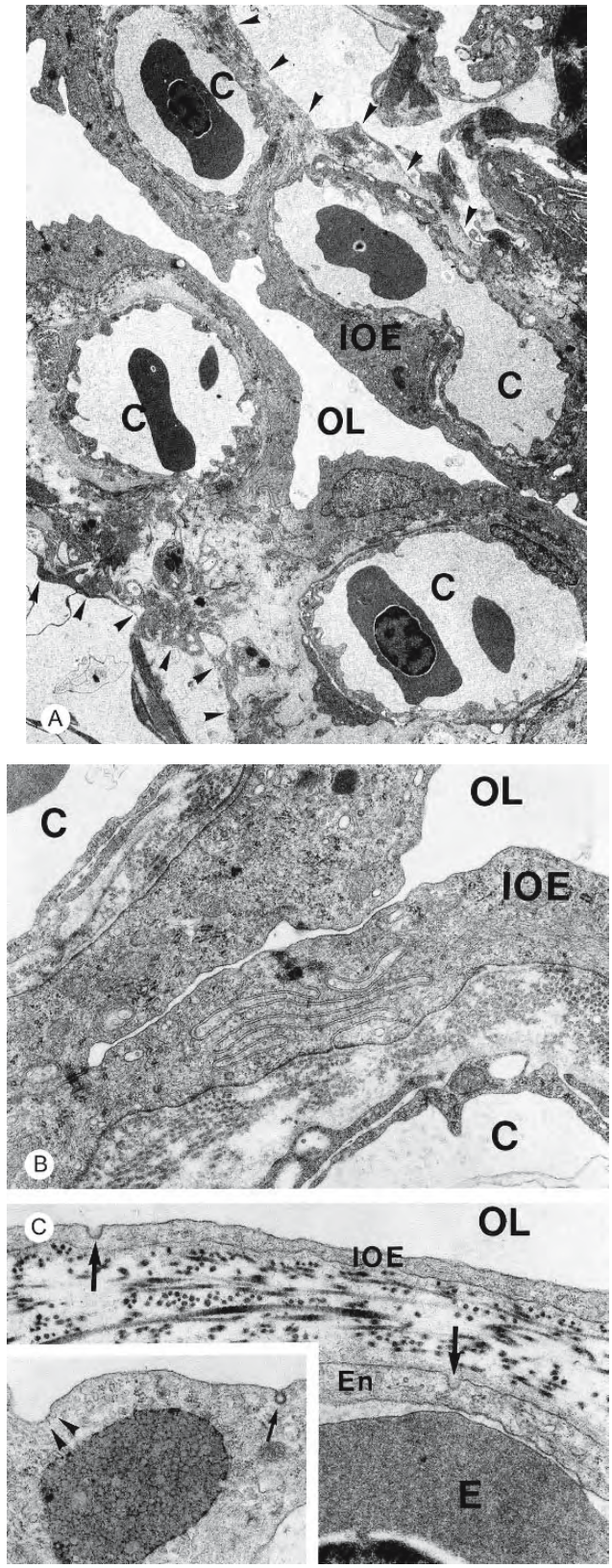

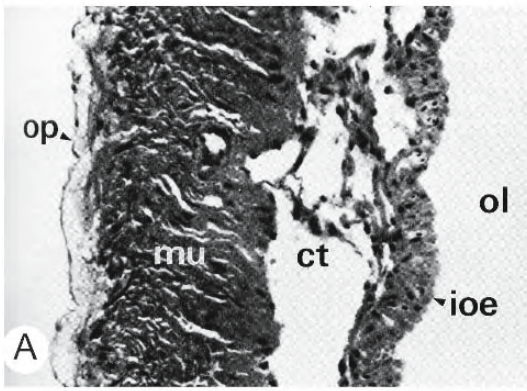

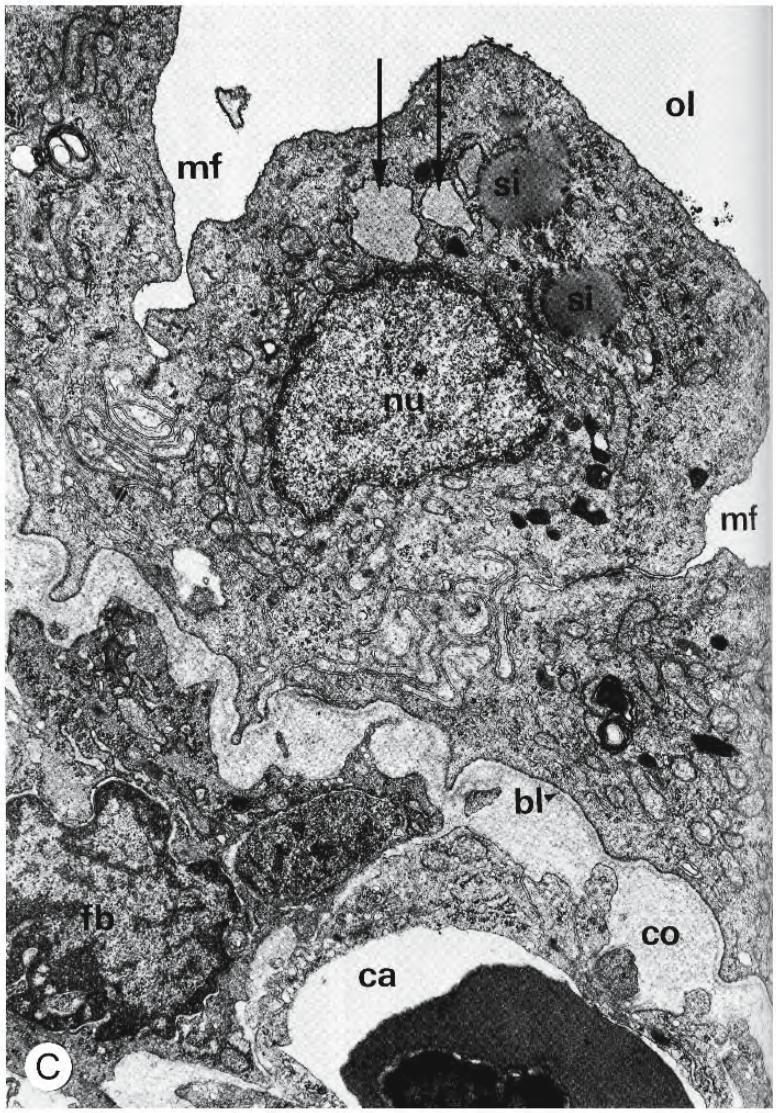

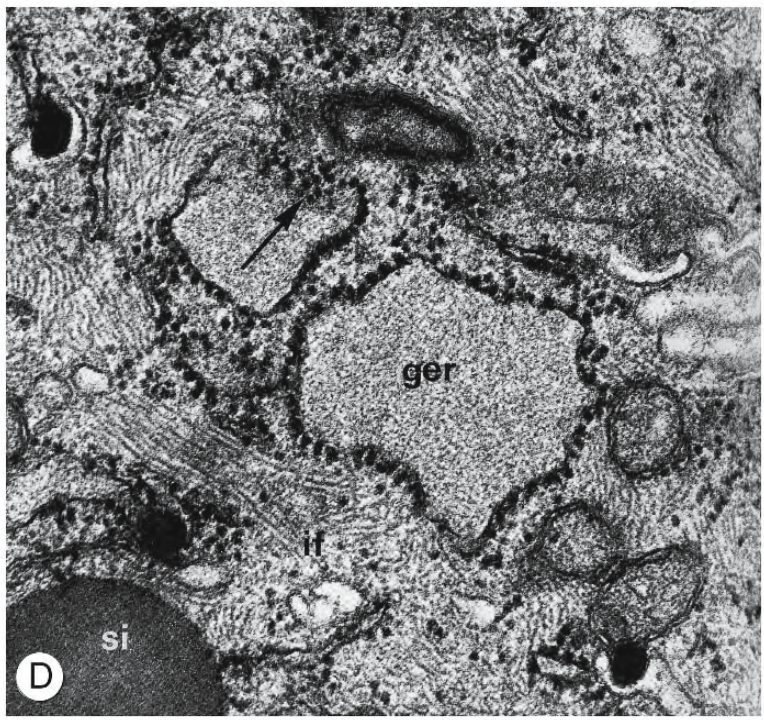

←——

Figure 6.93: Micrographs of sections of the near-term ovary of the goodeid *Ameca splendens.* (From Lombardi and Wourms, 1985a; © reproduced with permission of John Wiley & Sons, Inc.).

A. Photomicrograph of a longitudinal section through the ovarian wall. It is composed of four layers: the ovarian peritoneum (op), a muscular layer (mu) of outer longitudinal and inner circular muscle fibres, connective tissue stroma (ct), and the internal ovarian epithelium (ioe). ol, ovarian lumen X 100.

B. Scanning electron micrograph of the internal ovarian epithelium (ioe) that lines the ovarian lumen. The epithelium is thrown into a series of irregular folds; marginal clefts (arrows) delineate individual cells. X 150.

C. In this transmission electron micrograph, the internal ovarian epithelium is separated by a thin, moderately folded basal lamina (bl) from a connective tissue stroma containing a capillary (ca), collagenous fibres (co), and fibroblasts (fb). The lateral surfaces of the epithelial cell are interdigitated and sealed apically by junctional complexes. The cytoplasm of the epithelial cell contains large vesicles (arrows) derived from the granular endoplasmic reticulum. mf, marginal furrow; nu, nucleus; ol, ovarian lumen X 10,000.

D. Transmission electron micrograph of an internal ovarian epithelial cell containing vesicles that are studded with ribosomes (arrow). These vesicles are enlarged cisternae of the granular endoplasmic reticulum (ger) and have a moderately electron-dense granular matrix. Intermediate filaments are present in the surrounding cytoplasm. X 82,000.

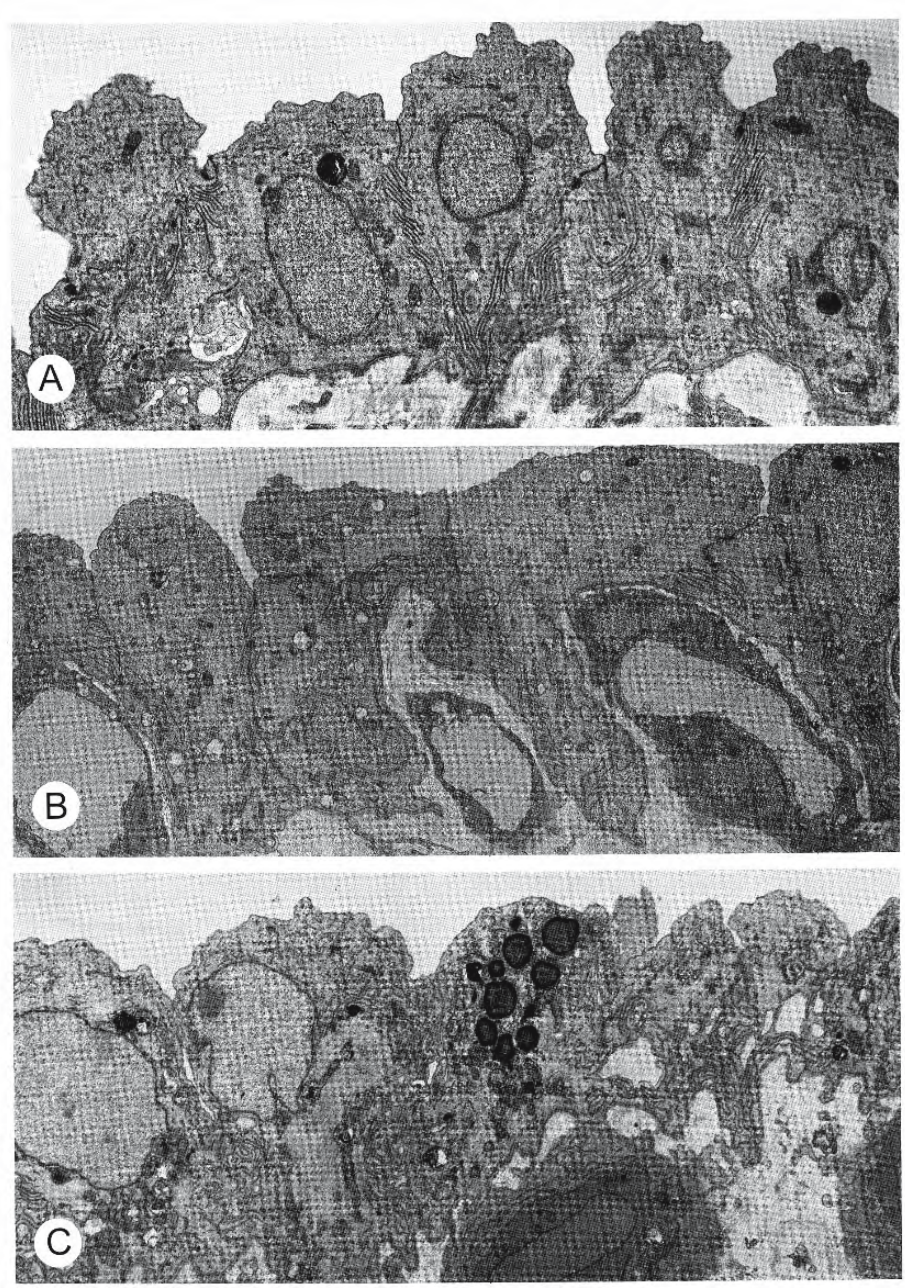

Figure 6.94: Transmission electron micrographs of representative sections of the internal ovarian epithelium from gravid females of three species of goodeid fish. All are simple epithelia with highly interdigitated lateral cell membranes. The domed epithelial cells are reminiscent of a transitional epithelium. All epithelia are well vascularized. (From Hollenberg and Wourms, 1995; © reproduced with permission of John Wiley & Sons, Inc.).

A. *Alloophorus robustus*. Note the apparent cytoplasmic budding from the apical region of the cell at the far left. X 4,800.

B. *Zoogoneticus quitzeoensis*. X 3,800.

C. *Goodea atripinnis*. Note the lipid accumulation in the centre cell. Dark annuli in the lipid droplets are the result of ferrocyanide postfixation. X 10,050.

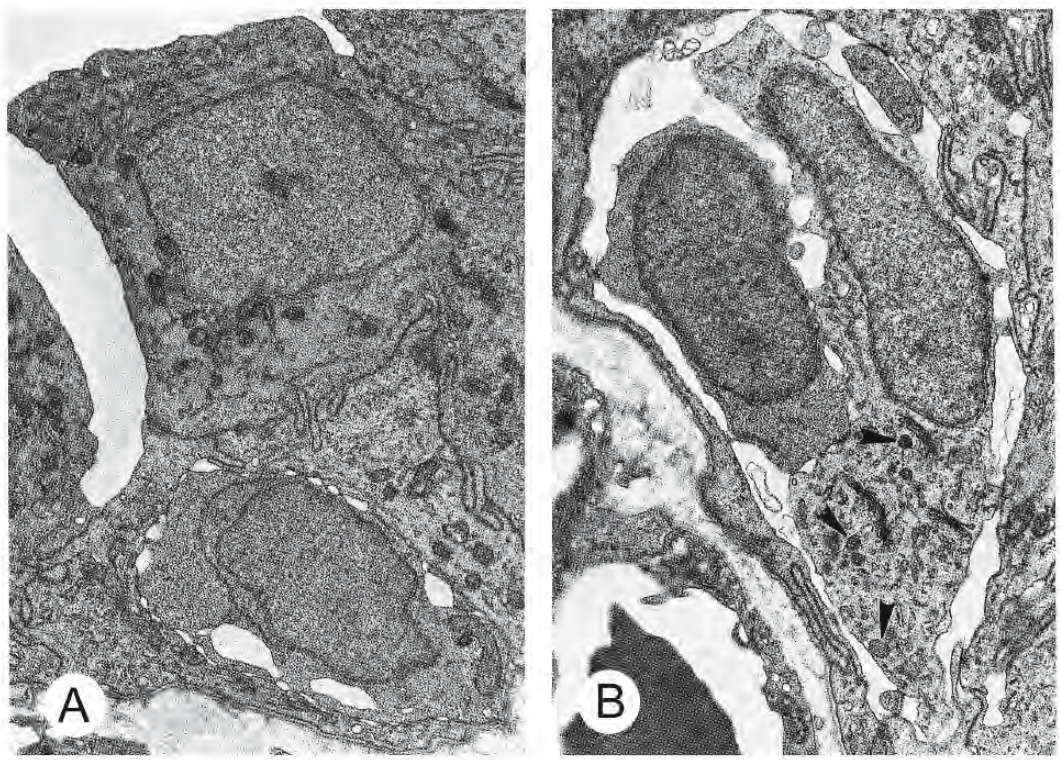

Figure 6.95: Transmission electron micrographs of the internal ovarian epithelium from a gravid female goodeid *Alloophorus robustus.* Intercellular spaces are often occupied by cells that are probably leucocytes. (From Hollenberg and Wourms, 1995; © reproduced with permission of John Wiley & Sons, Inc.).

A. X 8,400.

B. There are multiple Golgi complexes and small granules (arrowheads) in the cell on the right. X 8,700.

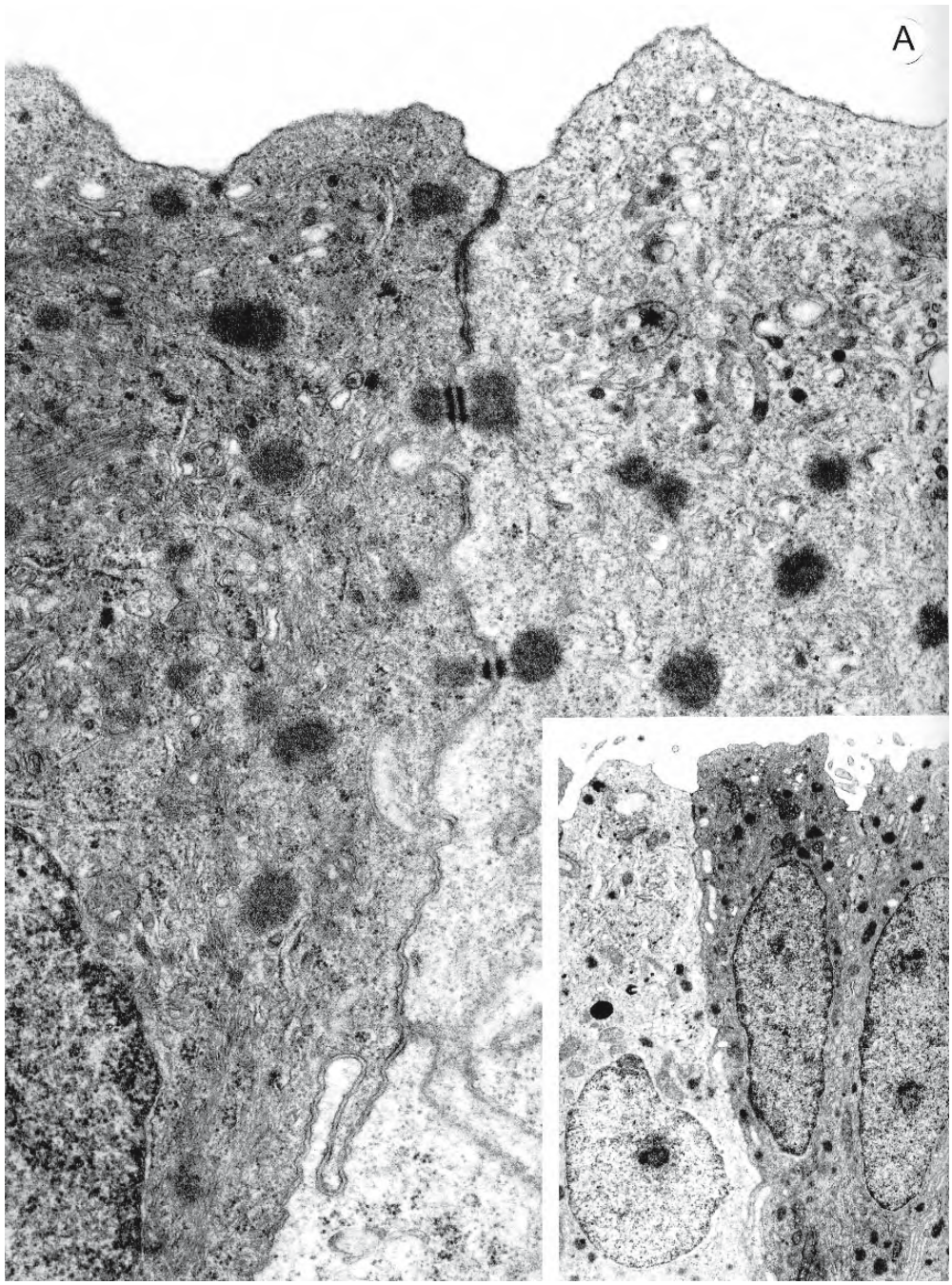

Figure 6.96: Transmission electron micrographs of internal ovarian epithelial cells in sections of the ovary of the goodeid teleost *Xenoophorus captivus.* (From Schindler, Kujat, and de Vries, 1988; reproduced with permission of the authors).

A. In a non-gravid ovary, the epithelial cells are cuboidal to columnar (inset) and are either compact and dark or oedematous and light. Apical tight junctions and large desmosomes of the junctional complexes are seen. Bundles of intermediate filaments criss-cross the cells, apparently converging on the desmosomal plaques. The cytoplasm contains conspicuous dense bodies without membranous demarcation. X 31,800.
Inset: X 7,890.

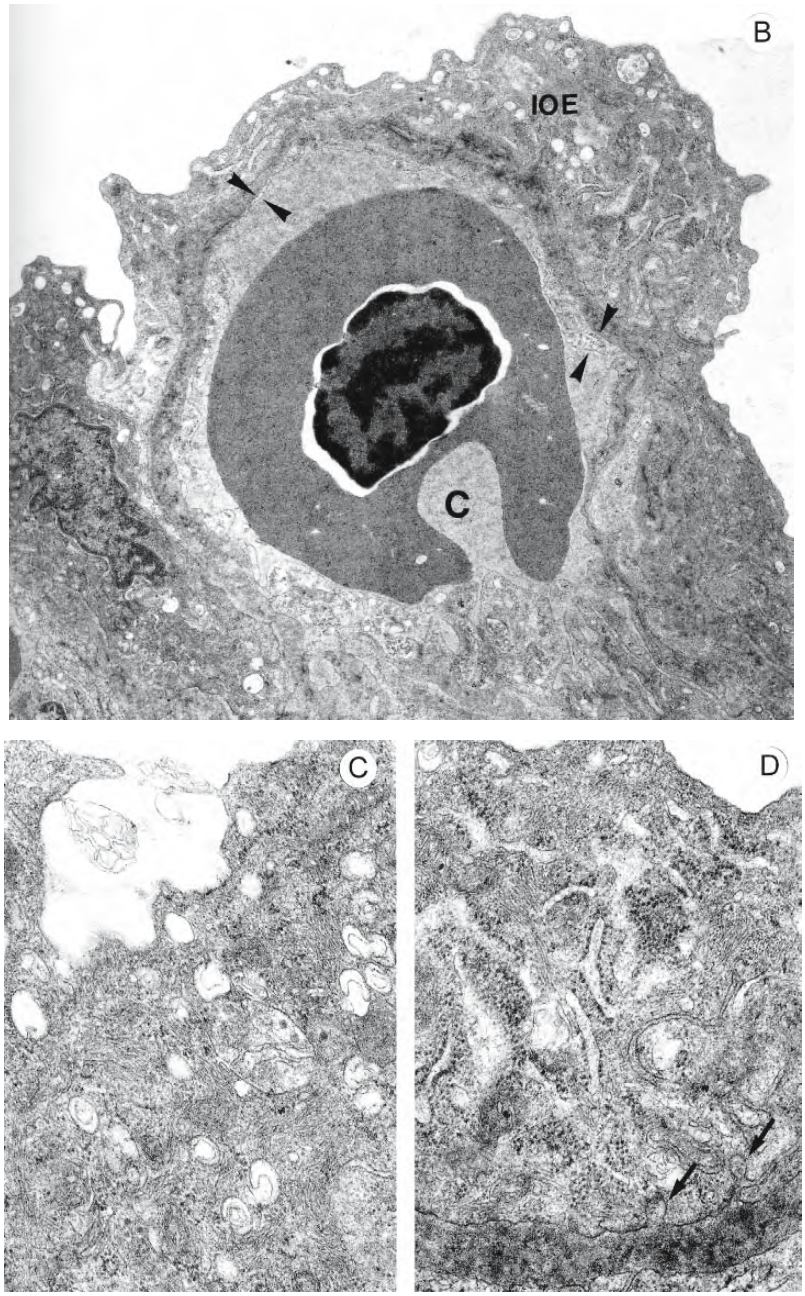

Figure 6.96: Continued.

B. The internal ovarian epithelium (IOE) of a gravid ovary becomes stretched due to swelling of the connective tissue thereby causing protrusion of capillaries (C) whose endothelium is shown between the arrowheads. Large numbers of vesicles and vacuoles are scattered throughout the cytoplasm of the epithelial cell. X 17,200.

C. The cytoplasm of an internal ovarian epithelial cell from a gravid ovary contains many invaginated vacuoles. Bundles of intermediate filaments criss-cross the cell. Bleb-like protrusions bud off from the luminal surface. X 41,000.

D. Several lamellae of granular endoplasmic reticulum are seen in the cytoplasm of this cell from the internal ovarian epithelium. Endocytotic activity is visible at the basal plasma membrane (arrows). The basal lamina is hardly distinguishable from the ground substance of the underlying connective tissue. X 45,000.

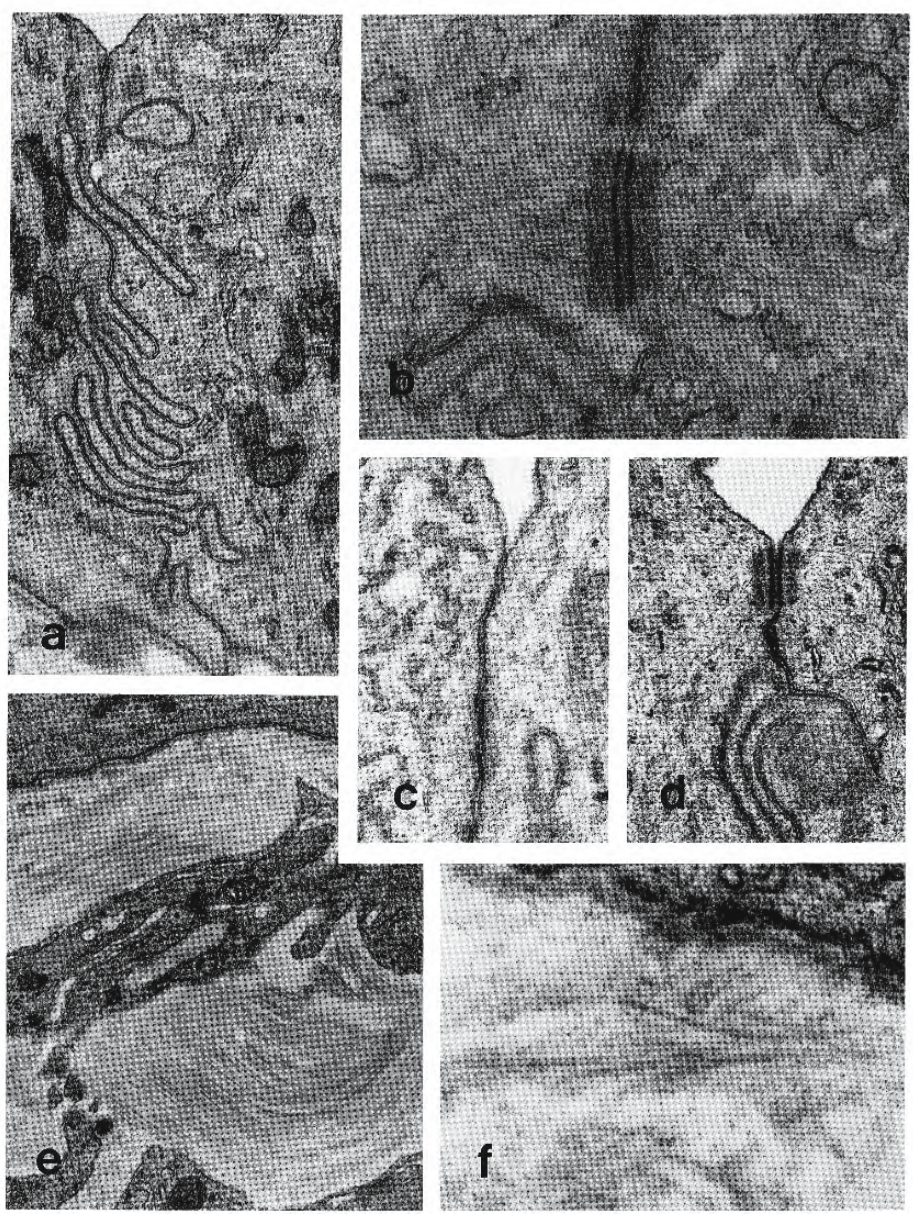

Figure 6.97: Transmission electron micrographs showing junctional and subepithelial features of the internal ovarian epithelium from gravid female goodeids. All are taken from *Alloophorus robustus* except **B** which is from *Zoogoneticus quitzeoensis.* (From Hollenberg and Wourms, 1995; © reproduced with permission of John Wiley & Sons, Inc.).

A. Highly interdigitated lateral cell membranes between adjacent cells. X 18,250

B. Desmosomes between cells are unusually prominent with thick attachment plaques on the cytoplasmic surfaces and bundles of intermediate filaments extending into the cytoplasm from the plaques. X 45,000.

C. Apical tight junctions are sometimes absent between cells. Lateral membranes maintain a constant distance from one another without fusion of the outer leaflets. X 39,000.

D. Desmosome immediately adjacent to the ovarian lumen. X 28,600.

E. Collagen bundles and a fibroblast in the subepithelial space. X 10,400.

F. Collagen fibres exhibiting their characteristic periodicity. X 46,650.

Figure 6.98: Transmission electron micrograph of bundles of tonofilaments (intermediate filaments) in a section of basal cytoplasm from a cell of the internal ovarian epithelium of a gravid female goodeid teleost *Goodea atripinnis.* Tonofilaments permeate the cytoplasm at all levels and in all orientations. X 47,150 (From Hollenberg and Wourms, 1995; © reproduced with permission of John Wiley & Sons, Inc.).

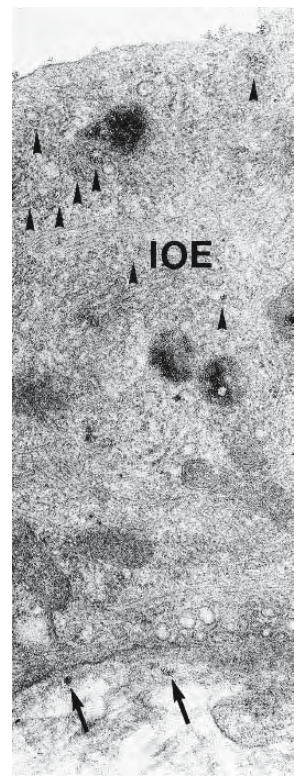

Figure 6.99: Transmission electron micrograph of a section of an internal ovarian epithelial cell of the goodeid *Xenotoca eiseni* after intraovarian exposure to cationized ferritin for six hours. Labelling of the apical surface occurs only at intervals. Intracellular localization of the tracer is most dense in large, somewhat multivesiculated vacuoles of the lysosomal apparatus. Some tracer is sequestered in relatively electron-lucent vesicles (arrowheads). Clusters of ferritin molecules are passing the basal lamina (arrows). X 54,000 (From Schindler, 1990; reproduced with permission).

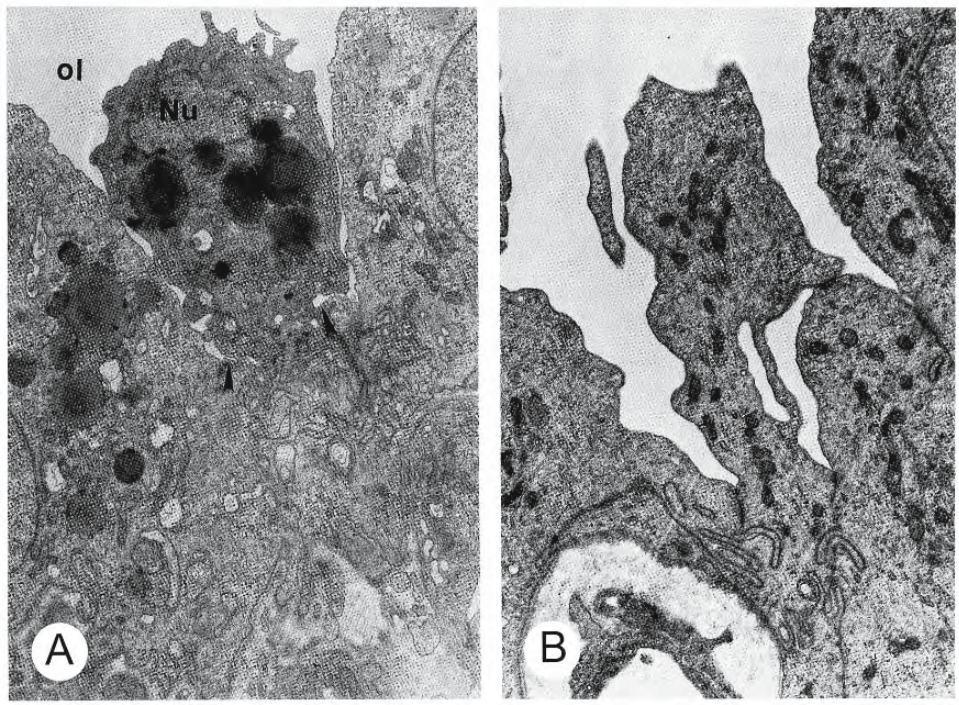

Figure 6.100: Transmission electron micrographs of possible apocrine secretion in internal ovarian epithelial cells of two species of gravid goodeids. (From Hollenberg and Wourms, 1995; © reproduced with permission of John Wiley & Sons, Inc.).

A. The apical portion of an epithelial cell from *Goodea atripinnis* contains lipid droplets and a nucleus (Nu). A large bleb appears to be about to pinch off from the rest of the cell (arrowheads) to be released into the ovarian lumen (ol). X 8,850.

B. A long, narrow cytoplasmic extension from an epithelial cell of *Zoogoneticus quitzeoensis* projects into the ovarian lumen. The cell junctions on the left and right lateral membranes are unusually close to one another suggesting that the extended cytoplasm may soon be sloughed. X 7,850.

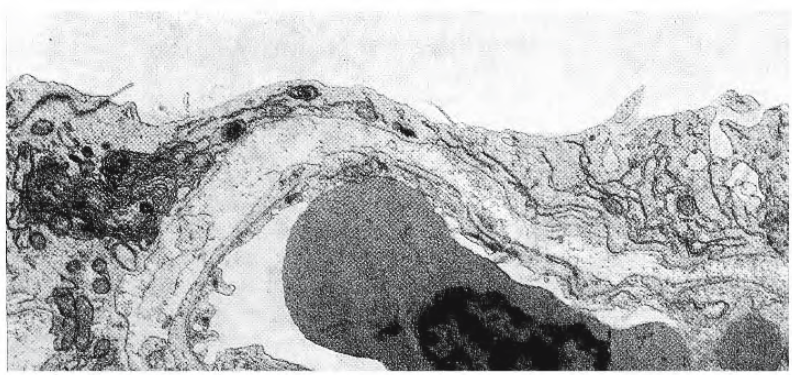

Figure 6.101: Transmission electron micrograph of a section of the internal ovarian epithelium of a gravid goodeid *Skiffia bilineata.* The epithelium overlying a capillary is attenuated. X 9,360 (From Schindler and Kujat, 1990; reproduced with permission).

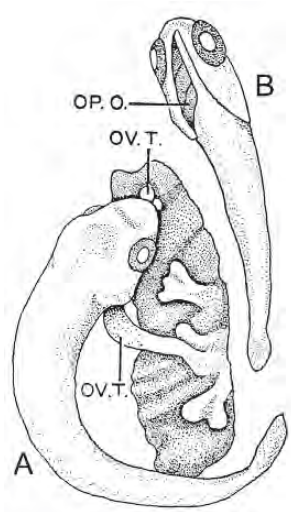

Figure 6.102: Drawings from the dissected gravid ovary of the jenynsiid *Jenynsia lineata* where embryos suckle on "nipples" formed from the luminal wall. Long, richly vascular, branching folds of the luminal wall form villi ovariales that grow into one opercular cleft of the embryo, establishing contact between maternal nutritive tissue and the embryonic digestive tract. (From Turner 1940d; © reproduced with permission of John Wiley & Sons, Inc.).

A. An embryo in late gestation attached to a villus ovarialis. The ovarian tissue extends through the opercular opening into the pharyngeal cavity and a small portion protrudes from the mouth.

B. An embryo in late gestation to illustrate an open opercular cleft.

Abbreviations: OP.O, opercular opening; OV.T, ovarian tissue.

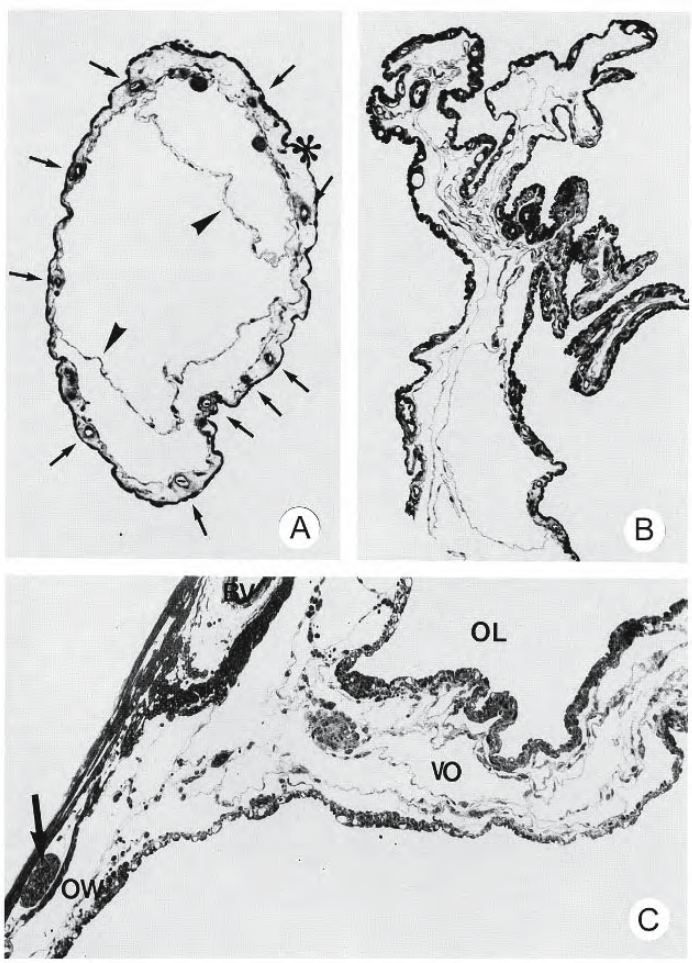

Figure 6.103: Photomicrographs of semithin sections of villi ovariales from the jenynsiid *Jenynsia lineata.* (From Schindler and de Vries, 1988b; © reproduced with permission of John Wiley & Sons, Inc.).

A. Cross section at the tip of a villus. Two intravillous septa (arrowheads) subdivide the core of the villus into loculi. The flat intraovarian epithelium (*) is underlain by a narrow band of connective tissue carrying capillaries (arrows). X 216.

B. An oblique section of a villus ovarialis. X 169.

C. A villus ovarialis (VO) extends from the ovarian wall (OW) into the ovarian lumen (OL). The ovarian wall contains a blood vessel (BV) and a nerve (arrow); loculi permeate the loose connective tissue of the villus. X 198.

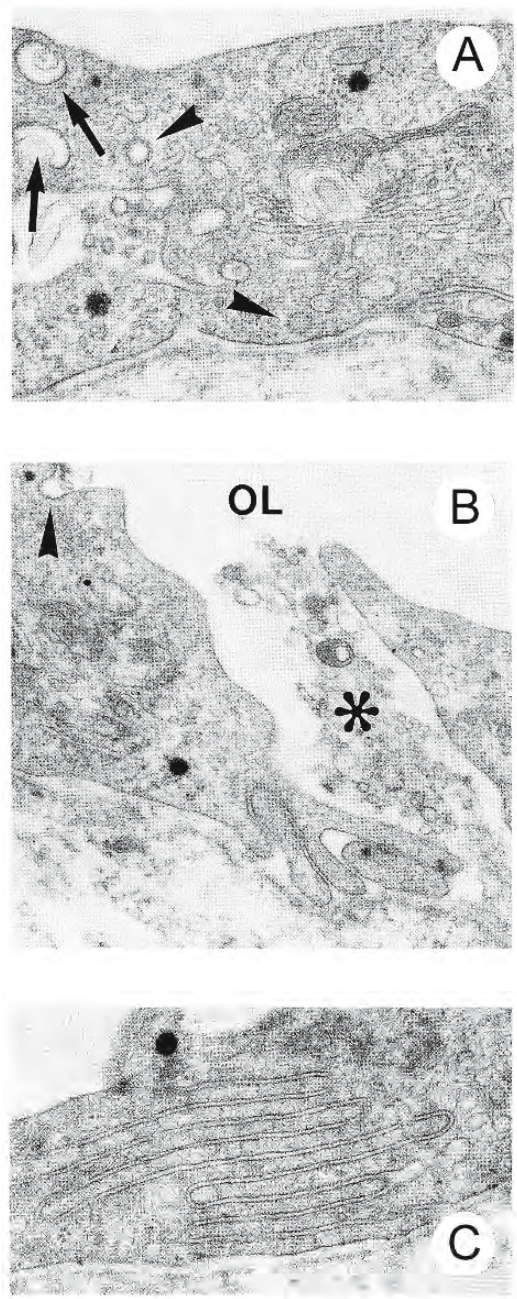

Figure 6.104: Transmission electron micrographs of epithelial cells on villi ovariales from the jenynsiid *Jenynsia lineata.* (From Schindler and de Vries, 1988b; © reproduced with permission of John Wiley & Sons, Inc.).

A. Endocytotic activity is indicated by numerous elements of a vacuolar complex including coated vesicles (arrowheads), cup-shaped vacuoles (arrows), and a Golgi complex. X 34,800.

B. The gap between intraovarian epithelial cells allows transepithelial passage of coarse material (*). Endocytotic activity (arrowhead) is evident at the surface of the ovarian lumen (OL). X 26,000.

C. Most adjacent cells of the intraovarian epithelium interdigitate. X 29,800.

Figure 6.105: Photographs of late term embryos of various species of goodeid fishes. Ribbon and rosette trophotaeniae extend from perianal lips. *Top*: *Alloophorus robustus; middle left*, *Zoogoneticus quitzeoensis* (the smallest goodeid species); *bottom left*: *Goodea atripinnis; bottom right; Ilyodon furcidens.* X 4 (From Hollenberg and Wourms, 1994; © reproduced with permission of John Wiley & Sons, Inc.).

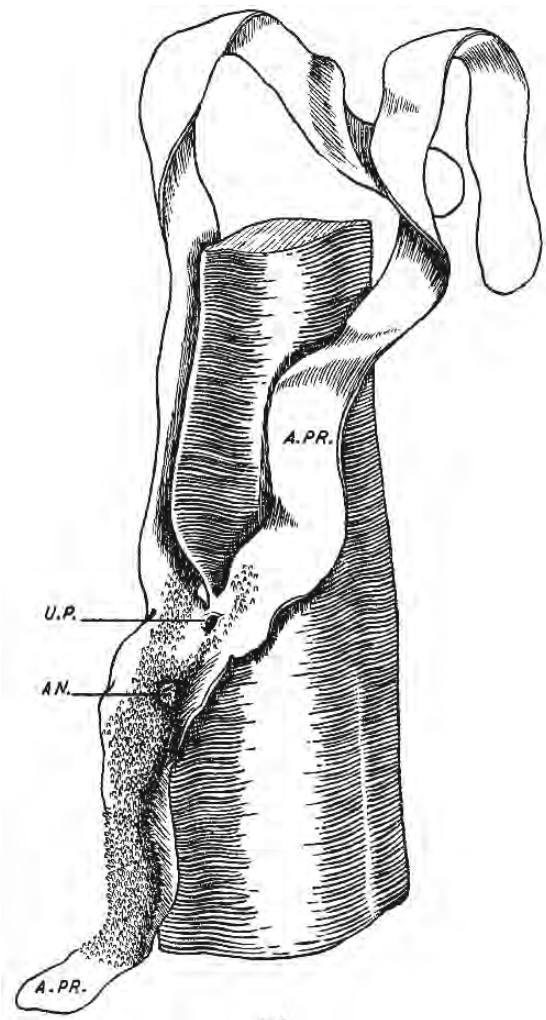

Figure 6.106: Drawing of a reconstruction of the absorptive processes and adjacent parts of an embryo of a zoarcid fish *Parabrotula dentiens.* X 150 (From Turner, 1936; © reproduced with permission of John Wiley & Sons, Inc.) *Abbreviations*: AN, anus; A.PR, absorptive processes; U.P, urinary pore.

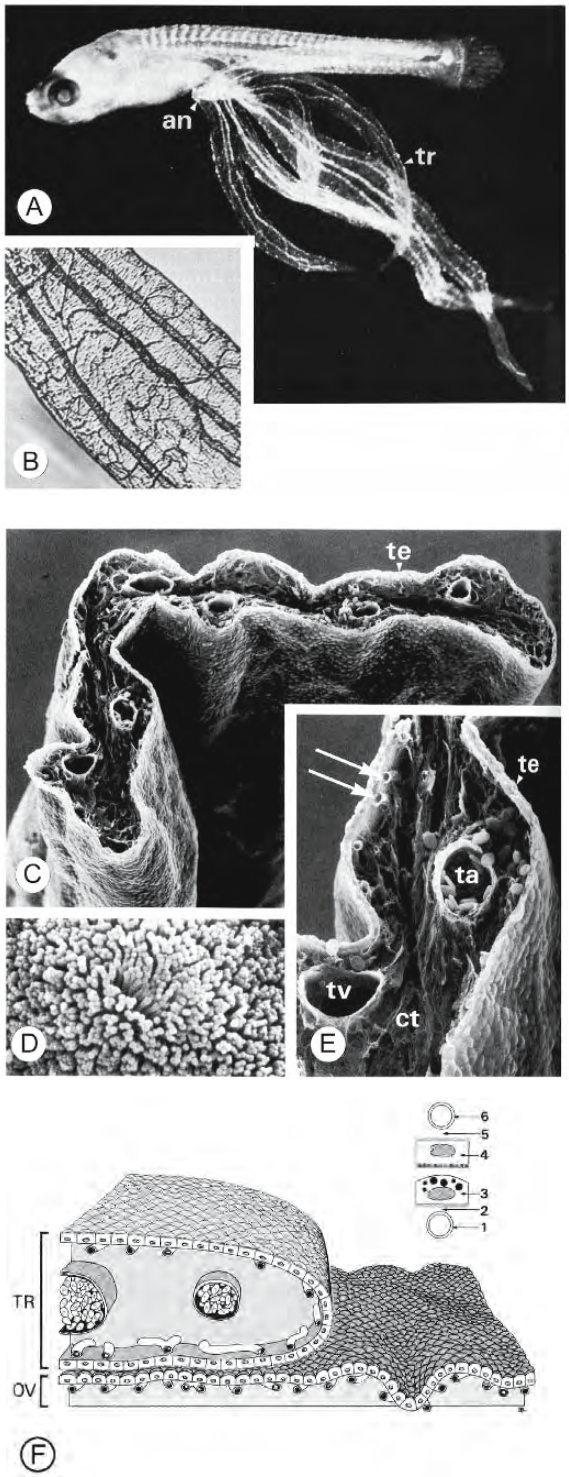

Figure 6.107: Depictions of trophotaeniae in the goodeid *Ameca splendens.* (From Lombardi and Wourms, 1985b; © reproduced with permission of John Wiley & Sons, Inc.).

A. Photomicrograph of a whole mount of a midterm embryo showing well developed, highly vascularized trophotaeniae (tr) extending from the anal region (an). X 10.

B. Photomicrograph of a glycerinated preparation of a trophotaenial ribbon from a midterm embryo. Elements of the vascular supply are visible within the connective tissue core: large vessels are oriented parallel to the trophotaenial axis while capillaries form a vascular bed beneath the outer epithelium. X 50.

C. Scanning electron micrograph of a cryofractured preparation revealing the internal structure of the caudal trophotaenial ribbon. Numerous blood vessels lie within the connective tissue core. te, trophotaenial epithelium X 100.

D. Scanning electron micrograph of the apical surface of a typical cell in the trophotaenial epithelium. Cells possess a dense mat of apical microvilli. X 6,000.

E. Detail of the preparation in Figure C. Peripheral capillaries (arrows) lie beneath the surface epithelium (te). Trophotaenial arteries (ta) and veins (tv) are embedded within the connective tissue core. Fibroblasts and a fibrous extracellular matrix are present within the connective tissue core (ct). X 250.

F. Schematic representation of tissue organization in the trophotaenial placenta. Some regions of the trophotaenial ribbons, seen here in cross section (TR), lie in direct apposition to the internal ovarian epithelium (OV) lining the ovarian lumen.

The six barriers to the transfer of materials from maternal to the embryonic bloodstream are shown in the upper right: (1) endothelial lining of capillaries within the ovarian connective tissue stroma; (2) ovarian connective tissue stroma; (3) internal ovarian epithelium; (4) trophotaenial epithelium; (5) trophotaenial connective tissue core; (6) endothelium of trophotaenial capillaries.

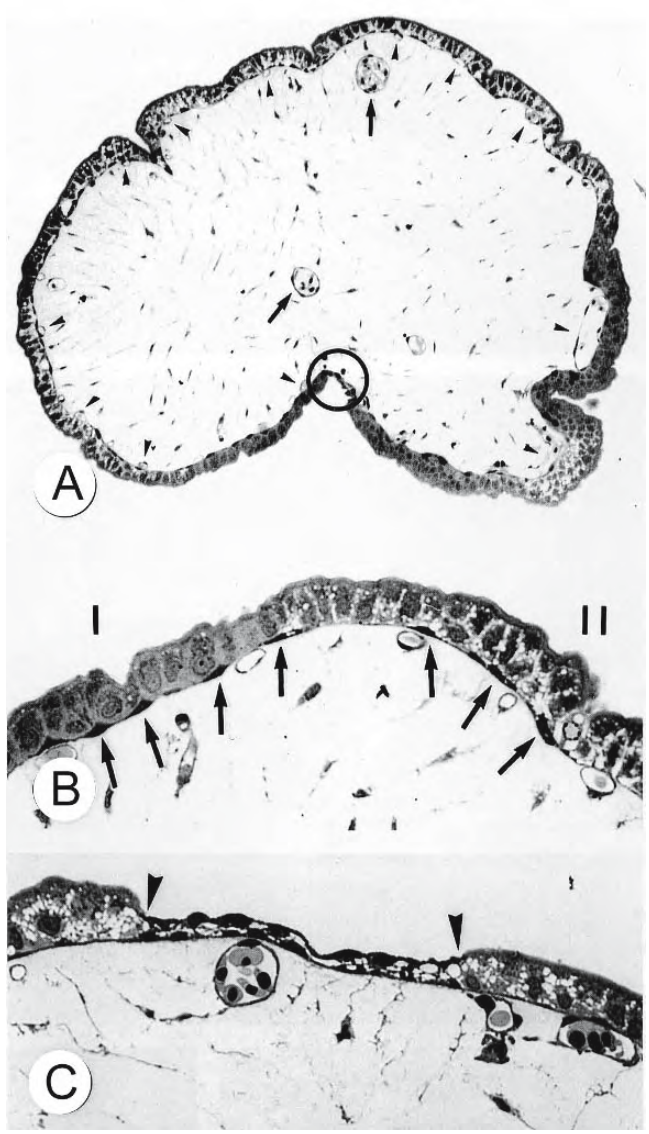

Figure 6.108: Photomicrographs of semithin sections of trophotaeniae of the goodeid *Xenoophorus captivus.* (From Schindler and de Vries, 1987b; reproduced with permission of the authors).

A. Kidney-shaped cross section of a trophotaenia. Its core consists of loose mesenchymal connective tissue containing thin-walled blood vessels (arrows) and a capillary plexus (arrowheads) beneath the epithelium. The circle indicates a small segment of stratified epithelium. X 220.

B. Trophotaenial epithelium showing closely apposed absorptive cells (I) and those isolated by large intercellular spaces (II). Densely stained basal cells (arrows) underlie most of the absorptive epithelium. X 400.

C. Segment of bilayered squamous epithelium (between arrowheads). Its level is slightly recessed below the surface of the bordering absorptive cells. X 440.

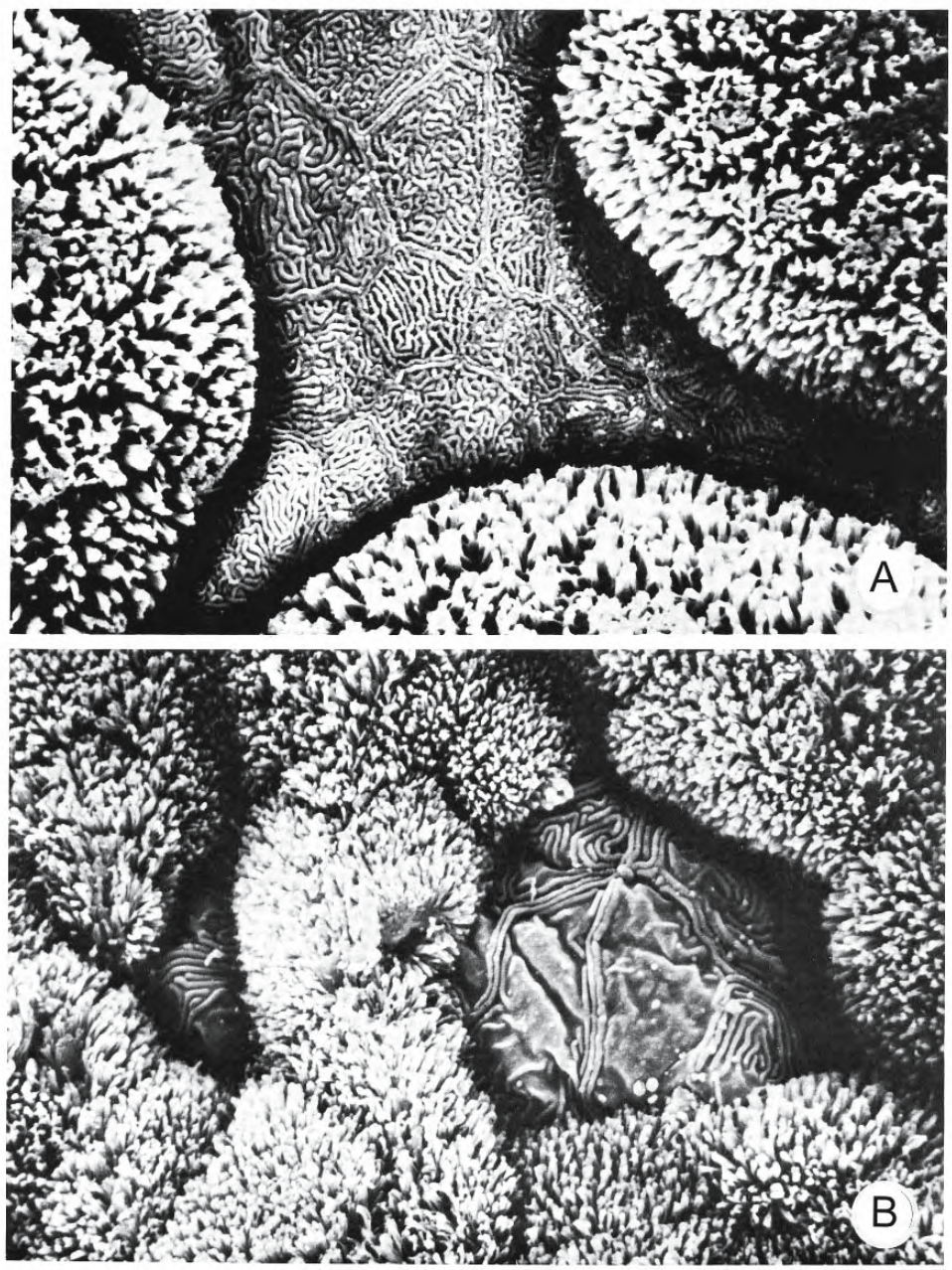

Figure 6.109: Scanning electron micrographs to illustrate the mosaic of absorptive cells and pavement cells on the surface of trophotaenia from near-term embryos of the goodeid *Girardinichthys viviparus.* (From Schindler and de Vries, 1986a; © reproduced with permission of John Wiley & Sons, Inc.).

A. The island of pavement cells at the centre is distinguished by the fingerprint pattern of microridges on the surface of individual cells whose boundaries are well defined. Forests of microvilli cover the surfaces of the surrounding absorptive cells. X 4,900.

B. Ridged pavement cells nestle singly and as clusters among the absorptive cells whose surface is studded with microvilli. X 4,900.

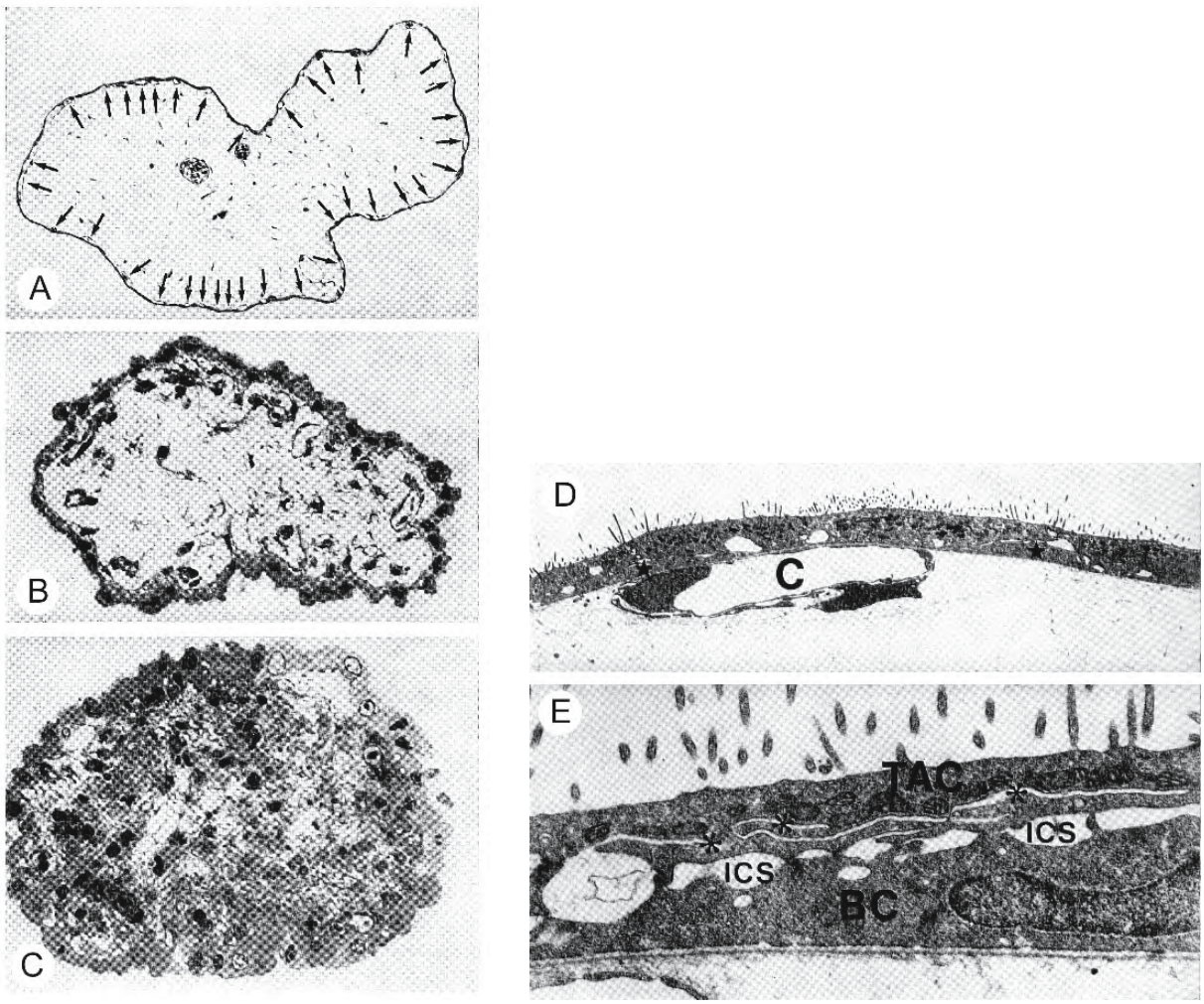

Figure 6.110: Micrographs of sections of trophotaeniae of the goodeid *Skiffia bilineata* to show the distribution of capillaries; **A** to **C** are photomicrographs, **D** and **E** are transmission electron micrographs. (From Schindler and Kujat, 1990; reproduced with permission).

A. Cross section through the middle of a trophotaenia. The core is filled with loose, mesenchymal connective tissue containing a few sinusoidal blood vessels. The external epithelium is thin and closely underlain by a capillary network (arrows). X 50.

B. Distal cross section of a trophotaenia. X 175.

C. The connective tissue core at the trophotaenial tip is relatively dense and contains several wandering cells. The external epithelium is composed of taller cells at this location. Many cells appear to be degenerating and sloughing off. X 200.

D. This segment of squamous external trophotaenial epithelium is underlain by a capillary (C). The monolayer of absorptive cells partly rests on flat basal cells (*). X 3,780.

E. Trophotaenial epithelium is composed of trophotaenial absorptive cells (TAC), with sparsely spaced microvilli, and underlying basal cells (BC) resting on the basement lamina. Deep channels (*) between the absorptive cells are open to the intercellular space (ICS). Basal cells lack invaginations of their membranes. X 30,500.

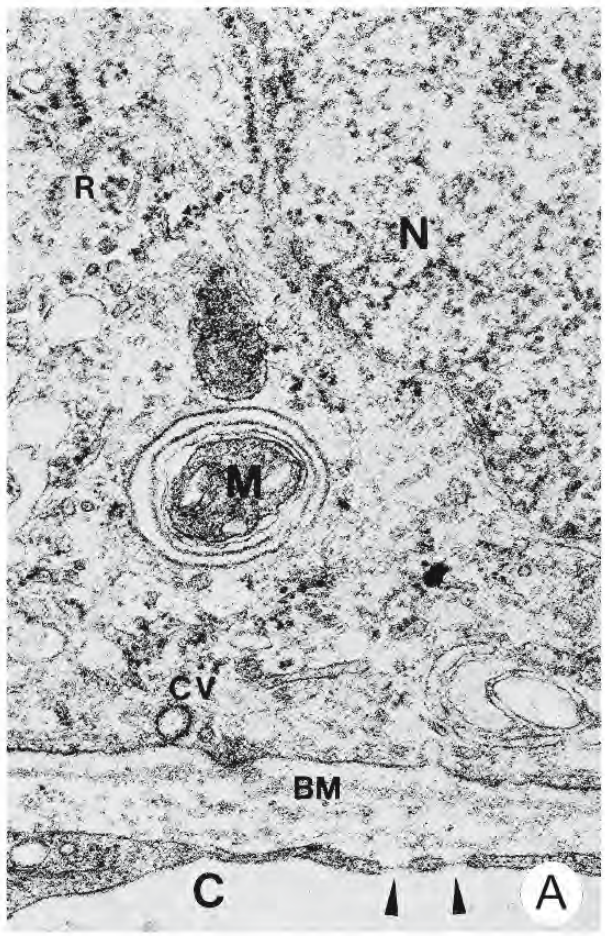

Figure 6.111: Transmission electron micrographs of sections through trophotaenial absorptive cells in a near-term embryo goodeid *Girardinichthys viviparus.* (From Schindler and de Vries, 1986a; © reproduced with permission of John Wiley & Sons, Inc.).

A. Micropinocytotic activity is evident in the basal region of an absorptive cell. The cell rests on a basal lamina (BM) and is underlain by a fenestrated (arrowheads) capillary (C). A coated vesicle (CV) is in contact with the basal plasmalemma. A mitochondrion (M) is encircled by an open bilayered membranous annulus. Free ribosomes (R) and the a portion of the nucleus (N) are shown. X 51,000.

B. Abundant mitochondria are packed in the apical cytoplasm of this absorptive cell, immediately beneath the brush border and a narrow band containing only small vesicles. The indented spherical nucleus (N) occupies the basal part of the cell. Adjacent cells are separated by bulges of the intercellular space (ICS). Membranous lamellae traverse the cytoplasm. Peripheral smooth membranes (arrowheads) resemble the plasmalemma rather than endoplasmic reticulum. X 15,600.

C. A stratified pavement epithelium forms irregular islands of ridged cells between the absorptive cells. This is a portion of a cell of the covering stratum of the multilayered epithelium. Below the peripheral fibrillar zone, the cytoplasm contains abundant, mostly agranular, slightly distended ergastoplasmic membranes elongated in parallel with the cell surface. Numerous small vesicles appear to be pinched off from the conspicuous Golgi complex (G). A slender cellular process bridges the expanded intercellular space (ICS) to the underlying stratum. X 9,770.

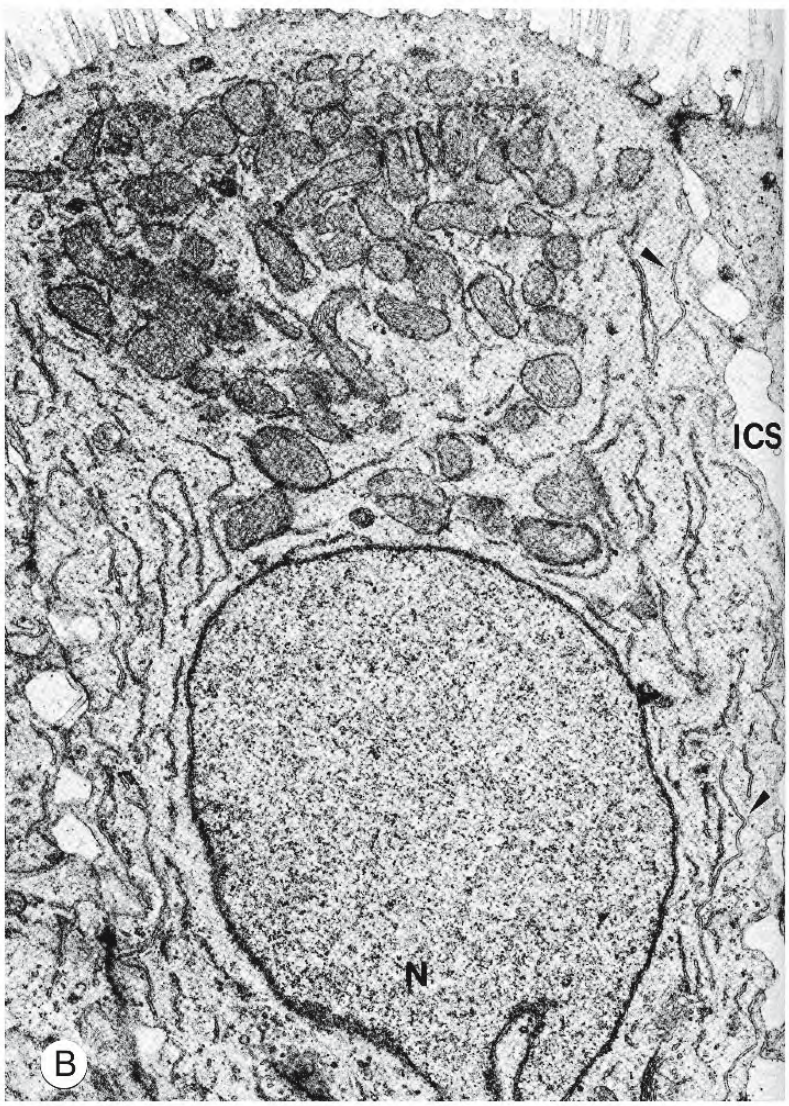

Figure 6.112: Transmission electron micrograph of a section through two types of trophotaenial epithelial cells from the goodeid *Xenoophorus captivus.* Basal cells have electron-dense cytoplasm and lie on the partly split basal lamina (arrows). The overlying absorptive cells show an apical microvillous border, apicolateral junctional complexes, and desmosomes between adjacent cells. A system of open lamellar membranes (arrowheads) parallels the lateral plasma membranes. The absorptive cells exhibit cytoplasmic zonation: *Zone I,* the endocytic apical zone comprises the exposed plasma membranes, including both the microvilli and the invaginations of the surface, vesicles, and vacuoles, and an osmiophilic tubular system; *Zone II,* the supranuclear zone is dominated by mitochondria and frequently by large electron-opaque bodies; *Zone III,* the nuclear zone usually has a Golgi complex (G) located basolateral to the nucleus; *Zone IV,* the basal zone, becomes increasingly devoid of organelles as gestation progresses and may be reduced to cytoplasmic processes penetrating the underlying basal cells. X 12,600 (From Schindler and de Vries, 1987b; reproduced with permission of the authors).

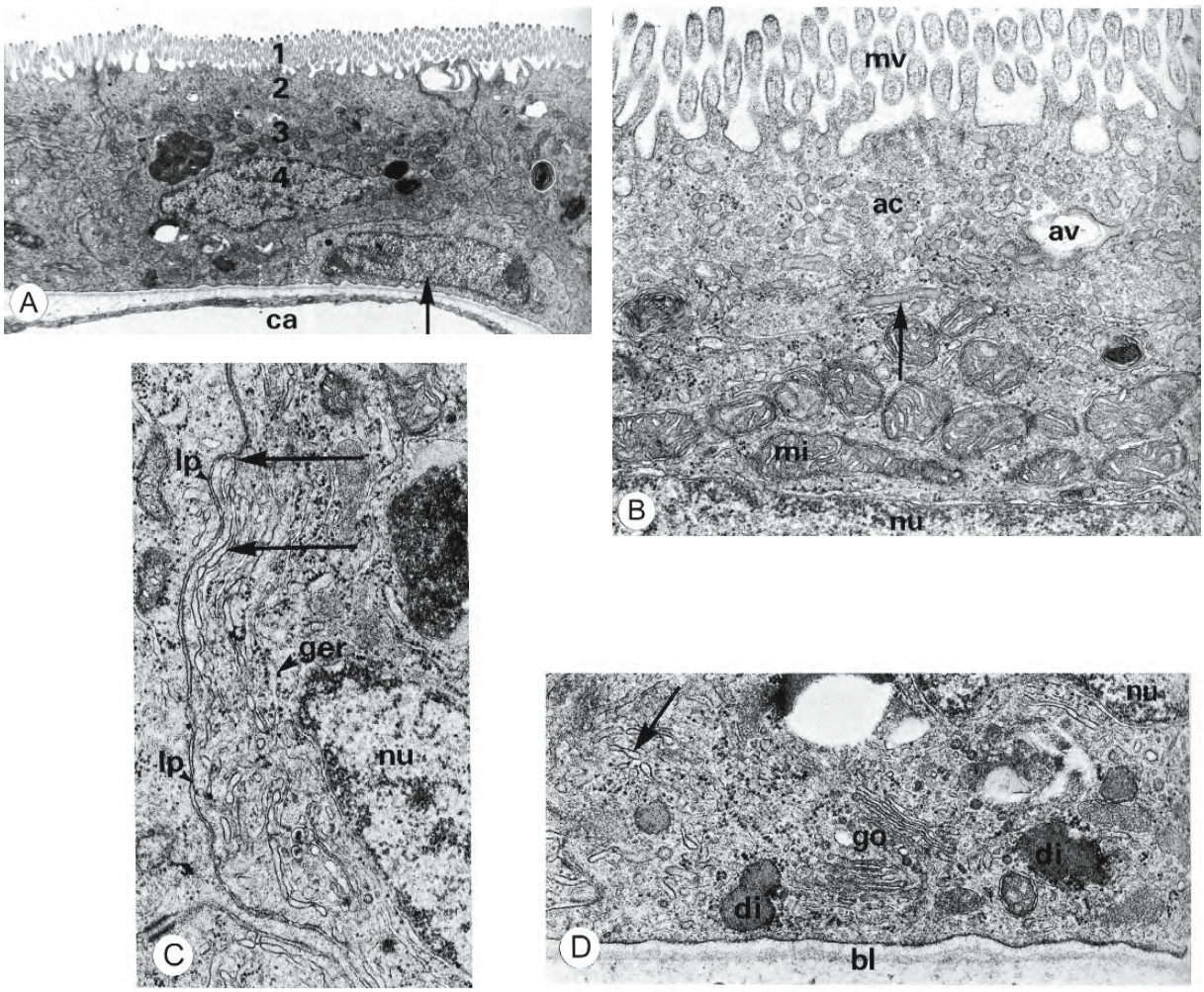

Figure 6.113: Transmission electron micrograph of sections through trophotaenial epithelial cells from the goodeid *Ameca splendens.* (From Lombardi and Wourms, 1985b; © reproduced with permission of John Wiley & Sons, Inc.).

A. An absorptive cell underlain by a squamous basal cell. Four areas of cytoplasmic zonation can be recognized in the absorptive cell: Zone 1, apical surface zone; Zone 2, apical cortical zone (endocytotic complex); Zone 3, supranuclear zone containing large membranous inclusions and mitochondria; and Zone 4, the nuclear-subnuclear zone. Agranular and granular endoplasmic reticulum occupies the paranuclear region. The Golgi complex lies in a lateral or basal position. The squamous basal cells possess electron-lucent cytoplasm (arrow). The epithelial cells are separated from a capillary (ca) by a delicate basal lamina. X 10,000.

B. Apical region of an absorptive cell. Microvilli (mv) extend from he convoluted cell surface. The outer leaflet of the plasmalemma is coated with a fine fibrillar material. The apical canalicular system (ac) contains tubular profiles (arrow) associated with collecting vesicles. Mitochondria (mi) of the supranuclear zone are numerous and situated adjacent to the nucleus (nu). av, apical vesicle X 20,000.

C. The lateral cytoplasm of adjacent absorptive cells contains the tubular cisternal complex (arrows) and elements of the granular endoplasmic reticulum (ger). lp, lateral plasmalemma; nu, nucleus X 30,000.

D. The subnuclear region of an absorptive cell contains numerous dense inclusions and a well developed Golgi complex (go). Invaginations of the lateral cell surfaces form elements of the tubular cisternal complex (arrow). The cells rest on a basal lamina (bl). di, dense inclusion X 30,000.

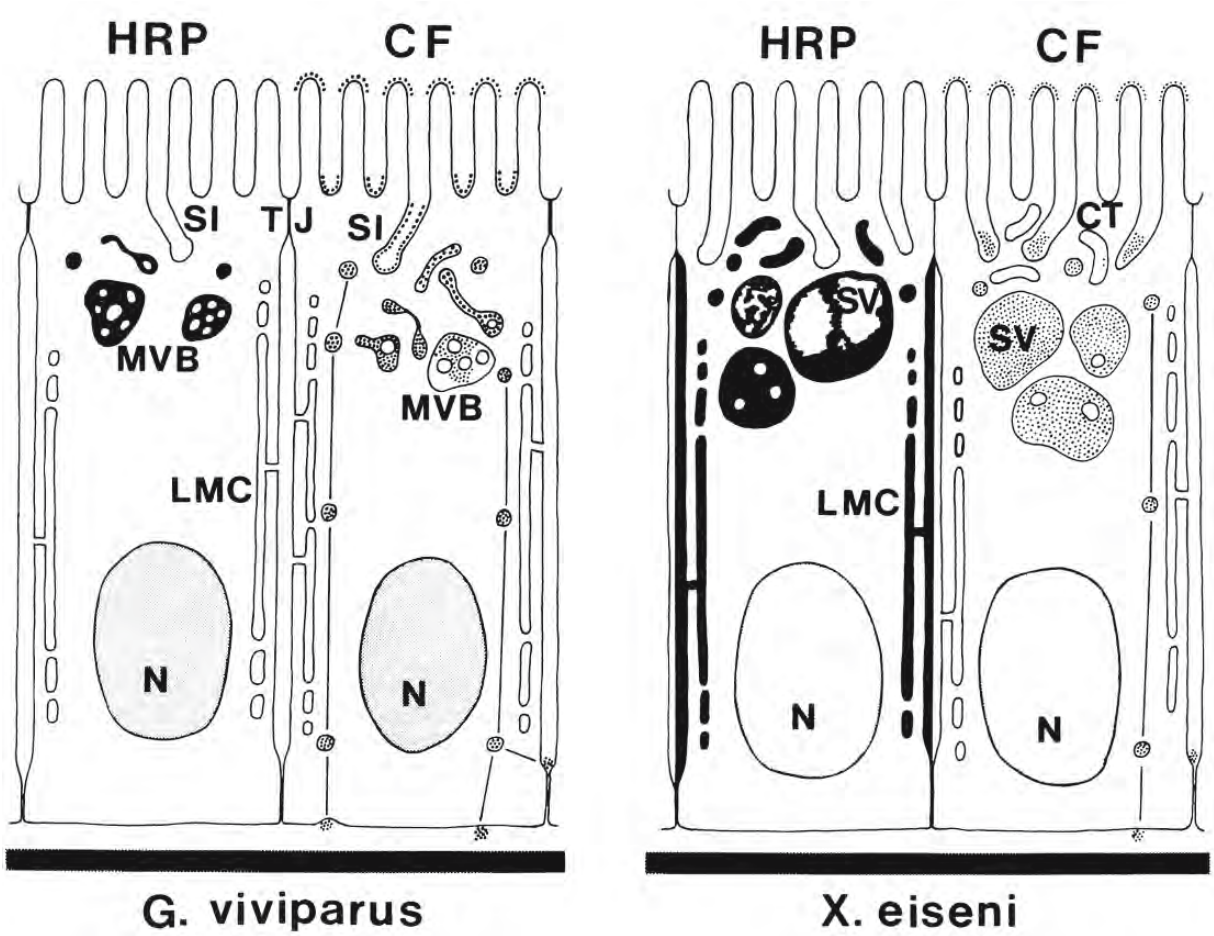

Figure 6.114: Diagrams to illustrate two morphologically distinct, species-specific lines of trophotaenial absorptive cells in the goodeids *Girardinichthys viviparus* and *Xenotoca eiseni* based on the presence or absence of a typical endocytotic apparatus and the uptake of cationized ferritin (CF) or horseradish peroxidase (HRP). Multivalent CF has an affinity for the tips of the microvilli and it adheres to the external plasmalemmal leaflet of the apical saccular membrane invaginations (SI) of the absorptive cells in *G. viviparus*. Internalized CF is accumulated in storage vacuoles (SV) or multivesicular bodies (MVB). Most of the endocytosed CF in *G. viviparus* but only some CF-containing vesicles in *X. eiseni* are transported across the trophotaenial absorptive cells, past the nucleus (N), and are exocytosed at the basolateral plasma membranes. Reaction product of HRP is accumulated in the multivesicular bodies located in the apical cytoplasm of the absorptive cells in *G. viviparus*. In *X. eiseni*, the reaction product of HRP partly fills large storage vacuoles, the apical dense cytoplasmic tubules (CT), and the lateral lamellar membrane complex (LMC). The borders of adjacent cells are sealed apically by tight junctions (TJ). (From Schindler and de Vries, 1987a; © reproduced with permission of John Wiley & Sons, Inc.).

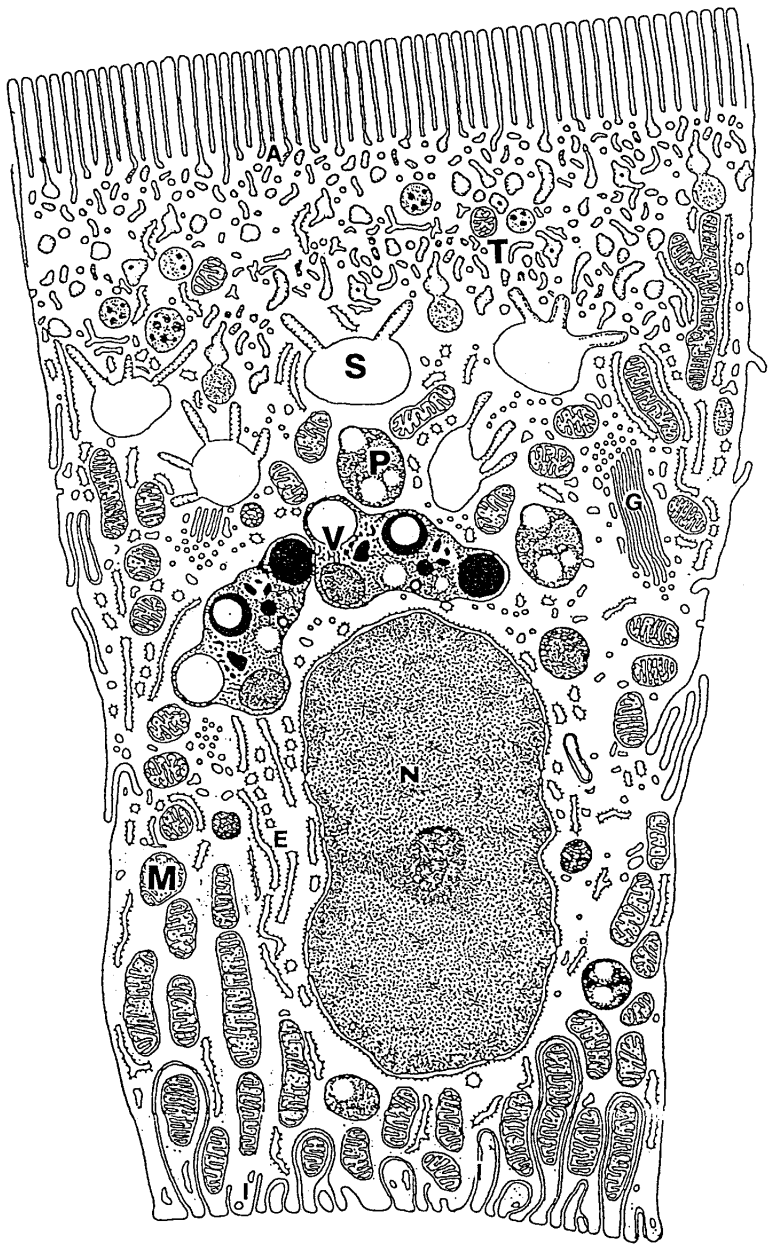

Figure 6.115: Diagrammatic representations of trophotaenial absorptive cells in two species of goodeid fishes. (From Kokkala and Wourms, 1994; © reproduced with permission of John Wiley & Sons, Inc.).

A. The absorptive cells in *Ameca splendens* are specialized for the endocytosis of macromolecules and can also transport small molecules. The cells have an apical brush border of microvilli. The apical cytoplasm contains smooth-surfaced invaginations of the plasmalemma (A) and associated vesicles as well as clathrin-coated pits and vesicles. Tubular (T) and spherical (S) endosomes are present. The region superior to the nucleus contains an array of endosomal-lysosomal (P,V) components. Mitochondria (M) occur both above and below the nucleus. Deep infoldings (I) of the basal plasmalemma are seen. E, endoplasmic reticulum; G, Golgi complex.

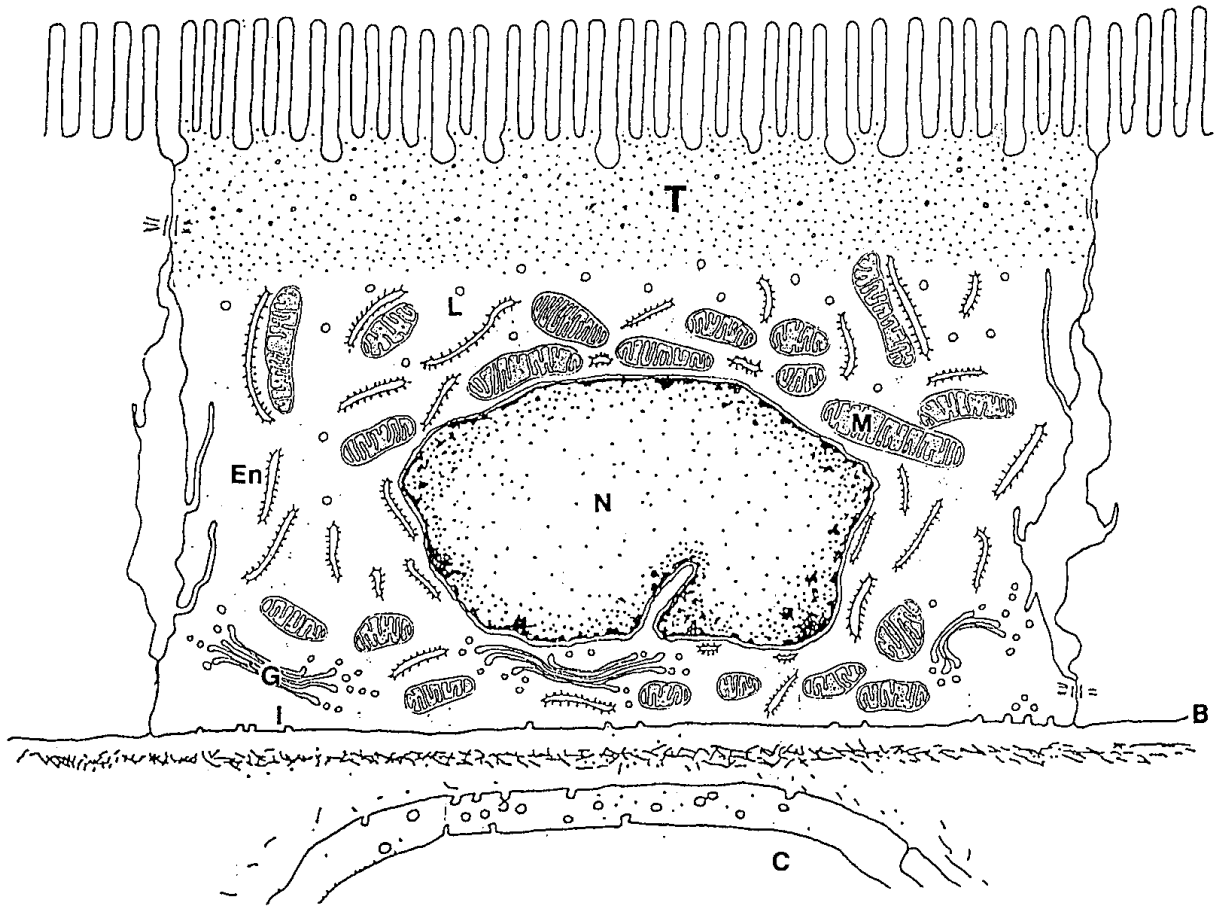

Figure 6.115: Continued.

B. The cuboidal epithelial cells in *Goodea atripinnis* are specialized for the transport of small molecules and do not endocytose large molecules; these cells lack an endocytic complex. Regularly spaced microvilli are subtended by a wide terminal web (T). Both apical and basal mitochondria (M) are associated with smooth endoplasmic reticulum (En). A basal Golgi complex (G) is shown. Only modest infoldings (I) of the basal plasmalemma are shown. The cell is separated from a capillary (C) by a thin basal lamina (B).

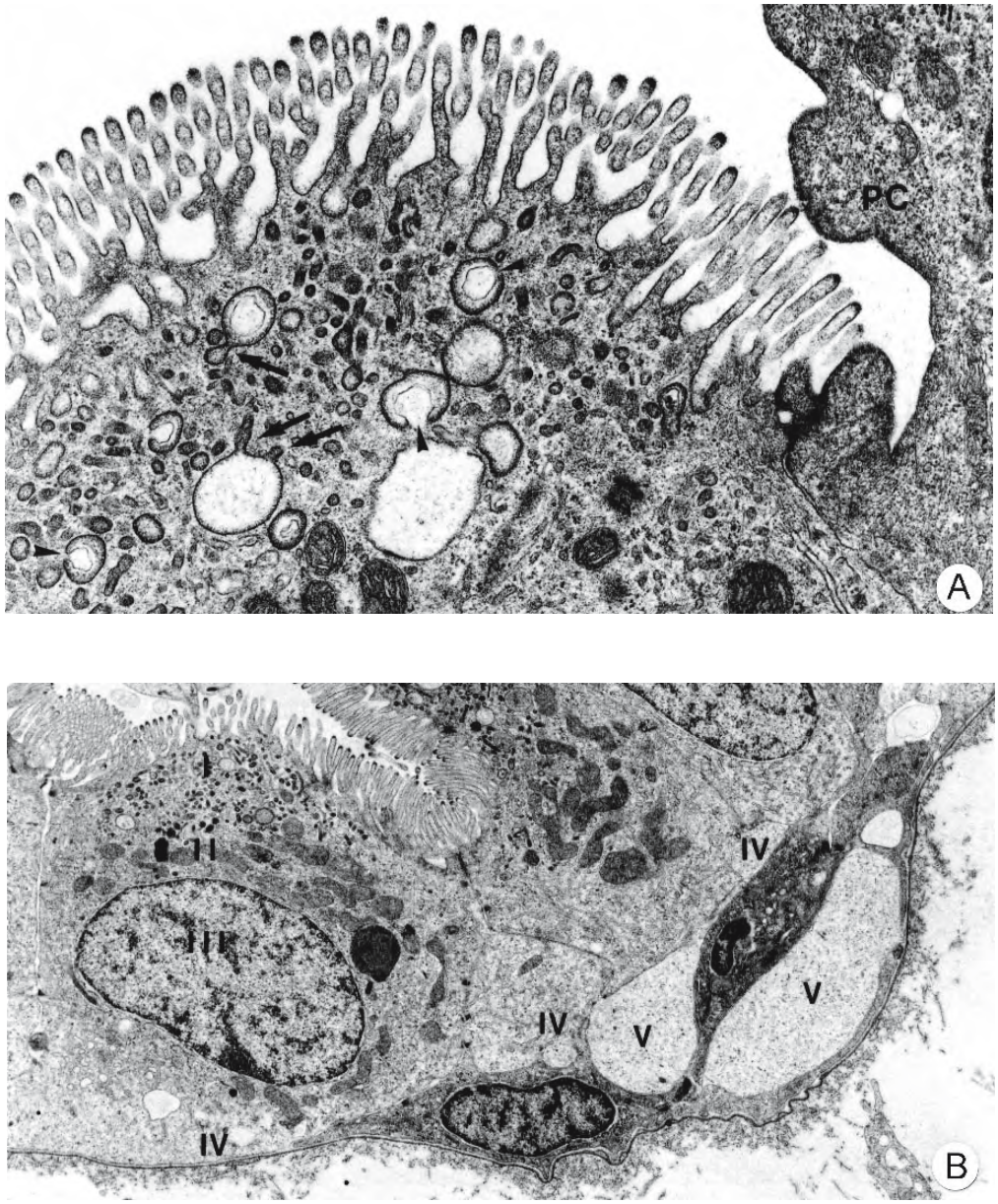

Figure 6.116: Transmission electron micrographs of sections through of trophotaenial absorptive cells in the goodeid *Xenoophorus captivus.* (From Schindler and de Vries, 1987b; reproduced with permission of the authors).

A. Tubular and saccular invaginations are numerous in the endocytic apical zone. Deeper in the cytoplasm are abundant vesicles, vacuoles, and dense tubular profiles. The vacuolar membranes are often invaginated on one side giving rise to crescent-shaped structures (arrowheads). Some profiles indicate either fusion or pinching off of tubules or vesicles from larger vacuoles (arrows). A pavement cell (PC) of the stratified epithelial component is shown at the right. X 27,000.

B. Two types of trophotaenial epithelial cells are shown: absorptive cells with a microvillous border overlie basal cells with an electron-dense cytoplasm. Zonation of the absorptive cells is shown by Roman numerals from the apical endocytic zone (I), supranuclear zone (II), nuclear zone (III), to the basal zone (IV). The basal zone contains two large vacuoles (V) of flocculent material. X 9,200.

Figure 6.117: Transmission electron micrographs of freeze-fracture replicas of the absorptive epithelium covering embryonic trophotaeniae in the goodeid *Xenotoca eiseni.* (From Schindler and de Vries, 1990; reproduced with permission of Springer-Verlag).

A. Survey view of the apical region of a trophotaenial absorptive cell. The fracture plane passes vertically through the supranuclear cytoplasm revealing the structural complexity of the endocytic complex that occupies a broad cortical zone below the microvillar border. Several mitochondria (M) occur in the deeper cytoplasm. Distended intraepithelial spaces (*) compress the middle of the cells. The lateral plasma membrane is underlain by a lamellar membrane complex (arrowheads). X 27,200.

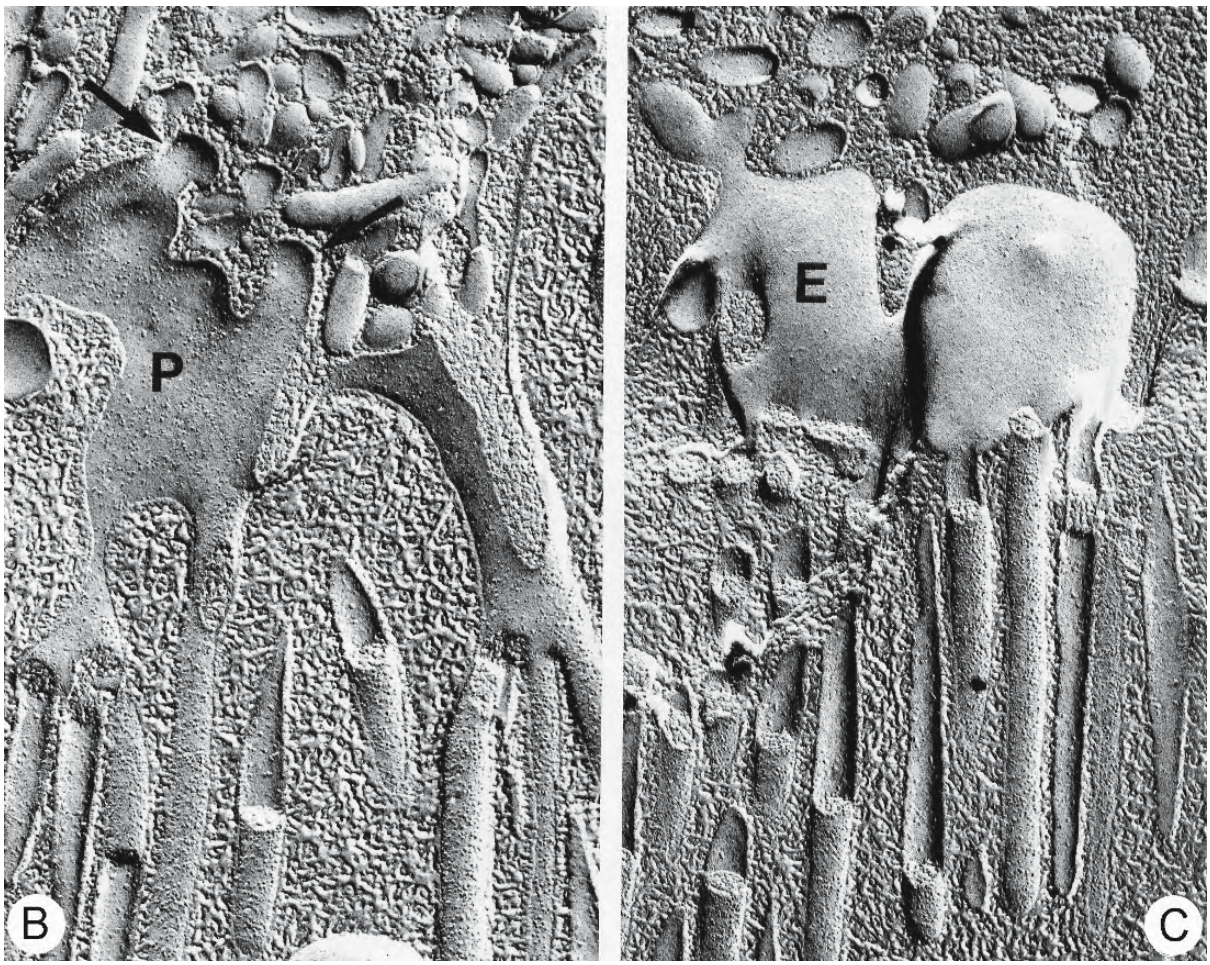

Figure 6.117: Continued.

B. This micrograph primarily illustrates the P-face appearance of the apical surface of a trophotaenial absorptive cell. Deep invaginations honeycomb the subsurface cytoplasmic matrix along with large numbers of small vesicles and tubules. The density of intramembranous particles is greatest on the P-faces of the microvilli. The continuation of their membrane on the intermicrovillous cell surface and beyond into the invaginations show reduced numbers of particles and it would appear that voluminous integral membrane proteins gain access to endocytic pits (arrows) only in small quantities. X 54,000.

C. Replica of the membrane of the microvillous and intermicrovillous regions of an absorptive cell. The invaginated surface illustrates the distribution of intramembranous particles in the E-face. Besides particle-free areas, only a few randomly scattered particles are present. X 54,000.

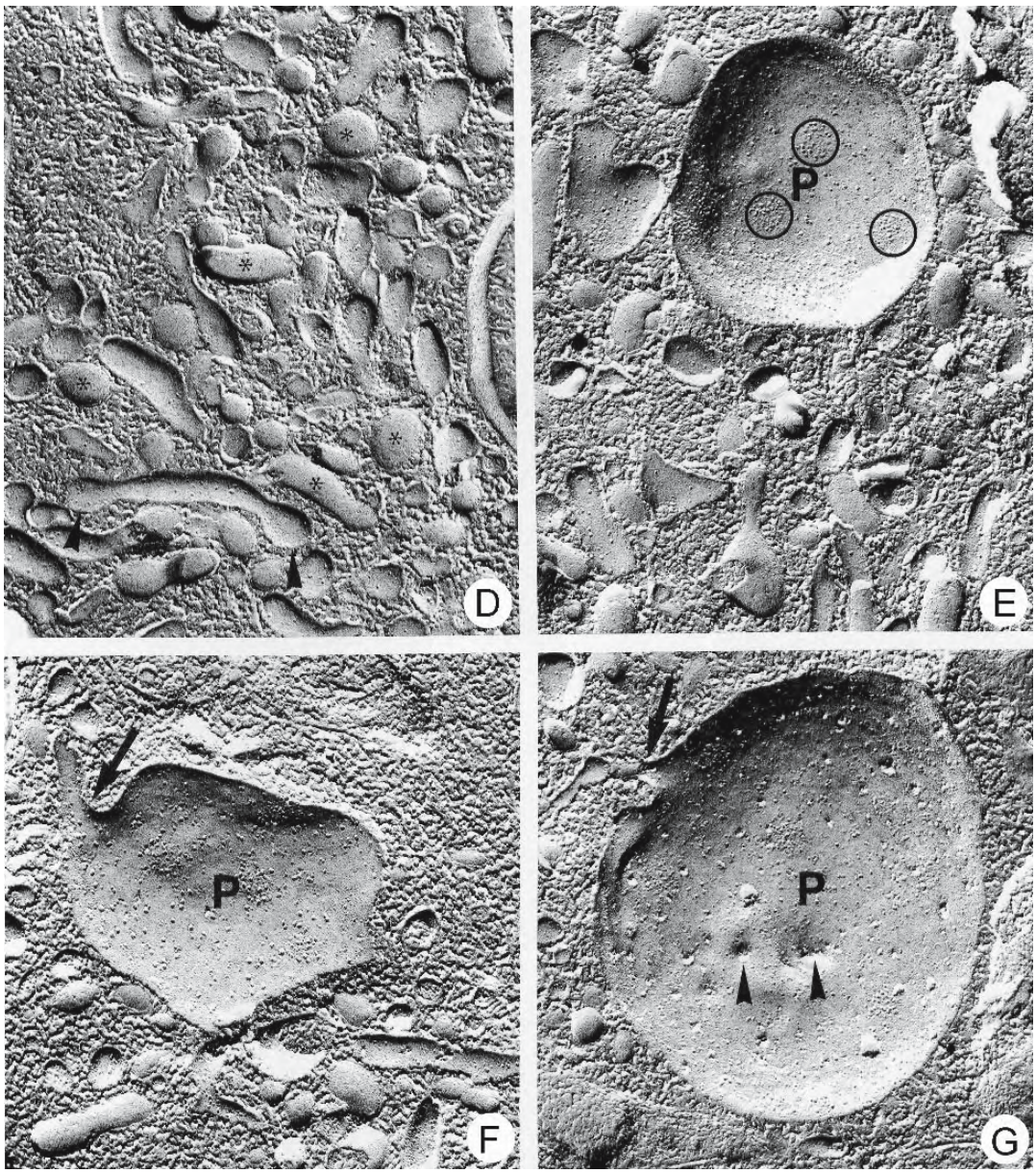

Figure 6.117: Continued.

D. The immediate subsurface cytoplasm contains an abundance of small vesicular and tubular structures. Their P-faces regularly show a few odd membrane-associated particles, whereas the corresponding E-faces (*) are almost devoid of intramembranous particles. Both ends of an apical tubule show bulbous distensions (arrowheads) indicating either fusion with or detachment of vesicles. X 63,000.

E. This replica shows the P-face of an endosome within the apical endocytic zone. Several intramembranous particles cluster in some membrane areas (circles). X 61,000.

F. The arrow indicates the connection between an endosome and an apical tubule. Intramembranous particles are clustered on the P-face. X 62,000.

G. This large endosome is connected to an apical tubule (arrow). Small pits (arrowheads) in the P-face indicate the presence of further connections within tubules. X 54,000.

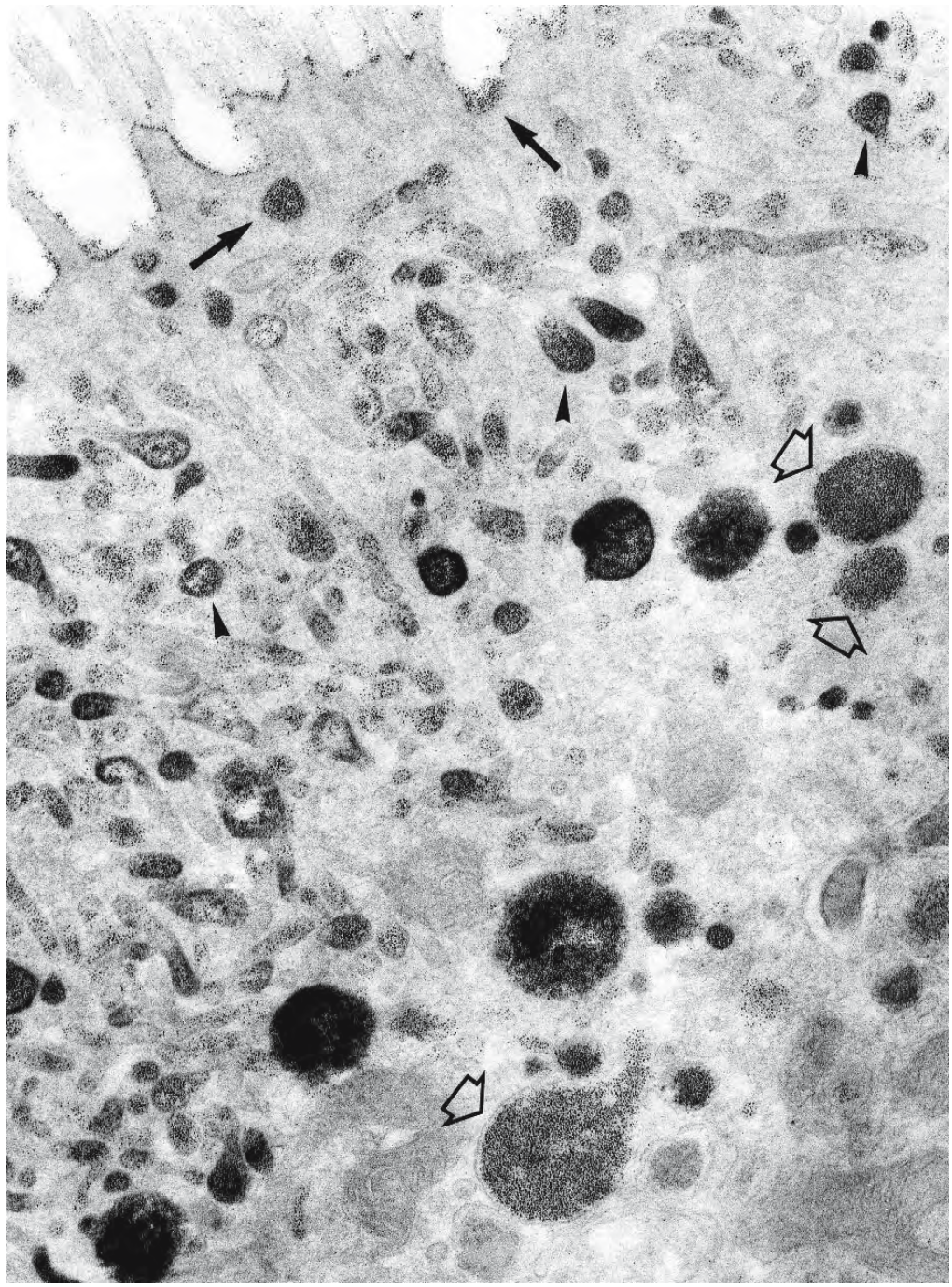

Figure 6.118: Transmission electron micrograph of a section through the apical portion of a trophotaenial absorptive cell of the goodeid *Xenoophorus captivus* after exposure to horseradish peroxidase and cationized ferritin for one hour. HRP-reaction product is enriched within some vacuoles in the deeper parts of the apical endocytic complex. Other vacuoles almost exclusively contain CF (light arrows). Surface invaginations and/or pinocytic vesicles (arrows) are filled with CF-agglomerates, Other vesicles of the same size are double-labelled (arrowheads). CF-molecules are present in most apical tubules. X 53,000 (From Schindler and de Vries, 1988a; reproduced with permission of the authors).

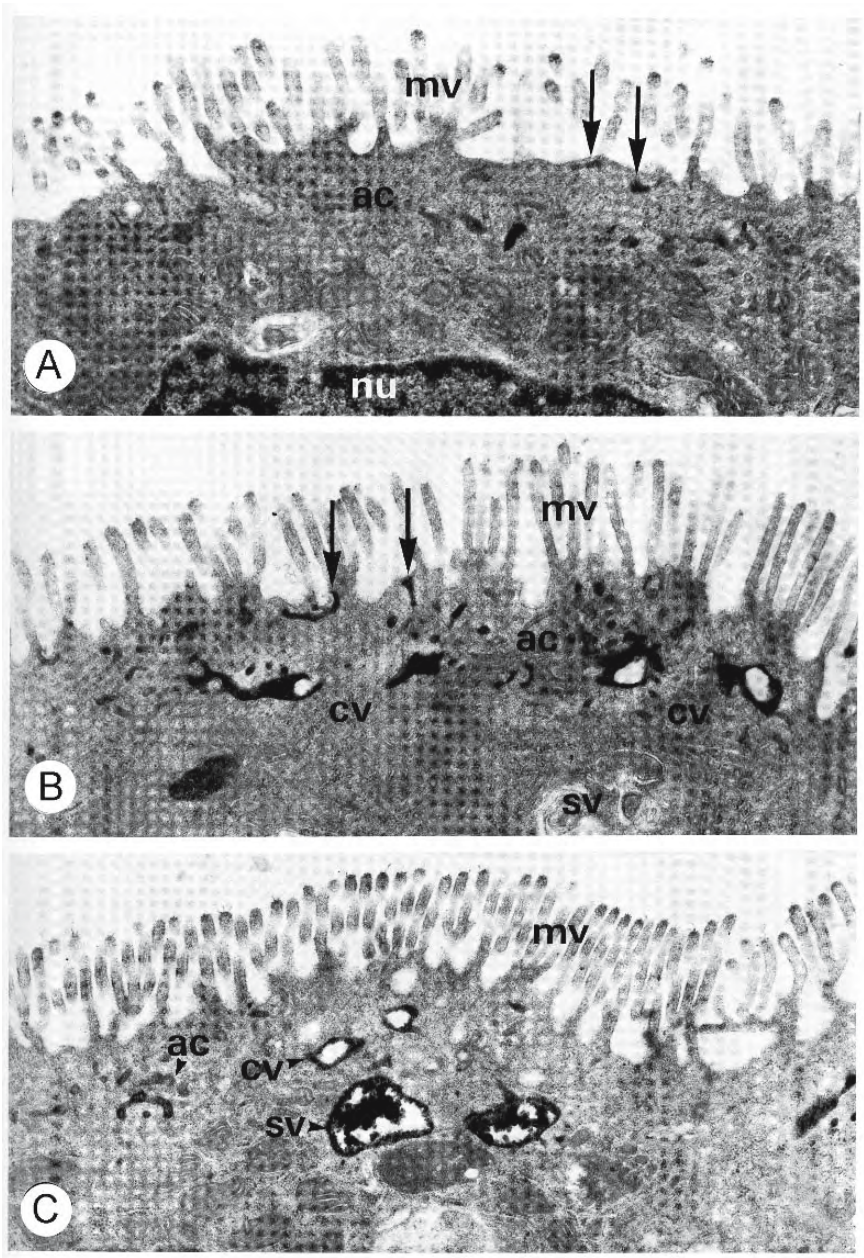

Figure 6.119: Transmission electron micrographs of sections through the apical regions of trophotaenial absorptive cells of the goodeid *Ameca splendens* fixed after a period of continuous exposure to horseradish peroxidase. (From Lombardi and Wourms, 1985c; © reproduced with permission of John Wiley & Sons, Inc.).

A. After 1.5 minutes' exposure, reaction product is present within a few apical vesicles and elements of the apical canalicular system (arrows) X 20,000.

B. After 10 minutes' exposure, uptake occurs by way of endocytosis of the apical plasma membrane (arrows). Reaction product is present within apical canaliculi and collecting vesicles. Large supranuclear lysosomes situated above the nucleus show no peroxidase activity. X 20,000.

C. After 15 minutes' exposure, the reaction product is present within apical canaliculi, collecting vesicles, and large supranuclear vesicles. X 20,000.

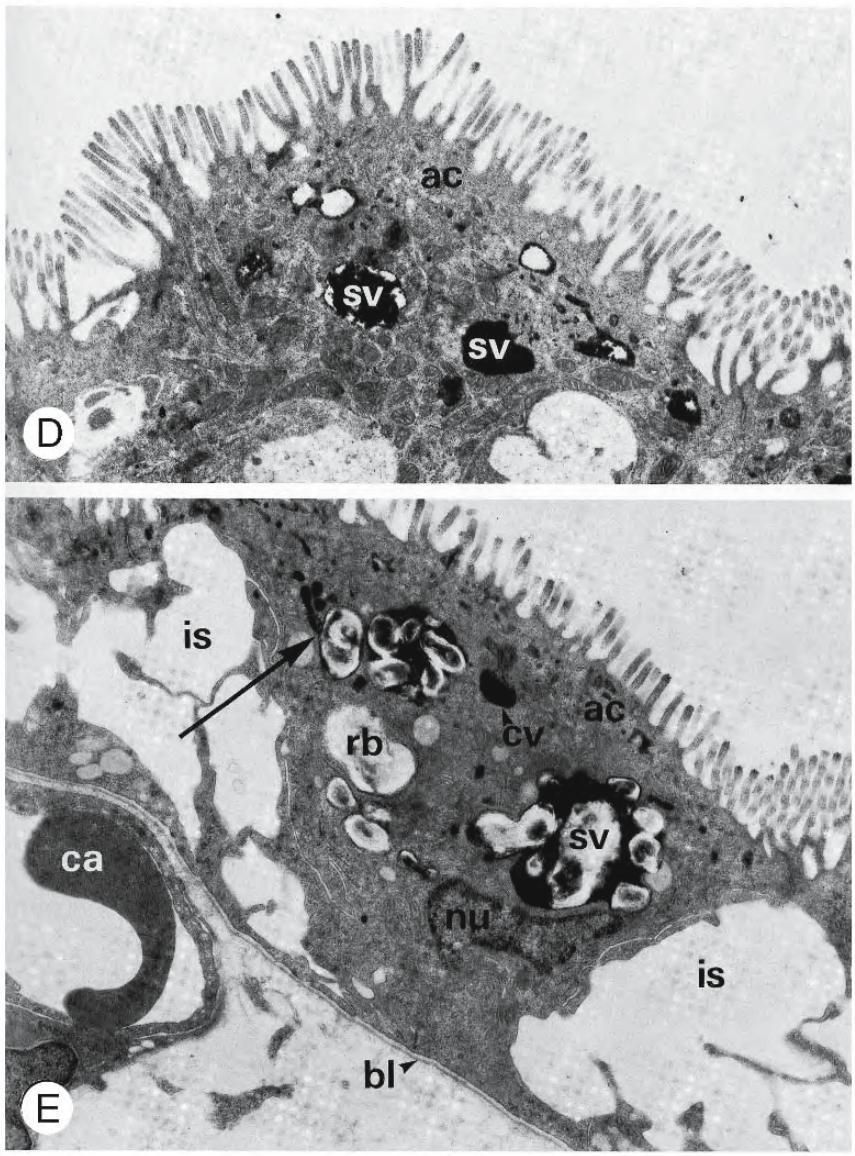

Figure 6.119: Continued.

D. After 30 minutes, the reaction product is present within the apical canalicular system, collecting vesicles, and enlarged supranuclear lysosomes. X 18,000.

E. An entire absorptive cell is shown after one hour's exposure. The reaction product is present within apical canaliculi, collecting vesicles, and greatly enlarged supranuclear lysosomes. Collecting vesicles fuse with supranuclear vesicles (arrow). Residual bodies containing flocculent material are present. Peroxidase activity is almost exclusively localized in the supranuclear region of the cell. Exogenous peroxidase activity is not detected within the trophotaenial connective tissue or vascular elements. X 18,000.

Abbreviations: ac, apical canaliculi; bl, basal lamina; ca, capillary; cv, collecting vesicles; is, intercellular space; mv, microvilli; nu, nucleus; rb, residual body; sv, supranuclear vesicles.

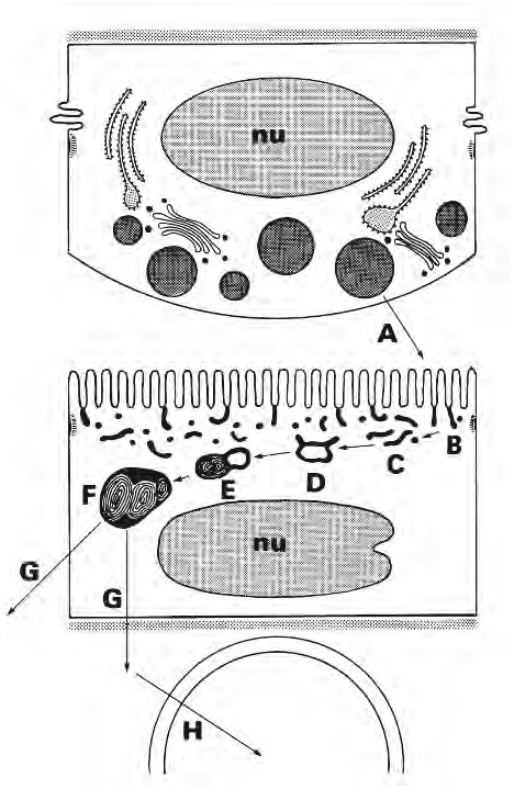

Figure 6.120: Diagrammatic summary of the proposed pathway by which proteins are transferred across the trophotaenial placenta in the goodeid *Ameca splendens.* A, the synthesis and release of protein-containing secretions by cells of the internal ovarian epithelium; B, uptake of ovarian secretions by the trophotaenial epithelium by endocytosis; C, transfer and passage of protein components through the apical canalicular system and its progressive accumulation in collecting vesicles; D, fusion of collecting vesicles with standing supranuclear secondary lysosomes; E, growth of standing lysosomes by accretion of collecting vesicles and/or other lysosomes; F, enzymatic hydrolysis of proteins within standing lysosomes; G, discharge of the products of protein hydrolysis (amino acids and peptides) via lateral and basal cell surfaces; H, passage of components of low molecular weight across the basal matrix and connective tissue core and their entry into the embryonic vascular system by transport across the capillary endothelium. (From Lombardi and Wourms, 1985c; © reproduced with permission of John Wiley & Sons, Inc.).

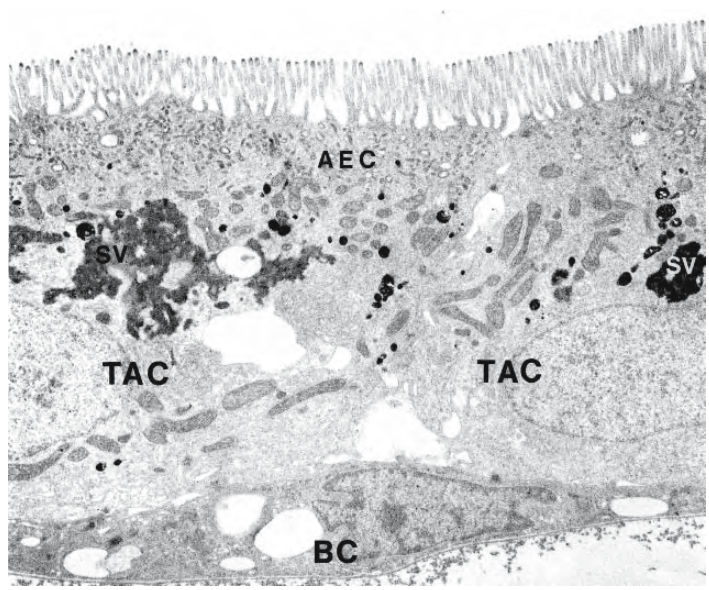

Figure 6.121: Transmission electron micrograph of a section through two trophotaenial absorptive cells overlying a basal cell in the trophotaenial epithelium of the goodeid *Xenoophorus captivus* following exposure to horseradish peroxidase. A system of intercellular spaces, continuous with the infoldings of the basolateral membranes of the absorptive cells, extends between the absorptive and basal cells. (From Schindler and de Vries, 1988a; reproduced with permission of the authors)
Abbreviations: AEC, apical endocytic complex; BC, basal cell; TAC, trophotaenial absorptive cell; SV, supranuclear vacuole. X 13,100.

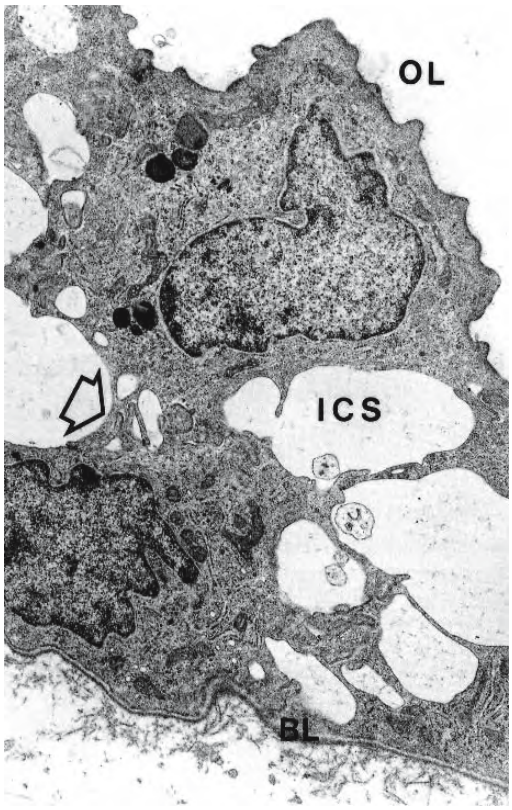

Figure 6.122: Transmission electron micrograph of a section through the stratified trophotaenial epithelium of the goodeid *Xenoophorus captivus.* The ovarian lumen (OL) is shown at the top. Huge intercellular spaces (ICS) have appeared between the stratified pavement cells. Adjoining cells are connected by cytoplasmic processes. The arrow indicates interdigitations between adjacent cells. The epithelium is separated from loose subepithelial connective tissue by a delicate basal lamina (BL). X 10,000 (From Schindler and de Vries, 1987b; reproduced with permission of the authors).

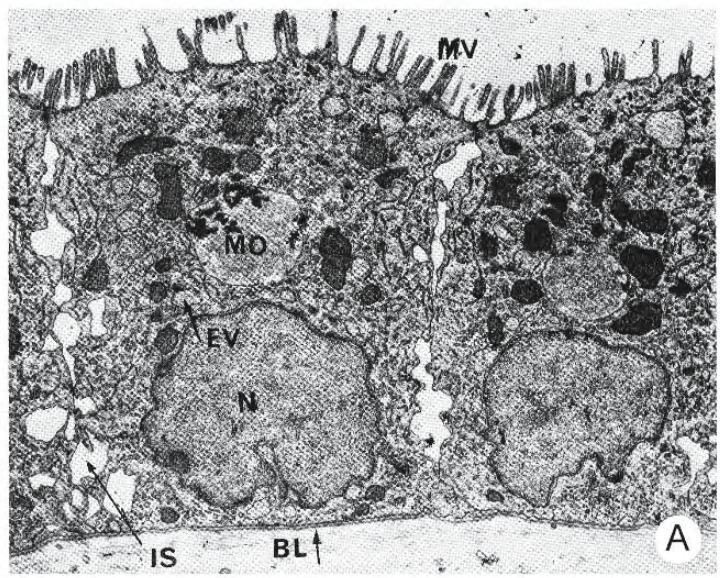

Figure 6.123: Transmission electron micrographs showing progressive distension of the intercellular spaces in the trophotaenial absorptive epithelium of a goodeid *"Characodon" eiseni.* (From Mendoza, 1972; © reproduced with permission of John Wiley & Sons, Inc.).

A. The trophotaenial epithelium at an early stage of its cell cycle. Intercellular spaces are slightly distended. Note the stratification of organelles. X 8,400.

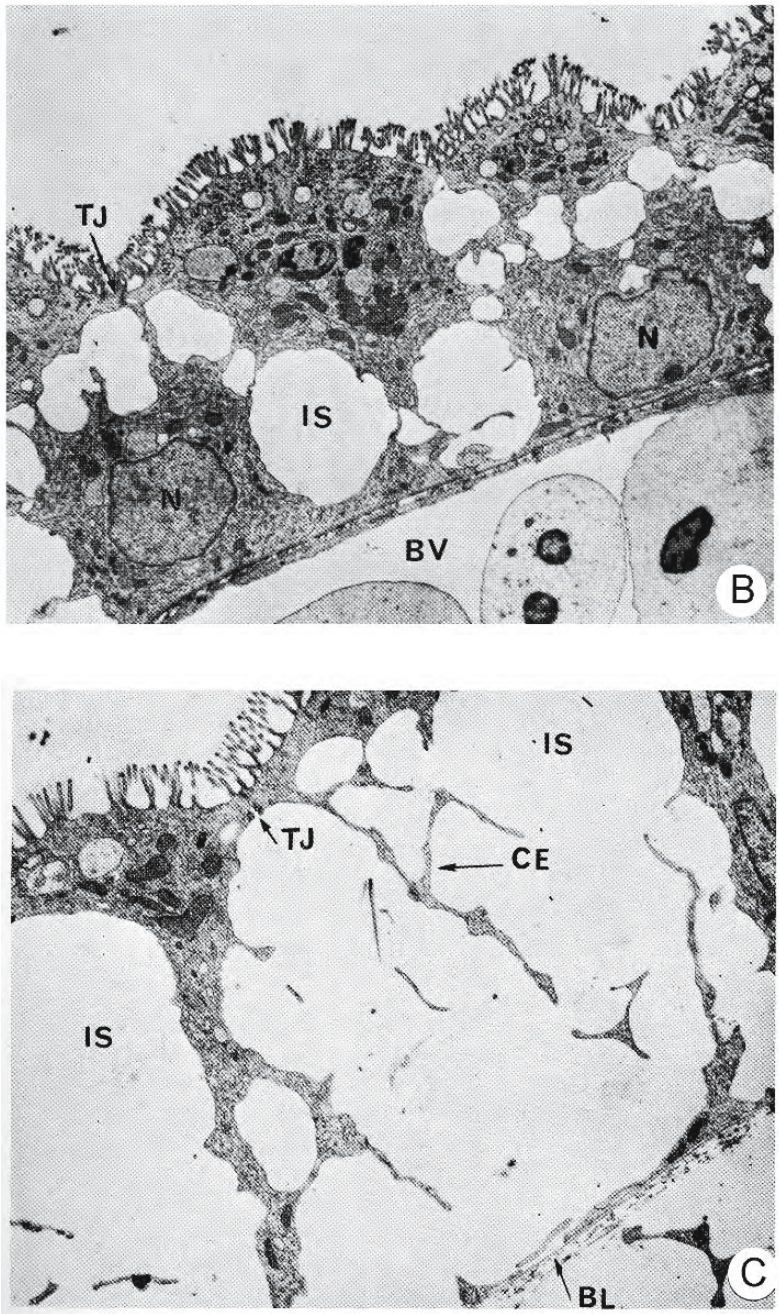

Figure 6.123: Continued.

B. A region of the epithelium with well developed intercellular spaces. A blood vessel is closely apposed to the basal lamina of the epithelium. X 3,750.

C. The epithelial cells are extremely distorted by the enlarged intercellular spaces. Epithelial contact with the basal lamina is minimal. The tight junction continues to seal the apical surface. X 9,000.

Abbreviations: BL, basal lamina; BV, blood vessel; CE, cellular extensions; EV, vesicle of the endoplasmic reticulum; IS, intercellular space; MO, "mottled vesicle"; MV, microvilli; N, nucleus; TJ, tight junction.

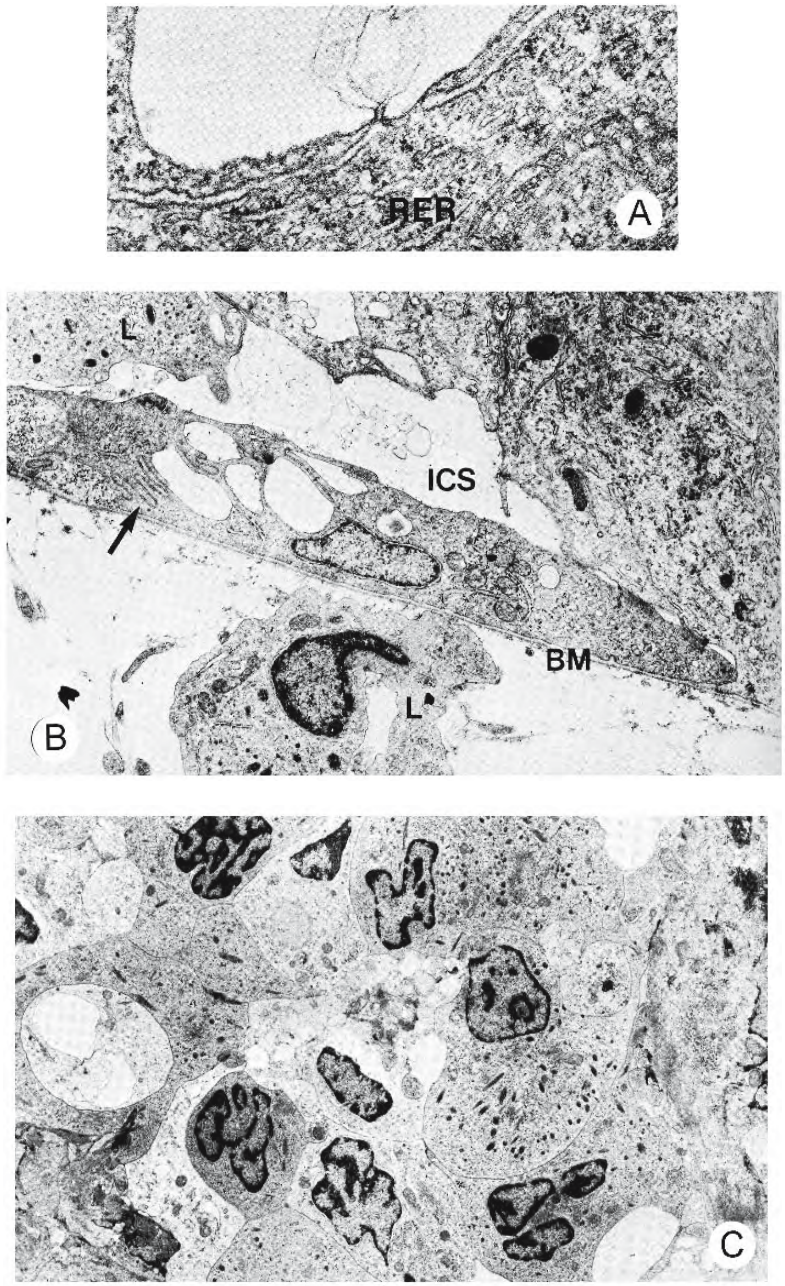

Figure 6.124: Intercellular spaces in the trophotaenial epithelium may have an excretory role in storing wastes or play a passive role in the acquisition of immunity. These are transmission electron micrograph of sections through of near-term embryos of the goodeid *Girardinichthys viviparus.* (From Schindler and de Vries, 1986a; © reproduced with permission of John Wiley & Sons, Inc.).

A. The lateral plasmalemmas of absorptive cells are lined with lamellar structures and membranous blebs are extruded into the intercellular space. RER, granular endoplasmic reticulum. X 54,000.

B. A single layer of flattened cells, resting on the basal lamina (BM), underlies the absorptive epithelium. These basal cells are connected by highly convoluted interdigitations (arrow). A leucocyte (L) can be seen in the intercellular spaces (ICS) between the two types of epithelial cells; another is present in the trophotaenial stroma. X 10,000.

C. Leucocytes, largely heterophilic granulocytes, occupy the connective tissue core of a trophotaenia. X 5,070.

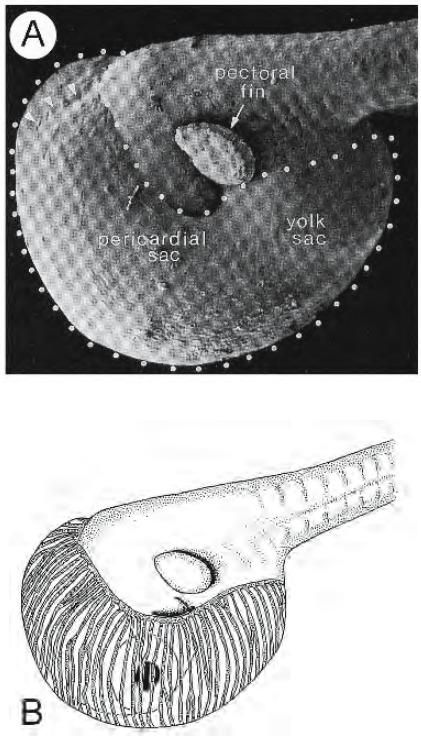

Figure 6.125: Embryos of the matrotrophic poeciliid, *Heterandria formosa.* (From Grove and Wourms, 1991; © reproduced with permission of John Wiley & Sons, Inc.).

A. Scanning electron micrograph of a mid-stage embryo. The hood-like expansion of the pericardial sac has invested the head of the embryo. Arrowheads indicate the position where the lateral margins of the expanded pericardial sac have fused dorsomedially. The portal plexus underlies the region outlined by dots. X 65.

B. Drawing of a mid-stage embryo illustrating the portal plexus underlying the yolk and pericardial sac surfaces and the extent to which the pericardial sac invests the head of the embryo.

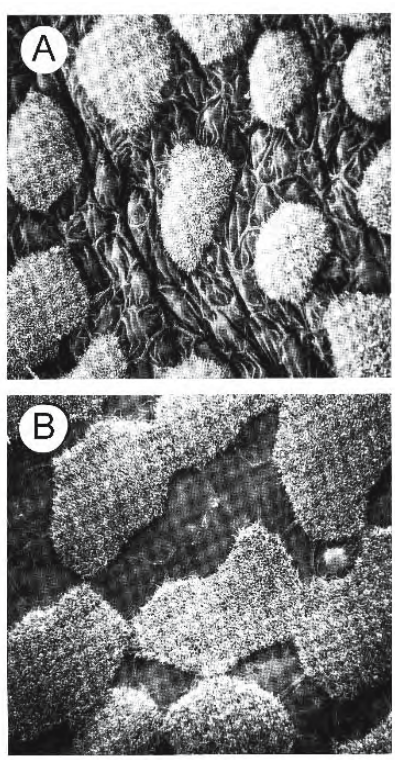

Figure 6.126: Scanning electron micrographs of the surface epithelium of a late-stage embryo of the matrotrophic poeciliid, *Heterandria formosa.* The epithelium is a patchwork of absorptive cells and cells that do not appear to be absorptive. (From Grove and Wourms, 1991; © reproduced with permission of John Wiley & Sons, Inc.).

A. The posterolateral surface consists of clusters of cells with microvilli interspersed among cells lacking microvilli. The cells lacking microvilli, however, display surface folds. X 750.

B. The lateral surface of the tail consists of cells with and without microvilli and those lacking microvilli display surface folds. X 650.

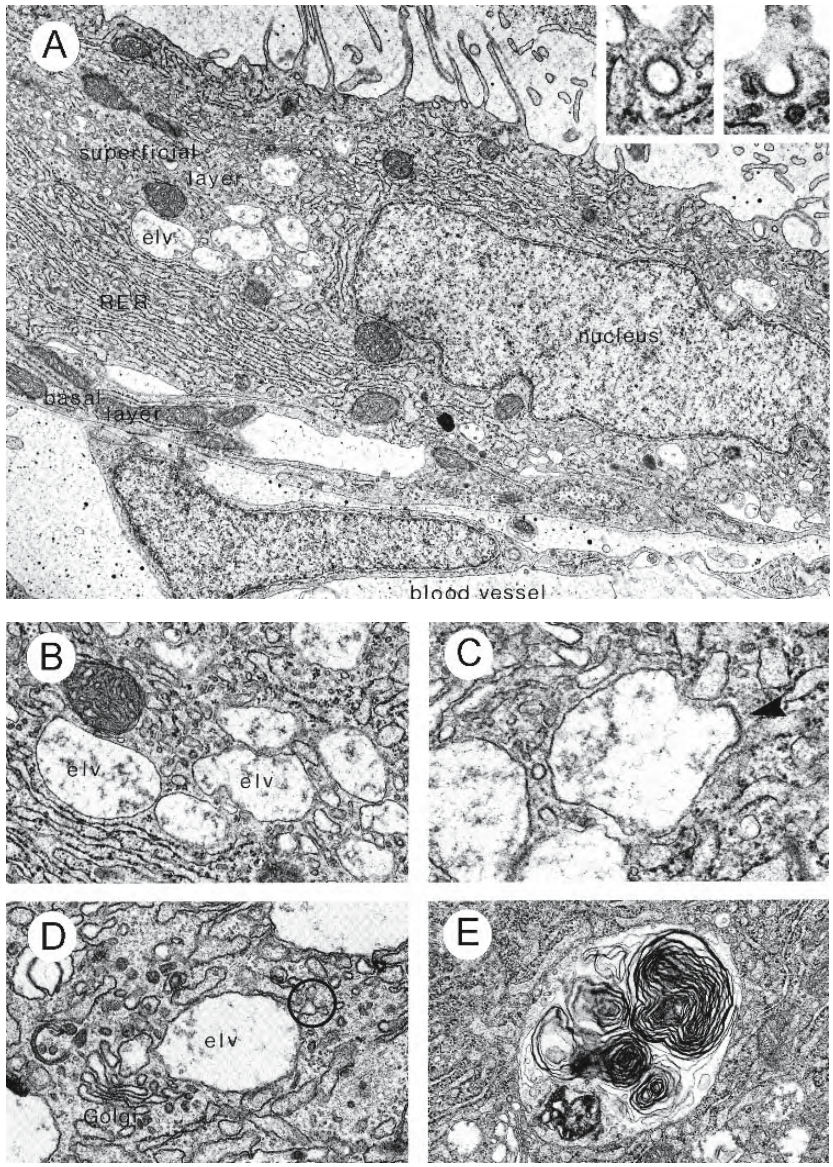

Figure 6.127: Transmission electron micrographs of sections of the surface epithelium of a mid-stage embryo of the matrotrophic poeciliid, *Heterandria formosa.* (From Grove and Wourms, 1991; © reproduced with permission of John Wiley & Sons, Inc.).

A. In the bilaminar surface epithelium covering the pericardial sac, the superficial cells possess apical microvilli, numerous electron-lucent vesicles (elv), and extensive granular endoplasmic reticulum (RER); the granular endoplasmic reticulum in the basal cytoplasm occurs as stacks of parallel cisternae. Basal cells are thinner and possess few organelles. The endothelium of a vessel of the portal plexus is closely associated with the surface epithelium. X 8,700
Inset: a coated vesicle and pit at the apical surface of the superficial cell. X 48,000.

B. Electron-lucent vesicles (elv) are shown in the cytoplasm of a superficial cell. X 17,300.

C. An electron-lucent vesicle in a superficial cell displays a coated region (arrowhead). X 39,000.

D. Electron-lucent vesicle (elv) with a bleb-like extension (circle). X 28,000.

E. An electron-lucent vesicle containing myelin figures. X 16,000.

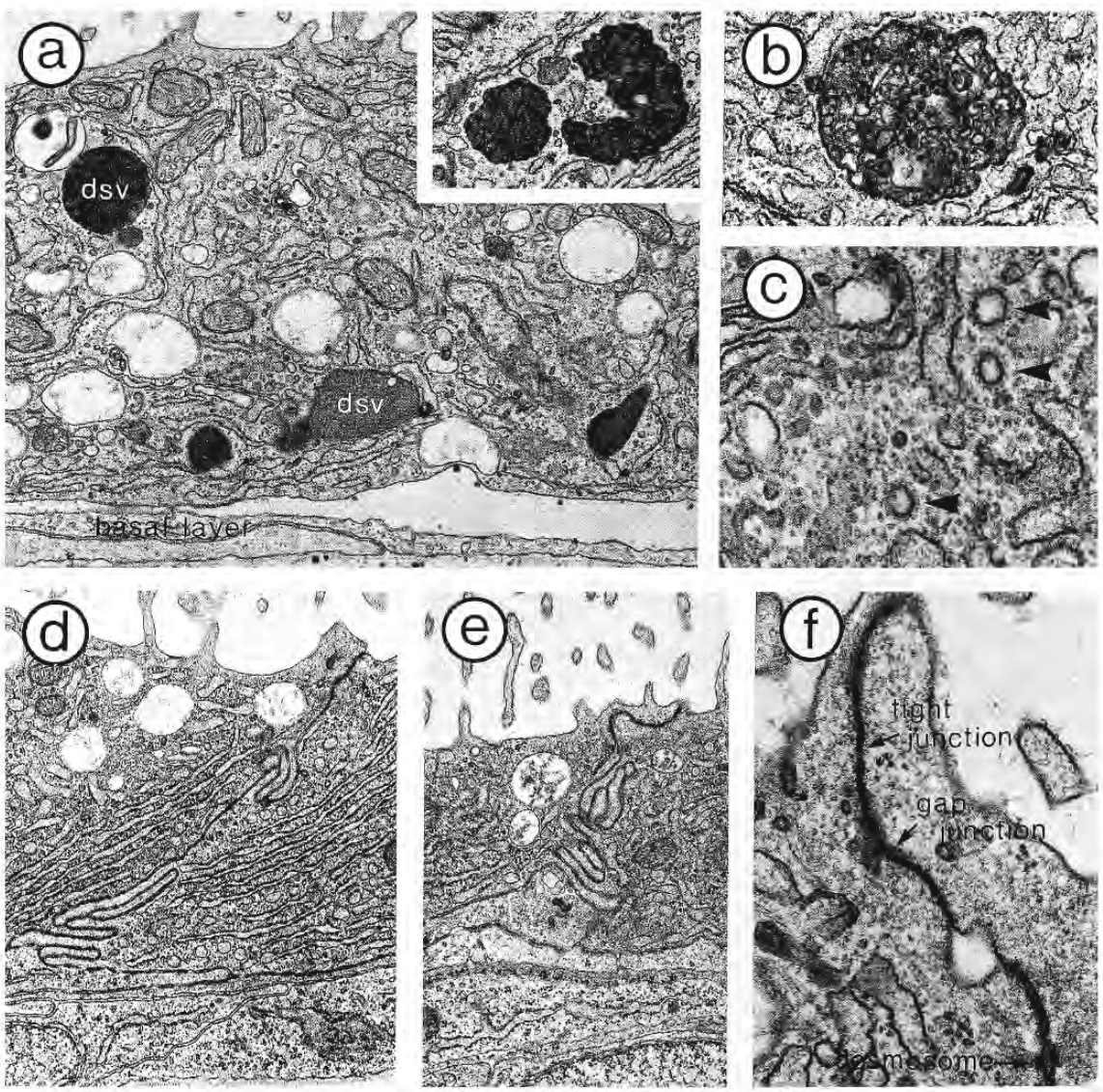

Figure 6.128: Transmission electron micrographs of sections of the surface epithelium covering the non-vascular, lateral surface of a mid-stage embryo, just caudal to the pectoral fin and dorsal to the pericardial and yolk sacs, of the matrotrophic poeciliid, *Heterandria formosa.* (From Grove and Wourms, 1991; © reproduced with permission of John Wiley & Sons, Inc.).

A. Superficial cell showing dense-staining (dsv) and electron-lucent vesicles. Dense-staining vesicles vary in the structure of their contents and in their shape. X 14,000.

Inset shows a dense-staining vesicle with heterogeneous contents. X 14,500.

B. A multivesicular body in a superficial epithelial cell. X 31,000.

C. Coated vesicles (arrowheads) in the cytoplasm of a superficial cell. X 43,000.

D,**E.** Contact between adjacent superficial cells is characterized by apical junctional complexes and extensive interdigitation of the lateral plasma membranes. X 11,000.

F. An apical junctional complex between adjacent superficial cells. X 37,000.

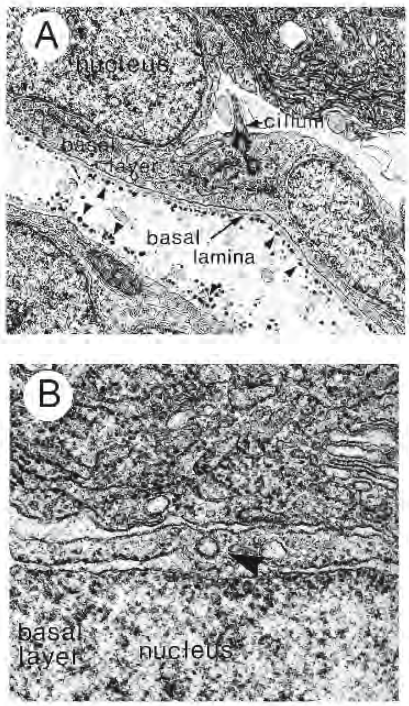

Figure 6.129: Transmission electron micrographs of sections of the surface epithelium of an embryo of the matrotrophic poeciliid, *Heterandria formosa.* (From Grove and Wourms, 1991; © reproduced with permission of John Wiley & Sons, Inc.).

A. Basal cell of the surface epithelium of a mid-stage embryo showing a cilium and its basal body. The dense extracellular granules (arrowheads) may represent yolk. X 10,000.

B. A basal cell from the surface epithelium of a mid-stage embryo showing a coated pit (arrowhead) at its apical surface. X 33,000.

C. Surface epithelium of a late stage embryo from a region similar to that shown in Figure 6.126A. The epithelium consists of superficial and basal cells. The superficial cells lack microvilli and are thinner than absorptive superficial cells with microvilli.
*Inset***:** cytoplasmic filaments (arrowhead) in the apical cytoplasm of a superficial cell. X 26,500.

D. Surface epithelium of a late stage embryo from a region similar to that shown in Figure 6.126A illustrating the junction between an absorptive cell bearing microvilli and a non-microvillous cell. Although the morphology of the two types of superficial cells differs strikingly, there is no apparent difference in the morphology of the basal cells. The basal lamina is indicated by arrowheads. X 9,500.

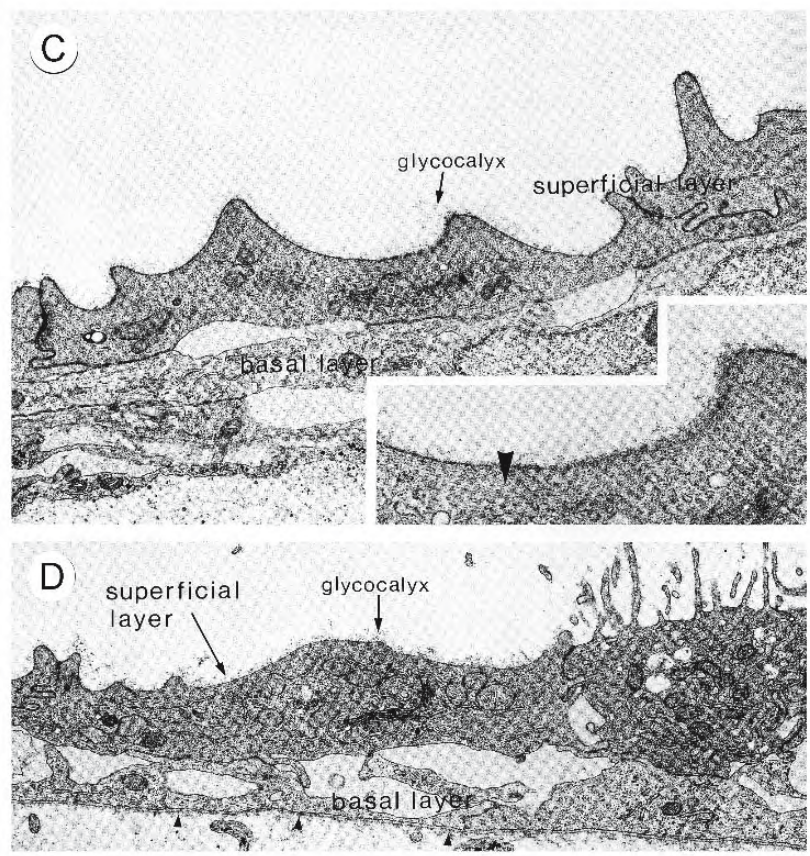

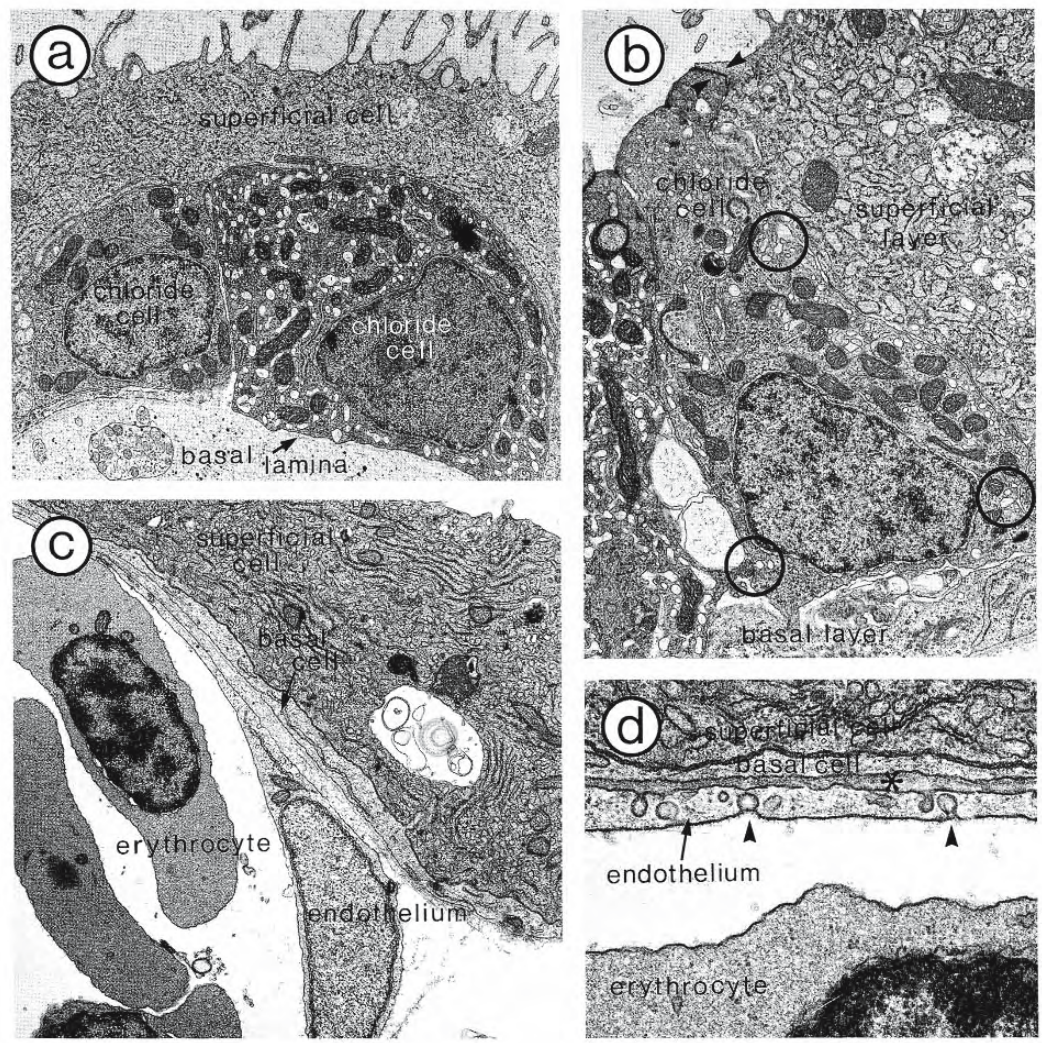

Figure 6.130: Transmission electron micrographs of sections of the surface epithelium of a mid-stage embryo of the matrotrophic poeciliid, *Heterandria formosa.* (From Grove and Wourms, 1991; © reproduced with permission of John Wiley & Sons, Inc.).

A,B. Putative chloride cells contain numerous mitochondria and an extensive system of tubular channels that communicate with the lateral and basal extracellular spaces (circles in B). Two chloride cells in A are in contact with the basal lamina. The chloride cells in B extend to the apical surface of the epithelium where they are connected to adjacent superficial cells by junctional complexes (arrowheads). X 7,800.

C. Blood vessel of the portal plexus is closely apposed to the basal surface of the surface epithelium. X 8,000.

D. An endothelial cell of the portal plexus is closely applied to a basal cell of the surface epithelium of the pericardial sac. The endothelial and epithelial cells are so close to one another that their two basal laminae (*) cannot be distinguished. Numerous pits and vesicles in the endothelial cell (arrowheads) suggest transcytotic movement across these cells. X 30,000.

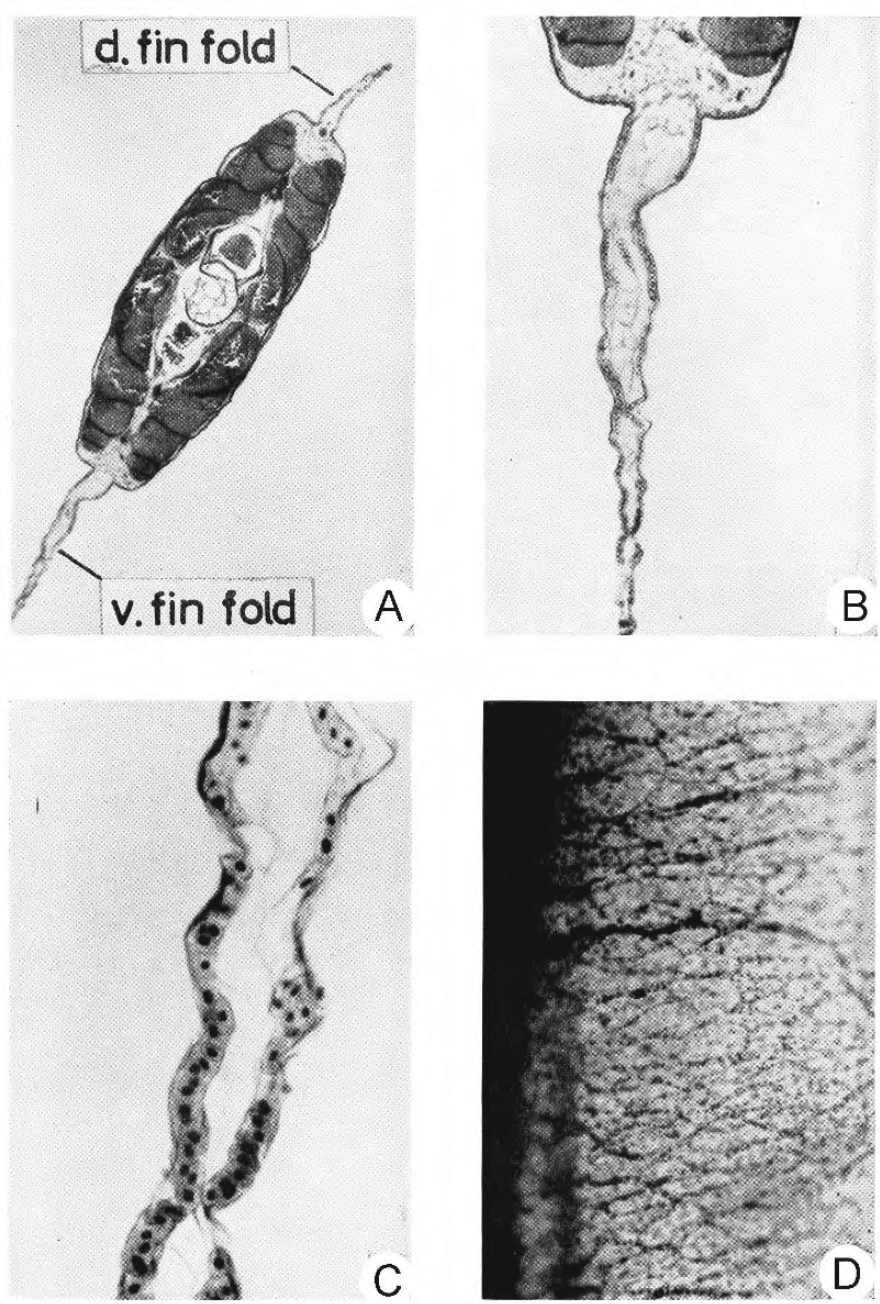

Figure 6.131: Exchange with the embryotroph takes place through skin covering the richly vascularized fin folds of goodeids. (From Mendoza, 1958; © reproduced with permission of John Wiley & Sons, Inc.).

Plate 1. Photomicrographs from *Goodea luitpoldii.*

A. Cross section of a 13-mm embryo showing the dorsal and ventral fin folds.

B. Section of the ventral fin fold showing the extensive subepithelial vascular stroma.

C. The same fin fold at a higher magnification.

D. Surface view of a stained whole mount of a fin fold of a 15-mm embryo showing its extensive vascularization. The base of the fold is at the left; the free edge at the right.

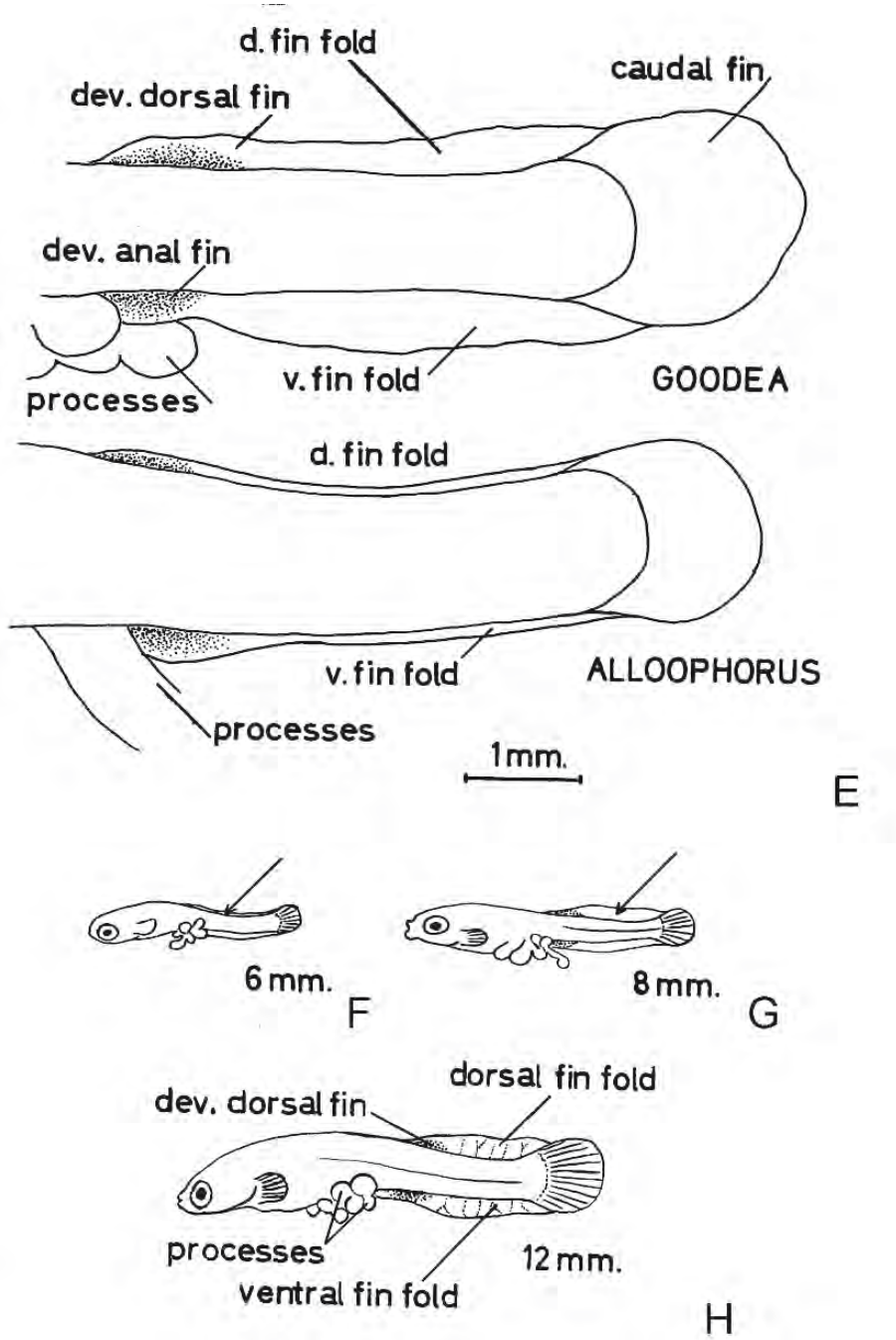

Plate 2. Drawings to illustrate fin folds.

E. Comparison of fin folds of 11-mm embryos of two goodeids *Goodea* and *Allophorus*.

F,G,H. Three stages of embryos of *Goodea luitpoldii* showing the development and resorption of the fin folds. The arrow indicates the dorsal fin fold.

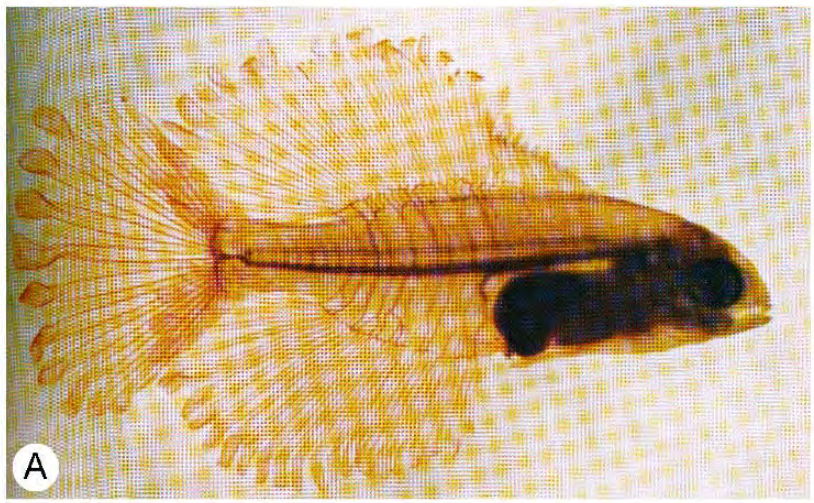

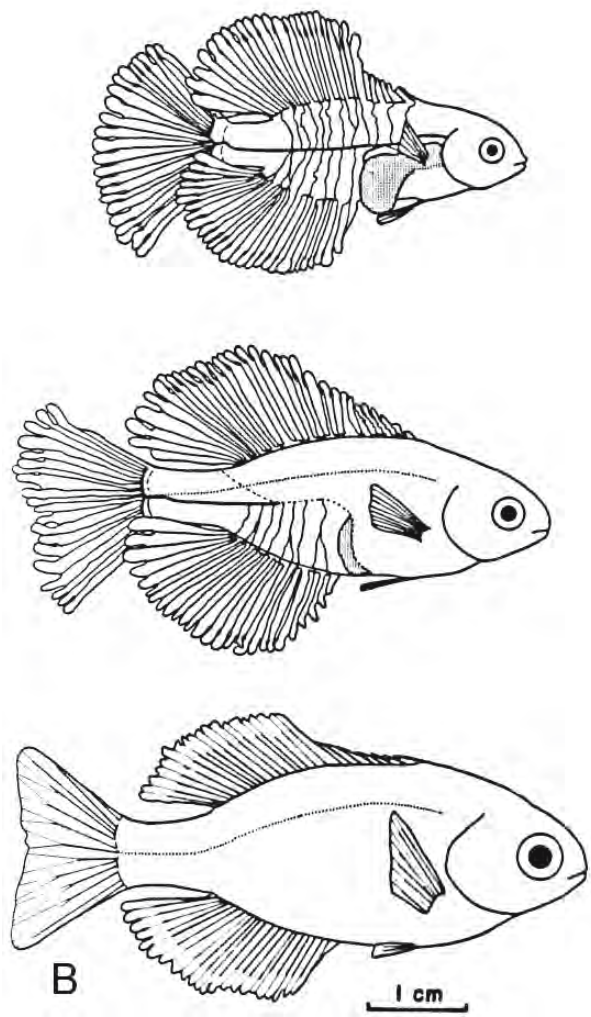

Figure 6.132: Vascularized spatulate expansions of the interradial fin web on the dorsal fin of embryos of embiotocids are presumed to function in maternal-foetal exchange. (From Webb, 1972; Fisheries and Oceans, Canada. Reproduced with the permission of the Minister of Public Works and Government Services, 2002).

A. Photograph showing the appearance of a young striped seaperch *Embiotoca lateralis* at the middle of gestation. The most prominent vessels (fin veins) anastomose at the base of the median and caudal fins, passing into the body to join the caudal vein. The lighter-appearing arteries leave the dorsal aorta, passing to the fins. The fin rays are transparent and cannot be distinguished. The gut can be clearly seen.

B. Drawings illustrating changes to young embiotocids during gestation.

Top: The striped seaperch *Embiotoca lateralis* at mid gestation showing the extensive venous system, particularly of the fins and spatulate extensions. The arterial system and fin rays have been omitted. The gut, shown stippled, still protrudes at this stage.

Centre: Late gestation pile perch *Rhacochilus vacca.* The veins in the fins are still prominent and the spatulate fin extensions are still present. Fin arteries and rays are omitted.

Bottom: The pile perch *Rhacochilus vacca* just after birth. The body is covered by scales. Vessels in the fins are reduced. Fin rays are shown. The spatulate extensions of the median and caudal fins have largely been absorbed.

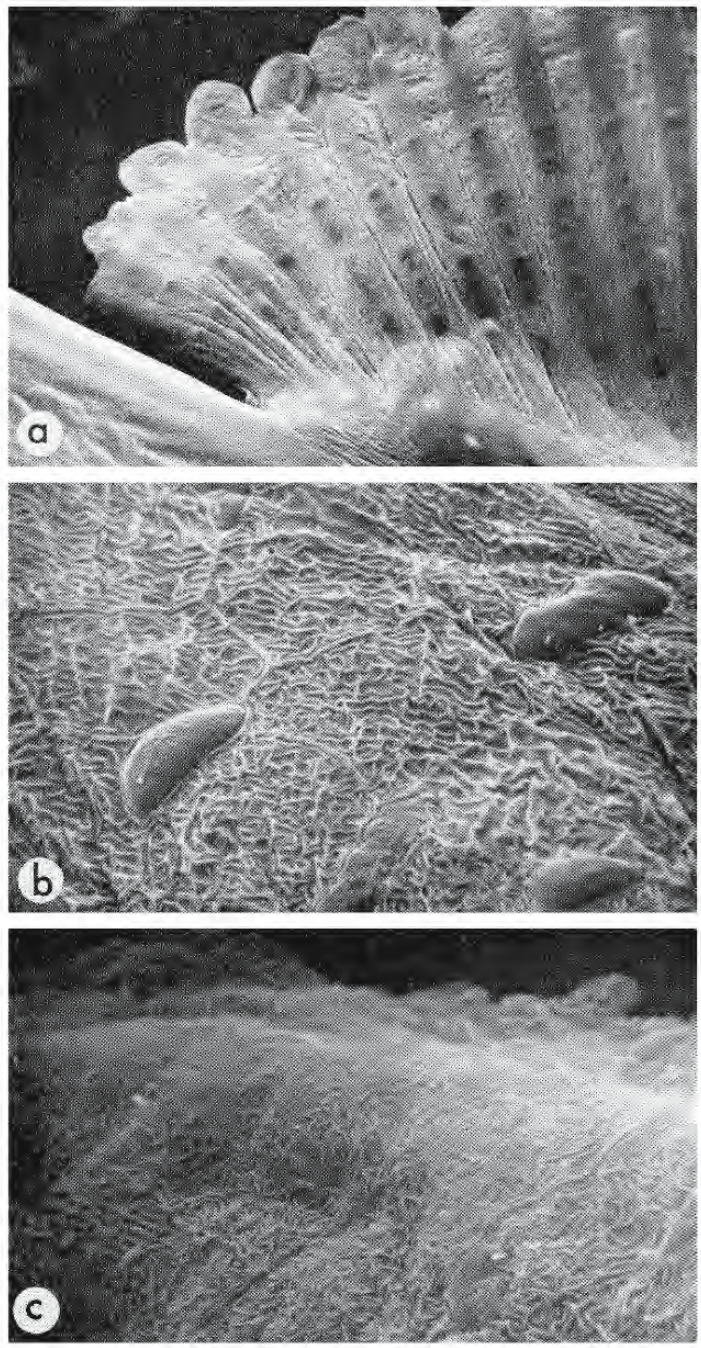

Figure 6.133: Scanning electron micrographs to illustrate adaptations facilitating respiratory exchange in the fins of the viviparous surfperch *Micrometrus minimus.* (From Dobbs, 1975; reproduced with permission from Elsevier Science).

A. Flaps on the posterior dorsal fin appear as expansions of the inter-radial fin web. X 48.

B. The apical plasmalemma of epidermal cells at the base of the dorsal fin bear microridges that increase the surface area for exchange. The bulges between the epidermal cells are probably mucous cells. X 1,800.

C. The surface of epidermal cells on the fin flaps bears microridges that resemble those on the epithelium covering gill filaments. X 1,850.

REFERENCES

Abraham, M. et al. 1984 The cellular envelope of oocytes in teleosts. Cell Tissue Res., **235:** 403 - 410.

Abraham, M. et al. 1993 Muco-follicle cells of the jelly coat in the oocyte envelope of the sheatfish *(Silurus glanis* L.). J. Morphol., **217:** 37 - 43.

Afzelius, B.A., L. Nicander, and I. Sjödén 1968 Fine structure of egg envelopes and the activation changes of cortical alevoli in the river lamprey, *Lampetra fluviatilis.* J. Embryol. Exper. Morphol., **19:** 311 - 318.

Alderdice, D.F., J.O.T. Jensen, and F.P.J. Velsen 1984 Measurement of hydrostatic pressure in salmonid eggs. Can. J. Zool., **62:** 1977 - 1987.

Aldridge, D.C. 1999 Development of European bitterling in the gills of freshwater mussels. J. Fish Biol., **54:** 138 - 151.

Amanze, D., and A. Iyengar 1990 The micropyle: a sperm guidance system in telost fertilization. Development, **109:** 495 - 500.

Anderson, E. 1967 The formation of the primary envelope during oocyte differentiation in teleosts. J. Cell Biol., **35:** 193 - 212.

Anderson, E. 1968 Cortical alveoli formation and vitellogenesis during oocyte differentiation in the pipefish, *Syngnathus fuscus* and the killifish, *Fundulus heteroclitus.* J. Morphol., **125:** 23 - 60.

Andreuccetti, P. et al. 1999 Intercellular bridges between granulosa cells and the oocyte in the elasmobranch *Raya asterias.* Anat. Rec., **255:** 180 - 187.

Aravindan, C.M., and K.G. Padmanabhan 1972 Formation of the micropyle in *Tilapia mossambica* Peters and *Stigmatogobius javanicus* (Blkr.). Acta Zool. (Stockh.), **53:** 45 - 47.

Asahina, K., K. Taguchi, and T. Hibiya 1987 *In vitro* effect of various steroids on final maturation in oocytes of agohaze-gobi *Chasmichthys dolichognathus* and Chichibu-goby *Tridentiger obscurus. In* Proceedings of the First Congress of the Asia and Oceania Society for Comparative Endocrinology (AOSCE), E. Ohnishi, Y. Nagahama, and H. Ishizaki eds. Nagoya: Nagoya University Corp., Printing Section, pp. 147 - 148.

Atz, J.W., 1964 Intersexuality in fishes, Chapter 3 *in* Intersexuality in Vertebrates Including Man, C.N. Armstrong and A.J. Marshall eds. London: Academic Press, pp. 145 - 232.

Azevedo, C. 1974 Évolution des enveloppes ovocytaires, au cours de l'ovogenèse chez un Téléostéen vivipare, *Xiphophorus helleri.* J. Microsc. (Paris), **21:** 43 - 54.

Azevedo, C., and A. Coimbra 1980 Evolution of nucleoli in the course of oogenesis in a viviparous teleost *(Xiphophorus helleri).* Biol. Cell., **38:** 43 - 48.

Babu, N., and N.B. Nair 1983 Follicular atresia in *Amblypharyngodon chakaiensis.* Z. Mikrosk.-Anat. Forsch., **97:** 499 - 504.

Bagenal, T.B., and E. Braum 1971 Eggs and early life history. Chapter 7 *in* Methods for Assessment of Fish Production in Fresh Waters, IBP Handbook no. 3, 2nd ed., W.E. Ricker, ed. Oxford: Blackwell Scientific Publications, pp. 166 - 198.

Ball, J.N. 1960 Reproduction in female bony fishes. Symp. Zool. Soc. London, **1:** 105 - 135.

Bara, G. 1965 Histochemical localization of Δ^5-3β-hydroxysteroid dehydrogenase in the ovaries of a teleost fish, *Scomber scomber* L. Gen. Comp. Endocrinol., **5:** 284 - 296.

Bara, G. 1974 Location of steroid hormone production in the ovary of *Trachurus mediterraneus.* Acta Histochem., **51:** 90 - 101.

Bartsch, P., and R. Britz 1997 A single micropyle in the eggs of the most basal living actinopterygian fish, *Polypterus* (Actinopterygii, Polypteriformes). J. Zool. Lond., **241:** 589 - 592.

Beams, H.W., and R.G. Kessel 1973 Oocyte structure and early vitellogenesis in the trout, *Salmo gairdneri.* Am. J. Anat., **136**: 105 - 122.

Begovac, P.C., and R.A. Wallace 1987 Ovary of the pipefish, *Syngnathus scovelli.* J. Morphol., **193:** 117 - 133.

Begovac, P.C., and R.A. Wallace 1988 Stages of oocyte development in the pipefish, *Syngnathus scovelli*. J. Morphol., **197:** 353 - 369.

Begovac, P.C., and R.A. Wallace 1989 Major vitelline envelope proteins in pipefish oocytes originate within the follicle and are associated with the Z3 layer. J. Exper. Zool., **251:** 56 - 73.

Bern, O., and R.R. Avtalion 1990 Some morphological aspects of fertilization in tilapias. J. Fish Biol., **36:** 375 - 381.

Berndtson, A.K., and F.W. Goetz 1986 Investigations on the control of *in vitro* spontaneous brook trout *(Salvelinus fontinalis)* ovulation. Gen. Comp. Endocrinol., **61:** 134 - 141.

Berndtson, A.K., and F.W. Goetz 1988 Protease activity in brook trout *(Salvelinus fontinalis)* follicle walls demonstrated by substrate-polyacrylamide gel electrophoresis. Biol. Reprod., **38:** 511 - 516.

Berndtson, A.K., and F.W. Goetz 1990 Metallo-protease activity increases prior to ovulation in brook trout *(Salvelinus fontinalis)* and yellow perch *(Perca flavescens)* follicle walls. Biol. Reprod., **42:** 391 - 398.

Berndtson, A.K., F.W. Goetz, and P. Duman 1989 *In vitro* ovulation, prostaglandin synthesis, and proteolysis in isolated ovarian components of yellow perch *(Perca flavescens):* effects of 17α,20β-dihydroxy-4-pregnen-3-one and phorbol ester. Gen. Comp. Endocrinol., **75:** 454 - 465.

Besseau, L., and E. Faliex 1994 Resorption of unemitted gametes in *Lithognathus mormyrus* (Sparidae: Teleostei): a possible synergic action of somatic and immune cells. Cell Tissue Res., **276:** 123 - 132.

Billard, R., and R. Breton 1978 Rhythms of reproduction in teleost fish. *In* Rhythmic Activity of Fishes, J.E. Thorpe, ed. London: Academic Press Inc., pp. 31 - 53.

Braekevelt, C.R., and D.B. McMillan 1967 Cyclic changes in the ovary of the brook stickleback *Eucalia inconstans* (Kirtland). J. Morphol., **123:** 373 - 396.

Breder, C.M. Jr., and D.E. Rosen 1966 Modes of Reproduction in Fishes. New York: Natural History Press, 941 pp.

Bretschneider, L.H., and J.J. Duyvené de Wit 1947 Sexual Endocrinology of Non-mammalian Vertebrates. New York: Elsevier Publishing Company, Inc.

Britz, R. 1997 Egg surface structure and larval cement glands in nandid and badid fishes with remarks on phylogeny and biogeography. American Museum Novitates, no. 3195.

Britz, R., M. Kokoscha, and R. Riehl 1995 The anabantoid genera, *Ctenops, Luciocephalus, Parasphaerichthys,* and *Sphaerichthys* (Teleostei: Perciformes) as a monophyletic group: evidence from egg surface structure and reproductive behaviour. Jap. J. Ichthyol., **42:** 71 - 79.

Brivio, M.F., R. Bassi, and F. Cotelli 1991 Identification and characterization of the major components of the *Oncorhynchus mykiss* egg chorion. Mol. Repr. Dev., **28:** 85 - 93.

Browning, H.C. 1973 The evolutionary history of the corpus luteum. Biol. Reprod., **8:** 128 - 157.

Brummett, A., and J. Dumont 1979 Initial stages of sperm penetration into the egg of *Fundulus heteroclitus.* J. Exper. Zool., **210:** 417 - 434.

Brummett, A., and J. Dumont 1981 Cortical vesicle breakdown in fertilized eggs of *Fundulus heteroclitus.* J. Exper. Zool., **216:** 63 - 79.

Brummett, A.R., J.N. Dumont, and J.R. Larkin 1982 The ovary of *Fundulus heteroclitus.* J. Morphol., **173:** 1 - 16.

Brummett, A.R., J.N. Dumont, and C.S. Richter 1985 Later stages of sperm penetration and second polar body and blastodisc formation in the egg of *Fundulus heteroclitus.* J. Exper. Zool., **234:** 423 - 439.

Bruslé, S. 1980 Fine structure of early previtellogenic oocytes in *Mugil (Liza) auratus* Risso, 1810 (Teleostei, Mugilidae). Cell Tissue Res., **207:** 123 - 134.

Bruslé, S. 1985 Fine structure of oocytes and their envelopes in *Chelon labrosus* and *Liza aurata* (Teleostei, Mugilidae). Zool. Sci., **2:** 681 - 693.

Bruslé, S., and J. Bruslé 1978 An ultrastructural study of early germ cells in *Mugil (Liza) auratus* Risso, 1810 (Teleostei: Mugilidae). Ann. Biol. Anim. Biochim. Biophys., **18:** 1141 - 1153.

Burns, J.R. et al. 1995 Internal fertilization, testis and sperm morphology in glandulocaudine fishes (Teleostei: Characidae: Glandulocaudinae). J. Morphol., **224:** 131 - 145.

Busson-Mabillot, S. 1966 Présence d'une thèque interne, glandulaire, dans le follicule primaire de la Lamproie de Planer *(L. planeri* Bloch), Vertébré cyclostome. C.R. Acad. Sci. Paris, Sér. D, **262:** 117 - 118.

Busson-Mabillot, S. 1967a Structure ovarienne chez la Lamproie adulte *Lampetra planeri* (Bloch). I. La zone pellucide. Morphogenèse et constitution histochimique. J. Microsc. (Paris), **6:** 577 - 598.

Busson-Mabillot, S. 1967b Structure ovarienne de la Lamproie adulte *(Lampetra planeri* Bloch). II. Les enveloppes de l'ovocyte: cellules folliculaires et stroma ovarien. J. Microsc. (Paris), **6:** 807 - 838.

Busson-Mabillot, S. 1967c Structure ovarienne chez la Lamproie de Planer adulte, *Lampetra planeri* (Bloch). Arch. Zool. Expér. Gen., **108:** 423 - 446.

Busson-Mabillot, S. 1973 Évolution des enveloppes de l'ovocyte et de l'oeuf chez un Poisson Téléostéen. J. Microsc. (Paris), **18:** 23 - 44.

Busson-Mabillot, S. 1977 Un type particulier de sécrétion exocrine: celui de l'appareil adhésif de l'oeuf d'un poisson Téléostéen. Biol. Cell., **30:** 233 - 244.

Busson-Mabillot, S. 1984 Endosomes transfer yolk proteins to lysosomes in the vitellogenic oocyte of the trout. Biol. Cell., **51:** 53 - 66.

Callard, I.P. et al. 1989 Endocrine regulation of reproduction in elasmobranchs: archetype for terrestrial vertebrates. J. Exper. Zoo. Suppl., **2:** 12 - 22.

Callard, I.P., L.A. Fileti, and T.J. Koob 1993 Ovarian steroid synthesis and the hormonal control of the elasmobranch reproductive tract. Env. Biol. Fishes, **38:** 175 - 185.

Callard, I., and T.J. Koob 1993 Endocrine regulation of the elasmobranch reproductive tract. J. Exper. Zool., **266:** 368 - 377.

Caporiccio, B., and R. Connes 1977 Étude ultrastructurale des enveloppes périovocytaires et périovulaires de *Dicentrarchus labrax* L. (Poisson, Téléostéen). Ann. Sci. Nat. Zool., **19:** 351 - 368.

Castro, J.I., and J.P. Wourms 1993 Reproduction, placentation, and embryonic development of the Atlantic sharpnose shark, *Rhizoprionodon terraenovae.* J. Morphol., **218:** 257 - 280.

Chan, S.T.H., A. Wright, and J.G. Phillips 1967 The atretic structures in the gonads of the rice-field eel *(Monopterus albus)* during natural sex-reversal. J. Zool. Lond., **153:** 527 - 539.

Chan, S.T.H., and W.S.B. Yeung 1983 Sex control and sex reversal in fish under natural conditions. Chapter 4 *in* Fish Physiology, vol. IXB, W.S. Hoar, D.J. Randall, and E.M. Donaldson, eds. New York: Academic Press, Inc., pp. 171 - 222.

Chen, K.C., K.T. Shao, and J.S. Yang 1999 Using micropylar ultrastructure for species identification and phylogenetic inference among four species of Sparidae. J. Fish Biol., **55:** 288 - 300.

Cherr, G.N., and W.H. Clark, Jr. 1982 Fine structure of the envelope and micropyles in the eggs of the white sturgeon, *Acipenser transmontanus* Richardson. Develop. Growth Differ., **24:** 341 - 352.

Cherr, G.N., and W.H. Clark, Jr. 1984 An acrosome reaction in sperm from the white sturgeon, *Acipenser transmontanus.* J. Exper. Zool., **232:** 129 - 139.

Cherr, G.N., and W.H. Clark, Jr. 1985 An egg envelope component induces the acrosome reaction in sturgeon sperm. J. Exper. Zool., **234:** 75 - 85.

Chieffi, G. 1962 Integration of reproductive functions II: Endocrine aspects of reproduction in elasmobranch fishes. Gen. Comp. Endocrinol., Suppl. **1:** 275 - 285.

Chieffi, G. 1967 The reproductive system of elasmobranchs: developmental and endocrinological aspects. Chapter 37 *in* Sharks, Skates, and Rays, P.W. Gilbert, R.F. Mathewson, and D.P. Rall, eds. Baltimore: The Johns Hopkins Press, pp. 553 - 580.

Chieffi Baccari, G. et al. 1992 Ultrastructural investigation of the corpora atretica of the electric ray, *Torpedo marmorata.* Gen. Comp. Endocrinol., **86:** 72 - 80.

Clérot, J.-C. 1976 Les groupements mitochondriaux des cellules germinales des poissons Téléostéens Cyprinidés. I. Étude ultrastructurale. J. Ultrastruct. Res., **54:** 461 - 475.

Coello, S., and A.S. Grimm 1990 Development of Balbiani's vitelline body in the oocytes of the Atlantic mackerel, *Scomber scombrus* L. J. Fish Biol., **36:** 265 - 267.

Cornish, D.A. 1985 An autoradiographic study of the transfer of nutrients to the embryos of the teleost *Clinus dorsalis.* S. Afr. J. Sci., **81:** 393 - 394.

Cornish, D.A., and W.J. Veith 1987 The chemical composition of the follicular fluid of the teleost *Clinus dorsalis* (Perciformes: Clinidae). Comp. Biochem. Physiol., **88A:** 599 - 602.

Cotelli, F. et al. 1986 Studies on the composition, structure and differentiation of fish egg chorion. Cell Biol. Int. Repts., **10:** 471.

Cotelli, F. et al. 1988 Structure and composition of the fish egg chorion *(Carassius auratus).* J. Ultrastruct. Molec. Struct. Res., **99:** 70 - 78.

Coux, Olivier, Keiji Tanaka, and Alfred L. Goldberg 1996 Structure and functions of the 20S and 26S proteasomes. Ann. Rev. Biochem., **65:** 801 - 847.

Craik, J.C.A. 1978a The effects of oestrogen treatment on certain plasma constituents associated with vitellogenesis in the elasmobranch *Scyliorhinus canicula* L. Gen. Comp. Endocrinol., **35:** 455 - 464.

Craik, J.C.A. 1978b Plasma levels of vitellogenin in the elasmobranch *Scyliorhinus canicula* L. (lesser spotted dogfish). Comp. Biochem. Physiol., **60B:** 9 - 18.

Craik, J.C.A. 1978c Effects of hypophysectomy on vitellogenesis in the elasmobranch *Scyliorhinus canicula* L. Gen. Comp. Endocrinol., **36:** 63 - 67.

Craik, J.C.A. 1978d An annual cycle of vitellogenesis in the elasmobranch *Scyliorhinus canicula.* J. Marine Biol. Assoc. U.K., **58:** 719 - 726.

Craik, J.C.A. 1978e Kinetic studies of vitellogenin metabolism in the elasmobranch *Scyliorhinus canicula* L. Comp. Biochem. Physiol., **61A:** 355 - 361.

Craik, J.C.A., and S.M. Harvey 1984 Biochemical changes occurring during final maturation of eggs of some marine and freshwater teleosts. J. Fish Biol., **24:** 599 - 610.

Craik, J.C.A., and S.M. Harvey 1986 Phosphorus metabolism and water uptake during final maturation of ovaries of teleosts with pelagic and demsersal eggs. Marine Biol., **90:** 285 - 289.

Davenport, J., S. Lønning, and E. Kjørsvik 1981 Osmotic and structural changes during early development of eggs and larvae of the cod, *Gadus morhua* L. J. Fish Biol., **19:** 317 - 331.

Davenport, J., S. Lønning, and E. Kjørsvik 1986 Some mechanical and morphological properties of the chorions of marine teleost eggs. J. Fish Biol., **29:** 289 - 301.

Dépêche, J. 1973 Infrastructure superficielle de la vésicule vitelline et du sac péricardique de l'embryon de *Poecilia reticulata* (Poisson Téléostéen). Application à l'étude du rôle de "cellules à chlorure" dans l'osmoregulation embryonnaire. Z. Zellforsch. Mikrosc. Anat., **141:** 235 - 253.

Dobbs, G.H. 1975 Scanning electron microscopy of intraovarian embryos of the viviparous teleost, *Micrometrus minimus* (Gibbons), (Perciformes: Embiotocidae). J. Fish Biol., **7:** 209 - 214.

Dodd, J.M. 1977 The structure of the ovary of nonmammalian vertebrates. Chapter 5 *in* The Ovary, 2nd ed., vol. I: General Aspects. S. Zuckerman and B.J. Weir, eds. New York: Academic Press, pp. 219 - 263.

Dodd, J.M. 1983 Reproduction in cartilaginous fishes (Chondrichthyes). Chapter 2 *in* Fish Physiology, vol. IXA, W.S. Hoar, D.J. Randall, and E.M. Donaldson, eds. New York: Academic Press, Inc., pp. 31 - 95.

Dodd, J.M., and M.H.I. Dodd 1985 Evolutionary aspects of reproduction in cyclostomes and cartilaginous fishes, *in* Evolutionary Biology of Primitive Fishes, vol. 103, NATO ASI Series, Series A: Life Sciences. New York: Plenum Press, pp. 295 - 319.

Dodd, M.H.I., and J.M. Dodd 1980 Ultrastructure of the ovarian follicle of the dogfish *Scyliorhinus canicula.* Gen. Comp. Endocrinol., **40:** 330 - 331.

Dodd, J.M., and J.P. Sumpter 1984 Fishes, Chapter 1 *in* Marshall's Physiology of Reproduction, 4th ed., vol. 1, G.E. Lamming, ed. Edinburgh: Churchill Livingstone, pp. 1 - 126.

Donovan, M.J., and N.H. Hart 1982 Uptake of ferritin by the mosaic egg surface of *Brachydanio.* J. Exper. Zool., **223:** 299 - 304.

Donovan, M.J., and N.H. Hart 1986 Cortical granule exocytosis is coupled with membrane retrieval in the egg of *Brachydanio rerio.* J. Exper. Zool., **237:** 391 - 405.

Droller, M.J., and T.F. Roth 1966 An electron microscope study of yolk formation during oogenesis in *Lebistes reticulatus* Guppyi. J. Cell Biol., **28:** 209 - 232.

Drummond, C.D. et al. 2000 Postovulatory follicle: a model for experimental studies of programmed cell death or apoptosis in teleosts. J. Exper. Zool., **287:** 176 - 182.

Duffey, R.J., and F.W. Goetz 1980 The *in vitro* effects of 17α-hydroxy-20β-dihydroprogesterone on germinal vesicle breakdown in brook trout *(Salvelinus fontinalis)* oocytes. Gen. Comp. Endocrinol., **41:** 563 - 565.

Dumont, J.N., and A.R. Brummet 1980 The vitelline envelope, chorion, and micropyle of *Fundulus heteroclitus* eggs. Gamete Res., **3:** 25 - 44.

Erickson, D.L., and E.K. Pikitch 1993 A histological description of shortspine thornyhead, *Sebastolobus alascanus,* ovaries: structures associated with the production of gelatinous egg masses. Environ. Biol. Fishes, **36:** 273 - 282.

Fänge, R. 1977 Size relations of lymphomyeloid organs in some cartilaginous fish. Acta Zool. (Stockh.), **58:** 125 - 128.

Fänge, R., and A. Mattisson 1981 The lymphomyeloid (hemopoietic) system of the Atlantic nurse shark, *Ginglymostoma cirratum.* Biol. Bull., **160:** 240 - 249.

Fänge, R., and A. Pulsford 1983 Structural studies on lymphomyeloid tissues of the dogfish, *Scyliorhinus canicula* L. Cell Tissue Res., **230:** 337 - 351.

Fasano, S., R. Pierantoni, and G. Chieffi 1989 Reproductive biology of elasmobranchs with emphasis on endocrines. J. Exper. Zool., Suppl. **2:** 53 - 61.

Feng, D., and D.P. Knight 1992 Secretion and stabilization of the layers of the egg capsule of the dogfish *Scyliorhinus canicula.* Tissue & Cell, **24:** 773 - 790.

Feng, D., and D.P. Knight 1994a The effect of pH on fibrillogenesis of collagen in the egg capsule of the dogfish, *Scyliorhinus canicula.* Tissue & Cell, **26:** 649 - 659.

Feng, D., and D.P. Knight 1994b Structure and formation of the egg capsule tendrils in the dogfish *Scyliorhinus canicula.* Phil. Trans. Roy. Soc. London, B, **343:** 285 - 302.

Fernholm, B. 1972 Is there any steroid hormone formation in the ovary of the hagfish, *Myxine glutinosa?* Acta Zool. (Stockh.), **53:** 235 - 242.

Fernholm, B. 1975 Ovulation and eggs of the hagfish *Eptatretus burgeri.* Acta Zool. (Stockh.), **56:** 199 - 204.

Fishelson, L. 1977 Ultrastructure of the epithelium from the ovary wall of *Dendrochirus brachypterus* (Pteroidae, Teleostei). Cell Tissue Res., **177:** 375 - 381.

Flegler, C. 1977 Electron microscopic studies on the development of the chorion of the viviparous teleost *Dermogenys pusillus* (Hemirhamphidae). Cell Tissue Res., **179:** 255 - 270.

Flügel, H. 1964a Electron microscopic investigations on the fine structure of the follicular cells and the zona radiata of trout oocytes during and after ovulation. Naturwissenschaften, **51:** 564 - 565.

Flügel, H. 1964b Desmosomes in the follicular epithelium of growing oocytes of the eastern brook trout *Salvelinus fontinalis* (electron microscopic investigations). Naturwissenschaften, **51:** 566.

Flügel, H. 1967a Elektronenmikroskopische Untersuchungen an den Hüllen der Oozyten und Eier des Flußbarsches *Perca fluviatilis.* Z. Zellforsch. Mikrosk. Anat., **77:** 244 - 256.

Flügel, H. 1967b Licht- und elektronenmikroskopische Untersuchungen an Oozyten und Eiern einiger Knochenfische. Z. Zellforsch. Mikrosk. Anat., **83:** 82 - 116.

Foscarini, R. 1989 A comparative study of the skin and gill structure in oviparous and viviparous freshwater fish larvae. J. Fish Biol., **34:** 31 - 40.

Franchi, L.L. 1962 The structure of the ovary. Chapter 2B *in* The Ovary, vol. 1, S. Zuckerman, ed. London: Academic Press, pp. 121 - 142.

Franchi, L.L., A.M. Mandl, and S. Zuckerman 1962 The development of the ovary and the process of oogenesis. Chapter 1 *in* The Ovary, vol. 1, S. Zuckerman, ed. London: Academic Press, pp. 1 - 88.

Fraser, E.A., and R.M. Renton 1940 Observation on the breeding and development of the viviparous fish, *Heterandria formosa.* Quart. J. Microsc. Sci., **81:** 479 - 520.

Fujita, T., A. Takemura, and K. Takano 1998 Immunochemical detection of precursor proteins of yolk and vitelline envelope, and their annual changes in the blood of *Diodon holocanthus.* J. Fish Biol., **52:** 1229 - 1240.

Fukada, S. et al. 1994 Steroidogenesis in the ovarian follicle of medaka *(Oryzias latipes,* a daily spawner) during oocyte maturation. Develop. Growth Differ., **36:** 81 - 88.

Gardiner, D.M. 1978 Cyclic changes in fine structure of the epithelium lining the ovary of the viviparous teleost, *Cymatogaster aggregata* (Perciformes: Embiotocidae). J. Morphol., **156:** 367 - 380.

Geraudie, J., and S. Chilmonczyk 1976 Étude comparative du repli natatoire d'un embryon de téléostéen ovipaire *(Salmo gairdneri)* et d'un embryon de téléostéen vivipaire *(Goodea atripinnis).* Bull. Soc. Zool. Fr., **101:** 481 - 488.

Gevers, P. et al. 1992 Origin of primordial germ cells, as characterized by the presence of nuage, in embryos of the teleost fish *Barbus conchonius.* Eur. J. Morphol., **30:** 195 - 204.

Giersberg, H., and P. Rietschel 1968 Vergleichende Anatomie der Wirbeltiere, vol. 2. Jena: Gustav Fischer. As cited by van Tienhoven, 1983.

Gilbert, P.W., and D.A. Schlernitzauer 1966 The placenta and gravid uterus of *Carcharhinus falciformis.* Copeia, **1966:** 451 - 457.

Gilkey, J.C. et al. 1978 A free calcium wave traverses the activating egg of the medaka, *Oryzias latipes.* J. Cell Biol., **76:** 448 - 466.

Gilkey, J.C. 1981 Mechanism of fertilization in fishes. Am. Zool., **21:** 359 - 375.

Ginsburg, A. 1961 The block to polyspermy in sturgeon and trout with special reference to the role of cortical granules (alveoli). J. Embryol. Exper. Morphol., **9:** 173 - 190.

Ginsburg, A.S., and T.A. Dettlaff 1991 The Russian sturgeon *Acipenser güldenstädti.* Part I. Gametes and early development up to time of hatching. Chapter 2 *in* Animal Species for Developmental Studies, vol. 2: Vertebrates, T.A. Dettlaff and S.G. Vassetzky, eds. New York: Consultants Bureau, pp. 15 - 65.

Giulianini, P.G. et al. 2001 Can goby spermatozoa pass through the filament adhesion apparatus of laid eggs? J. Fish Biol., **58:** 1750 - 1752.

Giulianini, P.G., and E.A. Ferrero 2000 Ultrastructural aspects of the ovarian follicle and egg envelope of the sea-grass goby *Zosterisessor ophiocephalus* (Osteichthyes, Gobiidae). Ital. J. Zool., **68:** 29 - 37.

Goetz, F.W. 1983 Hormonal control of oocyte final maturation and ovulation in fishes. Chapter 3 *in* Fish Physiology, vol. IXB, W.S. Hoar, D.J. Randall, and E.M. Donaldson, eds. New York: Academic Press, Inc., pp. 117 - 170.

Goetz, F.W. et al. 1987 The mechanism and hormonal regulation of ovulation: the role of prostaglandins in teleost ovulation. *In* Proceedings of the Third International Symposium on the Reproductive Physiology of Fish, St. John's Newfoundland, Canada, D.R. Idler, L.W. Crim, and J.M. Walsh, eds., pp. 235 - 238.

Goetz, F.W. et al. 1989a The role of prostaglandins in the control of ovulation in yellow perch, *Perca flavescens.* Fish Physiol. Biochem., **7:** 163 - 168.

Goetz, F.W. et al. 1989b Prostaglandin F and E synthesis by specific tissue components of the brook trout *(Salvelinus fontinalis)* ovary. J. Exper. Zool., **250:** 196 - 205.

Goetz, F.W., and G. Theofan 1979 *In vitro* stimulation of germinal vesicle breakdown and ovulation of yellow perch *(Perca flavescens)* oocytes. Effects of 17α,20β-dihydroprogesterone and prostaglandins. Gen. Comp. Endocrinol., **37:** 273 - 285.

Goodrich, E.S. 1930 Studies on the Structure & Development of Vertebrates. London: Macmillan and Co., Limited. 837 pp.

Gothilf, Y. et al. 1997 Preovulatory changes in the levels of three gonadotropin-releasing hormone-encoding messenger ribonucleic acids (mRNAs), gonadotropin β-subunit mRNAs, plasma gonadotropin, and steroids in the female gilthead seabream, *Sparus aurata.* Biol. Reprod., **57:** 1145 - 1154.

Götting, K.-J. 1965 Die Feinstruktur der Hüllschichten reifender Oocyten von *Agonus cataphractus* L. (Teleostei, Agonidae). Z. Zellforsch. Mikrosk. Anat., **66:** 405 - 414.

Götting, K.-J. 1967 Der Follikel und die peripheren Strukturen der Oocyten der Teleosteer und Amphibien. Eine vergleichende Betrachtung auf der Grundlage elektronenmikroskopischer Untersuchungen. Z. Zellforsch. Mikrosk. Anat., **79:** 481 - 491.

Grandi, G., and G. Colombo 1997 Development and early differentiation of gonad in the European eel *(Anguilla anguilla* [L.], Anguilliformes, Teleostei): a cytological and ultrastructural study. J. Morphol., **231:** 195 - 216.

Greeley, M.S. et al. 1986 Oocyte maturation in the mummichog *(Fundulus heteroclitus):* effects of steroids on germinal vesicle breakdown of intact follicles *in vitro.* Gen. Comp. Endoctrinol., **62:** 281 - 289.

Greeley, M.S., D.R. Calder, and R.A. Wallace 1986 Changes in teleost yolk proteins during oocyte maturation: correlation of yolk proteolysis with oocyte hydration. Comp. Biochem. Physiol., **84B:** 1 - 9.

Grier, H. 2000 Ovarian germinal epithelium and folliculogenesis in the common snook, *Centropomus undecimalis* (Teleostei: Centropomidae). J. Morphol., **243:** 265 - 281.

Grierson, J.P., and A.C. Neville 1981 Helicoidal architecture of fish egg-shell. Tissue & Cell, **13:** 819 - 830.

Greenwood, P.H. 1975 J.R. Norman: a History of Fishes, 3rd ed. London: Ernest Benn Limited, 467 pp.

Große Wichtrup, L., and H. Greven 1985 Uptake of ferritin by the trophotaeniae of the goodeid fish. *Ameca splendens* Miller and Fitzsimons 1971 (Teleostei, Cyprinodontiformes). Cytobios, **42:** 33 - 40.

Große Wichtrup, L., and H. Greven 1986 Ultrastructural aspects of the trophotaenial epithelium in *Ameca splendens* Miller and Fitzsimons (Teleostei, Cyprinodontiformes) revealed by electron dense stains. Cytobios, **45:** 175 - 183.

Grove, B.D., and J.P. Wourms 1991 The follicular placenta of the viviparous fish, *Heterandria formosa.* I. Ultrastructure and development of the embryonic absorptive surface. J. Morphol., **209:** 265 - 284.

Grove, B.D., and J.P. Wourms 1994 Follicular placenta of the viviparous fish, *Heterandria formosa.* II. Ultrastructure and development of the follicular epithelium. J. Morphol., **220:** 167 - 184.

Guraya, S.S. 1963 Histochemical studies on the yolk-nucleus in fish oogenesis. Z. Zellforsch. Mikrosk. Anat., **60:** 659 - 666.

Guraya, S.S. 1972 Histochemical observations on the interstitial gland cells of dogfish ovary. Gen. Comp. Endocrinol., **18:** 409 - 412.

Guraya, S.S. 1979 Recent advances in the morophology, cytochemistry, and function of Balbiani's vitelline body in animal oocytes. Int. Rev., Cytol., **59:** 249 - 321.

Guraya, S.S. 1982 Recent progress in the structure, origin, composition, and function of cortical granules in animal egg. Int. Rev. Cytol., **78:** 257 - 360.

Guraya, S.S. 1986 The Cell and Molecular Biology of Fish Oogenesis. Monographs in Developmental Biology, vol. 18, H.W. Sauer, ed. Basel: S. Karger AG, 223 pp.

Guraya, S.S., and S. Kaur 1982 Cellular sites of steroid synthesis in the oviparous teleost fish *(Cyprinus carpio* L.): a histochemical study. Proc. Indian Acad. Sci. (Anim. Sci.), **91:** 587 - 597.

Hagenmaier, H.E. 1973 The hatching process in fish embryos: III. The structure, polysaccharide and protein cytochemistry of the chorion of the trout egg, *Salmo gairdneri* (Rich.). Acta Histochem., **47:** 61 - 69.

Hagiwara, S., and L.A. Jaffe 1979 Electrical properties of egg cell membranes. Ann. Rev. Biophys. Bioeng., **8:** 385 - 416.

Häcker, G. 2000 The morphology of apoptosis. Cell Tissue Res., **301:** 5 - 17.

Haider, S. 1990 Further experimental evidence in support of the involvement of ovarian follicles in oocyte maturation of the Indian catfish, *Mystus vittatus.* Gen. Comp. Endocrinol., **80:** 80 - 84.

Hamaguchi, S. 1982 A light- and electron-microscopic study on the migration of primordial germ cells in the teleost, *Oryzias latipes.* Cell Tissue Res., **227:** 139 - 151.

Hamaguchi, S. 1985 Changes in the morphology of the germinal dense bodies in primordial germ cells of the teleost, *Oryzias latipes.* Cell Tissue Res., **240:** 669 - 673.

Hamazaki, T.S. et al. 1989 A glycoprotein from the liver constitutes the inner layer of the egg envelope (zona pellucida interna) of the fish, *Oryzias latipes.* Dev. Biol., **133:** 101 - 110.

Hamazaki, T., I. Iuchi, and K. Yamagami 1985 A spawning female-specific substance reactive to anti-chorion (egg-envelope) glycoprotein antibody in the teleost, *Oryzias latipes.* J. Exper. Zool., **235:** 269 - 279.

Hamazaki, T.S., I. Iuchi, and K. Yamagami 1987 Production of a "spawning female-specific substance" in hepatic cells and its accumulation in the ascites of the estrogen-treated adult fish, *Oryzias latipes.* J. Exper. Zool., **242:** 325 - 332.

Hamlett, W.C. 1986 Prenatal absorptive surfaces in selachians. *In* Indo-Pacific Fish Biology: Proceedings of the Second International Conference on Indo-Pacific Fishes. T. Uyeno, R. Arai, T. Taniuchi, and K. Matsuura, eds. Tokyo: Ichthyological Society of Japan, pp. 333 - 344.

Hamlett, W.C. 1987 Comparative morphology of the elasmobranch placental barrier. Arch. Biol. (Brux.), **98:** 135 - 162.

Hamlett, W.C. 1989 Evolution and morphogenesis of the placenta in sharks. J. Exper. Zool., Suppl. **2:** 35 - 52.

Hamlett, W.C. 1993 Ontogeny of the umbilical cord and placenta in the Atlantic sharpnose shark, *Rhizoprionodon terraenovae.* Environ. Biol. Fishes, **38:** 253 - 267.

Hamlett, W.C. et al. 1985 Permeability of external gill filaments in the embryonic shark. Electron microscopic observations using horseradish peroxidase as a macromolecular tracer. J. Submicrosc. Cytol., **17:** 31 - 40.

Hamlett, W.C. et al. 1993a Uterogestation and placentation in elasmobranchs. J. Exper. Zool., **266:** 347 - 367.

Hamlett, W.C.et al. 1993b Fine structure of the term umbilical cord in the Atlantic sharpnose shark, *Rhizoprionodon terraenovae.* J. Submicrosc. Cytol. Pathol., **25:** 547 - 557.

Hamlett, W.C. et al. 1996a Ultrastructure of uterine trophonemata, accommodation for uterolactation, and gas exchange in the southern stingray, *Dasyatis americana.* Can. J. Zool., **74:** 1417 - 1430.

Hamlett, W.C. et al. 1996b Ultrastructure of the oviducal gland in the yellow spotted stingray, *Urolophus jamaicensis* with observations on a novel inclusion. J. Anat., **188:** 224 - 225.

Hamlett, W.C. et al. 1998a Survey of oviducal gland structure and function in elasmobranchs. J. Exper. Zool., **282:** 399 - 420.

Hamlett, W.C. et al. 1998b Reproductive accommodations for gestation in the Atlantic guitarfish, *Rhinobatos lentiginosus,* Rhinobatidae. J. Elisha Mitchell Sci. Soc., **114:** 199 - 208.

Hamlett, W.C., and M.K. Hysell 1998 Uterine specializations in elasmobranchs. J. Exper. Zool., **282:** 438 - 459.

Hamlett, W.C., M. Jezior, and R. Spieler 1999 Ultrastructural analysis of folliculogenesis in the ovary of the yellow spotted stingray, *Urolophus jamaicaensis.* Ann. Anat., **181:** 159 - 172.

Hamlett, W.C., and T.J. Koob 1999 Female reproductive system. Chapter 15 *in* Sharks, Skates, and Rays: the Biology of Elasmobranch Fishes, W.C. Hamlett, ed. Baltimore: The Johns Hopkins University Press, pp. 398 - 443.

Hamlett, W.C., M.A. Miglino, and L.J.A. DiDio 1993 Subcellular organization of the placenta in the Atlantic sharpnose shark, *Rhizoprionodon terraenovae.* J. Submicrosc. Cytol. Pathol., **25:** 535 - 545.

Hamlett, W.C., F.J. Schwartz, and L.J.A. DiDio 1987 Subcellular organization of the yolk syncytial-endoderm complex in the preimplantation yolk sac of the shark, *Rhizoprionodon terranovae.* Cell Tissue Res., **247:** 275 - 285.

Hamlett, W.C., and J.P. Wourms 1984 Ultrastructure of the pre-implantation shark yolk sac placenta. Tissue & Cell, **16:** 613 - 625.

Hamlett, W.C., J.P. Wourms, and J.S. Hudson 1985a Ultrastructure of the full-term shark yolk sac placenta. I. Morphology and cellular transport at the fetal attachment site. J. Ultrastruct. Res., **91:** 192 - 206.

Hamlett, W.C., J.P. Wourms, and J.S. Hudson 1985b Ultrastructure of the full-term shark yolk sac placenta. II. The smooth, proximal segment. J. Ultrastruct. Res., **91:** 207 - 220.

Hamlett, W.C., J.P. Wourms, and J.S. Hudson 1985c Ultrastructure of the full-term shark yolk sac placenta. III. The maternal attachment segment. J. Ultrastruct. Res., **91:** 221 - 231.

Hamlett, W.C., J.P. Wourms, and J.W. Smith 1985 Stingray placental analogues: structure of trophonemata in *Rhinoptera bonasus.* J. Submicrosc. Cytol., **17:** 541 - 550.

Harder, W. 1975 Anatomy of Fishes, Part I. Text; Part II. Figures and Plates. Stuttgart: E. Schweizerbart'sche Verlagsbuchhandlung, 612 pp.; 132 pp. and 13 plates.

Hardisty, M.W. 1971 Gonadogenesis, sex differentiation and gametogenesis. Chapter 8 *in* The Biology of Lampreys, vol. I, M.W. Hardisty and I.C. Potter, eds. London: Academic Press, Inc., pp. 295 - 359.

Hart, N.H. 1990 Fertilization in teleost fishes: mechanisms of sperm-egg interactions. Int. Rev. Cytol., **121:** 1 - 66.

Hart, N.H., and G.C. Collins 1991 An electron-microscope and freeze-fracture study of the egg cortex of *Brachydanio rerio.* Cell Tissue Res., **265:** 317 - 328.

Hart, N.H., and M. Donovan 1983 Fine structure of the chorion and site of sperm entry in the egg of *Brachydanio.* J. Exper. Zool., **227:** 277 - 296.

Hart, N.H., R. Pietri, and M. Donovan 1984 The structure of the chorion and associated surface filaments in *Oryzias* — evidence for the presence of extracellular tubules. J. Exper. Zool., **230:** 273 - 296.

Hart, N.H., and J.S. Wolenski 1988 Actin in the cortex of the teleost egg. J. Cell Biol., **107:** 174a.

Hart, N.H., and S.F. Yu 1980 Cortical granule exocytosis and cell surface reorganization in eggs of *Brachydanio.* J. Exper. Zool., **213:** 137 - 159.

Hart. N.H., S.-F. Yu, and V. Greenhut 1977 Observations on the cortical reaction in eggs of *Brachydanio rerio* as seen with the scanning electron microscope. J. Exper. Zool., **201:** 325 - 331.

Henderson, N.E. 1967 The urinary and genital systems of trout. J. Fish. Res. Bd. Canada, **24:** 447 - 449.

Hirai, A. 1988 Fine structures of the micropyles of pelagic eggs of some marine fishes. Jap. J. Ichthyol., **35:** 351 - 357.

Hirai, A. 1993 Fine structure of the egg membranes in four species of Pleuronectinae. Jap. J. Ichthyol., **40:** 227 - 235.

Hirai, A., and T. Yamamoto 1986 Micropyle in the developing eggs of the anchovy, *Engraulis japonica.* Jap. J. Ichthyol., **33:** 62 - 66.

Hirose, K. 1972 The ultrastructure of the ovarian follicle of medaka, *Oryzias latipes.* Z. Zellforsch. Mikrosk. Anat., **123:** 316 - 329.

Hirose, K. et al. 1975 *In vitro* bioconversions of steroids in the mature ovary of the hagfish, *Eptatretus burgeri.* Comp. Biochem. Physiol., **51B:** 403 - 408.

Hirose, K., and R. Ishida 1974 Effects of cortisol and human chorionic gonadotrophin (HCG) on ovulation in ayu *Plecoglossus altivelis* (Temminck & Schlegel) with special respect to water and ion balance. J. Fish Biol., **6:** 557 - 564.

Hisaw, F.L., Jr., and F.L. Hisaw 1959 Corpora lutea of elasmobranch fishes. Anat Rec., **135:** 269 - 277.

Hoar, W.S. 1955 Reproduction in teleost fish. Mem. Soc. Endocrinol., **4:** 5 - 24.

Hoar, W.S. 1957 The gonads and reproduction. Chapter VII *in* The Physiology of Fishes, vol. I, M.E. Brown, ed. New York: Academic Press, Inc., pp. 287 - 321.

Hoar, W.S. 1969 Reproduction. Chapter 1 *in* Fish Physiology, vol. III, W.S. Hoar and D.J. Randall, eds. New York: Academic Press, Inc., pp. 1 - 72.

Hoar, W.S., and Y. Nagahama 1978 The cellular sources of sex steroids in teleost gonads. Ann. Biol. Anim. Bioch. Biophys., **18:** 893 - 898.

Hogan, J.C. 1978 An ultrastructural analysis of "cytoplasmic markers" in germ cells of *Oryzias latipes.* J. Ultrastruct. Res., **62:** 237 - 250.

Hollenberg, F., and J.P. Wourms 1994 Ultrastructure and protein uptake of the embryonic trophotaeniae of four species of goodeid fishes (Teleostei: Atheriniformes). J. Morphol., **219:** 105 - 129.

Hollenberg, F., and J.P. Wourms 1995 Embryonic growth and maternal nutrient sources in goodeid fishes (Teleostei: Cyprinodontiformes). J. Exper. Zool., **271:** 379 - 394.

Hosokawa, K. 1983 Electron microscopic observation of the formation of the chorion in *Pagras major.* Zool. Mag., **92:** 77 - 89.

Hosokawa, K. 1985 Electron microscopic observation of chorion formation in the teleost, *Navodon modestus.* Zool. Sci., **2:** 513 - 522.

van den Hurk, R., and J. Peute 1979 Cyclic changes in the ovary of the rainbow trout, *Salmo gairdneri,* with special reference to sites of steroidogenesis. Cell Tissue Res., **199:** 289 - 306.

van den Hurk, R., and J. Peute 1985 Functional aspects of the postovulatory follicle in the ovary of the African catfish, *Clarias gariepinus,* after induced ovulation. An ultrastructural and enzyme histochemical study. Cell Tissue Res., **240:** 199 - 208.

Hurley, D.A., and K.C. Fisher 1966 The structure and development of the external membrane in young eggs of the brook trout, *Salvelinus fontinalis* (Mitchill). Can. J. Zool., **44:** 173 - 190.

Hyllner, S.J. et al. 1991 Oestradiol-17β induces the major vitelline envelope proteins in both sexes in teleosts. J. Endocrinol., **131:** 229 - 236.

Hyllner, S.J., B. Norberg, and C. Haux 1994 Isolation, partial characterization, induction, and the occurrence in plasma of the major vitelline envelope protein in the Atlantic halibut *(Hippoglossus hippoglossus)* during sexual maturation. Can. J. Fish. Aquat. Sci., **51:** 1700 - 1707.

Hyllner, S.J., C. Silversand, and C. Haux 1994 Formation of the vitelline envelope precedes the active uptake of vitellogenin during oocyte development in the rainbow trout, *Oncorhynchus mykiss.* Mol. Reprod. Dev., **39:** 166 - 175.

Inoue, S. et al. 1987 Localization of polysialoglycoprotein as a major glycoprotein component in cortical alveoli of the unfertilized eggs of *Salmo gairdneri.* Dev. Biol., **123:** 442 - 454.

Inoue, S., and Y. Inoue 1986 Fertilization (activation)-induced 200- to 9-kDa depolymerization of polysialoglycoprotein, a distinct component of cortical alveoli of rainbow trout eggs. J. Biol. Chem., **261:** 5256 - 5261.

Ishijima, S., Y. Hamaguchi, and T. Iwamatsu 1993 Sperm behavior in the micropyle of the medaka egg. Zool. Sci., **10:** 179 - 182.

Iuchi, I., K. Masuda, and K. Yamagami 1991 Change in component proteins of the egg envelope (chorion) of rainbow trout during hardening. Develop. Growth Differ., **33:** 85 - 92.

Iuchi, I., and K. Yamagami 1976 Major glycoproteins solubilized from the teleostean egg membrane by the action of the hatching enzyme. Biochim. Biophys. Acta, **453:** 240 - 249.

Iwamatsu, T. 1992 Morphology of filaments on the chorion of oocytes and eggs in the medaka. Zool. Sci., **9:** 589 - 599.

Iwamatsu, T. 1994 Medaka oocytes rotate within the ovarian follicles during oogenesis. Dev. Growth Differ., **36:** 177 - 186.

Iwamatsu, T. 1998 Studies on fertilization in the teleost. I. Dynamic responses of fertilized medaka eggs. Develop. Growth. Differ., **40:** 475 - 483.

Iwamatsu, T. 2000 Fertilization in fishes. Chapter 3 *in* Fertilization in Protozoa and Metazoan Animals, J.J. Tarín and A. Cano eds. Berlin, Heidelberg: Springer-Verlag.

Iwamatsu, T. et al., 1997 Effect of micropylar morphology and size on rapid sperm entry into the eggs of the medaka. Zool. Sci., **14:** 623 - 628.

Iwamatsu, T. et al. 1976 Studies of oocyte maturation of the medaka, *Oryzias latipes.* III. Cytoplasmic and nuclear changes of oocyte during *in vitro* maturation. Annot. Zool. Jap., **49:** 28 - 37.

Iwamatsu, T. et al. 1988 Oogenesis in the medaka *Oryzias latipes* — stages of oocyte development. Zool. Sci., **5:** 353 - 373.

Iwamatsu, T. et al. 1991 Time sequence of early events in fertilization in the medaka egg. Develop. Growth Differ., **33:** 479 - 490.

Iwamatsu, T. et al. 1997 Effect of micropylar morphology and size on rapid sperm entry into the eggs of the medaka. Zool. Sci., **14:** 623 - 628.

Iwamatsu, T., S. Ishijima, and S. Nakashima 1993 Movement of spermatozoa and changes in micropyles during fertilization in medaka eggs. J. Exper. Zool., **266:** 57 - 64.

Iwamatsu, T., and H. Keino 1978 Scanning electron microscopic study on the surface change of eggs of the teleost, *Oryzias latipes,* at the time of fertilization. Develop. Growth Differ., **20:** 237 - 250.

Iwamatsu, T., and S. Nakashima 1996 Dynamic growth of oocytes of the medaka, *Oryzias latipes.* I. A relationship between establishment of the animal-vegetal axis of the occyte and its surrounding granulosa cells. Zool. Sci., **13:** 873 - 882.

Iwamatsu, T., S. Nakashima, and K. Onitake 1993 Spiral patterns in the micropylar wall and filaments on the chorion in eggs of the medaka, *Oryzias latipes.* J. Exper. Zool., **267:** 225 - 232.

Iwamatsu, T., and T. Ohta 1976 Breakdown of the cortical alveoli of medaka eggs at the time of fertilization, with a particular reference to the possible role of spherical bodies in the alveoli. Roux's Arch., **180:** 297 - 309.

Iwamatsu, T., and T. Ohta 1977 Fine structure of loach oocytes during maturation *in vitro.* Develop. Growth Differ., **19:** 213 - 226.

Iwamatsu, T., and T. Ohta 1978 Electron microscopic observation on sperm penetration and pronuclear formation in the fish egg. J. Exper. Zool., **205:** 157 - 180.

Iwamatsu, T., and T. Ohta 1981a On a relationship between oocyte and follicle cells around the time of ovulation in the medaka, *Oryzias latipes.* Annot. Zool. Jap., **54:** 17 - 29.

Iwamatsu, T., and T. Ohta 1981b Scanning electron microscopic observations on sperm penetration in teleostean fish. J. Exper. Zool., **218:** 261 - 277.

Iwamatsu, T., Y. Shibata, and T. Kanie 1995 Changes in chorion proteins induced by the exdate released from the egg cortex at the time of fertilization in the teleost, *Oryzias latipes.* Develop. Growth Differ., **37:** 747 - 759.

Iwamatsu, T., Y. Yoshimoto, and Y. Hiramoto 1988a Cytoplasmic Ca^{2+} release induced by microinjection of Ca^{2+} and effects of microinjected divalent cations on Ca^{2+} sequestration and exocytosis of cortical alveoli in the medaka egg. Dev. Biol., **125:** 451 - 457.

Iwamatsu, T., Y. Yoshimoto, and Y. Hiramoto 1988b Mechanism of Ca^{2+} release in medaka eggs microinjected with inositol 1,4,5-triphosphate and Ca^{2+}. Dev. Biol., **129:** 191 - 197.

Iwamatsu, T., N. Yoshizaki, and Y. Shibata 1997 Changes in the chorion and sperm entry into the micropyle during fertilization in the teleostean fish, *Oryzias latipes.* Develop. Growth Differ., **39:** 33 - 41.

Iwasaki, Y. 1973 Histochemical detection of Δ^5-3β-hydroxysteroid dehydrogenase in the ovary of the medaka, *Oryzias latipes,* during annual reproductive cycle. Bull. Fac. Fish. Hokkaido Univ., **23:** 177 - 184.

Jaffe, L.F. 1980 Calcium explosions as triggers of development. Ann. N.Y. Acad. Sci., **339:** 86 - 101.

Jalabert, B. 1976 In vitro oocyte maturation and ovulation in rainbow trout *(Salmo gairdneri),* northern pike *(Esox lucius),* and goldfish *(Carassius auratus).* J. Fisheries Res. Bd, Canada, **33:** 974 - 988.

Jalabert, B., and R. Billard 1969 Étude ultrastructurale du site de conservation des spermatozoïdes dans l'ovaire de *Poecilia reticulata* (Poisson Téléostéen). Ann. Biol. Anim. Bioch. Biophys., **9:** 273 - 280.

Jalabert, B, and D. Szöllösi 1975 In vitro ovulation of trout oocytes: effect of prostaglandins on smooth muscle-like cells of the theca. Prostaglandins, **9:** 765 - 778.

Jiang, J.-Q. et al. 1996 Organization of cytoplasmic microtubules during maturation of goldfish oocytes. Zool. Sci., **13:** 899 - 907.

Johnson, E.Z., and R.G. Werner 1986 Scanning electron microscopy of the chorion of selected freshwater fishes. J. Fish Biol., **29:** 257 - 265.

Johnston, P.M. 1951 The embryonic history of the germ cells of the largemouth black bass, *Micropterus salmoides salmoides* (Lacépède). J. Morphol., **88:** 471 - 542.

Jollie, W.P., and L.G. Jollie 1964a The fine structure of the ovarian follicle of the ovoviviparous poeciliid fish, *Lebistes reticulatus.* I. Maturation of follicular epithelium. J. Morphol., **114:** 479 - 502.

Jollie, W.P., and L.G. Jollie 1964b The fine structure of the ovarian follicle of the ovoviviparous poeciliid fish, *Lebistes reticulatus.* II. Formation of the follicular pseudoplacenta. J. Morphol., **114:** 503 - 526.

Jollie, W.P., and L.G. Jollie 1967a Electron microscopic observations on the yolk sac of the spiny dogfish, *Squalus acanthias.* J. Ultrastruct. Res., **18:** 102 - 126.

Jollie, W.P., and L.G. Jollie 1967b Electron microscopic observations on accommodations to pregnancy in the uterus of the spiny dogfish, *Squalus acanthias.* J. Ultrastruct. Res., **20:** 161 - 178.

Kagawa, H. et al. 1982 Estradiol-17β production in amago salmon *(Oncorhynchus rhodurus)* ovarian follicles: role of the thecal and granulosa cells. Gen. Comp. Endocrinol., **47:** 440 - 448.

Kagawa, H., and Y. Nagahama 1981 *In vitro* effects of prostaglandins on ovulation in goldfish *Carassius auratus.* Bull. Jap. Soc. Sci. Fisheries., **47:** 1119 - 1121.

Kagawa, H., and K. Takano 1979 Ultrastructure and histochemistry of granulosa cells of pre- and post-ovulatory follicles in the ovary of medaka, *Oryzias latipes.* Bull. Fac. Fish. Hokkaido Univ., **30:** 191 - 204. [In Japanese with English abstract and figure legends]

Kagawa, H., K. Takano, and Y. Nagahama 1981 Correlation of plasma estradiol-17β and progesterone levels with ultrastructure and histochemistry of ovarian follicles in the white-spotted char, *Salvelinus leucomaenis.* Cell Tissue Res., **218:** 315 - 329.

Kanamori, A., S. Adachi, and Y. Nagahama 1988 Developmental changes in steroidogenic responses of ovarian follicles of amago salmon *(Oncorhynchus rhodurus)* to chum salmon gonadotropin during oogenesis. Gen. Comp. Endocrinol., **72:** 13 - 24.

Kanamori, A., and Y. Nagahama 1988a Developmental changes in the properties of gonadotropin receptors in the ovarian follicles of amago salmon *(Oncorhynchus rhodurus)* during oogenesis. Gen. Comp. Endocrinol., **72:** 25 - 38.

Kanamori, A., and Y. Nagahama 1988b Involvement of 3',5'-cyclic adenosine monophosphate in the control of follicular steroidogenesis of amago salmon *(Oncorhynchus rhodurus).* Gen. Comp. Endocrinol., **72:** 39 - 53.

Karasaki, S. 1967 An electron microscope study on the crystalline structure of the yolk platelets of the lamprey egg. J. Ultrastruct. Res., **18:** 377 - 390.

Kessel, R.G. 1992 Annulate lamellae: a last frontier in cellular organelles. Int. Rev. Cytol., **133:** 43 - 120.

Kessel, R.G. et al. 1985 The presence and distribution of gap junctions in the oocyte-follicle cell complex of the zebrafish, *Brachydanio rerio.* J. Submicrosc. Cytol., **17:** 239 - 253.

Kessel, R.G., H.W. Beams, and H.N. Tung 1984 Relationships between annulate lamellae and filament bundles in oocytes of the zebrafish, *Brachydanio rerio.* Cell Tissue Res., **236:** 725 - 727.

Kessel, R.G., R.L. Roberts, and H.N. Tung 1988 Intercellular junctions in the follicular envelope of the teleost, *Brachydanio rerio.* J. Submicrosc. Cytol. Pathol., **20:** 415 - 424.

Khoo, K.H. 1975 The corpus luteum of goldfish *(Carassius auratus* L.) and its functions. Can. J. Zool., **53:** 1306 - 1323.

Khoo, K.H. 1979 The histochemistry and endocrine control of vitellogenesis in goldfish ovaries. Can. J. Zool., **57:** 617 - 626.

Kille, R.A. 1960 Fertilization of the lamprey egg. Exper. Cell Res., **20:** 12 - 27.

King, W. et al. 1994 Plasma levels of gonadal steroids during final oocyte maturation of striped bass, *Morone saxatilis* L. Gen. Comp. Endocrinol., **95:** 178 - 191.

King, M.V., D.L. Berlinsky, and C.V. Sullivan 1995 Involvement of gonadal steroids in final oocyte maturation of white perch *(Morone americana)* and white bass *(M. chrysops): in vivo* and *in vitro* studies. Fish Physiol. Biochem., **14:** 489 - 500.

King, W., P. Thomas, and C.V. Sullivan 1994 Hormonal regulation of final maturation of striped bass oocytes *in vitro.* Gen. Comp. Endocrinol., **96:** 223 - 233.

Kitajima, K. et al. 1988 Comparative structures of the apopolysialoglycoproteins from unfertilized and fertilized eggs of salmonid fishes. Biochemistry, **27:** 7141 - 7145.

Kitajima, K., and S. Inoue 1988 A proteinase associated with cortices of rainbow trout eggs and involved in fertilization-induced depolymerizatrion of polysialoglycoproteins. Dev. Biol., **129:** 270 - 274.

Kitajima, K., S. Inoue, and Y. Inoue 1989 Isolation and characterization of a novel type of sialoglycoproteins (hyosophorin) from eggs of medaka, *Oryzias latipes:* nonapeptide with a large N-linked glycan chain as a tandem repeat unit. Dev. Biol., **132:** 544 - 553.

Kitajima, K., Y. Inoue, and S. Inoue 1986 Polysialoglycoproteins of *Salmonidae* fish eggs. Complete structure of 200-kDa polysialoglycoprotein from the unfertilized eggs of rainbow trout *(Salmo gairdneri).* J. Biol. Chem., **261:** 5262 - 5269.

Kjesbu, O.S. et al. 1991 Fecundity, atresia, and egg size of captive Atlantic cod *(Gadus morhua)* in relation to proximate body composition. Can. J. Fish. Aquat. Sci., **48:** 2333 - 2433.

Kjesbu, O.S., and H. Kryvi 1989 Oogenesis in cod, *Gadus morhua* L., studied by light and electron microscopy. J. Fish Biol., **34:** 735 - 746.

Kjesbu, O.S.,H. Kryvi, and B. Norberg 1996 Oocyte size and structure in relation to blood plasma steroid hormones in individually monitored, spawning Atlantic cod. J. Fish Biol., **49:** 1197 - 1215.

Knight, D.P. et al. 1993 Changes in macromolecular organization in collagen assemblies during secretion in the nidamental gland and formation of the egg capsule wall in the dogfish *Scyliorhinus canicula.* Phil. Trans. Roy. Soc. London B, **341:** 419 - 436.

Knight, D.P. et al. 1996 Spinnerets in fish extrude sheet material with complex molecular orientations. Biomimetics, **4:** 105 - 120.

Knight, D.P., and D. Feng 1992 Formation of the dogfish egg capsule, a coextruded, multilayer laminate. Biomimetics, **1:** 151 - 175.

Knight, D.P., and D. Feng 1994a Interaction of collagen with hydrophobic protein granules in the egg capsule of the dogfish *Scyliorhinus canicula.* Tissue & Cell, **26:** 155 - 167.

Knight, D.P., and D. Feng 1994b Some observations on the collagen fibrils of the egg capsule of the dogfish, *Scyliorhinus canicula.* Tissue & Cell, **26:** 385 - 401.

Knight, D.P., D. Feng, and M. Stewart 1996 Structure and function of the selachian egg case. Biol. Rev., **71:** 81 - 111.

Knight, D.P., and S. Hunt 1974 Fibril structure of collagen in egg capsule of dogfish. Nature, **249:** 379 - 380.

Knight, D.P., and S. Hunt 1976 Fine structure of the dogfish egg case: a unique collagenous material. Tissue & Cell, **8:** 183 - 193.

Knight, D.P., and S. Hunt 1986 A kinked molecular model for the collagen-containing fibrils in the egg case of the dogfish *Scyliorhinus canicula.* Tissue & Cell, **18:** 201 - 208.

Knight, F.M. et al. 1985 Follicular placenta and embryonic growth of the viviparous four-eyed fish *(Anableps).* J. Morphol., **185:** 131 - 142.

Kobayashi, D. et al. 1996 Steroidogenesis in the ovarian follicles of the medaka *(Oryzias latipes)* during vitellogenesis and oocyte maturation. Zool. Sci., **13:** 921 - 927.

Kobayashi, M. et al. 1988 Development of sensitivity to maturation-inducing steroids in the oocytes of the daily spawning teleost, the kisu *Sillago japonica.* Gen. Comp. Endocrinol., **72:** 264 - 271.

Kobayashi, W. 1985a Electron microscopic observation of the breakdown of cortical vesicles in the chum salmon egg. J. Fac. Sci. Hokkaido Univ., Ser. VI, Zool., **24:** 87 - 102.

Kobayashi, W. 1985b Communications of oocyte-granulosa cells in the chum salmon ovary detected by transmission electron microscopy. Develop. Growth Differ., **27:** 553 - 561.

Kobayashi, W., and T.S. Yamamoto 1981 Fine structure of the micropylar apparatus of the chum salmon egg, with a discussion of the mechanism for blocking polyspermy. J. Exper. Zool., **217:** 265 - 275.

Kobayashi, W., and T.S. Yamamoto 1985 Fine structure of the micropylar cell and its change during oocyte maturation in the chum salmon, *Oncorhynchus keta.* J. Morphol., **184:** 263 - 276.

Kobayashi, W., and T.S. Yamamoto 1987 Light and electron microscopic observations of sperm entry in the chum salmon egg. J. Exper. Zool., **243:** 311 - 322.

Kobayashi, W., and T.S. Yamamoto 1993 Factors inducing closure of the micropylar canal in the chum salmon egg. J. Fish Biol., **42:** 385 - 394.

Koch, E.A. et al. 1993 The hagfish oocyte at late stages of oogenesis: structural and metabolic events at the micropylar region. Tissue & Cell, **25:** 259 - 273.

Kokkala, I., and J.P. Wourms 1994 In vivo fluorescence imaging of the functional organization of trophotaenial placental cells of goodeid fishes. J. Morphol., **219:** 35 - 46.

Koob, T.J. 1991 Deposition and binding of calcium and magnesium in egg capsules of *Raja erinacea* Mitchill during formation and tanning in utero. Copeia, **1991:** 339 - 347.

Koob, T.J., and I.P. Callard 1991 Reproduction in female elasmobranchs. *In* Comparative Physiology, vol. 10: Oogenesis, Spermatogenesis and Reproduction, R.K.H. Kinne, ed. Basel: Karger, pp. 155 - 209.

Koob, T.J., and I.P. Callard 1999 Reproductive endocrinology of female elasmobranchs: lessons from the little skate *(Raja erinacea)* and spiny dogfish *(Squalus acanthias).* J. Exper. Zool., **284:** 557 - 574.

Koob, T.J., and D.L. Cox 1988 Egg capsule catechol oxidase from the little skate *Raja erinacea* Mitchill, 1825. Biol. Bull., **175:** 202 - 211.

Koob, T.J., and D.L. Cox 1990 Introduction and oxidation of catechols during the formation of the skate *(Raja erinacea)* egg capsule. J. Marine Biol. Assoc. U.K., **70:** 395 - 411.

Koob, T.J., and D.L. Cox 1993 Stabilization and sclerotization of *Raja erinacea* egg capsule proteins. Env. Biol. Fishes, **38:** 151 - 157.

Koob, T.J., and W.C. Hamlett 1998 Microscopic structure of the gravid uterus in the little skate, *Raja erinacea.* J. Exper. Zool., **282:** 421 - 437.

Korsgaard, B. 1983 The chemical composition of follicular and ovarian fluids of the pregnant blenny *(Zoarces viviparus* (L.)). Can. J. Zool., **61:** 1101 - 1108.

Kosmath, I., R.A. Patzner, and H. Adam 1981 The structure of the micropyles of the eggs of *Myxine glutinosa* and *Eptatretus burgeri* (Cyclostomata). Zool. Anz., **206:** 273 - 278.

Kosmath, I., R.A. Patzner, and H. Adam 1983a Regression im Ovar von *Myxine glutinosa* L. (Cyclostomata). II. Elektronenmikroskopische Untersuchungen an den atretische Follikeln. Z. Mikrosk.-Anat. Forsch., **97:** 667 - 674.

Kosmath, I., R.A. Patzner, and H. Adam 1983b Regression im Ovar von *Myxine glutinosa* L. (Cyclostomata). IV. Histochemische Untersuchungen an den atretischen Follikeln. Z. Mikrosk.-Anat. Forsch., **97:** 941 - 947.

Kosmath, I., R.A. Patzner, and H. Adam 1984a Regression im Ovar von *Myxine glutinosa* L. (Cyclostomata). III. Untersuchungen der Feinstruktur post-ovulatorischer Follikel. Zool. Anz., **212:** 129 - 138.

Kosmath, I., R.A. Patzner, and H. Adam 1984b Regression im Ovar von *Myxine glutinosa* L. (Cyclostomata). V. Histochemische Untersuchungen an den post-ovulatorischen Follikeln. Zool. Anz., **212:** 309 - 316.

Koya, Y., T. Hamatsu, and T. Matsubara 1995 Annual reproductive cycle and spawning characteristics of the female kichiji rockfish *Sebastolobus macrochir.* Fisheries Sci., **61:** 203 - 208.

Koya, Y., and T. Matsubara 1995 Ultrastructural observations on the inner ovarian epithelia of kichjii rockfish *Sebastolobus macrochir* with special reference to the production of gelatinous material surrounding the eggs. Bull. Hokkaido Natl. Fish. Res. Inst., **59:** 1 - 16.

Koya, Y., H. Munehara, and K. Takano 1993 Secretion abilities of epithelia of ovarian wall and ovigerous lamella lining the ovarian cavity of masked greenling, *Hexagrammos octogrammus.* Jap. J. Ichthyol., **40:** 199 - 208.

Koya, Y., H. Munehara, and K. Takano 1997 Sperm storage and degradation in the ovary of a marine copulating sculpin, *Alcichthys alcicornis* (Teleostei: Scorpaeniformes): role of intercellular junctions between inner ovarian epithelial cells. J. Morphol., **233:** 153 - 163.

Koya, Y., K. Takano, and H. Takahashi 1993 Ultrastructural observations on sperm penetration in the egg of elkhorn sculpin, *Alcichthys alcicornis,* showing internal gametic association. Zool. Sci., **10:** 93 - 101.

Koya, Y., K. Takano, and H. Takahashi 1995 Annual changes in fine structure of inner epithelial lining of the ovary of a marine sculpin, *Alcichthys alcicornis* (Teleostei: Scorpaeniformes), with internal gametic association. J. Morphol., **223:** 85 - 97.

Krajhanzl, A., V. Horejsi, and J. Kocourek 1978a Studies on lectins. XLI. Isolation and characterization of a blood group B specific lectin from the roe of the powan *(Coregonus lavaretus maraena).* Biochim. Biophys. Acta, **532:** 209 - 214.

Krajhanzl, A., V. Horejsi, and J. Kocourek 1978b Studies on lectins. XLII. Isolation, partial characterization and comparison of lectins from the roe of five fish species. Biochim. Biophys. Acta, **532:** 215 - 224.

Krajhanzl, A. et al. 1984a Direct visualization of endogenous lectins in fish oocytes by glycosylated fluorescent cytochemical markers. Histochem. J., **16:** 426 - 428.

Krajhanzl, A. et al. 1984b An immunofluorescence study on the occurrence of endogenous lectins in the differentiating oocytes of silver carp *(Hypophthalmichthys molitrix* Valenc.) and tench *(Tinca tinca* L.). Histochem. J., **16:** 432 - 434.

Kristoffersson, R., S. Broberg, and M. Pekkarinen 1973 Histology and physiology of embryotrophe formation, embryonic nutrition and growth in the eel-pout, *Zoarces viviparus* (L.). Ann. Zool. Fenn., **10:** 467 - 477.

Kuchnow, K.P., and J.R. Scott 1977 Ultrastructure of the chorion and its micropyle apparatus in the mature *Fundulus heteroclitus* (Walbaum) ovum. J. Fish Biol., **10:** 197 - 201.

Kudo, S. 1976 Ultrastructural observations on the discharge of two kinds of granules in fertilized eggs of *Cyprinus carpio* and *Carassius auratus.* Develop. Growth Differ., **18:** 167 - 176.

Kudo, S. 1978 Enzymo-cytochemical observations on the cortical change in the eggs of *Cyprinus carpio* and *Carassius auratus.* Develop. Growth Differ., **20:** 133 - 142.

Kudo, S. 1980 Sperm penetration and the formation of a fertilization cone in the common carp egg. Develop. Growth Differ., **22:** 403 - 414.

Kudo, S. 1982 Ultrastructure and ultracytochemistry of the fertilization envelope formation in the carp egg. Develop. Growth Differ., **24:** 327 - 339.

Kudo, S. 1992 Enzymatic basis for protection of fish embryos by the fertilization envelope. Experientia, **48:** 377 - 381.

Kudo, S. 1983a Ultracytochemical modifications of surface carbohydrates in fertilized eggs of the common carp. Dev. Growth Differ., **25:** 85 - 97.

Kudo, S. 1983b Response to sperm penetration of the cortex of eggs of the fish, *Plecoglossus altivelis.* Dev. Growth Differ., **25:** 163 - 170.

Kudo, S. 1998a Role of sperm head syndecan at fertilization in fish. J. Exper. Zool. **281:** 620 - 625.

Kudo, S. 1998b Presence of proteinase inhibitor in the vitelline envelope and its role in eggs of the fish *Tribolodon hakonensis.* J. Exper. Zool., **281:** 626 - 635.

Kudo, S. 1998c Thrombin induces assembly in vitro of vitelline envelope components of common carp eggs. J. Exper. Zool., **282:** 367 - 375.

Kudo, S., and M. Inoue 1986 A bactericidal effect of fertilization envelope extract from fish eggs. Zool. Sci., **3:** 323 - 329.

Kudo, S., and M. Inoue 1989 Bacterial action of fertilization envelope extract from eggs of the fish *Cyprinus carpio* and *Plecoglossus altivelis.* J. Exper. Zool., **250:** 219 - 228.

Kudo, S., and M. Inoue 1991 Enzyme activities responsible for the defense mechanism of the fertilization envelope. Naturwissenschaften, **78:** 172 - 173.

Kudo, S., and A. Sato 1985 Fertilization cone of carp eggs as revealed by scanning electron microscopy. Develop. Growth Differ., **27:** 121 - 128.

Kudo, S., A. Sato, and M. Inoue 1988 Chorionic peroxidase activity in eggs of the fish *Tribolodon hakonensis.* J. Exper. Zool., **245:** 63 - 70.

Kudo, S., and C. Teshima 1991 Enzyme activities and antifungal action of fertilization envelope extract from fish eggs. J. Exper. Zool., **259:** 392 - 398.

Kudo, S., and C. Teshima 1998 Assembly *in vitro* of vitelline envelope components induced by a cortical alveolus sialoglycoprotein of eggs of the fish *Tribolodon kakonensis.* Zygote, **6:** 193 - 202.

Kudo, S., and S. Yazawa 1995 Binding of bacterial toxins to glycoproteins in the envelopes of rainbow trout eggs. Histochem. J., **27:** 300 - 308.

Lahnsteiner, F., T. Weismann, and R.A. Patzner 1995 Composition of the ovarian fluid in 4 salmonid species: *Oncorhynchus mykiss, Salmo trutta lacustris, Salvelinus alpinus* and *Hucho hucho.* Reprod. Nutr. Dev., **35:** 465 - 474.

Lahnsteiner, F., T. Weismann, and R.A. Patzner 1997 Structure and function of the ovarian cavity and oviduct and composition of the ovarian fluid in the bleak, *Alburnus alburnus* (Teleostei, Cyprinidae). Tissue & Cell, **29:** 305 - 314.

Lambert, J.G.D. 1966 Location of hormone production in the ovary of the guppy, *Poecilia reticulata.* Experientia, **22:** 476 - 477.

Lambert, J.G.D. 1970a The ovary of the guppy *Poecilia reticulata.* The granulosa cells as sites of steroid biosynthesis. Gen. Comp. Endocrinol., **15:** 464 - 476.

Lambert, J.G.D. 1970b The ovary of the guppy *Poecilia reticulata.* The atretic follicle, a *corpus atreticum* or a *corpus luteum praeovulationis.* Z. Zellforsch. Mikrosk. Anat., **107:** 54 - 67.

Lambert, J.G.D., and P.G.W.J. van Oordt 1965 Preovulatory corpora lutea or corpora atretica in the guppy, *Poecilia reticulata.* A histological and histochemical study. Gen. Comp. Endocrinol., **5:** 693 – 694.

Lance, V., and I.P. Callard 1969 A histochemical study of ovarian function in the ovoviviparous elasmobranch, *Squalus acanthias.* Gen. Comp. Endocrinol., **13:** 255 - 267.

Lang, I. 1981a Electron microscopic and histochemical study of the postovulatory follicles of *Perca fluviatilis* L. (Teleostei). Gen. Comp. Endocrinol., **45:** 219 - 233.

Lang, I. 1981b Electron microscopic and histochemical investigations of the atretic oocyte of *Perca fluviatilis* L. (Teleostei). Cell Tissue Res., **220:** 201 - 212.

Lange, R.H. 1981 Are yolk phosvitins carriers for specific cations? Comparative microanalysis in vertebrate yolk platelets. Z. Naturforsch., **36c:** 686 - 687.

Lange, R.H. 1982 The lipoprotein crystals of cyclostome yolk platelets *(Myxine glutinosa* L., *Lampetra planeri* [Bloch], *L. fluviatilis* [L.]). J. Ultrastruct. Res., **79:** 1 - 17.

Lange, R.H. et al. 1983 Lipovitellin-phosvitin crystals with orthorhombic features: thin-section electron microscopy, gel electrophoresis, and microanalysis in teleost and amphibian yolk platelets and a comparison with other vertebrates. J. Ultrastruct. Res., **83:** 122 - 140.

Lange, R.H., Z. Grodzinski., and W. Kilarski 1982 Yolk-platelet crystals in three ancient bony fishes: *Polypterus bichir* (Polypteri), *Amia calva* L., and *Lepisosteus osseus* (L.) (Holostei). Cell Tissue Res., **222:** 159 - 165.

Lange, R.H., and H.-P. Richter 1981 A symmetric lipovitellin-phosvitin dimer in cyclostome yolk platelet crystals: structural and biochemical observations. J. Molec. Biol., **148:** 487 - 491.

Larsen, L.O. 1970 The lamprey egg at ovulation *(Lampetra fluviatilis* L. Gray). Biol. Reprod., **2:** 37 - 47.

Larsson, D.G.J., S.J. Hyllner, and C. Haux 1994 Induction of vitelline envelope proteins by oestradiol-17β in 10 teleost species. Gen. Comp. Endocrinol., **96:** 445 - 450.

Lehri, G.K. 1968 Cyclical changes in the ovary of the catfish, *Clarias batrachus* (Linn.). Acta Anat., **69:** 105 - 124.

Lepori, N.G. 1980 Sex differentiation, hermaphroditism and intersexuality in vertebrates including man. Padua: Piccin Medical Books, 345 pp.

Lessman, C.A. 1991 Metabolism of progestogens during in vitro meiotic maturation of follicle-enclosed oocytes of the goldfish *(Carassius auratus).* J. Exper. Zool., **259:** 59 - 68.

Levavi-Zermonsky, B., and Z. Yaron 1986 Changes in gonadotropin and ovarian steroids associated with oocytes maturation during spawning induction in the carp. Gen. Comp. Endocrinol., **62:** 89 - 98.

Lewis, J.C., and D.B. McMillan 1965 The development of the ovary of the sea lamprey *(Petromyzon marinus* L.). J. Morphol., **117:** 425 - 466.

Li, Y.H., C.C. Wu, and J.S. Yang 2000 Comparative ultrastructural studies of the zona radiata of marine fish eggs in three genera in Perciformes. J. Fish Biol., **56:** 615 - 621.

Linhart, O., and S. Kudo 1997 Surface ultrastructure of paddlefish eggs before and after fertilization. J. Fish Biol., **51:** 573 - 582.

Livni, N. 1971 Ovarian histochemistry of the fishes *Cyprinus carpio, Mugil capito* and *Tilapia aurea* (Teleostei). Histochem. J., **3:** 405 - 414.

Lombardi, J., and T. Files 1993 Egg capsule structure and permeability in the viviparous shark, *Mustelus canis.* J. Exper. Zool., **267:** 76 - 85.

Lombardi, J., and J.P. Wourms 1985a The trophotaenial placenta of a viviparous goodeid fish. I. Ultrastructure of the internal ovarian epithelium, the maternal component. J. Morphol., **184:** 277 - 292.

Lombardi, J., and J.P. Wourms 1985b The trophotaenial placenta of a viviparous goodeid fish. II. Ultrastructure of trophotaeniae, the embryonic component. J. Morphol., **184:** 293 - 309.

Lombardi, J., and J.P. Wourms 1985c The trophotaenial placenta of a viviparous goodeid fish. III. Protein uptake by trophotaeniae, the embryonic component. J. Exper Zool., **236:** 165 - 179.

Lønning, S. 1972 Comparative electron microscopic studies of teleostean eggs with special reference to the chorion. Sarsia, **49:** 41 - 48.

Lønning, S., and J. Davenport 1980 The swelling egg of the long rough dab, *Hippoglossoides platessoides limandoides* (Bloch). J. Fish Biol., **17:** 359 - 378.

Lønning, S., E. Kjørsvik, and J. Davenport 1984 The hardening process of the egg chorion of the cod, *Gadus morhua* L., and lumpsucker, *Cyclopterus lumpus* L. J. Fish Biol., **24:** 505 - 522.

Lønning, S., E. Kjørsvik, and I.-B. Falk-Petersen 1988 A comparative study of pelagic and demersal eggs from common marine fishes in northern Norway. Sarsia, **73:** 49 - 60.

Loureiro, M., and R.O. de Sá 1996 External morphology of the chorion of the annual fishes *Cynolebias* (Cyprinodontiformes: Rivulidae). Copeia, **1996:** 1016 - 1022.

Lupo di Prisco, C. 1968 Biosintesi di ormoni steroidi nell'ovario di due specie di selaci: *Scyliorhinus stellaris* (oviparo) e *Torpedo marmorata* (ovoviviparo). Riv. Biol., **61:** 113 - 146. [cited by Chieffi Baccari et al., 1992]

Lyngnes, R. 1930 Beiträge zur Kenntnis von *Myxine glutinosa* L. I. Über die Entwicklung der Eihülle bei *Myxine glutinosa.* Z. Morphol. Ökol. d. Tiere, **19:** 591 - 608.

Lygnes, R. 1931 Über atretische und hypertrophische Gebilde im Ovarium der *Myxine glutinosa* L. Biologisches Zentralblatt, **51:** 437 - 441.

Manning, A.J., and L.W. Crim 1998 Maternal and interannual comparison of the ovulatory periodicity, egg production and egg quality of the batch-spawning yellowtail flounder. J. Fish Biol., **53:** 954 - 972.

Manwell, C. 1963 Fetal and adult hemoglobins of the spiny dogfish *Squalus suckleyi.* Arch. Biochem. Biophys., **101:** 504 - 511.

Masuda, K., I. Iuchi, and K. Yamagami 1991 Analysis of hardening of the egg envelope (chorion) of the fish, *Oryzias latipes.* Develop. Growth Differ., **33:** 75 - 83.

Matsuyama, M., Y. Nagahama, and S. Matsuura 1991 Observations on ovarian follicle ultrastructure in the marine teleost, *Pagrus major,* during vitellogenesis and oocyte maturation. Aquaculture, **92:** 67 - 82.

Matthews, L.H. 1950 Reproduction in the basking shark, *Cetorhinus maximus* (Gunner). Phil. Trans. Roy. Soc. London, Ser. B, **234:** 247 - 316.

Mayer, I., S.E. Shackley, and J.S. Ryland 1988 Aspects of the reproductive biology of the bass, *Dicentrarchus labrax* L. I. An histological and histochemical study of oocyte development. J. Fish Biol., **33:** 609 - 622.

Meisner, A.D. et al. 2000 Morphology and histology of the male reproductive system in two species of internally inseminating South American catfishes, *Trachelyopterus lucenai* and *T. galeatus* (Teleostei: Auchenipteridae). J. Morphol., **246:** 131 - 141.

Meisner, A.D., and J.R. Burns 1997 Viviparity in the halfbeak Genera *Dermogenys* and *Nomorhamphus* (Teleostei, Hemiramphidae). J. Morphol., **234:** 295 - 317.

Mendoza, G. 1958 The fin fold of *Goodea luitpoldii,* a viviparous cyprinodont teleost. J. Morphol., **103:** 539 - 560.

Mendoza, G. 1972 The fine structure of an absorptive epithelium in a viviparous teleost. J. Morphol., **136:** 109 - 130.

Merson, R.R. et al., 2000 Oocyte development in summer flounder: seasonal changes and steroid correlates. J. Fish Biol., **57:** 182 - 196.

Metten, H. 1939 Studies on the reproduction of the dogfish. Phil. Trans. Roy. Soc. London, **230B:** 217 - 238.

Miranda, A.C.L. et al. 1999 Ovarian follicular atresia in two teleost species: a histological and ultrastructural study. Tissue & Cell, **31:** 480 - 488.

Mooi, R.D. 1990 Egg surface morphology of pseudochromoids (Perciformes: Percoidei), with comments on its phylogenetic implications. Copeia, **1990:** 455 - 475.

Mooi, R.D., R. Winterbottom, and M. Burridge 1990 Egg surface morphology, development, and evolution in the Congrogadinae (Pisces: Perciformes: Pseudochromidae). Can. J. Zool., **68:** 923 - 934.

Morin, R.P., and K.W. Able 1983 Patterns of geologic variation in the egg morphology of the fundulid fish, *Fundulus heteroclitus.* Copeia, **1983:** 726 - 740.

Munehara, H., K. Takano, and Y. Koya 1989 Internal gametic association and external fertilization in the elkhorn sculpin, *Alcichthys alcicornis.* Copeia, **1989:** 673 - 678.

Muñoz, M., M. Casadevall, and S. Bonet 1999 Annual reproductive cycle of *Helicolenus dactylopterus dactylopterus* (Teleostei: Scorpaeniformes) with special reference to the ovaries sperm storage. J. Marine Biol. Assoc. U.K., **79:** 521 - 529.

Mylonas, C.C. et al. 1997 Reproductive biology and endocrine regulation of final oocyte maturation of captive white bass. J. Fish Biol., **51:** 234 - 250.

Mylonas, C.C., L.C. Woods, and Y. Zohar 1997 Cyto-histological examination of post-vitellogenesis and final oocyte maturation in captive-reared striped bass. J. Fish Biol., **50:** 34 - 49.

Nagahama, Y. 1983 The functional morphology of teleost gonads. Chapter 6 *in* Fish Physiology, vol. IXA, W.S. Hoar, D.J. Randall, and E.M. Donaldson, eds. New York: Academic Press, Inc., pp. 223 - 275.

Nagahama, Y. 1984 Mechanism of gonadotropic control of steroidogenesis in the teleost ovarian follicle. Gunma Symp. Endocrinol., **21:** 167 - 182.

Nagahama, Y. 1987 Gonadotropin action on gametogenesis and steroidogenesis in teleost gonads. Zool. Sci., **4:** 209 - 222.

Nagahama, Y. et al. 1983 Relative *in vitro* effectiveness of 17α,20β-dihydroxy-4-pregnen-3-one and other pregnene derivatives on germinal vesicle breakdown in oocytes of ayu (*Plecoglossus altivelis),* amago salmon *(Oncorhynchus rhodurus),* rainbow trout *(Salmo gairderni),* and goldfish *(Carassius auratus).* Gen. Comp. Endocrinol., **51:** 15 - 23.

Nagahama, Y. et al. 1994 Regulation of oocyte maturation in fish. Chapter 13 *in* Fish Physiology, vol. XIII, N.M. Sherwood and C.L. Hew, eds. A.P. Farrell and D.J. Randall, series eds.). New York: Academic Press, Inc., pp. 393 - 439.

Nagahama, Y., and S. Adachi 1985 Identification of maturation-inducing steroid in a teleost, the amago salmon *(Oncorhynchus rhodurus).* Dev. Biol., **109:** 428 - 435.

Nagahama, Y., K. Chan, and W.S., Hoar 1976 Histochemistry and ultrastructure of pre- and postovulatory follicles in the ovary of the goldfish, *Carassius auratus.* Can. J. Zool., **54:** 1128 - 1139.

Nagahama, Y., W.C. Clarke, and W.S. Hoar 1978 Ultrastructure of putative steroid-producing cells in the gonads of coho *(Oncorhynchus kisutch)* and pink salmon *(Oncorhynchus gorbuscha).* Can. J. Zool., **56:** 2508 - 2519.

Nagahama, K., H. Kagawa, and G. Young 1982 Cellular sources of sex steroids in teleost gonads. Can. J. Fish. Aquat. Sci., **39:** 56 - 64.

Nakamura, M. et al. 1998 Gonadal sex differentiation in teleost fish. J. Exper. Zool., **281:** 362 - 372.

Nakamura, M., and Y. Nagahama 1985 Steroid producing cells duriung ovarian differentiation of the tilapia *Sarotherodon niloticus.* Dev. Growth Differ., **27:** 701 - 708.

Nakamura, M., J.L. Specker, and Y. Nagahama 1993 Ultrastructural analysis of the developing follicle during early vitellogenesis in tilapia, *Oreochromis niloticus,* with special reference to the steroid-producing cells. Cell Tissue Res., **272:** 33 - 39.

Nakamura, M., J.L. Specker, and Y. Nagahama 1996 Innervation of steroid-producing cells in the ovary of tilapia *Oreochromis niloticus.* Zool. Sci., **13:** 603 - 608.

Nakashima, S., and T. Iwamatsu 1989 Ultrastructureal changes in micropylar cells and formation of the micropyle during oogenesis in the medaka *Oryzias latipes.* J. Morphol., **202:** 339 - 349.

Nayyar, R.P. 1964 The yolk nucleus of fish oocytes. Quart. J. Microsc. Sci., **105:** 353 - 358.

Nedelea, M., and I. Steopoe 1970 Origine, caractères cytologiques et comportement des gonocytes primaires pendant l'embryogénèse et chez les jeunes larves de *Cyprinus carpio* L. (Téléostéens). Anat. Anz., **127:** 338 - 346.

Nelson, J.S. 1984 Fishes of the World, 2nd ed. New York: John Wiley & Sons, 523 pp.

Nicander, L., and I. Sjödén 1971 An electron microscopical study of the acrosomal complex and its role in fertilization in the river lamprey, *Lampetra fluviatilis.* J. Submicrosc. Cytol., **3:** 309 - 317.

Nicholls, T.J., and G. Maple 1972 Ultrastructural observations on possible sites of steroid biosynthesis in the ovarian follicular epithelium of two species of cichlid fish, *Cichlasoma nigrofasciatum* and *Haplochromis multicolor.* Z. Zellforsch. Mikrosk. Anat., **128:** 317 - 335.

Nieuwkoop, P.D., and L.A. Sutasurya 1979 Primoridal Germ cells in the Chordates: Embryogenesis and Phylogenesis. Cambridge: Cambridge University Press, 187 pp.

Nosek, J. 1984 Biogenesis of the cortical granules in fish oocyte. Histochem. J., **16:** 435 - 437.

Nosek, J., A. Krajhanzl, and J. Kocourek 1983 Studies on lectins. LVII. Immunofluorescence localization of lectins present in fish ovaries. Histochemistry, **79:** 131 - 139.

Nosek, J., A. Krajhanzl, and J. Kocourek 1984 Binding of the cortical granule lectin to the jelly envelope in mature perch ova. Histochem. J., **16:** 429 - 431.

Nuccitelli, R. 1980a The electrical changes accompanying fertilization and cortical vesicle secretion in the medaka egg. Dev. Biol., **76:** 483 - 498.

Nuccitelli, R. 1980b The fertilization potential is not necessary for the block to polyspermy or the activation of development in the medaka egg. Dev. Biol., **76:** 499 - 504.

Ohta, H. et al. 1983 Ultrastructure of the chorion and the micropyle of the Japanese eel *Anguilla japonica.* Bull. Jap. Soc. Scientific Fisheries, **49:** 501.

Ohta, H., and T. Teranishi 1982 Ultrastructure and histochemistry of granulosa and micropylar cells in the ovary of the loach, *Misgurnus anguillicaudatus* (Cantor). Bull. Fac. Fish. Hokkaido Univ., **33:** 1 - 8.

Ohta, T. 1985 Electron microscopic observations on sperm entry into eggs of the bitterling during cross fertilization. J. Exper. Zool., **233:** 291 - 300.

Ohta, T. 1991 Initial stages of sperm-egg fusion in the freshwater teleost, *Rhodeus ocellatus ocellatus.* Anat. Rec., **229:** 195 - 202.

Ohta, T. et al. 1990 Cortical alveolus breakdown in eggs of the freshwater teleost *Rhodeus ocellatus ocellatus.* Anat. Rec., **227:** 486 - 496.

Ohta, T., and T. Iwamatsu 1983 Electron microscopic observations on sperm entry into eggs of the rose bitterling, *Rhodeus ocellatus.* J. Exper. Zool., **227:** 109 - 119.

Ohta, T., and C. Nashirozawa 1996 Sperm penetration and transformation of sperm entry site in eggs of the freshwater teleost *Rhodeus ocellatus ocellatus.* J. Morphol., **229:** 191 - 200.

Okkelberg, P. 1921 The early history of the germ cells in the brook lamprey, *Entosphenus wilderi* (Gage), up to and including the period of sex differentiation. J. Morphol., **35:** 1 - 151.

Oppen-Berntsen, D.O., et al. 1994 Plasma level of zr-proteins, estradiol-17β, and gonadotropins during an annual reproductive cycle of Atlantic salmon *(Salmo salar).* J. Exper. Zool., **268:** 59 - 70

Oppen-Berntsen, D.O., E. Gram-Jensen, and B.T. Walther 1992 Zona radiata proteins are synthesized by rainbow trout *(Oncorhynchus mykiss)* hepatocytes in response to oestradiol-17β. J. Endocrinol., **135:** 293 - 302.

Oppen-Berntsen, D.O., J.V. Helvik, and B.T. Walther 1990 The major structural proteins of cod *(Gadus morhua)* eggshells and protein crosslinking during teleost egg hardening. Dev. Biol., **137:** 258 - 265.

Oshiro, T., and T. Hibiya 1975 Presence of ovulation-inducing enzymes in the ovarian follicles of loach. Bull. Jap. Soc. Sci. Fisheries, **41:** 115.

Oshiro, T., and T. Hibiya 1981 Water absorption of oocytes in the plaice *Limanda yokohamae* during meiotic maturation and its role in rupturing follicles. Bull. Jap. Soc. Sci. Fisheries, **47:** 835 - 841.

Oshiro, T., and T. Hibiya 1982 Protease secretion of ovarian follicles in the loach *Misgurnus anguillicaudatus,* suggesting the presence of ovulation-inducing enzymes. Bull. Jap. Soc. Sci. Fisheries, **48:** 623 - 628.

Otake, T., and K. Mizue 1985 The fine structure of the placenta of the blue shark, *Prionace glauca.* Jap. J. Ichthyol., **32:** 52 - 59.

Otake, T., and K. Mizue 1986 The fine structure of the intra-uterine epithelium during late gestation in the blue shark, *Prionace glauca.* Jap. J. Ichthyol., **33:** 162 - 167.

Pankhurst, N.W. 1997 *In vitro* steroid production by isolated ovarian follicles of the striped trumpeter. J. Fish Biol., **51:** 669 - 685.

Pant, M.C. 1968 The process of atresia and the fate of the discharged follicle in the ovary of *Glyptothorax pectinopterus.* Zool. Anz., **181:** 153 - 160.

Parmentier, H.K., J.G.M. van den Boogaart, and L.P.M. Timmermans 1985 Physiological compartmentation in gonadal tissue of the common carp *(Cyprinus carpio* L.). A study with horseradish peroxidase and monoclonal antibodies. Cell Tissue Res., **242:** 75 - 81.

Parmentier, H.K., and L.P.M. Timmermans 1985 The differentiation of germ cells and gonads during development of carp *(Cyprinus carpio* L.). A study with anti-carp sperm monoclonal antibodies. J. Embryol. Exper. Morphol., **90:** 13 - 32.

Patiño, R., and H. Kagawa 1999 Regulation of gap junctions and oocyte maturational competence by gonadotropin and insulin-like growth factor-I in ovarian follicles of red seabream. Gen. Comp. Endocrinol., **115:** 454 - 462.

Patiño, R., and P. Thomas 1990 Effects of gonadotropin on ovarian intrafollicular processes during the development of oocyte maturational competence in a teleost, the Atlantic croaker: evidence for two distinct stages of gonadotropic control of final oocyte maturation. Biol. Reprod., **43:** 818 - 827.

Patzner, R.A. 1974 Die frühen Stadien der Oogenese bei *Myxine glutinosa* L. (Cyclostomata). Licht- und elektronenmikroskopische Untersuchungen. Norw. J. Zool., **22:** 81 - 93.

Patzner, R.A. 1975 Die fortschreitende Entwicklung und Reifung der Eier von *Myxine glutinosa* L. (Cyclostomata). Licht- und elektronenmikroskopische Untersuchungen. Norw. J. Zool., **23:** 111 - 120.

Patzner, R.A. 1978 Cyclical changes in the ovary of the hagfish *Eptatretus burgeri* (Cyclostomata). Acta Zool. (Stockh.), **59:** 57 - 61.

Patzner, R.A. 1984 The reproduction of *Blennius pavo* (Teleostei, Blenniidae). II. Surface structures of the ripe egg. Zool. Anz., **213:** 44 - 50.

Pendergrass, P., and P. Schroeder 1976 The ultrastructure of the thecal cell of the teleost, *Oryzias latipes,* during ovulation in vitro. J. Reprod. Fert., **47:** 229 - 233.

Peter, R.E., and K.L. Yu 1997 Neuroendocrine regulation of ovulation in fishes: basic and applied aspects. Rev. Fish Biol. Fisheries, **7:** 173 - 197.

Petrino, T.R. et al. 1989 Steroidogenesis in *Fundulus heteroclitus.* II. Production of 17α-hydroxy-20β-dihydroprogesterone, testosterone, and 17β-estradiol by various components of the ovarian follicle. Gen. Comp. Endocrinol., **76:** 230 - 240.

Petrino, T.R. et al. 1993 Steroidogenesis in *Fundulus heteroclitus.* V. Purification, characterization, and metabolism of 17α,20β-dihydroxy-4-pregnen-3-one by intact follicles and its role in oocyte maturation. Gen. Comp. Endocrinol., **92:** 1 - 15.

Pinter, J., and P. Thomas 1999 Induction of ovulation of mature oocytes by the maturation-inducing steroid 17α,20β,21-trihydroxy-4-pregnen-3-one in the spotted seatrout. Gen. Comp. Endocrinol., **115:** 200 - 209.

Potter, H., and C.R. Kramer 2000 Ultrastructural observations on sperm storage in the ovary of the platyfish, *Xiphophorus maculatus* (Teleostei: Poeciliidae): the role of the duct epithelium. J. Morphol., **245:** 110 - 129.

Potts, W.T.W., and P.P. Rudy, Jr. 1969 Water balance in the eggs of the Atlantic salmon *Salmo salar.* J. Exper. Biol., **50:** 223 - 237.

Pratt, H.L. 1988 Elasmobranch gonad structure: a description and survey. Copeia, **1988:** 719 - 729.

Pratt, H.L. 1993 The storage of spermatozoa in the oviducal glands of western North Atlantic sharks. Environ. Biol. Fishes, **38:** 139 - 149.

Prisco, M., L. Ricchiari, and P. Andreuccetti 2001 An ultrastructural study of germ cells during ovarian differentiation in *Torpedo marmorata.* Anat. Rec., **263:** 239 - 247.

Pusey, B.J., and T. Stewart 1989 Internal fertilization in *Lepidogalaxias salmandroides* Mees (Pisces: Lepidogalaxiidae). Zool. J. Linnean Soc., **97:** 69 - 79.

Qasim, S.Z. 1955 Time and duration of the spawning season in some marine teleosts in relation to their distribution. Journal du Conseil (Conseil Permanent International pour l'Exploration de la Mer), **21:** 144 - 155.

Rai, B.P. 1966 The corpora atretica and the so-called corpora lutea in the ovary of *Tor (Barbus) tor* (Ham.). Anat. Anz., **119:** 459 - 465.

Rastogi, R.K. 1969 The occurrence and significance of ovular atresia in the fresh water mud-eel, *Amphipnous cuchia* (Ham.). Acta Anat., **73:** 148 - 160.

Rideout, R.M., M.P.M. Burton, and G.A. Rose 2000 Observations on mass atresia and skipped spawning in northern Atlantic cod, from Smith Sound, Newfoundland. J. Fish Biol., **57:** 1429 - 1440.

Ridgway, E.B., J.C. Gilkey, and L.F. Jaffe 1977 Free calcium increases explosively in activating medaka eggs. Proc. Natl. Acad. Sci. USA, **74:** 623 - 627.

Riehl, R. 1977 Licht- und elektronenmikroskopische Untersuchungen zu Bau und Entwicklung der Mikropylen von *Noemacheilus barbatulus* (L.) und *Gobio gobio* (L.) (Pisces, Teleostei). Zool. Anz., **198:** 313 - 327.

Riehl, R. 1980 Micropyle of some salmonins and coregonins. Environ. Biol. Fishes, **5:** 59 - 66.

Riehl, R., and M. Kokoscha 1993 A unique surface pattern and micropylar apparatus in the eggs of *Luciocephalus* sp. (Perciformes, Luciocephalidae). J. Fish Biol., **43:** 617 - 620.

Rusaouën, M. 1976 The dogfish shell gland, a histochemical study. J. Exper. Marine Ecol., **23:** 267 - 283.

Rusaouën, M. 1978 Étude ultrastructurale des zones à sécrétions protéiques et glycoprotéiques de la glande nidamentaire de la Roussette, à maturité. Arch d'Anat. Microsc., **67:** 107 - 119.

Rusaouën, M. et al. 1976 Evidence of collagen in the egg capsule of the dogfish, *Scyliorhinus canicula.* Comp. Biochem. Physiol., **53B:** 539 - 543.

Rusaouën-Innocent, M. 1990a Tannage quinonique de la capsule ovigère de la Rousette *Scyliorhinus canicula* (Linné). Can. J. Zool., **68:** 2553 - 2563.

Rusaouën-Innocent, M. 1990b A radioautographic study of collagen secretion in the dogfish nidamental gland. Tissue & Cell, **22:** 449 - 462.

Saidapur, S.K. 1978 Follicular atresia in the ovaries of non-mammalian vertebrates. Int. Rev. Cytol., **54:** 225 - 244.

Saidapur, S.K., and V.B. Nadkarni 1976 Steroid synthesizing cellular sites in the ovary of catfish, *Mystus cavasius:* a histochemical study. Gen. Comp. Endocrinol., **30:** 457 - 461.

Sakai, Y.T. 1961 Method for removal of chorion and fertilization of the naked egg in *Oryzias latipes.* Embryologia, **5:** 357 - 368.

Scapigliati, G. et al. 1995 Characterization of the main egg chorion proteins of the whitefish *Coregonus lavaretus* L. (Osteichthyes, Salmonidae). Comp. Biochem. Physiol., **112B:** 169 - 175.

Schalkoff, M.E., and N.H. Hart 1986 Effects of A23187 upon cortical granule exocytosis in eggs of *Brachydanio.* Roux Arch. Dev. Biol., **195:** 39 - 48.

Schindler, J.F. 1990 Retrograde trafficking of tracer protein by the internal ovarian epithelium in gravid goodeid teleosts. Anat. Rec., **226:** 177 - 186.

Schindler, J.F., and W.C. Hamlett 1993 Maternal-embryonic relations in viviparous teleosts. J. Exper. Zool., **266:** 378 - 393.

Schindler, J.F., and R. Kujat 1990 Structure and function of the trophotaenial placenta in the goodeid teleost, *Skiffia bilineata.* Z. Mikrosk.-Anat. Forsch., **104:** 241 - 257.

Schindler, J.F., R. Kujat, and U. deVries 1988 Maternal-embryonic relationships in the goodeid teleost, *Xenophorus captivus.* The internal ovarian epithelium and the embryotrophic fluid. Cell Tissue Res., **254:** 177 - 182.

Schindler, J.F., and U. deVries 1986a Ultrastructure of embryonic anal processes on *Girardinichthys viviparus* (Cyprinodontiformes, Osteichthyes). J. Morphol., **188:** 203 - 224.

Schindler, J.F., and U. deVries 1986b Surface ultrastructure of trophotaeniae, placental analogues appending to goodeid embryos. Z. Mikrosk.-Anat. Forsch., **100:** 939 - 949.

Schindler, J.F., and U. deVries 1987a Protein uptake and transport by trophotaenial absorptive cells in two species of goodeid embryos. J. Exper. Zool., **241:** 17 - 29.

Schindler, J.F., and U. deVries 1987b Maternal-embryonic relationships in the goodeid teleost, *Xenoophorus captivus.* Embryonic structural adaptations to viviparity. Cell Tissue Res., **247:** 325 - 338.

Schindler, J.F., and U. deVries 1988a Maternal-embryonic relationships in the goodeid teleost, *Xenoophorus captivus.* The vacuolar apparatus in trophotaenial absorptive cells and its role in macromolecular transport. Cell Tissue Res., **253:** 115 - 128.

Schindler, J.F., and U. deVries 1988b Ovarian structural specializations facilitate aplacental matrophy in *Jenynsia lineata* (Cyprinodontiformes, Osteichthyes). J. Morphol., **198:** 331 - 339.

Schindler, J.F., and U. deVries 1990 Membrane differentiations of an absorptive epithelium covering embryonic trophotaeniae in a goodeid teleost. Cell Tissue Res., **259:** 321 - 330.

Schlernitzauer, D.A., and P.W. Gilbert 1966 Placentation and associated aspects of gestation in the bonnethead shark, *Sphryna tiburo.* J. Morphol., **120:** 219 - 231.

Schmehl, M.K., and E.F. Graham 1987 Comparative ultrastructure of the zona radiata from eggs of six species of salmonids. Cell Tissue Res., **250:** 513 - 519.

Schoonen, W.G.E.J. et al. 1989 Steroidogenesis during induced oocyte maturation and ovulation in the African catfish, *Clarias gariepinus.* Fish Physiol. Biochem., **6:** 61 - 78.

Schoots, A.F.M. et al. 1982 Hatching in teleostean fishes: fine structural changes in the egg envelope during enzymatic breakdown *in vivo* and *in vitro.* J. Ultrastruct. Res., **80:** 185 - 196.

Schroeder, P.C., and P. Pendergrass 1976 The inhibition of in-vitro ovulation from follicles of the teleost, *Oryzias latipes,* by cytochalasin B. J. Reprod. Fert., **48:** 327 - 330.

Schulz, R. 1986 Immunohistological localization of 17β-estradiol and testosterone in the ovary of the rainbow trout *(Salmo gairdneri* Richardson) during the preovulatory period. Cell Tissue Res., **245:** 629 - 633.

Scott, A.P., and A.V.M. Canario 1987 Status of oocyte maturation-inducing steroids. *In* Proceedings of the Third International Symposium on the Reproductive Physiology of Fish, St. John's Newfoundland, Canada, D.R. Idler, L.W. Crim, and J.M. Walsh, eds., pp. 224 - 234.

Scott, D.B.C. 1974 The reproductive cycle of *Mormyrus kannume* Forsk. (Osteoglossomorpha, Mormyriformes) in Lake Victoria Uganda. J. Fish Biol., **6:** 447 - 454.

Seiler, K., R. Seiler, and R. Claus 1981 Histochemical and spectrophotometric demonstration of hydroxysteroid dehydrogenase activity in the presumed steroid producing cells of the brook lamprey *(Lampetra planeri* Bloch) during metamorphosis. Endokrinologie, **78:** 297 - 300.

Seko, A. et al. 1989 Structural studies of fertilization-associated carbohydrate-rich glycoproteins (hyosophorin) isolated from the fertilized and unfertilized eggs of flounder, *Paralichthys olivaceus.* J. Biol. Chem., **264:** 15922 - 15929.

Selman, K. et al. 1993 Stages of oocyte development in the zebrafish, *Brachydanio rerio.* J. Morphol., **218:** 203 - 224.

Selman, K., and R.A. Wallace 1982a Oocyte growth in the sheepshead minnow: uptake of exogenous proteins by vitellogenic oocytes. Tissue & Cell, **14:** 555 - 571.

Selman, K., and R.A. Wallace 1982b The inter- and intracellular passage of proteins through the ovarian follicle in teleosts. *In* Proceedings of the International Symposium on Reproductive Physiology of Fish, Wageningen, the Netherlands, 2 - 6 August 1982, C.J.J. Richter and H.J.T. Goos, eds. Wageningen: Centre for Agricultural Publishing and Documentation, pp. 151 -157.

Selman, K., and R.A. Wallace 1983 Oogenesis in *Fundulus heteroclitus.* III. Vitellogenesis. J. Exper. Zool., **226:** 441 - 457.

Selman, K., and R.A. Wallace 1986 Gametogenesis in *Fundulus heteroclitus.* Am. Zool., **26:** 173 - 192.

Selman, K., and R.A. Wallace 1989 Review: Cellular aspects of oocyte growth in teleosts. Zool. Sci., **6:** 211 - 231.

Selman, K., R.A. Wallace, and V. Barr 1986 Oogenesis in *Fundulus heteroclitus.* IV. Yolk vesicle formation. J. Exper. Zool., **239:** 277 - 288.

Selman, K., R.A. Wallace, and V. Barr 1988 Oogenesis in *Fundulus heteroclitus.* V. The relationship of yolk vesicles and cortical alveoli. J. Exper. Zool., **246:** 42 - 56.

Selman, K., R.A. Wallace, and D. Player 1991 Ovary of the seahorse, *Hippocampus erectus.* J. Morphol., **209:** 285 - 304.

Shackley, S.E., and P.E. King 1977 Oogenesis in a marine teleost, *Blennius pholis* L. Cell Tissue Res., **181:** 105 - 128.

Shackley, S.E., and P.E. King 1979 Lipid yolk synthesis in a marine teleost, *Blennius pholis* L. Cell Tissue Res., **204:** 507 - 512.

Shelton, W.L. 1978 Fate of the follicular epithelium in *Dorosoma petenense* (Pisces: Clupeidae). Copeia, **1978:** 237 - 244.

Shrivastava, S.S. 1969 Formation of the corpora atretica in *Notopterus notopterus* (Pallas). Acta Zool. (Stockh.), **50:** 77 - 89.

Smith, C.L., and S.R. Haley 1987 Evidence of steroidogenesis in postovulatory follicles of the tilapia, *Oreochromis mossambicus.* Cell Tissue Res., **247:** 675 - 687.

Smith, C.L., et al. 1975 *Latimeria,* the living coelacanth is ovoviviparous. Science, **190:** 1105 - 1106.

Song, Y., K. Kitajima, and Y. Inoue 1990 New tandem-repeating peptide structures in polysialoglycoproteins from the unfertilized eggs of kokanee salmon. Arch. Biochem. Biophys., **283:** 167 - 172.

Srivastava, S.J., and A.K. Saxena 1996 Morphological changes in hepatocytes in relation to reproductive cycle of a freshwater female catfish, *Heteropneustes fossilis* (Bloch). J. Anv. Zool., **17:** 98 - 104.

Stanley, H.P. 1963 Urogenital morphology in the chimaeroid fish *Hydrolagus colliei* (Lay and Bennett). J. Morphol., **112:** 99 - 124.

Stehr, C.M., and J.W. Hawkes 1979 The comparative ultrastructure of the egg membrane and associated pore structures in the starry flounder, *Platichthys stellatus* (Pallas), and pink salmon, *Oncorhynchus gorbuscha* (Walbaum). Cell Tissue Res., **202:** 347 - 356.

Stehr, C.M., and J.W. Hawkes 1983 The development of the hexagonally structured egg envelope of the C-O sole, *(Pleuronichthys coenosus).* J. Morphol., **178:** 267 - 284.

Suzuki, K., E.S.P. Tan, and B. Tamaoki 1989 Change of steroidogenic pathways in the ovary of a tropical catfish, *Clarias macrocephalus,* Gunther, after hCG treatment. Gen. Comp. Endocrinol., **76:** 223 - 229.

Szöllösi, D., and R. Billard 1974 The micropyle of trout eggs and its reaction to different incubation media. J. Microsc. (Paris), **21:** 55 - 62.

Szöllösi, D., and B. Jalabert 1974 La thèque du follicule ovarien de la Truite. J. Microsc. (Paris), **20:** 92a.

Szöllösi, D., B. Jalabert, and B. Breton 1978 Postovulatory changes in the theca folliculi of the trout. Ann. Biol. Anim. Bioch. Biophys., **18:** 883 - 891.

Taguchi, T. et al. 1993 Structural studies of a novel type of tetraantennary sialoglycan unit in a carbohydrate-rich glycopeptide isolated from the fertilized eggs of Indian medaka fish, *Oryzias melastigma.* J. Biol. Chem., **268:** 2353 - 2362.

Takahashi, H., and K. Takano 1971 Sex hormone-induced precocious hypertrophy and ciliation of epithelial cells in the ovarian lumen of the goldfish. Annot. Zool. Jap., **44:** 32 - 41.

Takano, K. 1964 On the egg formation and the follicular changes in *Lebistes reticulatus.* Bull. Fac. Fish. Hokkaido Univ., **15:** 147 - 155.

Takano, K. 1968 Fine structure of the wall of the ovarian lumen in the teleost, *Oryzias latipes.* Bull. Fac. Fish. Hokkaido Univ., **19:** 76 - 82.

Takano, K., and H. Ohta 1982 Ultrastructure of micropylar cells in the ovarian follicles of the pond smelt, *Hypomesus transpacificus nipponensis.* Bull. Fac. Fish. Hokkaido Univ., **33:** 65 - 78.

Takemura, A., and K. Takano 1995 Lysozyme in the ovary of tilapia *(Oreochromis mossambicus):* its purification and some biological properties. Fish Physiol. Biochem., **14:** 415 - 421.

Tang, F., B. Lofts, and S.T.H. Chan 1974 Δ^5 3β-hydroxysteroid dehydrogenase activities in the ovary of the rice-field eel, *Monopterus albus* (Zuiew). Experientia, **30:** 316 - 317.

Teshima, K. 1975 Studies on sharks — VIII. Placentation in *Mustelus griseus.* Jap. J. Ichthyol., **22:** 7 - 12.

Teshima, K., M. Ahmad, and K. Mizue 1978 Studies on sharks — XIV. Reproduction in the Telok Anson shark collected from Perak River, Malaysia. Jap. J. Ichthyol., **25:** 181 - 189.

Teshima, K., and K. Mizue 1972 Studies on sharks. I. Reproduction in the female sumitsuki shark *Carcharhinus dussumieri.* Marine Biol., **14:** 222 - 231.

Tesoriero, J.V. 1977a Formation of the chorion (zona pellucida) in the teleost, *Oryzias latipes.* I. Morphology and early oogenesis. J. Ultrastruct. Res., **59:** 282 - 291.

Tesoriero, J.V. 1977b Formation of the chorion (zona pellucida) in the teleost, *Oryzias latipes.* II. Polysaccharide cytochemistry of early oogenesis. J. Histochem. Cytochem., **25:** 1376 - 1380.

Tesoriero, J.V. 1978 Formation of the chorion (zona pellucida) in the teleost, *Oryzias latipes.* III. Autoradiography of [^{3}H] proline incorporation. J. Ultrastruct. Res., **64:** 315 - 326.

Tesoriero, J.V. 1980 The distribution and fate of ^{3}H-glucose and ^{3}H-galactose in oocytes of *Oryzias latipes.* Cell Tissue Res., **209:** 117 - 129.

TeWinkel, L.E. 1972 Histological and histochemical studies of post-ovulatory and pre-ovulatory atretic follicles in *Mustelis canis.* J. Morphol., **136:** 433 - 458.

Theofan, G., and F.W. Goetz 1981 The *in vitro* effects of actinomycin D and cyclohexamide on germinal vesicle breakdown and ovulation of yellow perch *(Perca flavescens)* oocytes. Comp. Biochem. Physiol., **69A:** 557 - 561.

Thiaw, O.T., and X. Mattei 1991 Morphogenesis of the secondary envelope of the oocyte in a teleostean fish of the family Cyprinodontidae: *Aphyosemion splendopleure.* J. Submicrosc. Cytol. Pathol., **23:** 419 - 426.

Thiaw, O.T., and X. Mattei 1992 Perimicropylar filaments in eggs of Cyprinodontidae (Pisces, Teleostei). Can. J. Zool., **70:** 1064 - 1068.

Thiaw, O.T., and X. Mattei 1996 Ultrastructure of the secondary egg envelope of Cyprinodontidae of the Genus *Epiplatys* Gill, 1862 (Pisces, Teleostei). Acta Zool. (Stockh.), **77:** 161 - 166.

Thibault, R.E., and R.J. Schultz 1978 Reproductive adaptations among viviparous fishes (Cyprinodontiformes: Poeciliidae). Evolution, **32:** 320 - 333.

Thomas, P., and R. Patiño 1991 Changes in 17α,20β,21-trihydroxy-4-pregnen-3-one membrane receptor concentrations in ovaries of spotted seatrout during final oocyte maturation. *In* Proceedings of the Fourth International Symposium on the Reproductive Physiology of Fish, A.P. Scott, J.P. Sumpter, D.E. Kime, and M.S. Rolfe, eds. Sheffield U.K.: FishSymp 91, pp. 122 - 124.

Thomas, P., and J.M. Trant 1989 Evidence that 17α,20β,21-trihydroxy-4-pregnene-3-one is a maturation-inducing steroid in spotted seatrout. Fish Physiol. Biochem., **7:** 185 - 191.

Thorsen, A., and H.J. Fyhn 1996 Final oocyte maturation *in vivo* and *in vitro* in marine fishes with pelagic eggs; yolk protein hydrolysis and free amino acid content. J. Fish Biol., **48:** 1195 - 1209.

van Tienhoven, A. 1983 Reproductive Physiology of Vertebrates, 2nd ed. Ithaca: Cornell University Press, 491 pp.

Timmermans, L.P.M., and N. Taverne 1989 Segregation of primordial germ cells: their numbers and fate during early development of *Barbus conchonius* (Cyprinidae, Teleostei) as indicated by ^{3}H-thymidine incorporation. J. Morphol., **202:** 225 - 237.

Tokarz, R.R. 1978 Ooogonial proliferation, oogenesis, and folliculogenesis in nonmammalian vertebrates. Chapter 5 *in* The Vertebrate Ovary: Comparative Biology and Evolution, R.E. Jones, ed. New York: Plenum Press, pp. 145 - 179.

Tokumoto, T. 1999 Nature and role of proteasomes in maturation of fish oocytes. Int. Rev. Cytol., **186:** 261 - 294.

Tokumoto, M. et al. 1997 Involvement of 26S proteasome in oocyte maturation of goldfish *Carassius auratus.* Zool. Sci., **14:** 347 - 351.

Toshimori, K., and F. Yasuzumi 1979a Tight junctions between ovarian follicle cells in the teleost *(Plecoglossus altivelis).* J. Ultrastruct. Res., **67:** 73 - 78.

Toshimori, K., and F. Yasuzumi 1979b Gap junctions between microvilli of an oocyte and follicle cells in the teleost *(Plecoglossus altivelis).* Z. Mikrosk.-Anat. Forsch., **93:** 458 - 464.

Trant, J.M., and P. Thomas 1989a Isolation of a novel maturation-inducing steroid produced *in vitro* by ovaries of Atlantic croaker. Gen. Comp. Endocrinol., **75:** 397 - 404.

Trant, J.M., and P. Thomas 1989b Changes in ovarian steroidogenesis *in vitro* associated with final maturation of Atlantic croaker oocytes. Gen. Comp. Endocrinol., **75:** 405 - 412.

Trant, J.M., P. Thomas, and C.H.L. Shackleton 1986 Identification of 17α,20β,21-trihydroxy-4-pregnen-3-one as the major ovarian steroid produced by the teleost *Micropogonias undulatus* during final oocyte maturation. Steroids, **47:** 89 - 99.

Treasurer, J.W. 1990 The annual reproductive cycle of pike, *Esox lucius* L., in two Scottish lakes. J. Fish Biol., **36:** 29 - 46.

Treasurer, J.W., and F.G.T. Holliday 1981 Some aspects of the reproductive biology of perch *Perca fluviatilis* L. A histological description of the reproductive cycle. J. Fish Biol., **18:** 359 - 376.

Truscott, B. et al. 1992 Steroids involved with final oocyte maturation in the winter flounder. J. Steroid Biochem. Molec. Biol., **42:** 351 - 356.

Tsang, P., and I.P. Callard 1983 *In vitro* steroid production by ovarian granulosa cells of *Squalus acanthias.* Bull. Mount Desert Island Biol. Labs., **23:** 78 - 79.

Tsang, P., and I.P. Callard 1992 Regulation of ovarian steroidogenesis in vitro in the viviparous shark, *Squalus acanthias.* J. Exper. Zool., **261:** 97 - 104.

Tsukahara, J. 1971 Ultrastructural study on the attaching filaments and villi of the oocyte of *Oryzias latipes* during oogenesis. Develop. Growth Differ., **13:** 173 - 180.

Tsuneki, K., and A. Gorbman 1977 Ultrastructure of the ovary of the hagfish *Eptatretus stouti.* Acta Zool. (Stockh.), **58:** 27 - 40.

Turner, C.L. 1933 Viviparity superimposed upon ovo-viviparity in the Goodeidae, a family of cyprinodont teleost fishes of the Mexican Plateau. J. Morphol., **55:** 207 - 251.

Turner, C.L. 1936 The absorptive processes in the embryos of *Parabrotula dentiens,* a viviparous deep-sea brotulid fish. J. Morphol., **59:** 313 - 325.

Turner, C.L. 1937 Reproductive cycles and superfetation in pœciliïd fishes. Biol. Bull., **72:** 145 - 164.

Turner, C.L. 1938a Adaptations for viviparity in embryos and ovary of *Anableps anableps.* J. Morphol., **62:** 323 - 349.

Turner, C.L. 1938b Histological and cytological changes in the ovary of *Cymatogaster aggregatus* during gestation. J. Morphol., **62:** 351 - 368.

Turner, C.L. 1940a Pseudoamnion, pseudochorion, and follicular pseudoplacenta in poecilid fishes. J. Morphol., **67:** 59 - 89.

Turner, C.L. 1940b Follicular pseudoplacenta and gut modifications in anablepid fishes. J. Morphol., **67:** 91 - 105.

Turner, C.L. 1940c Pericardial sac, trophotaeniae, and alimentary tract in embryos of goodeid fishes. J. Morphol., **67:** 271 - 289.

Turner, C.L. 1940d Adaptations for viviparity in jenynsiid fishes. J. Morphol., **67:** 291 - 297.

Turner, C.L. 1947 Viviparity in teleost fishes. Sci. Monthly, **65:** 508 - 518.

Turner, C.L. 1952 An accessory respiratory device in embryos of the embiotocid fish, *Cymatogaster aggregata,* during gestation. Copeia, **1952:** 146 - 147.

Ulrich, E. 1969 Étude des ultrastructures au cours de l'ovogenèse d'un poisson Téléostéen, le Danio *Brachydanio rerio* (Hamilton-Buchanan). J. Microsc. (Paris), **8:** 447 - 478.

Veith, W.J. 1979a The chemical composition of the follicular fluid of the viviparous teleost *Clinus superciliosus.* Comp. Biochem. Physiol., **63A:** 37 - 40.

Veith, W.J. 1979b Reproduction in the live-bearing teleost *Clinus superciliosus.* S. Afr. J. Zool., **14:** 208 - 211.

Veith, W.J. 1980 Viviparity and embryonic adaptations in the teleost *Clinus superciliosus.* Can. J. Zool., **58:** 1 - 12.

Venkatesh, B. et al. 1992 Steroid metabolism by ovarian follicles and extrafollicular tissue of the guppy *(Poecilia reticulata)* during oocyte growth and gestation. Gen. Comp. Endocrinol., **86:** 378 - 394.

Venkatesh, B., C.H. Tan, and T.J. Lam. 1992a Steroid production by ovarian follicles of the viviparous guppy *(Poecilia reticulata),* and its regulation by precursor substrates, dibutyryl cAMP and forskolin. Gen. Comp. Endocrinol., **85:** 450 - 461.

Venkatesh, B., C.H. Tan, and T.J. Lam 1992b Prostaglandin synthesis in vitro by ovarian follicles and extrafollicular tissue of the viviparous guppy *(Poecilia reticulata)* and its regulation. J. Exper. Zool., **262:** 405 - 413.

de Vlaming, V. et al. 1983 Aspects of embryo nutrition and excretion among viviparous embiotocid teleosts: potential endocrine involvements. Comp. Biochem. Physiol., **76A:** 189 - 198.

Wake, M.H. 1985 Oviduct structure and function in non-mammalian vertebrates. Fortschr. Zool., **30:** 427 - 435.

Wallace, R.A. 1978 Oocyte growth in nonmammalian vertebrates. Chapter 13 *in* The Vertebrate Ovary: Comparative Biology and Evolution, R.E. Jones, ed. New York: Plenum Press, pp. 469 - 502.

Wallace, R.A. 1985 Vitellogenesis and oocyte growth in nonmammalian vertebrates. *In* Developmental Biology: a Comprehensive Synthesis, vol. 1, L.W. Browder, ed. New York: Plenum Press, pp. 127 - 177.

Wallace, R.A., and K. Selman 1978 Oogenesis in *Fundulus heteroclitus.* I. Preliminary observations on oocyte maturation *in vivo* and *in vitro.* Dev. Biol., **62:** 354 - 369.

Wallace, R.A., and K. Selman 1980 Oogenesis in *Fundulus heteroclitus.* II. The transition from vitellogenesis into maturation. Gen. Comp. Endocrinol., **42:** 345 - 354.

Wallace, R.A., and K. Selman 1981 Cellular and dynamic aspects of oocyte growth in teleosts. Am. Zool., **21:** 325 - 343.

Wallace, R.A., and K. Selman 1985 Major protein changes during vitellogenesis and maturation of *Fundulus* oocytes. Dev. Biol., **110:** 492 - 498.

Walvig, F. 1963 The gonads and formation of sex cells. *In* The Biology of *Myxine.* A. Brodal and R. Fänge, eds. Oslo, Universitetsforlaget, pp. 530 - 580.

Webb, P.W., and J.R. Brett 1972 Respiratory adaptations of prenatal young in the ovary of two species of viviparous seaperch, *Rhacochilus vacca* and *Embiotoca lateralis.* J. Fisheries Res. Bd. Canada, **29:** 1525 - 1542.

Weichert, C.K. 1970 Anatomy of the Chordates, 4th ed. New York: McGraw-Hill Book Company, 814 pp.

Weisbart, M. et al. 1980 The presence of steroids in the sera of the Pacific hagfish, *Eptatretus stouti,* and the sea lamprey, *Petromyzon marinus.* Gen. Comp. Endocrinol., **41:** 506 - 519.

Weisbart, M., J.H. Youson, and J.P. Wiebe 1978 Biochemical, histochemical, and ultrastructural analyses of presumed steroid-producing tissues in the sexually mature sea lamprey, *Petromyzon marinus* L. Gen. Comp. Endocrinol., **34:** 26 - 37.

Widakowich, V. 1907 Über eine Verschlußvorrichtung im Eileiter von *Squalus acanthias.* Zool. Anz., **31:** 636 - 643.

Wiebe, J.P. 1968 The reproductive cycle of the viviparous seaperch, *Cymatogaster aggregata* Gibbons. Can. J. Zool., **46:** 1221 - 1234.

Wiegand, M.D. 1982 Vitellogenesis in fishes. *In* Proceedings of the International Symposium on Reproductive Physiology of Fish, Wageningen, the Netherlands, 2 - 6 August 1982, C.J.J. Richter and H.J.T. Goos, eds. Wageningen: Centre for Agricultural Publishing and Documentation, pp. 136 - 146.

van Winkoop, A. et al. 1992 Ultrastructural changes in primordial germ cells during early gonadal development of the common carp (*Cyprinus carpio* L., Teleostei). Cell Tissue Res., **267**: 337 – 346.

Wolenski, J.S., and N.H. Hart 1987a Scanning electron microscope studies of sperm incorporation into the zebrafish *(Brachydanio)* egg. J. Exper. Zool., **243:** 259 - 273.

Wolenski, J.S., and N.H. Hart 1987b Visualization of actin with rhodamine phalloidin in the zebrafish egg. Biol. Bull., **173:** 573.

Wolenski, J.S., and N.H. Hart 1988a Effects of cytochalasin B and D on the fertilization of zebrafish *(Brachydanio)* eggs. J. Exper. Zool., **246:** 202 - 215.

Wolenski, J.S., and N.H. Hart 1988b Sperm incorporation independent of fertilization cone formation in the danio egg. Develop. Growth Differ., **30:** 619 - 628.

Wolff, R.G. 1991 Functional Chordate Anatomy. Lexington, Massachusetts: D.C. Heath and Company, 752 pp.

Wourms, J.P. 1976 Annual fish oogenesis. I. Differentiation of the mature oocyte and formation of the primary envelope. Dev. Biol., **50:** 338 - 354.

Wourms, J.P. 1977 Reproduction and development in chondrichthyan fishes. Am. Zool., **17:** 379 - 410.

Wourms, J.P. 1981 Viviparity: the maternal-fetal relationship in fishes. Am. Zool., **21:** 473 - 515.

Wourms, J.P. 1993 Maximization of evolutionary trends for placental viviparity in the spadenose shark, *Scoliodon laticaudus.* Environ. Biol. Fishes, **38:** 269 - 294.

Wourms, J.P., J.W. Atz, and M.D. Stribling 1991 Viviparity and the maternal-embryonic relationship in the coelacanth *Latimeria chalumnae.* Environ. Biol. Fishes, **32:** 225 - 248.

Wourms, J.P., and D.M. Cohen 1975 Trophotaeniae, embryonic adaptations, in the viviparous ophidioid fish, *Oligopus longhursti:* a study of museum specimens. J. Morphol., **147:** 385 - 402.

Wourms, J.P., B.D. Grove, and J. Lombardi 1988 The maternal-embryonic relationship in viviparous fishes. Chapter 1 *in* Fish Physiology, vol. XIB, W.S. Hoar and D.J. Randall, eds. London: Academic Press, Inc., pp. 1 - 134.

Wourms, J.P., and H. Sheldon 1976 Annual fish oogenesis. II. Formation of the secondary egg envelope. Dev. Biol., **50:** 355 - 366.

Yamagami, K. 1981 Mechanisms of hatching in fish: secretion of hatching enzyme and enzymatic choriolysis. Am. Zool., **21:** 459 - 471.

Yamamoto, K. 1963 Cyclical changes in the wall of the ovarian lumen in the medaka, *Oryzias latipes.* Annot. Zool. Jap., **36:** 179 - 186.

Yamamoto, K., and I. Oota 1967 Fine structure of yolk globules in the oocyte of the zebrafish, *Brachydanio rerio.* Annot. Zool. Jap., **40:** 20 - 27.

Yamamoto, K., and H. Onozato 1968 Steroid-producing cells in the ovary of the zebrafish, *Brachydanio rerio.* Annot. Zool. Jap., **41:** 119 - 128.

Yamamoto, K., and F. Yamazaki 1966 Hormonal control of ovulation and spermiation in goldfish. Gunma Symp. Endocrinol., **4:** 131 - 145.

Yamamoto, M. 1964 Electron microscopy of fish development. III. Changes in the ultrastructure of the nucleus and cytoplasm of the oocyte during its development in *Oryzias latipes.* J. Fac. Sci. Univ. Tokyo, Sect. IV, Zool., **10:** 335 - 346.

Yamamoto, T.S. 1961 Physiology of fertilization in fish eggs. Int. Rev. Cytol., **12:** 361 - 405.

Yamamoto, T.S., and W. Kobayashi 1992 Closure of the micropyle during embryonic development of some pelagic fish eggs. J. Fish Biol., **40:** 225 - 241.

Yanagimachi, R. et al. 1992 Factors controlling sperm entry into the micropyles of salmonid and herring eggs. Develop. Growth Differ., **34:** 447 - 461.

Yaron, Z. 1971 Observations on the granulosa cells of *Acanthobrama terrae-sanctae* and *Tilapia nilotica* (Teleostei). Gen. Comp. Endocrinol., **17:** 247 - 252.

Yoneda, M. et al. 1998 Ovarian structure and batch fecundity in *Lophiomus setigerus.* J. Fish Biol., **52:** 94 - 106.

York, W.S., R. Patiño, and P. Thomas 1993 Ultrastructural changes in follicle cell-oocyte associations during development and maturation of the ovarian follicle in Atlantic croaker. Gen. Comp. Endocrinol., **92:** 402 - 418.

Yorke, M.A., and D.B. McMillan 1979 Nature and cellular origin of the adhesive coats of the lamprey egg *(Petromyzon marinus).* J. Morphol., **162:** 313 - 325.

Yorke, M.A., and D.B. McMillan 1980 Structural aspects of ovulation in the lamprey, *Petromyzon marinus.* Biol. Reprod., **22:** 897 - 912.

Yoshimoto, Y. et al. 1986 The wave pattern of free calcium release upon fertilization in medaka and sand dollar eggs. Develop. Growth Differ., **28:** 583 - 596.

Young, G., S. Adachi, and Y. Nagahama 1986 Role of ovarian thecal and granulosa layers in gonadotropin-induced synthesis of a salmonid maturation-inducing substance (17α,20β-dihydroxy-4-pregnen-3-one). Dev. Biol., **118:** 1 - 8.

Young, G., H. Kagawa, and Y. Nagahama 1982 Secretion of aromatizable Δ^4 androgens by thecal layers during estradiol-17β production by ovarian follicles of amago salmon *(Oncorhynchus rhodurus) in vitro.* Biomed. Res., **3:** 659 - 667.

Young, G., H. Kagawa, and Y. Nagahama 1983 Evidence for a decrease in aromatase activity in the ovarian granulosa cells of amago salmon *(Oncorhynchus rhodurus)* associated with final oocyte maturation. Biol. Reprod., **29:** 310 - 315.

Yu, J.Y.-L. et al. 1981 Vitellogenesis and its hormonal regulation in the Pacific hagfish, *Eptatretus stouti* L. Gen. Comp. Endocrinol., **43:** 492 - 502.

Zapata, A. 1981 Ultrastructure of elasmobranch lymphoid tissue. 2. Leydig's and epigonal organs. Dev. Comp. Immunol., **5:** 43 - 52.

Zapata, A.G. et al. 1996 Structure of the lymphoid organs of elasmobranchs. J. Exper. Zool., **275:** 125 - 143.

Zotin, A.I. 1958 The mechanism of hardening of the salmonid egg membrane after fertilization or spontaneous activation. J. Embryol. Exper. Morphol., **6:** 546 - 568.

INDEX